ELECTRODIALYSIS OF SALTS,

ACIDS AND BASES

BY ELECTRO-OSMOTIC PUMPING

by

J J Schoeman

CONTENTS

ELECTRODIALYSIS OF SALTS, ACID AND BASES
BY ELECTRO-OSMOTIC PUMPING

EXECUTIVE SUMMARY

Electro-osmotic pumping (EOP) is a variant of conventional electrodialysis (ED) that should be suitable for concentration/desalination of saline waters. In EOP, brine is not circulated through the brine compartments, but is evolved in a closed cell. Brine enters the cell as electro-osmotic and osmotic water and leaves the cell by electro-osmotic pumping. This leads to very high concentration factors (high brine concentration) and thus high recovery of product water and small volume of brine to be disposed of. The relatively simple design of an EOP-ED stack and the possibility that an EOP-ED stack may be cheaper than conventional ED are the major advantages of EOP-ED.

Electro-osmotic pumping of sodium chloride solutions has been described in the literature. Water and salt fluxes were studied through ion-exchange membranes as a function of current density and feed concentration and mathematical models were developed to describe the experimental data. It has been reported that current efficiency determined in EOP experiments was close to the value expected from transport number determinations when sodium chloride solutions were electrodialyzed. It has also been reported that apparent transport numbers gave a lower estimate of current efficiency in ED. However, only results for sodium chloride solutions and one commercially available ion-exchange membrane, viz. *Selemion* AMV and CMV were reported. It would be very useful if membrane performance for concentration/desalination applications could be accurately predicted from transport numbers obtained from simple potential measurements. Information in this regard for ion-exchange membranes to be used for saline, acidic and basic effluent treatment, is insufficient.

A sealed-cell ED (SCED) laboratory stack (EOP-ED stack) was also developed and evaluated for desalination/concentration of sodium chloride solutions. However, a membrane type that is not commercially available, viz., polysulphone based membrane, has been used in the SCED studies. Only desalination/concentration of sodium chloride solutions has been reported in the studies. Saline, acidic and alkaline effluents frequently occur in industry. These effluents have the potential to be treated with EOP-ED for water and chemical recovery and effluent volume reduction. No information, however, could be found in the literature regarding EOP characteristics (brine volume, current efficiency, electro-osmotic coefficients, etc.) of membranes suitable for EOP-ED of acidic and alkaline solutions. Little information is also available in the literature regarding EOP characteristics of membrane types to be used for EOP-ED of saline solutions. Consequently, information regarding EOP characteristics of commercially available ion-exchange membranes suitable for saline, acidic and basic effluent treatment

is insufficient and information in this regard will be necessary to select membranes suitable for EOP-ED of saline, acidic and basic effluents. No information also exists regarding the performance of an EOP-ED stack for concentration/desalination of industrial effluents.

Much information, on the other hand, is available in the literature regarding electro-osmosis in general and factors affecting water transport through ion-exchange membranes. Much information is also available in the literature regarding concentration/desalination of saline solutions and saline industrial effluents with conventional ED and electrodialysis reversal (EDR). Conventional ED and EDR, however, are established processes for water and wastewater treatment. These processes are applied with success for water and wastewater treatment.

The objectives of this study were therefore to:

a) consider and fully document the relevant EOP-ED and ED theory;

b) study the EOP-ED characteristics (transport numbers, brine concentration, current efficiency, current density, electro-osmotic coefficients, etc.) of commercially available and other membranes in a single cell pair (cp) with the aim of identifying membranes suitable for EOP-ED;

c) develop a simple method and to evaluate existing models with which membrane performance for concentration by EOP-ED can be predicted;

d) evaluate EOP-ED for industrial effluent treatment in a conventional ED and in a sealed-cell ED (SCED) membrane stack.

A conventional ED membrane stack which was converted into an EOP-ED stack performed satisfactorily for concentration/desalination of sodium chloride-, hydrochloric acid- and caustic soda solutions. Dialysate concentrations of less than 500 mg/ℓ could be obtained in the feed water and cell pair voltage ranges from 1 000 to 10 000 mg/ℓ and 0,5 to 4,0 V/cp. Small brine volumes were obtained. Brine volume varied between 1,5 and 4,0%; 2,4 and 7,8%; and between 2,3 and 7,3% in the case of sodium chloride-, hydrochloric acid- and caustic soda solutions (1 000 to 5 000 mg/ℓ feed). Current efficiency was high. Current efficiency varied between 75,2 and 93,6%; 29,2 and 46,3%; and between 68,9 and 81,2% when sodium chloride-, hydrochloric acid- and caustic soda solutions were electrodialyzed, respectively. Low electrical energy consumptions were obtained. Electrical energy consumption was less than 2,5 kWh/m^3 product for sodium chloride solutions in the 1 000 to 3 000 mg/ℓ feed concentration range; approximately 0,2 kWh/m^3 product at 1 000 mg/ℓ hydrochloric acid feed concentration; and between 0,4 and 2,2 kWh/m^3 product for caustic soda in the 1 000 to 3 000 mg/ℓ feed concentration range. Water yield increased with increasing cell pair voltage and increasing linear flow velocity through the stack and decreased with decreasing feed water concentration. It would

be advantageous to operate an EOP-ED stack at the highest possible linear flow velocity.

Sealed-cell ED should be very effectively applied for concentration/desalination of relatively dilute (500 to 3 000 mg/ℓ TDS) non-scaling forming salt solutions. Product water with a TDS of less than 300 mg/ℓ could be produced in the feed water concentration range from 500 to 10 000 mg/ℓ TDS. Electrical energy consumption of 0,27 to 5,9 kWh/m^3 product was obtained (500 to 3 000 mg/ℓ feed water concentration range). Brine volume comprised approximately 2% of the initial feed water volume. Therefore, brine disposal cost should be reduced significantly with this technology. Sealed-cell ED became less efficient in the 5 000 to 10 000 mg/ℓ TDS feed water concentration range due to high electrical energy consumption (3,3 to 13,0 kWh/m^3 product). However, SCED may be applied in this TDS range depending on the value of the product that can be recovered.

A relatively concentrated ammonium nitrate effluent (TDS 3 600 mg/ℓ) could be successfully treated with SCED. Brine volume comprised only 2,8% of the treated water volume. Electrical energy consumption was determined at 2,7 kWh/m^3 product. Both the brine and the treated water should be reused in the process. Membrane fouling, however, may affect the process adversely and this matter needs further investigation. Treatment of scale forming waters will affect the process adversely because scale will precipitate in the membrane bags which cannot be opened for cleaning. Membrane scaling may be removed by current reversal or with cleaning solutions. However, this matter needs further investigation. Scale forming waters, however, should be avoided or treated with ion-exchange or nanofiltration prior to SCED treatment.

Sealed-cell ED has potential for treatment of relatively dilute (< 3 000 mg/ℓ TDS) non-scaling waters for chemical and water recovery for reuse. However, high TDS waters (up to approximately 16 000 mg/ℓ) should also be treated depending on the value of the product that can be recovered. The successful application of SCED technology seems to depend on the need to apply this technology in preference to conventional ED for specific applications where high brine concentrations and small brine volumes are required. Capital cost of SCED equipment should be less than that of conventional ED due to the simpler design of the SCED stack. The membrane utilization factor of 95% is much higher than in conventional ED (approximately 80%).

Electro-osmotic pumping studies in a single cell pair have shown the following:

Brine concentration increased with increasing current density and increasing feed water concentration and levels off at high current density dependent on the electro-osmotic coefficients of the membranes. Current efficiency was nearly constant over a wide range of current densities and feed water concentrations in the case of the *Selemion-* (salt and acid concentration) and *Raipore* membranes (salt

concentration). However, all the other membranes showed a slight decrease in current efficiency indicating that the limiting current density was exceeded. Water flow through the membranes (salt and base concentration) increased with increasing current density and increasing feed water concentration. Increasing water flow increased current efficiency significantly, especially in the case of the more porous heterogeneous membranes. It will therefore not be necessary for membranes to have very high permselectivities (> 0,9) for use in EOP·ED. Consequently, water flow through ED membranes also has a positive effect in ED and this effect is often neglected. The electro-osmotic coefficients decreased with increasing feed water concentration until a constant value was obtained at high current density. Osmotic flow in EOP·ED decreased with increasing current density while the electro-osmotic flow increased relative to the osmotic flow. Osmotic flow contributes significantly to the total water flow in EOP·ED. Membrane permselectivity decreased with increasing brine and feed concentration and increasing concentration gradient across the membranes.

Selemion AMV and CMV and *Ionac* membranes; *Selemion* AAV and CHV and the newly developed Israeli ABM membranes; and *Selemion* AMV and CMV, *Selemion* AMP and CMV and *Ionac* membranes performed well for salt-, acid- and base concentration, respectively. Current efficiencies varied between 62 and 91% (*Selemion* AMV and CMV); 34 and 60% (ABM-3 and *Selemion* CHV); and between 47 and 76% (*Selemion* AMV and CMV) for salt-, acid- and base concentration, respectively, in the feed water concentration range from 0,05 to 1,0 mol/ℓ.

A simple membrane potential measurement has been shown to function satisfactory to predict membrane performance for salt-, acid- and base concentration. Membrane performance could be predicted with an accuracy of 10; 20 and 20% and better for salt-, acid- and base concentration, respectively. Brine concentration could be predicted satisfactorily from apparent transport numbers and water flows. Maximum brine concentration, c_b^{max}, could be predicted satisfactorily from two simple models.

The correct Onsager relationships to be used for potential measurements and for the transport number are at zero current and zero volume flow, and at zero concentration gradient and zero volume flow, respectively. In practical ED, measurements are conducted at zero pressure and in the presence of concentration gradients and volume flows. These factors will influence the results considerably in all systems in which volume flow is important and where the concentration factor is high as encountered in EOP·ED. In measurement of membrane potential, the volume flow is against the concentration potential and in general will decrease potential. In ED water flow helps to increase current efficiency, but the concentration gradient decreases current efficiency.

Models describe the system satisfactorily for concentration of salt, acid and base solutions. Brine

concentration approached a limiting value (plateau) at high current density independent of current density and dependent on the electro-osmotic coefficients of the membranes. A constant slope (electro-osmotic coefficient) was obtained when water flow was plotted against current density. Straight lines were obtained when cell pair resistance was plotted against the specific resistance of the dialysate. Current efficiency increased with increasing flow of water through the membranes and decreased when the concentration gradient was high and the apparent transport numbers were low.

The contract objectives have been achieved in this study. It was shown that:

a)   EOP·ED should be effectively applied for concentration/desalination of relatively dilute (< 3 000 mg/ℓ TDS) non-scaling waters for chemical and water recovery and effluent volume reduction;

b)   a simple membrane potential measurement should be effectively used to predict membrane performance for potential salt-, acid- and base concentration/desalination applications;

c)   commercially available and other membranes could be identified which would be suitable for salt-, acid- and base concentration/desalination with EOP·ED and conventional ED;

d)   water transport in ED not only has a negative effect on process performance, but also has a significant positive effect on process performance by increasing current efficiency - an aspect which is neglected in ED;

e)   it will not be necessary for membranes to have very high permselectivities in EOP·ED because efficiency will be increased with an increasing feed concentration or increasing water flow through the membranes;

f)   in measurement of membrane potential the volume is against the concentration potential and in general will decrease potential;

g)   in ED water flow helps to increase current efficiency, but the concentration gradient decreases current efficiency;

h)   existing models for salt concentration describe the system satisfactorily for acid- and base concentration.

The relevant EOP·ED and ED theory were also fully documented.

This report offers the following to potential users of ED technology:

a)   it identifies membranes and membrane characteristics suitable for salt-, acid- and base concentration with EOP·ED and conventional ED;

b)   it describes a simple method that can be used to evaluate membrane performance for salt-, acid- and base EOP·ED and conventional ED applications;

c)   it demonstrates how existing models can be used to predict membrane performance for salt-, acid- and base concentration/desalination;

v

d)   it describes and explains relevant EOP-ED and ED theory;

e)   it shows how membranes can be characterized;

f)   it highlights potential ED applications.

The following actions will be taken as a result of this study:

a)   the simple membrane potential method that was developed in this study to predict membrane performance for potential salt-, acid- and base concentration/desalination applications would be used to predict membrane performance of other commercially available and newly developed membranes;

b)   EOP-ED in a conventional ED stack will be evaluated for metal and water recovery from electroplating effluents;

c)   EOP-ED and conventional ED will be evaluated for potential salt-, acid- and base concentration/desalination applications in industry;

d)   several publications will be written and submitted to refereed journals;

e)   a PhD thesis will be submitted to the University of Pretoria.

The following recommendations can be made as a result of this study:

a)   EOP-ED and ED technology should be more exploited for industrial effluent treatment for chemical and water recovery and effluent volume reduction;

b)   An EOP-ED membrane stack should be constructed from materials (gaskets, spacers, electrodes) available in South Africa for subsequent testing as an effluent concentrator;

c)   EOP-ED should be evaluated for metal and water recovery from electroplating effluents;

d)   EOP-ED and conventional ED should be evaluated for acid and caustic soda recovery from industrial effluents;

e)   heterogeneous membranes should be made and the EOP-ED characteristics should be determined;

f)   EOP-ED of other commercially available membranes should also be evaluated;

g)   existing models should be tested on other commercially and newly developed membranes.

ACKNOWLEDGEMENTS

1. INTRODUCTION

Electro-osmotic pumping (EOP) is a variant of conventional electrodialysis (ED) that should be suitable for concentration/desalination of saline waters[1]. In EOP, brine is not circulated through the brine compartments, but is evolved in a closed cell. Brine enters the cell as electro-osmotic and osmotic water and leaves the cell by electro-osmotic pumping. This leads to very high concentration factors (high brine concentration) and thus high recovery of product water and small volume of brine to be disposed of. The relatively simple design of an EOP-ED stack, the possibility that an EOP-ED stack may be cheaper than conventional ED and the small brine volume produced, are the major advantages of EOP-ED[1].

Electro-osmotic pumping of sodium chloride solutions has been described by Garza[1]; Garza and Kedem[2]; Kedem *et al.* [3]; Kedem and Cohen[4] and Kedem and Bar-On[5]. Water and salt fluxes were studied through ion-exchange membranes as a function of current density and feed concentration and mathematical models were developed to describe the experimental data[1]. Kedem has reported that current efficiency determined in EOP experiments was close to the value expected from transport number determinations when sodium chloride solutions were electrodialyzed[5]. Kedem has also reported that apparent transport numbers gave a lower estimate of current efficiency in ED[2]. However, only results for sodium chloride solutions and one commercially available ion-exchange membrane, viz. *Selemion* AMV and CMV were reported. It would be very useful if membrane performance for concentration/desalination applications could be accurately predicted from transport numbers obtained from simple potential measurements. Information in this regard for ion-exchange membranes to be used for saline, acidic and basic effluent treatment, is limited.

A sealed-cell ED (SCED - membranes are sealed together at the edges) laboratory stack (EOP-ED stack) was also developed for evaluation of desalination/concentration of sodium chloride solutions[3, 4, 5]. However, only one membrane type that is presently not commercially available, viz., polysulphone based membranes, have been used in the SCED studies. Only desalination/concentration of sodium chloride solutions has been reported in the studies. Saline, acidic and alkaline effluents frequently occur in industry. These effluents have the potential to be treated with EOP-ED for water and chemical recovery and effluent volume reduction. No information, however, could be found in the literature regarding EOP characteristics (brine volume, current efficiency, electro-osmotic coefficients, etc.) of membranes suitable for EOP-ED of acidic and alkaline solutions. In addition, little information is available in the literature regarding EOP characteristics of membrane types to be used for EOP-ED of saline solutions. Consequently, information regarding EOP characteristics of commercially

available ion-exchange membranes suitable for saline, acidic and basic solution treatment is insufficient and information in this regard will be necessary to select membranes suitable for EOP-ED of saline, acidic and basic effluents. In addition, no information exists regarding the performance of an EOP-ED stack for industrial effluent treatment. Information on the theory of EOP-ED and ED is scattered throughout the literature[1 - 5, 6 - 19] and is not well documented in any single publication.

Much information, on the other hand, is available in the literature regarding electro-osmosis in general and factors affecting water transport through ion-exchange membranes[5, 20 - 32]. Much information is also available in the literature regarding concentration/desalination of saline solutions and saline industrial effluents with conventional ED[6, 7, 33 - 37] and electrodialysis reversal (EDR)[8]. Conventional ED and EDR, however, are established processes for brackish water desalination and to a lesser extent for wastewater treatment. These processes are applied with success, especially for brackish water treatment for potable use[6, 8, 38, 39]. Conventional ED and EDR, however, have the potential to be applied more for industrial effluent treatment.

The objectives of this study were therefore to:

- Consider and document the relevant EOP-ED theory properly;
- Study the EOP-ED characteristics (transport numbers, brine concentration, current density, current efficiency, electro-osmotic coefficients, etc.) of commercially available ion-exchange and other membranes in a single cell pair with the aim to identify membranes suitable for saline, acidic and alkaline effluent treatment;
- Determine whether membrane performance can be predicted effectively from simple transport number determinations and existing models;
- Study EOP-ED of saline solutions in a conventional ED stack;
- Study EOP-ED of saline solutions and industrial effluents in a SCED stack.

2

2. LITERATURE SURVEY

2.1 Electro-osmotic Pumping of Salt Solutions with Homogeneous Ion-Exchange Membranes

Garza[1] and Garza and Kedem[2] have described electro-osmotic pumping of salt solutions with homogeneous membranes in a single cell pair. Brine concentrations, volume flows and current efficiencies were determined at different current densities (0 - 60 mA/cm^2) for three different sodium chloride feed water concentrations (0,01; 0,1 and 0,5 mol/ℓ). *Selemion* AMV and CMV and polyethylene-based membranes, however, were the only membranes used.

It was found that model calculations described the system in an appropriate way. The results predicted important results such as:

a) approaching of a limiting (plateau) value of the maximum brine concentration (c_b^{max}) as the current density is increased;

b) dependence of c_b^{max} on the electro-osmotic coefficient (EOC) of the membranes;

c) approaching of a limiting value (plateau) of current efficiency (ϵ_p) at high current density (below its limiting value);

d) approaching of a constant slope for curves of volume flow (J) through the membranes versus effective current density (I_{eff}).

It was experimentally found [1,2] that graphs of brine concentration (c_b) versus current density levelled off at high values of current and that c_b approached a maximum plateau, c_b^{max}, which depended only on the electro-osmotic coefficients (β) of the membrane pair ($c_b^{max} = \frac{1}{2} F\beta$). The smaller the ratio between the osmotic and electro-osmotic water flows, the smaller the current necessary to reach this plateau.

Graphs of volume flow versus effective current density became straight lines at high values of the current. The electro-osmotic and osmotic coefficients could be determined from the slope and the intercept of the lines, respectively. The results have agreed quite well with values obtained from a standard method[1] which is very time consuming.

The average value of the apparent transport number for the different membrane pairs

($\overline{\Delta t}$'s) was determined from the membrane potential for a concentration difference similar to that obtained in the EOP experiments at high current densities[2]. It was found to give a good (lower) estimate of the actual Coulomb efficiency of the process at a salt concentration of 0,1 mol/ℓ. However, no results at higher or lower concentrations were reported. *Selemion* AMV and CMV ion-exchange membranes were the only commercially available membranes used.

The maximum brine concentration, c_b^{max}, was predicted from the following two relationships[2]:

a) $\quad c_b^{max} = \dfrac{1}{2\beta F} \quad$ and $\qquad\qquad\qquad\qquad\qquad$ (2.1)

b) $\quad c_b^{max} = c_b (1 + J_{osm}/J_{elosm}) \qquad\qquad\qquad\qquad$ (2.2)

(Note: $J = J_{osm} + J_{elosm}$).

Good correlations between the two methods were obtained with the membranes and the salt solutions used.

The EOP results have shown that with appropriate membranes and control of polarization, EOP may be used as a good alternative to conventional ED for desalination/concentration of saline solutions. Laboratory scale EOP experiments may also be conducted as an alternative and convenient way of determining osmotic and electro-osmotic coefficients.

Experimental results were obtained for non-porous membranes. Current efficiencies were in the range of 60 - 85%. It was suggested by Garza[1] that a current efficiency of 90% could be obtained with a porous ion-exchange membrane. However, no other results were reported.

Most of the energy consumption in the EOP system will take place in the dialysate compartments[1]. Therefore, to reduce it and to suppress concentration polarization, it would be advisable to combine the membranes with open dialysate compartments containing ion-conducting spacers.

It was suggested by Garza[1] that EOP would have the following advantages in relation to conventional ED when used for desalination:

a) $\qquad$ the capital cost of the equipment would be decreased due to the simpler

construction of the unit-cell stack compared to the conventional plate-and-frame stack;

b)   the membrane utilization factor in the membrane bags could be about 95% compared to about 70 to 75% for membranes in conventional ED stacks;

c)   higher current densities would be possible in unit-cell stacks because of the higher linear flow velocities that could be obtained. These higher current densities would result in higher production rates;

d)   there would be a decrease in brine volume, and as a consequence, less brine disposal problems.

The only disadvantages could be the fact that more electrical energy per unit of product water would be experienced in the unit-cell stack because higher current densities were used. However, the increased cost for electrical energy would be more than off-set by the decrease in the cost of membrane replacement and amortization of the capital investment, according to Garza[1].

No information could be found in the literature regarding EOP characteristics (brine concentration, current efficiency, electro-osmotic coefficient, etc.) of membranes for acid and alkaline solution treatment in a single cell pair similar to that described for saline solutions.

2.2   Electro-Osmotic Pumping of Saline Solutions in a Unit-Cell Stack

The so-called unit-cell stack was described by Nishiwaki[6] for the production of concentrated brine from seawater by ED. It consisted of envelope bags formed of cation- and anion-exchange membranes sealed at the edges and provided with an outlet, alternated with feed channels. The direction of volume flow through the stack was such to cause ionic flow into the membrane bags. The only water entering the bags was the electro-osmotic water drawn along with the ions plus the osmotic flow caused by the higher pressure of the brine compared to the feed. This variant of ED is called electro-osmotic pumping (EOP) and is used for production of concentrated brine from seawater for salt production.

A simple sealed-cell ED stack (SCED) was described by Kedem et al.[3] in 1978. This cell consisted of thermally sealed polyethylene based membranes (21 bags, 5 x 9 cm). The membranes were not very selective at high salt concentration. It was found that smooth continuous operation was obtained with stable voltage and pH in the

concentration range from 0,01 to 0,04 mol/ℓ and current densities from 5 to 20 mA/cm^2.

Kedem and Cohen[4] have described the performance of a laboratory SCED unit for desalination/concentration of sodium chloride solutions. Heterogeneous ion-exchange membranes were used. The selectivity of these membranes, however, were lower than that of commercially available membranes. Nevertheless, it was demonstrated that various sodium chloride feed concentrations could be desalinated effectively. The results are shown in Table 2.1.

Table 2.1: Desalination of sodium chloride solutions at various cell pair voltages.

c_{feed}	$c_{product}$	Output	Energy Consumption	c_{brine}	Recovery	V_{cp}	d_{eff}
mg/ℓ	mg/ℓ	$\dfrac{m^3}{m^2 day}$	$\dfrac{kWh}{m^3}$	mg/ℓ	%	Volt	mm
2 670	810	3,25	1,55	82 780	98	1	1,13
1 910	320	1,86	1,33	60 610	97,3	1	1,13
1 570	570	2 60	0,56	45 800	97,8	0,72	1,07
1 910	540	1,62	0,54	46 040	97	0,5	0,82

c_f : feed concentration
c_p : product concentration
c_b : brine concentration
V_{cp} : cell pair voltage
d_{eff} : effective thickness of dialysate compartment (polarization factor).

Product water yield (output), electrical energy consumption, brine concentration, c_b, water recovery, cell pair voltage, V_{cp}, and the polarization factor (d_{eff}) are also shown in Table 2.1.

Kedem and Bar-on[5] have reported results on the desalination of sodium chloride solutions with a SCED stack using heterogeneous ion-exchange membranes. The results are shown in Table 2.2.

Table 2.2: Desalination of sodium chloride solutions at a linear flow velocity of 14,4 cm/s.

V_{cp}	c_f mg/ℓ	c_p mg/ℓ	Energy consumption kWhr/m³	Output m³/day	n_c %	c_b mg/ℓ	d_{eff} mm
0,9	2 200	100	1,01	1,41	77,0		1,24
	1 500	500	0,51	3,68	76,5	68 390	1,10
	1 000	300	0,35	3,62	79,5		0,85
0,7	2 100	100	0,80	1,16	78		0,97
	1 500	500	0,39	3,06	78,5	59 620	0,83
	1 000	300	0,27	3,05	77		0,80
0,5	2 500	500	0,53	1,22	80		0,88
	1 500	500	0,27	1,95	80	60 200	0,71
	1 000	300	0,19	2,62	80		0,60

V_{cp}	:	cell pair voltage
c_f	:	feed concentration
c_p	:	product concentration
n_c	:	current efficiency
c_b	:	brine concentration
d_{eff}	:	effective thickness of dailysate compartment (polarization factor).

The current efficiency (n_c) is shown for varying cell pair voltages and feed water concentrations. It was mentioned by Kedem and Bar-on[5] that the permselectivity of the ion-exchange membranes that were used decreased substantially at high salt concentration. This, however, is not reflected in the data on the current efficiency that was obtained in the SCED stack (Table 2.2). It appears therefore, according to Kedem and Bar-on, that electro-osmosis contributes to salt transfer and helps to maintain current efficiency.

At constant cell pair voltage (V_{cp}), polarization is nearly constant and plots of cell pair resistance (R_{cp}) versus specific resistance of the dialysate (ρ) give straight lines in a rather wide concentration range[5]. As shown in Figure 2.1, this is not true for the whole range covered. Polarization decreases slightly with increasing current. For the estimated effective thickness of the dialysate compartment, d_{eff}, this is approximated by straight lines for parts of this range.
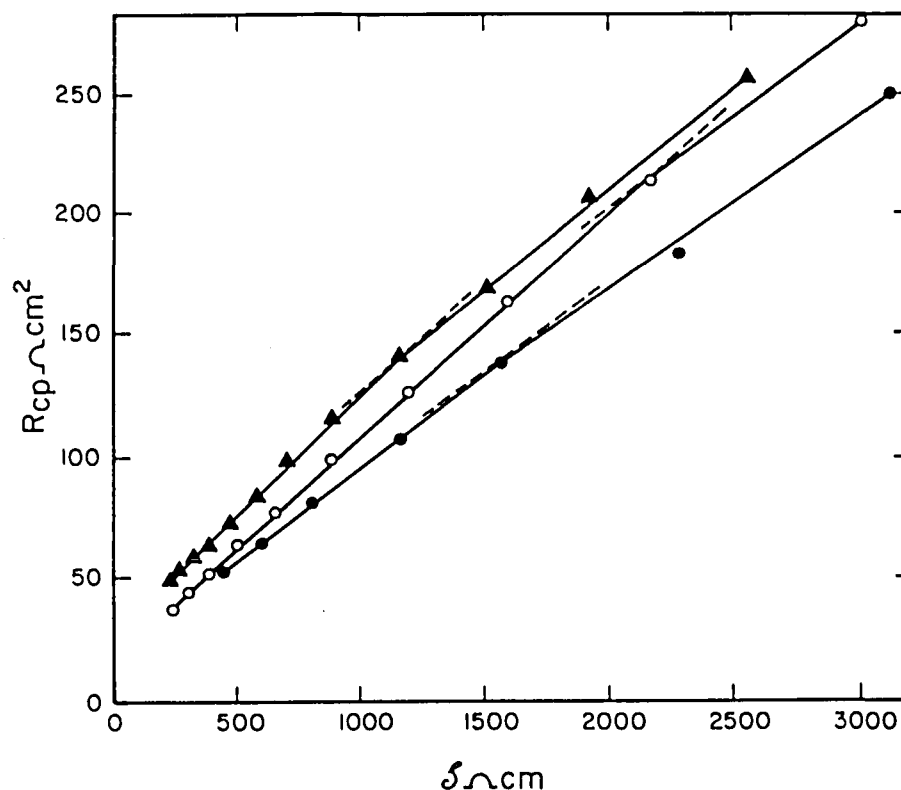
Figure 2.1: Apparent resistance per cell pair as a function of the specific resistance of the dialysate solution. V_{cp} - 0,7 V.

Membrane potentials and ohmic resistance for a pair of membranes are shown in Table 2.3. Membrane potentials were measured with calomel electrodes between stirred cells. Column 4 shows the potentials for ideal permselectivity (absolute values). Membrane resistance (AC) was measured in 0,5 and 0,1 mol/ℓ sodium chloride solutions.

Table 2.3: Membrane potential and ohmic resistance of a heterogeneous cation-exchange membrane (c) and a similar anion-exchange membrane (a)

Solutions	Membrane Potential				Solution Concentration	Membrane Resitance	
NaCl	$\Delta\psi_m^c$	$\Delta\psi_m^a$	$\Delta\psi_m^0$	$\dfrac{\Delta\psi_m^c + |\Delta\psi_m^a|}{2\Delta\psi_m^0}$	NaCl	C	A
mol/ℓ	mV	|mV|	|mV|	%	mol/ℓ	Ωcm^2	Ωcm^2
0,02/0,04	15,6	14,9	16,7	91	0,5	9,5	9,8
0,1/0,2	14,8	14,4	16,3	89	0,1	37,1	26,6
0,5/1,0	13,2	11,9	16,8	75			
1,0/2,0	12,4	11,1	18,2	64			
0,02/1,0	80,0	72,6	93,0	82			

$\Delta\psi_m^c$: membrane potential of cationic membrane
$\Delta\psi_m^a$: membrane potential of anionic membrane
$\Delta\psi_m^0$: membrane potential for ideal permselectivity.

2.3   Electro-Osmotic and Osmotic Flows

Electro-osmosis of different salt, acid and alkaline solutions have been studied extensively through a wide variety of membranes[5, 20 - 27, 28 -32, 40, 41].

Brydges and Lorimer[20] showed that when current density is varied, water transport number can:

a)   increase at low current density because osmotic water flow has been superimposed on water transport by the electric field;

b)   decrease at higher current density because of accumulation of salt in the membrane;

c)   decrease more at current densities near or above the limiting value because of an increased contribution of hydrogen and hydroxide ions to transport. These phenomena arise from a combination of diffusion (film) at both the membrane-solution interface and from the dependence of counter-ions and water transport numbers on external salt concentration.

Kruissink[21] has showed that with *Nafion* 170 membranes under practical conditions (concentrated alkali (≥ 10 mol/ℓ) and 5 mol/ℓ sodium chloride), that electro-osmotic water transport caused the maximum current efficiency to increase from 0,45 (electro-osmotic water transport number zero) to about 0,75 to 0,80 (at electro-osmotic water transport number of 1).

Hidalgo-Alvarez *et al.*[22] have found that at low electric current, the electro-osmotic coefficient undergoes a sharp elevation. This effect was very similar to that found by Lakshminarayanaiah[40]. At high electric current the electro-osmotic coefficient tends toward a constant value. This value depends on the concentration of the solution. When the concentration increases, the electro-osmotic permeability decreases.

Ceynowa[23] has indicated that the water transport number depends on many factors, such as experimental conditions (current density, stirring, difference in the concentration which occurs in the course of electrolysis on both sides of a membrane) as well as membrane parameters such as cross-linking, water content, ion-exchange capacity. Consequently, the resulting water transport number may sometimes be questionable and its properties complex.

The decrease of the water transport number with an increase in concentration of the external solution is usually given as the main non-controversial property[23]. However, Tombalakian et al.[24] found constant values of the water transport number for the homogeneous sulphonic acid membranes of high cross-linking and low water content in hydrochloric acid solution. Demarty et al.[41] stated the same for the heterogeneous *Ionac* MC 3470 XL membrane in hydrochloric acid solutions. Similarly Oda and Yawataya[27] reported that in some membranes in the presence of hydrochloric acid solution the water transport number remained constant at about 1,0 and the hydrogen ion transfer number only drops from 1,0 to 0,99. They also suggested that membranes deswell with increasing electrolyte concentration.

Ceynowa[23] found that the water and ion transport numbers at low sulphuric acid concentrations were in a wide range (5 - 70 mA/cm^2) independent of current density in the case of the heterogeneous MRF-26 ion-exchange membrane. However, at high concentration (2,26 mol/kg water) the increase in water transport number with current density was remarkable. It was also found that the water transport number in the MRF membrane decreased with increasing concentration (0,5 to 2,0 mol/kg water). With Nafion-120 membrane the water transport number remained almost constant with increasing feed concentration.

Rueda et al.[25] stated that the decrease of water transport number with increase in external salt concentration could be attributed to the decrease of the selectivity of the membrane. At very dilute solutions, the current is carried by the cations because the anions are almost completely excluded from the cationic cellulose acetate membrane. As the external solution concentration increases, the permselectivity of the membrane decreases. Anions are now present in the membrane and cations and anions participate in the transport of current across the membrane in opposite directions. Obviously, water transport will be reduced. An increase of external salt concentration leads to an increase of charge concentration in the neighbourhood of the matrix and consequently a decreasing of the electro-osmotic permeability.

Electro-osmotic permeability of several cellulose acetate membranes have been determined using solutions of alkali-chlorides[25]. The electro-osmotic permeability has been studied as a function of the external electrolyte concentration (0,001 to 0,1 mol/ℓ) and of current density applied. The results showed that the electro-osmotic permeability depended on the thickness of the membranes and the nature of the cations. The electro-osmotic permeability has been found to be strongly dependent

on the external salt concentration. However, the electro-osmotic permeability was not significantly affected by current density.

Tasaka et al.[66] have also studied electro-osmosis in charged membranes. At low electrolytic concentrations the direction of electro-osmosis is the same as that of counter-ion flow, because most of the movable ions in the membrane are counter-ions. With increasing external salt concentration the concentration of co-ions in the membrane increases, and then electro-osmosis decreases. In many instances electro-osmosis tends towards zero at the limit of high electrolyte concentrations.

Oda and Yawataya[27] have found that the electro-osmotic coefficient of hydrochloric acid through a cation-exchange membrane remains almost constant over the concentration range from 0,5 to 4,0 mol/ℓ. In hydrochloric acid solutions the electro-osmotic water transference is merely about one mole water per Faraday through a membrane.

Narebska et al.[28] have investigated the isothermal transport of ions and water across the perfluorinated Nafion 120 membrane in contact with sodium chloride solutions at a concentration of 0,05 up to 4 mol/ℓ based on irreversible thermodynamics of transport. It was found that the specific conductivity of the membrane increased at low external electrolyte concentration. The apparent transport number of the cation decreased significantly at higher external electrolyte concentration. The electro-osmotic coefficient also decreased significantly at higher external electrolytic concentration. The osmotic volume flux, and salt diffusion flux increased with increasing electrolyte concentration while the hydrodynamic volume flow decreased with increasing electrolytic concentration. The membrane also deswelled significantly with increasing electrolyte concentration.

Narebska and Koter[29] have studied the conductivity of ion-exchange membranes on the grounds of irreversible thermodynamics of transport. They have found that convection conductivity covers 50 to 55% of the total membrane conductivity and even more at increased temperature. This means that the flowing water doubles the ability of the membrane to transport the ionic current. This confirms the substantial role that water plays in the transport behaviour of a membrane.

Narebska et al.,[30] have performed a detailed analysis of membrane phenomena in the system Nafion 120/NaOH$_{aq}$. They have determined the phenomenological resistance -

(r_ik) and friction coefficient (f_ik). They have found that the resistance imposed by the membrane on the permeating OH⁻ ions is much lower that that for Cl⁻ ions. The three factors contributing to this effect - i.e. the frictions imposed by the cation (f_{21}), water (f_{2w}) and the polymer matrix (f_{2m}) - influence the flow of OH⁻ and Cl⁻ to a different degree. Chloride ions are hindered mainly by water, especially at increasing sorption. The flow of OH⁻ ions in diluted solution is hindered by the matrix and, at a higher concentration, by the cation and then by water.

Considering these results, it is apparent that the easy flow of NaOH results not only from the high mobility of OH⁻ ions, but also from the low osmotic flux (2 to 3 times less than in NaCl solutions) opposing the stream of electrolyte and the very low friction of the OH⁻ ions with water.

The water transport number decreased from 10 mol/Faraday to 2 mol/Faraday over the concentration range of 0,05 to 4 mol/ℓ. The apparent transport number (Δt^c) also decreased significantly with increasing caustic soda concentration.

The transport of aqueous NaCl solutions across the perfluorinated Nafion 120 membrane have been studied on the basis of irreversible thermodynamics by Narebska et al.[31]. The straight resistance coefficients r_{ii}, partial frictions f_{ik} and diffusion indexes have been determined.

Since the Donnan equilibrium and TMS theory were published, it is a well known and documented fact that co-ions are rejected from a charged polymer by the high potential of the polymer network. It was found by Narebska et al., that friction of this co-ion with the charged polymer was not the main force which resisted the flow of negative ions in the negatively charged polymer network. Except at 289 K and m_{ext} = 0,5, the anion-polymer frictional force (2m) was below the friction with water (2w) and it decreases with increasing electrolyte concentration and temperature. As a result, at high temperature and m_{ext}, the resistance against flowing anions is imposed by water; the lower the amount of water in the membrane, the higher this resistance.

Koter and Narebska[32] have investigated the mobilities of Na⁺, Cl⁻ and OH⁻ ions and water in Nafion 120 membranes. They have found that the interactions of Na⁺ and Cl⁻ ions running in opposite directions are negligible in the whole concentration range (0,05 to 4 mol/ℓ) studied. However, hydroxide ions impede cations, particularly at higher external concentrations (high sorption). This fact can be attributed to the higher

partial friction between Na^+ and OH^- ions caused by the phenomenon called "local hydrolysis".

The mobility of hydroxide ions exceeds that of chloride ions even more in the membrane than in the free solution. The mobility of hydroxide ions is much more sensitive to concentration than that of chloride ions. The mobility of the hydroxide ions declines much more rapidly than the mobility of the chloride ions. This reflects the dehydration of the membrane with increasing sorption of an electrolyte.

Kedem and Bar-on[5] have mentioned that the current efficiency (n_c) for a single membrane pair was sometimes equal to and even higher than the apparent transport number of the membrane pair $(\overline{\Delta t})$ measured with calomel electrodes. According to them, this is due to the substantial influence of electro-osmotic and osmotic flow into the brine cells during ED which increase the current efficiency. Both osmotic and electro-osmotic water flow enters the brine cell through both membranes. It increases the flows of counter-ions leaving the brine. The total effect of volume flow into a brine cell is increased salt flow. There will also be a slight influence of osmotic flow on the potential measurements. This will decrease the potential measurement and therefore the apparent transport number[5].

2.4   Structural Properties of Membrane Ionomers

Mauritz and Hopfinger[42] have described structural properties of ion-exchange membranes. Common functionalities of ion-exchange membranes are: $-SO_3^-$; $-COO^-$; $-NH_3^+$; $=NH_2^+$. These hydrophillic groups are responsible for the swelling of the hydrophobic network of ion-exchange membranes on exposure to water. Swelling of ion-exchange membranes may be inhibited by the presence of crystalline domains within the membrane matrix.

The approach to equilibrium for an initially dry ion-exchange membrane (in a given counter-ion salt form and containing no co-ions) that is subsequently immersed in pure water, can be visualized in the following way: Although the interaction between the organic polymer backbone is endothermic and may influence the rate of swelling, the strongly exothermic tendency of the counter-ions and ionogenic side chains to hydrate results in having the initially arrived water molecules strongly bound in ionic solvation shells resulting in little or no volume expansion of the network. In the truly dry state, the counter-ions are strongly bound by electrostatic forces in contact ion pairs. Further

uptake of water beyond that which is barely required for maximum occupancy of all the hydration shells results in moving the association - dissociation equilibrium between bound and unbound counter-ions toward increased counter-ion mobility. The driving force for swelling is the tendency for the water to dilute the polymer network. Stated in precise thermodynamic formalism, the difference between the water activity in the interior ($\bar{a}_w < 1$) and exterior ($a_w = 1$) of the membrane gives rise to a membrane internal osmotic pressure, Π, that results in a deformation of the polymer chain network:

$$\Pi v_w = RT \ln \bar{a}_w \qquad (2.4.1)$$

This equation is a statement of the free energy balance across the membrane - water interface at equilibrium and that v_w the partial molar volume of the internal water component may, in reality, not be the same as for the bulk water, nor be of a uniform value throughout the polymer because of local structuring effects.

As the water uptake proceeds, the increased side-chain counter-ion dissociation allows for more complete ionic hydration. The deformation of the polymer chain network upon further incorporation of water molecules also proceeds by a shift in the distribution of rotational isomers to higher energy conformations and changes in other intra-molecular, as well as inter-molecular interactions. Consequently, the increased overall energy state, for a given membrane water content of n moles, per equivalent of resin, is manifested by polymer chain retractive forces that resist expansion of the network. Accordingly, the configurational entropy decreases as less conformations become available within the matrix. Eventually, an equilibrium water content, n_o, is reached at which the osmotic swelling pressure is balanced by the cohesive energy density.

A qualitative set of rules that describe the equilibrium water swelling of polymeric ion-exchangers are as follows according to Mauritz and Hopfinger:

a)   Increasing the cross-link density reduces the swelling by decreasing the average inter-chain separation;

b)   Swelling will greatly depend on the pK of the ionogenic groups as well as their number per unit volume. For example, the equilibrium water uptake for strong acid resins exceeds that of resins containing the less hydrophillic weak acid groups;

14

c)   The nature of the counter-ion can influence swelling in a number of ways. Firstly, water uptake naturally increases with increasing hydrative capacity of the counter-ion.   In general, for alkali counter-ion forms, the following progression is noted: $Li^+ > Na^+ > K^+ > Rb^+ > Cs^+$.   Increased valence reduces swelling by: (i)   reducing the number of counter-ions in the resin through the electroneutrality requirement;   (ii)   forming ionic cross-links;   and (iii)   reducing the hydrative capacities by the formation of triplet associations such as: $-SO_3^- \cdots Ca^{2+} \cdots SO_3^-$;

d)   The internal resin osmotic pressure is enhanced as the association - dissociation equilibrium between bound and unbound counter-ions shifts to greater dissociation by allowing for more complete hydration shell formation.

Narebska and Wodzki[43] have investigated water and electrolyte sorption (sulphuric acid) in perfluorosulphonic and polyethylene-poly (styrene sulphonic acid) membranes of different cross-linking in the temperature range of 293 to 333 K and a concentration of external electrolyte up to 5,7 mol/kg H_2O. As the hydration of the membranes is an exothermic process, a decrease of swelling with increasing temperature could be predicted. Also due to the nature of sulphuric acid one could expect dehydration of the membranes with an increasing concentration of acid. It was found that an increase of both variables, i.e. temperature and concentration, caused deswelling of the membranes in a higher degree when the cross-linking is lower.   Only for the membranes with a low degree of cross-linking (2 and 5% DVB) equilibrated with diluted solutions of sulphuric acid, a small increase of swelling is visible at a temperature range of 293 to 303 K.

Narebska et al.,[44] have studied swelling and sorption equilibria for Nafion membranes in concentrated solutions of sodium chloride (0 to 6 mol/kg H_2O), and sodium hydroxide (0 to 18 mol/kg H_2O), at 293 to 363 K. It was found that significant deswelling of the membranes took place with increasing electrolyte concentration. Increasing temperature (above 333 K), also caused a loss of water. Narebska et al., have stated that deswelling of a membrane depends on the kind of membrane, temperature and the nature of the external electrolyte.

2.5 Measurement of Transport Number

The efficiency with which a membrane transport selectively any particular ionic species may be inferred by measuring the transport number of the species in the membrane. Two methods are normally used to determine membrane transport number. They are:

a)   the emf method[45] and;

b)   the Hittorf's method[45]. In these methods different concentrations of electrolyte exist on either side of the membrane, even though in the Hittorf's method one might start initially with the same concentration. Therefore, the transport number values derived by these methods cannot be directly related to a definite concentration of the external solution.

Membrane potentials measured using concentrations c' and c" on either side of the membrane may be used in the following equation to derive an average transport number:

$$E/E_{max} = 2\bar{t}_+ - 1; \quad \bar{t}_+ = (E/E_{max}) + 0,5 \qquad (2.5.1)$$

If Ag-AgCl electrodes immersed in two chloride solutions are used, $\bar{t}_+$ is derived from[45]:

$$E = 2\bar{t}_{+(app)} \frac{RT}{F} \ln \frac{a'}{a''} \qquad (2.5.2)$$

The derived transport number value has been called the apparent transport number because in this type of measurement water transport has not been taken into account. This apparent value will be close to the true value when very dilute solutions are used.

In the Hittorf's method a known quantity of electricity is passed through the membrane cell containing two chambers filled with the same electrolyte separated by a membrane. Cations migrate to the cathode and anions migrate to the anode. The concentration change brought about in the two chambers, which is not more than about 10%, is estimated by the usual analytical methods. The transport number is calculated from $t_i = FJ_i/I$.

The determination of meaningful transport numbers for any membrane-electrolyte system calls for careful control of a number of factors. The important factors for the

control of the concentration of the donating or receiving side are[45]:

a)   external concentration;

b)   current density; and

c)   difference in concentration on either side of the membrane.

The effect of current density on the values of $\bar{t}_i$ has been demonstrated by Kressman and Tye[46] using multi-compartment cells and by Lakshminarayanaih and Subrahmanyan[47] using simple cells. When external concentrations are small (< 0,1 mol/ℓ) an increase of current density decreases $\bar{t}_i$ values. This is attributed to polarization effects at the membrane-solution interface facing the anode.

The amount of polarization decreases as the concentration is increased. When the external concentration is 0,1 mol/ℓ, $\bar{t}_i$ exhibits a maximum at a certain current density below which the $\bar{t}_i$ values decrease as the current density is decreased and above which also $\bar{t}_i$ values decreased as the current density is increased. The decrease as the current density is lowered is attributed to back diffusion of the electrolyte[47].

When external concentrations > 0,1 mol/ℓ are used, polarization effects are negligible but back diffusion becomes dominant. As the quality of back flux due to diffusion is determined by the concentration differences allowed to build-up during electrodialysis, it should be made as small as possible to derive meaningful values for $\bar{t}_i$.

2.6   Transport Properties of Anion Exchange membranes in contact with Hydrochloric Acid Solutions. Membranes for Acid recovery by Electrodialysis

Boudet-Dumy et al.[48] have recently investigated chloride ion fluxes through Selemion AAV and ARA Morgane membranes specially designed for the recovery of acids by ED. In addition, measurement of the electrical conductance of the membranes and of the amount of sorbed electrolyte (HCl), at equilibrium, have been carried out. The analysis of the results suggested a low dissociation degree of acid present in the membrane. The lower dissociation of sorbed acid is a factor which decreases the proton leakage of the anion-exchange membrane. It was also shown that the flux of chloride ions from the anode to the cathode steadily increased as the amount of sorbed electrolyte increased. This result means that chloride ions are associated with the movement of positively charged species. This fact may be due to the formation of an aggregate form such as $(H_4OCl)^+$ resulting from the solvation of a proton by a water

molecule and an HCl molecule - ion association inside the membrane overcoming the state of a neutral HCl molecule. This result confirms the role of ion association in the membrane.

2.7   Electrodialysis Applications

Electrodialysis applications and potential applications[6 · 8, 33 · 39, 40 · 62] are widely discussed in the literature. Electrodialysis is a membrane based separation technique that is appealing because of its capability to deionize one stream while concentrating the electrolytes in another stream. Thus, ED produces a purified stream that can either be discharged or reused, and a concentrated electrolyte stream that can be disposed of or processed for reclamation of the dissolved salt. Some applications of ED include desalination of brackish waters[56], desalting of whey and stabilization of wine[57], purification of protein solutions[58], recovery of metals from plating rinse waters[38], recovery of acids[59], recovery of heavy metals from mining mill process[60], and the treatment of cooling-tower blowdown for water recovery and effluent volume reduction[61].

When concentration polarization is absent in ED, there are two main causes of the decrease in current efficiency[62]:   Co-ion intrusion and counter-ion backdiffusion. Co-ion intrusion is the passage of co-ions through an ion-exchange membrane from the concentrate to the diluate, and is due to the electrical potential and concentration gradients across the membrane. Counter-ion backdiffusion is the backward passage of counter-ions through an ion-exchange membrane from the concentrate to the diluate due to a high concentration gradient across the membrane. The effects of counter-ion backdiffusion can be decreased by increasing stack voltage, that is, increasing the electrical potential driving force. However, such an increase in stack voltage is limited by the limiting current density and high energy costs. Co-ion intrusion can be reduced by using ion-exchange membranes that exclude co-ions to a greater degree.

Kononov et al.[33] have described the removal of hydrochloric acid from waste waters containing organic products. The possibility was demonstrated of concentrating hydrochloric acid by ED. The model effluent contained 4,4 g/ℓ hydrochloric acid, 58 g/ℓ sofolene-3 and 20 g/ℓ chlorohydrin. At a current density of 10 mA/cm² a brine was obtained containing 51 g/ℓ acid with a current efficiency of 35%. The low current efficiency is explained by diffusion of acid from the brine into the dialysate and the decrease in the selectivity of the membranes in contact with concentrated hydrochloric

18

acid solution (50 g/ℓ).

Korngold[34] has described the recovery of sulphuric acid from rinsing waters used in a pickling process. Sulphuric acid was concentrated from 9 100 mg/ℓ to 34 300 mg/ℓ while the diluate contained 3 700 mg/ℓ sulphuric acid. Approximately 70% of the sulphuric acid in the rinsing water could be recovered by ED treatment.

Urano et al.[37] have described concentration/desalination of model hydrochloric and sulphuric acid solutions in a laboratory scale conventional electrodialyzer. Newly developed Selemion AAV anion-exchange membrane were used. The transport number for hydrogen ions of this membrane is much smaller than that of conventional anion-exchange membranes with the result that the acid could be efficiently concentrated. However, no acid feed and brine concentrations were given.

The concentration of carbonate solutions by ED was reported by Laskorin et al.[35]. The feed solution had the following composition: sodium carbonate (4 to 7 g/ℓ); sodium bicarbonate (4 - 7 g/ℓ) and sodium sulphate (2 to 3 g/ℓ). The total salt content of the solution did not exceed 15 g/ℓ. The first series of experiments was carried out with liquid circulation in both the diluating and concentrating compartments. A linear liquid velocity and a current density of 5 to 6 cm/s and 20 mA/cm² was used, respectively. The duration of the desalting cycle was 1,5 to 2,0 hour. A fresh portion of feed was introduced after each desalting cycle. The portion of concentrate remained unchanged for 10 cycles. MKK cation- and MAK anion selective membranes were used. The brine concentration was increased from 22,9 g/ℓ at the end of the first cycle to 87, 8 g/ℓ at the end of the 10th cycle at a current efficiency of 81%. The diluate concentration at the end of the cycles varied between 0,16 and 0,47 g/ℓ.

A second series of experiments was conducted without circulation of liquid through the brine compartments. The solvent entered the brine compartments as a result of electro-osmotic transport through the membranes. The brine salt content reached a value of 182,8 g/ℓ after 3 cycles. The current efficiency varied between 70 and 75% and the electrical energy consumption was approximately 2,7 kWh/kg salt. A higher brine concentration was obtained without circulation of brine through the brine compartments.

Smagnin and Chukkin[36] have described concentration of caustic soda and sodium

chloride with ED. Caustic soda and sodium chloride concentrations of 0,07 and 1,07 mol/ℓ, respectively, were chosen as the feed solutions. No circulation of brine was used in a conventional ED stack. The change of brine concentration in relation to the current density was determined. MA-40 and MK-40 ion-exchange membranes were used. Maximum brine concentrations of 346 g/ℓ caustic soda and 365 g/ℓ sodium chloride were obtained at current densities of 249 and 117 mA/cm^2, respectively.

3. THEORY

3.1 Theories of Membrane Transport

3.1.1 Nernst-Planck and Pseudo-Thermodynamic Treatments

Theories of membrane transport and the application of non-equilibrium thermodynamics to transport processes have been described by Meares *et al.*[9].

Many of the earlier treatments of membrane transport use the Nernst-Planck equations to describe the relationships between the flows of the permeating species and the forces acting on the system[10, 63] according to Meares *et al.* According to these equations the flux J_i of species i at any point is equal to the product of the local concentration c_i of i, the absolute mobility u_i of i, and the force acting on i. This force has been identified with the negative of the local gradient of the electrochemical potential μ_i of i. Thus, at a distance x from a reference plane at right angles to the direction of unidimensional flow through a membrane

$$J_i = -c_i u_i \, d\mu_i/dx \tag{3.1.1.1}$$

The electrochemical potential of i can be divided into its constituent parts giving in place of equation eq. (3.1.1.1)

$$J_i = -c_i u_i \left(RTd \, \ell n \, c_i/dx + RTd \, \ell n \, \gamma_i/dx + \bar{V}_i dp/dx + z_i \, Fd\psi/dx \right) \tag{3.1.1.2}$$

where γ_i, $\bar{V}_i$, z_i, p, and ψ represent the activity coefficient, the partial molar volume, the valence charge on i, the hydrostatic pressure, and the electrical potential, respectively. R is the gas constant, T the absolute temperature, and F the Faraday. It is apparent from eq. (3.1.1.2) that the Nernst-Planck equations make use of the Nernst-Einstein relation between the absolute mobility u_i and the diffusion coefficient D_i of species i. This is

$$D_i = u_i RT \tag{3.1.1.3}$$

On replacing the electrochemical mobility in eq. (3.1.1.2) by the diffusion coefficient, the more usual form of the Nernst-Planck flux equation is obtained according to Meares *et al.*

$$J_i = -D_i \left(\frac{dc_i}{dx} + c_i \frac{d \ln \gamma_i}{dx} + \frac{c_i \tilde{V}_i}{RT} \frac{dp}{dx} + \frac{c_i z_i F}{RT} \frac{d\psi}{dx} \right)$$

(3.1.1.4)

On the basis of the Nernst-Planck equations, the flow of species i is regarded as unaffected by the presence of any other permeating species except in so far as the other species either influences the force acting on i by, for example, affecting the values of γ_i or ψ, or alters the state of the membrane and hence alters the value of D_i.

To obtain relationships between the flows of the permeating species and the observable macroscopic differences in concentration, electrical potential, and hydrostatic pressure between the solutions on the two sides of the membrane, it is necessary to integrate the Nernst-Planck equation (eq. 3.1.1.4) for each mobile component across the membrane and the membrane/solution boundaries. In order to carry out this integration an additional assumption has to be made. The differences between the various treatments derived from the Nernst-Planck equations lie in the different assumptions used. For example, in the theory of Goldman [63], which is widely applied to biological membranes, it is assumed that the gradient of electrical potential $d\psi/dx$ is constant throughout the membrane. It is usually assumed also that thermodynamic equilibrium holds across the membrane/solution interfaces and that the system is in a steady state so that the flows J_i are constant throughout the membrane. Generally these integrations do not lead to linear relationships between the flows and the macroscopic differences of electrochemical potential between the two bathing solutions.

The main disadvantage of the Nernst-Planck approach according to Meares [9] is that it fails to allow for interactions between the flows of different permeating species. Such interactions are most obvious when a substantial flow of solvent, usually water, occurs at the same time as a flow of solute. For example, during the passage of an electric current across a cation-exchange membrane, the permeating cations and anions both impart momentum to the water molecules with which they collide. Since the number of cations is greater than the number of anions, the momentum imparted to the water by the cations is normally greater than the momentum imparted by the anions and an electro-osmotic flow of water is set up in the direction of the cation current. The

resultant bulk flow of the water has the effect of reducing the resistance to the flow of cations and increasing the resistance to the flow of anions. This flow of water occurs under the difference of electrical potential and in the absence of a concentration gradient of water. The appropriate Nernst-Planck equation would predict no flow of water under these conditions according to Meares *et al.* Furthermore the flows of cations and anions differ from those which would be predicted from the respective Nernst-Plank equations on account of the effect of the water flow on the resistances to ionic flow.

This effect of solvent flow on the flows of solute molecules or ions can be allowed for by adding a correction term to the Nernst-Planck equations[9]. Thus, it can be written

$$J_i = -c_i u_i \ d\mu_i/dx + c_i v \qquad (3.1.1.5)$$

where v is the velocity of the local centre of mass of all the species[11]. The term $c_i v$ is often called the convective contribution to the flow of i and some authors have preferred to define v as the velocity of the local centre of volume.

The addition of this convection term to the Nernst-Planck equation for the flow of a solute is probably a sufficient correction in most cases involving only the transport of solvent and nonelectrolyte solutes across a membrane in which the solvent is driven by osmotic or hydrostatic pressure according to Meares *et al.* The situation is much more complex when electrolyte solutes are considered according to Meares *et al.* Even at low concentrations the flows of cations and anions may interact strongly with each other. Interactions between the different ion flows may be of similar size to their interactions with the solvent flow. Under these circumstances the convection-corrected Nernst-Planck equations may still not give a good description of the experimental situation regarding the ion flows.

The theoretical difficulties arising from interacting flows can be formally overcome by the use of theories of transport based on nonequilibrium thermodynamics. Such theories are described in the next section.

3.1.2 Treatments based on Nonequilibrium Thermodynamics

Since the original papers of Staverman[12] and Kirkwood[64], many papers have appeared on the application of nonequilibrium thermodynamics to transport across synthetic and biological membranes. In particular, major contributions have been

made by Katchalsky, Kedem, and co-workers. In view of the appearance of extensive texts[13, 14], this account is intended only as a brief summary of the general principles.

3.1.2.1 The Phenomenological Equations

The theory of nonequilibrium thermodynamics allows that, in a system where a number of flows are occurring and a number of forces are operating, each flow may depend upon every force. Also, if the system is not too far from equilibrium, the relationships between the flows and forces are linear. Therefore, the flow J_i may be written as follows

$$J_i = \sum_{\text{all } k} L_{ik} X_k \qquad (3.1.1.6)$$

where the X_k are the various forces acting on the system and the L_{ik} are the phenomenological coefficients which do not depend on the sizes of the fluxes or forces. The flow J_i may be a flow of a chemical species, a volume flow, a flow of electric current, or a flow of heat. The forces X_k may be expressed in the form of local gradients or macroscopic differences across the membrane of the chemical potentials, electric potential, hydrostatic pressure, or temperature. If a discontinuous formulation is used so that the macroscopic differences in these quantities across the membrane are chosen as the forces, then the L_{ik} coefficients in eq. (3.1.1.6) are average values over the membrane interposed between a particular pair of solutions.

Equation (3.1.1.6) imply, for example, that the flow of a chemical species i is dependent not only on its conjugate force X_i, i.e., the difference or negative gradient of its own chemical or electrochemical potentials but also on the gradients or differences of the electrochemical potentials of the other permeating species. Hence eq. (3.1.1.6) imply that a difference of electrical potential may cause a flow of an uncharged species, a fact which, as previously indicated, the Nernst-Planck equations do not recognize according to Meares et al. In general, eq. (3.1.1.6) allow that any type of vectorial force can, under suitable conditions, give rise to any type of vectorial flow.

In a system where n flows are occurring and n forces are operating, a total of n^2 phenomenological coefficients L_{ik} are required to describe fully the transport properties of the system. This must be compared with the n mobilities used in the Nernst-Planck description of the system. A corresponding number n^2 experimental transport measurements would have to be made to permit the evaluation of all the L_{ik} coefficients.

Fortunately a simplification can be made with the help of Onsager's reciprocal relationship[13]. This states that under certain conditions

$$L_{ik} = L_{ki} \qquad (3.1.1.7)$$

The conditions required for eq. (3.1.1.7) to be valid are that the flows be linearly related to the forces and that the flows and forces be chosen such that

$$T\sigma = \Sigma_i \, J_i X_i \qquad (3.1.1.8)$$

where σ is the local rate of production of entropy in the system when the X_i are the local potential gradients. The quantity $T\sigma$ is often represented by the symbol Φ and called the dissipation function because it represents the rate at which free energy is dissipated by the irreversible processes. In fact there is no completely general proof of eq. (3.1.1.7) but its validity has been shown for a large number of situations[14].

With the help of the reciprocal relationship the number of separate L_{ik} coefficients required to describe a system of n flows and n forces is reduced from n^2 to ½n (n + 1).

This nonequilibrium thermodynamic theory holds only close to thermodynamic equilibrium. The size of the departure from equilibrium for which the linear relationship between flow and force, eq. (3.1.1.6), and the reciprocal relationship, eq. (3.1.1.7), are valid, depends upon the type of flow considered. Strictly, the range of validity must be tested experimentally for each type of flow process. In the case of molecular flow processes, electronic conduction, and heat conduction the linear and reciprocal relationships have been found to be valid for flows of the order of magnitude commonly encountered in membranes[65]. In describing the progress of chemical reactions the relationships are valid only very close to equilibrium. Systems in which chemical reactions are taking place will be excluded from this discussion.

3.1.2.2 The Choice of Flows and Forces

In an isothermal membrane system the most obvious choice of flows is the set of flows of the permeating species--solvent, nonelectrolyte solutes, and ions. The conjugate forces are then the differences or local gradients of the electrochemical potentials of these species. To accord with eq. (3.1.1.8), in which $T\sigma$ must be positive, increasing potentials in the direction of positive fluxes constitute negative forces. A set of

phenomenological equations corresponding to eq. (3.1.1.6) can be written relating the flows to the forces. The values of the L_{ik} coefficients appearing in these equations depend on the interactions occurring in the membrane, i.e., on the chemical nature of the permeating species and of the membrane, on the detailed microstructure of the membrane, and on the local concentrations of the permeating species.

In principle it should be possible to obtain values for the $\frac{1}{2}n(n + 1)$ L_{ik} coefficients by carrying out a suitable set of $\frac{1}{2}n(n + 1)$ independent experiments. For example, if all the forces except one, X_a, were held at zero and the flows J_i, J_j, etc. of all the n species were measured, then the values of the coefficients L_{ia}, L_{ja} etc. could be obtained directly. Similar experiments would give the values for the remaining L_{ik} coefficients. Other sets of experiments may be used, and one may combine experiments where some of the forces are kept at zero, experiments where some of the flows are kept at zero, and experiments where some forces and some flows are kept at zero[14].

Although the set of flows and conjugate forces outlined above may seem to be convenient for the molecular interpretation of the interactions occurring in a membrane system, the equations written in terms of these flows and forces are not convenient for the design of experiments for the evaluation of the L_{ik} coefficients. For example, the forces which are usually controlled experimentally are not differences of electrochemical potential, but differences of concentration, electrical potential, and hydrostatic pressure. Also, it may be more convenient to measure the total volume of the flows across a membrane rather than the flow of solvent, or to measure the electric current and one ionic flow rather than two ionic flows. For these reasons, sets of practical flows and forces are often chosen to describe membrane transport[14]. These practical sets of flows and their conjugate forces must satisfy the relationship of eq. (3.1.1.8), which gives the dissipation function.

A system involving the transport of water and a nonelectrolyte solute across a membrane can be described by giving the flows of water J_w and of solute J_s. The conjugate forces are then the differences, or the local gradients, of the chemical potentials of water μ_w and solute μ_s. The transport properties of this system are described by the following equations:

$$J_w = L_w \Delta \mu_w + L_{ws} \Delta \mu_s$$

<div align="right">(3.1.1.9)</div>

$$J_s = L_{sw} \Delta \mu_w + L_s \Delta \mu_s$$

where according to the reciprocal relationship $L_{sw} = L_{ws}$ and the dissipation function of the system is given by the expression

$$\Phi = J_w \Delta \mu_w + J_s \Delta \mu_s \qquad (3.1.1.10)$$

When considering ideal external solutions the forces $\Delta \mu_w$ and $\Delta \mu_s$ are often expanded into separate terms giving the contributions of the concentration differences and pressure difference to the total driving forces. Thus

$$\Delta \mu_w = (RT/c_w) \Delta \bar{c}_w) \Delta c_w + V_w \Delta p$$

Here V_w is an average partial molar volume of water and $\bar{c}_w$ is an average concentration of water. When $\Delta \mu_w$ and $\Delta \mu_s$ in eq. (3.1.1.10) are expanded in this way and the resulting concentration and pressure terms are grouped separately the expression for the dissipation function becomes[50]

$$\Phi = J_v \Delta p + J_D RT \Delta c_s \qquad (3.1.1.11)$$

where J_v the total volume flow is equal to $(\bar{V}_w J_w + \bar{V}_s J_s)$ and J_D is equal to $(J_s/\bar{c}_s - J_w/\bar{c}_w)$. J_D is sometimes called the exchange flow and represents the apparent mean velocity of the solute relative to the water. According to eq. (3.1.1.11) the system can be described in terms of J_v and J_D as flows and Δp and $RT \Delta c_s$ (or $\Delta \pi_s$) as their conjugate forces. Thus

$$J_v = L_p \Delta p + L_{pD} \Delta \pi_s$$

<div align="right">(3.1.1.12)</div>

$$J_D = L_{Dp} \Delta p + L_D \Delta \pi_s$$

where L_{Dp} equals L_{pD} and $\Delta \pi_s$ is the difference in osmotic pressure between the solutions. Experimentally it is easier to control the values of the forces appearing in eq. (3.1.1.12) than those appearing in eq. (3.1.1.9).

Similarly a system involving flows of water and a salt dissociated into a cationic species and an anionic species can be described in terms of the flows J_w, J_1, and J_2 of these molecular species or by the set comprising the total volume flow, the electric current, and the defined flow of salt, i.e., J_v, I and J_s.[14] In the former case the conjugate forces are the differences of the electrochemical potentials of the species across the membrane, in the latter case the conjugate forces are the pressure difference minus the osmotic pressure difference, the electrical potential difference, and the difference of the pressure-independent part of the chemical potential of the salt. Care must be taken in the precise definition of these forces, particularly of the electrical potential difference.[67]

Since the choice of flows and forces is to some extent open as long as the flows and forces satisfy eq. (3.1.1.8) a set can be chosen primarily for ease of theoretical interpretation of L_{ik} coefficients or for ease of experimental evaluation of the L_{ik} coefficients. Furthermore, given values of the L_{ik} coefficients relevant to one set of flows and forces, it is a straightforward operation to calculate the values of L_{ik} coefficients relevant to another set of flows and forces.[67]

It is of course possible and often convenient to describe the transport properties of a system in terms of flows and forces which are not conjugate and which do not obey eq. (3.1.1.8). The system where the membrane is permeated by a flow of water and a flow of a solute can be described in terms of the flow of water J_w, the flow of solute J_s, the pressure difference Δp, and the difference in concentration of the solute $RT\Delta c_s$ or $\Delta \pi_s$. These flows and forces are interrelated by the equations

$$J_v = L_p\Delta p - \sigma L_p \Delta \pi_s$$

(3.1.1.13)

$$J_s = \overline{c}_s(1 - \sigma)J_v + \omega\Delta \pi_s$$

Here L_p has the same significance as in eq. (3.1.1.12). σ is called the reflection coefficient of the solute and is equal to $\Delta p/\Delta \pi_s$ at zero J_v, ω is the solute permeability $J_s/\Delta \pi_s$ at zero J_v, and $\overline{c}_s$ is the average concentration of the solute in the two solutions.[67]

In practice eq. (3.1.1.13) may be easier to use than eq. (3.1.1.12) because the flows generally measured are J_v and J_s rather than J_v and J_D. However, eq. (3.1.1.13) are not

a proper set of phenomenological equations in the sense of eq. (3.1.1.6). Neither are σ and ω phenomenological coefficients in the sense used so far. They are related to the L_{ik} coefficients of eq. (3.1.1.12) by the relationships[66].

$$\sigma = -L_{pD}/L_p \text{ and } \omega = \bar{c}_s(L_pL_D - L_{pD}^2)/L_p$$

3.1.2.3 Uses and Limitations of the Theory

The theory of nonequilibrium thermodynamics has been applied to membranes in a number of papers where the aim has been to obtain general relationships between observable macroscopic flows and forces. Topics investigated in this way have included: isotopic tracer flows and flux ratios[68, 69], electrokinetic phenomena[70], the transport properties of complex membranes[14], and the coupling of transport processes with chemical reactions, so-called active transport[13]. However, the main concern of these investigations has been the transport of non-electrolyte solutes and ions across charged and uncharged membranes[12, 13, 46].

The L_{ik} coefficients obtained from experimental measurements of transport phenomena under one set of conditions can either be used to predict values of flows and forces under other sets of conditions or they can be analyzed for the purpose of interpreting, at a molecular level, the various interactions which occur between the permeating molecules and ions and the membrane material. This second use of the L_{ik} coefficients is especially interesting but it is by no means simple.

An inspection of any of the sets of phenomenological equations [(3.1.1.6), (3.1.1.9), (3.1.1.12), and (3.1.1.13)] shows that nowhere is any direct reference made to the membrane or its properties. The L_{ik} coefficients relate the flows of the permeating species to the gross thermodynamic forces acting on these species and, in general, no particular coefficient represents only the interaction of a permeating species with the membrane. Instead the properties of the membrane material affect the values of each of the L_{ik} coefficients to a greater or lesser extent.

The physical interpretation of measurements of transport properties is made more straightforward by inverting the matrix of the phenomenological equations [eq. (3.1.1.6)] to give the set of eqs. (3.1.1.14)

$$X_i =_{all}\Sigma_k \ R_{ik} \ J_k \qquad\qquad (3.1.1.14)$$

These represent the forces as linear functions of the flows. The R_{ik} and L_{ik} coefficients of eq's. (3.1.1.14) and (3.1.1.6) are related by the expression

$$R_{ik} = A_{ik} \ / \ |L| \qquad\qquad (3.1.1.15)$$

where A_{ik} is the minor of L_{ik} and $|L|$ is the determinant of the L_{ik} coefficients. If the reciprocal relation is valid for the L_{ik} coefficients, it is valid also for the R_{ik} coefficients. Whereas the L_{ik} coefficients have the dimensions of conductance (i.e., flow per unit force), the R_{ik} coefficients have the dimensions of resistance (i.e., force per unit flow) and are frequently called resistance coefficients.

The R_{ik} coefficients are easier to interpret at the molecular level than the L_{ik} coefficients. A non-zero R_{ik} ($i \neq k$) implies a direct interaction between i and k, that is, the molecular flow of k directly causes a force to act on species i. On the other hand, a non-zero L_{ik} ($i \neq k$) does not necessarily imply a direct molecular interaction between species i and k, it means that the force acting on k affects the flow of i, perhaps directly or indirectly.

In effect eq. (3.1.1.14) means that, in the steady state, the gross thermodynamic force X_i acting on species i is balanced by the forces $R_{ik}J_k$ summed over all species k, including i. The term $R_{ii}J_i$ is the drag force per mole which would act on i when moving at a rate J_i/c_i through a medium where there was no net flow of any other species. Thus the R_{ii} coefficients are still complex quantities including contributions from the interactions between i and all other species present, including the membrane. However, each R_{ik} ($i \neq k$) coefficient represents only the single interaction between the flows of i and k. The R_{ii} coefficients, like the L_{ii}, must always be positive but R_{ik} ($i \neq k$) and the L_{ik} coefficients may be positive, negative, or zero.

3.1.3 The Frictional Model of Membrane Transport

The frictional model of membrane transport has been described by Meares et al.[9]. The idea of describing steady-state transport processes in a membrane as balances between the gross thermodynamic forces acting on the system and frictional interactions between the components of the system is one of long standing. More recently, the term molecular friction coefficient has been applied to the coefficient which relates the frictional force between two components to the difference between their

velocities. This approach has been used to describe transport processes across membranes by several authors. The precise treatment that will be considered here is the frictional model as proposed by Spiegler[71].

The fundamental statement of the frictional model is that when the velocity of a permeating species has reached a constant value, the gross thermodynamic force X_i acting on one mole of that species must be balanced by the interactive forces, F_{ik}, acting between one mole of the same species and the other species present. Mathematically this is expressed by

$$X_i = - \frac{\Sigma}{k \neq i} F_{ik} \qquad (3.1.3.1)$$

Furthermore, these interactions are assumed to be frictional in character so that each force F_{ik} is equal to a friction coefficient f_{ik} multiplied by the difference between the velocities v_i and v_k of the two species. Thus

$$F_{ik} = -f_{ik}(v_i - v_k) \qquad (3.1.3.2)$$

and

$$X_i = \frac{\Sigma}{k \neq i} f_{ik}(v_i - v_k) \qquad (3.1.3.3)$$

It should be noted that f_{ik} is the force acting on one mole of i owing to its interaction with the amount of k normally in the environment of i and under unit difference between the mean velocities of i and k. In general the concentrations of i and k are not equal and consequently the coefficients f_{ik} and f_{ki} are not equal. When the balance of forces is taken over unit volume of the system it is readily seen that

$$c_i f_{ik} = c_k f_{ki} \qquad (3.1.3.4)$$

The quantity f_{ik}/c_k or f_{ki}/c_i represents the force acting between one mole of i and one mole of k at unit velocity difference. Its value obviously depends on the chemical types of the two species.

Besides containing a term such as $f_{ik}(v_i - v_k)$ for the interactions between i and each of the other permeating species, the right-hand side of eq. (3.1.3.3) also includes a term

$f_{im}(v_i - v_m)$ which allows for the interaction between i and the membrane. Usually the membrane is taken as the velocity reference so that v_m is zero.

With the help of the relationship

$$J_i = c_i v_i \qquad (3.1.3.5)$$

eq. (3.1.3.3) can be rearranged to

$$X_i = (J_i/c_i) \frac{\Sigma}{K \neq i} f_{ik} - \frac{\Sigma}{k \neq i} (J_k f_{ik}/c_k) \qquad (3.1.3.6)$$

Equation (3.1.3.6) has the same form as eq. (3.1.1.14) which relate the forces to the flows via the R_{ik} coefficients. Each R_{ii} coefficient can be equated to the corresponding $\Sigma f_{ik}/c_i$. This illustrates the complex nature of the R_{ii} coefficient. Each R_{ik} ($i=k$) coefficient is equivalent to the corresponding $-f_{ik}/c_k$.

In a system with n flows, (n - 1) friction coefficients are required to describe the interactions of any one permeating species with the other permeating species. One further coefficient is required to describe its interaction with the membrane. A total of n^2 friction coefficients is thus required to describe the transport properties of the system but with the use of eq. (3.1.3.4) this number is reduced to $\frac{1}{2}n(n + 1)$, i.e., the same as the minimum number of independent L_{ik} or R_{ik} coefficients. Hence the minimum number of experimental measurements required to characterize the system fully is the same whether it is described in terms of the L_{ik} coefficients, the R_{ik} coefficients, or the f_{ik} coefficients. The most convenient set of experimental parameters to be measured may depend on which set of coefficients is chosen to represent the properties of the system.

The choice of coefficients can be made mainly on the basis of experimental convenience because, having obtained values of one set of coefficients, it is no problem to obtain values for the other sets from these. The relationships between the R_{ik} and L_{ik} coefficients, and between these and the friction coefficients have already been given briefly above and are discussed in more detail elsewhere[9]. Direct relationships between the friction coefficients and experimentally measurable quantities have also been discussed in several papers[9]. The method of obtaining one such relationship is mentioned here as an illustration of Spiegler's treatment.

In a system consisting of a membrane, water, one species of univalent cation and one species of univalent anion, the electrical conductivity k is given by the expression

$$k = F(J'_1 - J'_2)$$

(3.1.3.7)

where J'_1 and J'_2 are the flows of univalent cations and anions per unit area, respectively, under an electrical potential gradient of 1 V cm^{-1}. Under these conditions the forces acting on the cations, anions and water are F, -F, and 0 J cm^{-1} mole^{-1}, respectively. On substituting these forces into the set of eqs. (3.1.3.6) describing the system, the equations can be solved for the flows J'_1 and J'_2 in terms of the friction coefficients and the concentrations of the ions and water. These expressions for J'_1 and J'_2 can then be substituted into eq. (3.1.3.7) to give an expression for k in terms of the friction coefficients operating in the system and the concentrations of the permeating species.

It is possible to obtain expressions for other transport parameters, such as the electro-osmotic permeability, transport numbers of the ions, and the self-diffusion coefficients of the permeating species in terms of the friction coefficients in a somewhat similar manner. A set of such expressions can then be solved to give the individual friction coefficients in terms of the transport parameters and the concentrations.

The procedure outlined above becomes rather tedious as the expressions giving the individual transport parameters in terms of the friction coefficients may be very complicated. Under certain circumstances a simpler procedure can be used to obtain values for the friction coefficients[9].

The main advantage claimed for the use of the frictional model to describe transport processes in membranes, is that each friction coefficient represents the interaction between a particular pair of flows. They are not complex combinations of several interactions as are the L_{ik} and R_{ii} coefficients. The model also permits a direct evaluation of the interactions between the various permeating species and the membrane, interactions which are hidden in treatments which use only the L_{ik} and R_{ik} coefficients.

It may be possible under favourable conditions to neglect some of the frictional interactions on the basis of previous knowledge of the properties of the membrane and permeants. A smaller number of experimental measurements is then necessary to describe the system. For example Spiegler[71] suggested that, in a system where a

cation-exchange membrane is in equilibrium with a dilute electrolyte solution, the friction coefficient f_{12} (where 1 represents cations and 2 represents anions) can be set equal to zero because of the low concentration of diffusible anions.

Simplifications such as that described above should be made only with great care. It is possible that even though f_{ik} may be negligibly small f_{ki} may be quite large because the ratio c_k/c_i [c.f. eq. (3.1.3.4)] may be large. In such a case the full number of experimental measurements must still be made.

The quantitative application of the frictional model to biological membrane systems is restricted by the difficulty of measuring or estimating values for the average or local concentrations of the permeating species in the membrane. These values are required for the calculation of the friction coefficients from the measured experimental parameters. Thus, although values for sets of L_{ik} coefficients (particularly L_p, σ, and ω) have been obtained for some biological systems, it has been possible to interpret these in terms of the friction coefficients in only a qualitative manner[9]. With homogeneous synthetic resin membranes the situation seems to be simpler. Some limited measurements of friction coefficients for such systems have been reported[9].

3.2   Conductance and Transport Number

3.2.1   Conductance and Transport Number and their Relation to Flows and Forces in Electrodialysis

The author has derived the following relationships for conductance and transport number and their relation to flows and forces in electrodialysis

Consider a system consisting of two aqueous solutions containing only one permeable electrolyte separated by a membrane[14]. Different concentrations, pressures, and electrical potentials are allowed on both sides of the membrane. Envisage further the operation of two forces with two conjugated flows which may pass from one side of the membrane to the other. The simplest choice of flows and forces would be the flow of cation J_1, driven by the difference in electrochemical potential $\Delta\tilde{\mu}_1$, and the flow of anion J_2, driven by the corresponding force $\Delta\tilde{\mu}_2$. The following simple phenomenological equations can then be set-up[13]. (see eq. 3.1.1.6)

34

$$J_1 = L_1 \Delta \tilde{\mu}_1 \tag{3.2.1}$$

$$J_2 = L_2 \Delta \tilde{\mu}_2 \tag{3.2.2}$$

where L_1 and L_2 are the phenomenological coefficients which characterize the system.

The chemical potential of the electrolyte, $\Delta \mu_s$, is equal to the electrochemical potentials of the cation and the anion[14].

$$\Delta \mu_s = \Delta \tilde{\mu}_1 + \Delta \tilde{\mu}_2 \tag{3.2.3}$$

The electrical current, I, through a membrane is related to the ionic flows by the relationship[13].

$$I = (z_1 J_1 + z_2 J_2)F \tag{3.2.4}$$

where z_1 = valence of cation; z_2 = valence of anion; F = Faraday's constant.

When $I = 0$, then $J_1 = J_2$

The electromotive force, E, acting on the system can be determined by introducing a pair of electrodes reversible to one of the ions, say ion 2, and measuring the potential difference. The value of E is related thermodynamically to the difference in electrochemical potential of ion 2[14]:

$$E = \frac{\Delta \tilde{\mu}_2}{z_2 F} \tag{3.2.5}$$

for NaCl, $z_2 = -1$

$$\text{and} \quad E = \frac{\Delta \tilde{\mu}_2}{-F} \tag{3.2.6}$$

$$\text{or} \quad EF = -\Delta \tilde{\mu}_2 \tag{3.2.7}$$

Membrane conductance is usually carried out under isothermal, isobaric conditions with constant salt concentrations across the membrane.

$$\text{when } \Delta\mu_s = 0, \text{ then } \Delta\tilde{\mu}_1 = -\Delta\tilde{\mu}_2 \qquad (3.2.8)$$

The electric current, I, through the membrane is:

$$I = F(J_1 - J_2) \qquad (3.2.9)$$

Substituting eq. (3.2.1) and (3.2.2) into eq. (3.2.9), gives

$$I = F(L_1\Delta\tilde{\mu}_1 - L_2\Delta\tilde{\mu}_2) \qquad (3.2.10)$$

$$\text{But, } \Delta\tilde{\mu}_1 = -\Delta\tilde{\mu}_2 \qquad \text{(see eq. 3.2.8)}$$

$$\therefore I = F(-L_1\Delta\tilde{\mu}_2 - L_2\Delta\tilde{\mu}_2) \qquad (3.2.11)$$

$$= -F\Delta\tilde{\mu}_2(L_1 + L_2) \qquad (3.2.12)$$

$$\text{But } EF = -\Delta\tilde{\mu}_2 \qquad \text{(see eq. 3.2.7)}$$

$$\therefore I = F^2E\ (L_1 + L_2)$$

$$\therefore \left[\frac{I}{E}\right]_{\Delta\mu_s\ =\ 0,\ Jv\ =\ 0} = F^2(L_1 + L_2) = \text{Conductance} \qquad (3.2.13)$$

when I = 0, then

$$J_1 - J_2 = 0 \qquad (3.2.14)$$

Substituting eqs. (3.2.1) and (3.2.2) into eq. (3.2.14) gives

$$L_1\Delta\tilde{\mu}_1 - L_2\Delta\tilde{\mu}_2 = 0 \qquad (3.2.15)$$

$$\text{But } \Delta\tilde{\mu}_1 = \Delta\mu_s - \Delta\tilde{\mu}_2 \qquad \text{(see eq. 3.2.3)}$$

$$L_1 (\Delta\mu_s - \Delta\tilde{\mu}_2) - L_2\Delta\tilde{\mu}_2 = 0 \qquad (3.2.16)$$

$$\text{and } \Delta\tilde{\mu}_2 = \frac{L_1}{L_1 + L_2} \Delta\mu_s \qquad (3.2.17)$$

$$\text{or } - EF = \frac{L_1}{L_1 + L_2} \Delta\mu_s \qquad (3.2.18)$$

$$\therefore \left[\frac{EF}{\Delta\mu_s}\right]_{I = 0, \ Jv = 0} = -\frac{L_1}{L_1 + L_2} \qquad (3.2.19)$$

$$\text{Consider } \left[J_1/I\right]_{\Delta\mu_s = 0} = \frac{L_1\Delta\tilde{\mu}_1}{F^2E(L_1 + L_2)} \qquad (3.2.20)$$

But $\Delta\tilde{\mu}_1 = -\Delta\tilde{\mu}_2$ and $EF = -\Delta\tilde{\mu}_2$

$$\therefore (J_1/I)_{\Delta\mu_s = 0} = \frac{L_1(-\Delta\tilde{\mu}_2)}{-\Delta\tilde{\mu}_2(L_1 + L_2) \cdot F} \qquad (3.2.21)$$

$$= \frac{1}{F} \cdot \frac{L_1}{L_1 + L_2} \qquad (3.2.22)$$

$$\therefore [JF/I]_{\Delta\mu_s = 0; \ Jv = 0} = \frac{L_1}{L_1 + L_2} \qquad (3.2.23)$$

$$= \Delta t \ \text{(transport number)} \qquad (3.2.23)$$

$$= -\left(\frac{EF}{\Delta\mu_s}\right)_{I = 0; \ Jv = 0} \qquad (3.2.24)$$

Note: The membrane potential $\Delta\psi$ is related to the electromotic force measured between reversible electrodes by the expression[13]:

$$\Delta\Psi = E - \frac{\Delta\tilde{\mu}_2}{z_2F}$$

37

3.3　Ion Coupling from Conventional Transport Coefficients

3.3.1　Ion Association and the Coupling of Flows

Kedem[15] has described ion association and coupling of flows, charged hydrophobic membranes and the association model, transport properties and transport coefficients in the absence of volume flows and transport coefficients in the absence of a pressure gradient.

Anions and cations will exist in part as neutral ion pairs or molecules when the dielectric constant of the membrane is low. Three mobile species can be identified in the membrane phase according to Kedem: free anion, free cation and ion pair (only a univalent electrolyte will be considered). The dissipation function for ion flows, in this case, can be expressed either in terms of the two stoichiometric ion flows, J_1 and J_2, or in terms of three species: free ion, J_1^* and J_2^*, and neutral molecule, J_s. Assuming dissociation equilibrium, the thermodynamic potential of the molecule is equal to that of the sum of the ions:

$$X_s = X_1 + X_2 \qquad (3.3.1)$$

The relation between J_i and J_i^* is:

$$J_1 = J_1^* + J_s$$

$$(3.3.2)$$

$$J_2 = J_2^* + J_s$$

and thus the two species dissipation function

$$\phi = J_1 X_1 + J_2 X_2$$

is equal to the three flow expression

$$\phi = J_1^* X_1 + J_2^* X_2 + J_s X_s = (J_1 - J_s)X_1 + (J_2 - J_s)X_2 + (X_1 + X_2)J_s.$$

Assuming that no frictional interactions exist between the free ions and the neutral molecule and that volume flow is either negligible or absent, a linear relationship between flows and forces can be described by the following set of equations:

$$X_1 = R_{11}^* J_1^*; \quad X_2 = R_{22}^* J_2^*; \quad X_s = R_s J_s \tag{3.3.3}$$

Equations (3.3.1), (3.3.2) and (3.3.3) give:

$$R_{11}^* (J_1 - J_s) + R_{22}^* (J_2 - J_s) = R_s J_s \tag{3.3.4a}$$

from which J_s is expressed in terms of individual resistance coefficients of the three mobile species and the flow of the free ions,

$$J_s = \frac{R_{11}^* J_1^* + R_{22}^* J_2^*}{\Sigma R} \tag{3.3.4b}$$

where $\Sigma R = R_s + R_{11}^* + R_{22}^*$.

From the relations one obtains the phenomenological equations which describe the total stoichiometric ionic flows and forces by means of the individual resistance coefficients of the free and associated mobile species:

$$X_1 = R_{11}^* \left(1 - \frac{R_{11}^*}{\Sigma R} \right) J_1 - \frac{R_{11}^* R_{22}^*}{\Sigma R} J_2$$

$$\tag{3.3.5}$$

$$X_2 = - \frac{R_{11}^* R_{22}^*}{\Sigma R} J_1 + R_{22}^* \left(1 - \frac{R_{22}^*}{\Sigma R} \right) J_2$$

The corresponding resistance coefficients are:

$$R_{11} = R_{11}^* \frac{R_{22}^* + R_s}{R_{11}^* + R_{22}^* + R_s}$$

$$R_{22} = R_{22}^* \frac{R_{11}^* + R_s}{R_{11}^* + R_{22}^* + R_s} \tag{3.3.6}$$

$$R_{12} = - \frac{R_{11}^* R_{22}^*}{R_{11}^* + R_{22}^* + R_s}$$

The relative importance of the ion-coupling, according to Kedem, is best expressed in terms of the degree of coupling, $q^2 = R_{12}^2 / R_{11} R_{22}$, where $q^2 = 1$ means that the coupling between the flows is complete, and $q^2 = 0$ indicates absence of coupling[72].

For the case of ion association, this coefficient is given by:

$$q^2 = \frac{R_{11}^* R_{22}^*}{(R_s + R_{11}^*)(R_s + R_{22}^*)} \tag{3.3.7}$$

If $R_s >> R_{11}^*$ and $R_s >> R_{22}^*$ then $R_{11} \approx R_{11}^*$, $R_{22} \approx R_{22}^*$ and $q^2 \to 0$; i.e. there is no significant coupling. If, on the other hand, R_s is much smaller than the R_{ii}^* terms, coupling can be practically complete.

The physical significance of these limits becomes clear if we introduce concentration and friction coefficients for the R's, $R_{ii} = f_{ii}/c_i$.

To discuss the orders of magnitude, let us take all f_{ii}'s approximately equal; then

$$q^2 \approx \frac{c_s^2}{(c_s + c_1^*)(c_s + c_2^*)} \tag{3.3.8}$$

Negligible coupling, i.e. $q^2 \to 0$, is found when the concentration of the free ion are much larger than the concentrations of associated molecules; on the other hand, strong association leads to a high degree of coupling, that is $q^2 \to 1$. In other words, the degree of coupling and degree of association are closely related.

Consider first a matrix, which does not carry fixed charges, i.e. $c_1^* = c_2^* = c^*$. The expression for the coupling coefficient will be given by

$$q^2 \cong \frac{c_s^2}{(c_s + c^*)^2} \qquad (3.3.9)$$

For slight association expected in high dielectric media, $c_s << c^*$ and:

$$q^2 \cong \frac{c_s^2}{2c_sc^* + c^{*2}} = \frac{(c_s/c^*)^2}{1 + 2\,c_s/c^*} \to 0 \qquad (3.3.10)$$

No coupling will thus be observed.

In these media q^2 also remains small in the presence of fixed charges, i.e.

$$c_1^* \neq c_2^*$$

For slight dissociation, as is to be expected in hydrophobic membranes, $c_s >> c^*$, and:

$$q^2 \cong \frac{1}{(1 + c^*/c_s)^2} \to 1 \qquad (3.3.11)$$

The presence of fixed charges in hydrophobic membranes complicates the analysis of coupling effects, according to Kedem and requires a detailed consideration of a model.

3.3.2 Charged Hydrophobic Membranes - The Association Model

Consider a polymeric membrane matrix with chemically bound ionizable groups at a total concentration of X_t, and low water content[73]. Several ion-exchange and dissociation equilibria are established when immersing such a membrane in an aqueous salt solution with a concentration c_s'.

aqueous solution   membrane   aqueous solution

$$X^* + c_1^* \to Xc_1$$
$$c_2^* + c_1^* \to c_s$$

c_s' c_s'
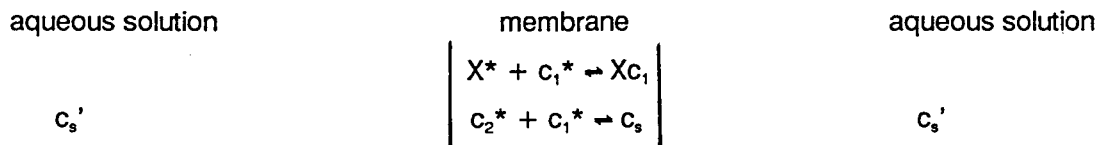
Assuming ideality in the aqueous solutions, dissolution equilibria of the free counter-ion c_1^* and free co-ion c_2^* between the membrane and the aqueous solution are obtained

by equating the electrochemical potentials in the two phases:

$$\tilde{\mu}_1' = \mu_1^{o\prime} + RT \ln c_1' + z_1 F \psi' = \mu_1^o + RT \ln c_1^* + z_1 F \psi = \tilde{\mu}_1$$

$$\tilde{\mu}_2' = \mu_2^{o\prime} + RT \ln c_2' + z_2 F \psi' = \mu_2^o + RT \ln c_2^* + z_2 F \psi = \tilde{\mu}_2.$$

(3.3.12)

Adding the respective terms and applying the condition for ion pair formation reaction in the membrane: $\mu_s = \tilde{\mu}_1 + \tilde{\mu}_2$, we obtain after rearrangement:

$$c_s = k \, c_3'^2$$

(3.3.13)

where c_s' is the concentration of the fully dissociated salt in water; c_s is the concentration of the undissociated salt in the membrane phase; c_1^*, c_2^* are the concentrations of free ions in the membrane; and $k = \exp[(\mu_s^o - \mu_1^{o\prime} - \mu_2^{o\prime})/RT]$.

Ion pair formation between the small ions is expressed by:

$$\frac{c_1^* c_2^*}{c_s} = K_d^s \qquad c_s = c_2^t - c_2^*$$

(3.3.14)

where c_2^t, c_s indicate the concentration of the total and the undissociated salt in the membrane phase. Ion pair formation at the fixed ionic sites is given by:

$$\frac{c_1^* X^*}{(X_t - X^*)} = K_d^f$$

(3.3.15)

where X_t is the total concentration of fixed groups and X^* is its free fraction. Introducing electroneutrality for the dissociated species, $c_1^* = c_2^* + X^*$, into the above expressions and rearranging the equations for the modified Donnan equilibrium for non-aqueous membranes, we obtain a polynomial of 3rd degree with respect to c_2^*:

$$K_d^f c_2^{*3} + (K_d^f X_t + \alpha) c_2^{*2} - K_d^f \alpha \, c_2^* - \alpha^2 = 0$$

(3.3.16)

$$\text{where } \alpha = K_d^s k c_s'^2$$

The adsorption isotherm of the co-ions, c_2^t, is given from the above relations by

$$c_2^t = c_2^* + c_s = c_2^* + \alpha/K_d^s$$

(3.3.17)

For analysis of the coupling coefficient, explicit expressions for the concentrations of the co-ion or counter-ion are obtained from eqs. (3.3.14) and (3.3.15) and the

electroneutrality condition:

for free co-ions:

$$c_2^* = \frac{K_d^s}{K_d^f} \left[\frac{c_2^t - c_2^*}{X_t - X^*} \right] X^*$$

(3.3.18)

for free counter-ions:

$$c_1^* = \left(\frac{K_d^s}{K_d^f} \left[\frac{c_2^t - c_2^*}{X_t - X^*} \right] + 1 \right) X^*$$

(3.3.19)

for small dissociation:

$c_2^* << c_2^t \cong c_s$ and $X^* << X_t$

At these conditions, free co-ion concentration becomes

$$c_2^* \cong m \, c_2^t \, a$$

(3.3.20)

where

$$m = K_d^s/K_d^f \text{ and } a = X^*/X_t <<1$$

Free counter-ion concentration is given by

$c_1^* \cong m \, c_2^t a + X^* = a(m \, c_2^t + X_t).$

(3.3.21)

Coupling coefficient is thus given by

$$q^2 = \frac{1}{(1 + c_1^*/c_s)(1 + c_2^*/c_s)} \cong \frac{1}{(1 + c_1^*/c_2^t)(1 + c_2^*/c_2^t)} \cong \frac{1}{1 + c_1^*/c_2^t}$$

(3.3.22)

High coupling $q^2 \to 1$ is obtained when $c_1^*/c_2^t << 1$;

$$\frac{c_1^*}{c_2^t} = a \frac{(m \, c_2^t + X_t)}{c_2^t} = a(m + X_t/c_2^t)$$

(3.3.23)

According to Kedem, high coupling will be observed in non-charged hydrophobic membranes with small salt dissociation constants; in charged hydrophobic membranes a high degree of coupling will be observed only in the case of large salt invasion.

3.3.3 Transport Properties and Transport Coefficients In the Absence of Volume Flow

Phenomenological equations for two stoichiometric ionic flows in the absence of volume flow is given by:

$$X_1 = R_{11}J_1 + R_{12}J_2$$

$$(3.3.24)$$

$$X_2 = R_{21}J_1 + R_{22}J_2$$

with $R_{12} = R_{21}$

Electric current, electric potential and concentration are measured in practice and the conventional transport coefficients are defined accordingly. The relation between the driving forces and the Rij's are obtained from the constraints imposed for each measurement. The expression for driving force for ion transport, i.e. the difference in the electrochemical potential for equal concentrations on both sides of the membrane, is given by:

$$X_i = \Delta\widetilde{\mu}_i = -z_i FE \qquad (3.3.25)$$

So that

$$X_1 + X_2 = 0 \qquad (3.3.26)$$

3.3.3.1 Electric conductance

Membrane conductance, κ, is:

$$\kappa = \left(\frac{I}{E}\right)_{\Delta\mu = 0; \ Jv = 0} \qquad \text{(see eq. 3.2.13)}$$

where the electric current, I, is given by

$$I = F(z_1 J_1 + z_2 J_2) \qquad \text{(see eq. 3.2.4)}$$

The current I can be expressed in terms of resistance coefficients and two driving forces by substituting eq. (3.3.24) into eq. (3.3.26).

$$\therefore \ J_2 = - \frac{R_{11} + R_{12}}{R_{22} + R_{12}} J_1 \qquad (3.3.27)$$

Introducing J_2 from eq. (3.3.27) into eq. (3.3.24), and rearranging, gives:-

$$X_1 = R_{11}J_1 - \frac{R_{12}(R_{11} + R_{12})J_1}{R_{22} + R_{12}} = \frac{R_{11}R_{22} - R_{12}^2}{R_{22} + R_{12}} J_1 \qquad (3.3.28)$$

From eqs. (3.2.4), (3.3.27) and (3.3.28), the current is

$$I = (J_1 - J_2) = \frac{R_{11} + R_{22} + 2R_{12}}{R_{11}R_{22} - R_{12}^2} X_1 \qquad (3.3.29)$$

and the conductance, κ, is

$$\frac{\kappa}{F^2} = \left(\frac{I}{E}\right)\frac{1}{F^2} = \frac{J_1 - J_2}{X_1} = \frac{R_{11} + R_{22} + 2R_{12}}{R_{11}R_{22} - R_{12}^2} \qquad (3.3.30)$$

3.3.3.2 Transport numbers

Transport numbers $t_{1,2}$ are defined as the fraction of the electric current carried by each of the ions, without concentration gradients. In practice, membrane potentials are measured assuming Onsager's symmetry.

The transport numbers in terms of the Rij's are:

$$t_1 = \frac{J_1}{J_1 - J_2} = \frac{R_{22} + R_{12}}{R_{11} + R_{22} + 2R_{12}} \qquad (3.3.31)$$

$$t_2 = 1 - t_1 = \frac{R_{11} + R_{12}}{R_{11} + R_{22} + 2R_{12}} \qquad (3.3.32)$$

The product of t_1 and t_2 is

$$t_1 t_2 = \frac{(R_{11} + R_{12})(R_{22} + R_{12})}{(R_{11} + R_{22} + 2R_{12})^2} \qquad (3.3.33)$$

3.3.3.3 Salt permeability

Salt permeability or salt "leak", ω_s, is measured in the absence of electric current, so that

$$J_1 = J_2 = J_s \qquad (3.3.34)$$

The driving force for salt flow is the gradient of its thermodynamic potential:

$$X_s = X_1 + X_2 \qquad (3.3.35)$$

Adding the respective terms from eq. (3.3.24) gives:

$$X_s = (R_{11} + R_{22} + 2R_{12}) \, J_s \qquad (3.3.36)$$

and

$$\frac{J_s}{X_s} = \omega_s \, c_s'^{\text{av}} = \frac{1}{R_{11} + R_{22} + 2R_{12}} \qquad (3.3.37)$$

where $c_s'^{\text{av}}$ is mean salt concentration on the two membrane sides.

3.3.3.4 Correlation between $\kappa_1, t_{1,2}$ and ω_s

In aqueous charged ion-exchange membranes where the total amount of co-ions is very small compared to that of the counter-ions, the electro-neutral salt leak will become a very small fraction of total membrane conductance. Comparing the expression for the leak-conductance (LC) ratio obtained from eqs. (3.3.30) and (3.3.37), the following equation is obtained:

$$\frac{\omega_s c_s^{av}}{\kappa/F^2} = \frac{R_{11} R_{22} - R_{12}^2}{(R_{11} + R_{22} + 2R_{12})^2} \qquad (3.3.38)$$

This and the expression for the product of the transport numbers, eq. (3.3.33), shows that

$$\frac{\omega_s c_s^{av}}{\kappa/F^2} = t_1 t_2 - \frac{R_{12}}{R_{11} + R_{22} + 2R_{12}} = t_1 t_2 - R_{12} \, \omega_s c_s^{av} \qquad (3.3.39)$$

In the case of zero volume flow and no coupling between the co- and counter-ions $R_{12} = 0$; a plot of the permeability ratio vs. the product of the two transport numbers should give a straight line with slope of 1, intersecting the origin:

$$\frac{\omega_s c_s^{av}}{\kappa/F^2} = t_1 t_2 \qquad (3.3.40)$$

In general, $R_{12} \neq 0$ should lead to a substantial deviation from this curve which will depend on the type and the extent of coupling.

Mutual drag reflects positive coupling between ion flows by any type of mechanism and is represented by a negative value of R_{12}. In this case the relation between the LC ratio and the product of the two transport numbers will be characterized by an inequality.

$$\frac{\omega_s c_s^{av}}{\kappa/F^2} > t_1 t_2 \qquad (3.3.41)$$

An estimate of R_{12} is readily obtained from measured values of salt leak, membrane conductance and transport numbers as is shown in eq. (3.3.42).

$$- R_{12} = \frac{1}{\kappa/F^2} - \frac{t_1 t_2}{\omega_s c_s'^{av}}$$ (3.3.42)

3.3.4 Transport Coefficients In the Absence of a Pressure Gradient

In practice, membrane conductance is usually measured in open cells with atmospheric pressure on both sides of the membrane and with equal salt concentrations. Under these conditions, volume flow is in general not zero. Thus in charged membranes, electro-osmotic volume flow is to be expected.

The electric conductance $(I/E)_{\Delta p = 0} \cong \kappa'$
is related to κ by[14]

$$\kappa' \equiv \frac{\kappa}{1 + P_E \beta}$$ (3.3.43)

where κ and P_E are the electric conductance and the electro-osmotic pressure respectively, measured under conditions of zero volume flow and salt gradient, and β is the electro-osmotic permeability, measured at zero pressure and salt gradient.

For a homogeneous charged membrane has β and P_E opposite signs[14], and

$$\beta = - \frac{P_E L_p}{\kappa}$$ (3.3.44)

L_p and κ are straight coefficients and therefore always positive. This implies that $\kappa' > \kappa$, i.e. electro-osmosis enhances membrane conductivity as a consequence of water-ion frictional drag; its direction is that of counter-ion flow. Similarly salt permeability is usually measured at zero pressure and osmotic flow is allowed to take place. In this case, however, volume flow is opposed to the direction of salt diffusion and therefore,

$$\frac{J_s}{X_s/c_s} \equiv \omega_s'' < \omega_s$$ (3.3.44)

where (') is used for measurement at $\Delta p = 0$. From eqs. (3.3.30), (3.3.43) and (3.3.44), the interaction between water flow and ion flows leads to the inequality.

$$\left(\frac{J_s}{X_s/c_s} \middle/ \frac{J_1 - J_2}{X_1} \right)_{\Delta p = 0} < \left(\frac{J_s}{X_s/c_s} \middle/ \frac{J_1 - J_2}{X_1} \right)_{Jv = 0} \qquad (3.3.45)$$

Therefore, salt diffusion in the presence of volume flow is less than salt diffusion in the absence of volume flow. The membrane potential at $\Delta p = 0$ in practice would also differ from that measured in the absence of water flow. In general, existence of volume flow would result in the flattening of the concentration difference between the two membrane-solution interfaces. In charged ion-exchange membranes, this will mostly affect the counter-ions, and therefore the observed membrane potential would be lowered by water flow, even with ideal stirring which would give in effect no unstirred layers. In real measurement, the existence of unstrirred layers would make this effect even larger. Maximum values of $t_1 t_2 = 0,25$ is obtained in completely non-permselective membranes, i.e. $t_1 = t_2 = 0,5$; in highly permselective membranes this product will approach zero. Volume flow will thus result in a smaller membrane potential of which will shift the measured data towards larger $t_1 t_2$ values.

In general, ion-water coupling, causes the experimental data to be shifted in the opposite direction to that affected by ion-ion coupling, according to Kedem.

Correlations (3.3.42) and (3.3.45) show that from customary measurements of conductance and membrane potential plus salt permeation, one gets a sharp distinction between ion-water coupling as found in usual ion-exchange membranes on the one hand, and ion-ion coupling as expected in hydrophobic membranes on the other hand. Zero coupling in the absence of volume flow was given by eq. (3.3.40).

3.4   Transport Processes Occurring During Electrodialysis

A number of transport processes occur simultaneously during ED, and these are illustrated in Figure 3.4.1[7].

Counter-ion transport constitutes the major electrical movement in the process; the counter-ions transport with them by electro-osmosis a certain quantity of water. Co-ion transport is comparatively small and is dependent upon the quality of the ion-selective membrane and upon the brine concentration. Water is also transported electro-osmotically with the co-ions. Diffusion of electrolyte occurs from the brine to the dialysate compartment because in the ED process the brine stream is usually more concentrated that the dialysate stream. Water transport is also associated with

electrolyte diffusion. Water transport due to osmosis takes place from the low concentration dialysate compartment into the higher concentration brine compartment.

$+$ $+$ $-$ $-$

counter - ion transport

Cl^- $(+H_2O)$ $Na^+(+H_2O)$

counter - ion transport

Na^+ $(+H_2O)$

co-ion transport

Cl^- $(+H_2O)$

$NaCl(+H_2O)$

diffusion

$NaCl(+H_2O)$

H_2O osmosis H_2O

Brine

Dialysate

Brine
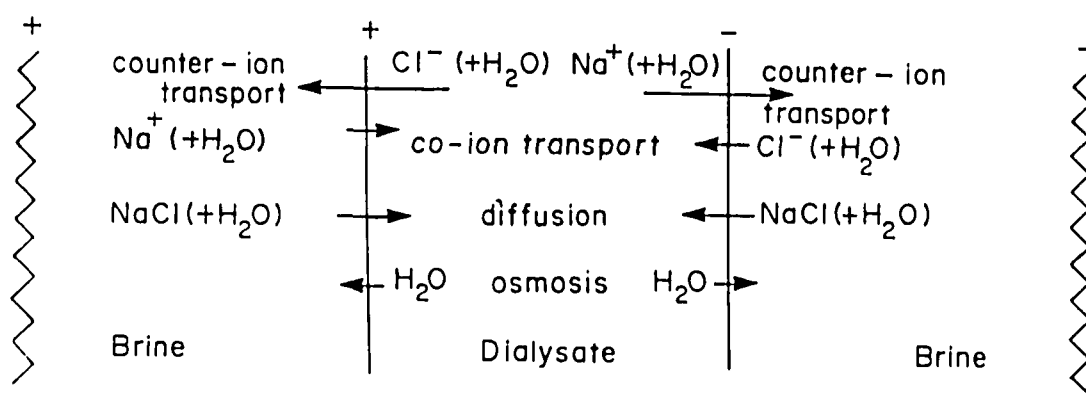
Figure 3.4.1: Illustration of transport processes which can occur simultaneously during the electrodialysis process.

The efficiency of demineralization of the liquid in the dialysate compartment may be considerably reduced by the counter effects of co-ion transport, diffusion, water transport associated with counter-ion movement and osmosis. The effect of these unwanted transfer processes can, however, be reduced by the correct selection of membranes and by the selection of the optimum operational procedure for a particular application[7]. Osmosis and electro-osmosis are effects which limit the usefulness of ED as a method of concentrating electrolyte solutions.

3.5 Current Efficiency and Transport Phenomena in Systems with Charged Membranes

The interaction between the current efficiency of electrodialytic separation with ion-exchange membranes and all the fluxes depressing selectivity, i.e., electric transport of co-ions, electro-osmotic flow of water, diffusion and osmosis have been described and experimentally examined by Koter and Narebska[17]. They have presented a simple definition of the current efficiency (CE) for a single ion-exchange membrane system. It allows for the estimation of CE from a determination of concentration changes in

cathode and anode solutions. With the proposed definition, CE can be expressed as a simple function of different kinds of transport taking place in the system. This fact makes it possible to examine the effects of these transports on current efficiency, that is to calculate the losses of CE due to:

a)   electric transport of co-ions;

b)   electro-osmotic flow of water;

c)   diffusion of a salt; and

d)   osmotic transport of water.

Thus, the full characteristics of a single ion-exchange membrane (cation- or anion-exchange) for a separation process like ED can be obtained. The mathematical solution has been examined for computing the current efficiency and its losses for the system $NaCl_{aq}$/Nafion 120 membrane and $NaOH_{aq}$/Nafion 120 membrane based on the experimental results published earlier[17].

3.5.1   Current Efficiency of a Membrane System - A Definition

Consider the one membrane system as shown in Figure 3.5.1. The ion-exchange membrane (M) separates two solutions of an Av_1Bv_2 electrolyte differing in concentrations. For the cation-exchange membrane (sign W =- 1) the cathode is on the more concentrated side whereas for the anion-exchange membrane (W =+ 1) it is on the diluted side. The electrodes and electrode reactions do not belong to the system. They are separated from the system by ideal membranes of reverse sign to the investigated membrane.

At t = 0, the concentration difference across the membrane is $\Delta c° = c°' - c°''$. After passing an electric current through the membrane for time t, the concentration difference changes to Δc^t. The ratio of ($\Delta c^t - \Delta c°$) for the real membrane to ($\Delta c^t - \Delta c'$) for the ideal membrane system (t_2, t_w, J_s, $J_w{}^{os}$ = 0) is a measure of the current efficiency:

$$CE = \frac{(\Delta c^t - \Delta c°)}{(\Delta c^t - \Delta c°)_{ideal}}$$ (3.5.1)

Rearrangement of this formula[17] leads to the following equation relating the current efficiency to the total counter-ions (J_1) and water (J_w) fluxes (see Appendix B).
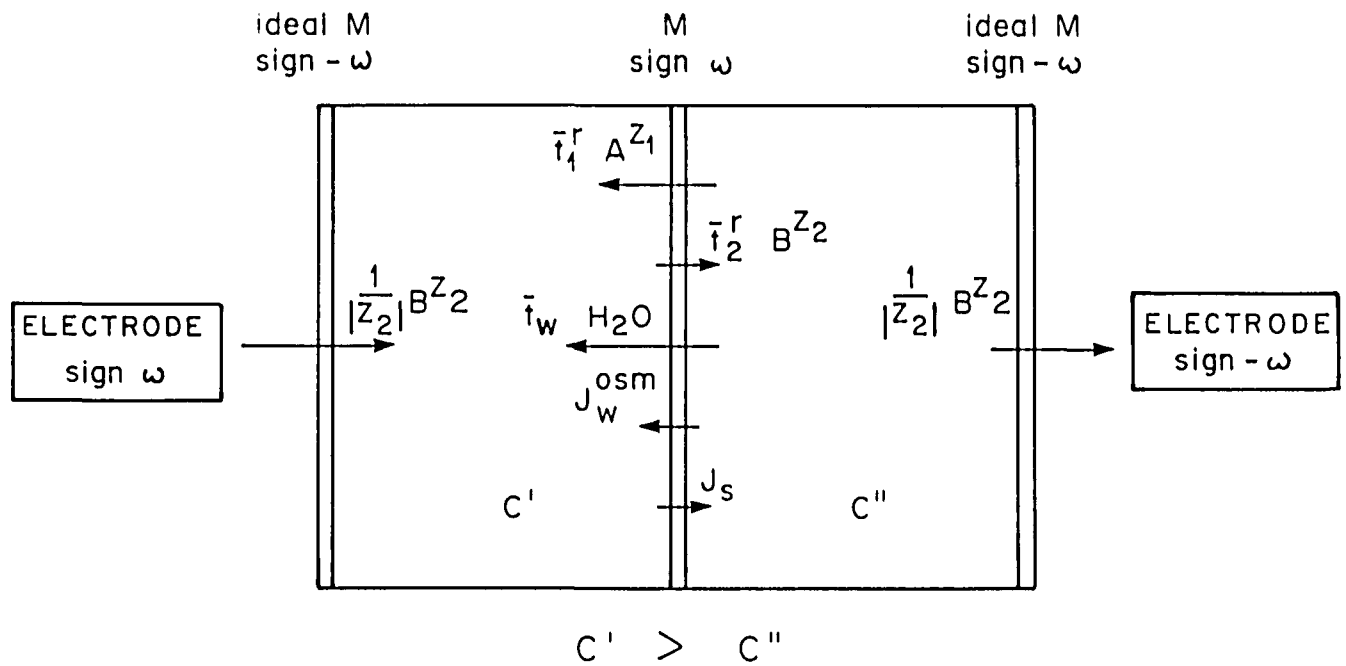
A – counter-ion
B – co-ion

Figure 3.5.1: Standard system for defining the current efficiency of an ion-exchange membrane in the isobaric condition ($\Delta p = 0$). The transport processes caused by the passage of 1 Faraday of electric charge ($\bar{t}_1$ and $\bar{t}_2$ are the electric transport of counter-ions and co-ions, respectively; $\bar{t}_w$ is the electro-osmotic transport of water) and by the concentration difference (J_s - diffusion of a salt, J^{os}_w = osmotic flux of water) are shown.

$$CE - \omega z_1 v_1 \ (J_1/v_1 - 0{,}018\widetilde{m}J_w)/I \tag{3.5.2}$$

Consider that the counter-ions are driven by the constant electric field and the chemical potential gradient, and that the same holds for water, eq. (3.5.2) can be rearranged to:

$$CE - z_1 v_1 (\bar{t}^r_1/v_1 - 0{,}018\widetilde{m}\bar{t}_w - \omega(J_s - 0{,}018\widetilde{m}J^{os}_w)F/I \tag{3.5.3}$$

where

$\bar{t}^r_1$	$=$	reduced transport number of counter-ions (eq. A2, Appendix B)
$\bar{t}_w$	$=$	transport number of water
$\widetilde{m}$	$=$	mean molality (eq. B17, Appendix B)
J_s, J_w^{os}	$=$	diffusion and osmotic fluxes
I	$=$	electric current
ω	$=$	-1 for cation-exchange membrane
	$=$	+1 for anion-exchange membrane

The formula indicating the fluxes that decrease current efficiency, is as follows:

	Electrical transport of co-ions	Electro-osmotic transport of water	Diffusion of salt	Osmotic flux of water	
$CE = 1 -$	$\bar{t}_2 - z_1$	$z_1 v_1 0.018\tilde{m}\tilde{t}_w -$	$z_1 v_1 \omega \ (J_s -$	$0.018\tilde{m}J_w^{os}) \ F/I$	(3.5.3a)

With the help of the transport equations of irreversible thermodynamics and the Gibbs - Duhem equation, the diffusion and osmotic fluxes, J, and J_w^{os}, can be expressed as a function of the difference of the chemical potential of a solute, $\Delta\mu_s$[9].

$$J_s - 0.018\tilde{m}J_w^{os} = \left[\left(\frac{J_s}{\Delta\mu_s}\right) - 0.018\tilde{m} \left(\frac{J_w^{os}}{\Delta\mu_s}\right) \right] \Delta\mu_s$$

$$= f(L_{ik}, \tilde{m})\Delta\mu_s \qquad (3.5.4)$$

Here f (L_{ik}, $\tilde{m}$) represents a combination of the phenomenological conductance coefficients L_{ik} and the mean molality, $\tilde{m}$, of a solute. Equation (3.5.3) and (3.5.4) clearly show that losses of selectivity due to osmotic and diffusion fluxes are dependent on the ratio of the chemical potential difference of solute and the current $\Delta\mu_s/I$.

3.5.2 Determination of Current Efficiency in a System with Electrode Reactions

Substituting the concentration changes for the system with ideal membrane, $(\Delta c^t - \Delta c^o)_{ideal}$ (eq. B15, Appendix B), and the equation

$$\Delta c^t - \Delta c^o = \omega(\Delta c_o^t - \Delta c_c^t) \qquad (3.5.5)$$

Into eq. (3.5.1), eq (3.5.6) is obtained:

$$CE = \frac{z_1 v_1 V^o F \ (\Delta c_c^t - \Delta c_a^t)}{2(1 - v_s c^o)I\Delta t} \qquad (3.5.6)$$

where Δc_a^t, Δc_c^t = concentration changes of anolyte and catholyte after time Δt

c^o = mean concentration of anolyte and catholyte at time $t = 0$,

$c^o = (c_a^o + c_k^o)/2$.

Equation (3.5.6) can only be applied to the standard system (Fig. 3.5.1) without any other effect but transport, i.e., without the electrode reactions. Actually, the experimentally determined variations of the concentrations of the cathodic and anodic solutions are produced by both the transport phenomena and the electrode reaction.

For computing the current efficiency related to the transport phenomena only, the concentration/volume effects of the electrode reactions should be accounted for. The use of electrodes makes it necessary to correct the numerator of eq. (3.5.6), i.e., the difference Δc_c - Δc_a. In the general form the formula for the membrane current efficiency determined in the practical system can be written as:

$$CE = \frac{z_1 v_1}{2(1 - \bar{v}_s \bar{c}^o)}\left[\frac{FV^o}{I}(\frac{\Delta c_c^t}{\Delta t} - \frac{\Delta c_a^t}{\Delta t})^{pract} + correction\right]$$

(3.5.7)

Some electrodes and the formulas for corrections are given by Koter and Narebska[17].

3.5.3 Relation Between Current Efficiency and Efficiency of Energy Conversion

Regarding the general formula for efficiency of energy conversion given by Kedem and Caplan[72], the efficiency of energy conversion, η_E, for the system studied here, takes the form

$$\eta_E = \omega \frac{J_1^w}{I} \frac{\Delta \mu_s}{\Delta E}$$

(3.5.8)

where J_1^w = $J_1/v_1 - 0{,}018 \, \tilde{m} \, J_w$ (3.5.9)

ΔE = is the difference of electrical potential measured with electrodes reversible to co-ions.

$$\Delta E = \Delta \tilde{\mu}_2/z_2 F$$

(3.5.10)

By comparing eq. (3.5.8) for J_1^w and eq. (3.5.3) for the current efficiency, it can be seen that η_E can be written as the product of current efficiency and the force-to-force ratio $\Delta \mu_s/\Delta E$:

$$\eta_E = \omega \frac{1}{z_1 v_1} CE \frac{\Delta \mu_s}{\Delta E} \qquad (3.5.11)$$

3.5.4 The Losses of Current Efficiency

To determine losses of current efficiency due to different kinds of transport (eq. 3.5.3a), four experiments can be performed. Results are here presented for the systems $NaCl_{aq}$/Nafion 120 and $NaOH_{aq}$/Nafion 120. All the experimental results used for computing CE have been published elsewhere[17].

Figures 3.5.2(a) and 3.5.2(b) present the effects of the conjugated fluxes on efficiency of electric transport of counter-ions across the cation-exchange membrane (Nafion 120) for two different values of concentration ratio; m'/m" and current density, i : m'/m" = 5, i = 100 A/m², and m'/m" = 10, i = 500 A/m².

On both figures the current efficiency corresponds to the abscissa (see eq. 3.5.3a)

$$CE = 1 - \Sigma \text{ losses}$$

and is dependent on the mean concentration $\tilde{m}$ (eq. B17, Appendix A). The effects which diminish current efficiency are[17]:

- Electric transport of co-ions, i.e., imperfect membrane permselectivity $(\bar{t}_2)$
- Diffusion of solute (J_s)
- Electro-osmotic flow $(\bar{t}_w)$
- Osmotic water fluxes (J_w^{os})

The following conclusions can be drawn from the figures[17]:

The imperfect selectivity $(\bar{t}_2)$, assumed to be one of the most important characteristics of a membrane, produces up to 8% (NaCl) and 35% (NaOH) of the CE losses at $\tilde{m}$ = 2. Similar to $\bar{t}_2$, the effect of electro-osmotic flow of water $(\bar{t}_w)$ increases with m. It plays a significant role in the system with NaCl where it diminishes CE up to 30%.

Depending on the working conditions, i.e., on the concentration ratio m'/m" and current density, the decrease of CE due to osmotic and diffusion flows can be larger than that caused by electric transport of co-ions and water. This effect is especially
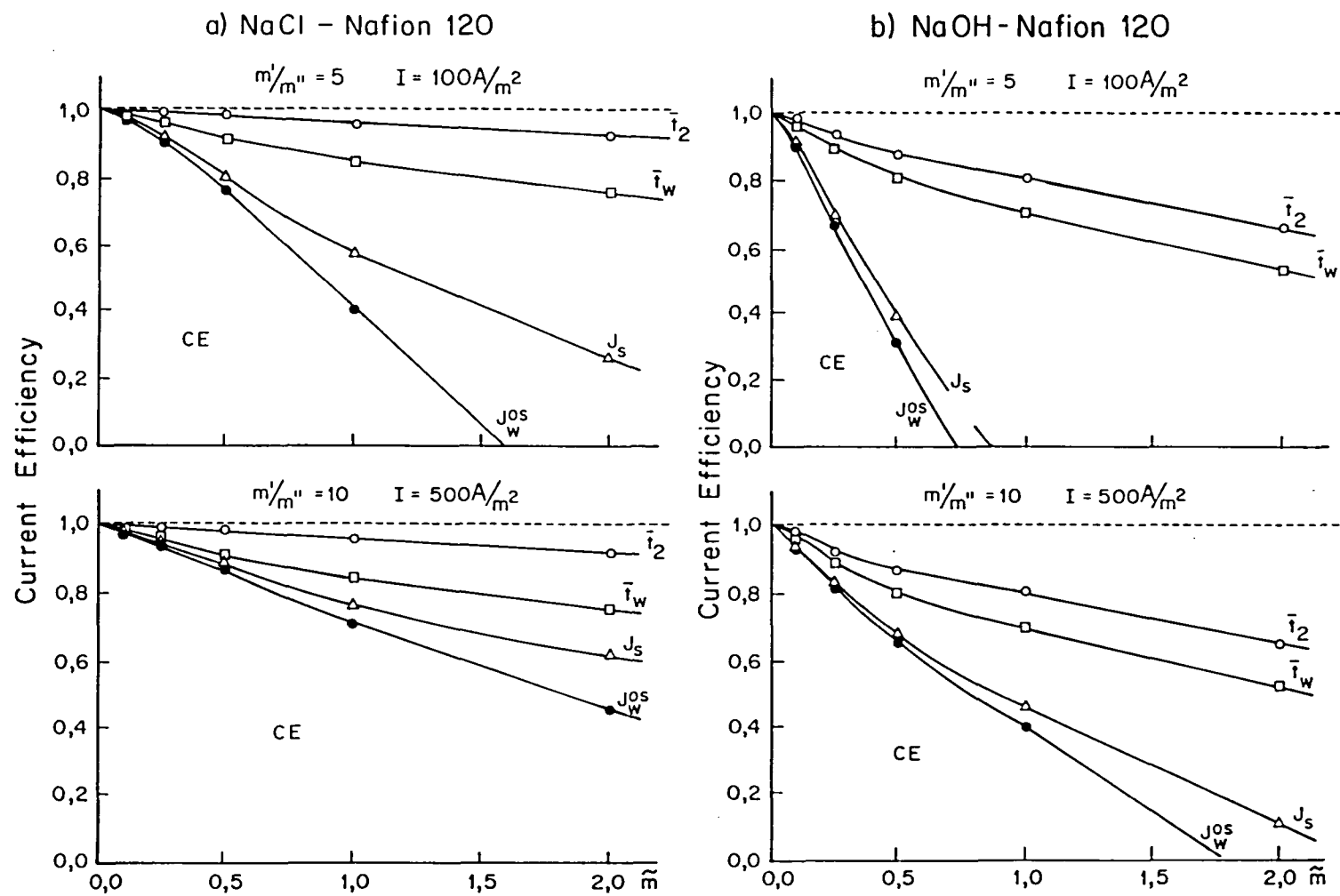
Figure 3.5.2: Losses of current efficiency due to imperfect selectivity of a membrane ($\bar{t}_2$), diffusion of a solute (J_s) and electro-osmotic flow ($\bar{t}_w$) and osmotic (J^{os}_w) fluxes. T = 298K.

seen at higher mean concentrations where the current efficiency can even be reduced to zero.

3.6   Efficiency of Energy Conversion in Electrodialysis

Efficiency of energy conversion in separation processes with Nafion 120 membranes from phenomenological transport coefficients has been described by Narebska and Koter[18].

In systems devised for desalination/concentration processes with ion-exchange membranes separating single electrolyte solutions of different concentrations, electrical energy is used to drive a solute against its concentration gradient. In these processes, the electrical energy is converted into free energy of mixing and in that way it is stored in the system. The efficiency of energy conversion (η) depends both on the degree of coupling between the driving process and the driven flow (q), as well as the operating conditions.

Kedem and Caplan[72] have defined η and q in terms of irreversible thermodynamics and outlined the methods available to access both parameters for thermocouples, fuel cells, osmionic batteries and desalination stacks by treating the system as a two-flow process. Later, Caplen[74] published some data on the overall degree of coupling q and η_{max} for hyperfiltration, concentration cells and ED, taking for the calculations the experimental results for a few points in dilute solutions.

Narebska and Koter[18] have presented results for the degree of coupling and efficiency of energy conversion calculated for the system composed of a perfluorinated Nafion 120 membrane and sodium chloride solutions of different concentrations. Their aim have been to conduct a detailed analysis of input-output relations by treating the system and the transport involved as a three-flow process and describing quantitatively the transport of water which consumes energy unprofitably.

The system consisted of a cation exchange membrane and aqueous solutions of 1 : 1 electrolyte of different concentrations in the adjacent compartments. Sodium are driven by the applied electrical potential difference opposite the concentration difference of NaCl.

3.6.1 Mathematical Formulation

3.6.1.1 The degree of coupling and the efficiency of energy conversion in the two-flow system (basic definitions)

The efficiency of energy conversion η is based in the dissipation function ϕ which for the two-flow system takes the general form:

$$\phi = J_1 X_1 + J_2 X_2 \geq 0 \tag{3.6.1}$$

According to Kedem and Caplan[72], with one flow producing entropy $(J_2 X_2)$, which is always positive and the other flow consuming entropy, being negative $(J_1 X_1)$, the efficiency of energy conversion can be expressed as:

$$\eta = - \frac{J_1 X_1}{J_2 X_2} \tag{3.6.2}$$

Denoting the force ratio as X_1/X_2 and the ratio of the straight conductance coefficients L_{ii} appearing in the flow equations

$$J_1 = L_{11} X_1 + L_{12} X_2$$

$$\tag{3.6.3}$$

$$J_2 = L_{21} X_1 + L_{22} X_2$$

as $Z^2 = L_{11}/L_{22}$, the efficiency function can be calculated with the equation:

$$\eta = - \frac{q + Zx}{q + 1/Zx} \tag{3.6.4}$$

q is the degree of coupling of the flows satisfying the relation $|q| \leq 1$.

The conversion of energy of process 2 to process 1 is only possible when the two flows are coupled, therefore, the degree of coupling can be defined as:

$$q^2 = 1 - \frac{(J_2)_{J_1 = 0}}{(J_2)_{X_1 = 0}} = 1 - \frac{(J_1)_{J_2 = 0}}{(J_1)_{X_2 = 0}} = \frac{L_{12}^2}{L_{11} L_{22}} \tag{3.6.5}$$

For electrodialysis, the dissipation function can be written in the form:

$$\varphi = J_1 \Delta \mu_s + IE \qquad (3.6.6)$$

where J_1 is the flux of counterions, $\Delta \mu_s$ the difference of chemical potential of an electrolyte, I the electric current and E the potential difference between the solutions on opposite sides of the membrane measured with electrodes reversible to the anions.

Kedem and Caplan have presented the general solution for the degree of coupling in ED. They admitted, however, that in their solution the contribution of water flow was neglected. This means that they have treated the process as a two-flow system.

3.6.1.2 Three-flow System

In any real system with a single electrolyte and the ion-exchange membrane separating solutions of different concentrations, the flow of water is another process which participates in the entropy production. Consequently, the equation describing the dissipation function should contain the third component, $J_w \Delta \mu_w$:

$$\varphi = J_1 \Delta \mu_s + J_w \Delta \mu_w + IE \geq 0 \qquad (3.6.7)$$

Thus, the efficiency of energy conversion for multiple-flow system can be defined as[74]:

$$\eta = -\frac{\sum_{i=1}^{n-1} J_i X_i}{J_n X_n} \qquad (3.6.8)$$

In eq. (3.6.8) $J_n X_n$ represents the driving process and $J_i X_i$ represents the driven flow.

As for ED $J_n X_n = IE$ and $\sum_i^{n-1} J X_i = J_1 \Delta \mu_s + J_w \Delta \mu_w$, one gets:

$$\eta = \left(-\frac{J_1 \Delta \mu_s}{IE} \right) + \left(-\frac{J_w \Delta \mu_w}{IE} \right) = \eta_{IE} + \eta_{wE} \qquad (3.6.9)$$

The first term of eq. (3.6.9) is the same as before, i.e. it expresses the storage of energy in producing a concentration difference in the permeant. The second term corresponds to the transport of water which acts opposite to the separation of the components. It causes a waste of energy by decreasing the concentration difference.

To find the degrees of coupling in both processes, the equations for transport of ions (J_1), water (J_w) and current (I) should be used in a general formula:

$$J_1 = L_{11}\Delta\mu_s + L_{1w}\Delta\mu_w + L_{1E}E$$

$$J_w = L_{1w}\Delta\mu_s + L_{ww}\Delta\mu_w + L_{wE}E \qquad (3.6.10)$$

$$I = L_{1E}\Delta\mu_s + L_{wE}\Delta\mu_w + L_EE$$

3.6.1.3 Degrees of coupling for the three-flow system

Defining the degree of coupling according to Kedem and Caplan, three coefficients for the three-flow system are obtained which denote sodium ion-current coupling (q_{iE}), water-current coupling (q_{wE}) and sodium ion-water coupling (q_{iw}).

$$q_{ik}^2 = 1 - \left[\frac{(J_i)_{J_k = 0}}{(J_i)_{X_k = 0}}\right]_{X_j = 0} = \frac{L_{ik}^2}{L_{ii}L_{kk}} \quad i,k = 1,w,E, \quad i \neq k \qquad (3.6.11)$$

All the degrees of coupling were calculated according to eq. (3.6.11) using conductance coefficients L_{ik}, of eq. (3.6.10).

For the more practical discussion of the input-output relation, such as finding the maximum output or the driven region for ED, the overall degree of coupling q_E is also helpful. This can be derived from the general formula

$$\bar{q}^2 = 1 - \frac{(J_n)_{J_i, n = 0}}{(J_n)_{X_i, n = 0}} \qquad (3.6.12)$$

For the system with three forces operating (ΔC, Δp, E, eq. (3.6.10), $\bar{q}_E$ takes the form:

$$\bar{q}_E^2 = 1 - \frac{(I)_{J_i, J_w = 0}}{(I)_{\Delta\mu_s, \Delta\mu_w = 0}} = \frac{q_{iE}^2 + q_{wE}^2 - 2q_{iE}q_{wE}q_{1w}}{1 - q_{1w}^2} \qquad (3.6.13)$$

At $\Delta p = 0$, which corresponds to operating conditions in ED, and applying the Gibbs-Duhem equation $c_s d\mu_s + c_w d\mu_w = 0$, the flow equations can be written in the form:

$$J_1 - \frac{c_s}{c_w} J_w = J_1^w = L_{11}' \Delta \mu_s + L_{IE}' E \qquad (3.6.14)$$

$$I = L_{IE}' \Delta \mu_s + L_E E$$

where

$$L_{11}' = L_{11} - 2\frac{c_s}{c_w} L_{1w} + \frac{c_s^2}{c_w^2} L_{ww} \qquad (3.6.15)$$

$$L_{IE}' = L_{IE} - \frac{c_s}{c_w} L_{wE}$$

For these equations the formula for the overall degree of coupling takes the form:

$$q_E^2 = 1 - \frac{(I)_{J_1^w = 0}}{(I)_{\Delta \mu_s = 0}} = \frac{L_{IE}^2}{L_{11}' L_E} \qquad (3.6.16)$$

3.6.1.4 Efficiency of Energy Conversion

Introducting eq. (3.6.10) into eq. (3.6.9) and assuming that $\Delta p = 0$, it is possible to derive the equations for both components of η (eq. 3.6.9), i.e. η_{IE} and η_{wE}

$$\eta_{IE} = - \frac{\left[Z_{IE} - \frac{c_s}{c_w} Z_{wE} q_{Iw}\right] X + q_{IE}}{q_{IE} - \frac{c_s}{c_w} Z_{w1} q_{wE} + \frac{1}{Z_{wE} x}} \qquad (3.6.17)$$

$$\eta_{wE} = \frac{c_s}{c_w} \frac{[Z_{IE} q_{1w} - \frac{c_s}{c_w} Z_{wE}] x + q_{wE}}{Z_{1w} q_{1w} - \frac{c_s}{c_w} q_{wE} + \frac{1}{Z_{wE}} x} \qquad (3.6.18)$$

The meaning of q_{ik} is as before eq. (3.6.11), $x = \Delta\mu_s/E$ and $Z_{ik} = \sqrt{L_{ij}/L_{kk}}$ where $i, k = 1, \omega, E, i \neq k$. These equations are appropriate for calculating η for ED.

3.6.2 The Two-Flow and Overall Degrees of Coupling

Model calculations have shown the following[18]:

Tight coupling, ranging up to 0.98, was found between the ion and current flows (q_{iE}) for solutions up to 0,5 mol/ℓ. (Fig 3.6.1).

The sodium transport number $\bar{t}_1$ was in the range 1,0 to 0,98 over this concentration range. The sodium transport number ($\bar{t}_1$) and q_{iE} decreased at higher concentrations.

The coupling of water-current flows (q_{wE}) was close to 0,5 at approximately 0,1 to 0,5 mol/ℓ (Fig. 3.6.1). In that region $q_{wE} \approx q_{1w}$ implying that q_{wE} represents the coupling of water to ion flow; known as electro-osmosis. In more concentrated solutions q_{wE} and q_{1w} diverge. Water-ion coupling becomes higher and water-current coupling becomes lower. At higher concentrations (> 0,5 mol/ℓ) the amount of "free" water in the membrane, the transport number of water $\bar{t}_w$ and the osmotic flow, decrease. Effects originating in the deswelling of the membrane at high external concentration may result in the observed decrease of the electro-osmotic flow and the increased coupling between ions and the amount of water crossing the membrane. The overall coupling coefficient q_E slightly exceeds q_{iE} and changes with external concentration similar to q_{iE}.
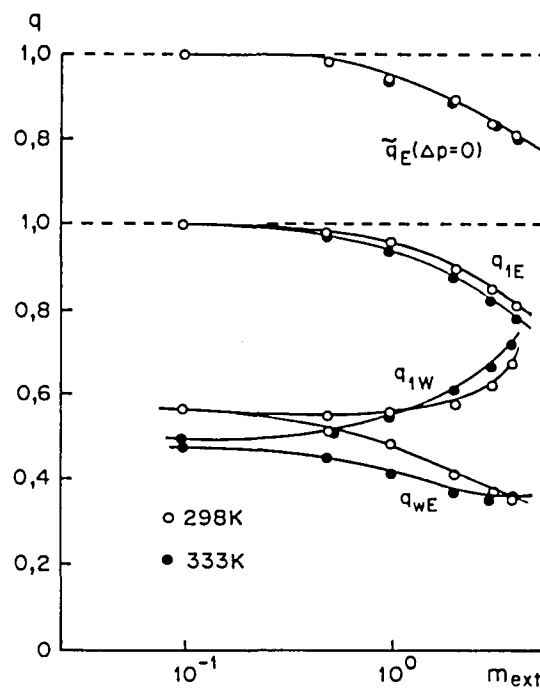
Figure 3.6.1: The concentration dependence of the degrees of coupling: sodium ions-current (q_{iE}), sodium ions-water (q_{1w}), water-current (q_{wE}), and the overall degree of coupling ($\bar{q}_E$) for the system $NaCl_{aq}$/Nafion 120 membrane.

3.6.3 Total Efficiency of Energy Conversion and its Components

The component efficiencies of energy conversion are not only of different meaning but of different sign (Fig. 3.6.2). The positive term η_{IE} indicates the fraction of the free energy of mixing produced by the driving process IE and stored in the system by the uphill transport of ions $J_1\Delta\mu_s$, against their spontaneous flow. The negative term η_{wE} means that the transport of water proceeds in the direction of the conjugated force $\Delta\mu_w$ (downhill). The energy input increases the rate of flow. Thus, this term causes the entropy of the system to increase and the energy supplied to the system to be wasted.

Both η_{IE} and η_{wE} change with the ratio $\Delta\mu_s/FE$ and with the concentration of electrolyte. The maximum in the η_{IE} curve means that for any concentration range of NaCl solutions there is an optimal concentration difference for which the efficiency of energy conversion is at a maximum.. There is no such maximum in the η_{wE} curve. The waste of energy due to water flow becomes much higher as the electrolyte becomes more concentrated and the concentration difference between the NaCl solutions in the adjacent compartments is higher.

The sum of η_{IE} and η_{wE} gives the total efficiency as η. The total efficiency, η, decreases with increasing concentration. The degree of coupling, $\bar{q}_E$, also decreases with increasing concentration.

Computations of q (coupling) and η (efficiency) employing the derived equations and phenomenological conductance coefficients determined for the system Nafion 120 membrane/sodium chloride solutions led to the following conclusions[18]:

- Coupling of the current to the flow of sodium ions (q_{IE}), of importance for the efficiency of energy conversion, is close to unity when the membrane is in contact with dilute solutions and is going down with increasing external concentration.

- Coupling of the current to the flow of water (q_{wE}), which is achieved by water-cation coupling (q_{Iw}), reaches a value as high as half that of q_{IE}, pointing to the unavoidable loss of energy during ED.

● The total efficiency of energy conversion (η) depends both on the concentration of separated electrolytes and on the ratio of thermodynamic forces ($\Delta\mu_s/FE$) acting in the system. The maximum of efficiency depends on the force ratio and decreases with increasing external concentration.

● The total efficiency of energy conversion is a complex quantity composed of a positive component (η_{IE}) related to the transport of cations and a negative one (η_{wE}) related to the transport of water; both components change with the external concentration to a different degree. The measure of the loss of energy (η_{wE}) may reach a value of as much as 70% of η_{max} in the more concentrated solutions.
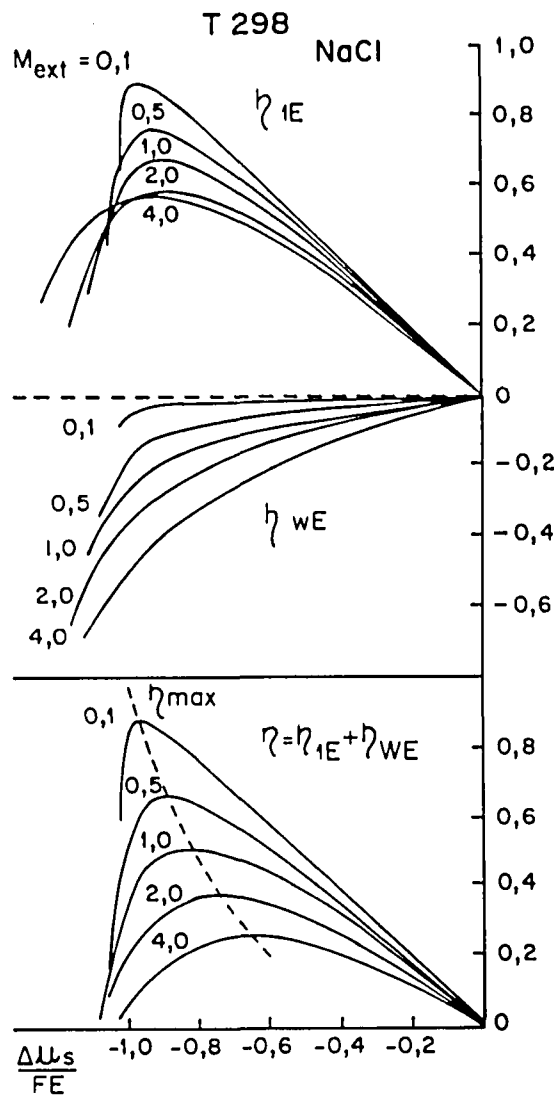
Figure 3.6.2: The efficiency of energy conversion η and the component efficiencies η_{IE}, η_{wE} and force ratio $\Delta\mu_s/FE$, at different concentrations NaCl in the external solution (T = 333 K).

3.7 Conversion of Osmotic into Mechanical Energy in Systems with Charged Membranes

Narebska et al.,[19] have described the problem of conversion of osmotic energy into mechanical energy within the framework of irreversible thermodynamics. Using the numerical results for the conductance coefficients for the system Nafion 120 membrane/single salt and alkali solutions, the couplings between the volume and the osmotic fluxes, q, and the efficiency of osmotic into mechanical energy conversion, η, have been computed.

The standard application of membrane systems is for separation of suspensions and molecular mixtures, gaseous or liquid, into components on an expense of supplied energy. Mechanical, thermal or electric energy can be used. More than twenty membrane separation techniques are known. In each of these systems, however, the difference in concentration of components on both sides of a membrane presents the effective source of osmotic energy, generating the spontaneous osmotic flux affecting the separation. For example, in ED, the osmotic flow of water dilutes the brine, thus lowering the energetic efficiency of desalination. In reverse osmosis, the osmotic pressure is a powerful force to overcome. Osmotic energy is thereby a native energy of a membrane system affecting both the income of energy and the separation process itself.

Conversion of osmotic energy into electric energy was postulated and theoretically described by Kedem and Caplan[72]. Systems converting osmotic energy into mechanical energy called "osmotic pumps" were proposed by Lee et al.,[75]. The energetic efficiency of the process, however, still seems to be a problem.

The work by Narebska et al.,[19] has been aimed at a theoretical analysis of osmotic into mechanical energy conversion, using irreversible thermodynamics as the underlying theory.

3.7.1 Theoretical

The system consists of an ion-exchange membrane separating electrolyte solutions of different molalities. Assuming ideal membrane permselectivity (totally impermeable to a solute) and the zero current condition, the only flow in the system should be the osmotic flow of water which is driven to the more concentrated side. However, for real

polymer membranes and particularly when they are in contact with concentrated solutions, diffusion of a solute across the membrane should be admitted as an additional phenomenon. The solute permeates the membrane towards the dilute solution side, that is, opposite to the osmotic flow.

In terms of irreversible thermodynamics the two flows

- the osmotic flow of water J_w and
- the diffusional flow of the solute J_s are described by the following equations:

$$J_s = L_s \Delta \mu_s + L_{sw} \Delta \mu_w \qquad (3.7.1a)$$

$$J_w = L_{ws} \Delta \mu_s + L_w \Delta \mu_w \qquad (3.7.1b)$$

$\Delta \mu_s$, $\Delta \mu_w$ are the differences of chemical potential of a solute and water, respectively. L_{ik} denotes the phenomenological conductance coefficients.

It is convenient to transform eq. (3.7.1a) and (3.7.1b) into another set of equations.

$$J_w' = L_w' \Delta \mu_w^c + L_{wp}' \Delta p \qquad (3.7.2a)$$

$$J_v = L_{pw}' \Delta \mu_w^c + L_p' \Delta p \qquad (3.7.2b)$$

Here J_w' denotes the flow of water against the flow of a solute conjugated to the concentration part of the chemical potential difference of water, $\Delta \mu_w^c$:

$$J_w' = J_w - \bar{c}_w / \bar{c}_s * J_s \qquad (3.7.3)$$

$$\Delta \mu_w^c = RT \ln (a_w'/a_w'') \qquad (3.7.4)$$

J_v of equation (3.7.2b) denotes the total volume flow conjugated to the difference of pressure in the compartments on the opposite sides of the membrane, Δp.

$$J_v = \bar{v}_s J_s + \bar{v}_w J_w \qquad (3.7.5)$$

The relation between the fluxes and forces of equations (3.7.1a and 3.7.1b) and of equations (3.7.2a and 3.7.2b) can be expressed in a matric form

$$\left|\begin{array}{c} J_w' \\ J_v \end{array}\right| = A * \left|\begin{array}{c} J_s \\ J_w \end{array}\right|, \quad \left|\begin{array}{c} \Delta\mu_w^c \\ \Delta_p \end{array}\right| = A^{-1T} * \left|\begin{array}{c} \Delta\mu_s \\ \Delta\mu_w \end{array}\right| \qquad \text{(3.7.6 and 3.7.7)}$$

$$L' = A * L * A^T \qquad (3.7.8)$$

where

$$A = \left|\begin{array}{cc} -\bar{c}_w/\bar{c}_s & 1 \\ \bar{v}_s & \bar{v}_w \end{array}\right|, \quad L = \left|\begin{array}{cc} L_s & L_{sw} \\ L_{ws} & L_w \end{array}\right|$$

With the flows of equations (3.7.2a and 3.7.2b) the dissipation function Φ consists of two components:

$$\Phi = \quad J_w^{\,'}\Delta\mu_w^c \quad + \quad J_v\Delta p$$

osmotic	mechanical	(3.7.9)
energy	energy	
component	component	

The efficiency of energy conversion, η, as defined by Kedem and Caplan[72], can be written as follows:

$$\eta = -\frac{J_v\Delta p}{J_w'\Delta\mu_w^c} \qquad (3.7.10)$$

$$0 < \eta < 1$$

For the system discussed here, η, means the output of mechanical energy produced by the input of unit osmotic energy. To acquire computational verification of various systems this equation should be transformed by substituting equations (3.7.2a and 3.7.2b) into equation (3.7.10) to give

$$\eta = -\frac{q + z * \Delta p/\Delta\mu_w^c}{q + 1/(Z * \Delta p/\Delta\mu_w^c)} \qquad (3.7.10\ a)$$

Here

$$q = L_{wp}'/(L_w'L'p)^{0,5}$$

$$Z = (L'_p/L'_w)^{0.5}$$

q is called a coupling coefficient. For energy conversion the size of q is fundamental. The value of q may vary between -1 and +1. A high value of q indicates tight coupling between the two processes involved in energy conversion. For the system discussed here, these are the spontaneous osmotic flow of water and the volume flow producing energy.

3.7.2 Transport Experiments and Computations

The perfluorinated cation-exchange membrane Nafion 120 (Du Pont de Nemours, USA), was used for measuring the membrane transport process as well as performing experiments with an osmotic unit. The measured membrane transport properties were the membrane electric conductivity, concentration potential, osmotic, electro-osmotic, diffusion and hydrodynamic flows. From these data the set of coefficients of equation (3.7.2), that is L'_w L'_p, L'_{wp} was calculated and then the coupling coefficient q (eq (3.7.11)) and the efficiency of energy conversion, η (eq. 3.7.10(1)) were found.

The theory was experimentally verified in a simple osmotic unit[19].

3.7.3 Osmotic and Diffusion Fluxes in Membrane Systems

For a given membrane, the flow of water and the diffusion of a solute, flowing in the opposite direction, depend strongly on the nature of the electrolyte. For the electrolytes used and the Nafion 120 membrane, the osmotic flow is low with sodium hydroxide solution, higher with sodium chloride and the highest with sulphuric acid solutions (Table 3.7.1). For the same system the diffusion fluxes change in the opposite direction. J_s of NaOH is about 25% of the osmotic flow; J_s of NaCl 4%; and J_s of H_2SO_4 is zero within the range of concentrations used.

Table 3.7.1: Osmotic and diffusion fluxes per unit of the chemical potential difference of a solute for systems with Nafion 120 membrane. m = 1, T = 25°C.

Flows	NaOH	NaCl	H_2SO_4
	($*10^{-10}$ mol^2/m^3 Ns)		
Osmotic flow of water ($-J_w/\Delta\mu_s$)	4,7	8,0	17,7
Diffusion of solute ($-J_s/\Delta\mu_s$)	1,1	0,33	- 0,16

3.7.4 Osmotic Energy Conversion

The coupling coefficient, q, and the efficiency of energy conversion, η, have been calculated with equations (3.7.10a) and (3.7.11). The couplings between the spontaneous osmotic flow (J_w^i) driven by the difference of solvent activity $(\Delta \mu_w^o)$ and the volume flow (J_v) producing the pressure (Δp) are shown as a function of the mean molalities of solutions bathing the membrane (Fig. 3.7.2). The coupling coefficient, q, is high for the system with sulphuric acid, ranging from 0,6 to 0,95 in 1 molar solution. For the other two electrolytes q does not exceed 0,4 (NaCl) or is even as low as 0,1 (NaOH). These results show the necessity of using membranes rejecting a solute almost perfectly. Even little diffusion as in the case of sodium chloride can disturb the coupling drastically.

This effect is even more pronounced as can be seen from the energy conversion, η (Fig. 3.7.3). Again, the η coefficient is the highest for the system with H_2SO_4 reaching 0,4. For this system the maximum of η is observed for the ratio of produced pressure to the osmotic one $\Delta p/\Delta \pi = 0,8$ (for ideal system it is one). In the case of the easily diffusing NaOH the energy conversion becomes negligible and decreased to 0,01 and the ratio $\Delta p/\Delta \pi$ for η_{max} is as low as 0,15.
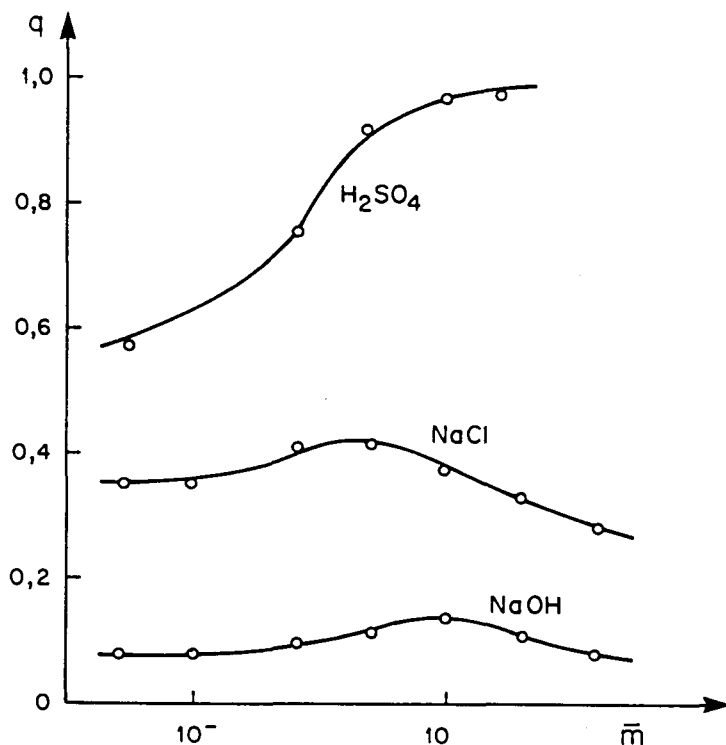
Figure 3.7.2: The concentration of coupling coefficient (eq. (3.7.11) for various electrolyte solutions and Nafion 120 membrane; 298 K.
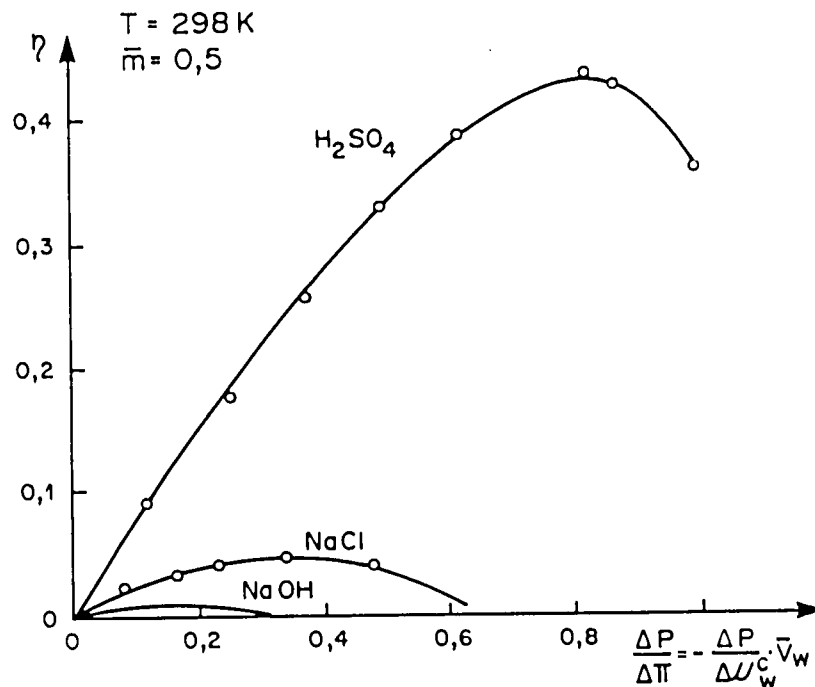
Figure 3.7.3: The dependence of the efficiency of osmotic into mechanical energy conversion (eq. 3.7.10) on the ratio $\Delta P/\Delta \Pi$; 298 K.

In order to examine the system further, the rate of fluxes for other electrolytes were measured (Table 3.7.2). These results confirm that only the solutes perfectly rejected by a membrane, like sulphuric acid, appears to be efficient in an osmotic pump. Only in the case of a membrane highly permselective to the given electrolyte, the free energy of mixing, which usually goes unexploited, can be put to effective use.

The following conclusions can be drawn[19]:

- A high degree of osmotic to mechanical energy conversion ranging from 0,4 to 0,5 can only be achieved in a system with a membrane, which rejects the solute almost entirely, that is with $\sigma \rightarrow 1$.

- A salt flux reaching even 4% of the osmotic flux of water (Table 3.7.1, NaCl) results in a vast decrease of the efficiency of energy conversion ($\eta < 0,1$).

- While in contact with an electrolyte which permeates Nafion 120 membrane more easily (like NaOH), the system cannot convert the osmotic energy to any remarkable degree ($\eta < 0,01$).

Table 3.7.2: Experimental volume fluxes in the systems with Nafion 120 membrane

ELECTROLYTE	J_v	$J_v/\Delta\pi$
	(* 10^{-8} m/s)	(* 10^{-8} m/s atm)
NaCl	10,8	0,236
Na_2SO_4	4,59	0,145
HCl	36,7	0,70
H_2SO_4	42,0	1,76
H_3PO_4	6,72	0,60

3.8 Donnan Exclusion

If a resin is allowed to equilibrate in an electrolyte solution rather than in pure water, the water uptake is comparatively less due to the lowered external water activity, $a_w(< 1)$. Specifically, the osmotic swelling pressure becomes[11]

$$\Pi = -(RT/v_w) \ln (\bar{a}_w/a_w) < -(RT/v_w) \ln \bar{a}_w \qquad (3.8.1)$$

In addition to the water fraction, the dissolved ions will distribute themselves across the membrane-solution interface according to a condition of free energy balance. Qualitatively, the driving force for electrolyte uptake is the initial solute chemical potential gradient across the interface. Considering this solely, the equilibrium concentrations within and exterior to the membrane would be equal were it not for the presence of the ionizable side-chains that through the constant of electro-neutrality, resist the co-ion uptake. A simple theory that explains the overall features of electrolyte uptake by ion-exchangers was outlined by Donnan[76].

Assuming complete ionization, equivalent interdiffusion, electro-neutrality, and the quality of single-ion activities and concentrations, the theoretical result for the free energy balance across the interface between a 1 : 1 electrolyte solution of concentration C (mol per litre) and cation-exchange membrane, in which the ionogenic side-chain density is R, is

$$\bar{C}(\bar{C} + R) = C^2 \qquad (3.8.2)$$

where $\bar{C}$ is the internal equilibrium electrolyte concentration and the membrane was originally in the salt form. Immediately, it is seen that $\bar{C} < C$ and that co-ion exclusion is enhanced by increasing R. As C becomes very large, the Donnan exclusion

mechanism becomes increasingly less effective.

3.9 Relationship Between True and Apparent Transport Numbers

The relationship between true and apparent transport numbers has been described by Laskshminarayanaiah[45].

The emf of a cell of the type shown in Figure 3.9.1 is given by the following equation which cannot be integrated without knowledge of how $\bar{t}_i$ and $\bar{t}_w$ vary with external electrolyte concentration.

$$E = - (2\ RT/F) \int_{,}^{"} (\bar{t}_i - 10^{-3}m_{\pm}\ M\bar{t}_w)d\ \ln a_{\pm} \tag{3.9.1}$$
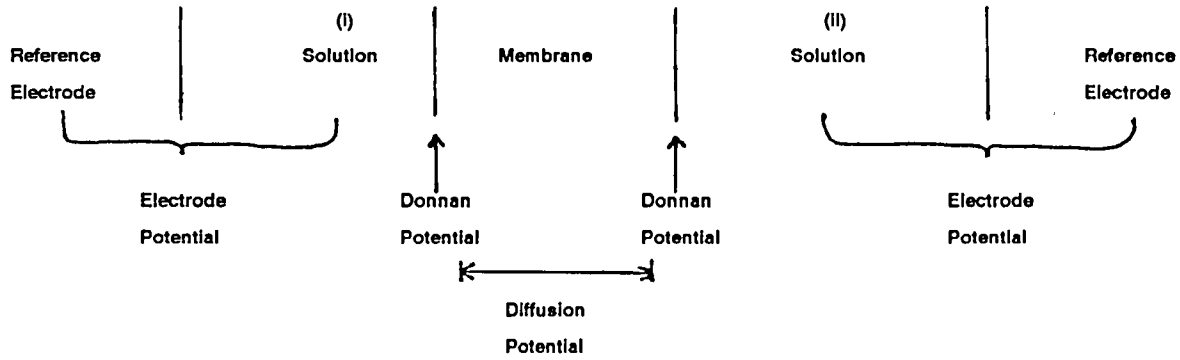
Figure 3.9.1:   Electric potentials across an ionic membrane separating different salt solutions.

$\bar{t}_+$ and $\bar{t}_w$ must be found by separate experiments and their values must be unambiguous without being influenced by factors such as current density and back diffusion. Even then, what relation these experimental values bear to $\bar{t}_+$ and $\bar{t}_w$ of eq. (3.9.1) is not clearly known.

However, an approximate approach can be made by integrating eq. (3.9.1) within narrow limits $a_{\pm}'$ and $a_{\pm}''$. On integration, eq. (3.9.1) takes the form:

$$E = - \frac{2RT}{F} (\bar{t}_{\pm} - 10^{-3}m_{\pm}\ M\bar{t}_w)\ \ln \frac{a_{\pm}'}{a_{\pm}''} \tag{3.9.2}$$

The emf of a cell of the type shown in Figure 3.9.1 can be calculated from the modified Nernst equation.

$$E = 2\bar{t}_{+(app)} \frac{RT}{F} \ln \frac{a'}{a''}$$

(3.9.3)

which can be equated to eq. (3.9.3) to give[77]:

$$\bar{t}_{+} = t_{+(app)} + 0,018m_{\pm}\bar{t}_{w}$$

(3.9.4)

Hale and McCouley tested eq. (3.9.4) using different heterogeneous membranes and found good agreement between true $\bar{t}_{+}$ measured directly and $\bar{t}_{+}$ calculated using eq. (3.9.4). Their measurements although confined to a number of different membranes, were made with one set of electrolyte solutions only (0,667 and 1,333 mol/ℓ NaCl). Lakshiminarayanaiah[78] checked eq. (3.9.4) over a wide concentration range. He found that the $\bar{t}_{+}$ values calculated from eq. (3.9.4) were higher than the measured values particularly in high electrolyte concentrations. This discrepancy existing in the case of strong solutions is difficult to reconcile in view of the fact that Lakshminarayanaiah and Subrahmanyas[47] showed that eq. (3.9.1) is able to generate values for E (however from measured values of t_{+} and t_{w}) agreeing with observed values. A more recent evaluation by Lakshminarayanaiah[79] has shown that eq. (3.9.4) is able to give values for $\bar{t}_{+}$ agreeing with those measured directly.

The relationship of $\bar{t}_{+(app)}$ obtained from emf measurements to $\bar{t}_{+}$ measured directly, unlike eq. (3.9.4), has been approached from a different standpoint by Oda and Yawataya[80]. The apparent transport number ($\bar{t}_{+(app)}$) calculated from emf data was related to the concentration of the external solution by an "interpolation technique". This consists in measuring E using two solutions, c' and c'', in the cell shown in Figure 3.9.1. In the first measurement of membrane potential, solution (') is so chosen that c'' is less than c' and in the second measurement c' is held constant and c'' is so chosen that it is now greater than c'. Each of the two values of $\bar{t}_{+(app)}$ calculated from the two measurements is now referred to that particular concentration of c' used in the experiment and plotted. The value of $\bar{t}_{+(app)}$ pertaining to c' which is kept constant in the two experiments is obtained by interpolation. Usually, $\bar{t}_{+(app)}$ is related to the mean external electrolyte concentration, i.e. (c' + c'')/2.

True values of $\bar{t}_{+}$ and $\bar{t}_{w}$ were determined by Oda and Yawataya from the same experiment by the mass method which consisted in estimating the mass changes in

both the salt and the water in the cathode chamber following the passage of a known quantity of current through the system, electrolyte solution (c) → membrane → electrolyte solution (c). The relationship between $\bar{t}_+$ and $\bar{t}_{+(app)}$ was derived in the following manner[80].

A selective membrane of fixed charge density $\bar{X}$ (equivalent per unit volume of swollen membrane) in equilibrium with an external electrolyte solution contains $\bar{X}(1 - \bar{s})$ equivalents of counter-ions and $\bar{X}\bar{s}$ equivalents of co-ions where $\bar{s}$ is the equivalent of co-ions per equivalent of fixed group present in the membrane. This arises from the Donnan absorption of the electrolyte by the membrane.

When an electric field is applied, ions and water move. In a membrane in which interactions between different membrane components, viz., counter-ion, co-ion, water and membrane, matrix, are absent, one may assume that the fixed water in the membrane is negligible and that all mobile water moves with the same velocity and in the same direction as the counter-ion. As a result, counter-ions move faster and co-ions move slower than they would otherwise if water stood still. Consequently, the mobilities (u's) of the counter-ion and co-ion may be written as:

$$\bar{u}_+' = \bar{u}_+ + \bar{u}_w \qquad (3.9.5)$$

$$\bar{u}_-' = \bar{u}_- - \bar{u}_w \qquad (3.9.6)$$

where +, -, and w stand for cation, anion and water, respectively. $\bar{u}_+'$ and $\bar{u}_-'$ are the increased and decreased mobilities due to the transport of water.

Due to water transport, the specific conductance of the membrane is increased. If k' is the membrane specific conductance, then

$$\bar{k}' = F[\bar{X} (1 + \bar{s}) \bar{u}_+' + \bar{X}\bar{s}\bar{u}_-'] \qquad (3.9.7)$$

On substituting from eqs. (3.9.5) and (3.9.6), eq. (3.9.7) becomes

$$\bar{k}' = F\bar{X}[(1 + \bar{s})\bar{u}_+ + \bar{s}\bar{u}_- + \bar{u}_w] \qquad (3.9.8)$$

If water transport is absent, the membrane conductance k is given by

$$\overline{k}' = Fx[(1 + \overline{s})\overline{u}_+ + \overline{s}\overline{u}_-]$$

(3.9.9)

It follows from eqs. (3.9.8) and (3.9.9) that the increase in conductance due to water transport is given by

$$\overline{k}' - \overline{k} = F\overline{X}\overline{u}_w$$

(3.9.10)

Transport numbers by definition are given by

$$t_+ = \frac{(1 + \overline{s})\overline{u}_+'}{(1 + \overline{s})\overline{u}_+ + \overline{s}\overline{u}_-'}$$

(3.9.11)

$$t_{+(app)} = \frac{(1 + \overline{s})\overline{u}_+}{(1 + \overline{s})\overline{u}_+ + \overline{s}\overline{u}_-'}$$

(3.9.12)

Substituting from eqs. (3.9.5) - (3.9.10) into eqs. (3.9.11) and (3.9.12) and remembering that $\overline{t}_{+(app)} + \overline{t}_{-(app)} = 1$, it can be shown that[80]:

$$\overline{t}_+ - \overline{t}_{+(app)} = (\overline{t}_{-(app)} + \overline{s})[(\overline{k}' - \overline{k})/\overline{k}']$$

(3.9.13)

Substituting from eq. (3.9.10), eq. (3.9.13) becomes

$$\overline{t}_+ - \overline{t}_{+(app)} = [\overline{t}_{-(app)} + \overline{s}][F\overline{X}\overline{u}_w/\overline{k}']$$

(3.9.14)

When a potential of E volts acts along length λ cm of a membrane capillary, the water in the pore moves with a mobility, u_w cm/s (i.e., E/ℓ is unity). The volume (millilitres) of water flowing per second through a membrane subject to unit potential gradient is given by β_E and is equal to $(u_w A)$ where A is the pore area. But β, the volume of water flowing per Coulomb is given by:

$$\beta = V/i$$

(3.9.15)

where V is millilitres of water flowing per second and i is the current in amperes. But $i = k_i A$ per unit potential gradient and k_i is the specific conductance of the pore liquid of an infinitely swollen membrane (k_i is really a modified membrane conductance). Consequently, it follows that

$$\beta_E = \bar{u}_w \, A = \bar{k}_i A \beta \tag{3.9.16}$$

Equation (3.9.16) differs from the original equation of Oda and Yawataya which is dimensionally incorrect[45].

Substitution of eq. (3.9.16) into eq. (3.9.14) gives

$$\bar{t}_+ = t_{+(app)} + (\bar{t}_{-(app)} + \bar{s})F\bar{X}\bar{k}_i\beta/\bar{k}' \tag{3.9.17}$$

But k' may be equated to $\varphi_w\bar{k}_i$ where φ_w is the volume fraction of water in the membrane. Equation (3.9.17), therefore, becomes

$$\bar{t}_+ = \bar{t}_{+(app)} + [\bar{t}_{-(app)} + \bar{s}]F\bar{X}_v\beta \tag{3.9.18}$$

where $\bar{X}_v = \bar{X}/\varphi_w$, equivalent of fixed groups per unit volume of interstitial water.

Since the method usually used to measure the transport number of water $\bar{t}_w$ which is equal to (F6/18), depends on following volume changes in the anode and cathode chambers, the observed volume changes, which measures only solution flow, have to be corrected for both salt transport and electrode reactions to give values for water flow only. If reversible Ag-AgCl electrodes are used, the passage of a Faraday of current produces at the cathode, a mole of Ag and $\bar{t}_+$ moles of MCl (M = univalent cation) and in the same time a mole of AgCl disappears. The actual increase in volume ΔV_c, which is equal to the volume decrease at the anode, due to water transport, is given by

$$\Delta V_C = \Delta V_o + \bar{V}_{AgCl} - \bar{V}_{Ag} - \bar{t}_+ \bar{V}_{MCl} \tag{3.9.19}$$

where the $\bar{V}$'s are partial molar volumes and ΔV_o is the observed volume change. As $V_{AgCl} = 25,77$ and $V_{Ag} = 10,28$, eq. (3.9.19) becomes

$$\Delta V_c = \Delta V_o + 15,5 - t_+\bar{V}_{MCl}$$

$\bar{V}_{MCl}$ values can be evaluated using the usual equations[81] and $\bar{t}_+$ values must be obtained by experiment using the appropriate concentration. Then

$$\bar{t}_w = \Delta V_c/\bar{V}_{H_2O} = \Delta V_c/18 \qquad\qquad (3.9.20)$$

$F\bar{X}_v\theta$ may be written as $\bar{t}_w/\bar{W}_c$

where $\bar{t}_w = F\theta/18$ and $\bar{W}_e = 1/18\bar{X}_v$; i.e., moles of water per equivalent of ion-exchange site. Substitution of these values in eq. (3.9.18) gives

$$t_+ = \begin{cases} \bar{t}_{+(app)} + [\bar{t}_{-(app)} + \bar{s}](\bar{t}_w/\bar{W}_e) \\ \\ \text{or} \\ \\ (\bar{t}_w/\bar{W}_e)(1 + \bar{s}) + \bar{t}_{+(app)}(1 - (\bar{t}_w/\bar{W}_e)) \end{cases} \qquad (3.9.21)$$

Oda and Yawataya computed $\bar{t}_+$ values from eq. (3.9.18) by measuring $\bar{t}_{+(app)}$, $\bar{s}$, $\bar{X}_v$ and θ. Although these values were lower than the observed values of $\bar{t}_+$, they considered the agreement good since the divergence of the calculated values from the observed values was within the limits of experimental error.

3.10 Electro-Osmotic Pumping - The Stationary State - Brine Concentration and Volume Flow

3.10.1 Ion Fluxes and Volume Flow

In the unit cell flow regime ED becomes a three-port system like reverse osmosis. The feed solution is introduced between the concentrating cells, passes between the cells and leaves the system. The permeate composition is completely determined by membrane performance under the conditions of the process. A schematic diagram of a unit cell showing ion and water fluxes in the system is shown in Figure 3.10.1[1]. For a uni-univalent salt-like sodium chloride, the current density through a cation-exchange membrane is related to the ion fluxes according to Garza [1] by:

$$I = F(z_1 j_1^c + z_2 j_2^c) \qquad\qquad (3.10.1)$$

$$= F(j_1^c - j_2^c) \qquad\qquad (3.10.2)$$

$$= F(|j_1^c| + |j_2^c|) \qquad\qquad (3.10.3)$$

where $z_1 = 1$ (cation)

and $z_2 = -1$ (anion)

and j_1^c and j_2^c are the cation and anion fluxes through the cation-exchange membrane respectively.

Effective transport numbers are defined as follows[1, 2]:

$$\bar{t}_1^c \quad = \quad |j_1^c|/(|j_1^c| + |j_2^c|) = (1 + \Delta t^c)/2 \tag{3.10.4}$$

$$\bar{t}_2^c \quad = \quad |j_2^c|/(|j_2^c| + |j_1^c|) = (1 - \Delta t^c)/2 \tag{3.10.5}$$

where $\Delta t^c = \bar{t}_1^c - \bar{t}_2^c$ \tag{3.10.6}

and $\bar{t}_1^c + \bar{t}_2^c = 1$ \tag{3.10.7}

Δt^c = difference between counter- and co-ion transport number or membrane permselectivity.

$\bar{t}_1^c \quad =$ cation transport number through cation membrane

$\bar{t}_2^c \quad =$ anion transport number through cation membrane

and the bar refers to the membrane phase.
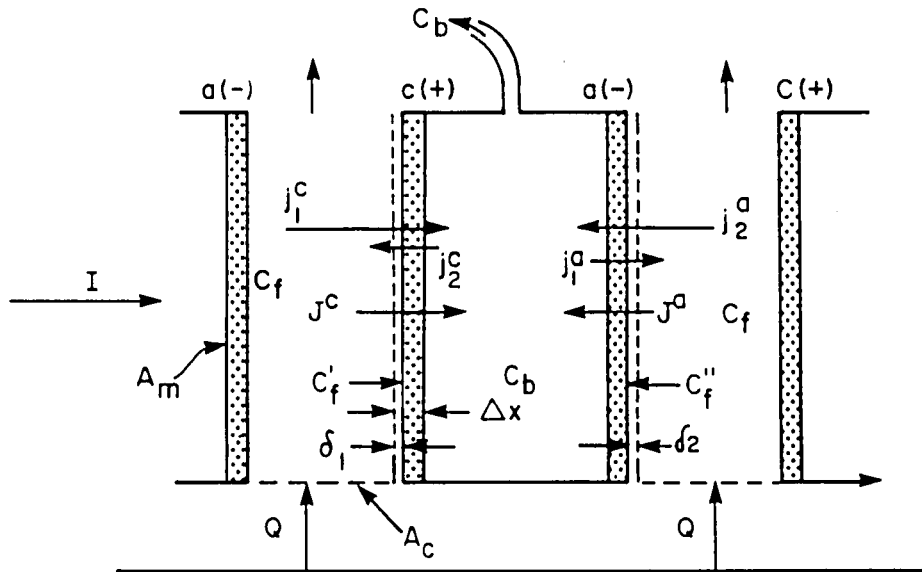
Figure 3.10.1: Representation of fluxes in the ED unit-cell system.
c and a indicate the cation- and anion-exchange membranes and subscripts 1 and 2 refer to the cations and anions, respectively (uni-univalent salts); Δx: membrane thickness; δ's: effective Nernst layers; c_f's: feed concentration; c_b: brine concentration; J^c and J^a: water fluxes; j^a and j^c anion and cation currents. A_m: effective membrane area; A_c: transversal area of the dialysate compartment; Q: flow of dialysate. The arrows show the direction of the fluxes.

Further,

$$j_1^c = \bar{t}_1^c \, (|j_1^c| + |j_2^c|) = \bar{t}_1^c \, I/F = (1 + \Delta t^c) \, I/2F \qquad (3.10.8)$$

$$j_2^c = \bar{t}_2^c \, (|j_1^c| + |j_2^c|) = \bar{t}_2^c \, I/F = (1 - \Delta t^c) \, I/2F \qquad (3.10.9)$$

(Note: Effective transport numbers are to be distinguished from the usual transport numbers which refer to the above ratio's in the absence of concentration gradients).

The brine concentration, c_b, can be obtained from the following material balance (Figure 3.10.1):

$$c_b = \frac{|j_1^c| - |j_1^a|}{|J^c| + |J^a|} = \frac{|j_2^a| - |j_2^c|}{|J^c| + |J^a|} \qquad (3.10.10)$$

where J^c and J^a are the water fluxes (flows) through the cation and anion membranes, respectively.

Consider,

$$c_b = \frac{|J_1^c| - |j_1^a|}{|J^c| + |J^c|} \qquad (3.10.11)$$

Substitute eq. (3.10.8) into eq. (3.10.11)

$$\therefore \quad c_b = \frac{(\bar{t}_1^c \, I/F) - (\bar{t}_1^a \, I/F)}{|J^c| + |J^a|} \qquad (3.10.12)$$

$$= \frac{(1 + \Delta t^c) \, I/2F - (1 - \Delta t^a) \, I/2F}{|J^c| + |J^a|} \qquad (3.10.13)$$

$$= \frac{I/2F \, [(1 + \Delta t^c) - (1 - \Delta t^a)]}{|J^c| + |J^c|} \qquad (3.10.14)$$

$$= \frac{I \, (\Delta t^c + \Delta t^a)}{2F(|J^c| + |J^a|)} \qquad (3.10.15)$$

$$c_b = \frac{I \, \Delta \bar{t}}{F \, (|J^c| + |J^a|)} \qquad (3.10.16)$$

$$= \frac{I \Delta \bar{t}}{2FJ} \qquad (3.10.17)$$

$$\Delta \bar{t} = \frac{\Delta t^c + \Delta t^a}{2} \qquad\qquad (3.10.18)$$

and $\quad 2J = |J^c| + |J^a| \qquad\qquad (3.10.19)$

The volume flow through every membrane is equal to the sum of the electro-osmotic and osmotic contributions[2].

Therefore $\quad J = J_{elosm} + J_{osm} \qquad\qquad (3.10.20)$

The electro-osmotic water flow for the cation and anion membrane is given by[2]:

$$J^c_{elosm} = (\beta_1{}^c t_1{}^c - \beta_2{}^c t_2{}^c)I \qquad\qquad (3.10.21)$$
$$J^a_{elosm} = (\beta_2{}^a t_2{}^a - \beta_1{}^a t_1{}^a)I \qquad\qquad (3.10.22)$$

The assumption here according to Garza & Kedem[2] is that the electro-osmotic water flow is governed by the drag exerted by the ions. The β's are 'drag' coefficients. They represent the amount of water dragged along with every type of ion by electro-osmosis. For tight membranes, the value of the β's should not be very different from the primary hydration water associated with the ions. For porous membranes, however, the value of the β's may be several ten folds larger.

The osmotic contribution is given by[2]:

$$J_{osm} = 2RT \sigma L_p \Delta(g\, c_s) \qquad\qquad (3.10.23)$$

where R is the universal gas constant, T the absolute temperature, g the osmotic coefficient, σ the reflection coefficient and L_p the hydraulic permeability.

Therefore,

$$J^c_{osm} + J^a_{osm} = 2RT(g_b c_b - g_f c_f)(\sigma^c L_p{}^c + \sigma^a L_p{}^a) \qquad\qquad (3.10.24)$$

Introduction of equations (3.10.20); (3.10.21); (3.10.22) into equation (3.10.16) and neglecting the terms $(\beta_1{}^c - \beta_2{}^c)\bar{t}_2{}^c$ and $(\beta_2{}^a - \beta_1{}^a)\bar{t}_1{}^a$ in comparison with $\beta_1{}^c \Delta t^c$ and $\beta_2{}^a \Delta t^a$, gives: (note: use was made of eq.(3.10.6)

$$c_b = \frac{I(\Delta t^c + \Delta t^a)2}{FI(\beta_1^c \Delta t^c + \beta_2^a \Delta t^a) + 2RT(g_b c_b - g_f c_f)\sigma^c L_p^c + \sigma^a L_p^a)} \qquad (3.10.25)$$

$$= \frac{(\Delta t^c + \Delta t^a)/2}{F(\beta_1^c \Delta t^c + \beta_2^a \Delta t^a) + 2FRT(g_b c_b - g_f c_f)\sigma^c L_p^c + \sigma^a L_p^a)/I} \qquad (3.10.26)$$

Equation (3.10.26) is justified for very permselective membranes where t_2^c and t_1^a are small, or where $\beta_1^c \approx \beta_2^a$ and $\beta_2^c \approx \beta_1^a$.

For high current densities, the second term (osmotic contribution) in the denominater of equation (3.10.26) may be neglected.

Therefore,

$$c_b^{max} = \frac{(\Delta t^c + \Delta t^a)/2}{F(\beta^c \Delta t^c + \beta^a \Delta t^a)} \qquad (3.10.27)$$

For $\beta^c \approx \beta^a$ and $\Delta t^c \approx \Delta t^a$ (symmetric membranes), equation (3.10.27) becomes

$$c_b^{max} = \frac{1}{F(\beta_1^c + \beta_2^a)} = \frac{1}{2F\beta} \qquad (3.10.28)$$

where $2\beta = \beta_1^c + \beta_2^a$.

β_1^c and β_2^a are the drag coefficients associated with the counterions. These coefficients are identical with the electro-osmotic coefficient, $\beta = (J/I)_{\Delta p = \Delta T = 0}$ measured at low concentration where co-ion exclusion is practically complete, i.e.

$$t_{counter-ion} \approx 1, \, t_{co-ion} \approx 0.$$

The cases for which equation (3.10.28) applies (i.e. for very permselective and/or for approximately symmetric membranes, at high current densities) are of considerable interest and importance according to Garza and Kedem[2] since the brine concentration depends only on the electro-osmotic coefficients, β_1^c and β_2^a. c_b^{max} can also be determined from equations (3.10.26); (3.10.27) and (3.10.28)

$$c_b = \frac{I\Delta t}{F(J_{elosm} + J_{osm})} \qquad (3.10.29)$$

$$= \frac{I\Delta t}{F\, J_{elosm}(1 + J_{osm}/J_{elosm})} \qquad (3.10.30)$$

$$= \frac{c_b^{max}}{1 + J_{osm}/J_{elosm}} \qquad (3.10.31)$$

3.10.2 Symmetric cells

The theory of EOP in general leads to difficult computations which must be carried out numerically according to Garza[1]. However, there is one case in which results can be given in terms of simple closed formula. This case depends on the assumption of a symmetric cell[1]. In a symmetric cell the cation- and anion-exchange membranes have identical physical properties in all regards except for the sign of their fixed charges. Because of cell symmetry, the magnitudes of the counter-ion fluxes through both membranes are the same. When a symmetric salt is chosen like potassium chloride, the anion and cation have equal mobilities. In other words, the magnitude of the cation flux through the cation exchange membrane is the same as the magnitude of the anion flux through the anion-exchange membrane. Also the magnitudes of the co-ion fluxes through both membranes are the same, i.e., the magnitude of the anion flux through the cation-exchange membrane is the same as the magnitude of the cation flux through the anion-exchange membrane.

$$\left| j_1^c \right| = \left| j_2^a \right| \; ; \; \left| j_1^a \right| = \left| j_2^c \right| \qquad (3.10.32)$$

and thus

$$\bar{t}_1^c = \bar{t}_2^a \; ; \; \bar{t}_1^a = \bar{t}_2^c \; ; \; \Delta t^c = \Delta t^a = \Delta \bar{t} \qquad (3.10.33)$$

Water flows also are of equal magnitude and opposite direction:

$$\left| J^c \right| = \left| J^a \right| = J \quad \text{or} \quad J^c = -J^a = J \qquad (3.10.34)$$

The amount of salt leaving through the brine outlet per unit time and membrane area, $2J c_b$, is related to the cation flows by (eqs. 3.10.10 and 3.10.19):

$$2J c_b = \left| j_1^c \right| - \left| j_1^a \right| \qquad (3.10.35)$$

and in the symmetric system is :

$$J = I \Delta \bar{t}/2c_b F \qquad (3.10.36)$$

3.10.2.1   Current Efficiency

The amount of salt transferred per Faraday of current passed through a symmetric unit cell is given from equation 3.10.36 by

$$\varepsilon_p = \frac{2Jc_b}{I/F} = \Delta \bar{t}$$

(3.10.37)

The overall efficiency, ε, is, however, somewhat smaller than ε_p, since water is also lost with the salt. The effective current density, i.e. the purification of the product achieved, is given by[1]:

$$I_{eff} = F(\frac{Q}{A_m} - 2J)(c_f - c_p) = F(\frac{Q}{A_m} - 2J)(\Lambda c_f)$$

(3.10.38)

where Q is the amount of feed solution entering a channel per unit time, A_m the effective membrane area (Figure 3.10.1), Λ the degree of mineralization given by:

$$\Lambda = \frac{c_f - c_p}{c_f}$$

(3.10.39)

where

c_f is the concentration of the feed solution entering the stack, and c_p the concentration of the product leaving it.

The mass balance for the salt is:

$$\frac{Qc_f}{A_m} = (\frac{Q}{A_m} - 2J) \, c_p + 2Jc_b$$

(3.10.40)

Therefore

$$I_{eff}/F = (\frac{Q}{A_m} - 2J)(c_f - c_p) = 2J(c_b - c_f)$$

(3.10.41)

and

$$\varepsilon = \frac{I_{eff}}{I} = \Delta t(1 - \frac{c_f}{c_b}) = \varepsilon_p \times \varepsilon_\omega$$

(3.10.42)

where

$$\varepsilon_\omega = 1 - c_f/c_b \qquad\qquad (3.10.43)$$

As is customary in ED, the overall efficiency is presented as the product of two terms, one due to the lack of ideal permselectivity in the membranes, ε_p, the other reflecting the loss of water to the brine, ε_w.

3.10.2.2 Electro-Osmotic Flow

Electro-osmotic flow is measured under the restrictions[1]:

$$\Delta c = 0, \, du_w/dx = 0$$

Under these conditions are :

$$J_{elosm} = (j_1 \, \beta_1 + j_2 \, \beta_2)F \qquad\qquad (3.10.44)$$

Equation 3.10.44 can also be written as :

$$J_{elosm} = (\beta_1 t_1 - \beta_2 t_2)I \qquad\qquad (3.10.45)$$

$$= [\beta_1(t_1 - t_2) + (\beta_1 - \beta_2) \, t_2]I \qquad\qquad (3.10.46)$$

$$= [\beta_1 \Delta t + (\beta_1 - \beta_2)t_2]I \qquad\qquad (3.10.47)$$

For small values of t_2, or for $\beta_1 = \beta_2 = \beta$ equation (3.10.47) becomes :

$$J_{elosm} = \beta° \Delta t I \qquad\qquad (3.10.48)$$

where $\beta°$ is the customary electro-osmotic coefficient measured at low ionic strength where co-ion exclusion is high and $\Delta t \approx 1$, i.e.:

$$\beta° = (J/I)_{\Delta c = \Delta p = \Delta T = 0, \Delta t = 1} = (J_{elosm}/I)_{\Delta t = 1}$$

3.10.2.3 Osmotic Flow at High Co-Ion Exclusion

Osmotic flow is measured under the restrictions[1]:

$$I = \Delta p = 0, \, j_1 = j_2 = 0.$$

(absence of electric current, hydrostatic pressure and impermeable solutes). In this case is[1]:

$$J_{osm} = L_p \, \sigma \, \Delta \pi \tag{3.10.49}$$

3.10.2.4 Volume Flow in Electro-Osmotic Pumping

The volume flow into the membrane concentrating cells in EOP is the sum of the electro-osmotic and osmotic water flows and is given by[1]:

Therefore,

$$J = - L_p \, \sigma \, \Delta \Pi + \beta^\circ \, \Delta t \, I \tag{3.10.50}$$

3.10.3 Non-Symmetric Cell

3.10.3.1 Porous membranes

In the previous section a simplified theory of the electro-osmotic pumping process was given where only the symmetric cell case was treated. By 'symmetric cell' is meant that the cation- and anion-exchange membranes are assumed to have the same values for the physical properties of interest in the process, namely, absolute effective charge density, electro-osmotic coefficient, and hydraulic permeability. If this were not the case, the calculations would become much more complicated since Δt (difference between the effective transport numbers of counter- and co-ions) may have different values for the two types of membranes, and the expression for the brine concentration, c_b, will not be as simple as for the symmetric case[1]. c_b may be found in the general case from material balance considerations to be equal to : -

$$c_b = \frac{\left| j_1^c \right| - \left| j_1^a \right|}{\left| J^c \right| + \left| J^a \right|} \tag{3.10.11}$$

From the definition of 'effective' transport numbers given before (eqs. 3.10.4 and 3.10.5), it can be written :

$$\left| j_1^c \right| - \left| j_1^a \right| = \left| j_2^a \right| - \left| j_2^c \right|$$

$$= (1 + \Delta t^c)I/2F - (1 - \Delta t^a)I/2F$$

$$= (\Delta t^c + \Delta t^a)I/2F \qquad (3.10.51)$$

The volume flow is given by the sums of electro-osmotic and osmotic terms, namely:

$$J = J_{elosm} + J_{osm}$$
$$= (\beta_1 t_1 - \beta_2 t_2)I + 2RT\,\sigma\,L_p\,\Delta(\phi_s\,c_s) \qquad (3.10.52)$$

Therefore,

$$\left|J^c\right| + \left|J^a\right|$$
$$= I(\beta_1{}^c t_1{}^c - \beta_2{}^c t_2{}^c + \beta_2{}^a t_2{}^a - \beta_1{}^a t_1{}^a) + 2RT(\phi_b c_b - \phi_i c_i) \times (\sigma^c L_p{}^c + \sigma^a L_p{}^a)$$
$$= I[\beta_1{}^c(t_1{}^c - t_2{}^c) + (\beta_1{}^c - \beta_2{}^c)t_2{}^c + \beta_2{}^a(t_2{}^a - t_1{}^a) + (\beta_2{}^a - \beta_1{}^a)t_1{}^a] + \ldots + 2RT(\phi_b c_b - \phi_i c_i)$$
$$\times \quad (\sigma^c L_p{}^c + \sigma^a L_p{}^a) \qquad (3.10.53)$$

for small values of $t_2{}^c$ and $t_1{}^a$, or for $\beta_1{}^c = \beta_2{}^a = \beta_c{}^o$, and $\beta_2{}^c = \beta_1{}^a = \beta_a{}^o$; equation (3.10.53) becomes:

$$\left|J^c\right| + \left|J^a\right| = I(\beta_1{}^c\,\Delta t^c + \beta_2{}^a\,\Delta t^a) + 2RT(\phi_b c_b - \phi_i c_i) \times (\sigma^c L_p{}^c + \sigma^a L_p{}^a) \qquad (3.10.54)$$

Substituting equations (3.10.51) and (3.10.54) into (3.10.11), gives:

$$c_b = \frac{(\Delta t^c + \Delta t^a)/2}{F(\beta_1^c\,\Delta t^c + \beta_2^a\,\Delta t^a) + 2RT(\phi_b c_b - \phi_i c_i)(\sigma^c L_p^c + \sigma^a p^a)/I/F} \qquad (3.10.55)$$

In the case of high current density, the second term in the denominator of equation (3.10.55) can be neglected. Therefore,

$$c_b^{max} = \frac{(\Delta t_{max}^c + \Delta t_{max}^a)/2}{F(\beta_1^c \Delta t_{max}^c + \beta_2^a \Delta t_{max}^a)} \qquad (3.10.56)$$

Plots of Δt versus current density for every membrane are expected to have the same kind of behaviour as for the symmetric cell case, as no new elements have been added. The value of c_b, however, depends now on the properties of both membranes, and not on those of only one of them. Therefore, for high current densities the values of Δt become independent on I, and can be calculated[1]. Since the values of Δt depends on c_b, which in its turn depends on Δt^c and Δt^a, trial and error calculations are necessary according to Garza.

In conclusion, for the non-symmetric-cell case (as for the symmetric cell) the following is expected[1]:

- The Coulomb efficiency of the concentrating cell will reach a maximum (plateau) value at high current densities (below the limiting value of the current)

$$\varepsilon = \Delta t = t_1{}^c - t_1{}^a = (1 + \Delta t^c)/2 - (1 - \Delta t^a)/2$$
$$= (\Delta t^c + \Delta t^a)/2 \qquad\qquad (3.10.57)$$

- The brine concentration, c_b, to reach a maximum value (also at high current densities below the limiting value) independent of I and of the feed concentration;

- The volume flow (3.10.54) versus $I\Delta t$ plots will become straight lines at high current densities since the osmotic contribution becomes almost independent of current density when the latter is sufficiently high (because c_b becomes constant and c' - the concentration at the feed interface (Fig. 3.10.1) may be kept within certain limits by controlling concentration polarization); and the electro-osmotic contribution is directly proportional to $I\Delta\bar{t}$ ($\Delta\bar{t} = (\Delta\bar{t}^c + \Delta t^a)/2$, when either $\Delta t^c = \Delta t^a$ or $\beta_1{}^c = \beta_2{}^a$.

3.11 Flux Equations, Membrane Potentials and Current Efficiency

Flux equations, membrane potentials and current efficiency relevant to EOP-ED have been described by Kedem and Bar-On[5]. The total ED process comprises three independent flows and forces;   electric current and potential; volume flow and pressure/osmotic pressure; salt flow and concentration difference. For small flows and gradients linear equations can be written for each of the flows, including the influence of all gradients[14].

In practical ED, especially in EOP, flows and forces are large and one can not expect linear equations to hold, even if the usually defined membrane transport coefficients are constant, according to Kedem and Bar-on. In fact, transport coefficients may vary considerably in the concentration range between feed and brine. For an adequate discussion of flows under these conditions, Kedem and Bar-On have followed the analysis given previously for reverse osmosis[82].

In the schematic presentation shown in Figure 3.11.1, the membrane is broken down into differential elements, separated by uniform solution segments which are in equilibrium with the two contiguous membrane faces. All fluxes going from left to right are counted positive. The gradient of a scalar y, dy/dx, is taken as the value of the scalar on the right (double prime) minus the value on the left (single prime), divided by the distance. On the other hand, the operator Δ is defined with the opposite sign, in order to bring the notation used by Kedem and Bar-On in line with that of previous publications[5]:

$$\Delta c = c' - c'' \text{ and}$$

$$y = \int dy$$
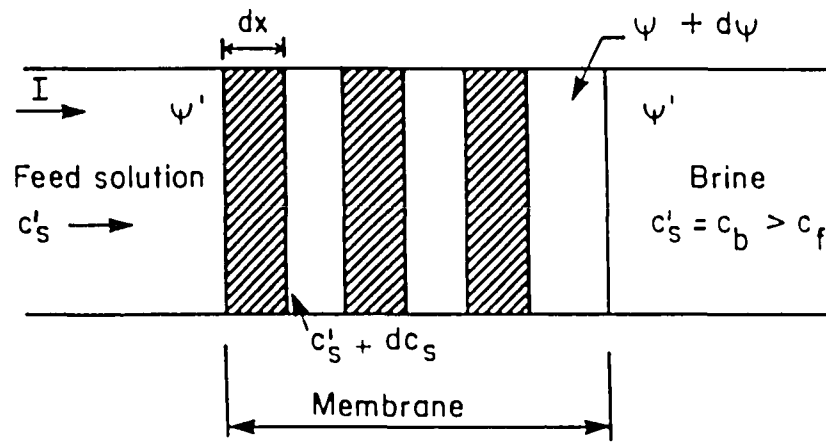
Figure 3.11.1: Schematic representation of cation-exchange membrane.

Salt flow across a differential layer of cation-exchange membrane can be written as a function of electric current, volume flow and concentration gradient according to Kedem and Katchalsky[14]:

$$S^c = \frac{J_1^c + J_2^c}{2} = C_s (1 - \sigma^c) J_v^c + \bar{P} \Delta c + \frac{\Delta t}{2} \frac{I}{F} \tag{3.11.1}$$

where

$$\Delta t^c = t_1^c - t_2^c = 2t_1^c - 1 \tag{3.11.2}$$

Equation (3.11.1) can be derived as follows according to Kedem and Bar-On[5]:

In a discontinuous system containing water and one uni-valent salt in the absence of hydrostatic pressure, the rate of free energy dissipation is :

$$\phi = j_1 \Delta\tilde{\mu}_1 + j_2\Delta\tilde{\mu}_2 + j_w \Delta\mu_w \tag{A1}$$

where the μ_i's are the electro-chemical potentials of ions 1 and 2.

$$\Delta\tilde{\mu}_1 + \Delta\tilde{\mu}_2 = \Delta\mu_s \tag{A2}$$

$$\Delta\tilde{\mu}_1 + \Delta\tilde{\mu}_2 = 2F\Delta\Psi(\Delta p = 0) \tag{A3}$$

$$I = F(J_1 - J_2) \tag{A4}$$

$$\Delta\mu_w = -\overline{V}_w \Delta\Pi s \tag{A5}$$

$$J_v = \overline{V}_w J_w \tag{A6}$$

Equation (A1) can be transformed to :

$$\phi = \frac{(J_1^c + J_2^c)}{2}\cdot\Delta\mu_s + I\Delta\Psi - J_v\Delta\pi_s \tag{A7}$$

because

$$\frac{J_1+J_2}{2}(\Delta\tilde{\mu}_1+\Delta\tilde{\mu}_2)+(J_1-J_2)\frac{(\Delta\tilde{\mu}_1-\Delta\tilde{\mu}_2)}{2}-J_v\Delta\pi_s$$

$$= \frac{J_1}{2}\Delta\tilde{\mu}_1+\frac{J_2}{2}\Delta\tilde{\mu}_1+\frac{J_1}{2}\Delta\tilde{\mu}_2+\frac{J_2}{2}\Delta\tilde{\mu}_2+\frac{J_1}{2}\Delta\tilde{\mu}_1-\frac{J_2}{2}\Delta\tilde{\mu}_1-\frac{J_1}{2}\Delta\tilde{\mu}_2+\frac{J_2}{2}\Delta\tilde{\mu}_2-J_v\Delta\pi_s$$

$$= J_1\Delta\tilde{\mu}_1 + J_2\Delta\tilde{\mu}_2 + J_w \Delta\mu_w$$

The salt flow was identified with J_1 (uni-valent cation). Therefore

$$J_2 = J_1 - I/F \tag{3.11.3}$$

The expressions for the ion fluxes in terms of the practical coefficients are[14]:

$$J_1 = \omega\Delta\Pi_s + c_s (1 - \sigma) Jv + t_1 I/F \tag{3.11.4}$$
and
$$J_2 = \omega\Delta\Pi_s + c_s (1 - \sigma) Jv - (1 - t_1) I/F \tag{3.11.5}$$

Therefore, the salt flow

$$\frac{J_1 + J_2}{2} = c_s(1-\sigma)Jv + \omega\Delta\pi_s + \frac{\Delta t}{2}I/F \qquad (3.11.6)$$

where ω = solute permeability

and $\Delta\pi_s$ = difference in osmotic pressure of permeable solute

Equation (3.11.1) is identical with equation (3.11.6).

$\bar{P}$ in equation (3.11.1) is the specific salt permeability, Δc the concentration difference and σ the reflection coefficient. In an ideally permselective cation-exchange membrane will $\Delta t^c \to 1$, $P \to 0$, $\sigma \to 1$, so that $S^c = 1/2F$. Similarly, in an ideal anion-exchange membrane will $\Delta t^a \to 0$, $P \to 0$, $\sigma \to 1$, and $-S^A = 1/2F$ and $\eta_c = 1$.

Consider now a cation-exchange membrane in which salt exclusion is not complete with co-ions carrying a significant fraction of the current[5]. In this case Δt will be smaller than 1 and will decrease with increasing c_s (salt concentration) as salt invasion becomes pronounced. Salt permeability will increase when c_s increases. If the influence of volume flow is negligible, a constant stationary value of S^c is possible only if the concentration profile is concave, i.e. dc/dx decreases from the feed to the brine surface[5]. A region of constant c_s may then develop near the brine surface at high current density. The upper limit of the partial current efficiency $\eta_c{}^c$ is then determined by Δt^c characterizing the membrane equilibrated with the brine solution. The same argument holds for the anion-exchange membrane. Therefore, according to Kedem and Bar-on, without the influence of volume flow

$$\eta_c < \frac{\Delta t^c(c_b) + \Delta t^a(c_b)}{2}) \qquad (3.11.7)$$

when back diffusion is overcome by high current density.

The conventional method for determination of transport numbers is the measurement of membrane potential, i.e. $\Delta\Psi$ between two solutions separated by the examined membrane without electric current. The potential across a differential layer is given by the expression[5]:

$$-F\frac{d\Psi}{dx} = \Delta t\frac{1}{2}\frac{d\mu_s}{dx} - F\frac{\beta}{L_p^R}J_v \qquad (3.11.8)$$

where β is the electro-osmotic coefficient and L_p is the hydraulic permeability. The last

term represents a streaming potential. If this can be neglected, the potential between feed and brine solution is given by :

$$\Delta \Psi_m = \frac{RT}{F} \int_{c_i}^{c_b} \Delta t (1 + \frac{d\ln\gamma\pm}{d\ln c_s}) \, d\ln c_s \tag{3.11.9}$$

for an ideal membrane is $\Delta t = 1$

$$\Delta \Psi_i = \frac{RT}{F} \ln \frac{(c_s\gamma^\pm)_b}{(c_s\gamma^\pm)_f} \tag{3.11.10}$$

where $\gamma^\pm$ is an activity coefficient and the average transport number is

$$\overline{\Delta t} = \frac{\Delta \Psi_m}{\Delta \Psi_i} \tag{3.11.11}$$

This average transport number, according to Kedem and Bar-on, is closer to the value for c_f than for c_b. The conclusion from equations (3.11.7), (3.11.9) and (3.11.11) is that for concentration dependent transport numbers, the actual current efficiency is expected to be less than predicted from membrane potentials, i.e.

$$\eta < \frac{\Delta \Psi_m^c + \left| \Delta \Psi_m^a \right|}{\left| 2\Delta \Psi_i \right|} \tag{3.11.12}$$

The correlation given by equation (3.11.12) is valid only if the influence of volume flow is negligible.

The potential per cell pair, V_{cp} (in volt), at a given current density ($i = I/cm^2$, mA/cm^2), is the sum of several terms[4]:

$$V_{cp} = V_n + i (R_m + R_p + R_d + R_b) \tag{3.11.13}$$

where V_n is the concentration potential, a counter driving force built up by the concentration process. Its magnitude depends on the concentration ratio between the brine and dialysate and the permselectivity of the membrane at the given conditions. V_n is measured during interruption of the current for a few seconds - long enough to disperse concentration gradients near the membranes, short enough to avoid changes of bulk concentration.

$\dfrac{V_{cp} - V_n}{i}$ is the resistance of the cell pair; R_m membrane resistance;

R_b brine compartment resistance; R_d dialysate compartment resistance; and R_p the ohmic resistance and additional counter potential due to polarization layers adjacent to the membrane surface facing the dialysate. In this system, R_b is negligible, since the brine is always more concentrated than the dialysate. For the simplest characterization of the system, it can be written[4]:

$$R_{cp} = \frac{V_{cp} - V_n}{I} = R_m + \rho d_{eff} \qquad (3.11.14)$$

where ρ is the specific resistance of the dialysate solution, and d_{eff} is the effective thickness of the dialysate compartment. In this simple representation the shadow effect of the spacer, polarization layers and any other possible disturbances are lumped into d_{eff}.

The measurement of voltage and current during desalination at a given circulating flow velocity gives the stack resistance as a function of concentration. If desalination is carried out at constant voltage, straight lines are obtained for a plot of cell pair resistance (R_{cp}) as a function of specific resistance of the bulk dialysate solution (ρ) in a wide range of currents and concentrations (c). This is due to nearly constant i/c, which determines, at given bulk flow, the polarization. Straight lines show not only that R_d, but also that the contribution of polarization, is an approximately linear function of bulk dialysate resistance.

3.12 Electrodialysis Theory

3.12.1 Basic Principles

An ED cell is shown in Figure 3.12.1. It comprises of a driven electrochemical cell containing electrodes at each end and a series of compartments or channels of typically 1 mm width, separated by membranes[8]. Alternate membranes are "anion permeable" ("A" in Fig. 3.12.1) and "cation-permeable" ("C" in Fig. 3.12.1). The membranes are thin sheets of polymer which have been treated with cationic and anionic groups to impart selective permeability. Under the influence of an applied potential between the electrodes, current flows within the ED cell, being carried by cations - which tend to migrate towards the negatively charged electrode (cathode) - and anions - which tend to move in the direction of the positively charged electrode (anode).
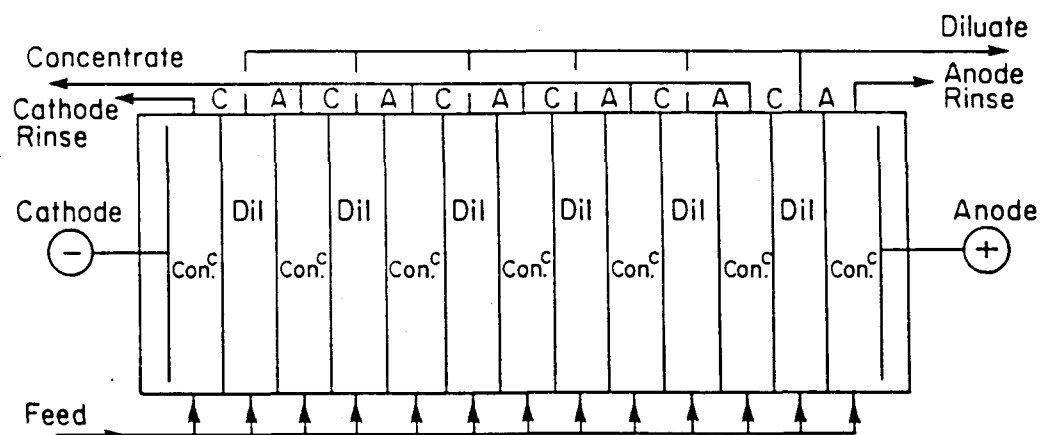
Figure 3.12.1: General layout of an ED stack. Dil = diluating compartments; Con.^{c} = concentrating compartments.

To see how water purification can occur in such a cell, consider the smaller set-up shown in Figure 3.12.2 and, in particular, the events in the compartment marked D_2. The various cations present in the water (say Na^+, Ca^{2+}, etc.) can pass freely through the cation-permeable membrane at one end of the compartment and the anions can pass through the anion-permeable membrane at the opposite end. However, neither the cations nor the anions can move out of the adjacent compartments F because the membranes towards which they move (under the influence of the applied potential) are of the wrong type (electrical charge) to allow passage of the ions. Ions, however, can escape from compartments D_2. The result of all this, in a multi-compartment cell, is that water is diluted and concentrated in alternate compartments (as noted in Fig. 3.12.1) - thus enabling the collection of the purer water from the so-called diluate channels.

During ED of a natural water, several electrode reactions are possible, but the most generally observed ones are[83]:

Hydrogen evolution,	$2H^+ + 2e = \uparrow H_2$ (cathode)	(3.12.1)
Oxygen evolution,	$4 (OH)^- = \uparrow O_2 + 2H_2O + 4e$ (anode)	(3.12.2)
or	$2H_2O = \uparrow O_2 + 4H^+ + 4e$ (anode)	(3.12.3)

93
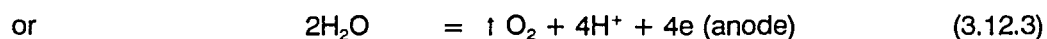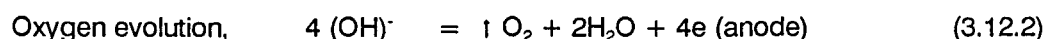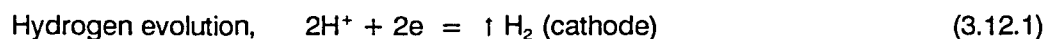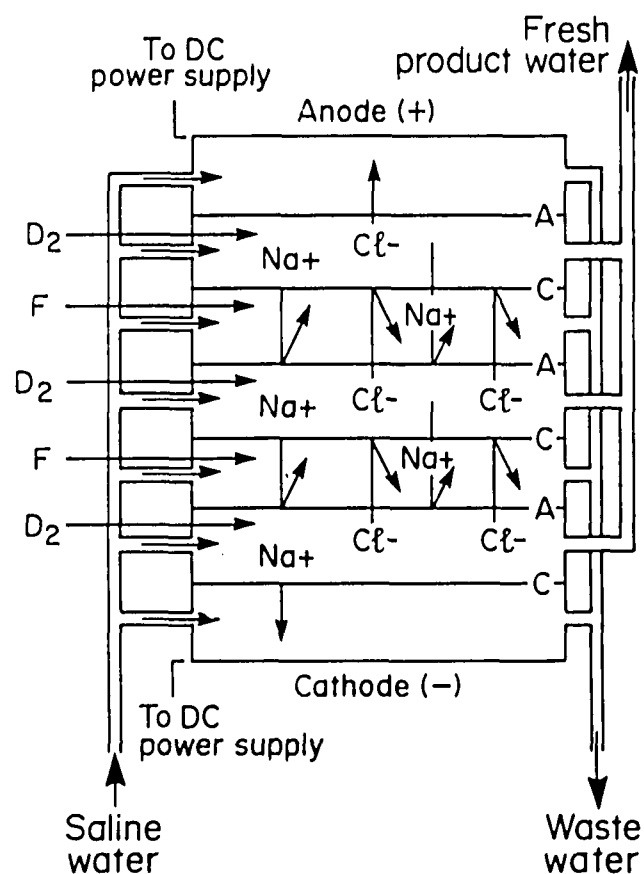
Figure 3.12.2: Ion movement during ED.

3.12.2 Desalting Rate

An important factor in any desalination process is the rate at which desalination occurs. In order to determine the factors which control the desalination rate in an ED unit, it is necessary to examine in some detail the ion-transport processes occurring in the cell[16] (and particularly within and around the membranes). This is done by considering the ion-transport numbers (i.e. the fraction of the current carried by the different kinds of ions in the cell), in particular, it is necessary to compare the transport numbers in the bulk solution and in the membranes. Consider, therefore, desalination of a solution of sodium chloride. In the bulk solution, away from the membranes, the current is carried by the opposite drift of Na^+ and Cl^- ions, in fact, 60% of the current is carried by the Cl^- ions and 40% by Na^+ ions, i.e. the transport numbers in the bulk solution are $t_1 = 0,4$ and $t_2 = 0,6$. In perfect membranes, however, only one type of ion can pass through a membrane and the total current is carried by that ion. The characteristics of perfect and practical ion-exchange membranes are shown in Table 3.12.1.

Table 3.12.1: Characteristics of perfect and practical ion-exchange membranes.

Membrane Type	Cation-permeable membrane (CPM)	Anion-permeable membrane (APM)
Perfect membrane	$\bar{t}^c_1 = 1,0;\ \bar{t}^c_2 = 0$	$\bar{t}^a_1 = 0;\ \bar{t}^a_2 = 1,0$
"Practical" membrane	$\bar{t}^c_1 \approx 1,0;\ \bar{t}^c_2 << 1$	$\bar{t}^a_1 << 1;\ \bar{t}^a_2 \approx 1,0$

where $\bar{t}^c_1$ = transport numbero of cations (Na$^+$) in CPM

$\bar{t}^c_2$ = transport number of anions (Cl$^-$) in CPM

$\bar{t}^a_1$ = transport number of cations in APM

$\bar{t}^a_2$ = transport number of anions in APM

The efficiency with which a membrane excludes a particular ion is expressed by the permselectivity of the membrane with respect to that ion. The permselectivity is defined as follows[7]:

For cation permeable membranes:

$$P^c = \frac{t_2 - \bar{t}_2}{t_2} = \frac{\bar{t}_1 - t_1}{1 - t_1} \qquad (3.12.4)$$

For anion permeable membranes:

$$P^a = \frac{t_1 - \bar{t}_1}{t_1} = \frac{\bar{t}_2 - t_2}{1 - t_2} \qquad (3.12.5)$$

Consider now the ion transport processes occurring within an ED unit and it is useful to begin with a simple cell containing sodium chloride solution with just one perfect membrane (a CPM) inserted (Fig. 3.12.3). In the situation depicted in Figure 3.12.3, chloride ions are drifting to the right and sodium ions to the left. At the membrane the sodium ion flux is proportional to the current I. Thus, as indicated in the magnified sketch of the membrane region (Fig. 3.12.3a),

$$\bar{t}_{Na+} = 1,0;\ \bar{t}_{Cl-} = 0,0$$

i.e. the Na$^+$ migration rate is I/F equiv/s where I is the current and F is Faraday's constant. In the bulk solution on either side of, but away from, the membrane,

$$t_{Na+} = 0,4 \text{ and } t_{Cl-} = 0,6$$

i.e. migration rates in equiv/s are 0,4 I/F of Na$^+$ and 0,6 I/F of Cl$^-$.

Consider now the two boundary-layer regions on either side of the membrane. The

ion flow due to the electrical current will produce the following mass balance for the passage of each Faraday of current.

R.H.S. Sodium

Inflow from solution   Outflow through membrane
         0,4   1,0

Sodium depletion   = 0,6 (equiv)

Chloride

Inflow from membrane   Outflow to solution
         0,0   0,6

Chloride depletion   = 0,6 (equiv)

Consequently, it appears that there is a deficiency in the salt mass balance on the R.H.S. of the membrane, when account is taken only of the electrical flow of ions. However, the nett efflux of salt from this region will reduce the concentration at the membrane surface and this will trigger an additional migration process, namely a diffusive flux of salt from the bulk solution into the depleted boundary region. In the steady state, the mass flux due to diffusion must be equivalent to sodium and chloride depletion rates of 0,6 (caused by the electrical flux) in order to maintain the salt concentrations in the boundary region.

L.H.S. Sodium

Inflow from membrane   Outflow to solution   Accumulation Rate
         1,0   0,4   0,6 (equiv)

Chloride

Inflow from solution   Outflow to membrane   Accumulation Rate
         0,6   0,0   0,6 (equiv)
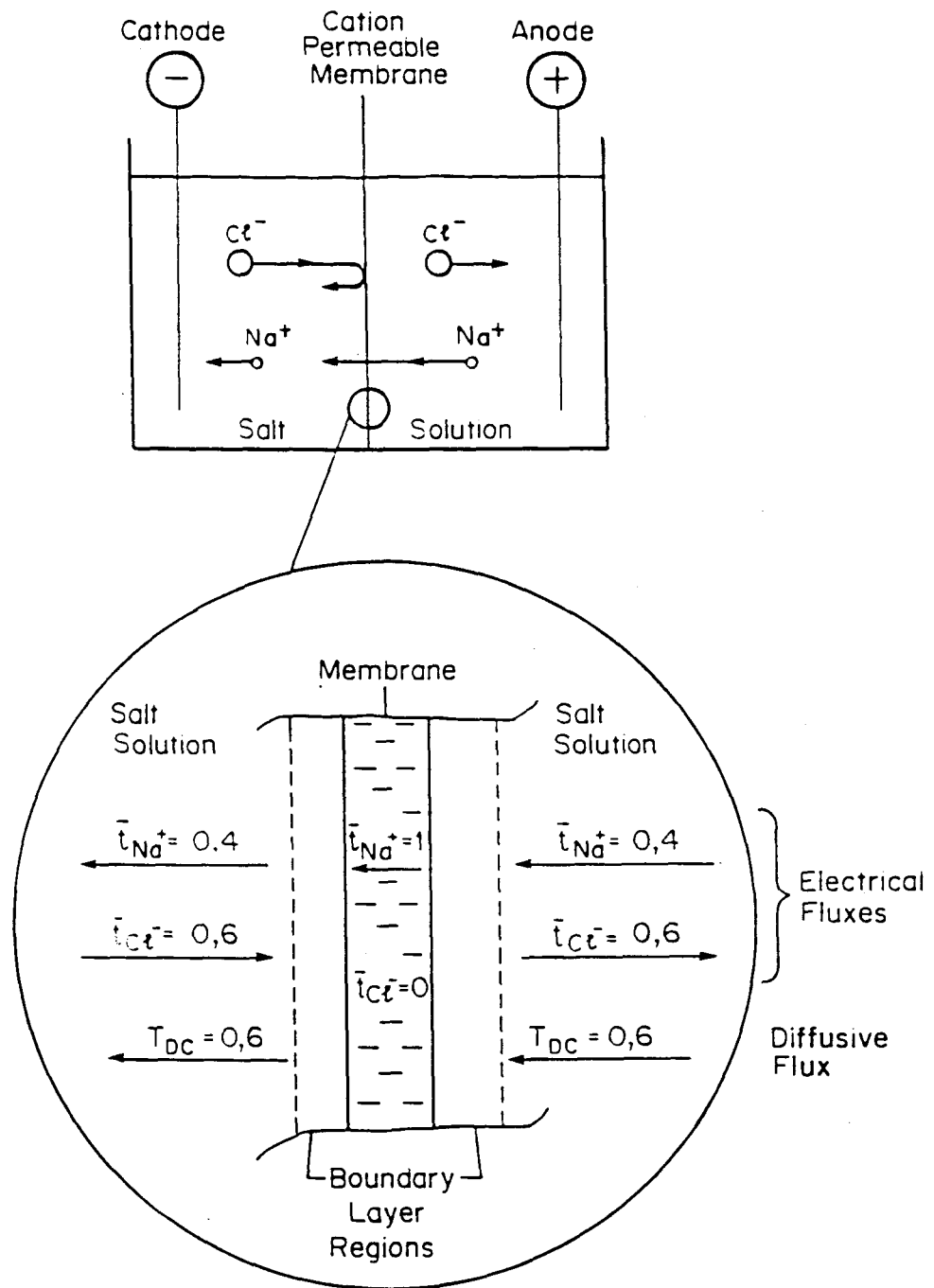
Figure 3.12.3 (Upper) and Figure 3.12.3(a) (Lower).
Processes occurring within and around a cation-permeable membrane in an electrochemical cell containing NaCl solution.

In a similar manner to the salt deficiency on the R.H.S. of the membrane as a result of Coulombic migration, there appears to be an accumulation of salt on the L.H.S. of the membrane equivalent to a transport number of 0,6. This imbalance of mass flow is again in the steady state, counted by a _diffusive_ flow of salt. This time the salt concentration is increased at the membrane surface by the electrical migration and the salt therefore diffuses away into the bulk of the solution. Comparing this situation with

the straightforward electrolysis process without the membrane, the nett effect of inserting the membrane is to produce an apparent diffusion of salt from right to left across the membrane. The rate (in equivs per Faraday) of this apparent diffusion transport number, T_{DC} may be expressed in terms of the transport numbers. For the present case, it is clear that $T_{DC} = 0,6$ equiv/Faraday, i.e. $T_{DC} = t_2$. However, in the general case for imperfect membranes, a similar analysis as that above leads to:

$$T_{DC} = t_2 - \bar{t}_2{}^c$$

A similar analysis and argument may be set up for an anion-permeable membrane. In this case, if the membrane was perfect (i.e. $\bar{t}_1{}^a = 0$ and $\bar{t}_2{}^a = 1,0$), there would appear to be a salt depletion on the L.H.S. To balance these there would have to be an apparent diffusion of salt from left to right across the membrane. In this case for an imperfect membrane, $T_{DA} = t_1 - \bar{t}_1{}^a$ which reduces to $T_{DA} = 0,4$ for the case of a perfect APM in a NaCl solution.

Consider now what will happen if an anion-permeable membrane is inserted on the right hand side of the cation permeable membrane in Figure 3.12.3. Such a set up is depicted in Figure 3.12.4. Passage of current through this system will produce an apparent effect of salt diffusion out of the space between the two membranes. For the simple example of perfect membranes in NaCl solution, the rates of these apparent diffusions will be

To the left across the C.P.M., $\quad T_{DC} = 0,6$
To the right across the A.P.M., $\quad T_{DA} = 0,4$

But, for the general case with imperfect membranes $T_{DC} = t_2 - \bar{t}_2{}^c$ and $T_{DA} = t_1 - \bar{t}_1{}^a$.

Therefore, the total apparent diffusive flux out of the central compartment of a set-up like Figure 3.12.4 is:

$$T_D = T_{DC} + T_{DA} \qquad = t_2 - \bar{t}_2{}^c + t_1 - \bar{t}_1{}^a \qquad (3.12.6)$$
$$= 1 - \bar{t}_2{}^c - \bar{t}_1{}^a \text{ equiv per Faraday} \qquad (3.12.7)$$
$$= 1 \text{ for perfect membranes.} \qquad (3.12.8)$$

T_D, the salt flux out of the central compartment, is clearly a measure of the desalting rate, i.e. for a current flow of I amp,

Desalting rate $=$ I/F $(T_{DC} + T_{DA})$ equiv/s   (3.12.9)

$=$ I/F equiv/s (for perfect membranes).   (3.12.10)

Hence, for a system with perfect membranes, the salt removal from the space between the membranes is exactly equivalent to the charge that is passed through the system. This is exactly equivalent to the decrease in salt concentration in sodium chloride in a simple electrolytic cell in which the electrode reactions involved sodium deposition (cathodic) and chlorine evolution (anodic). (Note: If the membranes been the other way round in Figure 3.12.4, the APM on the left and the CPM on the right, then the effect would be to concentrate rather than dilute the solution between the membranes).

Thus, the desalting rate increases with cell current. Another important factor is the number of membranes. As mentioned earlier, the above expressions apply to a simple ED cell containing just one pair of membranes. The system can be greatly improved by inserting many pairs of membranes because each pair produces an equivalent amount of desalination. Thus, the total desalination achieved per unit charge flow is
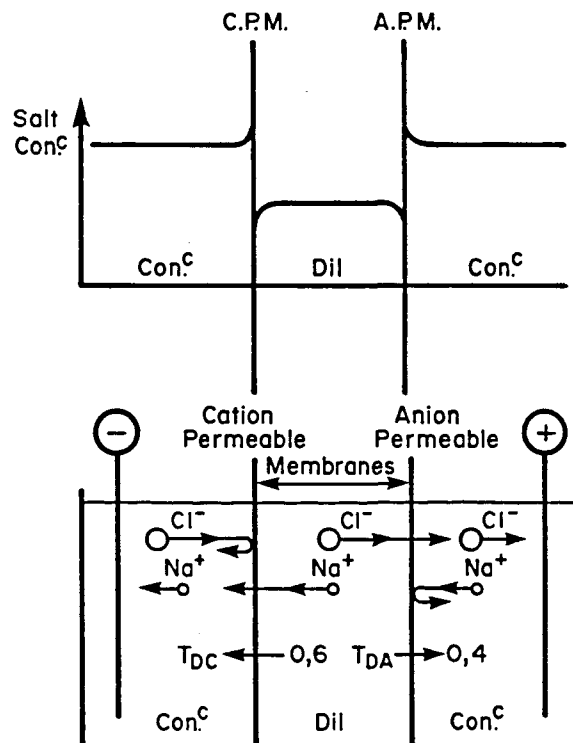
Figure 3.12.4: Cell containing a pair of membranes.

N times that in a one-pair set-up, where N is the number of membrane pairs, i.e.

$$\text{Desalting rate} = \frac{NI}{F} (T_{DC} + T_{DA}) \qquad (3.12.11)$$

Note that, in Figure 3.12.2, there are 6 membrane pairs giving a desalting rate of 6I/F equiv/s for perfect membranes.

3.12.3 Energy Requirements for Electrodialysis

In order to estimate the energy requirements for ED all the potential differences (or IR drops) in the cell must be investigated. The required applied voltage for ED comprises several elements[16]:

i)   a voltage necessary to drive the electrode reactions;

ii)   a voltage required to overcome the aqueous solution resistances in the ED cell;

iii)   a voltage necessary to overcome the membrane potentials;

The first of these is determined from the electrode potentials for the particular electrode reaction and increases with cell current due to polarisation of the electrode reactions. However, in commercial units, this component of the required applied voltage is usually small in comparison to those arising from (ii) and (iii). Therefore, the latter factors will be considered in more detail.

3.12.3.1 Solution Resistances

The resistivity of an aqueous electrolyte decreases with increasing ionic concentration. Therefore, IR drops through the diluate channels are considerably greater than those through the concentrate channels. A further complication, with consequences for ED energy requirements, is concerned with concentration changes which occur in the regions immediately adjacent to the membranes. These are summarized in Figure 3.12.5 which illustrates that salt depletion occurring in the boundary regions adjacent to the membranes in the diluate channels and enrichment occurring in the boundary layers on the concentrate side of the membranes. For a cation-permeable membrane,
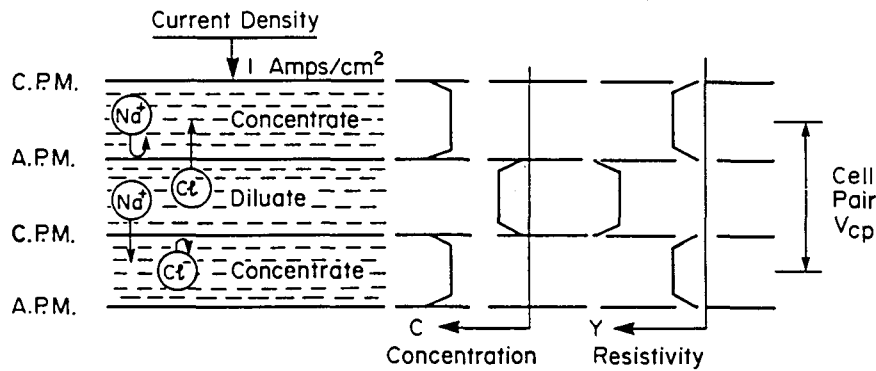
Figure 3.12.5: The cell pair showing salt depletion occurring in the boundary regions adjacent to the membranes in the diluate channels and salt enrichment occurring in the boundary layers on the concentrate side of the membrane.
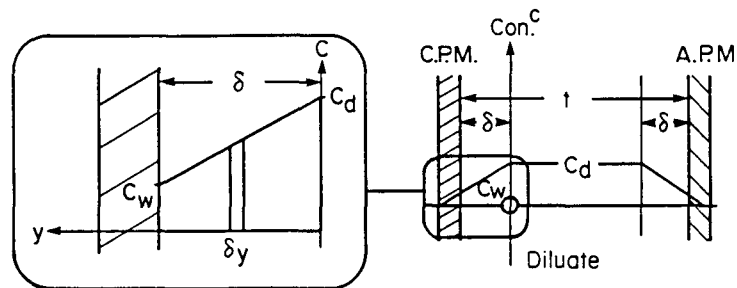
Figure 3.12.6: Concentration changes in boundary layers around membranes.

the concentration of salt in the "diluate boundary layer" is lower than the concentration of salt in the "main diluate stream", but the salt concentration is relatively enriched in the "concentrate boundary layer". Both these effects are clear on the concentration profiles shown in Figure 3.12.5. This phenomenon is very similar to concentration polarization processes which can occur around electrodes in electrochemical cells except that, in the present context, there is an unbalanced Faradaic transport in and around membranes which promotes additional diffusion fluxes to establish the steady-state concentration profile. Thus, these concentration-polarization phenomena around membranes in ED cells are a natural and inevitable result of the desalting mechanism i.e. of the change in electrical transport numbers at the membrane interface upon which the ED desalination process relies.

One important practical consequence of concentration polarization around membranes in ED units, indicated in Figure 3.12.5, is that the resistance of the diluate boundary layers is significantly greater than in the bulk diluate stream. Therefore, the occurrence

of concentration polarization increases the energy requirements for ED.

3.12.3.2 Membrane Potentials

When an ion-selective membrane separates two solutions of a salt at different concentrations, a potential difference is set-up across the membrane. This happens because, in the <u>absence</u> of any applied potentials, Na^+ ions will tend to migrate across the cation-exchange membrane from the concentrated solution to the diluate solution. This will lead to a charge imbalance across the membrane with the diluate side becoming positively charged relative to the concentrated side. Eventually this potential difference across the membrane will build up to such a level that further ion transfer is discouraged and the value of the potential difference at <u>this equilibrium condition</u> is known as the membrane potential. For a salt consisting of single-charged ions, and assuming that activities can be equated to concentrations, the magnitude of the membrane potential is given by

$$E_m = - (\bar{t}_1 - \bar{t}_2) \frac{RT}{F} \ln \left(\frac{C_{w1}}{C_{w2}}\right) \qquad (3.12.12)$$

where C_{w1} and C_{w2} are the concentrations of the salt in the concentrated and dilute solutions respectively.

The important point about the above is that natural flow across a membrane is from concentrate to diluate (i.e. the opposite to that required in desalination) and, to reverse this natural flow direction requires the <u>application</u> of a potential of magnitude greater than E_m, i.e. the membrane potential represents a potential drop which has to be overcome by the external applied voltage in order for desalination to occur. However, this is not the whole story. The magnitude of the membrane potential indicated by the above equation only applies to the equilibrium (i.e. infinitely-low current) state. As previously discussed, an inevitable consequence of desalination at finite currents is the occurrence of concentration polarization. The consequent concentrate enrichment and diluate depletions at the membrane/solution interface means that C_{w1} will be greater than the bulk concentrate composition and C_{w2} will be less than the bulk diluate concentrations. Therefore, another important effect of concentration polarization is to increase the membrane potential and hence the energy requirements for desalination.

3.12.3.3 The Cell-Pair Potential

The major part of the energy requirements for ED comprises the voltage necessary to overcome the solution resistances and membrane potentials. Estimation of the voltage is conveniently done by considering one cell pair which, as shown in Figure 3.12.5, encompasses a pair of membranes. The cell pair potential V_{cp}, is the sum of all the potential drops across the membranes and solutions comprising one cell pair.

Consider the basic conflict between attempts to maximise desalting rate and to minimize energy requirements. The flux of salts from the diluate channel is given by

$$T_D = 1 - \bar{t}_2^c - \bar{t}_1^a \qquad (3.12.13)$$

and that the desalting rate, d, is given by:

$$d = \frac{iT_D}{F} \text{ equiv cm}^{-2} \text{ s}^{-1} \qquad (3.12.14)$$

(using current density, i, instead of current I). The power required to drive a cell pair is:

$$P = V_{cp} \, i \text{ watts cm}^{-2} \qquad (3.12.15)$$

Therefore, increases in i, whilst raising the desalting rate, also lead to higher energy consumption - not only directly but also by increasing V_{cp} due to higher IR drops and concentration-polarization effects.

3.12.3.4 Resistances

The major contributor to V_{cp} is the resistance of the diluate stream. It is normal practice to keep the concentration of the concentrate high enough for its resistance to be negligible in comparison to that of the diluate. Modern membranes have, however, negligible small resistances. As a first approximation, it can be considered that the diluate stream is providing all the resistance. To calculate the resistance, the main stream and the boundary layers must be considered separately.

Considering the total thickness (including boundary layers) of the diluate stream to be 't' cm (typically 0,1 cm) (see Fig. 3.12.6). Let the thickness of the boundary layers (adjacent to the membranes) be δ (determined by hydrodynamic conditions and typically 0,01 cm).

3.12.3.5 Main stream of diluate

The resistance of 1 cm^2 cross section, d, is given by:

$$R_d = \frac{t - 2\delta}{\kappa} \quad ohm \tag{3.12.16}$$

with the conductivity, κ, expressed in units of $(ohm/cm)^{-1}$.

But the conductivity, κ, depends on the concentration C_d (equiv/cm^3) of the diluate stream via $\kappa = \Lambda C_d$ \hfill (3.12.17)

where Λ = equivalent conductivity in cm^2/ohm equiv.

$$\therefore \ R_d = \frac{t - 2\delta}{\Lambda C_d} \tag{3.12.18}$$

3.12.3.6 Boundary layers of diluate

Faradaic transport (i.e. under the influence of the applied electric field) of ions, across the membranes out of the diluate compartment, leads to a depletion of salt in the boundary layers which, in turn, causes a diffusion flux from the bulk diluate. The concentration gradient across the boundary layer stabilises (i.e. steady-state conditions are established) when the two fluxes are equal.

Consider the CPM boundary layer (left diagram on Fig. 3.12.6).

$$Faradaic\ Flux \ = \ i/F\ (t_2 - t_2^c) \ \approx \ (it_2/F) \tag{3.12.19}$$

$$Diffusion\ flux \ = \ -D\ \frac{dc}{dy} \tag{3.12.20}$$

Therefore, at steady state,

$$-D\ \frac{dc}{dy} \ = \ t_2\ i/F \tag{3.12.21}$$

Conductivity (and hence resistance) is concentration dependent. Therefore, to find the

boundary-layer resistance, R_{BC}, integration must be carried out across the layer.

$$\text{Resistance of element } \delta y = \frac{\delta y}{\kappa} = \frac{\delta y}{\Lambda c} \qquad \begin{array}{c}(3.12.22)\\ (\text{see Fig. } 3.12.6)\end{array}$$

Therefore, resistance of boundary layer,

$$R_{BC} = \int_0^\delta \frac{dy}{\Lambda c} \qquad (3.12.23)$$

Concentration gradient (assumed linear - see Figure 3.12.6) is:-

$$\frac{dc}{dy} = \frac{C_w - C_d}{\delta} \qquad (3.12.24)$$

Changing the integration variable limits:-

$$R_{BC} = \int_{C_d}^{C_w} \frac{\delta}{\left(\dfrac{C_w - C_d}{\Lambda C}\right)} dc = \frac{\delta}{(C_w - C_d)\Lambda} \ln\left(\frac{C_w}{C_d}\right) \qquad (3.12.25)$$

$$R_{BC} = \frac{\delta}{(C_d - C_w)\Lambda} \ln\left(\frac{C_d}{C_w}\right) \qquad (3.12.26)$$

(since $C_d - C_w = -(C_w - C_d)$ and $\ln x = -\ln 1/x$)

An alternative expression for R_{BC} can be produced by using the previously formulated steady-state relation.

$$-D \frac{dc}{dy} = t_2 \frac{i}{F} = -D \frac{(C_w - C_d)}{\delta} = \frac{D(C_d - C_w)}{\delta} \qquad (3.12.27)$$

$$\therefore C_d - C_w = \frac{t_2 \delta i}{FD} \qquad (3.12.28) \ (A)$$

$$\therefore R_{BC} = \frac{\delta FD}{t_2 \delta i \Lambda} \ln\left[\frac{C_d}{C_d - \left(\dfrac{t_2 \delta i}{FD}\right)}\right] \qquad (3.12.29)$$

$$= -\frac{FD}{t_2 i \Lambda} \ln\left(1 - \frac{t_2 \delta i}{FDC_d}\right) \qquad (3.12.30)$$

A similar analysis can be carried out to obtain an expression for the resistance, R_{BA}, of the diluate boundary layer at the APM (right hand side of Figure 3.12.6). This leads to the following expression:-

$$R_{BA} = -\frac{FD}{t_1 I \Lambda} \ln \left(1 - \frac{t_1 \delta I}{FDC_d}\right)$$

$$(3.12.31)$$

The depletion of solute in the boundary layers arises from the rapid flux of solute species through the membranes - this flux being directly proportional to the current flowing in the cell. In other words, as i increases from zero, the concentration gradient in the boundary layer increases (C_w decreases as i increases). It follows, therefore, that there are limits to the current that can be carried by the solute ions in an ED system - this limit being reached when C_w approaches zero.

As C_w approaches 0, equation (A) becomes:

$$C_d = \frac{t_2 \delta I_{max}}{FD}$$

$$(3.12.32)$$

and

$$I_{max} = \frac{C_d FD}{t_2 \delta}$$

$$(3.12.33) \quad (B)$$

which in turn, defines, for any given ED unit, a definite limit to the desalting rate -

$$\frac{N I_{max}}{F}$$

Another aspect of this "limiting current density phenomenon concerns the transport of H^+ and OH^- ions across CPM and APM membranes, respectively. At low current densities, the current is carried almost exclusively by solute ions rather than by H^+ and OH^-. This is because of the very low concentrations of H^+ and OH^- in neutral solution (10^{-7} mol/ℓ) - and is despite the approximately ten times higher mobilities of H^+ and OH^- compared with solute ions. But, as i increases, the flux of H^+ and OH^- across the membranes increases until, as i_{max} is approached, the flux of H^+ at the CPM and of OH^- at the APM becomes a substantial fraction of the total current. In rather more precise

terms, because of their tenfold higher mobilities, an appreciable fraction of the current will be carried by H^+ and OH^-, present at concentrations of 10^{-7} mol/ℓ, when the solute concentration at the membrane/diluate interface C_w, falls towards a value of about 5 x 10^{-6} mol/ℓ. Such a situation not only results in an obvious decreased efficiency of desalination but also in highly undesirable pH changes in the solutions. One consequence of such pH changes is that they can lead to an increased tendency towards scale precipitation if the pH increases significantly in any local region.

3.12.3.7 Membrane Potentials

The contribution of membrane potentials to the cell-pair potential is most conveniently predicted by considering ED of a solution of a single salt comprising of univalent ions. As was noted earlier, for this case the membrane potential was given by:

$$E_m = -(\bar{t}_1 - \bar{t}_2) \frac{RT}{F} \ln \frac{C_{w1}}{C_{w2}} \qquad (3.12.34)$$

where C_{w1} and C_{w2} now represent the bulk concentrations of the salt in the compartments on either side of the membrane. Note, though, that the membrane potential is determined by the salt concentrations at the membrane/salt interface. It was noted earlier that finite cell-current flow resulted in salt depletions and enrichments within the boundary region beside the membrane. In such circumstances, E_m will no longer be determined by the bulk-salt concentrations (C_{w1} and C_{w2}) but by the concentration-polarised membrane/boundary layer interfacial values (C_{wbc} and C_{wdc}, in the C.P.M. in Figure 3.12.7). Therefore, in order to obtain an expression for E_m in these practically-relevant conditions, it is necessary to estimate the concentrations C_{wbc} and C_{wdc} for C.P.M.and C_{wda} and C_{wba} for the A.P.M.. This exercise is considerably simplified if it is assumed (see Figure 3.12.7) that the four boundary layers have identical effective thickness, δ. If we assume a perfect cation permeable membrane (C.P.M.) and use the notation of Figure 3.12.7, the polarised C.P.M. membrane potential is given by:-

$$E_{mc} = -(1-0) \frac{RT}{F} \ln \frac{C_{wbc}}{C_{wdc}} \tag{3.12.35}$$

$$\text{Now} \quad C_d - C_{wdc} = \frac{t_2 \cdot \delta \cdot i}{FD} \tag{see A} \tag{3.12.36}$$

$$\therefore \quad C_{wdc} = C_d - \frac{t_2 \cdot \delta \cdot i}{FD} \tag{3.12.37}$$

$$\text{Similarly} \quad C_{wbc} = C_c + \frac{t_2 \cdot \delta \cdot i}{FD} \tag{3.12.38}$$

$$\text{hence} \quad E_{mc} = \frac{RT}{F} \ln \left[\frac{\dfrac{C_c}{C_d} + \dfrac{t_2 \cdot \delta \cdot i}{FDC_d}}{1 - \dfrac{t_2 \cdot \delta \cdot i}{FDC_d}} \right] \tag{3.12.39}$$

Similarly for the AMP.

$$E_{ma} = \frac{RT}{F} \ln \left[\frac{\dfrac{C_c}{C_d} + \dfrac{t_1 \cdot \delta \cdot i}{FDC_d}}{1 - \dfrac{t_1 \cdot \delta \cdot i}{FDC_d}} \right] \tag{3.12.40}$$
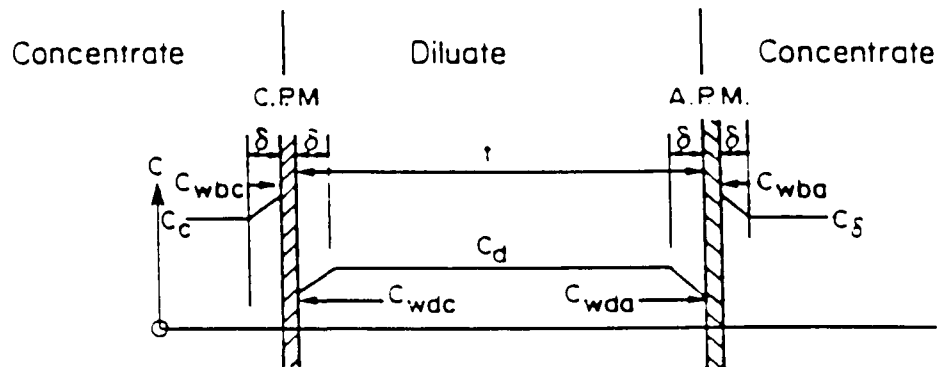
Figure 3.12.7: Concentration polarisation effects on membrane potential.

If the concentrate stream is several or more times as concentrated as the diluate stream, then

108

$$\frac{C_c}{C_d} >> \frac{t_2 \delta i}{FDC_d}$$

(3.12.41)

because $\dfrac{1}{i_{max}} = \dfrac{t_2 \delta}{FDC_d}$ (see equation B)

(3.12.42)

and $\dfrac{i}{i_{max}}$ has a maximum value of 1

All the relevant terms have now been covered, which, to a first approximation, contribute to the cell pair potential V_{cp}.

Cell pair potential V_{cp} is given by:

i.e. $V_{cp} = i (R_d + R_{BC} + R_{BA}) + E_{mc} + E_{ma}$

(3.12.43)

$$\therefore \quad V_{cp} = \frac{i(t-2\delta)}{\Lambda C_d} - \frac{FD}{t_2 \Lambda} \ln \left(1 - \frac{t_2 \delta i}{FDC_d} \right) - \frac{FD}{t_1 \Lambda} \ln \left(1 - \frac{t_1 \delta i}{FDC_d} \right)$$

$$+ \frac{RT}{F} \ln \left(\frac{C_c}{C_d} + \frac{t_2 \delta i}{FDC_d} \right) - \frac{RT}{F} \ln \left(1 - \frac{t_2 \delta i}{FDC_d} \right)$$

$$+ \frac{RT}{F} \ln \left(\frac{C_c}{C_d} + \frac{t_1 \delta i}{FDC_d} \right) - \frac{RT}{F} \ln \left(1 - \frac{t_1 \delta i}{FDC_d} \right)$$

(3.12.44)

Rearranging:-

$$V_{cp} = \frac{i(t - 2\delta)}{\Lambda C_d} - \left(\frac{FD}{t_2 \Lambda} + \frac{RT}{F} \right) \ln \left(1 - \frac{t_2 \delta i}{FDC_d} \right)$$

$$- \left(\frac{FD}{t_1 \Lambda} + \frac{RT}{F} \right) \ln \left(1 - \frac{t_1 \delta i}{FDC_d} \right)$$

$$+ \frac{RT}{F} \left[\ln \left(\frac{C_c}{C_d} + \frac{t_1 \delta i}{FDC_d} \right) + \ln \left(\frac{C_c}{C_d} + \frac{t_2 \delta i}{FDC_d} \right) \right]$$

(3.12.45)

Further simplification of the bottom line of the above expression it is necessary to recall that:-

$$\frac{C_c}{C_d} \gg \frac{t_2 \delta i}{FDC_d} \quad \left(\text{and similarly} \gg \frac{t_1 \delta i}{FDC_d}\right)$$

$$V_{cp} = \frac{i(t - 2\delta)}{\Lambda C_d} - \left(\frac{FD}{t_2\Lambda} + \frac{RT}{F}\right) \ln\left(1 - \frac{t_2 \delta i}{FDC_d}\right) - \left(\frac{FD}{t_1\Lambda} + \frac{RT}{F}\right) \ln\left(1 - \frac{t_1 \delta i}{FDC_d}\right) +$$

$$\frac{2RT}{F} \ln \frac{C_c}{C_d} \qquad\qquad (3.12.46)\ (C)$$

The order of magnitudes of some of the terms in the above relation is as follows by considering the desalination of sodium chloride:-

F = 96 500 Coulomb/equiv, t_2 = 0,6, R = 8,3 joule/°K

D (diffusion coefficient) = 1,5 x 10^5 cm²/s, t_1 = 0,4

Λ = 108,9 cm² ohm⁻¹ equiv⁻¹.

From which we can estimate the following terms:-

$$\frac{FD}{t_2\Lambda} = \frac{96\ 500 \times 1,5 \times 10^5}{0,6 \times 108,9} \left| \frac{\text{coulomb cm}^2 \text{ ohm equiv}}{\text{equiv s cm}^2} = \text{volts} \right.$$

$$= 0,02215 \text{ volt}$$

$$\frac{RT}{F} = \frac{8,3 \times 300}{96\ 500} = 0,0258 \text{ volt}$$

In short $\frac{FD}{t_2\Lambda}$ and $\frac{RT}{F}$ are of the same order

Also $\frac{FD}{t_1\Lambda}$ = 0,03323 volt

Remember also that $\frac{t_2\delta i}{FDC_d}$ and $\frac{t_1\delta i}{FDC_d}$ have maximum values of 1.

Of the remaining terms in equation (C) t,δ and C_c may be considered as design parameters which may be chosen and fixed. Therefore, in estimating the energy requirement for V_{cp}, it remains to find the most suitable combination of variables in V_{cp}, i and C_d. A convenient way of doing this is too recast equation (C) in a non-dimensional form. This operation can be done in several steps:-

110

(i)   Multiply both sides of (C) by F/RT.

This makes the L.H.S of (C) $\dfrac{V_{cp}F}{RT}$ which is a (voltage) non-dimensional term,

which we call V.

(ii)   The first term on the RHS of (C) now becomes

$$\frac{i(t-2\delta)}{C_d\Lambda}\frac{F}{RT}$$

If we multiply this term by $\dfrac{i_{max}}{i_{max}}$ $=$ $\dfrac{C_dFD}{t_2\delta}$ x $\dfrac{1}{i_{max}}$ (3.12.47)

we get $\dfrac{i}{i_{max}}$ $\dfrac{t-2\delta}{\delta}$ $\dfrac{F^2D}{\Lambda t_2 RT}$ $=$ $\beta\,\Lambda\,I$ (3.12.48)

when it is separated into three non-dimensional terms

I $=$ $\dfrac{i}{i_{max}}$ (3.12.49)

λ $=$ $\left(\dfrac{t-2\delta}{\delta}\right)$ (3.12.50)

β $=$ $\dfrac{F^2D}{\Lambda t_2 RT}$ (3.12.51)

(iii)   Replace C_c/C_d by C-another non-dimensional ("concentration ratio") term.

The substitution of the above non-dimensional terms into (C), together with some manipulation, gives the following non-dimensional equation:

Simple Resistance	Polarization	Useful	
V = $\beta\lambda I$	$-(1+\beta)$ ln $(1-I)-(1+\frac{t_2}{t_1}\beta)$ ln $(1-\frac{t_1}{t_2}I)$ $+2\ln C$	(3.12.52) (D)	

Possible ranges of values for λ I, and C

<u>Typical plant values</u>

$0 < \lambda < \text{large}$ 9

$0 < I < 1$ 0,95

$10 < C < 200$ 15 - 70

Equation (D) is divided into terms coming from <u>simple resistive losses</u> (since the $\beta\Lambda I$ term is derived from the first term on the RHS of equation (C) which represents the bulk dilate resistance), and <u>the work done against the membrane potentials</u> (said to be "useful" because it represents the minimum energy without polarization effects), and the <u>polarization-losses</u> (all these terms being derived from all the terms in (C) except the first and the last (simple membrane potential). These contributions to the cell pair potential may be plotted separately as they are in Figure 3.12.8. The "useful" potential is only a function of C and the two "loss" potentials are both functions of I, the resistive loss being a function of λ as well. This graph then covers the total likely range of conditions to be found in practical ED stacks. Thus, the various curves for different values of λ are plots of the contributions of the resistance loss ($\beta\lambda I$) to the V term for different values of λ (the cell to boundary layer thickness ratio). Note that, as λ increases (i.e. as the cell size increases) the energy requirements increase. Note also, that, for the calculations of the value of β (used in the λ-plots and also in the polarization plot) that a temperature of 300 °K has been used.

3.12.4 Estimation of Effects of Flow of Solution through Stack on Desalting Process

No account of the effects of flow of solution through the compartments of the ED stack have been taken up to now. This matter can be estimated by investigating how conditions vary as the diluate passes along its channel[16]. This procedure can be started by carrying out a salt mass balance on an element, dx, in which the concentration changes from C_d by a small amount dC_d (See Figure 3.12.9).

Area of element $=$ 1 x t $=$ t cm^2

Therefore, rate of salt flow into element is $C_d U_d t$ equiv s^{-1}.

Salt flux out of element along diluate channel is $(C_d + dC_d)$ t U_d equiv s^{-1}.

Flux of salt through membranes (= desalting rate)

$$= \quad \frac{i}{F} \quad \text{equiv/cm}^2 \text{ s}$$

$$= \quad \frac{i}{F} \quad dx \text{ equiv/s (out of element dx of membrane area dx cm}^2)$$

∴ Mass balance on salt gives:-

$$C_d t U_d \quad = (C_d + dC_d) tUd + idx/F \qquad (3.12.52)$$

$$\text{or, } - dC_d t U_d = idx/F \qquad (3.12.53)$$

$$-dC_d = \frac{i}{t} \frac{dx}{F U_d} \qquad (3.12.54)$$
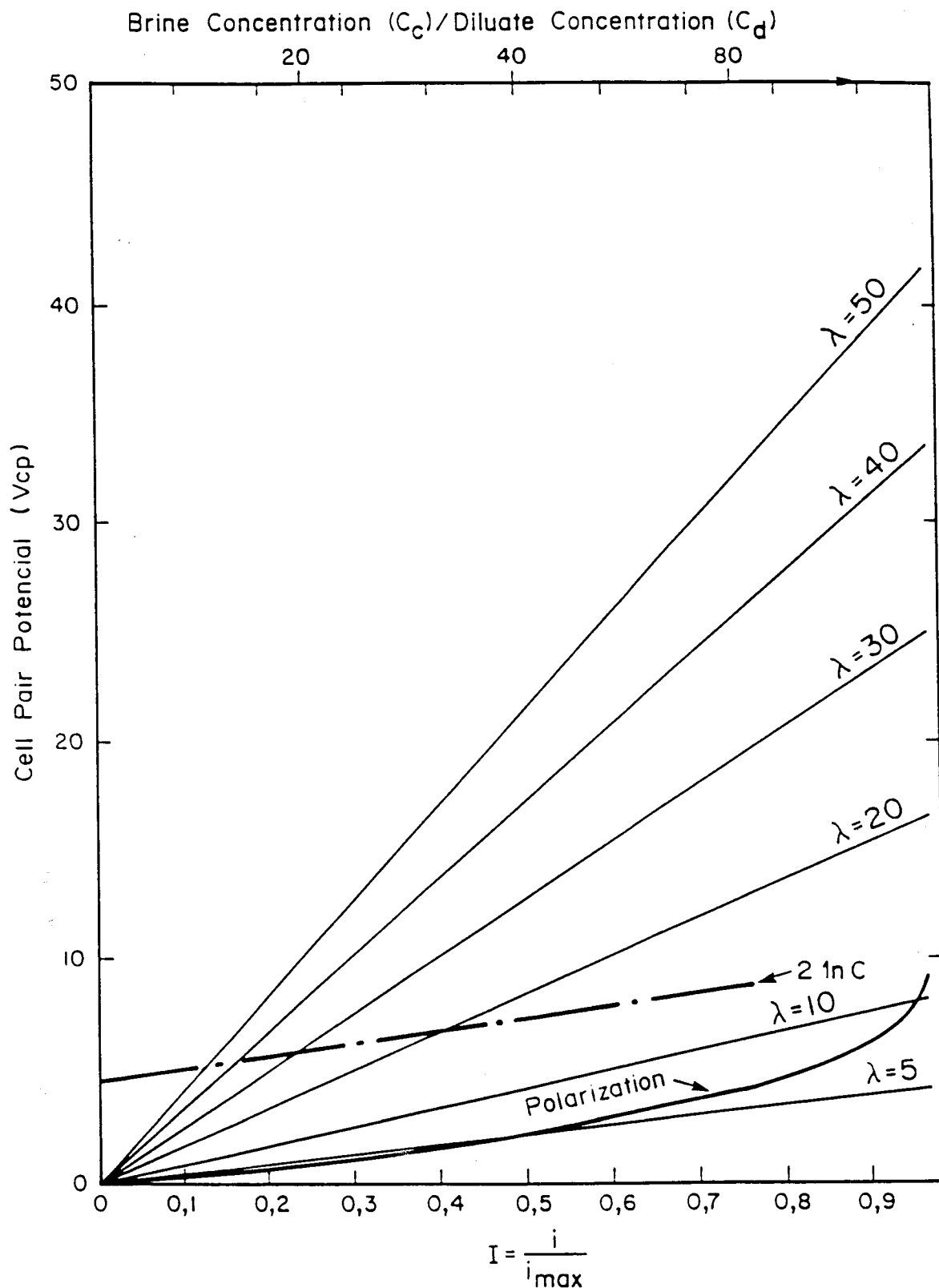
Figure 3.12.8: Effect of I on V_{cp} ($V_{cp} = \beta\lambda I$) at different cell to boundary layer thickness ratio's (λ) (simple resistive losses); effect of I on V_{cp} ($V_{cp} = -(1 + \beta)$ ln $(1 - I) - (1 + \underset{t_1}{t_2} \beta)$ ln $(1 - \underset{t_1}{t_1} I)$ (polarisation losses); effect of C (C_c/C_d) on V_{cp} ($V_{cp} = 2$ ln C) (useful potential).

If I in the above equation is replaced by the dimensionless current term $I = i/i_{max}$

$$\text{or} \qquad I = \frac{it_2\delta}{C_dFD} \qquad\qquad (3.12.55)$$

i.e. using the expression (derived earlier) for i_{max}:-

$$i_{max} = \frac{C_dFD}{t_2\delta} \qquad\qquad (3.12.56)$$

one obtain:

$$-dC_d = \frac{IC_dD}{t_2\delta} \times \frac{dx}{tU_d} \qquad\qquad (3.12.57)$$

or:

$$dx = -\frac{t_2\delta t\, U_d}{DI} \times \frac{dC_d}{C_d} \qquad\qquad (3.12.58)$$

$$\int_0^x dx = -\frac{t_2\delta tU_d}{DI} \int_{x-0}^x \frac{dC_d}{C_d} \qquad\qquad (3.12.59)$$

$$\therefore x = -\frac{t_2\delta tU_d}{DI} [\ln C_d(x) - \ln C_d(x=0)] \qquad\qquad (3.12.60)$$

$$= -\frac{t_2\delta tU_d}{DI} \ln \frac{C_d(x)}{C_d(x=0)} \qquad\qquad (3.12.61)$$

$$\text{and } C_d(x) = C_d(0)\, e^{-\left(\frac{DI}{t_2\delta tU_d}\right)x} \qquad\qquad (3.12.62)$$

$$= C_f\, e^{-\left(\frac{DI}{t_2\delta tU_d}\right)x} \qquad\qquad (3.12.63)$$
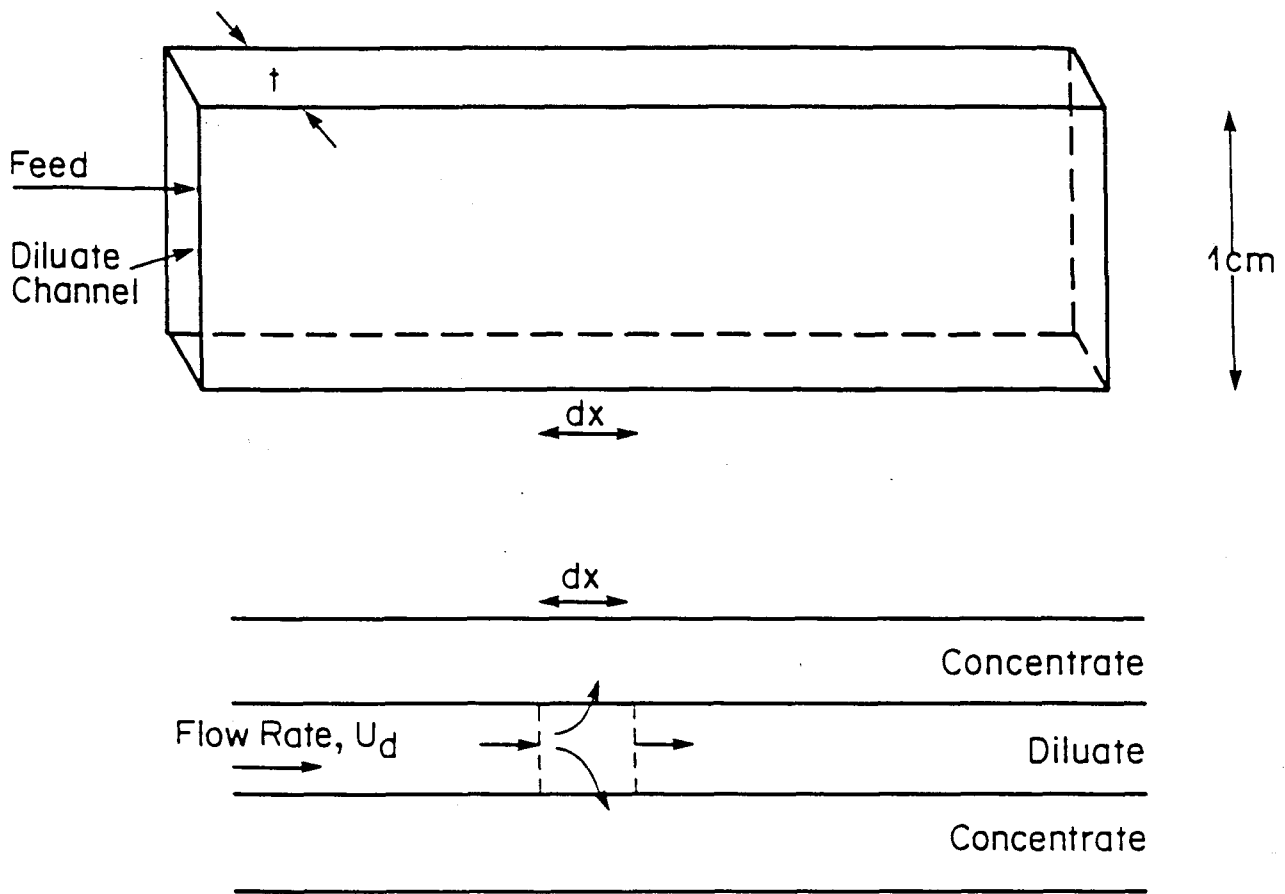
Figure 3.12.9: Flow through a diluate channel.

Now V_{cp} will be constant along the cell, but C_d and I will vary with x. Polarisation will be worse (i.e. highest value of I) at the stack entrance. Hence, if there is a "design" limit on polarisation it must be applied here (at x = 0). Hence, at this location $C_d = C_f$ (feed concentration) and $I = I_{max}$. It can therefore be worked out what the cell pair voltage will be at this point and this will be the value for the whole stack. Having settled on a value for V_{cp}, it can be examined how C_d and i (or I) vary with x. A typical result of such an analysis is shown in Figure 3.12.10.
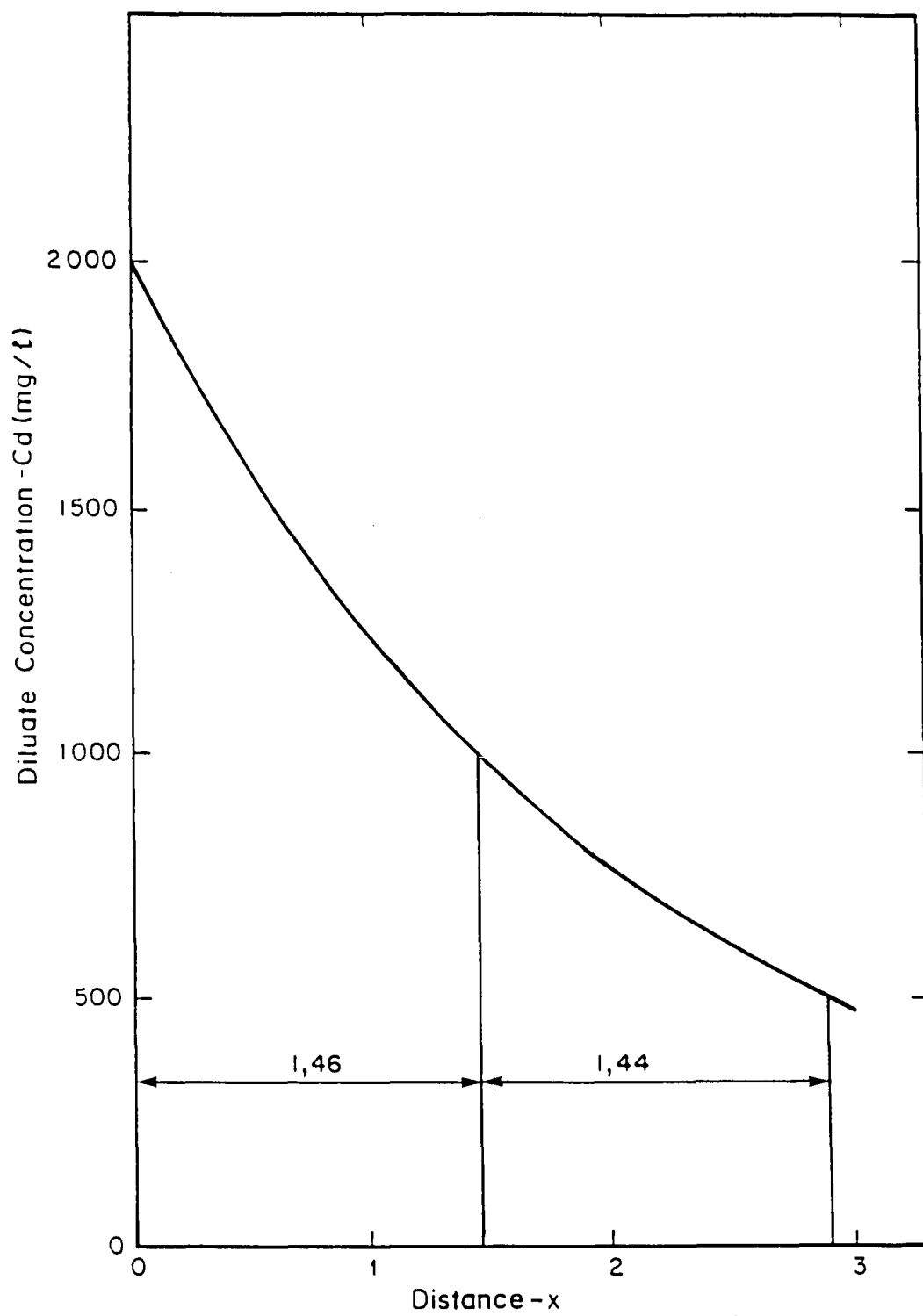
Figure 3.12.10: Variation of diluate concentration along cell pair.

4. ELECTRODIALYSIS IN PRACTICE

Electrodialysis technology has progressed significantly during the past 40 years since the introduction of synthetic ion-exchange membranes in 1949[53]. The first two decades of this period saw the development of classical or unidirectional standard electrodialysis. However, during the past decade, the main feature has been the development of the polarity reversal process - the so-called electrodialysis reversal (EDR)[84]. This form of electrodialysis desalination has virtually displaced unidirectional ED for most brackish water applications and is slowly gaining a significant share of this market.

EDR is at present mainly used for the desalination of brackish waters to produce fresh potable and industrial water. Unidirectional ED is used on a large scale in Japan for concentrating seawater to produce brine for salt production[85] and is also used on a small scale for seawater desalination[86] and for brackish water desalination[87].

Outside the water desalination field, ED is also being used on a large and increasing scale in North America and Europe to de-ash cheese whey to produce a nutritious high quality protein food supplement[53]. It is also finding application in the treatment of industrial waste waters for water recovery, reuse and effluent volume reduction[61, 88].

4.1 Electrodialysis Processes and Stacks

Different types of ED processes and stacks are used commercially for ED applications[6]. The filter-press- and the unit-cell stacks are the most familiar.

4.1.1 Filter-Press Stacks

The filter press stack configuration[6, 8] in which alternate cation- and anion-exchange membranes are arranged between compartment frames in a plate-and-frame filter press assembly is shown in Figure 4.1.

Salt solution flows between the alternately placed cation and anion permeable membranes in the ED stack. Direct current (DC) provides the motive force for ion migration through the ion-exchange membranes and the ions are removed or concentrated in the alternate water passage by means of permselective ion-exchange membranes. This process is called the standard ED process.
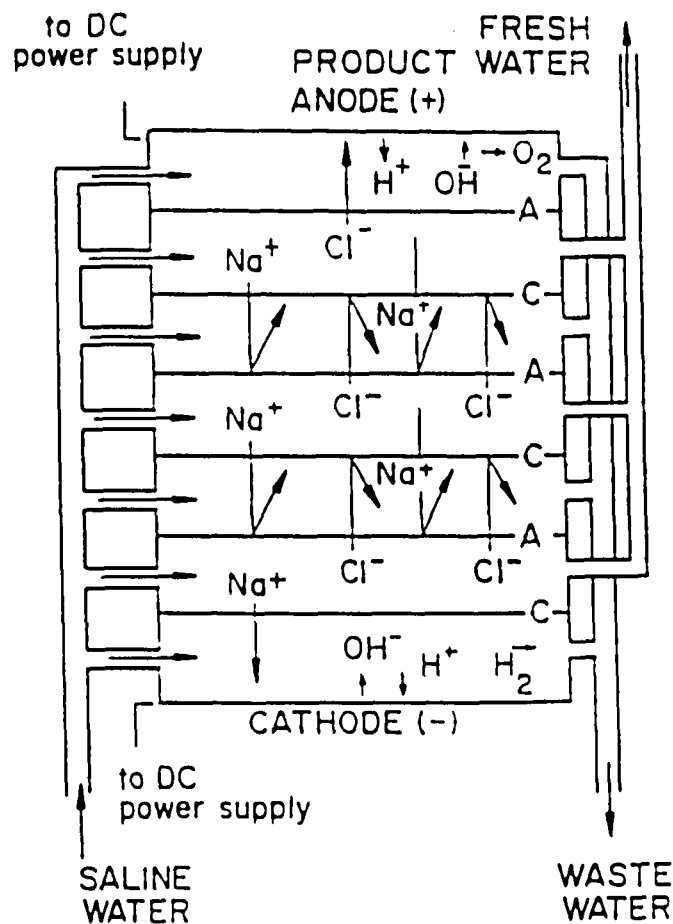
Figure 4.1: Plate-and-frame type EDR membrane stack.

C = cation membrane. A = anion membrane.

The standard ED process often requires the addition of acid and/or polyphosphate to the brine stream to inhibit the precipitation of sparsely soluble salts (such as $CaCO_3$ and $CaSO_4$) in the stack. To maintain performance, the membrane stack needs to be cleaned periodically to remove scale and other surface fouling matter. This can be done in two ways[8] by cleaning in-place (CIP); and stack disassembly.

Special cleaning solutions (dilute acids or alkaline brine) are circulated through the membrane stacks for in-place cleaning, but at regular intervals the stacks need to be disassembled and mechanically cleaned to remove scale and other surface-fouling matter. Regular stack disassembly is a time-consuming operation and is a disadvantage of the standard ED process.

The electrodialysis reversal process (EDR) operates on the same basic principles as the standard ED process. In the EDR process, the polarity of the electrodes is automatically reversed periodically (about three to four times per hour) and, by means of motor operated valves, the 'fresh product water' and 'waste water' outlets from the membrane stack are interchanged. The ions are thus transferred in opposite directions across the membranes. This aids in breaking up and flushing out scale, slime and other deposits from the cells. The product water emerging from the previous brine cells is usually discharged to waste for a period of one to two minutes until the desired water quality is restored.

The automatic cleaning action of the EDR process usually eliminates the need to dose acid and/or polyphosphate, and scale formation in the electrode compartments is minimized due to the continuous change from basic to acidic conditions. Essentially, therefore, three methods of removing scale and other surface fouling matter are used in the EDR process[8], viz., cleaning in place, stack disassembly as used in the standard ED process; and reversal of flow and polarity in the stacks. The polarity reversal system greatly extends the intervals between the rather time-consuming task of stack disassembly and reassembly, with an overall reduction in maintenance time.

The capability of EDR to control scale precipitation more effectively than standard ED is a major advantage of this process, especially for applications requiring high water recoveries. However, the more complicated operation and maintenance requirements of EDR equipment necessitate more labour and a greater skill level and may be a disadvantage of the process.

4.1.2   Unit-Cell Stack

A unit cell stack is shown in Figure 4.2. In this case the cation- and anion exchange membranes are sealed together at the edges to form a concentrating cell which has the shape of an envelope-like bag[6]. Many of these concentrating cells can be placed between electrodes in an ED stack.

The concentrating cells are separated by screen-like spacers. The feed flows between these concentrating cells and the direction of current through the stack is such as to cause ionic flow into the bags. Water flow into the cells is due to electro-osmosis (water is drawn along with the ions), and osmosis (water flows from the feed solution to the more concentrated brine). Small tubes are attached to each unit cell to allow

overflow of the brine. Because brine is pumped out of the cells mainly by the inflow of electro-osmotic water flow, this variant of ED is called electro-osmotic pumping ED.
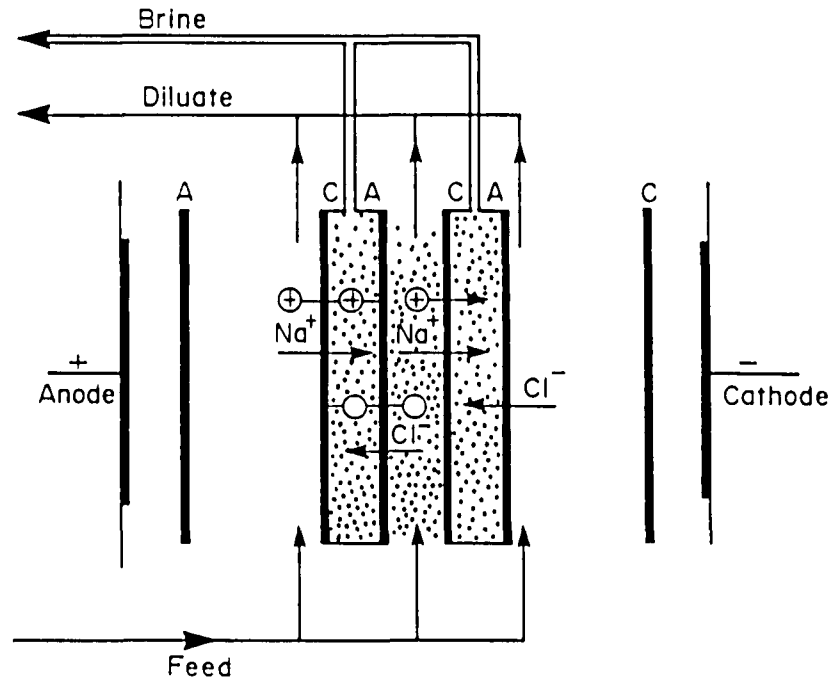
Figure 4.2: Schematic diagram of an ED unit cell stack.

C = cation membrane. A = anion membrane.

4.2 Ion-Exchange Membranes

Ion-exchange membranes are ion-exchangers in film form. There are two types: anion-exchange and cation-exchange membranes. Anion-exchange membranes contain cationic groups fixed to the resin matrix. The fixed cations are in electroneutrality with mobile anions in the interstices of the resin. When such a membrane is immersed in a solution of an electrolyte, the anions in solution can intrude into the resin matrix and replace the anions initially present, but the cations are prevented from entering the matrix by the repulsion of the cations affixed to the resin.

Cation-exchange membranes are similar. They contain fixed anionic groups that permit intrusion and exchange of cations from an external source, but exclude anions. This type of exclusion is called Donnan exclusion.

Details of methods for making ion-exchange membranes are presented in the literature[89 - 91] Heterogeneous membranes have been made by incorporating ion-exchange particles into film-forming resins (a) by dry molding or calendering mixtures of the ion-exchange and film-forming materials; (b) by dispersing the ion-exchange material in a solution of the film-forming polymer, then casting films from the solution and evaporating the solvent; and (c) by dispersing the ion-exchange material in a partially polymerized film-forming polymer, casting films, and completing the polymerization.

Heterogeneous membranes with usefully low electrical resistances contain more than 65% by weight of the cross-linked ion-exchange particles. Since these ion-exchange particles swell when immersed in water, it has been difficult to achieve adequate mechanical strength and freedom from distortion combined with low electrical resistance.

To overcome these and other difficulties with heterogeneous membranes, homogeneous membranes were developed in which the ion-exchange component forms a continuous phase throughout the resin matrix. The general methods of preparing homogeneous membranes are as follows[6]:

- Polymerization of mixtures of reactants (e.g., phenol, phenolsulfonic acid, and formaldehyde) that can undergo condensation polymerization. At least one of the reactants must contain a moiety that either is, or can be made, anionic or cationic.

- Polymerization of mixtures of reactants (e.g., styrene, vinylpyridine, and divinylbenzene) that can polymerize by additional polymerization. At least one of the reactants must contain an anionic or cationic moiety, or one that can be made so. Also, one of the reactants is usually a cross-linking agent to provide control of the solubility of the films in water.

- Introduction of anionic or cationic moieties into preformed films by techniques such as imbibing styrene into polyethylene films, polymerizing the imbibed monomer, and then sulfonating the styrene. A small amount of cross-linking agent (e.g., divinylbenzene) may be added to control leaching of the ion-exchange component. Other similar techniques, such as graft polymerization of imbibed monomers, have been used to attach ionized groups onto the molecular chains of preformed films.

- Casting films from a solution of a mixture of a linear film-forming polymer and

a linear polyelectrolyte, and then evaporating the solvent.

Membranes made by any of the above methods may be cast or formed around scrims or other reinforcing materials to improve their strength and dimensional stability.

The properties of some representative commercially available ion-exchange membranes as reported by the manufacturers are shown in Table 4.1[6].

Table 4.1: Reported Properties of Ion-Exchange Membranes*

Manufacturer and Designation	Type of Membrane	Area Resistance (ohm-cm²)	Transference Number of Counterion[a]	Strength	Approximate Thickness (mm)	Dimensional Changes on Wetting and Drying (%)	Size available
AMF[b]		(0,6 N KCl)		Mullen burst (kPa)			
C-60	Cat-exch	5 ± 2	0,80 (0,5/1,0 N KCl)	310	0,30		
C-100	Cat-exch	7 ± 2	0,90 (0,5/1,0 N KCl)	414	0,22	10 - 13	1,1 m wide rolls
A-60	An-exch	6 ± 2	0,80 (0,5/1,0 N KCl)	310	0,30		
A-100	An-exch	8 ± 2	0,90 (0,5/1,0 N KCl)	379	0,23	12 - 15	1,1 m wide rolls
ACI[c]		(0,5 N NaCl)		Tensile strength (kg/mm²)			
CK-1	Cat-exch	1,4	0,85 (0,25/0,5 N NaCl)		0,23		
DK-1	Cat-exch	1,8	0,85 (0,25/0,5 N NaCl)	2 to 2,4	0,23	15 - 23	1,1 x 1,1 m
CA-1	An-exch	2,1	0,92 (0,25/0,5 N NaCl)		0,23		
DA-1	An-exch	3,5	0,92 (0,25/0,5 N NaCl)	2 to 2,3	0,23	12 - 18	1,1 x 1,1 m
AGC[d]		(0,5 N NaCl)		Mullen burst (kPa)			
CMV	Cat-exch	3	0,93 (0,5/1,0 N NaCl)	1 241	0,15		
CSV	Cat-exch	10	0,92 (0,5/1,0 N NaCl)	1 241	0,30		
AMV	An-exch	4	0,95 (0,5/1,0 N NaCl)	1 531	0,15	< 2	1,1 m wide rolls
ASV	An-exch	5	0,95 (0,5/1,0 N NaCl)	1 531	0,15		
IC[f]		(0,1 N NaCl)		Mullen burst (kPa)			
MC-3142	Cat-exch	12	0,94 (0,/51,0 N NaCl)	1 379	0,20		
MC-3235	Cat-exch	18	0,95 (0,/10,2 N NaCl)	1 137	0,30	< 3[g]	1 x 3 m
MC-3470	Cat-exch	35	0,98 (0,/10,2 N NaCl)	1 379	0,20		
MA-3148	An-exch	20	0,90 (0,5/1,0 N NaCl)	1 379	0,20		
MA-3236	An-exch	120	0,93 (0,5/1,0 N NaCl)	1 137	0,30	< 3[g]	1 x 3 m
IM-12	An-exch[h]	12	0,96 (0,1/0,2 N NaCl)[g]	999	0,15[g]	Not given	
MA-3475R	An-exch	11	0,99 (0,5/1,0 N NaCl)	1 379	0,36	Not given	
II[i]				Mullen burst (kPa)			
CR-61	Cat-exch	11	0,93 (0,2 N NaCl)[b]	793	0,58	Cracks on	
AR-111A	An-exch	11	0,93 (0,1/0,2 N NaCl)	862	0,61	drying	0,5 x 1 m
TSC[j]			(by electrophoretic method in 0,5 N NaCl)	Mullen burst (kPa)			
CL-2,5T	Cat-exch	3	0,98	551	0,15		
CLS-25T	Cat-exch[k]	3	0,98	551	0,15	Not given	1 x 1,3 m
AV-4T	An-exch	4	0,98	1 034	0,18		
AVS-4T	An-exch[k]	5	0,98	965	0,18	Not given	1 x 1,3 m

4.3   Fouling

Fouling of ED membranes by dissolved organic and inorganic compounds may be a serious problem in practical electrodialysis[6, 92, 93] unless the necessary precautions (pretreatment) are taken.   Organic fouling is caused by the precipitation of large negatively charged anions on the anion-permeable membranes in the dialysate compartments.

Organic fouling of anion permeable membranes takes place in a number of ways[92]:

a)   The anion is small enough to pass through the membrane by electromigration but causes only a small increase in electrical resistance and a decrease in permselectivity of the membrane;

b)   The anion is small enough to penetrate the membrane, but its electromobility in the membrane is so low that its hold-up in the membrane causes a sharp increase in the electrical resistance and a decrease in the permselectivity of the membrane;

c)   The anion is too big to penetrate the membrane and accumulates on the surface (to some extent determined by the hydrodynamic conditions and also by a phase change which may be brought about by the surface pH).   The decrease in electrical resistance and permselectivity of the membrane is slight. The accumulation can be removed by cleaning.

In case (c) the electrodialysis process will operate without serious internal membrane fouling and only mechanical (or chemical) cleaning will be necessary. Case (b) would make it almost impossible to operate the electrodialysis process.   In case (a), the electrodialysis process can be used if the concentration of large anions in solution is low or if the product has a high enough value to cover the high electrical energy costs.

Inorganic fouling is caused by the precipitation (scaling) of slightly soluble inorganic compounds (such as $CaSO_4$ and $CaCO_3$) in the brine compartments and the fixation of multivalent cations (such as Fe and Mn) on the cation-permeable membranes. Organic anions or multivalent cations can neutralize or even reverse the fixed charge of the membranes, with a significant reduction in efficiency. Fouling also causes an increase in membrane stack resistance which, in turn, increases electrical consumption and adversely effects the economics of the process.

The following constituents are, to a greater of lesser extent, responsible for membrane fouling[94]:

- Traces of heavy metals such as Fe, Mn and Cu.
- Dissolved gases such as O_2, CO_2 and H_2S.
- Silica in diverse polymeric and chemical forms.
- Organic and inorganic colloids.
- Fine particulates of a wide range of sizes and composition.
- Alkaline earths such as Ca, Ba and Sr.
- Dissolved organic materials of both natural and man-made origin in a wide variety of molecular weights and compositions[92].
- Biological materials - viruses, fungi, algae, bacteria - all in varying stages of reproduction and life cycles.

Many of these foulants may be controlled by pretreatment steps which usually stabilize the ED process. However, according to Katz[94], the development of the EDR process has helped to solve the pretreatment problem more readily in that it provides self-cleaning of the vital membrane surfaces as an integral part of the desalting process.

4.4 Pretreatment

Pretreatment techniques for ED are similar to those used for RO[8]. Suspended solids are removed by sand and cartridge filters ahead of the membranes. Suspended solids, however, must be reduced to a much lower level for RO than for ED. The precipitation of slightly soluble salts in the standard ED process may be minimized by ion-exchange softening and/or reducing the pH of the brine through acid addition and/or the addition of an ihibiting agent.

Organics are removed by carbon filters, and hydrogen sulphide by oxidation and filtration. Biological growths are prevented by a chlorination-dechlorination step. The dechlorination step is necessary to protect the membranes from oxidation. Iron and manganese are removed by green sand filters, aeration, or other standard water treatment methods. It has been suggested that multivalent metal and organic ions, and hydrogen sulphide, however, must be reduced to a lower level for EDR than for RO[95].

The overall requirements for pretreatment in ED, may be somewhat less rigorous than for RO due to the nature of the salt separation and the larger passages provided[8].

In ED, the ions (impurities) move through the membranes, while in RO the water moves under a high pressure through the membranes while the salts are rejected. Salts with a low solubility can, therefore, more readily precipitate on spiral and hollow fine fibre RO membranes to cause fouling and to block the small water passages. Suspended solids can also more readily form a deposit. However, this might not be the case with tubular RO membranes. With the EDR process, precipitated salts in the brine compartments can be more readily dissolved and flushed out of the system using polarity reversal without the need for chemical pretreatment.

However, high removals of suspended solids, iron, manganese, organics and hydrogen sulphide are still critical to avoid fouling and suppliers of EDR equipment recommend pretreatment of the feed water[8], if it contains the following ions: $Fe > 0,3$ mg/ℓ; $Mn > 0,1$ mg/ℓ; $H_2S > 0,3$ mg/ℓ; free chlorine and turbidity > 2 NTU. In every case, of course, a careful examination of the prospective water would be necessary to determine suitability and pretreatment.

A certain degree of fouling is, however, unavoidable. Membranes should, therefore, be washed regularly with dilute acid and alkali solutions to restore performance.

4.5   Post-treatment

The EDR product water is usually less aggressive than the RO product because acid is usually not added in EDR for scale control[95]. Post-pH adjustment may, therefore, not be required as with RO. Non-ionic matter in the feed such as silica, particulates, bacteria, viruses, pyrogens and organics will not be removed by the ED process and must, if necessary, be dealt with during post-treatment.

4.6   Seawater Desalination

There is limited application of ED for seawater desalination because of high costs[8]. A small batch system (120 m³/d) has been in operation in Japan since 1974 to produce water of potable quality at a power consumption of 16,2 kWh/m³ product water[96]. A 200 m³/d seawater EDR unit was evaluated in China[97]. This unit operated at 31°C; its performance was stable; total electric power consumption was 18,1 kWh/m³ product water and the product water quality of 500 mg/ℓ TDS met all the requirements for potable water. When the stacks were disassembled for inspection, there were no signs of scale formation.

With the commercial ED units currently available, the energy usage for seawater desalination is relatively high compared with that of RO. However, work under the Office of Water Research and Technology (OWRT) programmes has indicated that high-temperature ED may possibly be competitive with RO[98]. Results have shown that the power consumption can be reduced to the levels required for seawater RO (8 kWh/m³) and that a 50% water recovery can probably be attained.

4.7 Brackish Water Desalination for Drinking-Water Purposes

A considerable number of standard ED plants for the production of potable water from brackish water are in operation[8, 87]. These plants are operating successfully. However, after the introduction of the reversal process in the early 1970's, Ionics Incorporated shifted almost all their production to this process[94].

The major application of the EDR process is for the desalination of brackish water. The power consumption and, to some degree, the cost of equipment required is directly proportional to the TDS to be removed from the feed water[8]. Thus, as the feedwater TDS increases, the desalination costs also increase. In the case of the RO process, a cost: TDS removal relationship also exists, but it is not as pronounced. Often the variation in the scaling potential of the feed water and its effect on the percentage of product water recovery can be more important than the cost: TDS relationship.

Thus, for applications requiring low TDS removals, ED is often the most energy-efficient method, whereas with highly saline feed waters RO may be expected to use less energy and is preferred. The economic crossover point between ED and RO based on operating costs is, however, difficult to define precisely and needs to be determined on a site-specific basis. Apart from local power costs, other factors must also be considered in determining the overall economics. Among these, to the advantage of ED, are the high recoveries possible (up to 90%), the elimination of chemical dosing (with EDR), and the reliability of performance that is characteristic of the ED process.

4.8 Energy Consumption

The energy consumption of a typical EDR plant is as follows[8]:

Pump   :   0,5 to 1,1 kWh/m³ product water
Membrane stack   :   0,7 kWh/m³ product water/1 000 mg of TDS removed
Power losses   :   5% of total energy usage

The major energy requirement, therefore, is for pumping the water through the ED unit and for the transport of the ions through the membranes.

4.9   Treatment of a High Scaling, High TDS Water with EDR

The successful performance of EDR on high calcium sulphate waters has been reported[84]. Brown[99] has described the performance of and EDR plant treating 300 m^3/d of a high calcium sulphate water with a TDS of 9 700 mg/ℓ. The only pretreatment applied was iron removal on green sand. The quality of the feed, product and brine is shown in Table 4.2

The water recovery and energy consumption were 40% and 7,7 kWh/m^3 of product water, respectively. No attempt was made to optimize water recovery. The stack resistance increased by only 3% after one year of operation, which clearly indicates the successful operation of the EDR unit in spite of the super saturated condition of the brine with respect to calcium sulphate. Membrane life times are estimated to be 10 years.

The main developments in EDR during the past few years have been the following:

- **EDR has achieved CaSO₄** saturation in the brine stream of up to 440% without performance decline on tests of several hundred hours' duration[99].

- EDR has desalted a hard (Ca^{2+} approx. 150 mg/ℓ) brackish water of 4 000 mg/ℓ TDS at water recoveries of up to 93% without cumbersome and expensive pre-softening[94].

- An EDR test unit has achieved 95% or greater recovery of a limited 4 000 mg/ℓ TDS brackish water resource by substituting a more abundant 14 000 mg/ℓ saline water in the brine stream[100]. The substitution of seawater in the brine stream would be freely available in coastal or island locations with limited high quality brackish water resources.

- The development, extensive field testing and subsequent large-scale commercial usage of a new family of thick (0,5 mm), rugged anti-fouling anion-permeable membranes in the USA with much higher current efficiencies and chlorine resistance than those formerly available[100].

Table 4.2:   Water Quality Before and After EDR Treatment

Constituent	Feed (mg/ℓ)	Product (mg/ℓ)	Brine (mg/ℓ)
Na$^+$	2 090	79	3 694
Ca^{++}	652	4	1 390
Mg^{++}	464	4	964
Cl$^-$	3 687	111	7 084
HCO$_3^-$	134	25	175
SO$_4^-$	2 672	19	5 000
TDS	9 727	242	18 307
pH	7,0	6,8	7,2

4.10   Brackish Water Desalination for Industrial Purposes

In the past most ED plants treated brackish waters of 1 000 to 10 000 mg/ℓ TDS and produced general purpose industrial product water of 200 to 500 mg/ℓ TDS. However, ED capital and construction costs have declined during recent years to the point where it is already feasible to treat water containing 200 to 1 000 mg/ℓ TDS and produce product water containing as little as 3 to 5 mg/ℓ TDS[101]. These low TDS levels are achieved by multistaging. The systems, which often employ ion-exchange (IX) units as 'polishers', are usually referred to as ED/IX systems.

4.11   ED/IX System

New and existing ion-exchange facilities can be converted to ED/IX systems by addition of ED units upstream of the ion-exchange units. The ED unit reduces chemical consumption, waste, service interruptions and resin replacement of the ion-exchanger in proportion to the degree of prior mineral removal achieved[101]. For small capacity systems (2 to 200 m³/d) the optimum ED demineralization will usually be 90% or greater; for larger installations, and particularly those where adequate ion-exchange capacity is already provided, the optimum demineralization via ED is more likely to be in the 60 to 80% range.

It must, however, be stressed that RO may also be used for the abovementioned application. RO may function better than ED because it removes silica and organic material better than ED. However, the choice of the treatment method (ED or RO) would be determined by the specific requirements and costs for a particular situation.

Honeywell in the USA, which manufactures printed circuit boards and does zinc plating and anodizing, used IX for the treatment of their process waters before they changed

over to an ED/IX system[102]. ED was chosen instead of RO because of lower membrane replacement costs. Process waters of varying degrees of purity are required, dissolved solids being the primary concern. Water with a TDS of about 50 mg/ℓ is suitable for zinc plating and anodizing and water with a TDS with a minimum specific resistance of 100 000 ohms is satisfactory for circuit board fabrication operations[102]. The purity of the treated water (raw water TDS - 250 to 500 mg/ℓ) after treatment with the ED/IX system was better than expected. Service runs have been up to ten times longer than before.

4.12 Industrial Wastewater Desalination for Water Reuse, Chemical Recovery and Effluent Volume Reduction

Large volumes of water containing varying amounts of salt, which are generated by washing and regenerating processes, blowdown from cooling towers, disposal of dilute chemical effluents, to name a few, present significant problems, particularly when zero effluent discharge is required. The problem is one of too much water carrying comparatively little salt, but still having a TDS content too great for acceptance to a receiving stream. Many industries face this problem today and have to consider the application of processes for concentrating salts or desalting water. The ED system for water recovery and brine concentration may be one of the best suited to alleviate the problem.

Some typical examples are given to illustrate this principle:

4.12.1 Electrodialysis of nickel plating solutions

During many plating operations, a substantial amount of bath solution adheres to plated work pieces as they leave the plating tank. In this manner valuable materials are lost as 'drag-out' into the subsequent rinse tank. This contaminated rinse solution can be passed through an ED system where these valuable materials can be recovered and returned to the plating tank.

One such opportunity of significant industrial importance is provided by nickel electroplating operations[103]. Earlier work by Trivedi and Prober[104] demonstrated the successful application of ED to nickel solutions. Later, Eisenmann[105] and Itoi[103] reported the use of ED to recover nickel from electroplating rinse waters.
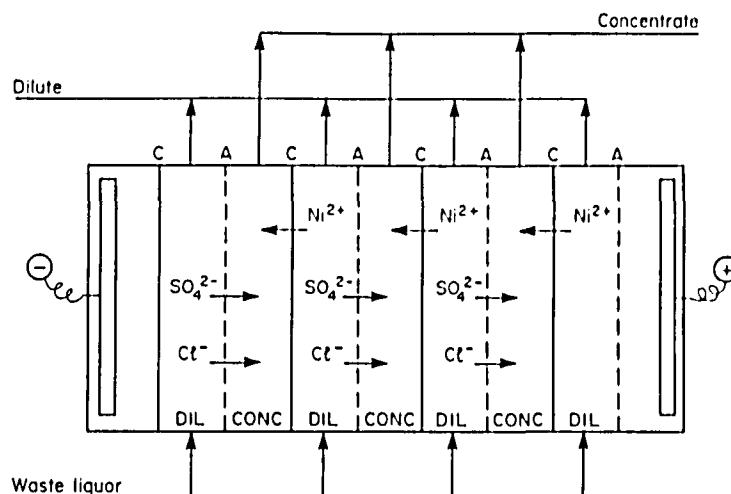
Figure 4.3: Electrodialysis of the washwater from a nickel galvanizing operation.

The wash water from a nickel galvanizing line is treated by ED as shown in Figure 4.3.

The results achieved in an existing facility are given in Table 4.3. The concentration ratio of the concentrated solution to the dilute solution is greater than 100. The concentrated solution is reused in the plating bath while the dilute solution is reused as wash water. The recovery of nickel discharged from the wash tank is approximately 90% or greater.

If organic electrolytes are present in the additives used in the galvanization bath, they must be removed prior to ED treatment to prevent organic fouling of the ED membranes.

Table 4.3: Electrodialysis of a Nickel Galvanization Effluent

Constituent	Effluent (g/ℓ)	Concentrate (g/ℓ)	Diluent (g/ℓ)
$NiSO_4$	12,47	133,4	1,27
$NiCl_2$	1,81	29,1	0,039

4.12.2 Treatment of cooling tower blowdown for water recovery and effluent volume reduction

The range of TDS levels encountered in cooling tower blowdown waters usually varies from about 1 500 to 4 000- mg/ℓ and higher levels at about 4 000 to 12 000- mg/ℓ

have also been reported[106]. The disposal of large volumes of this saline effluent can be a serious problem. The application of ED for the treatment of blowdown streams to recover good quality water for reuse and produce a small volume of concentrate promises to be the best prospective system available[107,108].

Blowdown waters from cooling towers can be concentrated tenfold or more using ED, while recovering and recycling the desalted water to the cooling tower at one-half its original concentration[88]. To accomplish this, blowdown is pretreated, filtered and passed through the ED system. By recirculation of the brine, it is possible to concentrate the salts into a small stream, while allowing for recovery of about 90% of the water.

The concentration of cooling blowdown waters in an EDR pilot plant at one of Eskom's power stations was evaluated[61]. Pretreatment of the blowdown water with lime softening, clarification, pH reduction, filtration and chlorination was found to be a basic precondition for successful operation. The operating experience on the EDR pilot plant was sufficiently positive to warrant full-scale application.

Detailed design studies and cost estimates for ED and several other alternative blowdown recovery/concentration systems have been reported[88]. The side stream process design which utilizes ED results in the lowest capital costs for the conditions specified. According to Wirth and Westbrook[88], it is expected that if the cost comparison were made on overall annual operating costs, the same results would occur.

4.13   Other Possible Industrial Applications

4.13.1 Concentration of sodium sulphate and its conversion into caustic soda and sulphuric acid

A pilot study has demonstrated the feasibility of the concentration of a sodium sulphate solution with ED in a first stage and the subsequent conversion into caustic soda and sulphuric acid in a second stage[109]. The sodium sulphate solution (20 to 40 g/ℓ) was treated in a multi-compartment electrodialyzer to yield a brine (260 - 320 g/ℓ, 10% of feed volume) and a product (2 g/ℓ, 90% of feed volume) which could be used as reclaimed water.

The brine was treated further in a three-compartment electrodialyzer to produce caustic soda and sulphuric acid at a concentration of 17 to 19% by mass and a power consumption of approximately 3,1 to 3,3 kWh/kg sodium sulphate decomposed. The sodium sulphate content of both products was about 1%.

4.13.2 Recovery of acid and caustic soda from ion-exchange regeneration wastes

Laboratory results of an electrodialytic process for acid and caustic recovery from ion-exchange regenerant wastes have been described[110]. The object of the study was to minimize the discharge of dissolved salts from a water treatment plant producing boiler feed water while recovering some of the pollution abatement process costs from the savings in regenerant chemical costs.

It was shown that the electrodialytic process for recovery of sulphuric acid and sodium hydroxide from ion-exchange regenerant wastes, and substantially reducing the amount of salt discharged to drain, is technically feasible. The nett costs for acid and caustic waste treatment was estimated at US $4,20 and $3,00/$m^3$ waste treated, respectively.

4.13.3 Concentration of dilute chemical effluents

Laboratory investigations have shown that dilute (approximately 2%) solutions of NH_4NO_3, Na_2SO_4, $NaNO_3$ and $NaCl$ can be concentrated to approximately 20% by ED at an energy consumption of about 1 kWh/kg salt[111]. The brine volumes were less than 10% of the original volume.

4.14 Polarisation

The current which is passed through an ED stack is carried almost exclusively by ions of the same sign. In the solution, all types of ions carry this current. The rate at which the current can pass through the solution is limited by the diffusion rate of ions to the membrane surface since there will inevitably be changes in the concentration of the solution close to the membrane surface. It is apparent that as the current density is increased, it becomes more difficult for the ions in the solution to carry the required current. This effect is know as concentration polarization[11]. The greater the current density used the greater are these polarization effects. Polarization also becomes a problem the more dilute the solution becomes.

The main effects of polarization are[6]:

i)   the differences in concentration result in increased membrane potentials and
        so the power required per unit charge passed is increased.

ii)   The current efficiency can also be reduced which means that the current
        required per unit of output is also increased.

iii)   When it is attempted to carry current in excess of the ions available to be
        transported through the membrane, the water "splits" into hydroxide and
        hydrogen ions. At the anion membrane the current is carried by hydroxide
        ions through the membrane and hydrogen ions are rejected to the solution.
        At the cation membrane the opposite effect occurs: hydroxide ions are
        transported to the membrane and are rejected to the solution. This effect is
        to be avoided since, firstly, both the current and the voltage efficiency are
        reduced (some of the current serves to split the water instead of desalting it
        and there is an increased voltage requirement) and secondly, when the water
        splits the pH in the boundary layer on the membrane surface can change
        increasing the likelihood of scale formation.

4.15   Cell Stack

It has already been shown that the basic unit in an ED plant is the cell pair where
cation and anion permeable membranes are alternately arranged so as to produce
adjacent diluate and concentrate streams. A number of cell pairs are located between
a pair of electrodes to form what is known as a cell stack. The number of cell pairs
varies depending on the manufacturer but is usually about 300.

In any cell pair the membranes are separated by a spacer. The hydrodynamic design
of the flow between the membranes is of extreme importance[6]. It is essential that as
far as it is practicable turbulent flow exists in individual cell pairs. Streamline flow
produces a relatively stagnant or slow moving layer on the membrane surface. Since
the current carrying ions have to diffuse through this film at low solution concentration,
polarization becomes more likely. There are a number of requirements a spacer must
meet. The fluid should flow at the same rate across the whole active membrane area
and should be turbulent within the limits of pressure drop. The manifold must supply
each spacer equally. The spacer should support the membrane, this being particularly

important in the region between the manifolds. The spacer material should be inert, should possess physical properties so as to permit a hydraulic seal when pressurised and be dimensionally stable.

The spacers are usually perforated PVC nets and, depending on the design, are 0,5 mm to 1 mm thick[6]. The size of the spacer depends on the size of the membrane used. In general, large components tend to cost less per unit of effective membrane area. However, practical considerations such as the ease of handling and mechanical strength must be taken into account. Components which are thin result in lower operating costs but there are difficulties in providing good flow distribution. It is apparent that the presence of the spacer reduces the active membrane area since it also serves to support the membrane. There is an advantage in utilising as much of the membrane surface area as possible but this results in difficulties in supporting and sealing the membranes. A membrane of about 1,5 m^2 is probably the maximum practicable, usually the area is 0,5 m^2 to 1 m^2. The effective membrane area is about 85 % of the total membrane area.

Stack sealing is of importance to stack operation. The spacer should seal easily since the lower compression force required to seal the stack, the less likely will be the chance of damaging components. This aspect of design becomes most complex in the region of manifolds. This area should be as small as possible but should not cause a high pressure drop. Also, since a seal must be made round this area the support in this region must be able to withstand the compressive scaling forces of the stack.

The stack itself should be easy to maintain. It often occurs that only a few cell pairs in the stack require maintenance. In a large stack it is desirable to be able to open the stack at any section and remove a cell pair without disturbing any of the other cell pairs.

The electrodes must be made of a material which is corrosion resistant, since at the cathode the flow becomes alkaline while at the anode gaseous chlorine and oxygen are formed. It is normal to have separate feeds to the anode and cathode, the anode rinse going to a drain while the cathode rinse is treated with acid and then recirculated. The maximum voltage across a stack is 3 volts per cell pair and so a normal stack voltage will be about 900 volts.

4.16   Process Design

Since the amount of desalting depends directly on the current level it is a straight-forward exercise to calculate the performance of a given stack at a particular current density. In order to achieve a given level of desalination the plant can either be run in a batch process or in a once-through process[6].

In a batch process, the water to be desalinated is stored in a tank and then partially desalted by passing it through the stack to a second tank having been further desalted. After each pass the concentration is checked and the process is repeated until the required level of demineralization is achieved. This method is often used when the feed water is subject to changes in composition. For example, in a lot of cases brackish well water is liable to increase in salinity at high pumping rates.

In a once-through system, the required desalting is achieved by passing the diluate stream through successive stacks arranged hydraulically in series. This process tends to be used in the higher capacity plants and requires less control systems. Where possible (i.e. where the feed water salinity can be guaranteed) a continuous type of plant is always to be preferred. Since plant operation is simpler, the likelihood of breakdown is reduced and the capital cost is reduced.

In both systems the concentrate streams are recycled to minimize blow-down and possible use of chemicals. The flow of the concentrate stream is normally 25% or less than that of the diluate stream. To minimize the electrical resistance of the stack it is desirable to have the concentrate stream at the maximum concentration possible (this also minimizes the blow-down to waste). The normal limiting factor for the degree of concentration is the solubility of calcium sulphate.

In both systems the limiting current density controls the amount of desalination possible. The onset of polarization manifests itself in the change of chemical conditions in the plant and also in an increase in the voltage requirements maintaining the current. The lower the salt content in the water, the lower will be the limiting current density. Electrodialysis, therefore, is not applicable in the production of high purity waters.

5. EXPERIMENTAL

5.1 Membranes

The membrane and membrane types shown in Table 5.1 were selected for the EOP study of sodium chloride-, hydrochloric acid- and caustic soda solutions.

Table 5.1 **Membrane and membrane types selected for EOP of Sodium Chloride-, Hydrochloric Acid- and Caustic Soda Solutions**

Membranes	Anionic (A) Cationic (C)	Type	Salt	Acid	Base
Selemion AMV	A	Homogeneous	✓	✓	✓
Selemion CMV	C	Homogeneous	✓	✓	✓
Ionac MA 3470	A	Heterogeneous	✓	✓	✓
Ionac MC 3475	C	Heterogeneous	✓	✓	✓
Raipore R 4030	A	Homogeneous	✓		
Raipore R 4010	C	Homogeneous	✓		
Ionics A 204 UZL 386	A	Homogeneous	✓		
Ionics C 61 CZL 386	C	Homogeneous	✓		
WTPSA-1	A	Heterogeneous	✓		
WTPSC-1	C	Heterogeneous	✓		
WTPVCA-2	A	Heterogeneous	✓		
WTPVCC-2	C	Heterogeneous	✓		
WTPSTA-3	A	Heterogeneous	✓		
WTPSTC-3	C	Heterogeneous	✓		
Selemion AAV	A	Homogeneous		✓	
Selemion CHV	C	Homogeneous		✓	
ABM-1	A	Homogeneous		✓	
Selemion CHV	C	Homogeneous		✓	
ABM-2	A	Heterogeneous		✓	
Selemion CHV	C	Homogeneous		✓	
ABM-3	A	Heterogeneous		✓	
Selemion CHV	C	Homogeneous		✓	
Selemion AMP	A	Homogeneous			✓
Selemion CMV	C	Homogeneous			✓

5.2 Membrane Preparation

The WTA (WATERTEK anion) and WTC (WATERTEK cation) ion-exchange membranes were prepared as follows:

Resin (strong acid and strong base) with a particle size of less than 70 μm was suspended in appropriate swelling, base and casting solutions and the membranes were cast on polypropylene support material. The membranes were dried for approximately 1 hour in a convection oven at temperatures from 65 to 80°C before use. Polysulphone (for WTPSA-1; WTPSC-1 membranes), polyvinyl chloride (for

WTPVCA-2, WTPVCC-2 membranes) and polystyrene (for WTPSTA-3, WTPSTC-3 membranes) were used as base materials. N- methyl-2 pyrolidone (NMP) was used as casting solution for the polysulphone (PS) based membranes while cyclohexanone was used as casting solution for the polyvinyl chloride and polystyrene based (PST) membranes.

The ABM membranes for acid EOP studies were supplied by the membrane research group of the Weizmann Institute of Science in Israel. The membranes used in the sealed-cell ED tests were also developed by the membrane research group of the Weizmann Institute of Science in Israel. The membranes were made from microbeads of styrene-divinylbenzene copolymer which were modified to cation- and anion-exchange particles. The cation-exchange particles were formed by chlorosulphonation with chlorosulphonic acid followed by hydrolysis to yield the sulphonated product. The anion-exchange particles were formed by chloromethylation followed by amination with triethylamine to yield the anion-exchange particles.

The ion-exchange membranes were formed by casting a suspension of the particles on a fabric. The suspension was evaporated to dryness to yield the dry membrane. The cation- and anion-exchange membranes were then heat-sealed to give the membrane bags.

5.3   Unit-Cell Construction

A unit cell can be constructed in the following number of ways : -

a)   glueing the membrane edges together with a suitable glue;

b)   glueing the membrane edges to either side of an injection moulded nylon ring (Figure 5.1) which has a brine exit within it[1];   and

c)   mounting of the membranes between gaskets as in the filter press stack design.

For experiment, the volume, however, of the brine compartment must be kept to a minimum in order to minimize time for achieving the steady state and for beginning to measure water flow. An injection moulded nylon ring (Figure 5.1) was used in the EOP experiments as the unit cell.
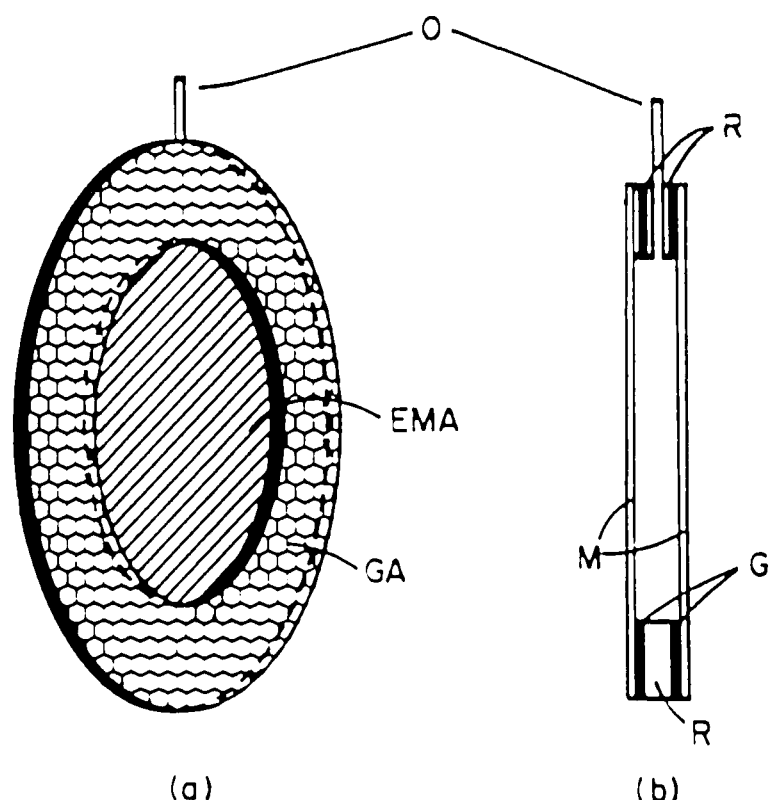
Figure 5.1: Schematic of injection moulded nylon ring that was used for construction of the membrane bag. The membranes are glued to both sides of the ring.

a : Front view   b : Lateral view
O : brine outlet   EMA : Effective membrane area
GA: Glueing area   M : Membrane
G : Glue   R : Nylon ring.

5.4 Determination of Brine Concentration, Current Efficiency and Water Flow as a Function of Feed Concentration and Current Density

The EOP cell used in the experiments was described by Oren and Litan[112] and is shown in Figure 5.2. It consists of two symmetric units, each of which contains a separate electrode. A carbon slurry was circulated through the electrode compartments and was used as electrode rinse solution. The membranes were attached to the nylon ring with silicon sealant and the nylon ring (membrane bag) was placed between the two circulation cells and rubber rings were used to secure sealing. Approximately 40 litres of solution containing salt, acid or base was circulated through the cell renewing its content approximately 60 times per minute. In this way an approximately constant feed concentration was maintained during the experiments.
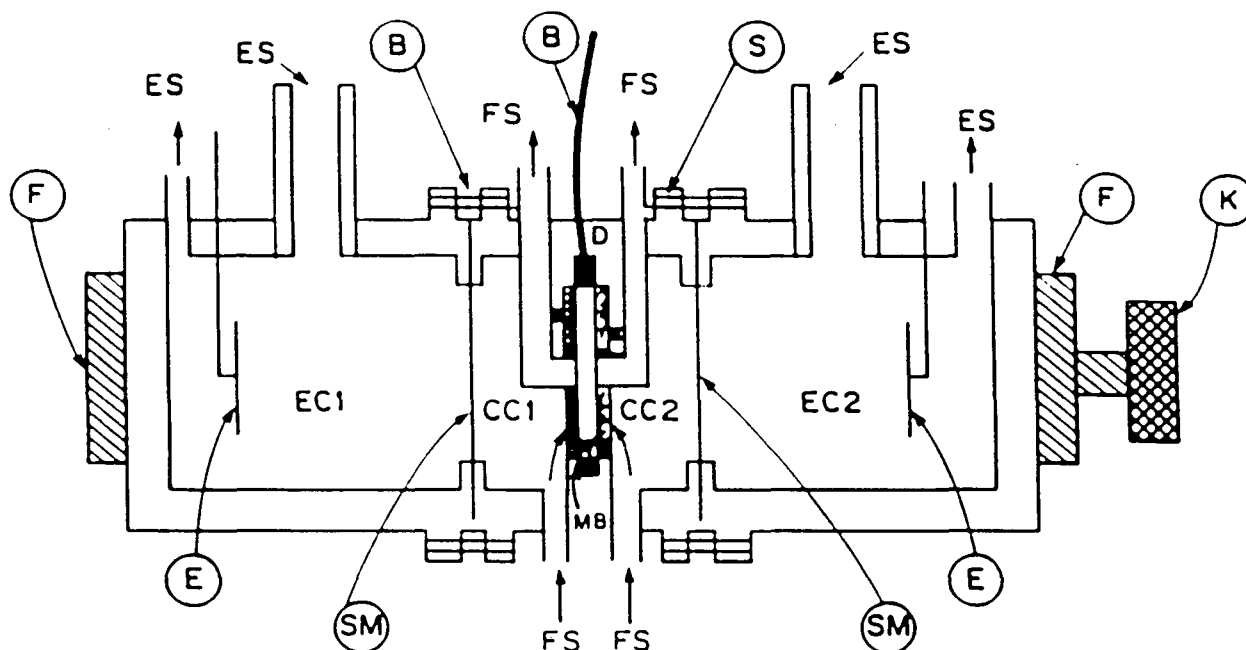
Figure 5.2: Schematic diagram of the apparatus used for the EOP experiments. EC1 and EC2: Electrode cells; CC1 and CC2: Circulation cells for the feed solution (FS); B: Brine outlet; MB: Membrane bag; SM: Membrane separating the electrode compartments from the feed solution; E: Electrodes; D: Perforated porous polypropylene disks; S: Stainless Steel Screws; F: Clamping frame; K: Tightening knob.

Efficient stirring and streaming of the solution in the cell were effected by the Meares and Sutton's method of forcing the solution onto the membrane surface through perforated polypropylene discs[112]. This has been shown to be a very efficient way of stirring. Constant current was supplied to the cell by a Hewlett Packard constant current source. Current was measured with a Hewlett Packard digital multimeter. Brine samples were collected at certain intervals and their volume and concentration determined. Each point on the plots of c_b versus I, and of J versus I_{eff} was the average of 3 to 5 measurements after the system had reached the stationary state. Concentration changes in the feed solution during the time of the experiments were found to be negligible.

Current efficiency, e_p, was calculated as follows[1]:

$$\epsilon_p = \frac{2Jc_b}{I/F} = \frac{c_b(V/t)}{I/F} \equiv \Delta\bar{t} \qquad \text{(see eq. 3.10.37)}$$

where c_b represents the brine concentration, V the volume of the solution that enters the bag per unit area (7,55 cm^2) in t seconds (V/t = 2J), I the applied current density (mA/cm^2) and F is Faraday's constant.

The maximum brine concentration, c_b^{max}, was determined from the following relation

$$c_b^{max} = \frac{1}{2\beta F}$$

(see eq. 3.10.28)

where 2β is the electro-osmotic coefficient determined from the slope of the J versus I_{eff} plots and F is Faraday's constant.

5.5   Determination of Membrane Characteristics

5.5.1   Membrane potential

The difference between the counter- and co-ion transport number, Δt, which is called the apparent transport number or membrane permselectivity, was measured as follows:

The potential ($\Delta\Psi_m$) of a membrane is usually measured between 0,1/0,2 mol/ℓ or 0,5/1,0 mol/ℓ sodium chloride solutions in a specially designed cell with calomel electrodes. The theoretical potential, $\Delta\Psi_i$, is calculated from the activities of the two solutions. Membrane permselectivity, Δt, can then be calculated from these values where $\Delta\Psi_m$ is the measured potential and a_s^{11}/a_s^1 is the ratio of salt activities on both sides of the membrane.

$$\Delta t = \frac{\Delta\Psi_m}{\Delta\Psi_i}$$

(see eq. 3.11.11)

where $\Delta t = 2t_1 - 1$ and

$$\Delta\Psi_i = \frac{RT}{F} \ln \frac{a_s^{11}}{a_s^1}$$

(see eq. 3.11.10)

5.5.2   Ion-Exchange Capacity

Membrane capacity was determined as follows[113]:

Approximately 3 g dried membrane sample (weighed accurately) was equilibrated with 150 ml 1 mol/ℓ hydrochloric acid for 16 hours at room temperature. The membrane

sample was rinsed free of chloride. The sample was then treated with 200 mℓ 4% sodium carbonate solution for 2 hours, neutralized to below pH 8,3 with 0,1 mol/ℓ sulphuric acid, potassium chromate (2 mℓ) added and the sample titrated with standardized 0,1 mol/ℓ silver nitrate and the total anion membrane exchange capacity calculated.

5.5.3 Gel Water Content

The gel water content of the membranes was determined as follows[113]:

Membrane samples (pretreated to their reference form[113]) were blotted dry with filter paper and mass recorded. The membrane sample was then dried at 105°C for 16 hours and the dried mass recorded. The gel water content (%) was calculated from the mass loss.

5.5.4 Membrane Resistance

Membrane resistance was measured between platinum electrodes coated with platinum black in a specially designed membrane resistance measurement cell with a resistance meter. Salt concentrations of 0,1 and 0,5 mol/ℓ sodium chloride were used. Membrane resistance was expressed in ohm.cm^2.

5.6 Determination of Salt and Acid Diffusion Rate through Membranes

Salt and acid diffusion rate through *Selemion* AMV and AAV membranes was determined in the cell shown in Figure 5.3. The cell consists of two half-cells containing stirrers with a volume of approximately 200 mℓ per half-cell. A membrane with an exposed area of 2,55 cm^2 was clamped between the two half-cells and salt or acid solution with a concentration difference of 0,05/2 mol/ℓ and 0,05/4 mol/ℓ was placed in the two half-cells. Diffusion was allowed to take place and the rate of concentration change in the two cells was determined.
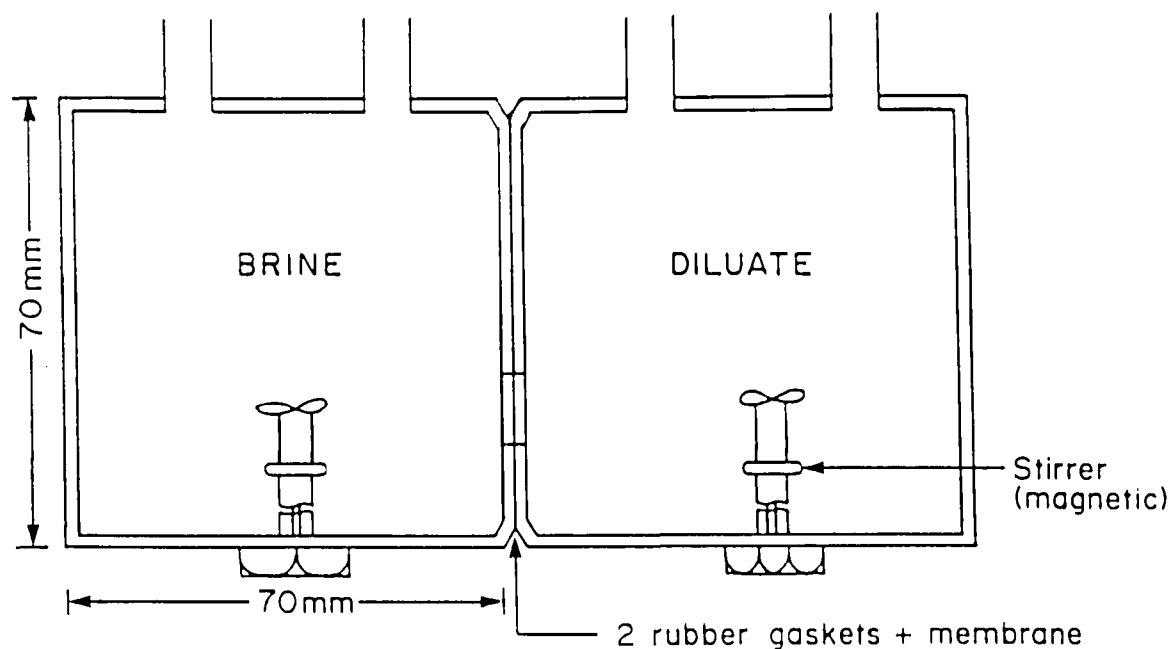
Figure 5.3: **Diagram of cell used for determination of diffusion of hydrochloric acid and sodium chloride through membranes (membrane area = 2,55 cm^2).**

5.7 Bench-Scale EOP-ED Stack

A bench-scale EOP-ED stack has been designed and constructed from materials available in South Africa. A simplified diagram of the membrane configuration in the stack is shown in Figure 5.4. The stack is similar to a conventional filter-press type ED stack. The only difference is that brine is not circulated through the brine compartments as is the case in conventional ED. Water enters the brine compartments by means of electro-osmosis and runs out of these compartments in a groove in the spacer at the top of each brine cell. The stack contained 10 cell pairs with an effective membrane area of 169 cm^2.

The end plates were made from PVC. A diagram of the end plates is shown in Figure 5.5. Water flow through the stack into the diluating and brine compartments was directed by the manifold shown in Figure 5.5. Gaskets made from polycarbonate (2 mm) and teflon (2 mm) were used in the stack to separate the membranes from each other. A diagramme of a gasket is shown in Figure 5.6. PVC spacers (0,3 mm) were used to separate the membranes from each other. Platinized titanium or graphite electrodes were used in the stack.

142

+ A C A C A C A C A C A C −

B B B B

Cl⁻

Na⁺

Cl⁻ Cl⁻ Na⁺ Na⁺

Na⁺ Na⁺

D D D D D Cl⁻ D

Cl⁻

Cl⁻ Cl⁻

Na⁺

Cl⁻

Figure 5.4: Simplified diagram of membrane configuration in EOP-ED stack.

B = brine compartment; D = diluating compartment.

10mm

|←— 55mm —→| →| |←

A ——— A

145mm

180mm

|←————— 200mm —————→|

Figure 5.5: End plates of EOP-ED stack.

143

a) Brine gasket   b) Diluating gasket
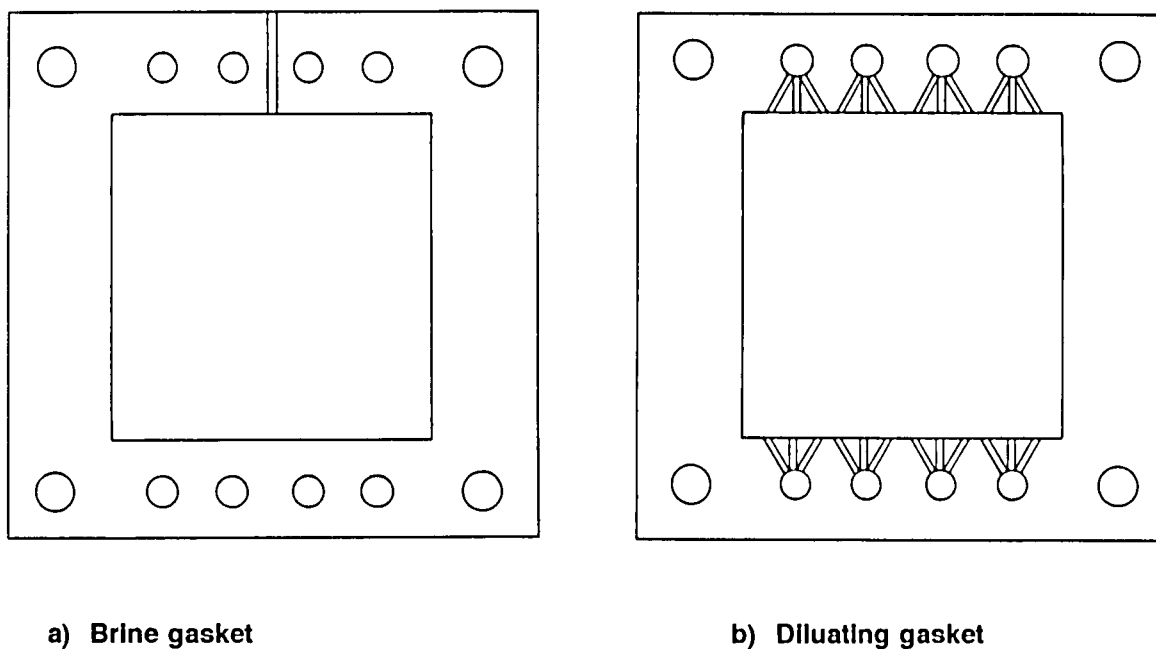
Figure 5.6:   Gaskets used In EOP-ED stack.

Ionac MA-3475 and MC-3470 membranes were used for concentration/desalination of sodium chloride solutions while *Selemion* AAV and CHV and *Selemion* AMV and CMV membranes were used for hydrochloric acid and caustic soda concentration/desalination, respectively.

Solutions of sodium chloride, hydrochloric acid and caustic soda in deionized water of different initial concentrations were concentrated/desalinated at different cell pair voltages in the stack. The experimental set-up is shown in Figure 5.7. Feed (c_f), product (c_p) and brine (c_b) concentrations were determined from conductivity measurements.

A typical ED experiment was conducted as follows:

Feed solution (12 ℓ) was circulated at a linear flow velocity of 1 cm/s through the dialysate compartments. The electrode solution consisted of 2 litre of a 2% carbon slurry in 1 mol/ℓ sodium chloride solution. The pH of this solution was adjusted to approximately 5 and circulated through the electrode compartments.

Direct current voltage of 0,5; 1,0; 1,5; 2,0; 3 and 4 volt was applied across a cell pair. Voltage between the cells was measured with platinum wire connected to a voltmeter. Platinum wire was inserted between the first and last brine cell. Current was recorded at 15 minute intervals and the concentration potential (V_n) was determined by interrupting the current for a few seconds. The final brine volume and the concentration of the desalinated feed (product water) and brine were determined at the end of the runs.

Current efficiency (CE), water recovery (WR), brine volume (BV), electrical energy consumption (EEC), concentration factor (CF), output (OP) (water yield), d_{eff} and R_{cp} were determined from the experimental data. Graphs were compiled of reduction in feed water concentration as a function of time and of cell pair resistance (V_{cp}) as a function of specific resistance (p) of the dialysate. An example of the calculations is shown in Appendix C.
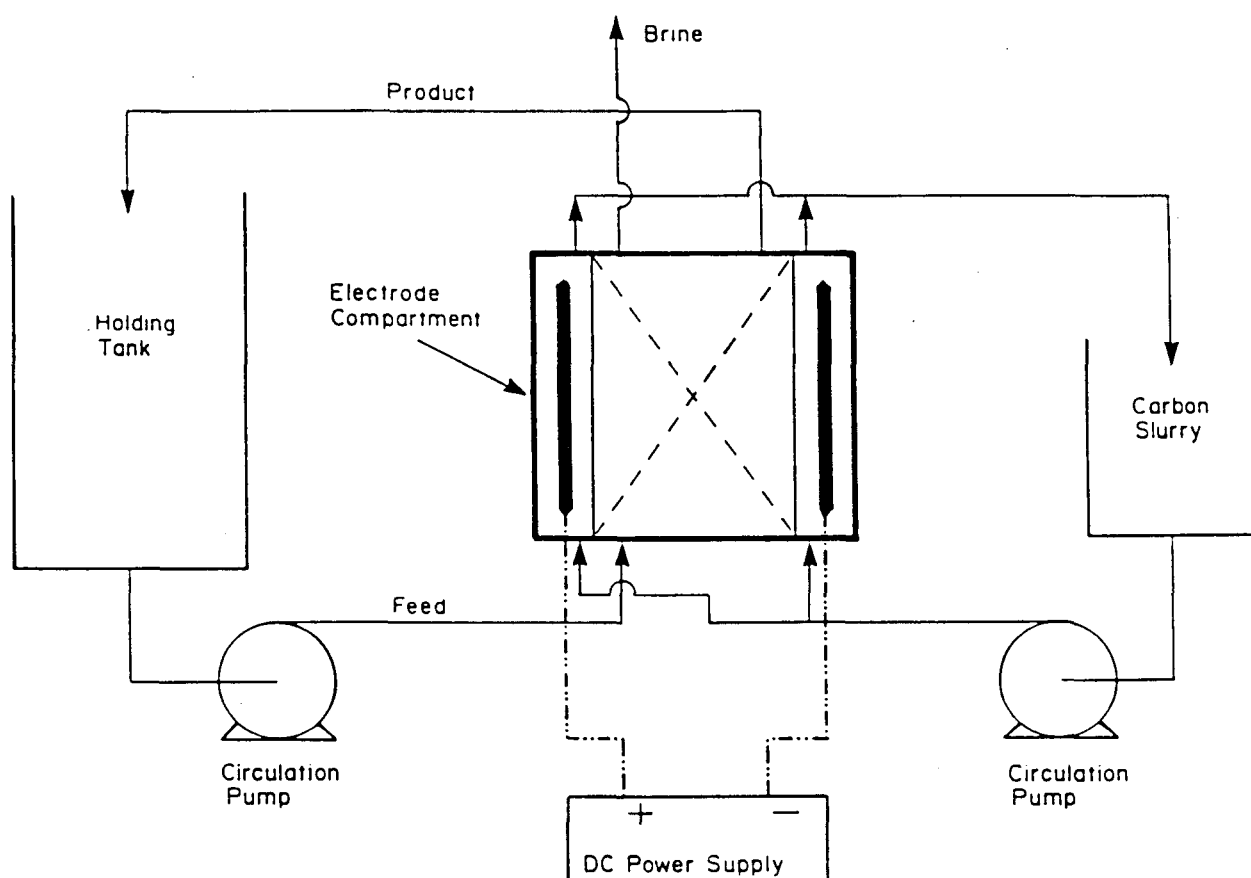
Figure 5.7: Experimental set-up for EOP-ED of sodium chloride, hydrochloric acid and caustic soda solutions.

5.8   Sealed-Cell ED Stack

A simplified diagram of the sealed-cell (SCED) membrane stack is shown in Figure 5.8. The brine sealed cells with outlets are arrayed in an open vessel, separated by spacers (0,3 mm). The dialysate enters through a suitable port at the bottom of the vessel and runs out through an overflow. Direct current is applied through carbon suspension electrodes[4]. The external dimensions of the sealed brine cells are 60 x 80 mm, giving an effective membrane area of 100 cm^2 per cell pair (cp).

Solutions of sodium chloride, ammonium nitrate, sodium sulphate, sodium nitrate and calcium chloride in deionized water of different initial concentrations were concentrated/desalinated at different cell pair voltages in the SCED unit. Feed (c_i), product (c_p) and brine (c_b) concentrations were determined from conductivity measurements. Various industrial effluents were also treated with SCED.

Feed solution (15 ℓ) was circulated at a linear flow velocity of 15 cm/s through the dialysate compartments. The electrode solution consisted of 2 ℓ of a 2 % carbon slurry in 1 mol/ℓ sodium chloride solution. The pH of the solution was adjusted to approximately 5 and circulated through the electrode compartments.

Electrodialysis was started by applying a DC voltage of approximately 0,5 Volt per cell pair across 17 membrane bags. Voltage between the membrane bags was measured with calomel electrodes connected to a salt bridge. Current was recorded at 10 or 20 minute intervals during ED and V_n was determined during interruption of the current for a short period. The final brine volume, concentration of the desalinated feed (product water) and brine were determined at the end of the runs.

Current efficiency (CE), water recovery (WR), brine volume (BV), electrical energy consumption (EEC), concentration factor (CF), output (OP) (water yield), effective thickness of dialysate compartment (d_{eff}), and membrane resistance (R_{cp}) were determined from the experimental data. Graphs were plotted of feed water concentration, brine concentration, current efficiency and electrical energy consumption as a function of time, and of cell pair voltage as a function of the specific resistance (p) of the dialysate.
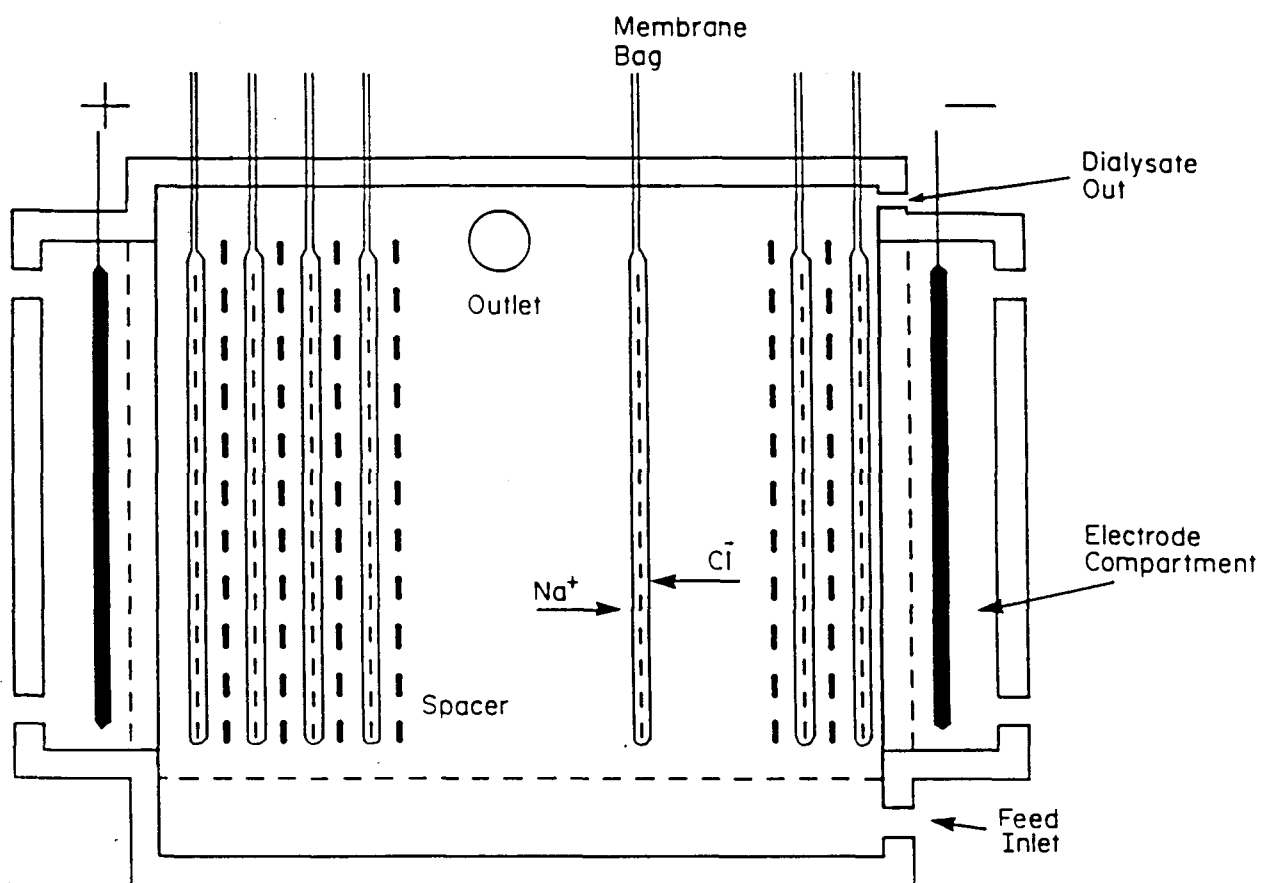
Figure 5.8:   Simplified diagram of SCED membrane stack.

6. ELECTRO-OSMOTIC PUMPING OF SODIUM CHLORIDE SOLUTIONS WITH DIFFERENT ION-EXCHANGE MEMBRANES

Brine concentrations, water flows and current efficiencies were determined at different current densities for different sodium chloride feed water concentrations. Membrane permselectivities (apparent transport numbers - Δt's) were measured at the same concentration differences as encountered during EOP experiments when brine concentration had reached the steady state. The EOP results are summarized in Tables 6.1 to 6.28 for the different membranes.

6.1 Brine Concentration

Brine concentration (c_b) as a function of current density (I) is shown in Figures 6.1 to 6.7. Initially brine concentration increases rapidly and then levels off at higher current densities. Brine concentration increases with increasing current density and increasing feed water concentration. Highest brine concentrations were obtained with *Selemion* and *Ionac* membranes (Table 6.29). Brine concentrations of 25,1 and 23,4% were obtained at high current density (0,1 mol/ℓ feed) with *Selemion* and *Ionac* membranes, respectively. Lower brine concentrations were obtained with the *Ionics* and WTPS membranes (19,0 and 20,9%, respectively) while the lowest concentrations were obtained with the *Raipore*, WTPVC and WTPST membranes (14,4, 15,1 and 15,4%, respectively). The concentration performance of the WTPS membranes compares favourably with that of the commercially available membranes.

It appears that the brine concentration will reach a maximum value, c_b^{max}. This was predicted from the flow equations[1]. Maximum brine concentration was nearly reached in the case of the *Raipore*- (Fig. 6.3), WTPVC- (Fig. 6.6) and WTPST- (Fig. 6.7) membranes at 0,05 mol/ℓ feed concentration at high current density. Maximum brine concentration was also nearly reached in the case of the *Selemion*- (Fig. 6.1), *Ionac*- (Fig. 6.2), *Raipore*- (Fig. 6.3), *Ionics*- (Fig. 6.4), WTPS- (Fig 6.5), WTPVC- (Fig. 6.6) and WTPST- (Fig. 6.7) membranes in the 0,1 to 1,0 mol/ℓ feed concentration range at high current densities.

Maximum brine concentration, c_b^{max}, was calculated from the following two relationships, viz.

$$c_b^{max} = \frac{1}{2\beta F} \qquad \text{(see eq. 3.10.28)}$$

Table 6.1 : Electro-osmotic pumping experimental conditions and results for 0,05 mol/ℓ sodium chloride (Selemion AMV and CMV)

Current Density	Brine concentration c_b, mol/l		Water flow	Current Efficiency	Effective Current Density	Transport Numbers				
I, mA/cm²	$c_{b\,exp.}$	$c_{b\,calc.}$	J, cm/h	e_p, %	I_{eff}, mA/cm²	Δt^c	Δt^a	$\overline{\Delta}t$	$\hat{t}_1^c$	$\hat{t}_2^a$
5	1,62	1,59	0,102	62,37	3,12	0,91	0,82	0,87	0,96	0,91
10	2,15	2,76	0,115	66,22	6,62	0,88	0,82	0,85	0,94	0,91
15	2,65	3,35	0,137	64,79	9,72	0,85	0,78	0,82	0,93	0,89
20	2,81	3,54	0,170	64,93	12,99	0,86	0,75	0,81	0,93	0,88
30	3,31	4,05	0,217	64,15	19,25	0,84	0,73	0,79	0,92	0,86

Electro-osmotic coefficient (2β) = 0,219 ℓ/F (slope = 0,008194 mℓ/mAh)
J_{osm} = y-intercept = 0,06023 cm/h
c_o^{max} = 4,55 mol/l
$\Delta t^c = t_1^c - t_2^c$

$\Delta t^a = t_2^a - t_1^a$
$\overline{\Delta}t$ = Average transport number of membrane pair
$\hat{t}_1^c$ = Transport number of cation through cation membrane
$\hat{t}_2^a$ = Transport number of anion through anion membrane.

Table 6.2 : Electro-osmotic pumping experimental conditions and results for 0,1 mol/ℓ sodium chloride (Selemion AMV and CMV)

Current Density	Brine concentration c_b, mol/l		Water flow	Current Efficiency	Effective Current Density	Transport Numbers				
I, mA/cm²	$c_{b\,exp.}$	$c_{b\,calc.}$	J, cm/h	e_p, %	I_{eff}, mA/cm²	Δt^c	Δt^a	$\overline{\Delta}t$	$\hat{t}_1^c$	$\hat{t}_2^a$
5	1,79	2,1	0,076	73,0	3,65	0,94	0,81	0,87	0,97	0,90
10	2,37	2,64	0,118	74,4	7,47	0,89	0,78	0,84	0,94	0,89
15	2,83	3,02	0,152	76,7	11,51	0,89	0,75	0,82	0,94	0,88
20	3,02	3,21	0,188	76,1	15,23	0,88	0,73	0,81	0,94	0,87
30	3,58	3,74	0,238	76,2	22,86	0,85	0,74	0,80	0,93	0,87
40	3,91	4,09	0,286	75,0	30,01	0,89	0,68	0,78	0,94	0,84
50	4,29	4,33	0,330	75,9	37,95	0,82	0,71	0,77	0,91	0,85

Electro-osmotic coefficient (2β) = 0,198 ℓ/F (slope = 0,00739 mℓ/mAh)
J_{osm} = y-intercept 0,067696 cm/h
c_o^{max} = 5,05 mol/l
$\Delta t^c = t_1^c - t_2^c$

$\Delta t^a = t_2^a - t_1^a$
$\overline{\Delta}t$ = Average transport number of membrane pair
$\hat{t}_1^c$ = Transport number of cation through cation membrane
$\hat{t}_2^a$ = Transport number of anion through anion membrane.

Table 6.3 : Electro-osmotic pumping experimental conditions and results for 0,5 mol/ℓ sodium chloride (Selemion AMV and CMV)

Current Density	Brine concentration c_b, mol/l		Water flow	Current Efficiency	Effective Current Density	Transport Numbers				
I, mA/cm²	$c_{b\,exp.}$	$c_{b\,calc.}$	J, cm/h	e_p, %	I_{eff}, mA/cm²	Δt^c	Δt^a	$\overline{\Delta}t$	$\hat{t}_1^c$	$\hat{t}_2^a$
5	1,72	1,71	0,0895	82,5	4,13	0,92	0,71	0,82	0,96	0,86
10	2,74	2,33	0,122	89,66	8,96	0,86	0,67	0,76	0,93	0,83
20	3,54	2,82	0,190	91,72	18,34	0,81	0,63	0,72	0,91	0,81
30	3,94	3,27	0,248	87,35	26,21	0,86	0,59	0,72	0,93	0,80
40	4,20	3,26	0,323	90,89	36,36	0,81	0,60	0,71	0,90	0,80
50	4,50	3,51	0,378	91,23	45,62	0,84	0,58	0,71	0,92	0,79
60	4,66	3,62	0,440	91,46	54,88	0,85	0,57	0,71	0,93	0,79

Electro-osmotic coefficient (2β) = 0,187 ℓ/F (slope = 0,006959 mℓ/mAh)
J_{osm} = y-intercept = 0,062409 cm/h
c_o^{max} = 5,36 mol/l
$\Delta t^c = t_1^c - t_2^c$

$\Delta t^a = t_2^a - t_1^a$
$\overline{\Delta}t$ = Average transport number of membrane pair
$\hat{t}_1^c$ = Transport number of cation through cation membrane
$\hat{t}_2^a$ = Transport number of anion through anion membrane.

Table 6.4: Electro-osmotic pumping experimental conditions and results for 1,0 mol/l sodium chloride (Selemion AMV and CMV)

Current Density	Brine concentration c_b, mol/l		Water flow	Current Efficiency	Effective Current Density	Transport Numbers				
I, mA/cm²	$c_{b\,exp.}$	$c_{b\,calc.}$	J, cm/h	e_p, %	I_{eff}, mA/cm²	Δt^a	Δt^c	$\overline{\Delta t}$	t_1^a	t_2^a
10	2,95	2,41	0,113	89,00	8,90	0,84	0,62	0,73	0,92	0,81
20	3,73	2,90	0,174	87,14	17,43	0,82	0,55	0,68	0,91	0,77
30	4,12	3,16	0,236	86,95	26,09	0,79	0,55	0,67	0,90	0,78
40	4,55	3,51	0,279	85,21	34,08	0,80	0,51	0,66	0,90	0,76
50	5,07	3,70	0,328	89,28	44,64	0,79	0,52	0,65	0,89	0,76
60	5,10	3,79	0,384	87,52	52,51	0,80	0,50	0,65	0,90	0,75

Electro-osmotic coefficient (2β) = 0,154 l/F (slope = 0,005757 ml/mAh)
J_{osm} = y-intercept = 0,078991 cm/h
c_b^{max} = 6,48 mol/l
$\Delta t^c = t_1^c \cdot t_2^c$

$\Delta t^a = t_1^a \cdot t_1^a$
$\overline{\Delta t}$ = Average transport number of membrane pair
t_1^c = Transport number of cation through cation membrane
t_2^a = Transport number of anion through anion membrane.

Table 6.5 : Electro-osmotic pumping experimental conditions and results for 0,05 mol/l sodium chloride (Ionac MA-3475 and MC-3470)

Current Density	Brine concentration c_b, mol/l		Water flow	Current Efficiency	Effective Current Density	Transport Numbers				
I, mA/cm²	$c_{b\,exp.}$	$c_{b\,calc.}$	J, cm/h	e_p, %	I_{eff}, mA/cm²	Δt^a	Δt^c	$\overline{\Delta t}$	t_1^a	t_2^a
5	1,50	1,82	0,0883	71,01	3,55	0,93	0,80	0,86	0,96	0,90
10	2,16	2,80	0,1112	64,41	6,44	0,91	0,76	0,83	0,95	0,88
15	2,60	3,45	0,1324	61,54	9,23	0,90	0,73	0,82	0,95	0,87
20	2,87	4,05	0,1456	56,04	11,21	0,83	0,74	0,79	0,92	0,87
25	3,25	4,60	0,1589	55,39	13,85	0,86	0,71	0,78	0,93	0,85

Electro-osmotic coefficient (2β) = 0,186 l/F (slope = 0,0069464 ml/mAh)
J_{osm} = y-intercept = 0,0657676 cm/h
c_b^{max} = 5,37 mol/l
$\Delta t^c = t_1^c \cdot t_2^c$

$\Delta t^a = t_1^a \cdot t_1 a$
$\overline{\Delta t}$ = Average transport number of membrane pair
t_1^c = Transport number of cation through cation membrane
t_2^a = Transport number of anion through anion membrane.

Table 6.6 : Electro-osmotic pumping experimental conditions and results for 0,1 mol/l sodium chloride (Ionac MA-3475 and MC-3470)

Current Density	Brine concentration c_b, mol/l		Water flow	Current Efficiency	Effective Current Density	Transport Numbers				
I, mA/cm²	$c_{b\,exp.}$	$c_{b\,calc.}$	J, cm/h	ϵ_p, %	I_{eff}, mA/cm²	Δt^a	Δt^c	$\overline{\Delta t}$	t_1^a	t_2^a
5	1,92	2,29	0,0662	68,17	3,41	0,89	0,73	0,81	0,95	0,87
10	2,49	2,94	0,0997	64,19	6,42	0,88	0,70	0,79	0,94	0,85
15	2,89	3,65	0,1186	61,70	9,25	0,86	0,68	0,77	0,93	0,84
20	3,18	3,84	0,14834	63,23	12,65	0,86	0,67	0,76	0,93	0,83
30	3,4	4,27	0,1977	60,09	18,03	0,84	0,67	0,75	0,92	0,83
40	3,81	4,89	0,2295	58,62	23,45	0,84	0,66	0,75	0,92	0,83
50	4,00	5,32	0,2649	56,81	28,40	0,85	0,66	0,76	0,93	0,83

Electro-osmotic coefficient (2β) = 0,206 l/F (slope = 0,0076844 ml/mAh)
J_{osm} = y-intercept = 0,0503481 cm/h
c_b^{max} = 4,85 mol/l
$\Delta t^c = t_1^c \cdot t_2^c$

$\Delta t^a = t_2^a \cdot t_1^a$
$\overline{\Delta t}$ = Average transport number of membrane pair
t_1^c = Transport number of cation through cation membrane
t_2^a = Transport number of anion through anion membrane.

Table 6.7 : Electro-osmotic pumping experimental conditions and results for 0,5 mol/ℓ sodium chloride (Ionac MA-3475 and MC-3470)

Current Density	Brine concentration c_b, mol/l		Water flow	Current Efficiency	Effective Current Density	Transport Numbers				
I, mA/cm²	$c_{b\,exp.}$	$c_{b\,calc.}$	J, cm/h	e_p, %	I_{eff}, mA/cm²	Δt^c	Δt^a	$\overline{\Delta}t$	$\bar{t}_1^c$	$\bar{t}_2^a$
5	2,37	1,69	0,07568	96,17	4,81	0,80	0,57	0,69	0,90	0,79
10	2,95	2,57	0,097	76,81	7,68	0,80	0,54	0,67	0,90	0,77
20	3,69	3,03	0,1589	78,61	15,72	0,78	0,52	0,65	0,89	0,76
30	3,99		0,205	73,19	21,95					
40	4,05	3,84	0,2472	67,10	26,84	0,77	0,50	0,64	0,88	0,75
50	4,37	4,42	0,26136	61,23	30,62	0,75	0,49	0,62	0,87	0,75
60	4,51	4,91	0,2825	56,93	34,16	0,73	0,51	0,62	0,87	0,75
70	4,59	5,05	0,3178	55,87	39,11	0,73	0,50	0,61	0,86	0,75

Electro-osmotic coefficient (2β) = 0,190 ℓ/F (slope = 0,0070843 mℓ/mAh)
J_{osm} = y-intercept = 0,0454963 cm/h
c_b^{max} = 5,26 mol/l
$\Delta t^c = t_1^c \cdot t_2^c$

$\Delta t^a = t_2^a \cdot t_1^a$
$\overline{\Delta}t$ = Average transport number of membrane pair
$\bar{t}_1^c$ = Transport number of cation through cation membrane
$\bar{t}_2^a$ = Transport number of anion through anion membrane.

Table 6.8: Electro-osmotic pumping experimental conditions and results for 1,0 mol/ℓ sodium chloride (Ionac MA-3475 and MC-3470)

Current Density	Brine concentration c_b, mol/l		Water flow	Current Efficiency	Effective Current Density	Transport Numbers				
I, mA/cm²	$c_{b\,exp.}$	$c_{b\,calc.}$	J, cm/h	e_p, %	I_{eff}, mA/cm²	Δt^c	Δt^a	$\overline{\Delta}t$	$\bar{t}_1^c$	$\bar{t}_2^a$
20	3,96	2,76	0,1766	93,73	18,75	0,76	0,54	0,65	0,88	0,77
40	4,47	3,36	0,286	85,70	34,28	0,75	0,54	0,64	0,88	0,77
60	4,56	3,62	0,411	83,648	50,19	0,78	0,55	0,67	0,89	0,78
80	4,91	3,68	0,5033	82,804	66,24	0,73	0,51	0,62	0,87	0,76

Electro-osmotic coefficient (2β) = 0,187 ℓ/F (Slope 0,0069749 mℓ/mAh)
J_{osm} = y-intercept = 0,0487359 cm/h
c_b^{max} = 5,35 mol/l
$\Delta t^c = t_1^c \cdot t_2^c$

$\Delta t^a = t_2^a \cdot t_1^a$
$\overline{\Delta}t$ = Average transport number of membrane pair
$\bar{t}_1^c$ = Transport number of cation through cation membrane
$\bar{t}_2^a$ = Transport number of anion through anion membrane.

Table 6.9 : Electro-osmotic pumping experimental conditions and results for 0,05 mol/ℓ sodium chloride (Ralpore R4030 anion and R4010 cation)

Current Density	Brine concentration c_b, mol/l		Water flow	Current Efficiency	Effective Current Density	Transport Numbers				
I, mA/cm²	$c_{b\,exp.}$	$c_{b\,calc.}$	J, cm/h	e_p, %	I_{eff}, mA/cm²	Δt^c	Δt^a	$\overline{\Delta}t$	$\bar{t}_1^c$	$\bar{t}_2^a$
5	0,86	1,44	0,1059	48,85	2,44	0,79	0,84	0,82	0,90	0,92
10	1,19	1,84	0,1589	50,70	5,07	0,74	0,82	0,78	0,87	0,91
15	1,47	2,32	0,1827	48,02	7,20	0,71	0,81	0,76	0,85	0,90
20	1,55	2,50	0,2225	46,23	9,25	0,70	0,80	0,75	0,85	0,90
30	1,62	2,57	0,317	46,01	13,80	0,67	0,79	0,73	0,83	0,90

Electro-osmotic coefficient (2β) = 0,547 ℓ/F (slope = 0,0204201 mℓ/mAh)
J_{osm} = y-intercept = 0,0348506
c_b^{max} = 1,83 mol/l
$\Delta t^c = t_1^c \cdot t_2^c$

$\Delta t^a = t_2^a \cdot t_1^a$
$\overline{\Delta}t$ = Average transport number of membrane pair
$\bar{t}_1^c$ = Transport number of cation through cation membrane
$\bar{t}_2^a$ = Transport number of anion through anion membrane.

Table 6.10: Electro-osmotic pumping experimental conditions and results for 0,1 mol/l sodium chloride (Ralpore R4030 anion and R4010 cation)

Current Density	Brine concentration c_b, mol/l		Water flow	Current Efficiency,	Effective Current Density	Transport Numbers				
I, mA/cm²	$c_{b,sup}$	$c_{b,sol}$	J, cm/h	e_p, %	I_{eff}, mA/cm²	Δt^a	Δt^c	$\overline{\Delta t}$	t_1^c	t_2^a
5	0,99	1,35	0,1148	60,62	3,03	0,83	0,83	0,83	0,92	0,92
10	1,37	1,72	0,172	63,23	6,32	0,78	0,80	0,79	0,89	0,90
20	1,86	2,28	0,251	62,74	12,55	0,75	0,77	0,76	0,88	0,89
30	2,16	2,57	0,3192	61,61	18,48	0,71	0,75	0,73	0,86	0,88
40	2,33	2,68	0,3973	62,04	24,82	0,71	0,72	0,71	0,85	0,86
50	2,47	2,86	0,467	61,97	30,99	0,70	0,73	0,72	0,85	0,86

Electro-osmotic coefficient (2ß) = 0,320 l/F (slope = 0,0119546 ml/mAh)
J_{osm} = y-intercept = 0,0985769 cm/h
c_b^{max} = 3,13 mol/l
Δt^c = t_1^c - t_2^c

Δt^a = t_2^a - t_1^a
$\overline{\Delta t}$ = Average transport number of membrane pair
t_1^c = Transport number of cation through cation membrane
t_2^a = Transport number of anion through anion membrane.

Table 6.11 : Electro-osmotic pumping experimental conditions and results for 0,5 mol/l sodium chloride (Ralpore R4030 anion and R4010 cation)

Current Density	Brine concentration c_b, mol/l		Water flow	Current Efficiency	Effective Current Density	Transport Numbers				
I, mA/cm²	$c_{b,sup}$	$c_{b,sol}$	J, cm/h	e_p, %	I_{eff}, mA/cm²	Δt^a	Δt^c	$\overline{\Delta t}$	t_1^c	t_2^a
5	1,28	1,89	0,0894	61,11	3,05	0,98	0,83	0,90	0,99	0,91
10	1,65	2,21	0,1456	64,36	6,44	0,92	0,80	0,86	0,96	0,90
20	2,07	2,51	0,2384	66,14	13,23	0,86	0,75	0,80	0,93	0,87
30	2,38	2,67	0,3178	67,59	20,27	0,81	0,71	0,76	0,91	0,85
40	2,62	2,76	0,3947	69,30	27,72	0,78	0,68	0,73	0,89	0,84
50	2,92	2,96	0,4450	69,66	34,83	0,77	0,64	0,71	0,89	0,82
60	3,08	3,22	0,4760	65,61	39,36	0,74	0,64	0,69	0,87	0,82
70	3,32	3,10	0,5615	71,35	49,95	0,71	0,62	0,67	0,86	0,81
90	3,46	3,24	0,6880	70,97	63,87	0,72	0,61	0,66	0,86	0,81

Electro-osmotic coefficient (2ß) = 0,251 l/F (slope 0,0093668 ml/mAh)
J_{osm} = y-intercept = 0,1117984 cm/h
c_b^{max} = 3,98 mol/l
Δt^c = t_1^c - t_2^c

Δt^a = t_2^a - t_1^a
$\overline{\Delta t}$ = Average transport number of membrane pair
t_1^c = Transport number of cation through cation membrane
t_2^a = Transport number of anion through anion membrane.

Table 6.12: Electro-osmotic pumping experimental conditions and results for 1,0 mol/l sodium chloride (Ralpore R4030 anion and R4010 cation)

Current Density	Brine concentration c_b, mol/l		Water flow	Current Efficiency	Effective Current Density	Transport Numbers				
I, mA/cm²	$c_{b,sup}$	$c_{b,sol}$	J, cm/h	e_p, %	I_{eff}, mA/cm²	Δt^a	Δt^c	$\overline{\Delta t}$	t_1^c	t_2^a
30	2.6	2.08	0.339	78.77	23.63	0.67	0.59	0.63	0,83	0,80
50	3.14	2.473	0.461	77.59	38.80	0.65	0.57	0.61	0,83	0,79
70	3.34	2.62	0.5934	75.89	53.13	0.64	0.56	0.60	0,82	0,78
90	3.48	2.96	0.7205	74.68	67.21	0.72	0.55	0.63	0,86	0,78

Electro-osmotic coefficient (2ß) = 0,236 l/F (Slope = 0,0087973 ml/mAh)
J_{osm} = y-intercept = 0,1265161 cm/h
c_b^{max} = 4,24 mol/l
Δt^c = t_1^c - t_2^c

Δt^a = t_2^a - t_1^a
$\overline{\Delta t}$ = Average transport number of membrane pair
t_1^c = Transport number of cation through cation membrane
t_2^a = Transport number of anion through anion membrane.

152

Table 6.13: Electro-osmotic pumping experimental conditions and results for 0,05 mol/l sodium chloride (Ionics A-204-UZL-386 and C-61-CZL-386)

Current Density	Brine concentration c_b, mol/l		Water flow	Current Efficiency	Effective Current Density	Transport Numbers				
I, mA/cm²	$c_{b\,exp.}$	$c_{b\,calc.}$	J, cm/h	e_p, %	I_{eff}, mA/cm²	Δt^c	Δt^a	$\bar{\Delta}t$	$\bar{t}_1^c$	$\bar{t}_2^a$
5	1,51	2,26	0,0662	53,61	2,68	0,78	0,82	0,80	0,89	0,91
10	1,87	2,69	0,1059	53,11	5,31	0,74	0,79	0,76	0,87	0,89
15	2,19	3,13	0,1324	51,84	7,78	0,72	0,76	0,74	0,86	0,88
20	2,52	3,72	0,1456	48,92	9,78	0,70	0,75	0,73	0,85	0,88
30	2,80	4,53	0,1766	44,18	13,25	0,69	0,74	0,71	0,85	0,87

Electro-osmotic coefficient (2ß) = 0,234 l/F (slope = 0,0087337 ml/mAh)
J_{osm} = y-intercept = 0,0612608 cm/h
$c_b{}^{max}$ = 4,27 mol/l
Δt^c = t_1^c - t_2^c

Δt^a = t_2^a - t_1^a
$\bar{\Delta}t$ = Average transport number of membrane pair
$\bar{t}_1^c$ = Transport number of cation through cation membrane
$\bar{t}_2^a$ = Transport number of anion through anion membrane.

Table 6.14: Electro-osmotic pumping experimental conditions and results for 0,1 mol/l sodium chloride (Ionics A-204-UZL-386 and C-61-CZL-386)

Current Density	Brine concentration c_b, mol/l		Water flow	Current Efficiency	Effective Current Density	Transport Numbers				
I, mA/cm²	$c_{b\,exp.}$	$c_{b\,calc.}$	J, cm/h	e_p, %	I_{eff}, mA/cm²	Δt^c	Δt^a	$\bar{\Delta}t$	$\bar{t}_1^c$	$\bar{t}_2^a$
5	1,55	1,97	0,0728	60,53	3,03	0,76	0,78	0,77	0,88	0,89
10	1,87	2,41	0,1165	58,43	5,84	0,74	0,76	0,75	0,87	0,88
15	2,24	2,81	0,1457	58,32	8,75	0,72	0,74	0,73	0.86	0,87
20	2,61	3,32	0,1589	55,60	11,11	0,70	0,72	0,71	0,85	0,86
30	3,00	3,95	0,1942	52,07	15,62	0,67	0,70	0,69	0,84	0,85
40	3,25	4,60	0,2207	48,07	19,23	0,66	0,70	0,68	0,83	0,85

Electro-osmotic coefficient (2ß) = 0,204 l/F (slope = 0,0076266 ml/mAh)
J_{osm} = y-intercept = 0,0748388 cm/h
$c_b{}^{max}$ = 4,89 mol/l
Δt^c = t_1^c - t_2^c

Δt^a = t_2^a - t_1^a
$\bar{\Delta}t$ = Average transport number of membrane pair
$\bar{t}_1^c$ = Transport number of cation through cation membrane
$\bar{t}_2^a$ = Transport number of anion through anion membrane.

Table 6.15: Electro-osmotic pumping experimental conditions and results for 0,5 mol/l sodium chloride (Ionics A-204-UZL-386 and C-61-CZL-386)

Current Density	Brine concentration c_b, mol/l		Water flow	Current Efficiency	Effective Current Density	Transport Numbers				
I, mA/cm²	$c_{b\,exp.}$	$c_{b\,calc.}$	J, cm/h	e_p, %	I_{eff}, mA/cm²	Δt^c	Δt^a	$\bar{\Delta}t$	$\bar{t}_1^c$	$\bar{t}_2^a$
10	2,42	2,20	0,1059	68,74	6,87	0,61	0,63	0,62	0,81	0,82
20	2,75	2,60	0,1766	65,09	13,02	0,61	0,62	0,62	0,81	0,81
30	3,08	2,97	0,2260	62,21	18,67	0,60	0,60	0,60	0,79	0,80
40	3,28	3,20	0,2754	60,56	24,22	0,59	0,59	0,60	0,79	0,80
50	3,48	3,43	0,3178	59,31	29,65	0,58	0,59	0,58	0,79	0,79
60	3,77	3,44	0,3443	58,00	34,80	0,56	0,57	0,57	0,78	0,79
70	3,8	3,70	0,3973	57,82	40,47	0,56	0,57	0,56	0,78	0,78
80	3,91	3,94	0,4291	56,22	44,98	0,56	0,57	0,57	0,78	0,79
90	3,94	4,00	0,4768	55,95	50,36	0,56	0,57	0,57	0,78	0,79
100	3,98	4,20	0,5033	53,70	53,70	0,56	0,57	0,57	0,78	0,79

Electro-osmotic coefficient (2ß) = 0,211 l/F (slope = 0,0078875 ml/mAh)
J_{osm} = y-intercept = 0,0780686 cm/h
$c_b{}^{max}$ = 4,73 mol/l
Δt^c = t_1^c - t_2^c

Δt^a = t_2^a - t_1^a
$\bar{\Delta}t$ = Average transport number of membrane pair
$\bar{t}_1^c$ = Transport number of cation through cation membrane
$\bar{t}_2^a$ = Transport number of anion through anion membrane.

Table 6.16: Electro-osmotic pumping experimental conditions and results for 1,0 mol/ℓ sodium chloride (Ionics A-204-UZL-386 and C-61-CZL-386)

Current Density	Brine concentration c_b, mol/l		Water flow	Current Efficiency	Effective Current Density	Transport Numbers				
I, mA/cm²	$c_{b\ sup.}$	$c_{b\ solo.}$	J, cm/h	e_p, %	I_{eff}, mA/cm²	Δt^a	Δt^c	$\bar{\Delta}t$	$\hat{t}_1^c$	$\hat{t}_2^a$
30	3,48	2,49	0,2472	76,88	23,06	0,58	0,52	0,55	0,79	0,76
50	3,72	2,72	0,3708	73,96	36,98	0,57	0,51	0,54	0,79	0,75
70	3,94	3,13	0,4450	67,15	47,00	0,57	0,50	0,53	0,78	0,75
90	4,08	3,46	0,5298	64,38	57,94	0,59	0,50	0,54	0,79	0,75

Electro-osmotic coefficient $(2\beta) = 0,216$ ℓ/F (slope $= 0,0080659$ mℓ/mAh)
$J_{osm} =$ y-intercept $= 0,0655084$ cm/h
$c_b^{max} = 4,63$ mol/l
$\Delta t^c = t_1^c - t_2^c$

$\Delta t^a = t_1^a - t_1^a$
$\bar{\Delta}t =$ Average transport number of membrane pair
$\hat{t}_1^c =$ Transport number of cation through cation membrane
$\hat{t}_2^a =$ Transport number of anion through anion membrane.

Table 6.17: Electro-osmotic pumping experimental conditions and results for 0,05 mol/ℓ sodium chloride (WTPSA-1, WTPSC-1)

Current Density	Brine concentration c_b, mol/l		Water flow	Current Efficiency	Effective Current Density	Transport Numbers				
I, mA/cm²	$c_{b\ sup.}$	$c_{b\ solo.}$	J, cm/h	e_p, %	I_{eff}, mA/cm²	Δt^a	Δt^c	$\bar{\Delta}t$	$\Delta\hat{t}_1^c$	$\hat{t}_2^a$
5	1,66	2,20	0,0695	61,88	3,09	0,82	0,83	0,82	0,91	0,91
10	1,99	2,36	0,1280	60,78	6,08	0,81	0,81	0,81	0,90	0,90
15	2,4	3,16	0,1390	59,64	8,95	0,78	0,79	0,79	0,89	0,89
20	2,85	3,85	0,1456	55,65	11,13	0,72	0,77	0,75	0,86	0,88
25	3,32	4,45	0,1523	54,22	13,55	0,70	0,75	0,73	0,85	0,86

Electro-osmotic coefficient $(2\beta) = 0,087$ ℓ/F (slope $= 0,0032427$ mℓ/mAh)
$J_{osm} =$ y-intercept $= 0,1090328$ cm/h
$c_b^{max} = 11,50$ mol/l
$\Delta t^c = t_1^c - t_2^c$

$\Delta t^a = t_2^a - t_1^a$
$\bar{\Delta}t =$ Average transport number of membrane pair
$\hat{t}_1^c =$ Transport number of cation through cation membrane
$\hat{t}_2^a =$ Transport number of anion through anion membrane.

Table 6.18: Electro-osmotic pumping experimental conditions and results for 0,1 mol/ℓ sodium chloride (WTPSA-1, WTPSC-1)

Current Density	Brine concentration c_b, mol/l		Water flow	Current Efficiency	Effective Current Density	Transport Numbers				
I, mA/cm²	$c_{b\ sup.}$	$c_{b\ solo.}$	J, cm/h	e_p, %	I_{eff}, mA/cm²	Δt^a	Δt^c	$\bar{\Delta}t$	$\hat{t}_1^c$	$\hat{t}_2^a$
5	1,68	2,06	0,0728	65,61	3,28	0,81	0,79	0,80	0,90	0,90
10	2,10	2,52	0,1165	65,46	6,55	0,79	0,78	0,79	0,89	0,89
15	2,53	3,07	0,1390	62,87	9,43	0,76	0,76	0,76	0,88	0,88
20	2,91	3,81	0,1456	56,82	11,36	0,74	0,74	0,74	0,87	0,87
30	3,42		0,1655	50,59	15,17					
40	3,58	5,74	0,1854	44,48	17,79	0,711	0,72	0,71	0,86	0,86

Electro-osmotic coefficient $(2\beta) = 0,156$ ℓ/F (slope $= 0,0058244$ mℓ/mAh)
$J_{osm} =$ y-intercept $= 0,0801568$ cm/h
$c_b^{max} = 6,41$ mol/l
$\Delta t^c = t_1^c - t_2^c$

$\Delta t^a = t_2^a - t_1^a$
$\bar{\Delta}t =$ Average transport number of membrane pair
$\hat{t}_1^c =$ Transport number of cation through cation membrane
$\hat{t}_2^a =$ Transport number of anion through anion membrane.

Table 6.19: Electro-osmotic pumping experimental conditions and results for 0,5 mol/ℓ sodium chloride (WTPSA-1, WTPSC-1)

Current Density	Brine concentration c_b, mol/l		Water flow	Current Efficiency	Effective Current Density	Transport Numbers				
I, mA/cm²	$c_{b\ exp.}$	$c_{b\ calc.}$	J, cm/h	e_p, %	I_{eff}, mA/cm²	Δt^c	Δt^a	$\bar{\Delta}t$	$\bar{t}_1^c$	$\bar{t}_2^a$
10	2,22	2,12	0,1218	72,51	7,25	0,72	0,66	0,69	0,86	0,83
20	3,17	3,034	0,1589	67,53	13,51	0,68	0,61	0,64	0,84	0,81
30	3,68	3,95	0,1766	58,06	17,42	0,65	0,60	0,62	0,82	0,80
40	3,77		0,2030	51,58	20,63					
50	3,90		0,2207	46,16	23,07					
60	4,01		0,2295	41,13	24,68					
80	4,1	6,951	0,2560	35,18	28,42	0,62	0,57	0,60	0,81	0,78
100	4,24	7,937	0,2825	32,11	32,11	0,63	0,57	0,60	0,81	0,78

Electro-osmotic coefficient (2β) = 0,175 ℓ/F (slope = 0,0065332 mℓ/mAh)
J_{osm} = y-intercept = 0,0699265 cm/h
c_b^{max} = 5,71 mol/l
$\Delta t^c = t_1^c - t_2^c$

$\Delta t^a = t_2^a - t_1^a$
$\bar{\Delta}t$ = Average transport number of membrane pair
$\bar{t}_1^c$ = Transport number of cation through cation membrane
$\bar{t}_2^a$ = Transport number of anion through anion membrane.

Table 6.20: Electro-osmotic pumping experimental conditions and results for 1,0 mol/ℓ sodium chloride (WTPSA-1, WTPSC-1)

Current Density	Brine concentration c_b, mol/l		Water flow	Current Efficiency	Effective Current Density	Transport Numbers				
I, mA/cm²	$c_{b\ exp.}$	$c_{b\ calc.}$	J, cm/h	e_p, %	I_{eff}, mA/cm²	Δt^c	Δt^a	$\bar{\Delta}t$	$\bar{t}_1^c$	$\bar{t}_2^a$
30	3,77	2,63	0,2225	74,96	22,49	0,54	0,51	0,52	0,77	0,75
50	4,06	3,50	0,2667	58,04	29,02	0,51	0,49	0,50	0,76	0,74
70	4,17	4,82	0,2790	44,56	31,19	0,53	0,50	0,51	0,76	0,75
90	4,27	5,78	0,2914	37,06	33,35	0,51	0,49	0,50	0,76	0,75

Electro-osmotic coefficient (2β) = 0,175 ℓ/F (slope = 0,0065210 mℓ/mAh)
J_{osm} = y-intercept = 0,0762254 cm/h
c_b^{max} = 5,72 mol/l
$\Delta t^c = t_1^c - t_2^c$

$\Delta t^a = t_2^a - t_1^a$
$\bar{\Delta}t$ = Average transport number of membrane pair
$\bar{t}_1^c$ = Transport number of cation through cation membrane
$\bar{t}_2^a$ = Transport number of anion through anion membrane.

Table 6.21: Electro-osmotic pumping experimental conditions and results for 0,05 mol/ℓ sodium chloride (WTPVCA-2, WTPVCC-2)

Current Density	Brine concentration c_b, mol/l		Water flow	Current Efficiency	Effective Current Density	Transport Numbers				
I, mA/cm²	$c_{b\ exp.}$	$c_{b\ calc.}$	J, cm/h	e_p, %	I_{eff}, mA/cm²	Δt^c	Δt^a	$\bar{\Delta}t$	$\bar{t}_1^c$	$\bar{t}_2^a$
5	0,99	1,36	0,1077	56,24	2,81	0,79	0,77	0,79	0,90	0,89
10	1,3	1,77	0,1562	54,46	5,44	0,75	0,74	0,74	0,87	0,87
15	1,64	2,18	0,1788	52,40	7,86	0,75	0,64	0,70	0,87	0,82
20	1,74	2,07	0,2119	49,42	9,88	0,68	0,49	0,59	0,84	0,75
30	1,85	2,7	0,2913	48,17	14,45	0,75	0,66	0,70	0,87	0,83

Electro-osmotic coefficient (2β) = 0,412 ℓ/F (slope = 0,0153695 mℓ/mAh)
J_{osm} = y-intercept = 0,0649212 cm/h
c_b^{max} = 2,43 mol/l
$\Delta t^c = t_1^c - t_2^c$

$\Delta t^a = t_2^a - t_1^a$
$\bar{\Delta}t$ = Average transport number of membrane pair
$\bar{t}_1^c$ = Transport number of cation through cation membrane
$\bar{t}_2^a$ = Transport number of anion through anion membrane.

Table 6.22: Electro-osmotic pumping experimental conditions and results for 0,1 mol/l sodium chloride (WTPVCA-2, WTPVCC-2)

Current Density	Brine concentration c_b, mol/l		Water flow	Current Efficiency	Effective Current Density	Transport Numbers				
I, mA/cm²	$c_{b\,aup}$	$c_{b\,aoto}$	J, cm/h	e_p, %	I_{eff}, mA/cm²	Δt^*	Δt^*	$\bar{\Delta}t$	$\hat{t}_1^*$	$\hat{t}_2^*$
5	1,05	0,94	0,1509	59,65	2,98	0,79	0,74	0,76	0,89	0,87
10	1,47	1,80	0,1483	58,45	5,85	0,73	0,70	0,71	0,86	0,85
15	1,72	2,12	0,1854	56,99	8,55	0,72	0,68	0,70	0,86	0,84
20	1,92	2,17	0,2219	54,53	10,91	0,66	0,63	0,65	0,83	0,81
30	2,26	2,92	0,256	51,71	15,51	0,70	0,64	0,67	0,85	0,82
40	2,58	3,47	0,2825	48,853	19,54	0,68	0,64	0,66	0,84	0,82

Electro-osmotic coefficient (2β) = 0,261 l/F (slope = 0,0097235 ml/mAh)
J_{osm} = (y-intercept = 0,0994504 cm/h
c_b^{max} = 3,84 mol/l
$\Delta t^c = t_1^c - t_2^c$

$\Delta t^* = t_2^* - t_1^*$
$\bar{\Delta}t$ = Average transport number of membrane pair
t_1^c = Transport number of cation through cation membrane
t_2^* = Transport number of anion through anion membrane.

Table 6.23: Electro-osmotic pumping experimental conditions and results for 0,5 mol/l sodium chloride (WTPVCA-2, WTPVCC-2)

Current Density	Brine concentration c_b, mol/l		Water flow	Current Efficiency	Effective Current Density	Transport Numbers				
I, mA/cm²	$c_{b\,aup}$	$c_{b\,aoto}$	J, cm/h	e_p, %	I_{eff}, mA/cm²	Δt^*	Δt^*	$\bar{\Delta}t$	$\hat{t}_1^*$	$\hat{t}_2^*$
5	1,43	1,23	0,0971	74,463	3,7231	0,6620	0,6148	0,6384	0,83	0,81
10	1,77		0,1562	74,153	7,4153					
15	2,08	1,70	0,1942	72,207	10,831	0,6128	0,5666	0,5897	0,81	0,78
20	2,26		0,2295	69,54	13,908					
30	2,58		0,2913	67,173	20,152					
40	2,81	2,33	0,3443	64,848	25,939	0,5696	0,5070	0,5383	0,78	0,75
60	3,02	2,581	0,429	57,9	34,74	0,5179	0,4715	0,4947	0,76	0,74

Electro-osmotic coefficient (2β) = 0,267 l/F (slope = 0,0099646 ml/mAh)
J_{osm} = y-intercept = 0,0869006 cm/h
c_b^{max} = 3,74 mol/l
$\Delta t^c = t_1^c - t_2^c$

$\Delta t^* = t_2^* - t_1^*$
$\bar{\Delta}t$ = Average transport number of membrane pair
t_1^c = Transport number of cation through cation membrane
t_2^* = Transport number of anion through anion membrane.

Table 6.24: Electro-osmotic pumping experimental conditions and results for 1,0 mol/l sodium chloride (WTPVCA-2, WTPVCC-2)

Current Density	Brine concentration c_b, mol/l		Water flow	Current Efficiency	Effective Current Density	Transport Numbers				
I, mA/cm²	$c_{b\,aup}$	$c_{b\,aoto}$	J, cm/h	e_p, %	I_{eff}, mA/cm²	Δt^c	Δt^*	$\bar{\Delta}t$	$\hat{t}_1^*$	$\hat{t}_2^*$
10	2,0	1,25	0,20	81,66	8,17	0,55	0,47	0,51	0,78	0,73
20	2,4	1,37	0,25	80,67	16,13	0,47	0,44	0,46	0,74	0,72
40	3,14	1,68	0,37	78,04	31,22	0,43	0,40	0,42	0,72	0,70
60	3,26	1,88	0,48	70,22	42,13	0,41	0,40	0,41	0,70	0,70

Electro-osmotic coefficient (2β) = 0,221 l/F (slope = 0,0082250 ml/mAh)
J_{osm} = y-intercept = 0,125719 cm/h
c_b^{max} = 4,54 mol/l
$\Delta t^c = t_1^c - t_2^c$

$\Delta t^* = t_2^* - t_1^*$
$\bar{\Delta}t$ = Average transport number of membrane pair
t_1^c = Transport number of cation through cation membrane
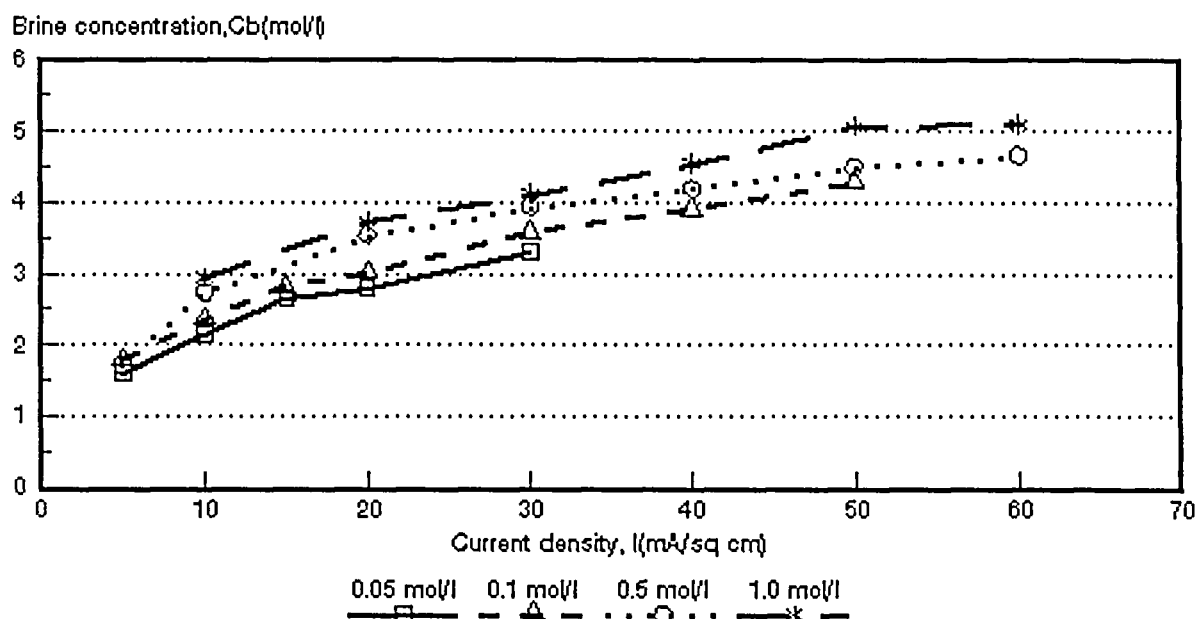t_2^* = Transport number of anion through anion membrane.

Table 6.25: Electro-osmotic pumping experimental conditions and results for 0,05 mol/ℓ sodium chloride (WTPSTA-3, WTPSTC-3)

Current Density	Brine concentration c_b, mol/l		Water flow	Current Efficiency	Effective Current Density	Transport Numbers				
I, mA/cm²	$c_{b\,exp.}$	$c_{b\,calc.}$	J, cm/h	e_p, %	I_{eff}, mA/cm²	Δt^c	Δt^a	$\overline{\Delta t}$	$\overline{t}_1^c$	$\overline{t}_2^a$
10	1,65	2,29	0,1368	60,53	6,05	0,87	0,81	0,84	0,93	0,90
15	1,92	2,65	0,1721	59,08	8,86	0,82	0,81	0,81	0,91	0,90
20	2,08	3,01	0,1960	54,65	10,93	0,81	0,78	0,80	0,90	0,90
25	2,11	3,20	0,2295	51,69	12,92	0,78	0,80	0,79	0,89	0,89
30	2,16	3,32	0,2649	51,13	15,34	0,79	0,78	0,79	0,89	0,89

Electro-osmotic coefficient (2β) = 0,371 ℓ/F (slope = 0,0138276 mℓ/mAh)
J_{osm} = y-intercept = 0,0502337 cm/h
c_b^{max} = 2,69 mol/l
$\Delta t^c = t_1^c - t_2^c$

$\Delta t^a = t_2^a - t_1^a$
$\overline{\Delta t}$ = Average transport number of membrane pair
$\overline{t}_1^c$ = Transport number of cation through cation membrane
$\overline{t}_2^a$ = Transport number of anion through anion membrane.

Table 6.26: Electro-osmotic pumping experimental conditions and results for 0,1 mol/ℓ sodium chloride (WTPSTA-3, WTPSTC-3)

Current Density	Brine concentration c_b, mol/l		Water flow	Current Efficiency	Effective Current Density	Transport Numbers				
I, mA/cm²	$c_{b\,exp.}$	$c_{b\,calc.}$	J, cm/h	e_p, %	I_{eff}, mA/cm²	Δt^c	Δt^a	$\overline{\Delta t}$	$\overline{t}_1^c$	$\overline{t}_2^a$
10	1,76	2,14	0,1404	66,24	6,62	0,83	0,77	0,80	0,92	0,89
15	1,87	2,31	0,1920	64,18	9,63	0,83	0,76	0,79	0,91	0,88
20	2,19	2,71	0,2154	63,24	12,65	0,82	0,75	0,78	0,91	0,88
30	2,35	2,90	0,2914	61,19	18,36	0,78	0,74	0,76	0,88	0,87
40	2,55	3,23	0,3496	59,75	23,90	0,78	0,74	0,76	0,89	0,87
50	2,64	2,96	0,4186	59,24	29,62	0,63	0,69	0,66	0,82	0,85

Electro-osmotic coefficient (2β) = 0,317 ℓ/F (slope = 0,011834 mℓ/mAh)
J_{osm} = y-intercept = 0,0691379 cm/h
c_b^{max} = 3,15 mol/l
$\Delta t^c = t_1^c - t_2^c$

$\Delta t^a = t_2^a - t_1^a$
$\overline{\Delta t}$ = Average transport number of membrane pair
$\overline{t}_1^c$ = Transport number of cation through cation membrane
$\overline{t}_2^a$ = Transport number of anion through anion membrane.

Table 6.27: Electro-osmotic pumping experimental conditions and results for 0,5 mol/ℓ sodium choiride (WTPSTA-3, WTPSTC-3)

Current Density	Brine concentration c_b, mol/l		Water flow	Current Efficiency	Effective Current Density	Transport Numbers				
I, mA/cm²	$c_{b\,exp.}$	$c_{b\,calc.}$	J, cm/h	e_p, %	I_{eff}, mA/cm²	Δt^c	Δt^a	$\overline{\Delta t}$	$\overline{t}_1^c$	$\overline{t}_2^a$
10	2,02	1,87	0,1377	74,96	7,50	0,74	0,65	0,69	0,87	0,82
20	2,45	2,23	0,2225	73,07	14,61	0,72	0,61	0,66	0,86	0,81
30	2,85	2,56	0.2826	71,96	21,59	0,70	0,59	0,65	0,85	0,80
40	2,91	2,56	0,3576	69,74	27,90	0,65	0,58	0,61	0,82	0,79
50	3,11	2,88	0,4026	67,13	33,57	0,67	0,57	0,62	0,83	0,79
70	3,29	2,75	0,5033	63,41	44,39	0,53	0,53	0,53	0,76	0,76
90	3,37	3,45	0,6093	61,15	55,04	0,65	0,60	0,63	0,82	0,80
110	3,41	3,59	0,7152	59,43	65,38	0,65	0,60	0,62	0,82	0,80

Electro-osmotic coefficient (2β) = 0,259 ℓ/F (slope = 0,0096672 mℓ/mAh)
J_{osm} = y-intercept = 0,0793991 cm/h
c_b^{max} = 3,86 mol/l
$\Delta t^c = t_1^c - t_2^c$

$\Delta t^a = t_2^a - t_1^a$
$\overline{\Delta t}$ = Average transport number of membrane pair
$\overline{t}_1^c$ = Transport number of cation through cation membrane
$\overline{t}_2^a$ = Transport number of anion through anion membrane.

Table 6.28: Electro-osmotic pumping experimental conditions and results for 1,0 mol/l sodium chloride (WTPSTA-3, WTPTSC-3)

Current Density	Brine concentration c_b, mol/l		Water flow	Current Efficiency	Effective Current Density	Transport Numbers				
I, mA/cm²	$c_{b\,a.p.}$	$c_{b\,ano.}$	J, cm/h	e_p, %	I_{eff}, mA/cm²	Δt^a	Δt^c	$\bar{\Delta}t$	t_i^c	t_i^a
30	2,94	2,02	0,3179	83,51	25,05	0,62	0,52	0,57	0,81	0,76
50	3,27	2,18	0,4715	82,67	41,33	0,61	0,49	0,55	0,81	0,75
70	3,41	2,45	0,5827	76,10	53,27	0,60	0,49	0,55	0,80	0,74
90	3,47	2,43	0,7159	73,92	66,53	0,54	0,49	0,52	0,77	0,75

Electro-osmotic coefficient (2β) = 0,257 l/F (slope = 0,0095674 ml/mAh)
J_{osm} = y-intercept = 0,0766808 cm/h
c_b^{max} = 3,90 mol/l
Δt^c = t_i^c - t_j^c

Δt^a = t_i^a - t_j^a
$\bar{\Delta}t$ = Average transport number of membrane pair
t_i^c = Transport number of cation through cation membrane
t_i^a = Transport number of anion through anion membrane.

Brine concentration,Cb(mol/l)

Current density, I(mA/sq cm)

0.05 mol/l   0.1 mol/l   0.5 mol/l   1.0 mol/l

Figure 6.1:   Brine concentration as a function of current density for 4 different NaCl feed concentrations. Selemion AMV and CMV membranes.

Brine concentration, Cb(mol/l)

Current density, I(mA/sq cm)

0.05 mol/l   0.1 mol/l   0.5 mol/l   1.0 mol/l
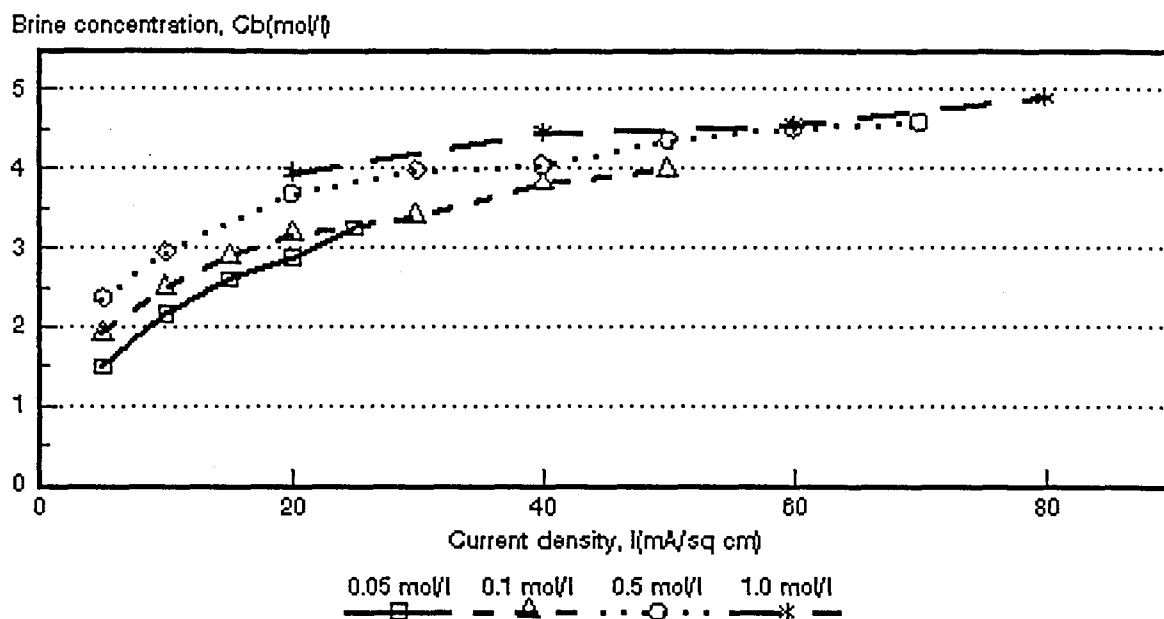
Figure 6.2: Brine concentration as a function of current density for 4 different NaCl feed concentrations. *Ionac* MA-3475 and MC-3470 membranes.

Brine concentration,Cb(mol/l)

Current density, I(mA/sq cm)

0.05 mol/l   0.1 mol/l   0.5 mol/l   1.0 mol/l
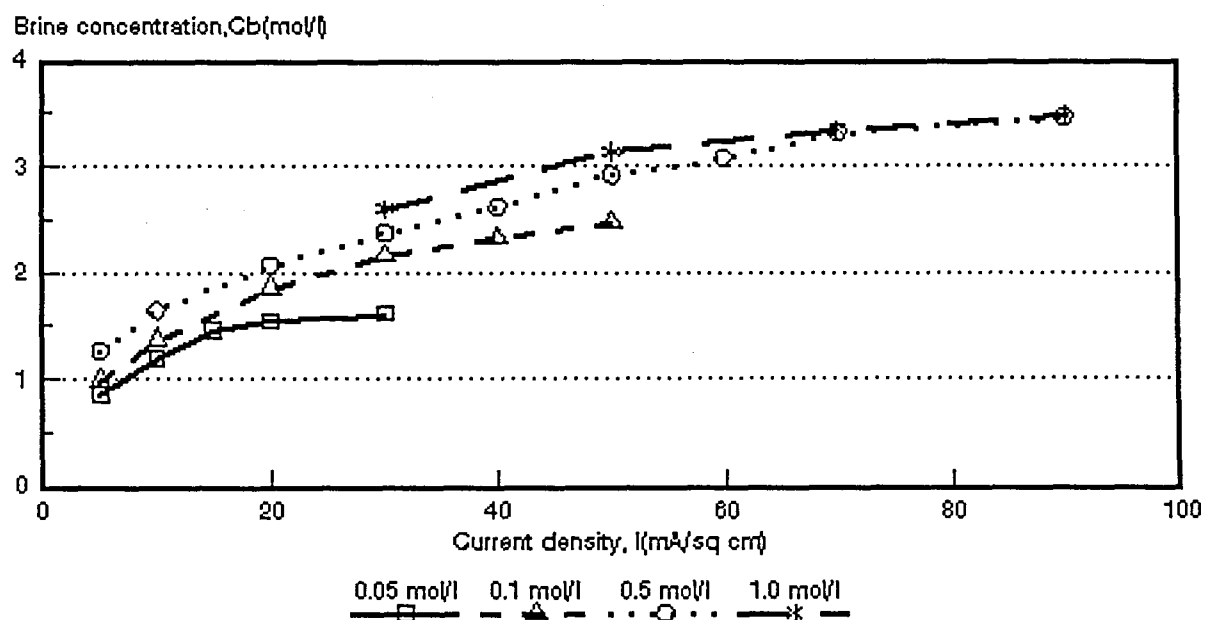
Figure 6.3: Brine concentration as a function of current density for 4 different NaCl feed concentrations. *Raipore* R4030 and R4010 membranes.

Brine concentration, (Cb mol/l)

Current density, I (mA/sq cm)

0.05 mol/l   0.1 mol/l   0.5 mol/l   1.0 mol/l
——⊟——   — ⚠ —   ··O··   ——✳ —
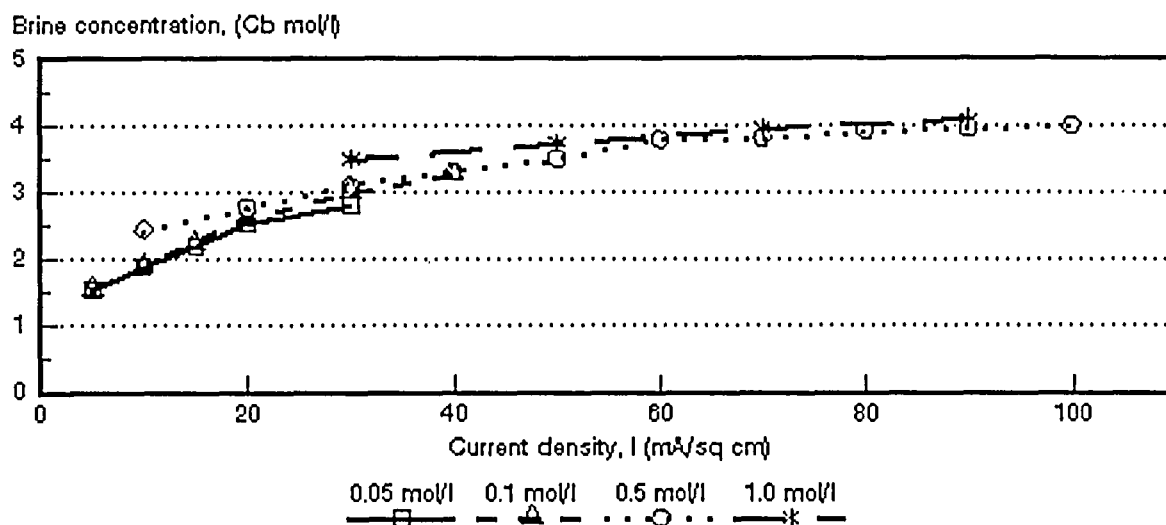
Figure 6.4:   Brine concentration as a function of current density for 4 different NaCl
feed concentrations. *Ionics* A-204-UZL-386 and C-61-CZL-386 membranes.

Brine concentration,Cb(mol/l)

Current density, I(mA/sq cm)

0.05 mol/l   0.1 mol/l   0.5 mol/l   1.0 mol/l
——⊟——   — ⚠ —   ··O··   ——✳ —
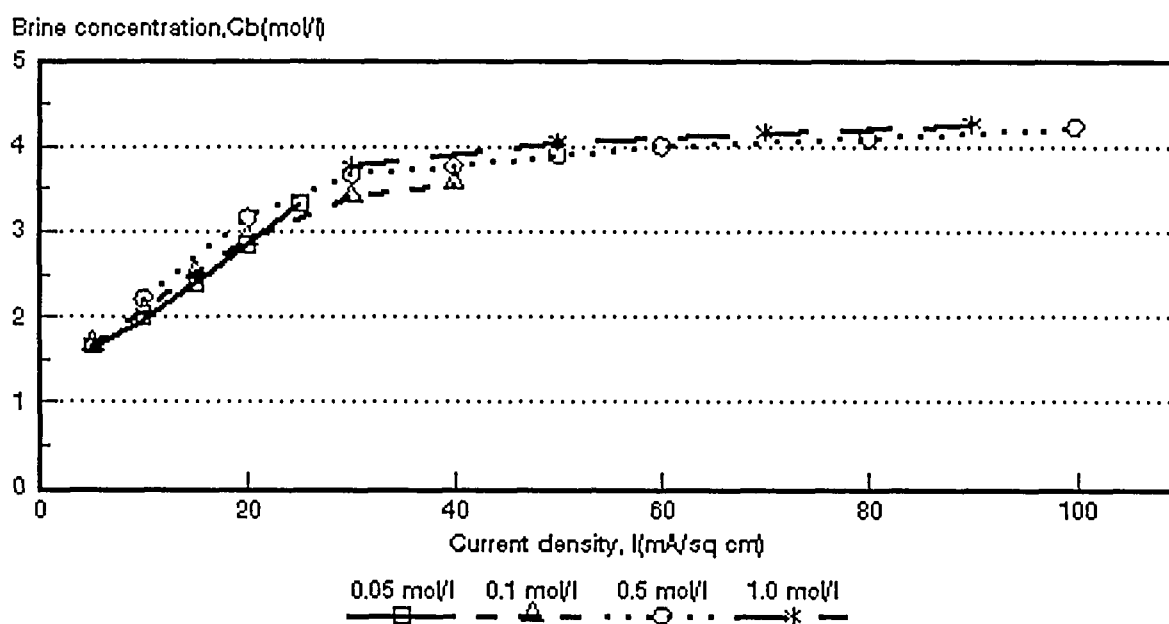
Figure 6.5:   Brine concentration as a function of current density for 4 different NaCl
feed concentrations. WTPSA-1 and WTPSC-1 membranes.

Brine concentration, Cb (mol/l)

Current density, I (mA/sq cm)

0.05 mol/l   0.1 mol/l   0.5 mol/l   1.0 mol/l
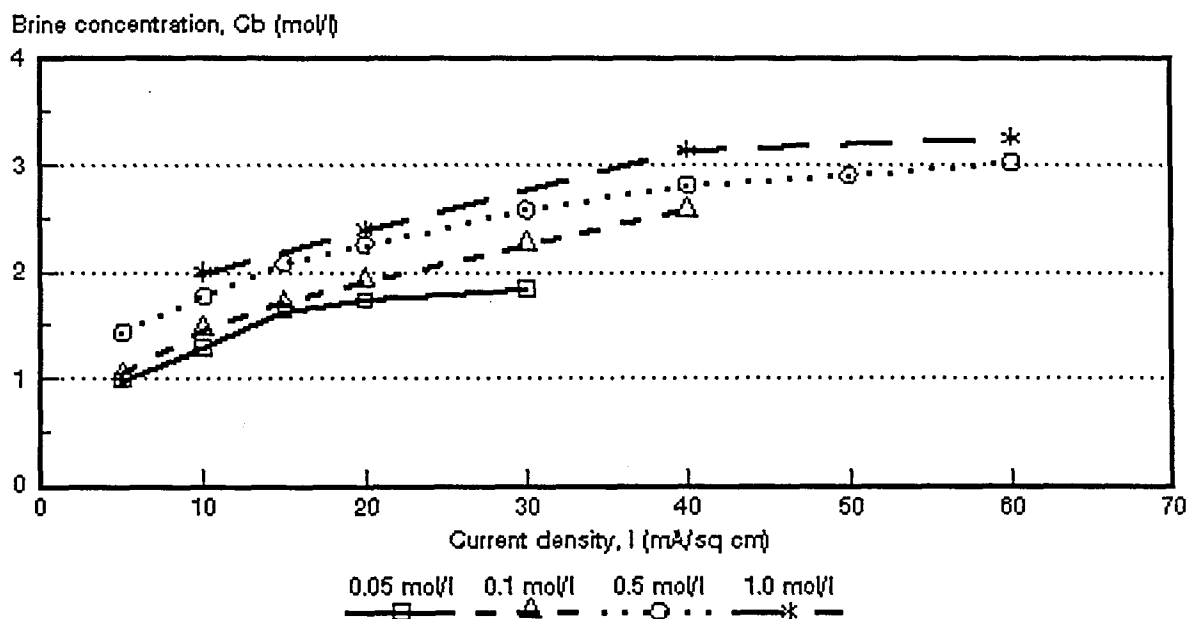
Figure 6.6: Brine concentration as a function of current density for 4 different NaCl feed concentrations. WTPVCA-2 and WTPVCC-2 membranes.

Brine concentration, Cb (mol/l)

Current density, I (mA/sq cm)

0.05 mol/l   0.5 mol/l   0.5 mol/l   1.0 mol/l
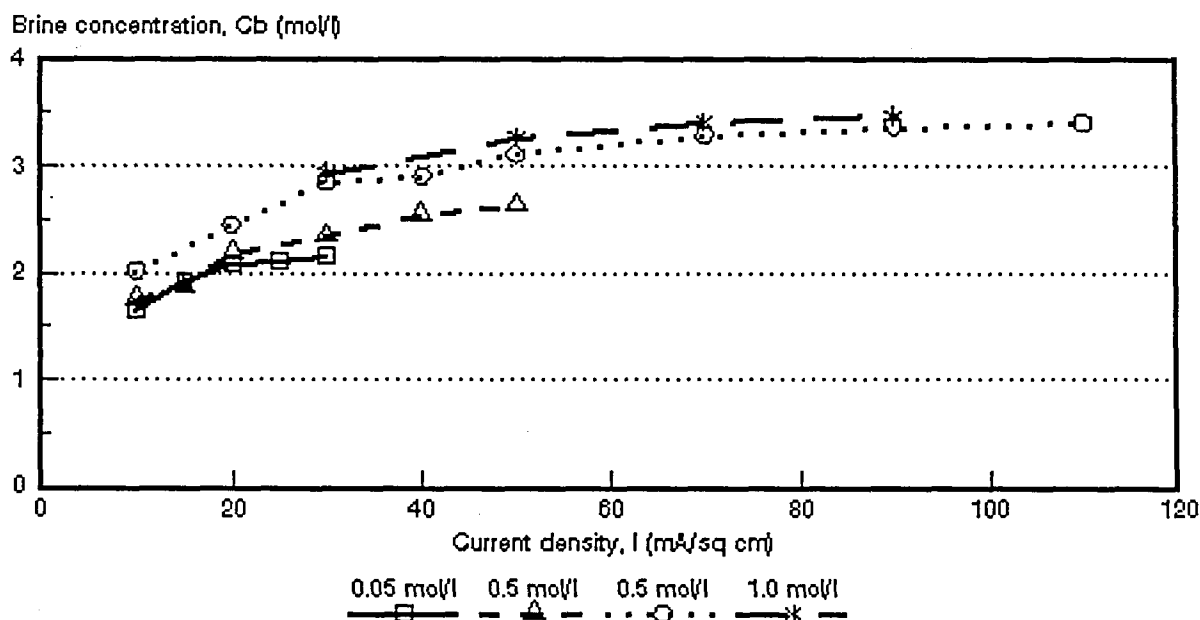
Figure 6.7: Brine concentration as a function of current density for 4 different NaCl feed concentrations. WTPSTA-3 and WTPSTC-3 membranes.

Table 6.29: Brine concentrations obtained at the highest current densities investigated for different sodium chloride feed concentrations

Feed Concentration mol/ℓ	Brine Concentration* (%)						
	Solemion	Ionac	Raipore	Ionics	WTPS	WTPVC	WTPST
0,05	19,3	19,0	9,5	16,4	19,4	10,8	12,6
0,10	25,1	23,4	14,4	19,0	20,9	15,1	15,4
0,50	27,2	26,8	20,2	23,3	24,8	17,7	19,9
1,0	29,8	28,7	20,3	23,8	25,0	19,1	20,3

* Brine concentrations obtained from data in Tables 6.1 to 6.28.

$$\text{and} \quad c_b^{max} = c_b(1 + J_{osm}/J_{closm}) \qquad \text{(see eq. 3.10.31)}$$

The results are shown in Tables 6.30 and Figures 6.8 to 6.14. Very good correlations were obtained with the above two relationships to determine c_b^{max}. Consequently, any one of these two methods can be used to determine c_b^{max}.

Maximum brine concentration seems to depend more on feed concentration in the case of the *Selemion-* (Fig. 6.8), *Raipore-* (Fig. 6.10), WTPS- (Fig. 6.12), WTPVC- (Fig. 6.13) and WTPST- (Fig. 6.14) membranes than has been experienced with the *Ionac-* (Fig. 6.9) and *Ionics-* (Fig. 6.11) membranes. This effect was especially pronounced for the *Selemion-*, *Raipore-* and WTPS membranes, and to a lesser extent for the WTPVC- and WTPST membranes. Much less change in maximum brine concentration as a function of feed concentration was experienced with the *Ionac-* (Fig. 6.9) and *Ionics* (Fig. 6.11) membranes. The *Ionac-* and *Ionics* membranes showed almost no dependence of maximum brine concentration on feed concentration in the feed concentration range of 0,05 to 1,0 mol/ℓ. It is interesting to note that the calculated maximum brine concentration has been very high at 0,05 mol/ℓ feed concentration in the case of the WTPS membranes (Fig. 6.12). The maximum brine concentration first declined very rapidly and then much slower to become almost independent of feed concentration in the 0,1 to 1,0 mol/ℓ feed concentration range. This opposite behaviour encountered with the more hydrophobic WTPS membranes can be ascribed to membrane swelling when the membranes come into contact with water[42].

Brine concentrations at different current densities were predicted from measured transport numbers and volume flows (J) with the relationship:

$$c_b = \frac{I\bar{\Delta}t}{2FJ} \qquad \text{(see eq. 3.10.17)}$$

The experimental and calculated brine concentrations are shown in Tables 6.1 to 6.28 and Figures 6.15 to 6.42. The calculated brine concentrations were determined from the average value of the apparent transport numbers (Δt's) of a membrane pair ($\bar{\Delta}$t) and from the water flows (J).

The correlation between the calculated and experimentally determined brine concentrations expressed as the ratio c_{bcalc}/c_{bexp} is shown in Table 6.31. The calculated brine concentrations were higher than the experimentally determined brine concentrations in the 0,05 to 0,1 mol/ℓ feed concentration range in the case of the *Selemion-, Ionac-, Ionics-*, WTPS-, WTPVC- and WTPST membranes (Figs. 6.15 to 6.42 and Table 6.31). The calculated brine concentration was still higher than the experimentally determined brine concentration at 0,5 mol/ℓ feed concentration for the *Raipore* membranes (Fig. 6.25). However, calculated brine concentrations became less than the experimentally determined brine concentrations in the 0,5 to 1,0 mol/ℓ feed concentration range in the case of the *Selemion-* (Fig's. 6.17 and 6.18), *Ionac-* (Fig's. 6.21 and 6.22), *Ionics-* (Fig's. 6.29 and 6.30), WTPVC- (Fig's. 6.37 and 6.38) and WTPST (Fig's. 6.41 and 6.42) membranes. Calculated brine concentration became less than the experimentally determined brine concentration at 1,0 mol/ℓ feed concentration for the *Raipore-* (Fig. 6.26) and WTPS- (Fig. 6.34) membranes.

Good correlations were obtained between the calculated and experimentally determined brine concentrations for all the membranes investigated depending on feed concentration and current density used (Table 6.31). For the *Selemion* membranes the ratio c_{bcalc}/c_{bexp} varied between 1,0 and 1,07 in the current density range from 15 to 50 mA/cm² (0,1 mol/ℓ feed). In the case of the *Ionac* membranes the ratio c_{bcalc}/c_{bexp} varied between 0,95 and 1,1 in the current density range from 40 to 70 mA/cm² (0,5 mol/ℓ feed). The c_{bcalc}/c_{bexp} ratio for the *Raipore* membranes varied between 0,93 and 1,05 in the 40 to 90 mA/cm² current density range (0,5 mol/ℓ feed). The correlation between c_{bcalc}/c_{bexp} for the *Ionics* membranes varied between 0,91 and 1,06 in the current density range from 10 to 100 mA/cm² (0,5 mol/ℓ feed). The WTPS membranes showed a very good correlation of 0,95 to 1,07 of c_{bcalc}/c_{bexp} in the current density range from 10 to 30 mA/cm² (0,5 mol/ℓ feed). However, a poor correlation was obtained at high current densities. The WTPVC membranes showed a correlation of c_{bcalc}/c_{bexp} of 0,82 to 0,86 in the 5 to 60 mA/cm² current density range (0,5 mol/ℓ

feed) while the WTPST membranes showed a correlation of 0,84 to 1,05 in the 10 to 110 mA/cm² current density range (0,5 mol/ℓ feed). Therefore, brine concentration should be reasonably accurately predicted from simple transport number and water flow determinations depending on feed water concentration and current density used.

Table 6.30: **Maximum brine concentration calculated from**

$$c_b^{max} = 1/2 \, F\beta^* \text{ and } c_b^{max} = c_b \, (1 + J_{osm}/J_{elosm})^{**}$$

Feed Concentration mol/ℓ	Maximum Brine Concentration, c_b^{max} (mol/ℓ)													
	Selemion		Ionac		Ralpore		Ionics		WTPS		WTPVC		WTPST	
	1	2	1	2	1	2	1	2	1	2	1	2	1	2
0,05	4,55	4,54	5,37	5,31	1,83	1,83	4,27	4,29	11,5	11,38	2,43	2,44	2,69	2,71
0,10	5,05	5,06	4,85	4,80	3,13	3,12	4,89	4,83	6,41	6,42	3,84	3,71	3,15	3,11
0,50	5,36	5,31	5,26	5,29	3,98	4,02	4,73	4,74	5,71	5,76	3,74	3,77	3,86	3,85
1,00	6,48	6,49	5,35	5,44	4,24	4,22	4,63	4,63	5,72	5,74	4,54	4,66	3,90	3,89

1   : $c_b^{max} = 1/2 \, F\beta$

2   : $c_b^{max} = c_b \, (1 + J_{osm} / J_{elosm})$

*   :   Calculated from electro-osmotic coefficients (Tables 6.1 to 6.28)

**   :   Calculated from $J_{elosm} = J - J_{osm}$ (y-intercept and the corresponding c_b values) (Tables 6.1 to 6.28).

Cb max

Cb max =1/2 FB   Cb max= Cb(1 + Josm/Jelosm)
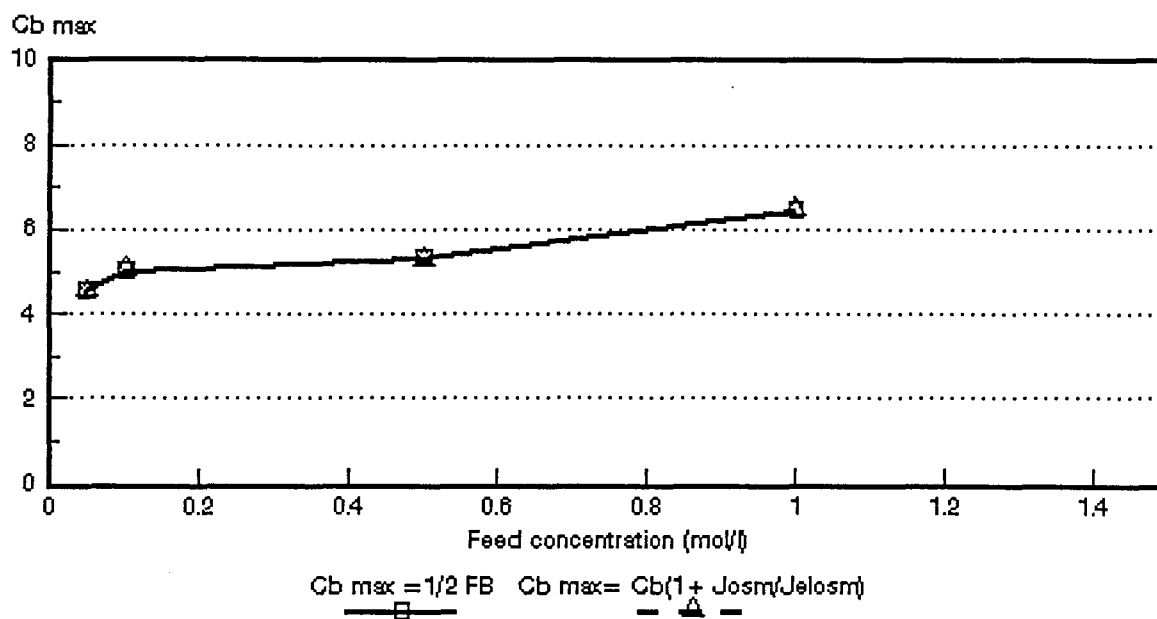
Figure 6.8: c_b^{max} as a function of feed concentration for different NaCl feed concentrations. *Selemion* AMV and CMV membranes.

Cb max

Cb max =1/2 FB   Cb max= Cb(1 + Josm/Jelosm)
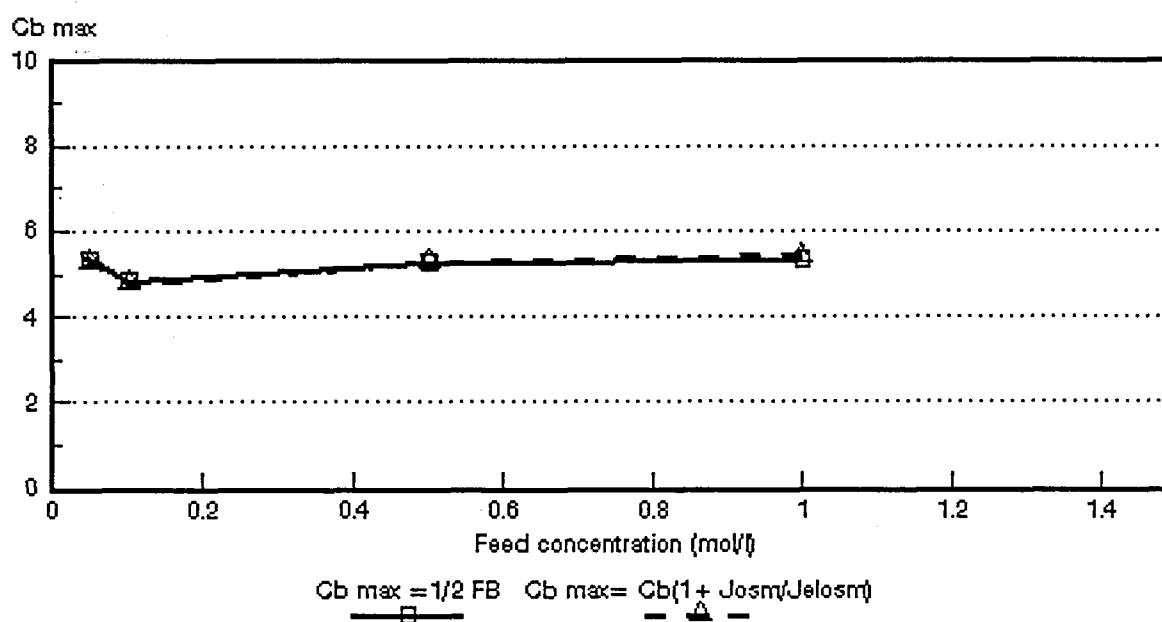
Figure 6.9: c_b^{max} as a function of feed concentration for different NaCl feed concentrations. *Ionac* MA-3475 and MC-3470 membranes.
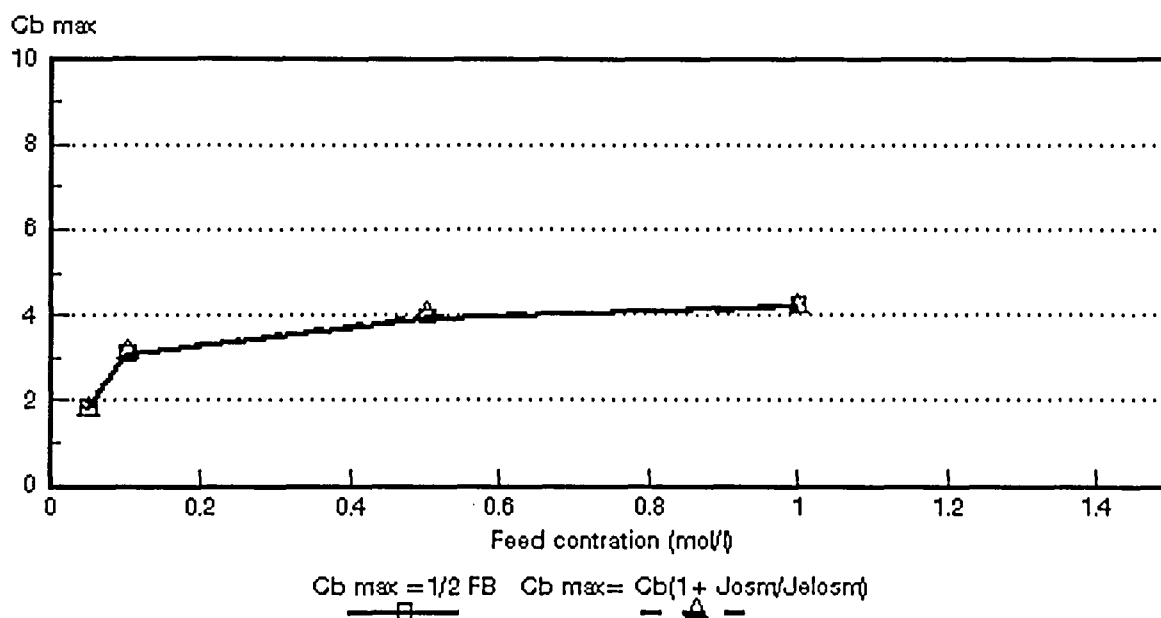
Figure 6.10: c_b^{max} as a function of feed concentration for different NaCl feed concentrations. *Ralpore* R4030 and R4010 membranes.
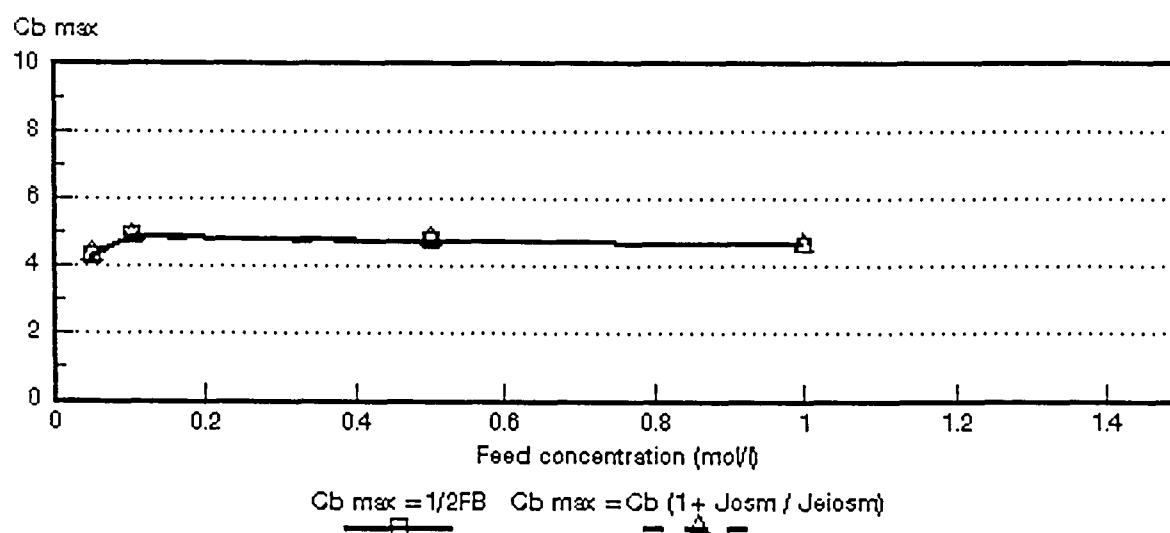
Figure 6.11: c_b^{max} as a function of feed concentration for different NaCl feed concentrations. *Ionics* A-204-UZL-386 and C-61-CZL-386 membranes.
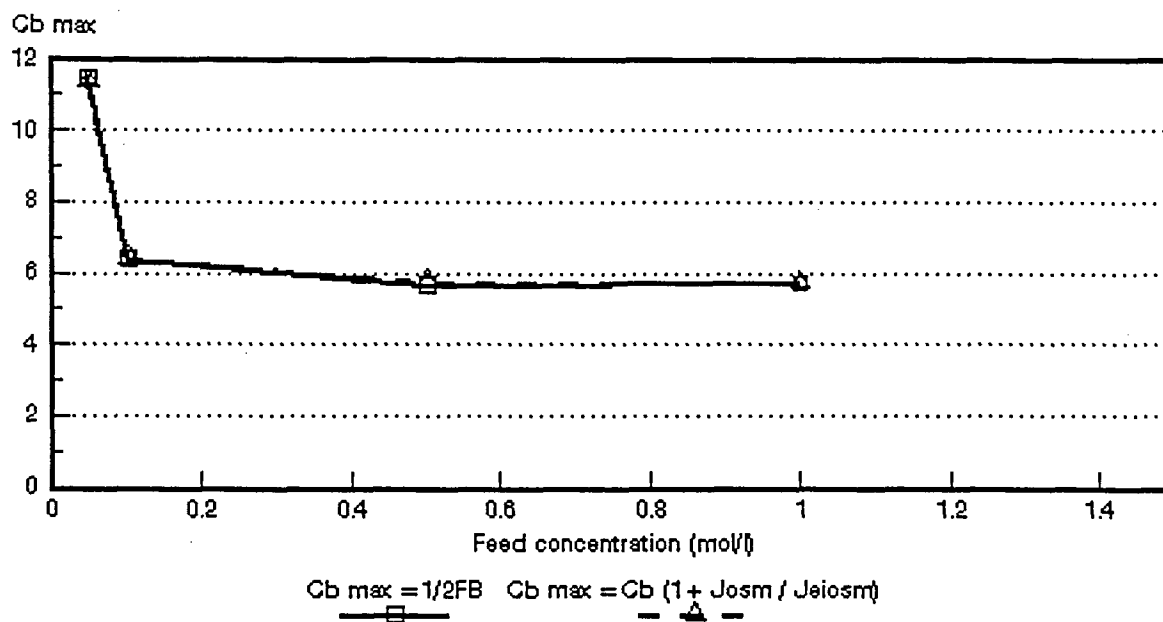
Figure 6.12: c_b^{max} as a function of feed concentration for different NaCl feed concentrations. WTPSA-1 and WTPSC-1 membranes.
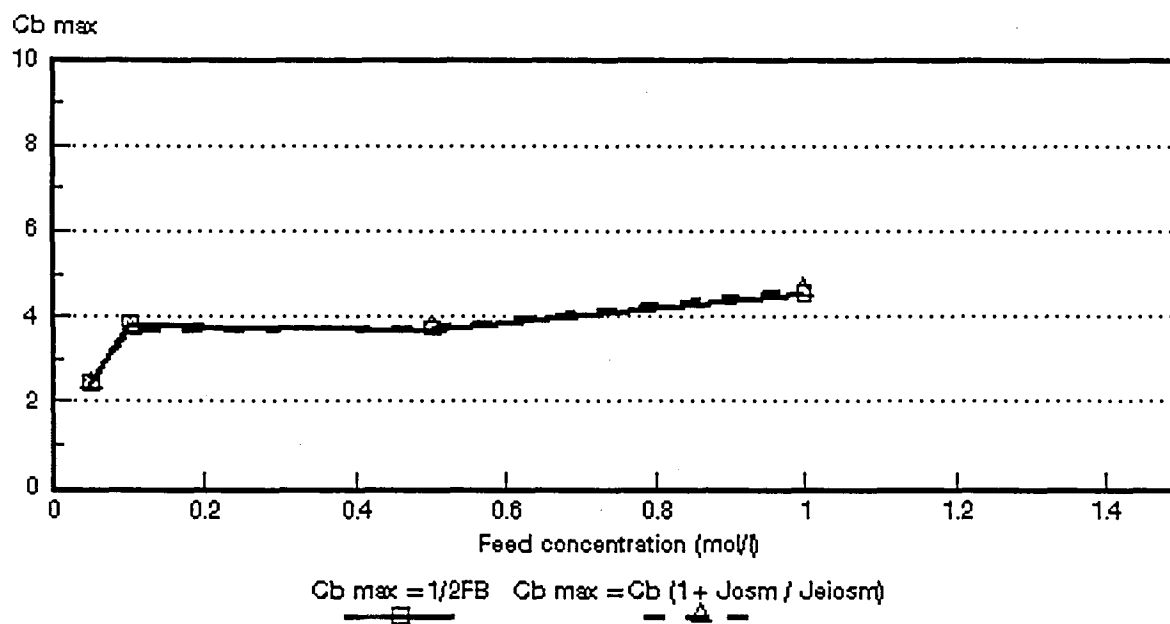
Figure 6.13: c_b^{max} as a function of feed concentration for different NaCl feed concentrations. WTPVCA-2 and WTPVCC-2 membranes.
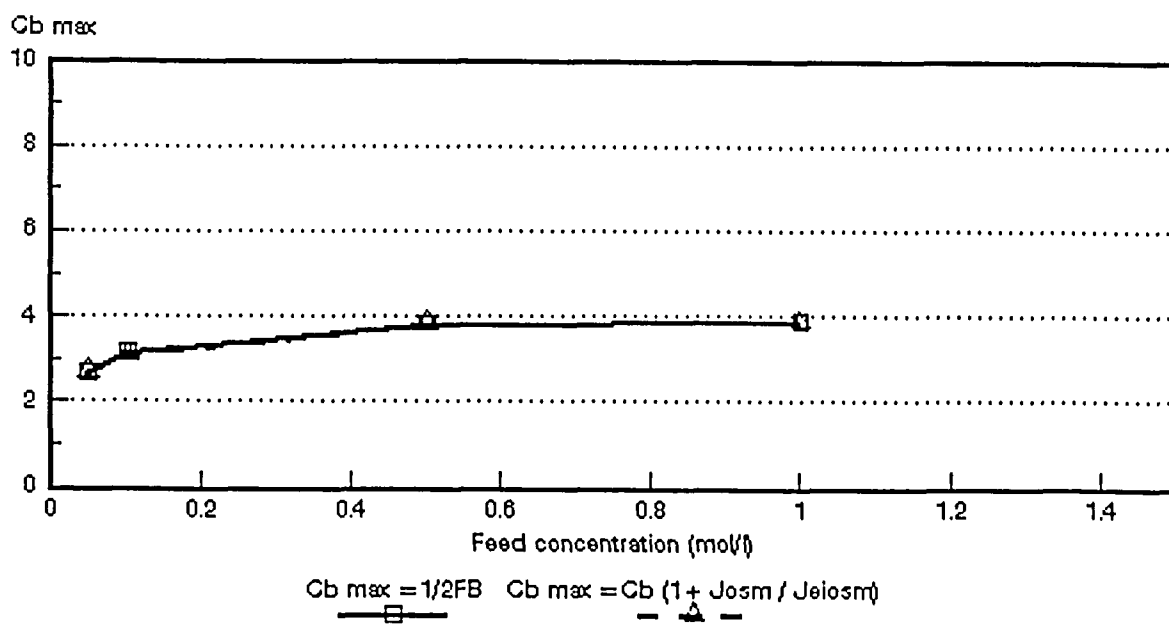
Figure 6.14: c_b^{max} as a function of feed concentration for different NaCl feed concentrations. WTPSTA-3 and WTPSTC-3 membranes.
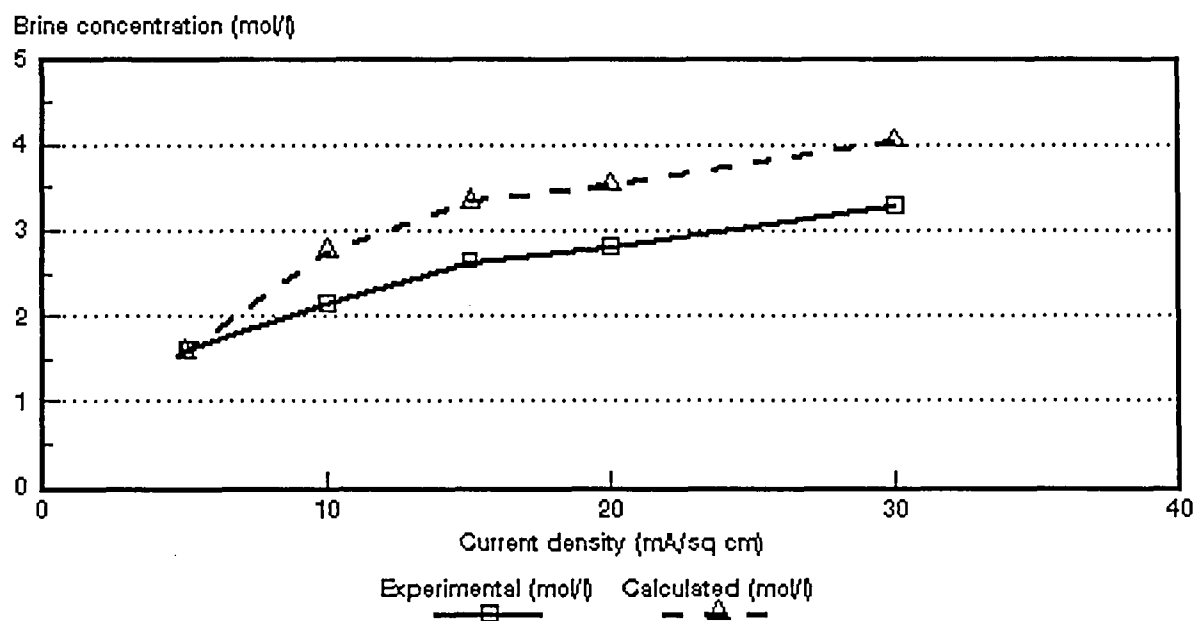
Figure 6.15: Experimental and calculated brine concentrations as a function of current density for 0,05 mol/ℓ NaCl feed solution. *Selemiom* AMV and CMV membranes.

168
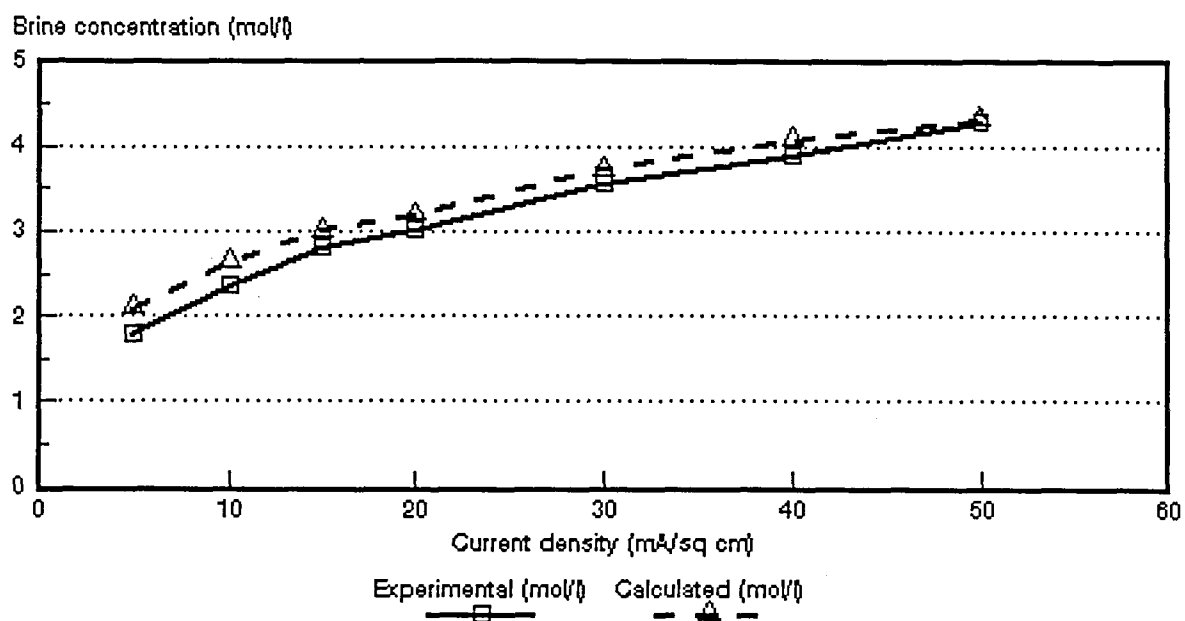
Figure 6.16: Experimental and calculated brine concentrations as a function of current density for 0,1 mol/ℓ NaCl feed solution. *Selemion* AMV and CMV membranes.
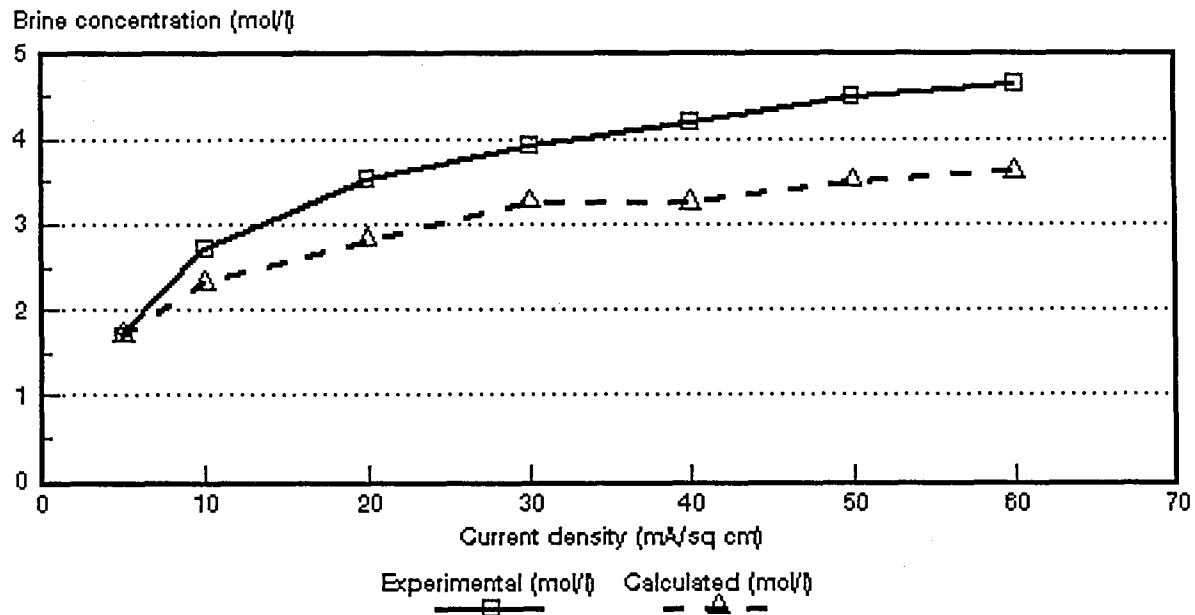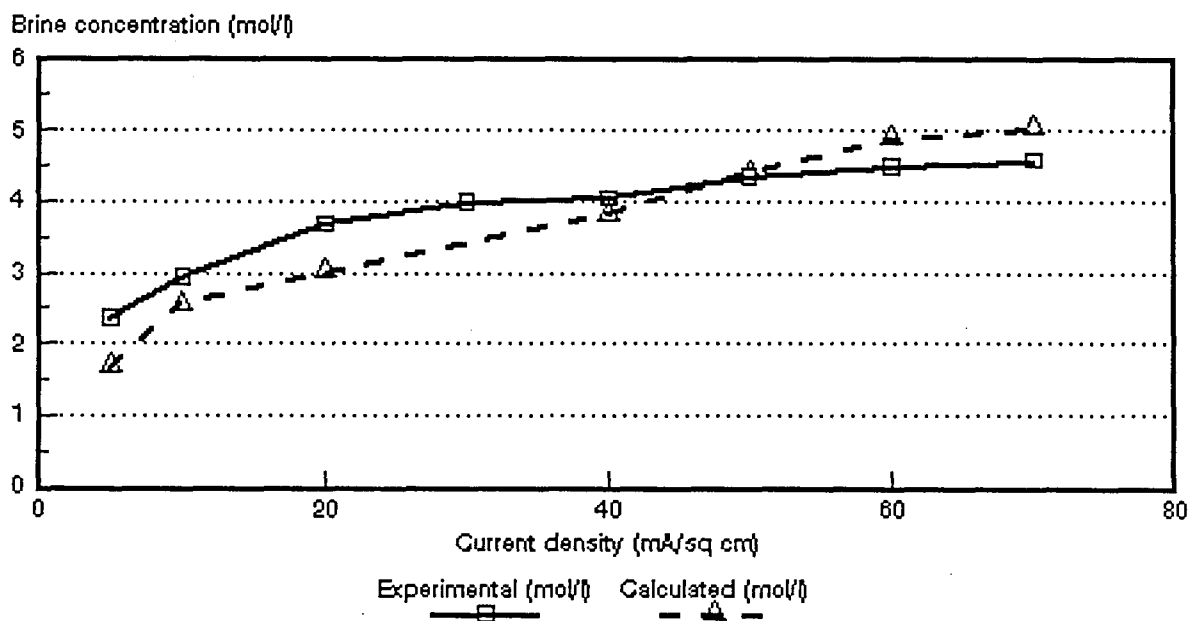

Figure 6.17: Experimental and calculated brine concentrations as a function of current density for 0,5 mol/ℓ NaCl feed solution. *Selemion* AMV and CMV membranes.

Brine concentration (mol/l)
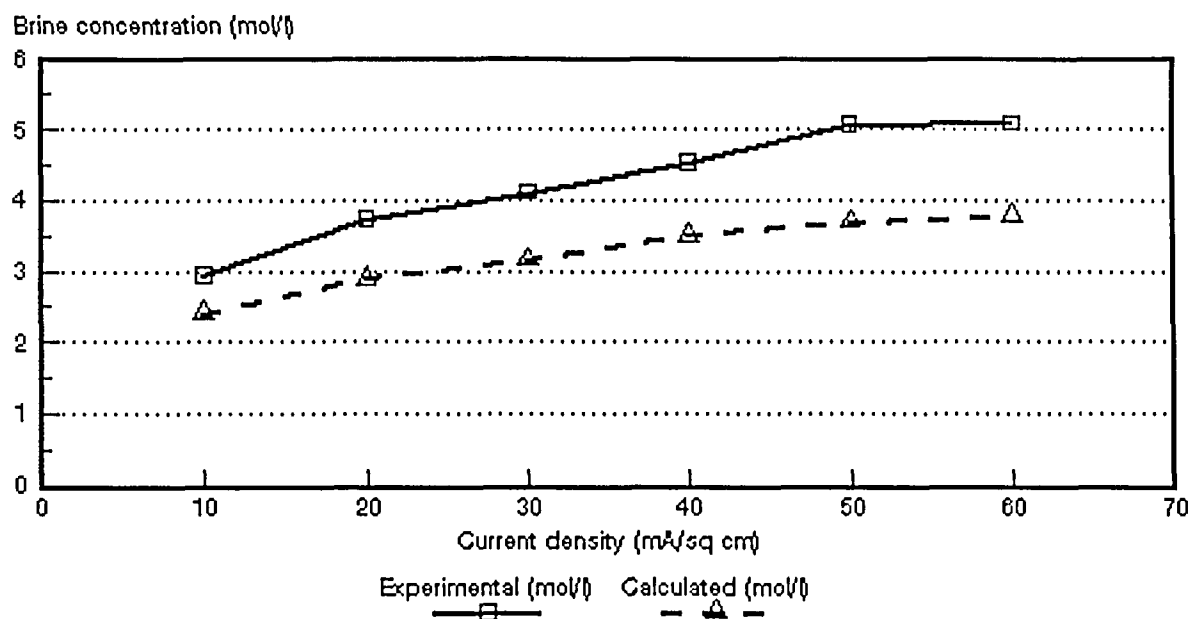
Figure 6.18: Experimental and calculated brine concentrations as a function of current density for 1,0 mol/ℓ NaCl feed solution. *Selemion* AMV and CMV membranes.

Brine concentration (mol/l)
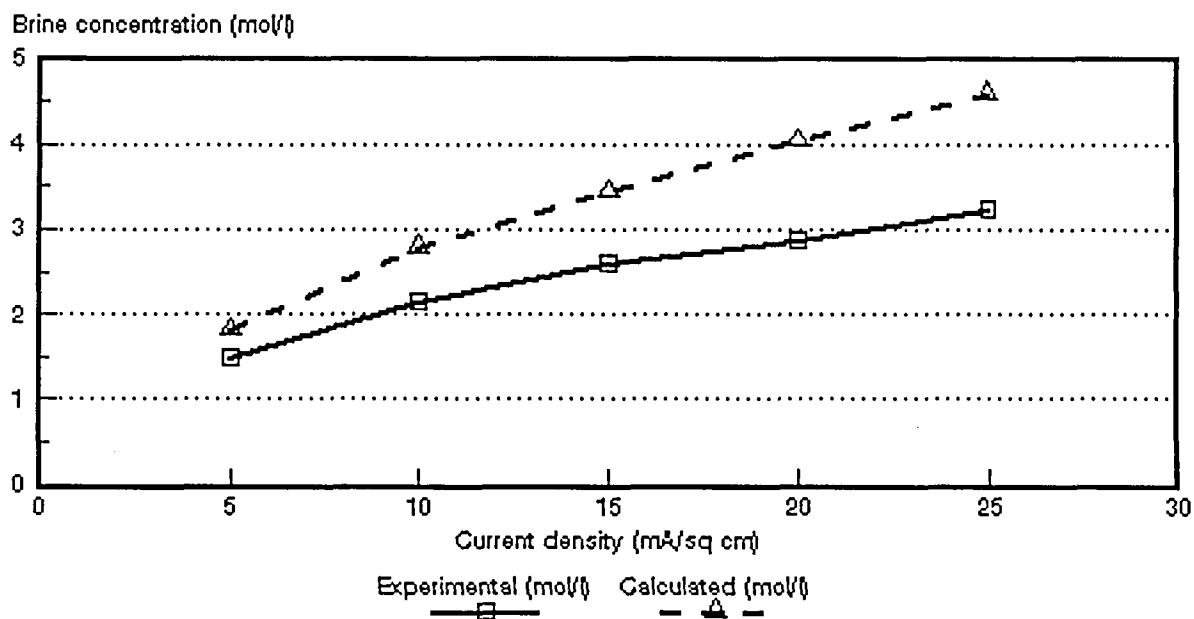
Figure 6.19: Experimental and calculated brine concentrations as a function of current density for 0,05 mol/ℓ NaCl feed solution. *Ionac* MA-3475 and MC-3470 membranes.
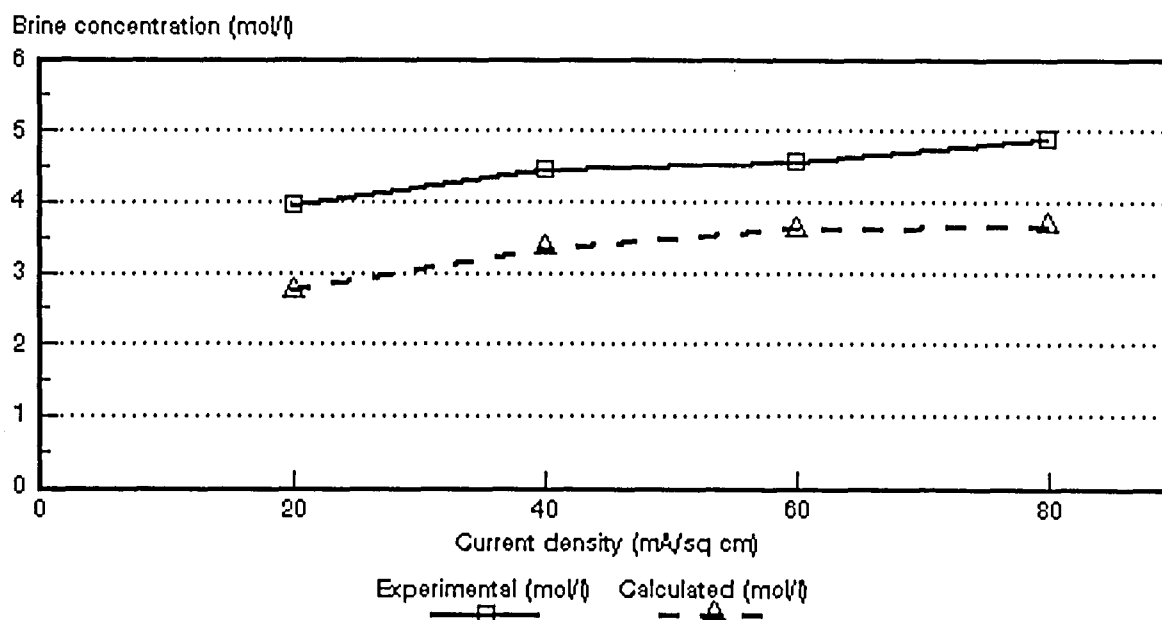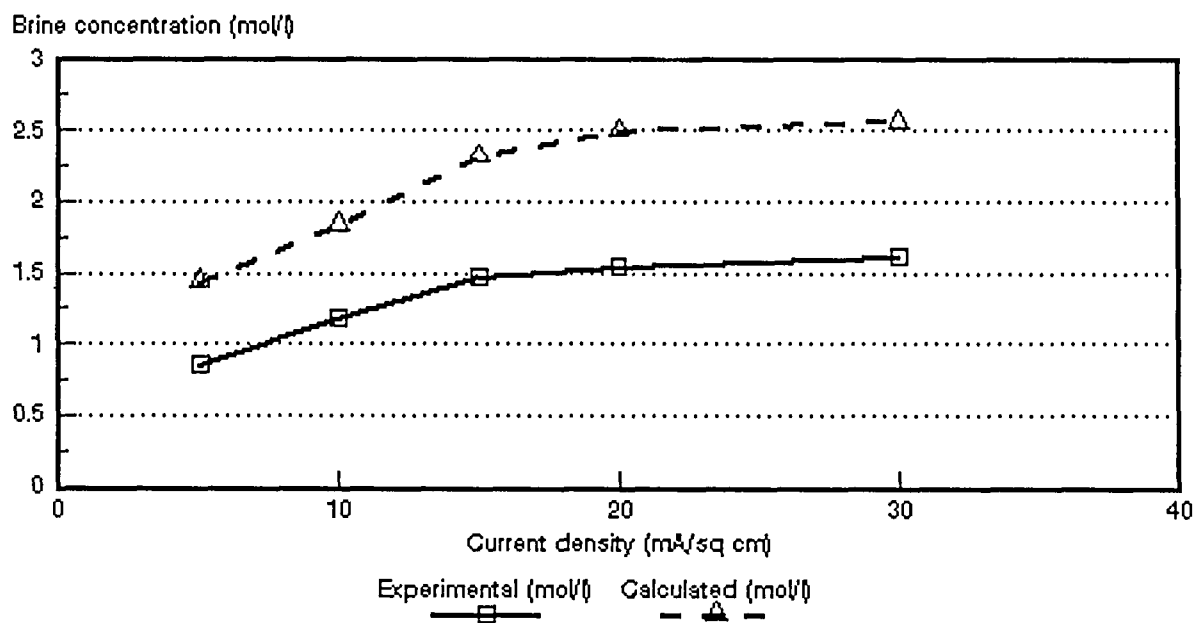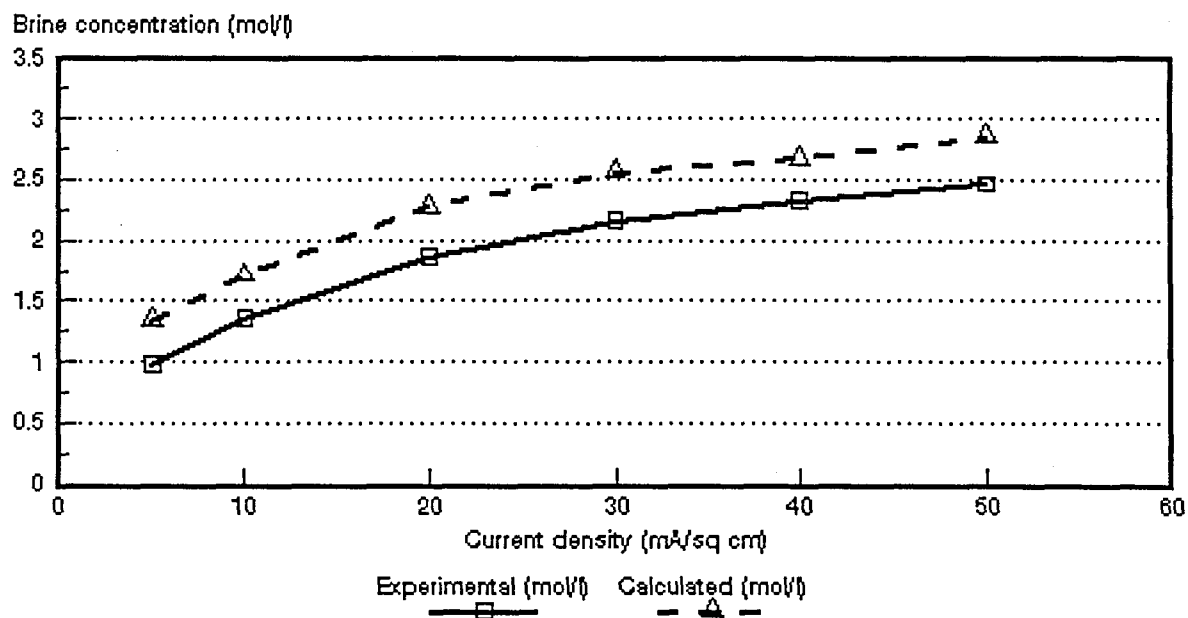
Brine concentration (mol/l)
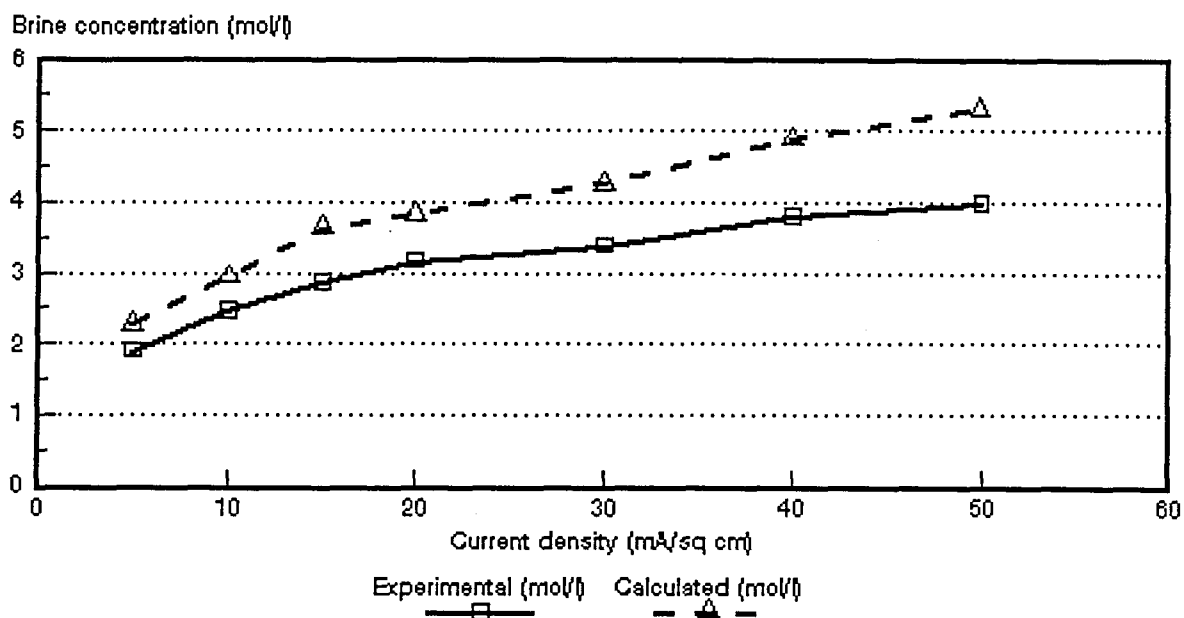
Figure 6.20:   Experimental and calculated brine concentrations as a function of current
density for 0,1 mol/ℓ NaCl feed solution. *Ionac* MA-3475 and MC-3470
membranes.

Brine concentration (mol/l)

Figure 6.21:   Experimental and calculated brine concentrations as a function of current
density for 0,5 mol/ℓ NaCl feed solution. *Ionac* MA-3475 and MC-3470
membranes.

Brine concentration (mol/l)

Figure 6.22:   Experimental and calculated brine concentrations as a function of current density for 1,0 mol/ℓ NaCl feed solution. *Ionac* MA-3475 and MC-3470 membranes.
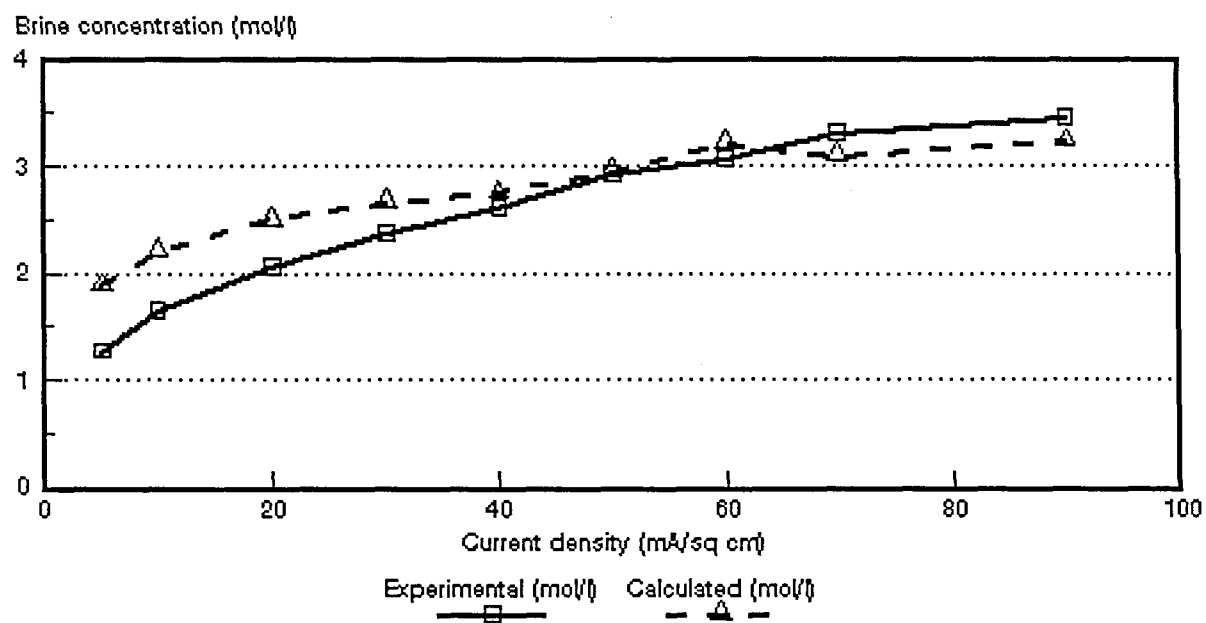
Brine concentration (mol/l)

Figure 6.23:   Experimental and calculated brine concentrations as a function of current density for 0,05 mol/ℓ NaCl feed solution. *Raipore* R4030 and R4010 membranes.
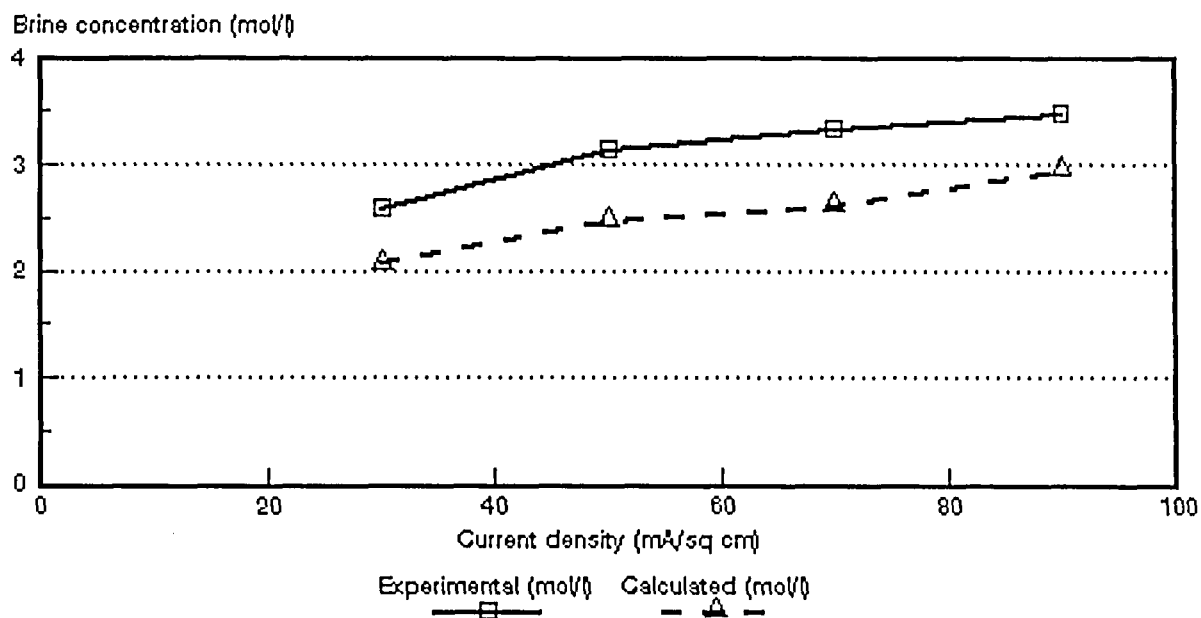
172

Brine concentration (mol/ℓ)

Figure 6.24: Experimental and calculated brine concentrations as a function of current density for 0,1 mol/ℓ NaCl feed solution. *Raipore* R4030 and R4010 membranes.

Brine concentration (mol/ℓ)

Figure 6.25: Experimental and calculated brine concentrations as a function of current density for 0,5 mol/ℓ NaCl feed solution. *Raipore* R4030 and R4010 membranes.
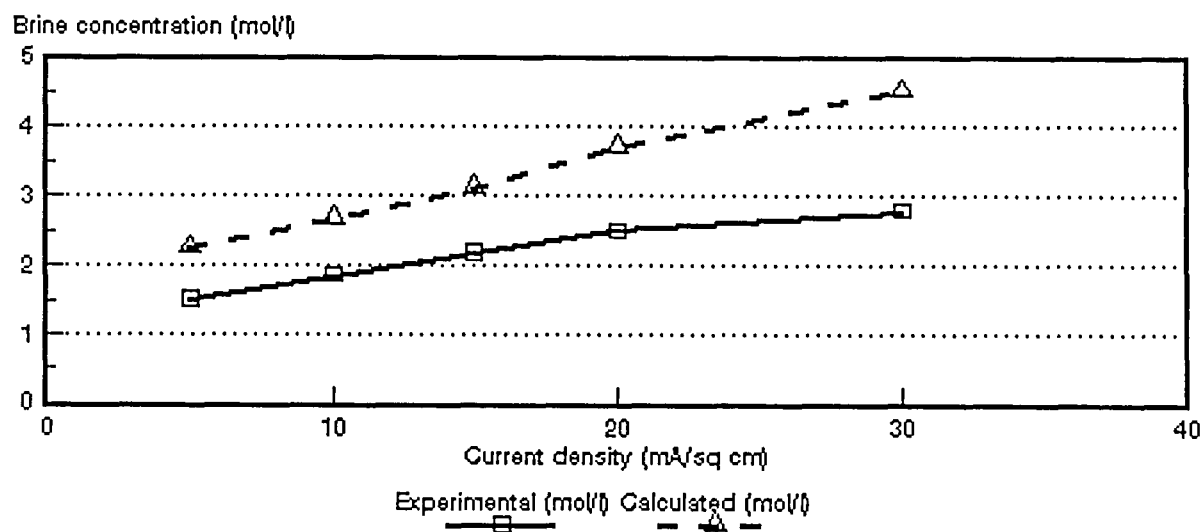
Brine concentration (mol/l)

Current density (mA/sq cm)

Experimental (mol/l)   Calculated (mol/l)

Figure 6.26: Experimental and calculated brine concentrations as a function of current density for 1,0 mol/ℓ NaCl feed solution. *Ralpore* R4030 and R4010 membranes.

Brine concentration (mol/l)

Current density (mA/sq cm)

Experimental (mol/l)   Calculated (mol/l)

Figure 6.27: Experimental and calculated brine concentrations as a function of current density for 0,05 mol/ℓ NaCl feed solution. *Ionics* A-204-UZL-386 and C-61-CZL-386 membranes.
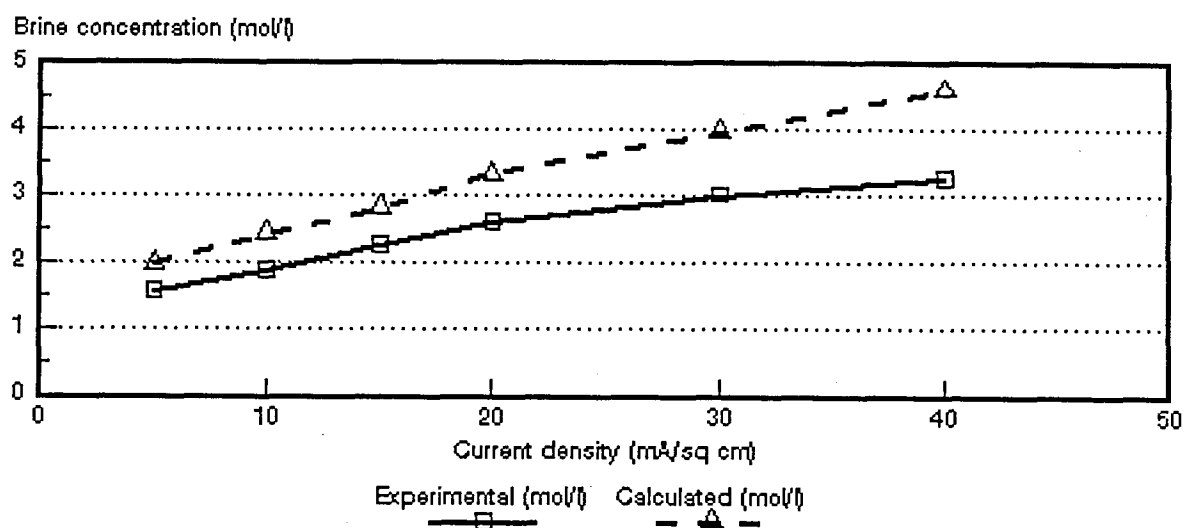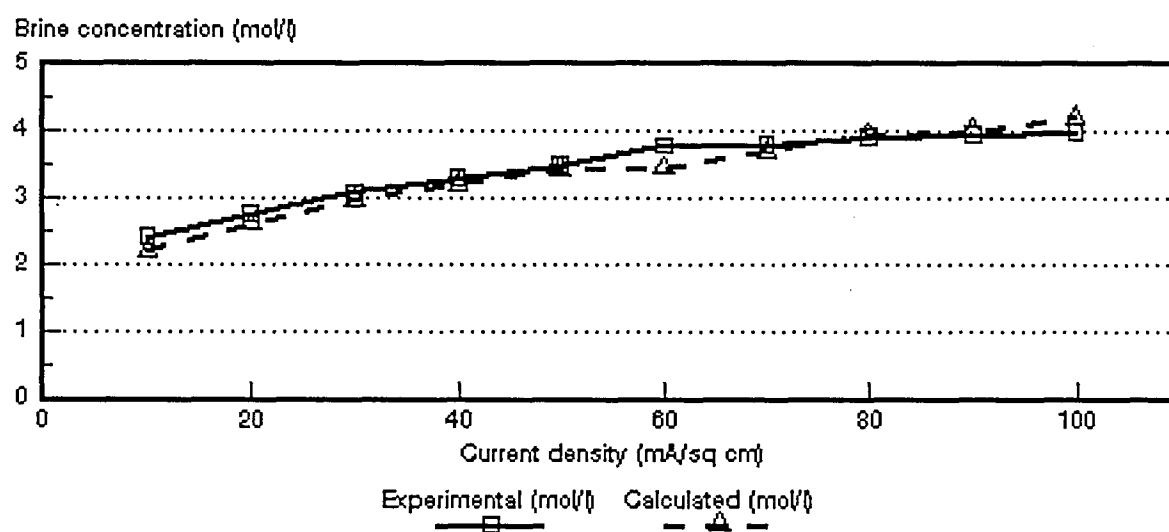
174

Brine concentration (mol/l)

Current density (mA/sq cm)

Experimental (mol/l)   Calculated (mol/l)

Figure 6.28: Experimental and calculated brine concentrations as a function of current density for 0,1 mol/ℓ NaCl feed solution. *Ionics* A-204-UZL-386 and C-61-CZL-386 membranes.

Brine concentration (mol/l)

Current density (mA/sq cm)

Experimental (mol/l)   Calculated (mol/l)

Figure 6.29: Experimental and calculated brine concentrations as a function of current density for 0,5 mol/ℓ NaCl feed solution. *Ionics* A-204-UZL-386 and C-61-CZL-386 membranes.
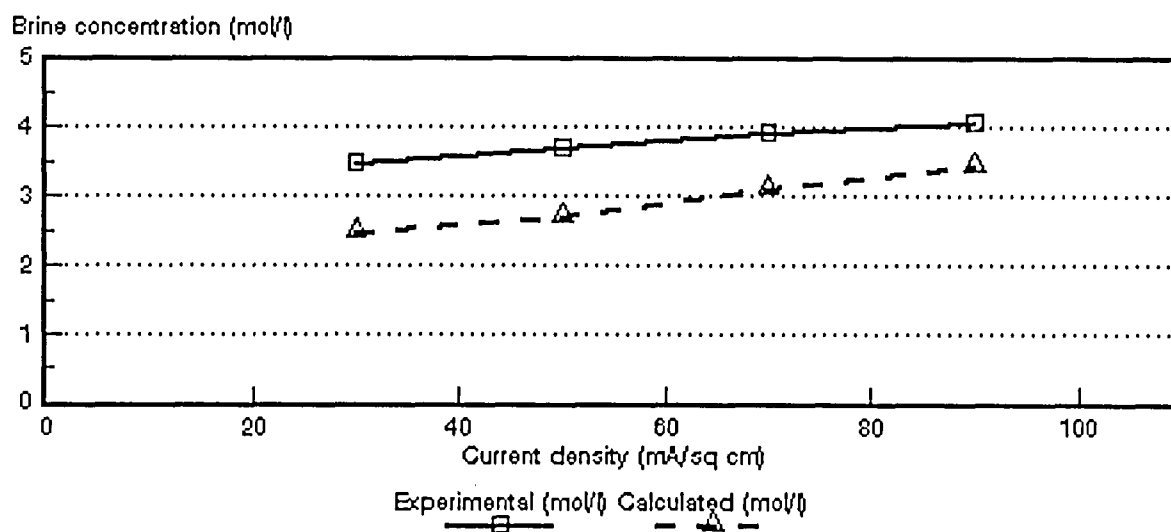
175

Brine concentration (mol/l)

Figure 6.30: Experimental and calculated brine concentrations as a function of current density for 1,0 mol/ℓ NaCl feed solution. *Ionics* A-204-UZL-386 and C-61-CZL-386 membranes.
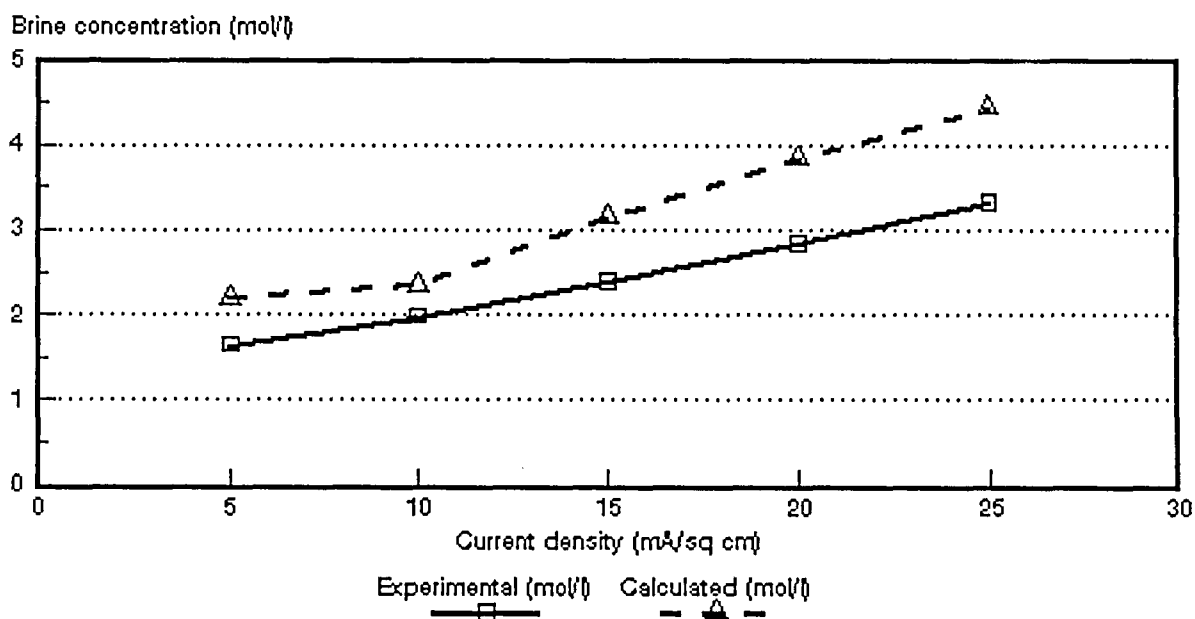
Brine concentration (mol/l)

Figure 6.31: Experimental and calculated brine concentrations as a function of current density for 0,05 mol/ℓ NaCl feed solution. WTPSA-1 and WTPSC-1 membranes.
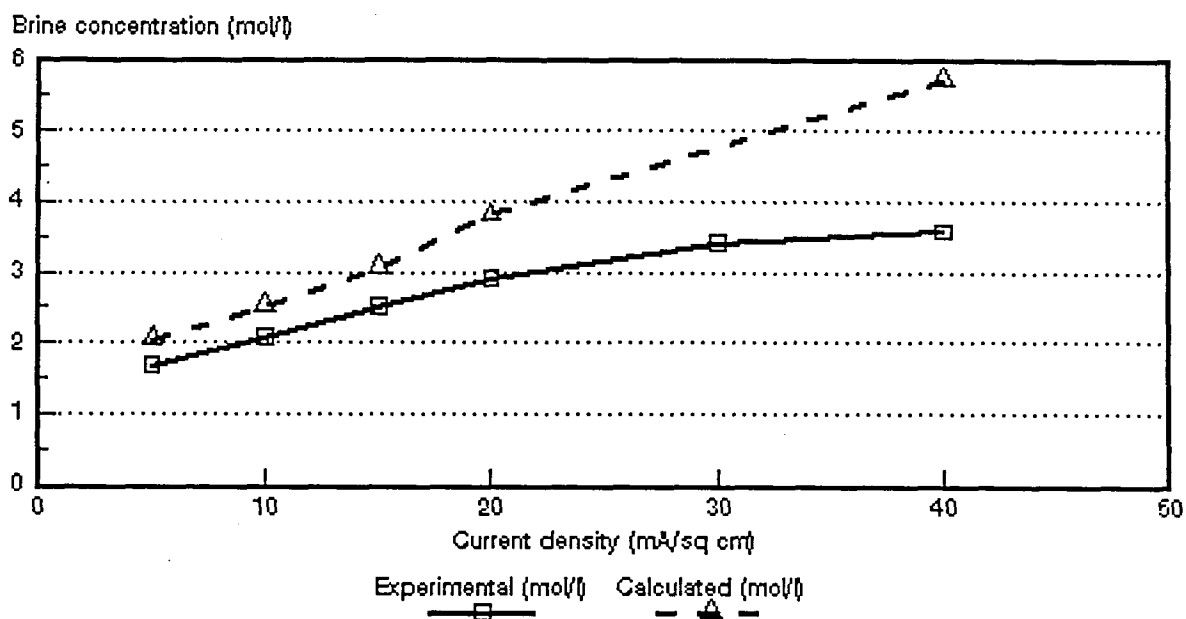
Brine concentration (mol/l)

Current density (mA/sq cm)

Experimental (mol/l)   Calculated (mol/l)

Figure 6.32: Experimental and calculated brine concentrations as a function of current density for 0,1 mol/ℓ NaCl feed solution. WTPSA-1 and WTPSC-1 membranes.

Brine concentration (mol/l)

Current density (mA/sq cm)

Experimental (mol/l)   Calculated (mol/l)

Figure 6.33: Experimental and calculated brine concentrations as a function of current density for 0,5 mol/ℓ NaCl feed solution. WTPSA-1 and WTPSC-1 membranes.
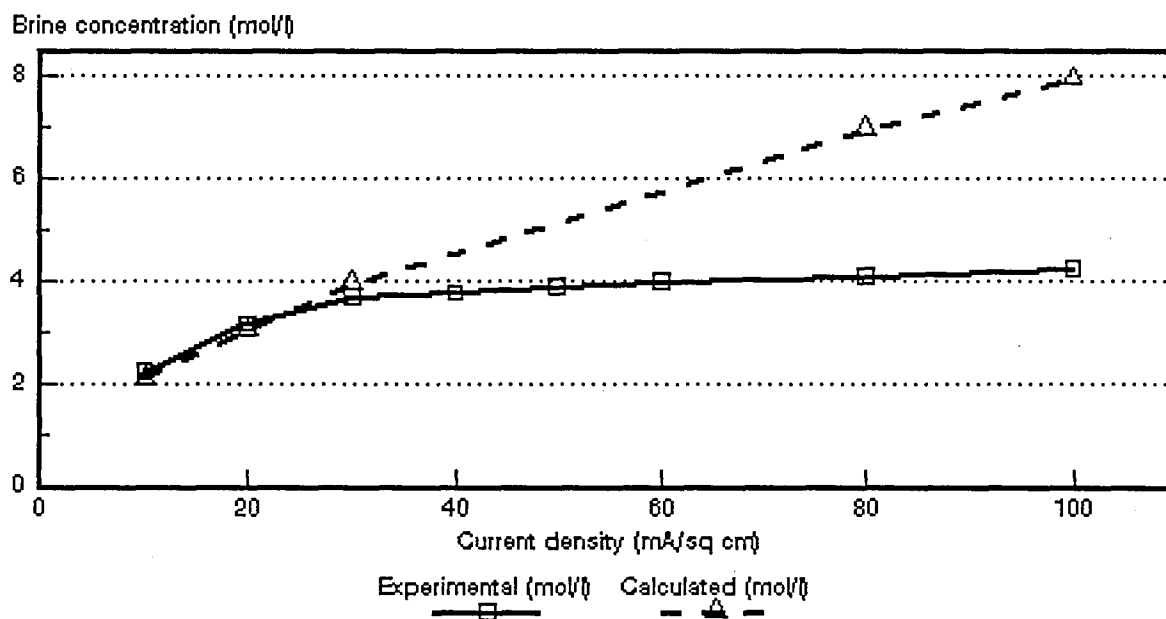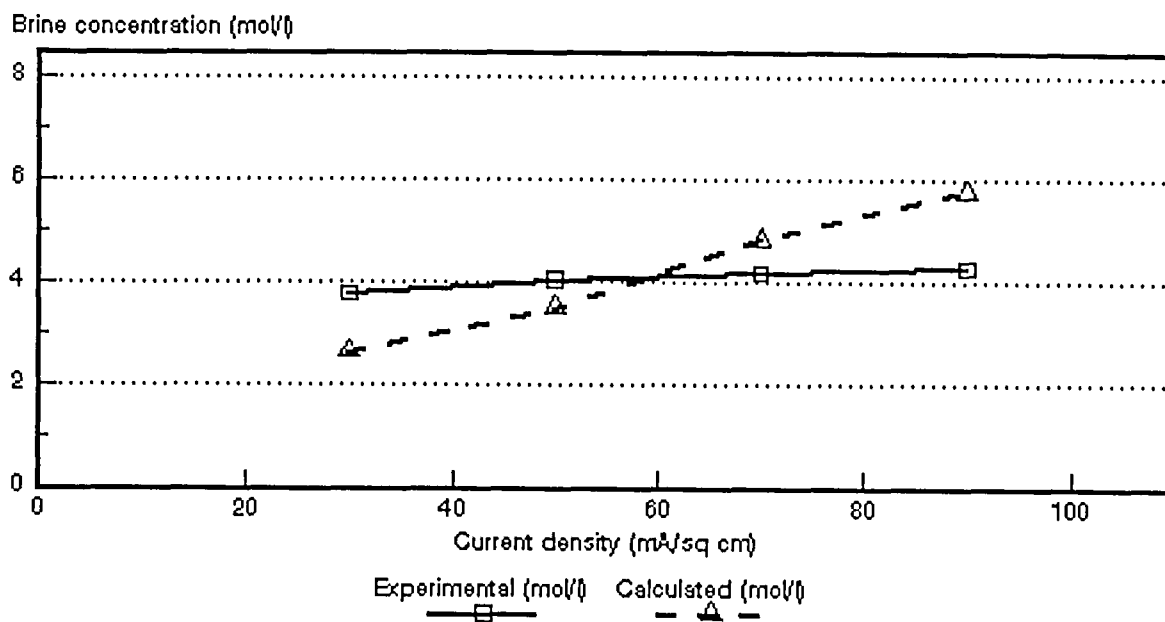
Brine concentration (mol/l)

Figure 6.34: Experimental and calculated brine concentrations as a function of current density for 1,0 mol/ℓ NaCl feed solution. WTPSA-1 and WTPSC-1
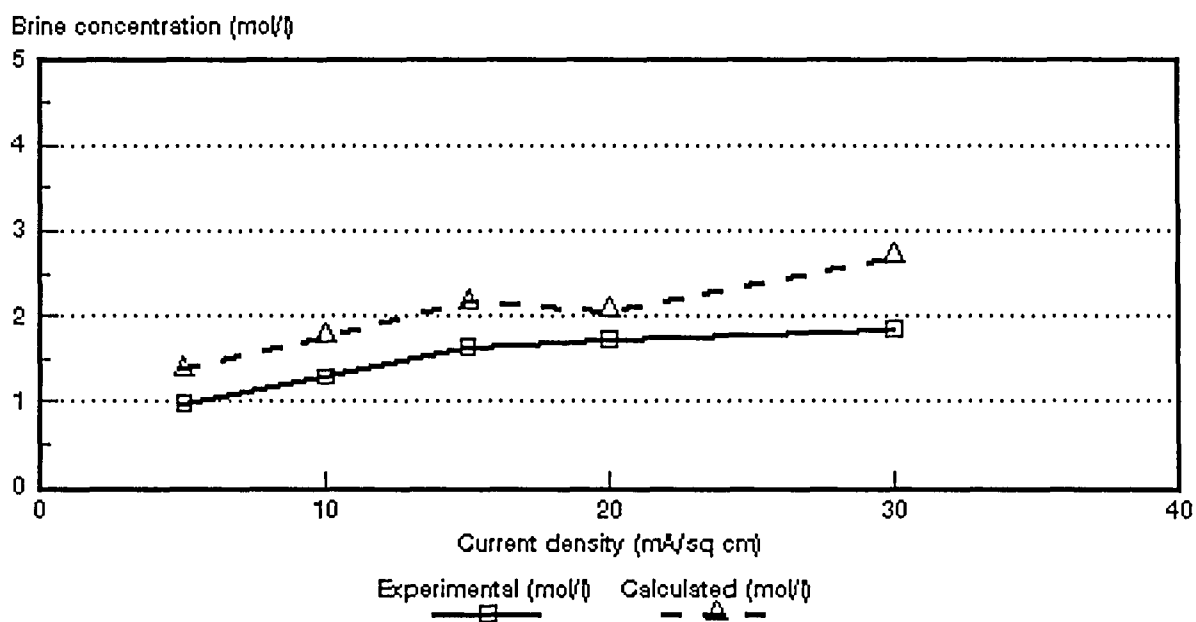
Brine concentration (mol/l)

Figure 6.35: Experimental and calculated brine concentrations as a function of current density for 0,05 mol/ℓ NaCl feed solution. WTPVCA-2 and WTPVCC-2 membranes.

Figure 6.36: Experimental and calculated brine concentrations as a function of current density for 0,1 mol/ℓ NaCl feed solution. WTPVCA-2 and WTPVCC-2 membranes.

Figure 6.37: Experimental and calculated brine concentrations as a function of current density for 0,5 mol/ℓ NaCl feed solution. WTPVCA-2 and WTPVCC-2 membranes.

Figure 6.38: Experimental and calculated brine concentrations as a function of current density for 1,0 mol/ℓ NaCl feed solution. WTPVCA-2 and WTPVCC-2 membranes.
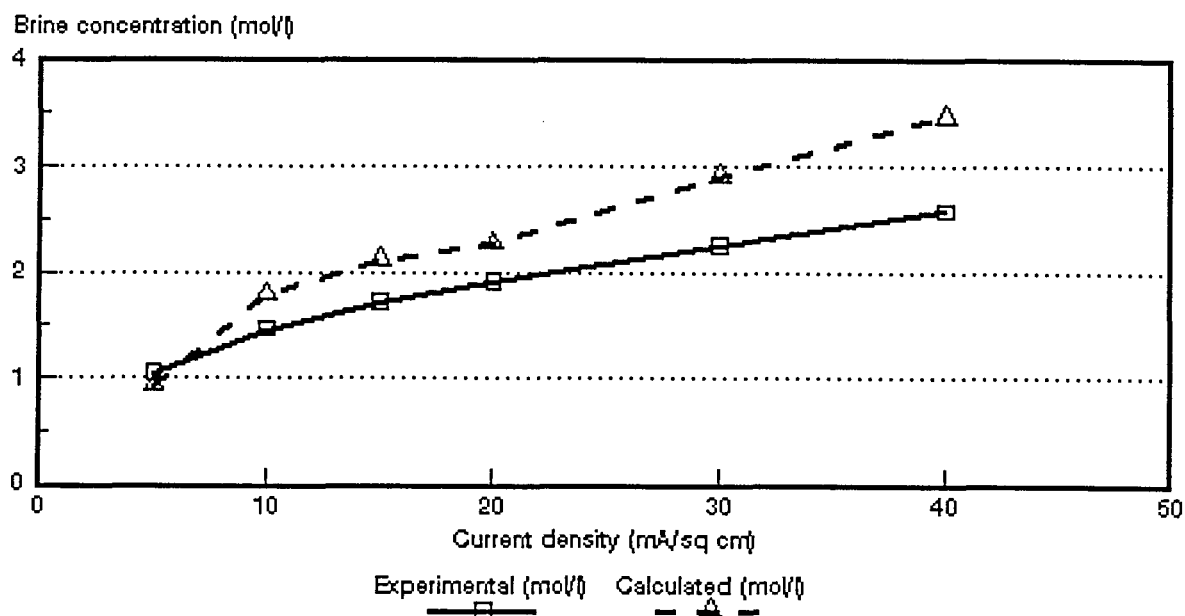

Figure 6.39: Experimental and calculated brine concentrations as a function of current density for 0,05 mol/ℓ NaCl feed solution. WTPSTA-3 and WTPSTC-3 membranes.

Brine concentration (mol/l)

Current density (mA/sq cm)

Experimental (mol/l)   Calculated (mol/l)

Figure 6.40: Experimental and calculated brine concentrations as a function of current density for 0,1 mol/l NaCl feed solution. WTPSTA-3 and WTPSTC-3 membranes.
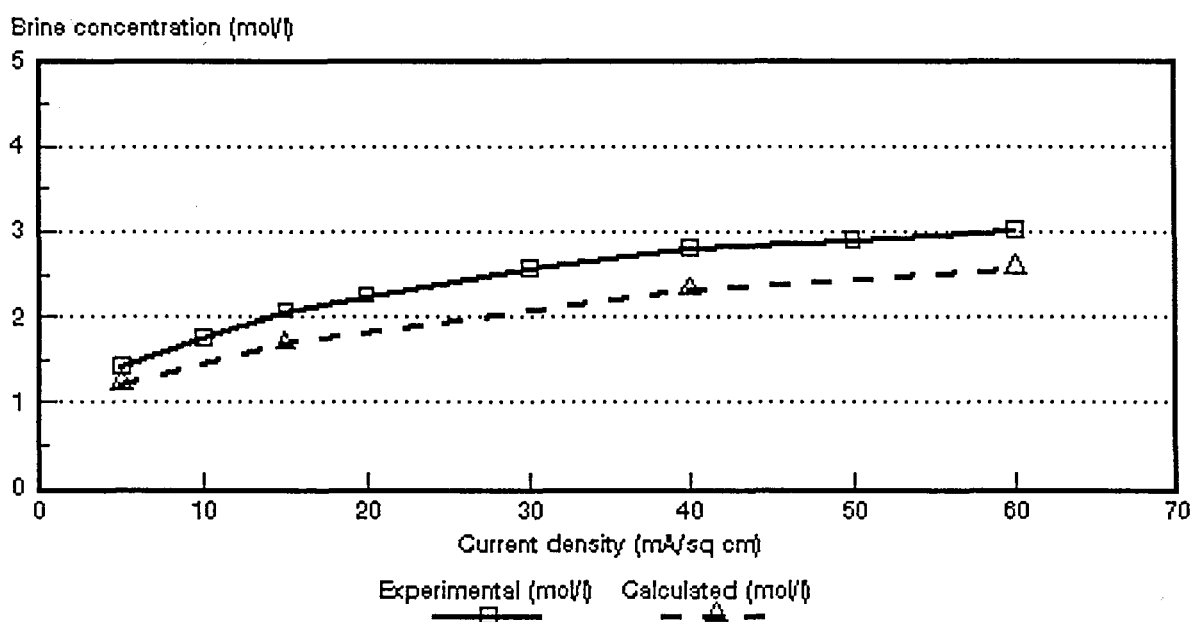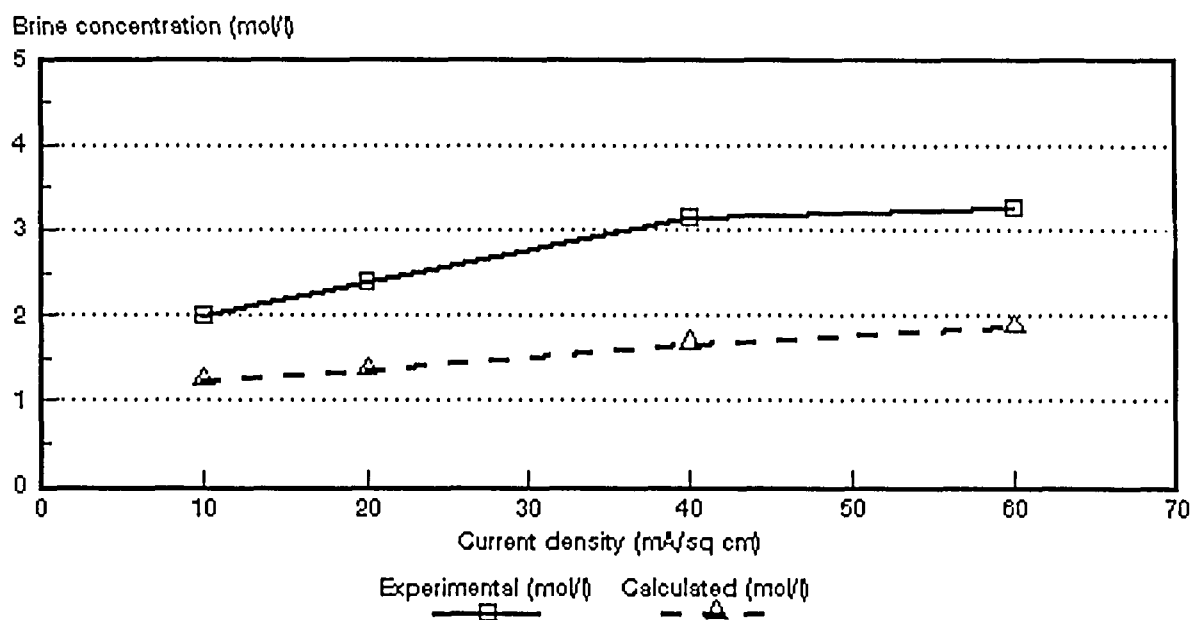
Brine concentration (mol/l)

Current density (mA/sq cm)

Experimental (mol/l)   Calculated (mol/l)

Figure 6.41: Experimental and calculated brine concentrations as a function of current density for 0,5 mol/l NaCl feed solution. WTPSTA-3 and WTPSTC-3 membranes.
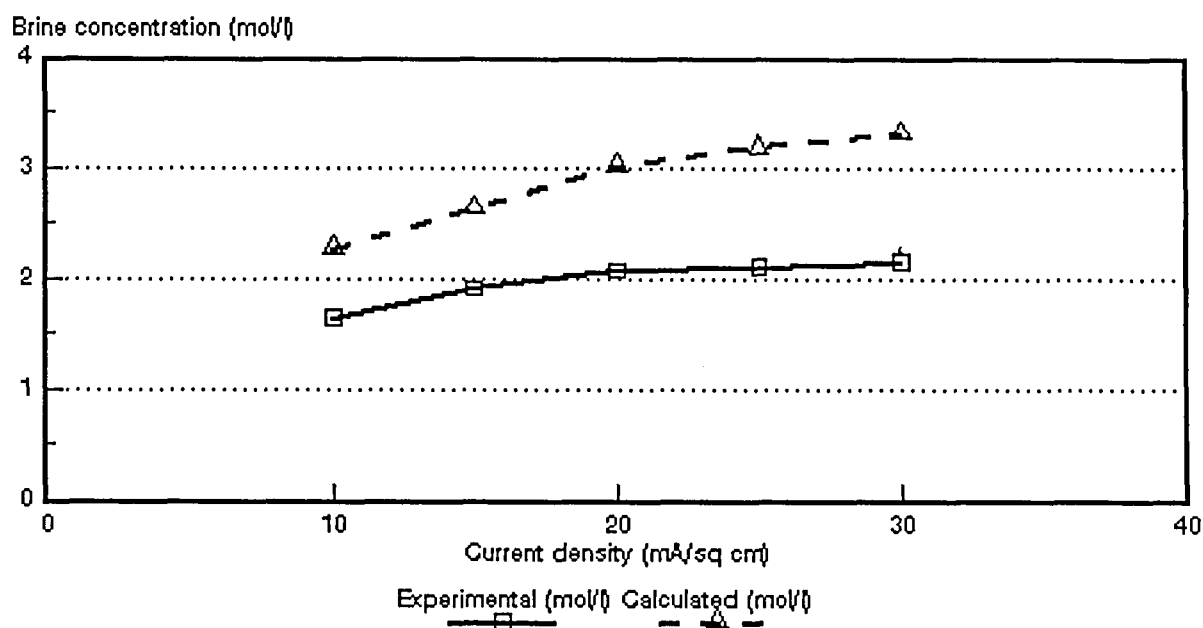
Figure 6.42: Experimental and calculated brine concentrations as a function of current density for 1,0 mol/ℓ NaCl feed solution. WTPSTA-3 and WTPSTC-3 membranes.

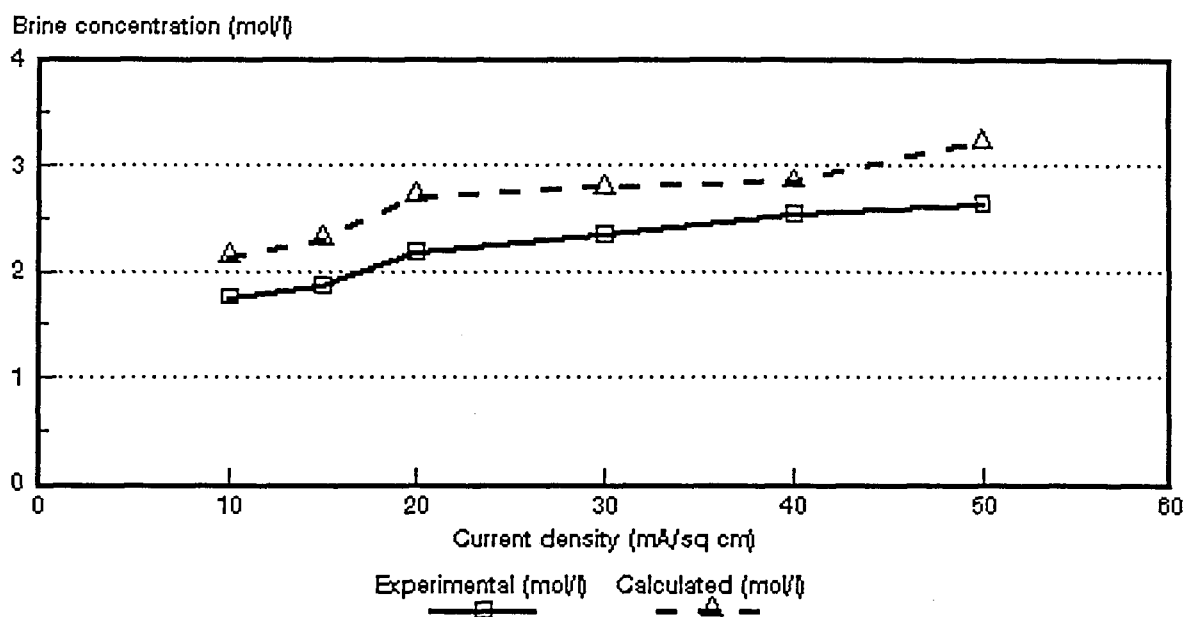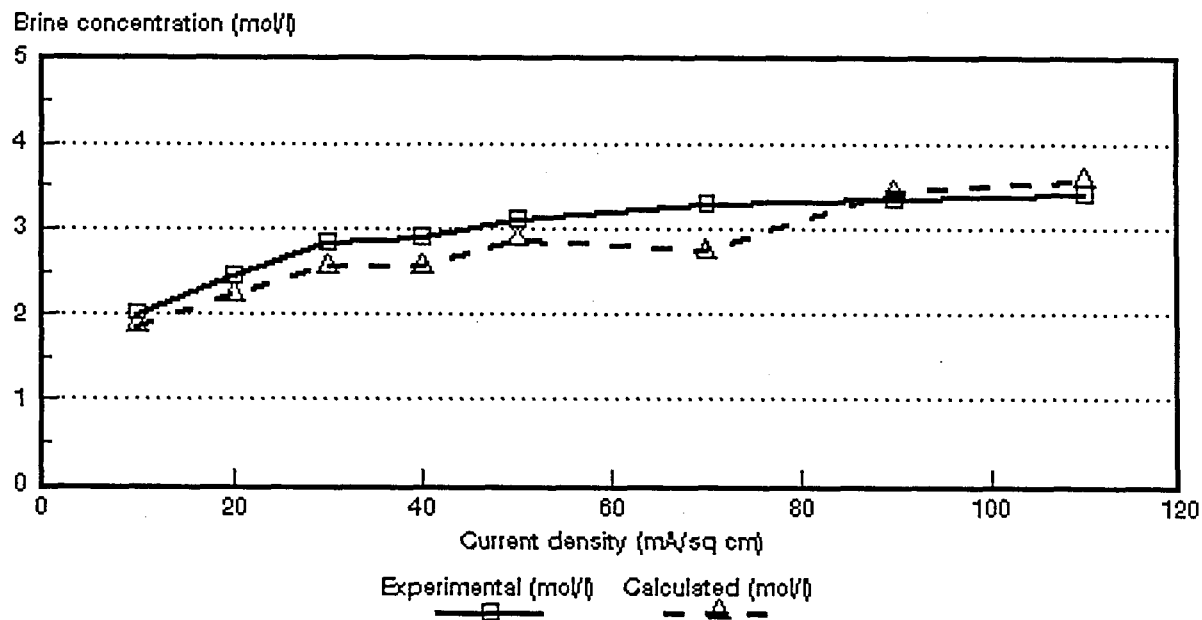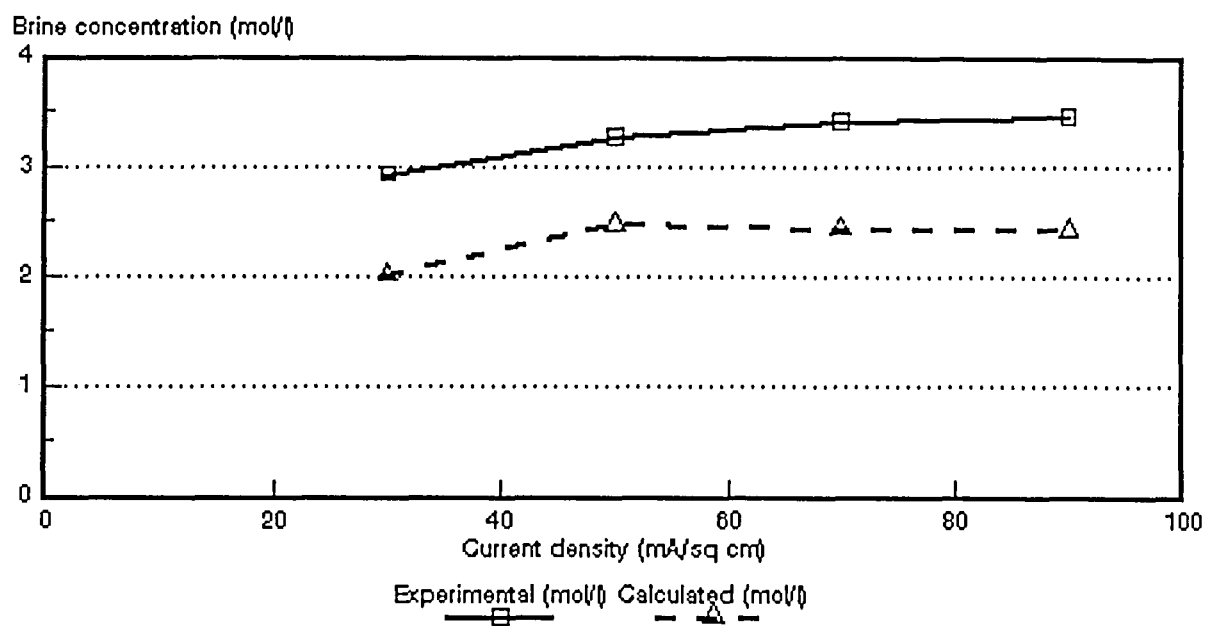**Table 6.31: Correlation between calculated ($c_{b\,calc}$) and experimentally ($c_{b\,exp}$) determined brine concentrations.**

c_{calc}/c_{exp}

Current Density	Selemion AMV & CMV Concentration, mol/l				Ionac MA-3475 & MC-3470 Concentration, mol/l				Raipore R4030 & R4010 Concentration, mol/l				Ionics A-204-UZL & C-61-CZL Concentration, mol/l				WTPS WTPSA & WTPSA Concentration, mol/l				WTPVC WTPVCA & WTPVCC Concentration, mol/l				WTPST WTPSTA & WTPSTC Concentration, mol/l			
mA/cm²	0,05	0,1	0,5	1,0	0,05	0,1	0,5	1,0	0,05	0,1	0,5	1,0	0,05	0,1	0,5	1,0	0,05	0,1	0,5	1,0	0,05	0,1	0,5	1,0	0,05	0,1	0,5	1,0
5	0,98	1,17	0,99		1,21	1,19	0,71		1,67	1,36	1,48		1,50	1,27			1,33	1,22			1,37	0,90	0,86					
10	1,28	1,11	0,85	0,82	1,30	1,18	0,87		1,54	1,26	1,34		1,43	1,29	0,91		1,19	1,20	0,95		1,36	1,22		0,63	1,39	1,22	0,93	
15	1,26	1,07			1,33	1,26			1,57				1,43	1,25			1,32	1,21			1,33	1,23	0,82		1,38	1,23		
20	1,26	1,06	0,79	0,78	1,41	1,21	0,82	0,70	1,61	1,23	1,21		1,48	1,27	0,95		1,35	1,31	0,96		1,19	1,13		0,57	1,45	1,24	0,91	
25					1,42												1,34								1,52			
30	1,22	1,04	0,83	0,77		1,26			1,58	1,19	1,12	0,80	1,62	1,31	0,96	0,72			1,07	0,70	1,46	1,29			1,54	1,23	0,99	0,69
40		1,05	0,77	0,77		1,28	0,95	0,75		1,15	1,05			1,42	0,98			1,60				1,34	0,83	0,54		1,27	0,88	
50		1,00	0,78	0,73		1,33	1,01			1,16	1,01	0,79			0,99	0,73				0,86						1,12	0,93	0,66
60			0,77	0,74			1,09	0,79			1,05				0,91								0,85	0,57				
70							1,10				0,93	0,78			0,97	0,79			1,16								0,84	0,72
80								0,75							1,01				1,70									
90											0,94	0,85			1,02	0,85			1,35								1,02	0,70
100															1,06				1,87									
110															1,05													

6.2   Current Efficiency

Current efficiency (ϵ_p) determined during the EOP experiments as a function of current density is shown in Figures 6.43 to 6.49 for the different membranes. Current efficiency increases with increasing feed water concentration in the concentration range from 0,05 to 1,0 mol/ℓ. However, current efficiency was slightly lower at the highest feed concentration in the case of the *Selemion* membranes (Fig 6.43). It is interesting to note that current efficiency has been significantly higher at the higher feed concentrations in the case of the *Ionac-* (Fig. 6.44), *Raipore-* (Fig. 6.45), *Ionics-* (Fig. 6.46), WTPS- (Fig. 6.47), WTPVC- (Fig. 6.48) and WTPST- (Fig 6.49) membranes.

No significant change in current efficiency was observed as a function of current density in the case of the *Selemion* membranes in the feed concentration range studied (Fig 6.43). This showed that the limiting current density was not reached in the range of current densities and feed water concentrations used for these membranes. However, changes in current efficiency, especially at the lower feed concentration levels (0,05 to 0,5 mol/ℓ), were experienced with the *Ionac-* (Fig. 6.44), *Raipore-* (Fig. 6.45, 0,05 mol/ℓ), *Ionics-* (Fig. 6.46, 0,05 to 1,0 mol/ℓ), WTPS- (Fig. 6.47, 0,05 to 1,0 mol/ℓ), WTPVC- (Fig. 6.48, 0,05 to 1,0 mol/ℓ) and WTPST- (Fig. 6.49, 0,05 to 1,0 mol/ℓ) membranes. This showed that the limiting current density was exceeded with increasing current density. A significant reduction in current efficiency was experienced in the case of the WTPS membranes at the higher feed concentrations at relatively low current densities (Fig. 6.47). This showed that the limiting current density was exceeded and that polarization was taking place.

The apparent transport numbers for a membrane pair $(\overline{\Delta t})$, for the anion- (Δt^a) and cation- (Δt^c) membranes, determined from membrane potential measurements for a concentration difference similar to that obtained in the EOP experiments at the different current densities and feed water concentrations used, are shown in Figures 6.50 to 6.77. The current efficiencies (ϵ_p) as determined by the EOP method and shown in Figures 6.43 to 6.49 are also shown in Figures 6.50 to 6.77. The correlation between the apparent transport numbers $(\overline{\Delta t}, \Delta t^a$ and $\Delta t^c)$ and the current efficiency (ϵ_p) is shown in Tables 6.32 to 6.34.

The apparent transport numbers $(\overline{\Delta t}, \Delta t^a, \Delta t^c)$ were higher than the current efficiencies at the lower feed water concentrations (0,05 to 0,1 mol/ℓ) (Tables 6.32 to 6.34 and Figs. 6.50 to 6.77). However, the apparent transport numbers became smaller than the
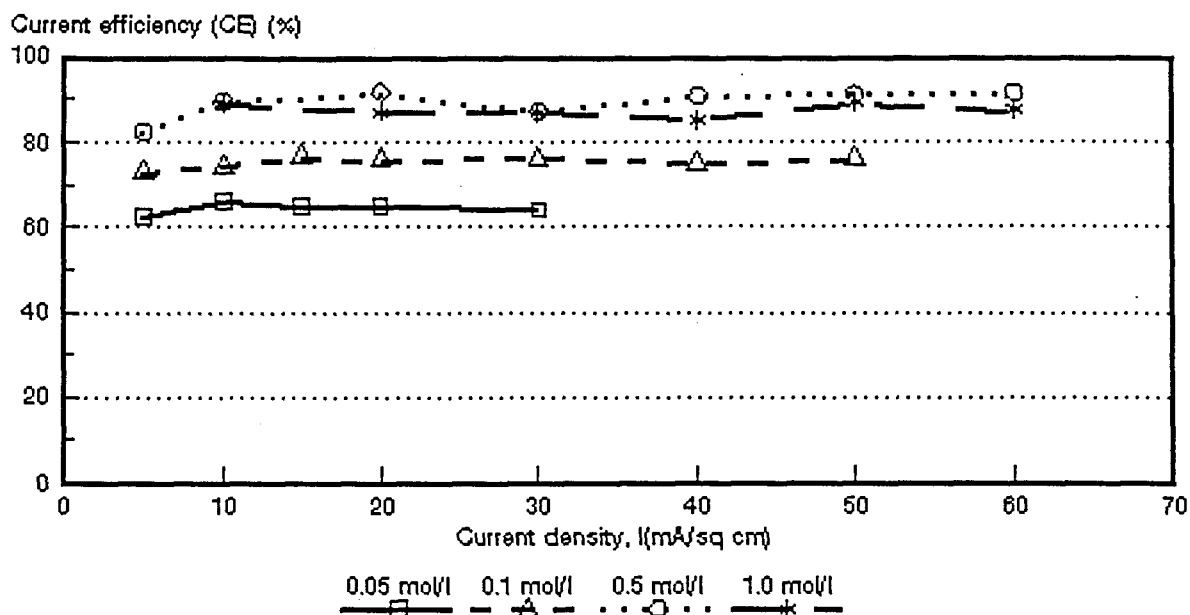
Current efficiency (CE) (%)

Figure 6.43: Current efficiency (ϵ_p) as a function of current density for 4 different NaCl feed concentrations. *Selemion* AMV and CMV membranes.
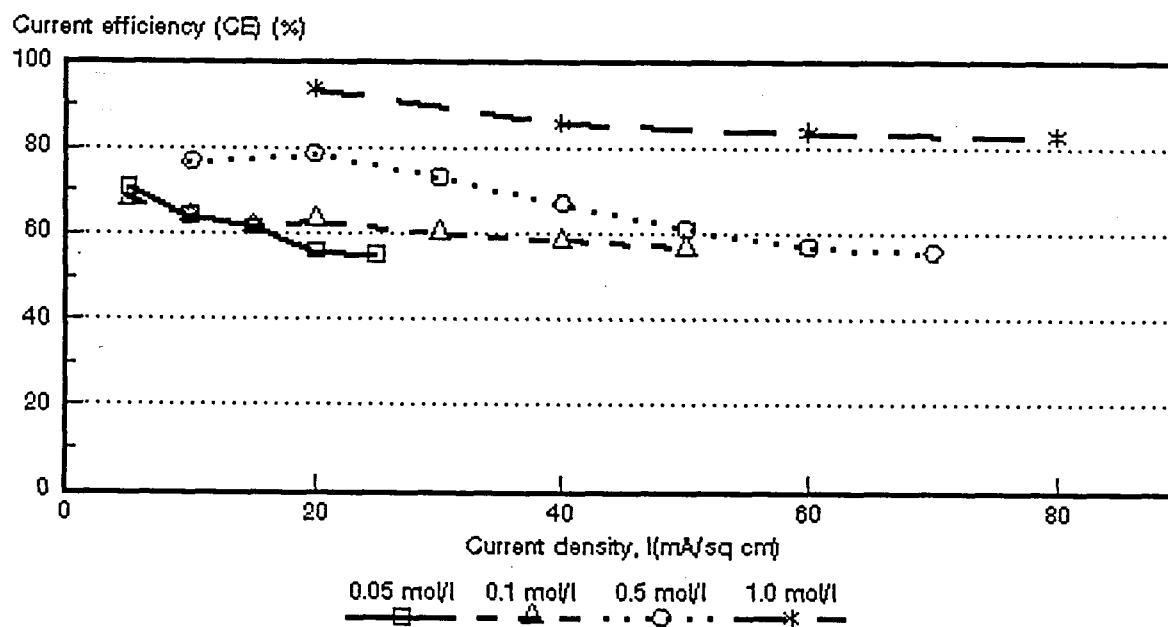
Current efficiency (CE) (%)

Figure 6.44: Current efficiency (ϵ_p) as a function of current density for 4 different NaCl feed concentrations. Ionac MA-3475 and MC-3470 membranes.
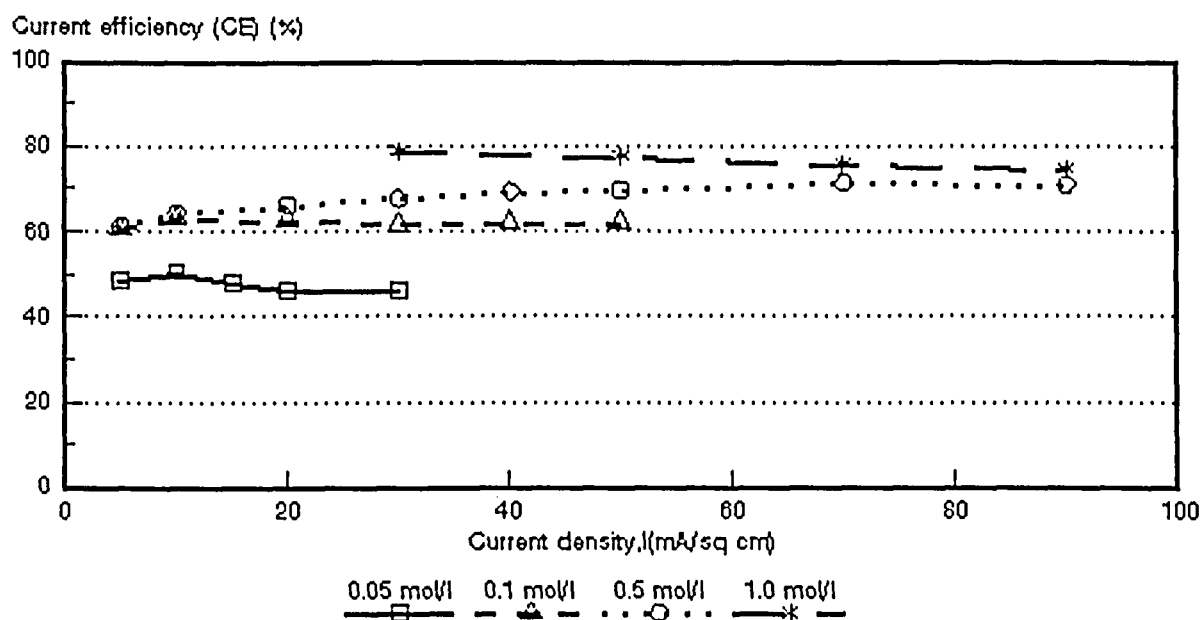
185

Figure 6.45: Current efficiency (ϵ_p) as a function of current density for 4 different NaCl feed concentrations. *Ralpore* R4030 and R4010 membranes.
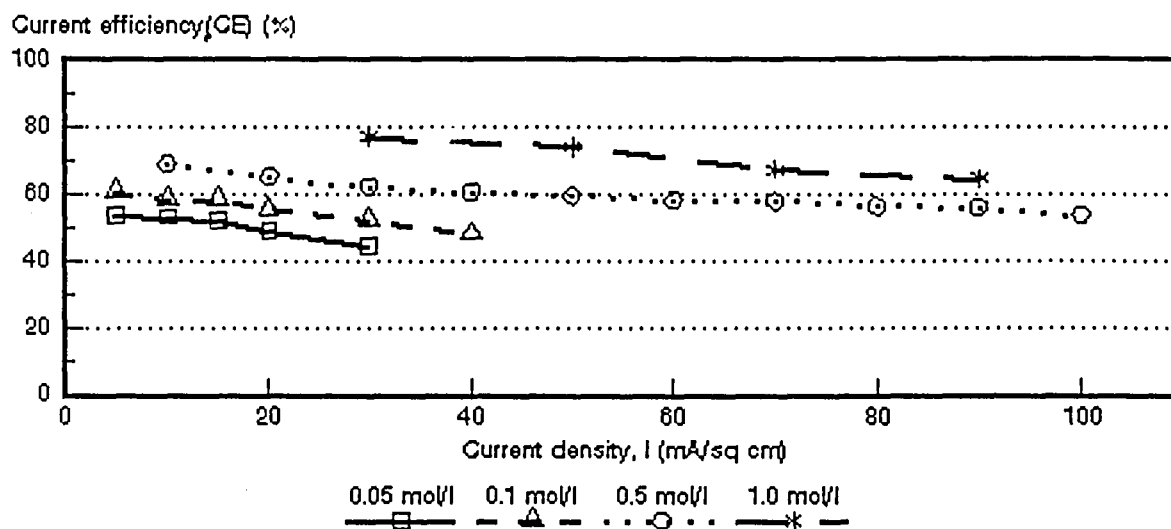

Figure 6.46: Current efficiency (ϵ_p) as a function of current density for 4 different NaCl feed concentrations. *Ionics* A-204-UZL-386 and C-61-CZL-386 membranes.

Current efficiency (CE) (%)

Figure 6.47: Current efficiency (ϵ_p) as a function of current density for 4 different NaCl feed concentrations. WTPSA-1 and WTPSC-1 membranes

Current efficiency (CE) (%)
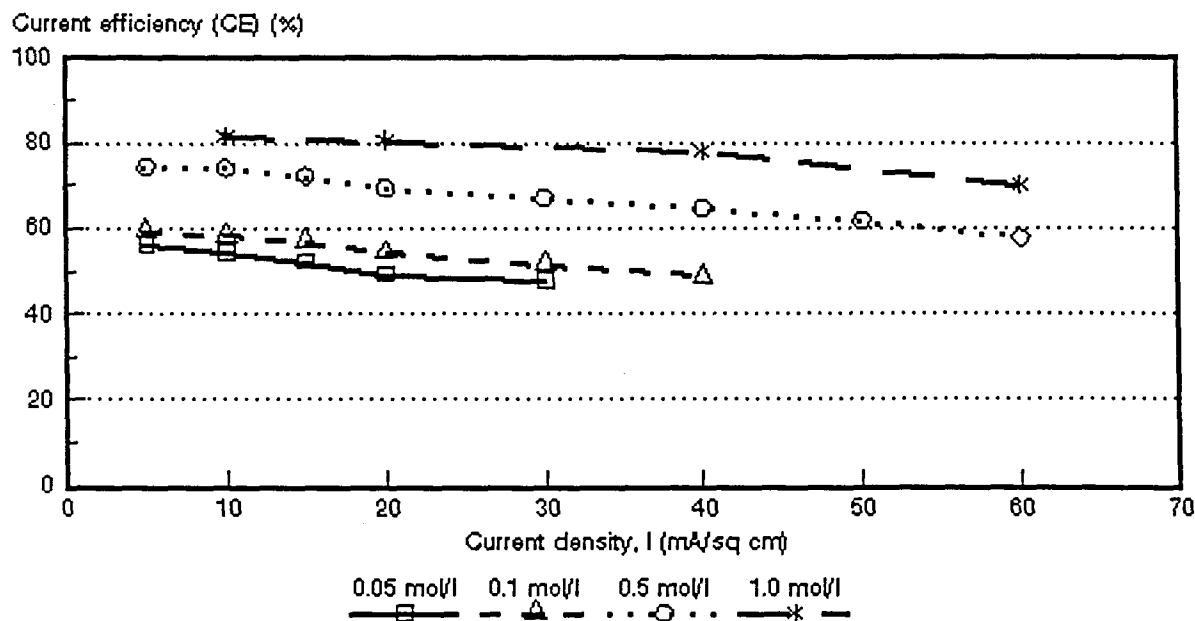
Figure 6.48: Current efficiency (ϵ_p) as a function of current density for 4 different NaCl feed concentrations. WTPVCA-2 and WTPVCC-2 membranes.
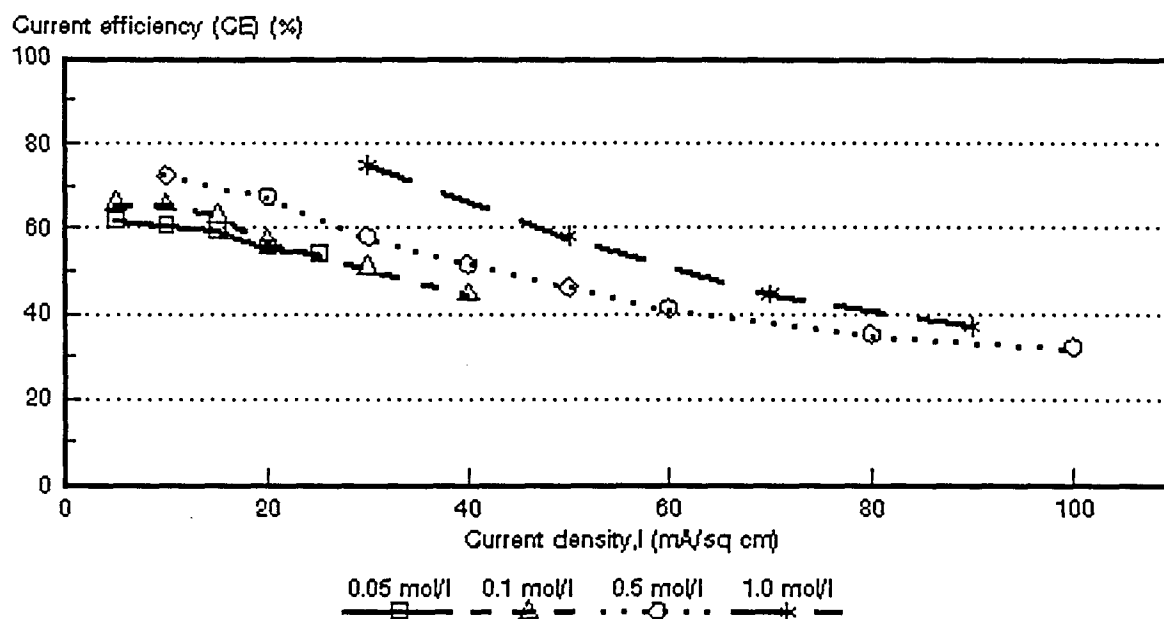
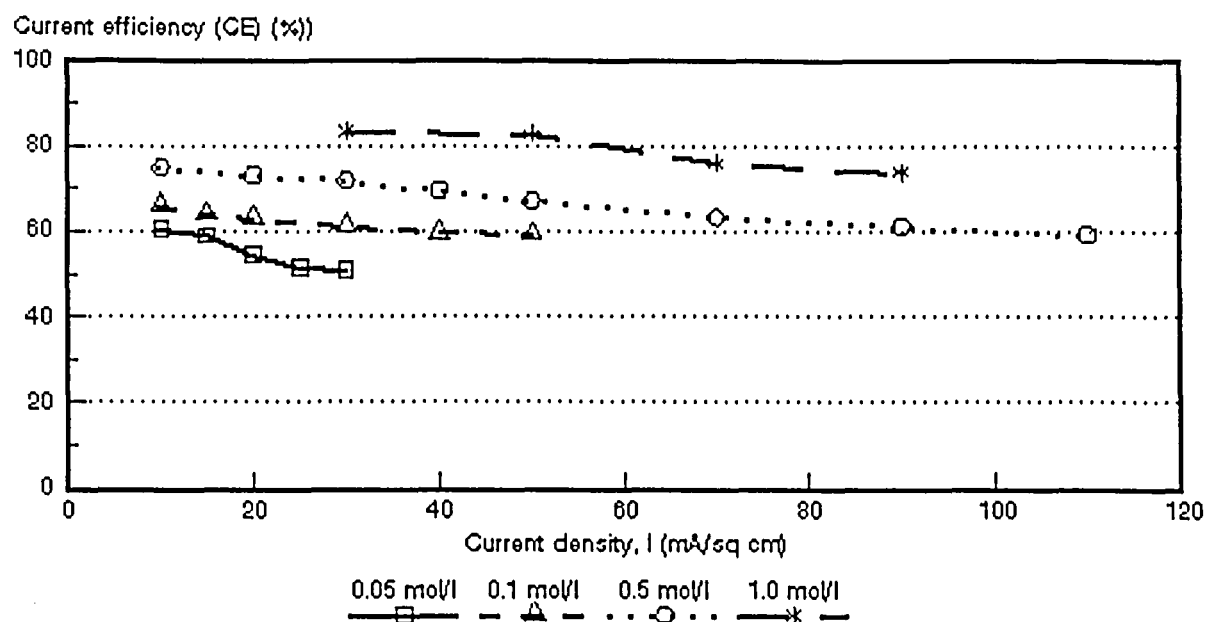**Figure 6.49:** Current efficiency (ϵ_p) as a function of current density for 4 different NaCl feed concentrations. WTPSTA-3 and WTPSTC-3 membranes.

Figure 6.50: Current efficiency (CE = ϵ_p) and apparent transport numbers as a function of current density for 0,05 mol/ℓ NaCl feed. *Selemion* AMV and CMV membranes. Delta t = $\bar{\Delta}$t; Delta ta = Δt^a; Delta tc = Δt^c.

CE ; Delta t ; Delta ta and Delta tc (%)

Figure 6.51: Current efficiency (CE = e_p) and apparent transport numbers as a function of current density for 0,1 mol/ℓ NaCl feed. *Selemion* AMV and CMV membranes. Delta t = $\bar{\Delta}t$; Delta ta = t^a; Delta tc = Δt^c.
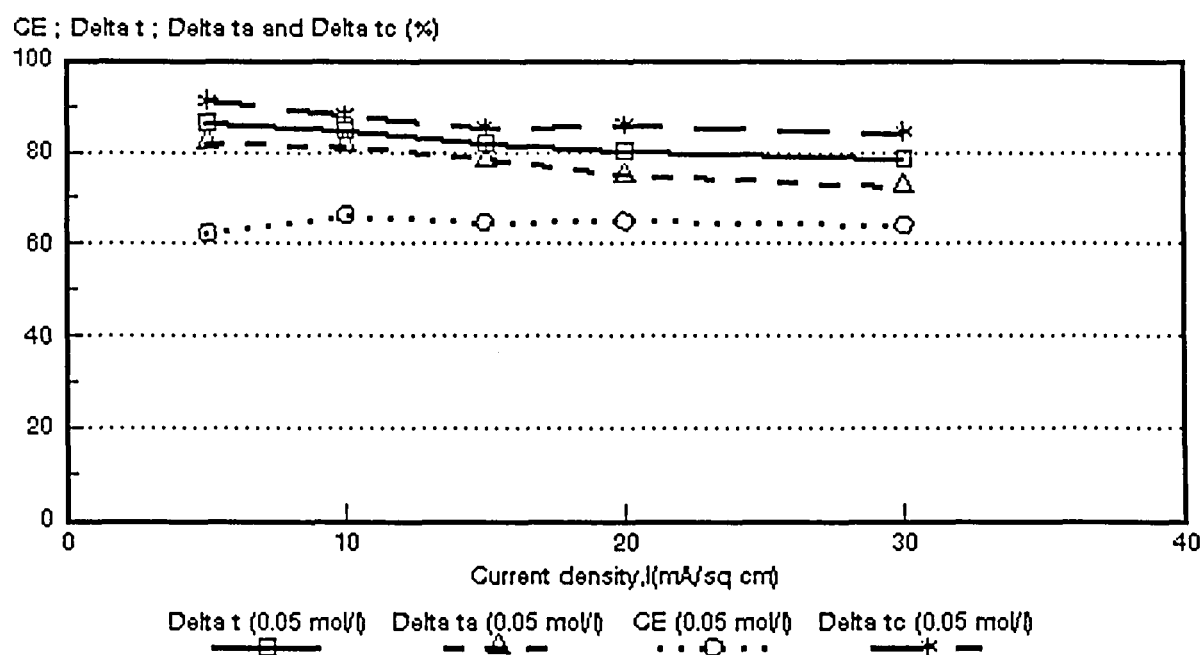
CE ; Delta t ; Delta ta and Delta tc (%)

Figure 6.52: Current efficiency (CE = e_p) and apparent transport numbers as a function of current density for 0,5 mol/ℓ NaCl feed. *Selemion* AMV and CMV membranes. Delta t = $\bar{\Delta}t$; Delta ta = Δt^a; Delta tc = Δt^c.

189

CE ; Delta t ; Delta ta and Delta tc (%)

Figure 6.53: Current efficiency (CE = ϵ_p) and apparent transport numbers as a function of current density for 1,0 mol/ℓ NaCl feed. *Selemion* AMV and CMV membranes. Delta t = $\bar{\Delta}t$; Delta ta = Δt^a; Delta tc = Δt^c.

CE ; Delta t ; Delta ta and Delta tc (%)

Figure 6.54: Current efficiency (CE = ϵ_p) and apparent transport numbers as a function of current density for 0,05 mol/ℓ NaCl feed. *Ionac* MA-3475 and MC-3470 membranes. Delta t = $\bar{\Delta}t$; Delta ta = Δt^a; Delta tc = Δt^c.

CE ; Delta t ; Delta ta and Delta tc (%)

Current density, I (mA/sq cm)

Delta t (0.1 mol/l)   Delta ta (0.1 mol/l)   CE (0.1 mol/l)   Delta tc (0.1 mol/l)
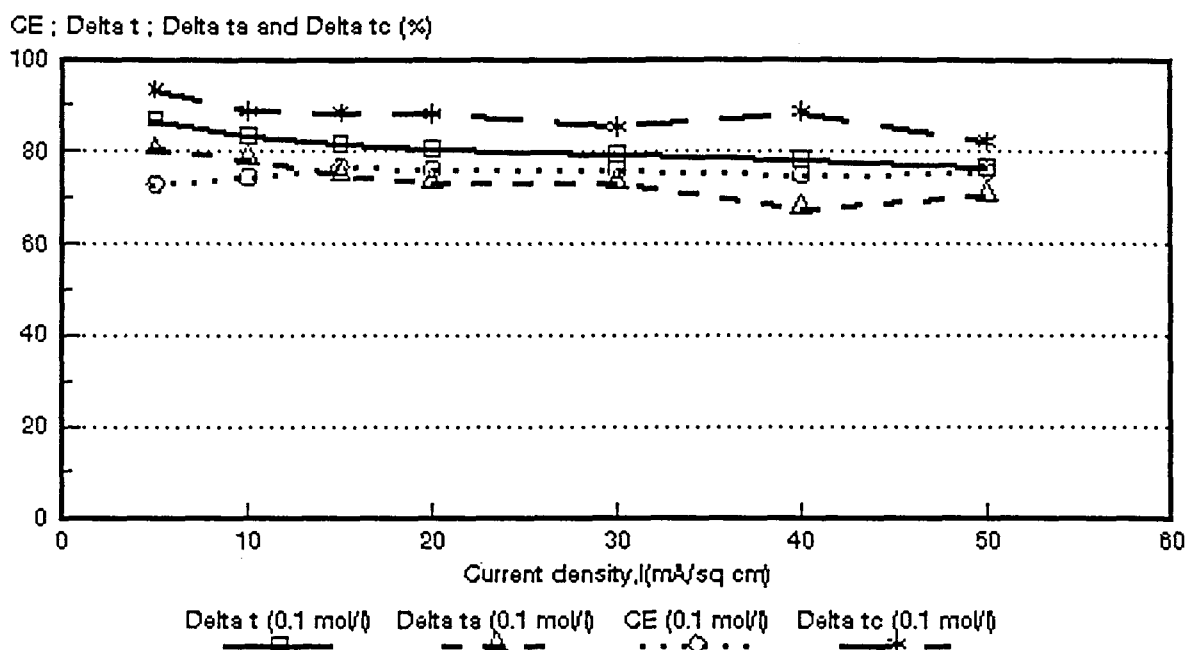——□——   — —△— —   · · ◇ · ·   ——✻ —

Figure 6.55: Current efficiency (CE = e_p) and apparent transport numbers as a function of current density for 0,1 mol/l NaCl feed. *Ionac* MA-3475 and MC-3470 membranes. Delta t = $\bar{\Delta}t$; Delta ta = Δt^a; Delta tc = Δt^c.

CE ; Delta t ; Delta ta and Delta tc (%)

Current density, I (mA/sq cm)

Delta t (0.5 mol/l)   Delta ta (0.5 mol/l)   CE (0.5 mol/l)   Delta tc (0.5 mol/l)
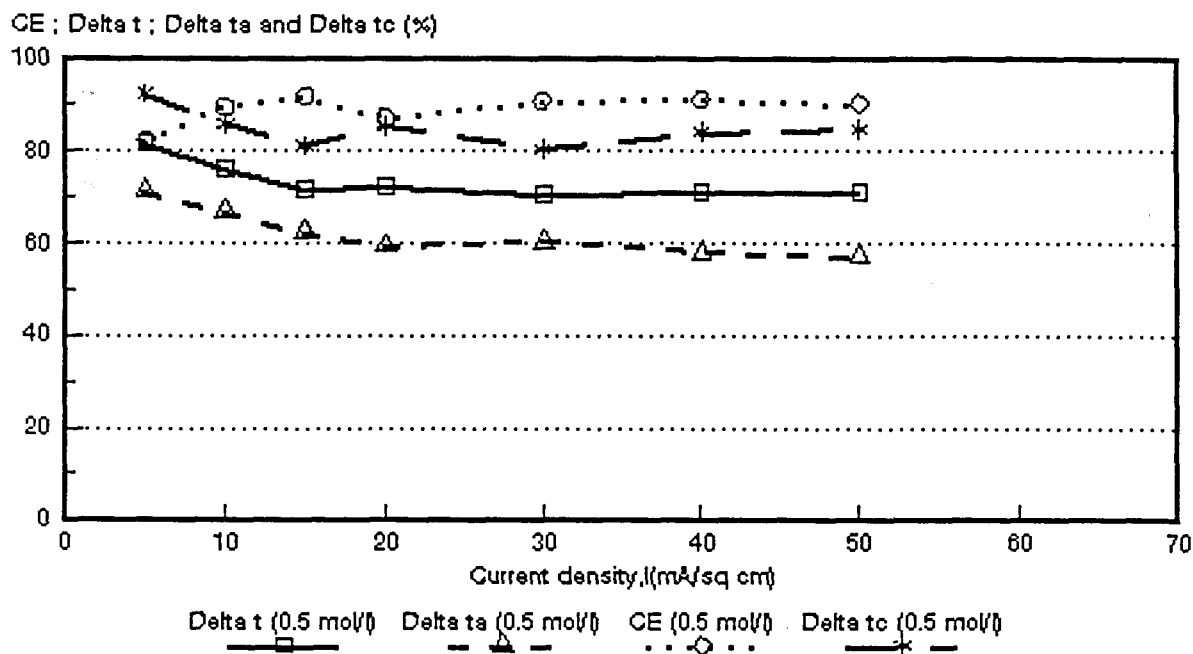——□——   — —△— —   · · ◇ · ·   ——✻ —

Figure 6.56: Current efficiency (CE = e_p) and apparent transport numbers as a function of current density for 0,5 mol/l NaCl feed. *Ionac* MA-3475 and MC-3470 membranes. Delta t = $\bar{\Delta}t$; Delta ta = Δt^a; Delta tc = Δt^c.
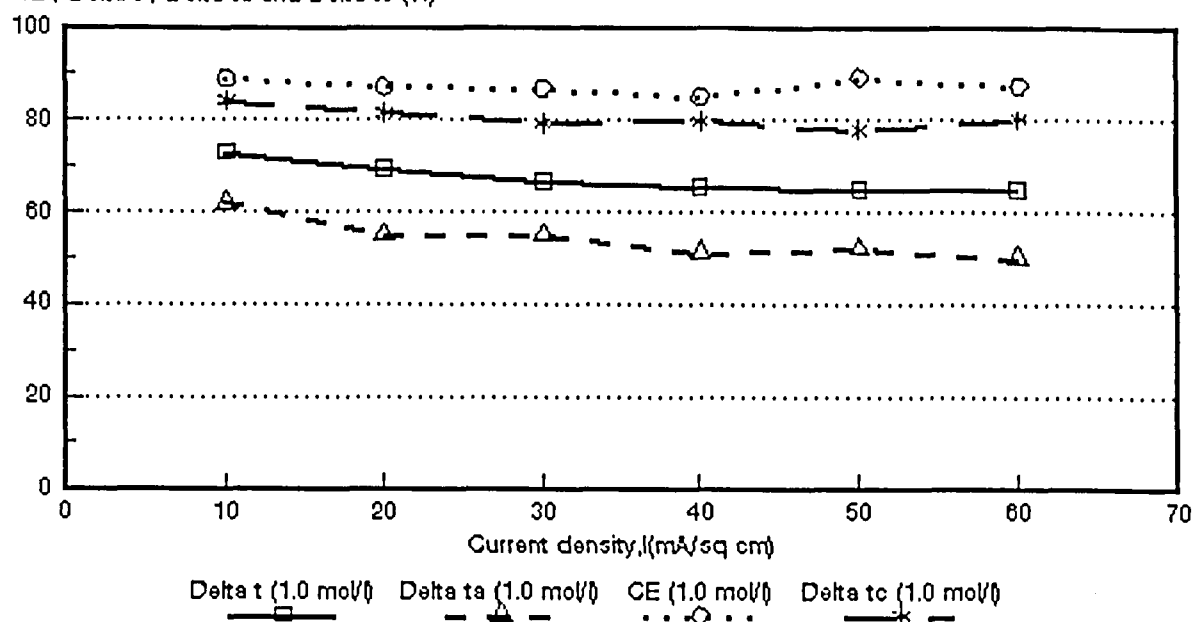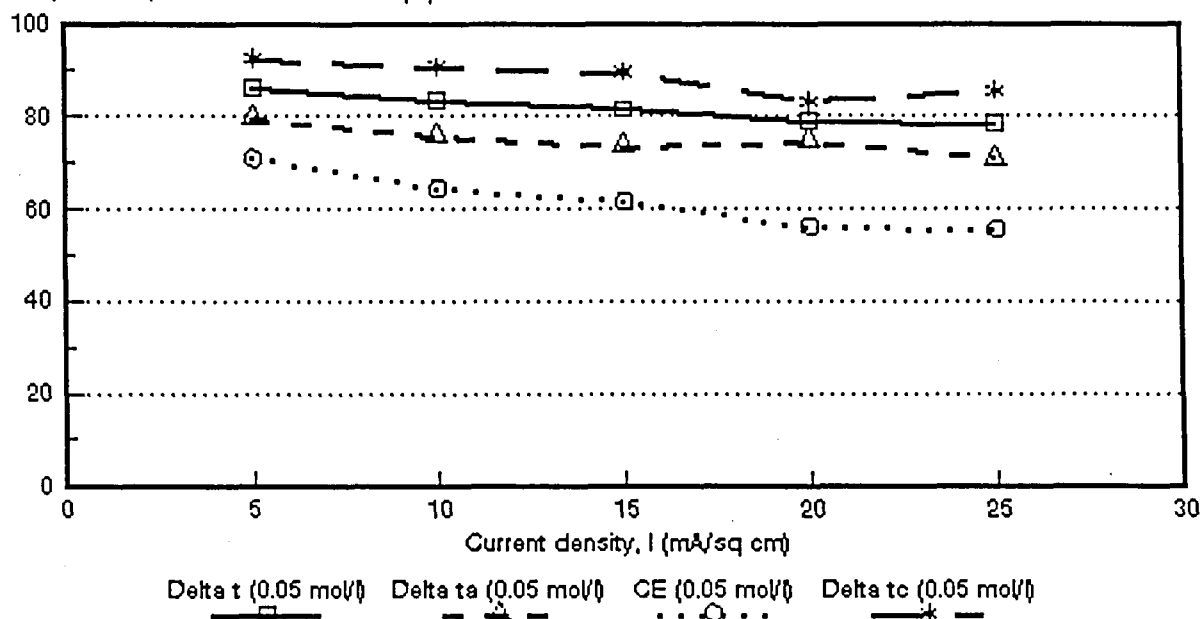
Figure 6.57: Current efficiency (CE = c_p) and apparent transport numbers as a function of current density for 1,0 mol/ℓ NaCl feed. *Ionac* MA-3475 and MC-3470 membranes. Delta t = $\bar{\Delta}t$; Delta ta = Δt^a; Delta tc = Δt^c.

Figure 6.58: Current efficiency (CE = ϵ_p) and apparent transport numbers as a function of current density for 0,05 mol/ℓ NaCl feed. *Raipore* R4030 and R4010 membranes. Delta t = $\bar{\Delta}t$; Delta ta = Δt^a; Delta tc = Δt^c.

Figure 6.59: Current efficiency (CE = e_p) and apparent transport numbers as a function of current density for 0,1 mol/ℓ NaCl feed. *Raipore* R4030 and R4010 membranes. Delta t = $\bar{\Delta}$t; Delta ta = Δt^a; Delta tc = Δt^c.
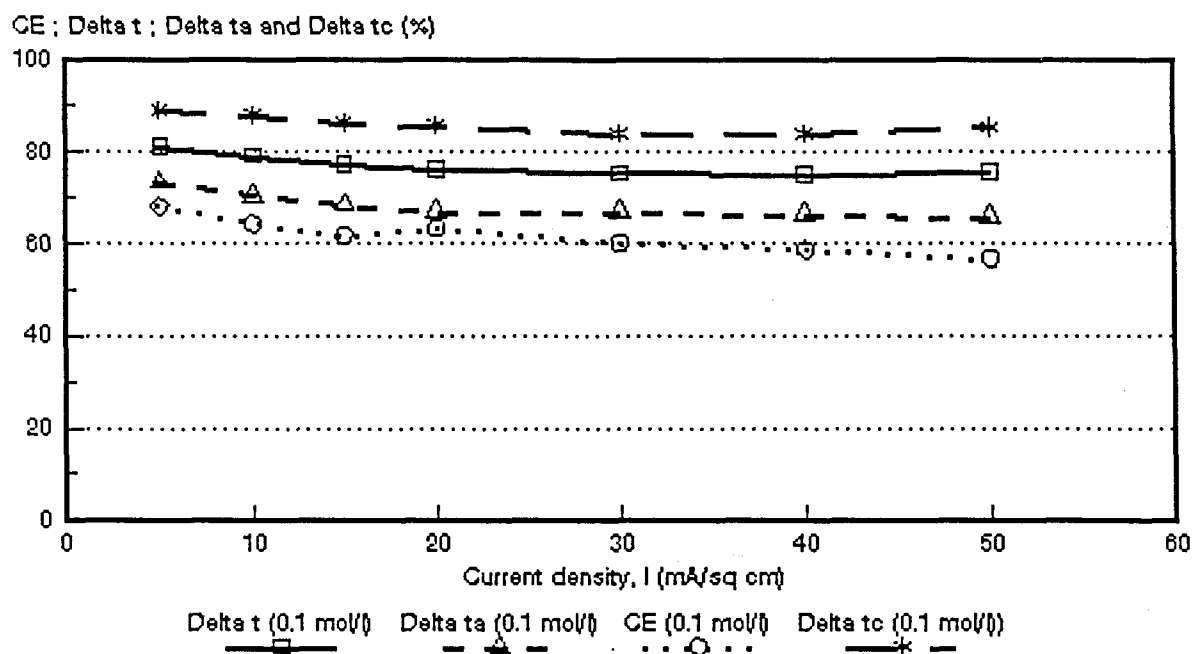

Figure 6.60: Current efficiency (CE = e_p) and apparent transport numbers as a function of current density for 0,5 mol/ℓ NaCl feed. *Raipore* R4030 and R4010 membranes. Delta t = $\bar{\Delta}$t; Delta ta = Δt^a; Delta tc = Δt^c.

CE ; Delta t ; Delta ta and Delta tc (%)

Figure 6.61: Current efficiency (CE = e_p) and apparent transport numbers as a function of current density for 1,0 mol/ℓ NaCl feed. *Ralpore* R4030 and R4010 membranes. Delta t = $\bar{A}$t; Delta ta = Δt^a; Delta tc = Δt^c.
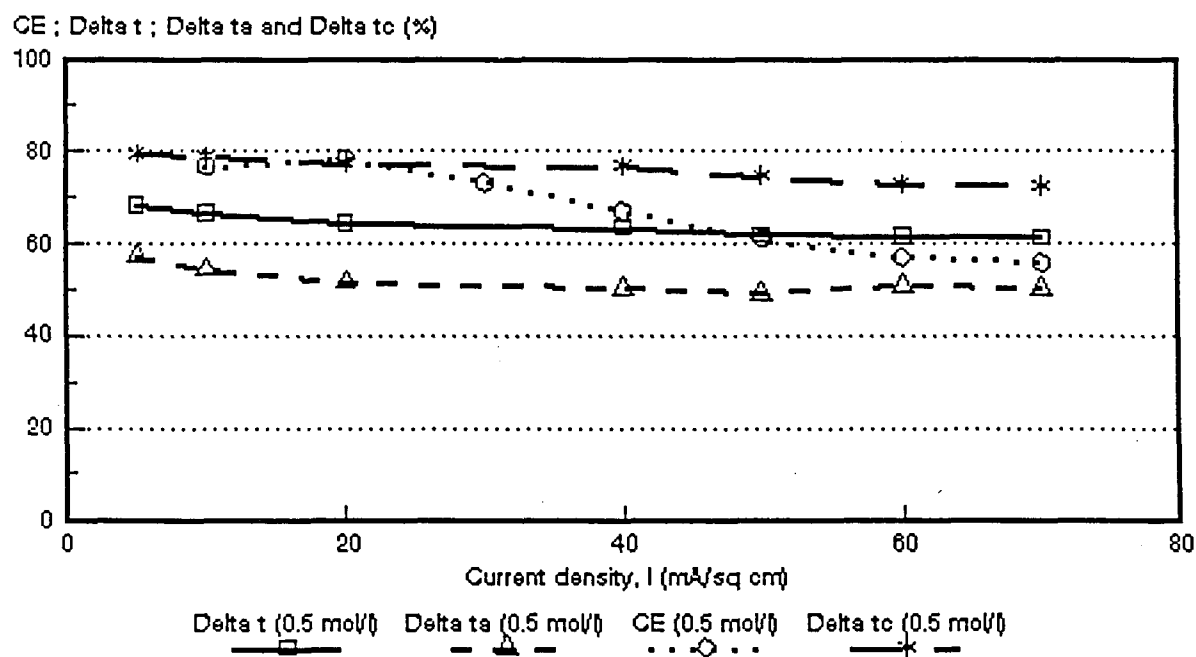
CE ; Delta t ; Delta ta and Delta tc (%)

Figure 6.62: Current efficiency (CE = e_p) and apparent transport numbers as a function of current density for 0,05 mol/ℓ NaCl feed. *Ionics* A-204-UZL-386 and C-61-CZL-386 membranes. Delta t = $\bar{A}$t; Delta ta = Δt^a; Delta tc = Δt^c.

Delta t (0.1 mol/l)   Delta ta (0.1 mol/l)   CE (0.1 mol/l)   Delta tc (0.1 mol/l)
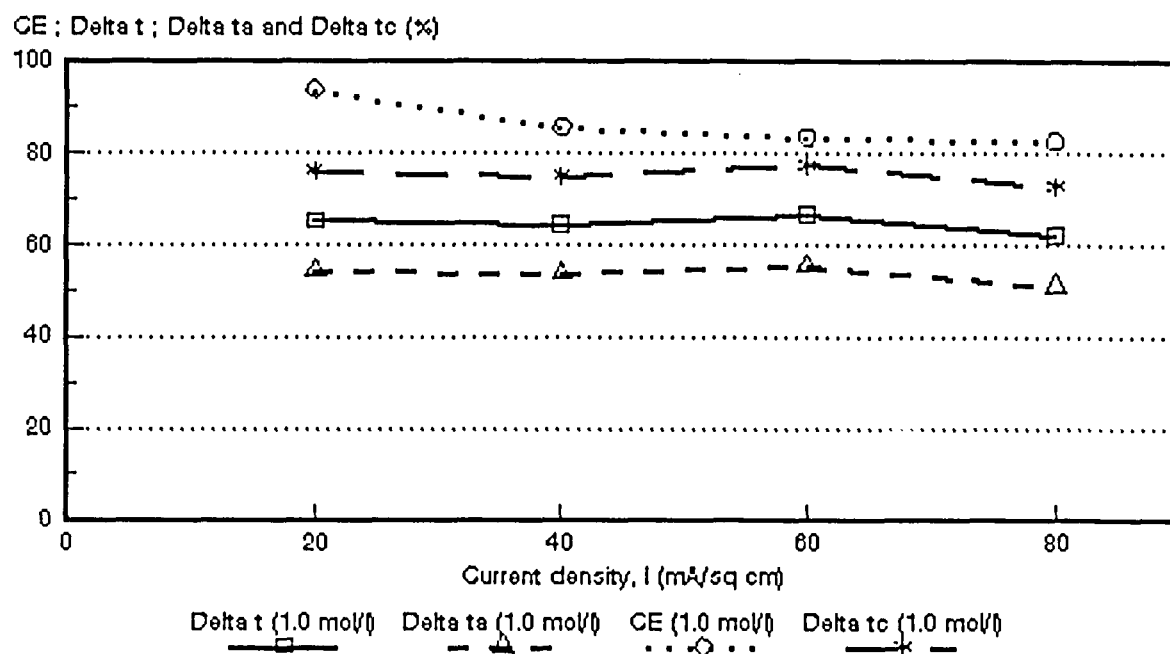
Figure 6.63: Current efficiency (CE = e_p) and apparent transport numbers as a function of current density for 0,1 mol/ℓ NaCl feed. *Ionics* A-204-UZL-386 and C-61-CZL-386 membranes. Delta t = $\overline{\Delta}$t; Delta ta = Δt^a; Delta tc = Δt^c.

CE ; Delta t ; Delta ta and Delta tc (%)

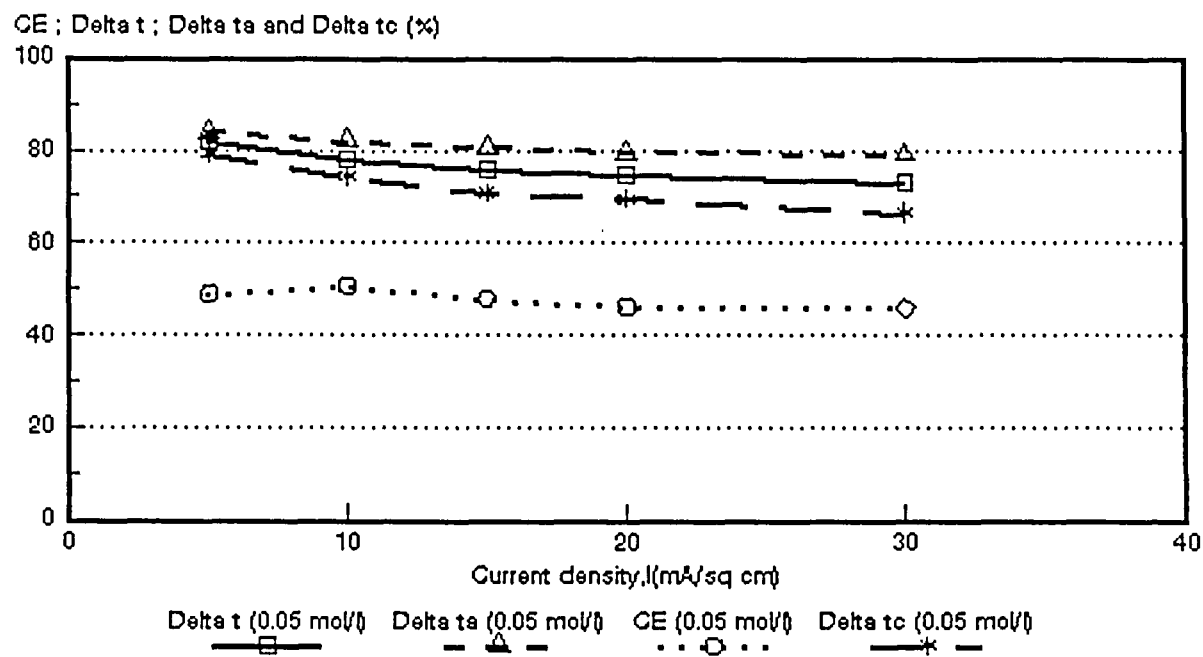Delta t (0.5 mol/l)   Delta ta (0.5 mol/l)   CE (0.5 mol/l)   Delta tc (0.5 mol/l)

Figure 6.64: Current efficiency (CE = e_p) and apparent transport numbers as a function of current density for 0,5 mol/ℓ NaCl feed. *Ionics* A-204-UZL-386 and C-61-CZL-386 membranes. Delta t = $\overline{\Delta}$t; Delta ta = Δt^a; Delta tc = Δt^c.
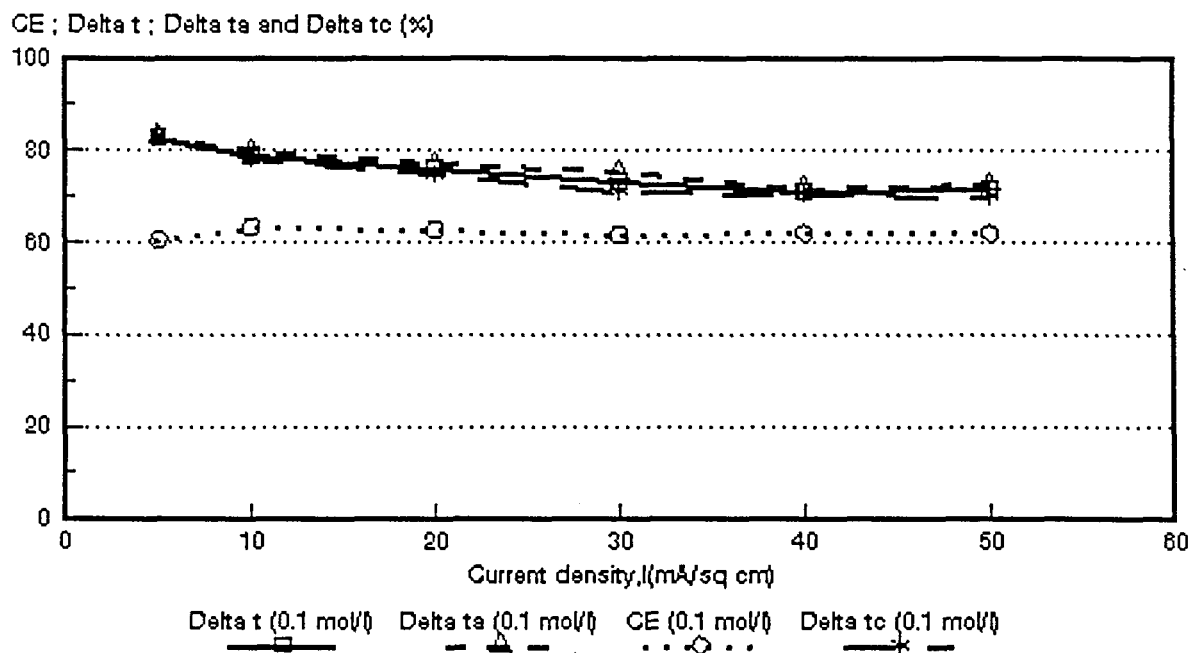
Figure 6.65: Current efficiency (CE = e_p) and apparent transport numbers as a function of current density for 1,0 mol/ℓ NaCl feed. *Ionics* A-204-UZL-386 and C-61-CZL-386 membranes. Delta t = $\bar{\Delta}$t; Delta ta = Δt^a; Delta tc = Δt^c.

Figure 6.66: Current efficiency (CE = e_p) and apparent transport numbers as a function of current density for 0,05 mol/ℓ NaCl feed. WTPSA-1 and WTPSC-1 membranes. Delta t = $\bar{\Delta}$t; Delta ta = Δt^a; Delta tc = Δt^c.

CE ; Delta t ; Delta ta and Delta tc (%)

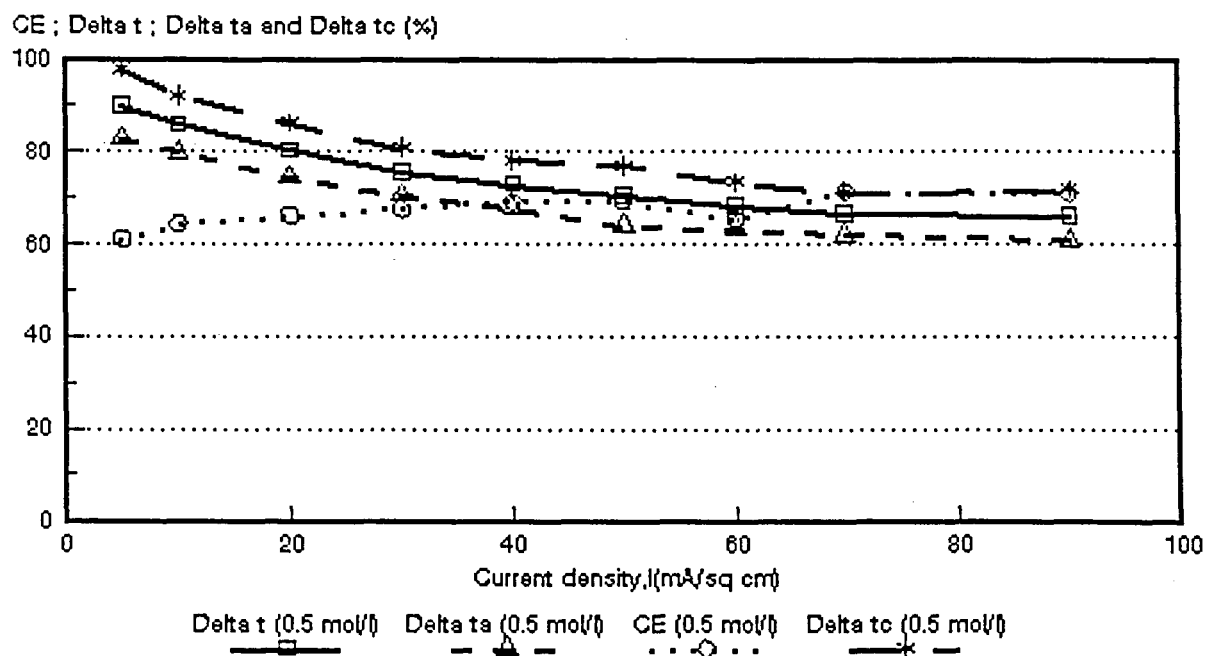Delta t (0.1 mol/l)   Delta ta (0.1 mol/l)   CE (0.1 mol/l)   Delta tc (0.1 mol/l)

Figure 6.67: Current efficiency (CE = e_p) and apparent transport numbers as a function of current density for 0,1 mol/l NaCl feed. WTPSA-1 and WTPSC-1 membranes. Delta t = $\bar{\Delta}$t; Delta ta = Δt^a; Delta tc = Δt^c.

CE ; Delta t ; Delta ta and Delta tc (%)

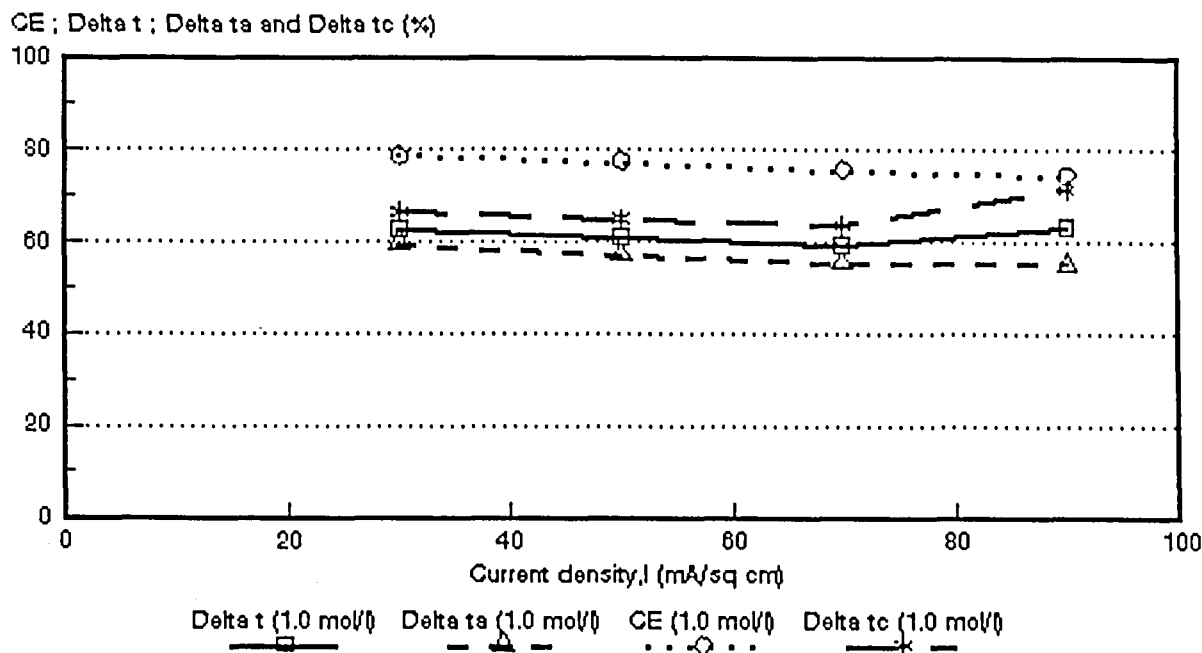Delta t (0.5 mol/l)   Delta ta (0.5 mol/l)   CE (0.5 mol/l)   Delta tc (0.5 mol/l)

Figure 6.68: Current efficiency (CE = e_p) and apparent transport numbers as a function of current density for 0,5 mol/l NaCl feed. WTPSA-1 and WTPSC-1 membranes. Delta t = $\bar{\Delta}$t; Delta ta = Δt^a; Delta tc = Δt^c.
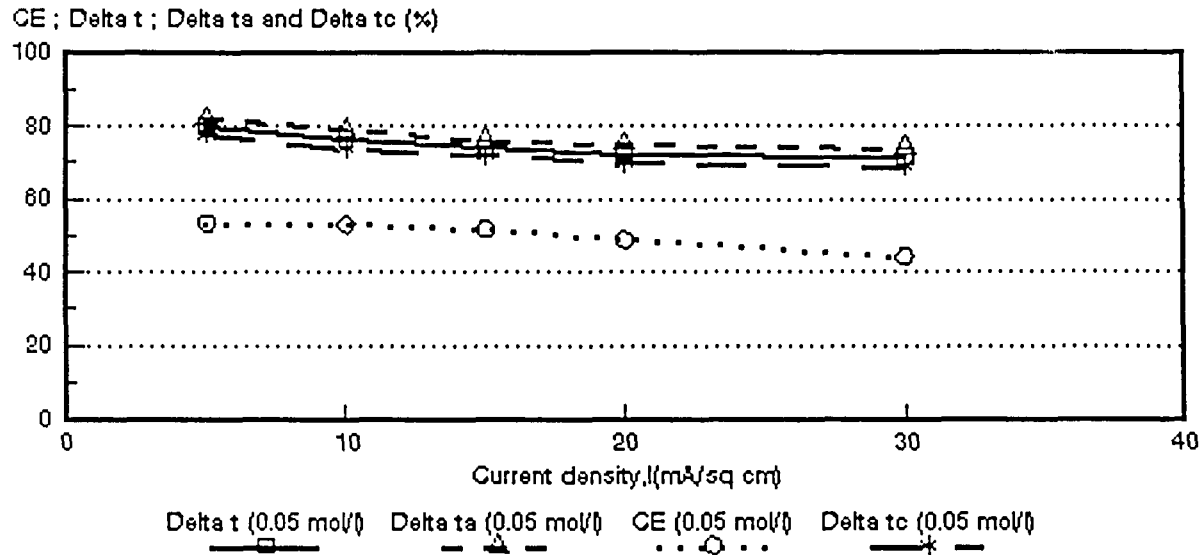
Figure 6.69: Current efficiency (CE = e_p) and apparent transport numbers as a function of current density for 1,0 mol/ℓ NaCl feed. WTPSA-1 and WTPSC-1 membranes. Delta t = $\overline{\Delta t}$; Delta ta = Δt^a; Delta tc = Δt^c.

Figure 6.70: Current efficiency (CE = e_p) and apparent transport numbers as a function of current density for 0,05 mol/ℓ NaCl feed. WTPVCA-2 and WTPVCC-2 membranes. Delta t = $\overline{\Delta t}$; Delta ta = Δt^a; Delta tc = Δt^c.

CE ; Delta t ; Delta ta and Delta tc (%)

Current density,I(mA/sq cm)

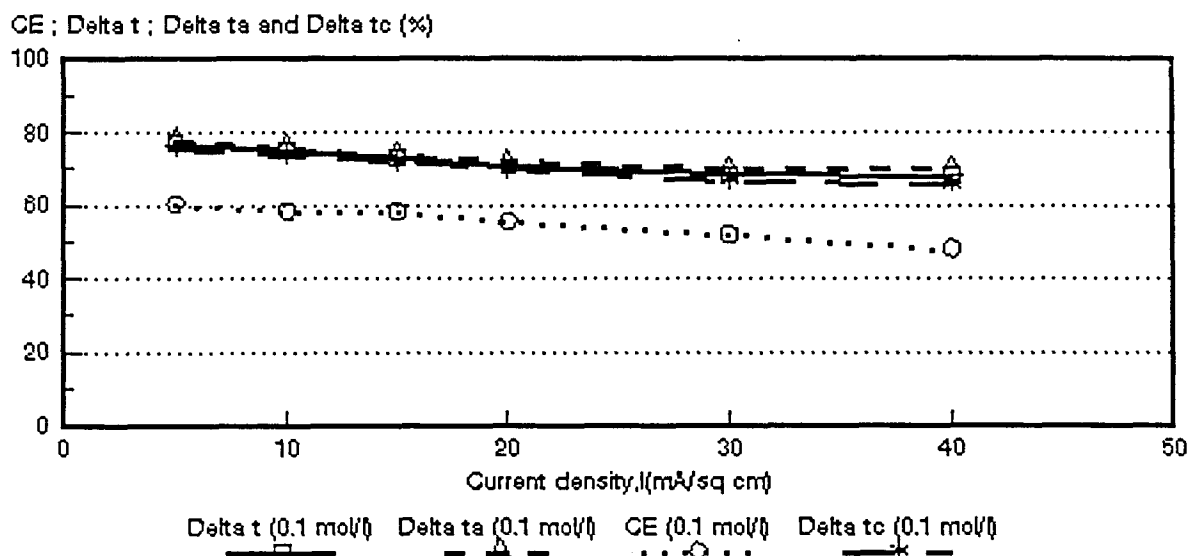Delta t (0.1 mol/l)   Delta ta (0.1 mol/l)   CE (0.1 mol/l)   Delta tc (0.1 mol/l)

Figure 6.71: Current efficiency (CE $= e_p$) and apparent transport numbers as a function of current density for 0,1 mol/l NaCl feed. WTPVCA-2 and WTPVCC-2 membranes. Delta t $= \bar{\Delta}t$; Delta ta $= \Delta t^a$; Delta tc $= \Delta t^c$.

CE ; Delta t ; Delta ta and Delta tc (%)

Current density,I(mA/sq cm)

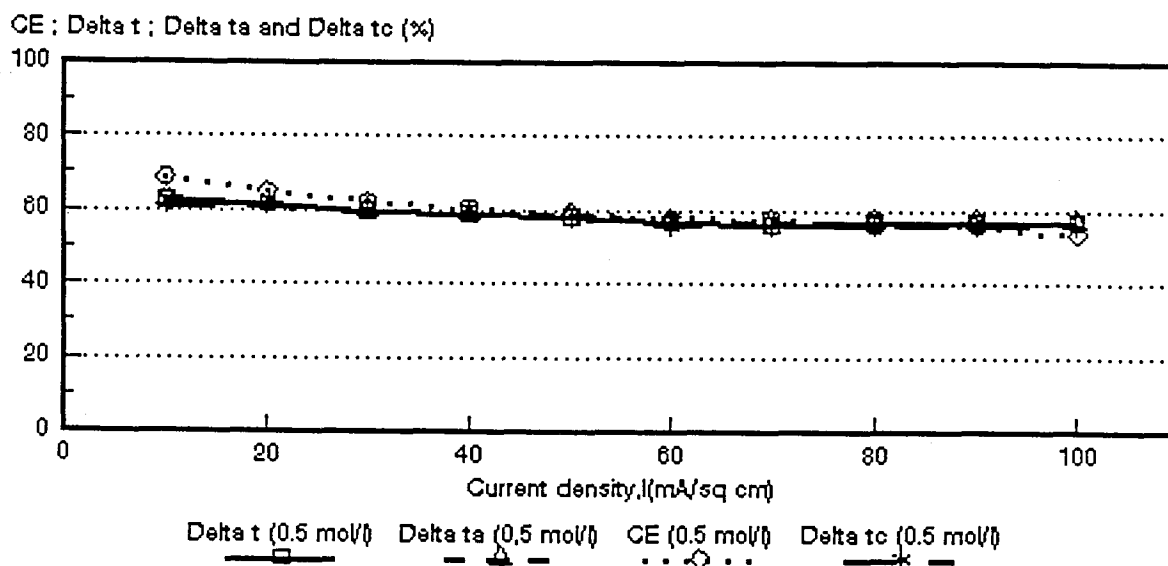Delta t (0.5 mol/l)   Delta ta (0.5 mol/l)   CE (0.5 mol/l)   Delta tc (0.5 mol/l)

Figure 6.72: Current efficiency (CE $= e_p$) and apparent transport numbers as a function of current density for 0,5 mol/l NaCl feed. WTPVCA-2 and WTPVCC-2 membranes. Delta t $= \bar{\Delta}t$; Delta ta $= \Delta t^a$; Delta tc $= \Delta t^c$.

199

CE ; Delta t ; Delta ta and Delta tc (%)

Current density,I(mA/sq cm)

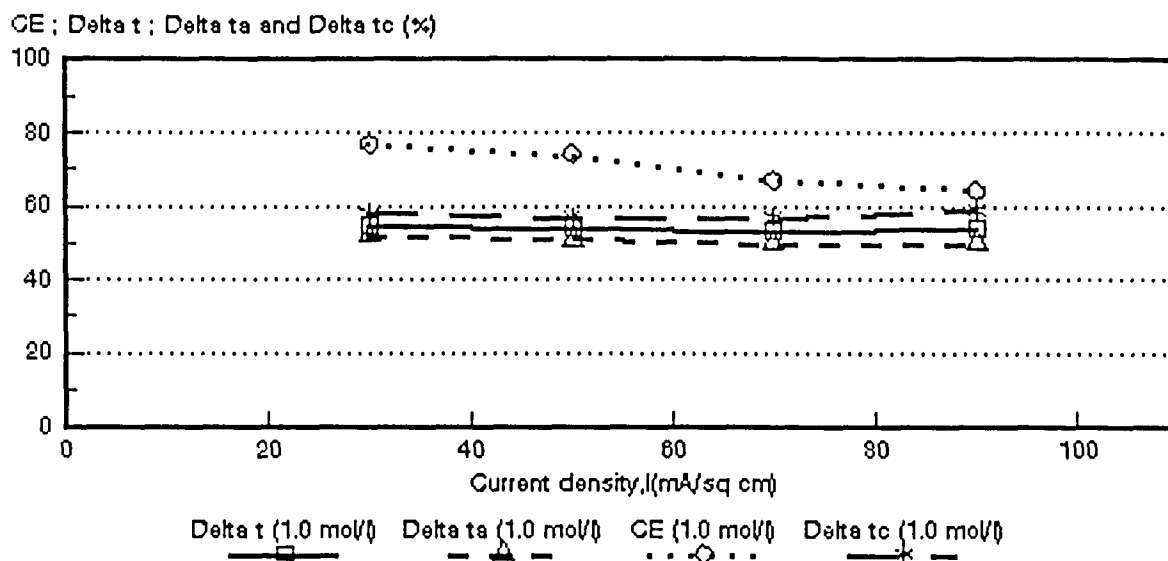Delta t (1.0 mol/l)   Delta ta (1.0 mol/l)   CE (1.0 mol/l)   Delta tc (1.0 mol/l)
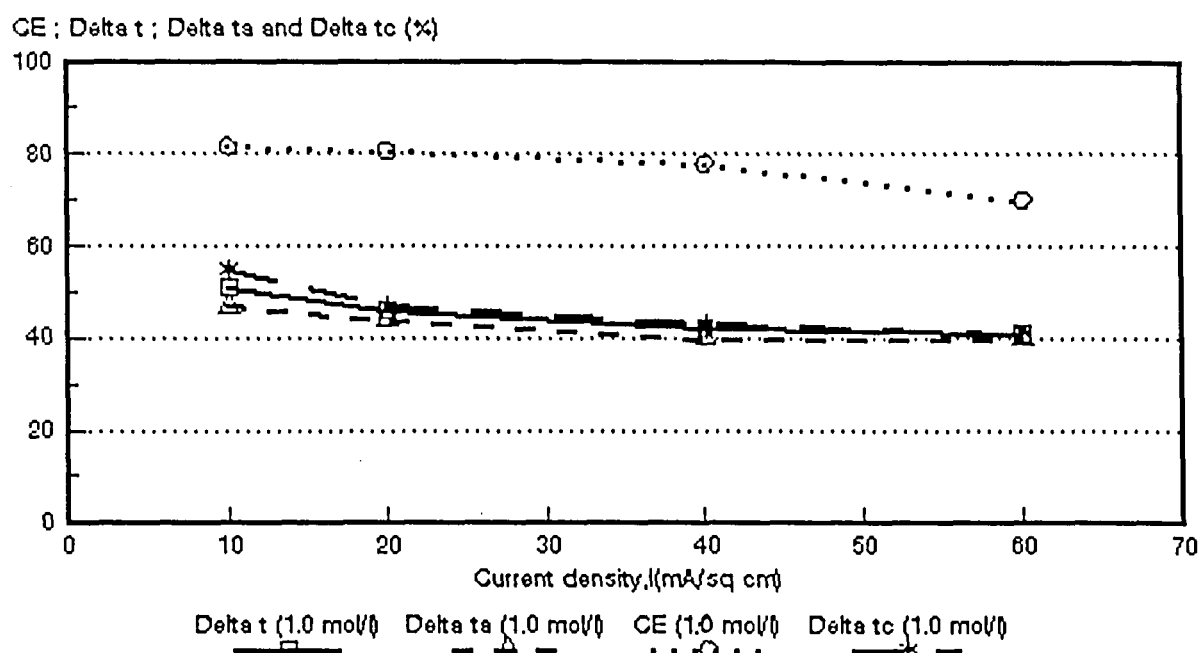
Figure 6.73: Current efficiency (CE = e_p) and apparent transport numbers as a function of current density for 1,0 mol/ℓ NaCl feed. WTPVCA-2 and WTPVCC-2 membranes. Delta t = $\bar{\Delta}$t; Delta ta = Δt^a; Delta tc = Δt^c.

CE ; Delta t ; Delta ta and Delta tc (%)

Current density,I(mA/sq cm)

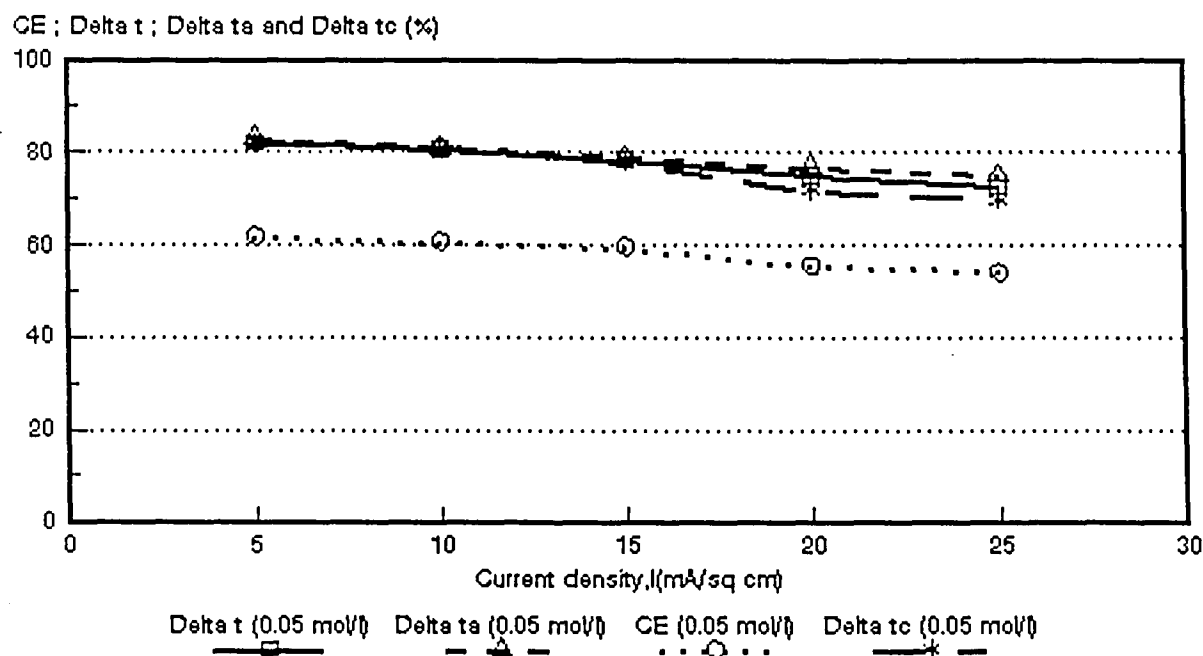Delta t (0.05 mol/l)   Delta ta (0.05 mol/l)   CE (0.05 mol/l)   Delta tc (0.05 mol/l)
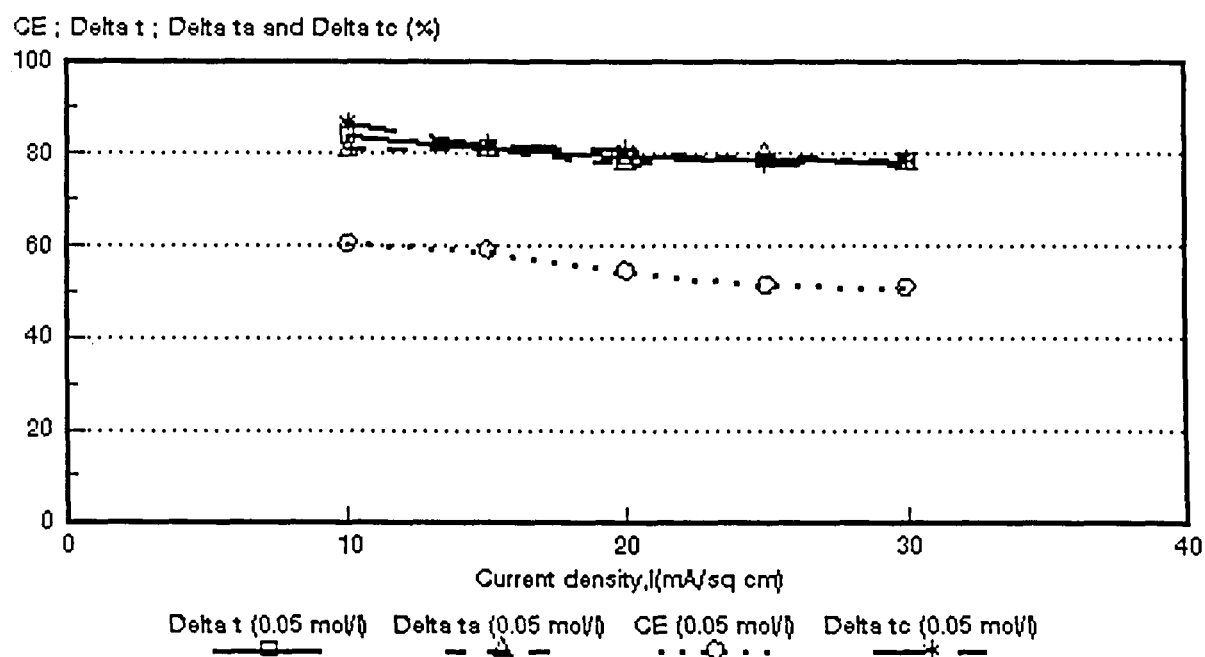
Figure 6.74: Current efficiency (CE = e_p) and apparent transport numbers as a function of current density for 0,05 mol/ℓ NaCl feed. WTPSTA-3 and WTPSTC-3 membranes. Delta t = $\bar{\Delta}$t; Delta ta = Δt^a; Delta tc = Δt^c.

200

CE ; Delta t ; Delta ta and Delta tc (%)

Current density,I(mA/sq cm)

Delta t (0.1 mol/l)   Delta ta (0.1 mol/l)   CE (0.1 mol/l)   Delta tc (0.1 mol/l)
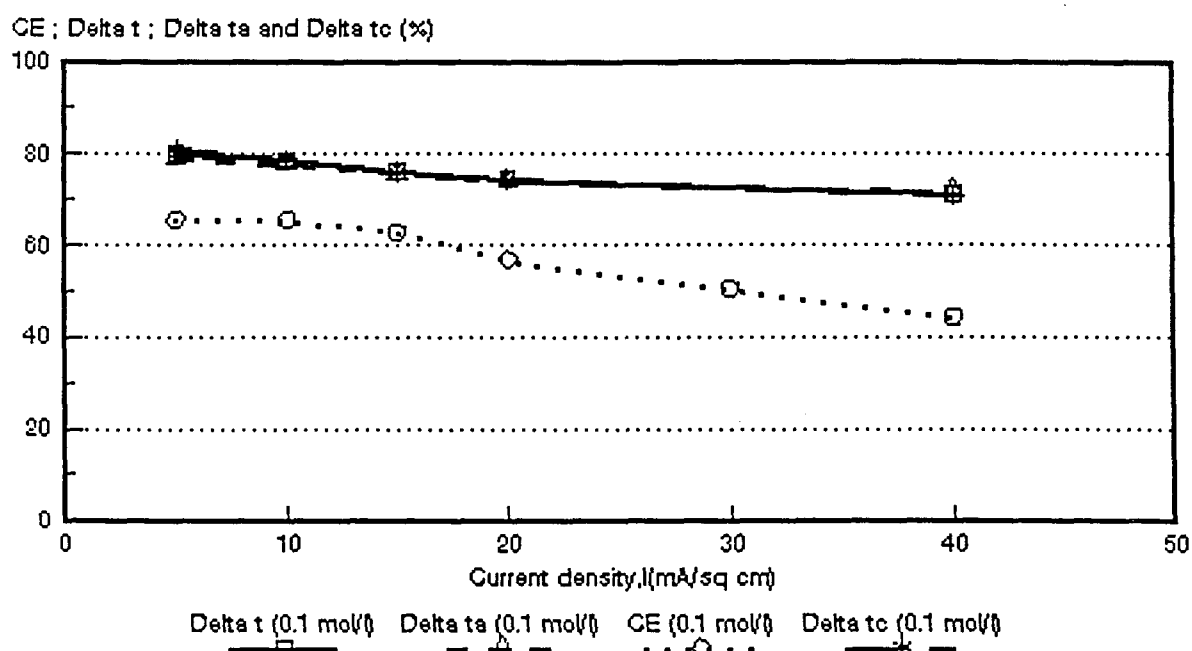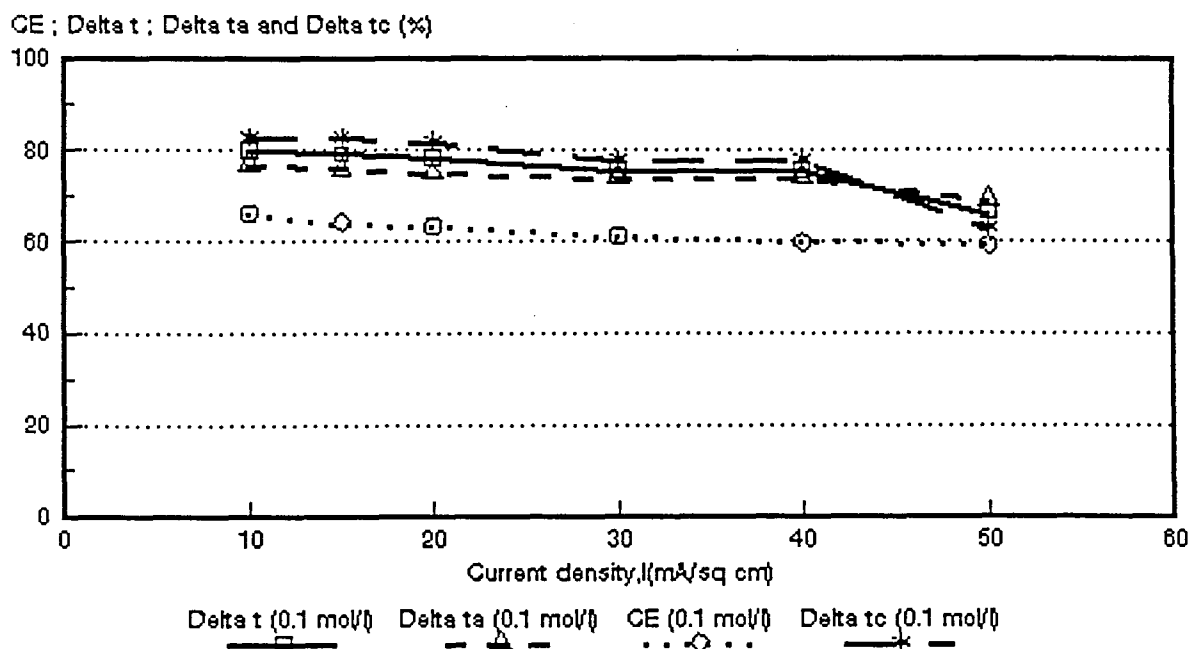
Figure 6.75: Current efficiency (CE = e_p) and apparent transport numbers as a function of current density for 0,1 mol/ℓ NaCl feed. WTPSTA-3 and WTPSTC-3 membranes. Delta t = $\overline{\Delta}$t; Delta ta = Δt^a; Delta tc = Δt^c.

CE ; Delta t ; Delta ta and Delta tc (%)

Current density,I(mA/sq cm)

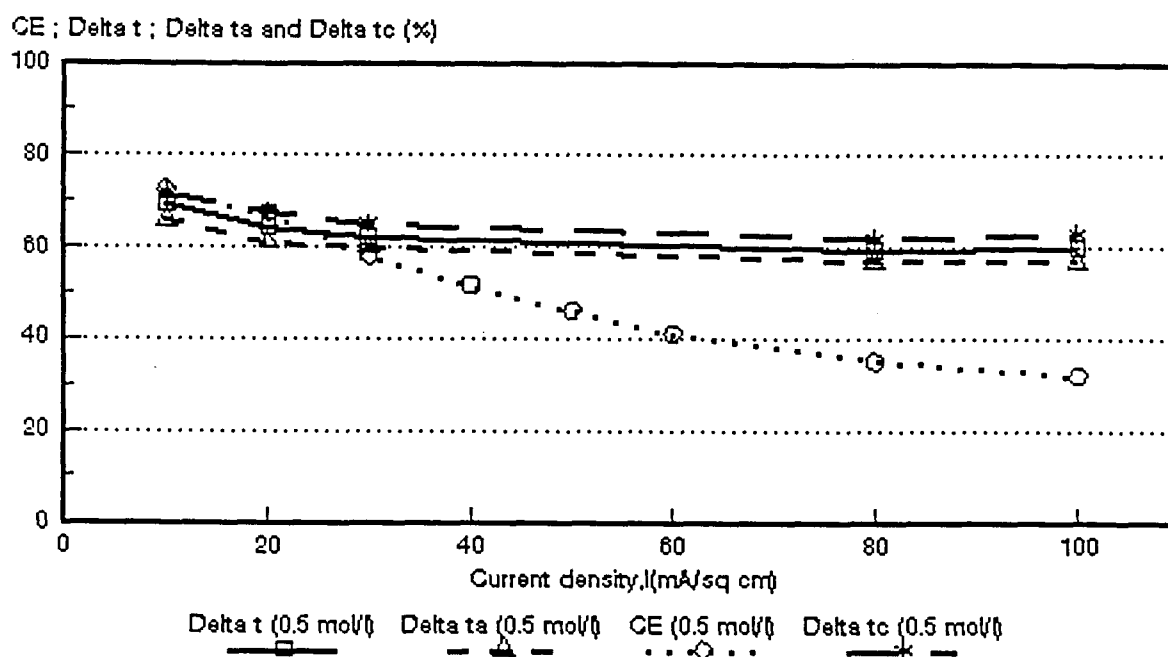Delta t (0.5 mol/l)   Delta ta (0.5 mol/l)   CE (0.5 mol/l)   Delta tc (0.5 mol/l)
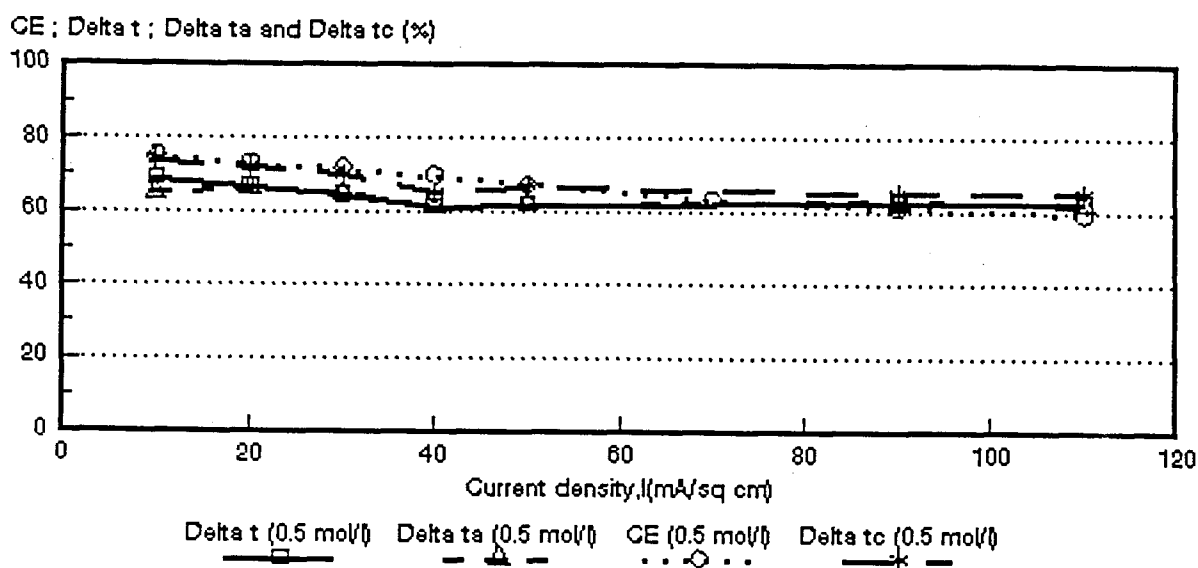
Figure 6.76: Current efficiency (CE = e_p) and apparent transport numbers as a function of current density for 0,5 mol/ℓ NaCl feed. WTPSTA-3 and WTPSTC-3 membranes. Delta t = $\overline{\Delta}$t; Delta ta = Δt^a; Delta tc = Δt^c.

201
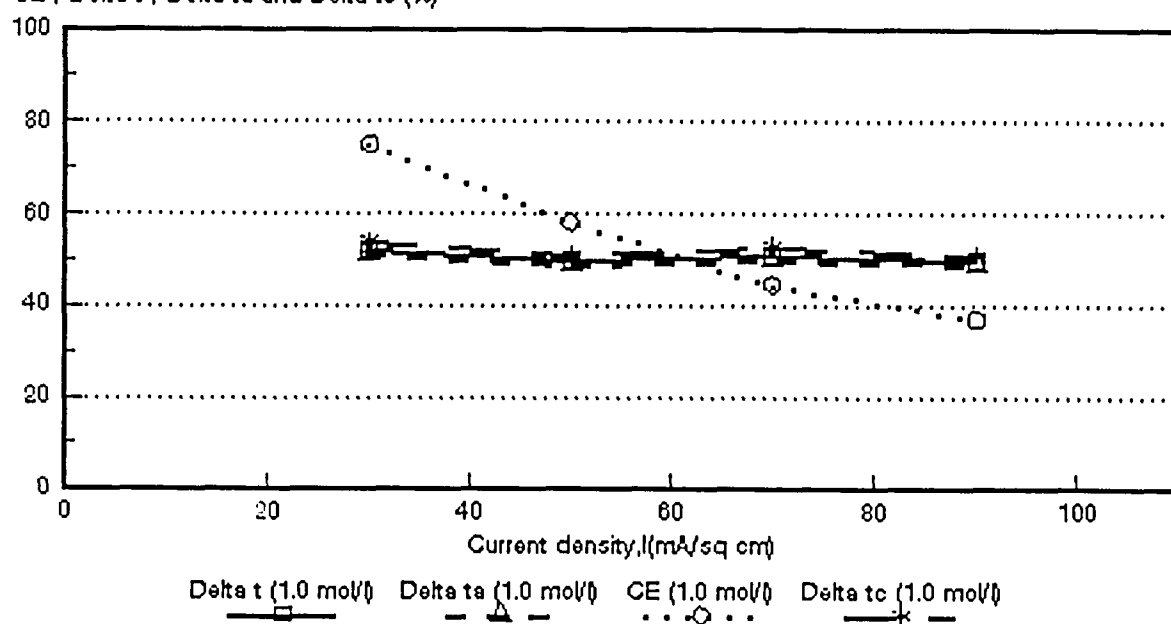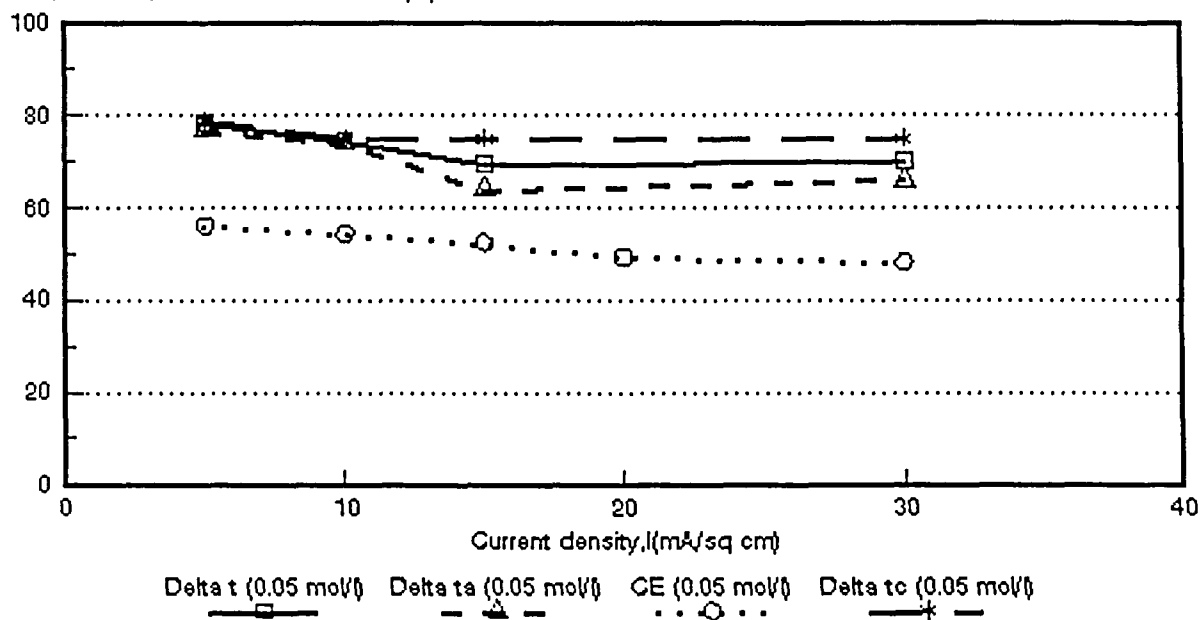
CE : Delta t : Delta ta and Delta tc (%)
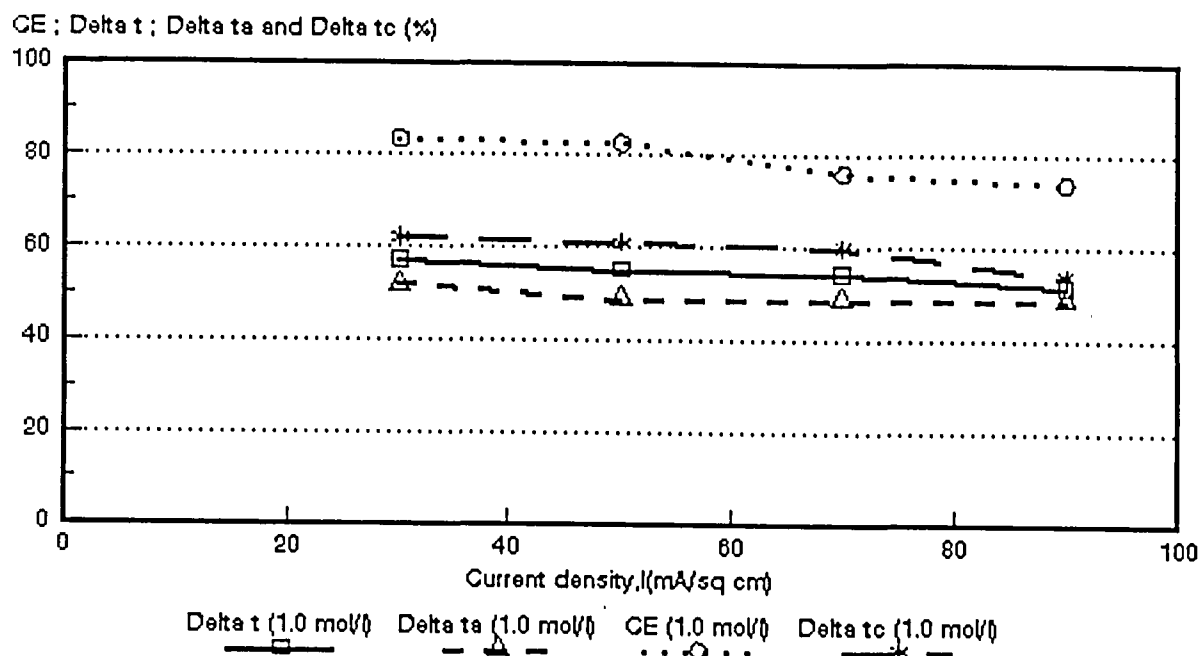
Figure 6.77: Current efficiency (CE = ϵ_p) and apparent transport numbers as a function of current density for 1,0 mol/ℓ NaCl feed. WTPSTA-3 and WTPSTC-3 membranes. Delta t = $\bar{\Delta}t$; Delta ta = Δt^a; Delta tc = Δt^c.
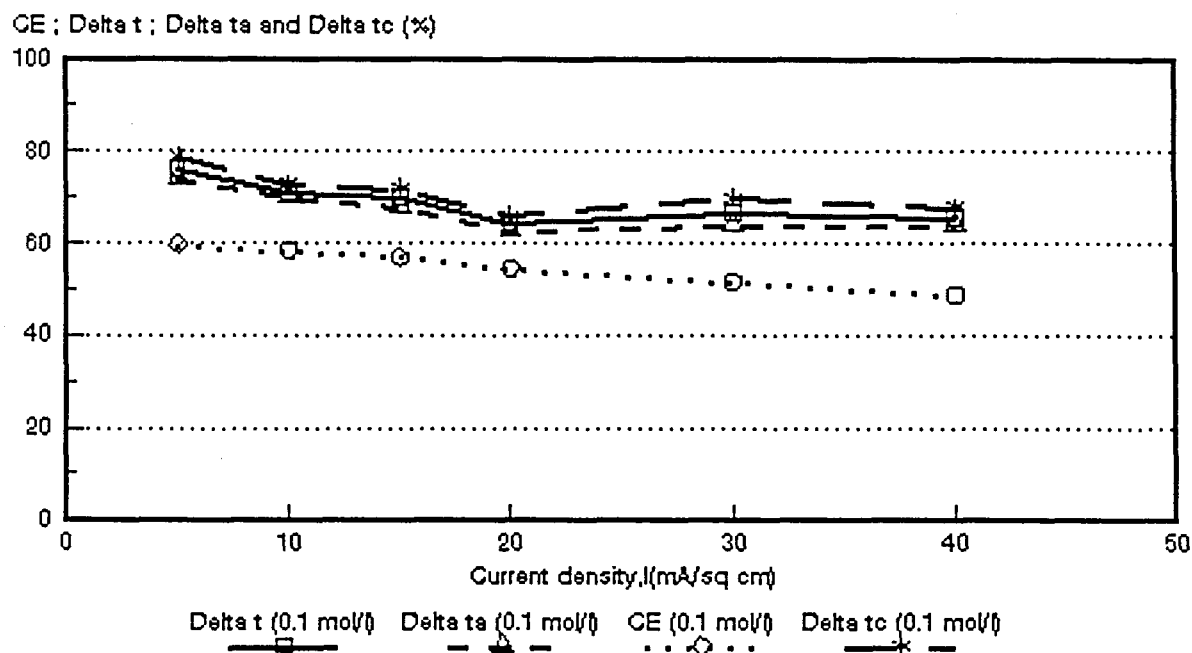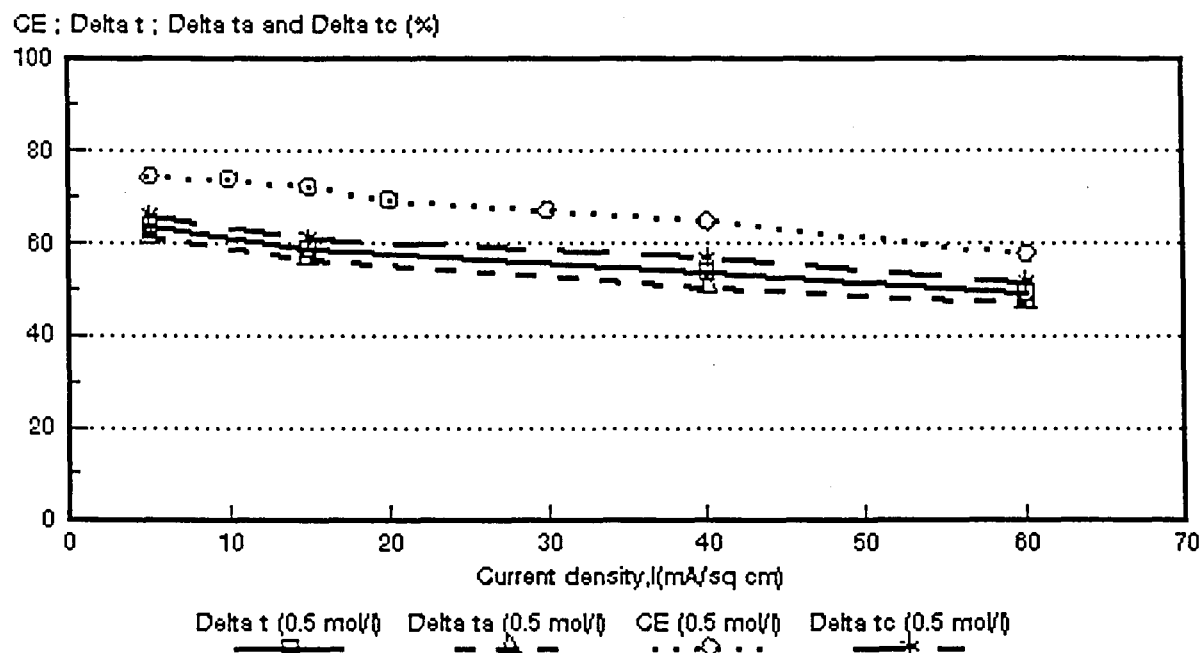
current efficiencies at the higher feed water concentrations (0,5 to 1,0 mol/ℓ). The only exception in this regard was obtained with the *Raipore* membranes where the apparent transport numbers became lower than the current efficiency at 1,0 mol/ℓ feed concentration.

Good correlations were obtained between the apparent transport number of a membrane pair ($\bar{\Delta}t$) and current efficiency (ϵ_p) for all the membranes investigated depending on the feed concentration and current density used (Table 6.32). The ratio between $\bar{\Delta}t/\epsilon_p$ for the *Selemion* membranes varied between 1,01 and 1,07 in the current density range from 15 to 50 mA/cm² (0,1 mol/ℓ feed). This ratio for the *Ionac* membranes varied between 0,95 to 1,09 in the current density range from 40 to 70 mA/cm² (0,5 mol/ℓ feed). For the *Raipore* membranes the ratio ($\bar{\Delta}t/\epsilon_p$) varied between 0,94 and 1,05 in the current density range from 40 to 90 mA/cm² (0,5 mol/ℓ feed). For the *Ionics* membranes the ratio varied between 0,95 and 1,02 in the current density range from 20 to 90 mA/cm² (0,5 mol/ℓ feed). A good correlation was obtained

between $\bar{\Delta}t$ and ϵ_p (0,95 to 1,07 at 0,5 mol/ℓ feed) for the WTPS membranes in the current density range from 10 to 30 mA/cm^2. The correlations, however, at high current densities (Table 6.32, 80 mA/cm^2) were not very good due to polarization that was taking place. Relatively good correlations were also obtained between $\bar{\Delta}t$ and ϵ_p for the WTPVC and WTPST membranes. The correlation varied between 0,82 to 0,86 (5 to 60 mA/cm^2, WTPVC) and between 0,88 and 1,04 (10 to 110 mA/cm^2, WTPST) at 0,5 mol/ℓ feed concentration. The ratio between $\bar{\Delta}t/\epsilon_p$ varied between approximately 0,82 and 1,09 in the feed concentration range from 0,1 to 0,5 mol/ℓ for the different membranes investigated. Therefore, it appears that apparent transport numbers determined from a simple membrane potential method should give a good approximate estimation of membrane performance for ED concentration/desalination applications. Membrane performance for concentration/desalination applications should be predicted with an accuracy of approximately 10% from membrane potential measurements depending on the feed concentration and current density used.

The apparent transport numbers of the anion- (Δt^a) and cation (Δt^c) membranes should also be used to predict membrane performance for concentration/desalination applications (Tables 6.33 and 6.34). However, the accuracy of the prediction will depend on the feed concentration and current density used.

Table 6.32: Correlation between apparent transport number for a membrane pair ($\overline{\Delta}t$) and current efficiency (e_p).

Current Density	Selemion AMV & CMV Concentration, mol/l				Ionac MA-3475 & MC-3470 Concentration, mol/l				Raipore R4030 & R4010 Concentration, mol/l				Ionics A-204-UZL & C-61-CZL Concentration, mol/l				WTPS WTPSA & WTPSC Concentration, mol/l				WTPVC WTPVCA & WTPVCC Concentration, mol/l				WTPST WTPSTA & WTPSTC Concentration, mol/l			
mA/cm²	0,05	0,1	0,5	1,0	0,05	0,1	0,5	1,0	0,05	0,1	0,5	1,0	0,05	0,1	0,5	1,0	0,05	0,1	0,5	1,0	0,05	0,1	0,5	1,0	0,05	0,1	0,5	1,0
5	1,39	1,19	0,99		1,21	1,19	0,72		1,68	1,37	1,47		1,49	1,27			1,32	1,22			1,41	1,27	0,86					
10	1,28	1,13	0,85	0,82	1,29	1,23	0,87		1,54	1,25	1,34		1,43	1,28	0,90		1,33	1,21	0,95		1,36	1,21		0,62	1,39	1,21	0,92	
15	1,27	1,07			1,33	1,25			1,58				1,43	1,25			1,32	1,21			1,34	1,23	0,82		1,37	1,23		
20	1,25	1,06	0,79	0,78	1,41	1,20	0,83	0,69	1,62	1,21	1,21		1,49	1,28	0,95		1,35	1,30	0,95		1,19	1,19		0,57	1,46	1,23	0,90	
25					1,41												1,35								1,52			
30	1,23	1,05	0,82	0,77		1,25			1,59	1,19	1,12	0,80	1,61	1,32	0,96	0,72			1,07	0,69	1,45	1,30			1,55	1,24	0,90	0,68
40		1,04	0,78	0,77		1,28	0,95	0,75		1,15	1,05			1,41	0,99			1,60				1,35	0,83	0,54		1,27	0,89	
50		1,01	0,78	0,73		1,34	1,01			1,16	1,02	0,79			0,98	0,73				0,86						1,11	0,92	0,67
60			0,78	0,74			1,09	0,80			1,05				0,99								0,85	0,58				
70							1,09				0,94	0,79			0,97	0,79				1,14							0,84	0,72
80								0,75							1,01				1,70									
90											1,03	0,84			1,02	0,84			1,35							1,03	0,70	
100															1,06				1,87									
110																										1,04		

Table 6.33: Correlation between apparent transport number of the anion membrane (Δt^a) and current efficiency (e_p).

$\Delta t^a/e_p$

Current Density mA/cm²	Selemion AMV & CMV Concentration, mol/l				Ionac MA-3475 & MC-3470 Concentration, mol/l				Raipore R4030 & R4010 Concentration, mol/l				Ionics A-204-UZL & C-61-CZL Concentration, mol/l				WTPS WTPSA & WTPSC Concentration, mol/l				WTPVC WTPVCA & WTPVCC Concentration, mol/l				WTPST WTPSTA & WTPSTC Concentration, mol/l			
	0,05	0,1	0,5	1,0	0,05	0,1	0,5	1,0	0,05	0,1	0,5	1,0	0,05	0,1	0,5	1,0	0,05	0,1	0,5	1,0	0,05	0,1	0,5	1,0	0,05	0,1	0,5	1,0
5	1,31	1,11	0,86		1,13	1,07	0,59		1,72	1,37	1,36		1,53	1,29			1,34	1,20			1,37	1,24	0,82					
10	1,24	1,04	0,75	0,70	1,18	1,09	0,70		1,62	1,27	1,24		1,49	1,30	0,92		1,33	1,19	0,91		1,36	1,20		0,58	1,34	1,16	0,87	
15	1,20	0,98			1,19	1,10			1,69				1,47	1,27			1,33	1,21			1,22	1,20	0,78		1,37	1,18		
20	1,16	0,96	0,69	0,63	1,32	1,06	0,66	0,58	1,73	1,23	1,13		1,53	1,29	0,95		1,38	1,30	0,90		0,99	1,16		0,55	1,43	1,19	0,83	
25					1,28												1,38								1,55			
30	1,14	0,97	0,68	0,61		1,11			1,72	1,22	1,05	0,75	1,67	1,34	0,96	0,68			1,03	0,68	1,37	1,24			1,53	1,21	0,82	0,62
40		0,91	0,66	0,60		1,13	0,75	0,63		1,16	0,98			1,46	0,97			1,62				1,31	0,77	0,51		1,24	0,83	
50		0,94	0,64	0,58		1,16	0,80			1,18	0,92	0,73			0,99	0,69				0,84						1,17	0,85	0,59
60			0,62	0,57			0,90	0,66			0,98				0,98								0,81	0,57				
70							0,89				0,87	0,74			0,99	0,74			1,12								0,84	0,64
80							0,62								1,01				1,62									
90											0,86	0,74			1,02	0,78			1,32								0,98	0,66
100															1,06				1,78									
110																										1,01		

Table 6.34: Correlation between apparent transport number of the cation membrane (Δt^c) and current efficiency (e_p).

$\Delta t^c/e_p$

Current Density mA/cm²	Selemion AMV & CMV Concentration, mol/l				Ionac MA-3475 & MC-3470 Concentration, mol/l				Raipore R4030 & R4010 Concentration, mol/l				Ionics A-204-UZL & C-61-CZL Concentration, mol/l				WTPS WTPSA & WTPSC Concentration, mol/l				WTPVC WTPVCA & WTPVCC Concentration, mol/l				WTPST WTPSTA & WTPSTC Concentration, mol/l			
	0,05	0,1	0,5	1,0	0,05	0,1	0,5	1,0	0,05	0,1	0,5	1,0	0,05	0,1	0,5	1,0	0,05	0,1	0,5	1,0	0,05	0,1	0,5	1,0	0,05	0,1	0,5	1,0
5	1,46	1,29	1,12		1,31	1,30	0,83		1,62	1,37	1,60		1,46	1,26			1,32	1,23			1,41	1,32	0.89					
10	1,33	1,20	0,96	0,94	1,41	1,37	1,04		1,48	1,23	1,43		1,40	1,27	0,89		1,33	1,21	0,99		1,38	1,25		0,67	1,44	1,26	0,99	
15	1,31	1,16			1,46	1,39			1,48				1,39	1,23			1,31	1,21			1,43	1,27	0,84		1,39	1,29		
20	1,33	1,16	0,88	0,94	1,48	1,36	0,99	0,81	1,52	1,20	1,30		1,43	1,26	0,94		1,29	1,30	1,01		1,38	1,21		0,58	1,48	1,30	0,98	
25	1,31				1,55												1,29								1,51			
30		1,12	0,98	0,91		1,40			1,46	1,15	1,20	0,85	1,56	1,29	0,96	0,75			1,17	0,72	1,56	1,35			1,55	1,27	0,97	0,74
40		1,19	0,89	0,94		1,43	1,15	0,88		1,15	1,13			1,37	0,97			1,60				1,39	0,86	0,55		1,30	0,93	
50		1,08	0,92	0,88		1,50	1,23			1,13	1,10	0,84			0,98	0,77							0,83			1,06	1,00	0,74
60			0,93	0,91			1,28	0,93			1,13				0,97								0,88	0,58				
70						1,31					0,99	0,84			0,97	0,85			1,19								0,84	0,79
80								0,88							1,00				1,76									
90											1,02	0,95			1,00	0,92			1,37								1,06	0,73
100															1,04				1,96									
110																										1,09		

206

6.3   Water Flow

Water flow (J) through the membranes as a function of current density and feed water concentration is shown in Figures 6.78 to 6.84. Water flow (J_i) through the membranes relative to the flow at $J_{0,5\ mol/\ell}$ and $J_{0,1\ mol/\ell}$ is shown in Table 6.35. Water or volume flow through the membranes increases as a function of both current density and feed water concentration. All the membranes showed an increase in water flow with increasing feed water concentration except the *Selemion* membranes at 1,0 mol/ℓ feed concentration (Table 6.35). It is further interesting to note that water flows are significantly higher at the highest feed concentration (1,0 mol/ℓ) in the case of the *Ionac-* (Fig 6.79), *Raipore-* (Fig. 6.80), *Ionics-* (Fig. 6.81), WTPS- (Fig. 6.82), WTPVC- (Fig. 6.83) and WTPST- (Fig. 6.84) membranes. Current efficiencies for these membranes were also the highest at the highest feed concentration when more water flowed through the membranes (see Figs. 6.43 to 6.49). Therefore, it appears that increasing current efficiency is caused by increasing water flow through the membranes.   This effect was especially pronounced for the more porous heterogeneous *Ionac-*, WTPS-, WTPVC- and WTPST membranes.

Water flow (J) through the membranes as a function of effective current density, I_{eff}, (actual current density times Coulomb efficiency) and feed water concentration for the different membranes are shown in Figures 6.85 to 6.91. Straight lines were obtained at higher values of I_{eff}. The slope of these lines corresponds to the combined electro-osmotic coefficient (2β) of a membrane pair.   The electro-osmotic coefficients decreases significantly with increasing feed concentration in the case of the *Selemion-* (Fig. 6.85), *Raipore-* (Fig. 6.87), WTPS- (Fig. 6.89), WTPVC- (Fig. 6.90) and WTPST- (Fig. 6.91) membranes as can be seen from the slopes of the lines.

The electro-osmotic coefficients as a function of feed concentration are shown in Figures 6.92 to 6.98. The reduction in the electro-osmotic coefficients with increasing feed concentration can be ascribed to deswelling of the membranes at high feed concentration[27, 28, 42 - 44] and/or a reduction in membrane permselectivity at high feed concentration[25]. This effect was far less for the *Ionac-* and *Ionics* membranes. The WTPS membranes, on the other hand, showed an increase in the electro-osmotic coefficient with increasing feed concentration (Fig. 6.96). Therefore, it appears that this hydrophobic membrane starts to swell with increasing feed concentration in the feed concentration range from 0,05 to 0,5 mol/$\ell^{(42)}$.
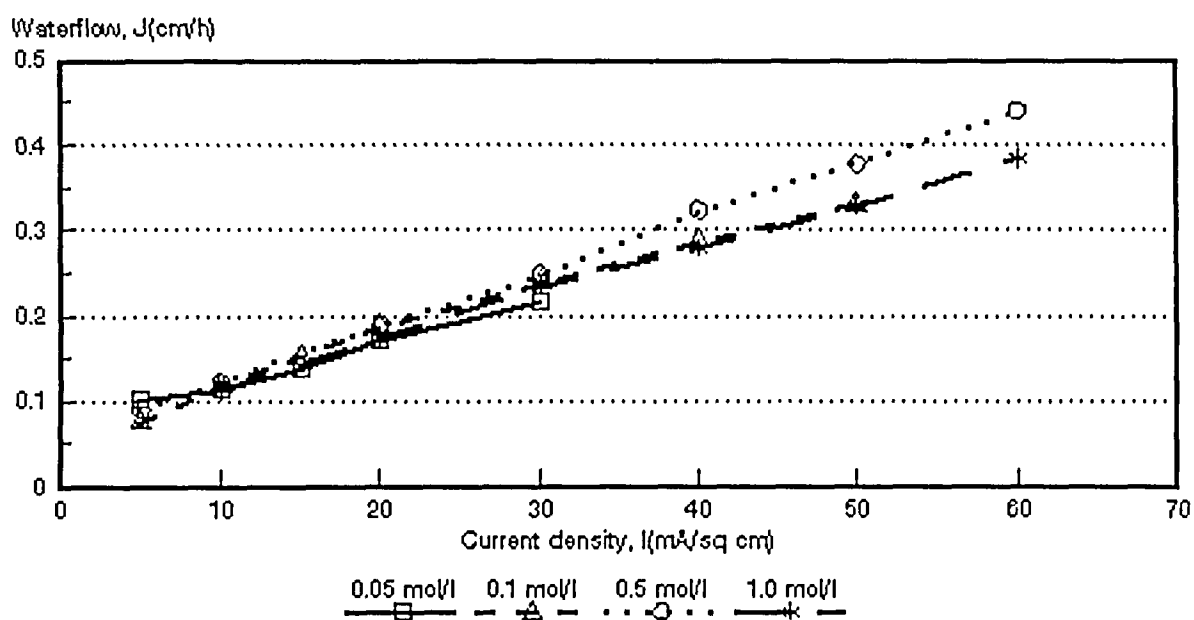
Figure 6.78:   Water flow through the Selemion AMV and CMV membranes as a function of current density and feed water concentration.

Figure 6.79:   Water flow through the Ionac MA-3475 and MC-3470 membranes as a function of current density and feed water concentration.

Figure 6.80: Water flow through the Raipore R4030 and R4010 membranes as a function of current density and feed water concentration.

Figure 6.81: Water flow through the Ionics A-204-UZL-386 and C-61-CZL-386 membranes as a function of current density and feed water concentration.

Figure 6.82: Water flow through the WTPSA-1 and WTPSC-1 membranes as a function of current density and feed water concentration.

Figure 6.83: Water flow through the WTPVCA-2 and WTPVCC-2 membranes as a function of current density and feed water concentration.
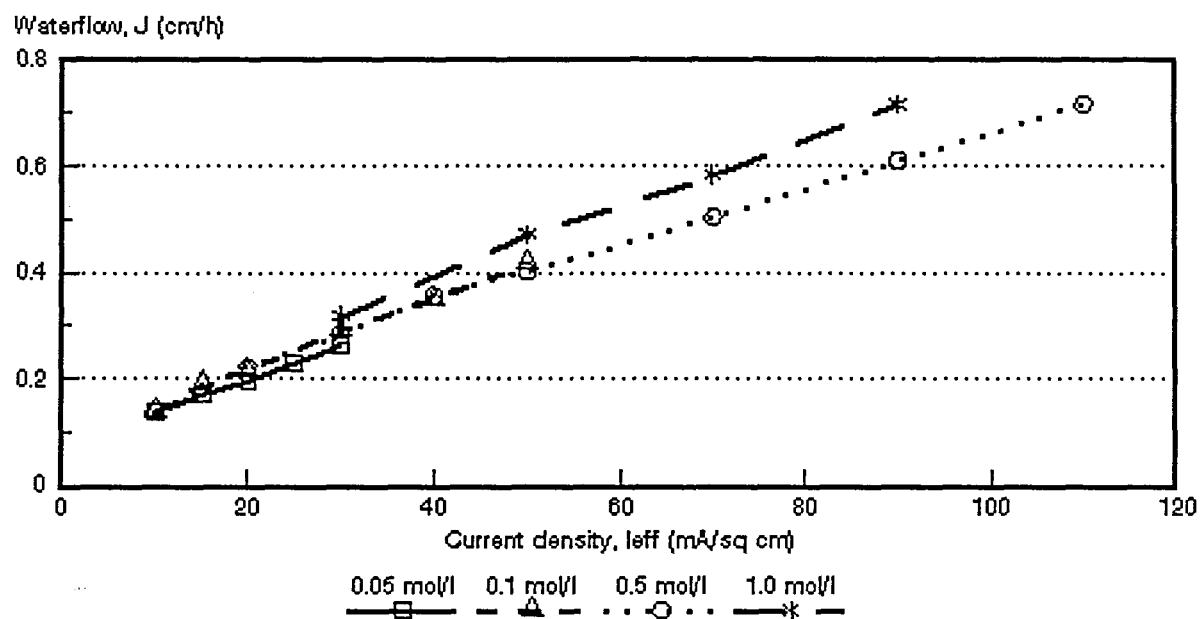
Figure 6.84: Water flow through the WTPSTA-3 and WTPSTC-3 membranes as a function of current density and feed water concentration.

Table 6.35: Water flow (J_i) through the membranes relative to the flow at $J_{0,5\ mol/l}$ or $J_{0,1\ mol/l}$

$J_i/J_{0,5\ mol/l}$

Current Density (mA/cm²)	Selemion AMV & CMV Concentration, mol/l				Ionac MA-3475 & MC-3470 Concentration, mol/l				Raipore R4030 & R4010 Concentration, mol/l				Ionics A-204-UZL & C-61-CZL Concentration, mol/l				WTPS WTPSA & WTPSC Concentration, mol/l				WTPVC WTPVCA & WTPVCC Concentration, mol/l				WTPST WTPSTA & WTPSTC Concentration, mol/l			
mA/cm²	0,05	0,1	0,5	1,0	0,05	0,1	0,5	1,0	0,05	0,1	0,5	1,0	0,05	0,1	0,5	1,0	0,05	0,1	0,5	1,0	0,05	0,1	0,5	1,0	0,05	0,1	0,5	1,0
5	1,14	0,85	1,0		1,17	0,87	1,0		1,18	1,28	1,0		1,0		1,0				1,0		1,11	1,55	1,0				1,0	
10	0,94	0,97	1,0	0,93	1,15	1,03	1,0		1,09	1,18	1,0		1,0	1,1	1,0		1,05	0,96	1,0		1,00	0,95	1,0	1,29	0,99	1,02	1,0	
15			1,0				1,0				1,0				1,0				1,0		0,92	0,95	1,0				1,0	
20	0,89	0,99	1,0	0,92	0,92	0,93	1,0	1,11	0,93	1,05	1,0		0,82	0,90	1,0		0,92	0,92	1,0		0,92	0,97	1,0	1,09	0,83	0,97	1,0	
25			1,0				1,0				1,0				1,0				1,0				1,0				1,0	
30	0,88	0,96	1,0	0,95		0,96	1,0		1,00	1,00	1,0	1,07	0,78	0,86	1,0	1,09		0,94	1,0	1,26	1,00	0,88	1,0		0,94	1,03	1,0	1,12
40		0,89	1,0	0,86		0,93	1,0	1,16		1,01	1,0			0,80	1,0		.	0,91	1,0			0,82	1,0	1,08		0,98	1,0	
50		0,87	1,0	0,87		1,01	1,0			1,05	1,0	1,04			1,0	1,17			1,0	1,21			1,0			1,04	1,0	1,17
60			1,0	0,87			1,0	1,45			1,0				1,0				1,0				1,0	1,12			1,0	
70 (5)*	(1,34)	(1,0)			(1,33)	(1,0)			(0,92)	(1,0)	1,0	1,06	(0,91)	(1,0)	1,0	1,12	(0,95)	(1,0)				1,0				1,0	1,0	1,15
80(10)*	(0,97)	(1,0)			(1,12)	(1,0)			(0,92)	(1,0)			(0,91)	(1,0)			(1,10)	(1,0)			(0,97)	(1,0)			(0,97)	(1,0)	1,0	
90(15)*	(0,90)	(1,0)			(1,11)	(1,0)			(0,89)	(1,0)	1,0	1,05	(0,91)	(1,0)	1,0	1,11	(1,00)	(1,0)			(0,90)	(1,0)			(0,90)	(1,0)	1,0	1,17
100(20)*	(0,90)	(1,0)			(0,98)	(1,0)			(0,89)	(1,0)			(0,91)	(1,0)			(1,00)	(1,0)			(0,91)	(1,0)			(0,91)	(1,0)	1,0	
110(30)*	(0,91)	(1,0)				(1,0)			(0,99)	(1,0)			(0,92)	(1,0)							(0,91)	(1,0)			(0,91)	(1,0)	1,0	

( )* : $J_{0,05} / J_{0,1}$

i = 0,05; 0,1; 0,5 and 1,0 mol/l

Figure 6.85: Water flow through the *Selemion* AMV and CMV membranes as a function of effective current density and feed water concentration.
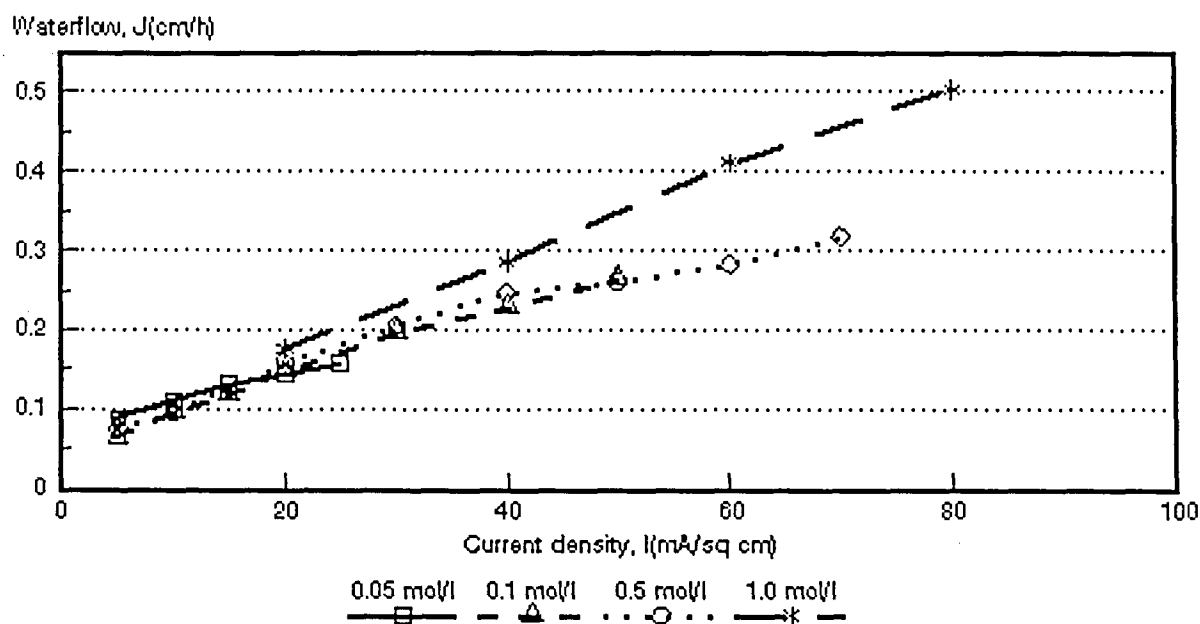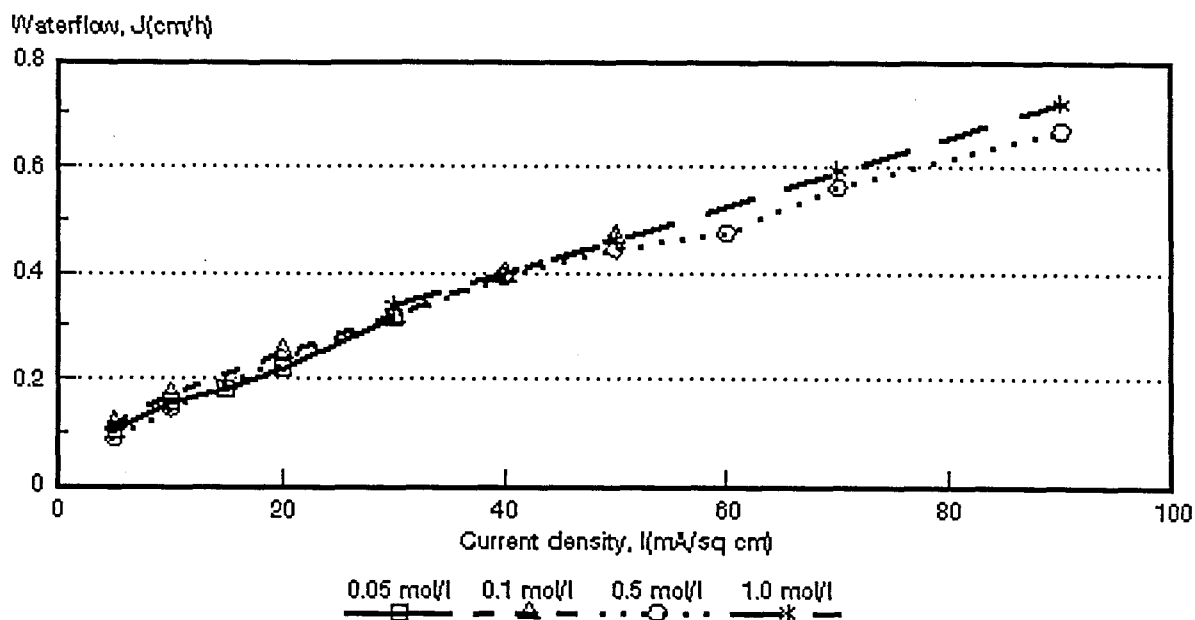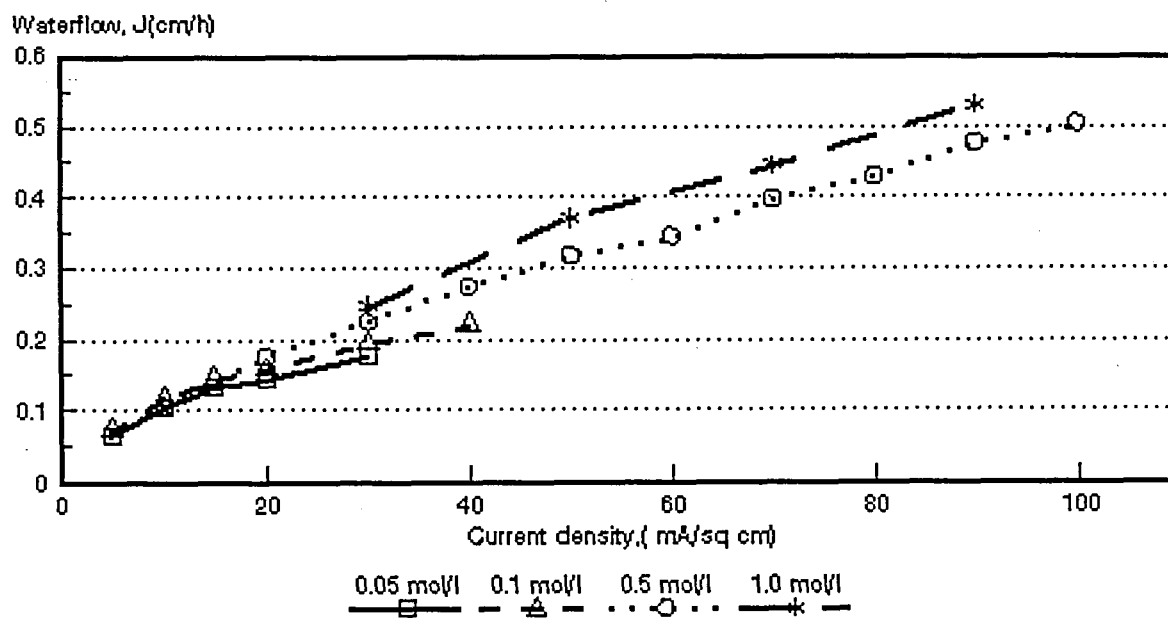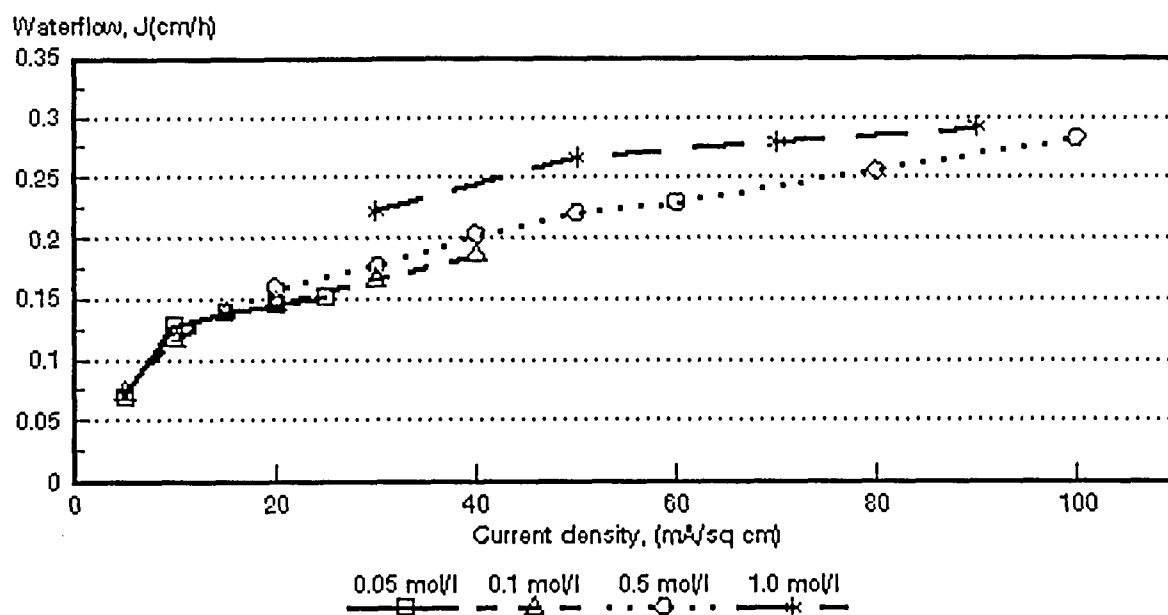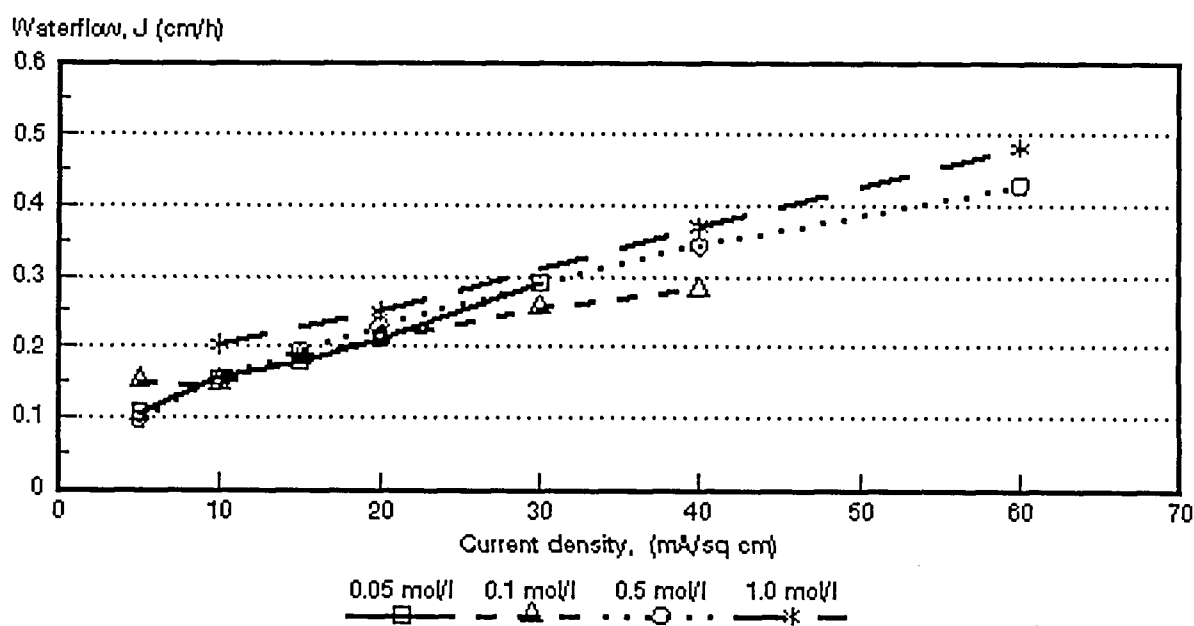

Figure 6.86: Water flow through the *Ionac* MA-3475 and MC-3470 membranes as a function of effective current density and feed water concentration.
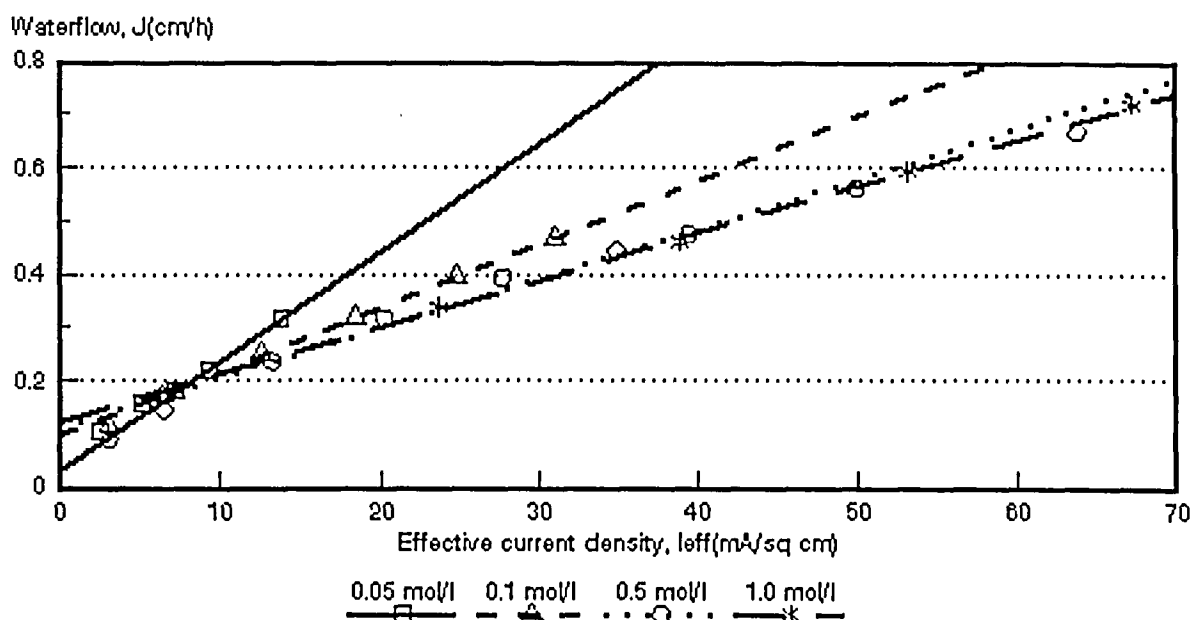
Figure 6.87: Water flow through the *Raipore* R4030 and R4010 membranes as a function of effective current density and feed water concentration.
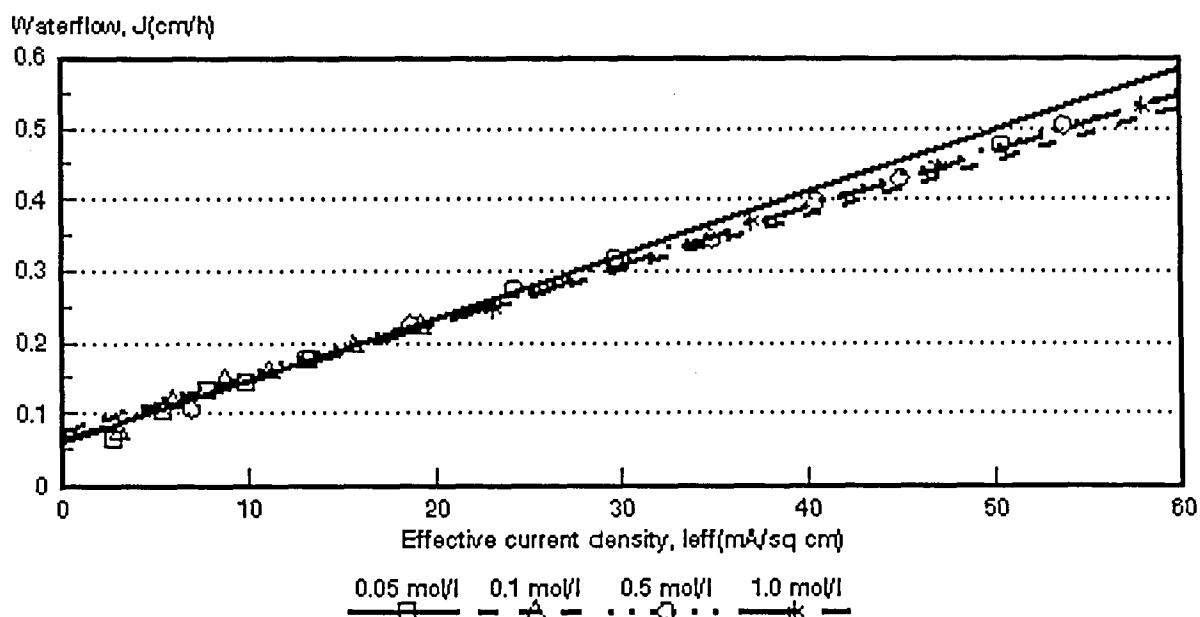
Figure 6.88: Water flow through the *Ionics* A-204-UZL-386 and C-61-CZL-386 membranes as a function of effective current density and feed water concentration.
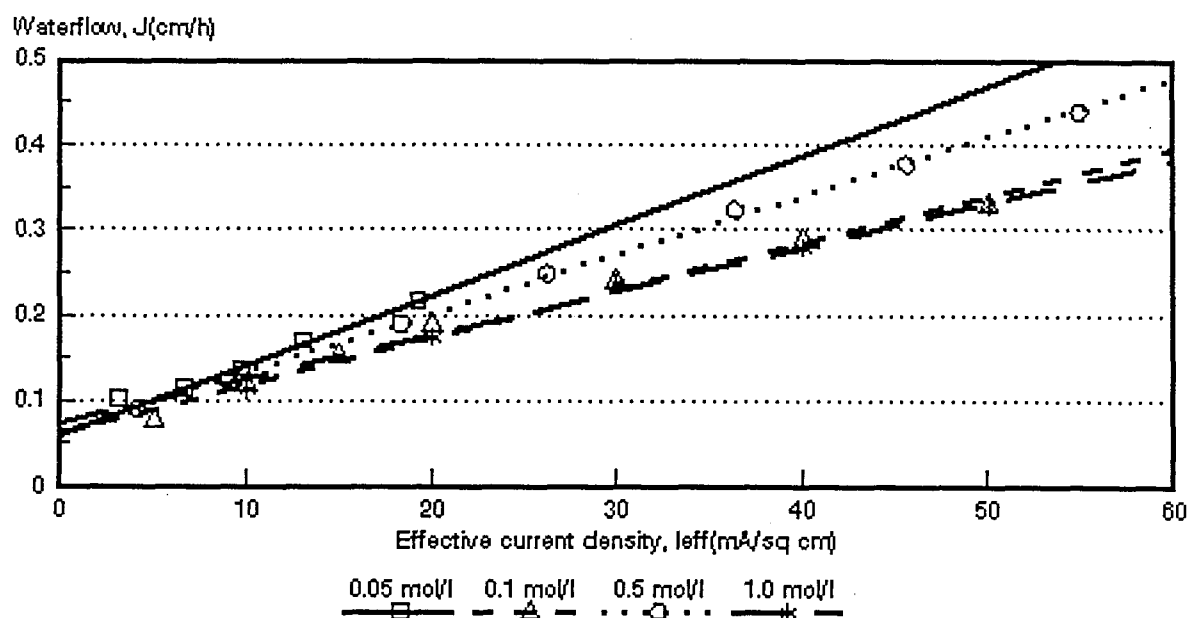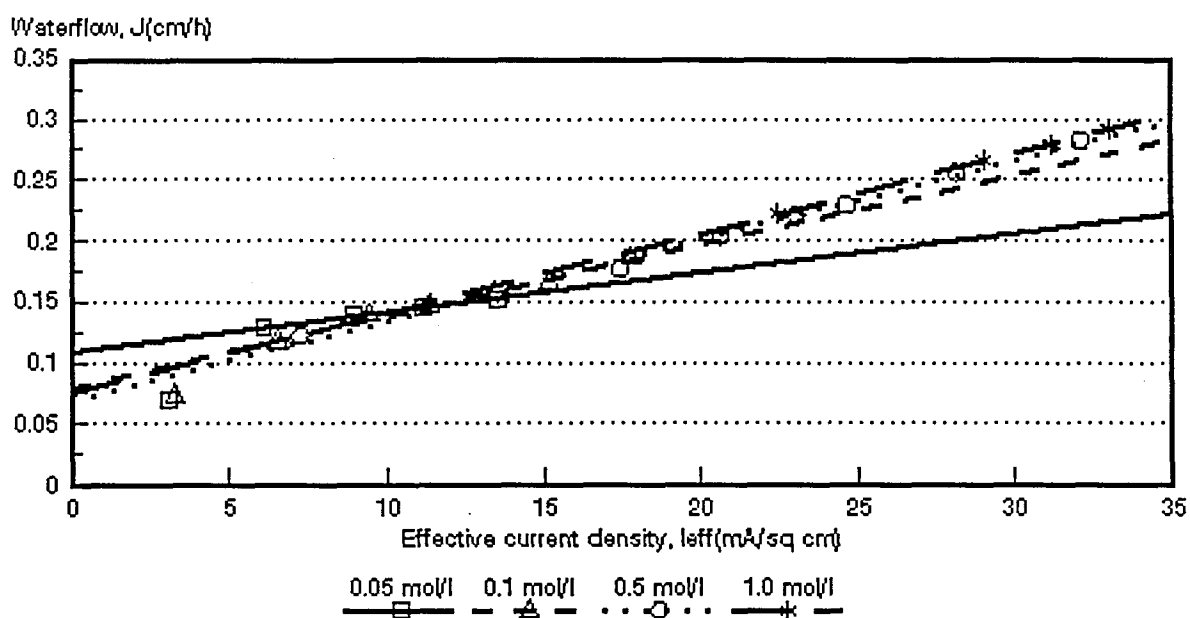
Figure 6.89: Water flow through the WTPSA-1 and WTPSC-1 membranes as a function of effective current density and feed water concentration.
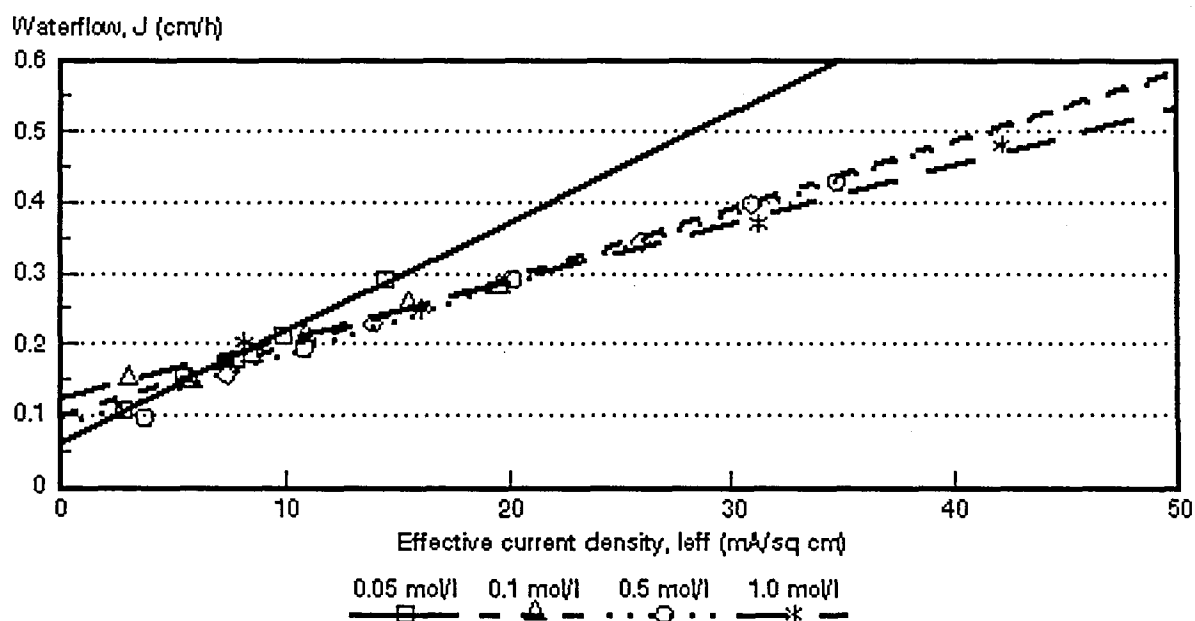
Figure 6.90: Water flow through the WTPVCA-2 and WTPVCC-2 membranes as a function of effective current density and feed water concentration.

Waterflow, J (cm/h)

Effective current density, Ieff (mA/sq cm)

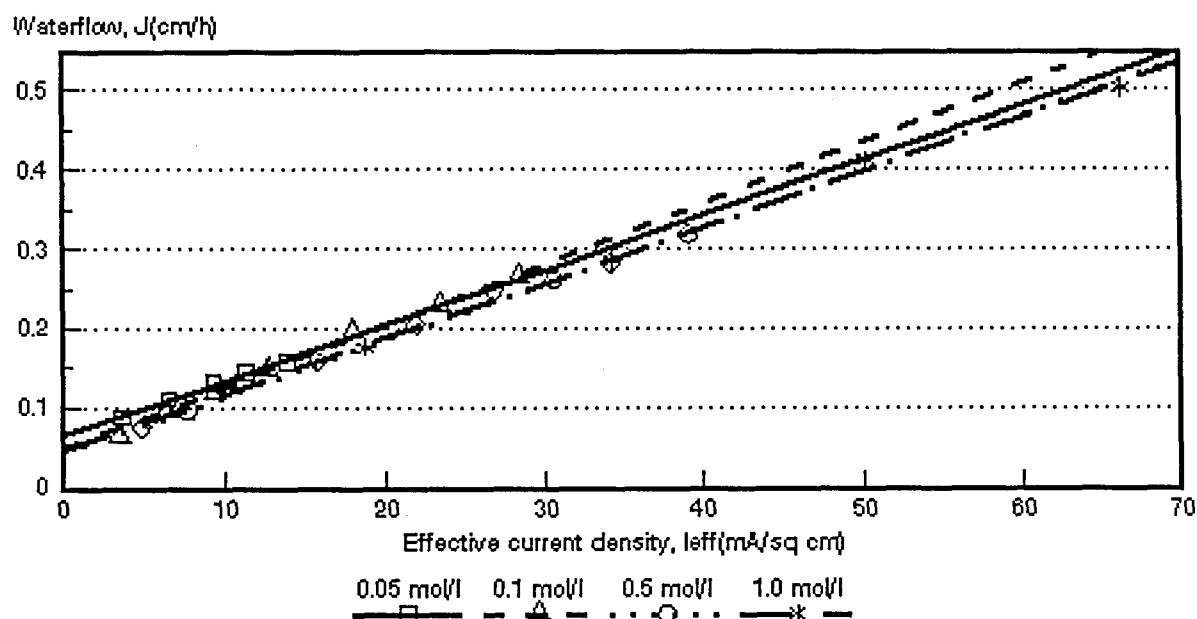0.05 mol/l   0.1 mol/l   0.5 mol/l   1.0 mol/l
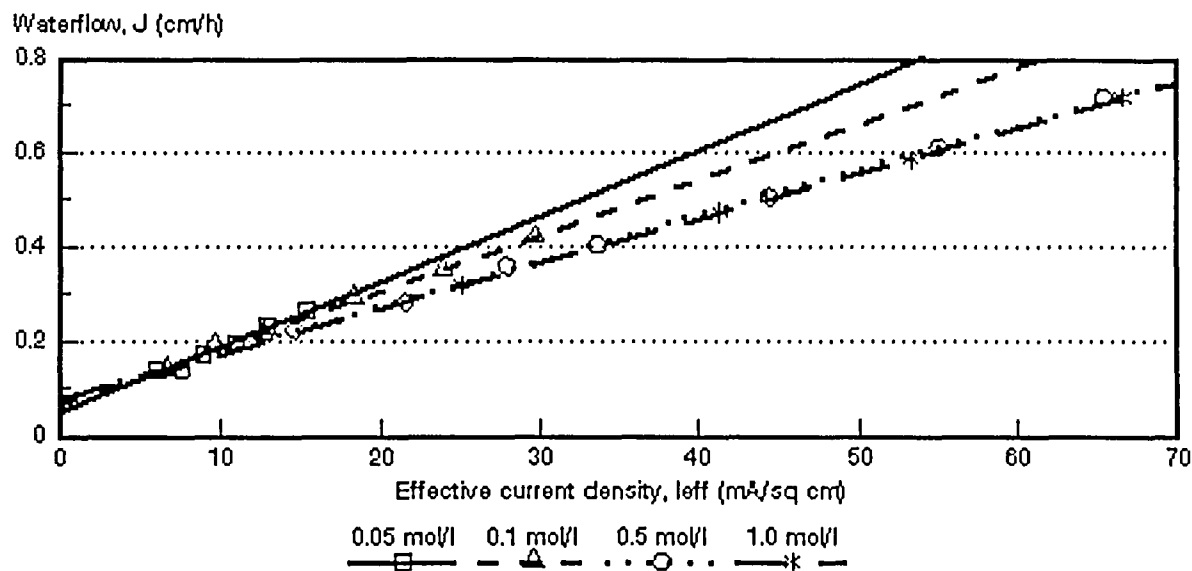
Figure 6.91:   **Water flow through the WTPSTA-3 and WTPSTC-3 membranes as a function of effective current density and feed water concentration.**

Electro-osmotic coefficient (l/Far)

Feed concentration (mol/l)
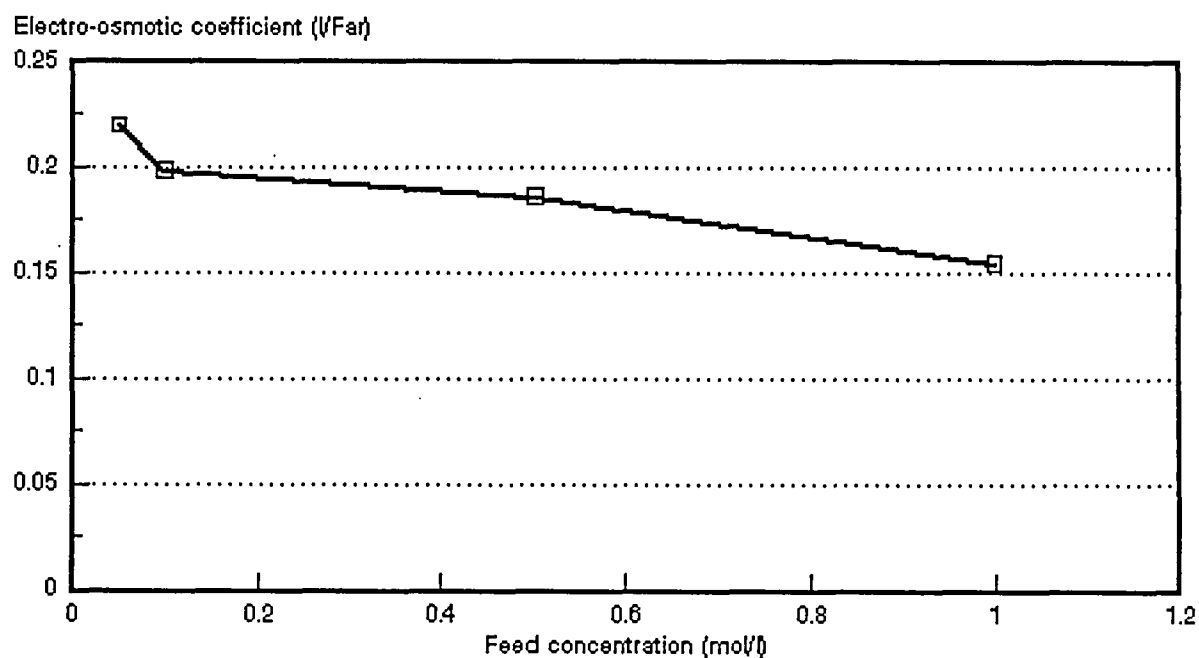
Figure 6.92:   **Electro-osmotic coefficient as a function of NaCl feed concentration. *Selemion* AMV and CMV membranes.**

216

Electro-osmotic coefficient (l/Far)
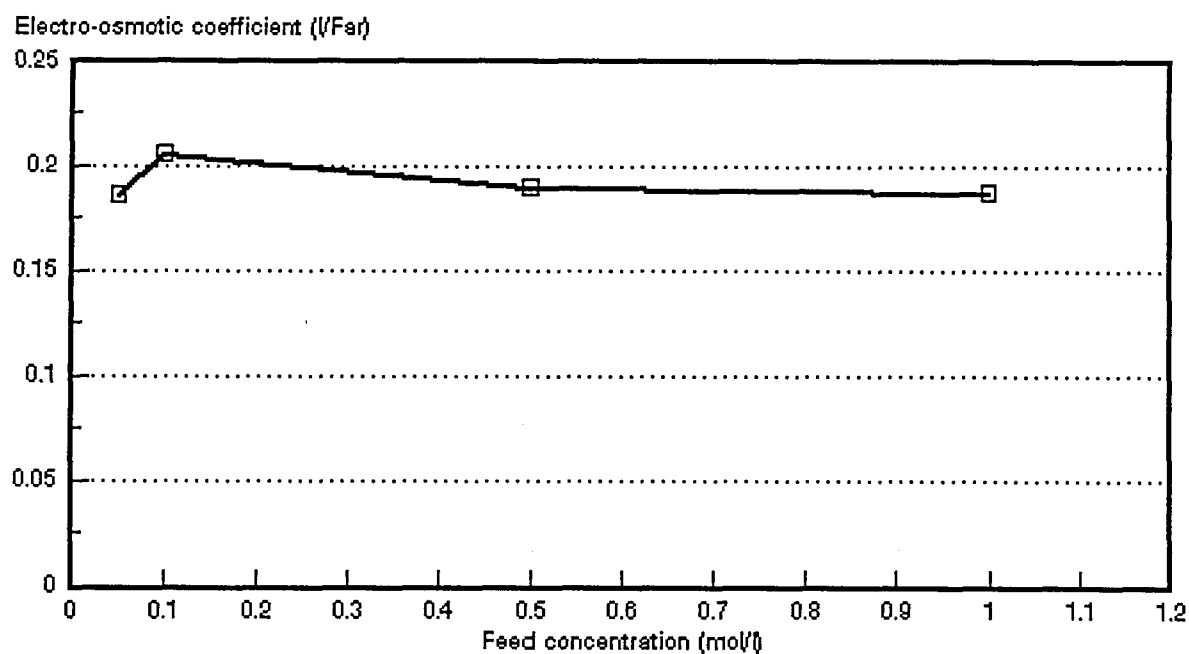
Figure 6.93:   Electro-osmotic coefficient as a function of NaCl feed concentrations.
Ionac MA-3475 and MC-3470 membranes.

Electro-osmotic coefficient (l/Far)
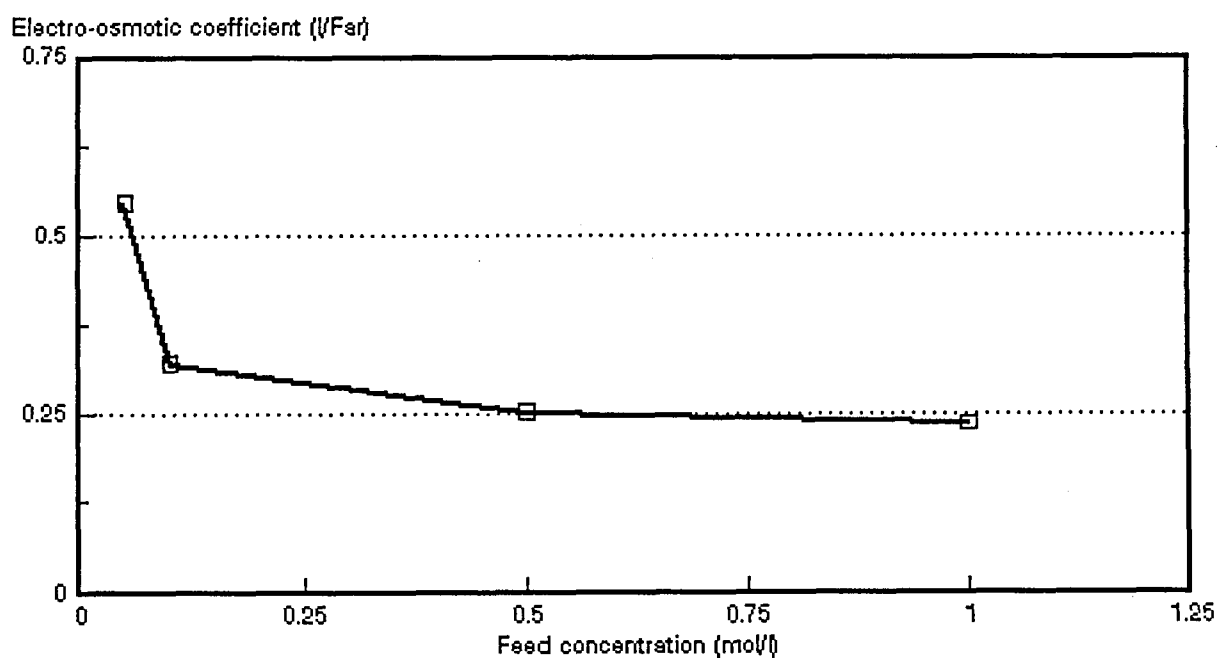
Figure 6.94   Electro-osmotic coefficient as a function of NaCl feed concentrations.
Raipore R4030 and R4010 membranes.

Electro-osmotic coefficient (l/Far)

Feed concentration (mol/l)
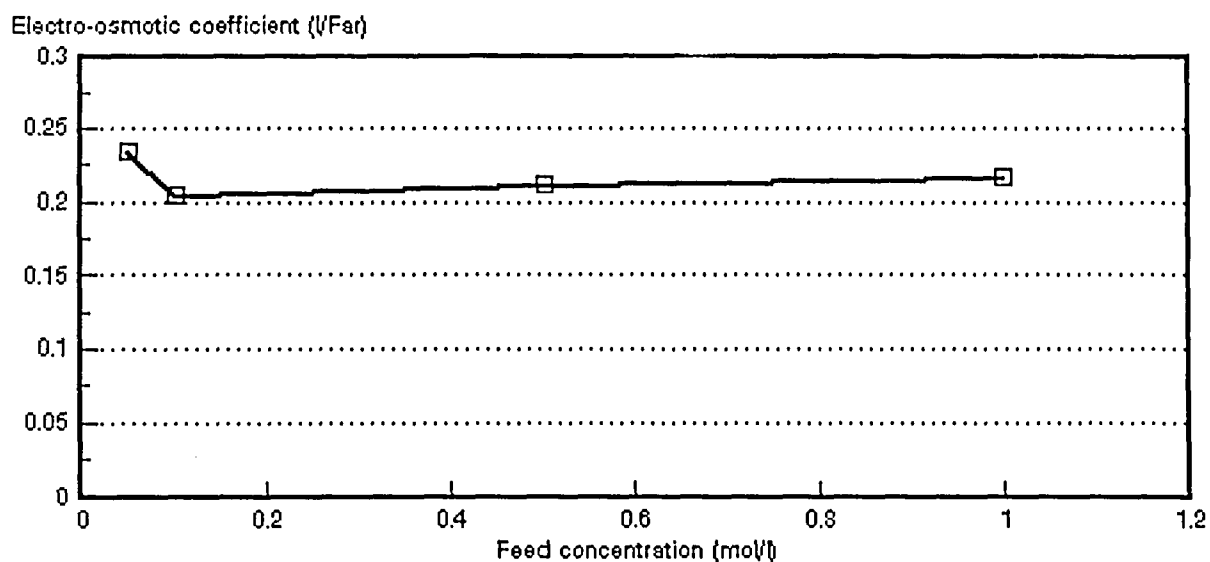
Figure 6.95: Electro-osmotic coefficient as a function of NaCl feed concentrations. *Ionics* A-204-UZL-386 and C-61-CZL-386 membranes.

Electro-osmotic coefficient (l/Far)

Feed concentration (mol/l)
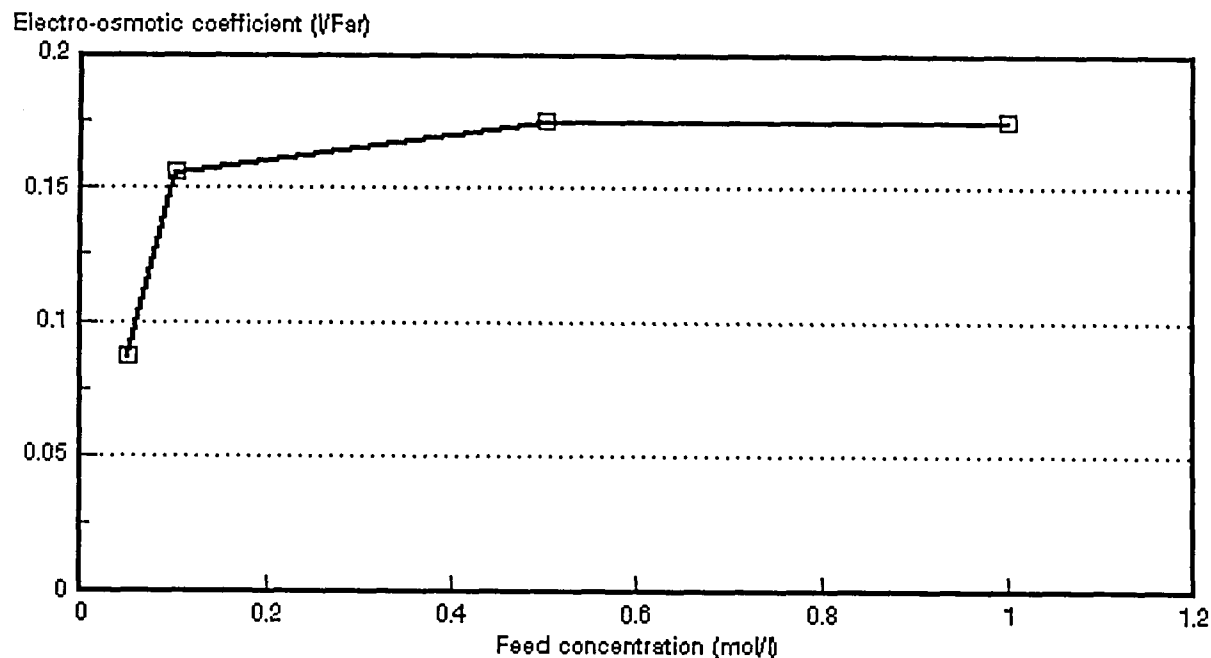
Figure 6.96: Electro-osmotic coefficient as a function of NaCl feed concentrations. WTPSA-1 and WTPSC-1 membranes.
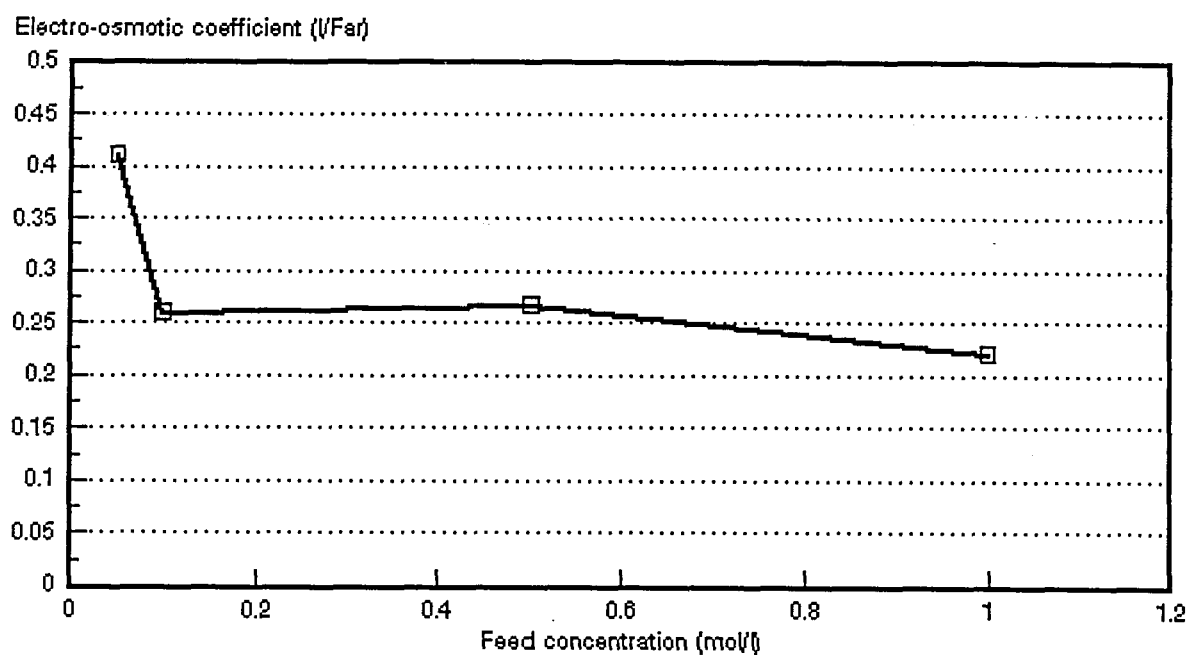
Figure 6.97: Electro-osmotic coefficient as a function of NaCl feed concentrations. WTPVCA-2 and WTPVCC-2 membranes.
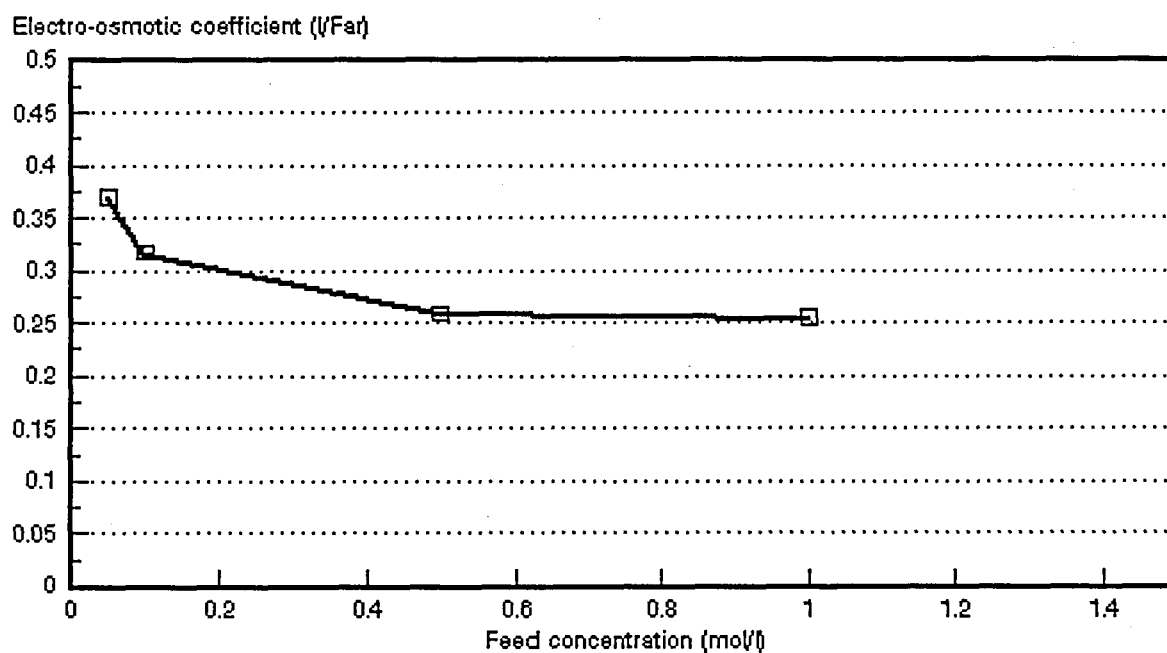
Figure 6.98: Electro-osmotic coefficient as a function of NaCl feed concentrations. WTPSTA-3 AND WTPSTC-3 membranes.

Table 6.36: Effect of the electro-osmotic coefficient (EOC)* on the maximum salt brine concentration, c_b^{max}.

| Membranes	Feed Concentration (mol/ℓ)	EOC ℓ/Faraday	c_b^{max} mol/ℓ	mol H_2O/Faraday
Selemion	0,05	0,219	4,55	12,2
AMV & CMV	0,10	0,198	5,05	11,0
	0,5	0,187	5,36	10,4
	1,0	0,154	6,48	8,6
Ionac	0,05	0,186	5,37	10,3
MA-3475 &	0,10	0,206	4,85	11,4
MC-3470	0,5	0,190	5,26	10,6
	1,0	0,187	5,35	10,4
Raipore	0,05	0,547	1,83	30,4
R4030 &	0,10	0,320	3,13	17,8
R4010	0,50	0,251	3,98	13,9
	1,0	0,236	4,24	13,1
Ionics A-204-UZL &	0,05	0,234	4,27	13,0
C-61-CZL-386	0,10	0,204	4,89	11,3
	0,5	0,211	4,73	11,7
	1,0	0,216	4,63	12,0
WTPS	0,05	0,087	11,5	4,8
WTPSCA-1 &	0,10	0,156	6,41	8,7
WTPSA-1	0,5	0,175	5,71	9,7
	1,0	0,175	5,72	9,7
WTPVC	0,05	0,412	2,43	22,8
WTPVCA-2 &	0,10	0,261	3,84	14,5
WTPVCC-2	0,5	0,267	3,74	14,8
	1,0	0,221	4,54	12,3
WTPST	0,05	0,371	2,69	20,6
WTPSTA-3 &	0,1	0,317	3,15	17,6
WTPSTC-3	0,5	0,259	3,86	14,4
	1,0	0,257	3,90	14,3

*   Data from Tables 6.1 to 6.28.

The effect of the electro-osmotic coefficient on the maximum brine concentration, c_b^{max}, is shown in Table 6.36. Maximum brine concentration increases with decreasing electro-osmotic coefficient. The electro-osmotic coefficients of the *Raipore* membranes were higher than the electro-osmotic coefficients of the other membranes. Consequently, lower brine concentrations were obtained with this membrane type. It is further interesting to note that the electro-osmotic coefficients of the WTPS membranes have been the lowest in the 0,05 to 0,5 mol/ℓ feed concentration range. Therefore, high brine concentrations could be obtained (Table 6.36).

Approximately 10 to 11 mol H_2O/Faraday passed through the *Selemion-*, *Ionac-* and *Ionics* membranes in the 0,1 to 0,5 mol/ℓ feed concentration range (Table 6.36).

Approximately 9 to 10 mol H_2O/Faraday passed through the WTPS membranes in this same feed concentration range. However, more water passed through the other membranes in this feed concentration range.

The osmotic flow (J_{osm}) relative to the total flow (J) through the membranes as a function of current density, is shown in Table 6.37. Osmotic flow decreases with increasing current density. The contribution of osmotic flow at a current density of 30 mA/cm^2 (0,1 mol/ℓ feed) in the case of the *Selemion-, Ionac-, Raipore-, Ionics-*, WTPS-, WTPVC- and WTPST membranes were 28,4%; 25,5%; 30,8%; 38,5%; 48,4%; 38,8% and 23,7% of the total flow through the membranes, respectively. Consequently, osmosis contributes significantly to water flow through the membranes especially at relatively low current density. The osmotic flow contribution to total water flow through the membranes was much less at high current density. Osmotic flow contribution to total flow through the membranes at a current density of 50 mA/cm^2 (0,1 mol/ℓ feed) was 20,5; 19,0; 21,1 and 16,5% for the *Selemion-, Ionac-, Raipore-* and WTPST membranes, respectively. Osmotic flow contribution was only 10,7% of total water flow in the case of the WTPST membranes at a current density of 110 mA/cm^2.

It is interesting to note that the water flow (J) versus the effective current density (I_{eff}) relationship becomes linear long before the maximum brine concentration, c_b^{max}, is reached.

Table 6.37: Osmotic flow* (J_{osm}) relative to the total flow (J) through the membranes as a function of current density.

Membranes	Current Density mA/cm²	J_{osm}/J (%) Feed Concentration (mol/ℓ)			
		0,05	0,1	0,5	1,0
Selemion AMV & CMV	10	52,3	57,4	51,2	69,9
	20	35,4	36,0	32,8	45,4
	30	27,7	28,4		33,5
	40			19,3	28,3
	50		20,5		
	60			14,1	20,6
Ionac MA-3475 & MC-3470	10	59,1	50,5	46,9	
	20	45,2	33,9	28,6	27,6
	30		25,5	22,2	17,0
	40		21,9	18,4	
	50		19,0		11,9
	60			16,1	9,7
	80				
Raipore R4030 & R4010	10	21,9	57,3	76,8	
	20	15,6	39,3	46,9	
	30	11,0	30,8	35,2	37,3
	40		24,8	28,3	
	50		21,1	25,1	27,4
	60		·	23,5	
	70			19,91	21,3
	90			16,2	17,6
Ionics A-204-UZL & C-61-CZL-386	10	37,8	64,2	73,7	
	20	42,1	47,1	44,2	
	30	34,7	38,5	34,5	26,5
	40		33,9	28,34	
	50			24,6	17,7
	60			22,7	
	80			18,2	
	90			16,4	12,3
	100			15,5	
WTPS WTPSA-1 & WTPSC-1	10	85,2	68,8	57,4	
	20	74,9	55,1	44,0	
	30		48,4	39,6	34,3
	40		43,2	34,4	
	50			31,7	28,5
	60			30,5	
	70				27,3
	80			27,3	
	90				26,2
	100			24,7	
WTPVC WTPVCA-2 & WTPVCC-2	10	41,6	67,1	55,6	62,8
	20	30,6	44,8	37,9	50,2
	30	22,2	38,8	29,8	
	40		35,2	25,2	34,0
	60			20,3	26,2
WTPST WTPSTA-3 & WTPSTC-3	10	36,7	49,2	57,7	
	20	25,6	32,1	35,7	
	30	19,0	23,7	27,7	24,1
	40		19,8	22,2	
	50		16,5	19,7	16,3
	70			15,8	
	90			13,0	13,2
	110			11,1	10,7

* Data from Tables 6.1 to 6.28.

6.4   Membrane Permselectivity

Membrane permselectivity ($\overline{\Delta}t$) as a function of brine concentration for various initial feed concentrations, is shown in Figures 6.99 to 6.105. Membrane permselectivity decreased with increasing brine concentration for all the membranes investigated. Permselectivity decreased with increasing feed concentration in the case of the *Selemion-*, *Ionac-*, WTPS-, WTPVC- and WTPST membranes. However, permselectivity was slightly higher at 1,0 mol/ℓ feed concentration than at 0,5 mol/ℓ feed concentration in the case of the Ionac membranes (Fig. 6.100). Permselectivity showed an increase with increasing feed concentration in the case of the *Raipore* membrane (Fig. 6.101).

Figure 6.99:   Membrane permselectivity ($\overline{\Delta}t$) as a function of brine concentration for different NaCl feed concentrations. *Selemion* AMV and CMV membranes.

Figure 6.100: Membrane permselectivity ($\bar{\Delta}t$) as a function of brine concentration for different NaCl feed concentrations. *Ionac* MA-3475 and MC-3470 membranes.
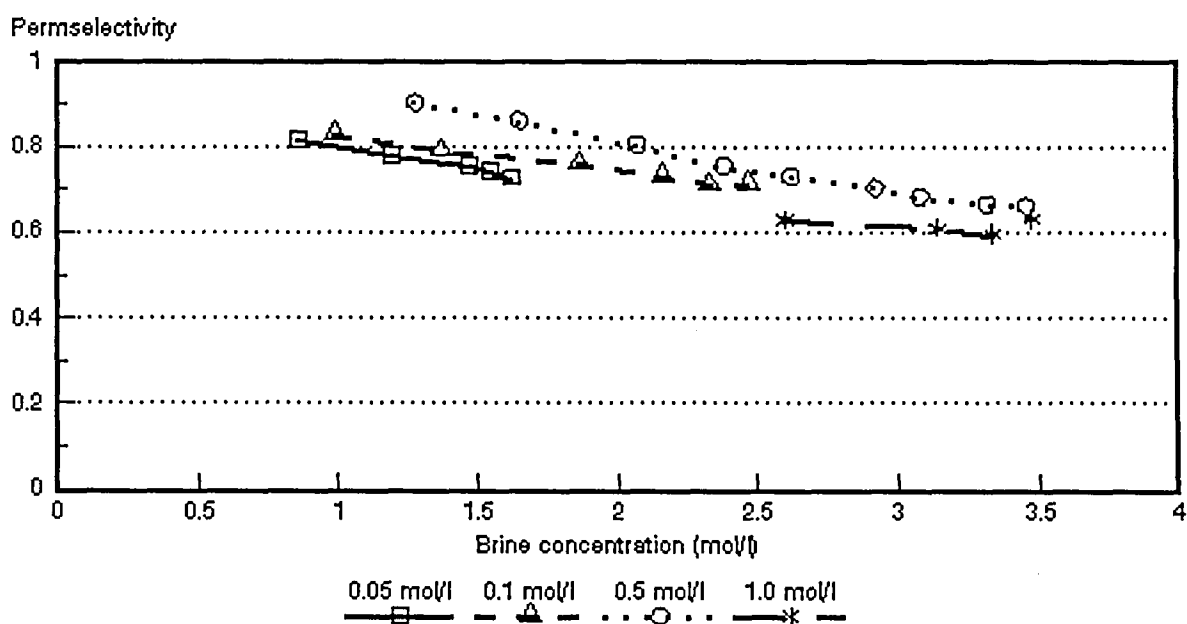
Figure 6.101: Membrane permselectivity ($\bar{\Delta}t$) as a function of brine concentration for different NaCl feed concentrations. *Raipore* R4030 and R4010 membranes.
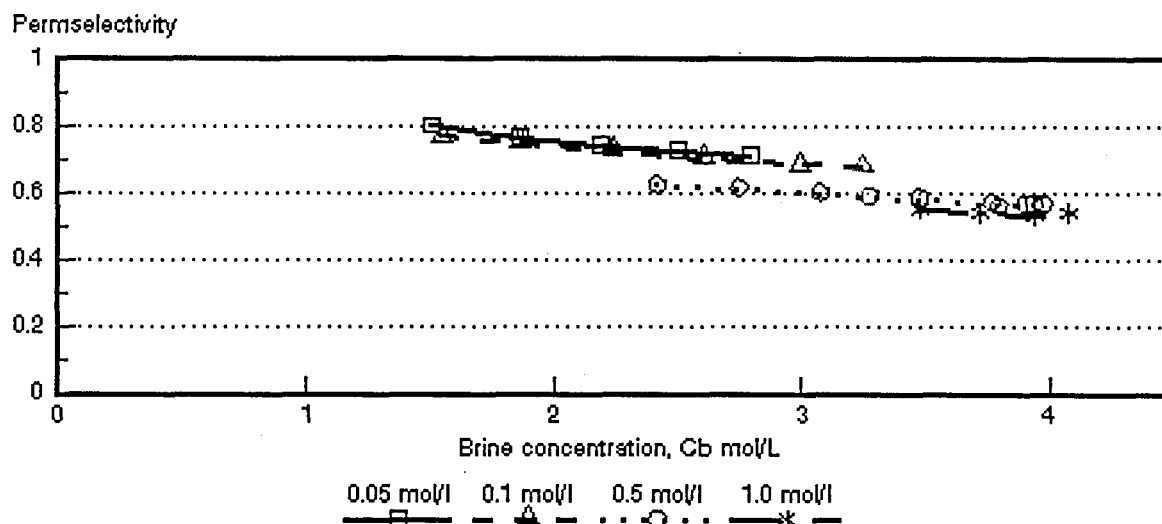
Permselectivity

Figure 6.102: Membrane permselectivity ($\overline{\Delta t}$) as a function of brine concentration for different NaCl feed concentrations. *Ionics* A-204-UZL-386 and C-61-CZL-386 membranes.
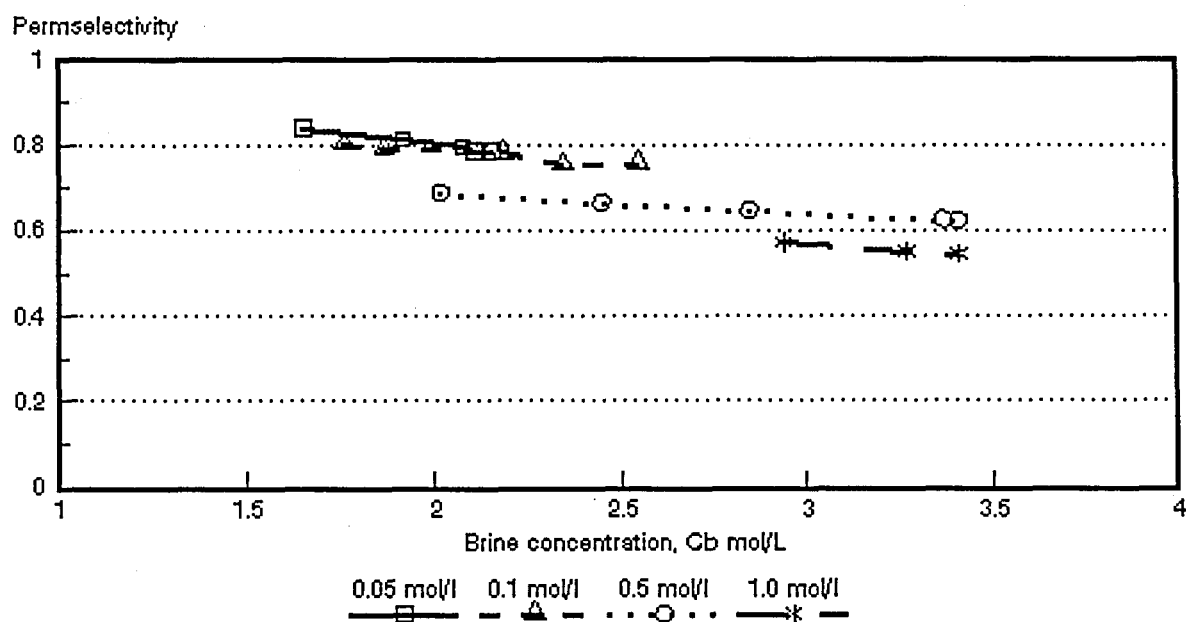
Permselectivity

Figure 6.103: Membrane permselectivity ($\overline{\Delta t}$) as a function of brine concentration for different NaCl feed concentrations. WTPSA-1 and WTPSC-1 membranes.
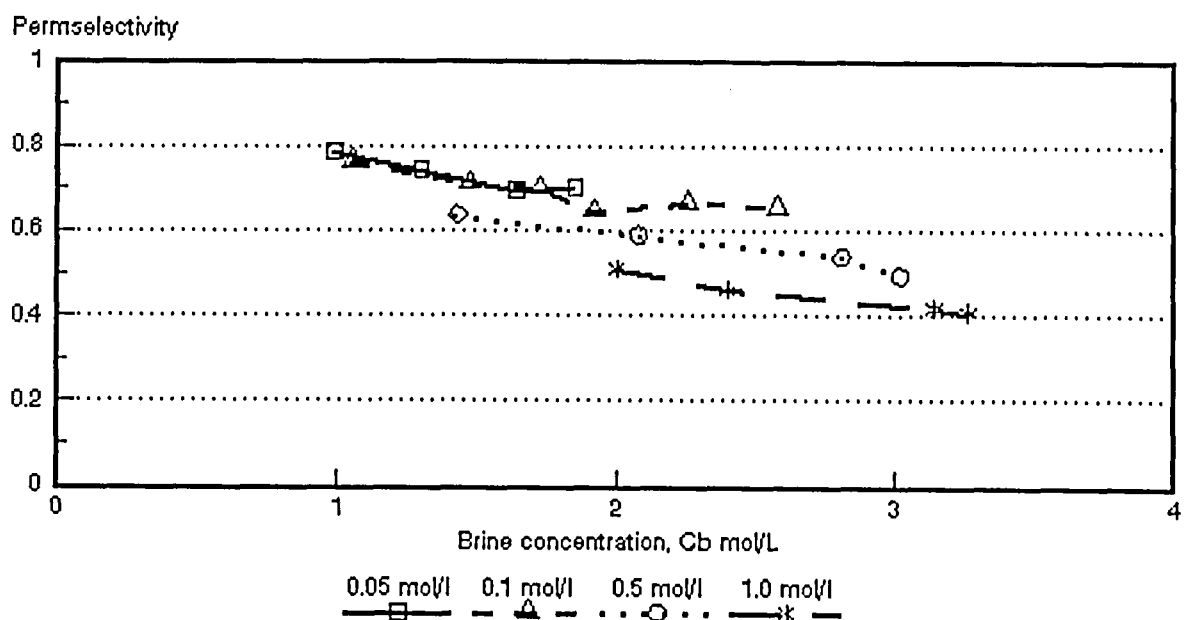
Figure 6.104: Membrane permselectivity ($\overline{\Delta}t$) as a function of brine concentration for different NaCl feed concentrations. WTPVCA-2 and WTPVCC-2 membranes.
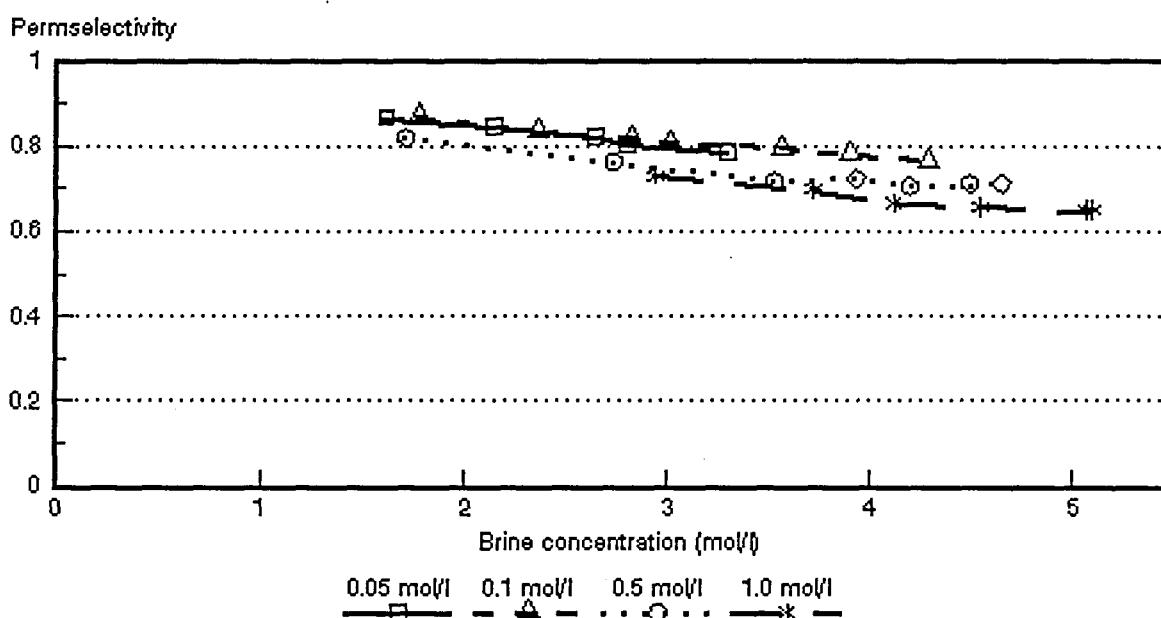

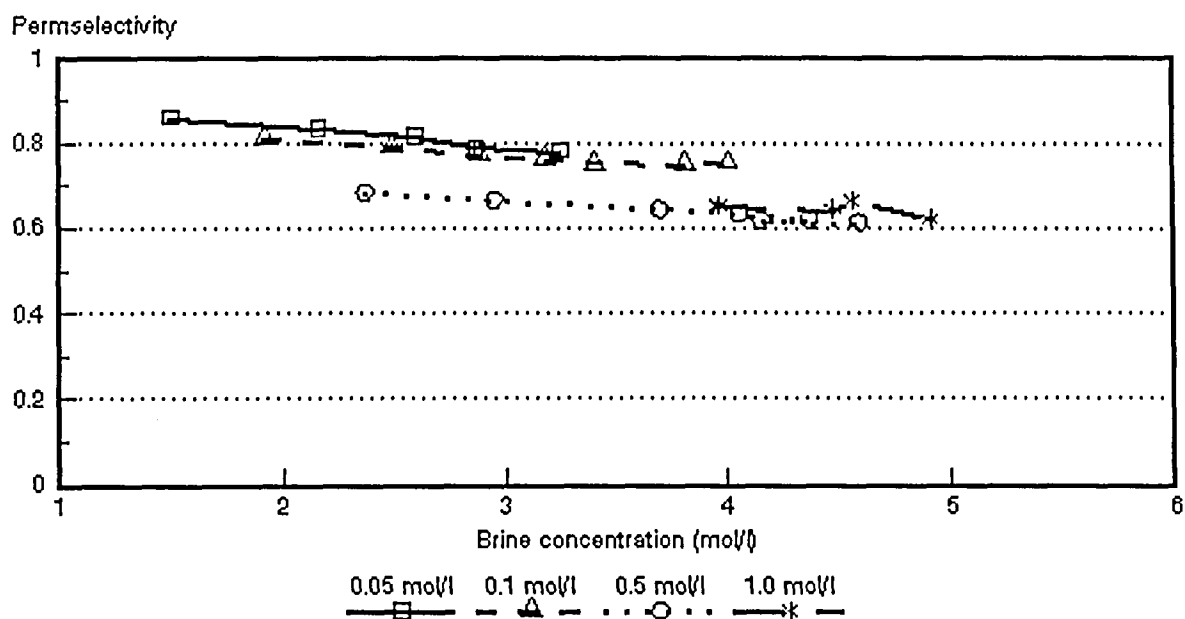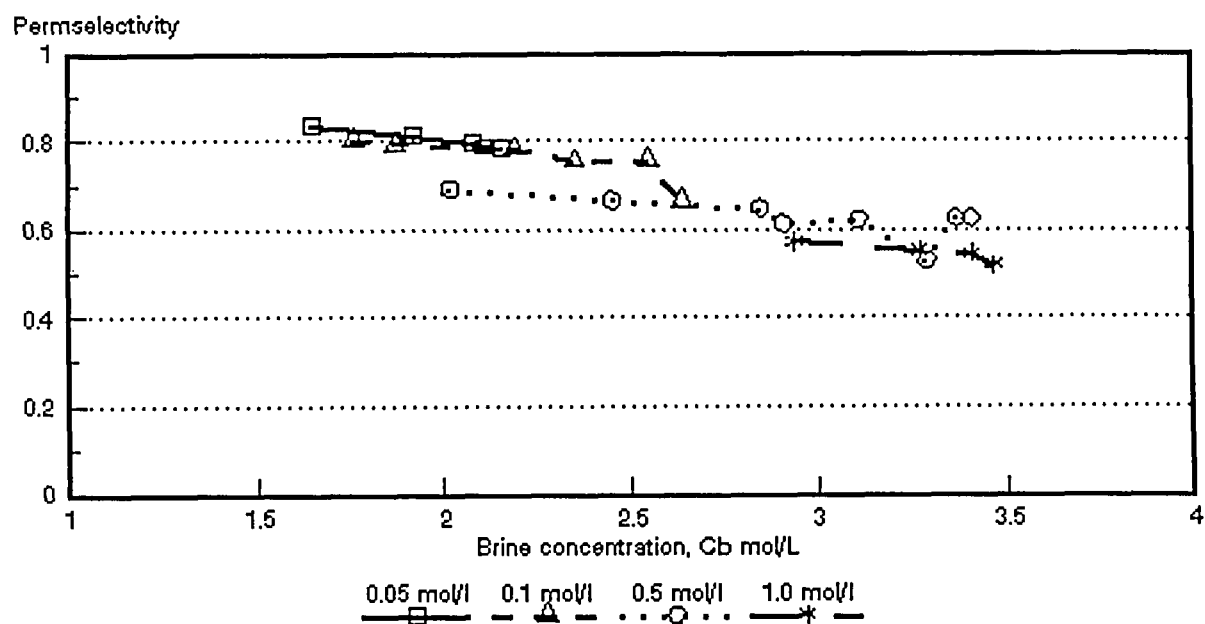**Figure 6.105:** Membrane permselectivity ($\overline{\Delta}t$) as a function of brine concentration for different NaCl feed concentrations. WTPSTA-3 and WTPSTC-3 membranes.

6.5 Membrane Characteristics

6.5.1 Membrane resistance

Membrane resistances are summarized in Table 6.38.

Table 6.38: Membrane resistances of the membranes used for EOP of sodium chloride solutions

Membrane	Resistance - ohm·cm²	
	0,1 mol/ℓ NaCl	0,5 mol/ℓ NaCl
Selemion AMV	4,7	1,5
Selemion CMV	3,8	1,0
Ionac MA-3475	36,6	19,4
Ionac MC-3470	42,0	24,3
Raipore R4030	3,1	1,0
Raipore R4010	1,3	-
Ionics A-204-UZL-386	13,4	12,3
Ionics C-61-CZL-386	14,2	15,2
WTPSA-1	97,9	60,3
WTPSC-1	12,8	8,6
WTPVCA-2	21,1	11,1
WTPVCC-2	24,9	14,9
WTPSTA-3	83,3	49,3
WTPSTC-3	24,9	14,3

6.5.2 Gel water contents and ion-exchange capacities of the membranes used for EOP of sodium chloride solutions

The gel water contents and the ion-exchange capacities are summarized in Table 6.39.

Table 6.39: Gel water contents and Ion-exchange capacities of the membranes used for the EOP of sodium chloride solutions.

Membrane	Gel Water Content (%)	Ion-exchange capacity me/dry g
Selemion AMV	18,4	1,26
Selemion CMV	22,7	2,4
Ionac MA-3475	17,8	1,06
Ionac MC-3470	18,5	1,82
Ionics A-204-UZL-386	22,9	1,49
Ionics C-61-CZL-386	23,7	1,51
WTPSA-1	26,4	0,54
WTPSC-1	43,4	1,75
WTPVCA-2	15,9	1,15
WTPVCC-2	29,8	0,76
WTPSTA-3	35,57	1,13
WTPSTC-3	31,44	0,61

6.5.3 Permselectivities of the membranes used for the EOP of sodium chloride solutions

The permselectivities of the membranes at different salt gradients are summarized in Table 6.40.

Table 6.40: Membrane perselectivities of the membranes used for EOP of sodium chloride solutions at different salt gradients

Membrane	Δt(1)*	Δt(2)**	Δt(3)***
Selemion AMV	0,86	0,75	0,71
Selemion CMV	1,00	0,99	0,88
Ionac MA-3475	0,83	0,66	0,64
Ionac MC-3470	1,00	0,91	0,78
Raipore R4030	0,85	0,72	0,66
Raipore R4010	0,96	0,85	0,63
Ionics A-204-UZL-386	0,92	0,75	0,67
Ionics C-61-CZL-386	0,94	0,82	0,70
WTPSA-1	0,92	0,75	0,68
WTPSC-1	0,90	0,77	0,58
WTPVCA-2	0,86	0,65	0,50
WTPVCC-2	0,90	0,71	0,54
WTPSTA-3	0,91	0,73	0,65
WTPSTC-3	0,89	0,72	0,69

(1)* : 0,1/0,2 mol/ℓ   (2)** : 0,5/1,0 mol/ℓ
(3)*** : 0,1/4,0 mol/ℓ NaCl

7. ELECTRO-OSMOTIC PUMPING OF HYDROCHLORIC ACID SOLUTIONS WITH DIFFERENT ION-EXCHANGE MEMBRANES

Acid brine concentrations, water flows and current efficiencies were determined at different current densities for different hydrochloric acid feed water concentrations. Membrane permselectivities (apparent transport numbers) were measured at concentration differences similar to those obtained during EOP experiments. The results are summarized in Tables 7.1 to 7.17.

7.1 Brine Concentration

Acid brine concentration (c_b) as a function of current density is shown in Figures 7.1 to 7.5. Acid concentration increases more rapidly in the beginning as has been experienced with the salt solutions and then starts to level off. The levelling off in acid concentration is more pronounced at the lower acid feed concentrations (0,05 mol/ℓ, Figs. 7,3 and 7,5). The acid concentration curves were steeper than the curves obtained during sodium chloride concentration. Higher current densities could be obtained easier with the acid feed solutions.

Acid brine concentration increases with increasing current density and increasing acid feed water concentration as has been the case with sodium chloride solutions. The highest acid concentrations were obtained with the *Selemion* AAV and CHV membranes followed by the ABM-3 and CHV and ABM-2 and CHV membranes (Table 7.18). Acid brine concentrations of 25,0; 22,6 and 22,9% could be obtained from 0,5 mol/ℓ feed solutions with *Selemion* AAV and CHV, ABM-3 and CHV and ABM-2 and CHV membranes, respectively. The ABM-1 and CHV membranes did not perform as well as the other membranes for acid concentration while very low acid brine concentrations were obtained with the *Selemion* AMV and CMV membranes. The reason for the low acid concentrations obtained with the *Selemion* AMV and CMV membranes compared to the other anion membranes could be ascribed to the very low permselectivity of the *Selemion* AMV membrane for chloride ions (Tables 7.1 to 7.17). The permselectivity (Δt^a) of the *Selemion* AMV membrane was only 0,2 at 0,1 mol/ℓ hydrochloric acid feed (20 mA/cm^2) compared to 0,64 for the *Selemion* AAV; 0,62 for the ABM-3; approximately 0,5 for the ABM-2 and 0,57 for the ABM-1 membranes (Tables 7.1; 7.5; 7.9; 7.13; 7.16). The concentration gradients across the *Selemion* AAV, ABM-3, ABM-2 and ABM-1 membranes were also much higher than the concentration gradient across the *Selemion* AMV membrane during determination

Table 7.1 : Electro-osmotic pumping experimental conditions and results for 0,1 mol/l hydrochloric acid (Selemion AMV and CMV)

Current Density	Brine concentration c_b, mol/l		Water flow	Current Efficiency	Effective Current Density	Transport Numbers				
I, mA/cm²	$c_{b\ exp}$	$c_{b\ calc}$	J, cm/h	e_p, %	I_{eff}, mA/cm²	Δt^a	Δt^c	$\bar{\Delta t}$	$\bar{t_1^c}$	$\bar{t_2^a}$
10	0,88	4,36	0,0555	13,15	1,32	1,00	0,30	0,65	1,00	0,65
20	1,17	4,67	0,093	14,57	2,91	0,96	0,20	0,58	0,98	0,60
30	1,45	5,14	0,121	15,63	4,69	0,97	0,13	0,55	0,99	0,57
40	1,62	5,49	0,140	15,20	6,08	0,95	0,08	0,52	0,98	0,54
50	1,78	5,43	0,170	16,21	8,11	0,95	0,04	0,50	0,97	0,52
60	1,95	5,58	0,189	16,46	9,88	0,92	0,02	0,47	0,96	0,51

Electro-osmotic coefficient (2β) = 0,357 l/F (slope = 0,013304 ml/mAh)
J_{osm} = y-intercept = 0,059376 cm/h
c_b^{max} = 2,80 mol/l
$\Delta t^c = t_1^c - t_2^c$

$\Delta t^a = t_2^a - t_1^a$
$\bar{\Delta t}$ = Average transport number of membrane pair
$\bar{t_1^c}$ = Transport number of cation through cation membrane
$\bar{t_2^a}$ = Transport number of anion through anion membrane.

Table 7.2: Electro-osmotic pumping experimental conditions and results for 0,54 mol/l hydrochloric acid (Selemion AMV and CMV)

Current Density	Brine concentration c_b, mol/l		Water flow	Current Efficiency	Effective Current Density	Transport Numbers				
I, mA/cm²	$c_{b\ exp}$	$c_{b\ calc}$	J, cm/h	e_p, %	I_{eff}, mA/cm²	Δt^a	Δt^c	$\bar{\Delta t}$	$\bar{t_1^c}$	$\bar{t_2^a}$
10	1,07	4,42	0,047	13,40	1,34	0,96	0,15	0,56	0,98	0,58
20	1,37	4,99	0,074	13,60	2,72	0,95	0,04	0,50	0,97	0,52
30	1,58	5,17	0,103	15,58	4,37	0,92	0,02	0,47	0,96	0,51
40	1,75	5,33	0,126	14,73	5,89	0,90	0,02	0,46	0,95	0,51
50	1,91	5,96	0,155	15,85	7,93	0,90	0,06	0,48	0,95	0,53
60	2,05	6,16	0,176	16,10	9,66	0,90	0,08	0,49	0,95	0,54

Electro-osmotic coefficient (2β) = 0,371 l/F (slope = 0,0138374 ml/mAh)
J_{osm} = y-intercept = 0,0436566 cm/h
c_b^{max} = 2,70 mol/l
$\Delta t^c = t_1^c - t_2^c$

$\Delta t^a = t_2^a - t_1^a$
$\bar{\Delta t}$ = Average transport number of membrane pair
$\bar{t_1^c}$ = Transport number of cation through cation membrane
$\bar{t_2^a}$ = Transport number of anion through anion membrane.

Table 7.3: Electro-osmotic pumping experimental conditions and results for 1,0 mol/l hydrochloric acid (Selemion AMV and CMV)

Current Density	Brine concentration c_b, mol/l		Water flow	Current Efficiency	Effective Current Density	Transport Numbers				
I, mA/cm²	$c_{b\ exp}$	$c_{b\ calc}$	J, cm/h	e_p, %	I_{eff}, mA/cm²	Δt^a	Δt^c	$\bar{\Delta t}$	$\bar{t_1^c}$	$\bar{t_2^a}$
10	1,36	5,39	0,0336	12,40	1,24	0,88	0,09	0,49	0,94	0,55
20	1,62	5,63	0,0608	13,17	2,63	0,81	0,11	0,46	0,91	0,55
30	1,79	5,51	0,0940	15,03	4,51	0,82	0,11	0,46	0,91	0,55
40	1,97	7,03	0,1095	14,45	5,78	0,87	0,17	0,52	0,93	0,58
50	2,15	6,82	0,1280	14,69	7,35	0,81	0,13	0,47	0,90	0,57
60	2,29	7,65	0,1480	15,20	9,12	0,82	0,19	0,51	0,91	0,60
70	2,42	8,04	0,1630	15,10	10,57	0,82	0,18	0,50	0,91	0,59

Electro-osmotic coefficient (2β) = 0,306 l/F (slope = 0,011409 ml/mAh)
J_{osm} = y-intercept = 0,043319 cm/h
c_b^{max} = 3,27 mol/l
$\Delta t^c = t_1^c - t_2^c$

$\Delta t^a = t_2^a - t_1^a$
$\bar{\Delta t}$ = Average transport number of membrane pair
$\bar{t_1^c}$ = Transport number of cation through cation membrane
$\bar{t_2^a}$ = Transport number of anion through anion membrane.

Table 7.4: Electro-osmotic pumping experimental conditions and results for 0,05 mol/ℓ hydrochloric acid (Selemion AAV and CHV)

Current Density	Brine concentration c_b, mol/l		Water flow	Current Efficiency	Effective Current Density	Transport Numbers				
I, mA/cm²	$c_{b\ exp.}$	$c_{b\ calc.}$	J, cm/h	e_p, %	I_{eff}, mA/cm²	Δt^c	Δt^a	$\bar{\Delta}t$	$\bar{t}_1^c$	$\bar{t}_2^a$
10	2,59	4,88	0,062	42,91	4,29	0,95	0,67	0,81	0,98	0,83
20	3,25	6,13	0,093	40,38	8,08	0,91	0,61	0,76	0,96	0,81
30	3,69	6,83	0,123	40,66	12,20	0,91	0,59	0,75	0,95	0,80
40	4,12	7,66	0,141	39,01	15,60	0,90	0,55	0,72	0,95	0,77
50	4,45	8,27	0,160	38,16	19,08	0,89	0,53	0,71	0,94	0,76
60	4,70	9,64	0,178	37,41	22,45	0,88	0,49	0,69	0,94	0,75
70	5,01	9,04	0,196	37,52	26,26	0,87	0,49	0,68	0,93	0,74

Electro-osmotic coefficient (2β) = 0,140 ℓ/F (slope = 0,00523 mℓ/mAh)
J_{osm} = y-intercept = 0,059609 cm/h
c_b^{max} = 7,14 mol/l
$\Delta t^c = t_1^c - t_2^c$

$\Delta t^a = t_2^a - t_1^a$
$\bar{\Delta}t$ = Average transport number of membrane pair
$\bar{t}_1^c$ = Transport number of cation through cation membrane
$\bar{t}_2^a$ = Transport number of anion through anion membrane.

Table 7.5 : Electro-osmotic pumping experimental conditions and results for 0,1 mol/ℓ hydrochloric acid (Selemion AAV and CHV)

Current Density	Brine concentration c_b, mol/l		Water flow	Current Efficiency	Effective Current Density	Transport Numbers				
I, mA/cm²	$c_{b\ exp.}$	$c_{b\ calc.}$	J, cm/h	e_p, %	I_{eff}, mA/cm²	Δt^c	Δt^a	$\bar{\Delta}t$	$\bar{t}_1^c$	$\bar{t}_2^a$
10	2,68	5,12	0,060	43,4	4,34	0,94	0,71	0,83	0,97	0,85
20	3,36	6,76	0,086	38,88	7,78	0,91	0,64	0,78	0,96	0,82
30	3,84	7,17	0,117	40,05	12,02	0,90	0,59	0,75	0,95	0,80
40	4,41	7,86	0,140	41,36	16,54	0,89	0,59	0,74	0,94	0,79
50	4,63	8,47	0,157	38,95	19,48	0,88	0,54	0,71	0,94	0,77
60	4,87	8,67	0,180	39,05	23,43	0,88	0,51	0,70	0,94	0,76
70	5,12	8,64	0,211	41,29	28,90	0,88	0,51	0,70	0,94	0,76
80	5,33	9,03	0,225	40,18	32,14	0,87	0,51	0,69	0,94	0,76
100	5,73	9,62	0,264	40,48	40,48	0,88	0,48	0,68	0,94	0,74

Electro-osmotic coefficient (2β) = 0,141 ℓ/F (slope = 0,005249 mℓ/mAh)
J_{osm} = y-intercept = 0,055129 cm/h
c_b^{max} = 7,09 mol/l
$\Delta t^c = t_1^c - t_2^c$

$\Delta t^a = t_2^a - t_1^a$
$\bar{\Delta}t$ = Average transport number of membrane pair
$\bar{t}_1^c$ = Transport number of cation through cation membrane
$\bar{t}_2^a$ = Transport number of anion through anion membrane.

Table 7.6: Electro-osmotic pumping experimental conditions and results for 0,5 mol/ℓ hydrochloric acid (Selemion AAV and CHV)

Current Density	Brine concentration c_b, mol/l		Water flow	Current Efficiency	Effective Current Density	Transport Numbers				
I, mA/cm²	$c_{b\ exp.}$	$c_{b\ calc.}$	J, cm/h	e_p, %	I_{eff}, mA/cm²	Δt^c	Δt^a	$\bar{\Delta}t$	$\bar{t}_1^c$	$\bar{t}_2^a$
10	2,62	5,87	0,050	35,45	3,55	0,89	0,69	0,79	0,94	0,84
20	3,53		0,089	42,24	8,45	0,87	0,62	0,75	0,94	0,81
30	4,03	6,95	0,115	41,45	12,44	0,86	0,57	0,71	0,93	0,79
40	4,39		0,138	40,65	16,26	0,81	0,56	0,70	0,92	0,78
50	4,72	8,01	0,160	40,34	20,17	0,83	0,55	0,69	0,91	0,77
60	5,10		0,173	39,33	23,60	0,82	0,52	0,67	0,91	0,76
70	5,35	8,83	0,195	39,90	27,93	0,78	0,54	0,66	0,89	0,77
80	5,67		0,213	40,46	32,37	0,84	0,59	0,71	0,92	0,80
100	5,96	8,80	0,258	41,26	41,26	0,73	0,49	0,61	0,86	0,75
120	6,35		0,289	41,08	49,30	0,82	0,47	0,64	0,91	0,73
140	6,84	9,50	0,304	39,78	55,69	0,76	0,54	0,65	0,88	0,77

Electro-osmotic coefficient (2β) = 0,126 ℓ/F (slope = 0,004688 mℓ/mAh)
J_{osm} = y-intercept = 0,061762 cm/h
c_b^{max} = 7,93 mol/l
$\Delta t^c = t_1^c - t_2^c$

$\Delta t^a = t_2^a - t_1^a$
$\bar{\Delta}t$ = Average transport number of membrane pair
$\bar{t}_1^c$ = Transport number of cation through cation membrane
$\bar{t}_2^a$ = Transport number of anion through anion membrane.

Table 7.7: Electro-osmotic pumping experimental conditions and results for 1,0 mol/l hydrochloric acid (Selemion AAV and CHV)

Current Density	Brine concentration c_b, mol/l		Water flow	Current Efficiency	Effective Current Density	Transport Numbers				
I, mA/cm²	c_b exp.	c_b calc.	J, cm/h	e_p, %	I_eff, mA/cm²	Δt^a	Δt^c	$\overline{\Delta t}$	t_1^c	t_2^a
10	2,87	5,47	0,051	39,30	3,93	0,91	0,59	0,75	0,96	0,79
20	3,58		0,085	40,89	8,18	0,82	0,56	0,69	0,91	0,78
30	4,10	6,69	0,111	40,60	12,18	0,82	0,50	0,66	0,91	0,75
40	4,63		0,135	42,00	16,80	0,80	0,50	0,65	0,90	0,75
50	5,01	7,95	0,149	40,13	20,07	0,80	0,47	0,64	0,90	0,73
60	5,31	8,08	0,172	40,85	24,51	0,81	0,44	0,62	0,90	0,72
80	5,86	8,69	0,209	40,96	32,77	0,76	0,46	0,61	0,88	0,73
100	6,19	9,50	0,245	40,73	40,73	0,75	0,50	0,62	0,88	0,75
140	7,00	10,40	0,299	40,08	56,11	0,71	0,48	0,60	0,86	0,74
180	7,44	11,42	0,351	38,94	70,09	0,70	0,49	0,60	0,85	0,75

Electro-osmotic coefficient $(2\beta) = 0,125$ l/F (slope $= 0,004674$ ml/mAh)
$J_{osm} =$ y-intercept $= 0,055604$ cm/h
$c_b^{max} = 8,00$ mol/l
$\Delta t^c = t_1^c - t_2^c$

$\Delta t^a = t_2^a - t_1^a$
$\overline{\Delta t} =$ Average transport number of membrane pair
$t_1^c =$ Transport number of cation through cation membrane
$t_2^a =$ Transport number of anion through anion membrane.

Table 7.8: Electro-osmotic pumping experimental conditions and results for 0,05 mol/l hydrochloric acid (ABM-3 and Selemion CHV)

Current Density	Brine concentration c_b, mol/l		Water flow	Current Efficiency	Effective Current Density	Transport Numbers				
I, mA/cm²	c_b exp.	c_b calc.	J, cm/h	e_p, %	I_eff, mA/cm²	Δt^a	Δt^c	$\overline{\Delta t}$	Δt_1^c	Δt_2^a
10	2,47	4,55	0,064	42,53	4,25	0,90	0,66	0,78	0,95	0,83
20	2,91	5,79	0,098	38,42	7,68	0,93	0,60	0,77	0,97	0,80
30	3,33	7,13	0,117	34,81	10,44	0,90	0,59	0,74	0,95	0,79
40	3,78	7,69	0,138	34,89	13,96	0,90	0,53	0,71	0,95	0,76
50	4,00	8,44	0,154	33,06	16,53	0,89	0,50	0,70	0,95	0,75
60	4,16	8,68	0,176	32,70	19,62	0,88	0,48	0,68	0,94	0,74

Electro-osmotic coefficient $(2\beta) = 0,171$ l/F (slope $= 0,0063924$ ml/mAh)
$J_{osm} =$ y-intercept $= 0,0495041$ cm/h
$c_b^{max} = 5,85$ mol/l
$t^c = t_1^c - t_2^c$

$t^a = t_2^a - t_1^a$
$\overline{\Delta t} =$ Average transport number of membrane pair
$t_1^c =$ Transport number of cation through cation membrane
$t_2^a =$ Transport number of anion through anion membrane.

Table 7.9: Electro-osmotic pumping experimental conditions and results for 0,1 mol/l hydrochloric acid (ABM-3 and Selemion CHV)

Current Density	Brine concentration c_b, mol/l		Water flow	Current Efficiency	Effective Current Density	Transport Numbers				
I, mA/cm²	c_b exp.	c_b calc.	J, cm/h	e_p, %	I_eff, mA/cm²	Δt^a	Δt^c	$\overline{\Delta t}$	t_1^c	t_2^a
10	2,27	4,76	0,0675	41,01	4,1	0,97	0,75	0,86	0,99	0,88
20	2,90	5,95	0,0976	37,80	7,56	0,94	0,62	0,78	0,97	0,81
30	3,41	6,80	0,119	36,32	10,90	0,92	0,52	0,72	0,96	0,76
40	3,78	7,09	0,147	37,31	14,92	0,92	0,48	0,70	0,96	0,74
50	3,99	7,46	0,166	35,42	17,71	0,90	0,43	0,66	0,95	0,71
60	4,38	9,00	0,178	34,99	20,99	0,89	0,55	0,72	0,94	0,77

Electro-osmotic coefficient $(2\beta) = 0,166$ l/F (slope $= 0,0061880$ ml/mAh)
$J_{osm} =$ y-intercept $= 0,0523128$ cm/h
$c_b^{max} = 6,02$ mol/l
$t^c = t_1^c - t_2^c$

$t^a = t_2^a - t_1^a$
$\overline{\Delta t} =$ Average transport number of membrane pair
$t_1^c =$ Transport number of cation through cation membrane
$t_2^a =$ Transport number of anion through anion membrane.

Table 7.10 : Electro-osmotic pumping experimental conditions and results for 0,5 mol/ℓ hydrochloric acid (ABM-3 and Selemion CHV)

Current Density, I, mA/cm²	Brine concentration, c_b, mol/l		Water flow, J, cm/h	Current Efficiency, Ep, %	Effective Current Density, I_{eff}, mA/cm²	Transport Numbers				
	$C_{b\,exp.}$	$C_{b\,calc.}$				Δt^c	Δt^a	$\overline{\Delta}t$	$\bar{t}_1^c$	$\bar{t}_2^a$
10	2,41	4,64	0,062	40,42	4,04	0,92	0,64	0,78	0,96	0,82
20	3,04	5,70	0,093	38,05	7,61	0,90	0,53	0,71	0,95	0,76
30	3,61	6,48	0,114	36,88	11,06	0,86	0,46	0,66	0,93	0,73
40	3,97		0,138	36,65	14,64	0,85	0,40	0,62	0,92	0,70
50	4,35	7,36	0,152	35,52	17,76	0,84	0,36	0,60	0,92	0,68
70	5,30	8,52	0,172	34,95	24,47	0,82	0,30	0,56	0,91	0,65
90	5,50	8,81	0,212	34,72	31,25	0,83	0,29	0,56	0,91	0,64
110	5,95	8,76	0,252	36,09	40,14	0,82	0,26	0,54	0,91	0,63
120	6,18	8,34	0,284	37,13	48,27	0,82	0,24	0,53	0,91	0,62

Electro-osmotic coefficient (2β) = 0,124 ℓ/F (slope = 0,0046224 mℓ/mAh)
J_{osm} = y-intercept = 0,0643752 cm/h
c_b^{max} = 8,06 mol/l
$t^c = t_1^c - t_2^c$

$t^a = t_2^a - t_1^a$
$\overline{\Delta}t$ = Average transport number of membrane pair
$\bar{t}_1^c$ = Transport number of cation through cation membrane
$\bar{t}_2^a$ = Transport number of anion through anion membrane.

Table 7.11: Electro-osmotic pumping experimental conditions and results for 1,0 mol/ℓ hydrochloric acid (ABM-3 and Selemion CHV)

Current Density I, mA/cm²	Brine concentration c_b, mol/l		Water flow J, cm/h	Current Efficiency ϵ_p, %	Effective Current Density I_{eff}, mA/cm²	Transport Numbers				
	$C_{b\,exp.}$	$C_{b\,calc.}$				Δt^c	Δt^a	$\overline{\Delta}t$	$\bar{t}_1^c$	$\bar{t}_2^a$
20	3.05	4.07	0.145	59.558	11.911	1.00	0.57	0.79	1,00	0,78
40	4.19	5.81	0.184	51.694	20.678	0.93	0.50	0.72	0,97	0,75
60	4.66	6.41	0.238	49.634	29.780	0.93	0.44	0.68	0,96	0,71
80	5.4	7.87	0.261	47.291	37.833	0.91	0.47	0.69	0,95	0,73

Electro-osmotic coefficient (2β) = 0,125 ℓ/F (slope = 0,0046471 mℓ/mAh)
J_{osm} = y-intercept =   cm/h
c_b^{max} = 8.03 mol/l
$\Delta t^c = t_1^c - t_2^c$

$\Delta t^a = t_2^a - t_1^a$
$\overline{\Delta}t$ = Average transport number of membrane pair
$\bar{t}_1^c$ = Transport number of cation through cation membrane
$\bar{t}_2^a$ = Transport number of anion through anion membrane.

Table 7.12 : Electro-osmotic pumping experimental conditions and results for 0,05 mol/ℓ hydrochloric acid (ABM-2 and Selemion CHV)

Current Density, I, mA/cm²	Brine concentration, c_b, mol/l		Water flow, J, cm/h	Current Efficiency, E_p, %	Effective Current Density, I_{eff}, mA/cm²	Transport Numbers				
	$C_{b\,exp.}$	$C_{b\,calc.}$				Δt^c	Δt^a	$\overline{\Delta}t$	$\bar{t}_1^c$	$\bar{t}_2^a$
10	3,15	5,2	0,050	42,87	4,29	0,90	0,51	0,71	0,95	0,76
20	3,92		0,076	40,01	8,00					
30	4,40	7,6	0,095	37,49	11,24	0,88	0,40	0,64	0,94	0,70
40	4,72		0,117	36,86	14,74					
50	4,80		0,143	36,81	18,40					
60	4,90	9,1	0,145	31,89	19,14	0,87	0,32	0,59	0,93	0,66

Electro-osmotic coefficient (2β) = 0,170 ℓ/F (slope = 0,0063345 mℓ/mAh)
J_{osm} = y-intercept = 0,0245486 cm/h
c_b^{max} = 5,88 mol/l
$t^c = t_1^c - t_2^c$

$t^a = t_2^a - t_1^a$
$\overline{\Delta}t$ = Average transport number of membrane pair
$\bar{t}_1^c$ = Transport number of cation through cation membrane
$\bar{t}_2^a$ = Transport number of anion through anion membrane.

Table 7.13 : Electro-osmotic pumping experimental conditions and results for 0,1 mol/l hydrochloric acid (ABM-2 and Selemion CHV)

Current Density I, mA/cm²	Brine concentration c_b, mol/l		Water flow J, cm/h	Current Efficiency e_p, %	Effective Current Density I_{eff}, mA/cm²	Transport Numbers				
	$c_{b\,exp}$	$c_{b\,calc}$				Δt^a	Δt^c	$\bar{\Delta}t$	t_i^c	t_i^a
10	2,1	3,3	0,091	51,13	5,11	0,06	0,65	0,81	0,97	0,82
20	2,95		0,117	46,08	9,21					
30	3,40		0,132	40,24	12,07					
40	3,82	6,8	0,146	37,29	14,91	0,88	0,45	0,66	0,94	0,55
50	4,28		0,152	34,95	17,48					
60	4,42		0,172	34,00	20,40					
80	4,82		0,198	32,08	25,6					
100	5,18	10,02	0,230	31,87	31,87	0,07	0,36	0,62	0,93	0,68

Electro-osmotic coefficient (2β) = 0,133 l/F (slope = 0,0049643 ml/mAh)
J_{osm} = y-intercept = 0,0704871 cm/h
c_b^{max} = 7,51 mol/l
$t^c = t_1^c - t_2^c$

$t^a = t_2^a - t_1^a$
$\bar{\Delta}t$ = Average transport number of membrane pair
t_i^c = Transport number of cation through cation membrane
t_i^a = Transport number of anion through anion membrane.

Table 7.14: Electro-osmotic pumping experimental conditions and results for 0,5 mol/l hydrochloric acid (ABM-2 and Selemion CHV)

Current Density I, mA/cm²	Brine concentration c_b, mol/l		Water flow, J, cm/h	Current Efficiency, E_p, %	Effective Current Density, I_{eff}, mA/cm²	Transport Numbers,				
	$c_{b\,exp}$	$c_{b\,calc}$				Δt^a	Δt^c	$\bar{\Delta}t$	t_i^c	t_i^a
10	2,88	4,3	0,0625	48,26	4,83	0,90	0,55	0,73	0,95	0,77
20	4,06		0,086	46,85	9,37					
30	4,44		0,1130	44,43	13,33					
40	5,02	6,3	0,127	42,81	17,12	0,82	0,25	0,53	0,90	0,62
60	5,30		0,1576	37,32	22,39					
80	5,70		0.194	37,1	29,68					
100	5,95	7,5	0,229	36,61	36,61	0,75	0,17	0,46	0,87	0,58
120	6,30		0,256	36,03	43,24					

Electro-osmotic coefficient (2β) = 0,131 l/F (slope = 0,0049116 ml/mAh)
J_{osm} = y-intercept = 0,0465110 cm/h
c_b^{max} = 7,6 mol/l
$\Delta t^c = t_1^c - t_2^c$

$\Delta t^a = t_2^a - t_1^a$
$\bar{\Delta}t$ = Average transport number of membrane pair
t_i^c = Transport number of cation through cation membrane
t_i^a = Transport number of anion through anion membrane.

Table 7.15 Electro-osmotic pumping experimental conditions and results for 0,05 mol/l hydrochloric acid (ABM-1 and Selemion CHV)

Current Density I, mA/cm²	Brine concentration c_b, mol/l		Water flow J, cm/h	Current Efficiency e_p, %	Effective Current Density I_{eff}, mA/cm²	Transport Numbers				
	$c_{b\,exp}$	$cC_{b\,calc}$				Δt^a	Δt^c	$\bar{\Delta}t$	t_i^c	t_i^a
10	2,00	4,24	0,0675	36,24	3,621	0,98	0,55	0,77	0,99	0,76
20	2,65	5,86	0,0927	32,93	6,586	0,96	0,50	0,73	0,98	0,75
30	3,1		0,1336	29,35	8,805					
40	3,1		0,1456	30,267	12,106					
50	3,7		0,1483	29,425	14,712					
60	3,95	10,15	0,1509	26,645	15,987	0,92	0,45	0,68	0,96	0,72
80	4,00		0,1854	24,852	19,882					

Electro-osmotic coefficient (2β) = 0,188 l/F (slope = 0,0070105 ml/mAh)
J_{osm} = y-intercept = 0,0465611 cm/h
c_b^{max} = 5,32 mol/l
$\Delta t^c = t_1^c - t_2^c$

$\Delta t^a = t_2^a - t_1^a$
$\bar{\Delta}t$ = Average transport number of membrane pair
t_i^c = Transport number of cation through cation membrane
t_i^a = Transport number of anion through anion membrane.

Table 7.16 : Electro-osmotic pumping experimental conditions and results for 0,1 mol/ℓ hydrochloric acid (ABM-1 and Selemion CHV)

Current Density	Brine concentration c_b, mol/l		Water flow	Current Efficiency	Effective Current Density	Transport Numbers				
I, mA/cm²	$c_{b\,exp.}$	$c_{b\,calc.}$	J, cm/h	e_p, %	I_{eff}, mA/cm²	Δt^c	Δt^a	$\bar{\Delta}t$	$\bar{t}_1^c$	$\bar{t}_2^a$
10	2,2	3,00	0,0675	39,84	3,98	0,92	0,16	0,54	0,96	0,58
20	2,85	6,0	0,0927	35,42	7,08	0,91	0,57	0,74	0,95	0,79
30	3,3		0,1324	35,05	11,72					
40	3,5	6,6	0,1483	34,79	13,91	0,87	0,45	0,66	0,93	0,73
50	3,9		0,1655	34,62	17,31					
60	4,15	7,03	0,1942	36,02	21,6	0,86	0,35	0,61	0,93	0,68
80	4,5		0,211	31,95	25,56					
100	4,9	8,76	0,247	32,47	32,47	0,85	0,30	0,58	0,93	0,65

Electro-osmotic coefficient (2β) = 0,152 ℓ/F (slope = 0,0056523 mℓ/mAh)
J_{osm} = y-intercept = 0,0692712 cm/h
c_b^{max} = 6,58 mol/l
$\Delta t^c = t_1^c - t_2^c$

$\Delta t^a = t_2^a - t_1^a$
$\bar{\Delta}t$ = Average transport number of membrane pair
$\bar{t}_1^c$ = Transport number of cation through cation membrane
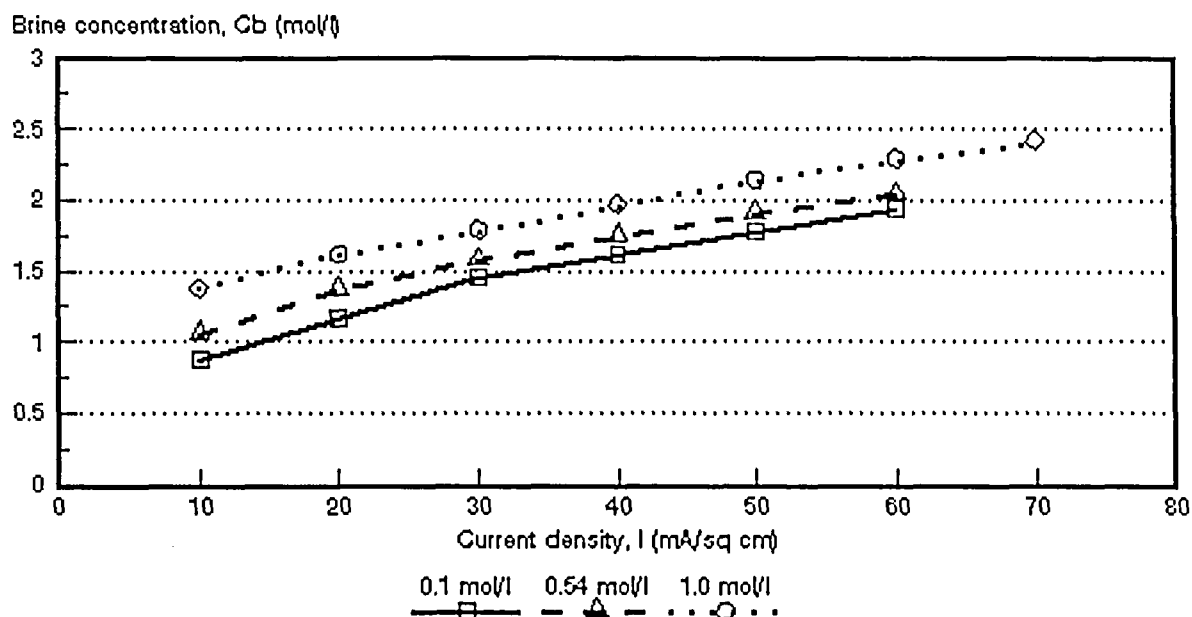$\bar{t}_2^a$ = Transport number of anion through anion membrane.

Table 7.17 : Electro-osmotic pumping experimental conditions and results for 0,5 mol/ℓ hydrochloric acid (ABM-1 and Selemion CHV)

Current Density	Brine concentration c_b, mol/l		Water flow	Current Efficiency	Effective Current Density	Transport Numbers				
I, mA/cm²	$c_{b\,exp.}$	$c_{b\,calc.}$	J, cm/h	e_p, %	I_{eff}, mA/cm²	Δt^c	Δt^a	Δt	$\bar{t}_1^c$	$\bar{t}_2^a$
10	2,35		0,0635	40,05	4,00					
20	2,80	5,2	0,0971	36,45	7,29	0,87	0,46	0,67	0,94	0,73
30	3,3		0,1165	34,36	10,31					
40	3,62	6,2	0,1456	35,34	14,14	0,84	0,35	0,60	0,92	0,68
60	4,2	6,2	0,1854	34,79	20,88	0,83	0,18	0,51	0,92	0,59
80	4,65		0,2119	33,02	26,42					
100	5,1	7,8	0,2613	35,73	35,73	0,79	0,12	0,46	0,90	0,56
120	5,25		0,291	34,17	41,00					

Electro-osmotic coefficient (2β) = 0,149 ℓ/F (slope = 0,0055429 mℓ/mAh)
J_{osm} = y-intercept = 0,0647860 cm/h
c_b^{max} = 6,71 mol/l
$\Delta t^c = t_1^c - t_2^c$

$\Delta t^a = t_2^a - t_1^a$
Δt = Average transport number of membrane pair
$\bar{t}_1^c$ = Transport number of cation through cation membrane
$\bar{t}_2^a$ = Transport number of anion through anion membrane.

235

Brine concentration, Cb (mol/l)

Current density, I (mA/sq cm)

0.1 mol/l   0.54 mol/l   1.0 mol/l

Figure 7.1:   Acid concentration as a function of current density for 3 different HCl feed concentrations. *Selemion* AMV and CMV membranes.
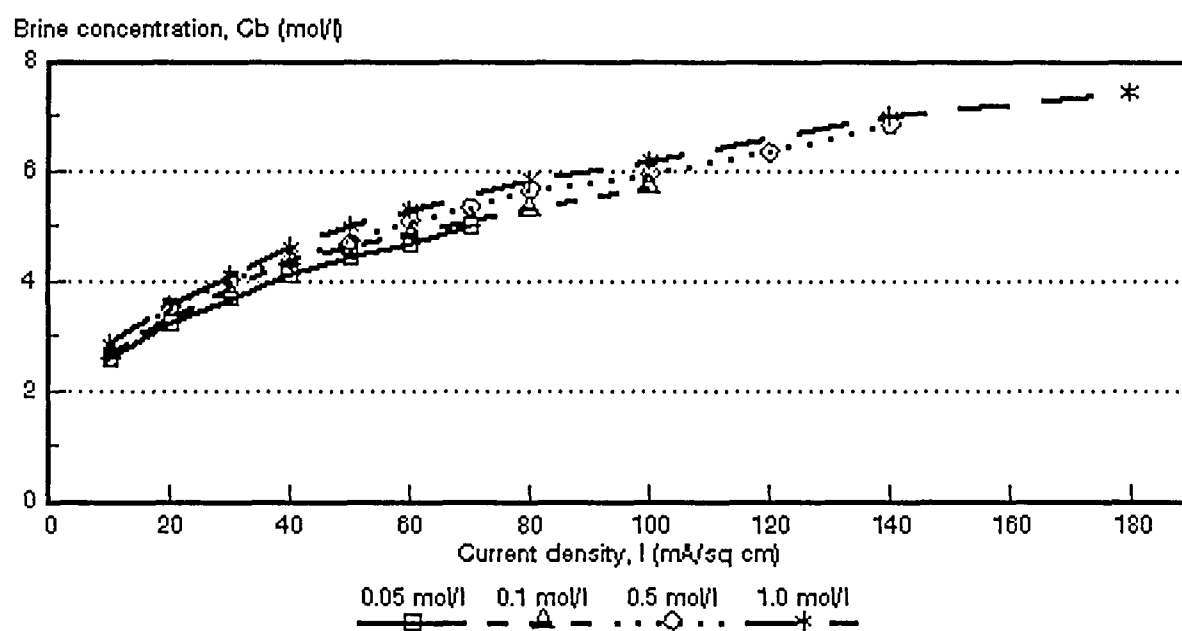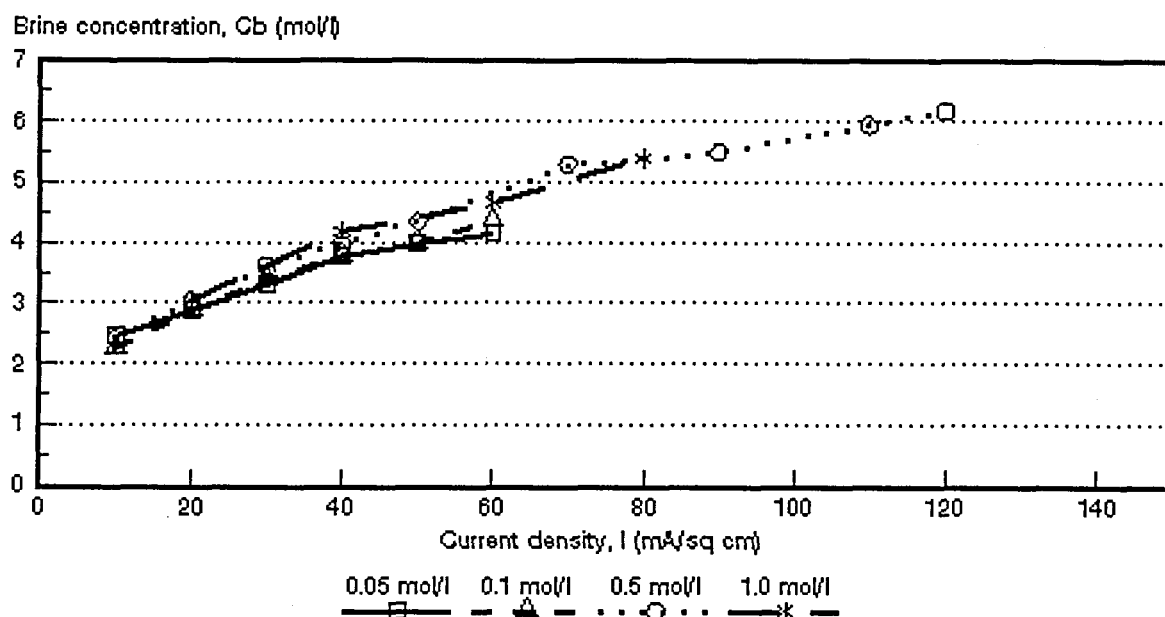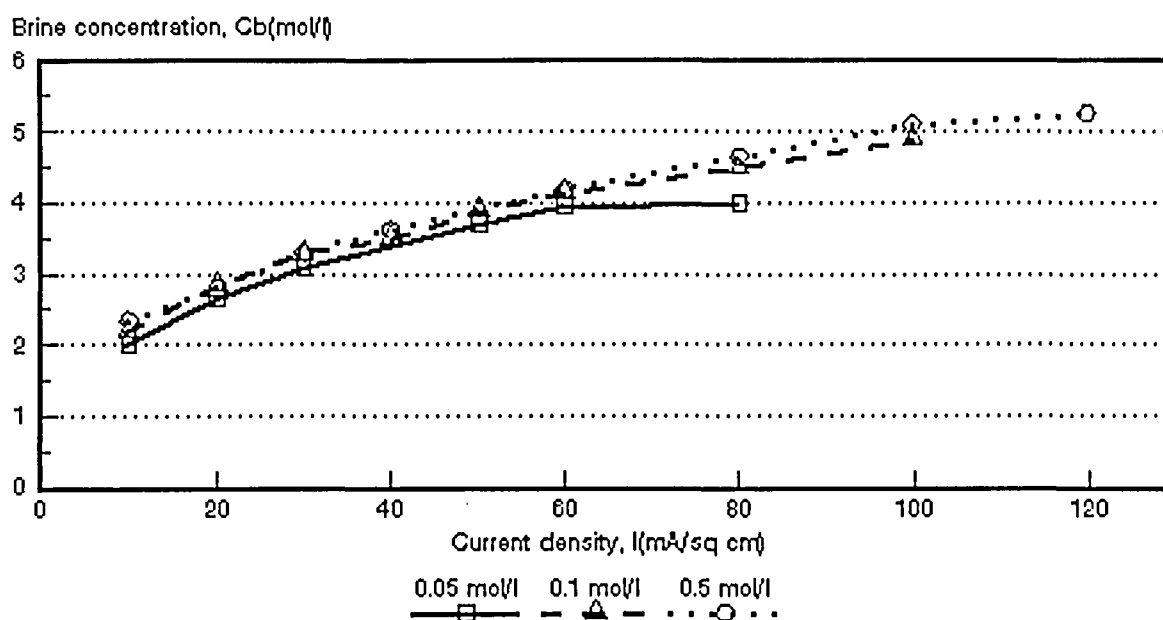
Brine concentration, Cb (mol/l)

Current density, I (mA/sq cm)

0.05 mol/l   0.1 mol/l   0.5 mol/l   1.0 mol/l

Figure 7.2:   Acid concentration as a function of current density for 4 different HCl feed concentrations. *Selemion* AAV and CHV membranes.

Brine concentration, Cb (mol/l)

Figure 7.3: Acid concentration as a function of current density for 3 different HCl feed concentrations. ABM-3 and *Selemion* CHV membranes.

Brine concentration,Cb(mol/l)
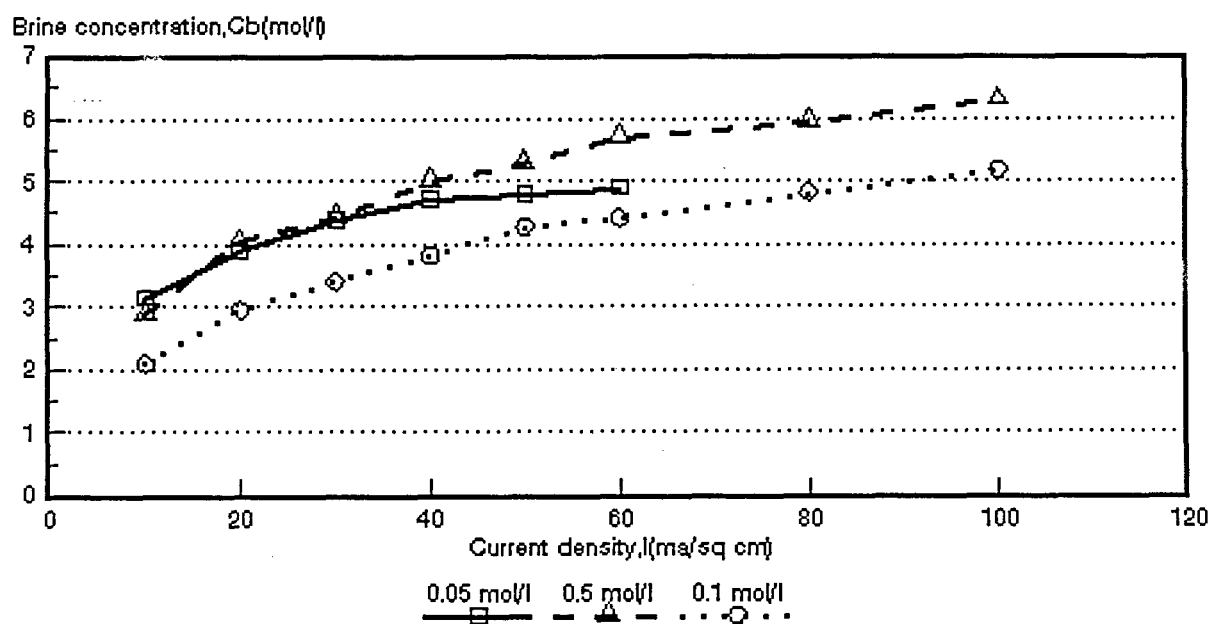
Figure 7.4 Acid concentration as a function of current density for 3 different HCl feed concentrations. ABM-2 and *Selemion* CHV membranes.

Brine concentration, Cb(mol/l)

Figure 7.5: Acid concentration as a function of current density for 3 different HCl feed concentrations. ABM-1 and *Selemion* CHV membranes.

Table 7.18 Acid brine concentrations obtained at the highest current densities investigated for different hydrochloric acid feed concentrations.

Feed Concentration	Brine Concentration* (%)				
	Selemion	Selemion	Israeli & Selemion	Israeli & Selemion	Israeli & Selemion
mol/*l*	AMV & CMV	AAV & CHV	ABM-3 & CHV	ABM-2 & CHV	ABM-1 & CHV
0,05	-	18,3	15,2	17,9	14,6
0,10	7,1	20,9	16,0	18,9	17,9
0,50**	7,5	25,0	22,6	22,9	19,2
1,0	8,8	27,2	19,7***		

*   Brine concentrations obtained from the data in Tables 7.1 to 7.17.

** 0,54 mol/*l* for AMV and CMV.

*** Lower current density.

238

of membrane permselectivity. Adsorbed hydrochloric acid and ion association are factors which decrease the proton leakage of anion exchange membranes[48].

It also appears as has been experienced with sodium chloride solutions that acid brine concentration will approach a maximum value, c_b^{max}. The maximum brine concentration, c_b^{max}, will be reached faster for the lower acid feed concentrations than for the higher acid feed concentrations (Figs. 7.3, 7.4 and 7.5). However, it appears that the maximum brine concentration for acid, especially at the higher acid feed concentrations, will be reached at much higher current densities than has been the case with the sodium chloride solutions. Maximum acid brine concentrations were calculated from the same relationships as used in 6.1. The results are shown in Table 7.19 and Figures 7.6 to 7.10. Very good correlations were obtained by the two methods.

The maximum acid brine concentration that can be obtained depends on the acid feed concentration. This was evident for all the membranes investigated. However, the maximum acid brine concentration remained almost constant in the case of the *Selemion* AAV and CHV membranes at 0,5 and 1,0 mol/ℓ feed concentration (Table 7.19, Fig. 7.7). The same behaviour was observed for the ABM-3 and CHV membranes (Fig. 7.8). Maximum acid brine concentration for the ABM-2-, ABM-1- and CHV membranes remained constant at 0,1 and 0,5 mol/ℓ feed concentration (Figs. 7.9 and 7.10).

Acid brine concentration at different current densities was predicted from measured transport numbers (Δt's) and volume flows with the same relationship as used in 6.1. The experimental and calculated acid brine concentrations are shown in Tables 7.1 to 7.17 and Figures 7.11 to 7.27.

The calculated acid brine concentrations were determined from the average apparent transport number of a membrane pair ($\overline{\Delta t}$). The correlations between the calculated and the experimentally determined acid brine concentrations were not satisfactory as could be seen from Figures 7.11 to 7.27 and Table 7.20. The calculated acid brine concentrations were much higher than the experimentally determined concentrations. The calculated acid brine concentrations were approximately 3 to 4 times higher for the *Selemion* AMV and CMV membranes than the experimentally determined concentrations (Table 7.20). The calculated acid brine concentrations were approximately 1,5 to 2 times higher for the *Selemion* AAV and CHV membranes than

the experimentally determined values in the feed concentration and current density ranges studied. Approximately the same results were obtained for the ABM-3, ABM-2 and ABM-1 membranes. Therefore, it appears that simple membrane potential measurements for a membrane pair ($\overline{\Delta}$t) cannot be applied effectively to predict acid brine concentration accurately. The reason for this may be ascribed to backdiffusion of acid during EOP experiments which reduces current efficiency and therefore acid brine concentration.

Table 7.19: Maximum acid brine concentration calculated from $c_b^{max} = 1/2\ F\beta^*$ and $c_b^{max} = c_b\ (1 + J_{osm}/J_{eiosm})^{**}$

Feed Concentration	Maximum Acid Brine Concentration, c_b^{max} (mol/ℓ)									
	Selemion		Selemion		Israeli & Selemion		Israeli & Selemion		Israeli & Selemion	
mol/ℓ	AMV & CMV		AAV & CHV		ABM-3 & CHV		ABM-2 & CHV		ABM-1 & CHV	
	1	2	1	2	1	2	1	2	1	2
0,05			7,1	7,1	5,9	5,8	5,9	5,9	5,3	5,2
0,10	2,8	2,8	7,1	7,4	6,0	5,8	7,5	7,5	6,6	6,7
0,50	2,7	2,7	7,9	8,1	8,1	8,0	7,6	7,6	6,7	6,6
1,00	3,3	3,3	8,0	8,2	8,0	8,0				

1 : $c_b^{max} = 1/2\ F\beta$
2 : $c_b^{max} = c_b\ (1 + J_{osm}/J_{eiosm})$
* : calculated from electro-osmotic coefficients (Tables 7.1 to 7.17)
** : Calculated from $J_{eiosm} = J - J_{osm}$ (y-intercept and the corresponding c_b values) (Tables 7.1 to 7.17)

Cb max =1/2FB   Cb max =Cb (1 + Josm / Jeiosm)
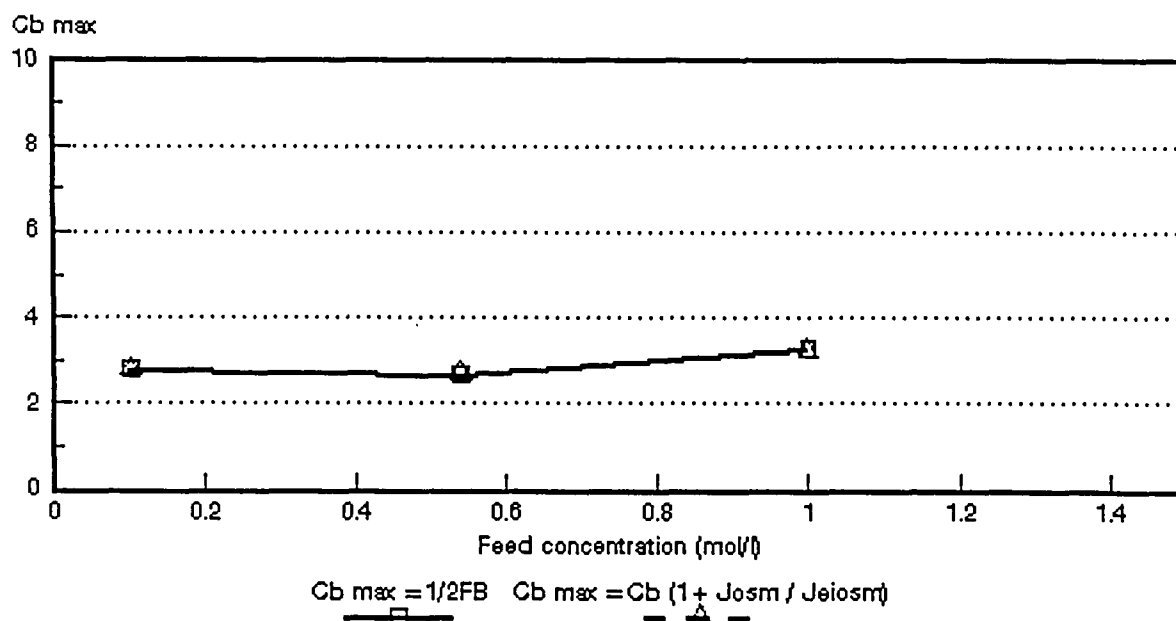
Figure 7.6: Maximum acid brine concentration as a function of feed concentration for different HCl feed concentrations. Selemion AMV and CMV membranes.
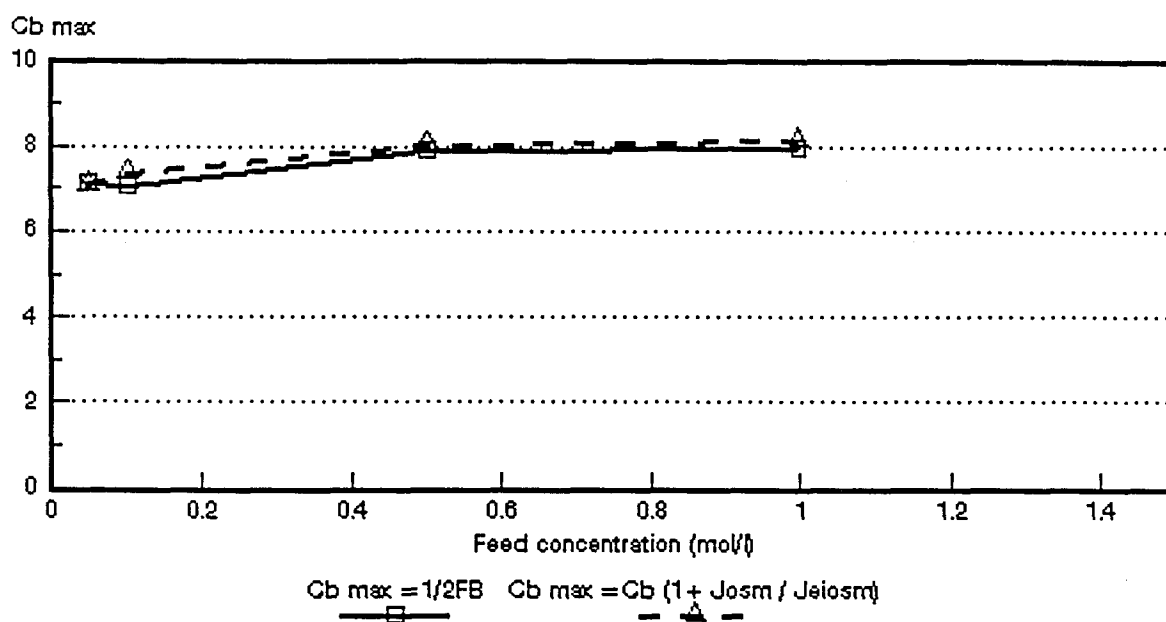
Figure 7.7: Maximum acid brine concentration as a function of feed concentration for different HCl feed concentrations. *Selemion* AAV and CHV membranes.
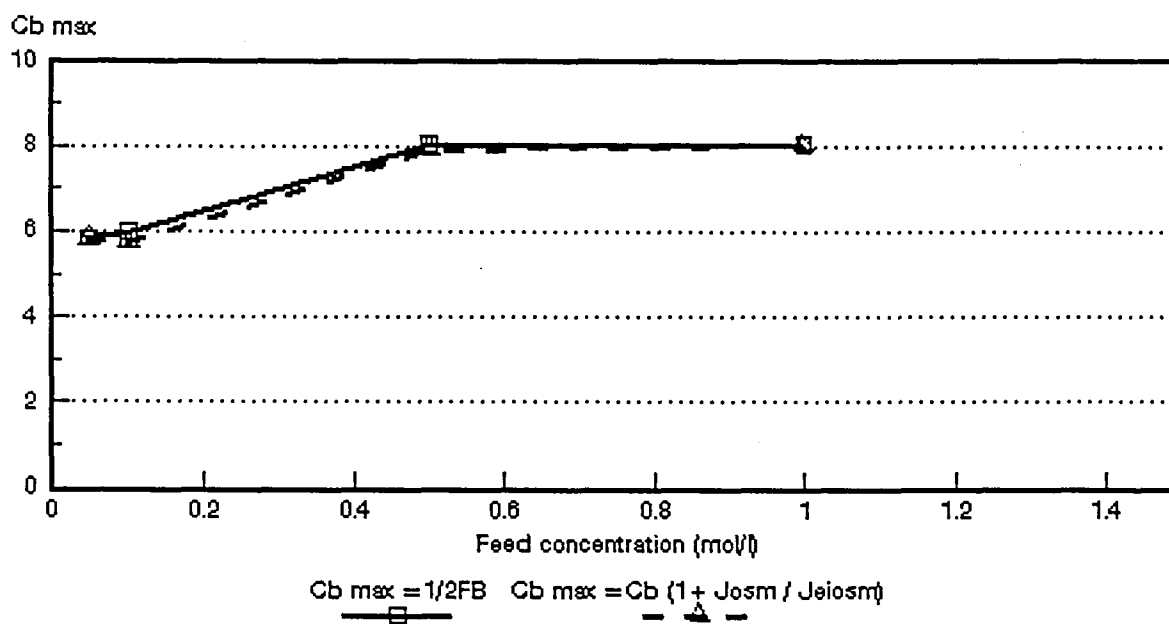
Figure 7.8: Maximum acid brine concentration as a function of feed concentration for different HCl feed concentrations. ABM-3 and *Selemion* CHV membranes.
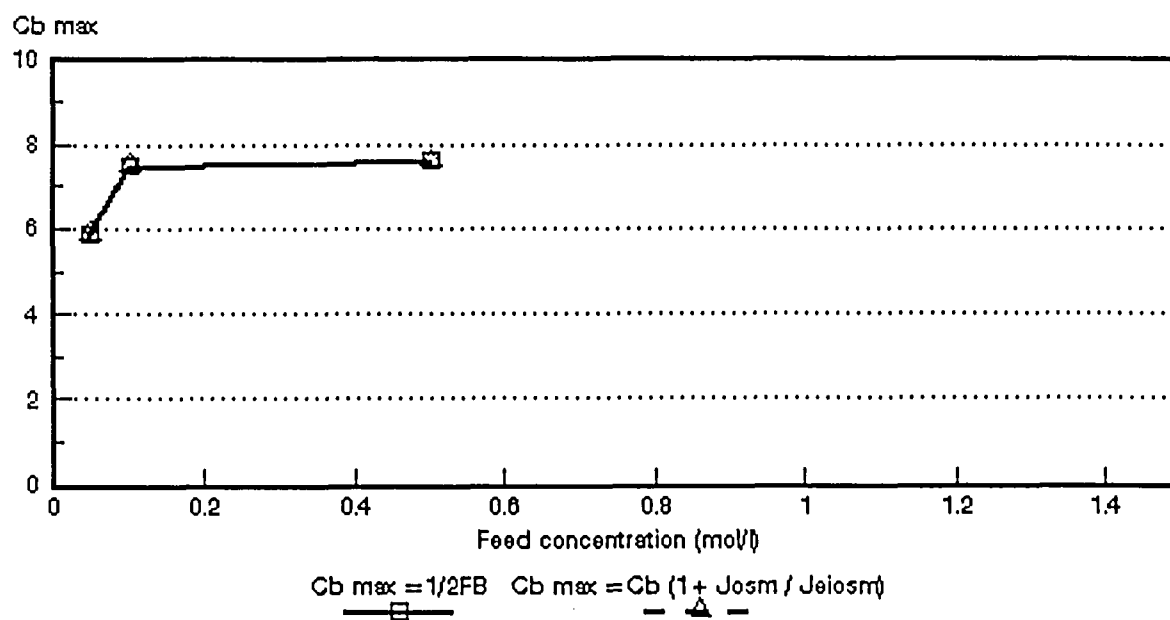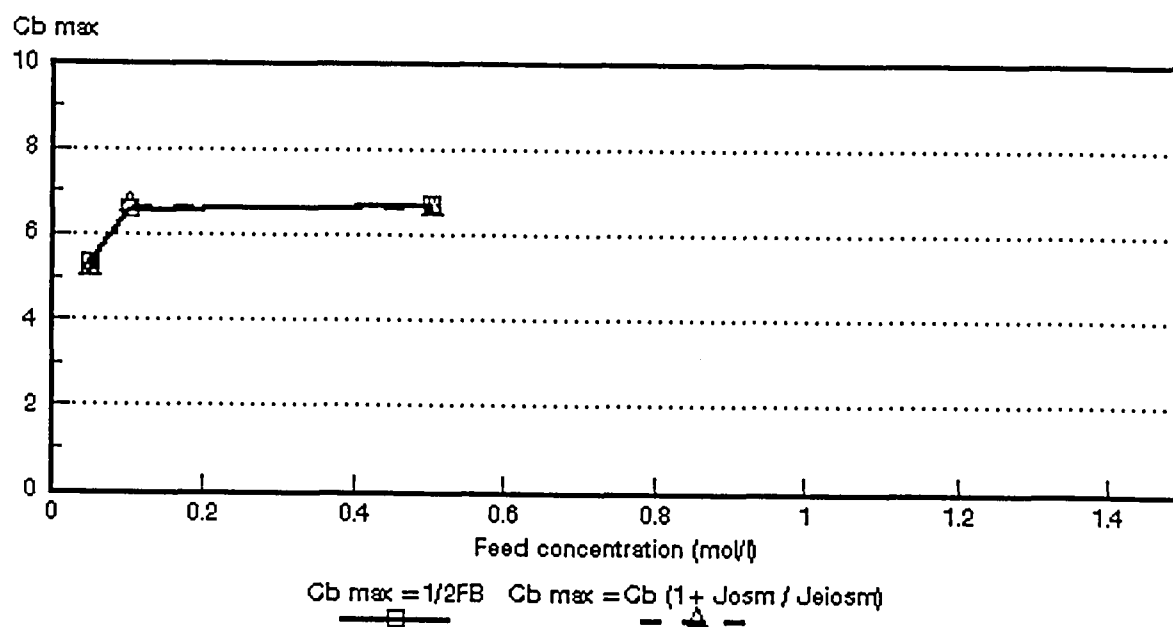
Cb max

Cb max = 1/2FB   Cb max = Cb (1 + Josm / Jeiosm)

Figure 7.9: Maximum acid brine concentration as a function of feed concentration for different HCl feed concentrations. ABM-2 and *Selemion* CHV membranes.

Cb max

Cb max = 1/2FB   Cb max = Cb (1 + Josm / Jeiosm)

Figure 7.10: Maximum acid brine concentration as a function of feed concentration for different HCl feed concentrations. ABM-1 and *Selemion* CHV membranes.

242
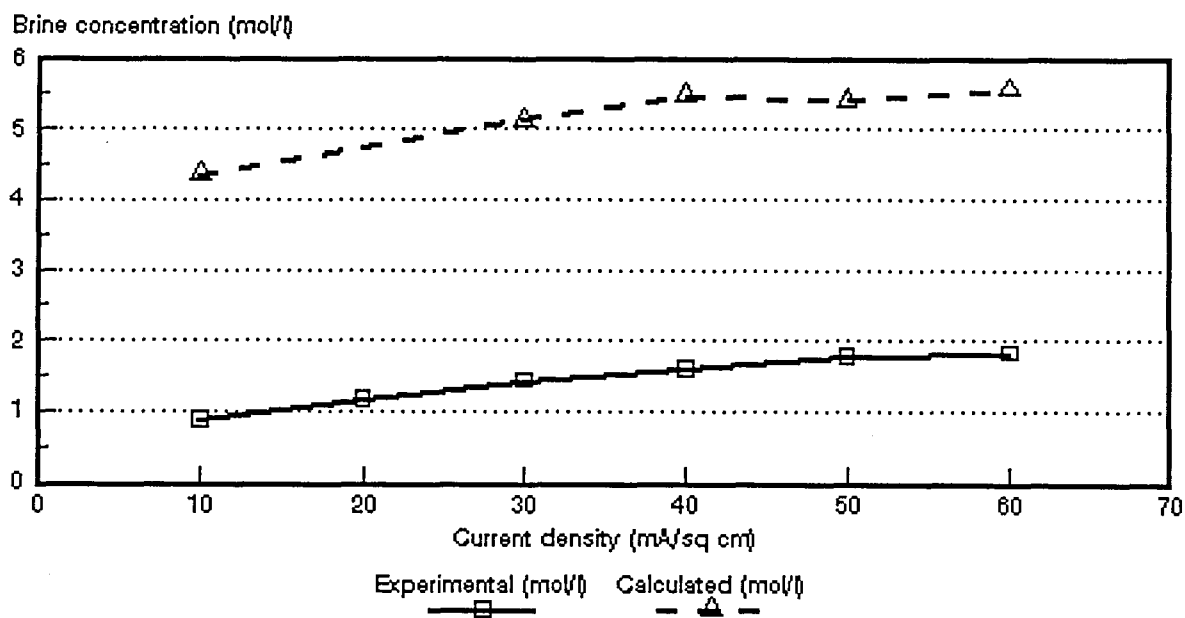
Figure 7.11: Experimental and calculated acid brine concentrations as a function of current density for 0,1 mol/ℓ HCl feed solution. *Selemion* AMV and CMV membranes.
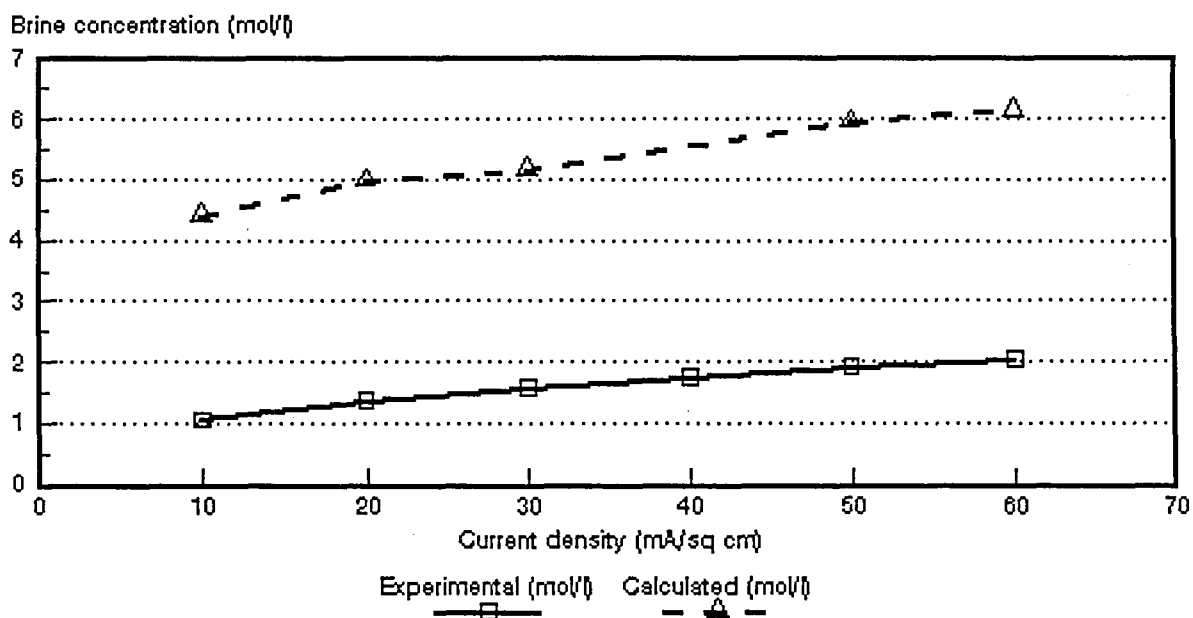
Figure 7.12: Experimental and calculated acid brine concentrations as a function of current density for 0,54 mol/ℓ HCl feed solution. *Selemion* AMV and CMV membranes.
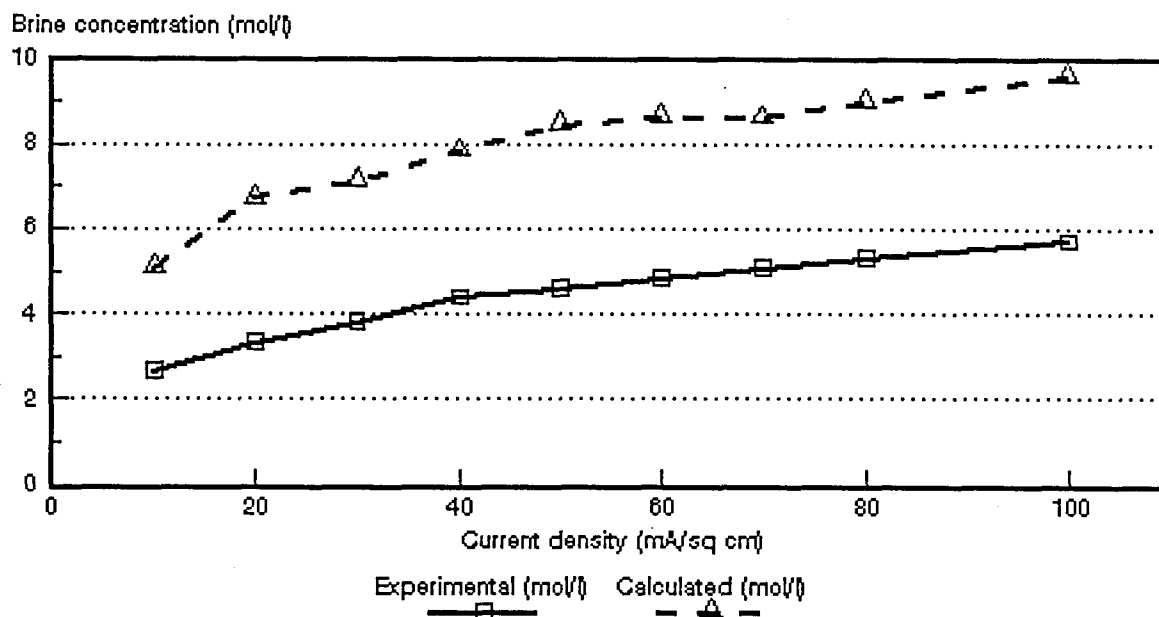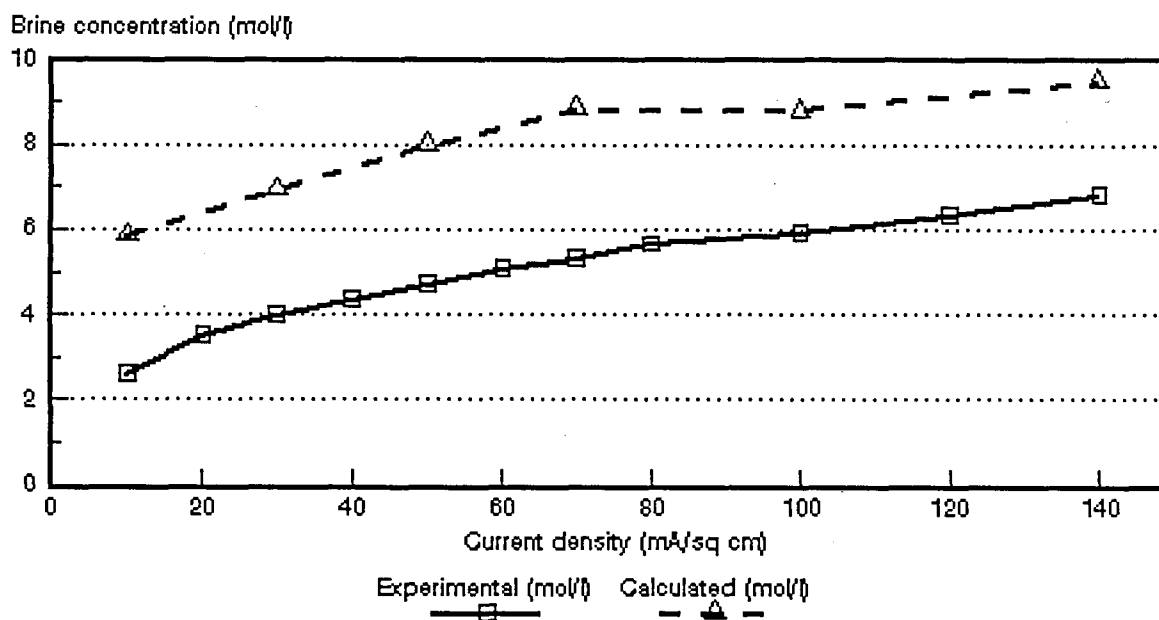
243

Brine concentration (mol/l)

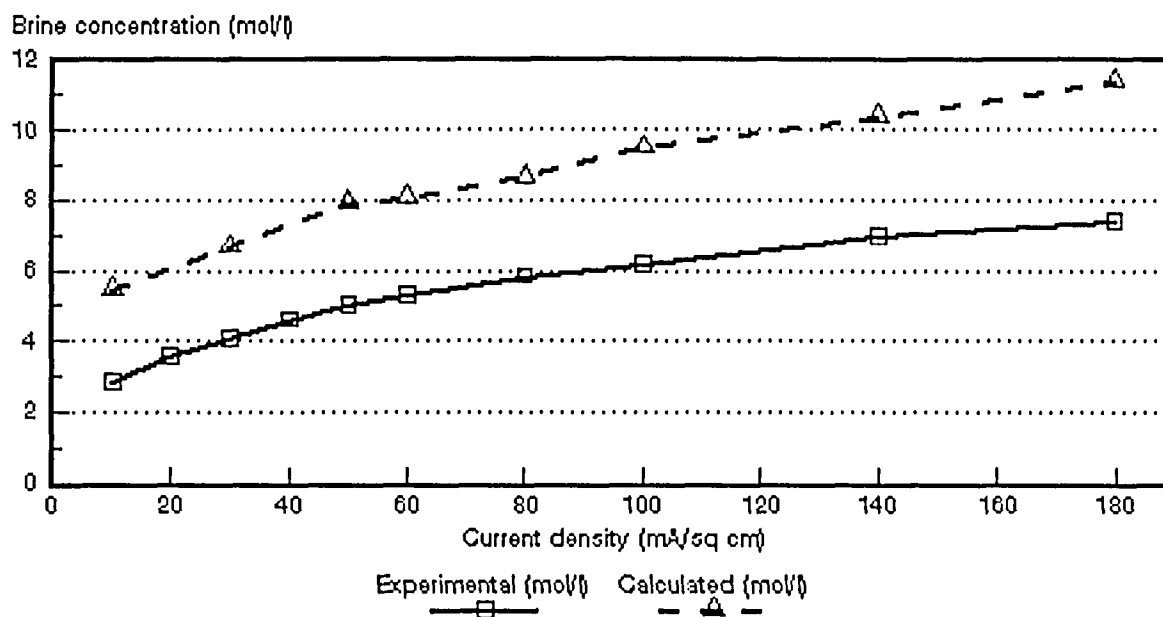

Experimental (mol/l)   Calculated (mol/l)
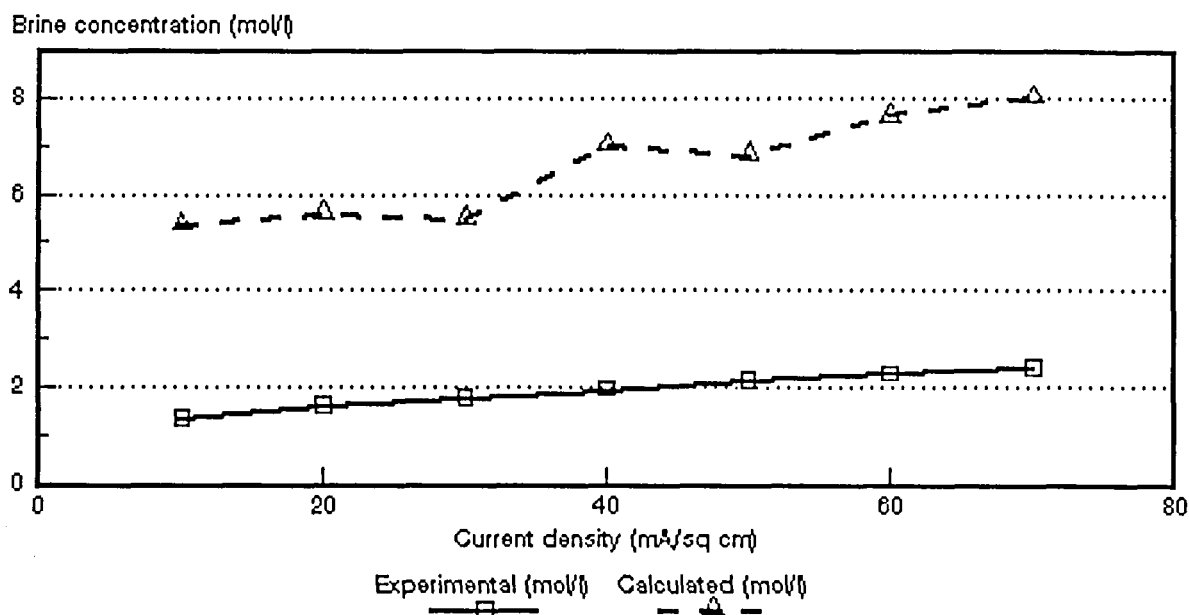
Figure 7.13: Experimental and calculated acid brine concentrations as a function of current density for 1,0 mol/ℓ HCl feed solution. *Selemion* AMV and CMV membranes.

Brine concentration (mol/l)

Experimental (mol/l)   Calculated (mol/l)
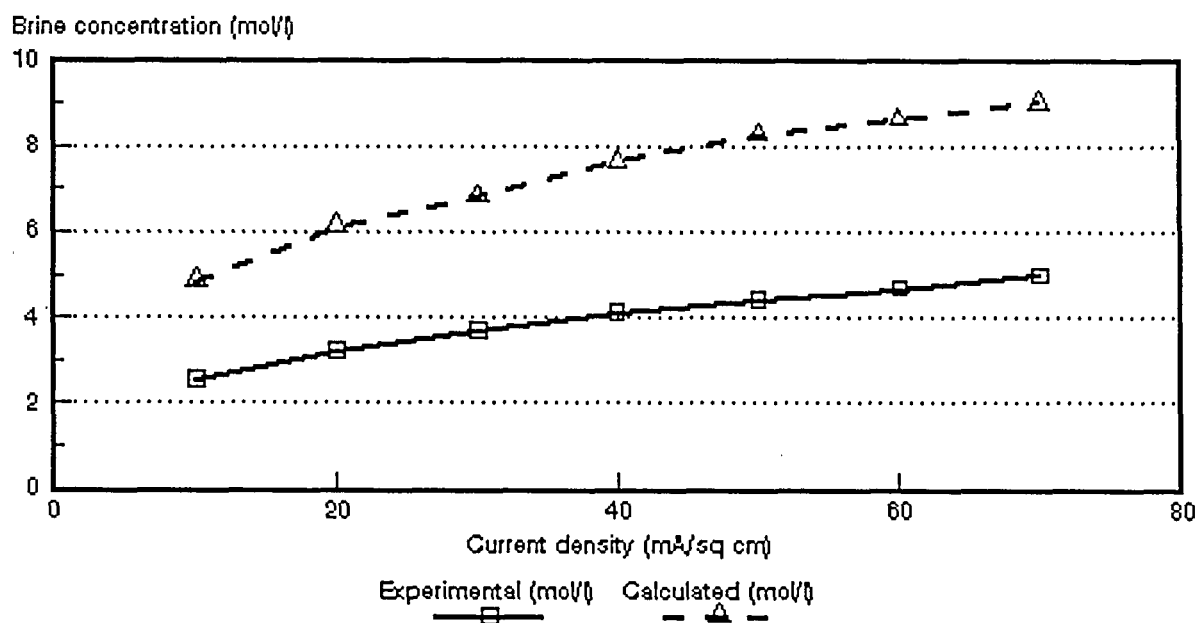
Figure 7.14: Experimental and calculated acid brine concentrations as a function of current density for 0,05 mol/ℓ HCl feed solution. *Selemion* AAV and CHV membranes.
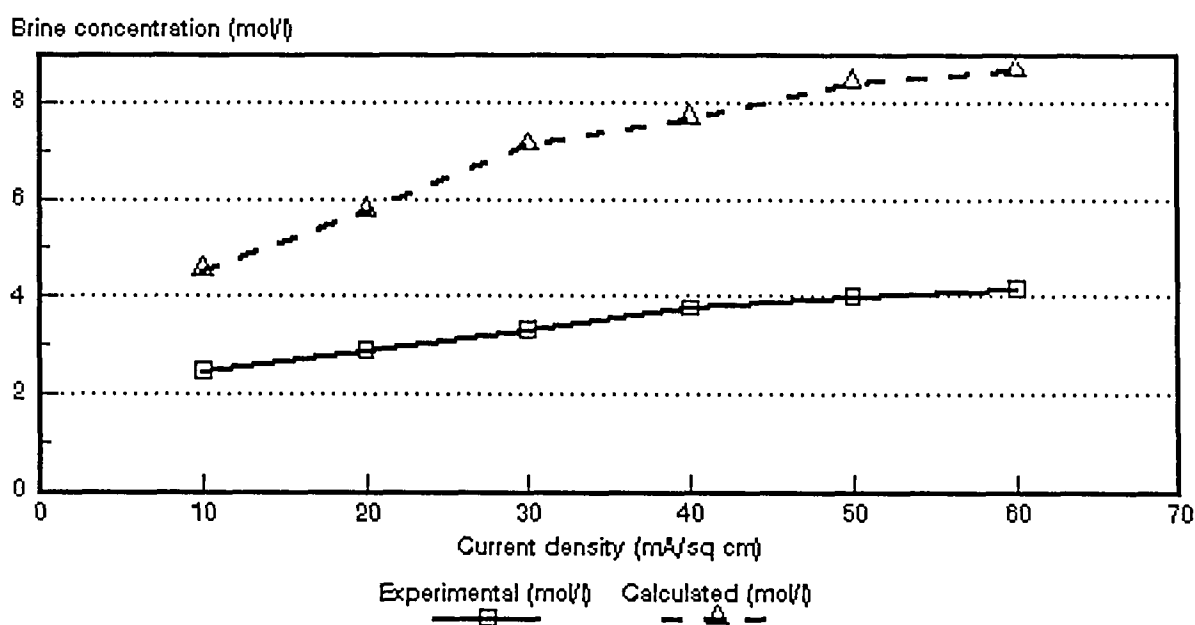
Brine concentration (mol/ℓ)

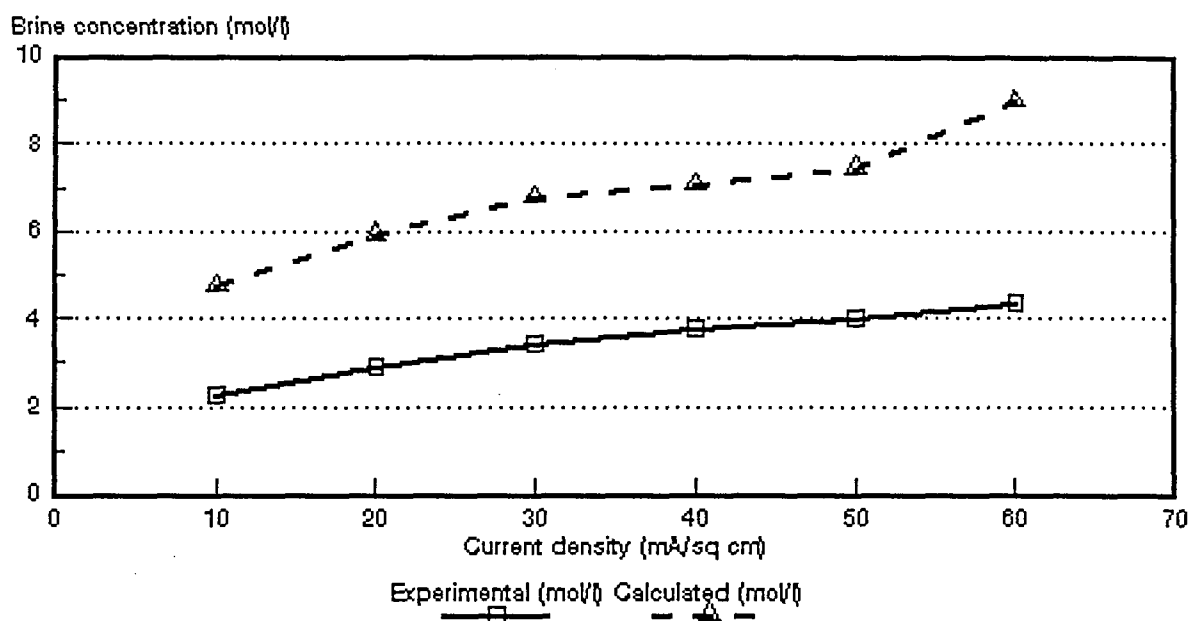Current density (mA/sq cm)

Experimental (mol/ℓ)   Calculated (mol/ℓ)

Figure 7.15: Experimental and calculated acid brine concentrations as a function of current density for 0,1 mol/ℓ HCl feed solution. *Selemion* AAV and CHV membranes.

Brine concentration (mol/ℓ)

Current density (mA/sq cm)

Experimental (mol/ℓ)   Calculated (mol/ℓ)

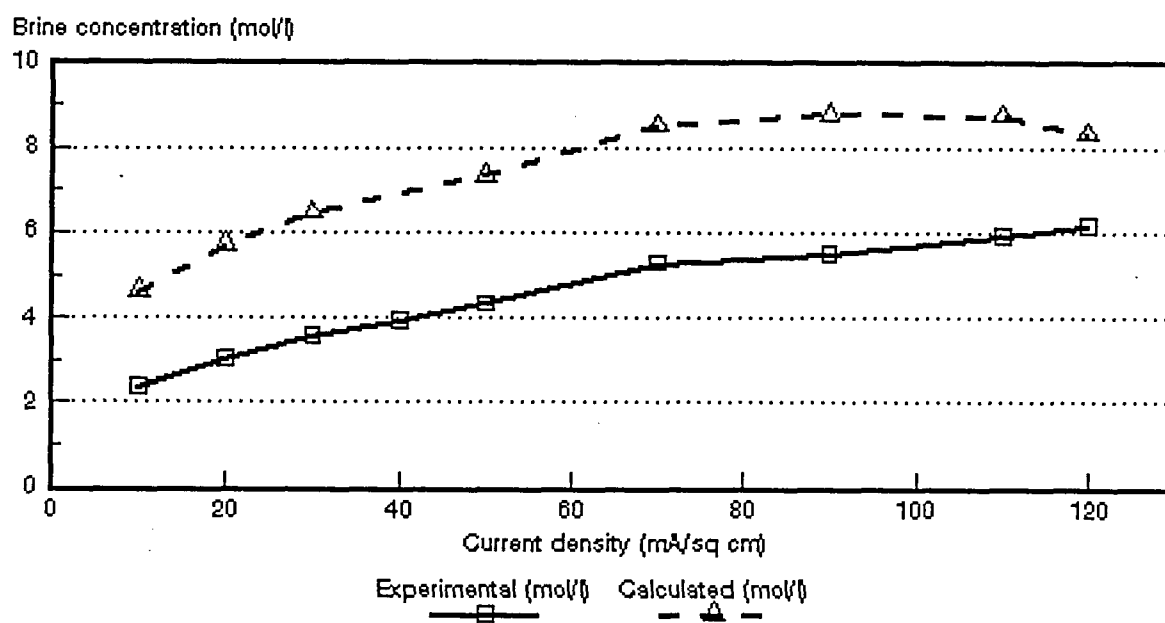**Figure 7.16:** Experimental and calculated acid brine concentrations as a function of current density for 0,5 mol/ℓ HCl feed solution. *Selemion* AAV and CHV membranes.

Brine concentration (mol/l)

Current density (mA/sq cm)

Experimental (mol/l)   Calculated (mol/l)

Figure 7.17:   Experimental and calculated acid brine concentrations as a function of
current density for 1,0 mol/l HCl feed solution. *Selemion* AAV and CHV
membranes.

Brine concentration (mol/l)

Current density (mA/sq cm)

Experimental (mol/l)   Calculated (mol/l)

Figure 7.18:   Experimental and calculated acid brine concentrations as a function of
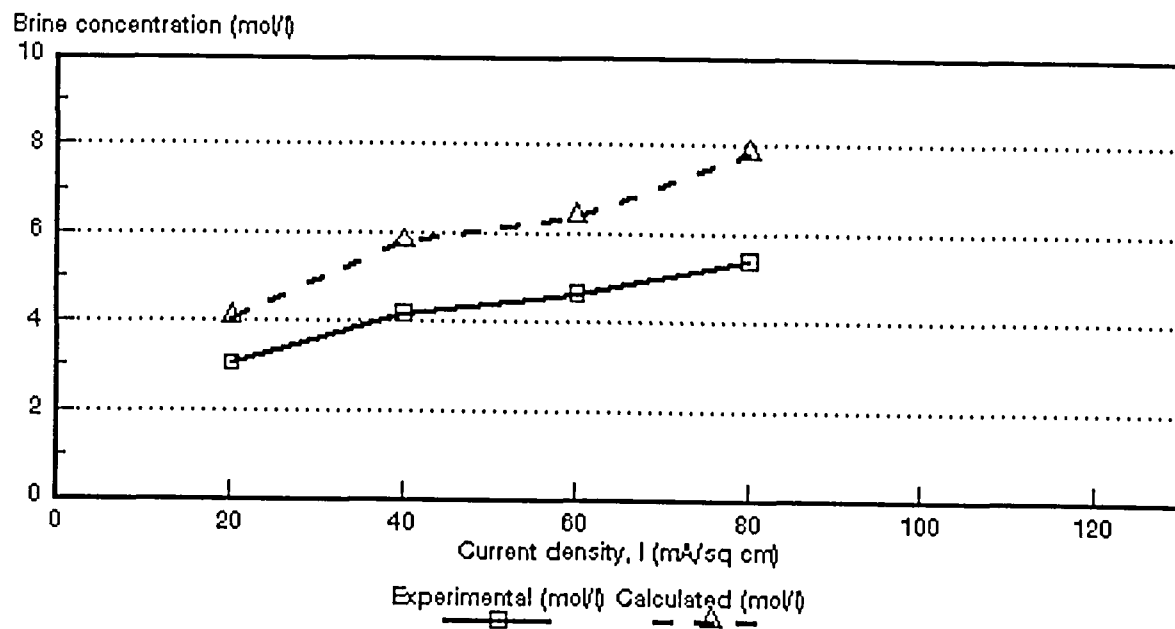current density for 0,05 mol/l HCl feed solution. ABM-3 and CHV
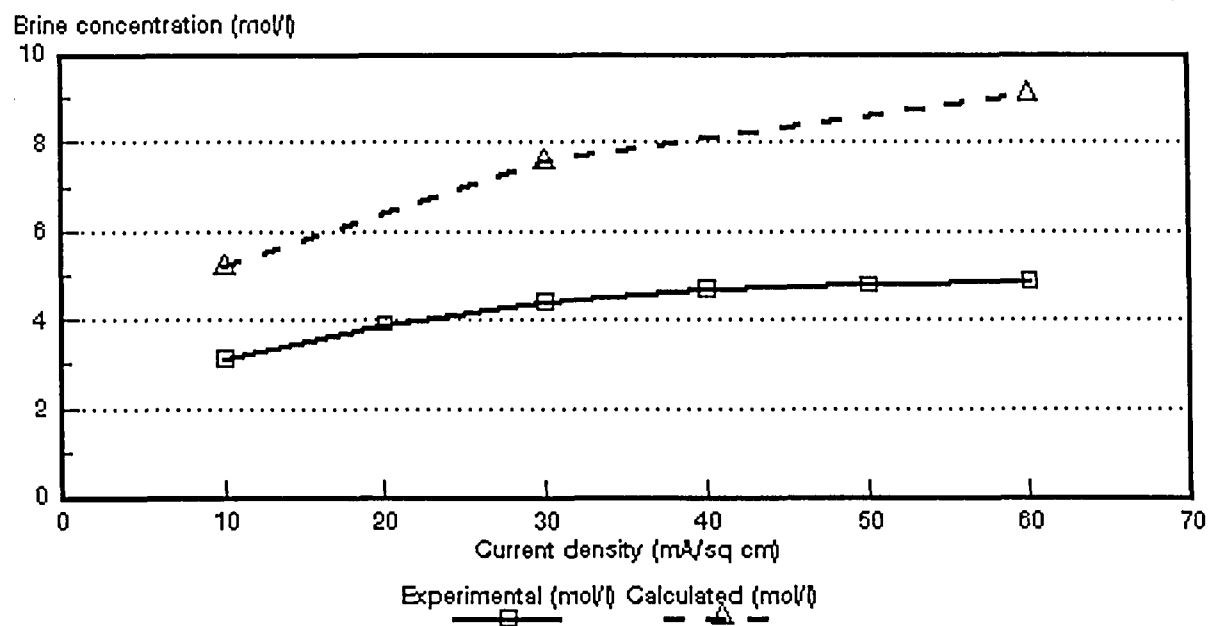membranes.

Figure 7.19: Experimental and calculated acid brine concentrations as a function of current density for 0,1 mol/ℓ HCl feed solution. ABM-3 and CHV membranes.

Figure 7.20: Experimental and calculated acid brine concentrations as a function of current density for 0,5 mol/ℓ HCl feed solution. ABM-3 and CHV membranes.

Figure 7.21: Experimental and calculated acid brine concentrations as a function of current density for 1,0 mol/ℓ HCl feed solution. ABM-3 and CHV membranes.

Figure 7.22: Experimental and calculated acid brine concentrations as a function of current density for 0,05 mol/ℓ HCl feed solution. ABM-2 and CHV membranes.
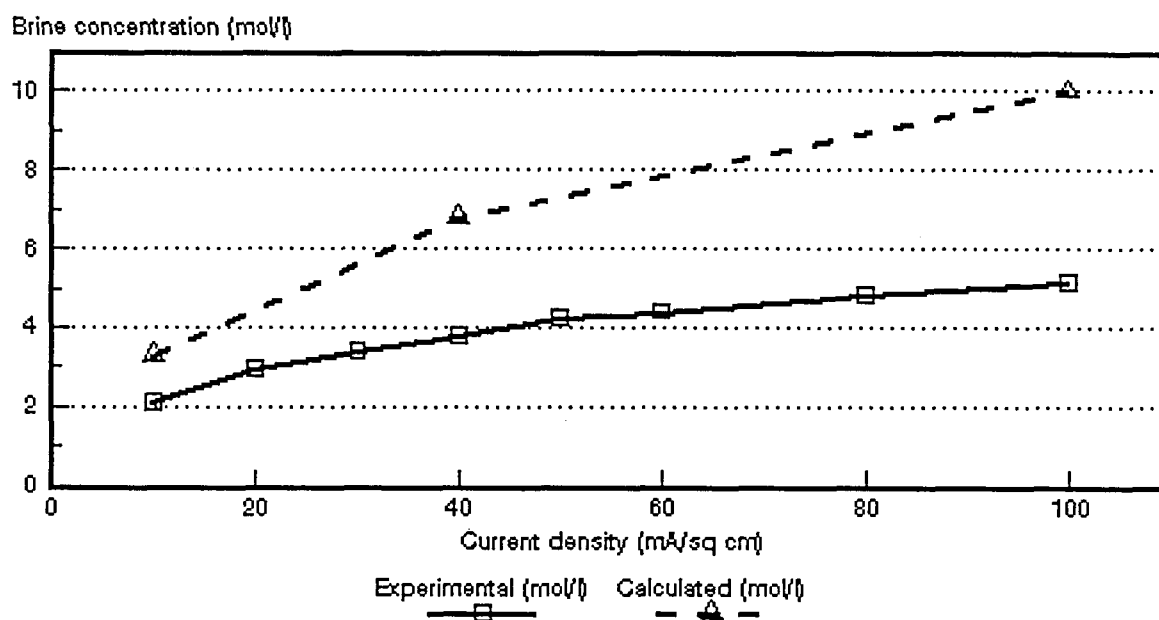
248

Figure 7.23: Experimental and calculated acid brine concentrations as a function of current density for 0,1 mol/ℓ HCl feed solution. ABM-2 and CHV membranes.
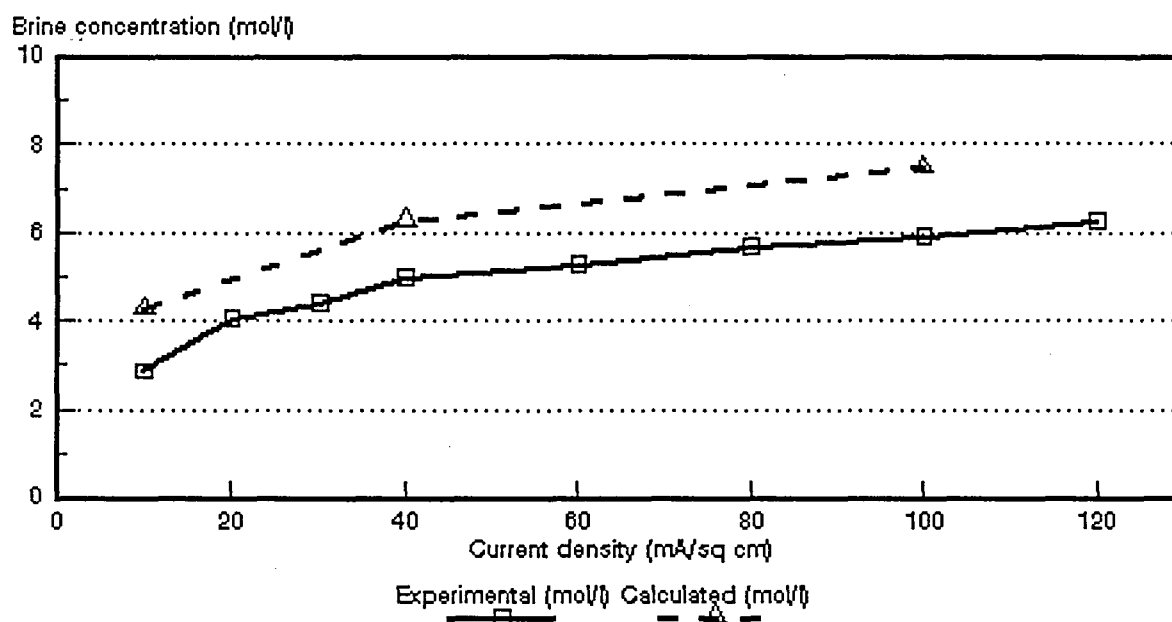

Figure 7.24: Experimental and calculated acid brine concentrations as a function of current density for 0,5 mol/ℓ HCl feed solution. ABM-2 and CHV membranes.
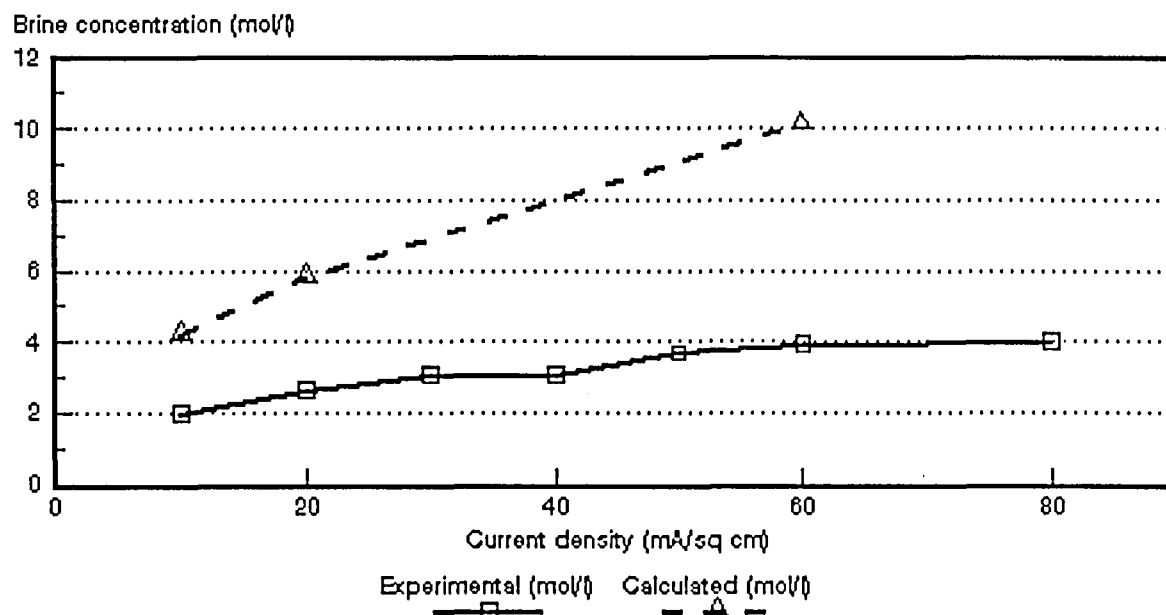
Figure 7.25: Experimental and calculated acid brine concentrations as a function of current density for 0,05 mol/ℓ HCl feed solution. ABM-1 and CHV membranes.

Figure 7.26: Experimental and calculated acid brine concentrations as a function of current density for 0,1 mol/ℓ HCl feed solution. ABM-1 and CHV membranes.

Brine concentration (mol/l)

Current density (mA/sq cm)

Experimental (mol/l)   Calculated (mol/l)

Figure 7.27: Experimental and calculated acid brine concentrations as a function of current density for 0,5 mol/ℓ HCl feed solution. ABM-1 and CHV membranes.
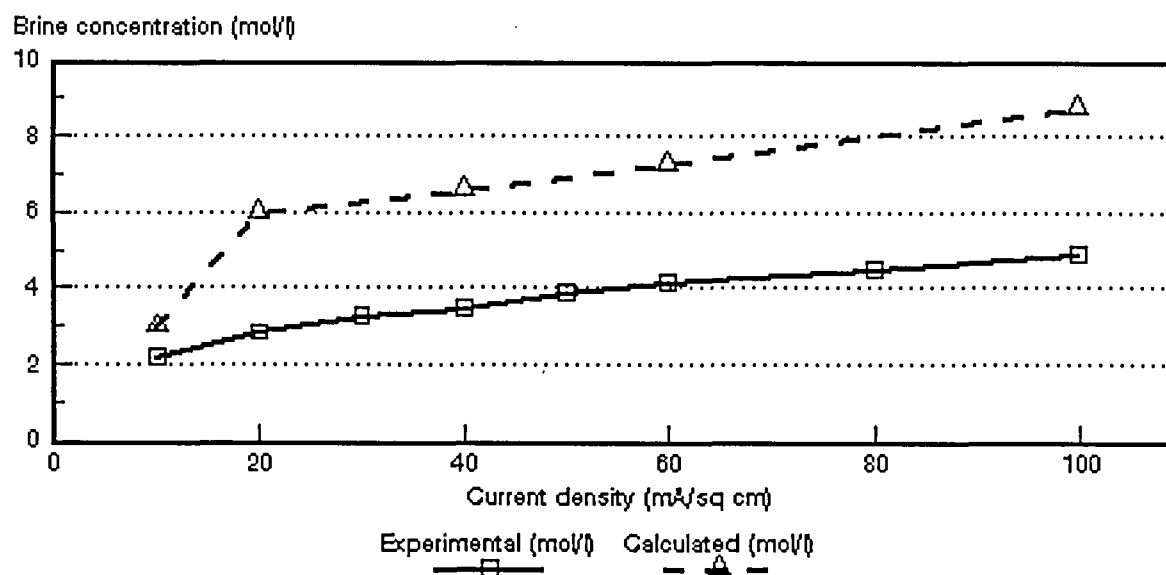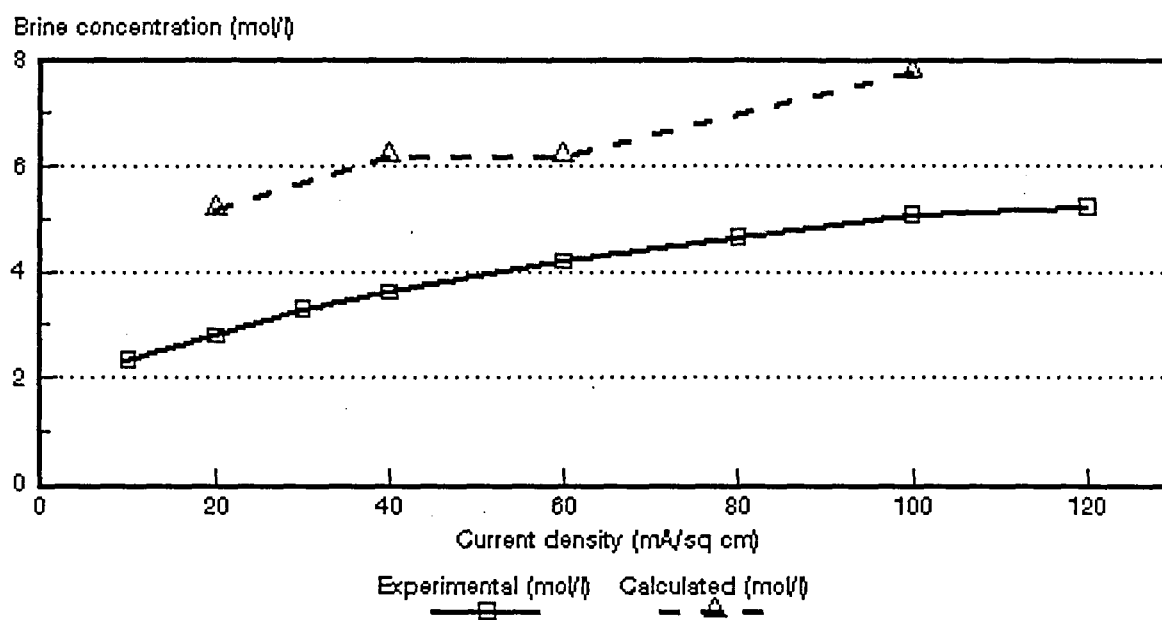
Tabel 7.20: Correlation between calculated (c_{bcalc}) and experimentally (c_{bexp}) determined acid brine concentrations.

Current Density	c_{bcalc}/c_{bexp} Selemion AMV & CMV Concentration, mol/l				Selemion AAV & CHV Concentration, mol/l				Israeli & Selemion ABM-3 & CHV Concentration, mol/l				Israeli & Selemion ABM-2 & CHV Concentration, mol/l				Israeli & Selemion ABM-1 & CHV Concentration, mol/l			
mA/cm²	0,05	0,1	0,5	1,0	0,05	0,1	0,5	1,0	0,05	0,1	0,5	1,0	0,05	0,1	0,5	1,0	0,05	0,1	0,5	1,0
10		4,95	4,13	3,96	1,88	1,91	2,24	1,91	1,84	2,10	1,93		1,65	1,57	1,49		2,12	1,36		
20		3,99	3,64	3,48	1,89	2,01			2,00	2,05	1,88	1,33					2,21	2,11	1,86	
30		3,54	3,27	3,08	1,85	1,87	1,72	1,63	2,14	1,99	1,80		1,73							
40		3,39	3,05	3,57	1,86	1,78			2,03	1,88		1,39		1,78				1,89	1,71	
50		3,05	3,12	3,17	1,86	1,83	1,70	1,59	2,11	1,87	1,69				1,25					
60		2,86	3,00	3,34	2,05	1,78		1,52	2,09	2,05		1,38	1,86				2,57	1,69	1,48	
70				3,32	1,80	1,69	1,65				1,61									
80						1,69		1,48				1,46								
90											1,60									
100						1,68	1,48	1,53						1,26				1,79	1,53	
110											1,47			1,93						
120											1,35									
130																				
140							1,40	1,49												
150																				
160																				
170																				
180								1,53												

252

7.2 Current Efficiency

Current efficiency (e_p) determined during EOP experiments as a function of current density is shown in Figures 7.28 to 7.32. Current efficiency was determined to be very low (approximately 13 to 16%) for the *Selemion* AMV and CMV membranes (Fig. 7.28). This low current efficiency can be ascribed to the low permselectivity of the *Selemion* AMV membranes for chloride ions (proton leakage) (Tables 7.1 to 7.3). The permselectivity (Δt^a) of the *Selemion* AMV membrane was shown to vary between 0,3 and 0,02 at 0,1 mol/ℓ acid feed concentration at different concentration gradients in the current density range from 10 to 60 mA/cm². Permselectivities varied from 0,15 to 0,08 and from 0,09 to 0,18 at 0,54 and 1,0 mol/ℓ acid feed concentration, respectively. Therefore, the *Selemion* AMV membrane has a very low permselectivity for chloride ions.

Current efficiencies obtained with the *Selemion* AAV and CHV membranes were much higher than current efficiencies obtained with the *Selemion* AMV and CMV membranes (Fig. 7.29). Current efficiency of the *Selemion* AAV and CHV membranes was determined at approximately 40%. The apparent transport numbers of the anion-exchange membrane were much higher in this case (Table 7.4 to 7.7) than in the case of the Selemion AMV membrane. The apparent transport numbers for the AAV anion-exchange membrane (Δt^a) varied between 0,67 and 0,49 at 0,05 mol/ℓ feed concentration (Table 7.4). Approximately the same values were obtained for the apparent transport number of the *Selemion* AAV membrane in the 0,1 to 1,0 mol/ℓ feed concentration range. Current efficiencies obtained for the ABM-3 and CHV membranes were slightly lower than that obtained for the *Selemion* AAV and CHV membranes in the 0,05 to 0,5 mol/ℓ feed concentration range (Fig. 7.30). Current efficiency was determined at approximately 37%. However, current efficiency for the ABM-3 and CHV membranes was much higher at 1,0 mol/ℓ feed concentration. Current efficiency varied between 60 and 47%. Current efficiency for the ABM-2 and CHV membranes was initially higher than 40% (Fig. 7.31) but then decreased to between 30 and 40%. Current efficiency for the ABM-1 and CHV membranes was determined at between 25 and 40%. It is interesting to note that current efficiency has increased with increasing acid feed concentration in the case of the ABM and CHV membranes.

Current efficiency remained almost constant with increasing current density and increasing acid feed concentration in the case of the *Selemion* AMV and CMV and

Selemion AAV and CHV membranes (Figs. 7.28 and 7.29). However, current efficiency decreased somewhat with increasing current density in the case of the ABM-3, ABM-2 and ABM-1 membranes (Fig's. 7.30 to 7.32). This was more pronounced at the lower acid feed concentrations. Therefore, it appeared that the limiting current density was exceeded. However, current efficiency remained approximately constant at the higher acid feed concentrations (0,5 mol/ℓ) at high current densities showing that polarization was absent.

The apparent transport numbers ($\overline{\Delta t}$, Δt^a and Δt^c) for a concentration difference similar to that obtained in the EOP experiments are shown in Figures 7.33 to 7.49. The current efficiencies (e_p) as determined by the EOP method and shown in Figures 7.28 to 7.32 are also shown in Figures 7.33 to 7.49. The correlation between the apparent transport numbers ($\overline{\Delta t}$, Δt^a, Δt^c) and current efficiency is shown in Tables 7.21 to 7.23.

The apparent transport numbers ($\overline{\Delta t}$'s) were much higher than the current efficiencies (e_p's) as determined by the EOP method (Tables 7.21 to 7.23 and Figs. 7.33 to 7.49). The apparent transport numbers were from 3 to 5 times higher than the current efficiencies in the case of the *Selemion* AMV and CMV membranes in the acid feed concentration and current density ranges investigated (Table 7.21). In the case of the Selemion AAV and CHV membranes the apparent transport numbers were 1,5 to 2 times higher than the current efficiencies. Much the same results were found for the ABM and CHV membranes. Therefore, it appears that a simple membrane potential measurement cannot be used effectively in the case of acids to predict membrane performance accurately. The reason for the big difference between the apparent transport number and the current efficiency may be ascribed to backdiffusion of acid during EOP of acids.

It is interesting to note that much better correlations have been obtained between the apparent transport numbers of the anion membranes (Δt^a) and current efficiencies (Table 7.22). The apparent transport numbers were approximately 1,3 to 1,4 times higher than the current efficiencies in the case of the *Selemion* AAV and CHV membranes in the current density range from 30 to 70 mA/cm² (0,5 mol/ℓ feed). An even better correlation was obtained at 1,0 mol/ℓ feed concentration in the current density range from 40 to 140 mA/cm². The apparent transport numbers were from 1,05 to 1,19 times higher than current efficiencies in this range. The ratio between apparent transport number and current efficiency ($\Delta t^a/e_p$) varied between 1,22 and 0,86 for the ABM-3 and CHV membranes in the current density range from 30 to 70
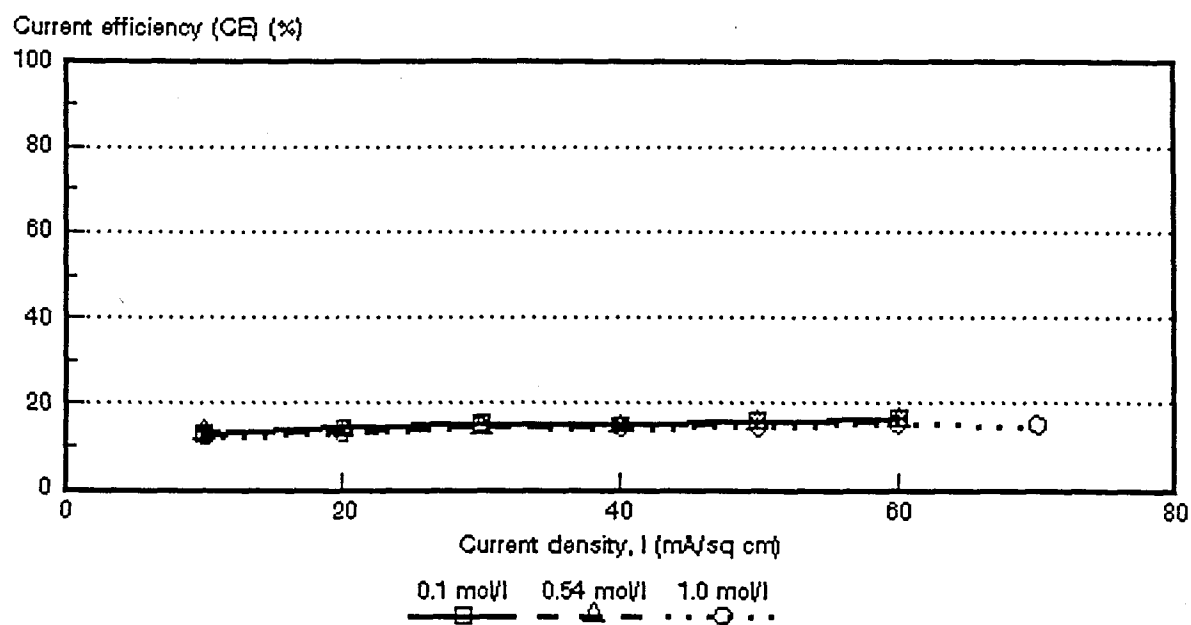
Current efficiency (CE) (%)

Figure 7.28: Current efficiency (ε_p) as a function of current density for 3 different HCl feed concentrations. *Selemion* AMV and CMV membranes.
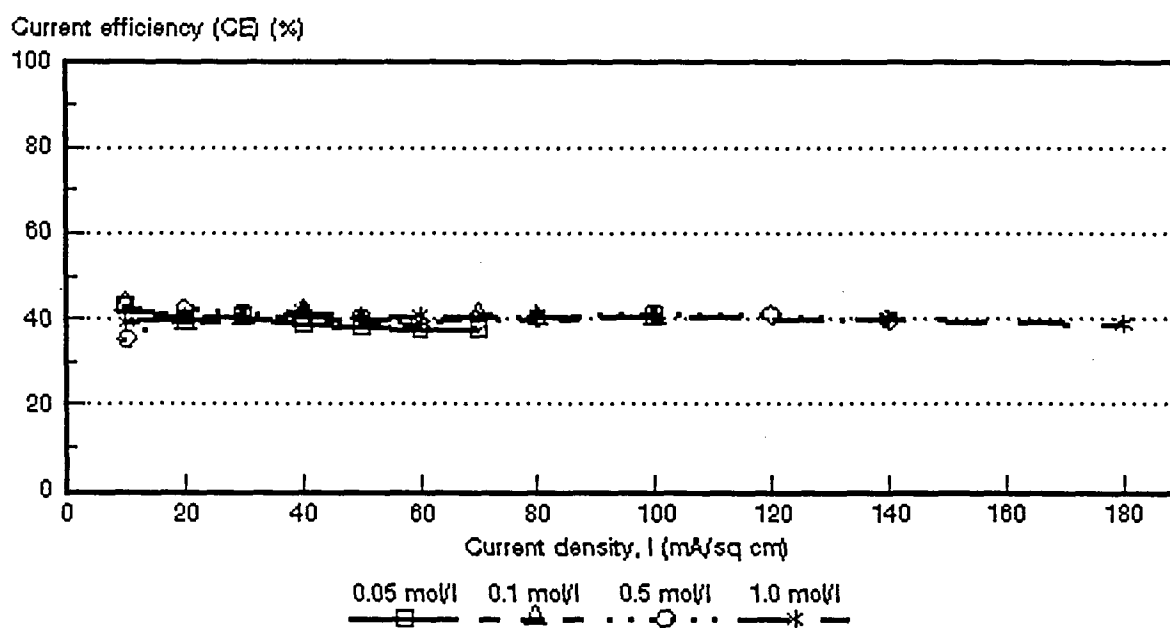
Current efficiency (CE) (%)

Figure 7.29: Current efficiency (ε_p) as a function of current density for 4 different HCl feed concentrations. *Selemion* AAV and CHV membranes.

255

Current efficiency (CE) (%)

Current density,I(mA/sq cm)
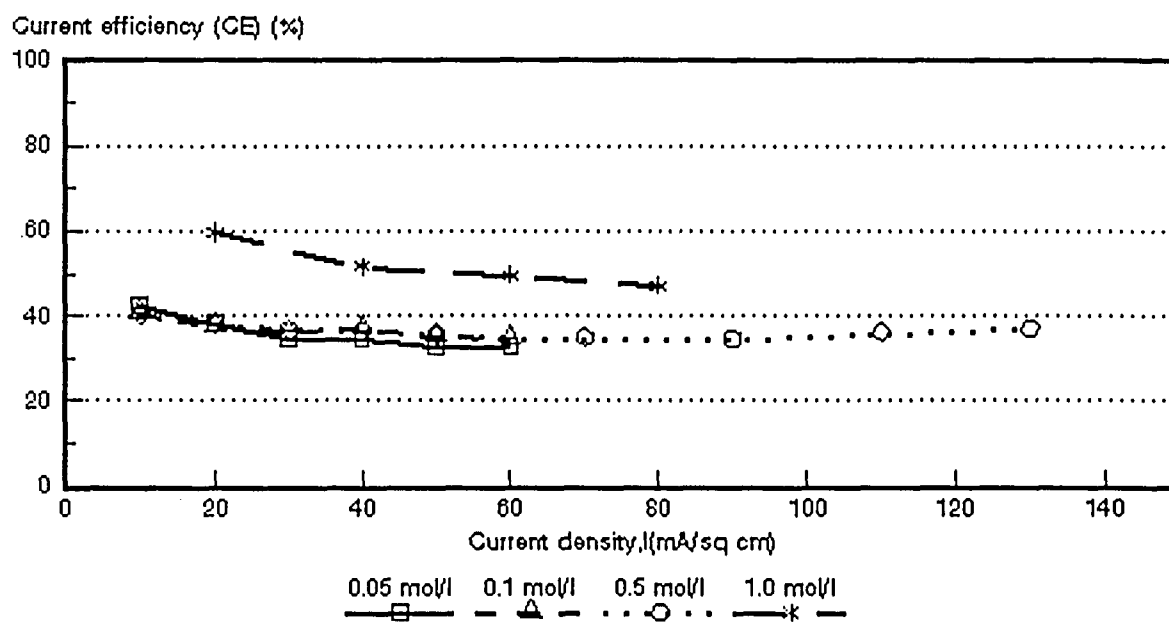
0.05 mol/l   0.1 mol/l   0.5 mol/l   1.0 mol/l

Figure 7.30:   Current efficiency (ϵ_p) as a function of current density for 4 different HCl feed concentrations. ABM-3 and *Selemion* CHV membranes.
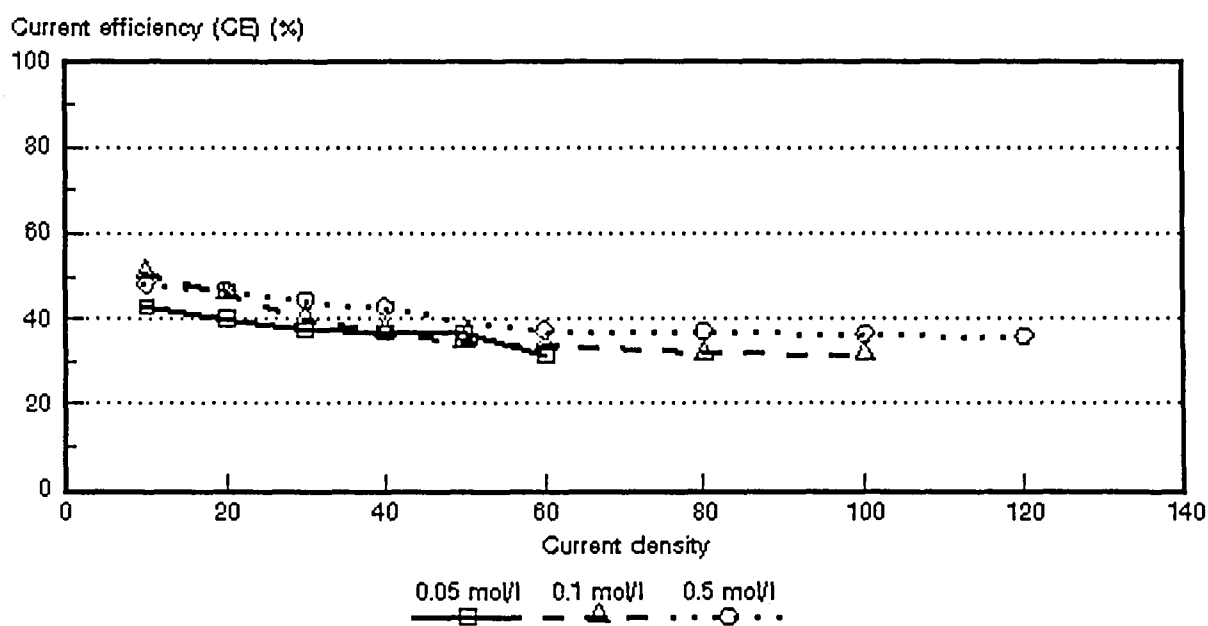
Current efficiency (CE) (%)

Current density

0.05 mol/l   0.1 mol/l   0.5 mol/l

Figure 7.31:   Current efficiency (ϵ_p) as a function of current density for 3 different HCl feed concentrations. ABM-2 and *Selemion* CHV membranes.
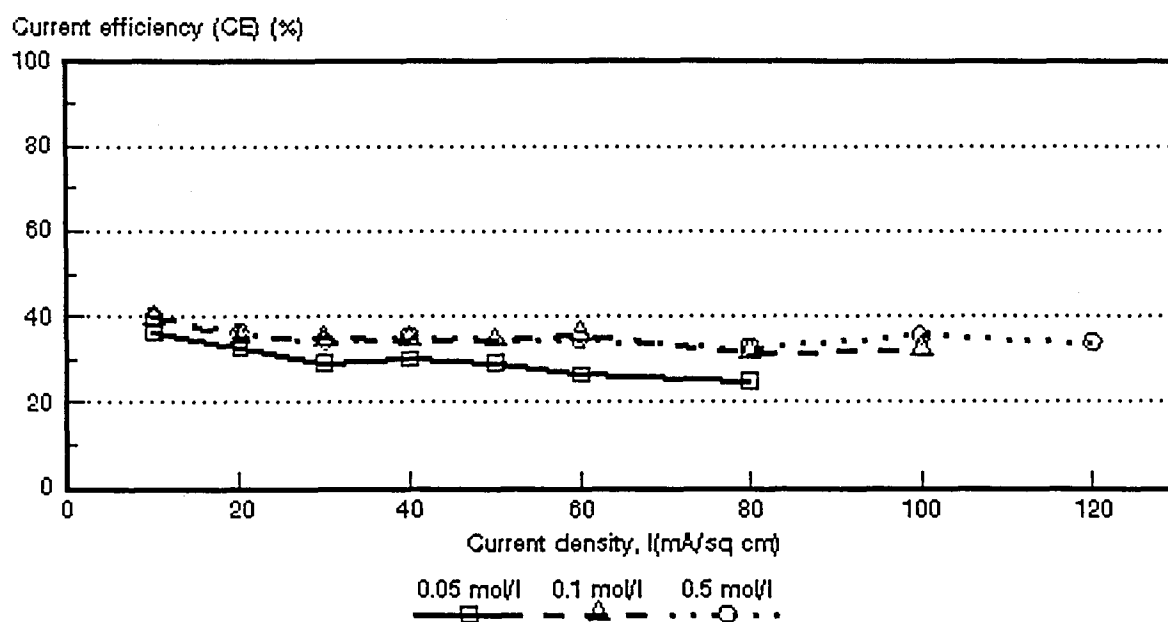
Current efficiency (CE) (%)

Current density, I(mA/sq cm)

0.05 mol/l   0.1 mol/l   0.5 mol/l

Figure 7.32: **Current efficiency (ε_p) as a function of current density for 3 different HCl feed concentrations. ABM-1 and *Selemion* CHV membranes.**

CE ; Delta t ; Delta ta and Delta tc (%)

Current density,I(mA/sq cm)

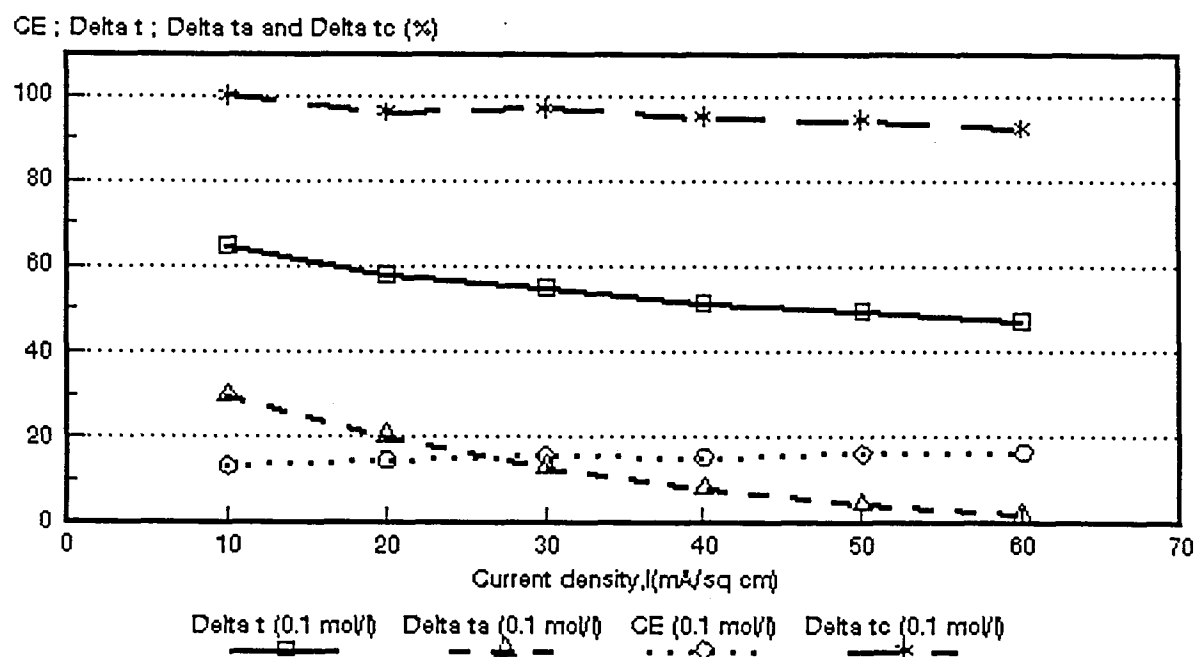Delta t (0.1 mol/l)   Delta ta (0.1 mol/l)   CE (0.1 mol/l)   Delta tc (0.1 mol/l)

Figure 7.33: **Current efficiency (CE = ε_p) as a function of current density for 0,1 mol/ℓ HCl feed. *Selemion* AMV and CMV membranes. Delta t = $\overline{\Delta}$t; Delta ta = Δt^a; Delta tc = Δt^c**
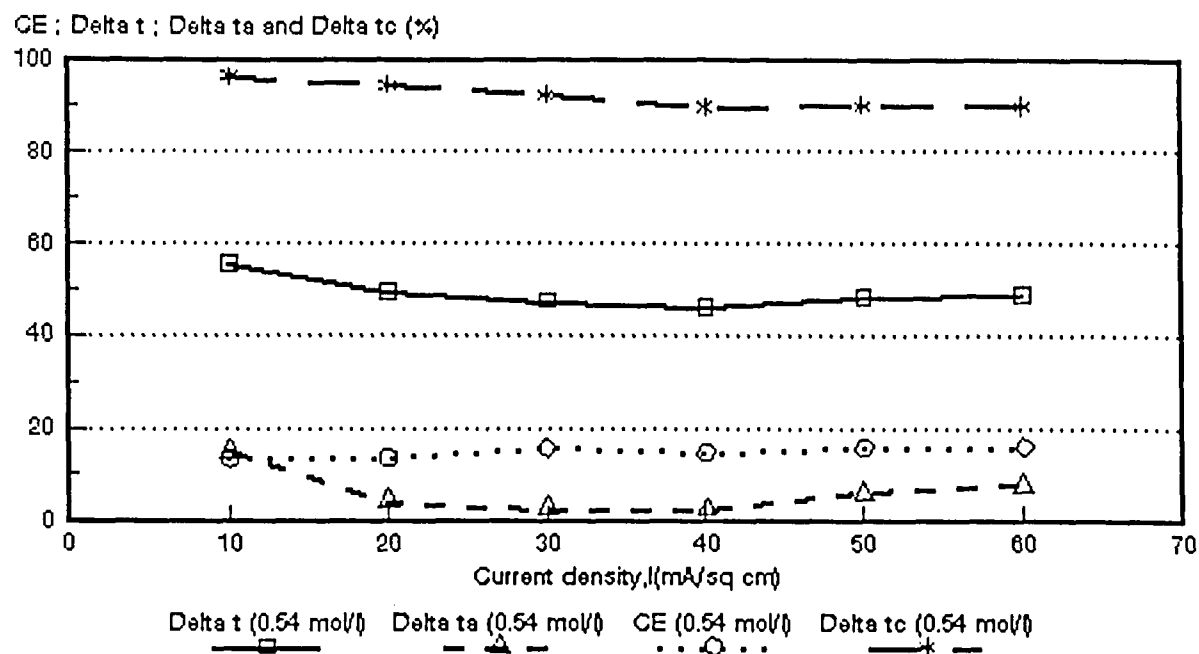
Figure 7.34: Current efficiency (CE = c_p) as a function of current density for 0,54 mol/ℓ HCl feed. *Selemion* AMV and CMV membranes. Delta t = $\overline{\Delta}$t; Delta ta = Δt^a; Delta tc = Δt^c
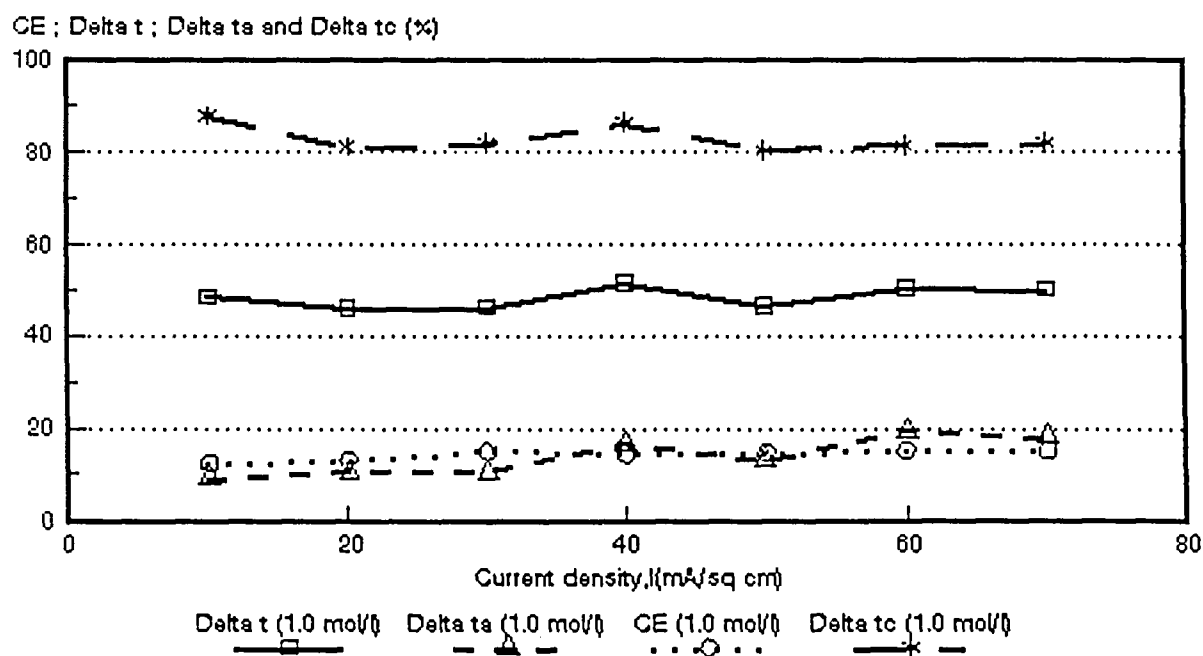
Figure 7.35: Current efficiency (CE = ϵ_p) as a function of current density for 1,0 mol/ℓ HCl feed. *Selemion* AMV and CMV membranes. Delta t = $\overline{\Delta}$t; Delta ta = Δt^a; Delta tc = Δt^c

CE ; Delta t ; Delta ta and Delta tc (%)

Current density,I(mA/sq cm)

Delta t (0.05 mol/l)   Delta ta (0.05 mol/l)   CE (0.05 mol/l)   Delta tc (0.05 mol/l)

Figure 7.36: Current efficiency (CE $= e_p$) as a function of current density for 0,05 mol/ℓ HCl feed. *Selemion* AMV and CMV membranes. Delta t $= \bar{\Delta}$t; Delta ta $= \Delta t^a$; Delta tc $= \Delta t^c$
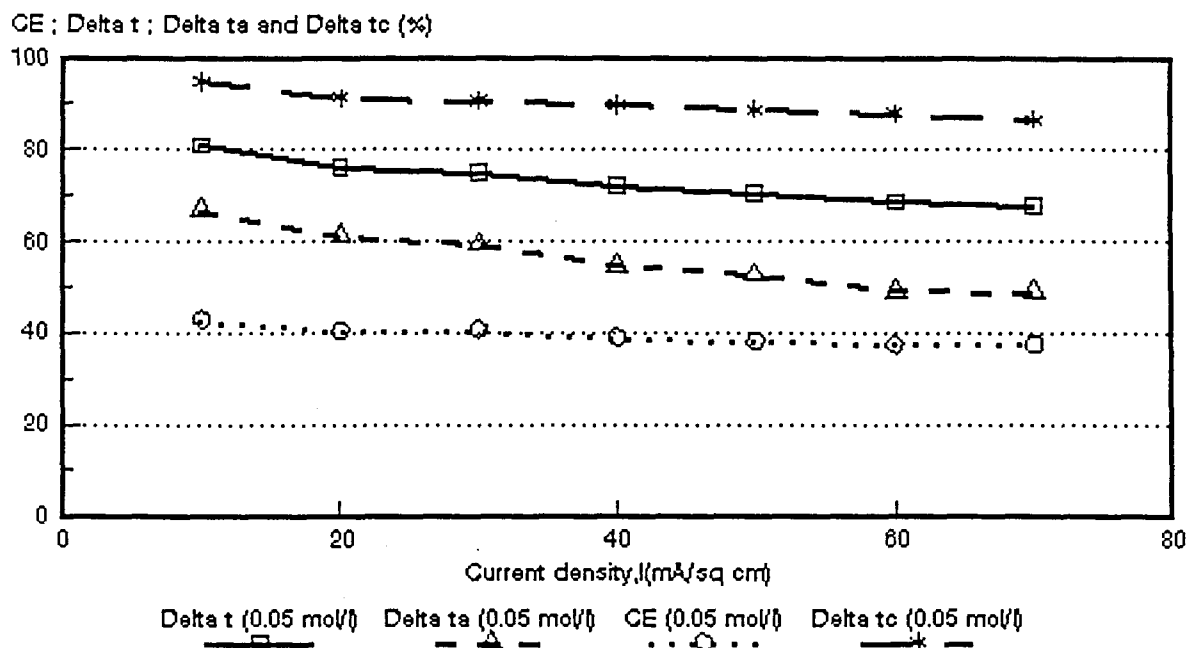
CE ; Delta t ; Delta ta and Delta tc (%)

Current density,I(mA/sq cm)

Delta t (0.1 mol/l)   Delta ta (0.1 mol/l)   CE (0.1 mol/l)   Delta tc (0.1 mol/l)

Figure 7.37: Current efficiency (CE $= e_p$) as a function of current density for 0,1 mol/ℓ HCl feed. *Selemion* AAV and CHV membranes. Delta t $= \bar{\Delta}$t; Delta ta $= \Delta t^a$; Delta tc $= \Delta t^c$

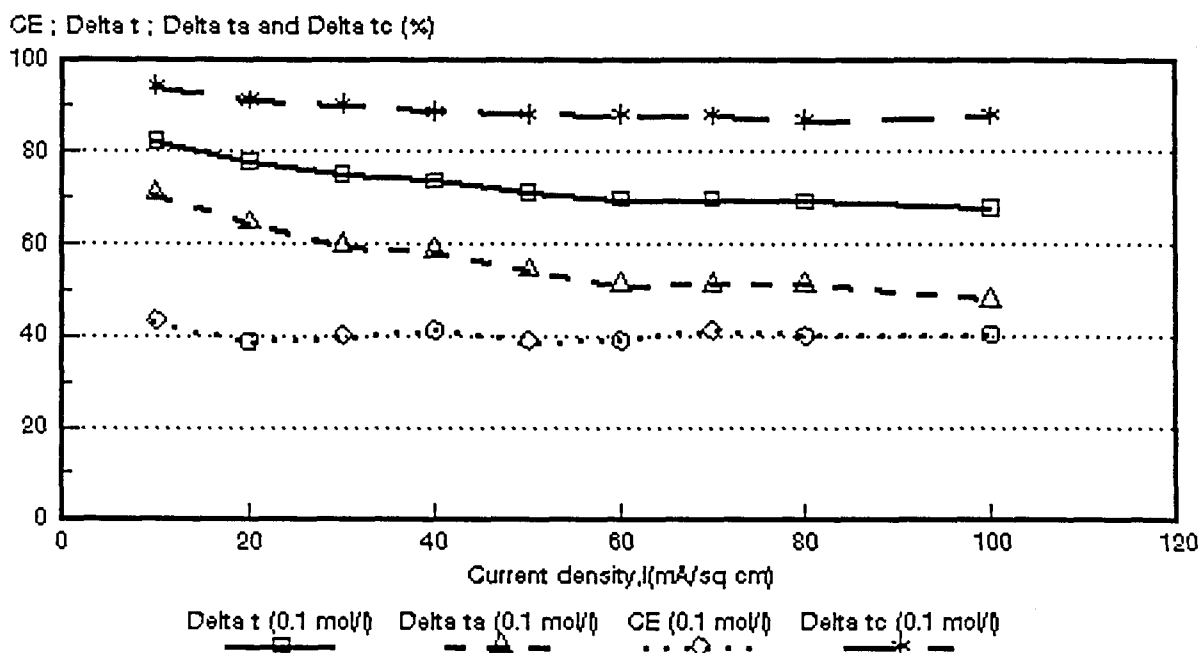CE ; Delta t ; Delta ta and Delta tc (%)

Figure 7.38:   Current efficiency (CE = e_p) as a function of current density for 0,5 mol/ℓ
HCl feed. *Selemion* AAV and CHV membranes. Delta t = $\overline{\Delta}$t;
Delta ta = Δt^a;   Delta tc = Δt^c
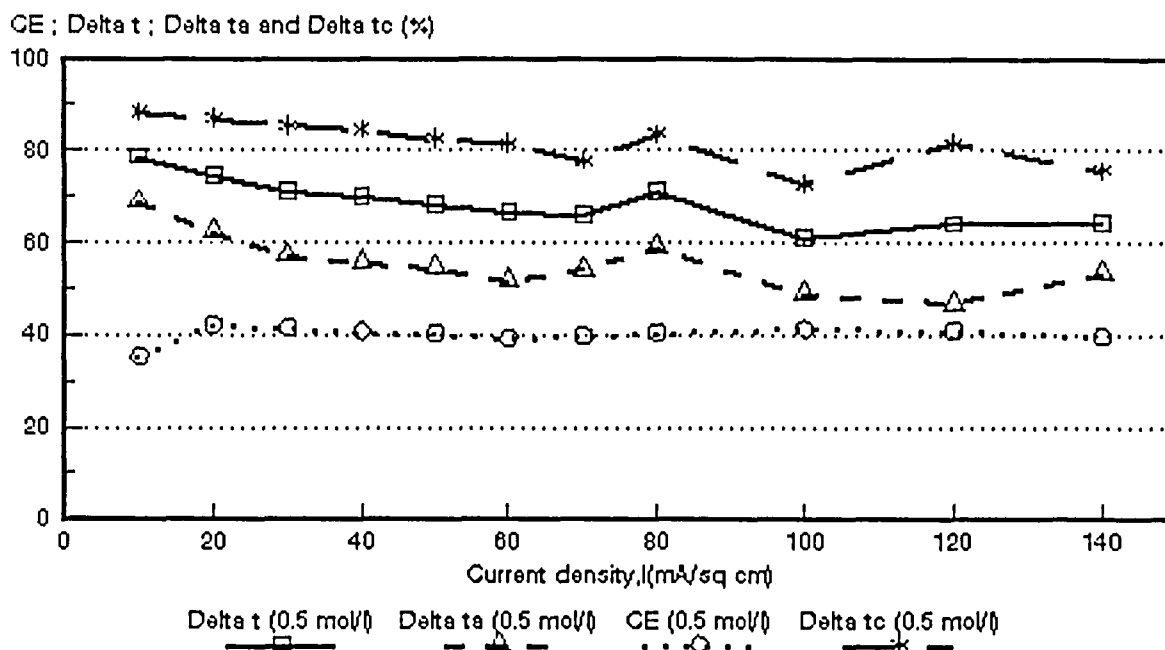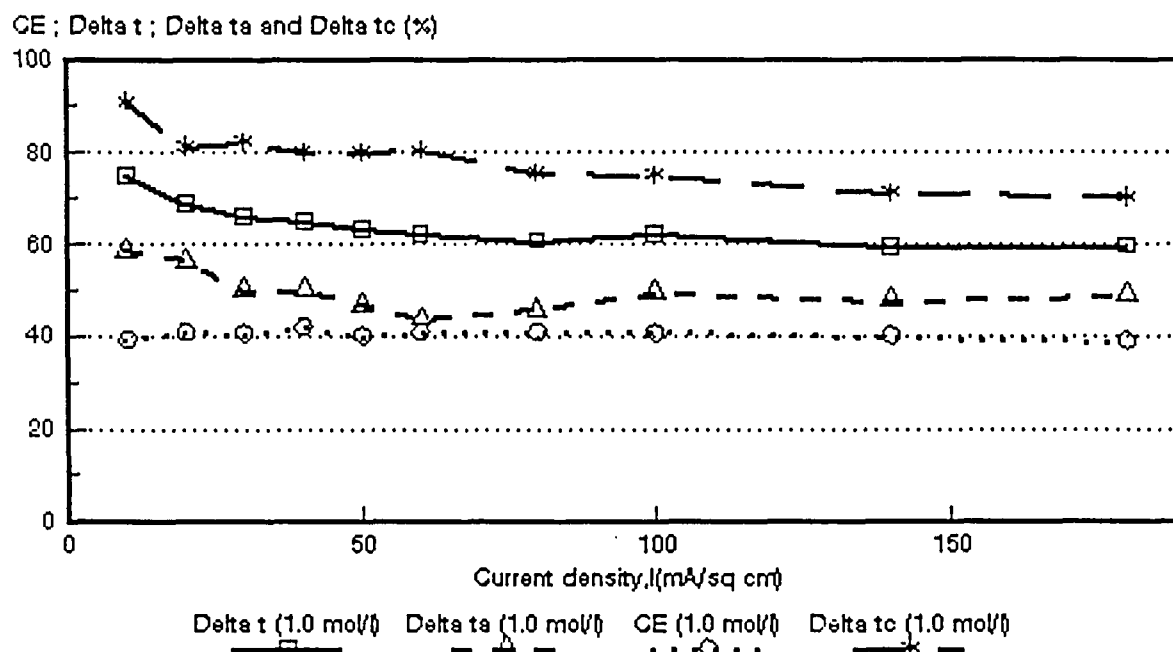
CE ; Delta t ; Delta ta and Delta tc (%)

Figure 7.39:   Current efficiency (CE = e_p) as a function of current density for 1,0 mol/ℓ
HCl feed. *Selemion* AAV and CHV membranes. Delta t = $\overline{\Delta}$t;
Delta ta = Δt^a;   Delta tc = Δt^c

260

Figure 7.40: Current efficiency (CE = ϵ_p) as a function of current density for 0,05 mol/ℓ HCl feed. *Selemion* ABM-3 and CHV membranes. Delta t = $\overline{\Delta}$t; Delta ta = Δt^a; Delta tc = Δt^c

Figure 7.41: Current efficiency (CE = ϵ_p) as a function of current density for 0,1 mol/ℓ HCl feed. ABM-3 and *Selemion* CHV membranes. Delta t = $\overline{\Delta}$t; Delta ta = Δt^a; Delta tc = Δt^c
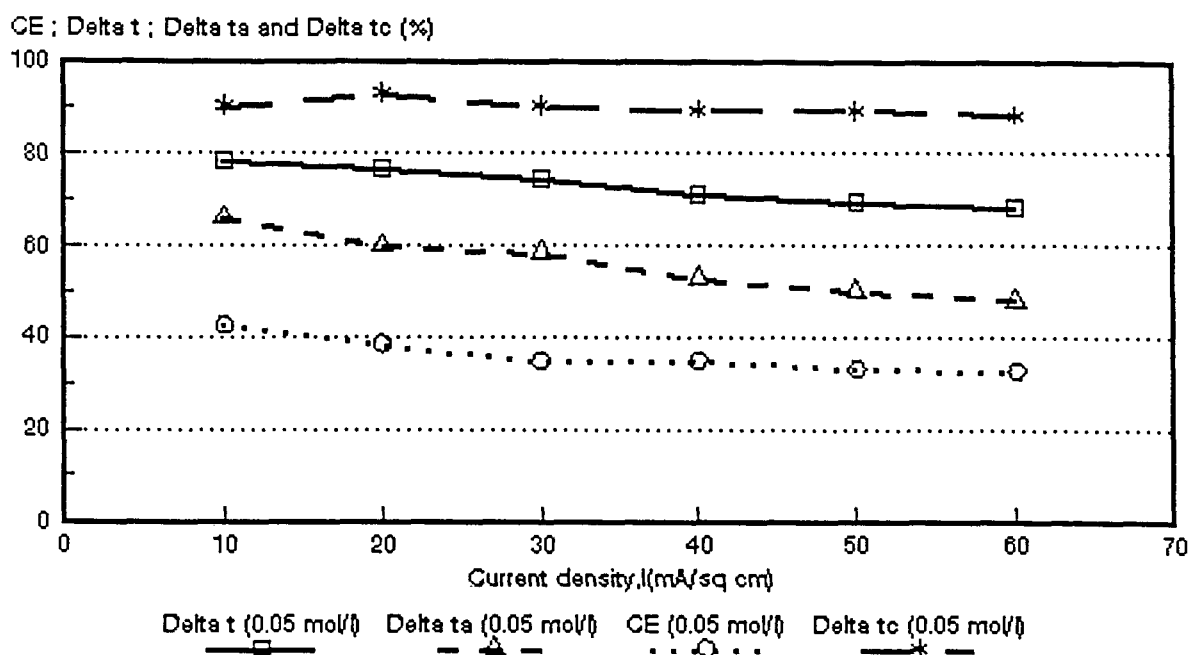
CE ; Delta t ; Delta ta and Delta tc (%)

Figure 7.42: Current efficiency (CE = ϵ_p) as a function of current density for 0,5 mol/ℓ HCl feed. *Selemion* ABM-3 and CHV membranes. Delta t = $\bar{\Delta}$t; Delta ta = Δt^a; Delta tc = Δt^c

CE ; Delta t ; Delta ta and Delta tc (%)

Figure 7.43: Current efficiency (CE = ϵ_p) as a function of current density for 1,0 mol/ℓ HCl feed. ABM-3 and *Selemion* CHV membranes. Delta t = $\bar{\Delta}$t; Delta ta = Δt^a; Delta tc = Δt^c
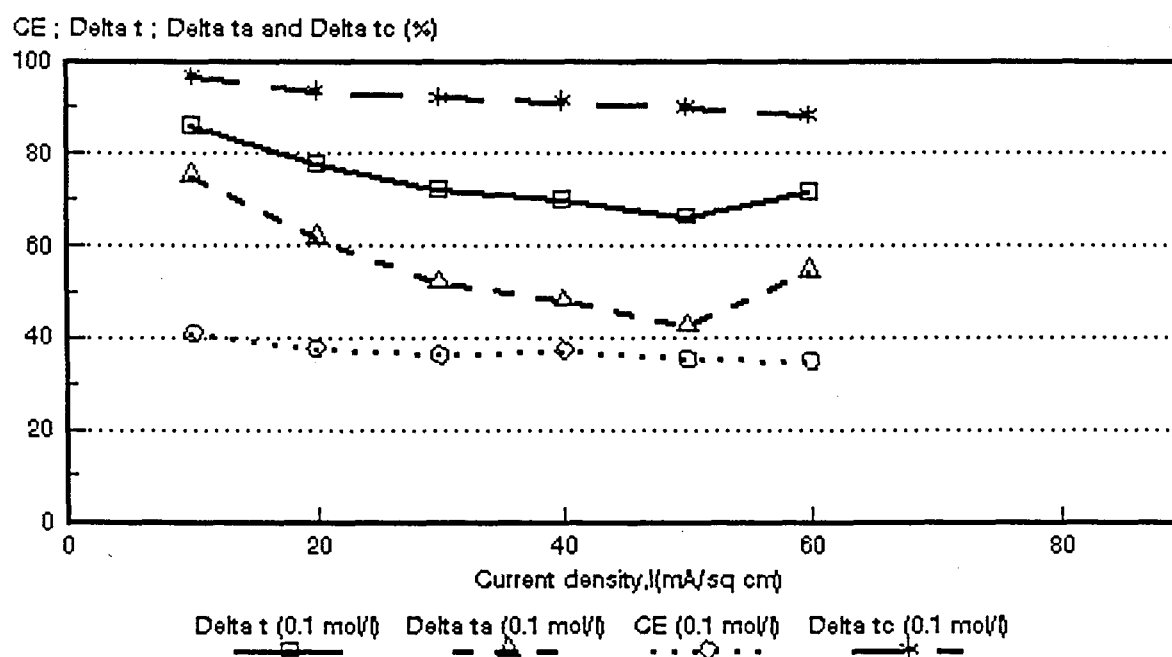
Figure 7.44: Current efficiency (CE = e_p) as a function of current density for 0,05 mol/ℓ HCl feed. ABM-2 and *Selemion* CHV membranes. Delta t = $\bar{\Delta}$t; Delta ta = Δt^a; Delta tc = Δt^c

Figure 7.45: Current efficiency (CE = e_p) as a function of current density for 0,1 mol/ℓ HCl feed. ABM-2 and Selemion CHV membranes. Delta t = $\bar{\Delta}$t; Delta ta = Δt^a; Delta tc = Δt^c
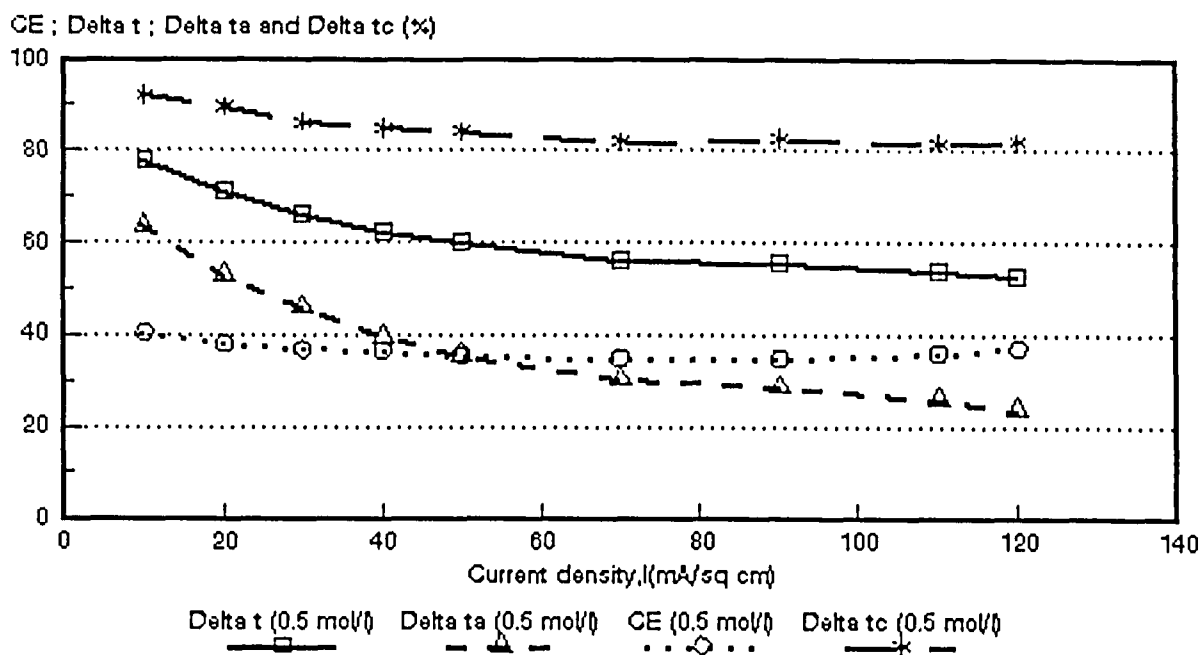
CE ; Delta t ; Delta ta and Delta tc (%)

Figure 7.46: Current efficiency (CE = ϵ_p) as a function of current density for 0,5 mol/ℓ HCl feed. ABM-2 and *Selemion* CHV membranes. Delta t = $\bar{\Delta}$t; Delta ta = Δt^a; Delta tc = Δt^c.

CE ; Delta t ; Delta ta and Delta tc (%)

Figure 7.47: Current efficiency (CE = ϵ_p) as a function of current density for 0,05 mol/ℓ HCl feed. ABM-1 and *Selemion* CHV membranes. Delta t = $\bar{\Delta}$t; Delta ta = Δt^a; Delta tc = Δt^c.

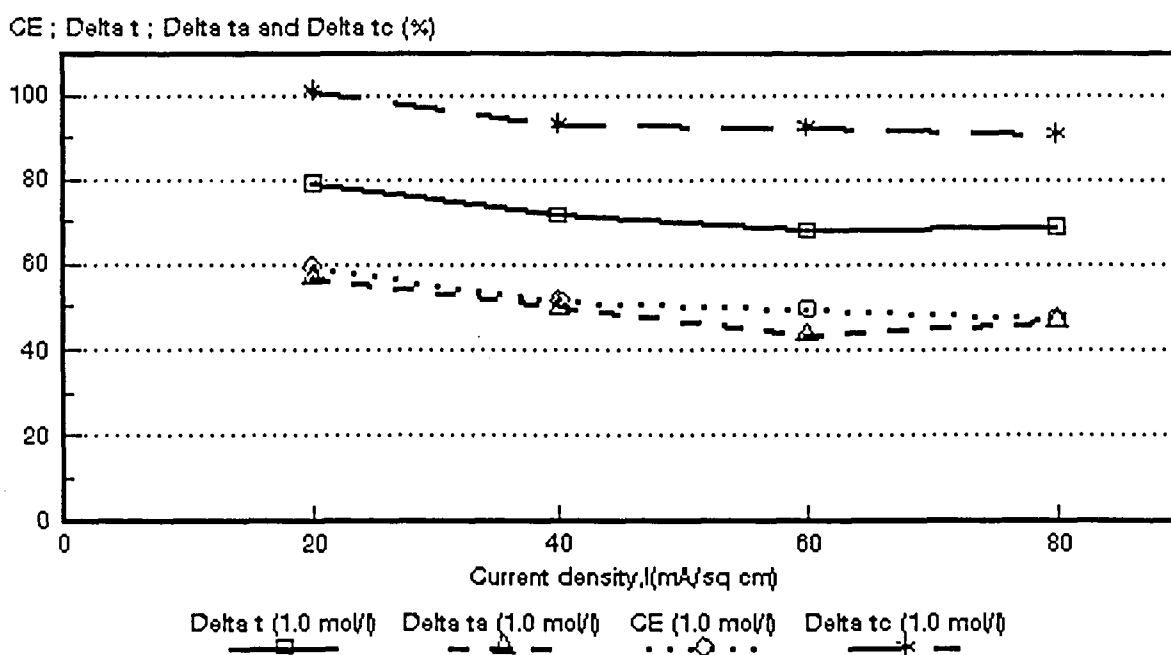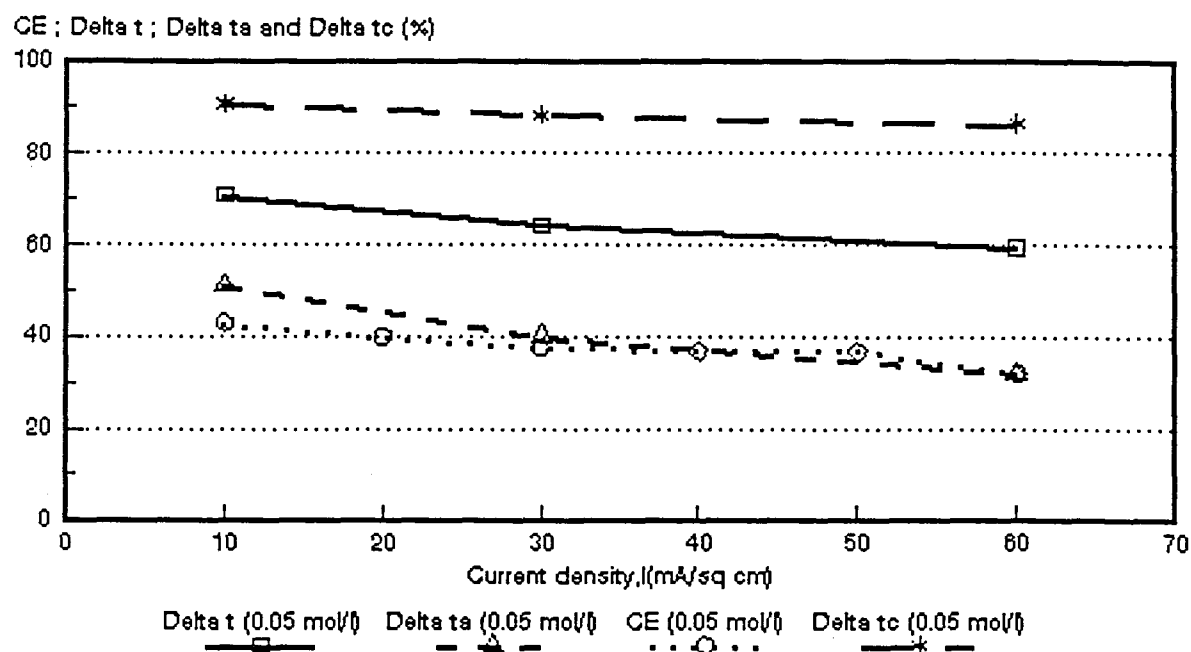CE ; Delta t ; Delta ta and Delta tc (%)

Figure 7.48: Current efficiency (CE = e_p) as a function of current density for 0,1 mol/ℓ HCl feed. ABM-1 and *Selemion* CHV membranes. Delta t = $\bar{\Delta}$t; Delta ta = Δt^a; Delta tc = Δt^c.
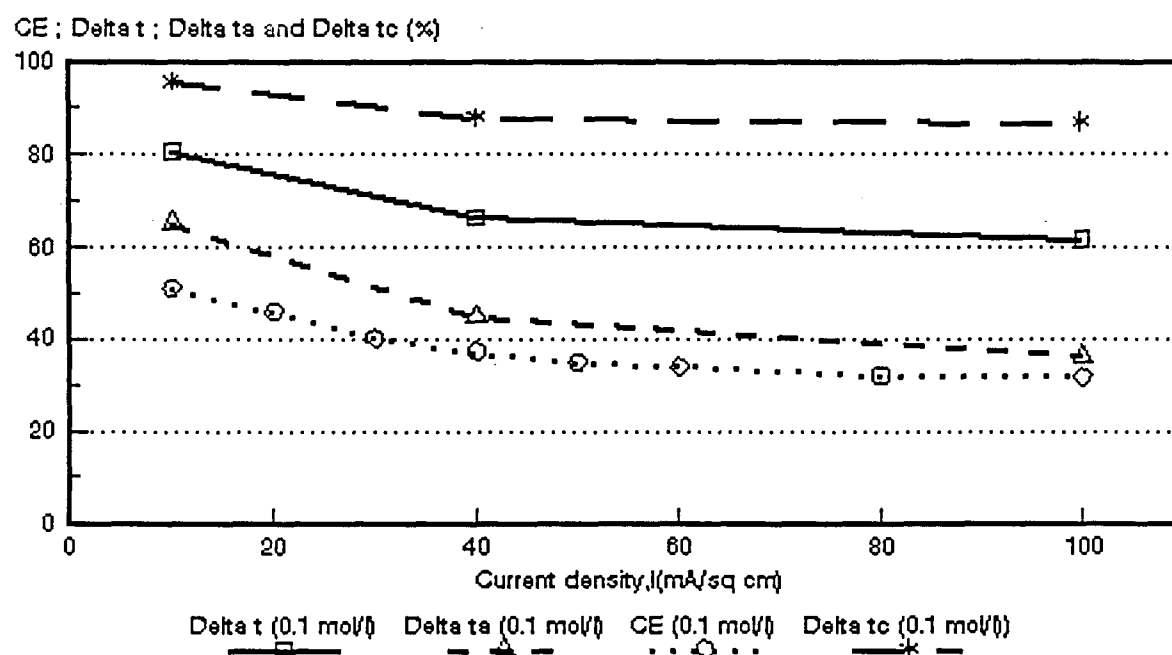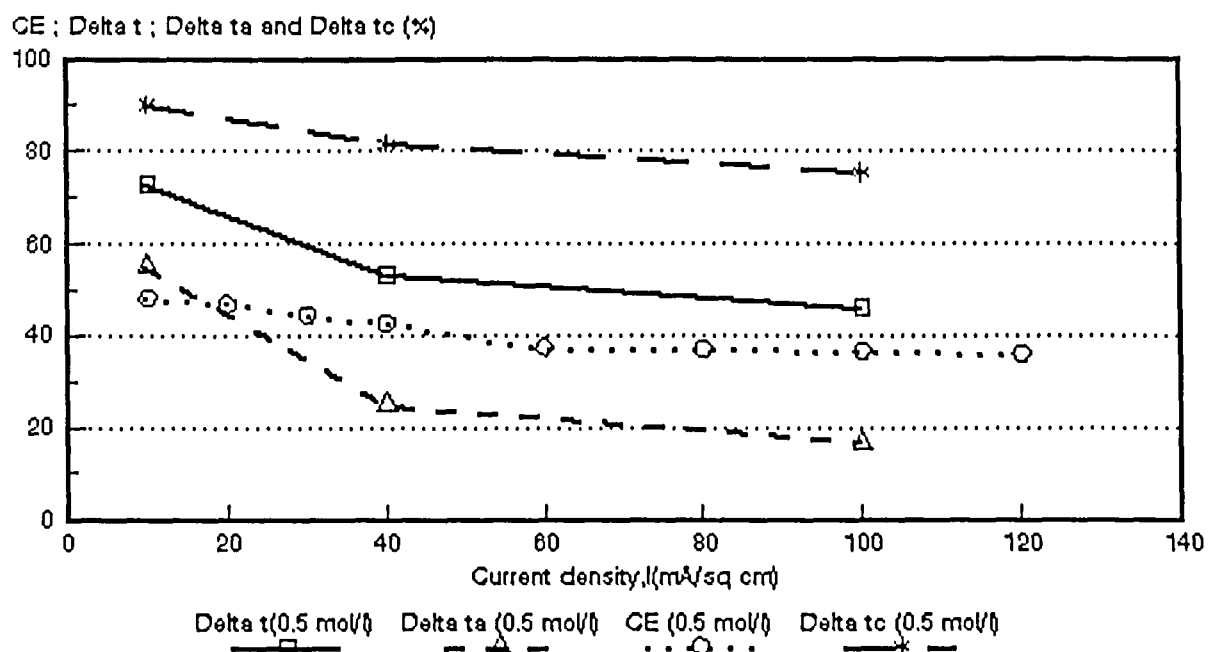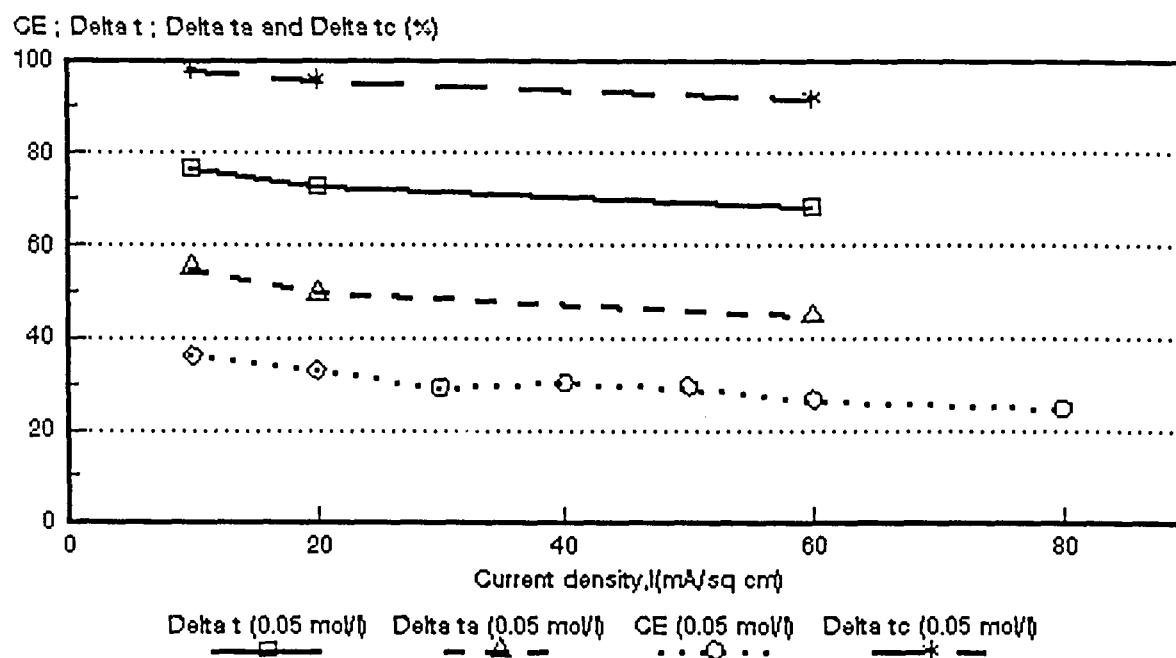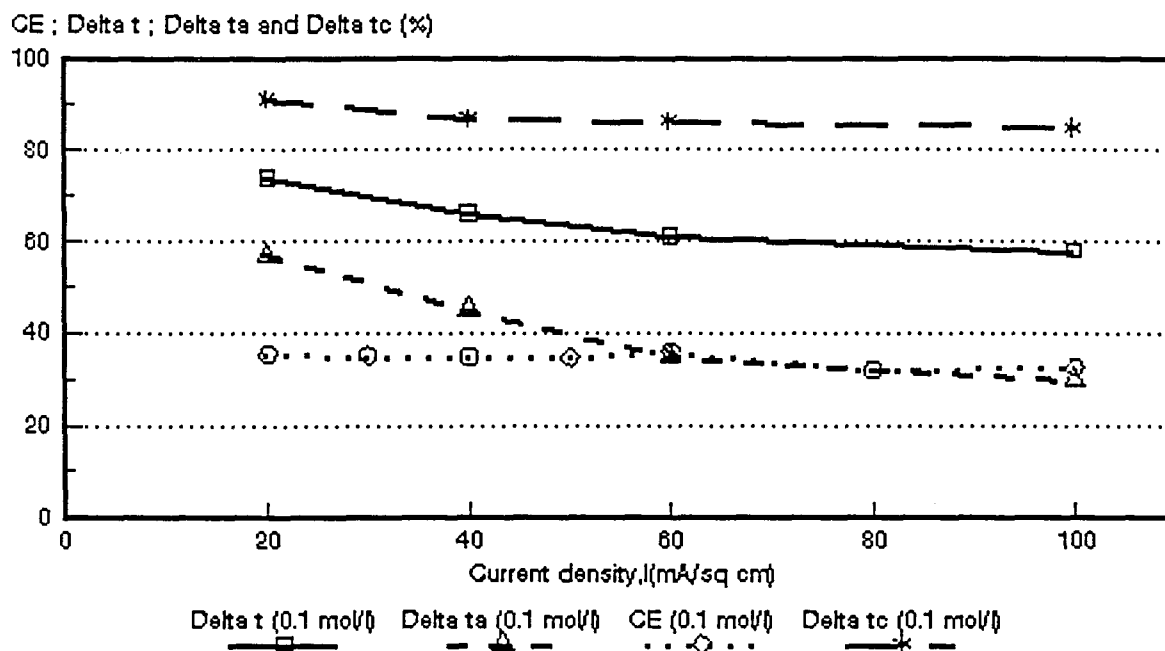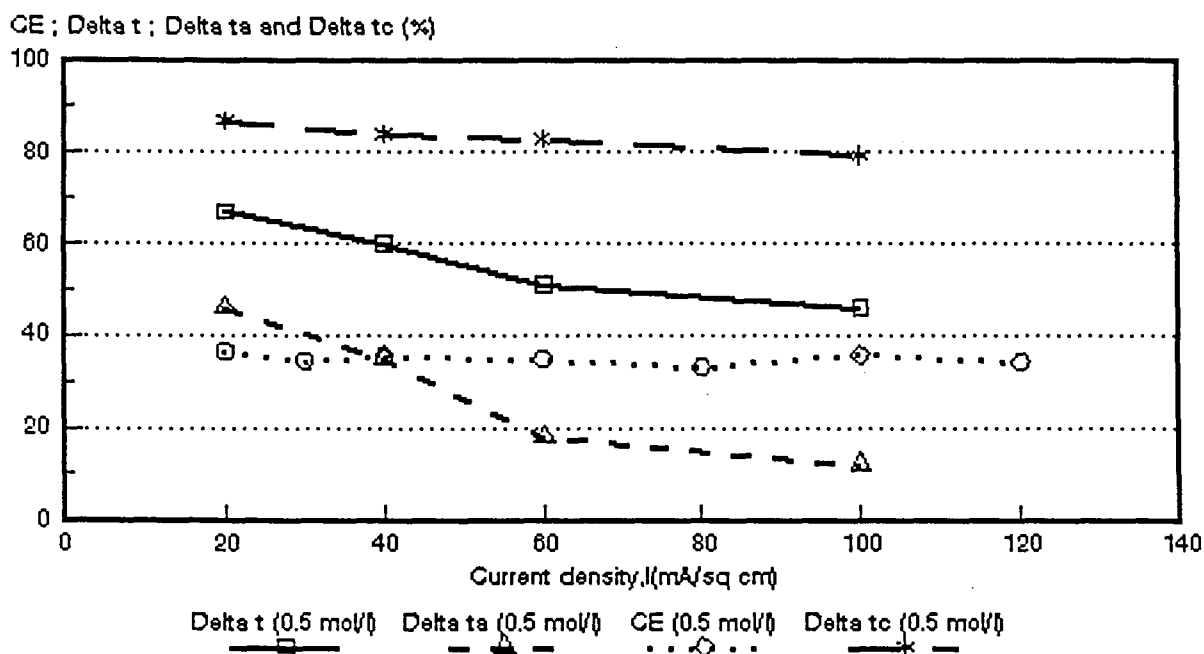
CE ; Delta t ; Delta ta and Delta tc (%)

Figure 7.49: Current efficiency (CE = e_p) as a function of current density for 0,5 mol/ℓ HCl feed. ABM-1 and *Selemion* CHV membranes. Delta t = $\bar{\Delta}$t; Delta ta = Δt^a; Delta tc = Δt^c.

Tabel 7.21: Correlation between apparent transport number of the membrane pair ($\overline{\Delta t}$) and current efficiency (e_p).

Current Density	$\overline{\Delta t}/e_p$																			
	Selemion AMV & CMV Concentration, mol/ℓ				Selemion AAV & CHV Concentration, mol/				Israeli & Selemion ABM-3 & CHV Concentration, mol/ℓ				Israeli & Selemion ABM-2 & CHV Concentration, mol/ℓ				Israeli & Selemion ABM-1 & CHV Concentration, mol/ℓ			
mA/cm²	0,05	0,1	0,5	1,0	0,05	0,1	0,5	1,0	0,05	0,1	0,5	1,0	0,05	0,1	0,5	1,0	0,05	0,1	0,5	1,0
10		4,92	4,18	3,87	1,89	1,89	2,20	1,88	1,84	2,10	1,91		1,66	1,57	1,49		2,10	1,36		
20		3,97	3,68	3,41	1,88	1,98	1,75	1,69	1,98	2,04	1,86	1,33					2,19	2,11	1,84	
30		3,53	3,01	3,07	1,84	1,85	1,71	1,63	2,13	1,98	1,79		1,71							
40		3,42	3,13	3,52	1,85	1,76	1,72	1,55	2,03	1,85	1,69	1,37		1,77	1,24			1,90	1,70	
50		3,09	3,02	3,13	1,83	1,83	1,69	1,57	2,08	1,86	1,66						2,28			
60		2,85	3,04	3,36	1,82	1,76	1,68	1,52	2,08	2,03		1,37	1,85				2,56	1,69	1,47	
70				3,31	1,79	1,67	1,63				1,60									
80						1,72	1,75	1,47				1,44								
90											1,59									
100						1,68	1,45	1,52						1,91	1,26			1,78	1,29	
110											1,47									
120							1,56				1,40									
130																				
140							1,61	1,47												
150																				
160																				
170																				
180								1,52												

Tabel 7.22: Correlation between apparent transport number of the anion membrane (Δt^a) and current efficiency (e_p).

Current Density mA/cm²	Selemion AMV & CMV Concentration, mol/ℓ				Selemion AAV & CHV Concentration, mol/ℓ				Israeli & Selemion ABM-3 & CHV Concentration, mol/ℓ				Israeli & Selemion ABM-2 & CHV Concentration, mol/ℓ				Israeli & Selemion ABM-1 & CHV Concentration, mol/ℓ			
	0,05	0,1	0,5	1,0	0,05	0,1	0,5	1,0	0,05	0,1	0,5	1,0	0,05	0,1	0,5	1,0	0,05	0,1	0,5	1,0
10		2,27	1,12	0,73	1,54	1,61	1,92	1,48	1,55	1,83	1,56		1,19	1,27	1,14		1,52			
20		1,37	0,29	0,83	1,51	1,65	1,47	1,37	1,56	1,61	1,36	0,94					1,49	1,61	1,26	
30		0,83	0,13	0,73	1,45	1,47	1,37	1,23	1,67	1,43	1,22		1,07							
40		0,53	0,14	1,17	1,38	1,40	1,35	1,19	1,49	1,29	1,06	0,97		1,18	0,56			1,30	0,99	
50		0,25	0,38	0,88	1,36	1,39	1,34	1,15	1,51	1,19	0,99									
60		0,12	0,50	1,25	1,31	1,30	1,30	1,05	1,47	1,55		0,87	1,00				1,65	0,97	0,52	
70				1,19	1,28	1,23	1,35				0,86									
80						1,27	1,46	1,10				0,97								
90											0,81									
100						1,19	1,19	1,20						1,23	0,44			0,92	0,34	
110											0,69									
120							1,12				0,62									
130																				
140							1,33	1,17												
150																				
160																				
170																				
180								1,26												

Tabel 7.23: Correlation between apparent transport number of the cation membrane (Δt^c) and current efficiency (e_p).

Current Density mA/cm²	Selemion AMV & CMV Concentration, mol/ℓ				Selemion AAV & CHV Concentration, mol/ℓ				Israeli & Selemion ABM-3 & CHV Concentration, mol/ℓ				Israeli & Selemion ABM-2 & CHV Concentration, mol/ℓ				Israeli & Selemion ABM-1 & CHV Concentration, mol/ℓ			
	0,05	0,1	0,5	1,0	0,05	0,1	0,5	1,0	0,05	0,1	0,5	1,0	0,05	0,1	0,5	1,0	0,05	0,1	0,5	1,0
10		7,58	7,16	7,10	2,21	2,17	2,48	2,32	2,12	2,37	2,28		2,10	1,86	1,86		2,71	2,31		
20		6,58	6,99	6,14	2,25	2,34	2,06	1,98	2,42	2,46	2,34	1,68					2,92	2,57	2,38	
30		6,22	5,90	5,47	2,21	2,24	2,05	2,02	2,59	2,53	2,33		2,35							
40		6,25	6,12	6,00	2,31	2,13	2,06	1,90	2,55	2,44	2,29	1,80		2,36	1,89			2,50	2,38	
50		5,86	5,66	5,51	2,30	2,26	2,03	2,00	2,69	2,54	2,37									
60		5,58	5,59	5,39	2,35	2,25	2,06	1,96	2,69	2,52		1,85	2,73				3,46	2,39	2,39	
70				5,43	2,29	2,13	1,93				2,32									
80						2,16	2,05	1,83				1,90								
90											2,36									
100						2,17	1,74	1,84						2,73	2,05			2,62	2,21	
110											2,24									
120							1,97				2,18									
130																				
140							1,88	1,77												
150																				
160								1,80												
170																				
180																				

mA/cm² (0,1 mol/ℓ feed). The correlation was even better at 1,0 mol/ℓ feed concentration and varied between 0,97 and 0,84 in the 20 to 80 mA/cm² current density range.

A satisfactory correlation was obtained between the apparent transport number (Δt^a) and current efficiency at 0,05 mol/ℓ feed concentration in the case of the ABM-2 and CHV membranes (30 to 60 mA/cm²). The ratio of $\Delta t^a/\epsilon_p$ varied between 1,07 and 1,0. The ratio was approximately 1,18 at 0,1 mol/ℓ feed concentration in the same current density range. A very poor correlation, however, was obtained at 0,5 mol/ℓ feed concentration for the same membranes.

The ABM-1 and CHV membranes showed the best correlation (0,92 to 0,97) at 0,1 mol/ℓ feed concentration in the current density range from 60 to 100 mA/cm². A poor correlation, however, was obtained with the Selemion AMV and CMV membranes.

The correlations between the apparent transport numbers of the cation membrane (Δt^c) and current efficiencies (Table 7.23) were not as good as the correlations obtained between the apparent transport numbers of the membrane pair ($\bar{\Delta}t$) (Table 7.21) and that of the anion membrane (Δt^a) and current efficiency (Fig. 7.22). It therefore seems that the best correlation between transport numbers and current efficiency for acid can be obtained from the apparent transport number of the anion membrane. It also seems that the apparent transport number of the anion membrane gives the best approximate estimation of the performance of membranes for acid concentration/desalination. However, accuracy of performance depends on the acid feed concentration used. The performance of a membrane for acid concentration should be estimated with an accuracy of approximately 20% from the apparent transport number of the anion membrane, depending on the acid feed concentration used.

7.3 Water Flow

Water flow (J) through the membranes as a function of current density and acid feed water concentration is shown in Figures 7.50 to 7.54. Water flow (J_i) through the membranes relative to the flow at $J_{0,5\ mol/\ell}$ is shown in Table 7.24. Water flow through the membranes decreased significantly with increasing acid feed concentration in the case of the *Selemion* AMV and CMV membranes. A slight decrease in water flow was also experienced in the case of the *Selemion* AAV and CHV membranes. Therefore, there appeared to be no support (water flow) to improve current efficiency as had been experienced with the sodium chloride solutions (see Figs. 7.28 and 7.29 and Figs. 6.43 to 6.49). However, a definite increase in water flow was observed for the ABM-3 and CHV membranes, especially at the highest feed concentration (Table 7.24) and an increase in current efficiency was experienced for this membrane type at 1,0 mol/ℓ feed concentration (see Fig. 7.30). Increase in water flows were also experienced for the ABM-2, ABM-1 and CHV membranes with increasing acid feed concentration. Current efficiency also increased slightly in these cases (see Figs. 7.31 and 7.32). The high water flow that was experienced with the ABM-2 membranes at 0,1 mol/ℓ feed concentration may be ascribed to membrane leakage due to a partially torn membrane.

Water flow (J) through the membranes as a function of effective current density, I_{eff}, and feed water concentration are shown in Figures 7.55 to 7.59. Straight lines were obtained at higher values of I_{eff} as were experienced with the sodium chloride solutions. The slope of these lines corresponds to the combined electro-osmotic coefficient (2β) of a membrane pair. The electro-osmotic coefficients decreased as a function of increasing acid feed concentration in the feed concentration range from 0,05 to 1,0 mol/ℓ (Figs. 7.60 to 7.64). The electro-osmotic coefficient of the *Selemion* AMV and CMV membranes remained almost constant in the 0,1 to 0,5 mol/ℓ feed concentration range and then decreased more significantly to a lower value at 1,0 mol/ℓ feed concentration (Fig. 7.60). The electro-osmotic coefficient of the *Selemion* AAV and CHV membranes remained constant in the 0,05 to 0,1 mol/ℓ feed range (Fig. 7.61) and then decreased somewhat to remain almost constant in the 0,5 to 1,0 mol/ℓ feed concentration range. The electro-osmotic coefficients of the ABM-3 and CHV membranes decreased significantly in the 0,05 to 0,5 mol/ℓ feed concentration range and then remained constant (Fig. 7.62). Both the ABM-2 and ABM-1 membranes showed a reduction in the electro-osmotic coefficient in the 0,05 to 0,1 mol/ℓ feed concentration ranges and then remained constant in the 0,1 to 0,5 mol/ℓ feed

concentration range (Figs. 7.62 to 7.63). It, therefore, appears that the membranes deswell somewhat with increasing acid feed concentration.

The effect of the electro-osmotic coefficient on the maximum acid brine concentration c_b^{max}, is shown in Table 7.25. Maximum acid brine concentration increases with decreasing electro-osmotic coefficient. The electro-osmotic coefficients of the *Selemion* AMV and CMV membranes were much higher than that of the other membranes. The electro-osmotic coefficients of the *Selemion* AMV and CMV membranes were determined at 0,357 and 0,371 ℓ/Faraday at 0,1 and 0,54 mol/ℓ feed concentration, respectively. The electro-osmotic coefficients of the *Selemion* AAV and CHV; ABM-3 and CHV; ABM-2 and CHV and ABM-1 and CHV were determined at 0,141 and 0,126 ℓ/Faraday; 0,166 and 0,124 ℓ/Faraday; 0,133 and 0,131 ℓ/Faraday and 0,152 and 0,149 ℓ/Faraday under the same feed water conditions as above, respectively. Consequently, much higher acid brine concentrations could be obtained with these membranes.

Approximately 7 to 8 mol H_2O per Faraday passed through the *Selemion* AAV and CHV membranes in the acid feed concentration range from 0,1 to 0,5 mol/ℓ (Table 7.25). Approximately 7 to 9; 7 and 8 mol H_2O/Faraday passed through the ABM-3 and CHV; ABM-2 and CHV and ABM-1 and CHV membranes under the same feed conditions as above, respectively. Therefore, the newly developed Israeli ABM membranes compare favourably with the commercially available *Selemion* AAV and CHV membranes for acid concentration.

The osmotic water flow (J_{osm}) relative to the total water flow (J) through the membranes as a function of current density, is shown in Table 7.26. The osmotic flow (J_{osm}) relative to the total flow (J) decreases with increasing current density. Osmotic water flow contributes to approximately 50% of the total water flow through the membranes at a current density of 30 mA/cm² at 0,1 mol/ℓ feed concentration. However, the osmotic water flow contribution relative to the total water flow was much less at high current densities. Approximately 21% of the total water flow through the membranes was caused by osmosis in the case of the *Selemion* AAV and CHV membranes at a current density of 100 mA/cm² (0,1 mol/ℓ feed). The osmotic water flow contribution in the case of the ABM-3 and *Selemion* CHV membranes comprised 29,4% of the total water flow at a current density of 60 mA/cm² (0,1 mol/ℓ feed).
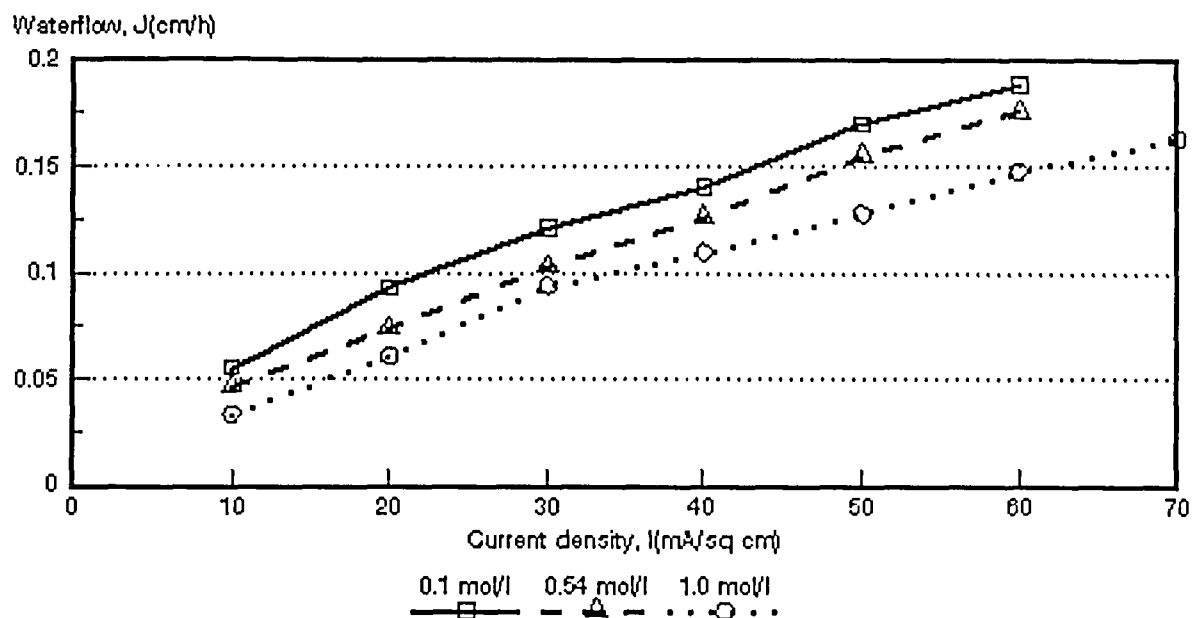
Figure 7.50: Water flow through the membranes as a function of current density and feed water concentration. *Selemion* AMV and CMV membranes.
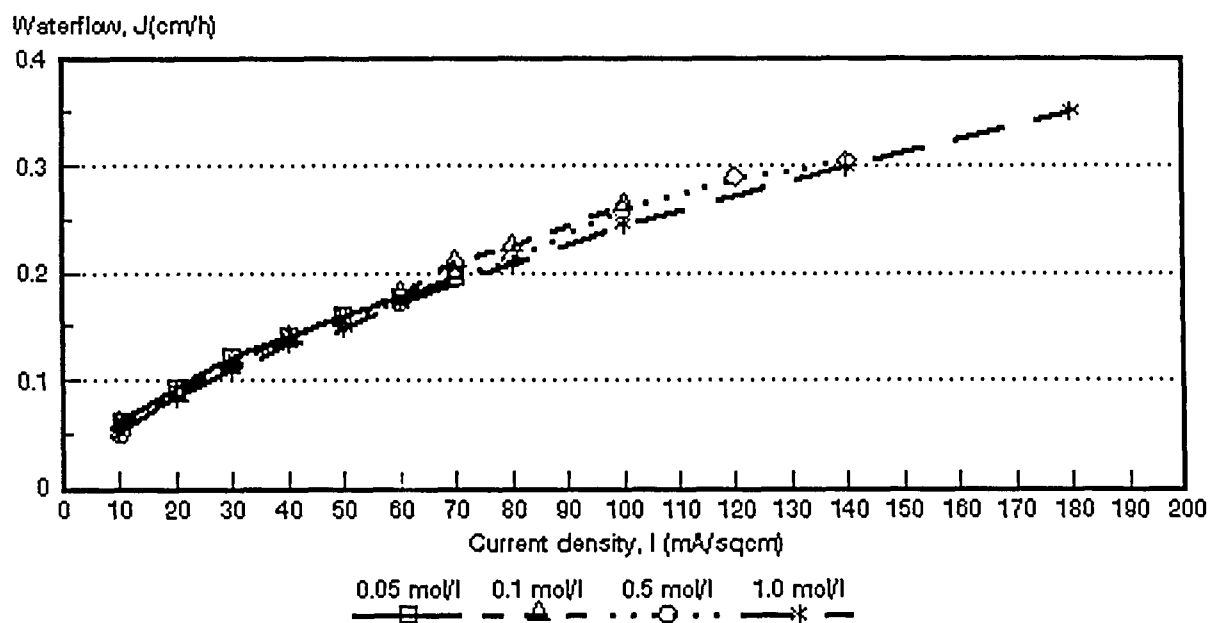

Figure 7.51: Water flow through the membranes as a function of current denisty and feed water concentration. *Selemion* AAV and CHV membranes.
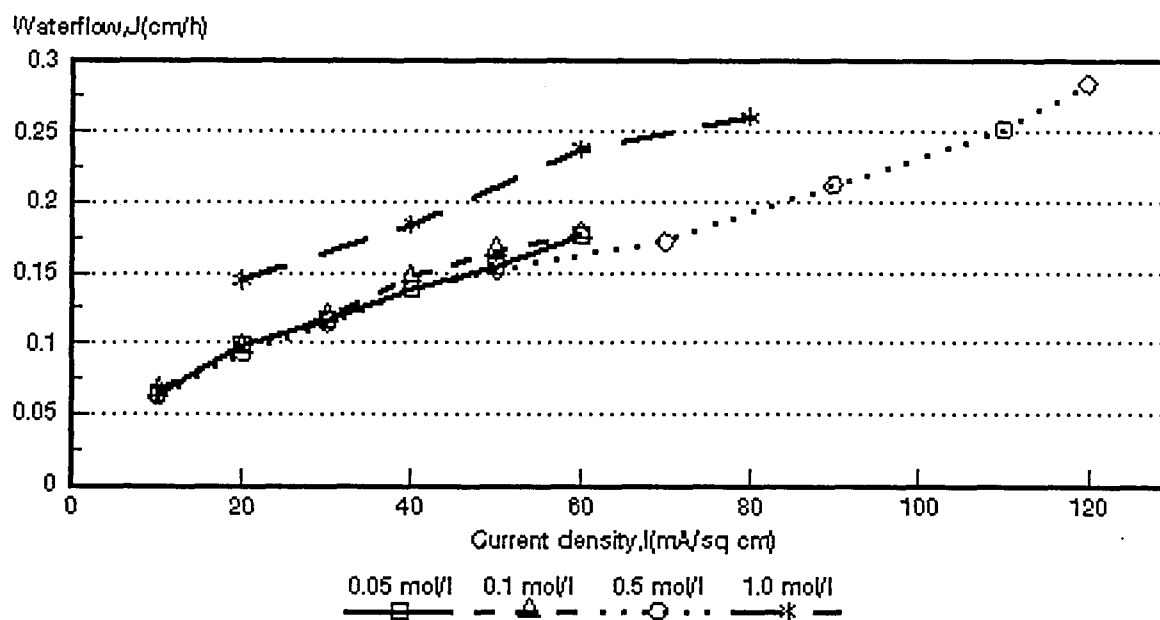
Figure 7.52: Water flow through the membranes as a function of current density and feed water concentration. ABM-3 and *Selemion* CHV membranes.
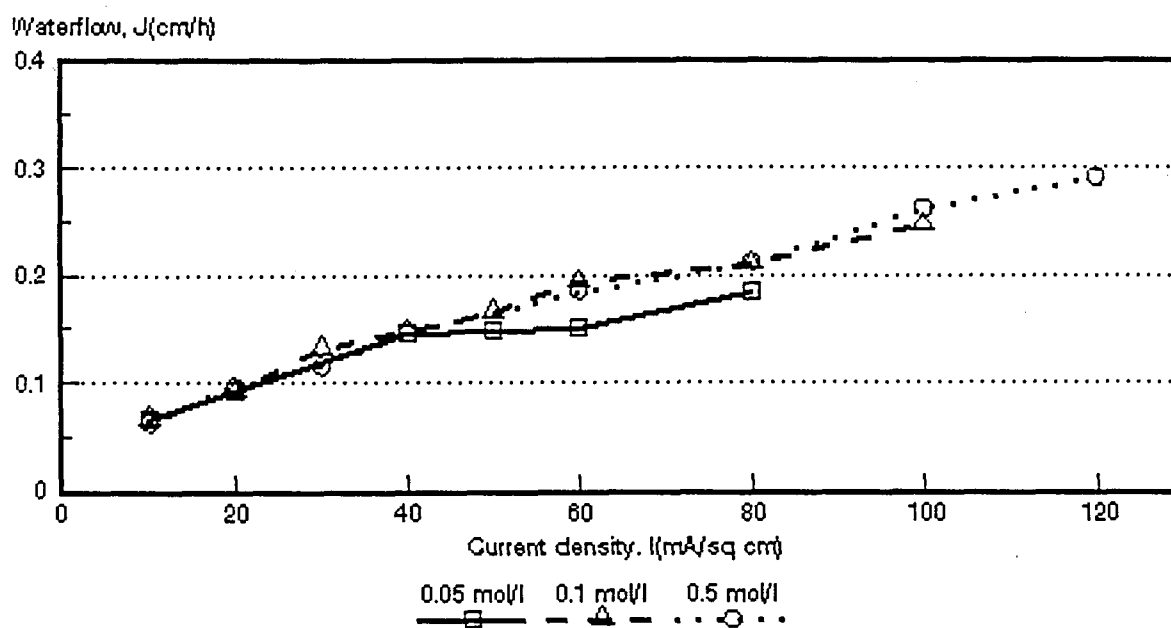

Figure 7.53: Water flow through the membranes as a function of current denisty and feed water concentration. ABM-2 and *Selemion* CHV membranes.
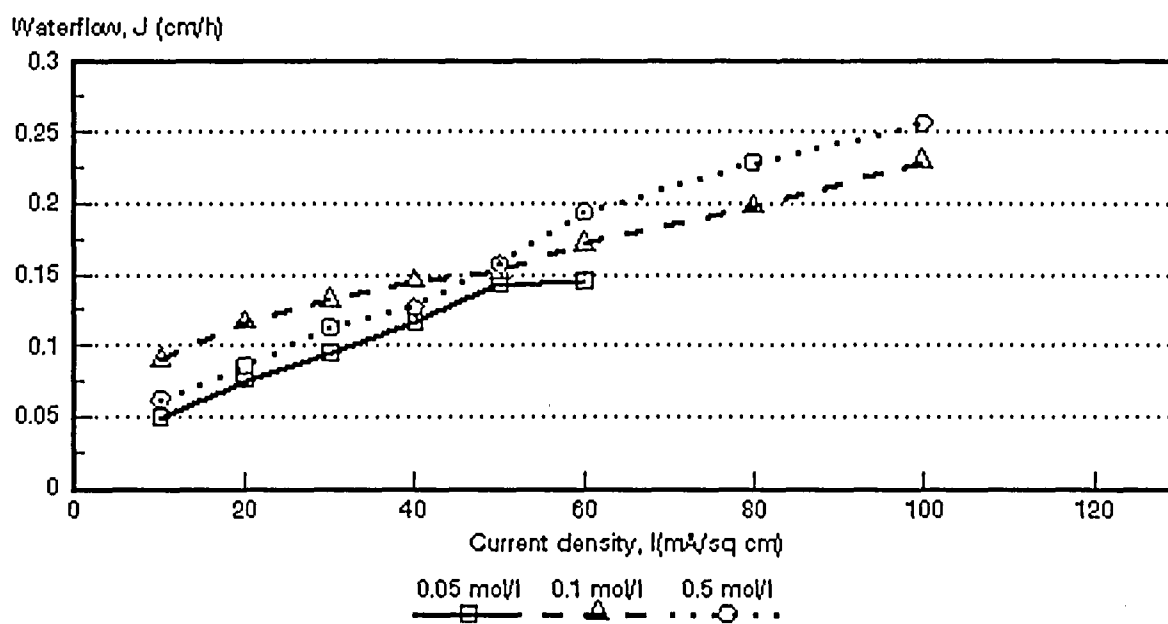
Figure 7.54: Water flow through the membranes as a function of current density and feed water concentration. ABM-1 and *Selemion* CHV membranes.

Waterflow, J(cm/h)

Effective current density, Ieff(mA/sq cm)

0.1 mol/l   0.54 mol/l   1.0 mol/l

Figure 7.55: Water flow through the membranes as a function of effective current density and HCl feed water concentration. *Selemion* AMV and CMV membranes.

Waterflow, J(cm/h)

Effective current density, Ieff (mA/sqcm)
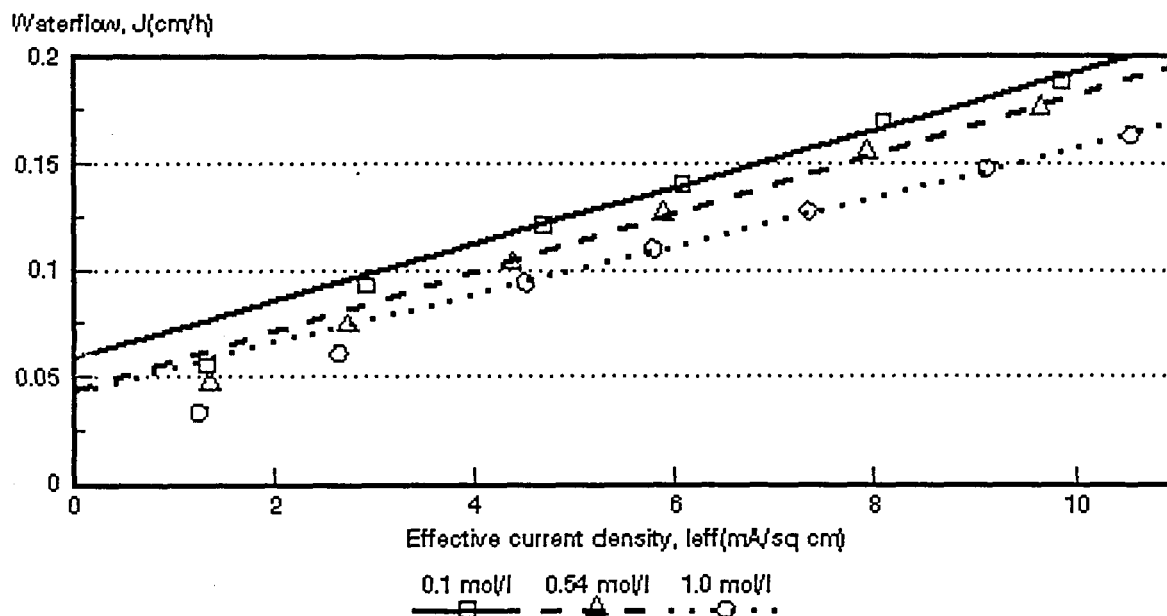
0.05 mol/l   0.1 mol/l   0.5 mol/l   1.0 mol/l

Figure 7.56: Water flow through the membranes as a function of effective current density and HCl feed water concentration. *Selemion* AAV and CHV membranes.

276

Figure 7.57: Water flow through the membranes as a function of effective current density and HCl feed water concentration. ABM-3 and *Selemion* CHV membranes.

Figure 7.58: Water flow through the membranes as a function of effective current density and HCl feed water concentration. ABM-2 and *Selemion* CHV membranes.

Waterflow, J(cm/h)

Effective current density, Ieff(mA/sq cm)

0.05 mol/l   0.1 mol/l   0.5 mol/l
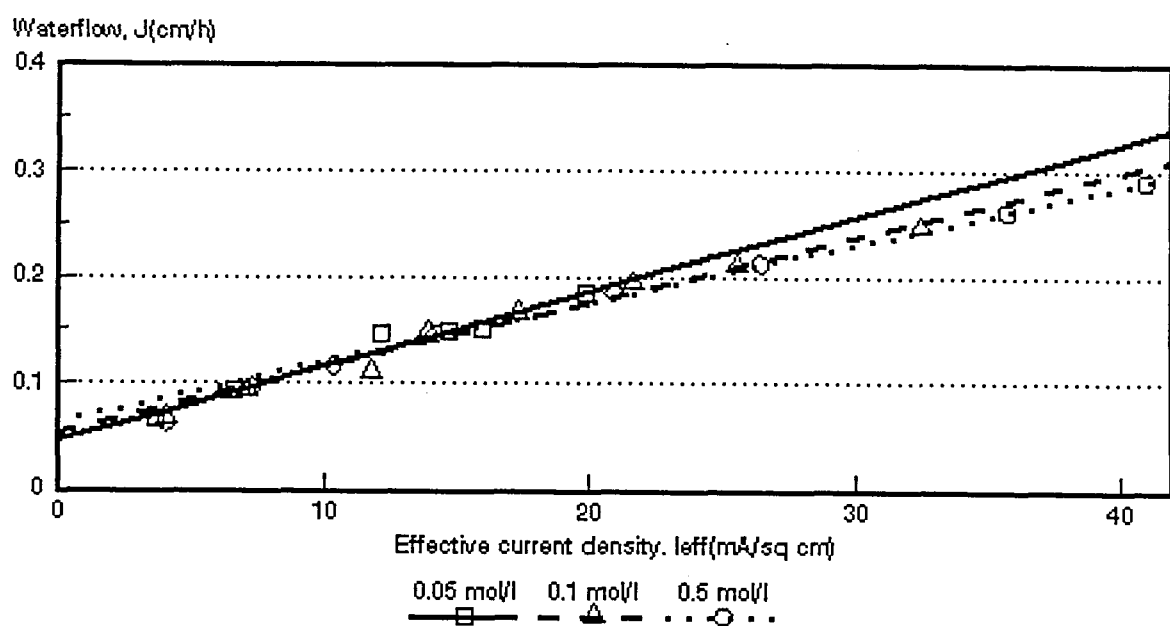
Figure 7.59:   Water flow through the membranes as a function of effective current density and HCl feed water concentration.   ABM-1 and *Selemion* CHV membranes.
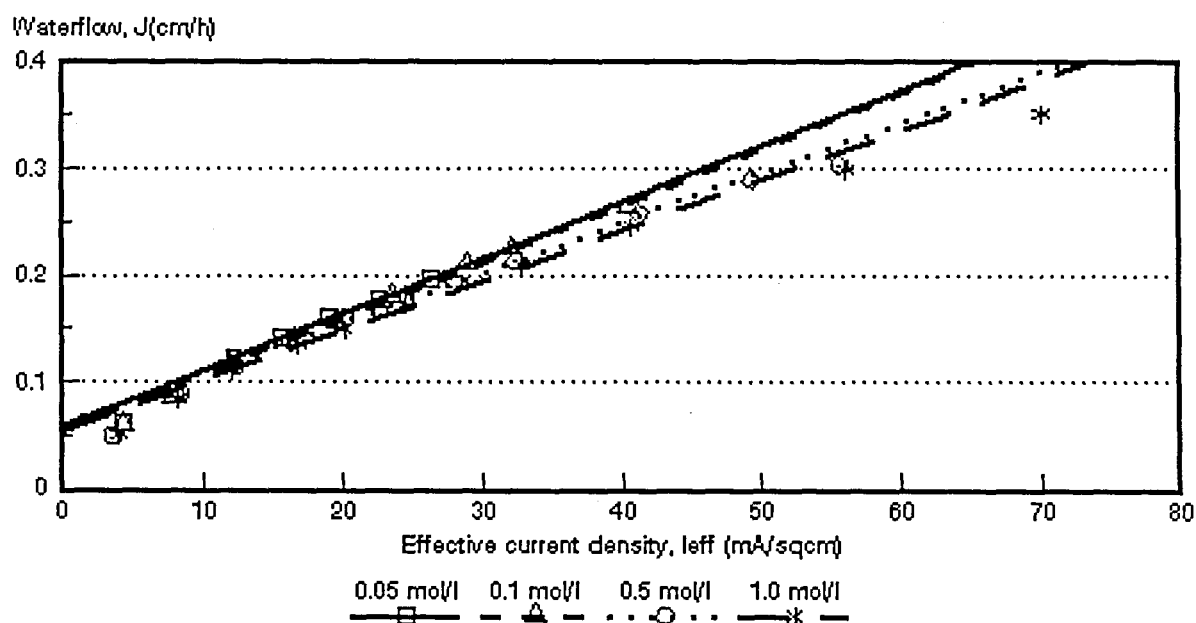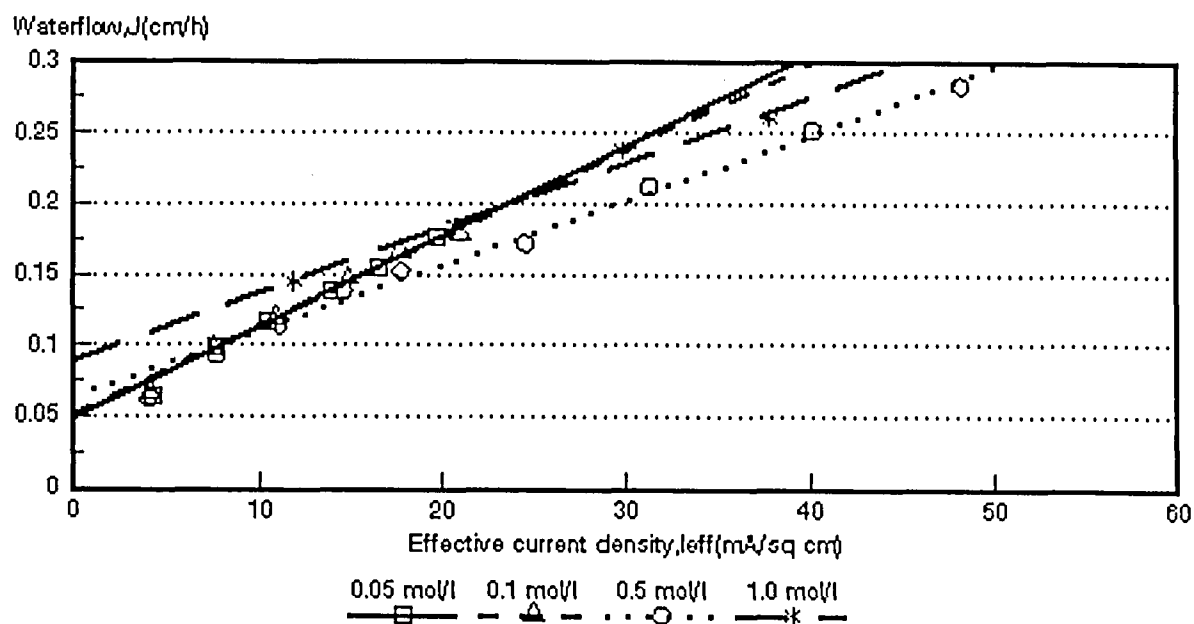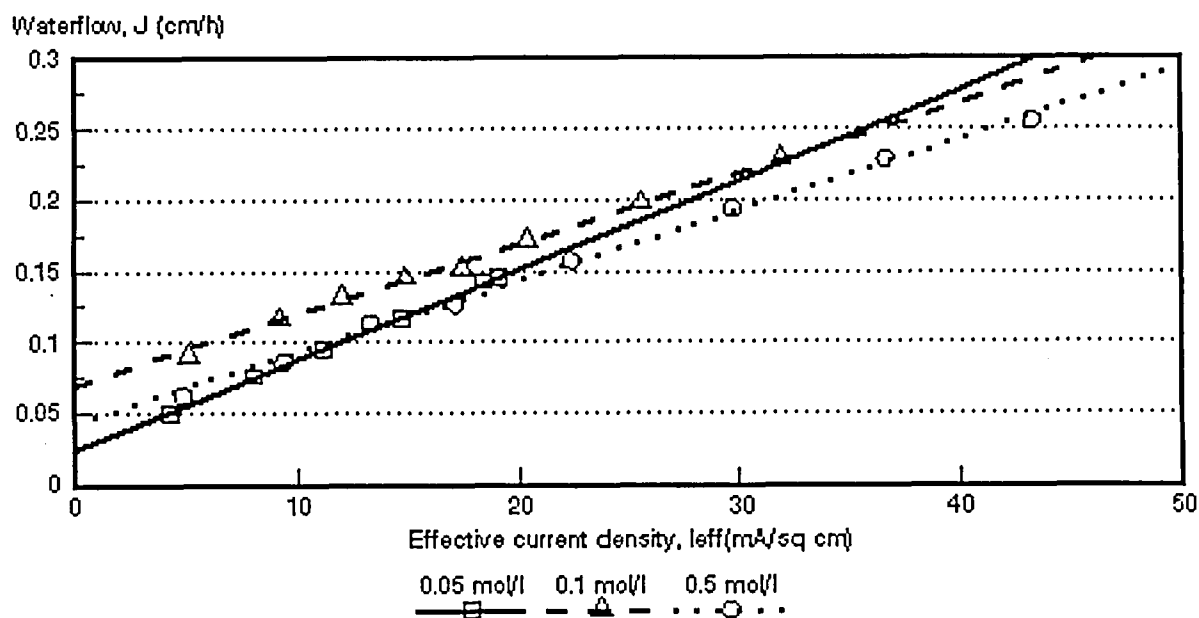
Electro-osmotic coefficient (l/Far)

Feed concentration (mol/l)
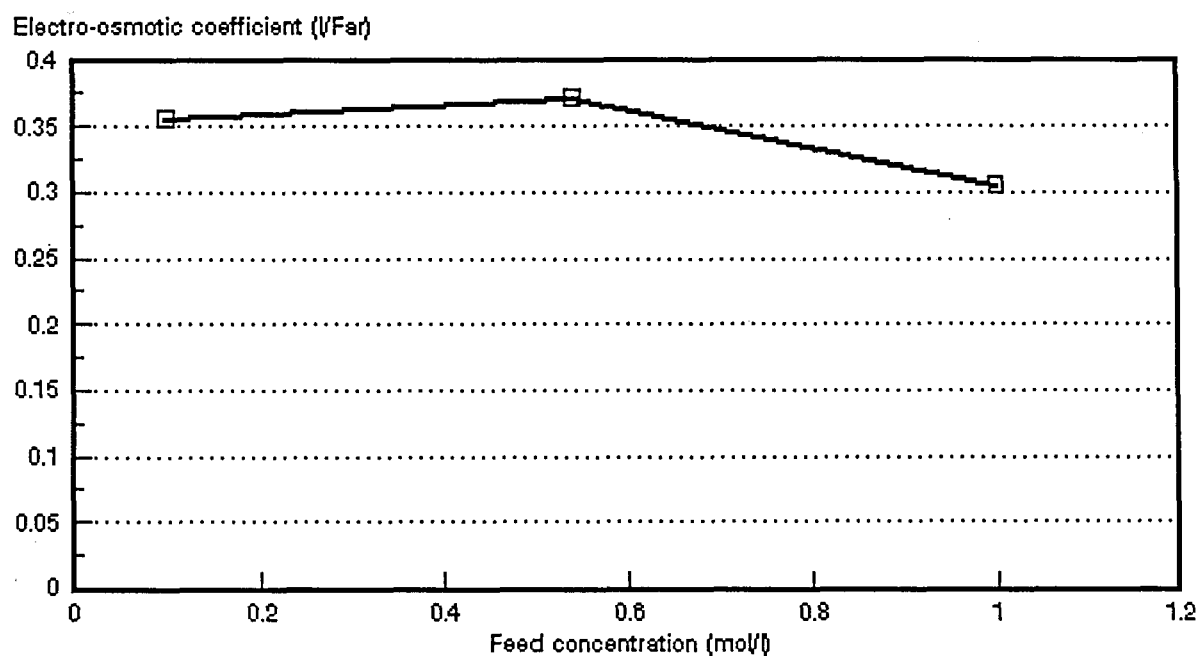
Figure 7.60:   Electro-osmotic coefficient as a function of HCl feed water concentration. *Selemion* AMV and CMV membranes.

Electro-osmotic coefficient (l/Far)
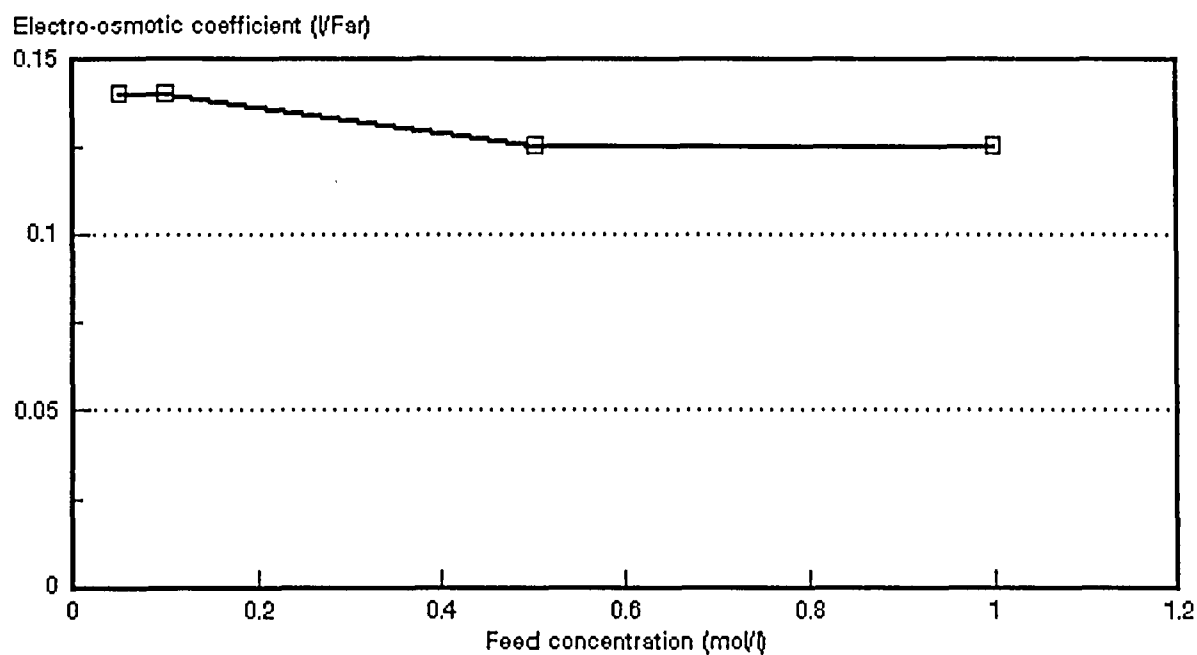
Figure 7.61: Electro-osmotic coefficient as a function of HCl feed water concentration. *Selemion* AAV and CHV membranes.

Electro-osmotic coefficient (l/Far)

Figure 7.62: Electro-osmotic coefficient as a function of HCl feed water concentration. ABM-3 and *Selemion* CHV membranes.

Electro-osmotic coefficient (I/Far)
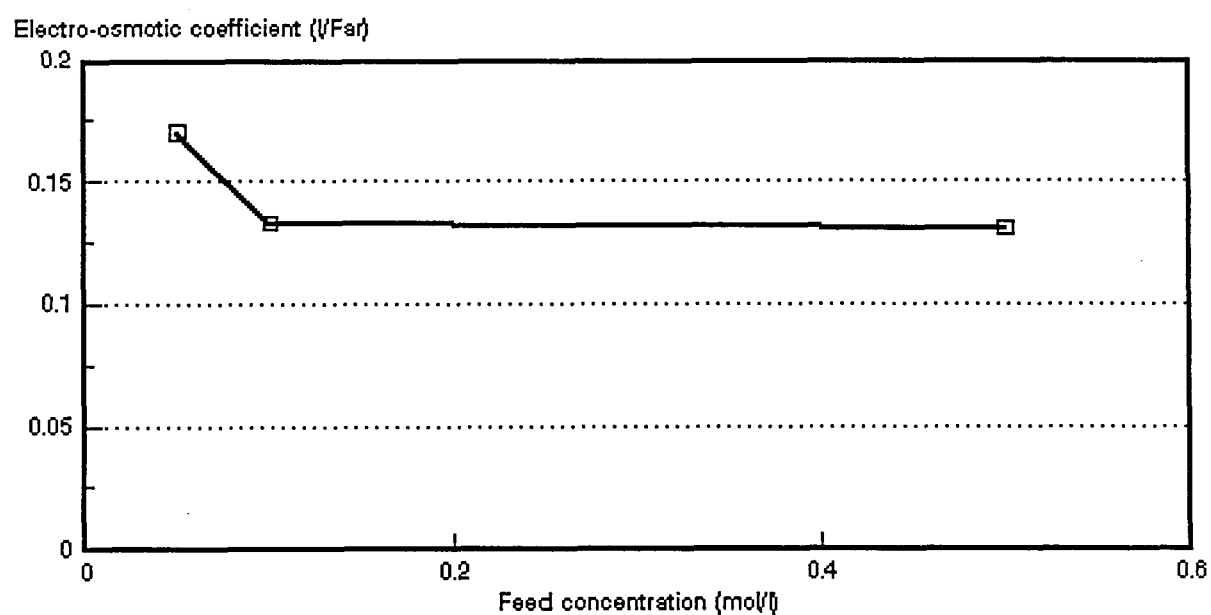
Figure 7.63:   Electro-osmotic coefficient as a function of HCl feed water concentration.
ABM-2 and *Selemion* CHV membranes.

Electro-osmotic coefficient (I/Far)

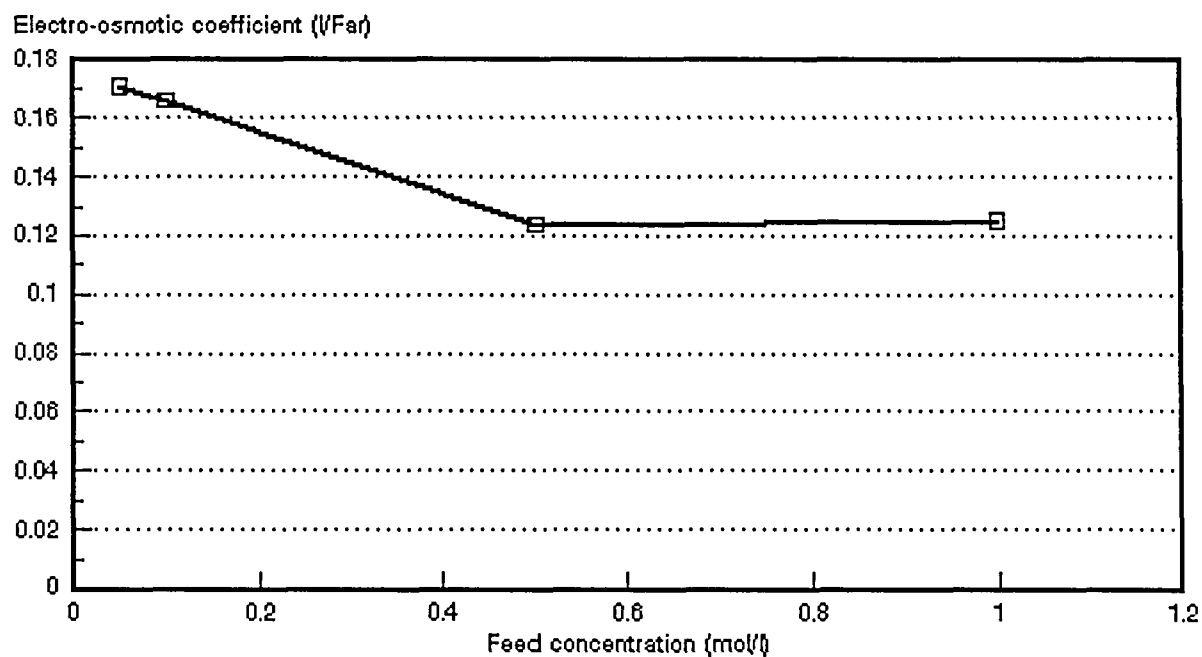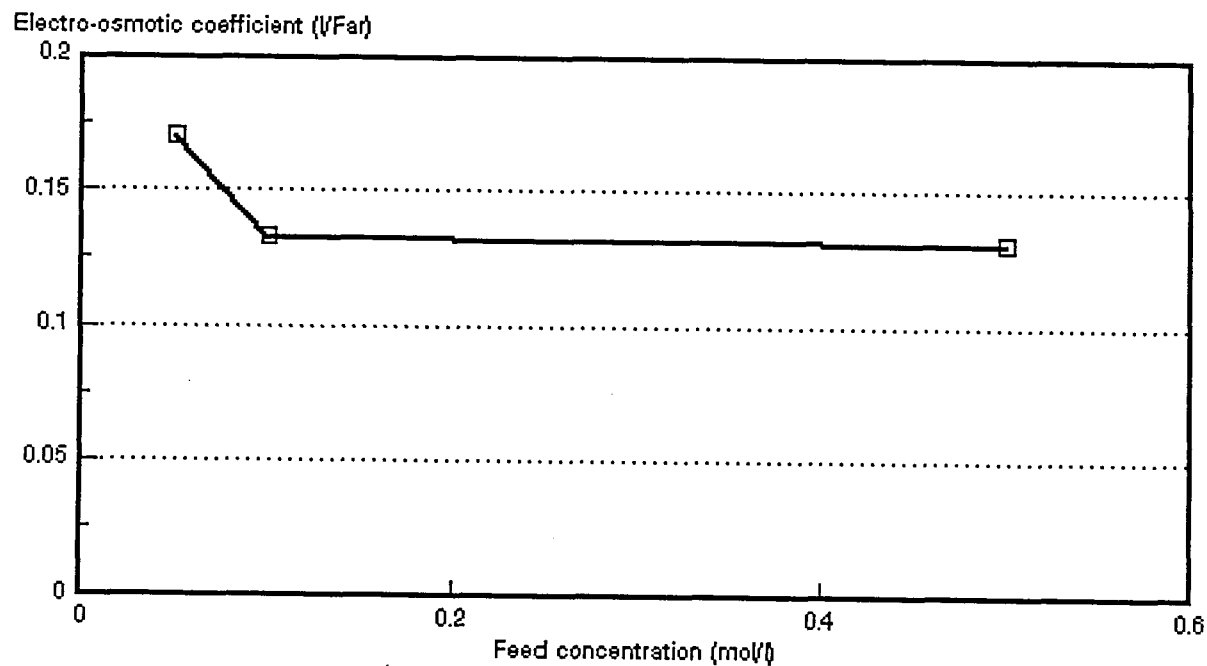Figure 7.64:   Electro-osmotic coefficient as a function of HCl feed water concentration.
ABM-1 and *Selemion* CHV membranes.

Table 7.25: Effect of the electro-osmotic coefficient (EOC)* on the maximum acid brine concentration, c_b^{max}.

Membranes	Feed Concentration mol/ℓ	EOC ℓ/Faraday	c_b^{max} mol/ℓ	mol H_2O/Faraday
Selemion	0,1	0,357	2,80	19,8
AMV & CMV	0,54	0,371	2,70	20,6
	1,0	0,306	3,27	17,0
Selemion	0,05	0,140	7,14	7,8
AAV & CHV	0,10	0,141	7,09	7,8
	0,50	0,126	7,93	7,0
	1,0	0,125	8,00	7,9
Israeli	0,05	0,171	5,85	9,5
ABM-3 &	0,10	0,166	6,02	9,2
Selemion CHV	0,50	0,124	8,06	6,9
	1,0	0,125	8,03	6,9
Israeli	0,05	0,170	5,88	9,4
ABM-2 &	0,10	0,133	7,51	7,4
Selemion CHV	0,50	0,131	7,6	7,3
Israeli	0,05	0,188	5,32	10,4
ABM-1 &	0,10	0,152	6,58	8,4
Selemion CHV	0,50	0,149	6,71	8,3

*   Data from Tables 7.1 to 7.17.

Table 7.26: Osmotic flow* (J_{oam}) relative to the total flow (J) through the membranes as a function of current density.

Membranes	Current Density mA/cm²	J_{oam}/J (%) Feed Concentration (mol/ℓ)			
		0,05	0,10	0,5	1,0
Selemion AMV & CMV	10		107,6	92,9	128,9
	20		63,8	58,9	71,2
	30		49,1	42,4	46,1
	40		42,4	34,6	39,6
	50		34,9	28,1	33,8
	60		31,4	24,8	26,6
Selemion AAV & CHV	10	96,1	91,9	123,5	109,0
	20	64,1	64,1	69,4	65,4
	30	48,5	47,1	53,7	50,1
	40	42,3	39,4	44,8	41,1
	50	37,3	35,1	38,6	37,3
	60	33,5	30,6	35,7	32,3
	70	30,4	26,1	31,7	
	80		24,5	29,0	26,6
	100		20,9	23,9	22,7
	120			21,4	
	140			20,3	18,6
	180				15,8
Israeli ABM-3 & Selemion CHV	10	77,4	77,5	103,8	
	20	50,5	53,6	69,2	
	30	42,3	44,0	56,4	
	40	35,9	35,6	46,6	
	50	31,1	31,5	42,4	
	60	28,1	29,4		
	70			37,4	
	90			30,4	
	110			25,5	
	120			22,7	
Israeli ABM-2 & Selemion CHV	10	49,1	77,5	74,4	
	20	32,3	60,2	54,1	
	30	25,8	53,4	41,2	
	40	21,0	48,3	36,6	
	50	17,2	46,4		
	60	16,9	41,0	29,5	
	80		35,6	24,0	
	100		30,6	20,3	
	120			18,1	
Israeli ABM-1 & Selemion CHV	10	69,0	102,6	102,0	
	20	50,2	74,7	66,7	
	30	34,9	52,3	55,6	
	40	32,0	46,7	44,5	
	50	31,4	41,9		
	60	30,9	35,7	34,9	
	80	25,1	32,8	30,6	
	100		28,0	24,8	
	120			22,3	

*   Data from Tables 7.1 to 7.17.

7.4   Membrane Permselectivity

Membrane permselectivities (from potential measurements) as a function of acid brine concentration for different acid feed concentrations are shown in Figures 7.65 to 7.69. Membrane permselectivity decreased with increasing acid brine concentration and increasing acid feed concentration in the case of Selemion AMV and CMV; Selemion AAV and CHV; ABM-2 and CHV and ABM-1 and CHV membranes. However, a higher permselectivity was obtained at the highest feed concentration (1,0 mol/ℓ feed) in the case of the ABM-3 and CHV membranes.

Permselectivity

Brine concentration (mol/ℓ)

0.1 mol/l   0.54 mol/l   1.0 mol/l
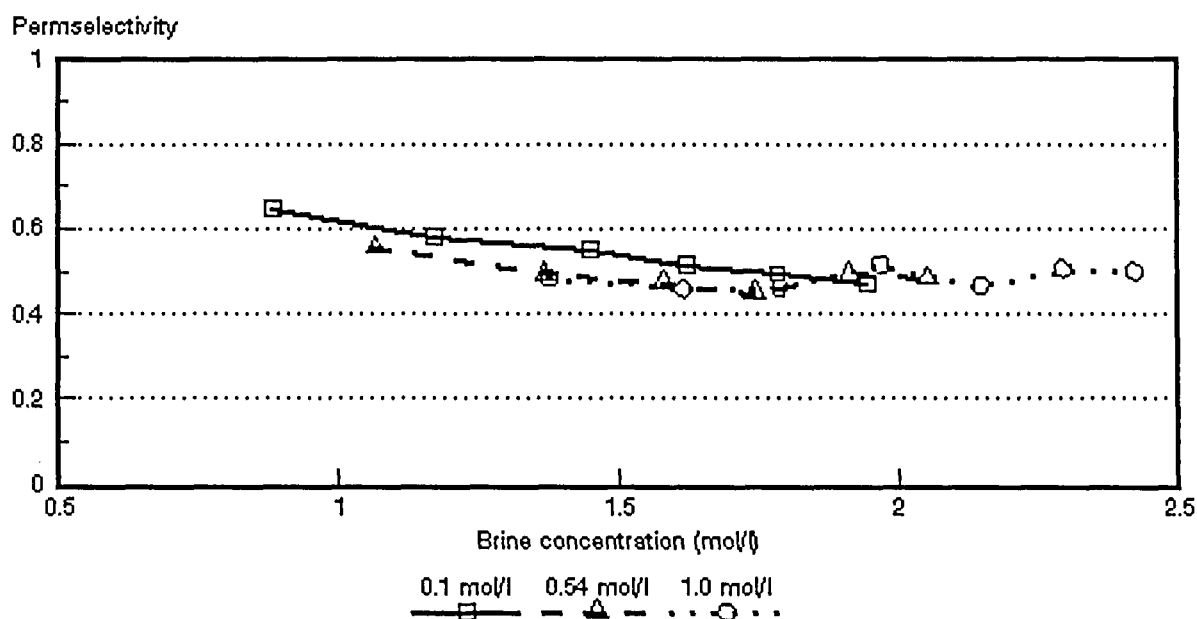
Figure 7.65:   Membrane permselectivity ($\overline{\Delta}$t) as a function of acid brine concentration for different HCl feed concentrations. Selemion AMV and CMV membranes.

Permselectivity

Figure 7.66: Membrane permselectivity ($\overline{\Delta}$t) as a function of acid brine concentration for different HCl feed concentrations. *Selemion* AAV and CHV membranes.

Permselectivity

Figure 7.67: Membrane permselectivity ($\overline{\Delta}$t) as a function of acid brine concentration for different HCl feed concentrations. ABM-3 and *Selemion* CHV membranes.

Figure 7.68: Membrane permselectivity ($\overline{\Delta}$t) as a function of acid brine concentration for different HCl feed concentrations. ABM-2 and *Selemion* CHV membranes.
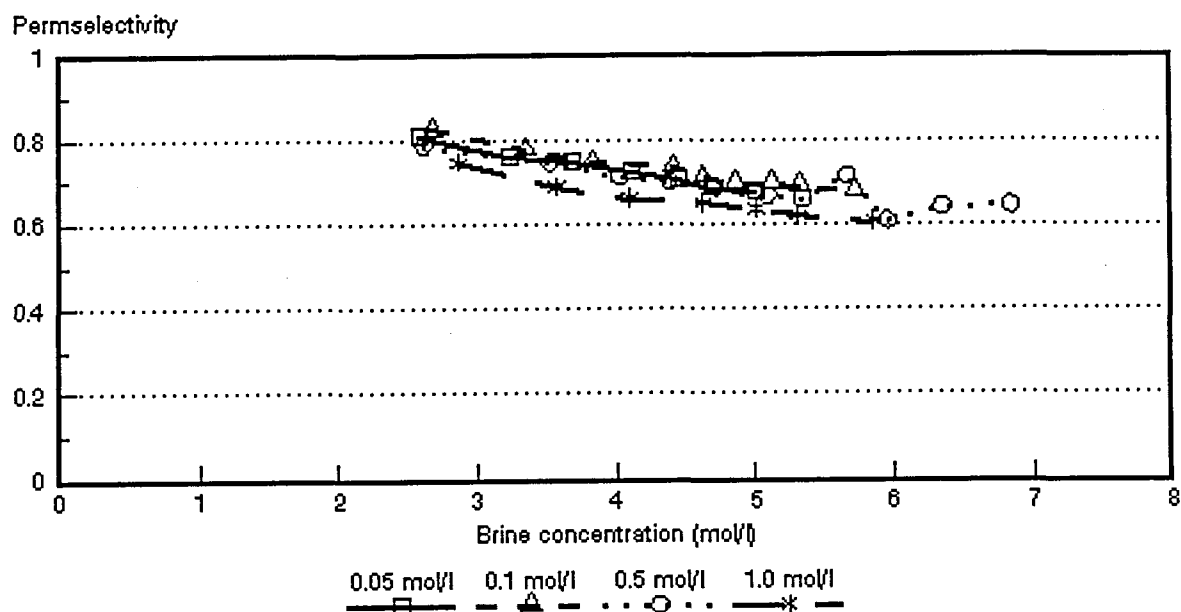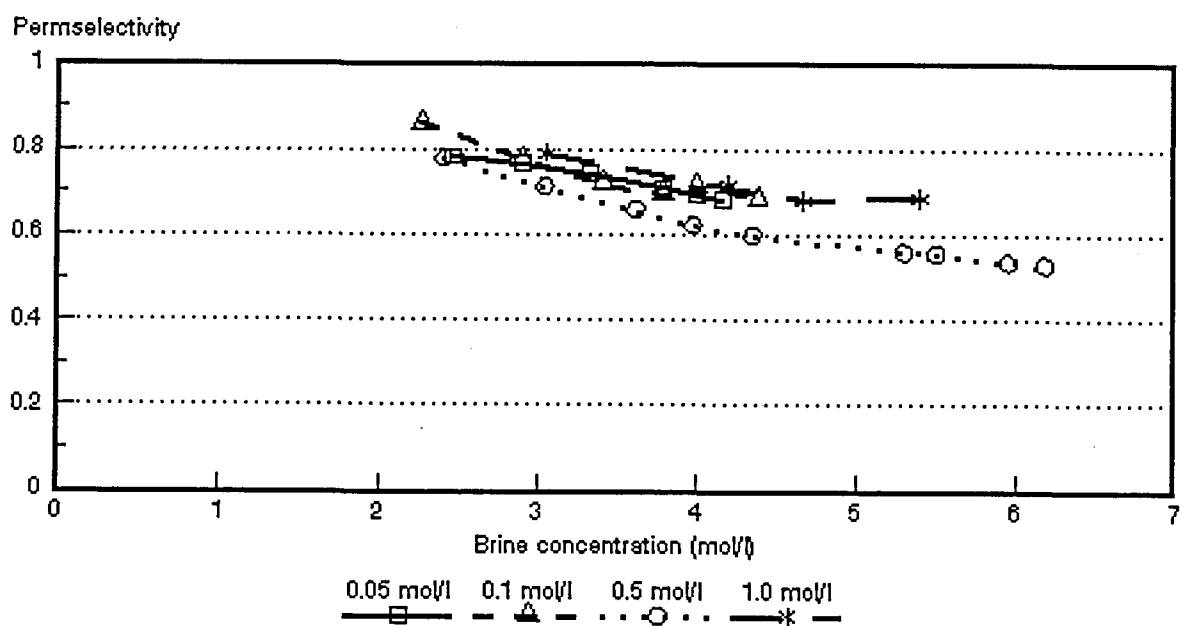

Figure 7.69: Membrane permselectivity ($\overline{\Delta}$t) as a function of acid brine concentration for different HCl feed concentrations. ABM-1 and *Selemion* CHV membranes.
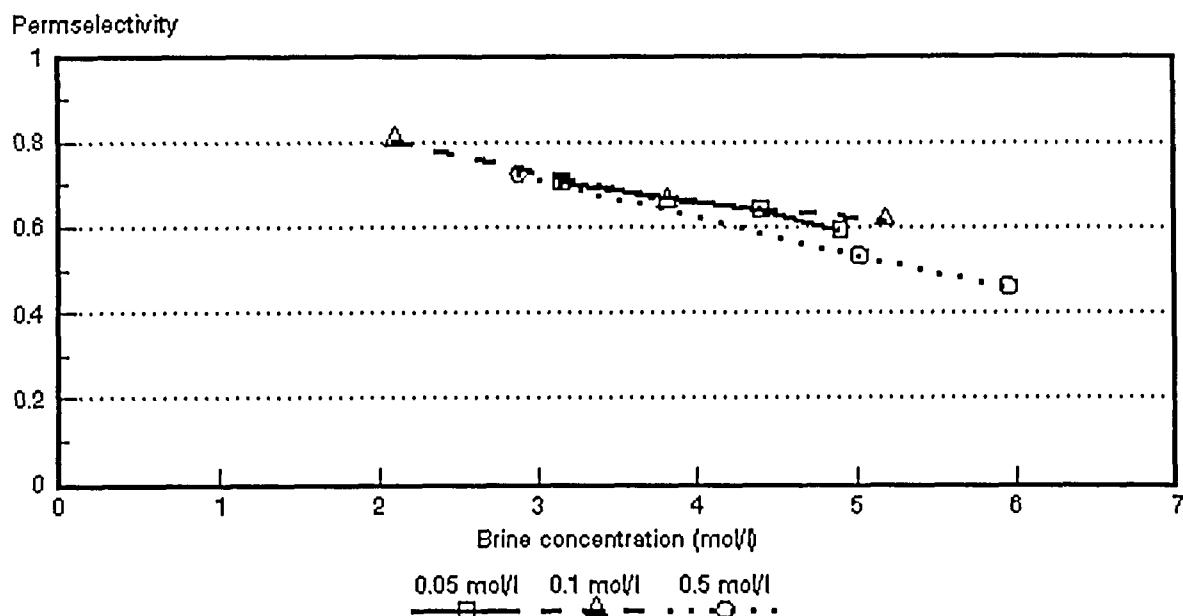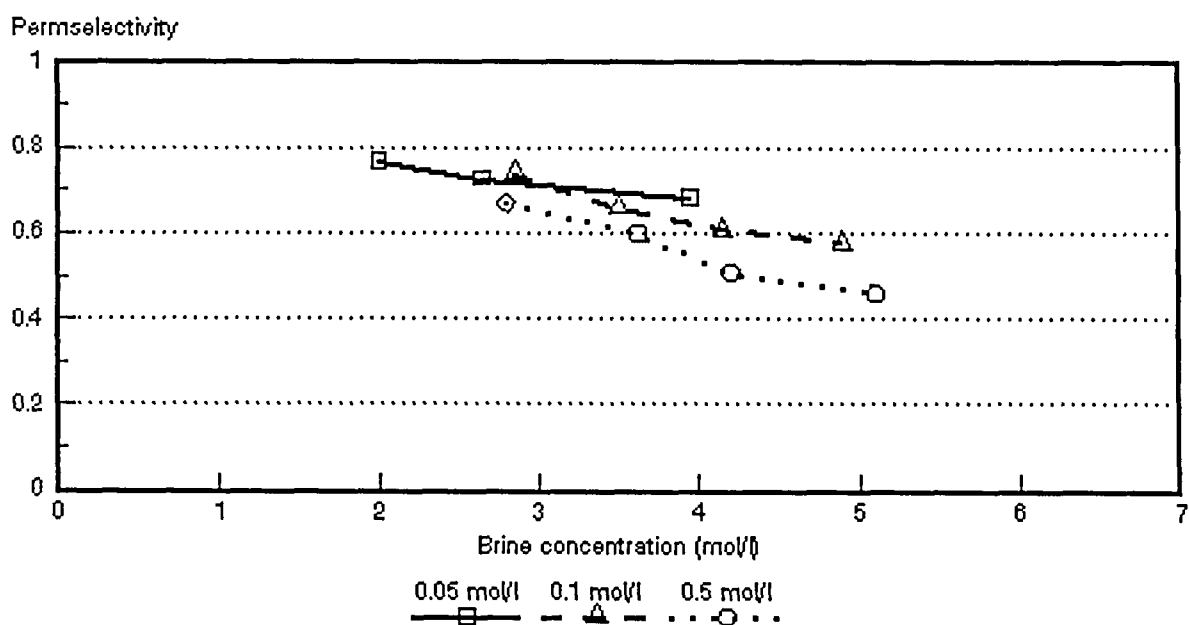
7.5 Acid and Salt Diffusion through Membranes

The diffusion rate of sodium chloride and hydrochloric acid solutions through *Selemion* AMV and AAV membranes was determined in an attempt to explain the difference that was obtained between the apparent transport numbers as determined by the potential method and the current efficiencies as determined by the EOP method. Salt and acid solutions of different concentrations were separated by the membranes and the change in diluate concentration as a function of time was determined. The rate of concentration change per unit time was determined from the results. The results are shown in Table 7.27.

Table 7.27: Change of concentration rate of sodium chloride and hydrochloric acid solutions through Selemion AMV and AAV membranes.

Initial Feed Concentration mol/ℓ	Initial Brine Concentration mol/ℓ	Rate of Concentration Change (ge/h)*			
		Selemion AMV		Selemion AAV	
		Salt Diluate	Acid Diluate	Salt Diluate	Acid Diluate
0,05	2	0,000568	0,005872	0,000165	0,000494
0,05	4	0,000390	0,002800	0,000145	0,002805

* gram equivalents per hour.

The rate of concentration increase in the more dilute compartment was much higher for the acid than for the salt solutions for both membrane types. Consequently, backdiffusion of acid from the brine into the diluate compartment will cause the current efficiency to decrease much more in the case of acids than in the case of salt solutions.

7.6   Membrane Characteristics

7.6.1   Membrane resistance

Membrane resistances are summarized in Table 7.28.

Table 7.28:   **Membrane resistances of the membranes used for EOP of hydrochloric acid solution.**

Membrane	Resistance - ohm cm²	
	0,1 mol/ℓ	0,5 mol/ℓ HCl
Selemion AMV	7,4	2,0
Selemion CMV	0,8	0,8
Selemion AAV	8,7	5,2
Selemion CHV	0,6	1,5
ABM-3	48,3	34,7
ABM-2	75,7	47,0
ABM-1	30,6	12,4

7.6.2   Gel water contents and Ion-exchange capacities of membranes used for EOP of hydrochloric acid solutions.

The gel water contents and ion-exchange capacities of the membranes used for EOP of hydrochloric acid solutions are shown in Table 7.29.

Table 7.29:   **Gel water contents and ion exchange capacities of the membranes used for EOP of hydrochloric acid solutions.**

Membrane	Gel Water Content %	Ion-Exchange Capacity me/dry g
Selemion AMV	18,4	1.26
Selemion CMV	22,7	2,4
Selemion AAV	9,1	0,48
Selemion CHV	13,4	1,98

7.6.3   Permselectivities of the membranes used for EOP of hydrochloric acid solutions

The permselectivities of the membranes at different hydrochloric acid concentration gradients are summarized in Table 7.30.

Table 7.30: Membrane permselectivities of the membranes used for EOP of hydrochloric acid solutions at different acid concentration gradients

Membrane	$\Delta t(1)^*$	$\Delta t(2)^{**}$	$\Delta t(3)^{***}$
Selemion AMV	0,74	0,46	0,13
Selemion CMV	1,00	0,88	0,88
Selemion AAV	0,97	0,83	0,54
Selemion CHV	0,99	0,87	0,87
ABM-3	0,88	0,63	0,44
ABM-2	0,92	0,77	0,49
ABM-1	0,84	0,60	0,40

(1)*   :   0,1 / 0,2 mol/ℓ HCl
(2)**   :   0,5 / 1,0 mol/ℓ HCl
(3)***   :   0,1 / 4,0 mol/ℓ HCl

8. ELECTRO-OSMOTIC PUMPING OF CAUSTIC SODA SOLUTIONS WITH DIFFERENT ION-EXCHANGE MEMBRANES

Caustic soda brine concentrations, water flows and current efficiencies were determined at different current densities for different caustic soda feed water concentrations. Membrane permselectivities (apparent transport numbers) were measured at the same concentrations differences as encountered during EOP experiments. The EOP results are summarized in Tables 8.1 to 8.11.

8.1 Brine Concentration

Caustic soda brine concentration (c_b) as a function of current density (I) is shown in Figures 8.1 to 8.3. Initially caustic soda brine concentration increases rapidly and then levels off at higher current densities similar to the results that have been obtained with sodium chloride and hydrochloric acid solutions. Brine concentration increases with increasing current density and increasing feed water concentration. Caustic soda brine concentrations obtained at the highest current densities studied are shown in Table 8.12.

Table 8.12: Caustic soda brine concentrations obtained at the highest current densities investigated for different caustic soda feed water concentrations.

Feed Concentration mol/ℓ	Brine Concentration* (%)		
	Selemion AMV & CMV	Selemion AMP & CMV	Ionac MA-3475 & MC-3470
0,05	14,3	15,4	15,7
0,1	17,7	19,9	18,0
0,5	20,1	22,4	21,7
1,0	24,2	-	16,0

* Data obtained from Tables 8.1 to 8.11.

Very high caustic soda brine concentrations were obtained for all the membranes investigated. Caustic soda brine concentrations of 17,7; 19,9 and 18,0% could be obtained from a 0,1 mol/ℓ caustic soda feed solution with *Selemion* AMV and CMV; *Selemion* AMP and CMV and *Ionac* MA-3475 and MC-3470 membranes, respectively. It is known from the literature that there is presently not an anion-exchange membrane commercially available that is stable at high caustic soda concentrations for long periods[114]. The *Selemion* AMP anion-exchange membrane is claimed by the manufacturers to be more resistant to caustic soda solutions than other commercially

Table 8.1: Electro-osmotic pumping experimental conditions and results for 0,05 mol/l caustic soda (Selemion AMV and CMV).

Current Density	Brine concentration c_b, mol/l		Water flow	Current Efficiency	Effective Current Density	Transport Numbers				
I, mA/cm²	$c_{b\,exp.}$	$c_{b\,calc.}$	J, cm/h	e_p, %	I_{eff}, mA/cm²	Δt^c	Δt^a	$\overline{\Delta t}$	$\bar{t}_1^c$	$\bar{t}_2^a$
10	2,30	3,15	0,0953	58,79	5,88	0,73	0,88	0,80	0,86	0,94
20	2,88	4,08	0,1413	54,43	10,89	0,68	0,87	0,77	0,84	0,94
30	3,18	4,59	0,1854	52,61	15,78	0,65	0,87	0,76	0,82	0,94
40	3,20	5,04	0,2251	48,29	19,31	0,65	0,87	0,76	0,83	0,93
50	3,58	5,50	0,2472	47,39	23,69	0,59	0,87	0,73	0,79	0,94

Electro-osmotic coefficient (2β) = 0,228 l/F (slope = 0,0085120 ml/mAh)
J_{osm} = y-intercept = 0,054571 cm/h
c_b^{max} = 4,39 mol/l
$\Delta t^c = t_1^c - t_2^c$

$\Delta t^a = t_2^a - t_1^a$
$\overline{\Delta t}$ = Average transport number of membrane pair
$\bar{t}_1^c$ = Transport number of cation through cation membrane
$\bar{t}_2^a$ = Transport number of anion through anion membrane.

Table 8.2: Electro-osmotic pumping experimental conditions and results for 0,1 mol/l caustic soda (Selemion AMV and CMV)

Current Density	Brine concentration c_b, mol/l		Water flow	Current Efficiency	Effective Current Density	Transport Numbers				
I, mA/cm²	$c_{b\,exp.}$	$c_{b\,calc.}$	J, cm/h	e_p, %	I_{eff}, mA/cm²	Δt^c	Δt^a	$\overline{\Delta t}$	$\bar{t}_1^c$	$\bar{t}_2^a$
10	2,16	2,67	0,1147	66,46	6,65	0,78	0,86	0,82	0,89	0,93
20	2,78	3,46	0,1721	64,04	12,81	0,74	0,85	0,80	0,87	0,93
30	3,45	4,31	0,1960	60,43	18,13	0,67	0,84	0,75	0,83	0,92
40	3,50		0,2578	60,48	24,19	0,68	0,84	0,76	0,84	0,92
50	3,69	4,63	0,2966	58,69	29,35	0,64	0,84	0,74	0,82	0,92
60	3,82		0,3108	53,04	31,83	0,67	0,81	0,74	0,83	0,90
80	4,33	5,59	0,3567	51,70	41,36	0,62	0,80	0,71	0,81	0,90
100	4,43	6,21	0,4203	49,85	49,85	0,60	0,80	0,70	0,80	0,90

Electro-osmotic coefficient (2β) = 0,179 l/F (slope = 0,0066710 ml/mAh)
J_{osm} = y-intercept = 0,0898921 cm/h
c_b^{max} = 5,59 mol/l
$\Delta t^c = t_1^c - t_2^c$

$\Delta t^a = t_2^a - t_1^a$
$\overline{\Delta t}$ = Average transport number of membrane pair
$\bar{t}_1^c$ = Transport number of cation through cation membrane
$\bar{t}_2^a$ = Transport number of anion through anion membrane.

Table 8.3 : Electro-osmotic pumping experimental conditions and results for 0,5 mol/l caustic soda (Selemion AMV and CMV).

Current Density	Brine concentration c_b, mol/l		Water flow	Current Efficiency	Effective Current	Transport Numbers				
I, mA/cm²	$c_{b\,exp.}$	$c_{b\,calc.}$	J, cm/h	e_p, %	I_{eff}, mA/cm²	Δt^c	Δt^a	$\overline{\Delta t}$	$\bar{t}_1^c$	$\bar{t}_2^a$
10	2,2	2,02	0,1457	66,39	6,64	0,78	0,80	0,79	0,89	0,90
20	2,33	3,32	0,1748	66,20	13,23	0,77	0,78	0,78	0,89	0,89
30	3,36	3,96	0,2120	63,62	19,89	0,73	0,77	0,75	0,87	0,88
40	3,56		0,2560	61,09	24,28	0,70	0,78	0,74	0,85	0,89
50	3,96	4,97	0,2649	56,24	28,12	0,65	0,76	0,71	0,83	0,88
60	4,13		0,2825	52,07	31,24	0,62	0,77	0,70	0,81	0,89
70	4,39	5,80	0,3072	51,65	36,16	0,59	0,78	0,68	0,79	0,89
80	4,53		0,3355	50,87	40,70	0,60	0,77	0,68	0,80	0,88
100	4,83	6,31	0,3920	50,71	50,71	0,57	0,76	0,66	0,79	0,88
120	5,03	6,40	0,459	51,54	61,85	0,58	0,73	0,66	0,79	0,87

Electro-osmotic coefficient (2β) = 0,152 l/F (slope = 0,0056728 ml/mAh)
J_{osm} = y-intercept = 0,1059033 cm/h
c_b^{max} = 6,58 mol/l
$\Delta t^c = t_1^c - t_2^c$

$\Delta t^a = t_2^a - t_1^a$
$\overline{\Delta t}$ = Average transport number of membrane pair
$\bar{t}_1^c$ = Transport number of cation through cation membrane
$\bar{t}_2^a$ = Transport number of anion through anion membrane.

Table 8.4: Electro-osmotic pumping experimental conditions and results for 1 mol/l NaOH (Selemion AMV and CMV)

Current Density	Brine concentration c_b, mol/l		Water flow	Current Efficiency	Effective Current Density	Transport Numbers				
I, mA/cm²	$c_{b\,exp}$	$c_{b\,calc}$	J, cm/h	e_p, %	I_{eff}, mA/cm²	Δt^a	Δt^c	$\overline{\Delta t}$	t_1^c	t_2^a
30	4,4	3,5	0,1943	76,37	22,91	0,57	0,75	0,66	0,78	0,87
50	5,2	4,55	0,2649	73,84	36,92	0,56	0,74	0,65	0,77	0,86
70	5,8	5,3	0,3046	67,66	47,36	0,50	0,74	0,62	0,75	0,86
90	6,05	6,3	0,3310	59,66	53,69	0,49	0,75	0,62	0,74	0,87

Electro-osmotic coefficient (2β) = 0,118 l/F (slope = 0,0044119 ml/mAh)
J_{osm} = y-intercept = 0,0962310 cm/h
c_b^{max} = 8,46 mol/l
$\Delta t^c = t_1^c - t_2^c$

$\Delta t^a = t_2^a - t_1^a$
$\overline{\Delta t}$ = Average transport number of membrane pair
t_1^c = Transport number of cation through cation membrane
t_2^a = Transport number of anion through anion membrane.

Table 8.5 : Electro-osmotic pumping experimental conditions and results for 0,05 mol/l caustic soda (Selemion AMP and CMV)

Current Density	Brine concentration c_b, mol/l		Water flow	Current Efficiency	Effective Current Density	Transport Numbers				
I, mA/cm²	c_b exp.	$c_{b\,calc}$	J, cm/h	e_p, %	I_{eff}, mA/cm²	Δt^a	Δt^c	$\overline{\Delta t}$	t_1^c	t_2^a
10	1,92	2,55	0,118	61,07	6,11	0,74	0,87	0,81	0,87	0,93
20	2,48	3,64	0,172	57,06	11,41	0,82	0,86	0,84	0,91	0,93
30	2,76	3,58	0,235	57,92	17,38	0,67	0,85	0,75	0,84	0,92
40	3,16	3,94	0,268	56,66	22,66	0,57	0,84	0,71	0,79	0,92
50	3,44	4,61	0,293	54,06	27,03	0,61	0,84	0,72	0,80	0,92
60	3,84	5,31	0,297	50,90	30,54	0,59	0,82	0,71	0,79	0,91

Electro-osmotic coefficient (2β) = 0,176 l/F (slope = 0,0065825 ml/mAh)
J_{osm} = y-intercept = 0,1094348 cm/h
$\overline{\Delta t}$ = Average transport number of membrane pair
c_b^{max} = 5,68 mol/l

$\Delta t^a = t_2^a - t_1^a$
$\Delta t^c = t_1^c - t_2^c$
t_1^c = Transport number of cation through cation membrane
t_2^a = Transport number of anion through anion membrane.

Table 8.6 : Electro-osmotic pumping experimental conditions and results for 0,1 mol/l caustic soda (Selemion AMP and CMV)

Current Density	Brine concentration c_b, mol/l		Water flow	Current Efficiency	Effective Current Density	Transport Numbers				
I, mA/cm²	$c_{b\,exp}$	$c_{b\,calc}$	J, cm/h	e_p, %	I_{eff}, mA/cm²	Δt^a	Δt^c	$\overline{\Delta t}$	t_1^c	t_2^a
10	2,14	2,53	0,117	67,34	6,73	0,76	0,83	0,79	0,88	0,91
20	2,88	3,33	0,169	65,00	13,00	0,70	0,81	0,76	0,85	0,91
30	3,35	3,69	0,221	66,21	19,86	0,65	0,80	0,73	0,83	0,90
40	3,62		0,248	60,12	24,05	0,59	0,80	0,70	0,80	0,90
50	3,90	4,63	0,282	59,04	29,52	0,59	0,81	0,70	0,80	0,90
60	4,38		0,298	58,32	34,99	0,58	0,79	0,69	0,79	0,89
70	4,41	5,24	0,333	56,20	39,34	0,54	0,79	0,67	0,77	0,90
80	4,61		0,366	56,41	45,13	0,54	0,78	0,66	0,77	0,89
90	4,67	5,61	0,396	55,08	49,57	0,53	0,79	0,66	0,77	0,89
100	4,97	5,82	0,404	53,82	53,82	0,48	0,78	0,63	0,74	0,89

Electro-osmotic coefficient (2β) = 0,155 l/F (slope = 0,0057673 ml/mAh)
J_{osm} = y-intercept = 0,1036958 cm/h
c_b^{max} = 6,45 mol/l
$\Delta t^c = t_1^c - t_2^c$

$\Delta t^a = t_2^a - t_1^a$
$\overline{\Delta t}$ = Average transport number of membrane pair
t_1^c = Transport number of cation through cation membrane
t_2^a = Transport number of anion through anion membrane.

Table 8.7 : Electro-osmotic pumping experimental conditions and results for 0,50 mol/ℓ caustic soda (Selemion AMP and CMV)

Current Density	Brine concentration c_b, mol/l		*Water flow	Current Efficiency	Effective Current Density	Transport Numbers				
I, mA/cm²	$c_{b\,exp.}$	$c_{b\,calc.}$	J, cm/h	e_p, %	I_{eff}, mA/cm²	Δt^c	Δt^a	$\overline{\Delta}t$	$\bar{t}_1^a$	$\bar{t}_2^a$
10	2,29	2,62	0,110	67,75	6,78	0,76	0,79	0,77	0,88	0,89
20	3,02	3,36	0,159	64,33	12,87	0,66	0,78	0,72	0,83	0,89
30	3,57	4,05	0,196	62,63	18.79	0,65	0,77	0,71	0,83	0,88
40	3,98		0,236	62,99	25,20	0,56	0,77	0,67	0,78	0,88
50	4,12	4,71	0,265	58,58	29,29	0,60	0,74	0,67	0,80	0,88
60	4,43	5,02	0,295	58,42	35,05	0,58	0,74	0,66	0,79	0,87
70	4,89		0,282	52,83	36,98	0,47	0,75	0,61	0,74	0,87
80	4,83	5,67	0,331	53,59	42,87	0,53	0,72	0,63	0,77	0,86
100	5,19	5,59	0,399	55,46	55,46	0,48	0,72	0,60	0,74	0,86
120	5,59	6,29	0,419	52,76	63,31	0,47	0,70	0,59	0,74	0,85

Electro-osmotic coefficient (2ß) = 0,137 ℓ/F (slope = 0,0051179 mℓ/mAh)
J_{osm} = y-intercept = 0,1068910 cm/h
c_b^{max} = 7,30 mol/l
$\Delta t^c = t_1^c - t_2^c$

$\Delta t^a = t_2^a - t_1^a$
$\overline{\Delta}t$ = Average transport number of membrane pair
$\bar{t}_1^c$ = Transport number of cation through cation membrane
$\bar{t}_2^a$ = Transport number of anion through anion membrane.

Table 8.8 : Electro-osmotic pumping experimental conditions and results for 0,05 mol/ℓ caustic soda (Ionac MA-3475 and MC-3470)

Current Density	Brine concentration c_b, mol/l		Water flow	Current Efficiency	Effective Current Density	Transport Numbers				
I, mA/cm²	$c_{b\,exp.}$	$c_{b\,calc.}$	J, cm/h	e_p, %	I_{eff}, mA/cm²	Δt^c	Δt^a	$\overline{\Delta}t$	$\bar{t}_1^a$	$\bar{t}_2^a$
10	2,77	2,79	0,0927	68,8	0,8196	0,57	0,82	0,69	0,78	0,91
20	3,4	3,61	0,1391	63,37	12,6	0,55	0,80	0,67	0,77	0,90
30	3,76	3,96	0,1854	62,29	18,6	0,51	0,80	0,66	0,76	0,90
40	3,92	4,14	0,2344	61,59	24,63	0,51	0,79	0,65	0,75	0,90

Electro-osmotic coefficient (2ß) = 0,212 ℓ/F (slope = 0,0079229 mℓ/mAh)
J_{osm} = y-intercept = 0,0388302 cm/h
c_b^{max} = 4,72 mol/l
$\Delta t^c = t_1^c - t_2^c$

$\Delta t^a = t_2^a - t_1^a$
$\overline{\Delta}t$ = Average transport number of membrane pair
$\bar{t}_1^c$ = Transport number of cation through cation membrane
$\bar{t}_2^a$ = Transport number of anion through anion membrane.

Table 8.9 : Electro-osmotic pumping experimental conditions and results for 0,1 mol/ℓ caustic soda (Ionac MA-3475 and MC-3470)

Current Density	Brine concentration c_b, mol/l		* Water flow,	Current Efficiency	Effective Current Density	Transport Numbers				
I, mA/cm²	$c_{b\,exp.}$	$c_{b\,calc.}$	J, cm/h	e_p, %	I_{eff}, mA/cm²	Δt^c	Δt^a	$\overline{\Delta}t$	$\bar{t}_1^c$	$\bar{t}_2^a$
10	2,63	2,58	0,1033	72,22	7,22	0,61	0,81	0,71	0,81	0,91
20	3,4	3,38	0,1522	69,38	13,88	0,57	0,80	0,69	0,79	0,90
30	3,71	3,69	0,200	66,77	20,03	0,52	0,80	0,66	0,76	0,90
40	4,1		0,247	67,93	27,17	0,48	0,79	0,64	0,74	0,89
50	4,26	4,04	0,279	64,50	32,25	0,43	0,78	0,60	0,71	0,89
60	4,15		0,318	58,93	35,35					
70	4,45	4,37	0,371	63,19	44,23	0,45	0,79	0,62	0,73	0,89
75	4,51		0,371	59,71	44,78	0,43	0,79	0,61	0,71	0,89

Electro-osmotic coefficient (2ß) = 0,193 ℓ/F (slope = 0,0071947 mℓ/mAh)
J_{osm} = y-intercept = 0,0529144 cm/h
c_b^{max} = 5,18 mol/l
$\Delta t^c = t_1^c - t_2^c$

$\Delta t^a = t_2^a - t_1^a$
$\overline{\Delta}t$ = Average transport number of membrane pair
$\bar{t}_1^c$ = Transport number of cation through cation membrane
$\bar{t}_2^a$ = Transport number of anion through anion membrane.

Table 8.10 : Electro-osmotic pumping experimental conditions and results for 0,5 mol/l caustic soda (Ionac MA-3475 and MC-3470)

Current Density	Brine concentration c_b, mol/l		Water flow	Current Efficiency	Effective Current Density	Transport Numbers				
I, mA/cm²	$c_{b\,exp.}$	$c_{b\,calc}$	J, cm/h	e_p, %	I_{eff}, mA/cm²	Δt°	Δt^*	$\bar{\Delta t}$	t_1°	t_2°
10	2,63	2,13	0,0993	70,56	7,06	0,37	0,76	0,57	0,68	0,88
20	3,40	2,86	0,1378	62,77	12,55	0,32	0,73	0,53	0,66	0,87
30	3,98	3,14	0,1854	65,86	19,76	0,32	0,72	0,52	0,66	0,86
40	4,33	3,35	0,2296	66,65	26,66	0,22	0,72	0,47	0,61	0,86
50	4,50		0,2560	61,77	30,88	0,20	0,72	0,46	0,60	0,86
60	4,55		0,3178	64,62	38,77					
70	4,98	3,50	0,3443	65,67	45,97	0,22	0,70	0,46	0,61	0,85
80	5,00		0,3921	65,68	52,55					
90	5,23	3,71	0,4132	64,31	57,88	0,21	0,70	0,46	0,61	0,85
100	5,20		0,4503	62,77	62,77					
110	5,43		0,14768	63,04	69,34					

Electro-osmotic coefficient (2β) = 0,176 l/F (slope = 0,0065599 ml/mAh)
J_{osm} = y-intercept = 0,0526844 cm/h
c_b^{max} = 5,68 mol/l
$\Delta t^c = t_1^c - t_2^c$

$\Delta t^* = t_2^* - t_1^*$
$\bar{\Delta t}$ = Average transport number of membrane pair
t_1° = Transport number of cation through cation membrane
t_2° = Transport number of anion through anion membrane.

Table 8.11: Electro-osmotic pumping experimental conditions and results for 1,0 mol/l caustic soda (Ionac MA-3475 and MC-3470)

Current Density	Brine concentration c_b, mol/l		Water flow	Current Efficiency	Effective Current Density	Transport Numbers				
I, mA/cm²	$c_{b\,exp.}$	$c_{b\,calc}$	J, cm/h	e_p, %	I_{eff}, mA/cm²	Δt°	Δt^*	$\bar{\Delta t}$	t_1°	t_2°
10	2,75	1,80	0,0971	71,60	7,16	0,20	0,73	0,47	0,60	0,87
20	3,44	2,50	0,1378	63,51	12,70	0,21	0,71	0,46	0,61	0,86
30	3,84	2,70	0,1854	63,62	19,09	0,20	0,68	0,44	0,60	0,84
40	4,02	3,40	0,1986	53,52	21,4	0,18	0,73	0,46	0,59	0,87

Electro-osmotic coefficient (2β) = 0,193 l/F (slope = 0,0072079 ml/mAh)
J_{osm} = y-intercept = 0,0459504 cm/h
c_b^{max} = 5,18 mol/l
$\Delta t^c = t_1^c - t_2^c$

$\Delta t^* = t_2^* - t_1^*$
$\bar{\Delta t}$ = Average transport number of membrane pair
t_1° = Transport number of cation through cation membrane
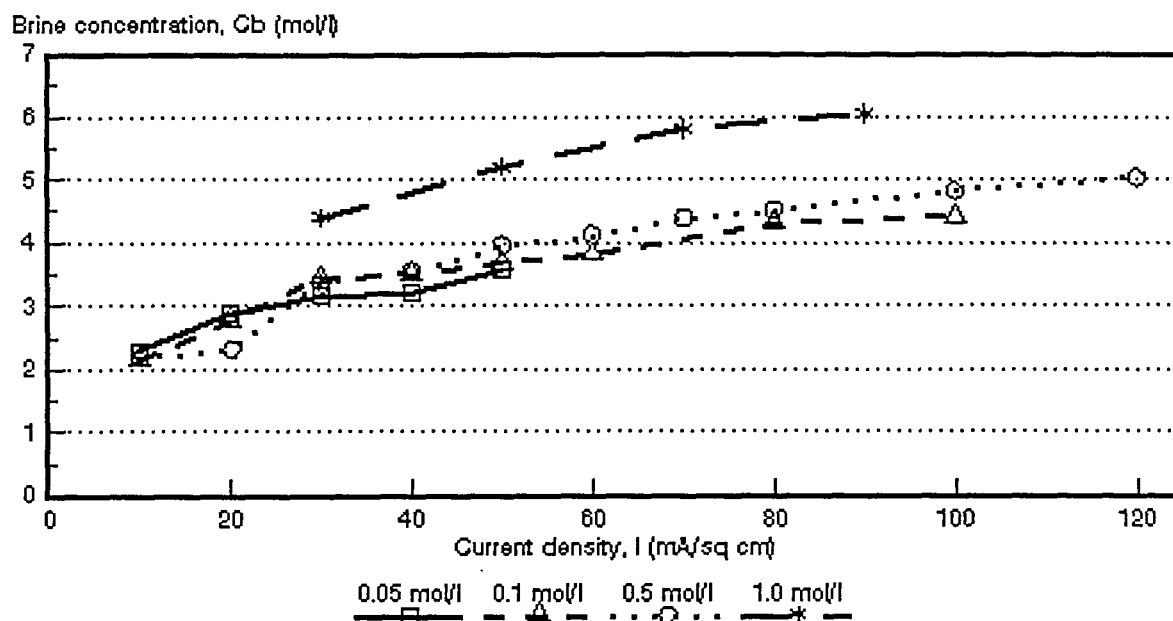t_2° = Transport number of anion through anion membrane.

Figure 8.1: Caustic soda concentration as a function of current density for 4 different NaOH feed water concentrations. *Selemion* AMV and CMV membranes.
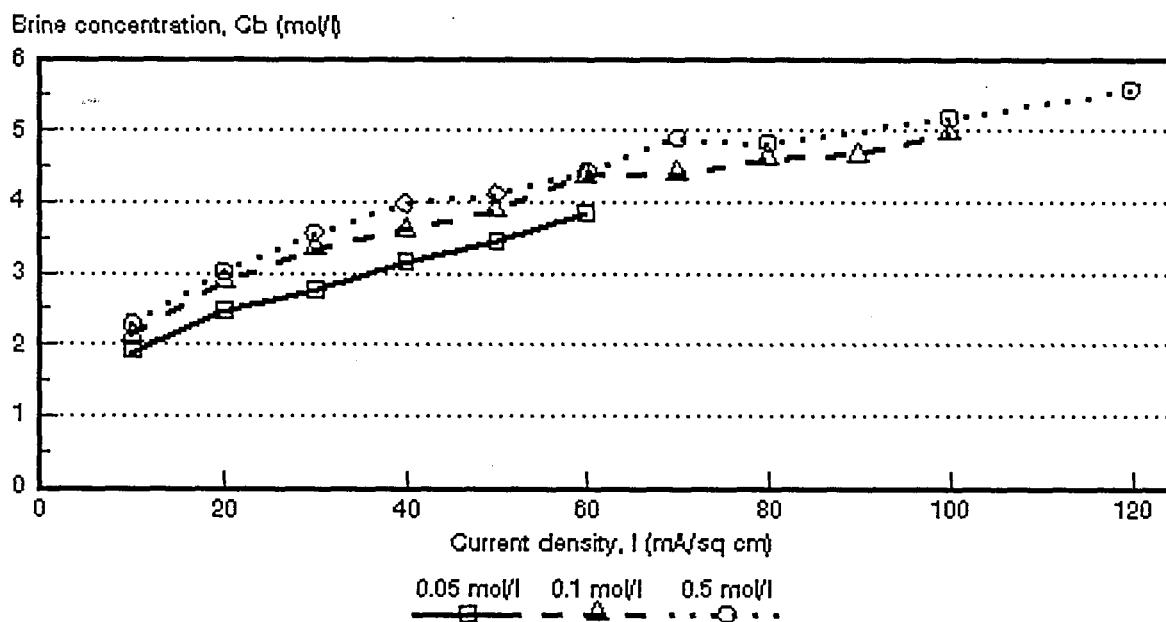

Figure 8.2: Caustic soda concentration as a function of current density for 3 different NaOH feed water concentrations. *Selemion* AMP and CMV membranes.
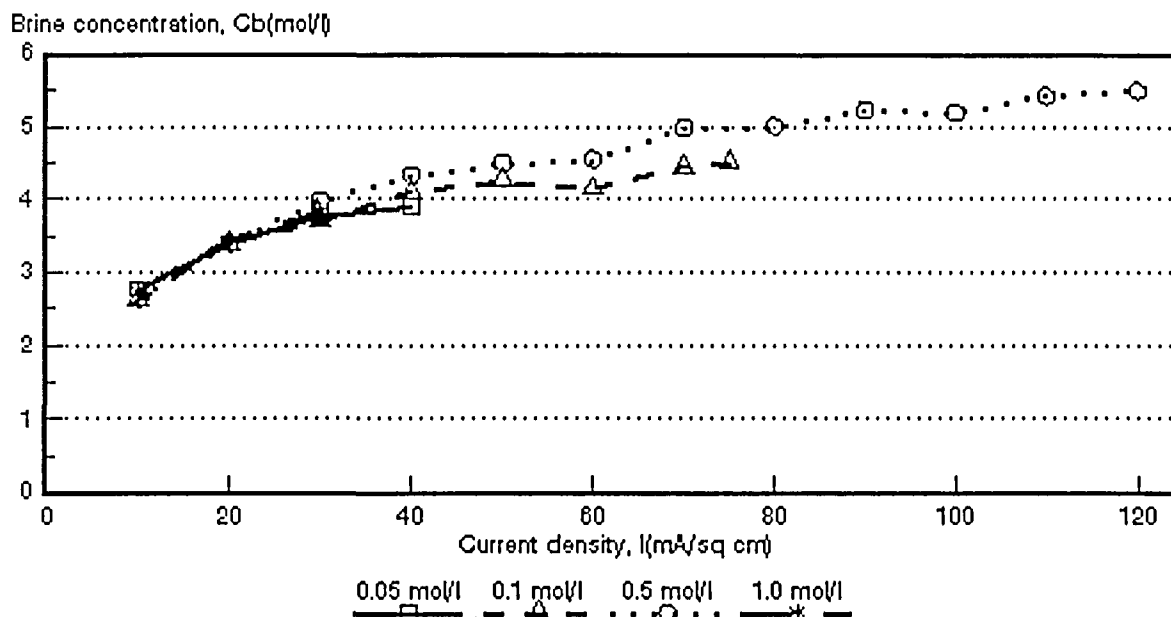
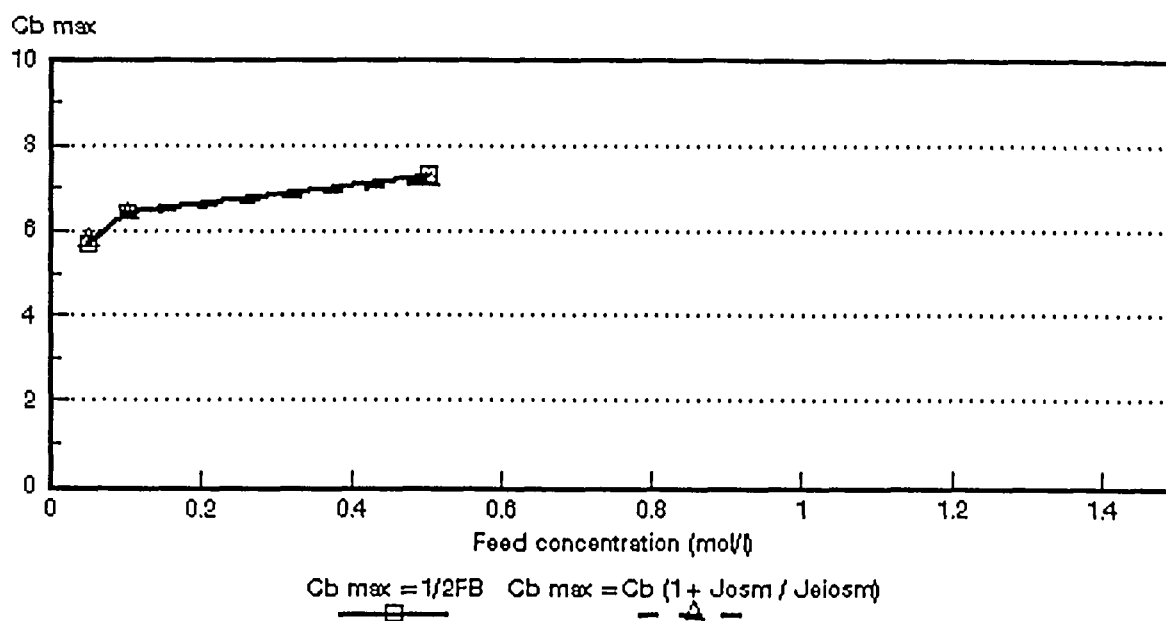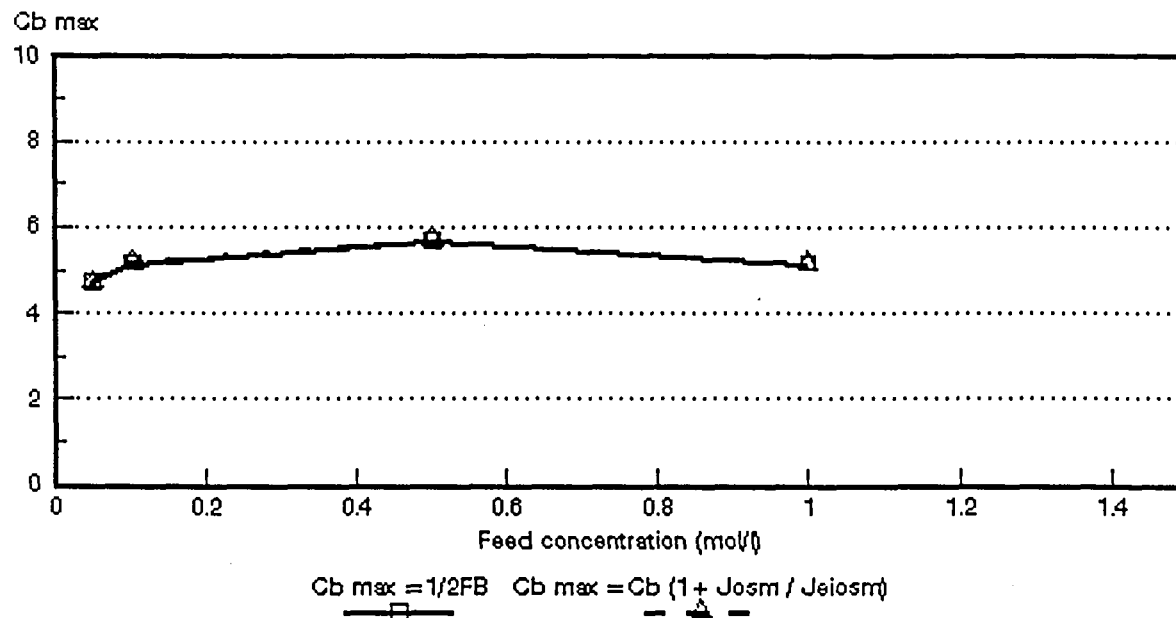Brine concentration, Cb(mol/l)

Figure 8.3:   Caustic soda concentration as a function of current density for 4 different NaOH feed water concentrations. *Ionac* MA-3475 and MC-3470 membranes.

available anion-exchange membranes. Consequently, membrane life time will be a problem when caustic soda solutions are electrodialyzed with conventional ion-exchange membranes. However, the value of the product recovered by ED might be of such a nature that a relatively short membrane life time could be tolerated.

It appears that the caustic soda brine concentration will reach a maximum value, c_b^{max}, as has been experienced with sodium chloride and hydrochloric acid solutions. This maximum value, however, was not reached even at the lowest caustic soda feed concentrations that were used (Figs. 8.1 to 8.3). It appears, however, that the maximum caustic soda brine concentration will be reached at relatively low current densities at the lowest feed water concentrations used. Maximum caustic soda brine concentration for higher caustic soda feed concentrations (0,1 to 1,0 mol/ℓ) will be reached at high current densities.

Maximum caustic soda brine concentration, c_b^{max}, was calculated from the same relationships as used in 6.1. The results are shown in Tables 8.13 and Figures 8.4 to 8.6.   Maximum caustic soda brine concentration depends somewhat on feed concentration. The *Selemion* AMV and CMV membranes showed an increase in the maximum brine concentration as a function of feed concentration in the feed

Table 8.13: Maximum caustic soda brine concentration, c_b^{max}, calculated from

$$c_b^{max} = 1/2\, F\beta* \text{ and } c_b^{max} = c_b\,(1 + J_{osm}/J_{eiosm})**$$

Feed Concentration mol/ℓ	Maximum Brine Concentration, c_b^{max}					
	AMV and CMV		AMP and CMV		MA-3475 and MC-3470	
	1	2	1	2	1	2
0,05	4,4	4,6	5,7	5,8	4,7	4,7
0,10	5,6	5,4	6,5	6,4	5,2	5,2
0,50	6,6	6,5	7,3	7,2	5,7	5,7
1,0	8,5	8,5			5,2	5,2

1   : $c_b^{max} = 1/2\, F\beta$

2   : $c_b^{max} = c_b\,(1 + J_{osm}/J_{eiosm})$

*   :   Calculated from electro-osmotic coefficients (Tables 8.1 - 8.11)

**   :   Calculated from $J_{eiosm} = J - J_{osm}$ (y-intercept and the corresponding c_b values) (Tables 8.1 - 8.11).

Cb max =1/2FB   Cb max =Cb (1+ Josm / Jeiosm)
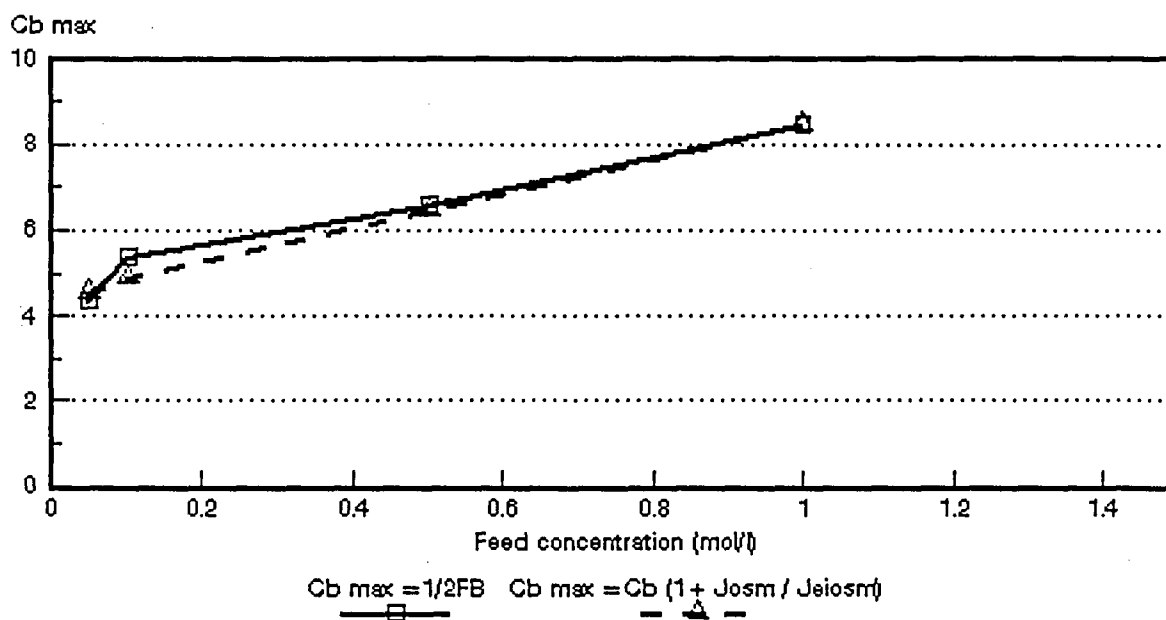
Figure 8.4: Maximum caustic soda brine concentration as a function of feed concentration for different NaOH feed water concentrations. *Selemion* AMV and CMV membranes.

296

Figure 8.5: Maximum caustic soda brine concentration as a function of feed concentration for different NaOH feed water concentrations. *Selemion* AMP and CMV membranes.

Figure 8.6: Maximum caustic soda brine concentration as a function of feed concentration for different NaOH feed water concentrations. *Ionac* MA-3475 and MC-3470 membranes.

concentration range from 0,05 to 1,0 mol/ℓ (Fig. 8.4). A similar trend was observed for the Selemion AMP and CMV membranes (Fig. 8.5) while the *Ionac* membranes first showed an increase and then a slight decrease in c_b^{max} at high feed concentration (Fig. 8.6). A very good correlation was again obtained by the two methods that were used to calculate the maximum caustic soda brine concentration (Table 8.13).

Caustic soda brine concentrations obtained at different current densities and feed water concentrations were predicted from measured transport numbers and volume flows (J) with the same relationship as used in 6.1. The experimental and calculated caustic soda brine concentrations are shown in Tables 8.1 to 8.11. and Figures 8.7 to 8.17. The calculated caustic soda brine concentrations were determined from the average value of the apparent transport number of a membrane pair ($\overline{\Delta t}$) and from water flows. The correlations between the calculated and experimentally determined brine concentrations, expressed as the ratio c_{bcalc}/c_{bexp}, are shown in Table 8.14.

The calculated caustic soda brine concentrations were significantly higher than the experimentally determined brine concentrations at a caustic soda feed concentration of 0,05 mol/ℓ in the case of the *Selemion* AMV and CMV and *Selemion* AMP and CMV membranes (Table 8.14). The calculated caustic soda brine concentration was from 1,36 to 1,54 times higher than the experimentally determined brine concentration in the case of the *Selemion* AMV and CMV membranes and from 1,25 to 1,47 higher in the case of the *Selemion* AMP and CMV membranes. However, a much better correlation was obtained at 0,1 and 0,5 mol/ℓ caustic soda feed concentration for both membrane pairs. The ratio c_{bcalc}/c_{bexp} varied between 1,23 and 1,25 (10 to 50 mA/cm², 0,1 mol/ℓ feed) and between 0,92 and 1,25 (10 to 50 mA/cm², 0,5 mol/ℓ feed) for the *Selemion* AMV and CMV membranes. The same ratio for the *Selemion* AMP and CMV membranes varied between 1,10 and 1,19 (10 to 50 mA/cm², 0,1 mol/ℓ feed) and between 1,11 and 1,14 (10 to 50 mA/cm², 0,5 mol/ℓ feed). Therefore, a higher estimation of caustic soda brine concentration can be obtained from measured transport numbers and water flows in this case.

A very good correlation was obtained between the calculated and experimentally determined caustic soda brine concentrations in the case of *Ionac* membranes at 0,05 and 0,1 mol/ℓ feed concentration. The ratio c_{bcalc}/c_{bexp} varied between 1,01 and 1,06 (10 to 40 mA/cm², 0,05 mol/ℓ feed) and between 0,95 and 0,99 (10 to 70 mA/cm², 0,1 mol/ℓ feed). Therefore, an excellent correlation was obtained. However, the correlations at 0,5 and 1,0 mol/ℓ feed for the same membranes were not very good (Table 8.14).
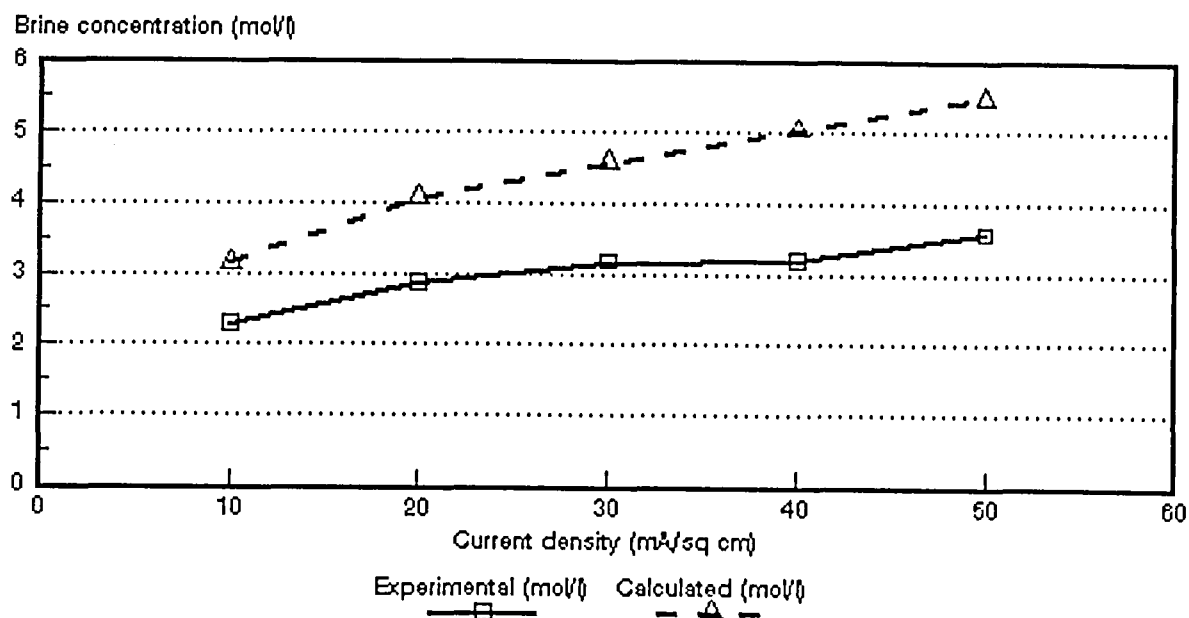
Figure 8.7: Experimental and calculated caustic soda brine concentrations as a function of current density for 0,05 mol/ℓ NaOH feed solution. *Selemion* AMV and CMV membranes.
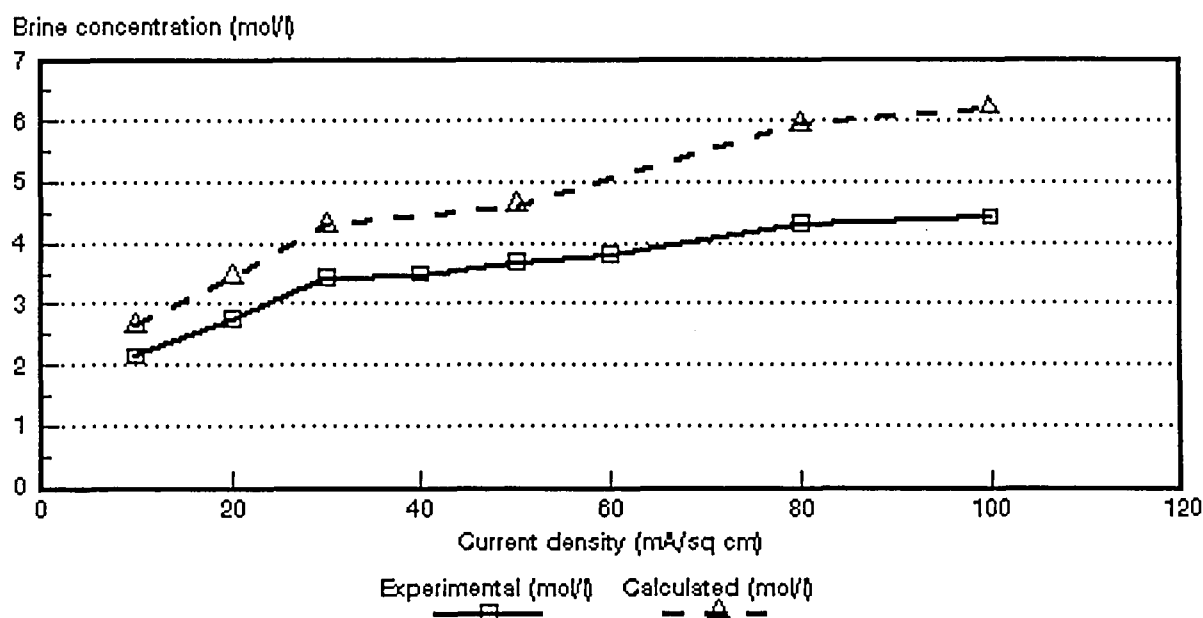

Figure 8.8: Experimental and calculated caustic soda brine concentrations as a function of current density for 0,1 mol/ℓ NaOH feed solution. *Selemion* AMV and CMV membranes.
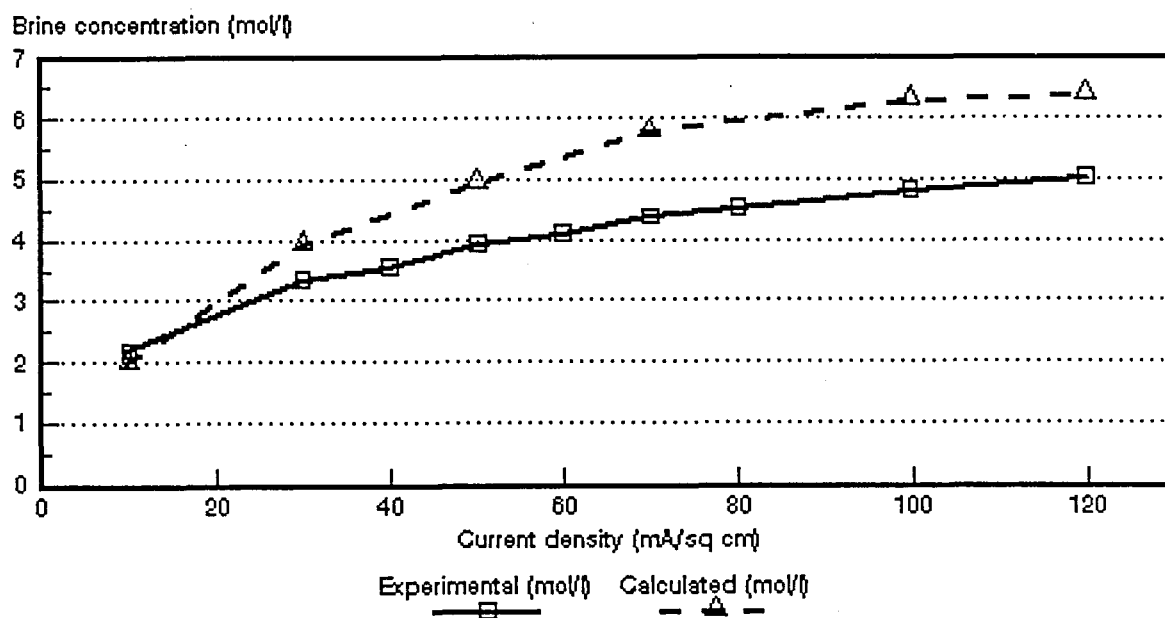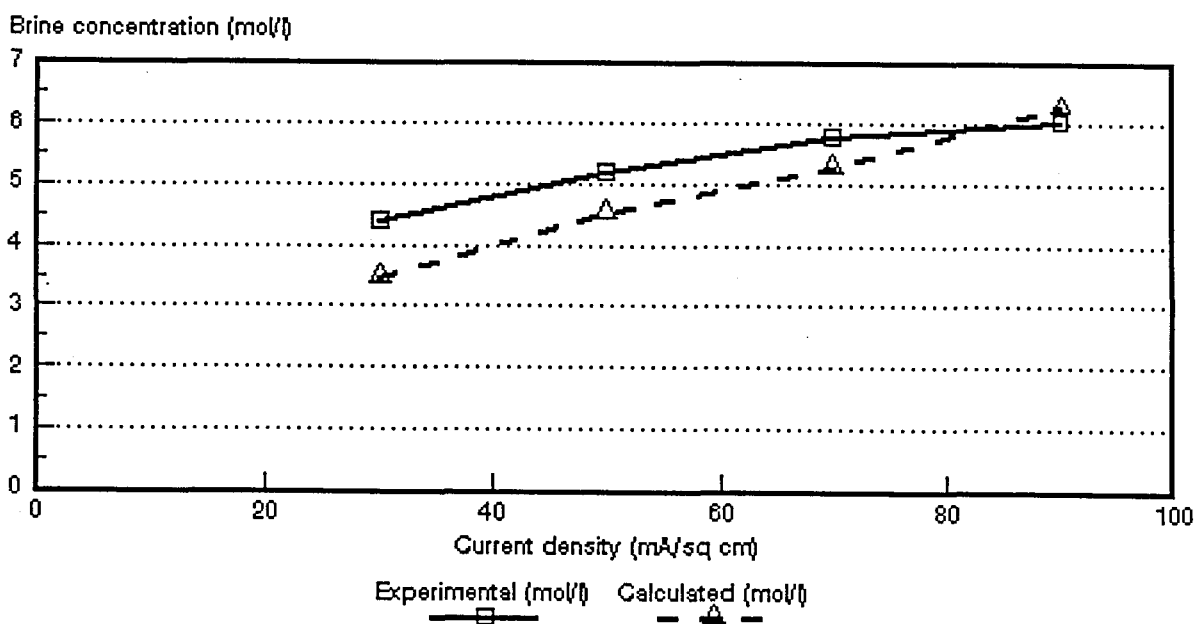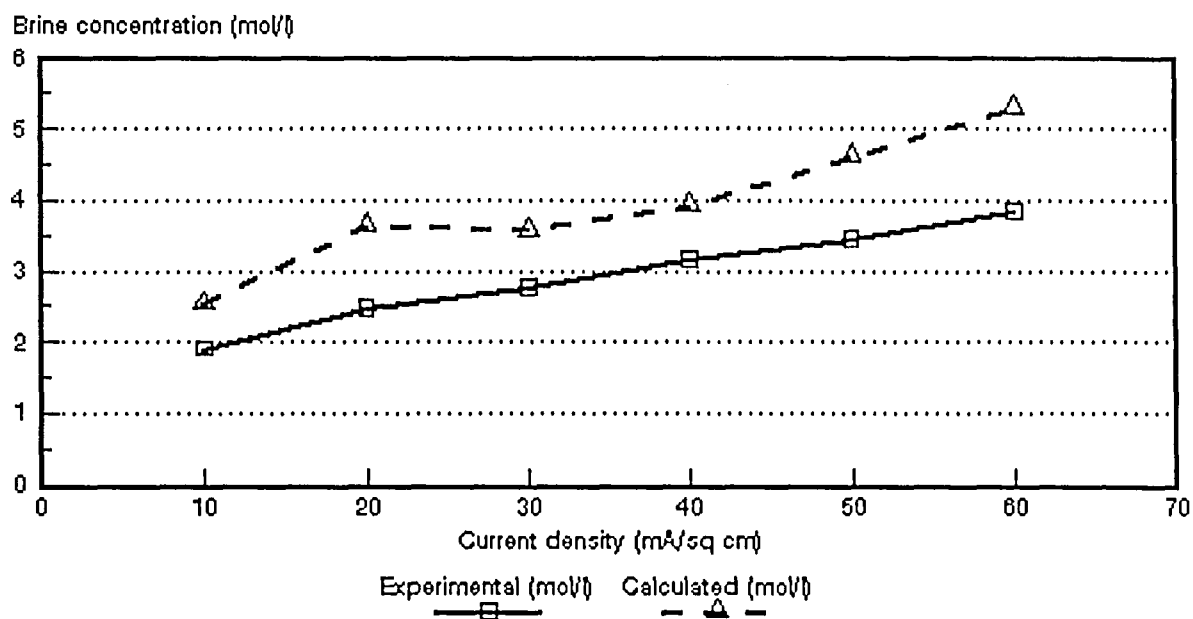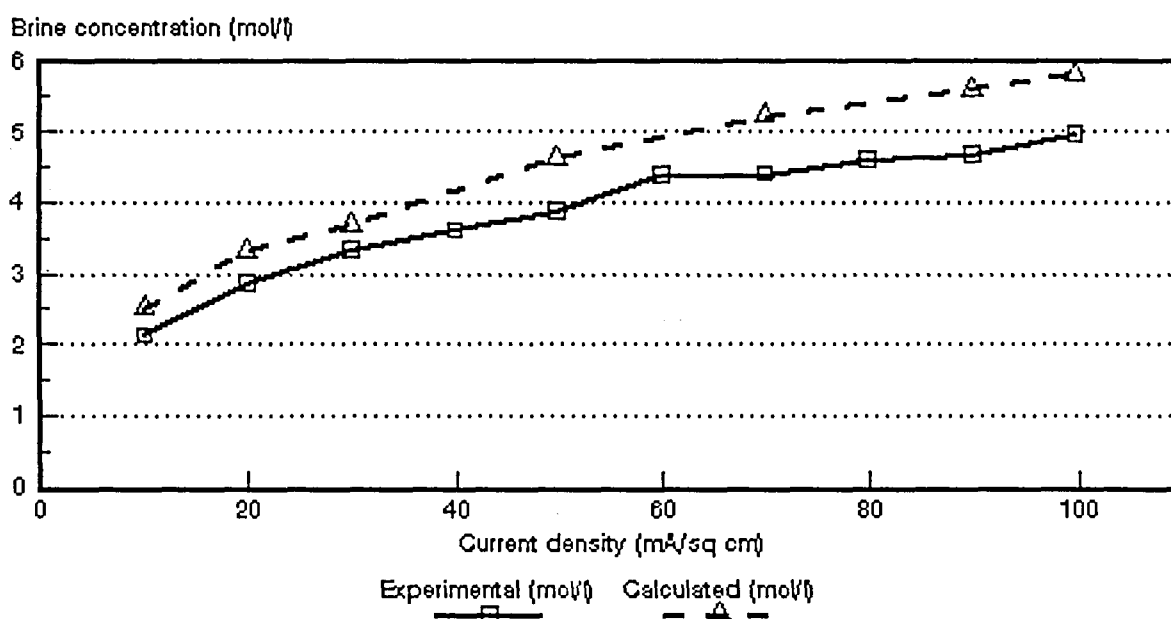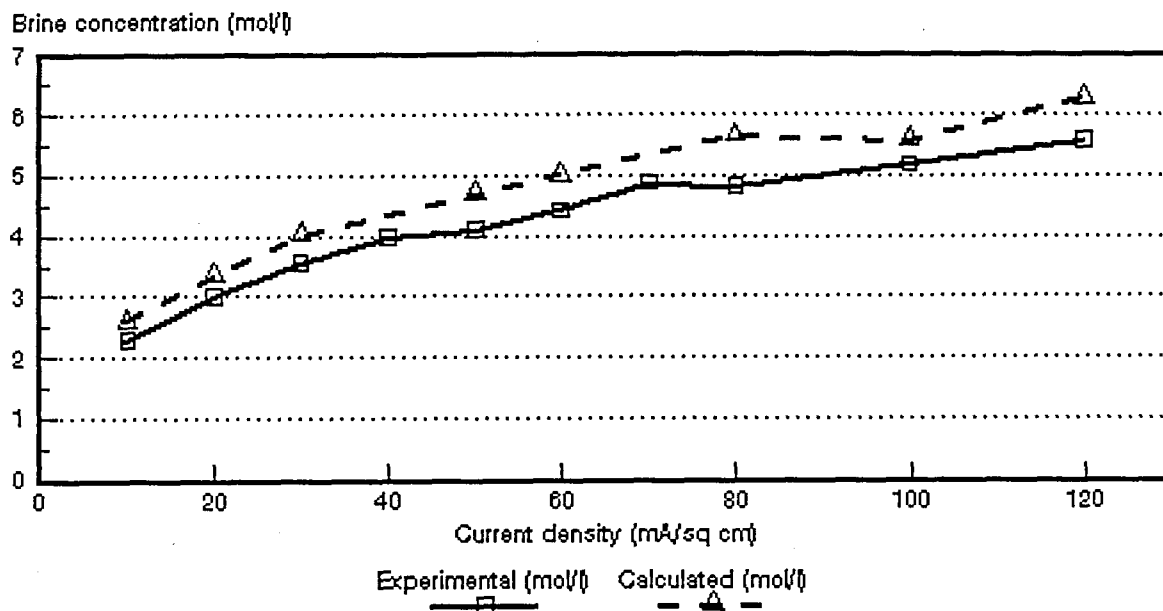
Brine concentration (mol/l)

Figure 8.9: Experimental and calculated caustic soda brine concentrations as a function of current density for 0,5 mol/l NaOH feed solution. *Selemion* AMV and CMV membranes.

Brine concentration (mol/l)

Figure 8.10: Experimental and calculated caustic soda brine concentrations as a function of current density for 1,0 mol/l NaOH feed solution. *Selemion* AMV and CMV membranes.
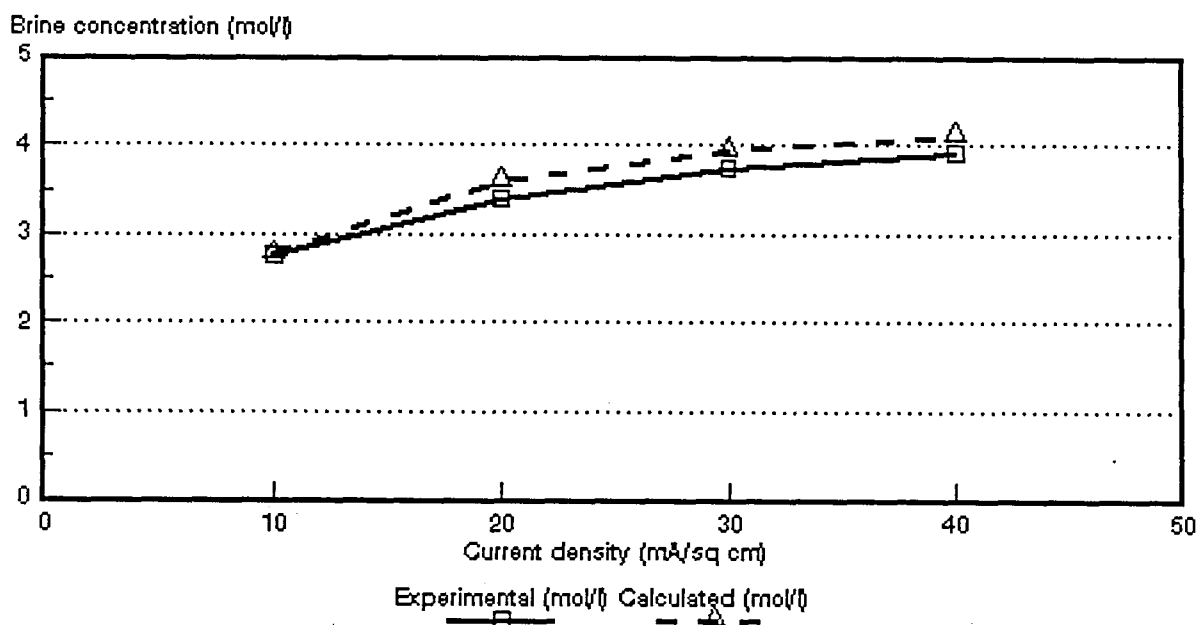
300

Brine concentration (mol/l)

Figure 8.11: Experimental and calculated caustic soda brine concentrations as a function of current density for 0,05 mol/ℓ NaOH feed solution. *Selemion* AMP and CMV membranes.

Brine concentration (mol/l)

Figure 8.12: Experimental and calculated caustic soda brine concentrations as a function of current density for 0,1 mol/ℓ NaOH feed solution. *Selemion* AMP and CMV membranes.

Brine concentration (mol/l)

Figure 8.13: Experimental and calculated caustic soda brine concentrations as a function of current density for 0,5 mol/ℓ NaOH feed solution. *Selemion* AMP and CMV membranes.

Brine concentration (mol/l)

Figure 8.14: Experimental and calculated caustic soda brine concentrations as a function of current density for 0,05 mol/ℓ NaOH feed solution. *Ionac* MA-3475 and MC-3470 membranes.
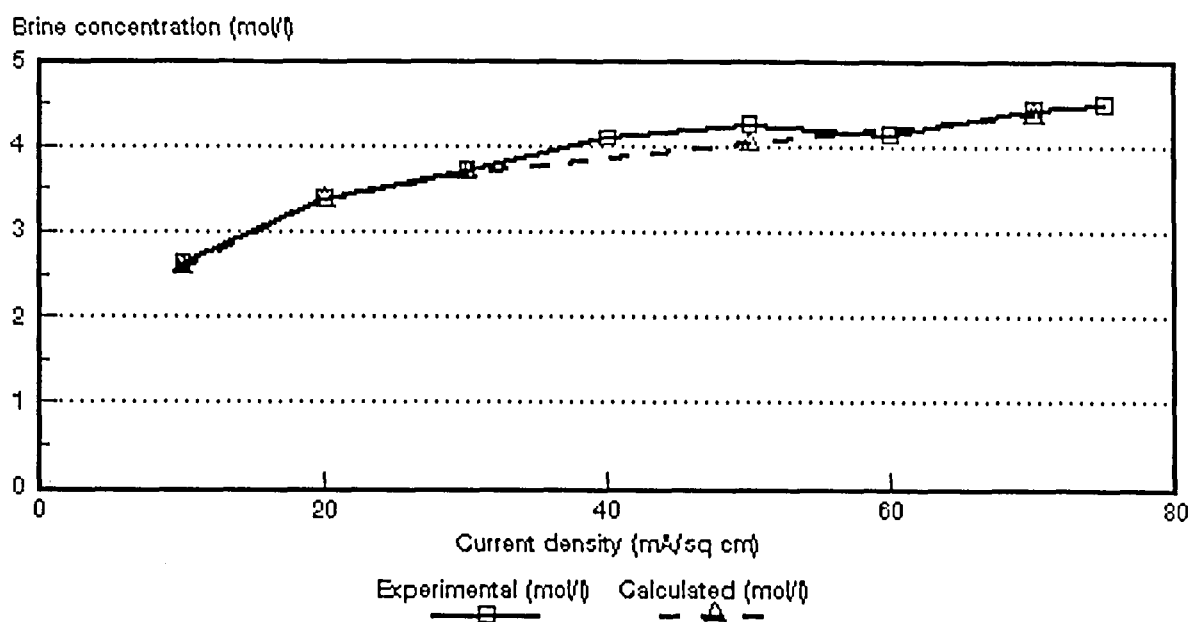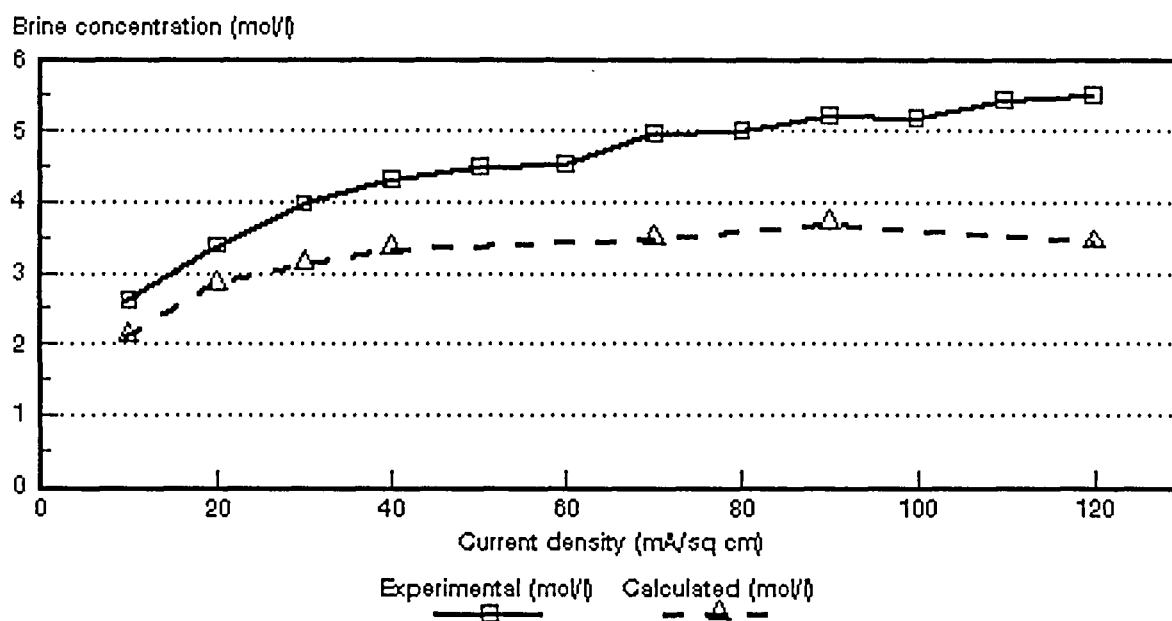
Figure 8.15: Experimental and calculated caustic soda brine concentrations as a function of current density for 0,1 mol/ℓ NaOH feed solution. *Ionac* MA-3475 and MC-3470 membranes.

Figure 8.16: Experimental and calculated caustic soda brine concentrations as a function of current density for 0,5 mol/ℓ NaOH feed solution. *Ionac* MA-3475 and MC-3470 membranes.
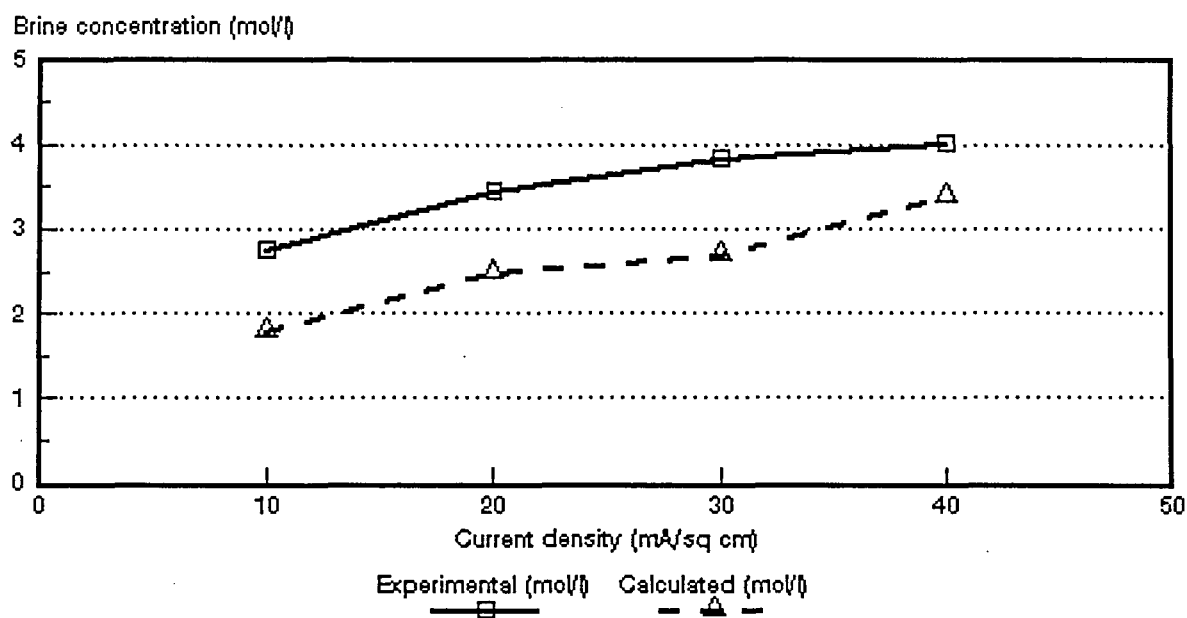
Figure 8.17: Experimental and calculated caustic soda brine concentrations as a function of current density for 1,0 mol/ℓ NaOH feed solution. *Ionac* MA-3475 and MC-3470 membranes.

Table 8.14: Correlation between calculated (c_{bcalc}) and experimentally (c_{bexp}) determined brine concentrations.

Current Density mA/cm²	c_{bcalc}/c_{bexp}										
	Selemion AMV & CMV Concentration, mol/ℓ				Selemion AMP & CMV Concentration, mol/ℓ			Ionac MA-3475 & MC-3470 Concentration, mol/ℓ			
	0,05	0,1	0,5	1,0	0,05	0,1	0,5	0,05	0,1	0,5	1,0
10	1,36	1,23	0,92		1,33	1,18	1,14	1,01	0,98	0,81	0,65
20	1,42	1,24	1,42		1,47	1,16	1,11	1,06	0,99	0,84	0,73
30	1,44	1,25	1,18	0,80	1,30	1,10	1,13	1,05	0,99	0,79	0,70
40	1,58				1,25			1,06		0,77	0,85
50	1,54	1,25	1,25	0,88	1,34	1,19	1,14		0,95		
60					1,38		1,13				
70			1,32	0,91		1,19			0,98	0,70	
75											
80		1,29					1,17				
90				1,04		1,20				0,71	
100		1,40	1,30			1,17	1,08				
110											
120							1,13				

305

8.2   Current Efficiency

Current efficiency (ε_p) determined during the EOP experiments as a function of current density and caustic soda feed water concentration is shown in Figures 8.18 to 8.20. Current efficiency increases with increasing feed water concentration in the caustic soda feed concentration range from 0,05 to 1,0 mol/ℓ. However, very little difference in current efficiency was experienced in the 0,1 to 0,5 mol/ℓ feed concentration range. Current efficiency was significantly higher at 1,0 mol/ℓ caustic soda feed concentration in the case of the *Selemion* AMV and CMV membranes (Fig. 8.18). This phenomena was not observed in the case of the *Selemion* AMP and CMV (Fig. 8.19) and the *Ionac* membranes (Fig. 8.20).

Current efficiency decreased slightly with increasing current density. This was observed even at the highest caustic soda feed concentration (1,0 mol/ℓ) in the case of the *Selemion* AMV and CMV membranes (Fig. 8.18). Current efficiency, however, appeared to remain reasonably constant in the 0,1 to 0,5 mol/ℓ feed water concentration range for all the membranes investigated.

The apparent transport numbers ($\overline{\Delta}t$, Δt^a and Δt^c) for a concentration difference similar to that obtained in the EOP experiments are shown in Figures 8.21 to 8.31. The current efficiencies (ε_p) as determined by the EOP method and shown in Figures 8.18 to 8.20 are also shown in Figures 8.21 to 8.31. The correlation between the apparent transport numbers ($\overline{\Delta}t$, Δt^a, Δt^c) and the current efficiency is shown in Tables 8.15 to 8.17.

The apparent transport numbers ($\overline{\Delta}t$) were significantly higher than the current efficiencies in the case of the *Selemion* AMV and CMV and *Selemion* AMP and CMV membranes at 0,05 mol/ℓ feed concentration (Table 8.15). The apparent transport numbers were from 1,37 to 1,57 times higher than the current efficiency for the *Selemion* AMV and CMV membranes in the 10 to 40 mA/cm² current density range (0,05 mol/ℓ feed). The apparent transport numbers were from 1,30 to 1,48 times higher than current efficiency for the *Selemion* AMP and CMV membranes in the 10 to 60 mA/cm² current density range (0,05 mol/ℓ feed). However, better correlations were obtained in the 0,1 and 0,5 mol/ℓ feed concentration range for both membrane types. The apparent transport numbers were approximately 1,2 times higher than the current efficiency in the 0,1 and 0,5 mol/ℓ feed concentration range for the *Selemion* AMV and CMV membranes (10 to 50 mA/cm²) while the ratio $\overline{\Delta}t/\varepsilon_p$ was approximately 0,9 at 1,0
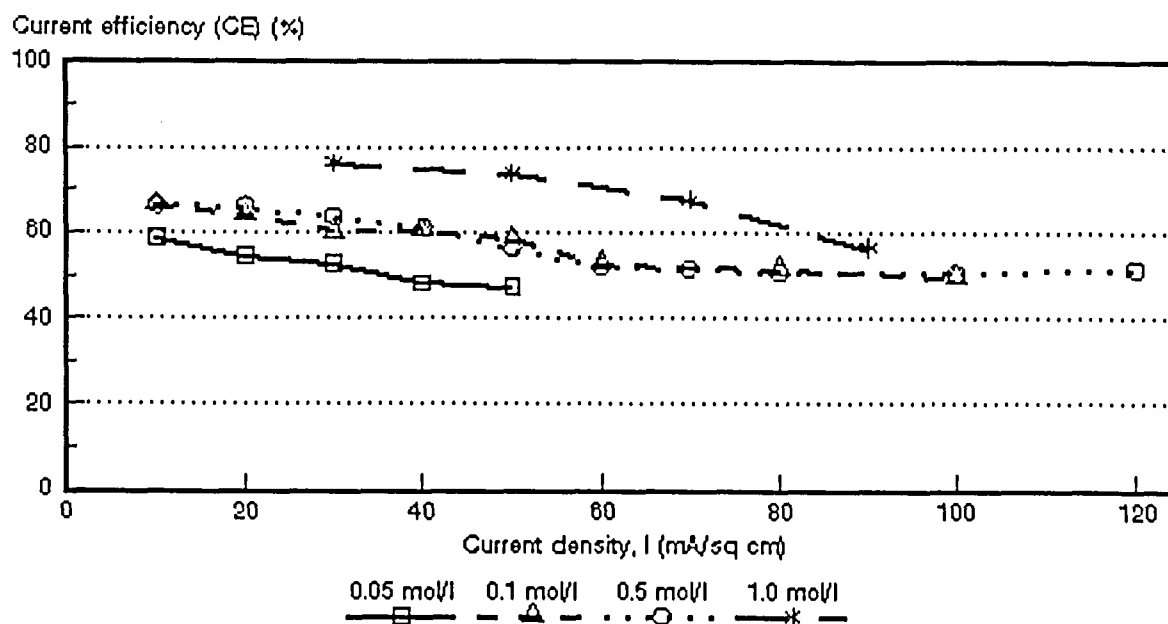
Current efficiency (CE) (%)

Figure 8.18: Current efficiency (ϵ_p) as a function of current density for 4 different NaOH feed water concentrations. *Selemion* AMV and CMV membranes.
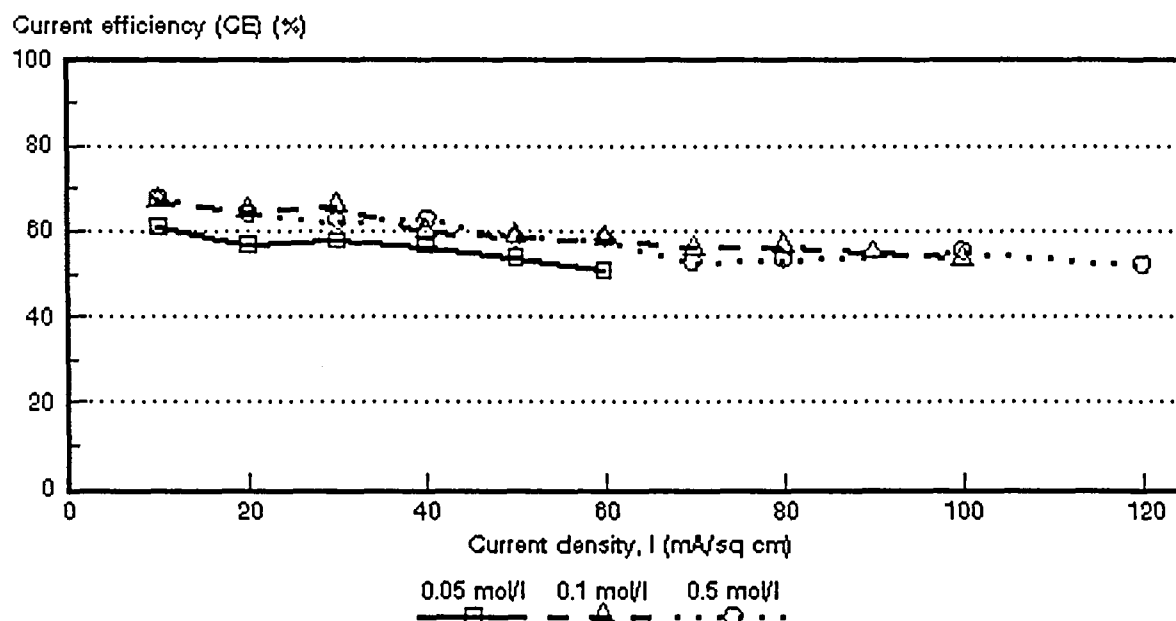
Current efficiency (CE) (%)

Figure 8.19: Current efficiency (ϵ_p) as a function of current density for 3 different NaOH feed water concentrations. *Selemion* AMP and CMV membranes.
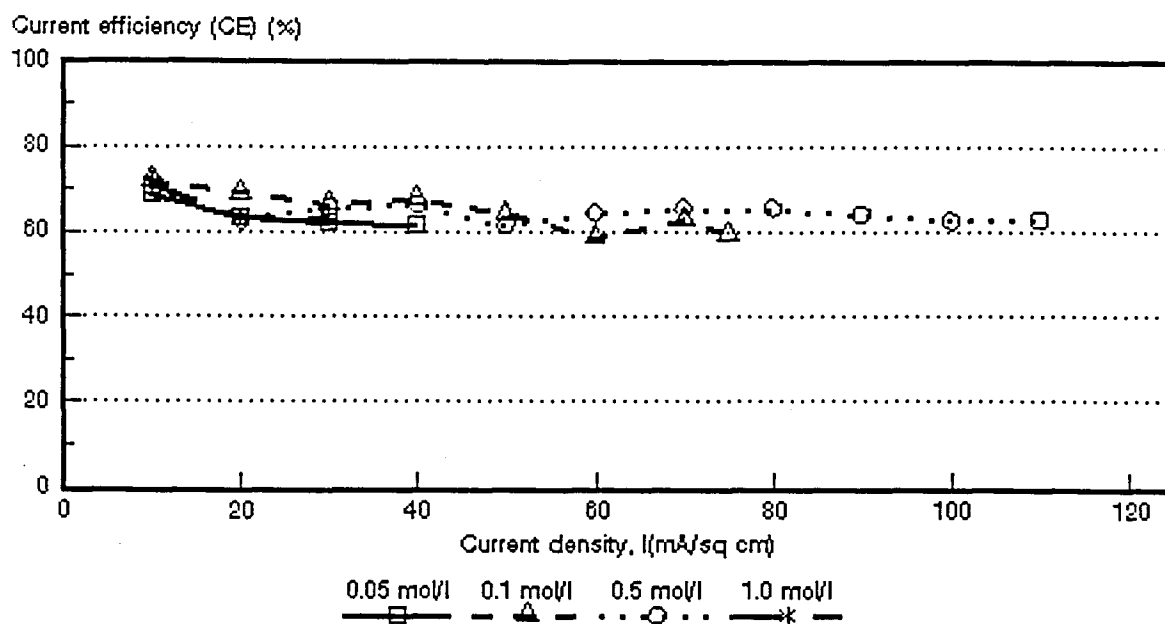
307

Current efficiency (CE) (%)

Figure 8.20: Current efficiency (ϵ_p) as a function of current density for 4 different NaOH feed water concentrations. *Ionac* MA-3475 and MC-3470 membranes.
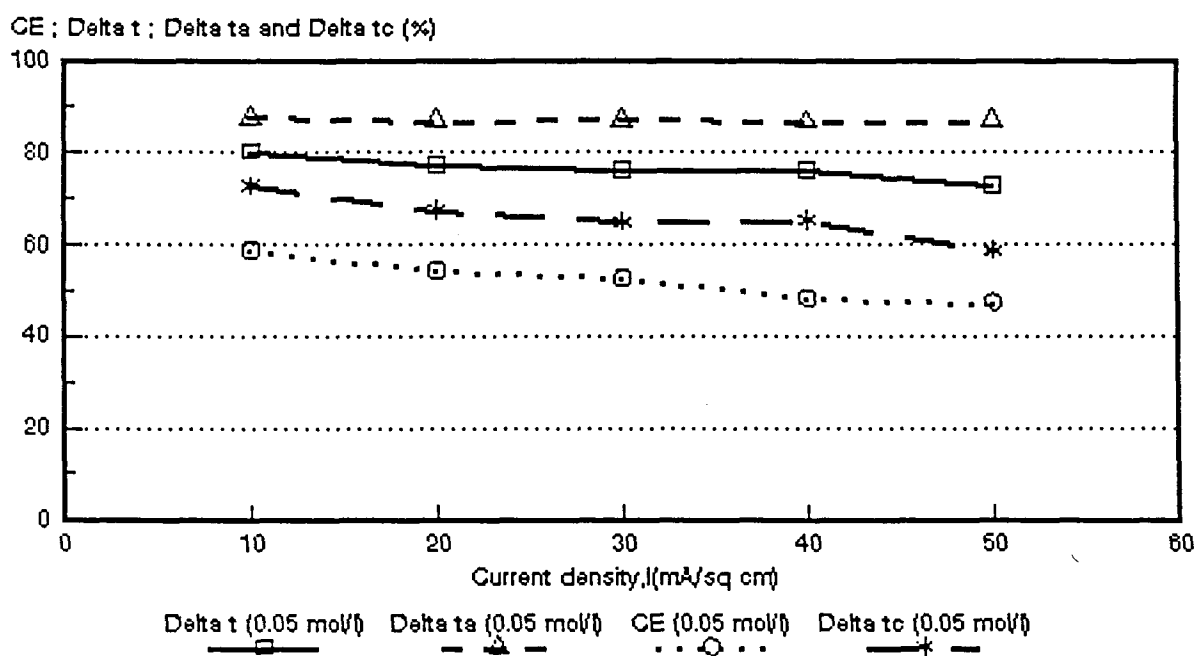
CE ; Delta t ; Delta ta and Delta tc (%)

Figure 8.21: Current efficiency (CE = ϵ_p) as a function of current density for 0,05 mol/ℓ NaOH feed. *Selemion* AMV and CMV membranes. Delta t = $\overline{\Delta}$t; Delta ta = Δt^a; Delta tc = Δt^c.
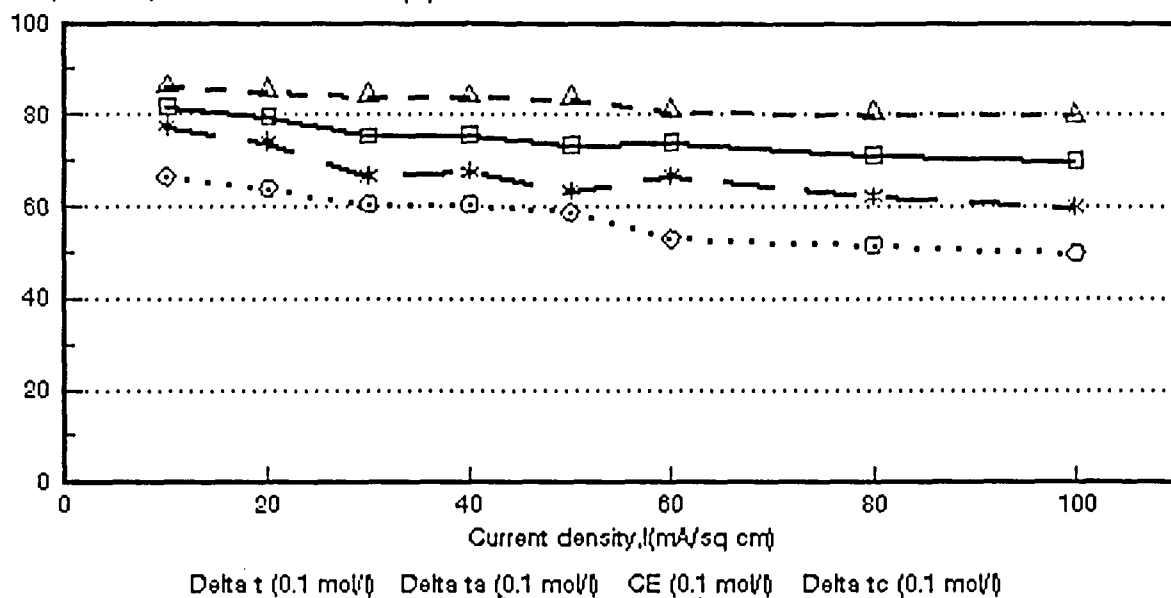
CE ; Delta t ; Delta ta and Delta tc (%)

Figure 8.22: Current efficiency (CE = ϵ_p) as a function of current density for 0,1 mol/ℓ NaOH feed. *Selemion* AMV and CMV membranes. Delta t = $\bar{\Delta}$t; Delta ta = Δt^a; Delta tc = Δt^c.
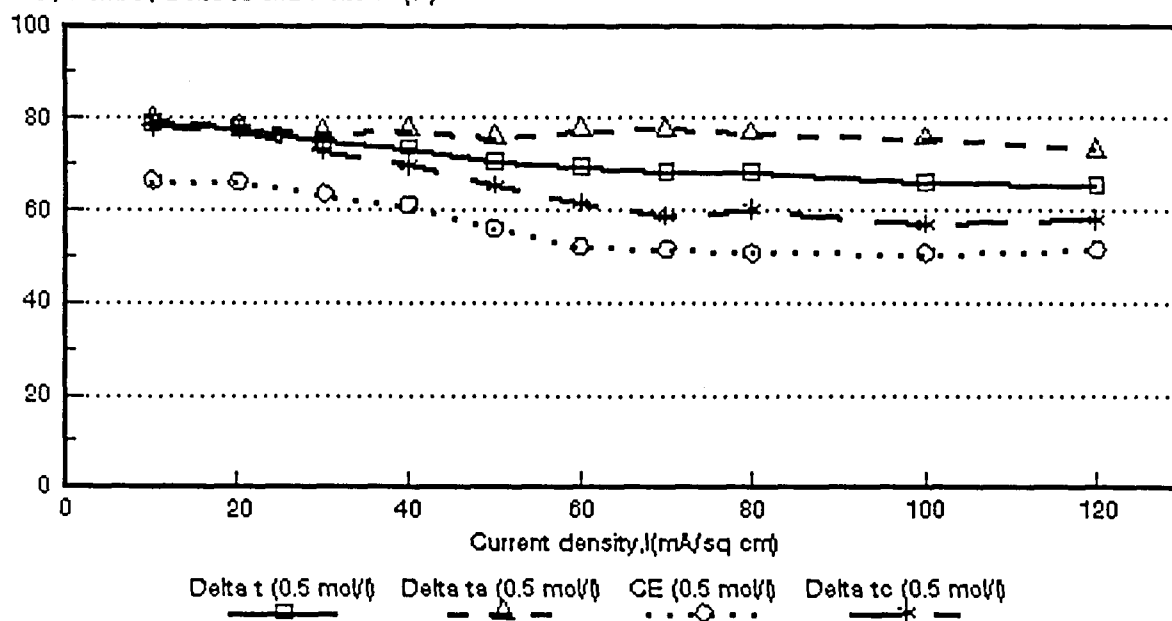
CE ; Delta t ; Delta ta and Delta tc (%)

Figure 8.23: Current efficiency (CE = ϵ_p) as a function of current density for 0,5mol/ℓ NaOH feed. *Selemion* AMV and CMV membranes. Delta t = $\bar{\Delta}$t; Delta ta = Δt^a; Delta = tc = Δt^c.

Figure 8.24: Current efficiency (CE = e_p) as a function of current density for 1,0 mol/ℓ NaOH feed. *Selemion* AMV and CMV membranes. Delta t = $\overline{\Delta}$t; Delta ta = Δt^a; Delta tc = Δt^c.
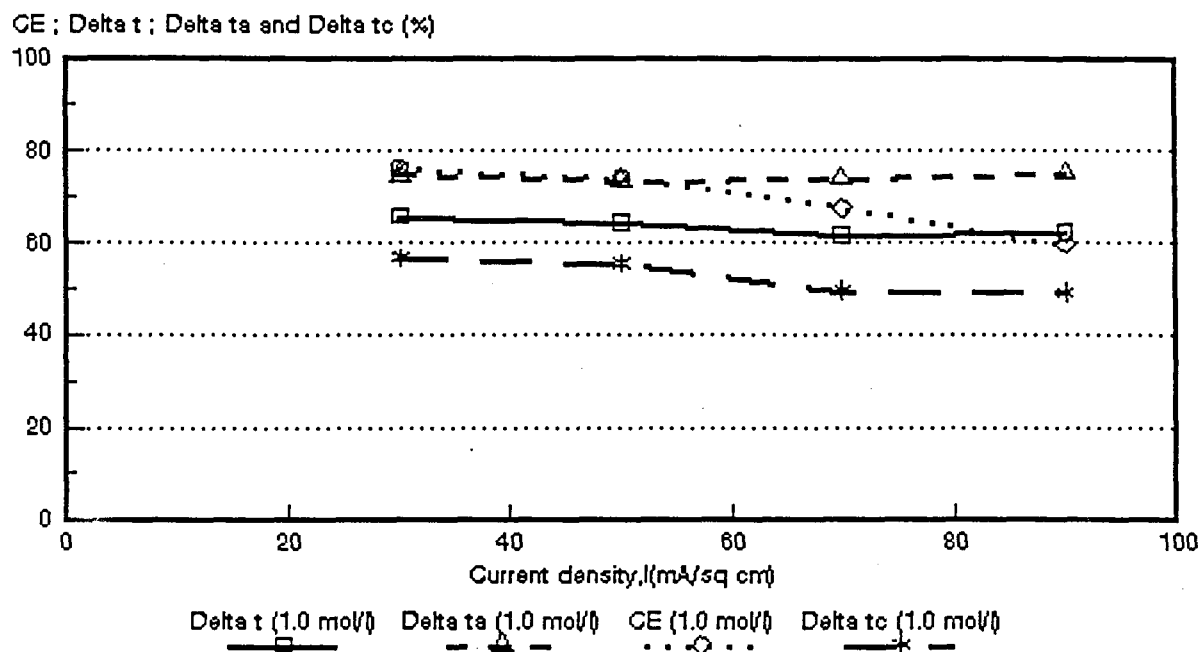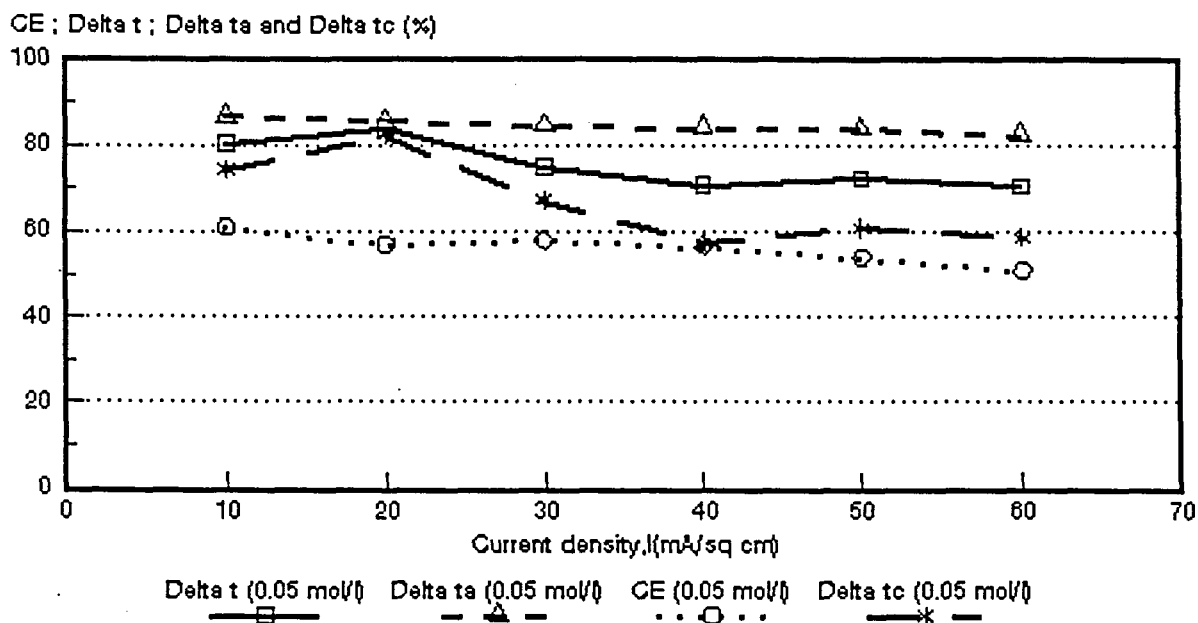

Figure 8.25: Current efficiency (CE = e_p) as a function of current density for 0,05 mol/ℓ NaOH feed. *Selemion* AMP and CMV membranes. Delta t = $\overline{\Delta}$t; Delta ta = Δt^c; Delta tc = Δt^c.

CE ; Delta t ; Delta ta and Delta tc (%)

Current density,I(mA/sq cm)

Delta t (0.1 mol/l)   Delta ta (0.1 mol/l)   CE (0.1 mol/l)   Delta tc (0.1 mol/l)

Figure 8.26: Current efficiency (CE = ϵ_p) as a function of current density for 0,1 mol/ℓ NaOH feed. *Selemion* AMP and CMV membranes. Delta t = $\bar{\Delta}$t; Delta tc = Δt^c; Delta ta = Δt^a.

CE ; Delta t ; Delta ta and Delta tc (%)

Current density,I(mA/sq cm)

Delta t (0.5 mol/l)   Delta ta (0.5 mol/l)   CE (0.5 mol/l)   Delta tc (0.5 mol/l)

Figure 8.27: Current efficiency (CE = ϵ_p) as a function of current density for 0,5 mol/ℓ NaOH feed. *Selemion* AMP and CMV membranes. Delta t = $\bar{\Delta}$t; Delta tc = Δt^c; Delta ta = Δt^a.
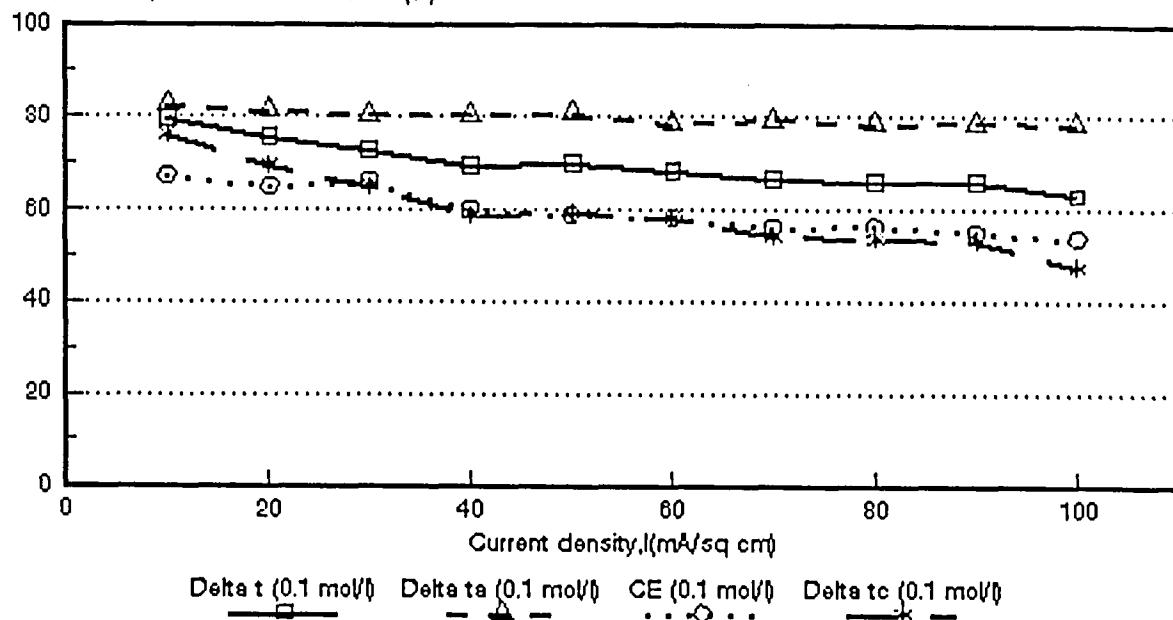
CE ; Delta t ; Delta ta and Delta tc (%)

Current density,I(mA/sq cm)

Delta t (0.05 mol/l)   Delta tc (0.05 mol/l)   CE (0.05 mol/l)   Delta ta (0.05 mol/l)

Figure 8.28: Current efficiency (CE = e_p) as a function of current density for 0,05 mol/l NaOH feed. *Ionac* MA-3470 and MC-3475 membranes. Delta t = $\bar{\Delta}$t; Delta tc = Δt^c; Delta ta = Δt^a.
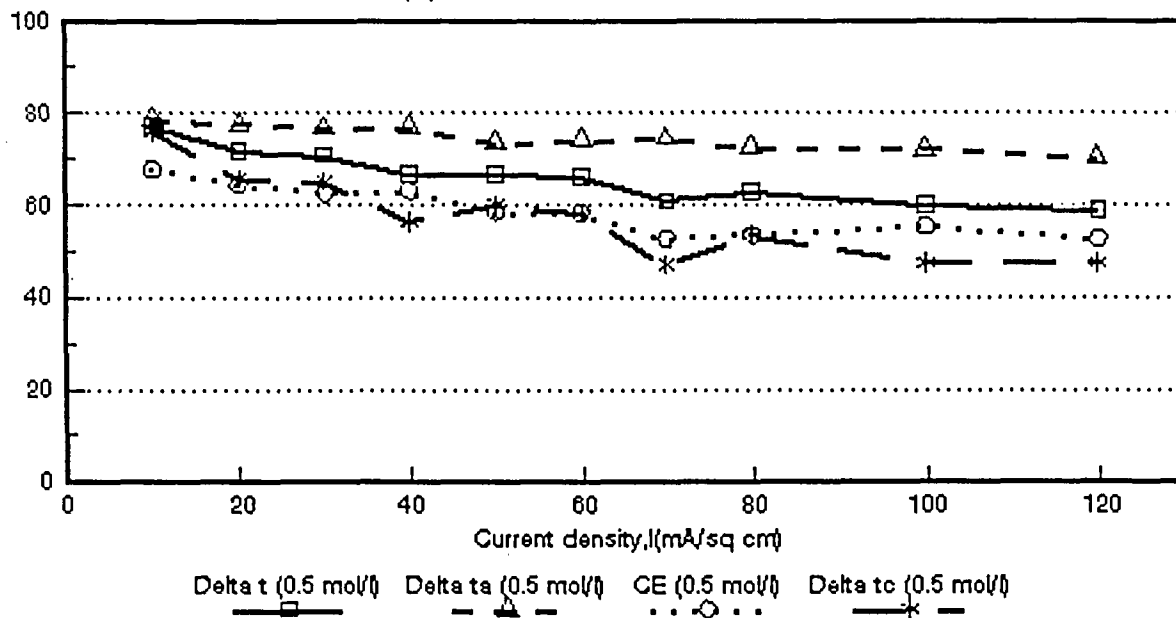
CE ; Delta t ; Delta ta and Delta tc (%)

Current density,I(mA/sq cm)

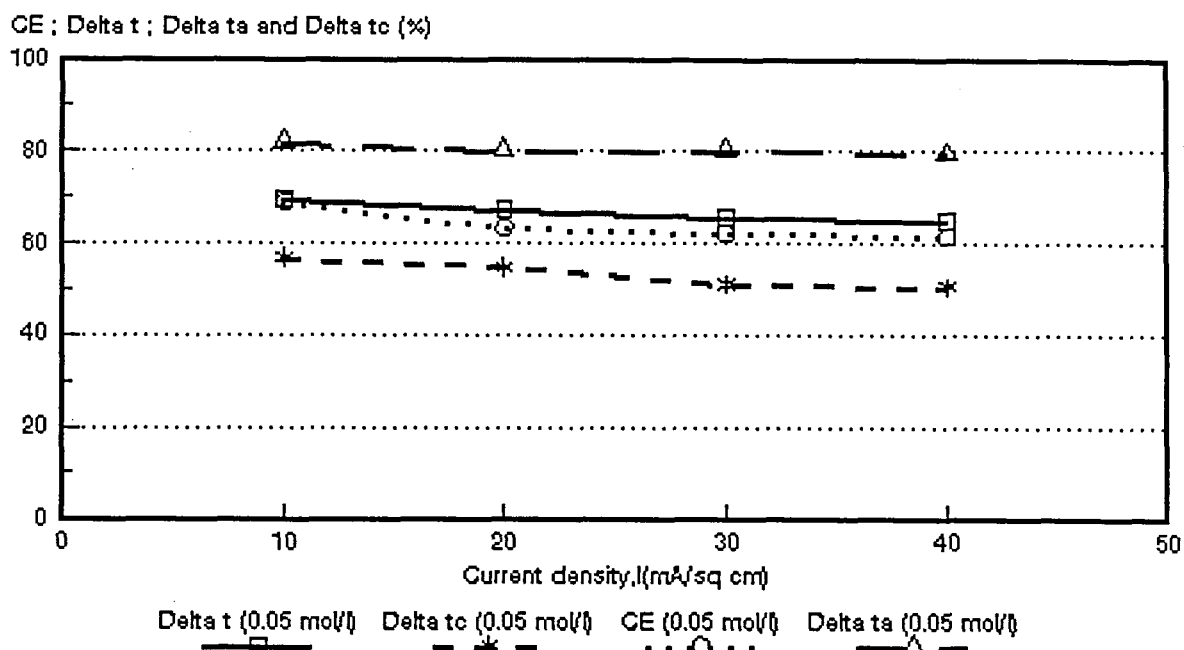Delta t (0.1 mol/l)   Delta tc (0.1 mol/l)   CE (0.1 mol/l)   Delta ta (0.1 mol/l)

Figure 8.29: Current efficiency (CE = e_p) as a function of current density for 0,1 mol/l NaOH feed. *Ionac* MA-3470 and MC-3475 membranes. Delta t = $\bar{\Delta}$t; Delta tc = Δt^c; Delta ta = Δt^a.
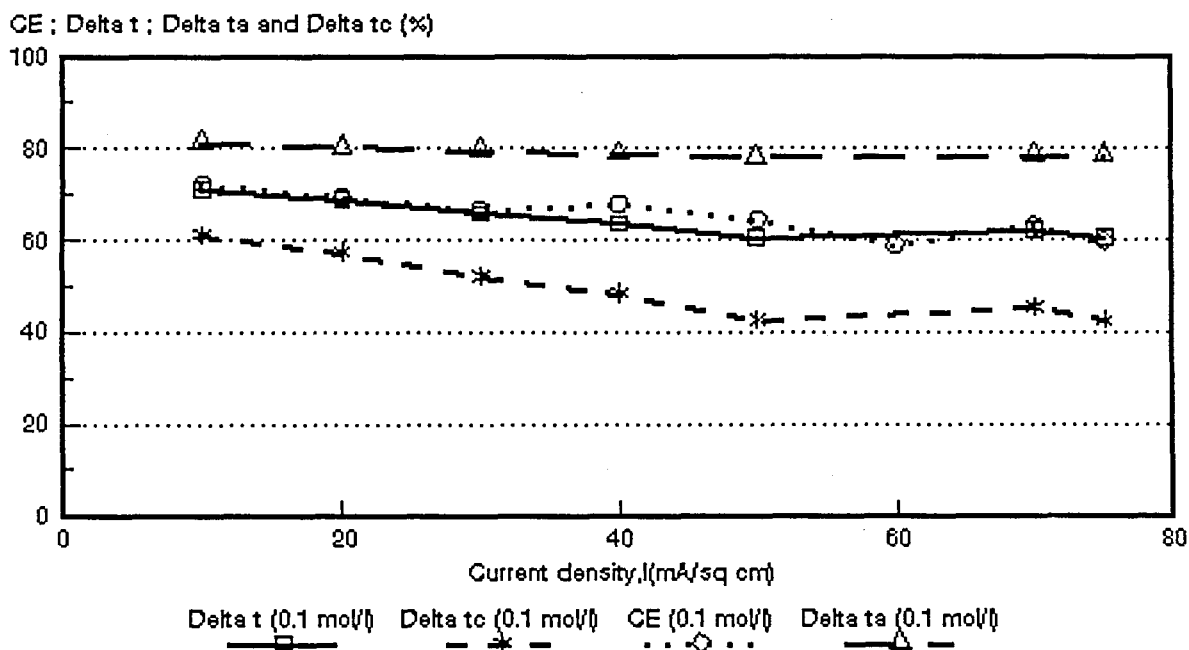
312

CE ; Delta t ; Delta ta and Delta tc (%)

Current density,I(mA/sq cm)

Delta t (0.5 mol/l)   Delta tc (0.5 mol/l)   CE (0.5 mol/l)   Delta ta (0.5 mol/l)

Figure 8.30   Current efficiency (CE = e_p) as a function of current density for 0,5 mol/ℓ NaOH feed. *Ionac* MA-3470 and MC-3475 membranes. Delta t = $\overline{\Delta}$t; Delta tc = Δ^c; Delta ta = Δt^a.

CE ; Delta t ; Delta ta and Delta tc (%)

Current density, I(mA/sq cm)

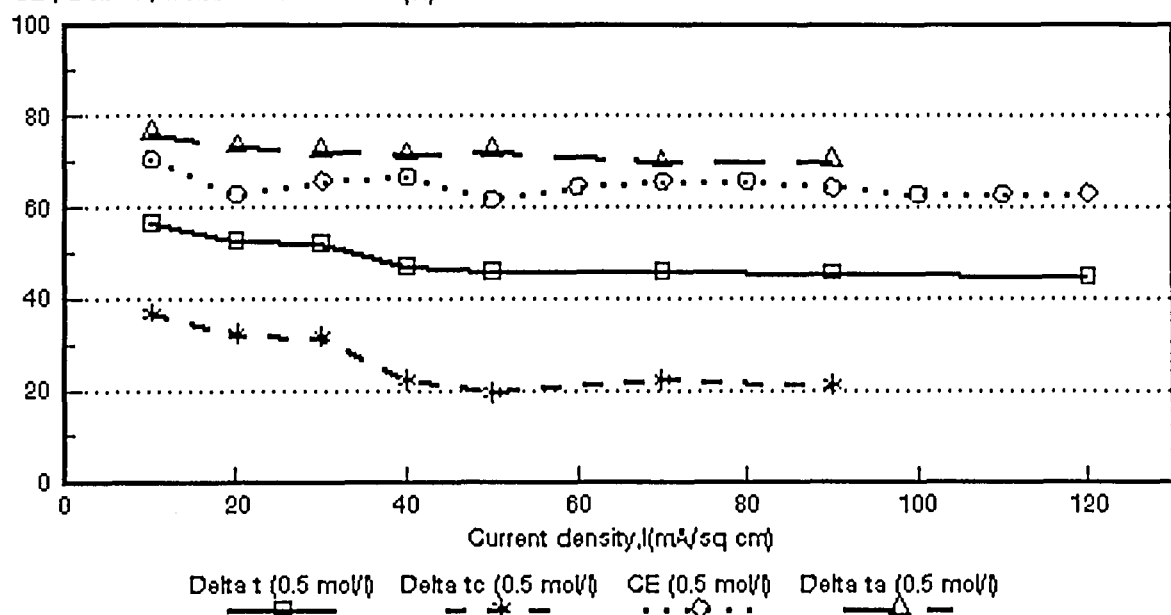Delta t (1.0 mol/l)   Delta tc (1.0 mol/l)   CE (1.0 mol/l)   Delta ta (1.0 mol/l)
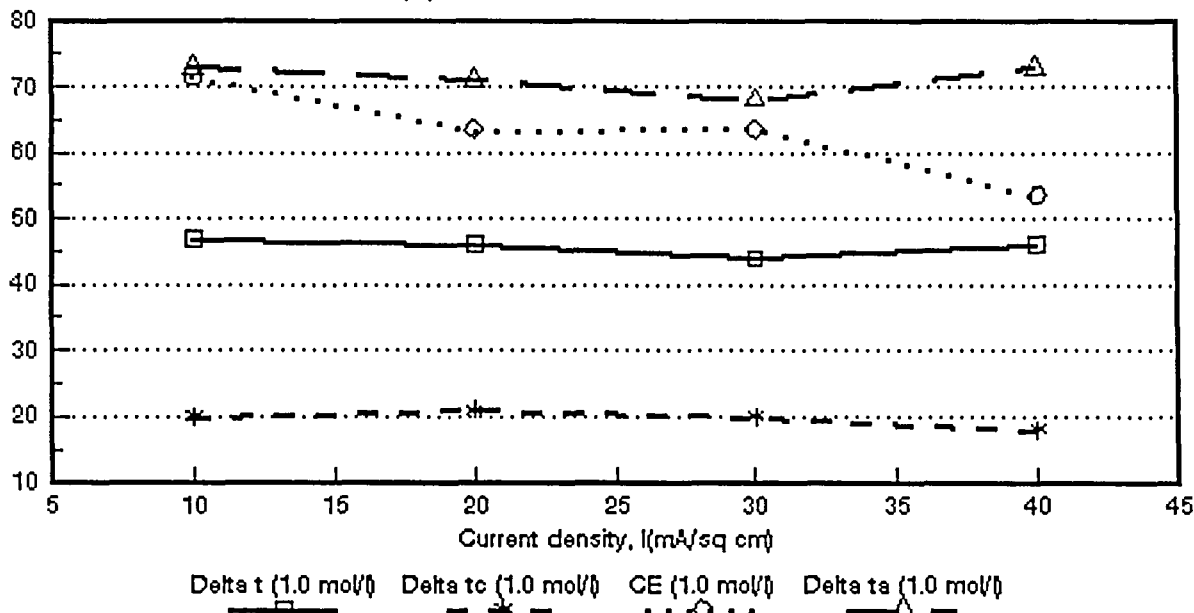
Figure 8.31   Current efficiency (CE = e_p) as a function of current density for 0,1 mol/ℓ NaOH feed. *Ionac* MA-3470 and MC-3475 membranes. Delta t = $\overline{\Delta}$t; Delta tc = Δt^c; Delta ta = Δt^a.

313

Table 8.15: Correlation between apparent transport number of a membrane pair ($\overline{\Delta t}$) and current efficiency (e_p).

Current Density mA/cm²	$\overline{\Delta t}/e_p$											
	Selemion AMV & CMV Concentration, mol/ℓ				Selemion AMP & CMV Concentration, mol/ℓ				Ionac MA-3475 & MC-3470 Concentration, mol/ℓ			
	0,05	0,1	0,5	1,0	0,05	0,1	0,5	0,05	0,1	0,5	1,0	
10	1,37	1,23	1,19		1,31	1,17	1,14	1,00	0,98	0,81	0,65	
20	1,42	1,23	1,16		1,47	1,15	1,10	1,06	0,98	0,84	0,72	
30	1,45	1,24	1,16	0,85	1,30	1,09	1,12	1,06	0,97	0,79	0,69	
40	1,57	1,24	1,19		1,48	1,15	1,05	1,06	0,93	0,71	0,84	
50		1,24	1,24	0,87	1,33	1,17	1,13		0,93	0,74		
60		1,38	1,32		1,37	1,17	1,13					
70			1,32	0,90		1,17	1,14		0,98	0,70		
75									1,01			
80		1,37	1,34			1,17	1,16					
90				1,04		1,20				0,70		
100		1,38	1,30			1,17	1,06					
110												
120			1,26				1,10					

Table 8.16:   Correlation between apparent transport number of the cation membrane (Δt^c) and current efficiency (ϵ_p).

Current Density mA/cm²	$\Delta t^c / \epsilon_p$										
	Selemion AMV & CMV Concentration, mol/ℓ				Selemion AMP & CMV Concentration, mol/ℓ			Ionac MA-3475 & MC-3470 Concentration, mol/ℓ			
	0,05	0,1	0,5	1,0	0,05	0,1	0,5	0,05	0,1	0,5	1,0
10	1,24	1,17	1,17		1,21	1,13	1,12	0,83	0,84	0,52	0,29
20	1,25	1,16	1,16		1,43	1,06	1,03	0,87	0,82	0,51	0,33
30	1,23	1,11	1,15	0,73	1,16	0,98	1,04	0,82	0,78	0,47	0,31
40	1,34	1,12	1,13		1,01	0,98	0,89	0,81	0,70	0,33	0,34
50	1,24	1,09	1,16	0,75	1,11	1,00	1,02		0,65	0,31	
60		1,26	1,17		1,14	0,99	0,99				
70			1,12	0,72		0,96	0,89		0,71	0,33	
75									0,70		
80		1,19	1,18			0,94	0,99				
90				0,82		0,96				0,33	
100		1,20	1,12			0,87	0,85				
110											
120			1,13				0,89				

Table 8.17: Correlation between apparent transport number of the anion membrane (Δt^*) and current efficiency (ε_p).

Current Density mA/cm²	$\Delta t^*/\varepsilon_p$ Selemion AMV & CMV Concentration, mol/ℓ				Selemion AMP & CMV Concentration, mol/ℓ			Ionac MA-3475 & MC-3470 Concentration, mol/ℓ			
	0,05	0,1	0,5	1,0	0,05	0,1	0,5	0,05	0,1	0,5	1,0
10	1,49	1,29	1,19		1,41	1,22	1,17	1,19	1,12	1,08	1,02
20	1,60	1,32	1,18		1,49	1,24	1,20	1,26	1,15	1,16	1,12
30	1,65	1,39	1,21	0,97	1,45	1,21	1,21	1,28	1,18	1,09	1,07
40	1,80	1,39	1,26		1,48	1,33	1,21	1,28	1,15	1,08	1,36
50	1,84	1,43	1,35	0,99	1,53	1,36	1,25		1,21	1,17	
60		1,53	1,48		1,61	1,34	1,27				
70		1,49		1,08		1,41	1,40		1,23	1,06	
75									1,31		
80		1,55	1,49			1,38	1,34				
90				1,26		1,42				1,09	
100		1,58	1,48			1,45	1,30				
110											
120			1,42				1,33				

mol/ℓ feed (30 to 50 mA/cm²). The ratio $\overline{\Delta t}/e_p$ for the *Selemion* AMP and CMV membranes varied between 1,1 and 1,2 (0,1 mol/ℓ feed, 10 to 70 mA/cm²) and was 1,1 at 0,5 mol/ℓ feed concentration (10 to 70 mA/cm²). Therefore, satisfactory correlations were obtained between the apparent transport numbers and current efficiency in the 0,1 to 0,5 mol/ℓ feed concentration ranges.

Very satisfactory correlations were obtained between $\overline{\Delta t}/e_p$ in the 0,05 to 0,1 mol/ℓ feed concentration range for the *Ionac* membranes (Fig's 8,28 and 8,29). The ratio $\overline{\Delta t}/e_p$ varied between 1 and 1,1 (10 to 40 mA/cm², 0,05 mol/ℓ) and between 0,9 and 1,0 (10 to 70 mA/cm², 0,1 mol/ℓ feed). The correlation, however, at 0,5 and 1,0 mol/ℓ feed concentration was not satisfactory. The ratio $\overline{\Delta t}/e_p$ varied between 0,7 and 0,8 at 0,5 mol/ℓ feed concentration and between 0,7 and 0,8 at 1,0 mol/ℓ feed concentration. Therefore, it should be possible to predict membrane performance for caustic soda concentration/desalination with ED with an accuracy of approximately 20% from the apparent transport numbers of the membrane pair. However, the accuracy of the predictions will depend on the feed concentration used.

Satisfactory correlations were obtained between the apparent transport numbers of the cation membrane (Δt^c) and current efficiency in the case of the *Selemion* and *Ionac* membranes (Table 8.16). The ratio between $\Delta t^c/e_p$ varied between 1,1 and 1,2 in the 0,1 to 0,5 mol/ℓ feed concentration range (10 to 120 mA/cm²) for the *Selemion* AMV and CMV membranes (Table 8.16). The same correlation was approximately 1,2 at 0,5 mol/ℓ feed concentration (10 to 50 mA/cm²) and varied between 0,7 and 0,8 at 1,0 mol/ℓ feed concentration (30 to 90 mA/cm²). The ratio between $\Delta t^c/e_p$ varied between 1,1 and 1,2 (0,05 mol/ℓ feed; 10 to 60 mA/cm²); 1,0 and 1,1 (0,1 mol/ℓ feed; 10 to 90 mA/cm²) and between 0,9 and 1,1 (0,5 mol/ℓ feed; 10 to 80 mA/cm²) for the *Selemion* AMP and CMV membranes. The ratio $\Delta t^c/e_p$ was approximately 0,8 (0,5 mol/ℓ feed; 10 to 40 mA/cm²) and varied between 0,7 and 0,8 (0,1 mol/ℓ feed; 10 to 70 mA/cm²) in the case of the *Ionac* membranes. However, a much poorer correlation was obtained at 0,5 and 1,0 mol/ℓ feed concentration as a result of the low selectivity of the cation membrane for sodium ions as a result of the high mobility of the hydroxyl ion[30] (Table 8.16). Therefore, it appears that membrane performance for caustic soda concentration/desalination can also be predicted from the apparent transport number of the cation membrane with an accuracy of approximately 20%.

Satisfactory correlations were obtained between the apparent transport number of the anion membrane (Δt^a) and current efficiency in the case of the *Selemion* AMV and CMV

- (1,0 mol/ℓ feed) and *Ionac* membranes (1,0 mol/ℓ feed) (Table 8.17). The ratio $\Delta t^a/e_p$ varied between approximately 1 and 1,1 in the case of the *Selemion* AMV and CMV membranes (30 to 70 mA/cm²). The ratio $\Delta t^a/e_p$ varied between 1 and 1,1 in the case of the *Ionac* membranes (10 to 30 mA/cm²). Poorer correlations of $\Delta t^a/e_p$ were obtained at the other feed concentrations (Table 8.17). Consequently, it should be possible to predict membrane performance for caustic soda concentration/desalination applications with an accuracy of approximately 10% from the apparent transport number of the anion membrane at high (1,0 mol/ℓ) feed concentration.

8.3 Water Flow

Water flow (J) through the membranes as a function of current density and feed water concentration is shown in Figures 8.32 to 8.34. Water flow (J_r) through the membranes relative to the flow at $J_{0,5\ mol/\ell}$ is shown in Table 8.18. Water flow through the membranes increases as a function of current density. Volume flow through the *Selemiom* AMV and CMV membranes increased in the 0,05 to 0,1 mol/ℓ feed concentration range (Table 8.18). However, volume flow decreased slightly in the 0,1 to 0,5 mol/ℓ feed concentration range at higher current densities and volume flow remained approximately constant at 1,0 mol/ℓ feed concentration. Current efficiency increased significantly in the 0,05 to 0,1 mol/ℓ feed concentration range (Fig. 8.18) as a result of the increased water flow. Current efficiency, however, was significantly higher at 1,0 mol/ℓ feed concentration (Fig. 8.18) than at 0,01 and 0,5 mol/ℓ feed, despite a slightly lower volume flow.

Volume flow decreased in the case of the *Selemion* AMP and CMV membranes in the feed concentration range from 0,05 to 0,5 mol/ℓ (Table 8.18). Current efficiencies, however, were approximately the same especially at the two higher feed concentrations (Fig. 8.19).

Volume flow was slightly higher at 0,1 mol/ℓ feed concentration in the case of the *Ionac* membranes in the beginning of the run. It is interesting to note that current efficiency has also been slightly higher at this feed concentration (Fig. 8.20). However, current efficiency was approximately the same in the feed concentration range from 0,05 to 1,0 mol/ℓ. Nevertheless, it also appears with caustic soda solutions as has been the case with sodium chloride solutions that increasing water flow can cause an increase in current efficiency.

Water flow (J) through the membranes as a function of effective current density, I_{eff}, and feed concentration is shown in Figures 8.35 to 8.37. Straight lines were obtained at higher values of I_{eff}. The slope of these lines corresponds to the combined electro-osmotic coefficient (2β) of a membrane pair. The electro-osmotic coefficients as a function of caustic soda feed water concentration is shown in Figures 8.38 to 8.40. The electro-osmotic coefficients decreased sharply with increasing feed concentration in the case of the *Selemion* AMV and CMV membranes (Figs. 8.38). It is interesting to note that the electro-osmotic coefficients have decreased over the entire feed concentration range from 0,05 to 1,0 mol/ℓ. A similar effect was observed with the *Selemion* AMP

and CMV membranes but the decrease in the electro-osmotic coefficients were far less (Fig. 8.39). These membranes, therefore, deswell less than the *Selemion* AMV and CMV membranes with increasing feed concentration. The *Ionac* membranes also showed less deswelling than the *Selemion* AMV and CMV membranes (Fig. 8.40).

The effect of the electro-osmotic coefficient on the maximum caustic soda brine concentration, c_b^{max}, is shown in Table 8.19. Maximum caustic soda brine concentration increases with decreasing electro-osmotic coefficient. The electro-osmotic coefficient of the *Selemion* AMP and CMV membranes were lower than that of the *Selemion* AMV and CMV and *Ionac* membranes. The electro-osmotic coefficient of the *Selemion* AMP and CMV membranes were determined at 0,155 ℓ/Faraday at 0,1 mol/ℓ feed concentration. The coefficients for the *Selemion* AMV and CMV and *Ionac* membranes at the same feed concentration were 0,179 and 0,193 ℓ/Faraday, respectively. Therefore, higher caustic soda brine concentrations could be obtained with the *Selemion* AMP and CMV membranes.

Approximately 8 to 9 mol H_2O/Faraday passed through the *Selemion* AMP and CMV membranes in the feed concentration range between 0,1 and 0,5 mol/ℓ (Table 8.19). Approximately 8 to 10 and 10 to 11 mol H_2O/Faraday passed through the membranes in the case of the *Selemion* AMV and CMV and *Ionac* membranes, respectively (0,1 to 0,5 mol/ℓ feed).

The osmotic flow (J_{osm}) relative to the total flow (J) through the membranes as a function of current density is shown in Table 8.20. The osmotic water flow through the membranes decreases with increasing current density. Osmotic water flow represented 45,9; 46,9 and 26,5% of the total flow through the membranes at a current density of 30 mA/cm² in the case of the *Selemion* AMV and CMV; *Selemion* AMP and CMV and *Ionac* membranes, respectively. Therefore, osmosis makes a significant contribution to water flow through the membranes at relative low current density. The osmotic contribution to total flow through the membranes (*Selemion* AMV and CMV and *Selemion* AMP and CMV) at a current density of 100 mA/cm² (0,1 mol/ℓ feed) was 21,4 and 25,7%, respectively. The osmotic contribution to the total flow in the case of the *Ionac* membranes at a current density of 70 mA/cm² (0,1 mol/ℓ feed) was 14,2%. Therefore, the contribution of osmotic water flow to total water flow through the membranes is much lower at high current density.
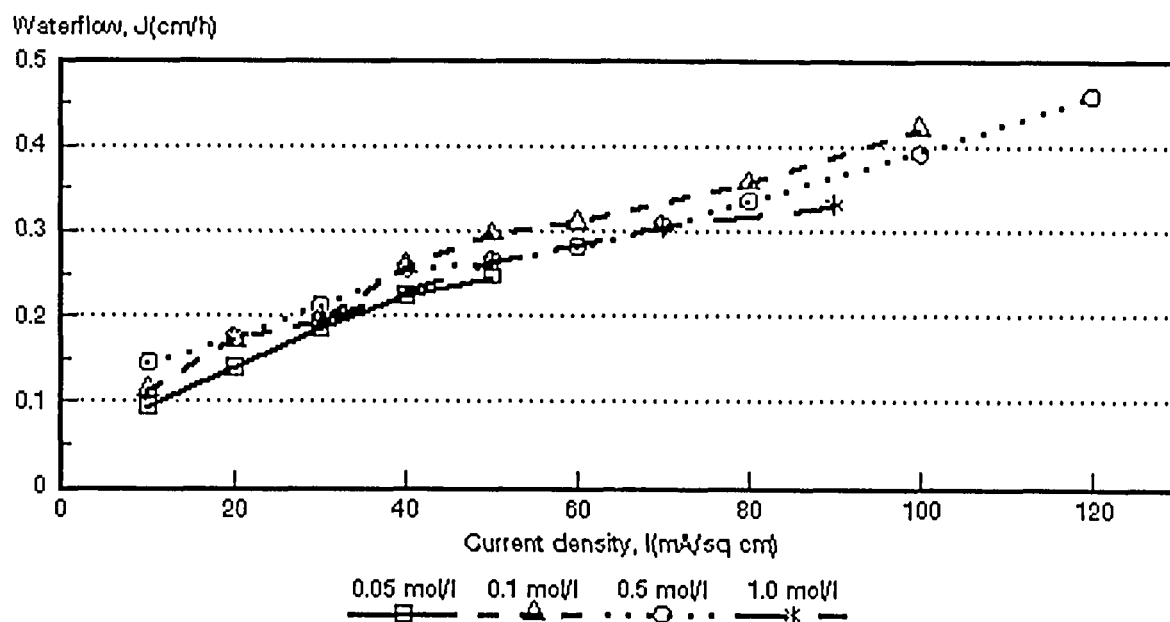
320

Waterflow, J(cm/h)

Figure 8.32   Water flow through the membranes as a function of current density and
feed water concentration. *Selemion* AMV and CMV membranes.
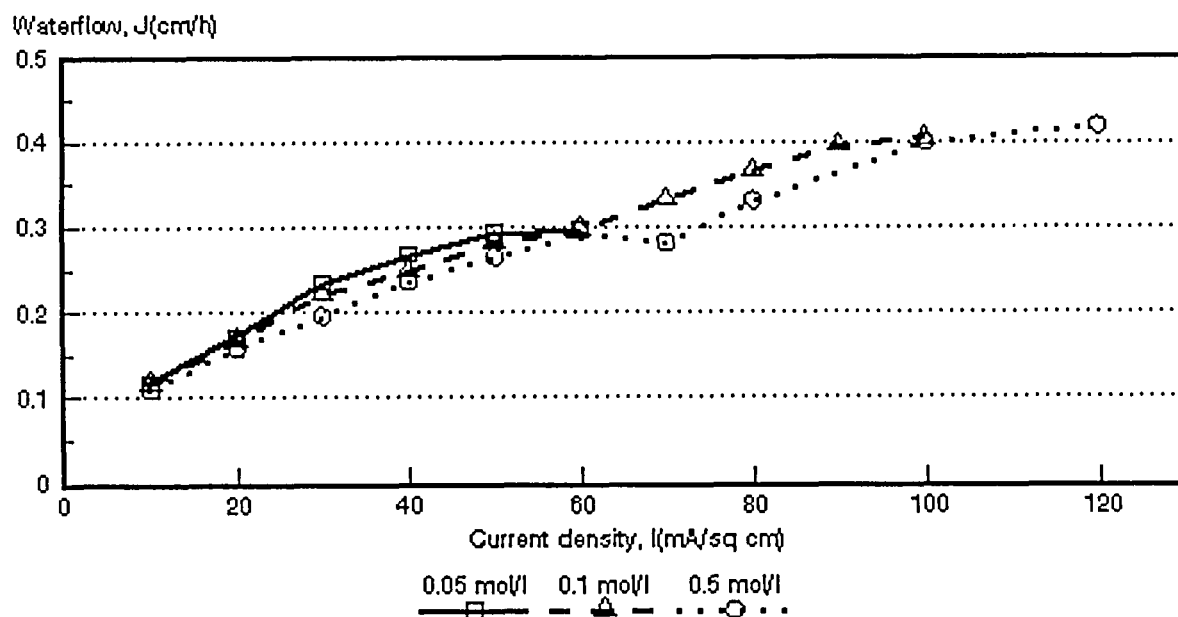
Waterflow, J(cm/h)

Figure 8.33:   Water flow through the membranes as a function of current density and
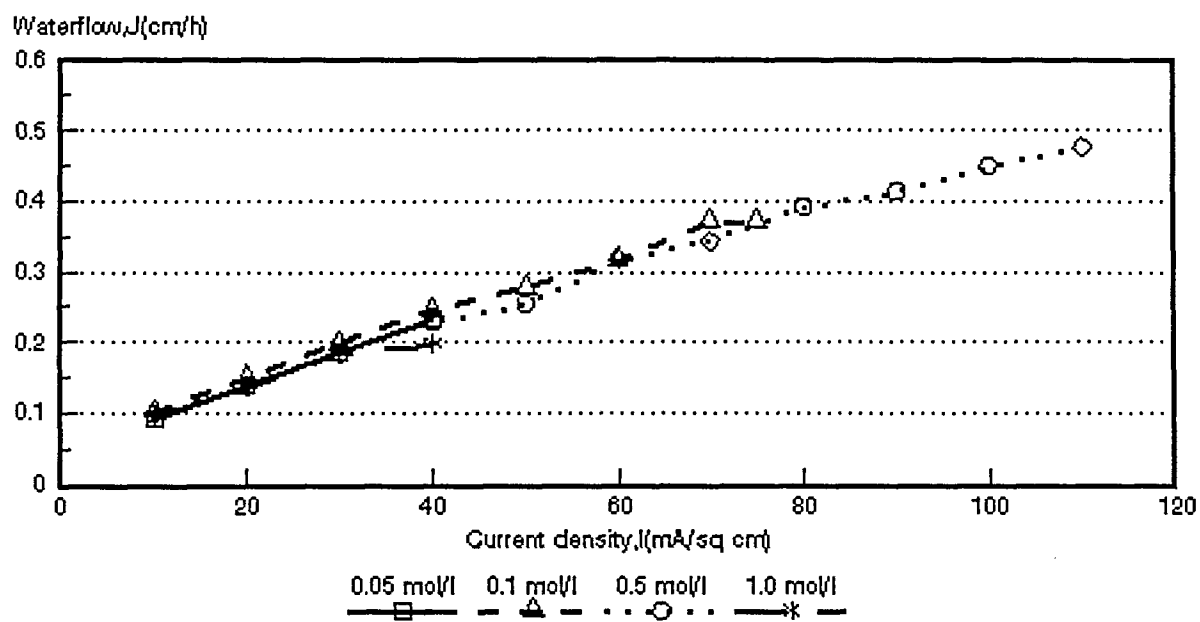feed water concentration. *Selemion* AMP and CMV membranes.

Figure 8.34: Water flow through the membranes as a function of current density and feed water concentration. *Ionac* MA-3475 and MC-3470 membranes.

Table 8.18: Water flow (J_i) through the membranes relative to the flow at $J_{0,5\ mol/l}$

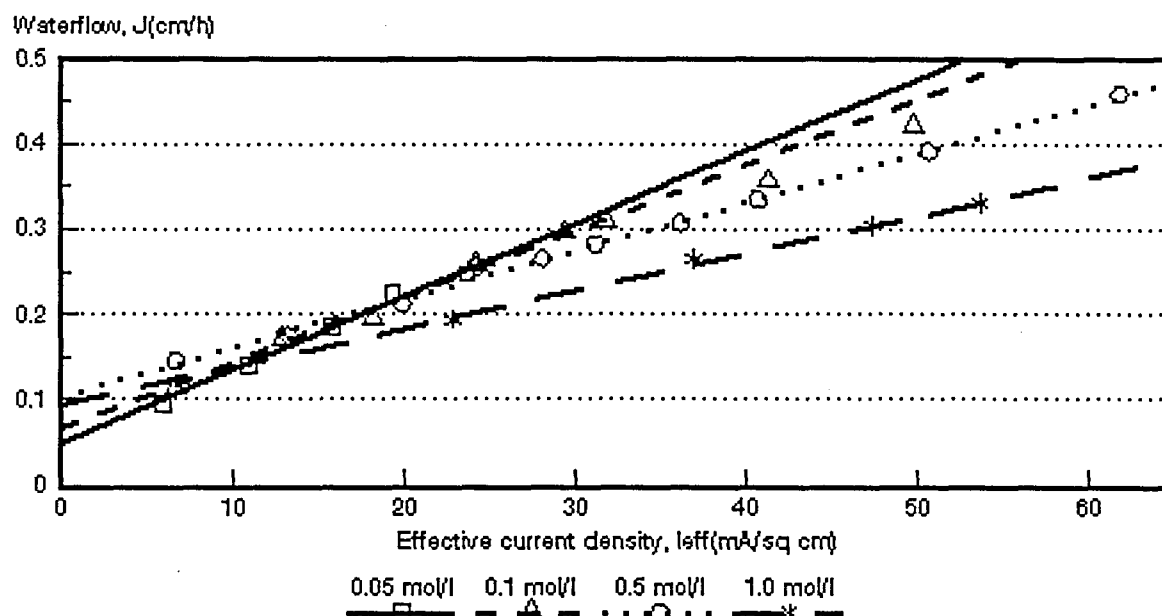| Current Density mA/cm²	$J_i/J_{0,5\ mol/l}$										
	Selemion AMV & CMV Concentration, mol/l				Selemion AMP & CMV Concentration, mol/l			Ionac MA-3475 & MC-3470 Concentration, mol/l			
	0,05	0,1	0,5	1,0	0,05	0,1	0,5	0,05	0,1	0,5	1,0
10	0,65	0,79	1,0		1,07	1,06	1,0	0,93	1,04	1,0	0,98
20	0,81	0,98	1,0		1,08	1,06	1,0	1,01	1,10	1,0	1,00
30	0,87	0,92	1,0	0,92	1,20	1,13	1,0	1,00	1,08	1,0	1,00
40	0,88	1,01	1,0		1,14	1,05	1,0	1,02	1,08	1,0	0,86
50	0,93	1,12	1,0	1,0	1,11	1,06	1,0		1,00	1,0	
60		1,10	1,0		1,01	1,01	1,0		1,08	1,0	
70		1,06	1,0	0,99		1,18	1,0				
75		1,07	1,0				1,0				
80						1,11	1,0				
90							1,0				
100						1,01	1,0				
110											
120											

i = 0,05; 0,1 and 1,0 mol/l

Figure 8.35: Water flow through the membranes as a function of effective current density and feed water concentration. *Selemion* AMV and CMV membranes.
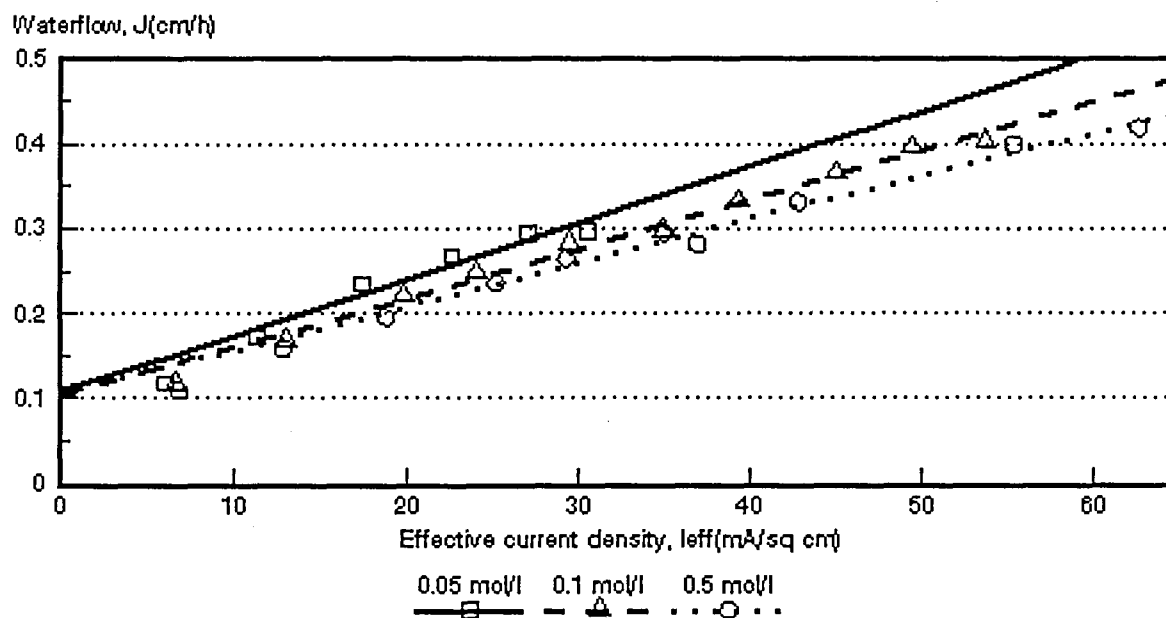

Figure 8.36: Water flow through the membranes as a function of effective current density and feed water concentration. *Selemion* AMP and CMV membranes.
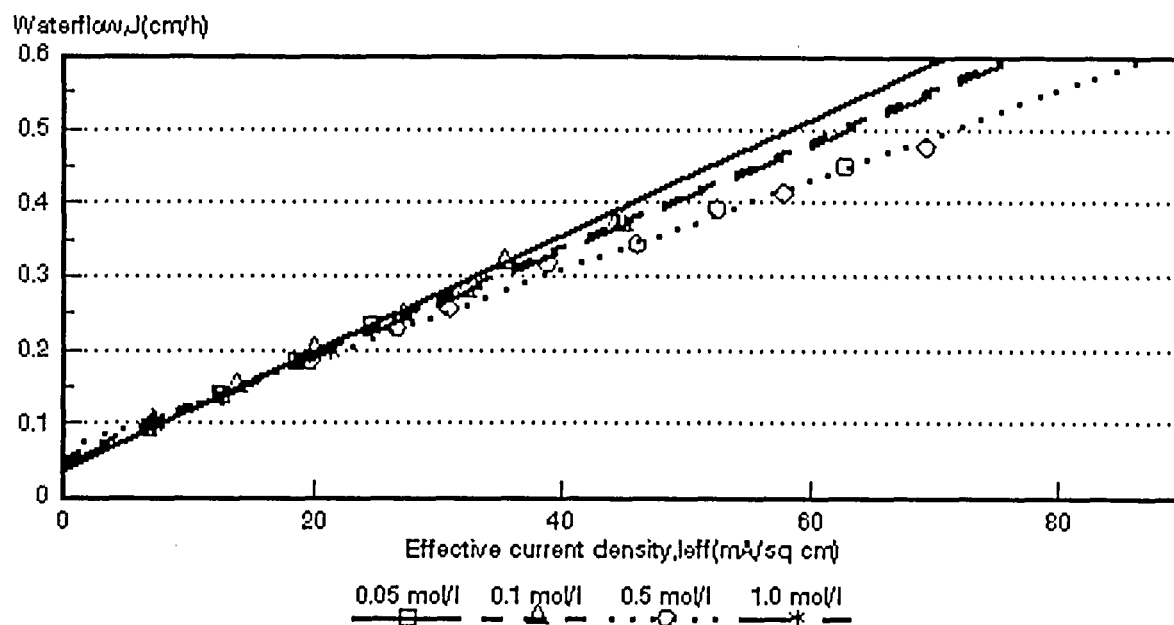
Waterflow,J(cm/h)

Effective current density,Ieff(mA/sq cm)

0.05 mol/l   0.1 mol/l   0.5 mol/l   1.0 mol/l

Figure 8.37:   Water flow through the membranes as a function of effective current density and feed water concentration. *Ionac* MA-3475 and MC-3470 membranes.
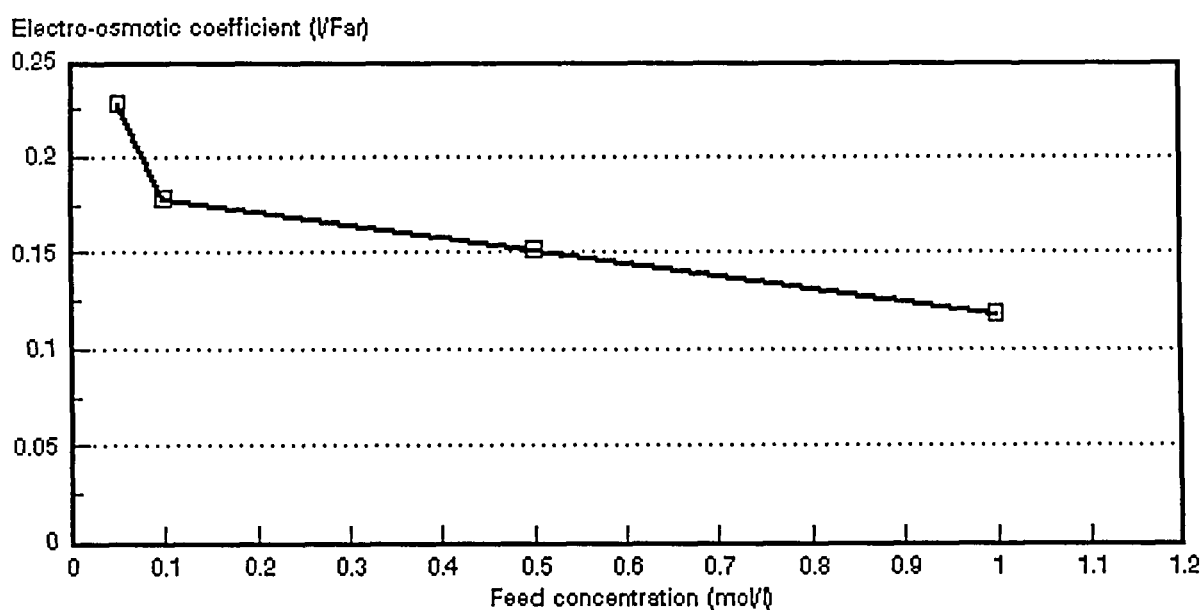
Electro-osmotic coefficient (l/Far)

Feed concentration (mol/l)

Figure 8.38:   Electro-osmotic coefficient as a function of NaOH feed concentration. *Selemion* AMV and CMV membranes.

Electro-osmotic coefficient (l/Far)

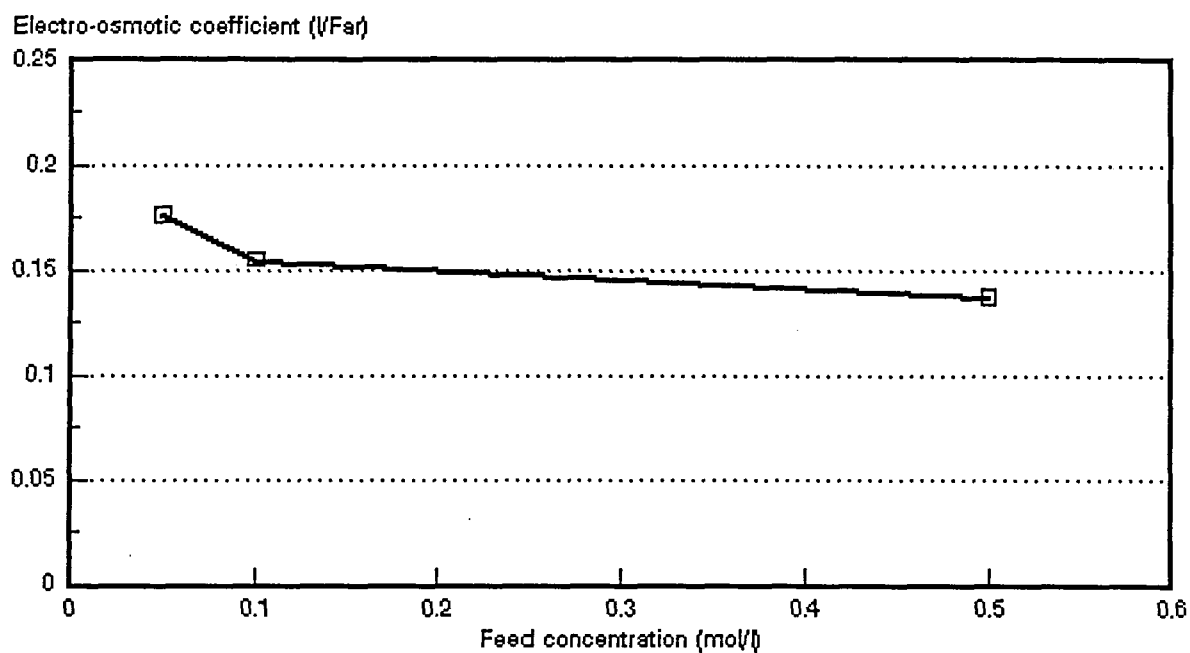

Figure 8.39: Electro-osmotic coefficient as a function of NaOH feed concentration. *Selemion* AMP and CMV membranes.
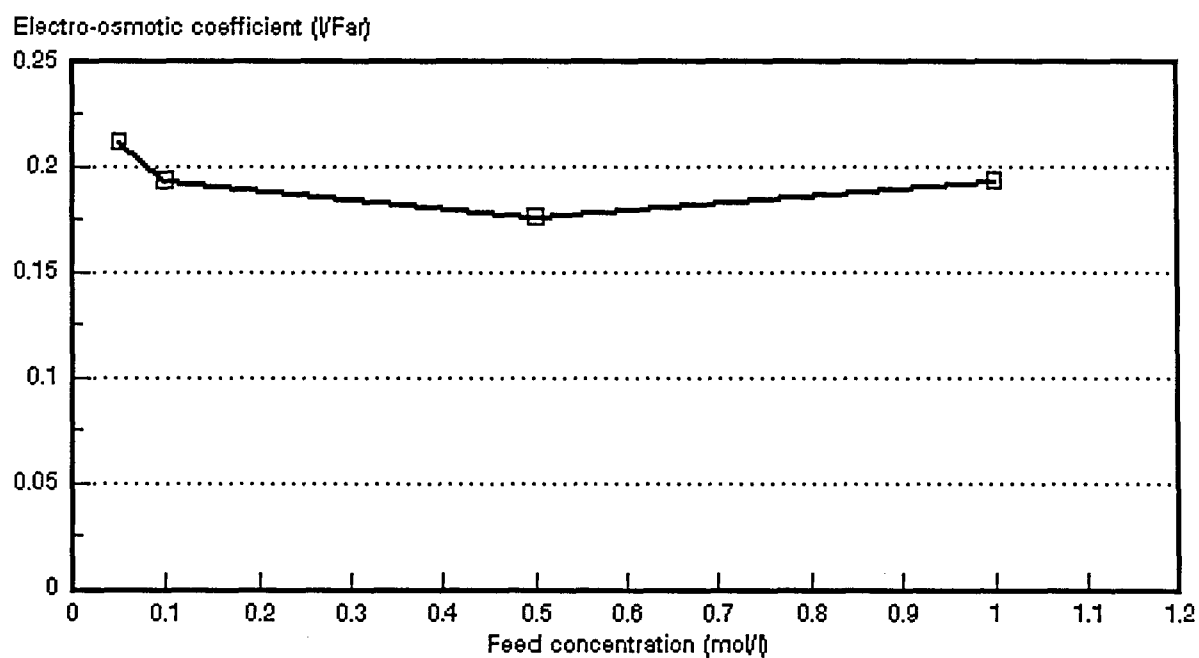
Electro-osmotic coefficient (l/Far)

Figure 8.40: Electro-osmotic coefficient as a function of NaOH feed concentration. *Ionac* MA-3475 and MC-3470 membranes.

Table 8.19: Effect of the electro-osmotic coefficient (EOC)* on the maximum caustic soda brine concentration, c_b^{max}.

Membranes	Feed Concentration mol/ℓ	EOC ℓ/Faraday	c_b^{max} mol/ℓ	mol H_2O/Faraday
Selemion AMV & CMV	0,05	0,228	4,39	12,7
	0,10	0,179	5,59	9,9
	0,50	0,152	6,58	8,4
	1,0	0,118	8,46	6,6
Selemion AMP & CMV	0,05	0,176	5,68	9,8
	0,10	0,155	6,45	8,6
	0,5	0,137	7,30	7,6
Ionac MA-3470 & MC-3475	0,05	0,212	4,72	11,8
	0,10	0,193	5,18	10,7
	0,50	0,176	5,68	9,8
	1,0	0,193	5,18	10,7

* Data from Tables 8.1 to 8.11.

Table 8.20: Osmotic flow* (J_{osm}) relative to the total flow (J) through the membranes as a function of current density.

Membranes	Current Density mA/cm²	J_{osm}/J (%) Feed concentration (mol/ℓ)			
		0,05	0,1	0,5	1,0
Selemion AMV & CMV	10	57,3	78,4	72,7	
	20	38,6	52,23	60,6	
	30	29,4	45,9	50,0	49,5
	40	24,2	34,9	41,4	
	50	22,1	30,3	40,0	36,3
	60		28,9	37,5	
	70				31,5
	80		25,2	31,6	
	90				29,07
	100		21,4	27,0	
	120			23,1	
Selemion AMP & CMV	10	92,7	88,6	97,1	
	20	63,6	61,4	67,2	
	30	46,6	46,9	54,5	
	40	40,8	41,8	45,3	
	50	37,3	36,8	40,3	
	60	36,8	37,8	36,2	
	70		31,1		
	80		28,3	32,3	
	90		26,2		
	100		25,7	26,7	
Ionac MA-3475 & MC-3470	10	41,9	51,2	53,1	47,3
	20	27,9	34,8	38,2	33,3
	30	20,9	26,5	28,4	24,8
	40	16,6	21,4	22,9	23,1
	50		18,9	20,6	
	60		16,6	16,6	
	70		14,2	15,3	
	80			13,4	
	100			11,7	

* Data from Tables 8.1 to 8.11.

8.4   Membrane Permselectivity

Membrane permselectivity (from membrane potential measurements) as a function of brine concentration at different initial feed water concentrations is shown in Figures 8.41 to 8.43.   Membrane permselectivity decreases with increasing caustic soda brine concentration and increasing feed water concentration. It is interesting to note that membrane permselectivity has not been much effected by increasing brine concentration in the case of the *Selemion* AMP and CMV membranes at 0,1 mol/ℓ feed concentration.
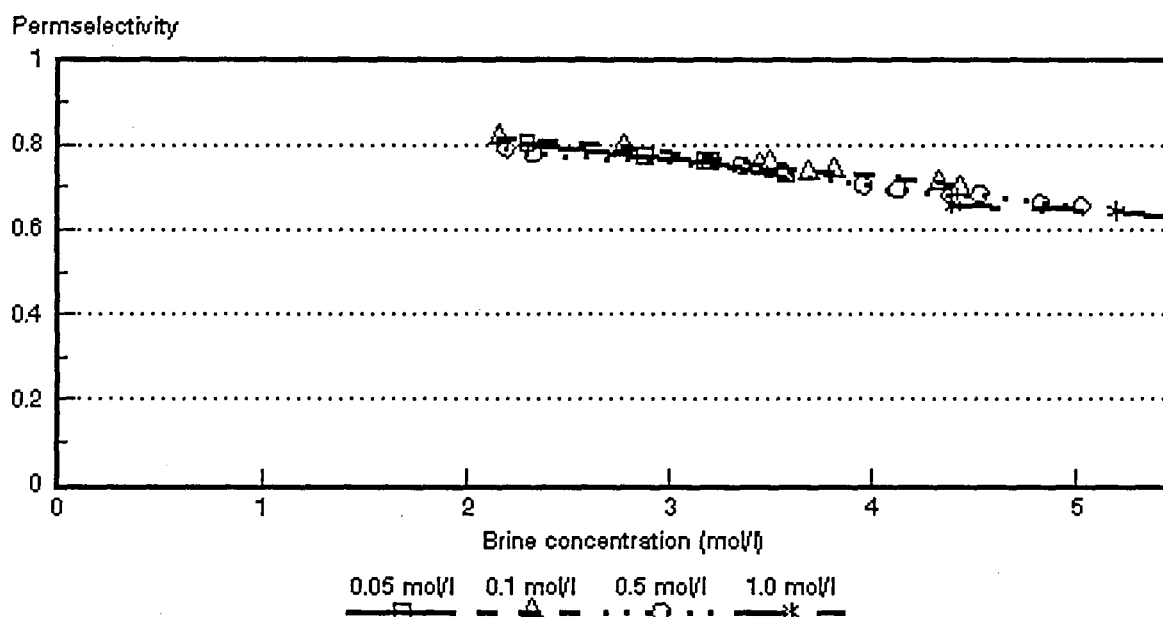
Figure 8.41:   Permselectivity ($\overline{\Delta}$t) as a function of brine concentration for different NaOH feed concentrations. *Selemion* AMV and CMV membranes.

Permselectivity

Brine concentration (mol/l)

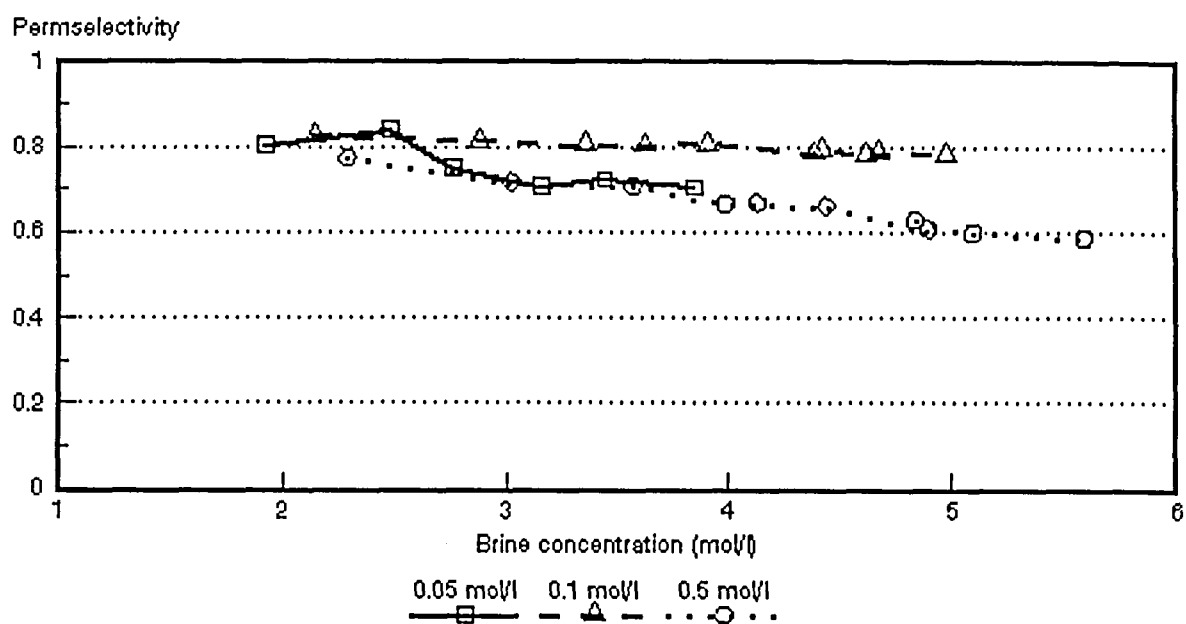0.05 mol/l   0.1 mol/l   0.5 mol/l

Figure 8.42: Permselectivity ($\bar{\Delta}t$) as a function of brine concentration for different NaOH feed concentrations. *Selemion* AMP and CMV membranes.
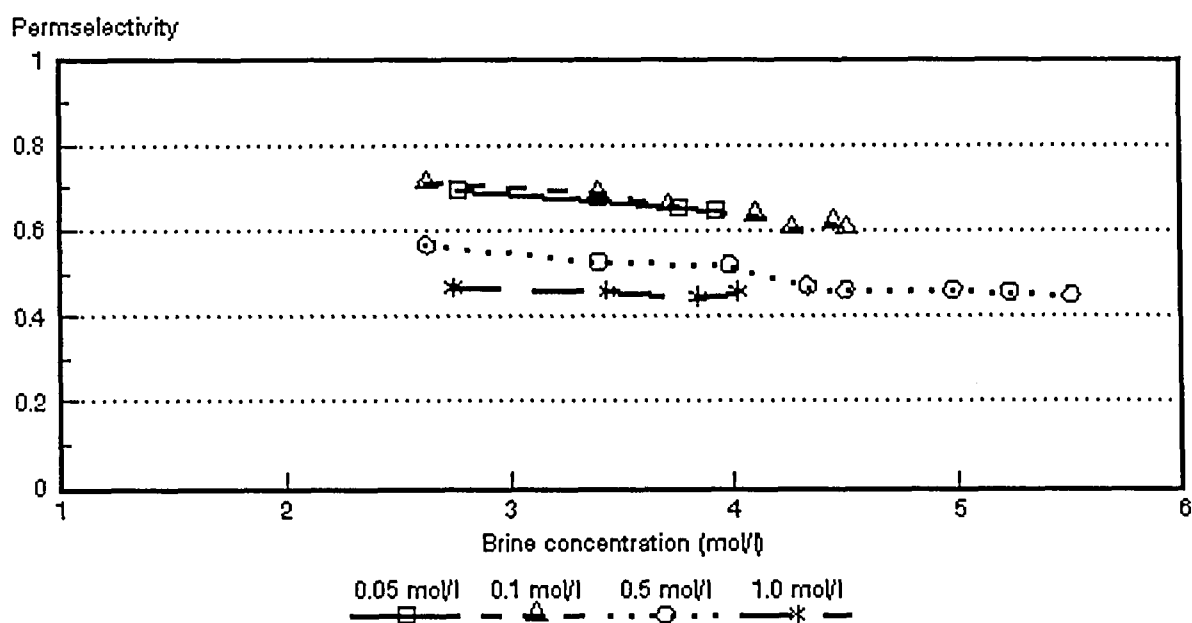
Permselectivity

Brine concentration (mol/l)

0.05 mol/l   0.1 mol/l   0.5 mol/l   1.0 mol/l

Figure 8.43: Permselectivity ($\bar{\Delta}t$) as a function of brine concentration for different NaOH feed concentrations. *Ionac* MA-3475 and MC-3470 membranes.

329

8.5   Membrane Characteristics

8.5.1   Membrane resistances of membranes used for EOP of caustic soda solutions

Membrane resistances of the membranes used for EOP of caustic soda solutions are summarized in Table 8.21.

Table 8.21:   Membrane resistances of the membranes used for EOP of caustic soda solutions.

Membrane	Resistance - ohm·cm²	
	0,1 mol/ℓ	0,5 mol/ℓ
Selemion AMV	4,1	0,5
Selemion AMP	9,6	1,5
Selemion CMV	5,1	1,2
Ionac MA-3475	15,7	7,1
Ionac MC-3470	26,9	15,7

8.5.2   Gel water contents and ion-exchange capacities of the membranes used for EOP of caustic soda solutions.

Gel water contents and ion-exchange capacities of the membranes used for EOP of caustic soda solutions are shown in Table 8.22.

Table 8.22:   Gel water contents and ion-exchange capacities of the membranes used for EOP of caustic soda solutions.

Membrane	Gel Water Content	Ion-exchange Capacity
	%	me/dry g
Selemion AMV	18,4	1,3
Selemion CMV	22,7	2,3
Selemion AMP	17,6	1,1
Ionac MA-3475	17,8	1,1
Ionac MC-3470	18,5	1,8

8.5.3 Permselectivities of the membranes used for EOP of caustic soda solutions.

Permselectivities of the membranes used for EOP of caustic soda solutions are shown in Table 8.23.

Table 8.23: **Membrane permselectivities of the membranes used for EOP of caustic soda solutions at different salt gradients.**

Membrane	$\Delta t(1)^{*}$	$\Delta t(2)^{**}$	$\Delta t(3)^{***}$
Selemion AMV	0,87	0,87	0,83
Selemion CMV	0,98	0,83	0,65
Selemion AMP	0,93	0,87	0,81
Ionac MA-3475	0,87	0,82	0,79
Ionac MC-3470	0,92	0,61	0,46

(1)*   :   0,1 / 0,2 mol/ℓ NaOH
(2)**   :   0,5 / 1,0 mol/ℓ NaOH
(3)***   :   0,1 / 4,0 mol/ℓ NaOH

9. ELECTRO-OSMOTIC PUMPING OF SODIUM CHLORIDE-, HYDROCHLORIC ACID- AND CAUSTIC SODA SOLUTIONS IN A CONVENTIONAL ELECTRODIALYSIS STACK

9.1 Concentration/Desalination of Sodium Chloride Solutions with *Ionac* MA-3475 and MC-3470 Membranes.

The concentration/desalination results of different sodium chloride feed water concentrations at different cell pair voltages are summarized in Table 9.1.

9.1.1 Brine and dialysate concentrations

Dialysate and brine concentrations as a function of time and cell pair voltage for different initial feed water concentrations are shown in Figures 9.1 to 9.8. Brine concentration as a function of feed water concentration and cell pair voltage is shown in Figure 9.9. A typical example of current as a function of time and cell pair voltage for an approximately 3 000 mg/ℓ feed water solution is shown in Figure 9.10.

Desalination/concentration rate increased with increasing cell pair voltage (Figs. 9.1 to 9.8 and 9.10). Brine concentration increased as a function of feed water concentration and cell pair voltage (Table 9.1 and Fig. 9.9). Brine concentrations of 2,1 to 14,0% could be obtained in the feed water concentration range from 1 000 to 10 000 mg/ℓ and cell pair voltage range from 0,5 to 4 volt per cell pair (Table 9.1). Product water concentrations of less than 500 mg/ℓ could be obtained in the same feed water concentration and cell pair voltage range.

The concentration factors (brine/feed) were relatively low (Table 9.1). This could be ascribed to the small volume of feed water (12 ℓ) that was used. Concentration factors decreased with increasing feed concentration. This shows that there is a limit to the brine concentration that can be obtained with ED. Brine concentration that can be obtained with ED depends inter alia on the permselectivity of the ion-exchange membranes and current density used and on the feed water concentration[6, 7]. Ion-exchange membranes tend to lose some of their permselectivity at high concentration.

9.1.2 Brine volume and water recovery

Low brine volume and high water recoveries were obtained (Table 9.1). Brine volume varied between 1,5 and 4% of the treated water volume in the feed water concentration

Table 9.1: Concentration/desalination results of sodium chloride solutions at different feed concentrations and cell pair voltages using Ionac MA-3475 and MC-3470 membranes.

Vcp	c_f mg/ℓ	c_p mg/ℓ	c_b mg/ℓ	CF	CE %	WR %	BV %	EEC kWh/m³	OP m³/m²·d	d_{eff} mm	R_{cp} ohm·cm²
0,5	992	212	21 981	22,2	93,6	98,1	1,9	0,192	0,37		
	2 906	488	73 460	25,3	84,3	97,1	2,9	0,662	0,28	4,23	49,2
1,0	933	193	30 814	33	81,8	98,5	1,5	0,417	0,45		
	3 224	503	82 025	25,4	81,1	97,2	2,8	1,55	0,35	6,76	80,2
	5 132	451	99 786	19,4	91,4	96,0	4,0	2,358	0,30	6,56	69,2
1,5	1 033	196	42 805	41,4	75,2	98,5	1,5	0,769	0,48		
	3 349	435	83 738	25,0	79,9	97,3	2,7	2,52	0,37	11,83	62,9
	3 045	450	86 893	28,5	81,3	97,6	2,4	2,21	0,55*	5,66	99,75
	3 058	433	104 475	34,16	83,01	97,6	2,4	2,18	0,67**	4,81	75,5
2	4 959	372	107 630	21,7	78,9	96,3	3,7	5,35	0,36	10,18	77,1
	10 709	548	136 933	12,8	93,3	93,7	6,3	10,03	0,32	12,11	31,8
3	3 515	430	100 868	28,7	69,4	97,3	2,7	6,14	0,51	11,95	128,8
	5 388	407	112 589	20,9	76,3	96,2	3,7	9,02	0,41	13,86	91,1
	10 364	487	139 637	13,5	86,90	94,2	6,8	15,7	0,36	15,22	50,3
4	10 364	409	139 637	13,5	77,6	94,0	6,0	23,6	0,38	15,49	79,7

*: 2,1 cm/s linear flow velocity; **: 2,73 cm/s linear flow velocity; other experiments conducted at a linear flow velocity approximately 1 cm/s

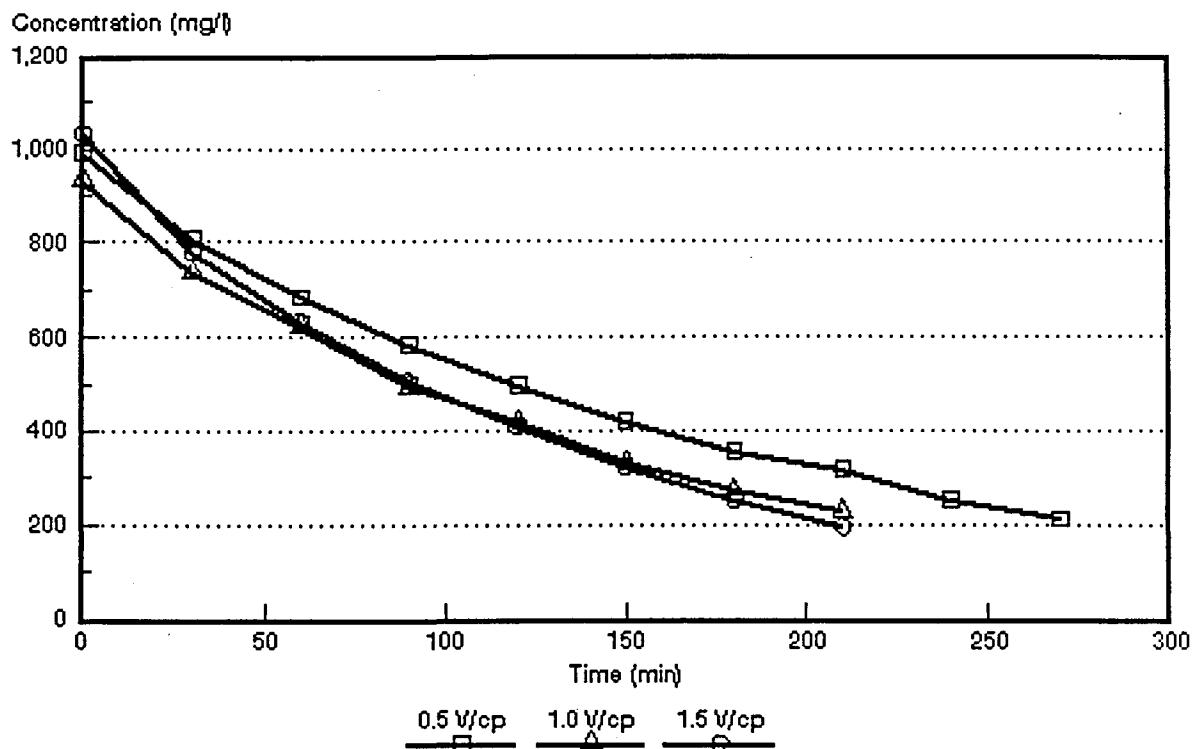|					
CF	=	concentration factor	OP	=	output (yield)
CE	=	current efficiency	WR	=	water recovery
BV	=	brine volume	EEC	=	electrical energy consumption

Concentration (mg/ℓ)

Figure 9.1: Dialysate concentration as a function of time and cell pair voltage for an approximately 1 000 mg/ℓ sodium chloride feed solution.
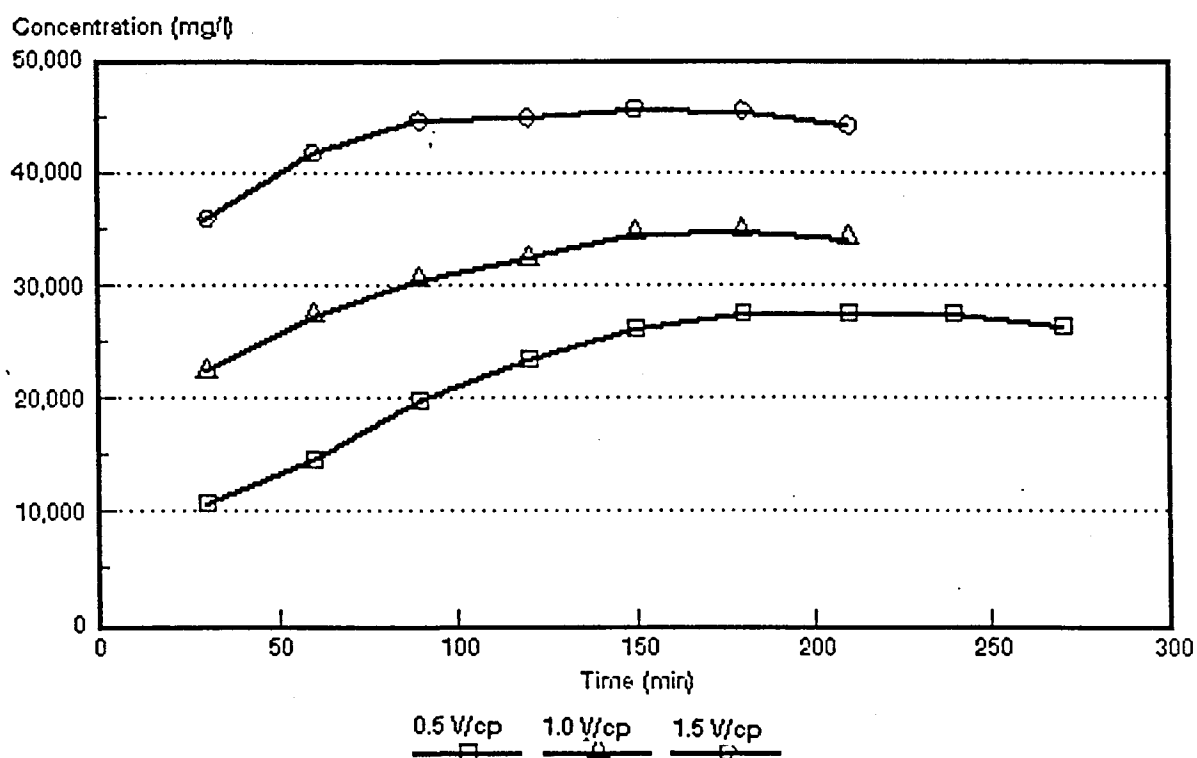

Figure 9.2: Brine concentration as a function of time and cell pair voltage for an approximately 1 000 mg/ℓ sodium chloride feed solution.
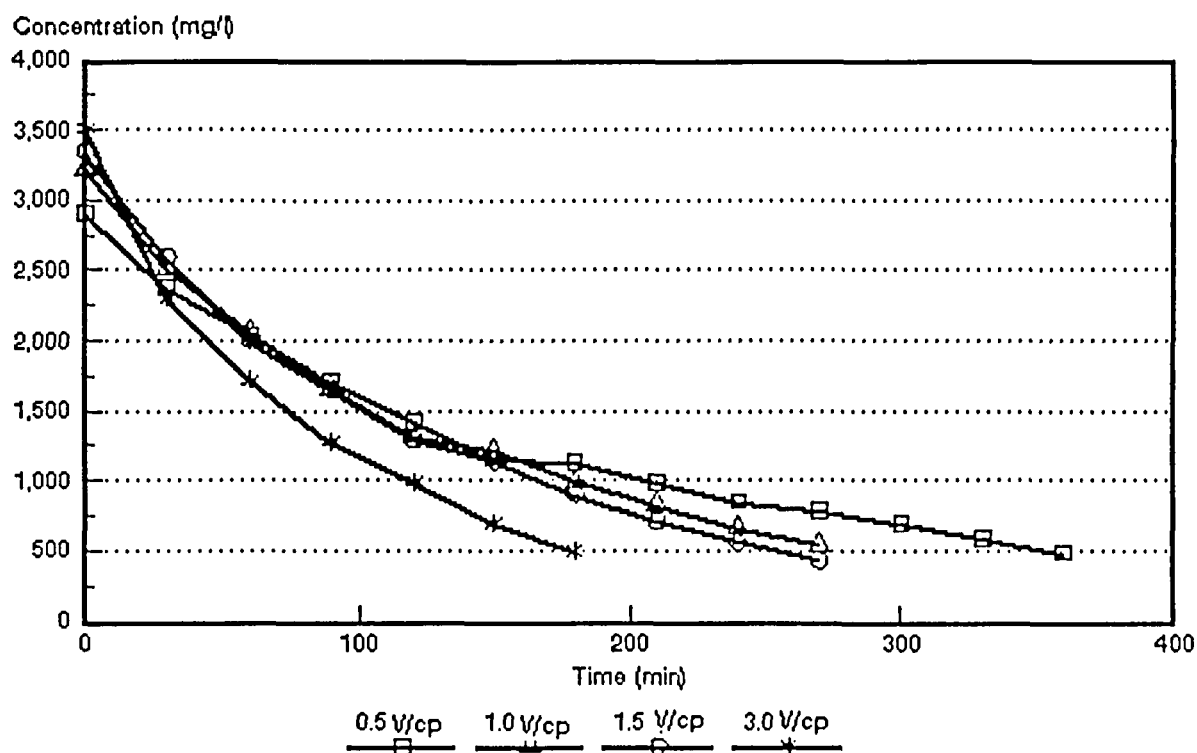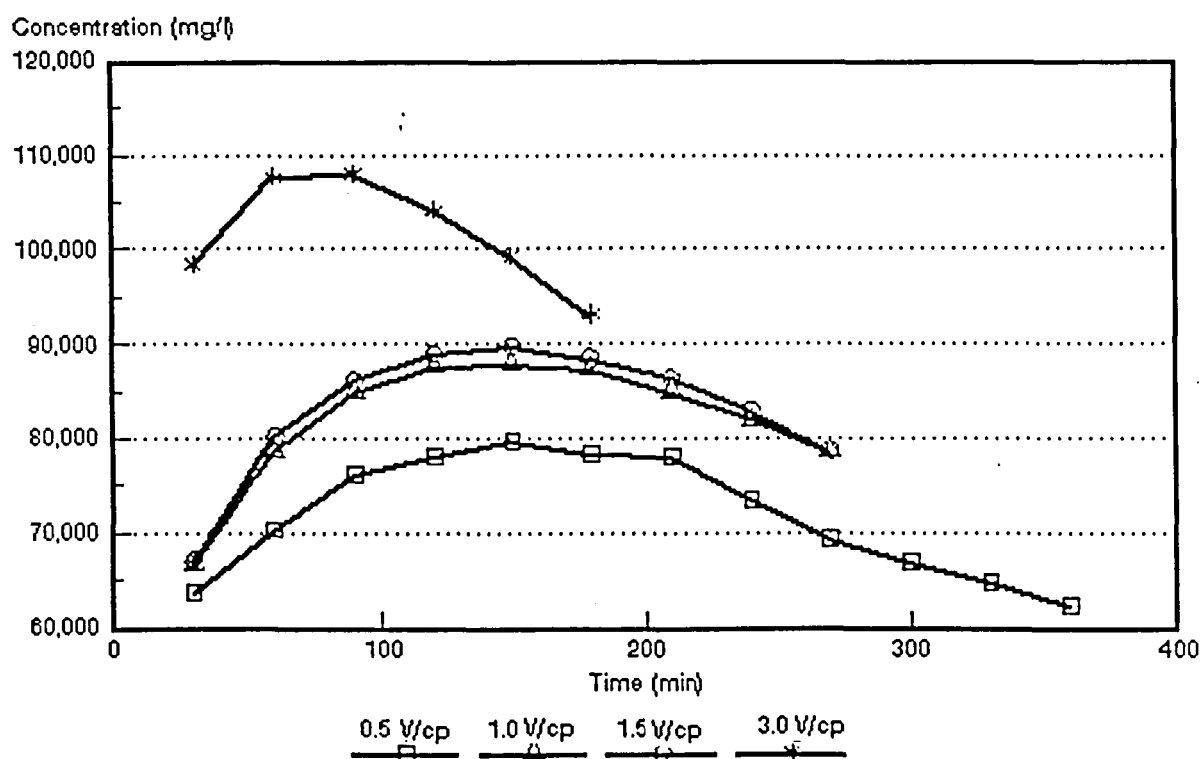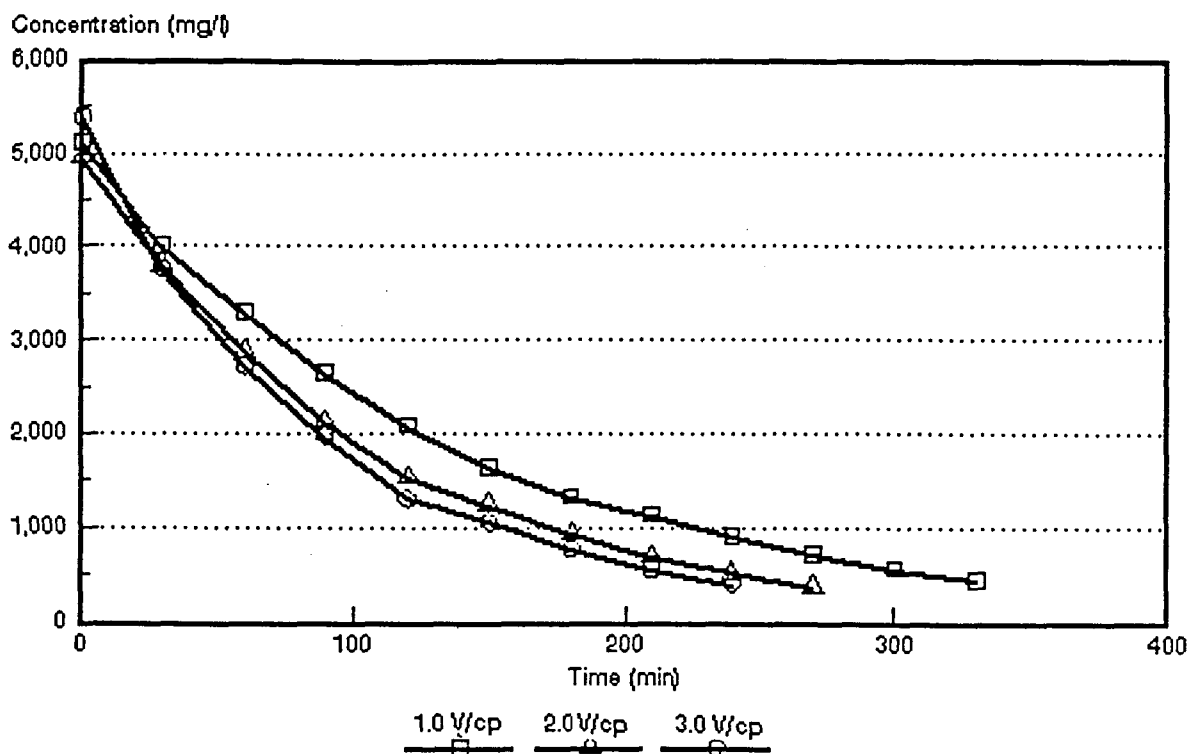
Figure 9.3: Dialysate concentration as a function of time and cell pair voltage for an approximately 3 000 mg/ℓ sodium chloride feed solution.
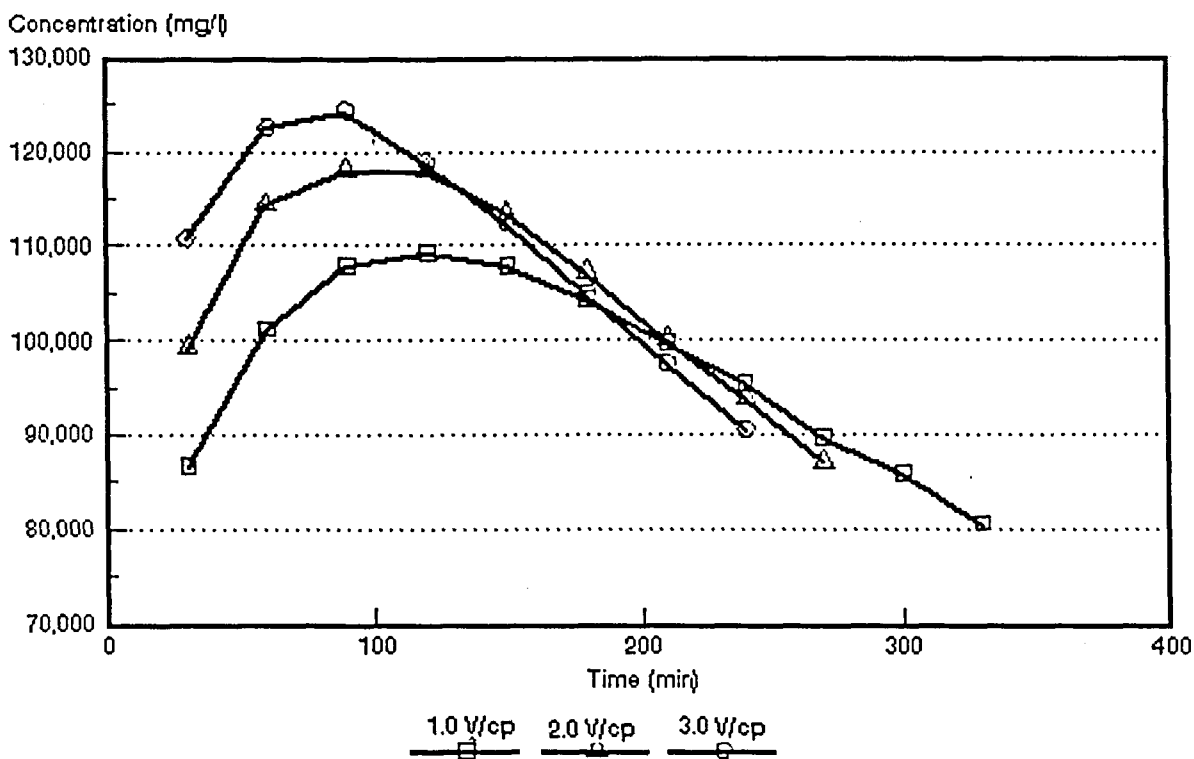

Figure 9.4: Brine concentration as a function of time and cell pair voltage for an approximately 3 000 mg/ℓ sodium chloride feed solution.

335

Concentration (mg/l)
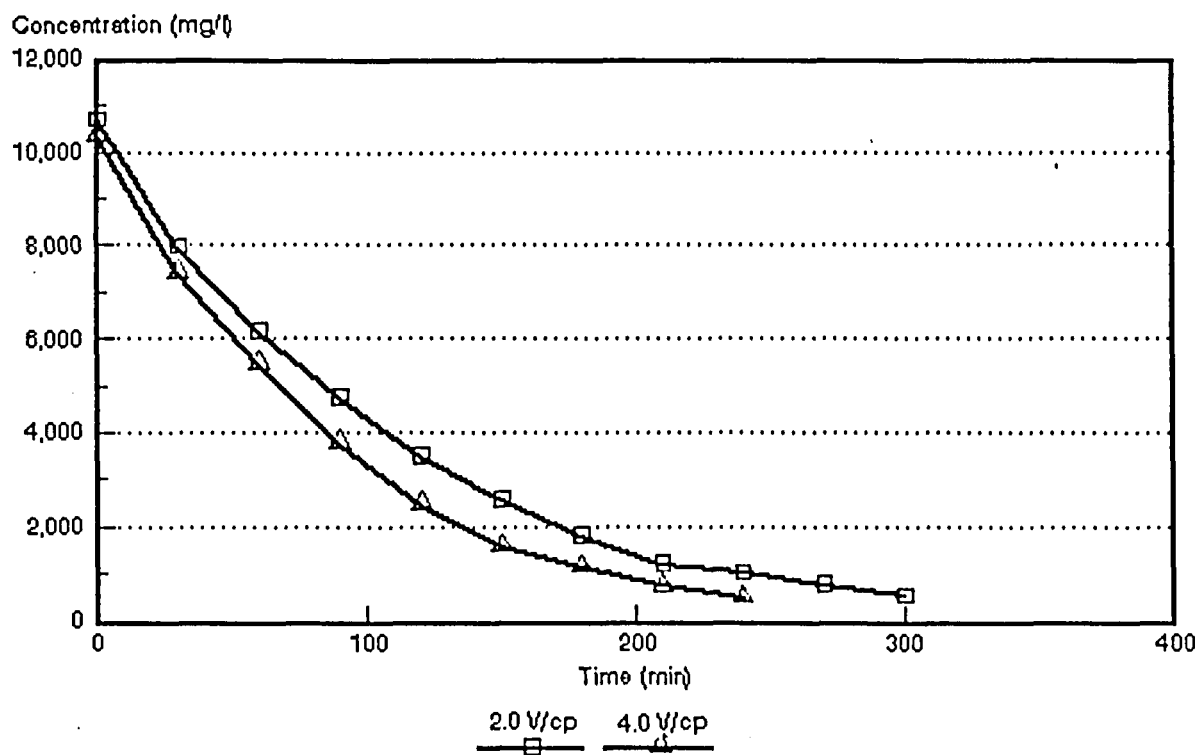

Figure 9.5:   Dialysate concentration as a function of time and cell pair voltage for an approximately 5 000 mg/ℓ sodium chloride feed solution.

Concentration (mg/l)

Figure 9.6:   Brine concentration as a function of time and cell pair voltage for an approximately 5 000 mg/ℓ sodium chloride feed solution.

Concentration (mg/ℓ)

Figure 9.7:   Dialysate concentration as a function of time and cell pair voltage for an approximately 10 000 mg/ℓ sodium chloride feed solution.
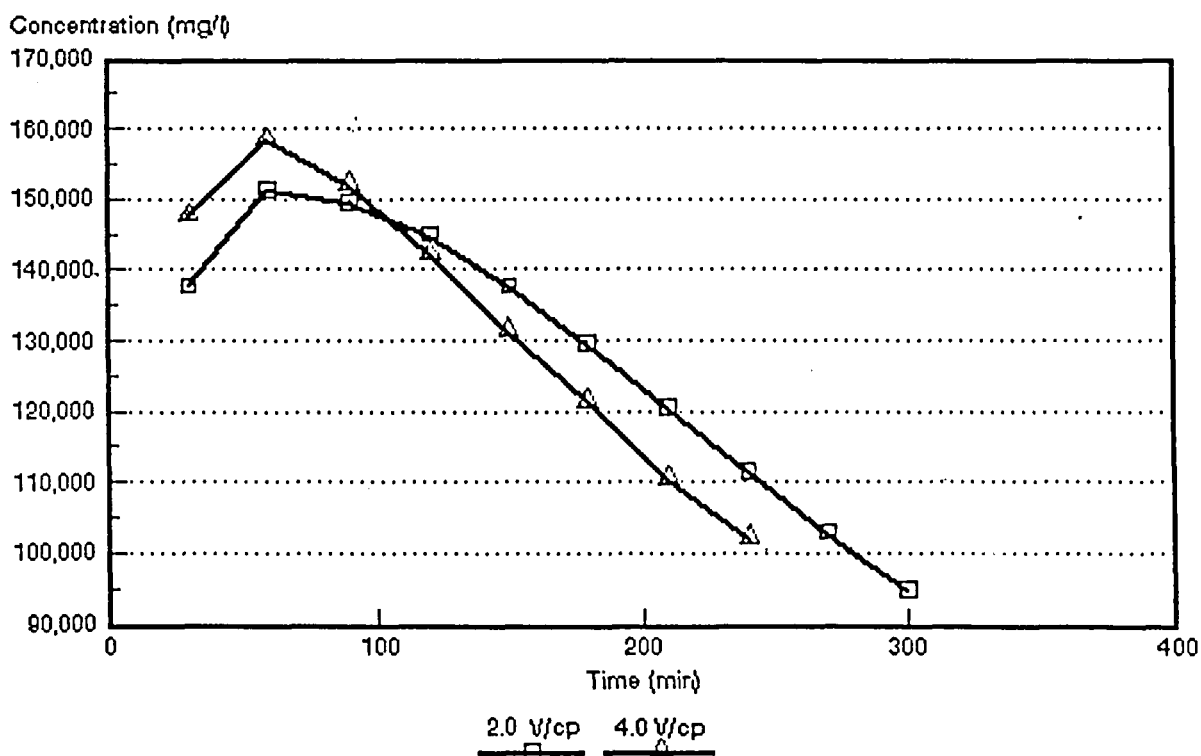
Concentration (mg/ℓ)

Figure 9.8:   Brine concentration as a function of time and cell pair voltage for an approximately 10 000 mg/ℓ sodium chloride feed solution.
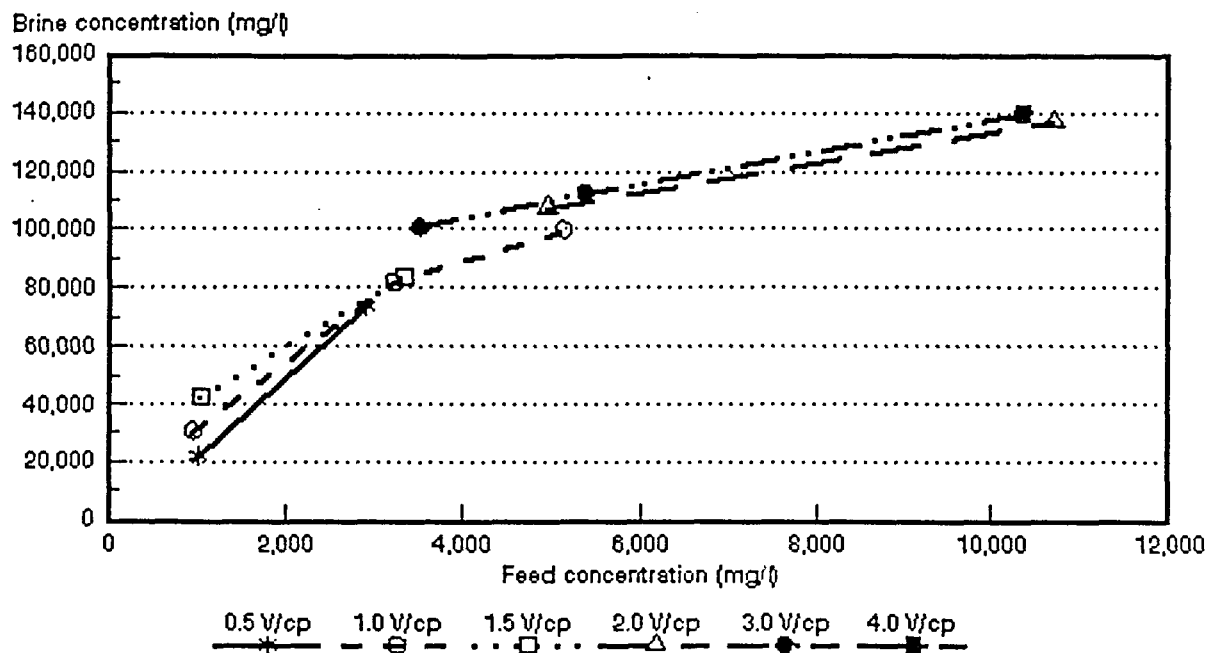
Brine concentration (mg/ℓ)

Figure 9.9: Brine concentration as a function of sodium chloride feed water concentration and cell pair voltage.
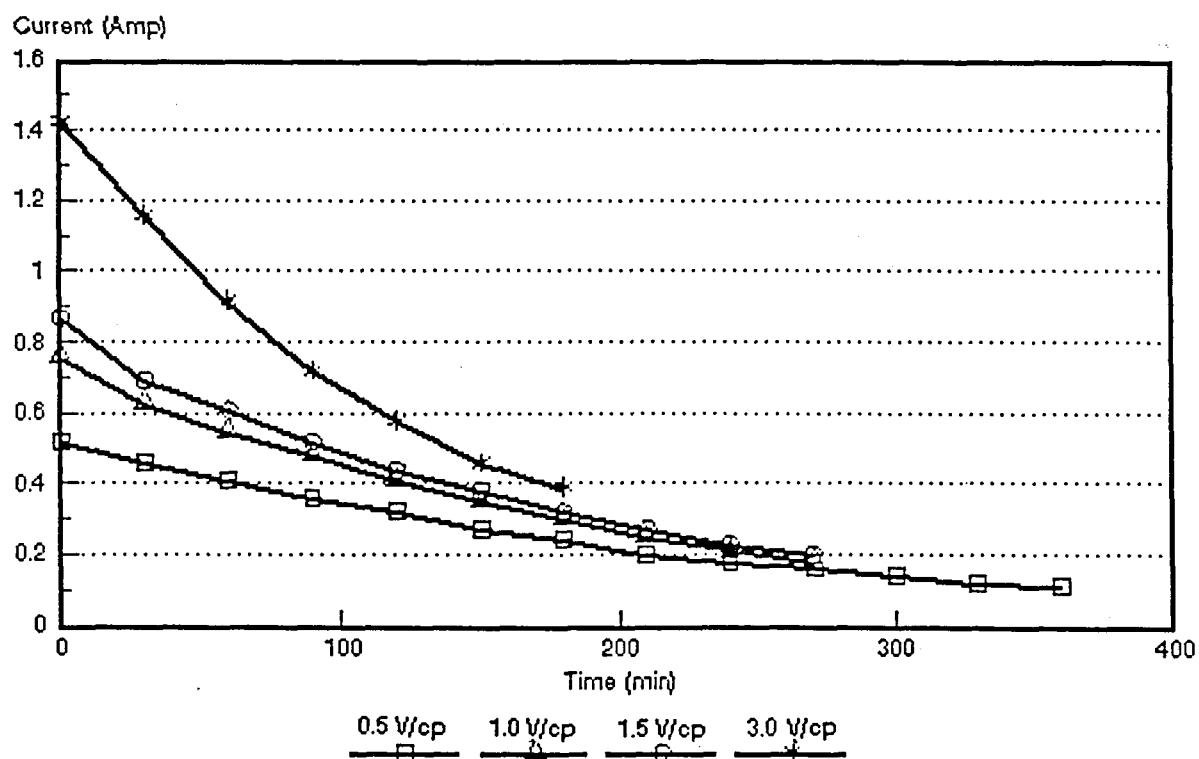
Current (Amp)

Figure 9.10: Electrical current as a function of time and cell pair voltage during desalination of an approximately 3 000 mg/ℓ sodium chloride solution.

338

range from 1 000 to 5 000 mg/ℓ (0,5 to 1,5 V/cp). Brine volume increased with increasing feed water concentration (Table 9.1) and a brine volume of 6,8% was obtained at a feed water concentration of approximately 10 000 mg/ℓ (3 V/cp). Water recoveries of approximately 96% were obtained in the feed water concentration range from 1 000 to 5 000 mg/ℓ. The lowest water recovery that was obtained was 93,7% (at approximately 10 000 mg/ℓ). Therefore, high water recoveries and low brine volumes could be obtained with EOP-ED.

9.1.3 Current efficiency

Current efficiency increased with increasing feed water concentration, especially at the higher cell pair voltages (Table 9.1 and Figure 9.11). This could be ascribed to an increasing flow of water through the membranes with increasing feed water concentration. Current efficiencies of 75,2 and 93,6% were obtained in the feed water and cell pair voltage ranges of 1 000 to 5 000 mg/ℓ and 0,5 to 1,5 V/cp, respectively. (Table 9.1). Current efficiencies of 69,4 to 86,9% were obtained in the feed water and cell pair voltage ranges of 3 000 to 10 000 mg/ℓ and 2 to 4 V/cp, respectively. Current efficiency further decreased with increasing cell pair voltage. This could be ascribed to increasing polarization that was taking place at the higher cell pair voltages.

9.1.4 Electrical energy consumption

Electrical energy consumption obtained during EOP-ED was low. Electrical energy consumption of less than 2,5 kWh/m^3 product water was obtained in the cell pair voltage and feed water concentration ranges of 0,5 to 1,5 V/cp (1 000 to 3 000 mg/ℓ)(Table 9.1), respectively. Electrical energy consumption further increased with increasing cell pair voltage and increasing feed water concentration (Fig. 9.12). Electrical energy consumption was 10 and 23,6 kWh/m^3 product water at 2 and 4 volt per cell pair, respectively (approximately 10 000 mg/ℓ feed). (Note: electrical energy consumption was only determined for ion transport).

9.1.5 Product water yield

Product water yield was low (Table 9.1). Product water yield varied between 0,28 and 0,67 m^3/m^2·d in the cell pair voltage and feed water concentration ranges studied. Water yield decreased as a function of feed water concentration and cell pair voltage (Table 9.1). A linear flow velocity of approximately 1 cm/s was used for most of the
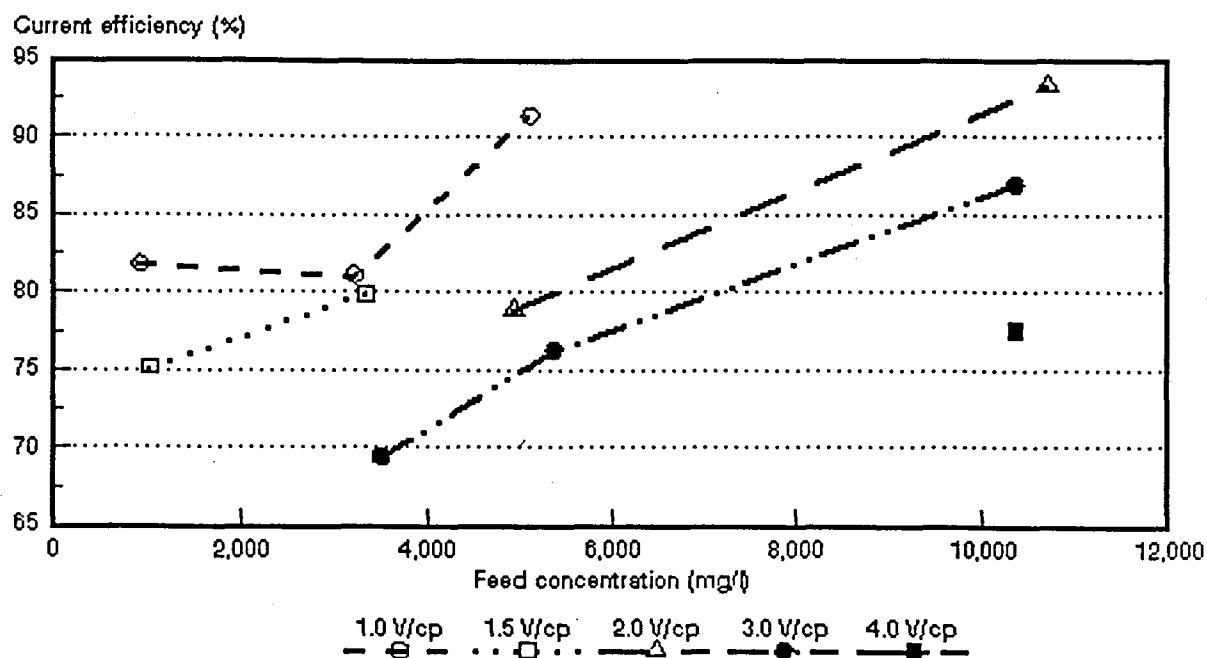
Current efficiency (%)

Figure 9.11: Current efficiency as a function of sodium chloride feed concentration and cell pair voltage.

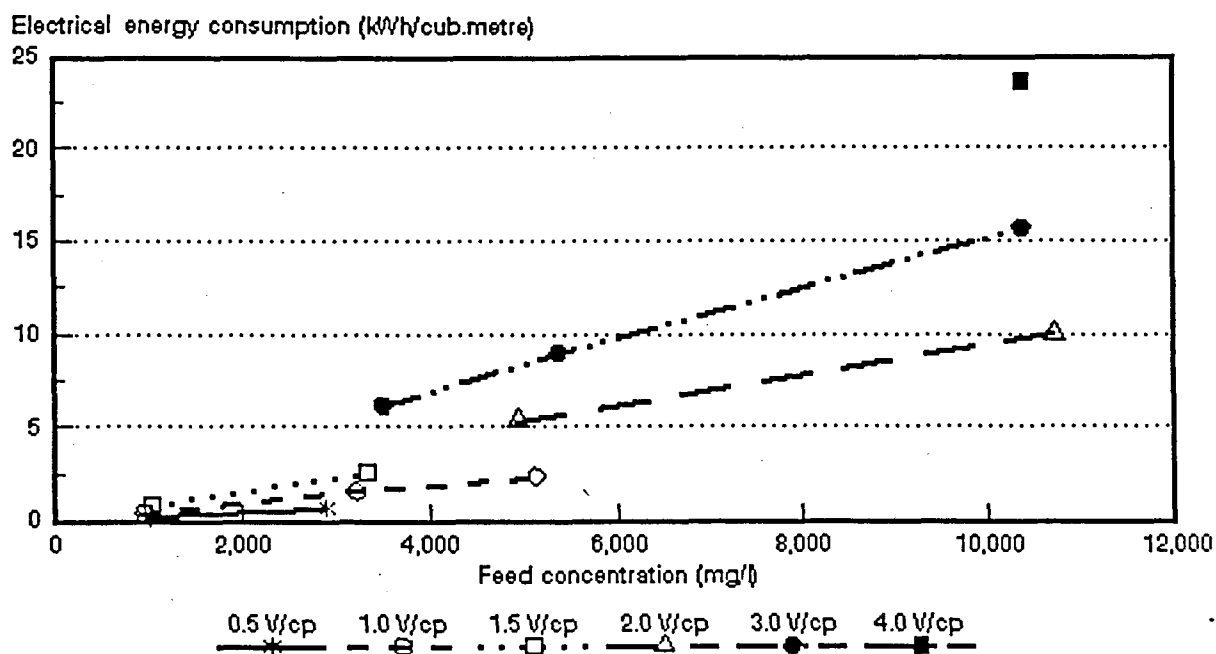Electrical energy consumption (kWh/cub.metre)

Figure 9.12: Electrical consumption as a function of sodium chloride feed concentration and cell pair voltage.

runs. However, linear flow velocity was increased to 2,1 cm/s and 2,7 cm/s at 3 000 mg/ℓ feed water concentration (1,5 V/cp)(Table 9.1). Product water yield was significantly increased when the linear flow velocity was increased.

9.1.6 Effective cell pair thickness and cell pair resistance

An example of cell pair resistance (R_{cp}) as a function of the specific resistance of the dialysate and cell pair voltage is shown in Figure 9.13. (Approximately 3 000 mg/ℓ feed). The lines through the linear region and extrapolation to the y-axis gives the cell pair resistance. The slope of the linear region gives the effective cell pair thickness, d_{eff}. The lines, however, deviate from linearity towards the end of the runs when the current is low and polarization is less. The effective cell pair thickness, d_{eff}, increased with increasing cell pair voltage and increasing feed water concentration. (Table 9.1). Cell pair resistance, R_{cp}, decreased with increasing feed water concentration and increased with increasing cell pair voltage (Table 9.1). The cell pair resistance increased slower than the specific resistance of the dialysate towards the end of the run because polarization is less. The effective thickness of the cell pair decreased significantly when the linear flow velocity was increased (Table 9.1).
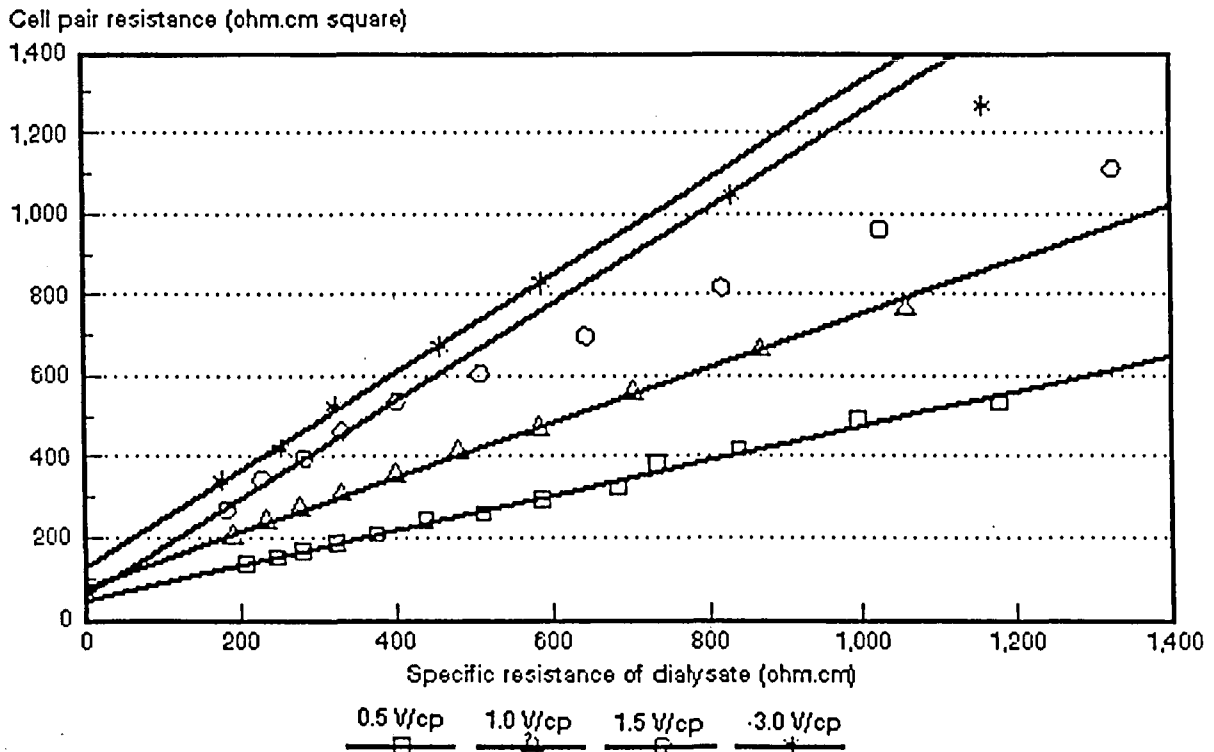

Figure 9.13: Cell pair resistance as a function of the specific resistance of the dialysate at different cell pair voltages (approximately 3 000 mg/ℓ sodium chloride feed).

341

9.2 Concentration/Desalination of Hydrochloric Acid Solutions with *Selemion* AAV and CHV Membranes

The concentration/desalination results of different hydrochloric acid feed water concentrations at different cell pair voltages are summarized in Table 9.2.

9.2.1 Acid brine and dialysate concentration

Dialysate and acid brine concentration as a function of time and cell pair voltage for different initial acid feed concentrations are shown in Figures 9.14 to 9.19. Acid brine concentration as a function of hydrochloric acid feed concentration and cell pair voltage is shown in Figure 9.20. Electric current as a function of time during concentration/desalination of an approximately 3 000 mg/ℓ hydrochloric acid feed solution is shown in Figure 9.21.

Faster and better acid removal was obtained at the higher cell pair voltages (Figs. 9.14, 9,16 and 9,18). Not much difference was experienced in the highest acid brine concentrations that could be obtained at the different cell pair voltages (Figs. 9.15, 9,17 and 9,19). Acid brine concentrations of 3,6 to 8,7% were obtained in the acid feed concentration range from approximately 1 000 to 5 000 mg/ℓ and cell pair voltage range from 0,5 to 4,0 volt per cell pair. Acid brine concentration further increased with increasing feed water concentration and increasing cell pair voltage (Fig. 9.20). Acid product water concentrations of less than 500 mg/ℓ could be obtained in the acid feed concentration and cell pair voltage range studied (Table 9.2).

Concentration factors were low. Concentration factors decreased as a function of acid feed concentration (Table 9.2).

9.2.2 Acid brine volume and water recovery

Low brine volumes and high water recoveries were obtained. Brine volume varied between 2,4 and 7,8% of the treated water volume in the acid feed concentration range of 1 000 to 5 000 mg/ℓ (0,5 to 4,0 V/cp) (Table 9.2). Brine volume also increased with increasing acid feed concentration and the highest acid brine concentration was obtained at an acid feed concentration of 5 000 mg/ℓ (1 V/cp). Water recovery was high. Water recovery of approximately 97% was obtained at an acid feed concentration of approximately 1 000 mg/ℓ (0,5 to 1 V/cp). The lowest water recovery obtained was 92,2% at an acid feed concentration of approximately 5 000 mg/ℓ (1,0

Table 9.2: Concentration/desalination results of hydrochloric acid solutions at different feed concentrations and cell pair voltages using Selemion AAV and CHV membranes.

Vcp	cf mg/ℓ	cp mg/ℓ	c_b mg/ℓ	CF	CE %	WR %	BV %	EEC kWh/m³	OP m³/m²·d	d_eff mm	Rcp ohm·cm²
0,5	1 130	197	36 460	32,3	37,8	97,1	2,9	0,182	0,33	5,1	15,1
0,5*	2 989	452	56 513	18,9	46,3	93,6	6,4	2,18	0,64	5,0	
1,0	1 021	175	36 460	35,7	29,2	97,6	2,4	2,14	0,39	7,90	58,4
1,0	3 281	452	67 451	20,6	35,6	94,6	5,4	5,90	0,36	13,80	1,9
1,0*	2 989	379	61 982	20,7	35,7	94,0	6,0	5,5	0,64	8,1	-1,6
1,0	5 032	510	85 681	17,0	32,0	92,2	7,8	10,5	0,31	13,50	
1,5	1 167	175	38 283	32,8	34,3	97,5	2,5	3,2	0,41	11,97	112,1
2,0	3 318	419	69 274	20,9	32,7	94,3	5,7	13,2	0,38	25,9	4,8
2,0*	3 099	510	43 752	14,12	38,6	92,5	7,5	10,83	0,70	21,4	-1,2
2,0	5 213	496	85 681	16,4	31,6	92,3	7,7	22,1	0,33	25,6	
3,0	3 354	467	72 920	21,7	33,9	94,6	5,4	18,99	0,43	37,3	3,5
3,0*	3 537	496	69 274	19,6	33,80	93,75	6,25	21,33	0,80	25,9	1,2
3,0	5 287	481	87 504	16,6	32,2	92,5	7,5	33,17	0,35	35,9	
4,0	3 208	423	72 920	22,7	33,3	94,9	5,1	24,76	0,46	46,8	13,2
4,0	4 958	467	85 681	17,2	31,3	92,8	7,2	42,58	0,40	44,9	3,9

*   Linear flow velocity ~ 5 cm/s. Other experiments conducted at a linear flow velocity of 1 cm/s.

CF	=	concentration factor	OP	=	output (yield)
CE	=	current efficiency	WR	=	water recovery
BV	=	brine volume	EEC	=	electrical energy consumption

Concentration (mg/l)

Figure 9.14: Dialysate concentration as a function of time and cell pair voltage for approximately 1 000 mg/ℓ hydrochloric acid solutions.
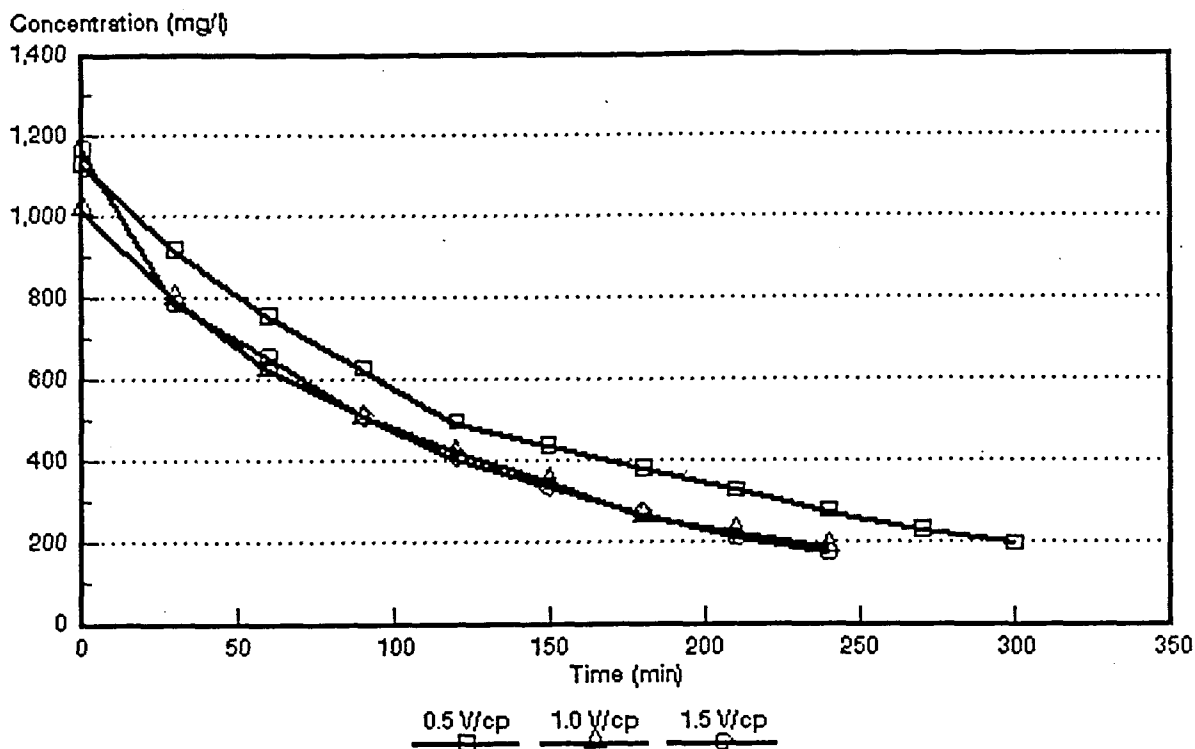
Concentration (mg/l)

Figure 9.15: Brine concentration as a function of time and cell pair voltage for approximately 1 000 mg/ℓ hydrochloric acid solutions.

Figure 9.16: Dialysate concentration as a function of time and cell pair voltage for approximately 3 000 mg/ℓ hydrochloric acid solutions.
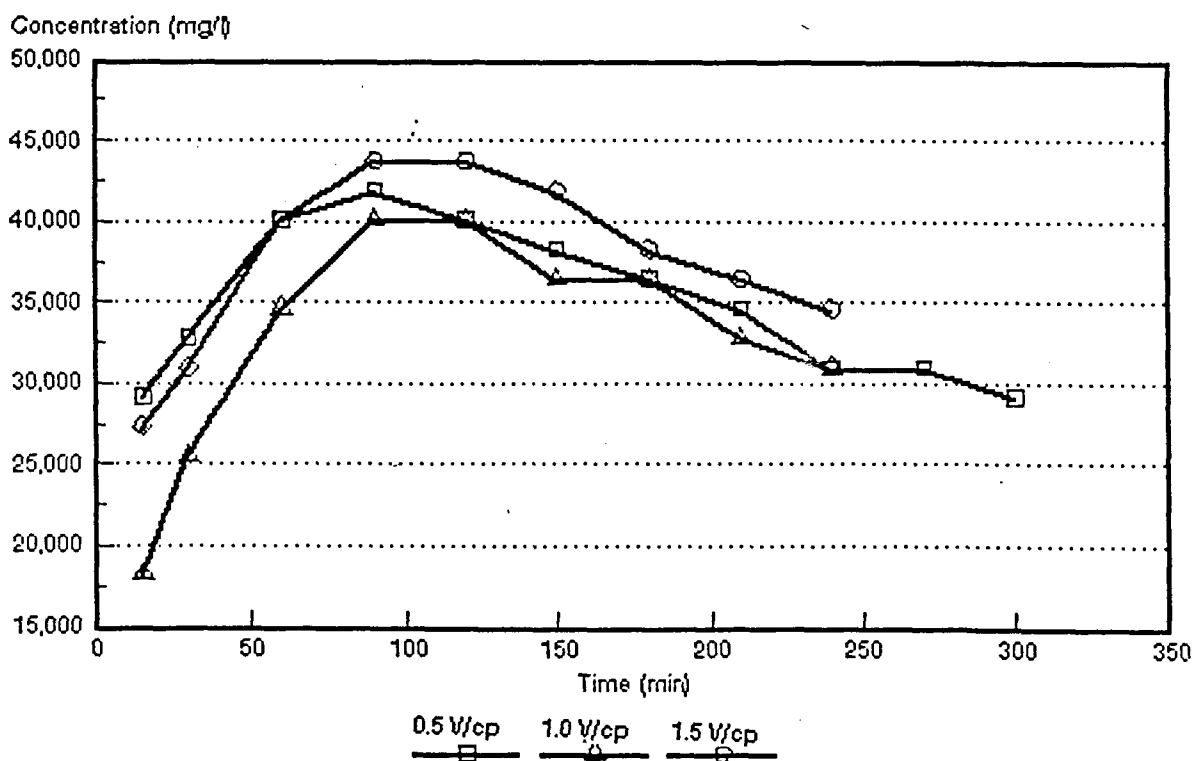

Figure 9.17: Brine concentration as a function of time and cell pair voltage for approximately 3 000 mg/ℓ hydrochloric acid solutions.
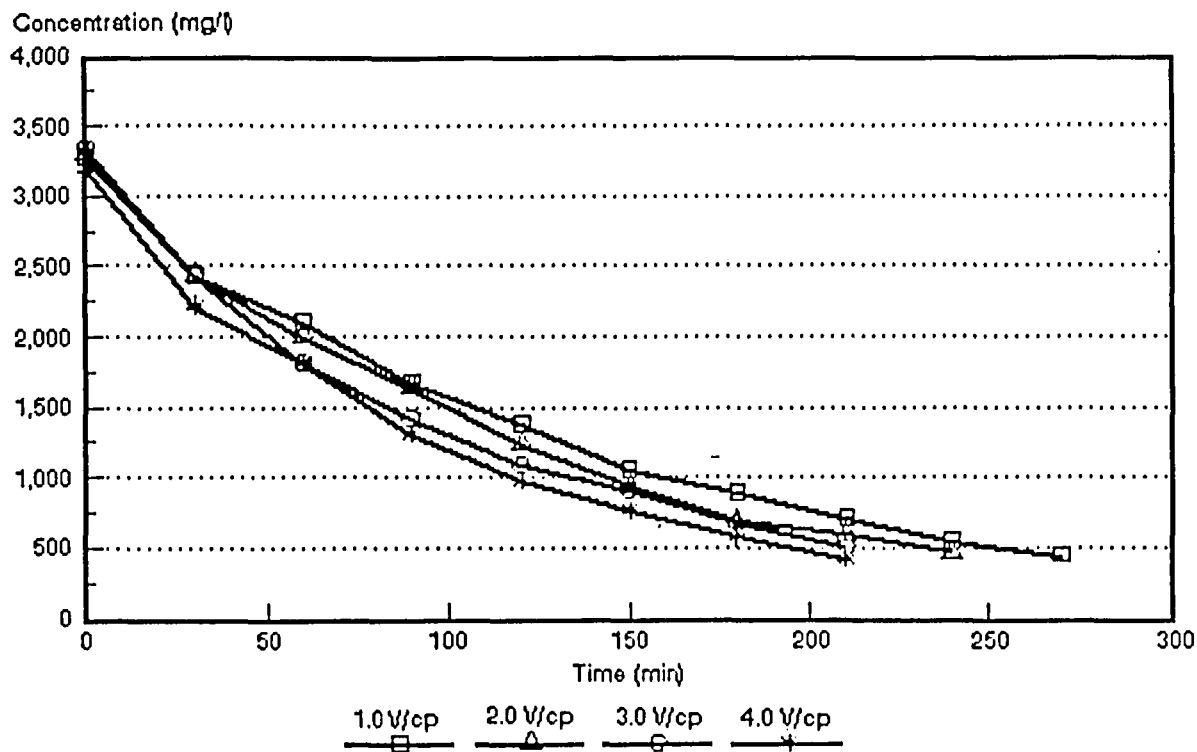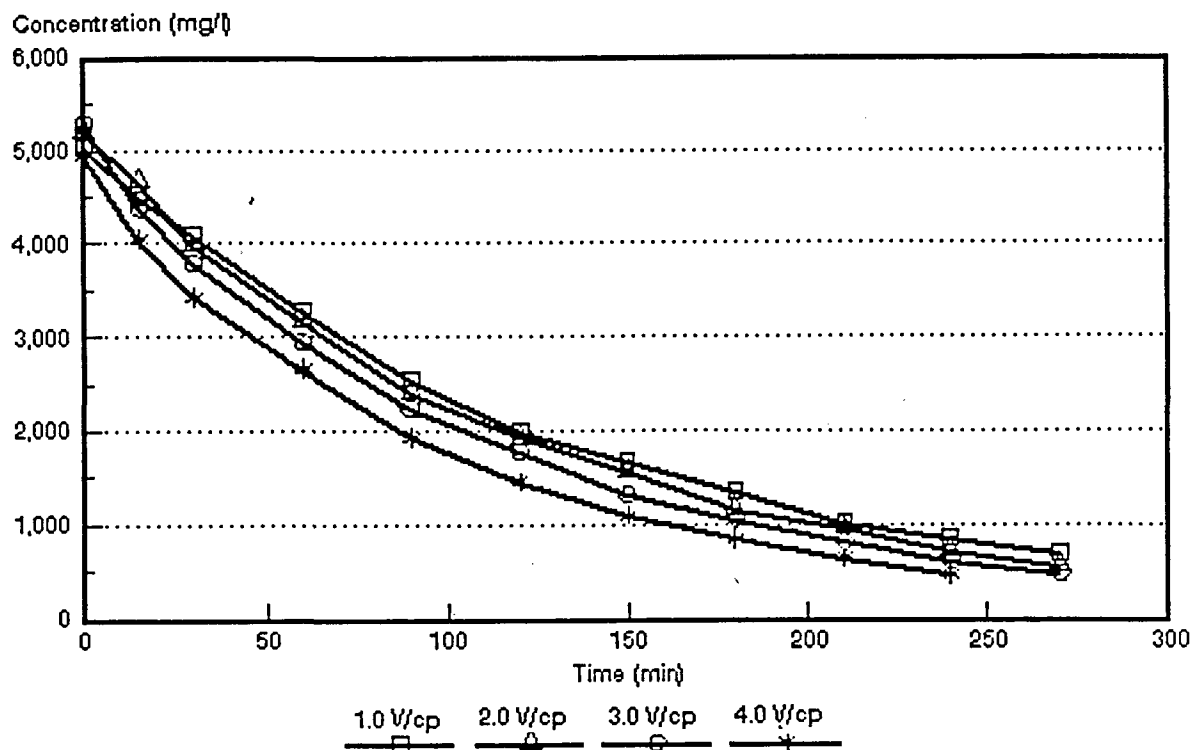
Figure 9.18: Dialysate concentration as a function of time and cell pair voltage for approximately 5 000 mg/ℓ hydrochloric acid solutions.
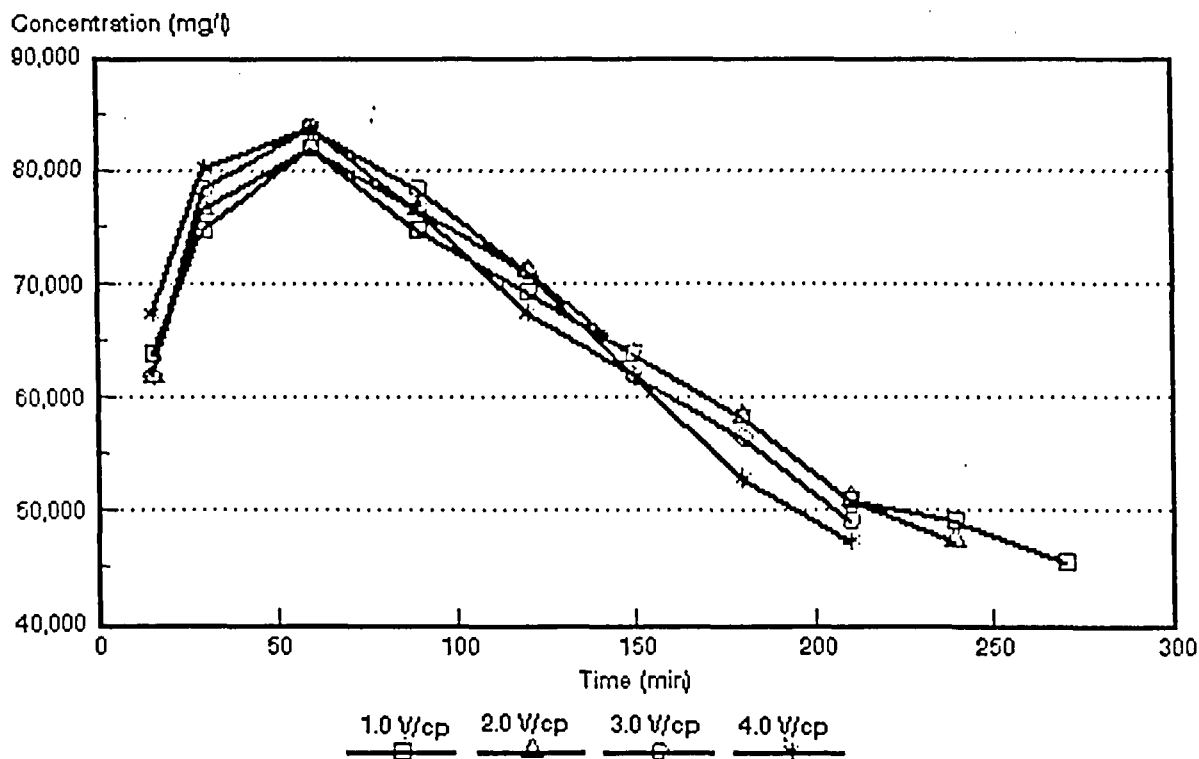

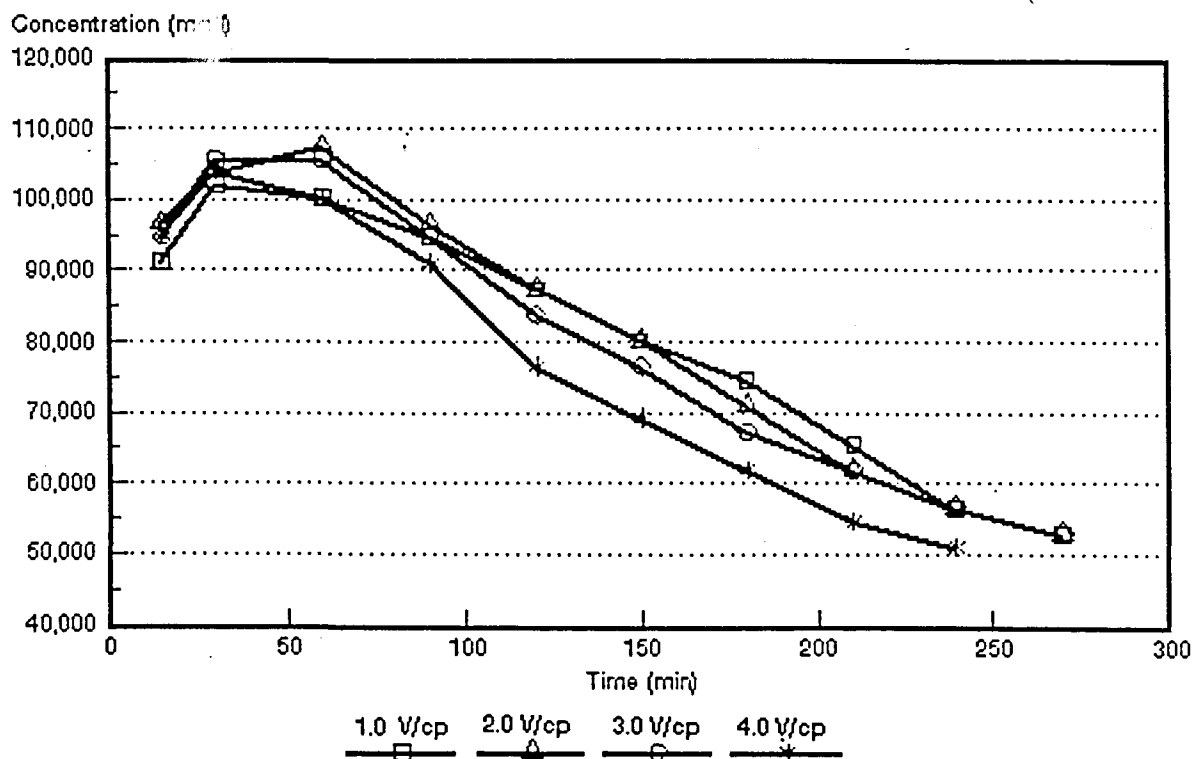**Figure 9.19:** Brine concentration as a function of time and cell pair voltage for approximately 5 000 mg/ℓ hydrochloric acid solutions.
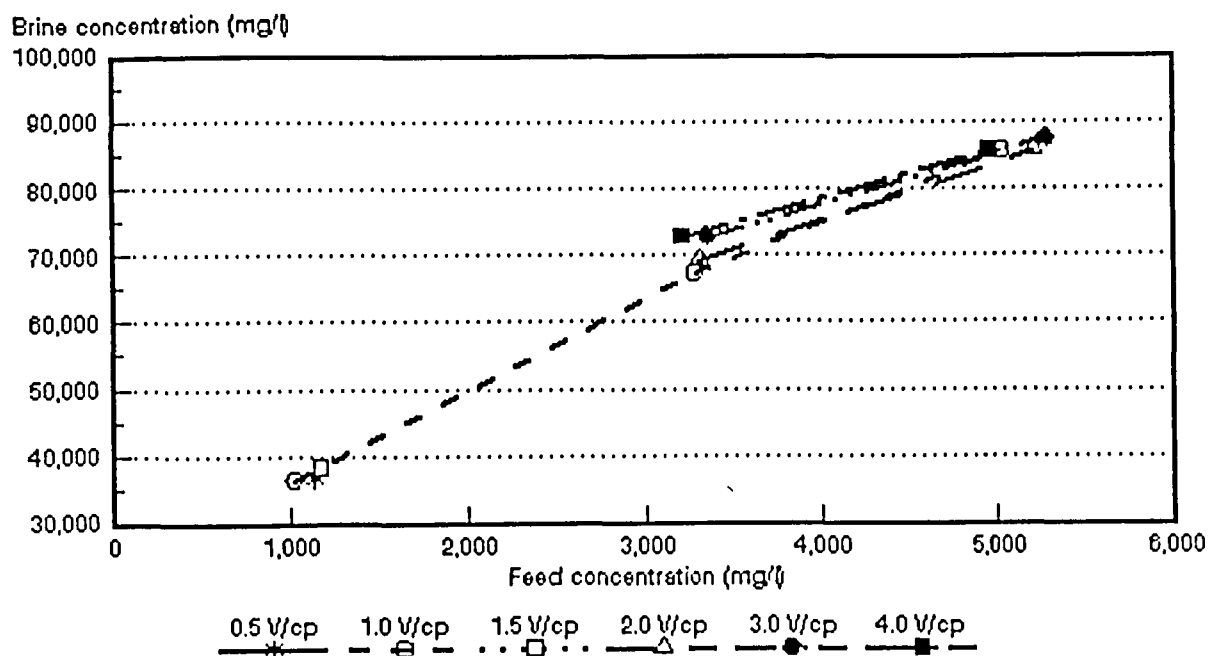
Figure 9.20: Brine concentration as as a function of hydrochloric acid feed concentration and cell pair voltage.
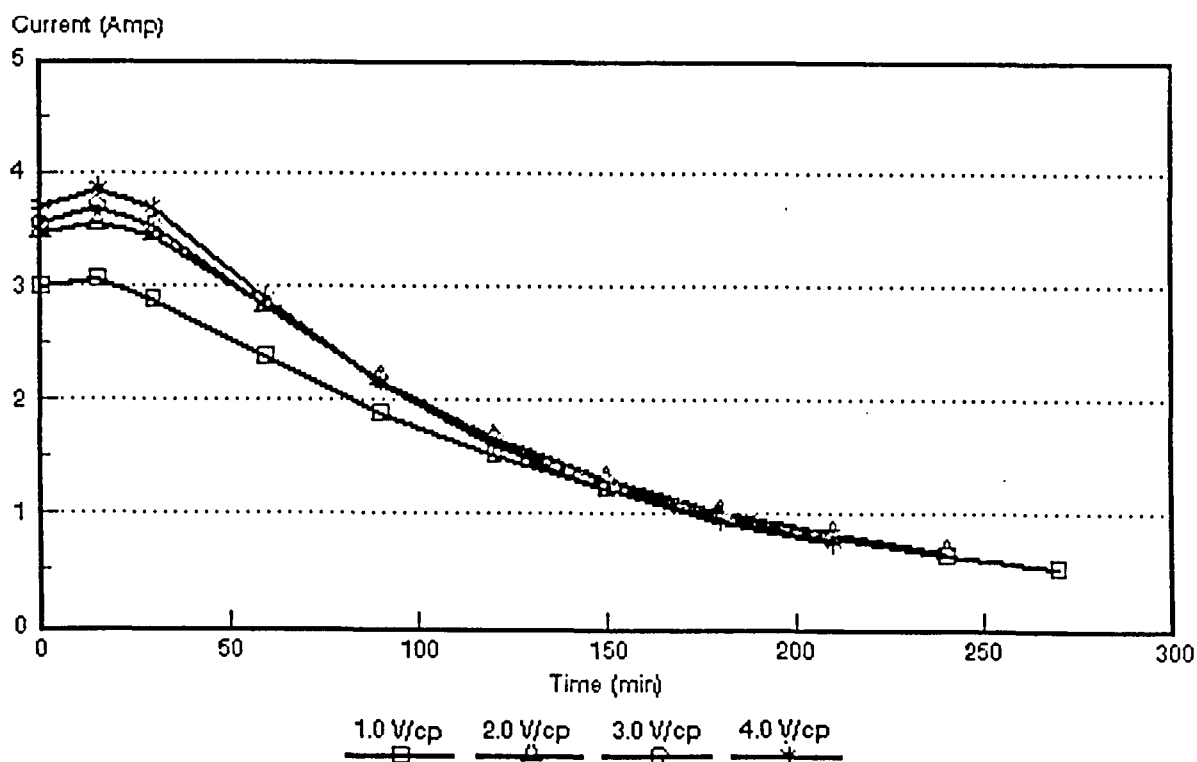

Figure 9.21: Electric current as a function of time and cell pair voltage during concentration/desalination of approximately 3 000 mg/ℓ hydrochloric acid solutions.

V/cp). Therefore, high water recoveries and low acid brine volumes could be obtained with EOP-ED of acidic solutions.

9.2.3 Current efficiency

Current efficiencies were low (Table 9.2). Current efficiency varied between 46,3 and 29,2% in the acid feed concentration and cell pair voltage ranges studied. Current efficiency did not change with increasing cell pair voltage and decreased with increasing feed water concentration especially at the higher acid feed concentrations (Fig. 9.22). This is contrary to what has been experienced during EOP-ED of sodium chloride solutions and can be ascribed to less water that permeates through the membranes at higher feed concentration. The low current efficiencies that were obtained with the acid solutions could be ascribed to the inability of the anion membranes to resist the passage of hydrogen ions. However, the permselectivity of the *Selemion* AAV membranes for hydrogen ions is much better than that of other membranes normally used for ED of saline solutions.

9.2.4 Electrical energy consumption

Electrical energy consumption increased with increasing cell pair voltage and increasing acid feed concentration (Table 9.2 and Fig. 9.23). Low electrical energy consumption was obtained at low cell pair voltages and low acid feed concentrations. Electrical energy consumptions of 0,2 to 3,2 kWh/m^3 product were obtained in the acid feed and cell pair voltage range of approximately 1 000 mg/ℓ and 0,5 to 1,5 V/cp, respectively. However, electrical energy consumption increased rapidly with increasing feed concentration and cell pair voltage. The electrical energy consumption at 2,0; 3,0 and 4,0 V/cp of an approximately 3 000 mg/ℓ hydrochloric acid solution was determined at 13,2; 18,9 and 24,8 kWh/m^3 product water, respectively.

9.2.5 Product water yield

Product water yield (output) increased with increasing cell pair voltage and decreased with increasing acid feed concentration (Table 9.2). Output also increased significantly with increasing linear flow velocity through the stack. Output was determined at 0,38 m^3/m^2·d at a linear flow velocity of 1 cm/s (2,0 V/cp). At a linear flow velocity of 5 cm/s, output was determined at 0,7 m^3/m^2·d (Table 9.2). Therefore, it would be advantageous to operate an EOP-ED stack at the highest possible linear flow velocity.
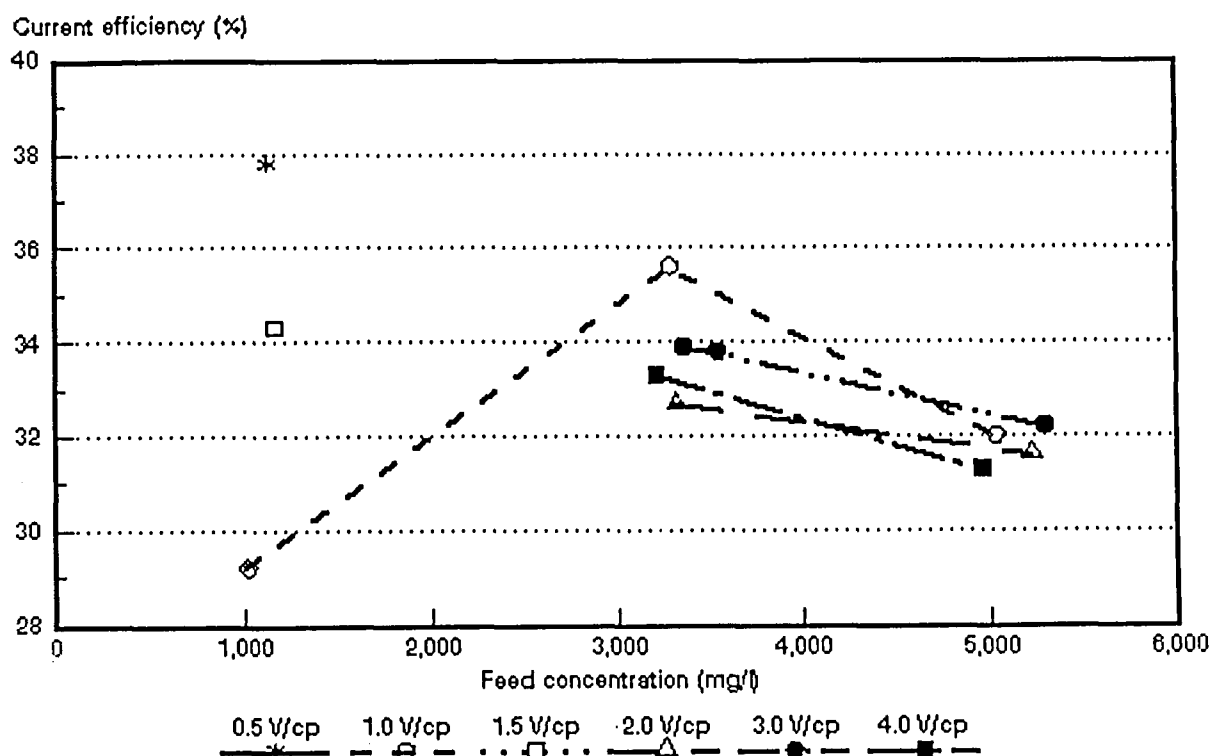
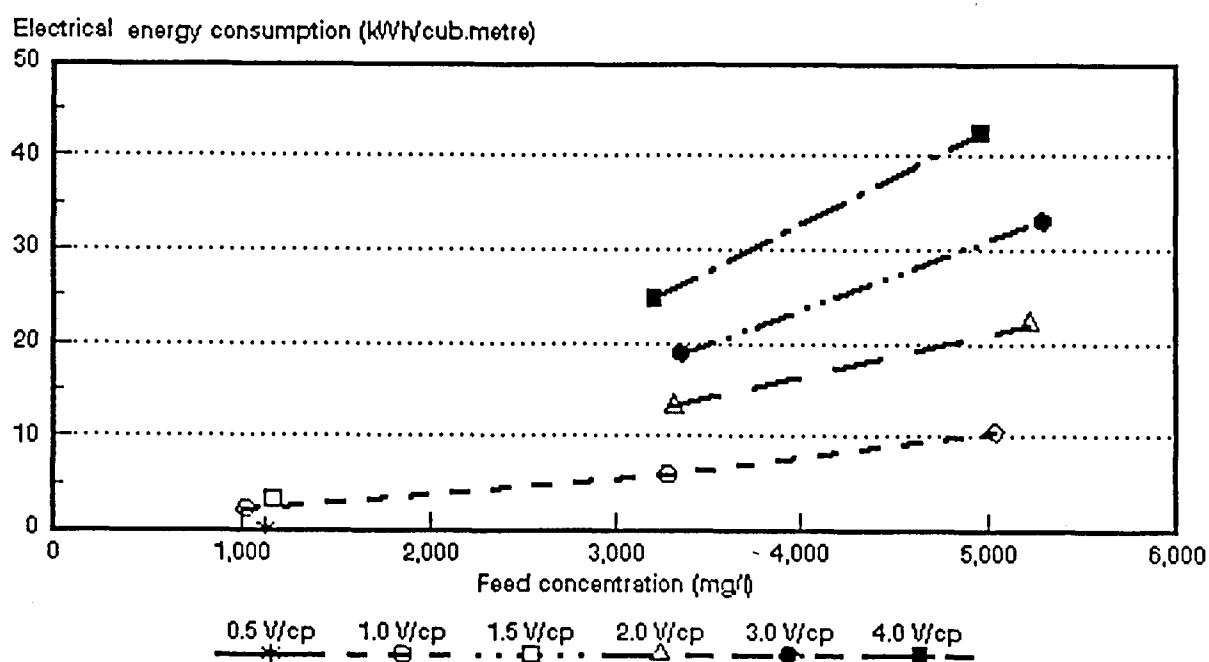**Figure 9.22:** Current efficiency as a function of hydrochiric acid feed concentration and cell pair voltage.

Figure 9.23: Electrical energy consumption as a function of hydrochloric acid feed concentration and cell pair voltage.

9.2.6 Effective cell pair thickness and cell pair resistance

An example of cell pair resistance (R_{cp}) as a function of the specific resistance of the dialysate and cell pair voltage is shown in Figure 9.24 for an approximately 5 000 mg/ℓ hydrochloric acid feed solution. Straight lines were obtained over the cell pair voltage range studied. The slope of the lines increased with increasing cell pair voltage as was experienced with sodium chloride solutions. However, the slopes of the lines were much steeper in the case of the acid especially at the higher cell pair voltages.

The effective cell pair thickness, d_{eff}, was determined at 13,5; 25,6; 35,9 and 44,9 mm at 1; 2; 3 and 4 V/cp, respectively (5 000 mg/ℓ feed) (Table 9.2). Effective cell pair thickness decreased significantly with increasing linear flow velocity. The effective cell pair thickness decreased from 13,8 mm to 8,1 mm at 1 V/cp (3 000 mg/ℓ feed).

Cell pair resistance, R_{cp}, decreased with increasing feed concentration and decreasing cell pair voltage. The negative cell pair resistances reported in Table 9.2 could be ascribed to experimental error due to the very low resistance of the cell pair.
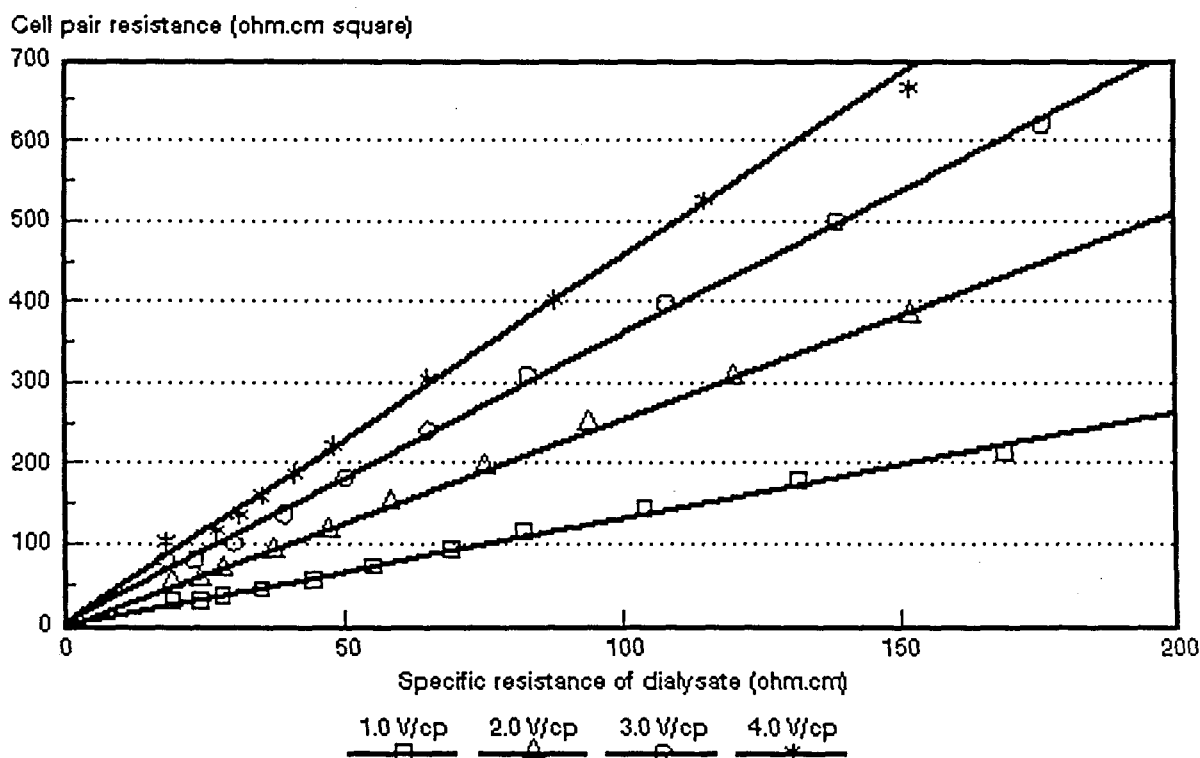

Figure 9.24: Cell pair resistance as a function of specific resistance of the dialysate and cell pair voltage for approximately 5 000 mg/ℓ hydrochloric acid solutions.

9.3 Concentration/Desalination of Caustic Soda Solutions with *Selemion* AMV and CMV Membranes

The concentration/desalination results of different caustic soda feed water concentrations at different cell pair voltages are summarized in Table 9.3.

9.3.1 Brine and dialysate concentration

Dialysate and brine concentrations as a function of time and cell pair voltage for different initial feed water concentrations are shown in Figs. 9.25 to 9.30. Caustic soda brine concentration as a function of feed concentration and cell pair voltage is shown in Figure 9.31. A typical example of electric current as a function of time and cell pair voltage for an approximately 5 000 mg/ℓ caustic soda feed solution is shown in Figure 9.32.

Desalination/concentration rate increased with increasing cell pair voltage (Figs. 9.25 to 9.30 and Fig. 9.32). Brine concentration increased as a function of feed concentration and cell pair voltage (Table 9.3 and Fig. 9.31). Caustic soda brine concentrations of 2,8 to 9,8% were obtained in the feed and cell pair voltage ranges of approximately 1 000 to 10 000 mg/ℓ and 0,5 to 3,0 V/cp, respectively.

Product water with a concentration of less than 400 mg/ℓ caustic soda could be produced (Table 9.3) from caustic soda feed waters in the feed and cell pair voltage ranges of 1 000 to 10 000 mg/ℓ and 0,5 to 3,0 V/cp, respectively. It was possible to produce a product water with a concentration of less than 100 mg/ℓ caustic soda.

Concentration factors increased with increasing cell pair voltage and decreased with increasing feed concentration as was experienced with sodium chloride and hydrochloric acid solutions.

9.3.2 Brine volume and water recovery

Low brine volumes and high water recoveries were again obtained (Table 9.3). Brine volume varied between 2,3 and 7,3% in the caustic soda feed water and cell pair voltage ranges of 1 000 to 5 000 mg/ℓ and 0,5 to 3 V/cp, respectively. Brine volume further increased with increasing caustic soda feed water concentration in the feed concentration range from 1000 to 10 000 mg/ℓ. The highest brine volume of 11,7%

351

Table 9.3: Concentration/desalination results of caustic soda solutions at different feed concentrations and cell pair voltages using Selemion AMV and CMV membranes.

Vcp	c_f mg/ℓ	c_p mg/ℓ	c_b mg/ℓ	CF	CE %	WR %	BV %	EEC kWh/m³	OP m³/m²·d	d_{eff} mm	Rcp ohm·cm²
0,5	1 008	168	30 000	29,8	75,1	97,7	2,3	0,77	0,42	6,03	56,1
1,0	1 056	120	28 000	26,5	68,96	97,55	2,45	0,91	0,44	11,6	54,8
	2 920	400	60 000	20,6	77,96	96,8	3,2	2,18	0,47		
	5 480	224	64 000	11,7	77,80	92,7	7,3	4,54	0,33		
	10 640	400	90 000	8,5	73,3	88,3	11,7	9,40	0,33	12,64	0,15
1,5	1 104	96	30 000	27,2	71,98	97,6	2,4	1,41	0,51	11,99	146,8
2,0	3 400	400	80 000	23,5	81,2	96,9	3,1	4,97	0,73		
	4 960	85	76 000	15,3	78,1	93,75	6,25	8,38	0,43		
	10 880	320	98 000	9,0	73,1	90,0	10,0	19,42	0,56	13,59	7,1
3,0	3 200	384	84 000	26,3	79,2	97,0	3,0	7,18	1,27		
	5 560	256	86 000	15,5	78,36	94,6	5,4	13,64	0,92		

Linear flow velocity 1 cm/s.

CF	=	concentration factor	OP	=	output (yield)
CE	=	current efficiency	WR	=	water recovery
BV	=	brine volume	EEC	=	electrical energy consumption

Concentration (mg/l)

Figure 9.25: Dialysate concentration as a function of time and cell pair voltage for an approximately 1 000 mg/l caustic soda feed solution.

Concentration (mg/l)

Figure 9.26: Brine concentration as a function of time and cell pair voltage for an approximately 1 000 mg/l caustic soda feed solution.

353

Figure 9.27: Dialysate concentration as a function of time and cell pair voltage for an approximately 3 000 mg/ℓ caustic soda feed solution.

Figure 9.28: Brine concentration as a function of time and cell pair voltage for an approximately 3 000 mg/ℓ caustic soda feed solution.
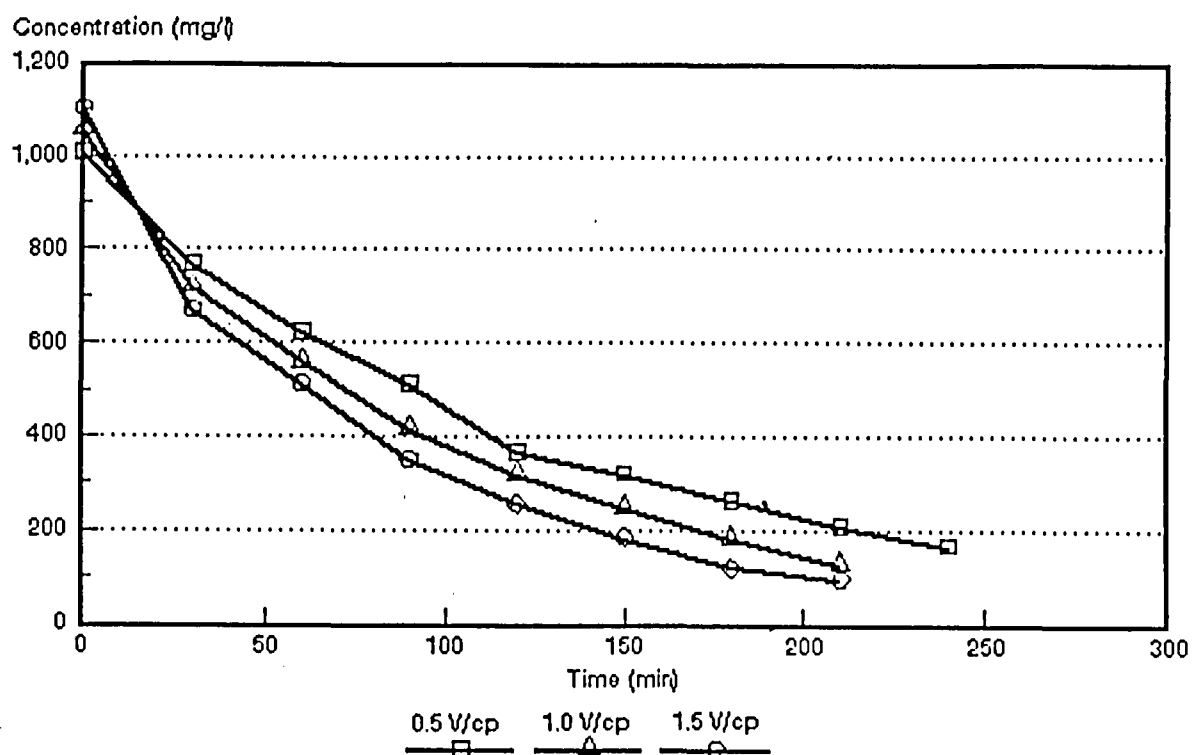
Figure 9.29: Dialysate concentration as a function of time and cell pair voltage for an approximately 5 000 mg/ℓ caustic soda feed solution.

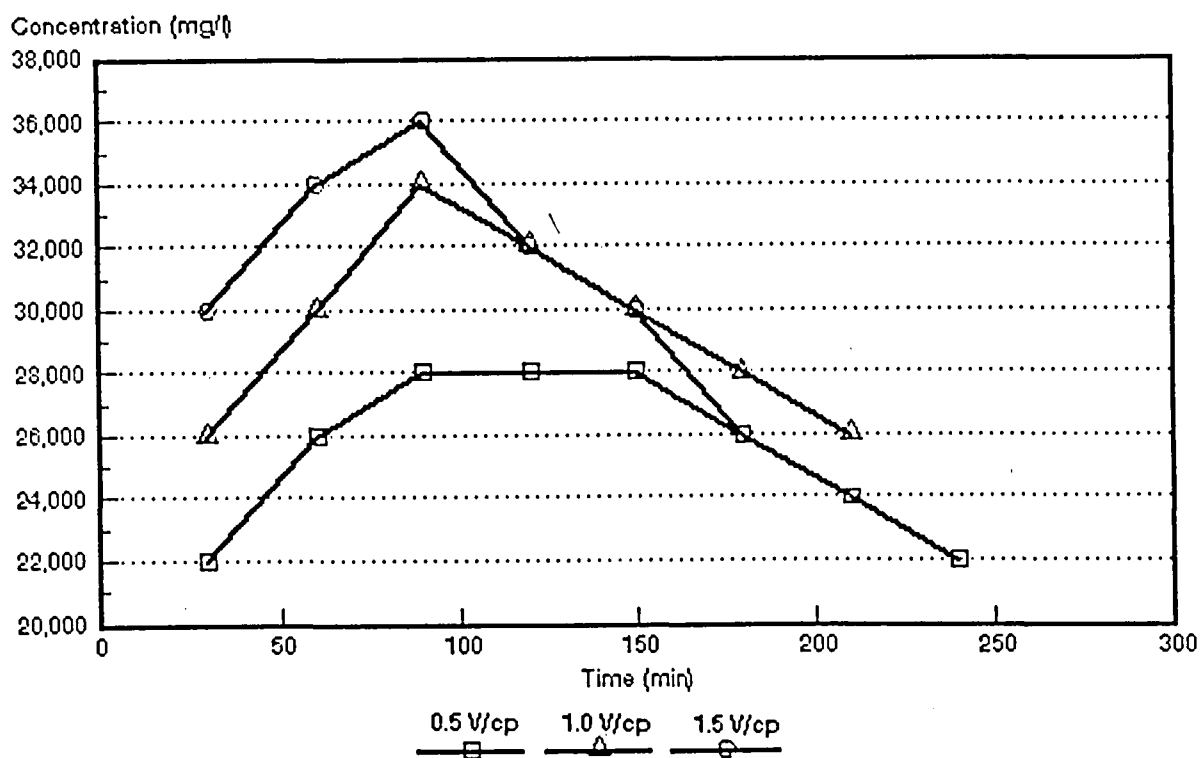**Figure 9.30:** Brine concentration as a function of time and cell pair voltage for an approximately 5 000 mg/ℓ caustic soda feed solution.
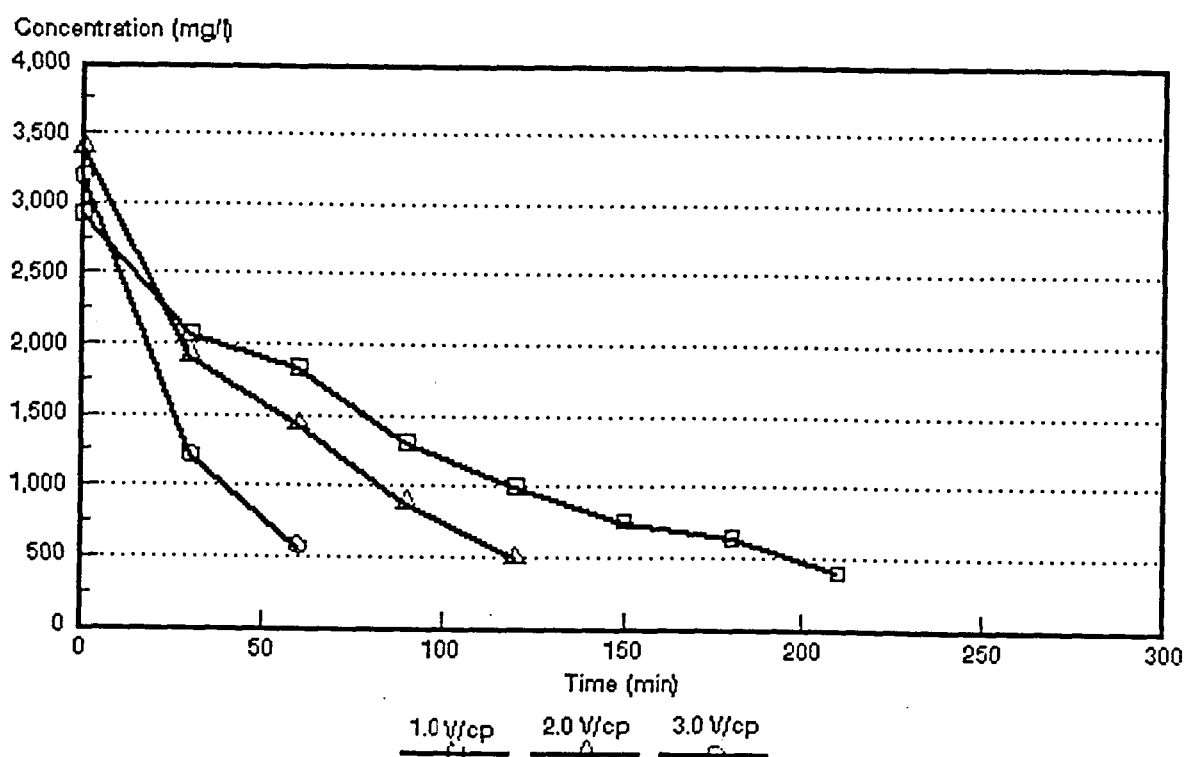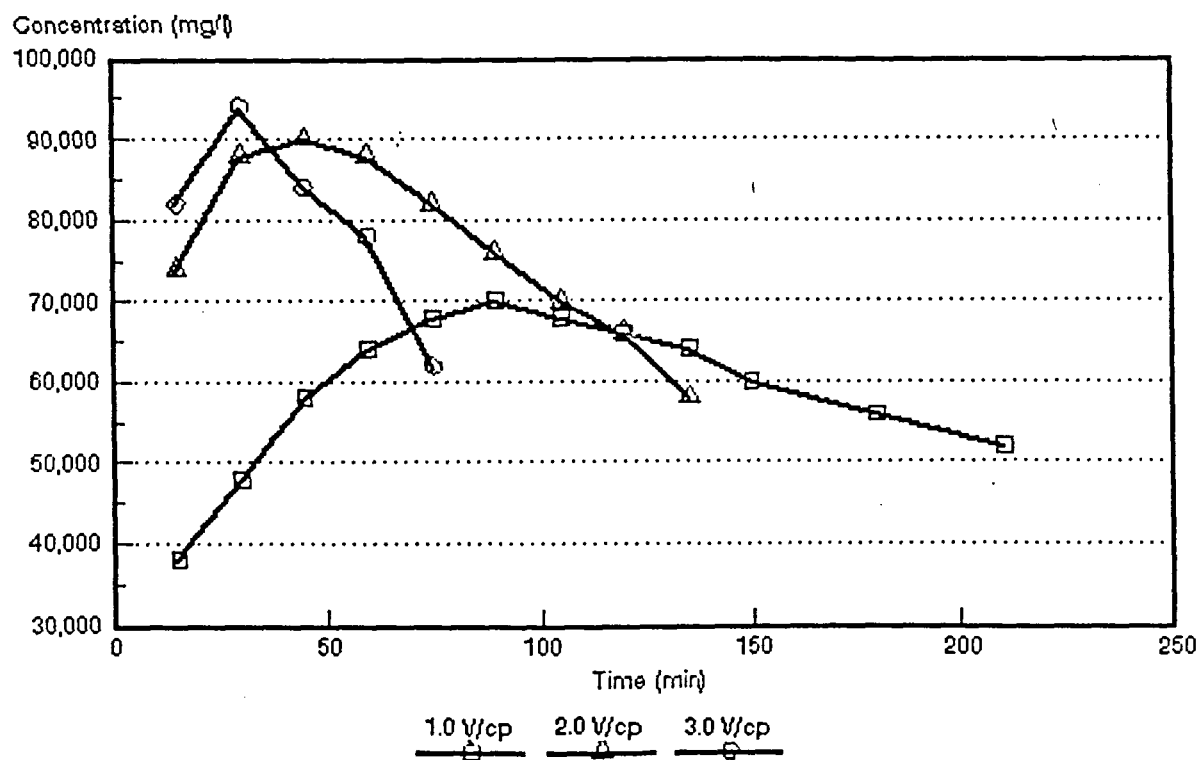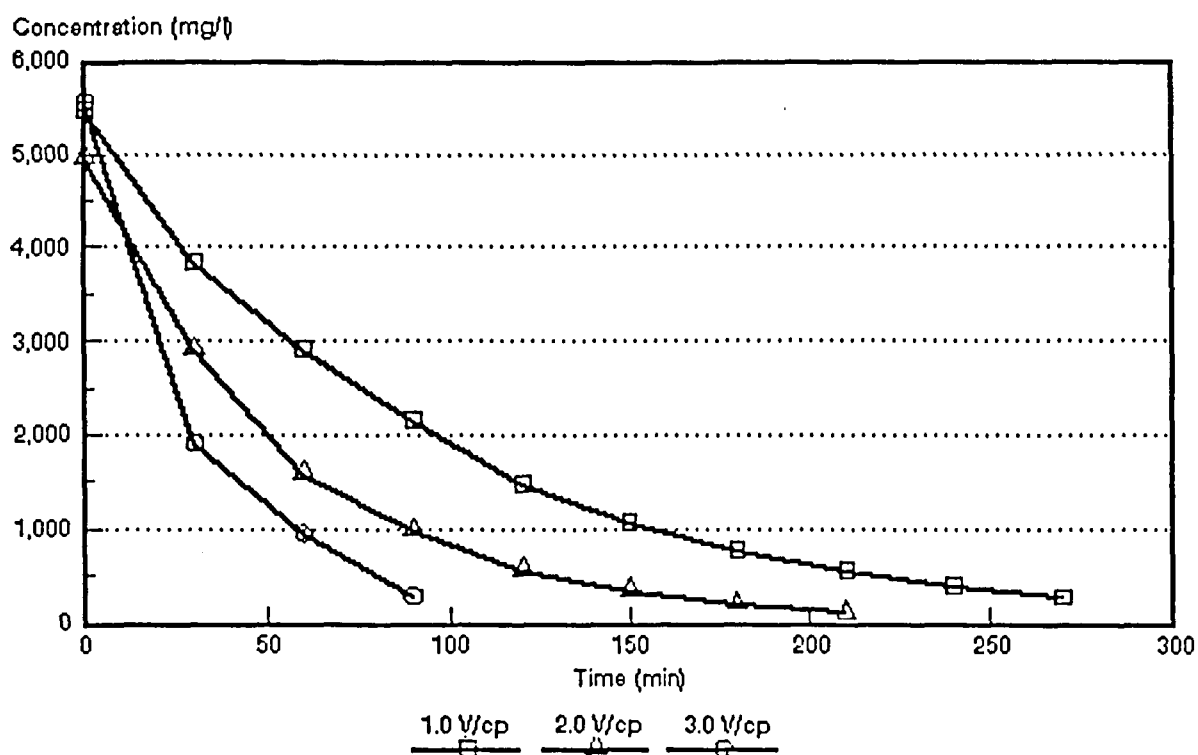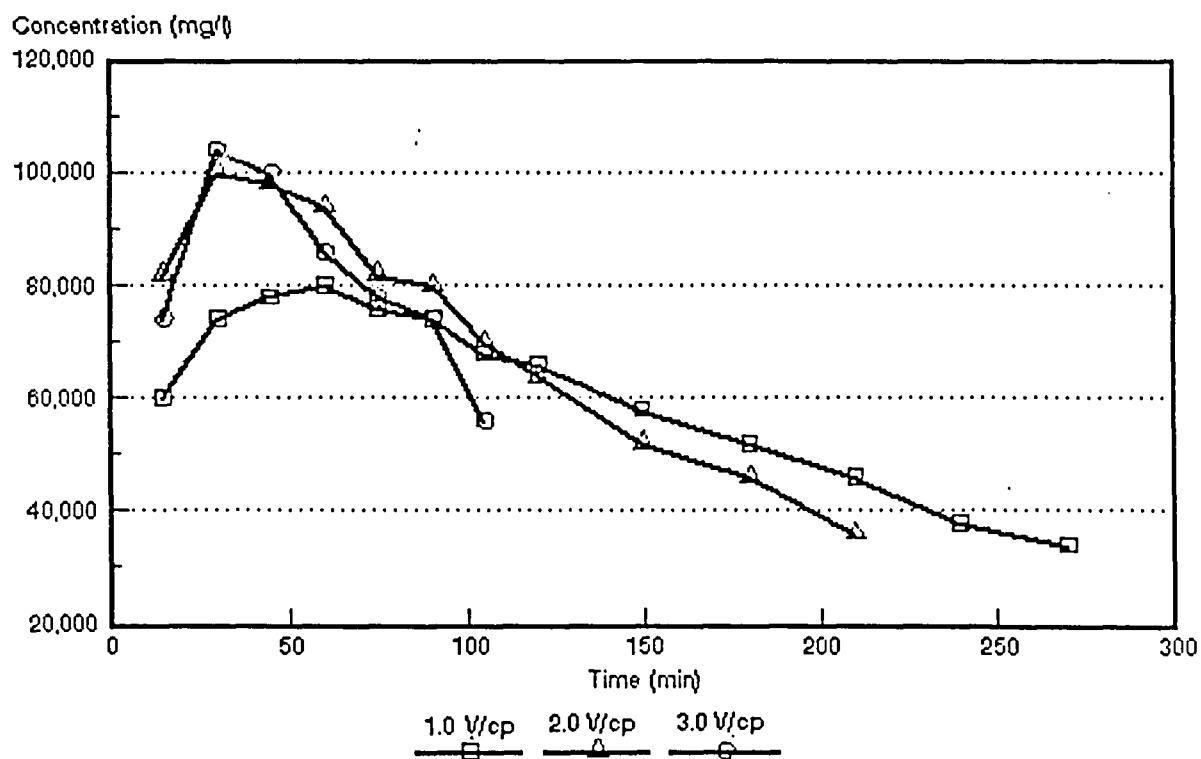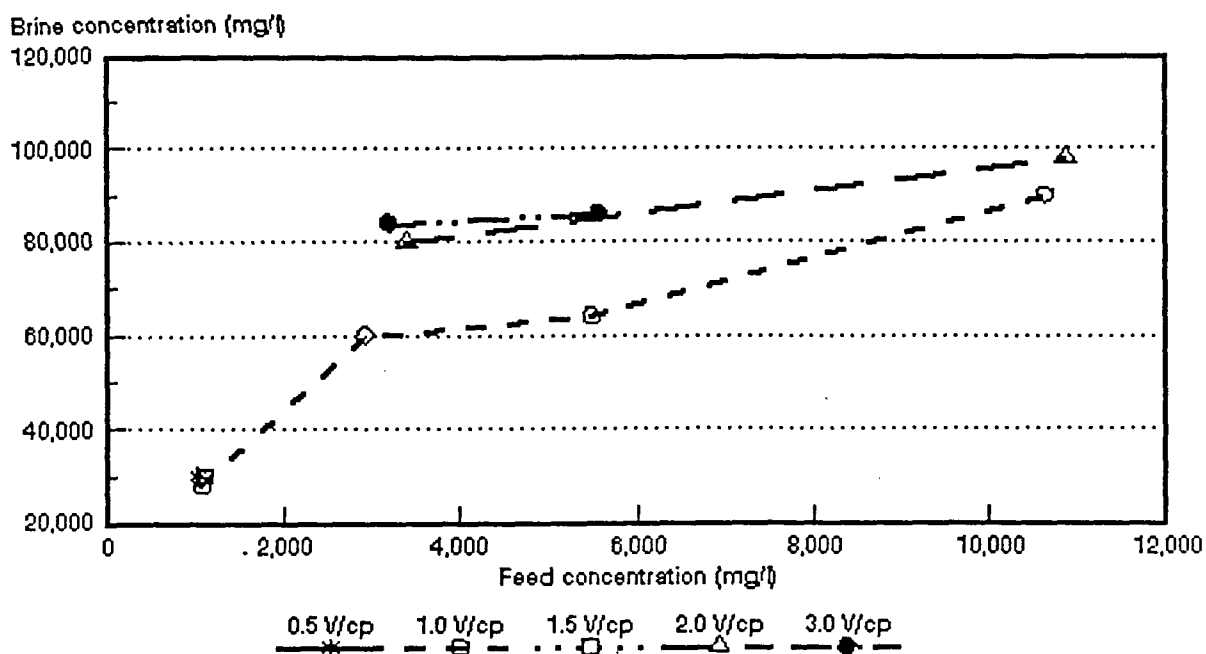
355

Figure 9.31: Brine concentration as a function of sodium hydroxide feed concentration and cell pair voltage.
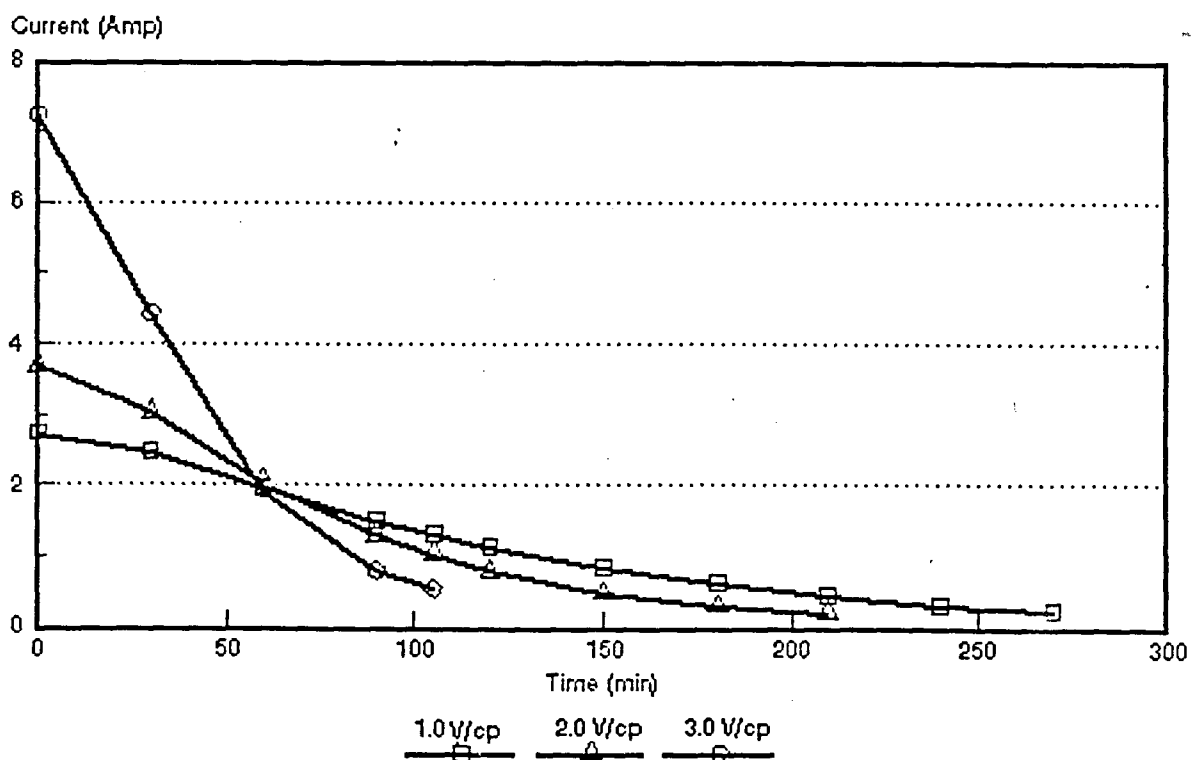
Figure 9.32: Current as a function of time and cell pair voltage for an approximately 5 000 mg/ℓ caustic soda solution.

was obtained at a caustic soda feed water concentration of approximately 10 000 mg/ℓ (1,0 V/cp). Water recoveries were high. Water recoveries of 93 to 97,5% were obtained in the caustic soda feed water concentration range from 1 000 to 5 000 mg/ℓ.

9.3.3 Current efficiency

Current efficiency increased with increasing caustic soda feed water concentration at 1,0 V/cp (Table 9.3 and Fig. 9.33). However, current efficiency slightly decreased with increasing caustic soda feed water concentration at the other cell pair voltages. Current efficiency did not decrease significantly with increasing cell pair voltage.

Current efficiencies of 73,3 to 77,9% were obtained in the caustic soda feed water and cell pair voltage ranges of 1 000 to 10 000 mg/ℓ and 0,5 to 1,5 V/cp, respectively. Current efficiencies of 73,1 to 81,2% were obtained in the caustic soda feed water and cell pair voltage ranges of 3 000 to 10 000 mg/ℓ and 2,0 to 3,0 V/cp, respectively.

9.3.4 Electrical energy consumption

Electrical energy consumption increased with increasing caustic soda feed water concentration and increasing cell pair voltage (Table 9.3 and Fig. 9.34). Electrical energy consumption was low at low cell pair voltages (0,5 to 1,5) and low feed concentrations (1 000 to 3 000 mg/ℓ). Electrical energy consumption varied between 0,4 and 2,2 kWh/m³ product water in this range. However, electrical energy consumption became higher at higher cell pair voltages and caustic soda feed water concentrations. An electrical energy consumption of 19,4 kWh/m³ product water was obtained at a cell pair voltage of 2,0 and a caustic soda feed water concentration of approximately 11 000 mg/ℓ.

9.3.5 Product water yield

Product water yield increased with increasing cell pair voltage and decreased with increasing feed concentration (Table 9.3).

9.3.6 Effective cell pair thickness and cell pair resistance

An example of cell pair resistance (R_{cp}) as a function of the specific resistance of the dialysate and cell pair voltage is shown in Figure 9.35 (approximately 1 000 mg/ℓ

Current efficiency (%)
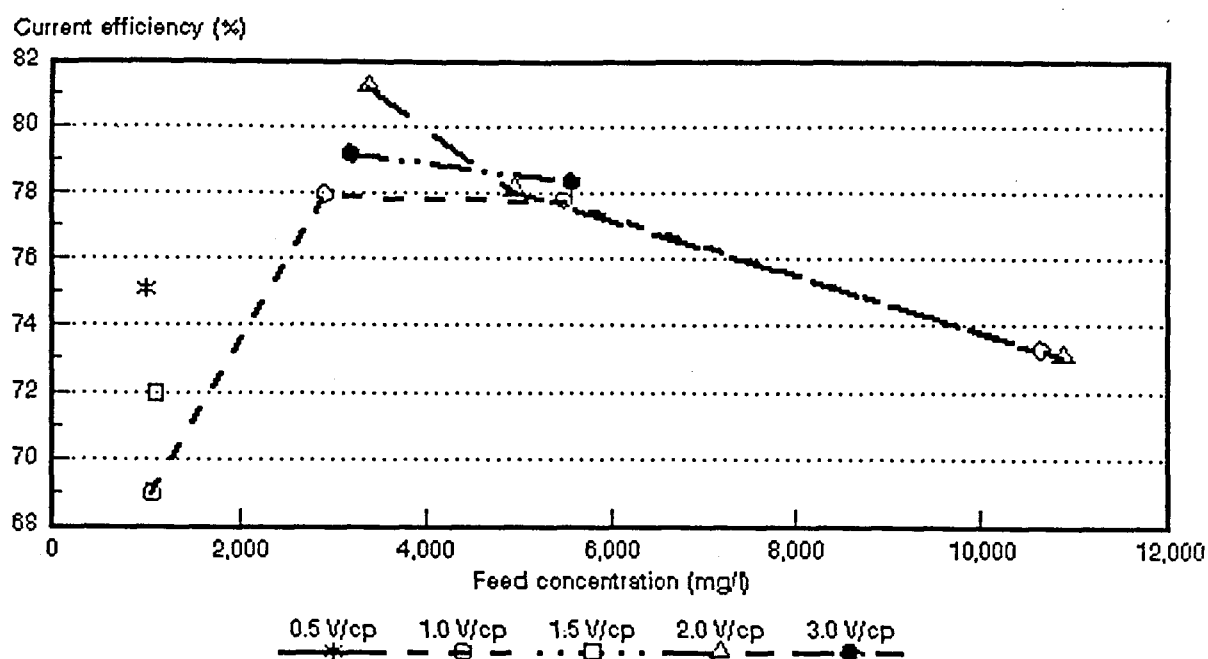
Figure 9.33: Current efficiency as a function of sodium hydroxide feed concentration and cell pair voltage.

Electrical energy consumption (kWh/cub.metre)
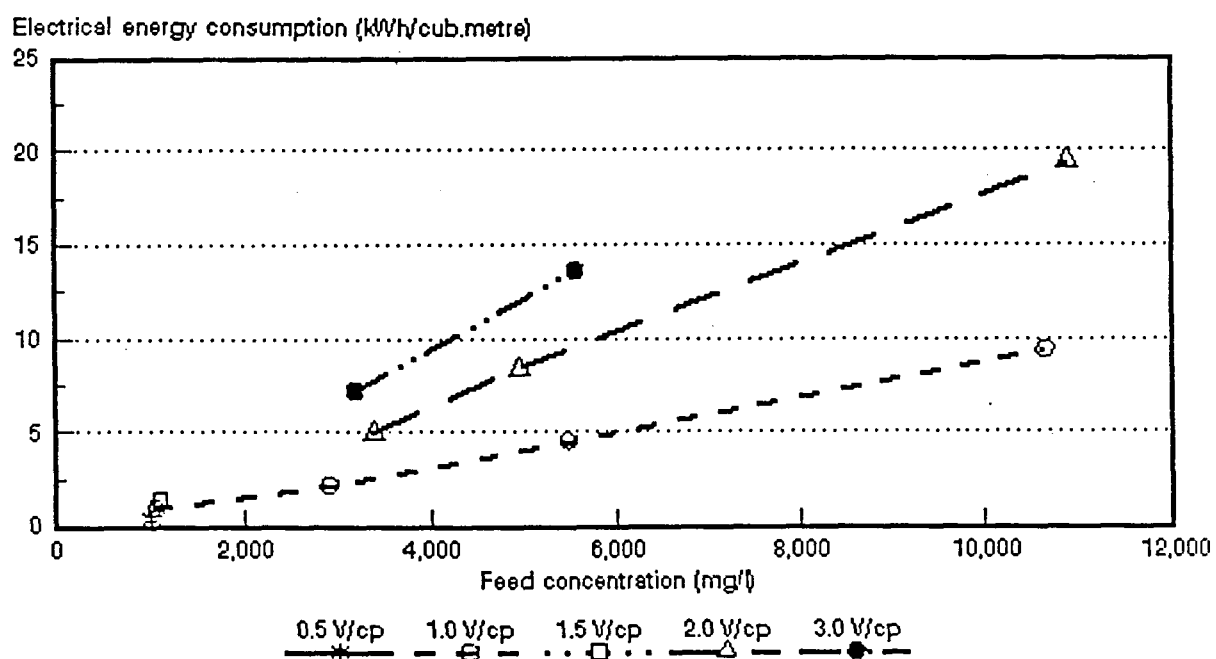
Figure 9.34: Electrical energy consumption as a function of sodium hydroxide feed concentration and cell pair voltage.

Cell pair resistance (ohm.cm square)
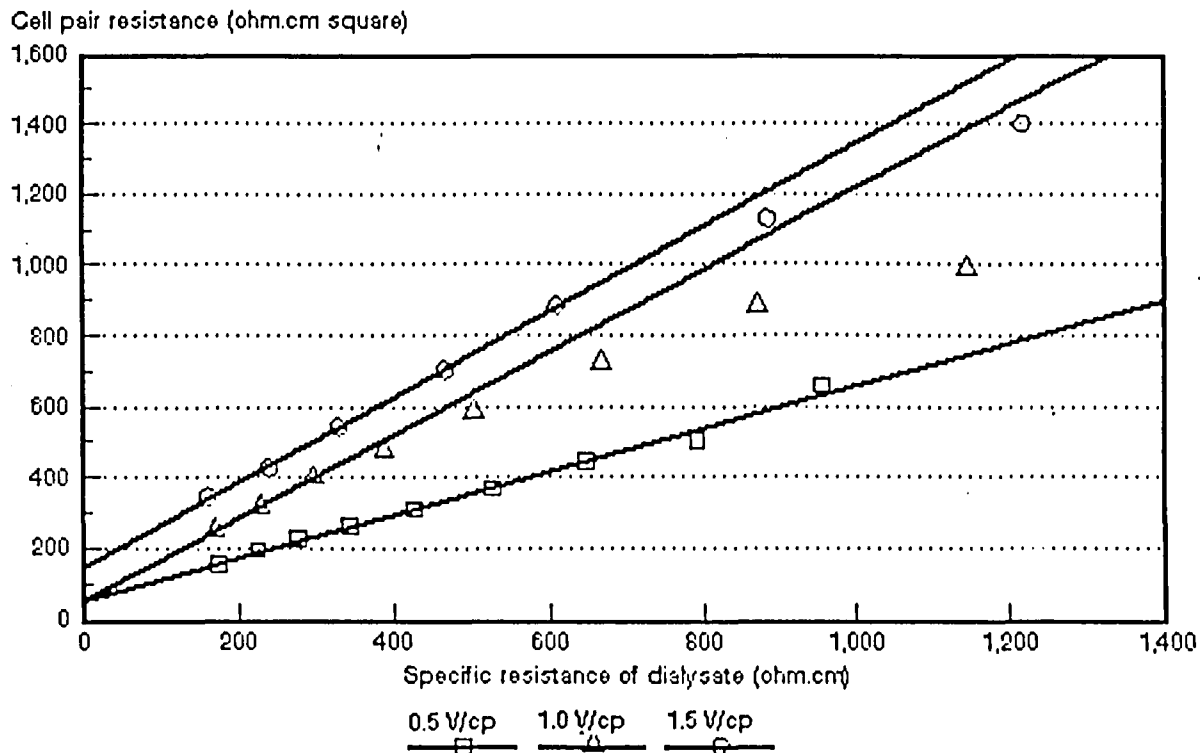
Figure 9.35: Cell pair resistance as a function of specific resistance of the dialysate and cell pair voltage for approximately 1 000 mg/ℓ caustic soda solution.

caustic soda feed). Polarization increased with increasing cell pair voltage in the cell pair voltage range from 0,5 to 1,0 V/cp. The effective cell pair thickness, d_{eff}, was determined at 6,03 mm at 0,5 V/cp (1 000 mg/ℓ feed). Cell pair thickness was 11,6 at 1,0 V/cp (1 000 mg/ℓ feed) and 11,99 at 1,5 V/cp (1 000 mg/ℓ feed). This showed that polarization was approximately the same at 1,0 and 1,5 V/cp.

Cell pair resistance decreased with increasing feed concentration (Table 9.3). A cell pair resistance of only 0,15 ohm·cm² was obtained at 10 000 mg/ℓ caustic soda feed concentration (1,0 V/cp).

10. CONCENTRATION/DESALINATION OF SALT SOLUTIONS AND INDUSTRIAL EFFLUENTS WITH SCED

10.1 Concentration of salt solutions

A summary of the concentration/desalination results of the different salt solutions is shown in Tables 10.1 to 10.5.

10.1.1 Desalination rate, product and brine concentration

Examples of the desalination/concentration of sodium chloride, ammonium nitrate and sodium sulphate solutions as a function of time at constant cell pair voltage are shown in Figures 10.1 to 10.3. The effect of increasing cell pair voltage on desalination/concentration of an approximately 1 000 mg/ℓ sodium sulphate solution is shown in Figure 10.4.

Desalination rate decreased with decreasing feed concentration (Figs. 10.1 to 10.3) and decreasing cell pair voltage (Figure 10.4). However, approximately the same initial desalination rate was obtained at 1,18 and 1,76 V/cp (Figure 10.4). The optimum cell pair voltage for desalination regarding polarization and electrical energy consumption should be determined for each feed concentration, because this information is required to operate an ED stack under optimum conditions. This, however, was not the main purpose of this investigation. The main purpose of this investigation was to evaluate the performance of the SCED unit for concentration/desalination of saline solutions at cell pair voltages normally applied in ED.

All the different salt solutions could be easily desalinated from approximately 10 000 mg/ℓ to 300 mg/ℓ and less (Figs. 10.1 to 10.3 and Tables 10.1 to 10.5). Product concentrations of less than 100 mg/ℓ could be obtained with ease in some cases. Therefore, SCED appears to be effective for the production of low TDS water.

Brine concentration increased with increasing feed concentration and increasing cell pair voltage (Tables 10.1 to 10.5 and Figure 10.5). Sodium chloride, ammonium nitrate, sodium sulphate, sodium nitrate and calcium chloride brine concentrations of 2,2 to 16,1%; 4,9 to 15%; 7,8 to 16,3%; 6,0 to 12,5% and 3,8 to 7,5% could be obtained, in the feed concentration and cell pair voltage range of 0,1 to 1% and 0,59 to 1,76 V/cp, respectively. Therefore, relatively high brine concentrations could be obtained

Table 10.1: Concentration/Desalination Results of Sodium Chloride Solutions at different cell pair voltages.

Vcp	Cf mg/l	Cp mg/l	Cb mg/l	CF	CE %	WR %	BV %	EEC kWh/m³	OP m³/m².d	d_eff mm	Rcp ohm-cm²
0,59	1010	282	22 450	22,20	72,20	96,00	4,00	0,34	1,22	0,95	38,8
1,18	950	35	31 000	35,40	66,70	96,30	3,70	0,77	1,53	1,01	39,2
	1 900	40	53 500	28,10	73,70	96,50	3,50	1,41	1,36	0,91	35,1
	3 400	125	72 000	21,20	56,40	96,40	3,60	3,26	1,36	0,97	21,3
	5 400	65	82 000	15,20	78,60	94,80	5,20	3,86	1,20	0,88	18,2
	10 200	195	161 000	15,80	67,90	93,50	6,50	8,04	1,19	0,87	14,4
1,76	985	25	37 000	37,70	63,90	96,70	3,30	1,25	1,75	1,09	46,5
	1 700	25	53 500	31,10	67,80	96,40	3,60	2,07	1,53	1,08	32,9
	2 700	48	72 000	27,40	55,20	96,50	3,50	3,74	1,75	1,05	26,7
	4 850	25	82 000	17,40	69,60	94,60	5,40	5,82	1,20	0,90	21,8
	9 400	120	161 000	18,10	71,90	94,00	6,00	11,10	1,49	0,95	15,1

Vcp = cell pair voltage
Cf = feed concentration
Cp = product concentration
Cb = brine concentration
CF = concentration factor
CE = current efficiency

WR = water recovery
BV = brine volume
EEC = electrical energy consumption
OP = output
d_eff = thickness of dialysate
Rcp = cell pair resistance

Table 10.2: Concentration/Desalination Results of Ammonia Nitrate Solutions at different cell pair voltages

Vcp	Cf mg/l	Cp mg/l	Cb mg/l	CF	CE %	WR %	BV %	EEC kWh/m³	OP m³/m².d	d_eff mm	Rcp ohm-cm²
0.59	580	240	58 000	100,00	29,70	99,30	0,70	0,23	1,58	0,97	25,6
	1 010	230	80 000	79,60	43,50	98,90	1,10	0,35	1,26	0,97	24,6
1.18	435	50	49 000	112,60	28 70	99,30	0,70	0,54	1,58	0,67	68,2
	1 100	55	87 500	79,60	51,80	98,80	1,20	0,80	1,39	0,84	38,6
	1 800	90	82 500	45,80	45,80	98,30	1,70	1,50	1,39	0,80	38,2
	3 100	125	117 630	30,70	48,20	98,00	2,00	2,45	1,38	0,75	20,2
	4 950	190	100 000	20,20	47,20	97,20	2,80	4,09	1,37	0,79	14,5
	9 100	320	146 000	16,00	49,40	95,30	4,70	7,37	1,21	0,85	14,7
1.76	420	42	64 500	153,50	22,40	99,00	1,00	1,00	1,58	0,85	45,3
	1 300	60	78 000	60,00	36,30	98,70	1,30	2,05	1,57	1,14	35,6
	1 800	35	120 000	66,70	41,70	98,50	1,50	2,54	1,39	0,87	28,8
	2 800	35	150 000	53,60	47,20	98,10	1,90	3,55	1,24	1,02	19,0
	4 525	45	136 500	30,20	47,20	97,30	2,70	6,78	1,24	1,06	12,8
	9 800	70	130 000	13,30	46,50	94,70	5,30	13,09	1,20	0,87	11,2

Table 10.3: Concentration/Desalination Results of Sodium Sulphate Solutions at different cell pair voltages.

Vcp	Cf mg/ℓ	Cp mg/ℓ	Cb mg/ℓ	CF	CE %	WR %	BV %	EEC kWh/m³	OP m³/m².d	d_eff mm	Rcp ohm·cm²
0.59	1 110	165	78 500	70,70	79,30	98,90	1,10	0,27	1,40	0,84	65,6
1.18	1 100	50	81 000	73,60	71,90	98,70	1,30	0,66	1,57	0,99	57,2
	2 100	70	120 000	57,10	71,70	98,50	1,50	1,28	1,39	0,99	47,7
	3 400	95	132 000	38,80	76,20	98,10	1,90	1,97	1,25	0,75	37,2
	5 350	445	133 000	24,80	62,30	97,50	2,50	3,59	1,24	1,02	32,3
	9 700	1 500	156 000	16,08	63,20	96,50	3,50	6,01	1,23	0,89	28,6
1.76	1 050	30	89 000	84,80	52,70	98,30	1,70	1,31	1,56	1,11	59,0
	1 900	35	123 000	64,60	63,40	98,50	1,50	1,99	1,39	1,25	42,8
	3 000	77	136 000	45,50	76,20	98,20	1,80	3,20	1,25	1,14	45,6
	4 950	65	134 000	27,10	62,30	97,50	2,50	4,75	1,24	1,25	29,9
	9 525	180	163 000	17,11	63,20	96,10	3,90	13,85	1,23	1,17	23,2

Table 10.4: Concentration/Desalination Results of Sodium Nitrate Solutions at different cell pair voltages

Vcp	Cf mg/ℓ	Cp mg/ℓ	Cb mg/ℓ	CF	CE %	WR %	BV %	EEC kWh/m³	OP m³/m².d	deff mm	Rcp ohm·cm²
0,59	1 100	465	65 000	59,30	41,50	98,90	1,10	0,28	1,57	1,01	28,8
1.18	1 000	90	63 500	63,3	47,0	98,6	1,40	0,73	1,57	0,99	32,1
	1 950	100	71 000	36,5	65,0,	98,4	1,60	1,07	1,39	1,01	30,4
	2 800	100	82 000	29,3	63,2	98,1	1,90	1,61	1,38	0,83	29,7
	5 000	140	102 000	20,5	56,67	97,3	2,70	3,29	1,24	0,86	19,3
	10 100	530	123 000	12,2	53,1	96,0	4,00	6,98	1,22	1,02	10,2
1.76	1 000	70	60 500	60,30	40,70	98,50	1,50	1,30	1,57	1,16	33,6
	2 100	60	69 500	33,10	51,30	98,20	1,80	2,25	1,39	1,12	28,3
	2 800	50	81 000	29,00	53,80	98,00	2,00	2,90	1,38	1,06	25,3
	5 200	90	117 000	22,50	55,00	97,10	3,90	5,34	1,23	1,27	17,0
	9 800	150	125 000	12,80	51,80	95,60	4,40	10,85	1,21	1,27	10,7

Table 10.5: Concentration/Desalination Results of Calcium Chloride Solutions at different cell pair voltages.

Vcp	Cf mg/l	Cp mg/l	Cb mg/l	CF	CE %	WR %	DV %	EEC kWh/m³	OP m³/m².d	deff mm	Rcp ohm·cm²
0,59	1 100	310	42 000	38,20	47,80	98,70	1,30	0,48	1,57	0,93	40,3
1.18	970	50	41 200	42,50	45,70	98,50	1,50	1,17	1,56	1,05	36,4
	2 100	110	51 000	24,30	49,70	97,80	2,20	2,34	1,38	1,15	27,5
	2 950	160	57 000	19,30	46,30	97,20	2,80	3,53	1,37	1,19	19,9
	5 000	230	75 000	14,00	45,70	95,80	4,20	6,21	1,22	1,19	15,4
	10 300	940	75 000	7,30	44,30	92,70	7,30	13,06	1,18	1,12	9,6
1.76	840	20	38 500	45,80	36,50	98,50	1,50	1,94	1,56	1,18	34,7
	2 000	35	45 500	22,80	48,10	97,80	2,20	3,57	1,38	1,32	28,2
	3 000	85	54 500	18,20	43,40	97,00	3,00	5,91	1,37	1,37	22,9
	5 050	65	73 000	14,50	43,20	95,60	4,40	10,31	1,22	1,31	14,0

Cf985mg/l;Cb37000mg/l   Cf1700mg/l;Cb53000mg/l   Cb2700mg/l;Cb74000mg/l

Cf4850mg/l;Cb84500mg/l   Cf9400mg/l;Cb170000mg/l
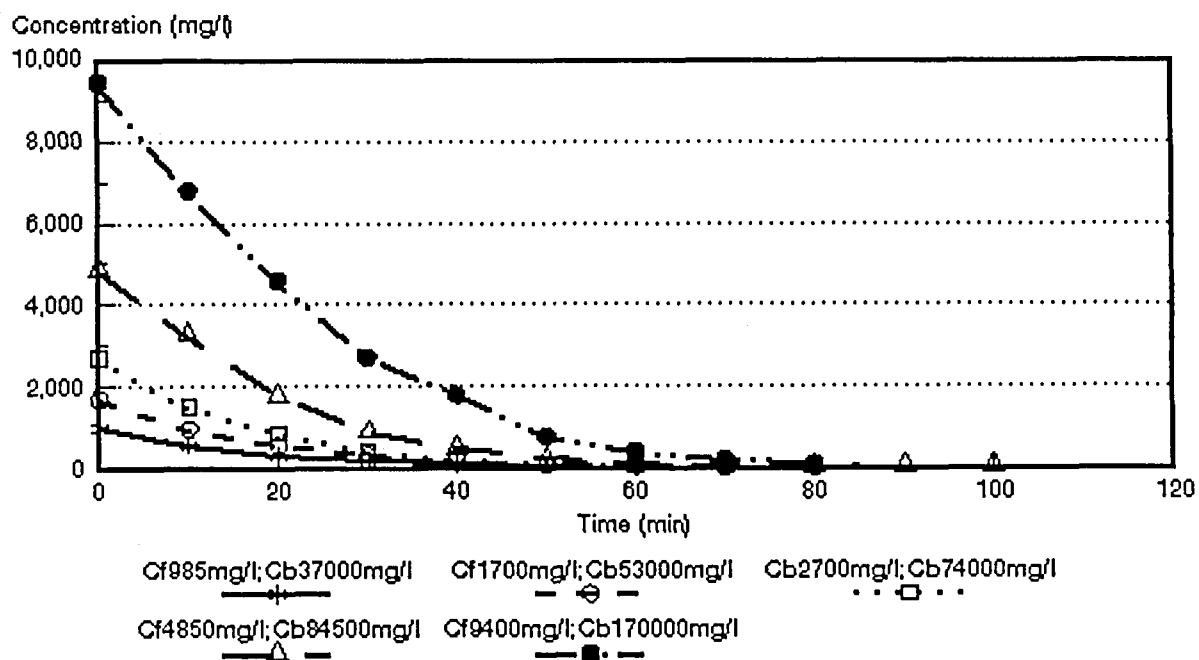
Figure 10.1: Concentration/desalination of different sodium chloride feed concentrations at 1,76 V/cp.
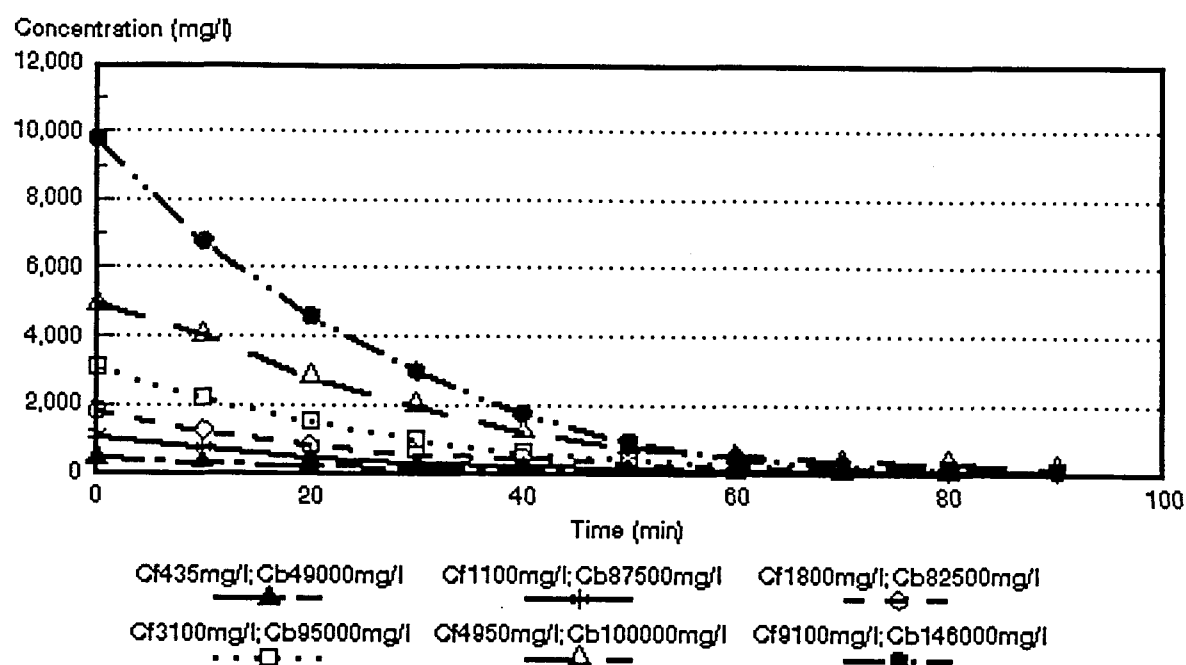
Figure 10.2: Desalination/concentration of different ammonium nitrate feed concentrations at 1,18 V/cp.
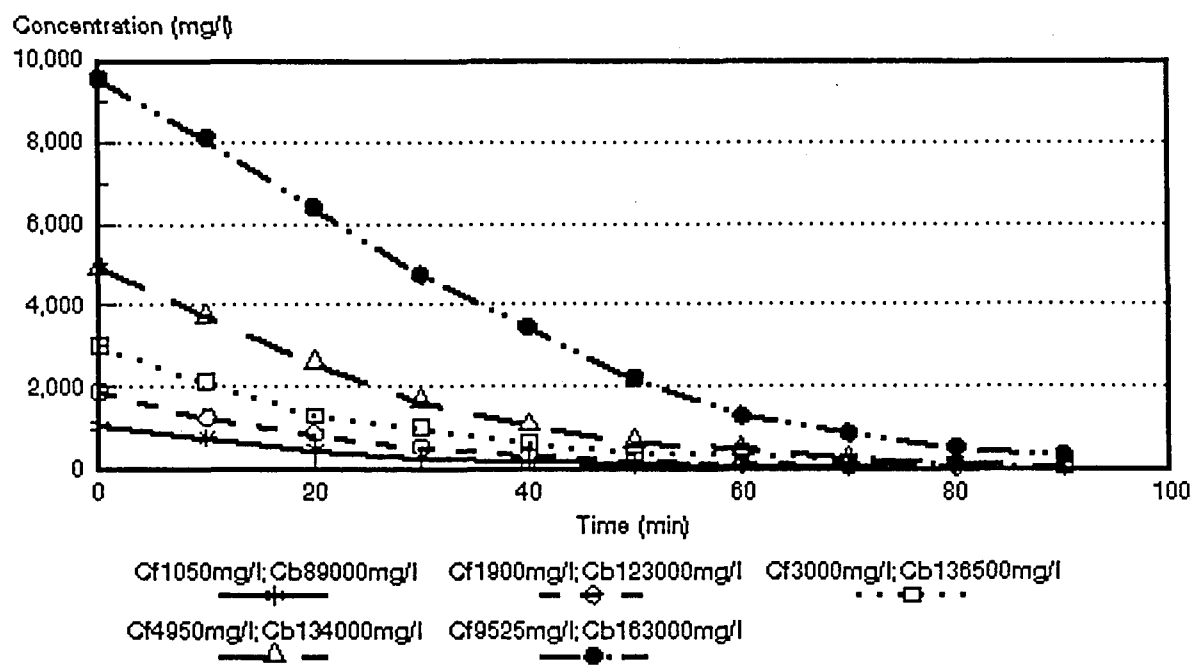
Figure 10.3: Desalination/concentration of different sodium sulphate feed concentrations at 1,76 V/cp.
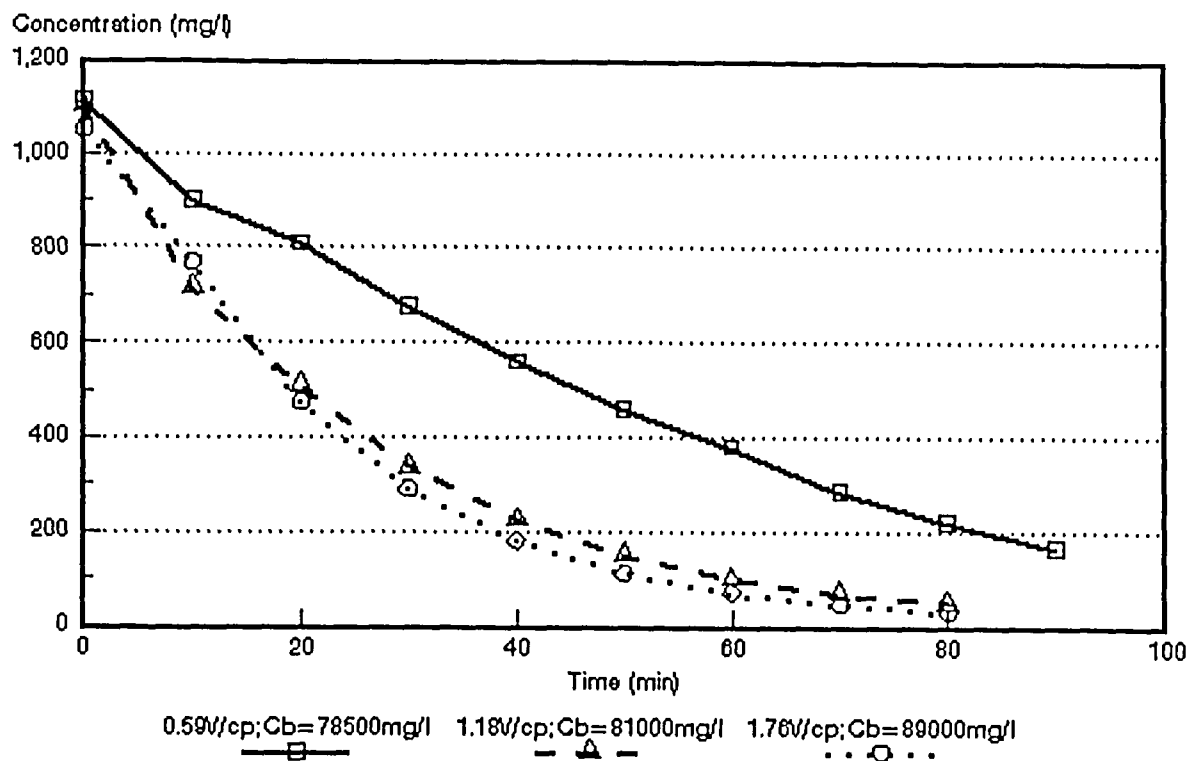
Concentration (mg/l)

0.59V/cp;Cb=78500mg/l   1.18V/cp;Cb=81000mg/l   1.76V/cp;Cb=89000mg/l

Figure 10.4: Desalination/concentration of sodium sulphate solutions at different cell pair voltages.

Brine concentration (mg/l)

Feed concentration (mg/l)

0.59 V/cp   1.18 V/cp   1.76 V/cp
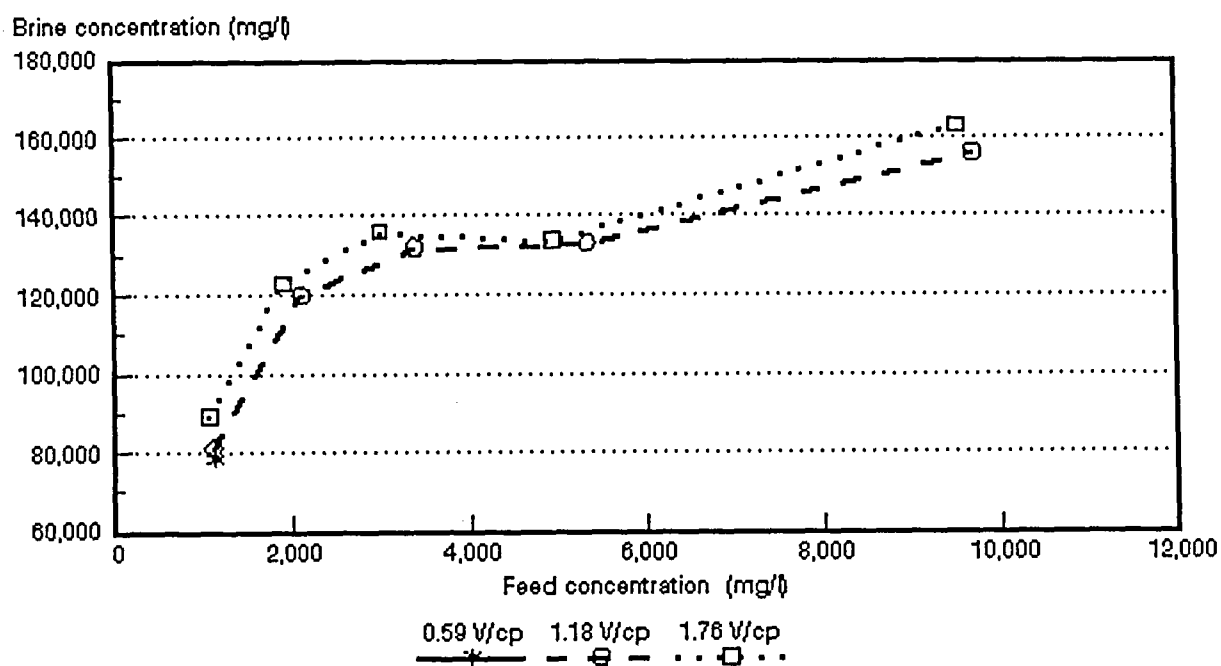
Figure 10.5: Brine concentration as a function of sodium sulphate feed concentration and cell pair voltage.

which would make the SCED technique suitable for concentration/desalination of industrial effluents. It is interesting to note that relatively low brine concentrations have been obtained with calcium chloride solutions (Table 10.5) in comparison with the other ions. However, the low current efficiency obtained with calcium chloride solutions explained the low brine concentrations that were obtained.

Concentration factors (brine/feed) decreased with increasing feed concentration (Tables 10.1 to 10.5). Therefore, there is a limit to the brine concentration that can be achieved. The brine concentration that can be obtained depends *inter alia* on the permselectivity of the ion-exchange membranes, feed concentration and current density used[6, 115]. Ion-exchange membranes tend to loose their permselectivity at high concentration due to backdiffusion of salt with the result that there is a limit to the brine concentration that can be achieved.

10.1.2 Current efficiency

Current efficiency increased with increasing feed concentration and decreasing cell pair voltage (Tables 10.1 to 10.5 and Figure 10.6). Current efficiency, however, decreased slightly at higher feed concentrations due to the lower permselectivity of the ion-exchange membranes at high feed concentration. Increasing current efficiency with increasing feed concentration may be ascribed to a higher flow of electro-osmotic water through the membranes at increasing feed concentration.

Current efficiencies of 55 to 74%; 30 to 52%; 53 to 79%; 42 to 65% and 37 to 50% were obtained with sodium chloride, ammonium nitrate, sodium sulphate, sodium nitrate and calcium chloride solutions, respectively, in the concentration and cell pair voltage ranges studied. Relatively low current efficiencies were obtained with ammonium nitrate and calcium chloride solutions. This shows that the ion-exchange membranes used do not have a very high permselectivity for ammonium nitrate and calcium chloride solutions.

10.1.3 Water recovery and brine volume

High water recovery and low brine volume were obtained at low to moderately high feed (1 000 to 3 000 mg/ℓ) concentrations (Tables 10.1 to 10.5). Brine volumes between 3 and 4%; 1 and 2%; 1 and 2%; 1 and 2% and 1 and 3% were obtained with sodium chloride, ammonium nitrate, sodium sulphate, sodium nitrate and calcium

chloride solutions, respectively. Higher brine volumes (3 to 7%), however, were obtained at higher feed concentrations (5 000 to 10 000 mg/ℓ). Therefore, very low brine volumes could be obtained with SCED. This low brine volume that is produced with SCED can reduce brine disposal cost significantly especially where brine is to be trucked away for disposal.

Excellent water recoveries were obtained. Water recoveries of approximately 96% were obtained in the feed concentration range of 1 000 to 3 000 mg/ℓ and of approximately 94% in the feed concentration range from 5 000 to 10 000 mg/ℓ. These high water recoveries and low brine volumes are significantly better than water recoveries of approximately 80% which is normally obtained with conventional electrodialysis.

10.1.4 Electrical energy consumption

Electrical energy consumption increased with increasing feed concentration and cell pair voltage (Figure 10.7 and Tables 10.1 to 10.5). Very low electrical energy consumptions (0,27 to 0,48 kWh/m^3 product water) were obtained at a cell pair voltage of 0,59 in the 1 000 mg/ℓ feed concentration range. Electrical energy consumptions of 0,66 to 5,91 kWh/m^3 were obtained in the feed concentration range of 1 000 to 3 000 mg/ℓ (1,18 to 1,76 V/cp range). Higher electrical energy consumption (3,29 to 13,06 kWh/m^3) was encountered in the feed concentration range from 5 000 to 10 000 mg/ℓ.

Electrical energy consumption was determined for ion transport only. The voltage drop across the electrode compartments was not taken into consideration because it is usually insignificant in a large membrane stack containing many membrane pairs (300 membrane pairs or more)[7]. The electrical energy consumption obtained during SCED usage would give a good indication of the operational cost that could be expected with SCED applications.

10.1.5 Product water yield

Product water yield (output) increased with increasing cell pair voltage and decreased with increasing feed concentration (Tables 10.1 to 10.5). Product water yield is a very important engineering design parameter because the membrane area required for a certain flow rate can be calculated from this figure.

Current efficiency (%)
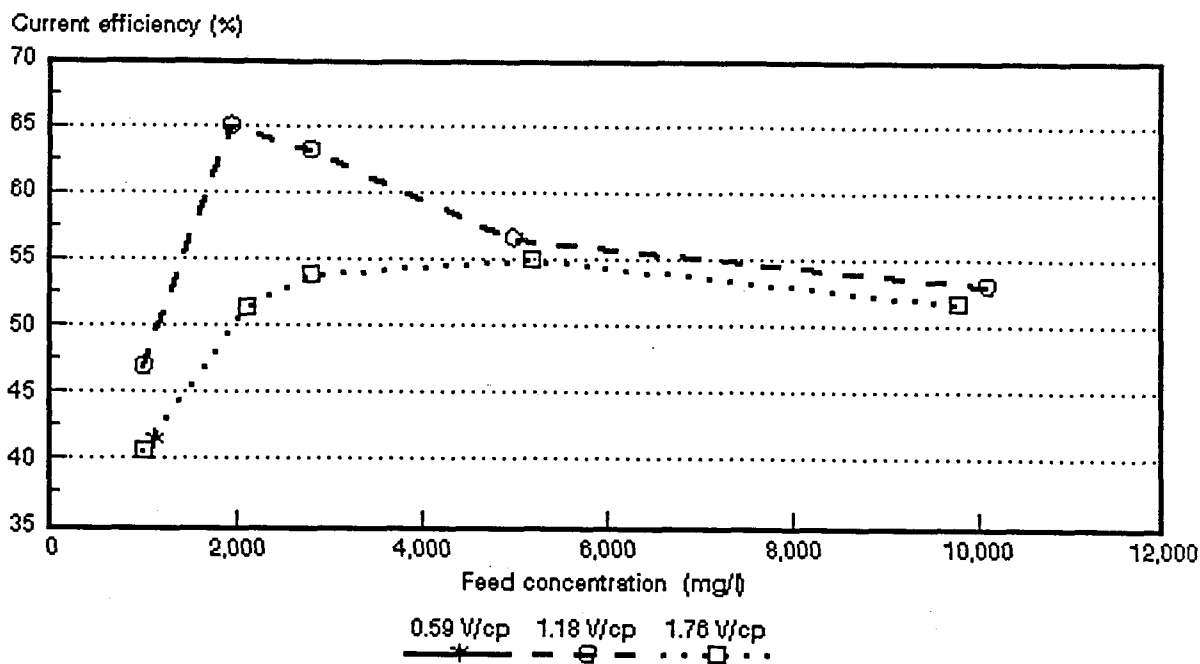

Figure 10.6:   Current efficiency as a function of sodium nitrate feed concentration and cell pair voltage.

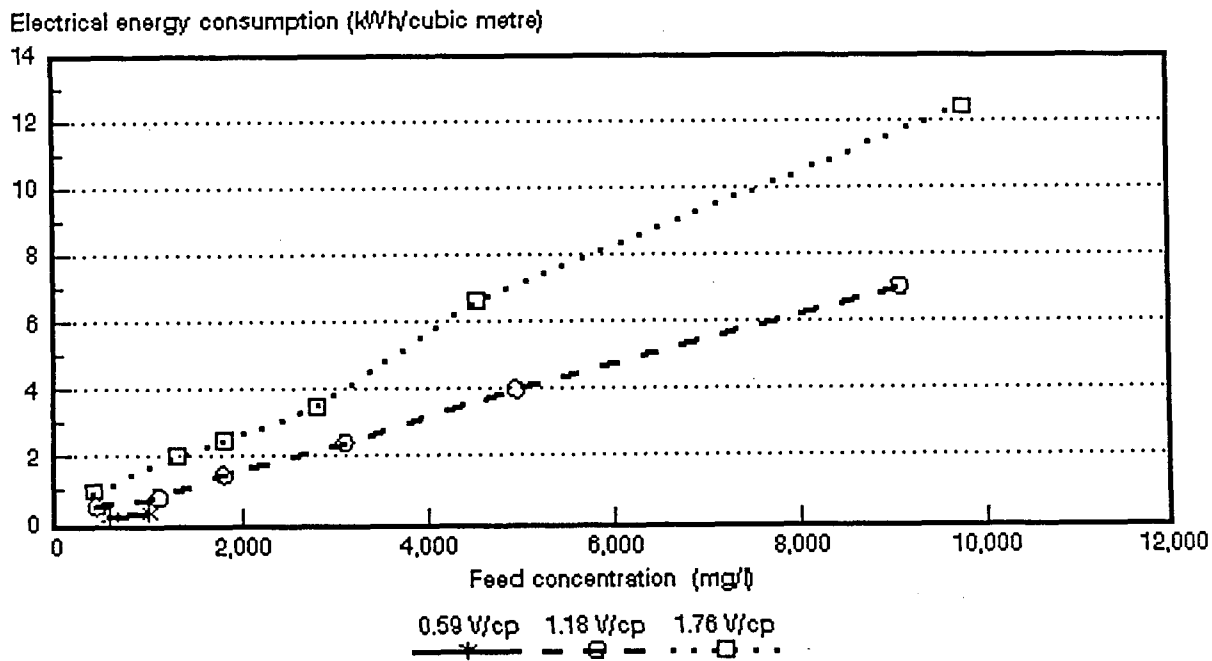Electrical energy consumption (kWh/cubic metre)

Figure 10.7:   Electrical energy consumption as a function of ammonium nitrate feed concentration and cell pair voltage.

10.1.6 Cell pair resistance (R_{cp}) and effective thickness (d_{eff}) of the dialysate compartment

Cell pair resistance as a function of the specific resistance of the dialysate for sodium sulphate solutions at different cell pair voltages is shown in Figure 10.8. Similar graphs were obtained for the other salt solutions. The lines consist of a linear region followed by a curved region[116]. The line starts to curve when the specific resistance of the dialysate becomes very high. Linear regression through the linear region of the lines gives d_{eff} (slope) and the cell pair resistance (R_{cp}) (y-intercept). The lines show that polarization and hence effective thickness of the dialysate compartment depends on cell pair voltage. The effective thickness of the dialysate compartment increased from 0,84 (at 0,59 V/cp), 0,99 mm (at 1,18 V/cp) to 1,11 mm (at 1,76 V/cp). Membrane resistance (R_{cp}) for the sum of the anion- and cation-exchange membranes was determined at 65,6 - (0,59 V/cp), 57,2 - (1,18 V/cp) and 59,0 ohm·cm² (at 1,76 V/cp). It was further found that R_{cp} decreased with increasing feed concentration (Tables 10.1 to 10.5). The cell pair resistance at 1,18 V/cp and an initial ammonium nitrate feed concentration of 9 100 mg/ℓ was determined at only 14,7 ohm·cm² (Table 10.2).

The model $R_{cp} = R_m + \rho d_{eff}$ is applicable not only to sodium chloride solutions but also to ammonium nitrate, sodium sulphate, sodium nitrate and calcium chloride solutions. However, care must be taken to use the linear portion of the curve (R_{cp} vs specific resistance) in the determination of R_{cp} and d_{eff}. This is also a method that can be used for the determination of cell pair resistance. Cell pair resistance, however, depends on the initial feed concentration. Therefore, feed concentration must be specified when cell pair resistance is given.

10.2 Concentration/Desalination of Industrial Effluents

10.2.1 Treatment of runoff from a fertilizer factory terrain with SCED

Runoff from an ammonium nitrate fertilizer factory terrain is presently stored in evaporation ponds. This runoff contains, amongst other ions, ammonium, nitrate and phosphate ions which have the potential to pollute the environment. Water and chemicals can also be recovered from the effluent for reuse. Sealed-cell ED was therefore investigated for treatment of this effluent[116].

The concentration/desalination results of the relatively dilute runoff are shown in Table 10.6.

Cell pair resistance (ohm.sq cm)
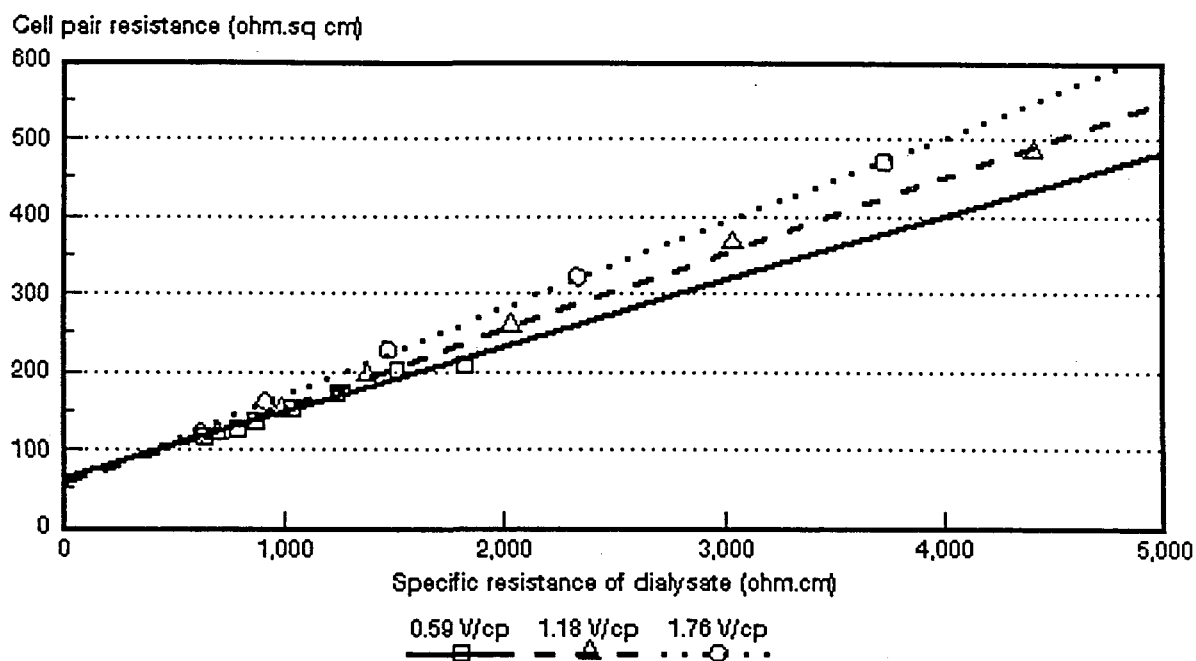
Figure 10.8: Cell pair resistance as a function of specific resistance of dialysate at different cell pair voltages for approximately 1 000 mg/ℓ Na_2SO_4 feed solutions.

Table 10.6: Concentration/desalination results of fertilizer run-off at different cell pair voltages

V_{cp}	C_f mS/m	C_p mS/m	C_b mS/m	% Conductivity Removal	CE %	WR %	BV %	EEC kWh/m³	OP m³/m²·d
1,18	545	29,8	10 724	94,5	56,9	97,2	2,8	2,7	1,03
0,88	556	48,9	10 312	91,2	63,3	97,2	2,8	2,0	0,77
0,59	520	53,3	8 830	89,7	-	96,9	3,1	1,24	0,54

Excellent salinity removals were obtained at the three cell pair voltages investigated. Salinity removal of 94,5% was obtained at a cell pair voltage of 1,18. Salinity removal decreased to only 89,7% at 0,59 V/cp.

Feed water conductivity was reduced from 545 mS/m to 29,8 mS/m at an electrical energy consumption of 2,7 kWh/m³ (1,18 V/cp). Brine volume comprised only 2,8% of the initial feed volume. Effluent volume could therefore be reduced significantly.

The chemical composition of feed, product and brine is shown in Table 10.7.

Table 10.7: **Chemical composition of feed, product and brine**

Constituent	Feed mg/ℓ	Product mg/ℓ	Brine mg/ℓ	% Removal
Sodium	111	25	3 758	77,50
Potassium	34	5	1 035	85,30
Calcium	93	24	3 404	74,20
Magnesium	64	8	2 121	87,50
Ammonium	621	30	16 638	95,20
Nitrate	1 936	73	63 783	96,30
Silica	7,70	4,60	54,40	40,30
Sulphate	299	48	8 469	83,90
Ortho-phosphate (P)	73,80	20,80	1 143	71,80
Chloride	187	14	5 371	92,50
Alkalinity (CaCO$_3$)	22	3	24	86,40
COD	219	19	587	91,30
Manganese	0,409	<0,025	18,90	42,90
Iron	<0,025	<0,025	0,91	
Fluoride	1,66	0,35	3,70	78,90
TDS (calculated)	3 602	296	108 114	91,80
pH	5,7	4,3	4,4	

TDS was reduced from 3 602 mg/ℓ to 296 mg/ℓ (1,18 V/cp) with ease. Therefore, a very good quality product water could be produced which might be reused at the factory. Very good ammonium (95,2%) and nitrate (96,3%) removals were obtained. Ammonium and nitrate were reduced from 621 and 1 936 mg/ℓ in the feed to 30 and 73 mg/ℓ in the product, respectively.

The brine had a TDS of 10,8%. Brine volume comprised only about 3% of the initial feed volume. Therefore, brine volume could be reduced significantly which means that smaller evaporation ponds would be required, or that the present ponds could last much longer. Ammonium and nitrate values may also be recovered from the brine for reuse. Potential pollution problems will therefore be reduced significantly.

The ion-exchange membranes used in the SCED unit performed well for treatment of the fertilizer runoff. However, membrane fouling or scaling in the long term may affect the process adversely. Therefore, membrane fouling and cleaning studies over an extended time period will be necessary to determine the effectiveness of SCED for this application.

10.2.2 Treatment of a concentrated Ammonium Nitrate Type effluent with SCED

The treatment of a more concentrated ammonium nitrate type effluent from a fertilizer manufacturing plant was also investigated with SCED. The pH of the effluent was approximately 11 and the effluent was neutralized with sulphuric acid prior to SCED treatment[116]. Concentration/desalination of the ammonium sulphate effluent was conducted in stages because of the high concentration of the effluent (13 230 mS/m or 123 700 mg/ℓ TDS). The product water after the first desalination stage was used as feed for the next concentration/desalination stage. The concentration/desalination results are shown in Table 10.8.

Table 10.8:   Concentration/desalination results of ammonium sulphate effluent

Vcp	Cf mS/m	Cp mS/m	Cb mS/m	% Conductivity Removal	CE %	WR %	BV %	EEC kWh/m³	OP m³/m²·d
0,53	13 230	8 452	26 313	36,1	43,1	84,7	15,3	23,3	0,448
0,53	8 751	2 437	18 952	72,2	-	78,8	21,2	28,9	0,318
1,18	2 424	6,2	17 416	99,8	46,9	91,6	8,4	17,9	0,282

Feed (13 230 mS/m) was first desalinated to 8 452 mS/m. Desalination rate was low due to the low cell pair voltage (0,53 V/cp) that could be applied as a result of excessive current that was drawn by the high conductivity of the feed solution[116]. It was only at the third desalination stage that a higher cell pair voltage could be applied.

The chemical composition of the feed, product and brine after the third desalination/concentration stage is shown in Table 10.9.

Table 10.9: Chemical composition of feed, product and brine (3rd stage desalination)

Constituent	Feed mg/ℓ	Product mg/ℓ	Brine mg/ℓ	% Removal
Sodium	268	12	2 787	95,52
Potassium	3	1	17	66,67
Calcium	7	1	60	85,71
Magnesium	1	4	13	
Kjeldahl-N	3 340	17	38 199	99,49
Ammonium	4 179	10	48 214	99,76
Nitrate	2 215	17	25 473	99,23
Silica	9,50	3,90	40,10	58,95
Sulphate	9 762	10	113 184	99,90
Total phosphate (P)	3,20	0,20	28,20	93,75
Chloride	103	28	1 167	72,82
COD	41	19	163	53,66
TDS (Calculated)	16 557	88	191 208	99,47
pH	3,6	4,9	2,9	

Very good ion removals were obtained. TDS was reduced from 16 557 mg/ℓ to 88 mg/ℓ, a 99,5% removal. Ammonium and nitrate removals were both approximately 99%. Brine with a TDS of 19,1% was obtained. Brine volume comprised 8,4% of the initial feed volume. Electrical energy consumption was determined at 17,9 kWh/m³ in this case. This energy consumption is high. However, an excellent quality product water was obtained which could be reused. This demonstrates that SCED may be effective for the treatment of relatively high TDS waters although the electrical energy consumption is high.

10.2.3 Treatment of an effluent saturated with Calcium Sulphate with SCED

Hydrochloric acid is used for extraction of calcium from activated carbon which is used for gold extraction by a gold recovery company. At times the effluent contains high concentrations of calcium (3 800 mg/ℓ), chloride (7 000 mg/ℓ) and sulphate (600 mg/ℓ). Sealed-cell ED was attempted for treatment of this high concentration calcium

sulphate effluent (TDS 23 000 mg/ℓ) for chloride recovery[116]. However, a white precipitate of calcium sulphate formed in the membrane bags shortly after the experiment was started. Therefore, calcium sulphate should be reduced to low levels to prevent calcium sulphate scaling during SCED treatment. This was done by treating another effluent sample (TDS 4 500 mg/ℓ) with barium carbonate. Sulphate was reduced from 339 mg/ℓ to 5 mg/ℓ.

The concentration/desalination results are summarized in Table 10.10.

Table 10.10: Concentration/desalination results of calcium chloride effluent

V_{cp}	C_f mS/m	C_p mS/m	C_b mS/m	% Conductivity Removal	CE %	WR %	BV %	EEC kWh/m³
1,18	1 182	362	13 548	69,4	32,5	97,0	3	6,4
1,18	383	51	9 609	86,7	28,8	97,7	2,3	3,1

Concentration/desalination was conducted in two stages. Conductivity was first reduced from 1 182 mS/m to 362 mS/m and then from 362 mS/m to 51 mS/m. Very low current efficiencies were obtained for the first (32,5%) and second (28,8%) desalination stages. Brine volume comprised approximately 3% (1st stage) and 2,3% (2nd stage) of the feed water volume and electrical energy consumption was determined at 6,4 and 3,1 kWh/m³ for the first and second desalination stages, respectively.

The chemical composition of the feed, product and brine for the second desalination stage is shown in Table 10.11.

Table 10.11: Chemical composition of feed, product and brine (2nd stage desalination)

Constituent	Feed mg/ℓ	Product mg/ℓ	Brine mg/ℓ	% Removal
pH	8,1	8,1	6,7	
Conductivity (mS/m)	383	51	9 609	86,7
Sodium	191	77	4 862	59,7
Potassium	9	3	162	66,7
Calcium	278	10	17 045	96,4
Magnesium	5	4	7	20,0
Ammonium	27	7	447	274,1
Nitrate	4	2	241	50,0
Sulphate	3	4	3	-
Chloride	783	113	46 412	85,6
Alkalinity (CaCO₃)	139	65	338	53,2
TDS (calculated)	1 469	299	102 180	79,6

A very good quality product water was obtained after the second desalination stage. TDS was reduced from 1 469 mg/ℓ to 299 mg/ℓ at an electrical energy consumption of 3,1 kWh/m³.

Chloride was effectively concentrated. The chloride concentration in the brine was 4,6%. This chloride may be converted into hydrochloric acid in an electrochemical cell. The recovered hydrochloric acid can then be used for removal of calcium from the spent activated carbon. This matter, however, warrants further investigation.

The high calcium concentration in the brine may cause scaling problems. However, no sign of scaling was detected during the laboratory tests. Membrane fouling and cleaning tests, however, should be conducted over an extended period of time to determine the practical feasibility of the process.

11.   GENERAL DISCUSSION

11.1   Requirements for ED Membranes

The customary requirements for ED membranes are:

a)   low electrical resistance[6] (< 20 ohm·cm^2);

b)   high permselectivity[6] ($> 0,9$);

c)   low electro-osmotic coefficient[7] (< 12 mol H_2O/Faraday);

d)   good chemical and dimensional stability[114];   and

e)   satisfactory polarization characteristics[7].

These requirements are also necessary for ED membranes for use in EOP. However, an additional requirement for EOP-ED is finite transport of water through the membranes. It has been shown that increasing flow of water through the membranes causes an increase in current efficiency.

It was shown by Narebska and Koter[18] that ion-water coupling became higher in more concentrated solutions (approximately 0,5 mol/ℓ). At higher concentrations ($> 0,5$ mol/ℓ), the amount of free water in the membrane, the water transport number and the osmotic flow decrease. Effects originating from the deswelling of the membrane at high external concentration, may result in the observed decrease of the electro-osmotic flow and the increased coupling between ions and the amount of water, crossing the membrane[18].

It has been found by Narebska et al.[31] that the resistance against flowing anions in a cation membrane is imposed by water;   the lower the amount of water in the membrane, the higher the resistance. Consequently, increased ion-water coupling causes increased resistance to the penetration of co-ions into the membrane matrix. The result is an increase in current efficiency. It is therefore not necessary for ED membranes for use in EOP to have very high permselectivities, because permselectivity will be increased with increasing flow of water through the membranes. This was especially observed for the more porous heterogeneous membranes at high feed concentration (1 mol/ℓ). Consequently, membranes with a relatively low permselectivity (approximately 0,6)   should be suitable for concentration of salt solutions with EOP-ED.

11.2   Permselectivity with Acids and Bases

An increasing amount of water flowed through the membranes with an increase in feed water concentration during EOP of salt solutions. However, a decrease in water flow was experienced with an increase in feed concentration during EOP of acid solutions. The anion membranes used for acid EOP had a very low permselectivity for chloride ions due to the very high mobility of the protons in the membrane[11]. Consequently, the protons which flowed in the opposite direction to the flow of water would inhibit water flow through the membranes. Therefore, very little water will pass through the anion membrane in the case of acid EOP.

The cation membranes used for acid EOP, on the other hand, had a very high permselectivity for protons (> 0,9). Back diffusion should be very low in this case because back diffusion would be inhibited by the opposite flow of protons[19]. Osmotic flow, however, can be high through the cation membrane[19].

The cation membranes had a lower current efficiency than the anion membranes during EOP of caustic soda solutions. This is due to the high mobility of the hydroxyl ion[30]. It was shown by Koter and Narebska[32] that hydroxide ions impeded cations, particularly at high external concentration, much more than chloride ions. This can be attributed to the higher partial friction between sodium and hydroxyl ions.

The resistance imposed by a membrane matrix on the permeating hydroxyl ions is much lower than that for chloride ions according to Narebska et al.[30]. Three factors contributing to this effect, viz: the friction imposed by the cation (f_{21}), water (f_{2w}); and the polymer matrix (f_{2m}) - influence the flow of hydroxyl and chloride ions to different degrees. Chloride ions are hindered mainly by water, especially at increasing sorption. The flow of hydroxyl ions in diluted solution is hindered by the matrix and at high concentration by the cation and then by water[30].

11.3   Brine Concentration, Electro-Osmotic and Osmotic Flows

Brine concentration increases with increasing feed water concentration and current density. This happens because the membranes become increasingly dewatered at high current density. Consequently, the electro-osmotic coefficient decreases.

The osmotic flow relative to the total flow through the membranes decreased with

increasing current density. Consequently, the relative amount of electro-osmotic flow through the membranes, increased as a function of current density. Osmotic flow, however, appears to contribute significantly to the total flow in EOP. The osmotic flow through the *Ionac* membranes at a current density of 20 mA/cm² (0,1 mol/ℓ feed) comprised 33,9% of the total flow through the membranes. Osmotic flow was reduced to 19,0% of the total flow at a current density of 50 mA/cm² (0,1 mol/ℓ feed). Osmotic flow through the *Selemion* AAV and CHV membranes contributed 64,1% to the total flow at a current density of 20 mA/cm² (0,1 mol/ℓ feed). Osmotic flow decreased to 20,9% at a current density of 100 mA/cm² (0,1 mol/ℓ feed). Osmotic flow through the *Selemion* AMP and CMV membranes contributed 61,4% to the total flow through the membranes at a current density of 20 mA/cm² (0,1 mol/ℓ feed). Osmotic contribution decreased to 25,7% at a current density of 100 mA/cm² (0,1 mol/ℓ).

Approximately 7 mol H₂O/Faraday permeated through the *Selemion* AAV and CHV membranes in the feed concentration range from 0,5 to 1,0 mol/ℓ. It is known that little water (< 1 mol/Faraday) can permeate acid blocking anion membranes[48]. Therefore, the water could have entered the membranes only through the cation membrane.

Osmotic flow increased with increasing feed water concentration. It was also observed that the osmotic flow decreased in some cases at the highest feed concentrations. This can be ascribed to stronger back diffusion at the highest feed water concentrations. It was also interesting to note that a decrease in osmotic flow had taken place with increasing feed water concentration in the case of the more hydrophobic *Ionac* and WTPS membranes. The osmotic flow also increased through the Israeli ABM and *Selemion* membranes with increasing feed concentration and higher current efficiencies were experienced.

11.4 Discrepancy between Transport Numbers Derived from Potential Measurements and Current Efficiency Actually Obtained

The correct relationships to be used when measuring membrane potential for the prediction of desalting in ED, are as follows:

$$[J/I]_{\Delta\mu_s;\ J_v\ =\ 0}\ =\ \Delta t/F$$

(see eqs. 3.2.23 and 3.2.24)

$$=-[\Delta\Psi/\Delta\mu_s]_{I\ =\ 0;\ J_v\ =\ 0}$$

The correct Onsager relationship for potential measured is at zero current and at zero volume flow, and for the transport number, at zero concentration gradient and zero volume flow[117]. In practical ED, measurements are conducted at zero pressure and in presence of concentration gradients and volume flows. These factors will influence the results considerably in all systems in which volume flow is important and where the concentration factor is high as is encountered in EOP. In the measurement of membrane potential, the volume flow is against the concentration potential and in general will decrease the potential. In ED water flow helps to increase current efficiency, but the concentration gradient acts against current efficiency.

In the case of sodium chloride solutions, the apparent transport number of the membrane pair $(\overline{\Delta t})$ was higher than current efficiency (e_p) at low feed water concentrations (approximately 0,05 mol/ℓ). This was predicted with the following relationship:

$$\eta\ <\ \frac{\Delta\Psi_m^c\ +\ |\ \Delta\Psi_m^a\ |}{|\ 2\Delta\Psi_I\ |}$$

(see eq. 3.11.12)

Equation (3.11.12) is valid if the influence of volume flow is negligible.

The apparent transport number $(\overline{\Delta t})$ decreased with increasing feed water concentration. Current efficiency, however, increased with increasing feed water concentration as a result of increasing water flow. Consequently, current efficiency became higher than the apparent transport number at higher feed water concentrations (0,5 to 1 mol/ℓ). Current efficiency, however, decreased at very high feed concentrations as a result of back diffusion. Similar results were obtained with EOP of caustic soda solutions.

Current efficiency was much lower than $\overline{\Delta t}$ during EOP of acid solutions. This can be ascribed to back diffusion of acid through the membranes during EOP which reduces current efficiency significantly.

Garza and Kedem[2] have found that the apparent transport number of a membrane

379

pair ($\widetilde{\Delta}$t) gave a good lower estimate of the actual Coulomb efficiency of the EOP process in the case of sodium chloride solutions (0,1 mol/ℓ feed) using *Selemion* AMV and CMV and polyethylene based membranes. However, it was found in this study that the apparent transport number of a membrane pair gave a higher estimate of the Coulomb efficiency of the EOP process in the 0,05 to 0,1 mol/ℓ feed concentration range. The apparent transport number of a membrane pair gave a lower estimation of the actual current efficiency in the feed water concentration range from approximately 0,5 to 1,0 mol/ℓ. However, the apparent transport number of a membrane pair gave a much too high estimation of current efficiency of the EOP process for hydrochloric acid concentration. The apparent transport number of the anion membrane, however, gave a much better estimation of current efficiency.

11.5   Current Efficiency and Energy Conversion in ED

The effects which diminish current efficiency in ED are the following[17]:

a)   electric transport of co-ions;

b)   diffusion of solute;

c)   electro-osmotic flow; and

d)   osmotic water flows.

The imperfect selectivity, $\bar{t}_2$, assumed to be one of the most important characteristics of a membrane can produce up to 8% (NaCl) and 35% (NaOH) of the current efficiency losses at $\widetilde{m}$ = $2^{(17)}$. Similar to $\bar{t}_2$, the effect of electro-osmotic flow of water ($\bar{t}_w$) increases with m. It plays a significant role in the system with sodium chloride where it diminishes current efficiency up to 30% according to Koter and Narebska[17]. However, it was found in this study that electro-osmotic flow of water increased current efficiency significantly in the 0,05 to 1,0 mol/ℓ feed concentration range.

Depending on the working conditions, i.e. on the concentration ratio m'/m" and current density, the decrease in current efficiency due to osmotic and diffusion flows can be larger than that caused by electric transport of co-ions and water. This effect is especially seen at the higher mean concentrations where the current efficiency can be reduced to zero[17].

Efficiency of energy conversion in ED consists of the following two terms, viz., η_{IE} (ion-current coupling) and η_{WE} (ion-water coupling) according to Narebska and Koter[18]. The first term expresses the storage of energy in producing a concentration difference

380

in the permeant. The second term corresponds to the transport of water, which acts opposite to the separation of the components. It causes a waste of energy by decreasing the concentration difference. This water flow has a negative effect on energy conversion in ED. However, electro-osmosis can also have a positive effect on ED by increasing current efficiency as has been demonstrated in this study.

11.6 Water Flow, Concentration Gradient and Permselectivity

Salt flux (S^c) through a cation-exchange membrane can be predicted with the following relationship:

$$S^c = \frac{J_1^c + J_2^c}{2} = c_s(1 - \sigma)J_v^c + \bar{P}\Delta C + \frac{\Delta t^c}{2} I/F \qquad \text{(see eq. 3.11.1)}$$

Salt flux (both cation and anion) through ion-exchange membranes depends on water flow (J_v) through the membranes, concentration gradient (ΔC) across the membrane and membrane permselectivity ($\overline{\Delta t}$). It was shown that increasing water flow through the membranes increased current efficiency. It was also shown that an increasing concentration gradient (ΔC) across the membranes decreased current efficiency. Current efficiency or salt flux was also low when the permselectivity of the membranes was low. The experimental data for salt, acid and base EOP can therefore be satisfactorily described by eq. (3.11.1).

Back diffusion through ion-exchange membranes in presence (at zero pressure) and absence of water flow can be predicted with the following relationship according to Kedem[15]:

$$\left[\frac{J_s}{X_s/C_s} \Big/ \frac{J_1 - J_2}{X_1} \right]_{\Delta p\, =\, 0} < \left[\frac{J_s}{X_s/C_s} \Big/ \frac{J_1 - J_2}{X_1} \right]_{J_v\, =\, 0} \qquad \text{(see eq. 3.3.45)}$$

Back diffusion of salt through a membrane is less when water flows from the opposite side (l.h.s. of eq. 3.3.45). However, back diffusion of salt is more in the absence of volume flow (r.h.s. of eq. 3.3.45). Therefore, current efficiency will be higher when salt diffusion is lower and this will occur when water flows through the membrane. This was illustrated especially during EOP of sodium chloride solutions.

A decreasing amount of water permeated the membranes during acid EOP with increasing acid feed water concentration. It was also found that back diffusion was

high during acid EOP. Therefore, the right hand side of equation (3.3.45) is applicable to the experimental data that have been observed with EOP of hydrochloric acid solutions.

11.7 Prediction of Brine Concentration

Maximum brine concentration, c_b^{max} was predicted with the following two relationships:

$$c_b^{max} = \frac{1}{2FB} \qquad \text{(see eq. 3.10.28)}$$

and

$$c_b^{max} = c_b(1 + J_{osm}/J_{elosm}) \qquad \text{(see eq. 3.10.31)}$$

Brine concentration (salt, acid or base) at high current density, c_b^{max}, appeared to attain a constant value, independent of current density and dependent on the feed water concentration. Maximum brine concentration was more dependent on feed concentration where the membranes deswelled more with increasing feed water concentration.

Maximum brine concentration could be predicted accurately with equations (3.10.28) and (3.10.31). Therefore, any one of these two methods can be used to predict c_b^{max}.

Brine concentration, c_b, was predicted from the water flow through the membranes and the apparent transport of the membrane pair ($\overline{\Delta t}$) with the following relationship:

$$c_b = \frac{I\overline{\Delta t}}{2FJ} \qquad \text{(see eq. 3.10.17)}$$

Brine concentration could be predicted more accurately in the case of sodium chloride and caustic soda solutions than in the case of hydrochloric acid solutions. This can be explained by back diffusion of acid that has been experienced during EOP of the hydrochloric acid solutions. However, a much better prediction of acid brine concentration should be obtained by using the apparent transport number of the anion membrane (Δt^a) in the above equation.

The permselectivity of the membranes ($\overline{\Delta t}$'s) decreased with increasing feed water concentration. Brine concentration, on the other hand, increased with increasing feed water concentration. Therefore, the ratio $c_{b\,calc}/c_{b\,exp}$ decreased with increasing feed

concentration. The accuracy of prediction of brine concentration will therefore depend on the feed concentration used for the determination of the apparent transport number.

11.8 Membranes for Sodium Chloride, Hydrochloric Acid and Caustic Soda Concentration

The *Selemion* and *Ionac* membranes performed satisfactorily for concentration of sodium chloride solutions. The *Raipore* membranes, however, did not perform well, due to the high water transport that was experienced with this membrane type. Consequently, lower concentrations and efficiencies were obtained. The *Ionics*, WTPS, WTPVC and WTPST membranes all gave good results in terms of brine concentration and current efficiency. However, serious polarization was experienced with the WTPS membranes and ways to improve the polarization characteristics of these membranes should be investigated.

The presently commercially available anion-exchange membranes are not stable for long periods when exposed to high pH values[114]. Consequently, the membranes that were evaluated for caustic soda concentration would have a relatively short life time when treating caustic soda effluents. Nevertheless, satisfactory results were obtained with the *Selemion* and *Ionac* membranes that were used for caustic soda concentration. Membrane life time studies, however, should be conducted to determine the effectiveness of these membranes for caustic soda concentration.

The newly developed Israeli ABM membranes compared favourably with the *Selemion* AAV membrane for acid concentration. The *Selemion* AAV membranes were specially designed for acid concentration. It was shown that the *Selemion* AAV membrane adsorbed a substantial amount of acid[48]. The low dissociation of sorbed acid in the membrane was shown to be a factor which was responsible for the decrease in proton leakage of this anion membrane.

A high degree of ion-coupling will be observed in the case of charged hydrophobic membranes when acid is absorbed by the membrane. It was shown that the flux of chloride ions from the anode to the cathode steadily increased as the amount of sorbed acid was increased[48]. This result showed that chloride ions are associated with the movement of positively charged species. This may be due to the formation of an aggregate form such as $(CH_4OCl)^+$ resulting from the solvation of a proton by a water and an hydrochloric acid molecule[48]. This shows that ion association is taking

place inside the membrane.

11.9   Conventional EOP-ED Stack

It was demonstrated that a conventional ED stack can be used as an EOP-ED stack for concentration of sodium chloride, hydrochloric acid and caustic soda solutions using commercially available ion-exchange membranes. Relatively high brine concentrations and low brine volumes were obtained. Electrical energy consumption was also low at low cell pair voltages.

An advantage of using a conventional ED stack as an EOP-ED stack is that the membranes can be taken out of the stack for cleaning purposes if it should be required. It is not possible to open sealed-cell ED membranes for cleaning. A disadvantage of using a conventional ED stack as an EOP-ED stack is that the membrane utilization factor will be low (approximately 80%). However, it should be possible to improve the membrane utilization factor with improved gasket design and this matter needs further investigation.

11.10   Sealed-Cell Electrodialysis

The sealed-cell ED unit performed satisfactorily for concentration/desalination of salt solutions and industrial effluents. High brine concentrations and low brine volumes were obtained. Low electrical energy consumptions were also obtained at low feed concentrations. Electrical energy consumptions obtained with the conventional EOP-ED stack were comparable to the electrical energy consumptions obtained with the sealed-cell ED stack.

The effective thickness of the dialysate compartment, d_{eff}, was much lower in the case of the sealed-cell ED unit than in the case of the EOP-ED stack. This can be ascribed to the thinner dialysate compartments that have been used in the sealed-cell unit and to the higher linear flow velocities used.

The advantages and disadvantages of SCED are as follows: The capital cost of SCED equipment should be less than that of a conventional plate-and-frame ED stack, because of the simpler construction of the SCED stack. The membrane utilization factor in the membrane bags is approximately 95% compared to approximately 80% for membranes in conventional ED stacks. Higher current densities can be used in

SCED than in conventional sheet flow ED because higher linear flow velocities can be obtained with ease. The higher current densities will result in higher water production rates. Brine volumes produced by SCED are smaller than those obtained with conventional ED. Therefore, the brine disposal problem will be reduced.

More electrical energy per unit of product water produced, will be used in the SCED stack due to the higher current densities used. However, the increased cost for electrical energy should be off-set by a decrease in capital cost. Scale may form more readily in the membrane bags because the SCED stack does not have a built-in self cleaning device such as encountered in the EDR system[8]. It will be difficult to remove scale from the membrane bags once it has formed because the bags cannot be opened for cleaning. Therefore, scale forming chemicals should be removed by ion-exchange or nanofiltration prior to SCED treatment. This will affect the economics of the process adversely, especially if large flows are involved.

Scale-up of a laboratory size SCED unit ($100 \, cm^2/cp$) to a pilot or full-scale plant would be possible. It would be possible to manufacture large-scale membrane bags commercially and the bags would be robust. An advantage of the membranes that were used in the SCED stack was that they could be stored dry. This is usually not the case with ion-exchange membranes normally used in conventional ED. The successful application of SCED technology seems to depend on the need to apply this technology in preference to conventional ED for specific applications where high brine concentrations and small brine volumes are required.

12. SUMMARY AND CONCLUSIONS

Salts, acids and bases frequently occur in industrial effluents. These effluents usually have a large pollution potential. Often the effluents also contain valuable chemicals and water that can be recovered for reuse. Effluent disposal cost can be high, especially where effluents must be trucked away for safe disposal. However, it would be possible to reduce disposal cost significantly if effluent volume could be reduced to a significant extent.

Electro-osmotic pumping ED has the potential to be applied for industrial effluent treatment. Preliminary work has indicated that small brine volumes and high brine concentrations could be achieved with EOP-ED at attractive electrical energy consumptions. However, it was determined that the following needs still existed regarding the application of EOP-ED for industrial effluent treatment:

a)   to consider and document the relevant EOP-ED and ED theory properly;

b)   to study the EOP-ED characteristics (transport numbers, brine concentration, current efficiency, current density, electro-osmotic coefficient, etc.) of commercially available and other ion-exchange membranes in a single cell pair with the aim to identify membranes suitable for EOP-ED;

c)   to develop a simple method and to evaluate existing models with which membrane performance for salt, acid and base EOP-ED, can be predicted; and

d)   to evaluate the EOP-ED process for industrial effluent treatment.

The following conclusions can be drawn as a result of this investigation:

●   A conventional ED stack which was converted into an EOP-ED stack performed satisfactorily for concentration/desalination of sodium chloride, hydrochloric and caustic soda solutions. Dialysate concentrations of less than 500 mg/ℓ could be obtained in the feed water and cell pair voltage ranges from 1 000 to 10 000 mg/ℓ and 0,5 to 4 V/cp, respectively. Brine concentrations of 2,1 to 14,0%; 3,6% to 8,7% and 2,3% to 7,3% were obtained for sodium chloride, hydrochloric acid and caustic soda solutions, respectively.

Current efficiency increased with increasing feed water concentration during EOP-ED of sodium chloride and caustic soda solutions. This is in contrast to what is usually happening. Increasing feed water concentration causes increasing water flow through the membranes which inhibits co-ion invasion. Therefore, higher current efficiency is obtained. This supported the results that were obtained in a single cell pair. Current

efficiencies varied between 75,2 and 93,6%; 29,2 and 46,3% and 68,9 and 81,2% for sodium chloride (1 000 to 5 000 mg/ℓ feed; 0,5 to 1,5 V/cp); hydrochloric acid (1 000 to 5 000 mg/ℓ feed; 0,5 to 4,0 V/cp); and caustic soda solutions (1 000 to 10 000 mg/ℓ feed; 0,5 to 3 V/cp), respectively.

Low brine volumes and high water recoveries were obtained. Brine volume increased with increasing feed water concentration and decreased with increasing cell pair voltage. Brine volume varied between 1,5 and 4,0% for sodium chloride (1 000 to 5 000 mg/ℓ feed; 0,5 to 1,0 V/cp); between 2,4 and 7,8% for hydrochloric acid (1 000 to 5 000 mg/ℓ feed; 0,5 to 1,5 V/cp); and between 2,3 to 7,3% for caustic soda solutions (1 000 to 5 000 mg/ℓ feed; 0,5 to 1,5 V/cp).

Electrical energy consumption was low at low feed water concentrations and low cell pair voltages. Electrical energy consumption increased with increasing feed water concentration and increasing cell pair voltage. Electrical energy consumption of less than 2,5 kWh/m^3 product water was obtained for sodium chloride (0,5 to 1,5 V/cp; 1 000 to 3 000 mg/ℓ feed); between 0,2 and 3,2 kWh/m^3 product for hydrochloric acid (0,5 to 1,5 V/cp; approximately 1 000 mg/ℓ feed); and between 0,4 and 2,2 kWh/m^3 product for caustic soda solutions (0,5 to 1,5 V/cp; 1 000 to 3 000 mg/ℓ feed).

Water yield increased with increasing cell pair voltage and decreased with decreasing feed water concentration. Water yield was 0,38 m^3/m^2.d at a linear flow velocity of 1 cm/s through the stack when hydrochloric acid was concentrated (2 V/cp; 3 000 mg/ℓ feed). Water yield was increased to 0,7 m^3/m^2.d when linear flow velocity was increased to 5 cm/s. A higher linear flow velocity will also depress polarisation. Therefore, it would be advantageous to operate an EOP-ED stack at the highest possible linear flow velocity.

● Sealed-cell ED should be effective for concentration/desalination of relatively dilute (500 to 3 000 mg/ℓ TDS) non-scaling forming salt solutions. Product water with a TDS of less than 300 mg/ℓ could be produced in the feed water concentration range from 500 to 10 000 mg/ℓ TDS. Electrical energy consumption of 0,27 to 5,9 kWh/m^3 product was obtained (500 to 3 000 mg/ℓ feed range). Brine volume comprised approximately 2% of the initial feed water volume. Therefore, brine disposal costs should be significantly reduced with this technology.

Sealed-cell ED became less efficient in the 5 000 to 10 000 mg/ℓ TDS feed water

concentration range due to high electrical energy consumption (3,3 to 13,0 kWh/m^3 product). However, SCED may be applied in this TDS range depending on the value of the products that can be recovered.

Treatment of scale forming waters will affect the process adversely because scale will precipitate in the membrane bags which cannot be opened for cleaning. Membrane scaling may be removed by current reversal or with cleaning solutions. However, this matter needs further investigation. Scale-forming waters, however, should be avoided or treated with ion-exchange or nanofiltration prior to SCED.

It was demonstrated that a relatively dilute ammonium nitrate effluent (TDS 3 600 mg/ℓ) could be successfully treated in the laboratory with SCED. Brine volume comprised only 2,8% of the treated water volume. Electrical energy consumption was determined at 2,7 kWh/m^3 product. Both the brine and the treated water could be reused. Membrane fouling or scaling, however, may affect the process adversely and this matter needs further investigation.

It was difficult to concentrate/desalinate a concentrated ammonium sulphate effluent (approximately 13 200 mS/m or 123 700 mg/ℓ TDS) with SCED. Concentration/desalination was conducted in stages. Nevertheless, it was possible to desalinate the effluent to 6,2 mS/m (88 mg/ℓ TDS). However, electrical energy consumption was high (59 kWh/m^3 product). Brine volume comprised 45% of the treated volume. A very high brine concentration (approximately 26 300 mS/m or 332 000 mg/ℓ TDS) could be obtained after the first desalination stage. However, a more dilute (16 557 mg/ℓ TDS) ammonium sulphate effluent (3rd stage) could be more easily concentrated/desalinated to 88 and 191 208 mg/ℓ TDS product water and brine, respectively, at water recovery and electrical energy consumption of 91,6% and 17,9 kWh/m^3, respectively. Therefore, SCED could also be effectively applied for the desalination/concentration of relatively high TDS waters.

It was not possible to concentrate/desalinate an effluent saturated with calcium sulphate with SCED due to membrane scaling which took place. However, it was possible to concentrate/desalinate the effluent effectively after sulphate removal by chemical precipitation. It was possible to concentrate/desalinate the effluent from 1 182 mS/m (4 461 mg/ℓ TDS) to 51 mS/m (299 mg/ℓ TDS) at an electrical energy consumption of 9,5 kWh/m^3 product. Brine volume comprised 5,3% of the treated feed. The cost effectiveness of these procedures need to be evaluated.

The ion-exchange membranes used in the SCED stack performed very well for ammonium and nitrate removal. Ammonium and nitrate ions were removed from 4 179 and 2 215 mg/ℓ in one case to 10 - (99,8% removal) and 17 mg/ℓ (99,2% removal), respectively.

Capital cost of SCED equipment should be less than that of conventional ED due to the simpler design of the SCED stack. The membrane utilization factor of 95% is much higher than in conventional (approximately 80%) ED.

Sealed-cell ED has potential for treatment of relatively dilute (< 3 000 mg/ℓ TDS) non-scaling waters for water and chemical recovery for reuse. However, high TDS (up to 16 000 mg/ℓ) waters can also be treated depending on the value of the products that can be recovered.

Studies in a single cell pair have shown the following:

- Brine concentration increased with increasing current density and increasing feed water concentration. Brine concentration appeared to attain a constant value at high current density dependent on the electro-osmotic coefficients of the membranes.

- Current efficiencies were nearly constant in a wide range of current densities (0 to 70 mA/cm²) and feed water concentrations (0,05 to 1,0 mol/ℓ) in the case of the *Selemion* and *Raipore* membranes used for sodium chloride concentration. The same phenomenon was observed for the *Selemion* membranes used for acid concentration. However, all the other membranes showed a slight decrease in current efficiency with increasing current density. This showed that the limiting current density was exceeded and that polarization was taking place. Significant polarization took place with the WTPS membranes at relatively low current density (> 20 mA/cm²).

- Water flow through the membranes increased with increasing current density. Water flow through the membranes also increased with increasing feed water concentration, especially for the membranes that were used for salt and caustic soda concentration. This increasing water flow improved current efficiency and water flow can therefore also have a positive effect on ED. However, water flow decreased through the *Selemion* membranes that were used for acid concentration when feed water concentration was increased and no increase in current efficiency was observed. Current efficiency,

however, increased through the Israeli ABM membranes when water flow increased.

The electro-osmotic coefficients were determined to be a function of feed water concentration. The coefficients decreased with increasing feed water concentration until a constant value was obtained at high current density. The decrease in electro-osmotic coefficients with an increase in feed water concentration can be ascribed to deswelling of the membranes with increasing feed water concentration or to a reduction in membrane permselectivity when the feed water concentration is increased.

Osmotic flow in EOP decreases relative to the total flow with increasing current density while the electro-osmotic flow increases relative to the osmotic flow. Osmotic flow, however, contributes significantly to the total water flow in EOP. Osmotic flow through the *Selemion* AAV and CHV membranes contributed 64,1% of the total flow through the membranes at a current density of 20 mA/cm^2 (0,1 mol/ℓ feed). Osmotic flow was 20,9% of the total flow at a current density of 100 mA/cm^2 (0,1 mol/ℓ feed).

- Membrane permselectivity decreased with increasing brine and feed water concentration and increasing concentration gradient across the membranes.

- *Selemion* AMV and CMV and *Ionac* membranes performed satisfactorily for concentration of sodium chloride solutions. Salt brine concentrations of 19,3%; 25,1%; 27,2% and 29,8% were obtained at feed water concentrations of 0,05; 0,1; 0,5 and 1,0 mol/ℓ, respectively, with the *Selemion* AMV and CMV membranes. Current efficiency in this feed water concentration range varied from 62 to 91%. Performance of the *Ionics* and WTPS membranes were poorer while the poorest results were obtained with the WTPVC, WTPST and *Raipore* membranes.

Satisfactory results were obtained with the *Selemion* AAV and CHV and newly developed Israeli ABM-3 and ABM-2 membranes for hydrochloric acid concentration. Acid brine concentrations of 18,3%; 20,9%; 25,0% and 27,2% were obtained at 0,05; 0,1; 0,5 and 1,0 mol/ℓ feed water concentration, respectively, for the *Selemion* AAV and CHV membranes. Current efficiency varied between 35 and 42%. Higher current efficiencies, however, were obtained with the Israeli ABM-3 membranes. Current efficiency varied between 34 and 60% in the same feed water concentration range.

Selemion AMV and CMV, *Selemion* AMP and CMV and *Ionac* membranes performed well for caustic soda concentration. Caustic soda brine concentrations of 14,3%;

17,7%; 20,1% and 24,4% were obtained at high current density at 0,05; 0,1; 0,5 and 1,0 mol/ℓ feed water concentration, respectively, with the *Selemion* AMV and CMV membranes. Current efficiency varied from 47 to 76%.

Membrane current efficiency in EOP increased with increasing water flow through the membranes. This was especially observed for the more porous heterogeneous membranes at high feed water (1,0 mol/ℓ) concentration. It will therefore not be necessary for membranes to have very high (> 0,9) permselectivities for use in EOP·ED.

- It has been found that a simple potential measurement can be used effectively to predict membrane performance for salt, acid and base concentration with ED. The ratio between the apparent transport number $(\bar{\Delta}t)$ and current efficiency (ε_p), however, depends on the feed concentration and current density used. Ratio's of $\bar{\Delta}t/\varepsilon_p$ varied between 1,0 and 1,07 (0,1 mol/ℓ feed, *Selemion* AMV and CMV, salt concentration); 0,95 to 1,09 (0,5 mol/ℓ feed, *Ionac*); 1,02 and 1,05 (0,5 mol/ℓ feed, *Raipore*); 0,95 and 1,02 (0,5 mol/ℓ, *Ionics*). Consequently, it should be possible to predict current efficiency for concentration of sodium chloride solutions with an accuracy of approximately 10% and better from the apparent transport number of the membrane pair.

Correlations obtained between the apparent transport number $(\bar{\Delta}t)$ and current efficiency for membranes used for acid concentration, were unsatisfactory. The apparent transport number of the membrane pair $(\bar{\Delta}t)$ was from 1,5 to 4 times higher than current efficiency in the feed acid concentration range from 0,05 to 1,0 mol/ℓ. Back diffusion of hydrochloric acid through the membranes caused the lower current efficiency. However, the apparent number of the anion membrane (Δt^a) gave a much better indication of membrane performance for acid concentration. Ratio's of $\Delta t^a/\varepsilon_p$ of 1,1 to 1,2 (1,0 mol/ℓ, *Selemion* AAV); 0,97 to 0,84 (1,0 mol/ℓ, ABM-2); 0,92 to 0,97 (0,1 mol/ℓ, ABM-1) were obtained. Consequently, it should be possible to predict current efficiency for concentration of hydrochloric acid solutions with an accuracy of approximately 20% and better from the apparent transport number of the anion membrane.

Correlations obtained between the apparent transport number $(\bar{\Delta}t)$ and current efficiency of the membranes investigated for caustic soda concentration were satisfactory. Ratio's of $\bar{\Delta}t/\varepsilon p$ of 1,0 to 1,1 (0,05 mol/ℓ, *Ionac*); 0,9 to 1,0 (0,1 mol/ℓ, *Ionac*); 0,9 (1,0 mol/ℓ, *Selemion* AMV and CMV); 1,1 to 1,2 (0,1 mol/ℓ, *Selemion* AMP

and CMV); 1,1 (0,5 mol/ℓ, *Selemion* AMP and CMV) were obtained. Therefore, it should be possible to predict current efficiency for concentration of caustic soda solutions with an accuracy of approximately 20% and better from the apparent transport number of the membrane pair. Good correlations were also obtained between the apparent transport number of the cation membrane (Δt^c) and current efficiency. Consequently, it should also be possible to predict current efficiency with an accuracy of approximately 20% and better from the apparent transport number of the cation membrane.

- The correct Onsager relationships to be used for potential measurement ($\Delta \Psi$) and for the transport number (JF/I) are at zero current and zero volume flow, and at zero concentration gradient and zero volume flow, respectively. In practical ED, measurements are conducted at zero pressure and in the presence of concentration gradients and volume flows. These factors will influence the results considerably in all systems in which volume flow is important and where the concentration factor is high as is encountered in EOP. In measurement of membrane potential, the volume flow is against the concentration potential and in general will decrease potential. In ED, water flow helps to increase current efficiency, but the concentration gradient is against current efficiency.

- Brine concentration can be predicted from apparent transport numbers ($\overline{\Delta t}$'s) and water flows through the membranes. The ratio c_{bcalc}/c_{bexp} decreased with increasing feed concentration.

- Maximum brine concentration, c_b^{max}, can be predicted from two simple models. A very good correlation was obtained by the two methods. Maximum brine concentration increased with increasing feed concentration and appeared to level off at high feed concentration (0,5 to 1,0 mol/ℓ).

- Models described the system satisfactorily for concentration of sodium chloride, hydrochloric acid and caustic soda solutions with commercially available membranes. Brine concentration approached a limiting value (plateau) at high current density dependent on the electro-osmotic coefficients of the membranes. A constant slope (electro-osmotic coefficient) was obtained when water flow was plotted against current density. Straight lines were obtained when cell pair resistance was plotted against the specific resistance of the dialysate. Current efficiency increased with increasing flow of water, decreased when back diffusion was high and transport numbers were low.

13. NOMENCLATURE

Sections 2.1 and 2.2

c_b^{max}	-	Maximum brine concentration (mol/ℓ)
e_p, η_c	-	current efficiency (%)
J	-	volume flow through membranes (cm/h)
I_{eff}	-	effective current density (Coulomb efficiency x current density)
c_b	-	brine concentration (mol/ℓ)
β	-	electro-osmotic coefficient (ℓ/Faraday)
F	-	Faraday's constant (96 500 Coulomb/ge)
J_{osm}	-	osmotic water flow (cm/h)
J_{elosm}	-	electro-osmotic water flow (cm/h) ($J = J_{osm} + J_{elosm}$)
c_f	-	feed concentration (mg/ℓ)
c_p	-	product concentration (mg/ℓ)
d_{eff}	-	effective thickness of dialysate compartment (mm) (polarisation factor)
V_{cp}	-	cell pair voltage (volt)
R_{cp}	-	cell pair resistance ($\Omega \cdot cm^2$)
ρ	-	specific resistance of dialysate ($\Omega \cdot cm$)
a	-	anion membrane
c	-	cation membrane
$\Delta \Psi_m$	-	membrane potential (mV)
$\overline{\Delta t}$	-	apparent transport number of membrane pair

Section 2.3

r_{ik}	-	phenomenological resistance coefficient
f_{ik}	-	phenomenological friction coefficient
f_{21}	-	friction imposed by cation (1) on anion
f_{2w}	-	friction imposed by water (w) on anion (2)
f_{2m}	-	friction imposed by polymer matrix (m) on anion (2)
r_{ii}	-	straight resistance coefficients
m_{ext}	-	external concentration
2m	-	anion-polymer frictional force
2w	-	anion-water frictional force
$\overline{\Delta t}$	-	apparant transport number of membrane pair

Section 2.4

$\bar{a}_w$	-	water activity in interior of membrane
a_w	-	water activity outside membrane
Π	-	membrane internal osmotic pressure
R	-	gas constant
T	-	absolute temperature
v_w	-	partial molar volume of internal water component of membrane
n_o	-	equilibrium water content

Section 2.5

E	-	membrane potential
E_{max}	-	maximum membrane potential
$\bar{t}_+$	-	transport number
$\bar{t}_{+(app)}$	-	apparent transport number
a'	-	activity on one side of the membrane
a"	-	activity on the other side of the membrane
F	-	Faraday's constant
I	-	electric current
J_i	-	ion flux of species i
$\bar{t}_i$	-	transport number of species i inside the membrane

Sections 3.1.1 and 3.1.2

J_i	-	Flux density of i ($mol/cm^{-2}s^{-1}$)
c_i	-	concentration of i ($mol\ cm^{-3}$)
μ_i	-	electrochemical potential of i
x	-	distance from reference plane in membrane
R	-	gas constant
T	-	absolute temperature
γ_i	-	activity coefficient of i
V_i	-	partial molar volume of i
p	-	pressure
z_i	-	number of positive charges per ion (valency)
F	-	Faraday's number
ψ	-	electrical potential

D_i	-	diffusion coefficient of i
u_i	-	absolute mobility of i
v	-	velocity of local center of mass
L_{ik}	-	phenomenological conductance coefficient
X_k	-	force on k per mole
σ	-	rate of entropy production, reflection coefficient
ϕ	-	dissipation function
n	-	number of components
J_D	-	exchange flow
π_s	-	osmotic pressure
L_p	-	phenomenological coefficient
L_{pD}	-	phenomenological coefficient
L_D	-	phenomenological coefficient
J_v	-	total volume flux density (cm/s^{-1})
ω	-	solute permeability
R_{ik}	-	phenomenological resistance coefficient
A_{ik}	-	minor of L_{ik} in $\lvert L \rvert$
$\lvert L \rvert$	-	determinant of L_{ik}
μ_s	-	chemical potential of electrolyte
I	-	electric current density (amp/cm^2)
E	-	electromotive force

Section 3.1.3

c_i	-	concentration of i (mol.cm^{-3})
F	-	Faraday's number
F_{ik}	-	frictional force of k on i per mol of i
f_{ik}	-	molar frictional coefficient of i with k
J_i	-	flux density of i (mol.cm^{-2}s^{-1})
k	-	specific electrical conductance
v_i	-	mean velocity of i
X_i	-	force on i per mol

Section 3.2

J_1	-	flow of cation J_1
J_2	-	flow of anion J_2

$\Delta\tilde{\mu}_i$	-	difference in electrochemical potential
L_i	-	phenomenological coefficient
$\Delta\mu_s$	-	chemical potential
I	-	electric current
z_1	-	valance of cation
z_2	-	valance of anion
F	-	Faraday's constant
E	-	electromotive force
J_v	-	volume flow
Δt	-	apparent transport number
$\Delta\Psi$	-	potential difference across the membrane

Section 3.3

a	-	$a = X^*/X_t$
c_2^t	-	total concentration of salt in membrane
c_s^*	-	salt concentration in the aqueous solution
c_s^{*av}	-	average concentration of salt in the two solutions adjacent to the membrane
c_1^*, c_2^*	-	concentration of the free counter- and co-ions in the membrane
c_s	-	concentration of associated salt in the membrane
E	-	electromotive force
F	-	Faraday's constant
f_{ij}	-	frictional coefficient
f_{12}	-	frictional coefficient between co- and counter-ions
I	-	electrical current
J_i	-	flow of species i
J_1, J_2	-	stoichiometric flows of counter-ions and co-ions, respectively
J_s	-	flow of salt
J_1^*, J_2^*	-	flow of free counter-ions and co-ions, respectively
k	-	distribution coefficient of salt between membrane and aqueous phases
K_d^s	-	dissociation constant of salt in the membrane
K_d^f	-	dissociation constant of fixed group in the membrane
L_p	-	filtration coefficient
m	-	$m = K_d^s/K_d^f$
Δp	-	pressure difference
P_E	-	electro-osmotic pressure measured at zero volume flow and the absence of salt gradients

q^2	-	degree of coupling
R_{11}^*,	-	straight resistance coefficients for transport of counter-ions, co-ions
R_{22}^*, R_s		and salt, respectively
R_{12}	-	coupling resistance coefficient between flows of ion 1 and 2
R	-	universal gas constant
T	-	absolute temperature
X_i	-	driving force for species i
X_1,	-	driving forces for transport of counter-ions, co-ions and salt,
X_2, X_s	-	respectively
X_t	-	total concentration of fixed groups in the membrane
X^*	-	concentration of dissociated fixed groups in the membrane
Xc_t	-	associated fixed groups in the membrane
z_i	-	valency of ion i
α	-	$\alpha = K_d^* \, kc_s^{'2}$
β	-	electro-osmotic permeability measured at zero pressure and salt gradient
t_1, t_2	-	transport number of counter-ions and co-ions, respectively
ψ', ψ	-	electric potential in aqueous and membrane phases
μ_i^o $\mu_i^{o'}$	-	standard chemical potential of species i in membrane and aqueous solution, respectively
$\tilde{\mu}_1$, $\tilde{\mu}_2$	-	electrochemical potential of counter-ion 1 and of co-ion 2 in membrane, respectively
$\Delta\tilde{\mu}_i$	-	difference in electrochemical potential of species i
$\tilde{\mu}_1'$, $\tilde{\mu}_2'$	-	electrochemical potential of counter-ion 1 and of co-ion 2 in aqueous solution, respectively
μ_s	-	chemical potential of salt in membrane
$\Delta\tilde{\mu}_i$	.	difference in electrochemical potentials of species i
κ	-	membrane conductance measured in the absence of salt gradient and volume flow
κ'	-	membrane conductance measured in the absence of a pressure gradient
ω_s	-	salt permeability defined for $J_v = 0$
ω_s'	-	salt permeability defined for $\Delta p - \Delta\pi = 0$ and $I = 0$
ω_s''	-	salt permeability defined for $\Delta p = 0$ and $I = 0$
$\dfrac{\omega_s c_s^{'av}}{\kappa F^2}$	-	leak conductance (LC) ratio defined for $J_v = 0$
σ	-	reflection coefficient

Section 3.5

Δc°	-	concentration difference across membrane at time t = 0
$c^{\circ\prime}$	-	concentration at one side of the membrane at time t = 0
$c^{\circ\prime\prime}$	-	concentration at other side of memtrane at time t = 0
Δc^t	-	concentration difference across membrane after time t
J_1	-	total counter-ions
J_w	-	water flux
$\bar{t}_2$	-	co-ion transport number
$\bar{t}_w$	-	water transport number
$\bar{t}_1$	-	counter-ion transport number
$\bar{t}_1{}^r$	-	reduced transport number of counter-ions
$\tilde{m}$	-	mean molality
J_s, $J_w{}^{os}$	-	diffusion and osmotic fluxes
I	-	electric current
ω	-	-1 for cation-exchange membrane; +1 for anion-exchange membrane
$f(L_{ik}, \tilde{m})$	-	combination of the phenomelogical conductance coefficient L_{ik} and the mean mobility, $\tilde{m}$, of a solute
$\Delta\mu_s$	-	chemical potential difference of the solute
I	-	electric current
$\Delta c_a{}^t$, $\Delta c_c{}^t$	-	concentration changes of anolyte and catholyte after time Δt
$\bar{c}^\circ$	-	mean concentration of anolyte and catholyte at time t = 0, $\bar{c}^\circ = (c_a{}^\circ + c_k{}^\circ)/2$
η_E	-	efficiency of energy conversion
$J_1{}^w$	-	$J_1/v_1 - 0{,}018 \, \tilde{m} \, J_w$
ΔE	-	difference of electrical potential measured with electrodes reversible to co-ions

Section 3.6

c_i	-	concentration of species i, $mol.m^{-3}$
E	-	potential difference. V
I	-	current density, $A{\cdot}m^2$
J_i	-	flux density of species i, $mol.m^{-2}.s^{-1}$
L_{ik}	-	conductance coefficients
m_{ext}	-	external molality of NaCl
q, q_{ik}	-	coupling coefficients
$\bar{t}_w$	-	transport number of water, mol per Faraday
X_i	-	thermodynamic force

x	-	force ratio
Z	-	square route of the straight conductance coefficients
η	-	efficiency of energy conversion
μ_i	-	chemical potential of species I, $J.mol^{-1}$
π	-	osmotic pressure, Pa
ϕ	-	dissipation function
1	-	sodium ions
s	-	solute
w	-	water

Section 3.7

J_w	-	osmotic flow of water
J_s	-	diffusion flow of solute
$\Delta\mu_s$, $\Delta\mu_w$	-	differences of chemical potential of solute and water, respectively
L_{ik}	-	phenomenological conductance coefficient
J_w'	-	flow of water against the flow of solute conjugated to the concentration part of the chemical potential difference of water, $\Delta\mu_w^c$
J_v	-	total volume flow conjugated to the difference of pressure in the compartments on the opposite side of the membrane, Δp
ϕ	-	dissipation function
η	-	efficiency of energy conversion
q	-	coupling coefficient
$\Delta\pi$	-	difference in osmotic pressure
σ	-	reflection coefficient

Section 3.8

Π	-	osmotic swelling pressure
$\bar{a}_w$	-	water activity in membrane
a_w	-	water activity outside membrane
R	-	gas constant
T	-	absolute temperature
$\bar{c}$	-	internal equilibrium electrolyte concentration
C	-	concentration mol/ℓ
v_w	-	partial molar volume of the internal water component

Section 3.9

E	-	total electromotic force of membrane cell
M	-	molecular mass of solvent
m	-	concentration
$\bar{t}_w$	-	water transport number
$\bar{t}_i$	-	transport number
R	-	gas constant
T	-	absolute temperature
F	-	Faraday
a	-	activity
$t_{+(app)}$	-	apparent transport number
t_+	-	true transport number
$\bar{X}$	-	fixed charge density (equivalent per unit volume of swollen membrane)
$\bar{s}$	-	equivalent of co-ions per equivalent of fixed group present in the membrane
$u's$	-	mobilities of ions
$\bar{k}'$	-	specific conductance of membrane
β	-	volume of water flowing per Coulomb
V	-	volume of water flowing per second (millilitre)
i	-	current in amperes
k_i	-	specific conductance of pore liquid
A	-	pore area
φ_w	-	volume fraction of water in the membrane
$\bar{X}_v$	-	equivalent of fixed groups per unit volume of interstitial water
ΔV_c	-	volume decrease at anode due to water transport
ΔV_o	-	observed volume change
$\bar{V}$	-	partial molar volume

Sections 3.10 and 3.11

a_i	-	activity of species i (mol/ℓ)
A_m	-	effective membrane area (cm^2)
c_i	-	concentration of species i (mol/ℓ)
F	-	Faraday's constant - 96 500 (amp.sec/mol)
F_i	-	driving force acting on species i
I	-	electric current density (amp/cm^2)
I_{eff}	-	effective current density (amp/cm^2)

j_i	-	flux of species i through a membrane ($mol/(sec.cm^2)$)
J	-	volume flow through a membrane ($cm/sec = cm^3/cm^2.sec$)
L_p	-	filtration coefficient
P	-	solute permeability
Q	-	amount of feed solution entering a diluate channel per unit time
R	-	universal gas constant
s^c	-	salt flux (cation)
s^a	-	salt flux (anion)
t_i	-	transport number of ionic species i
$\bar{t}_i$	-	effective transport number of the ionic species i
Δt	-	difference between counter-ion and co-ion effective transport members
$\overline{\Delta t}$	-	effective transport number of a membrane pair
T	-	absolute temperature, $^\circ K$
V_w	-	water flow through a membrane (cm/s)
V	-	volume of solution that enters a membrane bag per unit area
$\bar{V}$	-	molar volume of species i
Δx	-	membrane thickness
β_i	-	drag coefficients associated with the ionic species i
γ_i	-	activity coefficient of species i
δ	-	thickness of the unstirred layer next to a solid surface
ϵ_c	-	overall current efficiency
ϵ_p	-	Coulomb efficiency (current efficiency)
ϵ_w	-	efficiency associated with water transport through membranes
Λ	-	degree of demineralization
μ_i	-	chemical potential of ionic species i
$\tilde{\mu}_i$	-	electrochemical potential of ionic specie i
$\Delta\Psi_m$	-	electrical potential difference between reversible electrodes, due to a difference of concentration at both sides of the membrane
π	-	osmotic pressure
σ	-	reflection coefficient
ω	-	salt permeability
η	-	current efficiency
a	-	anion-exchange membrane
c	-	cation-exchange membrane
F	-	Faraday's constant (Coulomb $equiv^{-1}$)
I	-	current density, amp cm^{-2}
J	-	molar flux, $mol\ cm^{-2}\ sec^{-1}$

J_v	-	volume flux, $cm \cdot sec^{-1}$
L_p	-	hydraulic permeability $cm \cdot sec^{-1}$ per unit pressure
P	-	local solute permeability, $cm^2 \cdot sec^{-1}$
R	-	universal gas constant
R_{cp}	-	apparent resistance of cell pair ohm cm^2
R_m	-	resistance of membrane pair ohm cm^2
S	-	rate of salt removal, $mol/cm^2.s$
T	-	absolute temperature
V_{cp}	-	voltage per cell pair, volts
c_s	-	salt concentration, mol/cm^3
$c_b, c_f,$	-	concentration of brine, feed, product
c_p		respectively, mol/cm^3
d_{eff}	-	effective thickness of dialysate cell, mm
β	-	electro-osmotic coefficient, cm^3 Coulomb $^{-1}$
$\gamma\pm$	-	activity coefficient
μ_i	-	thermodynamic potential
$\bar{\mu}_i$	-	electrochemical potential
$\eta \ \eta_c$	-	efficiency, current efficiency
π	-	osmotic pressure
ρ	-	specific resistance of dialysate, ohm $\cdot$ cm
t	-	transport number
ψ	-	potential, volt
ω	-	Permeability coefficient

Section 3.12

t_1	-	transport number of cations in solution
t_2	-	transport number of anions in solution
$\bar{t}_1{}^c$	-	transport number of cations in CPM
$\bar{t}_2{}^c$	-	transport number of anions in CPM
$\bar{t}_1{}^a$	-	transport number of cations in APM
$\bar{t}_2{}^a$	-	transport number of anions in APM
T_{DC}	-	apparent diffusion transport number of anion near cation membrane
T_{DA}	-	apparent diffusion transport number of cation near anion membrane
N	-	number of membrane pairs
F	-	Faraday's constant
R	-	gas constant

T	-	absolute temperature
E_m	-	membrane potential
T_D	-	flux of salt from the diluate channel
d	-	desalting rate (equiv $cm^{-2}.s^{-1}$)
p^c	-	permselectivity of cation membrane
p^a	-	permselectivity of anion membrane
P	-	power required to drive cell pair
i	-	current density
V_{cp}	-	cell pair voltage
δ	-	thicknes of boundary layer
R_d	-	resistance 1 cm^2 cross section, d.
κ	-	conductivity $(ohm/cm)^{-1}$
C_d	-	concentration of diluate stream (equiv/cm^3)
C_c	-	brine concentration (equiv/cm^3)
C_c/C_d	-	C = non-dimentsional concentration ratio term
Λ	-	equivalent conductivity in cm^2/ohm equiv.
R_{BC}	-	boundary layer resistance at cation membrane
R_{BA}	-	boundary layer resistance at anion membrane
C_w	-	solute concentration at membrane/diluate interface
C_{w1}	-	bulk concentration of concentrated salt on one side of membrane
C_{w2}	-	bulk concentration of dilute salt solution on other side of membrane
C_{wbc}	-	concentration-polarized membrane/boundary layer concentration at brine side of cation membrane
C_{wdc}	-	concentration-polarization membrane/boundary layer concentration at diluate side of anion membrane
Ud	-	flow rate
λ	-	cell to boundary layer thickness ratio
D	-	diffusion coefficient (cm^2/s)
R	-	gas constnt
β	-	$\dfrac{F^2D}{\Lambda t_2RT}$

14. LITERATURE

1. Garza, G. (1973): Electrodialysis by Electro-Osmotic Pumping and Ion Separation with Charged Membranes. Thesis submitted to the Weizmann Institute of Science, Rehovot, Israel.

2. Garza, G., and Kedem, O. (1976): Electro-Osmotic Pumping in Unit-Cells. 5th International Symposium on Fresh Water from the Sea, 13, 79-87.

3. Kedem, O., Tanny, G. and Maoz, G. (1978): A simple Electrodialysis Stack. *Desalination*, 24, 313-319.

4. Kedem, O., and Cohen, J. (1983): EDS-Sealed-Cell Electrodialysis. *Desalination*, 46, 291-299.

5. Kedem, O., and Bar-On, Z. (1986): Electro-Osmotic Pumping in a Sealed-Cell ED Stack. AIChE Symposium Series, Industrial Membrane Processes, 248, 82, 19-27.

6. Nishiwaki, T. (1972): Concentration of Electrolytes prior to Evaporation with an Electromembrane Process, In: R.E. Lacey and S. Loeb (Ed.), Industrial Processing with Membranes, Wiley-Inter-Science, New York.

7. Wilson, J.R. (1960): Demineralization by Electrodialysis, London, Butterworth Scientific Publications.

8. U.S.A.I.D. Desalination Manual (1980). CH & M, International Corporation, 7201 NW, 11th Place, Gainesville, Florida, USA, 32601.

9. Meares, P., Thain, J.F., and Dawson, D.G. (1972): Transport Across Ion-Exchange Resin Membranes: The Frictional Model of Transport, In: Eisenmann, G. (Ed), Membranes, A Series of Advances, Volume 1, Macroscopic Systems and Models, Marcel Dekker, Inc. New York.

10. Teorell, T. (1953): Transport Processes and Electrical Phenomena in Ionic Membranes. *Progr. Biophys. Biophys. Chem.*, 3, 305.

11. Helfferich, F. (1962): *Ion-Exchange*, McGraw-Hill, New York, 344.

12.   Staverman, A.J. (1952): Non-Equilibrium Thermodynamics of Membrane Processes. *Trans. Faraday soc.*, 48, 176.

13.   Catchalsky, A., and Curren, P.F. (1965): Non-Equilibrium Thermodynamics In Biophysics, Harvard University Press, Cambridge Mass.

14.   Kedem, O., and Katchalsky, A. (1963): Permeability of Composite Membranes. *Trans. Faraday Soc.*, 59, 1918, 1931, 1941.

15.   Kedem, O. (1983): A Simple Procedure for Estimating Ion Coupling from Conventional Transport Coefficients. *Journal of Membrane Science*, 14, 249-262.

16.   Johnstone, B.L. (1987): Lecture on Basic Principles of Electrodialysis.

17.   Koter, S., and Narebska, A. (1989/90): Current Efficiency and Transport Phenomena in Systems with Charged Membranes. *Separation Science and Technology*, 24, (15), 1337-1354.

18.   Narebska, A., and Koter, S. (1987): Irreversible Thermodynamics of Transport Across Charged Membranes. Part III - Efficiency of Energy Conversion in Separation Processes with Nafion 120 Membrane from Phenomenological Transport Coefficients. *Journal of Membrane Science*, 30, 141 - 152.

19.   Narebska, A., koter, S., and Kujowski, W. (1990): Conversion of Osmotic Energy in Systems with Charged Membranes. *Journal Non-Equilibrium Thermodynamics*, 15, 1 - 10.

20.   Brydges, T.G., and Lorimer, J.W. (1983): The Dependence of Electro-Osmotic Flow on Current Density and Time. *Journal of Membrane Science*, 13, 291-305.

21.   Kruissink, C.H.A. (1983): The effect of Electro-Osmotic Water Transport on Current Efficiency and Cell Performance in Chlor-Alkali Membrane Electrolysis. *Journal of Membrane Science*, 14, 331-366.

22.   Hidalgo-Alvarez, R., de las Nieves, F.J. and Pardo, G. (1984): Anamalous Electro-Osmotic Flow through a Heteroporous Ion-Exchange Membrane - A Test Based upon the Reciprocity Relations. *Journal of Non-Equilibrium Thermodynamics*, 9, 157-1643.

23.   Ceynowa, Josef (1983): Electro-Osmosis in the System Ion-Exchange Membrane-Sulphuric
       Acid Solution. *Die Angewandte Makromolekulare Chemie,* 116, 165-174 (No 1824).

24.   Tombalakion, A.S., Barton, H.J., Graydon, W.F. (1962): *Journal Physical Chemistry,* 66, 1006.

25.   Rueda, C., Ruiz-Bauza, C., and Agular, J. (1977): Electro-Osmotic Permeability of Cellulose
       Acetate Membranes. *Journal Physical Chemistry,* 61, 789.

26.   Tasaka, Masayasu., Tamura, Staoski., and Takemura, Naota (1082): Concentration
       Dependence of Electro-Osmosis and Streaming Potential across Charged Membranes.
       Journal of Membrane Science, 12, 169-182.

27.   Oda, Goshio., and Yawataya, Tadaski (1957): On the Distribution and Behaviour of Water in
       Cation-Exchange Resin Membranes. *Bulletin of the Chemical Society of Japan,* 30,(3),
       213.

28.   Narebska, A., Koter, S., and Kujowski, W. (1984): Ions and Water Transport Across Charged
       Nafion Membranes. Irreversible Thermodynamic Approach. *Desalination,* 51, 3 - 17.

29.   Narebska, A. and Koter, S. (1987): Conductivity of Ion-Exchange Membranes - Convection
       Conductivity and Other Components. *Electro-Chimica Acta,* 32, (3), 449 - 453.

30.   Narebska, A., Kujowski, W., and Koter, S. (1987): Irreversible Thermodynamics of Transport
       Across Charged Membranes, Part II - Ion-Water Interactions in Permeation of Alkali.
       Journal of Membrane Science, 30, 125 - 140.

31.   Narebska, A., Koter, S., and Kujowski, W. (1985): Irreversible Thermodynamics of Transport
       Across Charged Membranes. 1. Macroscopic Resistance Coefficients for a System with
       Nafion 120 Membrane. *Journal of Membrane Science,* 25, 153 - 170.

32.   Koter, S., and Narebska, A. (1987): Conductivity of Ion-Exchange Membranes. *Electrochimica
       Acta,* 32, (3), 455 - 458.

33.   Kononov, A.N., Ponomarev, M.I., Shkaraputa, L.N., Grebenyuk, V.D., and Sklyar, V.T. (1984):
       Removal of Hydrochloric Acid from Waste Waters Containing Organic Synthesis
       Products. *Khimiya i Teckhnologiya Vody,* 6, (1), 66-68.

34. Korngold, E. (1978): Concentration of sulphuric and Hydrochloric Acids. *Electrodialysis in Advanced Waste Water Treatment,* 24, 129-139.

35. Laskorin, B.M., Smirnova, N.M., Tisov, Y., Gorina, G.N., and Borisov, A.V. (1973): Use of Electrodialysis with Ion-Selective Membranes for Concentrating Carbonate Solutions. *Zhurnal Prikladnoi Khimii,* 46, (9), 2117-2119.

36. Smagin, V.N., and Chukkin, V.A. (1975): Concentration of Brines of Desalination Plants with Electrodialysis. *5th International symposium on Fresh Water from the Sea,* 3, 139-148.

37. Urano, K., Ase, T., and Naito, Y. (1984): Recovery of Acid from Wastewater by Electrodialysis. *Desalination,* 51, 213-226.

38. Itoi, S., Nakamura, I., and Kawahara, T. (1980): Recovery of Metals from Plating Rinse Waters. *Desalination,* 32, 383.

39. Schoeman, J.J. (1985): The Status of Electrodialysis Technology for Brackish and Industrial Water Treatment. *Water SA,* 11, (2), 79-86.

40. Lakshminarayanaih, N. (1962): Electro-Osmotic Permeability of Ion-Exchange Resin Membranes. Proceedings Indian Academy, Sci., A55, 200.

41. Demarty, M., Maurel, A., and Selegny, E. (1974). *Journal Chim. Phys., Phys. Chim. Biol.,* 71, 811.

42. Mauritz, K.A., and Hopfinger, A.J. (1982): Structural Properties of Membrane Ionomers, In: *Modern Aspects of Electrochemistry,* 14, J.O.M. Bockris, B.E. Conway, and R.E. White, Eds., Plenum Publishing Corp., Ch.6.

43. Narebska, A., and Wodzki, R. (1982): Swelling Equilibria and Structure Variations of Nafion and Polyethylene (Polystyrene Sulphonic Acid) Membranes at High Electrolyte Concentrations and Increased Temperature. *Die Angewandte Makromolekulare Chemie,* 107, 51 - 60 (No. 1679).

44. Narebska, A., Wodzki, R., and Erdmann, K. (1983): Properties of Perflurosulphonic Acid Membranes in Concentrated Sodium Chloride and Sodium Hydroxide Solutions. *Die Angewandte Makromolekulare Chemie,* 111, 85 - 95 (No. 1711).

45. Lakshminarayanaih, N. (1969): Transport Phenomena In Membranes. Academic Press, Inc. 111 Fifth Avenue, New York, New York 10003.

46. Kressman, T.R.E., and Tye, F.L. (1956): *Discussions Farady Soc.* 21, 185.

47. Lakshminarayanaih, N., and Subrahmanyan, V. (1964): *J Polymer Sci. Pt. A* 2, 4491.

48. Boudet-Dumy, M., Lindheimer, A., and Gavach, C. (1991): Transport Properties of Anion-Exchange Membranes In Contact with Hydrochloric Acid Solutions. Membranes for Acid Recovery by Electrodialysis. *Journal of Membrane Science*, 57, 57-68.

49. Cherif, A.T., and Gavach, C. (1988): Sulphuric Acid Concentration with an Electrodialysis Process, *Hydrometallurgy*, 21, 191.

50. Huang, T.C., and Juang, R.S. (1986): Recovery of Sulphuric Acid with Multi-Compartment Electrodialysis. *Ind. Eng. Chem. Processes Des. Dev.*, 25, 537.

51. Nott, B.R. (1981): Electrodialysis for Recovering Acid and Caustic from Ion-Exhange Regeneration Wastes. *Ind. Eng. Chem. Prod. Res. Dev.*, 20, 170.

52. Grebenyuk, V.D., Penkalo, I.I., and Chalaya, L.M. (1986): Desalination of Water with Simultaneous Production of Alkali and Acid. *Khim. Teknol. Vody*, 8, 76.

53. Leitz, F.B. (1976): Electrodialysis for Industrial Water Clean-Up. *Environ. Sci. Technol.*, 10, 136.

54. Eisenmann, J.L. (1979): Membrane Processes for Metal Recovery from Electroplating Rinse Water. Second Conference on Advanced Pollution Control for the Metal Finishing Industry, E.P.A., Cincinnati, OH, 99.

55. Hanley, T.R., Chiu, H.K., and Urban, R.J. (1985): Phosphoric Acid Concentration by Electrodialysis. AIChE Symp. Ser., 82, 121.

56. McRae, W.A. (1983): In Desalination Technology, Developments and Practice (A. Porteous, ed), *Applied Science*, Chapter 8.

57.   Iaconelli, W.B. (1973): The Use of Electrodialysis in the Food Industry, Paper presented at the
        IFT Annual Meeting.

58.   Reed, P.B., (1984): *Chem. Eng. Prog.*, 47.

59.   Barney, J.J., and Hendrik, J.L., (1878): *Chem. Prod. Res. Dev.*, 17, 17.

60.   Bhagat (1980): *Water Pollution Control,* 11, 118.

61.   Melzer, J., and Van Deventer, D. (1983): Electrodialysis Used for Desalination of Waste Water
        in an Eskom Power Station. Presented at a Symposium on Desalination: New
        Developments and Industrial Application, CSIR Conference Centre, Pretoria, 27 October
        1983.

62.   Gering, K.L., and Scamehorn, J.F. (1988): Use of Electrodialysis to Remove Heavy Metals from
        Water. *Separation Science and Technology,* 23, (14 & 15), 2231-2267.

63.   Goldman, D.E. (1943): Potential, Impedance and Rectification in Membranes. *J. Gen.*
        Physiol., 27, 37.

64.   Kirkwood, J.G. (1954): In Ion Transport Across Membranes (H.T. Clarke, ed), Academic, New
        York, 119.

65.   Miller, D.G. (1960): Thermodynamics of Irreversible Processes. *Chem. Rev.,* 60, 15.

66.   Kedem, O., and Katchalsky, A. (1958): Thermodynamic Analysis of the Permeability of
        Biological Membranes to Non-Electrolytes. *Biochim. Biophys. Acta.* 27, 229.

67.   Krämer, H., and Meares, P. (1969): Correlation of Electrical and Permeability Properties of Ion-
        Selective Membranes. *Biophys. J.,* 9, 1006.

68.   Kedem, O., and Essig, A. (1965): Isotope Flows and Flux Ratios in Biological Membranes. *J.*
        Gen. Physiol., 48, 1047.

69.   Coster, H.G.L. and George, E.P. (1968): A Thermodynamic Analysis of Fluxes and Flux-Ration
        in Biological Membranes. *Biophys. J.,* 8, 457.

70.   Mazur, P. and Overbeek, J.T. (1951): On Electro-Osmosis and Streaming-Potentials in Diaphragms. *Rec. Trav. Chim.,* 70, 83.

71.   Spiegler, K.S. (1958): *Trans. Faraday Soc.,* 54, 1408.

72.   Kedem, O. and Caplan, S.R. (1965): Degree of Coupling and its Relation to Efficiency of Energy Conversion. *Trans. Faraday Soc.,* 61, (9), 1897.

73.   Kedem, O., and Perry, M. (1977): Proc. Symp. on the Behaviour of Ions in Macromolecular and Biological Systems, Colston, England, 134.

74.   Caplan, S.R. (1965): The Degree of Coupling and Efficiency of Fuel Cells and Membrane Desalination Processes. *J. Phys. Chem.,* 69, 3801.

75.   Lee, K.H., Baker, R.W., and Lonsdale, H.K. (1981): Membranes for Power Generation by Pressure Retarded Osmosis. *Jour. Membrane Science,* 8, 141.

76.   Donnan, F.G. (1924): *Chem Rev.* 1, 73.

77.   Hale, D.K., and McCauley, D.J. (1961): *Trans. Faraday Soc.* 57, 135.

78.   Lakshminarayanaiah, N. (1965): *Chem. Rev.* 65, 531.

79.   Lakshminarayanaiah, N. (1969): *J. Phys. Chem.* 73, 97.

80.   Oda, Y., and Yawataya, T. (1956): *Bull. Chem. Soc. Japan.* 29, 673.

81.   Harned, H.S., and Owen, B.B. (1958): "The Physical Chemistry of Electrolytic Solutions", 3rd ed., p. 359. Reinhold, New York.

82.   Spiegler, K.S., and Kedem, O. (1966): Thermodynamics of Hyperfiltration (Reverse Osmosis): Criteria for Efficient Membranes. *Desalination,* 1, 311-326.

83.   Ionics Pamphlet on EDR (1987).

84.   Katz, W.E. (1977): The Electrodialysis Reversal (EDR) Process. Presented at the International Congress on Desalination and Water Reuse, Tokyo, November/December 1977. Published by Ionics, Inc., 65 Grove Street, Watertown, MA, USA 02172 (Bulletin TP. 307).

85.   Leitz, F.B. and Eisenmann, J.L. (1981): Electrodialysis as a Separation Process. A.I.Ch.E. Symposium Series 77, 204-209.

86.   Tani, Y. (1981): Energy Saving Electrodialyzer for Seawater Desalination. Technical Proceedings, Ninth Annual Conference, National Water Supply Improvement Association, Washington, D.C. Published by NIWSA, 26 Newbury Road, Ipswich, NA, USA, 01938.

87.   Urano, K. (1977): Present Status of Electrodialysis Process in Japan. *Desalination*, 20, 365.

88.   Wirth, J.R. and Westbrook, G. (1977): Cooling Water Salinity and Brine Disposal Optimized with Electrodialysis Water Recovery/Brine Concentration System. *Combusion*, May, 33-37.

89.   Lakshminarayanaih, N. (1965): *Chem. Revs.* 65, 494.

90.   Friedlander, H.Z. and Rickles, R.N. (1966): *Anal, Chem.* 37, 27A.

91.   Molau, G.E. (1981): Heterogeneous Ion-Exchange Membranes. *Journ. of Membrane Science*, 8, 309-330.

92.   Korngold, E., De Körösy, F., Rahav, R. and Taboch, M.F. (1970): Fouling of Anion-Selective Membranes in Electrodialysis. *Desalination*, 8, 195.

93.   Van Duin, P.J. (1973): Poisoning of Electrodialysis Membranes. Proceedings of 4th International Symposium on Fresh Water from the Sea, 3, 253-259.

94.   Katz, W.E. (1982): Desalination by ED and EDR-State-of-the-Art in 1981. *Desalination*, 42, 129.

95.   Fraivillig, J.B. (1983): Reverse Osmosis/Electrodialysis Reversal Comparison. Permasep Products (Du Pont), Maylands Avenue, Hemel Hampstead, Herts, HP2-7DP.

96.   Miva, T. (1977). Desalting by Electrodialysis. *Desalination,* 20, 375.

97.   Song, Shi and Pei-Qi Chem (1983): Design and Field Trials of a 200 m³/day Seawater
        Desalination by Electrodialysis. *Desalination,* 46, 191.

98.   Parsi, E.J., Prato, T.A. and P'Donoghue, K. (1980): Status of High Temperature Electrodialysis.
        Presented at the Eighth Annual Conference of the National Water Supply Improvement
        Association, San Francisco, 6-10 July.

99.   Brown, D.R. (1981): Desalting High Salinity Water Using 10-Stage EDR. Proceedings of the
        Ninth Annual Conference and International Trade Fair of the National Water Supply
        Association, 2.

100.   Elyanow, D., Parent, R.G. and Mahoney, J. (1980): Parametric Tests of an Electrodialysis
        Reversal System with Aliphatic Anion Membranes. Report to WRT, US Department of
        the Interior (Contract No. 14-34-0001-9510),Washington, D.C.

101.   Katz, W.E. (1971): Electrodialysis for Low TDS Waters. *Ind. Water Engng.,* June/July (Bulletin
        TP.301).

102.   Highfield, W.H. (1980): Electrodialysis in Industrial Water Treatment. Presented at the 41st
        Annual Meeting of the International Water Conference, Pittsburgh, Pennsylvania,
        October, 1980. (Bulletin TP.316).

103.   Itoi, S. (1979): Electrodialysis of Effluents from Treatment of Metallic Surfaces. *Desalination*
        28, 193.

104.   Trivedi, D.S., and Prober, R. (1972): On the Feasibility of Recovering Nickel from Plating
        Wastes by Electrodialysis. *Ion Exch. Membr.,* 1, 37.

105.   Eisenmann, J.T. (1977): Recovery of Nickel from Plating Bath Rinse Waters by ED. *Plat. Surf.
        Finish.,* 64 (11), 34.

106.   Jordan, D.R., Bearden, M.D. and Mclhenny, W.R. (1975): Blowdown Concentration by
        Electrodialysis. *Chem. Engineering. Prog.,* 71(7), 77.

107. Jordan, D.R., McIhenny, W.F., and Westbrook, G.T. (1976): Cooling Tower Effluent Reduction by Electrodialysis. American Power Conference.

108. Westbrook, G.T. and Wirth, L.F. Jr. (1976): Water Reuse by Electrodialysis. *Ind. Water Engng.,* April/May 8.

109. Smirnova, N.M., Laskorin, B.N., Mishukova, J.S. and Borisov, A.V. (1983): The Application of Electrodialysis with Ion-Exchange Membranes for Treatment of Sodium Sulphate Solutions. *Desalination,* 46, 197.

110. Nott, B.R. (1981): Electrodialysis for Recovering Acid and Caustic Soda from Ion-Exchange Regeneration Wastes. *Ind. Engng. Chem. Product Des. and Dev.,* 20, (1).

111. Schoeman, J.J. and Botha, G.R. (1981): Behandeling van Industriële Uitvloeisels met Elektrodialise. Presented at a Symposium on Industrial Effluents, 23 November, Pretoria.

112. Oren, G. and Litan, J. (1974): The State of the Solution Membrane Interface during Ion Transport Across and Ion-Exchange Membrane. *Journ. Physical Chemistry,* 78, 1805.

113. Simon, G.P. and Calmon, C. (1986): Experimental Mehtods for the Determination of Non-Transport Properties of Membranes. *Desalination,* 59, 106, 103.

114. Kneifel, K., and Hattenbach, K. (1980): Properties and Long-Term Behaviour of Ion-Exchange Membranes. *Desalination,* 34, 77.

115. Schoeman, J.J., Hill, E., Enslin, G.M. and MacLeod, H. (1990): Electro-Osmotic Pumping of Salts, Acids and Bases. Contract Report to the Water Research Commission.

116. Schoeman, J.J. and Enslin, G.M. (1989): Evaluation of Sealed-Cell Electrodialysis for Industrial Effluent Treatment. Contract Report to the Water Research Commission.

117. Kedem, O. (1992): Private Communication.

1. DEFINITION OF TRANSPORT NUMBERS

a)   Transport number of ion i, t_i:

$$t_i = (z_i J_i F/I)_{\Delta c = 0}, \quad i = 1,2 \tag{A1}$$

where I is the electric current, J_i is the flux of species i, z_i is its charge, and F is the Faraday constant.

b)   Reduced transport number of species i (6), t_i^r.

For ions (i = 1,2):

$$t_i^r = \frac{1}{z_i} t_i = \left(\frac{FJ_i}{I}\right)_{\Delta c = 0}$$

For water:

$$t_w^r = t_w = \left(\frac{FJ_w}{I}\right)_{\Delta c = 0} \tag{A2}$$

1. DERIVATION OF THE FORMULA FOR THE CURRENT EFFICIENCY (Eq. 3.5.3, Fig. 3.5.1)

At $t = 0$ the concentrations of the anode ($i = a$) and the cathode ($i = c$) solutions are

$$c_i^o = n_i^o/V^o, \qquad i = a, c \tag{B1}$$

where n_i^o is the number of moles of an electrolyte in the "i" solution. The volumes of both solutions are equal and denoted by V^o. After passing the current I during time Δt, the concentrations in both compartments change to

$$c_i^t = (n_i^o + \Delta n_i) / (V^o + \Delta V_i), \qquad i = a, c \tag{B2}$$

where Δn_i and ΔV_i are the changes of the amount of an electrolyte and of the volume in the "i" compartment, respectively. Assuming $\Delta V_i << V^o$, from eqs. (B1) and (B2) we obtain

$$\Delta c_c^t - \Delta c_a^t = (\Delta n_c - \Delta n_a - c_c^o \Delta V_c + c_a^o V_a)/V^o \tag{B3}$$

For the standard system (Fig. 3.5.1), the changes of ΔV_i and Δn_i are as follows:

Real membrane:

$$
\begin{aligned}
\Delta n_i \quad &= \quad z_i(\Delta n^m + \Delta n^{mid}) \\
&= \quad z_i \omega J_1/v_1 \Delta t \quad \text{(moles of } Av_1 Bv_2) \tag{B4}
\end{aligned}
$$

$$
\begin{aligned}
\Delta V_i \quad &= \quad z_i(\Delta V^m + \Delta V^{mid}) \\
&= \quad z_i \omega(\bar{v}_s J_1/v_1 + \bar{v}_w J_s 1)\Delta t, \quad i = a \text{ or } c \tag{B5}
\end{aligned}
$$

where $z_a = 1$, $z_c = -1$

Δn^m and ΔV^m denote changes in the amounts of ions and of volume due to the transport across the investigated membrane, respectively

$$\Delta n^m = \omega J_1 \Delta t/v_1(Av_1 Bv_2) + x /| z_2 |(B^{z_2}) \tag{B6}$$

$$\Delta V^m = \left(\omega \bar{v}_s J_1/v_1 + \bar{v}_w J_w + \frac{\bar{v}_2}{|z_2|} \frac{I}{F} \right) \Delta t \tag{B7}$$

Δn^{mid} and ΔV^{mid} denote analogical effects of transport across ideal membranes surrounding the investigated membrane

$$\Delta n^{mid} = -x/|z_2|(B^{z_2})$$ (B8)

$$\Delta V^{mid} = -\frac{\bar{v}_2}{|z_2|}x$$ (B9)

$$x = I\Delta t/F$$ (B10)

$$J_1 = -\omega \bar{t}_1^r I/F + v_1 J_s$$ (B11)

$$J_w = -\omega \bar{t}_w I/F + J_w^{os}$$ (B12)

Ideal membrane ($\bar{t}_2$, $\bar{t}_w$, J_s, $J_w^{os} = 0$):

Equations (B4) and (B5) are simplified to

$$\Delta n_1 = -z_1 \frac{1}{z_1 v_1} x$$ (B13)

$$\Delta V_1 = -z_1 \frac{\bar{v}_s}{z_1 v_1} x$$ (B14)

By substituting eqs. (B13), (B14) and (B3) into eq. (5), we obtain :

$$(\Delta c^t - \Delta \bar{c}^o)_{Ideal} = \frac{2(1 - \bar{v}_s \bar{c}^o)x}{z_1 v_1 V^o}$$ (B15)

By substituting eqs. (B4) and (B5) through eqs. (B3) and (B15) in the formula defining the current efficiency (eq. 3.5.1), we obtain:

$$CE = \frac{z_1 v_1 F}{I}\left[\frac{J_1}{v_1} - \frac{c^o \bar{v}_w}{1 - \bar{v}_s \bar{c}^o}J_w\right]$$ (B16)

By introducing eqs. (B11) and (B12) into eq. (B16), we finally obtain:

$$CE = z_1 V_1 \left[\frac{\bar{t}_1^r}{V_1} - \left(\frac{\bar{c}_3}{\bar{c}_w} \right) \bar{t}_w - \omega \left(J_s - \left(\frac{\bar{c}_3}{\bar{c}_w} \right) J_w^{os} \right) F/I \right] \qquad (B16a)$$

where

$$\left(\frac{\bar{c}_3}{\bar{c}_w} \right) = \frac{\bar{V}_w \bar{c}^\circ}{1 - \bar{V}_s \bar{c}^\circ} = 0{,}018 \tilde{m} \qquad (B17)$$

$$\bar{c}^\circ = (c_a^\circ + c_k^\circ)/2 \qquad (B18)$$

2. THE SYSTEM WITH ELECTRODE REACTIONS

In practice, in any system there are electrodes and electrode reactions which cause additional variations in the concentrations in mol/dm^3 of the solutions. Consequently, the differences Δn_i^{cor} and ΔV_i^{cor} will appear:

$$\Delta n_i^{mld} = z_i \Delta n^{mld} = \Delta n_i^{el} + \Delta n_i^{cor}, \quad I = a, c \qquad (B19)$$

$$\Delta V_i^{mld} = z_i \Delta V^{mld} = \Delta V_i^{el} + \Delta V_i^{cor}, \quad I = a, c \qquad (B20)$$

where Δn_i^{el} and ΔV_i^{el} denote changes of amount of ions and volume due to electrode reactions.

By substituting eqs. (B19) and (B20) through eqs. (B3) and (B5) into eq. (6), we obtain:

$$CE = \frac{z_1 V_1}{2(1 - \bar{V}_s \bar{c}^\circ)} \left[V^\circ F \left(\frac{\Delta c_c^t}{\Delta t} - \frac{\Delta c_a^t}{\Delta t} \right)^{pract} \underbrace{+ \Delta \bar{n}_c^{cor} - \Delta \bar{n}_a^{cor} - c_c^\circ \Delta \bar{V}_c^{cor} + c_a^\circ \Delta \bar{V}^{cor}]}_{correction} \right] \qquad (B21)$$

where $\Delta \bar{n}_i^{cor} = \omega \Delta n_i^{cor}/x$; $\Delta \bar{V}_i^{cor} = 1 - \omega \Delta V_i^{cor}/x$, $i = a, c$

$\Delta \bar{n}_i^{cor}$ and $\Delta \bar{V}_i^{cor}$ for some systems are presented in Table 1. Substitution in the right-hand term of eq. (B21) gives the necessary corrections[17].

Table 1: Δn_i^{cor} and ΔV_i^{cor} for different electrode/electrolyte/membrane systems (eq. B21).

| Electrode | Cation-exchange membrane | | Anion-exchange membrane ($z_2 = z$) | |
| | $i = a, c$; $z_a = 1$; $z_c = -1$ | | | |
	$\Delta \bar{n}_i^{cor}$	ΔV_i^{cor}	Δn_i^{cor}	ΔV_i^{cor}
Ag/AgCl Solute: $MeCl_z$	0	$z_i(\bar{v}_{Ag} - \bar{v}_{AgCl})$	z_i/z_2	$z_i(\bar{v}_s/z_2 + \bar{v}_{Ag} - \bar{v}_{AgCl})$
Pt Solute: $Me(OH)_z$	0	c: $\bar{v}_w$ a: $-0.5\bar{v}_w$	z_i/z_2	c: $-\bar{v}_s/z_2 + \bar{v}_w$ a: $\bar{v}_s/z_2 - 0.5\bar{v}_w$
Pt Solute: H_2SO_4	$-z_i/2$	c: $0.5\bar{v}_s$ a: $-0.5(\bar{v}_s - \bar{v}_w)$	0	c: 0 a: $0.5\bar{v}_w$

Table 1: Electrodialysis desalination/concentration results of an approximately 1 000 mg/ℓ NaCl solution with Ionac MA-3475 and MC-3470 membranes at 0,5 V/cp (4 v/8 cp; 10V total).

Time min	Current amp	Cf mS/m	Cf mg/ℓ	Cb mS/m	Cb mg/ℓ	pH feed	pH brine
0	0,18	170	992			7,1	
15	0,17	151	880	1 197	7 855	6,6	7,2
30	0,16	139	809	1 610	10 709	6,8	7,3
45	0,15	128	744	1 980	11 429	7,0	7,3
60	0,14	118	685	2 340	14 675	7,4	7,3
75	0,13	109	632	2 660	17 560	7,5	7,1
90	0,12	101	585	2 910	19 814	7,5	7,0
105	0,11	93,6	542	3 180	22 248	7,6	6,9
120	0,10	86,3	499	3 320	23 511	7,6	6,8
135	0,09	79,0	456	3 500	25 133	7,8	7,1
150	0,09	73,1	420	3 610	26 125	7,8	6,8
165	0,08	68,2	392	3 720	27 117	7,6	6,9
180	0,08	62,2	357	3 760	27 478	7,7	6,8
195	0,07	58,5	335	3 770	27 568	7,5	6,8
210	0,07	55,5	317	3 770	27 568	7,6	6,9
225	0,06	48,0	273	3 760	27 478	7,4	6,9
240	0,06	44,3	251	3 760	27 478	7,5	6,9
255	0,05	41,5	235	3 760	27 478	7,3	7,0
270	0,05	37,6	212	3 640	26 396	7,0	7,0

Cross sectional area of diluating chamber is:

13 cm x 0,2 cm   =   2,6 cm²

For a linear flow rate of 1 cm/s:

2,6 cm² x 1 cm/s   =   2,6 cm³/s (flow rate)

Therefore, for 10 diluating chambers, the flow rate must be 1 560 mℓ/min.

Flow rate used	:	1 350 ml/min
∴ Linear flow velocity	:	0,87 cm/s
Feed volume (beginning)	:	12 l
Product volume (end)	:	11,25 l
Brine volume (end)	:	230 ml
Brine conductivity	:	3 150 mS/m
Brine concentration	:	21 981 mg/l

$\int f(x)\ dx$ = 15/2 (I_1 + 2 (I_2 + I_3 + + I_{n-1}) + I_n)

= 7,5 (3,69)

= 27,675 amp.min

= 1660,5 amp.s (coulombs).

Salt equivalents removed:

Beginning: 12 l x 992 mg/l = 11 904 mg

i.e. $\dfrac{11\ 904}{58,44}$ = 203,7 me

End : 11,77 x 212 mg/l = 2 495,24 mg

i.e. $\dfrac{2495,24}{58,44}$ = 42,7

∴ me removed = 161 me

= 0,161 ge

Current efficiency (%) = $\dfrac{96\ 500\ \text{C x 0,161 ge x 100}}{\text{ge}}$

10 cp x 1660,5 C

= 93,57%

Electrical energy consumption:

$$p = V \times I \times h \text{ (across membranes only)}$$

$$= \frac{5 \times 27{,}675}{60}$$

$$= 2{,}306 \text{ wh}$$

$$= 0{,}002306 \text{ kwh}$$

Energy consumption/m³ $= \dfrac{0{,}00231}{0{,}012}$

$$= 0{,}19219 \text{ kwh/m}^3 \text{ feed}$$

% water recovery $= \dfrac{11{,}77 \times 100}{12}$

$$= 98{,}08 \text{ %}$$

% Brine volume $= \dfrac{0{,}23 \times 100}{12}$

$$= 1{,}92 \text{ %}$$

Concentration factor $= \dfrac{21\ 981}{992}$

$$= 22{,}16$$

Water yield $= \dfrac{0{,}01177 \text{ m}^3 \times 1\ 440 \text{ min}}{0{,}169 \text{ m}^2 \times 270 \text{ min} \quad d}$

$$= 0{,}369 \text{ m}^3/\text{m}^2 \cdot d$$

(**Note:** membrane area is 169 cm², but there are 10 membrane pairs, therefore total membrane area is 0,169 m²).

Table 2: Electrodialysis concentration/desalination results of an approximately 3 000 mg/ℓ HCl solution with Selemium AAV and CHV membranes at 2 V/cp (16 V/8 cp).

Time min	Current amp	Vo V	Cf M	Cf mg/ℓ	Cb M	Cb mg/ℓ	V-Vo 10 cp	CD mA/cm²	Rcp	Specific resis- tance ohm·cm
0	3,48	1,08	0,091	3318			1,892	20,6	91,9	28
15	3,56	1,65	0,076	2771	1,7	61982	1,835	21,1	87,1	32
30	3,46	1,38	0,067	2463	2,1	76566	1,862	20,5	91,0	35
45	3,18	1,39	0,061	2224	2,2	80212	1,861	18,8	98,9	40
60	2,83	1,32	0,055	2005	2,25	82035	1,868	16,8	112	44
75	2,49	1,21	0,047	1714	2,25	82035	1,879	14,7	128	49
90	2,19	1,20	0,045	1641	2,1	76566	1,880	13,0	145	53
105	1,92	1,23	0,036	1313	2,0	72920	1,877	11,4	165	63
120	1,68	1,27	0,034	1240	1,95	71097	1,874	9,9	189	69
135	1,49	1,28	0,029	1057	1,85	67451	1,872	8,8	212	80
150	1,32	1,32	0,026	948	1,75	63805	1,868	7,8	239	85
165	1,16	1,42	0,022	802	1,65	60159	1,858	6,9	271	99
180	1,03	1,62	0,019	692	1,60	58336	1,838	6,1	302	111
195	0,93	1,86	0,018	656	1,50	54690	1,814	5,5	330	126
210	0,84	1,73	0,017	602	1,40	51044	1,827	5,0	368	139
225	0,75	1,83	0,014	510	1,35	49221	1,812	4,4	409	156
240	0,67	2,13	0,013	474	1,30	47398	1,787	4,0	451	174
255	0,61	2,13	0,012	419	1,2	43752	1,787	3,6	495	193

Linear flow velocity	:	0,87 cm/s
Feed volume (beginning)	:	12 ℓ
Product Volume (end)	:	11,32 ℓ
Brine Volume (end)	:	680 mℓ
Brine molarity	:	1, 9 M

$$\int f(x)\,dx \;=\; 15/2\,(I_1 + 2\,(I_2 + I_3 + \;\; + I_{n-1}) + I_n)$$

$$= 7,5\,(63,09)$$

$$= 473,175 \text{ amp·min}$$

$$= 28390,5 \text{ amp·s (coulombs)}$$

Acid equivalents removed:

Beginning   :   12 ℓ x 3318   mg/ℓ   =   39816 mg

i.e. $\dfrac{39816}{36,46}$ =   1092,05 me

End   :   11,32 ℓ x   419   mg/ℓ   =   4743,08 mg

i.e. $\dfrac{4743,08}{36,46}$ =   130,09 me

∴   me removed   =   1092,05 - 130,09

                     =   961,96 me

                     =   0,96196 ge

Current efficiency (%)   = $\dfrac{96500 \text{ C} \times 0,96196 \text{ ge} \times 100}{\text{ge}}$

                                 $10 \text{ cp} \times 28390,5 \text{ C}$

                           =   32,7 %

Energy Consumption (P)   =   V x I x h

                           = $20 \times \dfrac{473,175}{60}$

                           =   157,725 Wh

                           =   0,157725 kwh

∴ Energy   = $\dfrac{0,157725}{0,012}$
  Consumption/m³

                           =   13,15 kwh/m³ feed

% Water recovery   = $\dfrac{11,32 \times 100}{12}$

                           =   94,3%

% Brine volume   = $\dfrac{0,68 \times 100}{12}$

                           =   5,7 %

Concentration factor $\quad=\quad \dfrac{69274}{3318}$

$\qquad\qquad\qquad\qquad=\quad 20{,}9$

Water yield $\qquad\qquad=\quad \dfrac{0{,}01132 \times 1440}{0{,}169 \times 255}$

$\qquad\qquad\qquad\qquad=\quad 0{,}38\ \text{m}^3/\text{m}^2 \cdot \text{d}$

Rina Winter

From: Jane Zimmerman [jane@siyazisiza.co.za]

Sent: 02 June 2005 11:41

To: Rina Winter

Subject: Contribution of Aquaculture to Rural Livelihoods in South Africa

We would be very pleased to received a copy of **Contribution of Aquaculture to Rural Livelihoods in South Africa.**

With many thanks.

Jane Zimmerman

Executive Director

The Siyazisiza Trust

P.O. Box 67239
Bryanston
2021 South Africa
Telephone: +27 11 883-7407
Facsimile: +27 11 783-8395
Cell: 083 255 6797
Email: jane@pixie.co.za
jane@siyazisiza.co.za

From: Helen Watson [Watsonh@ukzn.ac.za]
Sent: 02 June 2005 11:21
To: Rina Winter
Subject: attention Rina Winter

Dear Rina,

Please will you send me a copy of report NoTT 238/05 and TT234/04 to the address below.

Many Thanks,
Helen

Dr Helen K Watson
Senior Lecturer
School of Environmental Sciences
Memorial Tower Building, Howard College Campus
University of KwaZulu-Natal
King George V Avenue,
Durban, 4041
Phone: 27 31 2601390
Fax: 27 31 2601391
Email: watsonh@ukzn.ac.za

<<<<gwavasig>>>>

NEW FILE

CHAMBER OF MINES RESEARCH ORGANIZATION

Report to the

WATER RESEARCH COMMISSION

on

THE EVALUATION OF SLURRY REVERSE OSMOSIS FOR

THE DESALINATION OF CALCIUM SULPHATE

SCALING MINE SERVICE WATER

by

R W Busby
G J G Juby
W Pulles
S Nel

Contract Report No. WRC 245/1/91

PRETORIA
October 1991

EVALUATION OF SLURRY REVERSE OSMOSIS FOR THE
.DESALINATION OF CALCIUM SULPHATE SCALING MINE
SERVICE WATER

R W BUSBY, G J G JUBY, W PULLES and S NEL

Underground Environment

KEYWORDS: ALGAE   MINE WATERS
                   BIODETERIORATION POTABLE WATER
                   CALCIUM SULPHATE REVERSE OSMOSIS
                   CRYSTAL GROWTH   WASTE WATER
                   DESALTING   WATER POLLUTION
                   EXPENSES   WATER TREATMENT
                   FOULING
                   HYDROCYCLONES
                   MEMBRANES

ACKNOWLEDGEMENT

PREFACE

The gold mining industry buys approximately 500 Ml/day of water from Water Boards for consumption within mines. Because of the ever increasing demands on South Africa's limited water resources and the gradually deteriorating water quality, the cost of high quality Water Board water is increasing steadily.

The use of water for mining results in significant increases in the salt content of the water, making it more corrosive and scale-forming and this in turn increases the maintenance costs of mine water reticulation systems. The most recent estimate for the cost penalty of poor quality service water in the gold mining industry is R300 million per annum. To limit the build-up of salts, up to 440 Ml per day of saline water is discharged from the mines. Some of this water may enter the surface or ground water environment and this practice is becoming increasingly unacceptable to the water authorities and public environmental lobby.

Reverse osmosis has been identified as a suitable technology for the desalination of mine service water. Mine waters may be classified into two categories, namely those which have a scaling potential with respect to calcium sulphate and those which do not. COMRO has, in 1986/87, carried out definitive research and shown that conventional tubular reverse osmosis is viable for the desalination of non-scaling brackish mine water.

This report describes the test work carried out on two alternative Slurry Reverse Osmosis pilot plants treating mine service water at the Hercules shaft of the ERPM gold mine at Boksburg. The mine water at ERPM is classified as "scaling" and it has a high calcium sulphate content. It is shown that, with appropriate pre-treatment, the Slurry Reverse Osmosis plant process is technically and economically viable on this type of mine water and gives a high quality product.

The work is considered definitive and no further test work on the slurry reverse osmosis process using this type of feed water is required. Sufficient data are now available to permit the design of a large scale process. A design and cost estimate has been prepared for a plant to produce 5,78 l/s (500 kl/day) of desalinated mine service water at a recovery of 90 per cent and is available on request as a separate report.

D G WYMER
Director
Underground Environment

SUMMARY

INTRODUCTION

The gold mining industry uses large quantities of water, notably for cooling and dust suppression in deep mining and stoping. Mine service water quality varies significantly from mine to mine, but has generally deteriorated since the Water Boards introduced restrictions during the droughts in the 1980's causing the mines to place more emphasis on recycling and reuse of the water. The latter in turn, has led to an increase in the corrosion and scaling potential of the mine waters.

Although there are no exact figures on the cost of poor quality service water in mines, the most recent estimate is up to R300 million per annum for the gold mining industry as a whole. Recent developments such as the use of hydro-power, as well as possible future implementation of more restrictive legislation on the discharge of waste waters, have highlighted the poor quality of mine service waters currently in use in reticulation systems, and the need for improving their quality in order that they can be reused or safely disposed of.

Mine waters can be broadly classified into two categories, namely those which have a scaling potential with respect to calcium sulphate and those which do not. Approximately 75 per cent of mine service waters are classified as "scaling" and 25 per cent as "non-scaling".

Previous work by COMRO (1987) has demonstrated that conventional reverse osmosis is a viable process for the desalination of "non-scaling" mine water containing a high concentration of sodium chloride.

The slurry reverse osmosis (SPARRO) process is one of the most promising technologies available for the desalination of calcium sulphate scaling mine waters. Previous pilot plant tests carried out by COMRO at ERPM gold mine (1984) have confirmed the technical viability of the process.

The aims of the study were to establish whether or not the seeded slurry process was a technically viable process for the full scale desalination of calcium sulphate scaling mine waters; to establish the product water recovery and salt rejection levels that could be achieved by the process; to establish those pre-treatment techniques which would be required to ensure good plant performance; to establish whether membrane fouling/scaling would occur while treating a mine water with a high calcium sulphate concentration; to evaluate and compare the alternative design features of two variants of the process; to obtain detailed design data; to establish the operating requirements; to prepare a design for a larger plant; and to estimate the capital and operating costs for a plant capable of producing 5,78 ℓ/s of desalinated mine service water.

FINDINGS AND DISCUSSIONS

The SPARRO (Slurry Precipitation and Recycle Reverse Osmosis) and MLT (Membrane Lifetime Test) and the common pre-treatment plant were operated on a continuous basis (24 hours per day), treating scaling mine water from the ERPM gold mine at Boksburg. The MLT plant was similar to that used in the previous COMRO work, while the SPARRO plant incorporated certain novel features. The units were operated from February 1989 to August 1990 for 8 549 hours (MLT) and 5 983 hours (SPARRO).

During 1989 the pre-treatment plant was designed and operated to remove iron and manganese hydroxides which may cause membrane degradation resulting in low salt rejections and low flux. This was accomplished by applying the following pre-treatment: raising the pH to 10 by the addition of caustic soda solution; oxidation of iron and manganese using potassium permanganate; removal of suspended solids and the products of oxidation by flocculation; and then filtration through dual media (sand/anthracite) filters. This special pre-treatment was followed by standard water conditioning for cellulose acetate membranes, i.e. pH adjustment to between five and six, and temperature control to 25 °C.

The performance of both the MLT and SPARRO plants during 1989 was unsatisfactory with membrane degradation which caused a drop in the salt rejection and increased flux. The SPARRO plant had additional problems which included restricted output from the slurry feed pump, difficulties in controlling reactor level, and blockages of the hydrocyclone purge.

The pre-treatment system was modified in December 1989 by discontinuing both the initial pH adjustment to 10 and the addition of potassium permanganate. This meant that no iron and manganese removal was taking place. Chlorination was introduced in November 1989. Operations on both plants were successful during 1990 and all major process problems were overcome. The performance of the membranes on the MLT plant was satisfactory and complied with the manufacturer's design data. The performance of the membranes on the SPARRO plant, though much improved, was inferior to the MLT plant. The SPARRO membranes required cleaning and restoration.

The single slurry feed pump system was found to be superior to the twin pump system in the SPARRO plant in terms of improved reactor level control and increased module life.

Typical values of raw mine water feed and desalinated product water quality are shown in Table 1.

Table 1   TYPICAL* FEED AND PRODUCT WATER QUALITIES FOR MLT AND SPARRO PLANTS

Determinand		Raw Mine	MLT Product	SPARRO Product
pH		4,63	5,1	5,09
Conductivity at 25 °C	(mS/m)	206	55	82
Suspended solids	(mg/ℓ)	54	0	0
Total dissolved solids (TDS)	(mg/ℓ)	2124	388	561
Ca^{2+}	(mg/ℓ)	361	14	17
Na^+	(mg/ℓ)	121	70	102
SO_4^{2-}	(mg/ℓ)	1211	147	244
$C\ell^-$	(mg/ℓ)	50	41	48

* 21st March 1990.

As indicated by Table 1, the product water from the MLT plant was of a high quality (conductivity 72 mS/m) and would be suitable for reuse after a slight upward pH adjustment. The product water is compared in Table 2 with that required for effluent discharge and the SABS maximum allowable limits for drinking water.

Table 2   COMPARISON OF PRODUCT WATER DETERMINANDS WITH STANDARD
EFFLUENT DISCHARGE AND DRINKING WATER REQUIREMENTS

Determinand	SPARRO Product Water	MLT Product Water	General Effluent Discharge Standards	SABS Maximum Allowable Limit
pH	5,09	5,1	5,5 - 9,5	5,5 - 9,5
Conductivity at 25 °C (mS/m)	82	55	Not to be increased by more than 75 mS/m above that of the intake water, i.e. 155 max*	300
Sodium (mg/l)	102	70	Not to be increased by more than 90 mg/l above that of the intake water, i.e. 106 max*	400
Manganese (mg/l)	2,1	1,0	0,4	0,1
Chloride (mg/l)	48	41	Not specified	600
Iron (mg/l)	0,1	0,6	Not specified	1,0
Sulphate (mg/l)	244	147	Not specified	600

*   Intake water refers to water supplied by the Water Board

With regard to discharging the product water to the environment, a slight upward adjustment of pH is required with further treatment to reduce manganese levels. For human consumption of the product water, a slight upward adjustment of pH and a further reduction of manganese is required to meet the SABS maximum allowable limits for chemical quality (health related parameters were not considered in this study).

Operating costs are estimated to be R1,34 c/kl (1990). The costs are made up of the following: membrane replacement (46 %); electricity consumption (34 %); pump maintenance (17 %); pre-treatment (3 %). The membrane cost is based on an estimated lifetime of two years.

The capital cost of a slurry reverse osmosis plant with a capacity of 5,78 l/s (500 kl/day) of product is estimated to be R2,58 million in 1990 terms. The detailed design and cost estimate are presented in a separate report which is available on request.

MAIN CONCLUSIONS

1. The seeded slurry reverse osmosis process was demonstrated to be capable of successfully desalinating calcium sulphate scaling mine water.

2. A module lifetime of at least two years can be achieved if the specified pre-treatment and operating procedures are followed.

3. The single slurry pump system as used in the MLT plant is superior to the twin pump system as used in the SPARRO plant in terms of reactor level control and module performance.

4. It is not necessary to remove iron and manganese in the pre-treatment stage.

5. The capital cost of a plant producing 5,78 ℓ/s (500 kℓ/day) of desalinated, scaling mine water is estimated to be R2,58 million in 1990 terms.

6. The operating costs of a slurry reverse osmosis plant operating on scaling mine water are estimated to be R1,34/kℓ in 1990 terms.

7. The product water produced by the plant was suitable for use in hydro-power systems, for human consumption or for effluent discharge after minor adjustments of certain water quality determinands. For continuous use as domestic water, further consideration would have to be given to health related water quality parameters.

8. It is felt that further pilot plant evaluation of the process in similar scaling water is not required. Data obtained from this study are sufficient to enable realistic operating cost estimates to be made for full scale plants.

CONTENTS

CONTENTS (Continued)

CONTENTS (Continued)

LIST OF TABLES

LIST OF FIGURES

1   INTRODUCTION

The South African gold mining industry circulates 5 500 Mℓ/day of water for mining operations[1]. Water is used for many purposes underground including drilling, dust suppression, sweeping, washing and cooling. The volumes of water recirculated and reused on mines has increased in recent years owing to restrictions imposed by the various Water Boards especially during droughts. Increased recirculation has led to a general increase in the dissolved solids content of the mine service waters, making them potentially more scaling and possibly more corrosive.

The main reasons for considering desalination in the gold mining industry include the following:

.   improving the quality of water in order that it can be cost-effectively reused as service water.

.   improving the quality of water for use in hydro-powered mining systems - where the hydrostatic head of water is used to power machinery underground[2, 3]

.   producing potable water as an alternative to purchasing board water.

.   producing potable water in emergencies when board water is unavailable due to drought

.   protecting water reticulation systems against corrosion and scale formation.

.   improving the quality of water to be discharged to the environment.

Mine waters can be broadly classified into two distinct groups, namely those that have a scaling potential with respect to calcium sulphate and those that do not. The latter are essentially sodium chloride waters and comprise only about 25 per cent of all mine service waters and are found predominantly in the Orange Free State gold fields. Previous work carried out by COMRO at the Beatrix Gold Mining Co. Ltd in 1987 showed that, with appropriate pretreatment, the conventional tubular reverse osmosis process operates well on non-scaling water[4]. Since calcium sulphate is a sparingly soluble salt (2,23 g/ℓ at 0°C), high calcium or sulphate concentration in mine water can lead to scaling problems. Data gathered from two extensive surveys of the service water in gold mines have revealed that about 75 per cent of them would become scaling when concentrated in a desalination process operating at 80 per cent water recovery[5, 6]. At the ERPM gold mine near Boksburg, the mine service water is brackish and is almost saturated with calcium sulphate. Conventional reverse osmosis and electrodialysis reversal processes are not suitable for use with water of this quality. The calcium sulphate slurry precipitation and recycle reverse osmosis (SPARRO) process which has been developed by COMRO has previously been shown in principle[7] and on a small scale to be suitable for the desalination of this type of scaling mine water. Two plants, namely the

0,7 ℓ/s SPARRO plant and the 0,17 ℓ/s Membrane Lifetime Test (MLT) plant, were installed at the ERPM gold mine to evaluate, optimize and develop the process so that it may be applied commercially on a larger scale.

This report describes the design changes, results and experience obtained during the operation of the two desalination pilot plants between February 1989 and August 1990. The common pretreatment section was also extensively modified and optimized during this period, and together with the desalination sections are evaluated in this report. A design and capital costing has been prepared for a larger plant with a capacity of 5,78 ℓ/s (500 kℓ/day) and is available as a separate report.

2   OBJECTIVES

1.   To develop and define the pretreatment process equipment and operating conditions required for the optimum operation of a slurry reverse osmosis desalination system.

2.   To establish the economic lifetime of tubular cellulose acetate membrane modules for desalinating scaling mine water in a seeded slurry mode.

3.   To develop and evaluate the performance and maintenance requirements of the NATIONAL and CROWN high pressure slurry feed pumps.

4.   To compare the twin high pressure feed pump system used in the SPARRO plant with the single pump system in the MLT plant.

5.   To evaluate the effect of contact time between pretreated water and calcium sulphate slurry on the performance of membrane modules.

6.   To evaluate the performance of the "tapered" versus the "straightthrough" module stack.

7.   To develop and evaluate the hydrocyclone system to control purge and suspended solids concentration.

8.   To develop and optimize operating and maintenance procedures.

9.   To establish operating costs.

10. To establish design data to be used in the design of a larger commercial plant.

11. To prepare a design and estimate the capital cost of a pretreatment and slurry reverse osmosis plant to produce 5,78 ℓ/s (500 kℓ/d) of desalinated mine water.

12. To promote the SPARRO process and seek applications within the mining industry.

---

3 SLURRY REVERSE OSMOSIS TECHNOLOGY BACKGROUND

3.1 Principles of Osmosis and Reverse Osmosis

Osmosis is a natural phenomenon involving fluid flow across a semi-permeable membrane. Such membranes are selective in that certain components of a solution, usually the solvent, can pass through them while others, usually the dissolved solids, are retained[8]. In osmosis, water molecules from pure water will pass through a semi-permeable membrane into salty water in order to equalize the salt concentrations on both sides of the membrane, as shown in Figure 1(a). Figure 1(b) shows the dynamic equilibrium established by the movement of the water; water from the pure water source is still passing into the salty water but the pressure differential between the two solutions, brought about by the change in volume, is causing water molecules to flow out of the salty source at the same rate. The differential pressure is known as the osmotic pressure, and it is defined as the externally applied pressure to the salty solution side necessary to establish equilibrium between the two solutions. If the external pressure applied to the salty water side is greater than the osmotic pressure, then water molecules will pass from the salty solution into the pure water side. This phenomenon is known as reverse osmosis (RO) and is illustrated in Figure 2.
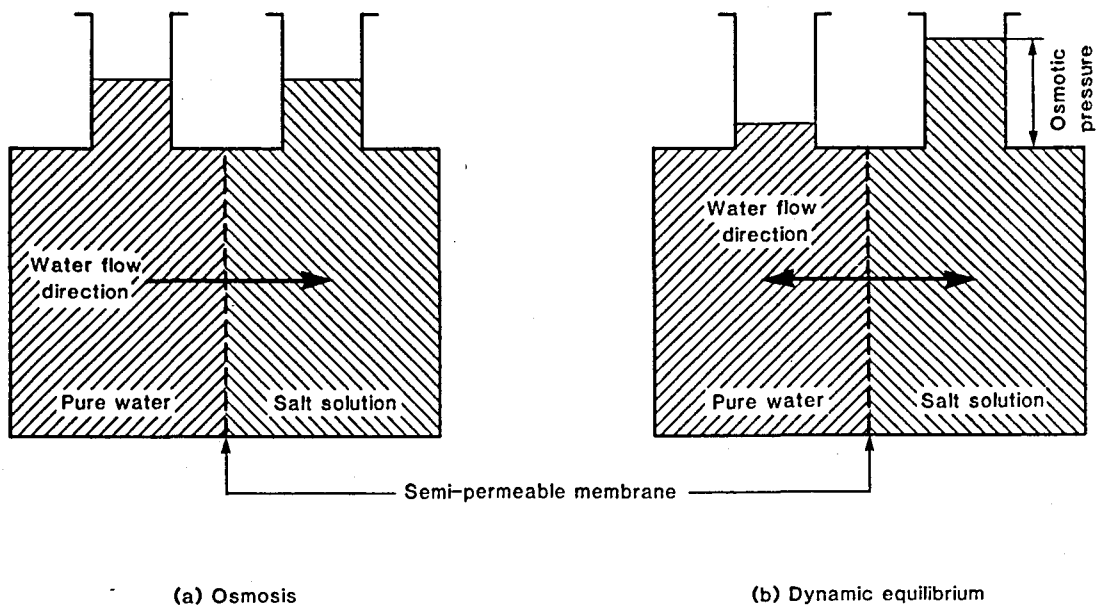

(a) Osmosis   (b) Dynamic equilibrium

Figure 1   PRINCIPLE OF OSMOSIS

PRESSURE VESSEL

FEED
WATER

High
pressure
pump

Salt
solution

Pure
water

Semi-permeable
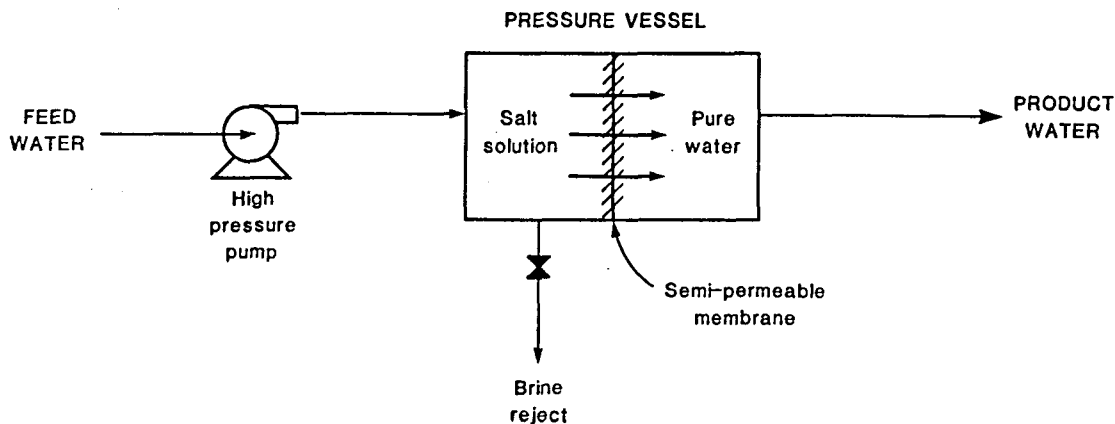membrane

Brine
reject

PRODUCT
WATER

Figure 2   PRINCIPLE OF RO FOR DESALINATION

In the early 1960s, the development of the asymmetric cellulose acetate membrane
permitted RO to become the successful practical process it is today. Currently, there are
three major membranes on the market: cellulose acetate, aromatic polyamide polymer,
and thin-film composite. The latter two membranes can tolerate wide pH variation
(pH 4-11) and are resistant to hydrolysis, but are very sensitive to chlorine degradation.
Cellulose acetate membranes, on the other hand, can tolerate chlorine levels of 0,5 to
1,0 mg/l continuously and 10 mg/l as a shock dose. They are usually used in
conjunction with chlorination to prevent biological attack of the membrane, to which they
are susceptible. Cellulose acetate hydrolyses at high and low pH, and high temperature,
as shown in Figure 3. For this reason the feed water temperature has to be controlled to
less than 30 ° C, and the pH to between 4,0 and 6,0.
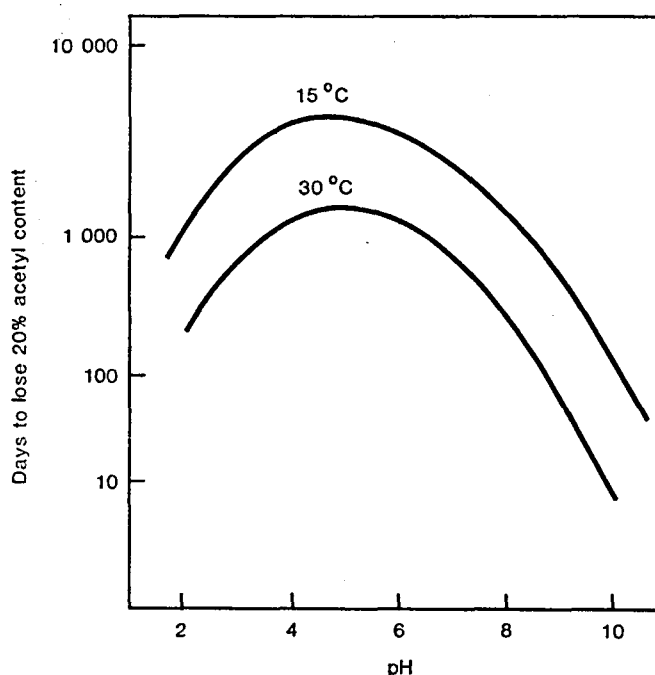
Figure 3   THE EFFECT OF TEMPERATURE AND pH ON THE HYDROLYSIS OF
            CELLULOSE ACETATE

Reverse osmosis membranes have been fabricated in three configurations: namely spiral-wound, hollow-fibre and tubular. As the name suggests, tubular reverse osmosis (TRO) membranes are in the form of tubes. The membrane material itself is coated onto the inside surface of a synthetic porous tube supported to withstand the high operating pressure required for the process (4 000 kPa).

The tubular membrane configuration offers certain advantages over the more conventional membrane arrangements of spiral-wound and hollow-fibre. It can tolerate feed waters with suspended solids, and the tubes facilitate easy cleaning of the membrane, both chemically and mechanically (sponge-ball cleaning). Effectively, this means that they can tolerate a lower degree of feed pretreatment in terms of suspended solids removal, compared to both hollow-fibre and spiral wound which require a high degree of suspended solids removal (i.e. sand filtration followed by cartridge filtration at micron level), which adds to the overall operating cost. Hollow-fibre membranes, and to a certain extent spiral-wound membranes, are difficult to clean chemically and nearly impossible to clean mechanically[9], particularly in situ. Tubular reverse osmosis membrane modules are manufactured in South Africa.

3.2   Principles of Slurry Reverse Osmosis

Conventional reverse osmosis (RO) systems, whether they are of spiral, hollow fibre, or tubular configuration, require feedwaters free from fouling and scaling components. In practice this requirement dictates that the feedwater be free of suspended solids, oils, grease, and colloidal materials such as iron and manganese. Further, the water recovery must be such that the solubility limit of the dissolved salts in the feedwater is not exceeded, in order to preclude the formation of scale on the membrane surfaces.

To date, most applications of reverse osmosis, and membrane desalination processes in general, have been limited to the desalination of relatively uncontaminated feed streams, such as brackish ground and surface waters or sea water. In most of these applications, the production of pure water was the major objective and hence the water recovery was not of prime importance.

Where RO has been used in waste water applications, "pretreatment" of the water feed to the plants has been a major consideration and important cost factor in the design and operation of the system. In many cases the pretreatment requirements have made the use of conventional RO membrane processes uneconomic. Gold mine service waters may be included in this category as they have relatively high concentrations of suspended solids, aluminium, iron, manganese, and silica, as well as significant amounts of oil and grease. In addition, they are in many cases nearly saturated with calcium sulphate, the principal factor which limits the water recovery of the system. For conventional membrane processes to work effectively on these waters, an extensive pretreatment system would be necessary. Suspended solids removal, reduction in iron and manganese concentration, and oil and grease removal would be required. In addition, to obtain a reasonable level of water recovery, chemical softening, using lime and soda ash,

would be required to precipitate calcium and magnesium and reduce silica levels. Pretreatment costs would thus tend to make the treatment of mine service waters by conventional reverse osmosis uneconomic.

The slurry reverse osmosis process was developed to overcome many of the difficulties encountered in the application of conventional RO processes to waste water treatment. The preferential seeding process is illustrated in Figure 4. In the simplest terms, a slurry of "seed" crystals, principally composed of calcium sulphate, is incorporated into the feed water of a tubular reverse osmosis system. These seed crystals then serve as preferential sites for the growth of additional crystals of calcium sulphate, silica and other salts and prevent the formation of scale on the surface of the membrane.

Figure 4 also shows that seed material is recycled from the concentrate to the feed. This seed material is added to the system at start-up. After the initial load is added, no further outside source of seed material is required as the process is self sustaining through the continuous crystallization of calcium sulphate. It should be noted that the total dissolved solids (TDS) of the seed slurry feed to the RO modules is much higher than the mine water feed TDS (as shown by the typical TDS values in Figure 4) because of the calcium sulphate recycle system.

Tubular reverse osmosis systems are required for the SRO process as slurries of 20 000 to 40 000 mg/ℓ solids are circulated continuously in the system. Such concentrations of suspended solids would rapidly result in complete blockage of either spiral or hollow fibre configuration RO modules. These high concentrations of suspended solids are achieved through the use of a hydrocyclone in the concentrate return stream. The fraction of the hydrocyclone-processed stream that is enriched in seed material is returned to the seed recycle tank: the seed depleted stream then becomes the waste and is purged to control the salinity of the system and the overall water recovery. This recycle of seed, plus the fact that SRO systems operate at high water recovery, results in high total suspended solids levels in an operating SRO system. The high recoveries can be achieved on waters saturated with calcium sulphate without producing excessively high osmotic pressures because the calcium sulphate content of the feedwater is precipitated in the seed slurry process.
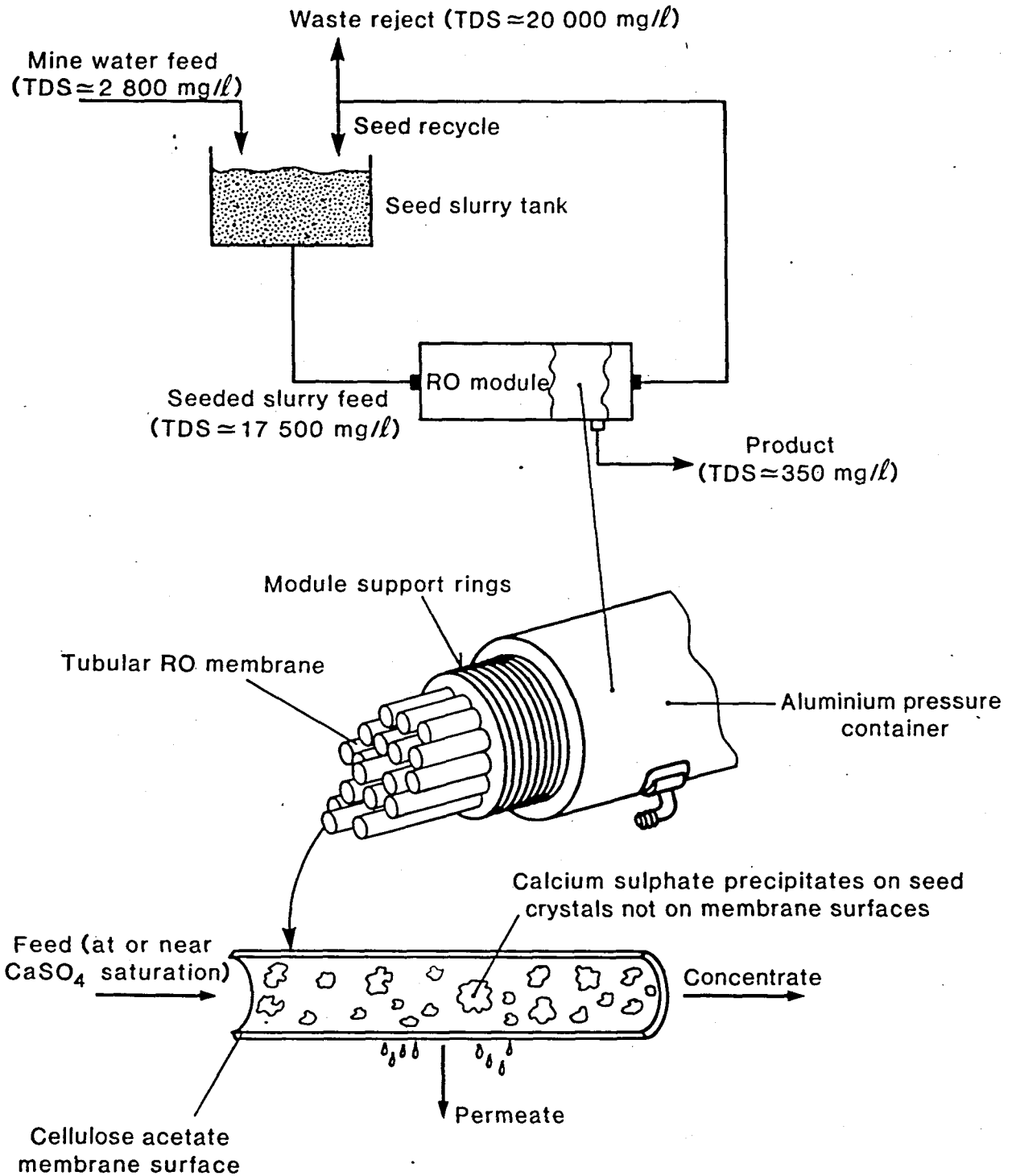
Waste reject (TDS ≈ 20 000 mg/ℓ)

Mine water feed
(TDS ≈ 2 800 mg/ℓ)

Seed recycle

Seed slurry tank

Seeded slurry feed
(TDS ≈ 17 500 mg/ℓ)

RO module

Product
(TDS ≈ 350 mg/ℓ)

Module support rings

Tubular RO membrane

Aluminium pressure
container

Calcium sulphate precipitates on seed
crystals not on membrane surfaces

Feed (at or near
CaSO₄ saturation)

Concentrate

Permeate

Cellulose acetate
membrane surface

Figure 4   SEEDED SLURRY PRECIPITATION REVERSE OSMOSIS PROCESS

3.3 Previous Research By COMRO (1983 -1987)

A feasibility study initiated by COMRO and prepared by Resources Conservation Company International (RCCI)[5] indicated that from technical, practical and economic considerations, the seeded reverse osmosis (SRO) process represents one of the most promising technologies available for the desalination of calcium sulphate scaling mine waters. Small-scale pilot plant tests (0,05 ℓ/s) were undertaken with the process at the East Rand Proprietary Mines (ERPM) by COMRO in 1984 in collaboration with RCCI and the Water Research Commission (WRC). These tests confirmed the technical viability of the process as applied to $CaSO_4$ scaling-type mine service waters[7].

Based on the promising small-scale pilot plant results and the potential wide ranging application possibilities for the process in the South African mining industry, the process was tested on a larger scale. COMRO operated a 0,5 ℓ/s pilot plant supplied by RCCI at ERPM in 1986. Numerous problems were experienced with this unit, with only 600 hours of operation being possible during 1986. The major problems were with the high pressure feed and interstage pumps and rapid failure of the membranes.

3.4 Previous Research By Resources Conservation Company International (RCCI)

The research[10] was carried out over a ten month period by RCCI for the Electric Power Research Institute (EPRI) at an electricity generating station of the Utah Power and Light Company. Power plant waste water treatment systems rarely incorporate membrane processes because the membranes often experience fouling due to inorganic scaling. Although a properly designed and operated pretreatment system can avoid this fouling, the capital and operating costs for the entire system are usually prohibitive. The study included operation at 80 per cent water recovery on cooling tower blowdown, operation at 65 per cent on a flue gas desulphurization thickener overflow feed, and a comparative evaluation of five different tubular cellulose acetate membranes.

Although the membranes showed no signs of fouling from inorganic scaling, they deteriorated rapidly during the first two test phases. The rapid failure was attributed to the presence of hard sharp particles of fly ash. Economic analysis indicated that, under certain circumstances, SRO could be more cost-effective than traditional waste water treatment processes such as brine concentration or conventional reverse osmosis with pretreatment. However, the cost and assumed lifetime of the membranes greatly affect estimates of capital and operating costs. It was concluded that the resolution of membrane fouling and deterioration concerns would permit seeded reverse osmosis to become an important part of integrated water management schemes.

3.5 Patents

Seeded slurry reverse osmosis was conceived and developed by RCCI, then further developed by COMRO. It is a proprietary process which allows high water recovery from scaling waters without the extensive pretreatment normally required for conventional

reverse osmosis systems. The RCCI process is protected by South African patent No. 85/0168 (dated 28 May 1986) which incorporates a previous USA patent No. 4207183 (dated 10 June 1980).

The inventions claimed by COMRO with reference to the SPARRO process are covered by South African patent application No. 89/3746 (dated 16 May 1990).

3.6 Collaborative Agreements

A memorandum of agreement in connection with the development of seeded reverse osmosis technology was signed on 24 June 1988 between COMRO, WRC, ISCOR and MEMBRATEK.

The agreement allocates the rights in respect of inventions and developments as a result of the collaboration during the period January 1988 to August 1990.

3.7 Licences

Under the terms of an agreement between RCCI and Membratek dated 11 September 1987, Membratek was appointed sole and exclusive licensor of RSA patent No. 85/0168 and all relevant proprietary information. The ownershipr of developments covered by RSA patent No. 89/3746 is shared by Membratek, COMRO and the Water Research Commission.

4 DESCRIPTION OF THE PILOT PLANTS AT ERPM (1989/1990)

4.1 Pretreatment (Figure 6)

The common pretreatment plant operates at up to 1,1 ℓ/s to treat the raw mine service water from the ERPM gold mine so that it becomes suitable for the MLT and SPARRO plants which are situated downstream. Some of the equipment and operating procedures were changed between February and December 1989. The first system used during 1989 is shown in Figure 5 and the final modified system which was used in 1990 is shown in Figure 6. The final system is described below and the changes are covered in Section 6.3.

(a) Raw Mine Water Storage. Mine water is pumped to the pretreatment plant during the night shift and is stored in two tanks with capacities of 50 m^3 and 20 m^3 giving a
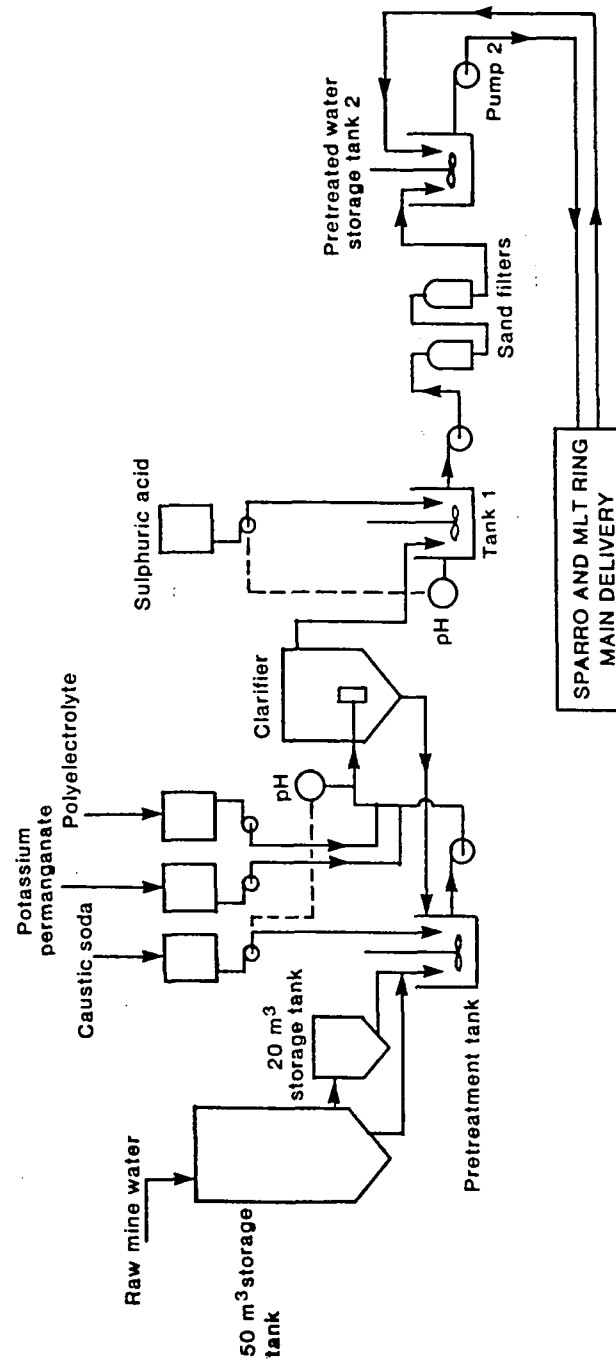
Figure 5   PROCESS FLOW DIAGRAM OF 1,1 ℓ/s PRETREATMENT PLANT BEFORE
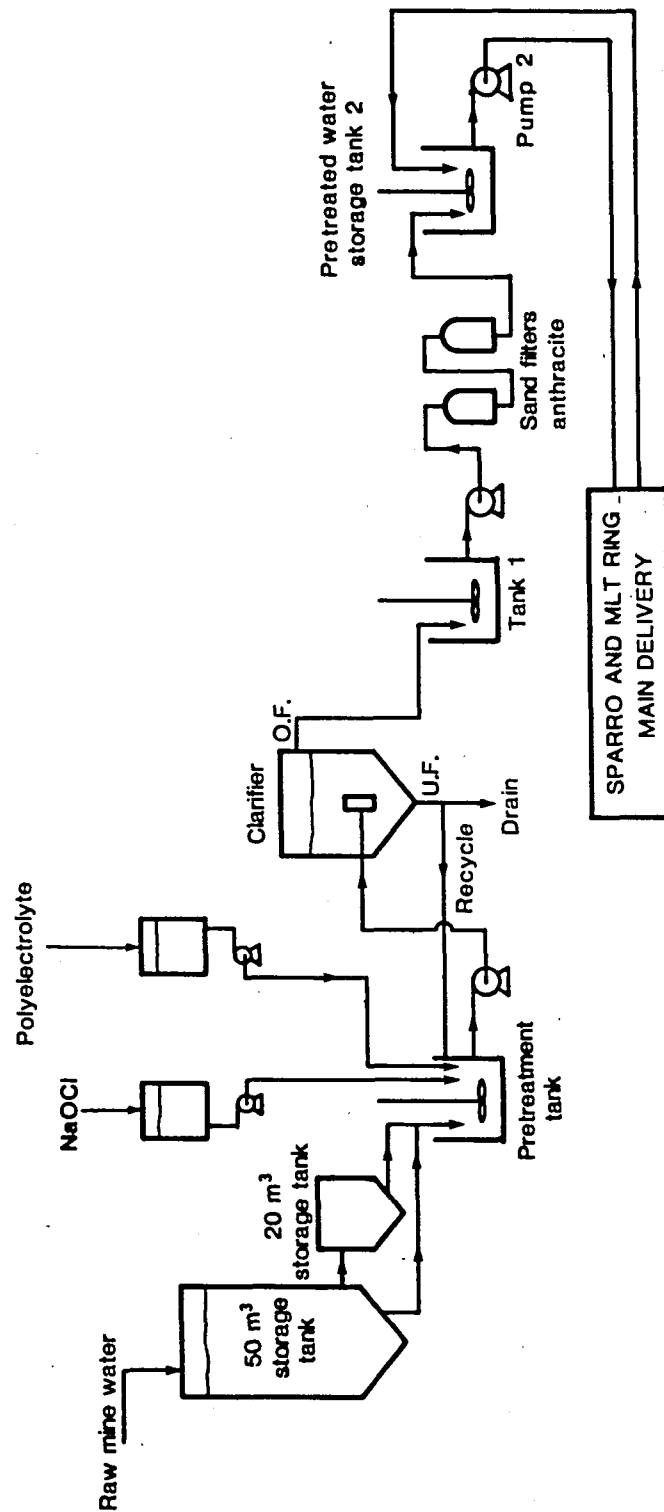MODIFICATION IN 1989 - FIRST SYSTEM

Figure 6   PROCESS FLOW DIAGRAM OF 1,1 ℓ/s (3,96 m^3/h) PRETREATMENT PLANT AFTER MODIFICATION IN 1990 - FINAL SYSTEM

total capacity of 70 m^3 and a reserve of 17 hours. The main 50 m^3 storage tank is made of epoxy painted carbon steel and the auxiliary 20 m^3 tank is constructed of stainless steel to prevent corrosion by the acid mine service water.

(b) Pretreatment Tank. Raw mine water flows by gravity on demand from the storage tanks into the 1,5 m^3 HDPE stirred pretreatment tank. Sodium hypochlorite and polyelectrolyte are added from a multiple head dosing pump. Sludge is recycled from the base of the clarifier which is situated immediately downstream. The polyelectrolyte solution can be added to the discharge line from the clarifier feed pump to prevent floc breakdown.

(c) Clarifier. Water is pumped from the pretreatment tank to the clarifier where the flocs develop and settle. The clarifier is made of GRP and has a diameter of 1 950 mm and a capacity of 6,3 m^3. The nominal upflow rate at a throughput of 1,1 ℓ/s is 1,3 m/h. The clarifier is fed from a central flocculating tube.

(d) pH Adjustment Tank. Clarified water overflows at the periphery of the clarifier and runs by gravity to the pH adjustment tank. The tank, which is made of rubber lined carbon steel, is stirred and has a capacity of 2,1 m^3. Provision is made for the pH to be controlled between pH 4-6 by the addition of caustic soda solution and sulphuric acid. This facility was not used from April to August 1990 as it was found that the pH of the water fed to the MLT and SPARRO plants was nearly always acceptable.

(e) Sand Filters. Water from the pH adjustment tank is pumped through two downflow sand/anthracite filters installed in parallel. The filters are backwashed from the pH adjustment tank once per shift.

(f) Pretreated Water Storage Tank. Filtered water is stored in a mild steel rubber lined tank with a capacity of 2,1 m^3. The tank provides a buffer storage of approximately half an hour when both the MLT and SPARRO plants are running. Water is supplied to the MLT and SPARRO plants by a ring main. The point of delivery for the MLT plant is into the reactor. The point of delivery for the SPARRO plant is into the raw feed water tank upstream of the high pressure mine water (MONO) pump.

4.2   Membrane Lifetime Test (MLT) Plant (Figure 7)

(a) Reactor. Pretreated water is pumped to the reactor on demand to maintain a constant level. The reactor which has a volume of 13 m^3 is made of GRP and is equipped with a central top mounted agitator. The reactor contains a suspension of fine calcium sulphate particles which are formed and grown by the crystallization of calcium sulphate from the supersaturated reject stream which is recirculated from the downstream membrane module bank. The residence time in the reactor is

Figure 7   PROCESS FLOW DIAGRAM OF 0.17 l/s (0.612 m³/h) MLT PLANT

13
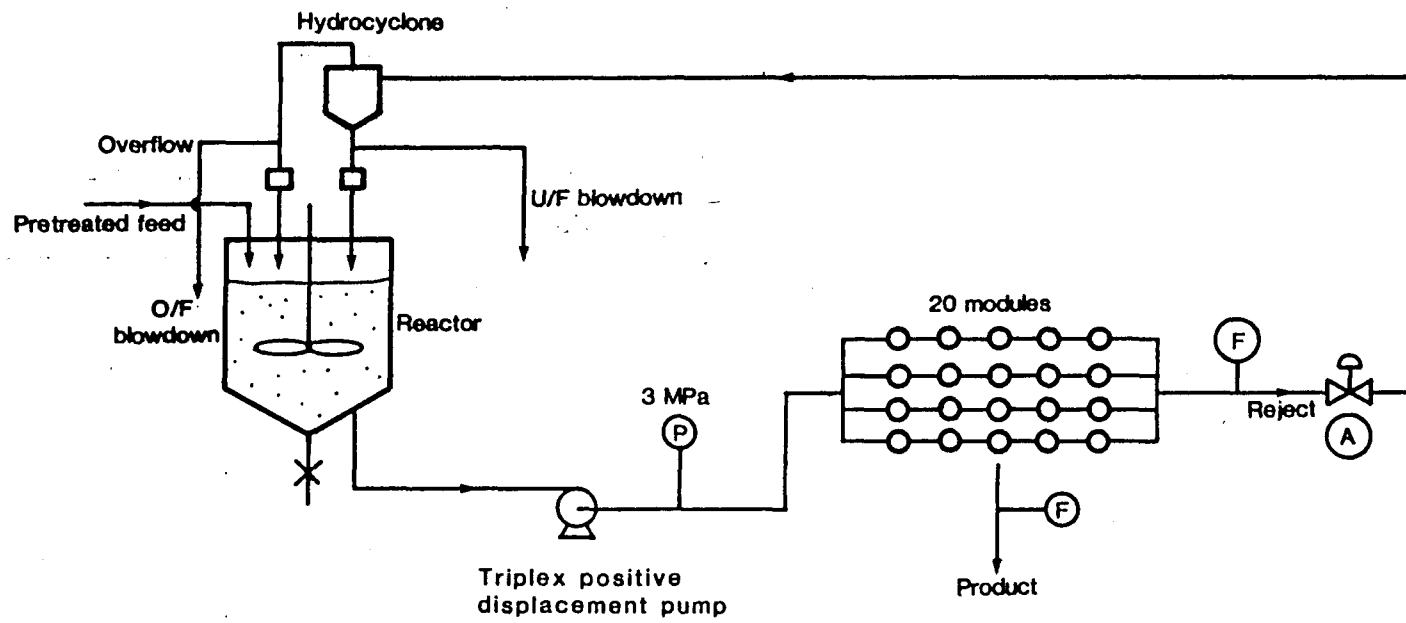
approximately four hours based on the rate at which the suspension is pumped from the bottom of the reactor to the membrane module bank. The target concentration of calcium sulphate is 20 000 - 40 000 mg/ℓ and the minimum level is 10 000 mg/ℓ.

(b) Slurry Feed Pump. The saturated suspension from the reactor is delivered to the membrane bank by the slurry feed pump at a pressure of 3 000 kPa. The pump is a Crown Chrome Plating Co. triplex pump Model 707 with three 38 mm diameter chromium plated plungers and fitted with rubber chevron gland seals. The output of the pump is 0,83 ℓ/s (3 m^3/h) at 243 rev/min.

(c) Membrane Module Bank. The bank is made up from 20 standard Membratek cellulose acetate tubular reverse osmosis modules. The modules are arranged with four passes in parallel and with five modules in series in each pass. The velocity of the suspension as it passes through the tubular membranes is approximately 2 m/s to prevent sedimentation which starts at < 0,5 m/s. The operating pressure of the membranes is limited to 3 000 kPa to prevent membrane compaction. The membranes are protected from over pressurization by the installation of bursting discs which rupture at 5 000 kPa.

The proportion of the total feed water to the bank that is withdrawn as product is termed the "pass conversion". The pass conversion on the MLT membrane bank was limited to 20 per cent to prevent precipitation of calcium sulphate scale on the membrane walls.

(d) Back Pressure Valve. The pressure of the module bank is controlled by a manually adjusted needle valve. A short narrow diameter spool pipe is installed immediately ahead of the valve to reduce the upstream pressure of the valve and prevent cavitation.

(e) Hydrocyclone. A 50 mm (two inch) hydrocyclone is installed on top of the reactor to concentrate the solids in the reject stream. The overflow from the hydrocyclone has a low concentration of solid particles whereas the underflow stream has a higher concentration. Smaller particles tend to enter the overflow stream and larger particles pass into the underflow stream. The efficiency of the hydrocyclone, which is affected inter alia by its dimensions and the flow rate, is characterized by the "d_{50} cut-off", this is the size of a particle in micrometers (10^{-6}m) which has an equal probability (i.e. 50 %) of going into either the overflow or underflow streams.

The underflow and overflow streams are diverted either to the reactor or to the purge drainage system by valves which are actuated by adjustable timers.

The purpose of the hydrocyclone is to:

(i)   Purge, from either the underflow or overflow streams, sufficient water to give the required overall water recovery from the plant, e.g. for a 90 per cent recovery, 10 per cent of the water fed to the plant from the pretreatment section must be purged to drain.

(ii)   Control the concentration of suspended solids, i.e. calcium sulphate seeds, in the reactor and the membrane modules. This is done by preferentially purging from the hydrocyclone overflow, which has a low concentration of suspended solids, and by preferentially recirculating the underflow which has a relatively high proportion of suspended solids. The target concentration of suspended solids is 20 000 - 40 000 mg/l and the minimum level to avoid damage to the membranes is 10 000 mg/l. If the required water recovery were maintained by purging only from the underflow, the level of suspended solids within the system would fall below 10 000 mg/l and the level would need to be maintained by "topping-up" from an external source of calcium sulphate seed.

4.3   <u>SPARRO Plant</u> (Figure 8)

(a)   Raw Water Feed Tank. Water from the pretreatment section is delivered on demand to the raw feed tank. The tank which is constructed of GRP has a buffer storage capacity of 2,6 m^3 which is sufficient for approximately one hours operation.

(b)   Raw Mine Water Pump. Water from the raw water feed tank is delivered to the inlet manifold of the module bank at a pressure of 3 000 to 4 000 kPa. The pump (P1A) is a Mono pump model RO 1000 which delivers 1,11 l/s (4 m^3/h). Since the plant operates in the range 0,55 - 0,69 l/s (2 - 2,5 m^3/h), it is necessary to depressurize and recycle some of the output back to the raw mine water tank to prevent the reactor overflowing when operating the module bank at the required pressure.

(c)   Slurry Recycle Pumps. There are two pumps fitted, P2A is supplied by National Pumps and P2B by Crown Chrome Plating. Since pump P2A has had an availability of less than 10 per cent and was never fully commissioned, only pump P2B is described at this stage. The pump is the same as that fitted on the MLT plant, i.e. a triplex positive displacement pump Model 707 fitted with three chromium plated plungers with all parts in contact with water being non-corrosive. The pump operates at a fixed speed of 295 rev/min and delivers 1,0 l/s (3,6 m^3/h). The pump delivers the suspension of calcium sulphate from the reactor to the inlet manifold of the module bank.

Figure 8   PROCESS FLOW DIAGRAM OF 0.7 ℓ/s (2.52 m³/h) SPARRO PLANT
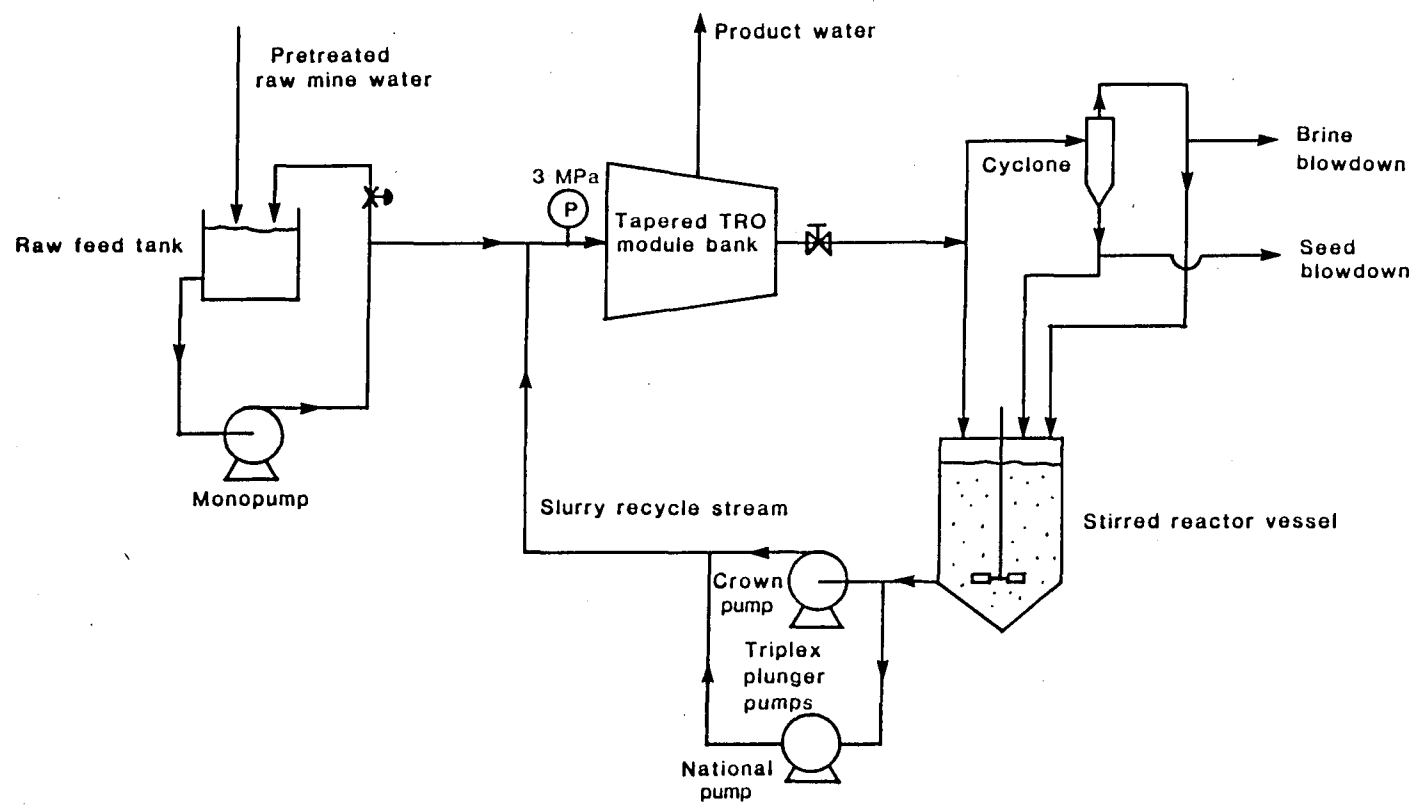
(d) Module Bank. The module bank contains 88 modules arranged in four sub-banks which are arranged in series and separated by manifolds. The first sub-bank contains 30 modules arranged with 10 parallel passes each with three modules in series. The second sub-bank has 24 modules arranged in eight parallel passes each with three modules in series. The third sub-bank has 24 modules in six parallel passes each with four modules in series. The fourth sub-bank has 10 modules in five parallel passes each with two modules in series. The fourth sub-bank was by-passed during 1990 to limit the pass conversion and prevent damage to the modules. The combined deliveries from the raw mine water pump and the slurry recycle pump enter the inlet manifold at a pressure of 3 000 - 4 000 kPa. The pressure is directly affected by the setting of the reject back pressure control valve, by the delivery rate of the raw mine water pump, and indirectly by the condition (flux) of the modules. Product water from each module is fed through a flexible tube into a common tundish. The pass conversion on the SPARRO plant was usually held in the range 35 - 40 per cent which is higher than the level of 20 per cent on the MLT plant.

(e) Reject Back Pressure Valve. The reject stream from the module bank is depressurized and recycled to the hydrocyclone which is installed on top of the reactor. The pressure control valve is remotely controlled from the instrument panel. The pressure in the membranes is actually controlled by the reject flow rate which is controlled by the setting of the valve. The valve is preceded by an orifice plate to reduce the upstream (inlet) pressure of the valve and to prevent cavitation.

(f) Hydrocyclone. The hydrocyclone is a 50 mm diameter Mozely cyclone and is the same as installed on the MLT plant. The function of the hydrocyclone is the same as on the MLT plant but the method of controlling the purge rate is different. The overflow and underflow from the cyclone normally discharge to the reactor. During purging, the two streams are diverted to drain on a time cycle and diverted back to the reactor when a measured quantity of water has been purged. The system is controlled by a Siemens modular programmable controller in the instrument panel.

(g) Reactor. The reactor has a volume of 5 m^3, is made of GRP, and is fitted with an agitator. The reactor only receives the reject stream from the module bank and not the raw mine water feed as is the case on the MLT plant. This means that the pretreated feed water bypasses the reactor and is not in contact with the slurry for four hours as is the case in the MLT plant.

5   PROGRAMME OF WORK

The pretreatment section and the two desalination test units, i.e the MLT and SPARRO plants, were operated from February/March 1989 to August 1990 on service water pumped from the ERPM gold mine.

After the initial commissioning phase which was completed in June 1989, every effort was made to operate all sections continuously. Sufficient operators were seconded from ERPM to cover "round-the-clock" operation on a "seven-day" working week.

As far as possible the plants were operated and monitored under fixed and consistent conditions to check membrane performance in terms of flux and salt rejections.

Equipment and procedures on all sections were compared and evaluated and modifications were made throughout to improve reliability, process control and operating costs. Particular attention was paid to methods of keeping the membrane flux and salt rejection at their specified levels and of extending the projected lifetime of the modules.

Process conditions were logged two or three times per shift and special samples were collected weekly for analysis in the COMRO laboratories. The data and knowledge gained during the several thousands of hours of operation formed the basis for the design and costing of a plant to desalinate 5,78 ℓ/s (500 kℓ/d) of scaling mine water.

6 PRETREATMENT PLANT RESULTS

6.1 Process Availability

An analysis of the availability (i.e. the reliability) of the pretreatment plant and the causes of breakdown is given in Appendix I. The plant was generally reliable and availabilities below 90 per cent occurred only during August and September 1989. The main causes of breakdown were electric failure of the motor and switchgear of the pretreated water delivery pump, the multiple head dosing pump and pH control. An availability of 99,6 per cent was achieved in 1990. The effect of operator absenteeism was overcome in August 1989 by the training of additional operators.

6.2 Operating Conditions

Graphs of process conditions are given in Appendix II.

6.2.1 Raw mine water conductivity (Graphs 1A and 1B)

The conductivity of raw mine water remained steady and was nearly always in the range 150 - 250 mS/m with an average of approximately 225 mS/m during 1989 and 1990. The apparent falls in conductivity in November 1989, between 5 000 and 6 000 hours elapsed time, and in February 1990, between 500 and 1 000 hrs elapsed time, were spurious and due to a faulty conductivity meter.

6.2.2 Clarifier overflow pH (Graphs 2A and 2B)

The specification of the pH of the clarifier overflow during 1989 was 9,5 to 10. During the first 2 000 hours of elapsed time, the control was poor with pH values as high as 12 or as

low as six. The control was significantly improved after 2 000 hours with pH generally in the range 8,5 to 10,5 with occasional excursions below pH of eight. No attempt was made to control the pH of the clarifier overflow after start-up in January 1990 and the pH was effectively governed by the raw mine water. The pH in 1990 was in the range of four to nine with the higher values coinciding with irregular doseage of lime underground.

6.2.3 Filter outlet pH (Graphs 3A and 3B)

The specified pH of the feed to the MLT and SPARRO plants is 5 - 6. During 1989 the pH was in the range 5 - 7 and during 1990, following changes in the process, the pH was slightly lower at 4 - 6. The pH rose to dangerously high levels of 7 - 8 after 1 000 hours in 1989 as a result of malfunctioning of the clarifier pH dosing system.

6.2.4 Filter outlet turbidity (Graphs 4A and 4B)

The specification is less than 1 NTU which is approximately equivalent to 2 mg/ℓ TSS. During the first 2 000 hours this objective was often not achieved. However, subsequent to the upgrading of the clarifier in May 1989, control improved markedly and turbidity was on average less than 1 NTU during the rest of 1989.

The turbidity during 1990 was adversely affected by the lower clarifier efficiency caused by the discontinuation of "two stage" pH control. The turbidity was usually below 3 NTU but numerous peaks of > 5 NTU were recorded as the filters had to remove a higher concentration of suspended solids. This may also be due to the negative effect of low pH on flocculation efficiency.

6.2.5 Chlorination

Chlorination was introduced in November 1989 to prevent the growth of algae in the system and particularly of biofouling on the membranes. The level of chlorine was maintained at 1 - 3 mg/ℓ (total chlorine) by dosing sodium hypochlorite solution containing 14 per cent of available chlorine into the pretreatment tank upstream of the clarifier.

6.2.6 Trace metals

Certain metals including iron, manganese, strontium and aluminium are known to damage cellulose acetate membranes in the conventional reverse osmosis process even when present at a concentration of about 1 mg/ℓ[4].

During 1989 the concentration of these potentially harmful metals was reduced by precipitation of their oxidized hydroxides at pH 10. The effect of "two-stage" and "single-stage" adjustments on the concentration of trace metals which could damage cellulose acetate modules is shown below in Tables 3 and 4.

Table 3   PERFORMANCE DATA FOR PRETREATMENT PLANT WITH TWO-STAGE pH
ADJUSTMENT

Parameter*	28/06/89		06/07/89		03/08/89		31/08/89		20/09/89	
	Feed	Prod	Feed	Prod	Feed	Prod	Feed	Prod	Feed	Prod
pH	4,48	5,61	4,37	5,47	4,57	5,64	4,53	6,28	4,93	4,11
pH (clarifier)	-	9,14	-	-	-	-	-	-	-	10,09
Suspended Solids	63	3	68	3	82	4	37	0	24	2
Iron	0,2	0,1	0,6	0,3	0,3	0,3	0,3	0,3	0,3	0,2
Manganese	5,1	0,2	7,8	0,3	5,2	0,4	4,7	0,2	4,0	0,1
Nickel	5,7	0,8	5,3	0,1	5,1	0,3	0,5	0,5	3,4	0,4
Zinc	1,3	0,2	1,8	0,2	1,9	0,3	1,4	0,2	1,1	0,2
Aluminium	3,1	0,0	2,2	0,4	2,4	1,8	3,8	0,8	3,5	0,2
Strontium	4,8	3,4	3,5	3,4	3,2	3,1	4,6	4,2	3,9	3,1

Table 4   EFFECT OF "TWO-STAGE pH ADJUSTMENT" AND "NO pH ADJUSTMENT"+

Parameter*	Two Stage pH Adjustment		No pH Adjustment	
	Raw Water	Feed Water	Raw Water	Feed Water
pH	4,94	6,17	4,49	4,56
Suspended Solids	16	0,5	95	5
TDS	1973	2034	2026	1991
Sulphate	1198	1101	1214	1188
Calcium	306	322	256	250
Sodium	112	190	111	122
Iron	0,3	0,3	0,7	0,4
Zinc	0,9	0,2	1,8	1,7
Manganese	4,4	0,2	8,9	8,6
Nickel	3,3	0,4	4,9	4,8
Aluminium	1,0	0,5	13,0	12,5

+ Typical values.

* All except pH in units of mg/ℓ.

6.3   Modifications and Plant Development (Figure 5 and 6)

6.3.1   Clarifier. The clarifier was initially incapable of operating at an output of 1,1 ℓ/s without
significant floc carry over. The clarifier was fitted with a single flocculating tube assembly
in May 1989 to permit a higher upward water flow rate[16]. The flocculating efficiency was
improved by the relocation of the neutralizing tank for use as a preseeding tank
immediately upstream of the clarifier. The potassium permanganate and polyelectrolyte
tanks were also relocated nearer to the clarifier and the dosing points moved to the
clarifier feed line. These changes led to a significant improvement but the clarifier still
needed careful attention to prevent carry over of the floc bed. It was intended to install a
continuous turbidity meter on the clarifier overflow to provide warning of clarifier
malfunction but this was not commissioned.

The flocculant was changed from ANIKEM 4816 to MAGNAFLOC 1011 to improve the consistency of the flocs as well as to improve the blow-down. A by-pass was installed to test whether the filters were capable of handling the solids load created by natural suspended solids and the precipitated heavy metals. However, it was found that the filter became overloaded within a short period and that a clarifier was essential.

6.3.2 pH Control

During 1989, the pH of the feed water to the clarifier was raised to pH 10 to precipitate the iron, manganese, and aluminium hydroxides in the clarifier. The adjustment was effected by dosing caustic soda solution into the preseeding tank. The pH of the clarifier overflow was then reduced to pH 5 - 6 by dosing sulphuric acid into the filter feed tank. (Section 6.2.6).

After start-up in January 1990, the pH was no longer adjusted to pH 10 to precipitate the metal hydroxides. The caustic dosing was transferred to the filter feed tank and was readjusted to control the filter feed pH to 5 - 6. The sulphuric acid dosing system was also retained in the filter feed tank to control pH in the range of 5 - 6. After April 7 1990, no attempt was made to control the pH at all and the pH remained within acceptable limits.

6.3.3 Potassium Permanganate Dosing

During 1989, potassium permanganate was dosed into the clarifier feed to oxidize iron, manganese, and aluminium to a higher valency to form an insoluble hydroxide which would precipitate in the clarifier. The dosing of potassium permanganate was discontinued in January 1990 with no negative effect on membrane life.

7 MLT PLANT RESULTS

Graphs of process conditions and derived data are given in Appendix II.

7.1 Process Availability

An analysis of the availability of the MLT plant and of the causes of breakdown is given in Appendix I. If planned shutdowns are allowed for, the availabilities achieved range from 41 per cent to 92 per cent with an average of 76 per cent, while the average availability in 1990 was 82 per cent. The main contributory causes of lost time excluding the pretreatment plant, planned stoppages and operator absences were: slurry feed pump, reject control valve, reactor agitator, and power failures. The slurry feed pump was the main reason for lost time.

7.2   Operating Conditions

7.2.1   Feed water conductivity (Graphs 5A and 5B)

The conductivity of the calcium sulphate slurry feed stream to the membrane module
bank was within the range 1 000 - 2 000 mS/m for the first 1 000 hours of operation. The
conductivity fell to 800 mS/m between 1 000 and 2 000 hours and gradually declined to
400 mS/m by the end of 1989. This was because of the high loss of salinity from the
system in the product stream as a result of low salt rejection of the modules.

The feed conductivity rose in January 1990 after new modules were installed and
fluctuated in the range 500 mS/m to 900 mS/m. The feed conductivity is not directly
controlled but is governed by the water recovery (i.e. purge rate) and by the condition of
the modules (i.e. salt rejection).

7.2.2   Feed water TSS (Graphs 6A and 6B)

The specification of feed suspended solids is 20 000 - 40 000 mg/ℓ with a minimum
concentration of 10 000 mg/ℓ. The TSS concentration is controlled by selective purging
from the hydrocyclone underflow and overflow streams. During 1989 and 1990, the
concentration of calcium sulphate was within the range 10 000 to 40 000 mg/ℓ. The
concentration of TSS fell below 10 000 mg/ℓ on several isolated occasions without
causing noticeable harm to the modules; this was because the concentration of TDS in
the feed had been so diluted by purging with fresh water that the process was not
operating under scaling conditions at these times.

7.2.3   Feed pH (Graphs 7A and 7B)

The specification for the pH of the feed to the module bank is 5 - 6. The control during the
first 1 200 hours in 1989 was poor after which the control was improved within a range of
pH 4 - 7. After the "single-stage" control system was introduced in January 1990, pH
control remained between pH 4 and 7 till April 1990. No control at all was applied
between April and August 1990 and the pH remained steadily in the range 4 - 6.

7.2.4   Product conductivity (Graphs 8A and 8B)

The product conductivity was very low (10 mS/m) at the beginning of the test because
the new membranes still had a high salt rejection, but steadily deteriorated to 80 mS/m by
2 000 hours. The product conductivity rose rapidly at 5 000 hours and remained in the
range 120 - 200 mS/m till the year end. The rise correlates with the rise in flux and drop in
salt rejection due to membrane degradation.

The product conductivity fell sharply following the replacement of half the module bank
with 10 new modules in January 1990 and remained within the range 10 - 100 mS/m. The
main variations in conductivity were due to gradual build-up in feed conductivity, followed

by a sharp drop after purging. The product conductivity is directly governed by the condition of the modules as defined by their "salt-rejection". The performance of the modules during 1990 was much better than in 1989 following changes to the pretreatment system, and improved methods of membrane preservation with formalin during long plant shutdowns.

7.2.5 Salt rejection (Graphs 9A and 9B)

The salt rejection at the beginning of the trials in March 1989 was very high, i.e. about 98 per cent but rapidly deteriorated over the first 2 000 hours to 87 per cent where it remained until 4 000 hours. The rejection fell sharply between 4 000 and 5 500 hours and then stabilized at 60 per cent till 7 000 hours in December 1989. The two sharp falls in rejection at 1 000 hours and 5 000 hours coincided with long plant shutdowns. It is probable that the drop in rejection during these shutdowns was due to algal fouling and inadequate preservation techniques. The introduction of chlorination in November may have prevented further loss of rejection.

Following the replacement of the 10 worst modules with 10 new modules in January 1990, the rejection rose to 90 - 95 per cent and remained fairly constant until the plant was shut down in August 1990 after a further 5 500 hours of operation. The apparent fall in rejection during the first 1 000 hours of operation in 1990 is spurious and is due to a faulty conductivity meter.

The rejection showed no sign of decline during 1990 and there is no reason to suppose that modules would fail because of hydrolysis within two years. This view is supported by Membratek, the suppliers of these modules

7.2.6 Corrected flux (Graphs 10A and 10B)

The membrane flux is corrected for temperature and pressure to the standard conditions of 25 ° C and 4 000 kPa. The manufacturers design flux is 550 ℓ/m^2d at the standard condition.

The flux started at 500 - 600 ℓ/m^2d in 1989, then increased steadily to about 750 $\ell/m^2.d$ and remained approximately at this level from 2 000 to 4 200 hours. The flux then rose sharply at 5 000 hours and restabilized at 900 - 1 000 $\ell/m^2.d$ for the remainder of 1989. The rises in flux exactly coincided with the fall in salt rejection which is a symptom of membrane hydrolysis (Table 13).

The flux remained high in 1990 when 10 new modules were installed, and then gradually declined to a constant level of 500 - 600 $\ell/m^2.d$ from 2 000 to 6 000 hours when the plant was shut down in August 1990. The stability of the flux at the design value of 500 - 600 $\ell/m^2.d$ indicates that the modules were not fouled, hydrolysed, or perforated.

7.2.7 Product water recovery

The average product water recovery during 1989, as estimated by daily spot checks, was 93 per cent. Following the installation of water meters in March 1990, the average water recoveries were as shown in Table 5.

Table 5   <u>MLT PLANT WATER RECOVERY</u>

Month	Water Recovery %	
	Gross	Nett
April 190	95	84
May 1990	93	92
June 1990	92	85
July 1990	98	92
August 1990	93	91
Average	94,2	88,8

The water recovery is defined as:

gross w.r. $= \dfrac{product}{feed} \times 100\ \%$

nett w.r. $= \dfrac{product}{feed + flush} \times 100\ \%$

The nett recovery is lower than the gross recovery because the quantity of water used to flush the modules is included with the quantity of the feed water in the denominator.

7.2.8 Analysis of feed, product, and brine streams

The pretreatment system was re-evaluated in December 1989 and it was decided to discontinue the removal of iron, manganese strontium and aluminium. This decision has been supported by the improved performance of the membranes in 1990.

Typical results for the period May to September 1989 are shown in Table 6. The effect of "high" vs "low" levels of water recovery on the composition of the feed and the product streams is shown in Table 7. The feed water concentration with "low" water recovery is lower than with "high" water recovery.

Table 6   MLT PLANT PERFORMANCE DATA

Parameter	19/05/89			28/06/89			09/08/89			20/09/89		
	Feed	Prod	Brine	Feed	Prod	Brine	Feed	Prod	Brine	Feed	Prod	Brine
pH	5,54	5,73	-	6,23	6,55	6,27	4,82	5,51	5,01	7,32	7,09	7,47
Suspended solids (mg/ℓ)	16 750	1	21 924	20 168	2	26 392	12 983	0	-	9 048	2	-
TDS (mg/ℓ)	8 052	763	9 717	7 014	102	8 542	5 949	532	6 221	3 233	552	3 791
Calcium (mg/ℓ as Ca)	320	5	422	433	7	467	478	20	522	500	63	629
Sodium (mg/ℓ as Na)	1 756	193	2 311	1 000	26	1 130	900	118	1 011	389	87	450
Sulphate (mg/ℓ as SO$_4$)	4 752	343	6 213	3 989	42	4 937	3 150	213	3 622	1 852	222	2 140
Iron (mg/ℓ as Fe)	0,3	0,2	0,6	0,2	0,1	0,2	0,4	0,3	0,4	0,2	0,1	0,2
Zinc (mg/ℓ as Zn)	0,8	0,1	-	1,2	0,1	-	1,1	0,2	-	0,2	0,1	0,2
Manganese (mg/ℓ as Mn)	3,1	0,2	-	8,9	0,1	9,8	3,1	0,2	3,6	0,3	0,1	0,3
Nickel (mg/ℓ as Ni)	2,8	-	-	8,9	-	-	2,7	-	-	0,7	-	-
Aluminium (mg/ℓ as Al)	4,0	0,3	-	1,0	0,0	-	6,0	0,2	-	0,2	0,1	-
Strontium (mg/ℓ as Sr)	17,5	0,8	-	10,3	0,1	-	8,6	0,4	-	11,4	1,1	-

Table 7   PERFORMANCE OF MLT PLANT IN TERMS OF REJECTION OF INDIVIDUAL IONS, pH AND TDS

Parameter*	Low Water Recovery 09/02/90			High Water Recovery 28/03/90		
	Feed	Product	Reject	Feed	Product	Reject
pH	5,04	5,52	5,02	4,62	5,07	4,69
TDS	5141	296	6240	7734	342	9013
Ca	722	19	733	428	16	450
Na	372	39	450	767	77	911
SO$_4$	2841	75	3514	4990	155	5971
Cl	149	28	184	191	17	235
Fe	0,4	0,3	0,4	0,4	0,1	0,4
Mn	9,4	0,3	11,9	27,5	0,7	32,2

* All except pH in units of mg/ℓ.
Low recovery 75 - 85 %
High recovery 85 - 95 %.

7.3   Modifications and Plant Development (Figure 7)

7.3.1   Slurry feed pump

Most of the lost time on the MLT plant was due to breakdown and maintenance of the slurry feed pump. In order to reduce lost time and maintenance costs, various types of plungers and gland packings were evaluated.

The performance of the seals and plungers used in the Crown Chrome Triplex pump is summarized in Table 8. The original CCP rope packing used with the pump was found to have a relatively short lifetime, i.e. about 300 - 400 hours, and required considerable downtime for repacking, i.e. two hours. The pump was modified to accept Chevron seals which have a lifetime of up to 500 hours and can be quickly replaced, limiting downtime to less then one hour.

Three types of plungers were evaluated, i.e. new stainless steel (R180/plunger), chromium plated and stainless steel sleeved. The potential lifetime of each of these types is approximately 1 000 hours. The cost of a rechromed plunger is R70 each, and the cost of resleeving is R60 each (i.e. labour R50 and material R10). The full life of the plungers was not utilized as they were changed prematurely whenever the packings were changed, to avoid damage to the new packings and to minimize the maintenance time and consequent loss of production. The material cost of maintaining the plungers and packings is 22,8c/kℓ. The use of very hard plunger surfaces such as ceramics has not been investigated to date but may be attractive if the packing wear can also be overcome.

The rate of wear of plungers fitted with stainless steel pipe sleeves was compared to that of chromium plated plungers and it was found that chromium wears at almost half the rate of a stainless steel surface.

Table 8   MLT PLANT SLURRY FEED PUMP PLUNGER LIFE

Date	Pump Hours	Plunger Hours	Maintenance
13.10.89	9262	-	Extra packing to plunger 1,3.
16.10.89	9290	1732	Replace plungers 1,3; New CCP (rope) packing.
10.11.89	9797	1088	Replace plunger 2; New chevron seal.
20.11.89	9992	702	Replace plungers 1, 3; Repack with CCP packing.
27.11.89	10124	327	Replace plunger 2; New chevron seal.
09.12.89	10341	-	Extra CCP in 1, 3; New chevron seal in 2.
16.01.90	10544	-	Glands 1, 3 to take chevron seals; Resleeved plungers installed in 1, 2 ,3.
23.01.90	10635	-	Replace chevron seals 1, 2.
12.02.90	11062	518	Resleeved plunger installed in 1, 2, 3,; New chevron seals.
18.03.90	11849	787	Resleeved plungers installed in 1, 2, 3.; New chevron sleeves
04.04.90	12195	346	Rechromed plungers installed in 1, 2, 3.; New chevron seals
30.04.90	12627	432	Resleeved plungers installed in 1, 2, 3.; New chevron seals
13.06.90	13214	587	Pump overhauled, new plungers fitted
20.07.90	13746	532	Changed plungers

7.3.2   Reject pressure control valve

The reject pressure control valve was changed from automatic to manual operation following problems with the control loop in September 1989. The modified system was more stable and easy to operate.

7.3.3 Module bank

The module bank was fitted with 20 new modules in March 1989 at the beginning of the trials. The salt rejection of each module was measured on 25 occasions during the following 18 months of operation and is recorded in Appendix III. The date of installation and removal is also recorded. A summary of the frequency of membrane replacement is given in Table 9.

The performance of the membranes during 1989 was unacceptable as indicated by measurements of salt rejection, product conductivity and membrane flux. Samples of membranes were removed from the stack after 1 000 and 2 000 hours of operation and sent to the University of Stellenbosch Institute for Polymer Science (USIPS) for inspection. The results are shown in Appendix VII and it was concluded that:

.   the membranes appeared to be physically eroded,
.   surface deposits containing mainly aluminium silicate were observed,
.   the membranes appeared to be hydrolysed.

Half of the modules in the bank were replaced in January 1990 as their salt rejections had declined to 50 per cent and the corrected flux had risen. The reasons for the module degradation include hydrolysis and possibly biological fouling.

The situation was much improved during 1990 and the performance of the module bank was acceptable following changes in the pretreatment system.

Table 9   MLT PLANT MEMBRANE REPLACEMENT

POSITION	MEMBRANE REPLACEMENTS																		Total
	'89 Mar.	'89 Apr.	'89 May	'89 June	'89 July	'89 Aug.	'89 Sept.	'89 Oct.	'89 Nov.	'89 Dec.	'90 Jan.	'90 Feb.	'90 Mar.	'90 Apr.	'90 May	'90 Jun.	'90 July	'90 Aug.	
1	1			2							1								4
2	1										1								2
3	1							1											2
4	1										1						1		3
5	1			1				1											3
6	1						.				1	1		1					4
7	1										1								2
8	1									1									2
9	1										1								2
10	1				1										1				3
11	1								1			1							3
12	1								1				1			1			4
13	1								1				1						3
14	1								1			1							3
15	1				1		1		1					2					6
16	1										1	1							3
17	1										1	1	1	1					5
18	2						1												3
19	1	1						1			1								4
20	1									1	1								3
TOTAL	21	1	0	3	2	0	2	3	5	2	10	5	3	4	1	1	1	0	64

During the 18 months of operation of the 20 module stack, a total of 64 modules were used. The reasons for replacement are given below:

Mechanical failure (23). This includes blocking and failure by bursting.

Low salt rejection (15). Modules were replaced in November 1989 (5) and in January 1990 (10). This was as a result of the poor pH control and inadequate preservation procedures in 1989.

Samples for analysis (6). Samples were sent to the University of Stellenbosch Institute for Polymer Science (USIPS) for analysis.

Initial installation	20
Mechanical failure	23
Low salt rejection	15
Samples for USIPS	6
Total	64
Modules in use 31/08/90	20
Modules used in trials	44

Average lifetime of a module before failure by bursting or blocking was 15,6 months (18 x 20/23). The longest operating module in use on 31 August 1990 had been in use for 5 421 plant hours. Production problems which led to mechanical failure of modules were identified and rectified by Membratek.

7.3.4   Hydrocyclone

The hydrocyclone installed on the MLT plant was 50 mm in diameter. The control of the diversion of the overflow and underflow to drain was by automatic timer and the system remained unchanged.
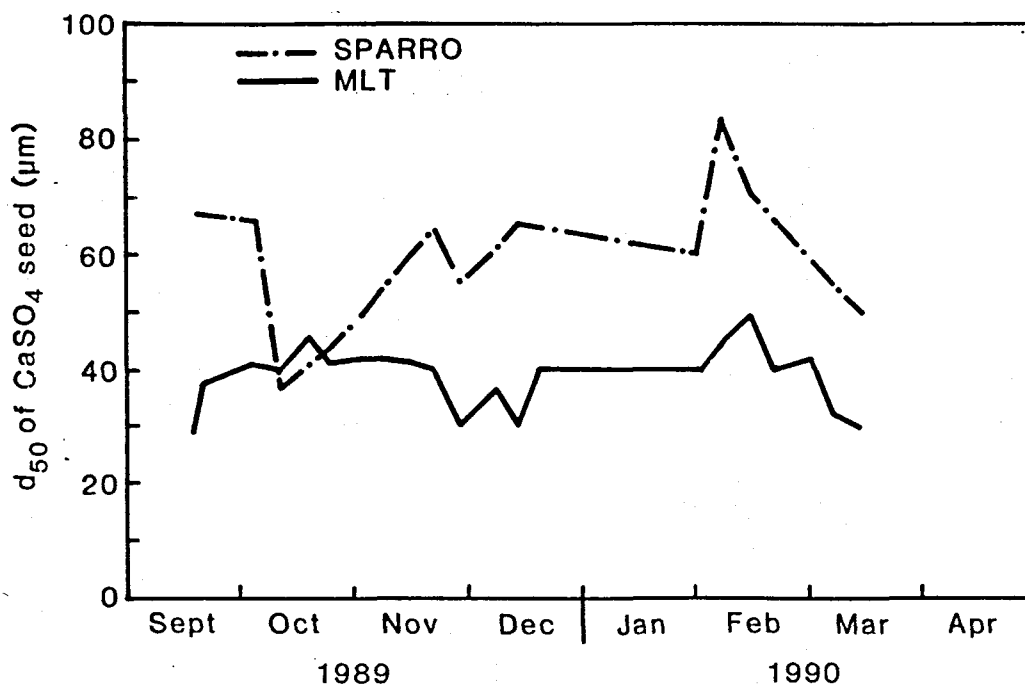
Figure 9   MLT PLANT AND SPARRO PLANT CaSO$_4$ SEED SIZE IN FEED TO

CYCLONE

The size distributions for the particles recirculated in the plant were analysed by COMRO and CSIR[15]. The average size of the seed in the feed to the cyclone as measured by COMRO between September 1989 and March 1990 is given in Figure 9.

Detailed results obtained by COMRO are given in Appendix IV.

A microscope photograph of conditioned seed from the MLT plant is given in Appendix VI.

8   SPARRO PLANT RESULTS

8.1   Process Availability

An analysis of the availability of the SPARRO plant and the causes of breakdown are given in Appendix I.

If planned shutdowns are discounted the availabilities range from 42 to 86 per cent with an average of 67 per cent. The availability in 1990 was 70 per cent. The main reasons for lost time excluding the pretreatment plant, planned stoppages and operator absence were: the slurry recycle pump, module replacement, module cleaning, module renovation, and instrumentation.

8.2   Operating Conditions

8.2.1   Feed water conductivity (Graphs 11A and 11B)

The feed water conductivity remained within the range of 200 and 400 mS/m throughout 1989, except for a brief initial period at 800 mS/m. This low range of values is attributed to the low salt rejection of the modules. The conductivity rose in 1990 and remained in the range 600 - 800 mS/m after the new modules were installed and the size of the module bank was reduced.

8.2.2   Total suspended solids (Graphs 12A and 12B)

The level of suspended solids during 1989 was between 2 000 and 25 000 mg/l. This parameter was difficult to maintain because the low salt rejection and feed conductivity inhibited the growth of calcium sulphate seed particles. It was frequently necessary to boost the seed concentration with surplus seed from the MLT plant and by adding commercial gypsum. The addition of commercial gypsum is not recommended because it blocks the inlet manifold of the slurry delivery pumps.

Following the replacement of the membranes in January 1990 and the adoption of procedures to maintain the efficiency of the modules, the TSS generally remained within the range 10 000 to 50 000 mg/l with an average of approximately 25 000 mg/l. However, on 8 July the seed concentration accidentally fell below 10 000 mg/l and this led to an immediate rise in the flux and a corresponding fall in the salt rejection. This process accident verifies the previously assumed lower concentration limit of 10 000 mg/l for normal operation with saturated feed water. This problem may also have occurred in 1989 but was not detected because of the poor condition of the module bank.

8.2.3   pH of feed (Graphs 13A and 13B)

The pH of the feed remained in the range four to seven with an average of 5,5 during 1989. The pH in 1990 was usually lower and most frequently in the range of 4 - 5. Short peaks of as high as 7 - 8 occurred which corresponded to the use of high pH flush water.

8.2.4   Product water conductivity (Graphs 14A and 14B)

The conductivity started at 100 - 140 mS/m and then rose to 160 - 190 after 3 000 hours when the modules were clearly degraded and exhibiting a low salt rejection. Module degradation is attributed to biofouling, poor pH control, high pass conversion and inadequate preservation during shutdowns (Table 13). Following the installation of 88 new modules in January 1990, the conductivity was initially 80 - 100 mS/m. The conductivity soon started to rise and reached 140 mS/m within 500 hours before the bottom section of the module bank was isolated to reduce the pass conversion. The

conductivity then fell and remained in the range 30 - 100 mS/m during 1990 with an average of approximately 70 mS/m. This level was governed by the salinity of the feed stream and the purge rate.

8.2.5 Salt rejection (Graphs 15A and 15B)

The membranes installed at start up in 1989 were not new. The initial rejection was 80 - 90 per cent but this steadily declined and had reached 50 per cent by the end of the year after 6 500 hours elapsed time due to module degradation (Table 13). The rejection was increased to 80 - 90 per cent after new modules were installed in January 1990, but this fell rapidly to 55 per cent after 500 hours. As a result of the isolation of the fourth section of the module bank, the salt rejection recovered and remained close to 90 per cent until shutdown in August after a further 4 000 hours had elapsed. The rejection dipped by approximately five per cent after 5 000 hours as a result of a brief period of operation with a TSS of less than 10 000 mg/ℓ. The modules were renovated and the rejection rose to 90 per cent and remained at that value till the end of the trials at 5 000 hours. The renovation procedure is discussed in Appendix VII.

8.2.6 Corrected Flux (Graphs 16A and 16B)

The flux increased to 1 000 ℓ/m^2.d during the first 2 000 hours and then to 1 300 ℓ/m^2.d after 4 000 hours, and stayed at this value till the end of 1989 (6 000 hours).

The high flux, which is approximately double the design value of 500 - 600 ℓ/m^2.d, shows that the modules had been degraded and coincides with the low salt rejection values during this period (Table 13). Following the replacement of the module bank in January 1990, the flux rose rapidly and erratically from 800 to 1 000 ℓ/m^2.d after 500 hours. When the fourth bottom bank of the modules was isolated, the flux fell immediately to 550 ℓ/m^2.d, indicating that the damaged modules were all in the bottom bank. The flux declined from 500 ℓ/m^2.d in April to 300 ℓ/m^2.d in June 1990 because of fouling. After the modules were cleaned with Biotex (1 %) and citric acid (2 %) the flux rose to 400 ℓ/m^2.d on 14 June. The flux declined again to 300 ℓ/m^2.d on 7 July when the seed concentration fell below 10 000 mg/ℓ. The flux then rose to 380 ℓ/m^2.d on 12 July and 420 ℓ/m^2.d on 16 July. After renovation, the plant was restarted on 10 August and the flux was 450 ℓ/m^2.d which fell to 350 ℓ/m^2.d on 16 August and remained steady at this level till shutdown on 31 August.

The SPARRO plant appears more susceptible to membrane fouling than the MLT plant, probably as a result of the foulants not being removed from the feed by contact with calcium sulphate seed in the reactor.

8.2.7 Product water recovery

The product water recovery was estimated by regular comparison of the purge rate with the plant feed rate during 1989 and up to May 1990 as no water meters were installed. Monitoring of the water recovery started in June 1990 and was delayed by difficulties in installing the water meter in the product line.

The results of the spot checks and the more accurate metered measurements show that the nett water recovery on the SPARRO plant was between 93 and 97 per cent.

8.2.8 Analysis of feed, product and brine streams

Typical analyses of the composition of the feed, product and brine streams are shown in Table 10. As stated in Section 7.2.8, the concentration of iron, manganese, strontium and aluminium was not considered to be so important in 1990 following the discontinuation of the "two-stage" pH adjustment system.

The effect of high feed salinity at high water recovery vs low feed salinity at low feed salinity is shown in Table 11.

Table 10 SPARRO PLANT PERFORMANCE DATA

Parameter	21/06/89			11/07/89			23/08/89			22/09/89		
	Feed	Prod	Brine	Feed	Prod	Brine	Feed	Prod	Brine	Feed	Prod	Brine
pH	6,39	6,46	6,77	6,48	6,25	6,79	5,83	5,85	5,83	7,32	7,31	7,35
Suspended solids (mg/ℓ)	12 040	0	21 438	9 400	0	16 290	9 767	0	16 638	13 496	1	32 746
TDS (mg/ℓ)	4 355	1 253	6 107	4 352	1 398	5 738	3 605	1 800	4 502	3 314	1 804	3 851
Calcium (mg/ℓ as Ca)	458	100	440	461	72	467	544	206	556	489	200	544
Sodium (mg/ℓ as Na)	542	158	829	683	311	994	433	256	578	406	227	556
Sulphate (mg/ℓ as SO$_4$)	2 354	643	3 436	2 373	788	3 220	1 975	869	2 500	1 864	1 017	2 246
Iron (mg/ℓ as Fe)	0,2	0,1	0,2	0,3	0,3	0,4	0,3	0,2	0,4	0,3	0,3	0,3
Zinc (mg/ℓ as Zn)	0,5	0,3	0,6	0,4	0,3	0,5	0,3	0,2	0,4	0,6	0,2	0,3
Manganese (mg/ℓ as Mn)	0,8	0,3	1,1	0,7	0,2	1,1	0,5	0,2	0,9	0,2	0,1	0,2
Nickel (mg/ℓ as Ni)	0,5	-	0,7	0,4	-	0,8	0,5	-	1,0	0,5	-	0,5
Aluminium (mg/ℓ as Al)	1,4	0,4	1,1	2,7	0,0	0,0	1,5	0,5	2,7	1,5	0,0	0,0
Strontium (mg/ℓ as Sr)	7,2	1,5	10,2	8,4	2,7	13,0	6,1	2,5	7,9	7,0	3,3	9,8

Table 11   PERFORMANCE OF SPARRO PLANT IN TERMS OF REJECTION OF
INDIVIDUAL IONS, pH AND TDS

Parameter*	Low Water Recovery 07/03/90			High Water Recovery 28/03/90		
	Feed	Product	Reject	Feed	Product	Reject
pH	4,44	4,96	4,44	5,35	5,45	5,23
TDS	5370	299	5660	11229	599	17255
Ca	511	17	656	433	19	422
Na	389	57	378	911	113	1411
SO$_4$	3500	131	3568	7853	278	12001
Cl	132	27	175	101	46	357
Fe	0,3	0,2	0,2	0,3	0,2	0,4
Mn	26	0,9	23	47	1,7	66

* All units in mg/ℓ except pH.
Low water recovery 90 - 95%
High water recovery 95 - 99%

8.3   Modifications and Plant Developments (Figure 8)

8.3.1   Mine water pumps P1

The two multi-stage centrifugal pumps (ex ISCOR SRO plant) which were initially fitted were mechanically unreliable and difficulties were experienced in obtaining replacements from the USA for the badly eroded impellers. The two pumps were replaced with a locally supplied Mono pump (Model RO-100) which is specially designed for reverse osmosis applications and constructed of a corrosion resisting steel. The Mono pump (P1A) proved very reliable and required only 74 hours of maintenance between June 1989 and August 1990, which gives an availability of over 99 per cent. The cause of the breakdown was due to the failure of the process instrument air supply which caused a restriction in the supply of water to the suction of the Mono pump.

8.3.2   Slurry recycle pumps

The slurry recycle pumps were the cause of most of the lost time. The National pump P2A was unreliable throughout, while the Crown Chrome pump (P2B) exhibited prolonged uninterrupted operation during the final six months of the trials in 1990. The initial problems experienced with the Crown pump P2B were inexplicable because an identical pump was operating well on the MLT plant in the same duty. The problems experienced are listed below.

. Air locking. The problem was manifested by a gradual loss of output after several hours of normal operation. The immediate problem was relieved by removing and cleaning the suction sieves, removing the valve covers and flushing out the air bubbles with water.

. Slow pick-up to full delivery rate. The pump took up to one hour to reach full output and the National pump P2A took longer. The problem was probably due to the presence of air bubbles in the cylinders.

. Pressure pulsations. This led to bursting disc failures.

. Gland packing maintenance. The time required for replacement of the rope packings was two hours.

. Blockage of inlet manifold. The inlet manifolds of the pumps were frequently blocked with settled calcium sulphate seed.

The following remedial actions were taken:

a. National Pump P2A. The pump operated well in only one month - October 1989 - when the Crown pump glands were being modified to take "chevron" seals. The pump was serviced in November 1989 by the suppliers and the glands modified to take PTFE (Teflon) packings. The pump was used again in February 1990 and could not achieve the required output. The valve seats were then reground by COMRO and the pump put back into use. The pump operated for only 44 hours before it was taken out of service again. The pump was overhauled again by the suppliers, but was only available for use in September 1990 after the SPARRO plant trials had been completed and therefore could not be re-evaluated in situ.

b. Crown Pump P2B.

   (i)   The output of the pump was uprated by 21 per cent from 0,85 ℓ/s to 1,01 ℓ/s by increasing the speed from 243 to 295 rev/min. Although this was done primarily to increase the feed rate to the membrane bank it may have been beneficial in the prevention of manifold blockages.

   (ii) The "rope" packings used in the gland seals were replaced by rubber "chevron" seals in October 1989. This reduced the time required for gland maintenance to less than one hour in 500 hours.

   (iii) The inlet manifold was drained each shift to prevent the accumulation of calcium sulphate seed which could restrict the feed of slurry to the pump.

c. Instrument Air Pressure. The diaphragm valve between the reactor and the Crown pump P2B was held open by the pressure of the instrument air supplied by ERPM gold mine. The pressure of the air must be 500 kPa to fully open the valve. It was observed that the air pressure frequently fell below 300 kPa, especially at night. The partial closure of the valve increases the hydraulic resistance between the pump suction and the reactor and reduces the NPSH (net positive suction head) below the

required 1 m (w.g). This could cause the ingress of air into the pump and the observed loss of output. The problem was overcome by replacing the unreliable mine air supply with bottled nitrogen gas.

d.   Suction Valve. The valve at the suction of the Crown pump was found to be defective and to have an air leak in the diaphragm which restricted the degree of opening. This was replaced.

e.   Addition of Gypsum Seed. The addition of gypsum seed to the reactor to boost the level of suspended solids was frequently carried out in 1989 because of the poor seed growth conditions, and was occasionally carried out in 1990 following excessive purging. It was observed that this was usually followed within several hours by a loss in output from the pump. The reason is that the large and irregular crystalline particles settle out quickly and form a stiff paste in the inlet sieves and inlet manifold. The use of commercial gypsum has been discontinued. A microscope photograph of coarse gypsum is shown in Appendix VI.

f.   Reactor Level. It was observed that if the level in the reactor fell below 1 m from the top, then the output of the pump fell. The reactor level was therefore maintained as high as possible without overflowing.

g.   Alternative Plungers/Packings. The lifetime of the plungers and packings in the Crown pump are shown in Table 12. The results were consistent with those given in Table 5 for the MLT plant. It appears that chromium plated plungers are the most cost-effective.

Table 12   SPARRO PLANT SLURRY FEED PUMP PLUNGER LIFE

Date	Pump Hours	Plunger Hours	Maintenance
09-11-89	988	-	Modified to use chevron seals, new plungers 1, 2, 3
09-12-89	1498	-	Replace chevron seals 1, 2, 3
16-02-90	1810	822	Replace chevron seals 1, 2, 3 replace plungers 1, 2, 3
02-03-90	1902	92	Fit sleeved plungers and packing 1, 2, 3
07-03-90	1996	-	Replace faulty plungers (not round) and chevron seals
31-03-90	2350	448	Replace plungers & packing 1, 2, 3 with hard chromed plungers
30-04-90	2779	429	Replace plungers & chevron seals (plungers - resleeved)
14-05-90	3033	254	Replaced plungers & chevron seals
18-05-90	3115	82	Replaced plungers 2, 3 & chevron seals 2, 3
25-05-90	3272	1 2 (239) (157)	Replaced plunger 1, 2 chevron seals 1, 2
05-06-90	3382	267	Replace plunger 3 chevron seal 3
20-06-90	3653	1 2 3 (381) (381) (271)	Replace plungers 1, 2, 3 chevron seals 1, 2, 3
02-07-90	3921	268	Replace plunger 3 chevron seal 3
09-07-90	4064	411	Replace plunger 2 chevron seal 2, 3
10-08-90	4231	578	Replace plunger 1 chevron seal 1
17-08-90	4356	-	Replace chevron seal 3
30-08-90	4628	-	Plant shutdown

8.3.3   Module bank

The initial 88 modules installed on the SPARRO plant in February 1989 were not all new as some of them had been used previously by ISCOR. As described in Section 8.2.4 and 8.2.5, the membranes degraded within the first 2 000 hours of elapsed time. It was decided, however, to leave the modules in to gain operating experience with the various novel design features of the SPARRO plant. It was also anticipated that the causes of membrane degradation would be identified and rectified. Following the changes to the pretreatment section, the introduction of chlorination in November 1989 and the adoption of improved module preservation procedures, a completely new set of 88 membranes was installed in January 1990. The modules were operating in the tapered four bank mode when the plant was restarted on 27 January as shown below.

Sub-bank	Position	Modules in		Total
		Parallel	Series	
1	Top inlet	10	3	30
2	Upper middle	8	3	24
3	Lower middle	6	4	24
4	Bottom outlet	5	2	10
Total				88

It became apparent within the first 1 000 hours that the modules in the fourth sub-bank (Nos 79 to 88) were showing a rapid loss in salt rejection and an increase in flux. This caused the product water quality to deteriorate. Microscopic inspection of the membranes showed perforation and crystal growth in the membranes. Microscopic photographs of the affected modules are given in Appendix V. The damage was attributed to the development of an excessively high degree of calcium sulphate supersaturation at the end of the module stack in sub-bank 4. The level of calcium sulphate supersaturation is affected inter-alia by the pass conversion of the module bank. The value of pass conversion adopted in the design of the SPARRO plant was 50 per cent, with a minimum value of 40 per cent based on previous pilot plant work. The actual value of the pass conversion during initial operation may have been as high as 60 per cent because of the high flux. The level recommended by Resources Conservation Company International (RCCI) based on work carried out for the Electric Power Research Institute (EPRI) was 30 - 40 per cent[10].

The pass conversion was reduced by removing the damaged bottom sub-bank of 10 modules and by increasing the output of the slurry delivery pump P2B from 0,85 l/s to 1,0 l/s. The reduction in module area of 11 per cent caused the product rate to fall to 0,69 l/s and the output of the pump rose from 0,85 l/s to 1,0 l/s. The combined effects of the changes caused a reduction in pass conversion to 40 per cent. The pass conversion gradually declined from February as the modules became fouled, and the product rate fell, and by April the pass conversion had reached 30 per cent.

The tapered stack performed reasonably well, but it was apparent that there were some distribution problems at the end of the inlet manifold as modules 10, 20, 30 became blocked twice in the first 1 500 hours of 1990.

The overall size of the module bank was reduced from 88 to 78 by isolating the 10 modules in the bottom sub-bank in February 1990. The isolation of modules 10, 20 and 30 in March 1990 further reduced the size to 75. As a result of a shortage of membranes in August, six more membrane positions were isolated which reduced the size to 69.

The main problem with the SPARRO module bank in 1990 was the decline in the corrected flux from 600 to 300 l/m^2.d in June. This is in contrast to the MLT plant where the flux stabilized at the design value of 500 - 600 l/m^2.d. The modules were cleaned in June with Biotex and citric acid solutions to remove organic and inorganic foulants.

The procedures for the cleaning of modules which were provided by Membratek are included in a separate report on the design of a 500 kℓ/day SPARRO plant. It is estimated that cleaning would be required every 500 hours to maintain an acceptable flux. This is probably a result of fouling of the membranes by colloidal material which has passed through the filter and which has not been absorbed by the seed particles as is thought to be the case on the MLT plant. The provision of an adequate contact period between pretreated water and the agitated slurry is an important design feature which is discussed in Sections 9 and 10.

As a result of the minor damage suffered by the module bank on 7 July 1990 when the concentration of seed fell below 10 000 mg/ℓ, it was decided to evaluate the membrane renovation procedures which had been developed by the University of Stellenbosch Institute for Polymer Research[11]. The principle of the restoration procedure is to lay a thin film of new polymer above the damaged membrane. The film is formed by the separate addition of polyvinyl methyl ether (PVME) and tannic acid in a series of controlled pH steps as described in detail in the separate design report.

A summary of common causes of membrane damage is shown below in Table 13.

Table 13   SUMMARY OF COMMON CAUSES OF MEMBRANE DAMAGE

	Symptoms	Cause	Restoration Procedures
Case I	1. Lower product water flow rate 2. Higher salt rejection	Membrane compaction accelerated by operating pressure greater than 3 450 kPa.	None. Requires element replacement when product water flow rate reaches an unacceptable level.
Case II	1. Higher product water flow rate 2. Lower salt rejection	Membrane hydrolysis 1. pH outside operating limits 2. Bacteria degradation 3. Temperature outside operating limits.	Injection of PVME and tannin or element replacement.
Case III	1. Lower product water flow rate 2. Lower salt rejection	Membrane fouling.	Element cleaning.
Case IV	1. Lower product water flow rate 2. High ΔP 3. High operating pressure	Membrane fouling.	Element cleaning.

The inlet pressure to the modules on the SPARRO plant was usually in the range 3 500 - 4 500 kPa, which may have contributed to module compaction.

8.3.4   Hydrocylone

A set of six 10 mm diameter hydrocyclones was initially installed. It was found that the walls of the cyclones were quickly worn by abrasive calcium sulphate seed. The underflow from the cyclones was sticky and dense which caused blockages. The set of

six was replaced by a single 25 mm hydrocyclone during commissioning. An attempt was made to predict the particle size distribution of the underflow and overflow streams using a computer model developed by COMRO and based on empirical cyclone modelling technology[12], but the results showed a marked variance from prediction.

The 25 mm hydrocyclone was replaced in March 1990 with a 50 mm hydrocyclone which was identical to that installed on the MLT plant. The pump blocking problem was overcome in March 1990 but it is unlikely that this was because of the new cyclone. As a result of the installation of water meters and the more accurate determination of the water recovery rate, the operation of the hydrocyclone at a water recovery of below 96 per cent was found to be impossible because of restrictions in the pipework and valves of the purge discharge system.

8.3.5 Reactor

The level control of the SPARRO plant reactor was troublesome throughout the trials. If the level rises then the reactor may overflow and the slurry may even become diluted below the lower concentration limit of 10 000 mg/ℓ. If the level falls, then the available suction head to the slurry recycle pumps falls below the 1 m(wg) required and the output falls, and this may also cause air bubbles to be drawn into the cylinders.

The level in the reactor is not automatically controlled as in the MLT plant. It is inherently unstable and requires frequent operator attention to adjust the process variables which maintain a constant level. The operator had to control the level by adjustment of the raw mine water feed rate from pump P1A, and the reactor pressure by adjustment of the reject control valve. If the reactor level fell, then the reactor pressure was in turn affected by the lower recycle slurry rate. The level of the reactor on the MLT plant is automatically controlled at one level -"full"- by a float valve which admits water on demand.

The main concern in the design of the reactor was that the residence time and the agitation should be sufficient for the supersaturated slurry to reach equilibrium before it was recycled to the membranes. The required time to dissipate supersaturation was estimated to be several minutes by plotting the decline of slurry conductivity in the reject stream from the module bank. This is less than the required residence time of one hour predicted from fundamental research into the kinetics of calcium sulphate precipitation carried out by the CSIR in 1988[14].

Measurements of seed concentration profiles in the reactor taken during December 1989 showed some maldistribution and this was rectified by installing an additional impeller in the middle of the agitator shaft.

8.3.6 Reject control valve

The original method of controlling the slurry flow rate through the membrane stack was indirect by adjusting the reject flow rate to control the inlet pressure. This proved

impractical and led to difficulties in controlling the level of the reactor. The reject flow control valve was disconnected from the reactor pressure loop and was then controlled directly to give the required flow rate. The reject flow rate, the recycle slurry feed rate, the raw mine water feed rate, the condition of the membranes, and the temperature of the water interact to control the product water rate, the membrane pressure and the reactor level.

9   PROCESS EVALUATION AND DISCUSSION

The evaluation of the process is focused on the primary objectives listed in Section 2. Both economic and non-economic criteria are taken into account, e.g.

a.   economic factors:
- membrane lifetime
- electric power consumption
- maintenance costs.

b.   non economic factors:
- process availability/reliability
- control
- flexibility.

Particular attention is paid to the comparison of the orthodox design of the MLT plant with the novel features included in the SPARRO plant. These include the twin pump delivery system, the tapered module bank and the hydrocyclone system.

9.1   Pretreatment Plant

It is necessary to pretreat the water to protect the membranes in the MLT and SPARRO plants by removing materials and conditions potentially harmful to the RO process such as:

- remove materials to prevent scaling and fouling
- adjust pH
- reduce temperature
- remove turbidity/suspended solids
- disinfect to prevent biological growth.

9.1.1   Removal of iron and manganese

During the previous work[7] by COMRO, no attempt was made to remove iron or to prevent it fouling the modules in the form of iron hydroxide. It was later suggested that the module life could be extended by removal of iron and other possible contaminants such as manganese, aluminium and strontium. Although it is claimed that the slurry

reverse osmosis process does not need the removal of iron and manganese, it was decided to remove them as this had proved beneficial in tests carried out with conventional RO on non-scaling mine water[4].

When the module salt rejection fell and the flux climbed during 1989 it was thought that this may possibly be due to the inadequate removal of iron, manganese or other unspecified trace metals. The removal of iron and manganese hydroxides was achieved by raising the raw mine water pH to 10 by the addition of caustic soda solution, together with addition of potassium permanganate to oxidise the metals.

It is evident, in the light of the acceptable performance of the modules during 1990, that the precipitation of hydroxides is not necessary. As well as being unnecessary, the removal of hydroxides at pH 10 in the clarifier is a potential hazard to the membranes, because the contents of the reactor could run through the membranes in the event of a failure of the second downstream stage of the pH adjustment and a clarifier malfunction. The cost of the two-stage adjustment process, i.e. from pH 5 to pH 10 and back to pH 5, in terms of caustic soda and sulphuric acid solution, is R0,16/kℓ which is an unnecessary expense.

9.1.2 Final pH

The target pH quoted by the suppliers of the membranes, Membratek, is pH 5 - 6. Examination of the cellulose acetate hydrolysis curve (Figure 3) shows that a range of pH 4 - 6 is also acceptable. The reason for quoting a range of 5 - 6 is to minimize the cost of reducing pH in alkaline water and does not imply that water with a pH 4 will damage the membranes.

The pH control system proved troublesome throughout the trials and it was dispensed with in April 1990. The problem was mainly due to the sensitivity and fragility of the probes rather than to the design of the system. It is therefore essential that the pH of the pretreated water be checked twice per shift by a laboratory pH meter which should be standardized regularly.

9.1.3 Temperature

The upper limit of temperature is 30 ° C and this did not cause any problems during the trials. The temperature can be reduced by the installation of a cooling tower in the pretreated water holding tank. The effect of heat addition through the dissipation of power in the high pressure slurry delivery pumps must be taken into account.

9.1.4 Removal of suspended solids

It has been claimed that it is not necessary to remove suspended solids at the pretreatment stage, because 20 000 mg/ℓ of calcium sulphate is present in the feed to the membranes. However, it must be appreciated that the nature of the quartzitic suspended

solids in raw mine water or other possible feed may be particularly harmful. It is reported by RCCI[10] that the presence of fly-ash is very damaging and that its removal was necessary to preserve membrane efficiency. It is also possible that abrasive solids could damage the high pressure pumps.

9.1.5 Disinfection

Reverse osmosis modules provide a large surface area for the attachment and growth of bacterial slimes and moulds. These organisms may cause membrane fouling or even module plugging. There is also some evidence that occasionally the enzyme systems of some organisms will attack the cellulose acetate membrane. The continuous application of chlorine to produce a 1 to 2 mg/ℓ chlorine residual will help inhibit or retard the growth of most of the organisms encountered. However, caution must be exercised since continuous exposure of the membrane to higher chlorine residuals will impair membrane efficiency. Shock concentrations of up to 10 mg/ℓ of chlorine may be applied from time to time.

The absence of chlorination between February and November 1989 was almost certainly a major reason for the poor performance of the modules in that period. Chlorination can be achieved by dosing sodium hypochlorite solution or by injecting chlorine gas. Chlorine gas is the more economic choice for large installations.

9.2 Membrane Life

The performance of the tubular cellulose acetate membranes is the key factor in the technical and economic viability of the process. The performance and projected lifetime of the modules are measured in terms of the salt rejections (based on the feed to the modules not to the plant) and of the corrected flux. Membranes require replacement after either mechanical failure, or when the salt rejection falls below a set level, e.g. 80 per cent, or the corrected flux falls below a set level e.g. 400 ℓ/m^2.d. The performance of the MLT module bank during 1990 indicates that a lifetime of at least two years (17 520 hours) is realistic provided that they are operated steadily and not mechanically damaged by blockage or bursting. Modules are guaranteed against rapid mechanical failure and will be replaced by the manufacturers.

The performance of the membranes in the SPARRO plant was not as good as in the MLT plant, mainly as a result of the fouling which occurred. The fouling is probably a result of the presence of fine solid particles and other foulants which may have passed through the pretreatment plant and which have not been removed by prolonged contact with calcium sulphate seed particles in the reactor. This is a major disadvantage of the SPARRO plant relative to the MLT plant. Nevertheless, the modules in the SPARRO plant configuration probably could achieve a lifetime of two years subject to a regular monthly cleaning with citric acid and Biotex solutions. Provisions for the periodic cleaning of the reverse

osmosis elements are included in the system design. This makes it possible to clean impurities off the membrane surface and restore normal flow rates in situ without removing the membranes from the stack.

The operating pressure has a bearing on the membrane life (Table 13). If the pressure exceeds 3 000 kPa then irreversible membrane compaction will occur. This probably contributed to the relatively inferior performance of the SPARRO plant in 1990 where the inlet pressure was usually in the range 3 500 - 4 500 kPa as the significance of the pressure was not appreciated.

Mechanical failure of the modules by blocking or by over-pressurization will probably not reduce the average module lifetime below two years on a commercial unit if the module bank is properly designed to prevent sedimentation and bypassing. It will be necessary to seek specialist advice on the design of the manifolds[13].

9.3   Tapered Module Stack

There are a number of aspects that need to be considered when considering the module configuration:

. tapered (SPARRO) versus straight through (MLT)
. manifolding
. minimum velocity
. number of modules
. pass conversion.

The major disadvantages of the straight through (rectangular) system is that there is a reduction in linear velocity through the tube bundle, and thus a high velocity is required at the inlet to achieve a required velocity in the last modules. The claimed advantages of a tapered system were:

. the linear velocity is maintained through the tube bundle which allows for a lower inlet velocity and the achievement of a high pass conversion.

. in the last part of the system where the greatest concentration is taking place there are fewer modules exposed to the higher feed salinity and therefore the overall product water quality should be better.

. the ability to increase the velocity of the brine in the last section of the taper reduces the risk of concentration polarization influencing the module performance. A more gradual pressure drop gives better overall fluxes.

With the setting of the maximum pass conversion at 30 per cent, the main advantage of the tapered module configuration is reduced. This is illustrated in the design prepared in separate design report where the inlet velocity of 2,3 m/s declines to only 1,7 m/s at the outlet in a stack containing seven modules in series and 10 modules in parallel.

Large module banks present piping and manifolding problems when dealing with a slurry. For this reason it was decided to design the pilot plant manifold to be similar to that of an anticipated full scale unit in order to assess its effectiveness. The module manifolds did not allow for smooth changes in velocities and were complicated by the need for intermediate manifolds and valves to give the required tapering. The inlet manifold design was not optimal[13] and probably contributed to the repeated blockage of modules 10, 20, and 30. The MLT stack which had five modules in series without intermediate manifolds and valves was less troublesome and could probably be extrapolated to seven modules as in the proposed design.

9.4   High Pressure Slurry Feed Pumps

a.   MLT. The CROWN CHROME triplex pump model 707 gave good service throughout. Most of the maintenance was for routine replacement of plungers and packing. Three different types of plunger were evaluated and it was found that rechromed surfaces were superior in wear resistance to either stainless steel sleeves, or new stainless steel. The potential lifetime of a chromed plunger is up to 1 000 hours and the replacement time is one hour. The pumps were modified to take rubberized chevron seals instead of the original rope packing. The normal lifetime of a chevron seal is 500 hours and the time to change a seal is one hour.

The optimum maintenance procedure is to change seals when they fail and to change the plungers only after 500 hours use except if they are obviously worn. The practice of changing plungers whenever seals are changed is wasteful.

b.   SPARRO. Compared with the MLT plant, the two high pressure slurry pumps were very troublesome. However, after several plant modifications, the CROWN CHROME triplex pump model 707 gave satisfactory service in 1990. The most important points to be considered are the provision of an adequate suction head from the reactor and the prevention of calcium sulphate seed blockages in the inlet manifold.

The NATIONAL triplex pump was never truly commissioned. Although it ran well in October 1989 this performance was never repeated. The absence of a reliable stand-by pump caused a significant loss in availability. While the NATIONAL pump may have been rectified by the final overhaul, it cannot be recommended at this stage.

9.5   "Twin" Versus "Single" High Pressure Feed Pumps

The twin pump system is the main difference between the two plants. The advantages claimed were:

.   maintenance costs would be reduced because a proportion of the water pressurised to 3 000 kPa would be clean and not a slurry.

.   the salinity of the combined stream at the manifold inlet could be reduced below saturation if the pretreated water was unsaturated.

.   capital costs could be reduced on large plants as large scale multi-stage centrifugal pumps have a lower specific cost than positive displacement pumps.

It is true that the MONO pump ran reliably (> 99 per cent availability) on clear water and that the centrifugal pumps would probably also have done if they had been repaired. However, these claimed advantages are negated by two much more significant disadvantages.

a.   Reactor level control

The twin pump system makes the control of the reactor level on the SPARRO plant inherently unstable, and complicates the control of the membrane pressure. These difficulties would be magnified on a large multiple unit.

The single pump system simplifies reactor level control, is reliable and is recommended for use in the design given in the separate design report.

b.   Contact between pretreated water and seed

During simultaneous "back-to-back" operation of the MLT and SPARRO plants in 1990 with the same feed water, it was found that the membrane bank in the MLT plant performed better than in the SPARRO plant. The MLT plant ran for several months without any appreciable deviation from the equilibrium flux rate of 550 l/m^2.d, whereas the SPARRO plant showed flux decline which is a sign of membrane fouling (Table 13) and would probably require cleaning on a monthly basis. The variation in the performance of the two pilot plants is attributed to the different durations of the contact time between the pretreated water and the stirred suspension before it reaches the modules. The residence time in the MLT plant was four hours whereas it was less than one minute in the SPARRO plant. This is because the pretreated water is injected by a second high pressure pump immediately upstream of the modules in the SPARRO plant instead of into the reactor. It is probable that colloidal material and other potential foulants present in

the pretreated water are removed by prolonged contact with the fine suspension of calcium sulphate particles and that they become incorporated during the process by crystallization, coprecipitation and aggregation.

The single pump system is recommended, thereby nullifying one of the claimed major advantages of the SPARRO process, i.e. reduced pumping costs as a result of the larger portion of the feed water (minewater) being pumped with a low cost pump.

The required duration of the contact between the pretreated water and seed cannot be defined on the basis of present knowledge. Four hours appears to be sufficient whereas one minute is evidently insufficient. This is a key parameter in the design of the reactor and is discussed below in Section 9.6.

9.6   Reactor

The reactor has four purposes:

.   to induce and complete the crystallization and desupersaturation of calcium sulphate in the reject stream from the membranes

.   to remove fine colloidal material and other potential foulants from the pretreated water stream thereby preventing membrane fouling. This is effectively the final stage of pretreatment

.   to provide a constant and adequate suction head for the slurry feed pumps (P2)

.   to act as a buffer storage.

The volume of the reactor in the SPARRO plant was sized[14] to provide one hour of residence time to complete the desupersaturation of the reject stream from the module bank. Conductivity measurements of the reject stream from the modules indicate that equilibrium is reached within several minutes and measurements taken from the recycled slurry show that desupersaturation has occurred.

As stated above (9.5), the required contact time to remove colloidal material is less than four hours. It is assumed that a residence time of one hour will be sufficient in the design of a large-scale plant.

The slurry feed pumps require a positive suction head to prevent air locks developing in the cylinders. If the level of the suspension in the reactor is maintained at 100 per cent full by admitting water on demand, then a head difference of 5 m will be adequate.

The provision of buffer storage will be met when the other criteria are met.

9.7   Hydrocyclone

The performance of the 50 mm hydrocyclone on the MLT plant was acceptable. The water recovery could be controlled between 80 - 100 per cent by manual adjustment of the timers which divert the overflow and underflow streams either to drain or back to the reactor.

Three different hydrocyclones were installed on the SPARRO plant in 1989 - 1990 and even then the system was not satisfactory. The purpose of the design was to produce a stream high in suspended solids to make the independent discharge of seed and brine possible. Unfortunately the initial choice of a 10 mm hydrocyclone bank gave a sticky and dense underflow which caused blockages which prevented gypsum blow down. The situation was improved by the installation of a 25 mm then a 50 mm diameter hydrocyclone. The computer controlled volume measuring system was probably more sophisticated then was required. The pipework around the hydrocyclones was undersized and this made it difficult to achieve a water recovery of less than 96 per cent without excessive loss of seed which upset the calcium sulphate balance. Experience on the MLT plant shows that the hydrocyclone system can work satisfactorily but the valves and pipework must be adequately sized.

10   DESIGN OF 5,78 ℓ/s SPARRO PLANT

A detailed design and costing of a 5,78 ℓ/s (500 kℓ/day) SPARRO plant was prepared. A summary of the basic design data used is given below and more detailed information is given in a separate desing report which is available on request.

10.1   Pretreatment

Quality of product water		
pH		4 - 6
Temperature (max)	°C	25
Suspended solids (max)	mg/ℓ	1
Turbidity (max)	NTU	1
Total chlorine (max)	mg/ℓ	3

10.2   Reactors

Seed concentration	mg/ℓ	20 - 40 000
Seed concentration (min)	mg/ℓ	10 000
Residence time	h	1

10.3   Hydrocyclones

Water recovery	%	80 - 99
Seed size (ave)	micron	50

10.4 Slurry Feed Pumps

Plunger life	h	500 - 1 000
Seal life (ave)	h	500

10.5 Membrane Banks

Slurry velocity (ave)	m/s	2
Slurry velocity (min)	m/s	1
Flux (at 25 ° C, 4 000 kPa)	ℓ/m^2.d	500 - 600
Salt rejection (m/m)	%	95
Operating pressure (max)	kPa	3 000
Pass conversion (max)	%	30
Module area (each)	m^2	1,75
Membrane life (min)	y	2

10.6 Operating Procedures

Preliminary operating procedures and membrane cleaning and renovating procedures are included in the design report.

11 COSTS

11.1 Operating Costs

Table 14   SPARRO PLANT OPERATING COSTS (1990)

Item	Unit Cost	Useage	Cost
Floc	1,5 g/kℓ	8 R/kg	1,2
Hypo	0,034 ℓ/k	0,88 R/kg	3,0
Elec.	5 kWh/kℓ	0,091 R/kWh	45,5
Plungers*	3/500 h	R79 each	18,2
Seals *	3/500 h	R19 each	4,6
Membranes	2 years	R300 each	<u>62,0</u>
			134,5 c/kℓ

* It is assumed in this cost estimate that the plungers and seals are changed
   simultaneously after 500 hours of use.

11.2 Capital Costs

Table 15 SPARRO PLANT (5,78 ℓ/s) CAPITAL COST ESTIMATE SUMMARY (1990)

	Item	R000's
1.	Civil Work	151,2
2.	Process equipment	1 296,48
3.	Structural steelwork	33,7
4.	Piping and valves	170,04
5.	Electric power, wiring and distribution	28,9
6.	Instruments	142,52
7.	Painting	30,0
8.	Engineering assembly	300,0
	Total	2 152,8
	Contingency (20 %)	430,56
	Total	2 583,36

*   Plant is designed for a 20 year life.

12 FURTHER RESEARCH

While it is considered that the design given in the separate design report is realistic and viable, certain areas require optimization. This may be carried out when a commercial plant is constructed, by application of work done on other projects (e.g. by ESCOM), or by small scale laboratory studies. The areas of future research are in the following fields:

a.   Reactor

The required contact time between the seed slurry and pretreated water has not been quantified. It is known that four hours is sufficient but this may be excessive. The type of reactions which occur in the reactor and their kinetics need to be determined.

b.   Manifolding

The delivery of slurry from a single pump to a number of separate module banks and the detailed design of the inlet manifolds require further attention. Problems of this kind have been experienced by ESCOM and the University of Natal have expertise in this field[13].

c. Hydrocyclone

A laboratory scale evaluation of various sizes of hydrocyclone operating with calcium sulphate slurries would provide valuable information. The behaviour of the cyclone could be correlated with a computer model[12]. This work does not need to be carried out on an operating plant.

13   POTENTIAL FOR APPLICATION

The most likely areas of application at this stage appear to be in the field of effluent treatment. Possible applications are in gold mining, coal mining, electricity generation, petroleum refining and the steel industry.

The widespread use of slurry reverse osmosis in the gold mining industry as a means of generating potable water or as a means of upgrading service water for hydro-power is unlikely in the near future.

14   CONCLUSIONS

1. The slurry reverse osmosis desalination process is technically viable for use with calcium sulphate scaling mine water.

2. In order to maintain an acceptable membrane life, mine water must be pretreated to pH 4 - 6, temperature < 25 °C, total suspended solids < 1 mg/l, and chlorinated.

3. It is not necessary to remove iron and manganese in the pretreatment stage.

4. A membrane life of at least two years is predicted provided specified operating procedures are maintained.

5. The corrected membrane flux on the MLT plant, at equilibrium, correlated closely with the predicted manufacturer's design value of 0,0064 l/m^2.s (550 l/m^2.d) at 25 °C and 4 000 kPa.

6. The membrane flux on the SPARRO plant declined below the design value, probably because of membrane degradation. It could be restored by cleaning with citric acid and Biotex solution to give a membrane life of two years.

7. The straight-through module bank (MLT) is preferred to the tapered bank, at the lower pass conversion of 30 per cent.

8. The single slurry feed pump system (MLT) is superior to the twin feed pump system (SPARRO) in terms of reactor level control, and membrane fouling.

9. The Crown Chrome triplex pump performed satisfactorily as a slurry feed pump.

10. A water recovery of 85 - 95 per cent was achieved.

11. A salt rejection of 90 - 95 per cent (wrt feed) and 75 per cent (overall) was achieved.

12. The product water was suitable for human consumption with respect to salinity.

13. The operating cost of a slurry reverse osmosis desalination plant is estimated to be R1,35/kℓ excluding capital charges (1990).

14. The capital cost of a slurry reverse osmosis plant to produce 5,78 ℓ/s (500 kℓ/d) at a water recovery of 90 per cent is estimated to be R2,58 million in 1990 terms, as designed for a 20 year life.

15   REFERENCES

1. Personal communication, W Pulles, COMRO 1990.

2. JOUGHIN, N.C. A system for providing mechanical and cooling power in deep mining, 13 CMMI Conference, Singapore, 1986.

3. MIDDLETON, N.T., VILJOEN, A. and WYMER, D.G. Hydro-power and its implications for the distribution and use of energy in mines : Symposium on Mine Water Systems, Mine Ventilation Society of S A, 6 - 8 March, 1985.

4. JUBY, G.J.G. and PULLES, W. Evaluation of tubular reverse osmosis for the desalination of brackish mine water. COMRO Reference Report, 1991.

5. RESOURCES CONSERVATION CO. INTERNATIONAL (RCCI). The development of an integrated mine service water treatment system, May 1985, Contract report submitted to COMRO.

6. COMRO, Survey of service water quality on ten gold mines, 1988 - 1989, Restricted Report in preparation.

7. HARRIES, R.C. A feasibility study of the use of seeded reverse osmosis to desalinate mine water. COMRO Research Report 50/84, August 1984.

8. APPLEGATE, L.E. Membrane Separation Processes, Chemical Engineering, June 1984.

9. SCHUTTE, C.F. Desalination : A South African Perspective, Water Research Commission, September 1983.

10. RESOURCES CONSERVATION CO. INTERNATIONAL (RCCI). Field demonstration of waste water concentration by seeded reverse osmosis. Electric Power Research Institute (EPRI), Project No. 2114-7, August 1988.

11. Personal communication. E. Jacobs. University of Stellenbosch IPS, 1990.

12. FLINTOFF, B.C. A mathematical model of the hydrocyclone classifier. CIM Bulletin, December 1976.

13. Personal communication. C. Buckley, University of Natal, 1990.

14. MAREE, J.P., WINTER, C.T. and ROBERTSON, P. Crystallization kinetics of calcium sulphate. CSIR, February 1988.

15. STREETER, J.H. Shape characteristics, specific surface area, and chemical composition of calcium sulphate. CSIR, September 1989.

16. PULLES, W., LUDWIG, J. and HAYWARD, B. Development and evaluation of a high rate settling process for the treatment of mine water. 5th World Filtration Congress, Nice, France, June 5-8 1990.

17. BUSBY, R.W., PULLES, W. and NEL, S. Design and costing of a 5,78 ℓ/s (500 kℓ/day) SPARRO seeded reverse osmosis plant for ERPM gold mine. COMRO Restricted Report No. 19/91, May 1991.

APPENDIX I   <u>ANALYSIS OF PRETREATMENT, MLT, AND SPARRO PLANTS</u>
<u>AVAILABILITIES FROM JULY 1989 TO AUGUST 1990</u>

APPENDIX I

<u>ANALYSIS OF MLT AND SPARRO PLANT AVAILABILITIES JULY 1989 TO AUGUST 1990</u>

<u>SUMMARY OF MLT PLANT OPERATING TIMES AND AVAILABILITIES</u>

MLT		Plant Run	Shutdown		Max Possible	Availability
			Not Planned	Planned		
		hrs	hrs	hrs	hrs	%
March	1989	Comm			744	Comm
April	1989	Comm			720	Comm
May	1989	Comm			744	Comm
June	1989	Comm			720	Comm
July	1989	656	88	0	744	88
August	1989	360	384	0	744	48
September	1989	207	297	216	720	41
October	1989	614	130	0	744	83
November	1989	562	158	0	720	78
December	1989	345	135	264	744	72
January	1990	291	36	417	744	89
February	1990	620	52	0	672	92
March	1990	681	63	0	744	92
April	1990	501	104	115	720	83
May	1990	582	114	48	744	84
June	1990	370	254	96	720	59
July	1990	576	168	0	744	77
August	1990	563	133	48	744	81
					Ave:	76

SUMMARY OF SPARRO OPERATING TIMES AND AVAILABILITIES

SPARRO		Plant Run	Shutdown		Max Possible	Availability
			Not Planned	Planned		
		hrs	hrs	hrs	hrs	%
February	1989	Comm			672	Comm
March	1989	Comm			744	Comm
April	1989	Comm			720	Comm
May	1989	Comm			744	Comm
June	1989	Comm			720	Comm
July	1989	344	400	0	744	46
August	1989	348	396	0	744	47
September	1989	370	134	216	720	73
October	1989	638	106	0	744	86
November	1989	454	266	0	720	63
December	1989	194	118	432	744	62
January	1990	60	10	674	744	86
February	1990	450	222	0	672	67
March	1990	517	227	0	744	69
April	1990	442	163	115	720	73
May	1990	595	101	48	744	85
June	1990	528	96	96	720	84
July	1990	314	430	0	744	42
August	1990	410	286	48	744	59
					Ave:	67

SUMMARY OF PRETREATMENT PLANT OPERATING TIMES AND AVAILABILITIES

PRETREATMENT		Shutdown	Max Possible	Availability
		Not Planned		
		hrs	hrs	%
March	1989		744	-
April	1989		720	-
May	1989		744	-
June	1989		720	-
July	1989	85	744	88
August	1989	336	744	54
September	1989	96	720	86
October	1989	42	744	94
November	1989	5	720	99
December	1989	38	744	94
January	1990	0	744	100
February	1990	16	672	97
March	1990	0	744	100
April	1990	0	720	100
May	1990	0	744	100
June	1990	0	720	100
July	1990	0	744	100
August	1990	0	744	100
			Ave:	93

ANALYSIS OF UNPLANNED STOPPAGES JULY 1989

Plant	Off-Line Time (Hours)
Pretreatment	
Operator absent	29
Air shortage	5
Delivery pump No 2	24
Clarifier pump	3
Clarifier	24
Total	85
MLT Plant	
Operator absent	29
Pretreatment plant breakdown	56
Slurry feed pump	3
Total	88
SPARRO Plant	
Operator absent	29
Pretreatment breakdown	56
Mine water pump P1A	100
Slurry recycle pumps P2A, B	200
Other	15
Total	400

ANALYSIS OF UNPLANNED STOPPAGES AUGUST 1989

Plant	Off-Line Time (Hours)
Pretreatment	
Operator absent	96
Dosing pump	168
Delivery pump No 2	72
Total	336
MLT Plant	
Operator absent	96
Pretreatment	240
Slurry feed pump	48
Total	384
SPARRO Plant	
Operator absent	96
Pretreatment	240
Slurry recycle pumps	60
Total	396

STOPPAGES ALLOCATED TO PREDOMINANT CAUSE

ANALYSIS OF UNPLANNED STOPPAGES SEPTEMBER 1989

Plant	Off-Line Time (Hours)
Pretreatment	
Delivery pump No 2	48
Caustic soda dosing	48
Total	96
MLT Plant	
Pretreatment breakdown	96
Reject flow control	201
Total	297
SPARRO Plant	
Pretreatment breakdown	96
Bursting discs	12
Pump P2A, P2B	26
Total	134

ANALYSIS OF UNPLANNED STOPPAGES OCTOBER 1989

Plant	Off-Line Time (Hours)
Pretreatment	
Water shortage	8
Floc dosing	10
Delivery pump No 2	24
Total	42
MLT Plant	
Pretreatment plant breakdown	42
Slurry feed pump	32
Modules	56
Total	130
SPARRO Plant	
Pretreatment breakdown	42
Slurry recycle pumps	64
Total	106

STOPPAGES ALLOCATED TO PREDOMINANT CAUSE

ANALYSIS OF UNPLANNED STOPPAGES NOVEMBER 1989

Plant	Off-Line Time (Hours)
Pretreatment	
pH control	5
Total	5
MLT Plant	
Pretreatment plant breakdown	5
Bursting disc	5
Power failure	8
Slurry feed pump	140
Total	158
SPARRO Plant	
Pretreatment breakdown	5
Bursting disc	5
Power failure	8
Slurry feed pump	248
Total	266

ANALYSIS OF UNPLANNED STOPPAGES DECEMBER 1989

Plant	Off-Line Time (Hours)
Pretreatment	
pH control	28
Operators absent	10
Total	38
MLT Plant	
Pretreatment plant breakdown	28
Operators absent	10
Modules	1
Slurry feed pump	96
Total	135
SPARRO Plant	
Pretreatment breakdown	28
Slurry feed pumps	90
Total	118

STOPPAGES ALLOCATED TO PREDOMINANT CAUSE

ANALYSIS OF UNPLANNED STOPPAGES JANUARY 1990

Plant	Off-Line Time (Hours)
MLT Plant	
Power failure	15
Operator absent	12
Slurry feed pump	4
Instrumentation	5
Total	36
SPARRO Plant	
Instrumentation	6
Slurry recycle pumps	4
Total	10

ANALYSIS OF UNPLANNED STOPPAGES FEBRUARY 1990

Plant	Off-Line Time (Hours)
Pretreatment	
pH meter	16
MLT Plant	
Pretreatment plant breakdown	16
Slurry feed pump	25
Modules failures, changes	11
Total off-line	52
SPARRO Plant	
Pretreatment	16
Generator	8
Feed pump P1	48
Slurry recycle pumps P2	25
Modules	83
Reject line blockage	42
Total	222

STOPPAGES ALLOCATED TO PREDOMINANT CAUSE

ANALYSIS OF UNPLANNED STOPPAGES MARCH 1990

Plant	Off-Line Time (Hours)
MLT Plant	
Slurry feed pump	49
Modules failure, changes	14
Total	63
SPARRO Plant	
Air pressure ex mine/mods	49
Slurry recycle pumps	150
Module failure, changes	20
Water meter installation	8
Total	227

ANALYSIS OF UNPLANNED STOPPAGES APRIL 1990

Plant	Off-Line Time (Hours)
MLT	
Slurry feed pump	90
Reactor	8
Power failure	6
Total	104
SPARRO	
Valves - low gas pressure	11
Slurry feed pump plungers	31
Power failure	2
Module change	10
Slurry feed pump electric overload	109
Total	163

STOPPAGES ALLOCATED TO PREDOMINANT CAUSE

ANALYSIS OF UNPLANNED STOPPAGES MAY 1990

Plant	Off-Line Time (Hours)
MLT	
Module burst	5
Slurry feed pump	109
Total	114
SPARRO	
Slurry feed pump	81
Valves - low gas pressure	5
Power failure	15
Total	101

ANALYSIS OF UNPLANNED STOPPAGES JUNE 1990

Plant	Off-Line Time (Hours)
MLT	
Slurry feed pump	254
Total	254
SPARRO	
Mono pump P1	26
Module cleaning	49
Instrumentation	21
Total	96

STOPPAGES ALLOCATED TO PREDOMINANT CAUSE

ANALYSIS OF UNPLANNED STOPPAGES JULY 1990

Plant	Off-Line Time (Hours)
MLT	
Slurry feed pump	42
Reactor agitator	120
Instrumentation	6
Total	168
SPARRO	
Module renovation	336
Instrumentation	6
Power failure	1
Slurry feed pump	70
Operator absent	17
Total	430

ANALYSIS OF UNPLANNED STOPPAGES AUGUST 1990

Plant	Off-Line Time (Hours)
MLT	
Reactor agitator	88
Operator absent	15
Power failure	30
Total	133
SPARRO	
Module renovation	192
Slurry feed pump	79
Operator absent	15
Total	286

STOPPAGES ALLOCATED TO PREDOMINANT CAUSE

APPENDIX II   GRAPHS OF PRETREATMENT, MLT AND SPARRO PLANTS
PERFORMANCE FROM FEBRUARY 1989 TO AUGUST 1990

APPENDIX II

<u>GRAPHS</u>

1.   Raw mine water conductivity
2.   Clarifier overflow pH
3.   Filter outlet pH
4.   Filter outlet turbidity
5.   MLT feed conductivity
6.   MLT feed total suspended solids
7.   MLT feed pH
8.   MLT product conductivity
9.   MLT rejection (wrt MLT feed)
10.   MLT corrected flux
11.   SPARRO feed conductivity
12.   SPARRO feed total suspended solids
13.   SPARRO feed pH
14.   SPARRO product conductivity
15.   SPARRO rejection (wrt SPARRO feed)
16.   SPARRO corrected flux

Graph A - 1989 elapsed hours
Graph B - 1990 elapsed hours

1 000 hours equivalent to 41,66 calendar days
31 days equivalent to 744 hours
Off-line time is shown by gap in graph.
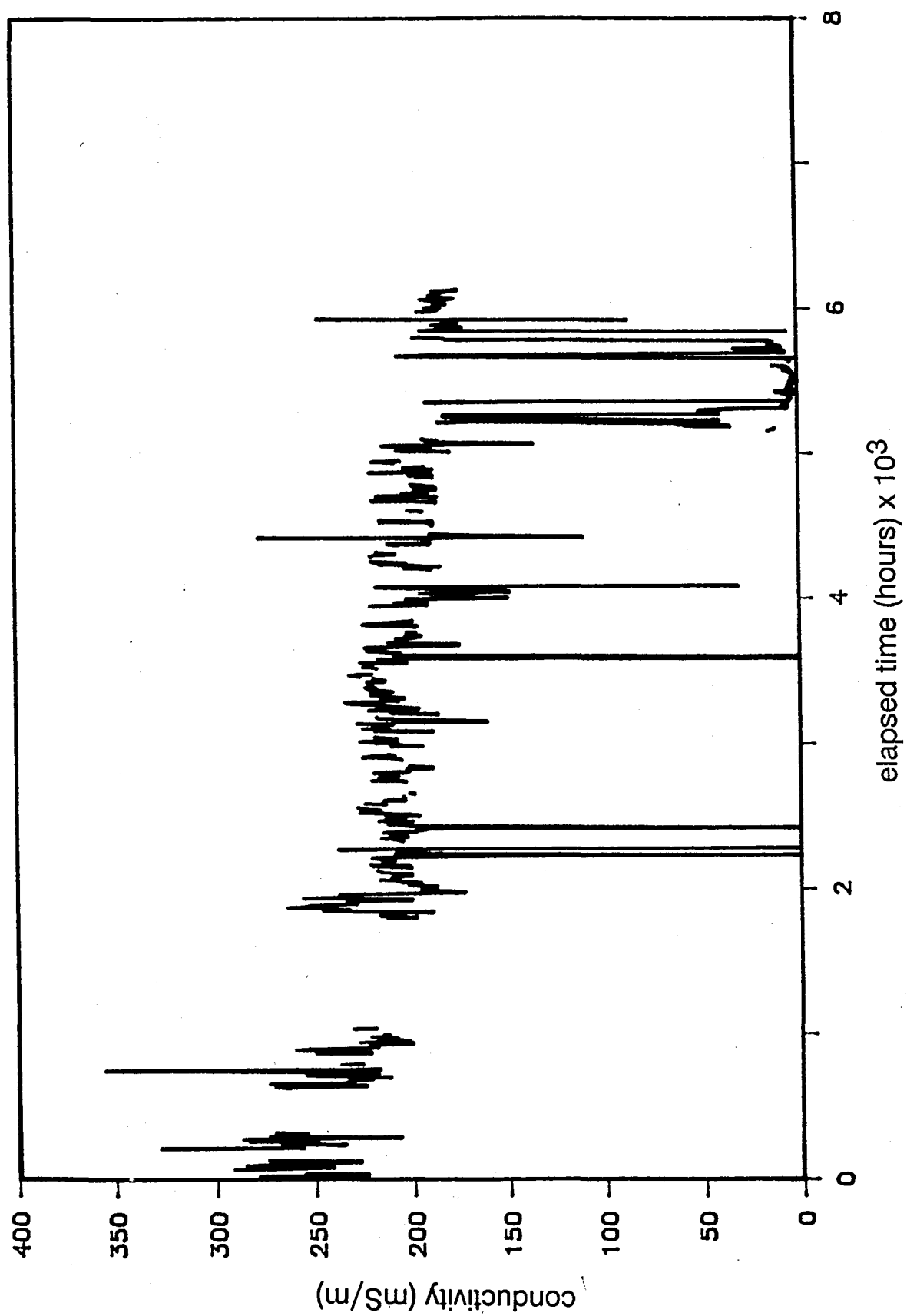
GRAPH 1A : Raw Mine Water Conductivity - 1989
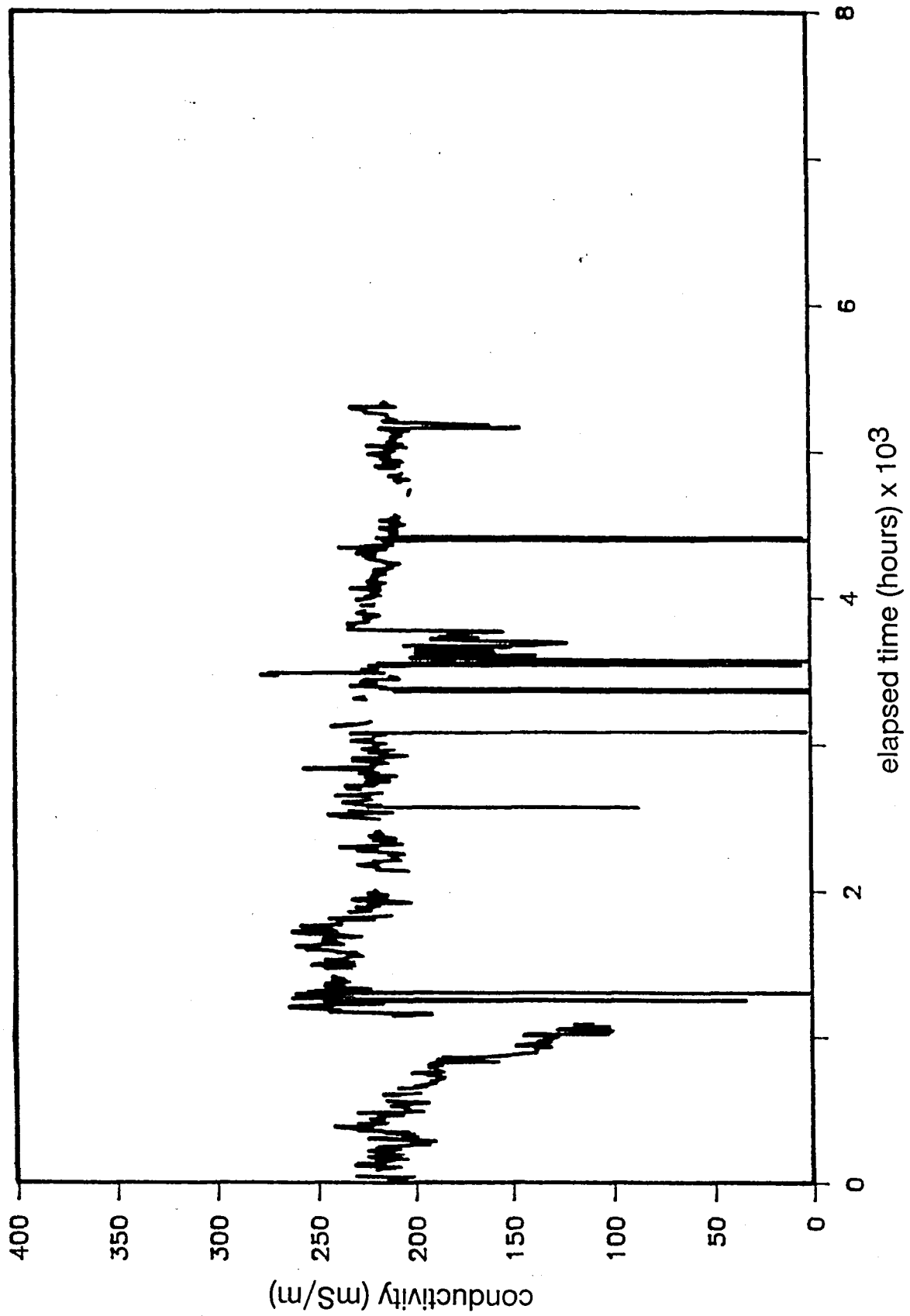
GRAPH 1B : Raw Mine Water Conductivity - 1990
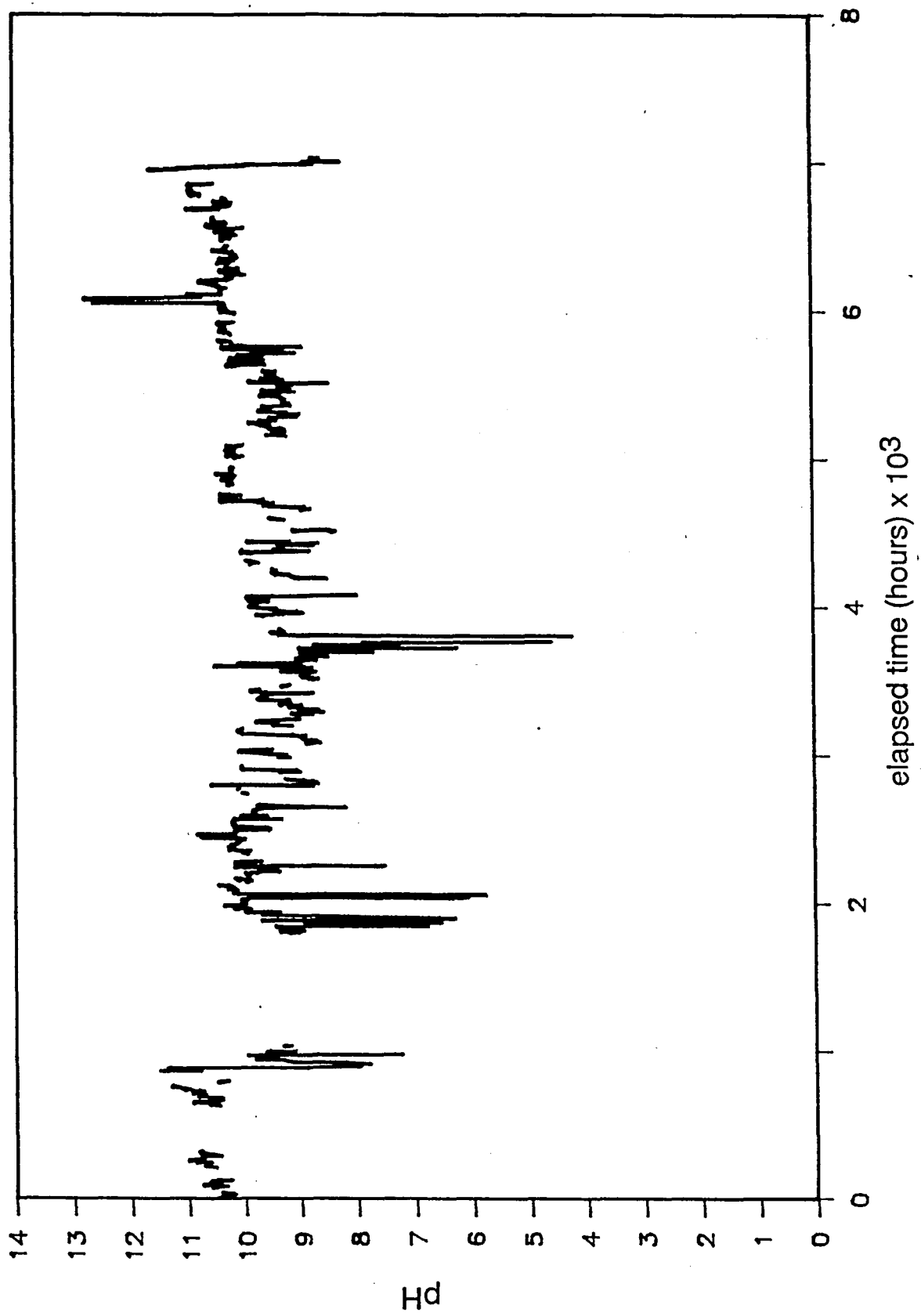
GRAPH 2A : Clarifier Overflow pH - 1989
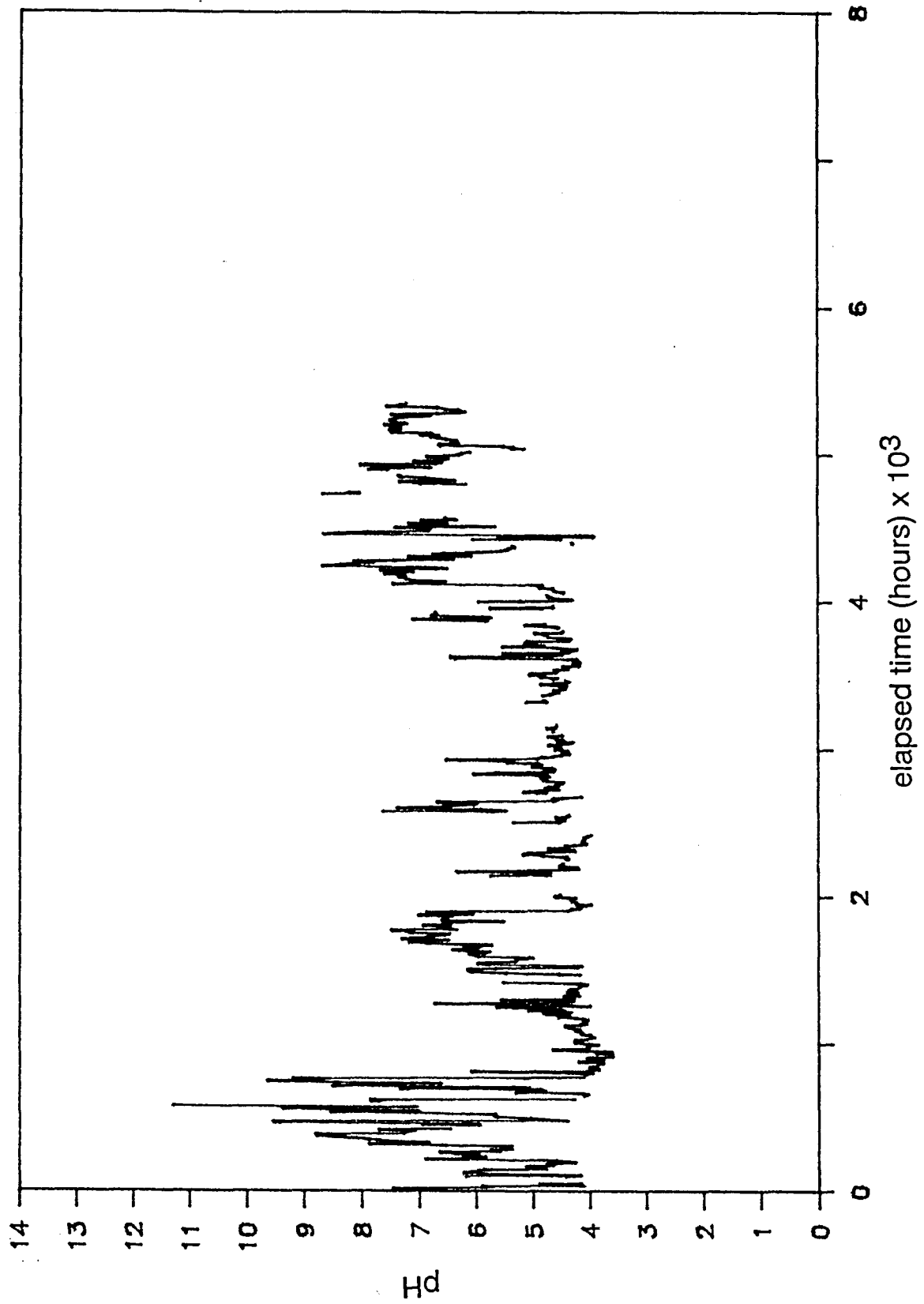
GRAPH 2B : Clarifier Overflow pH - 1990
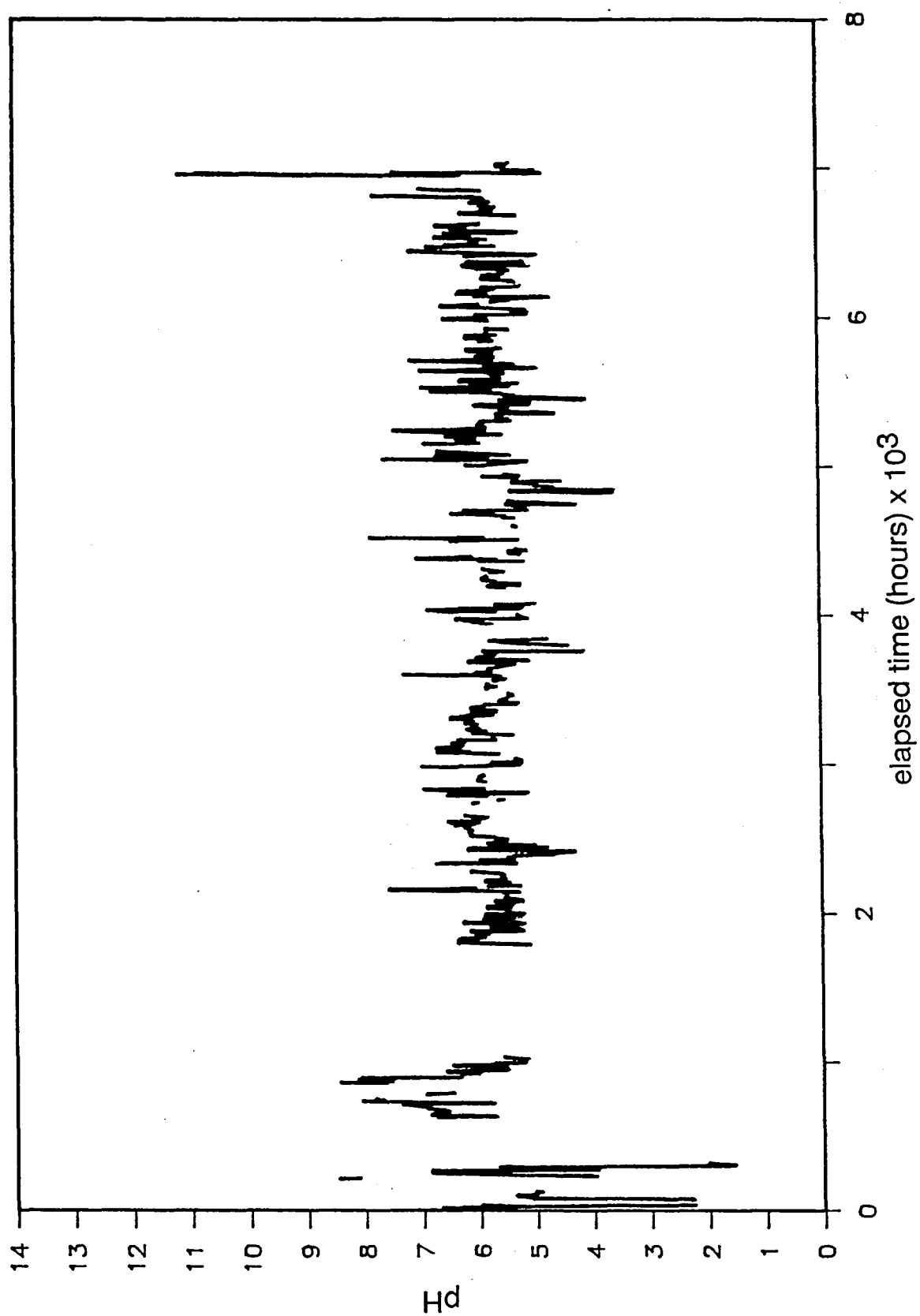
GRAPH 3A : Filter Outlet pH - 1989
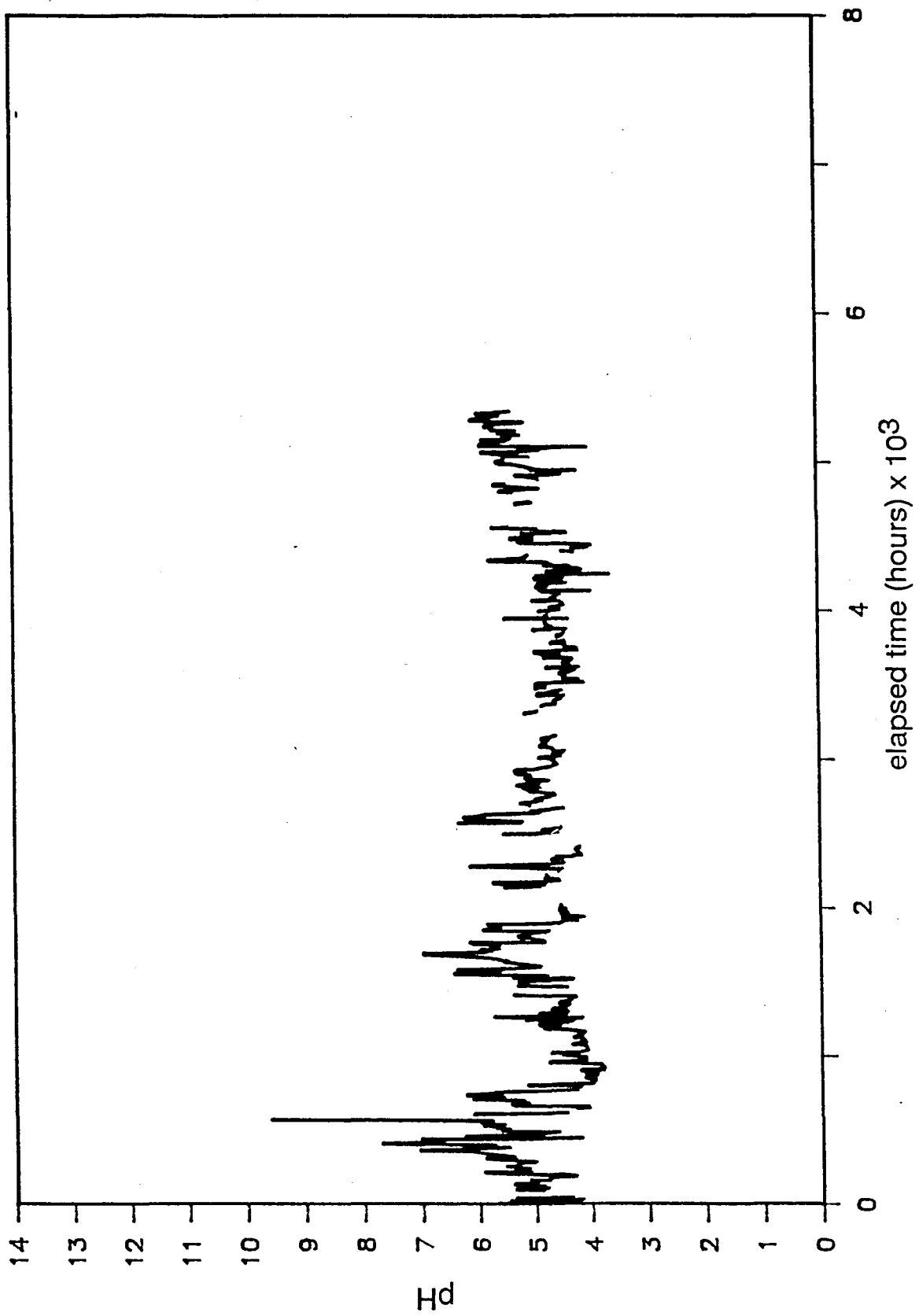
GRAPH 3B : Filter Outlet pH - 1990
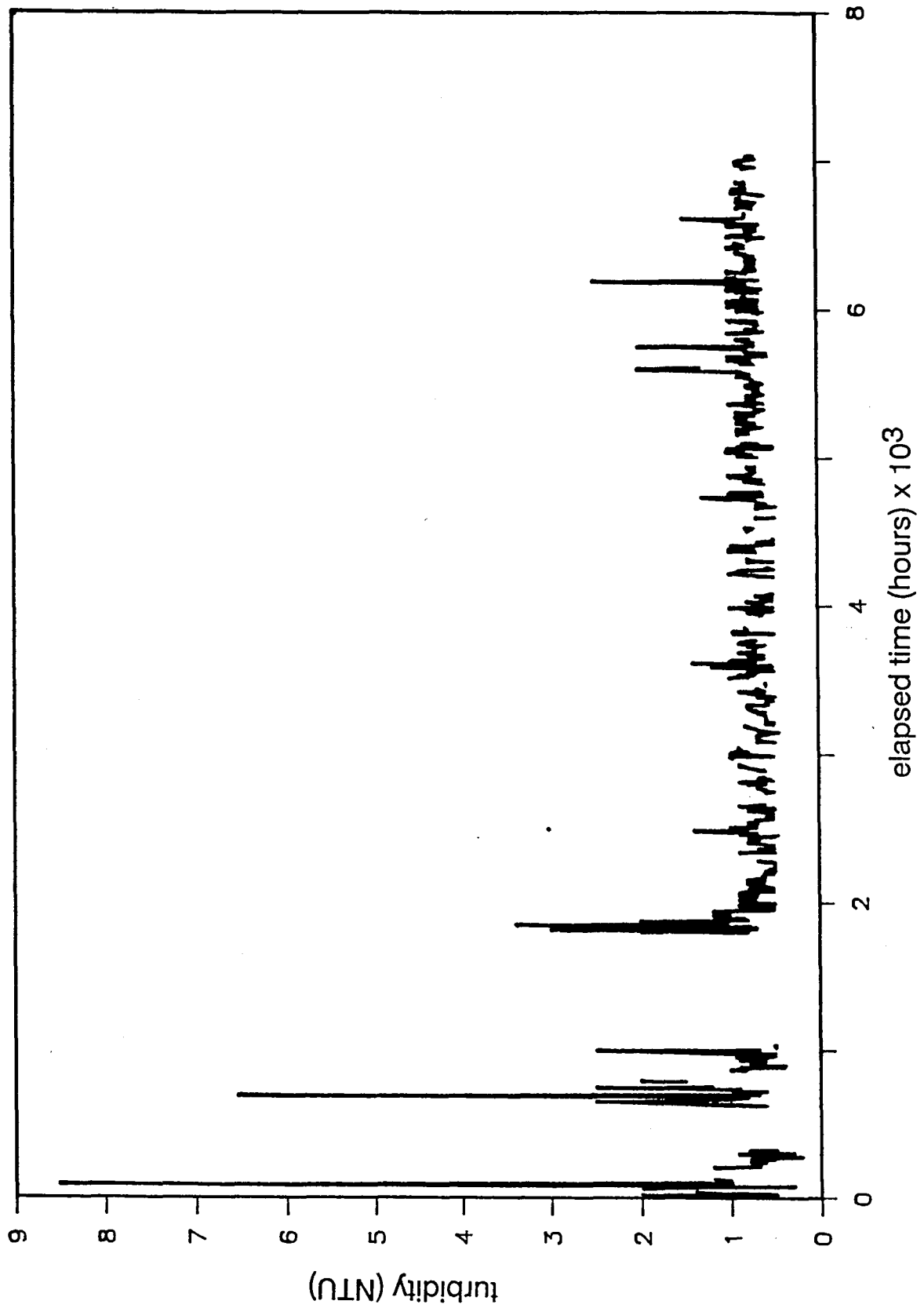
GRAPH 4A : Filter Outlet Turbidity - 1989
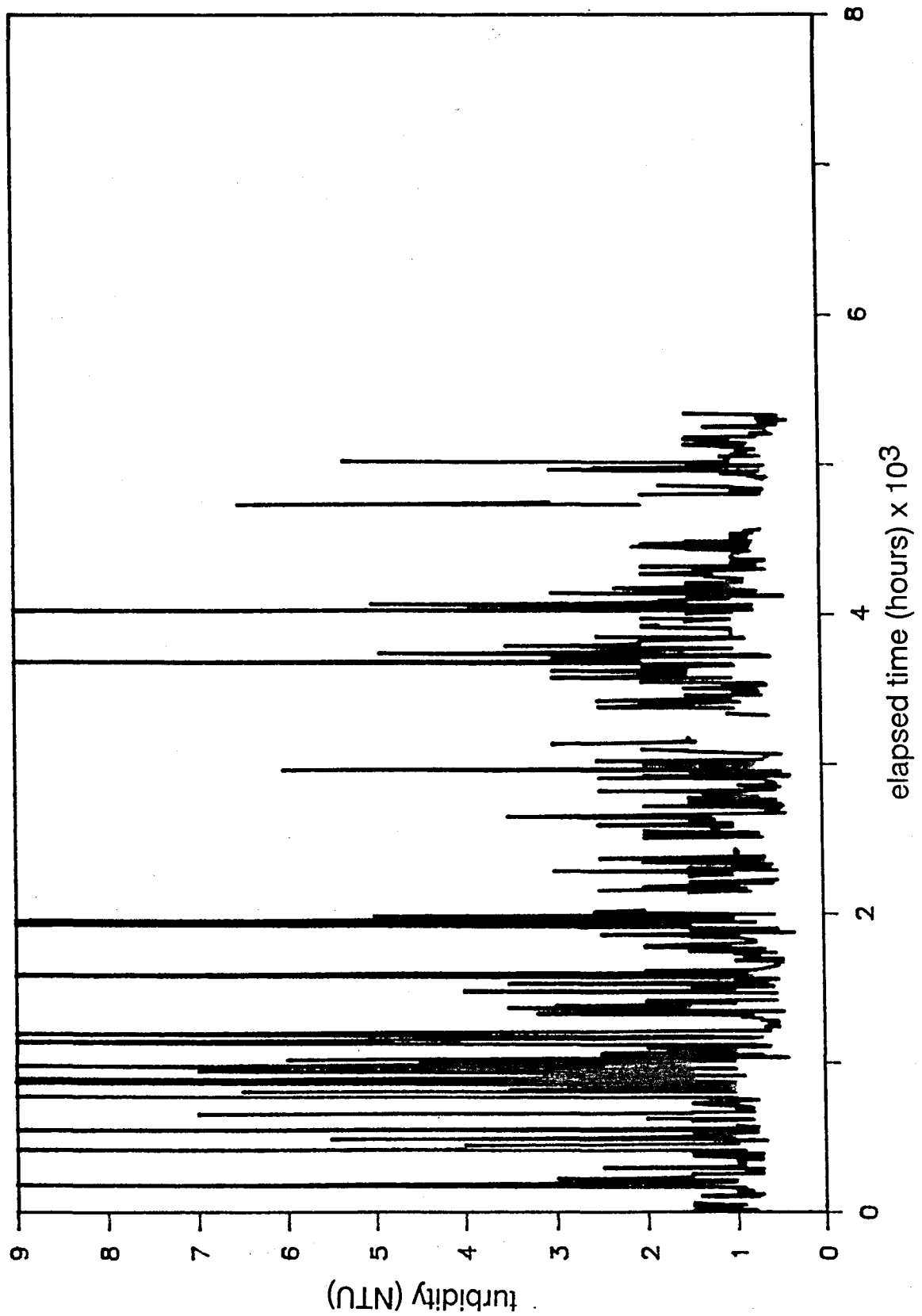
GRAPH 4B : Filter Outlet Turbidity - 1990
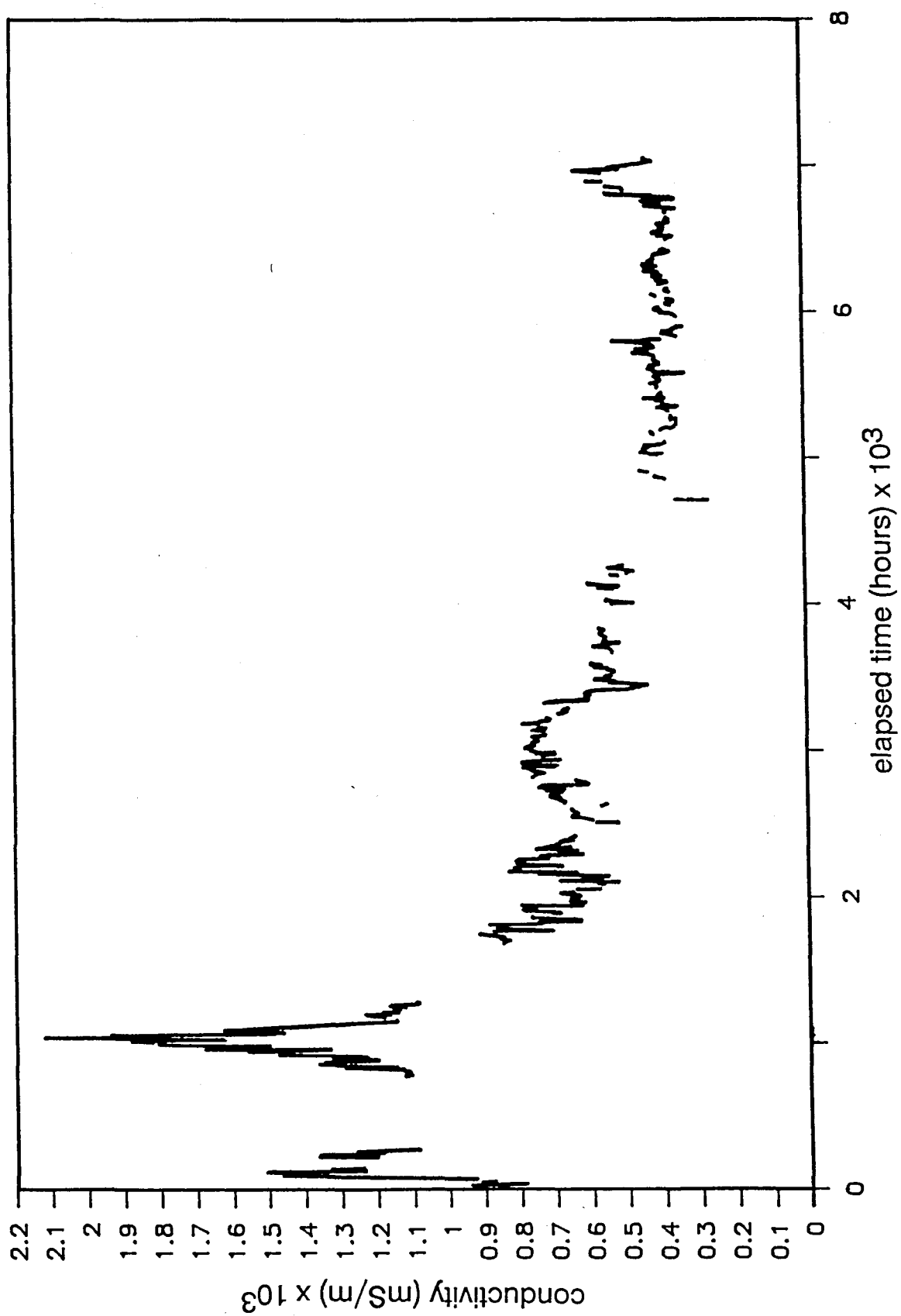
GRAPH 5A : MLT Feed Conductivity - 1989
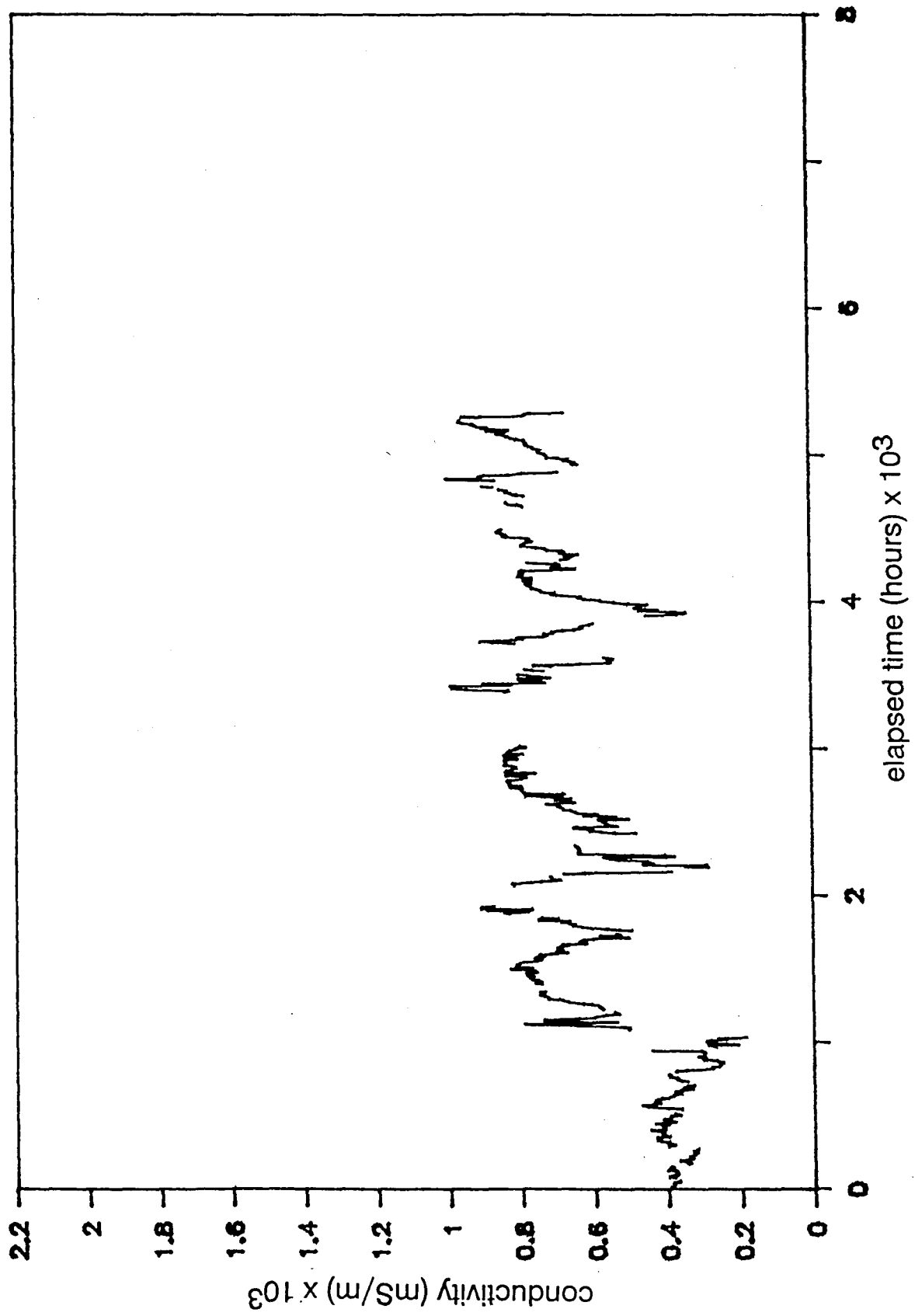
GRAPH 5B : MLT Feed Conductivity - 1990
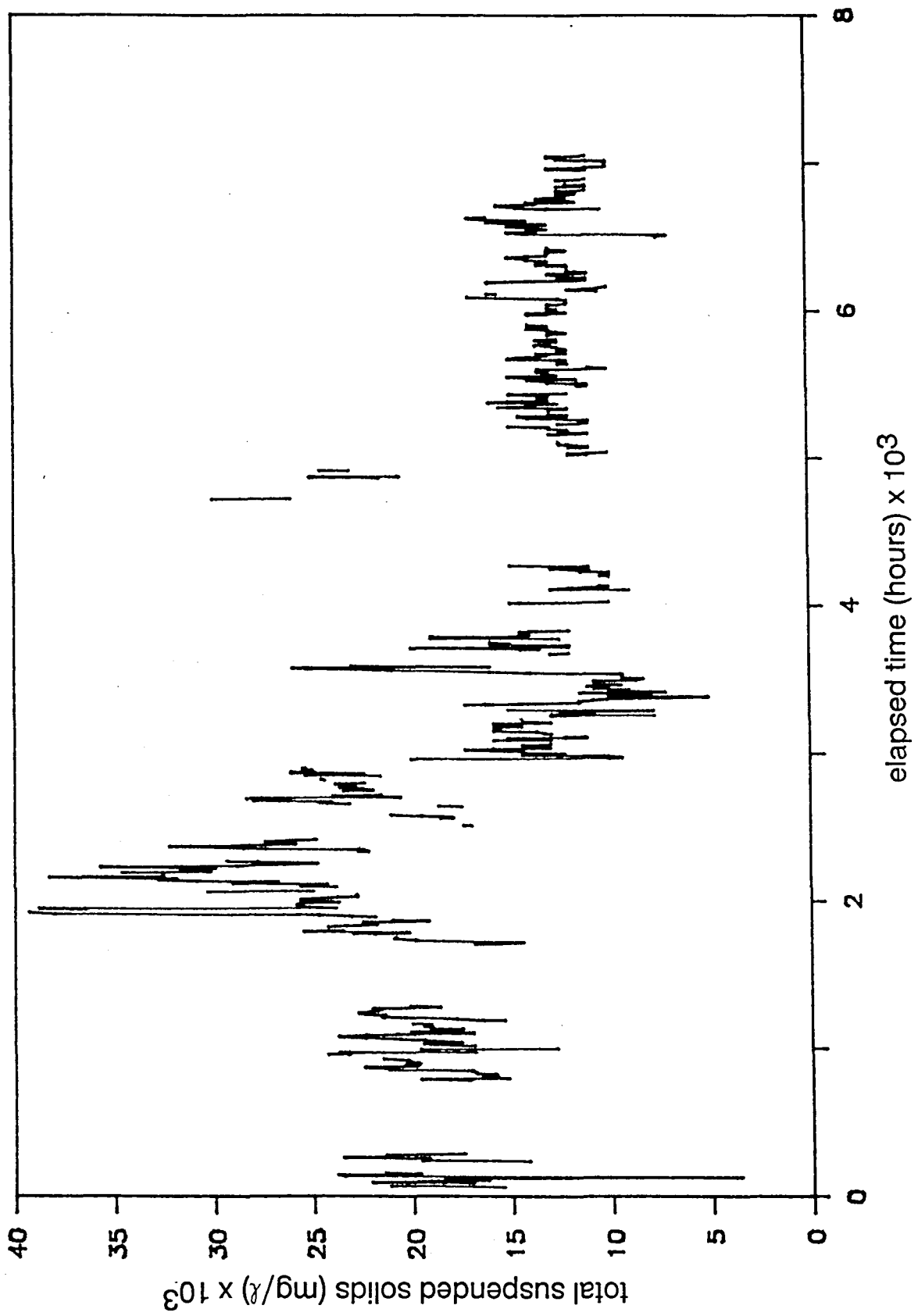
GRAPH 6A : MLT Feed Total Suspended Solids - 1989

GRAPH 6B : MLT Feed Total Suspended Solids - 1990

77
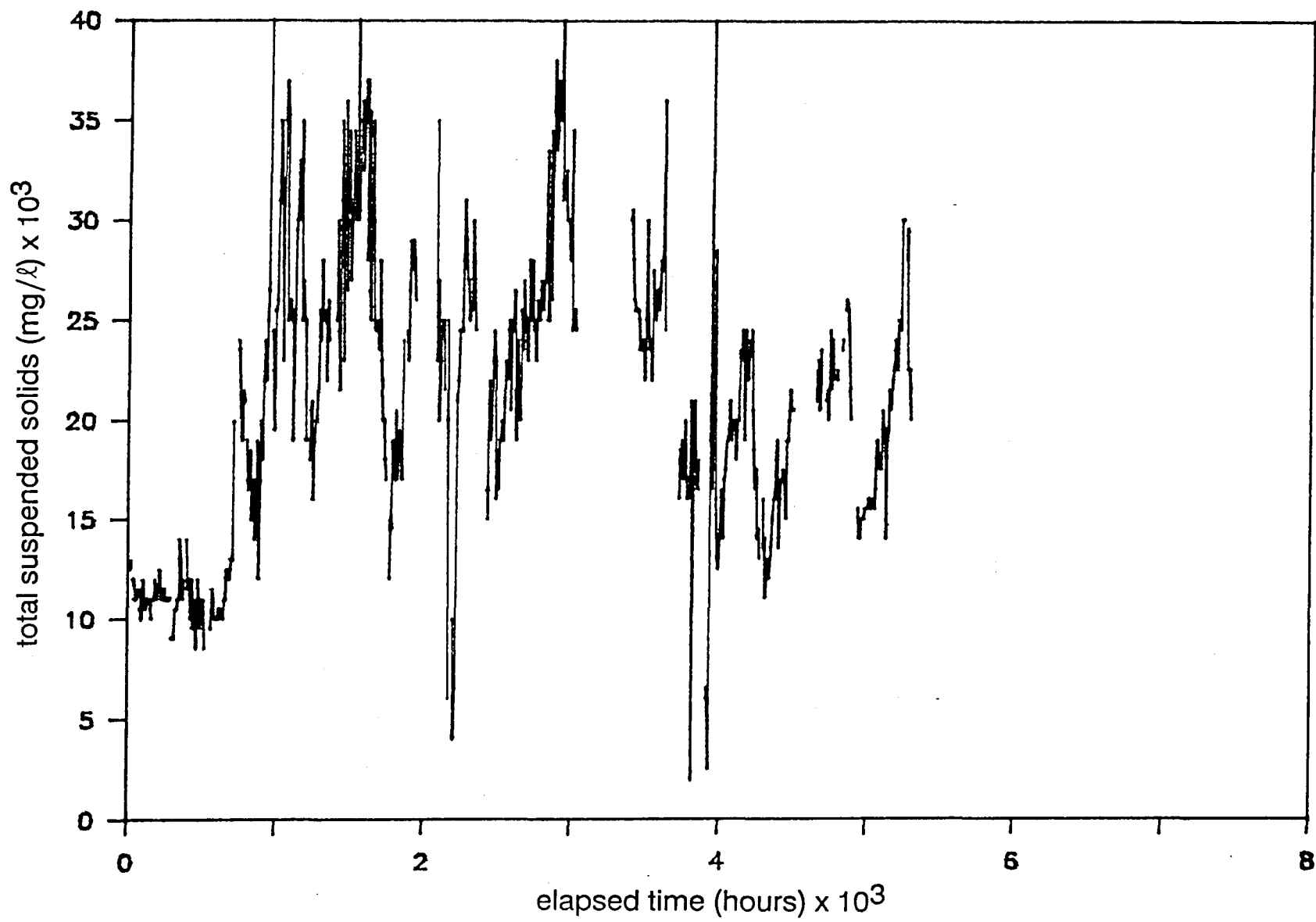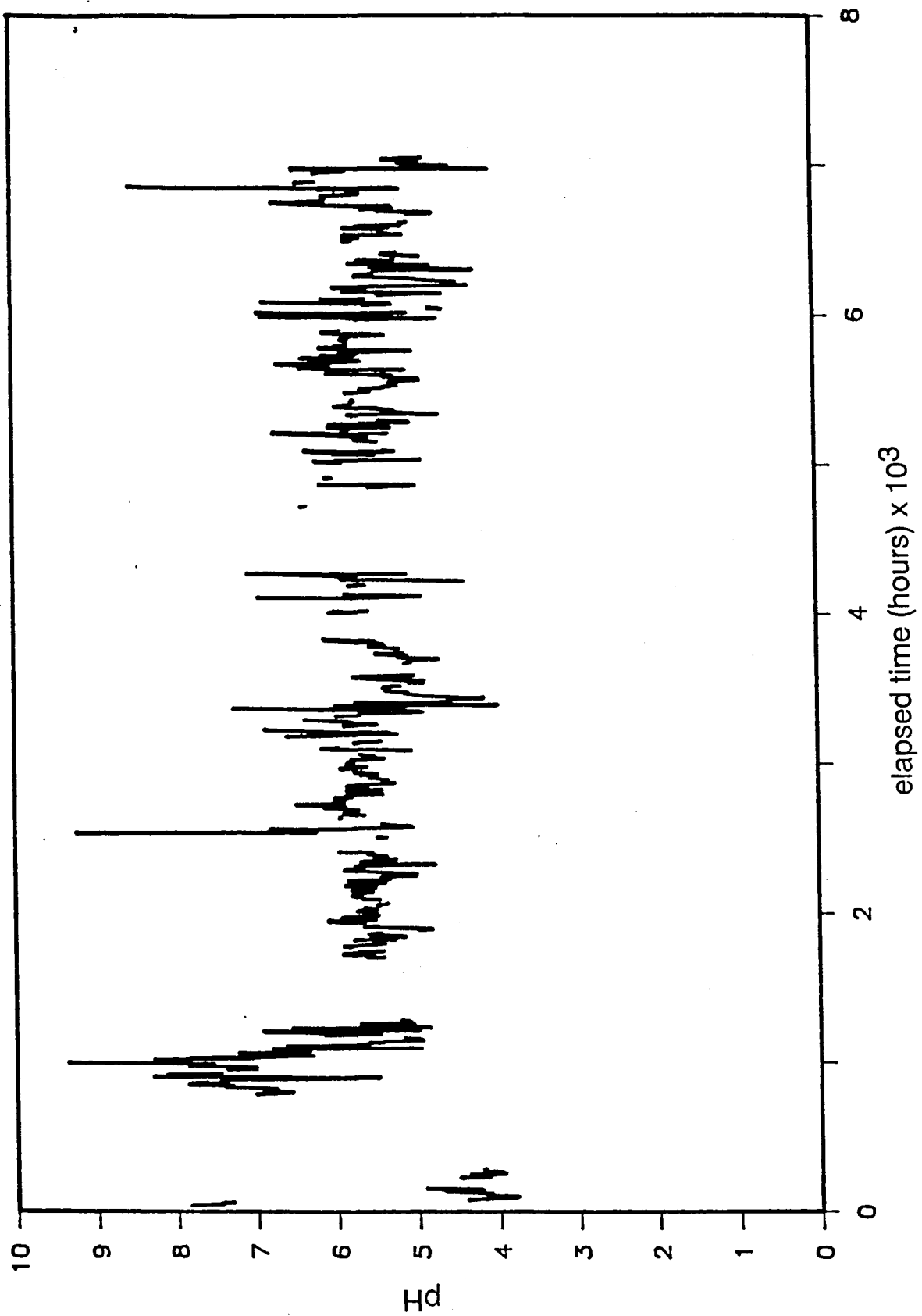
GRAPH 7A : MLT Feed pH - 1989
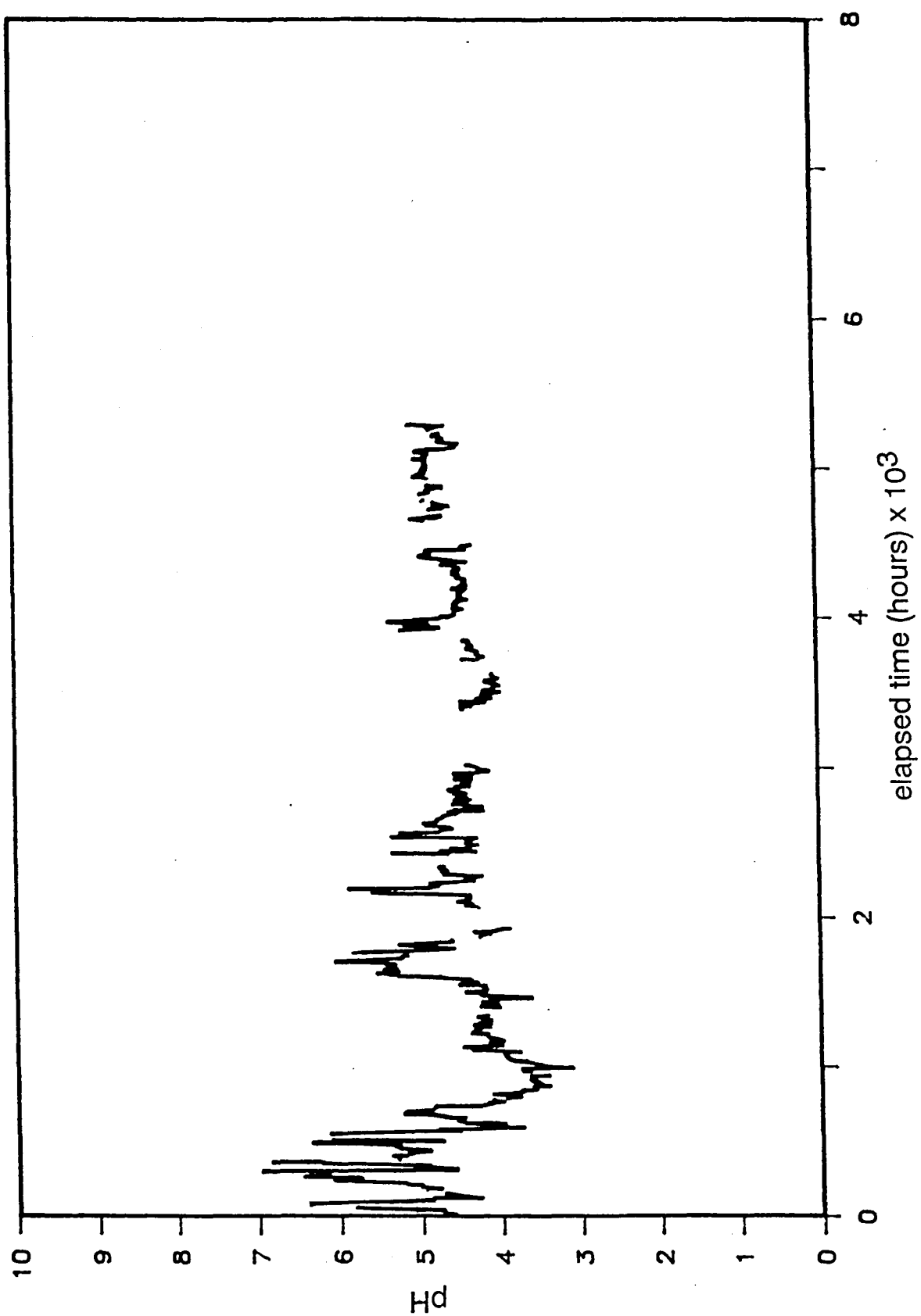
GRAPH 7B : MLT Feed pH - 1990
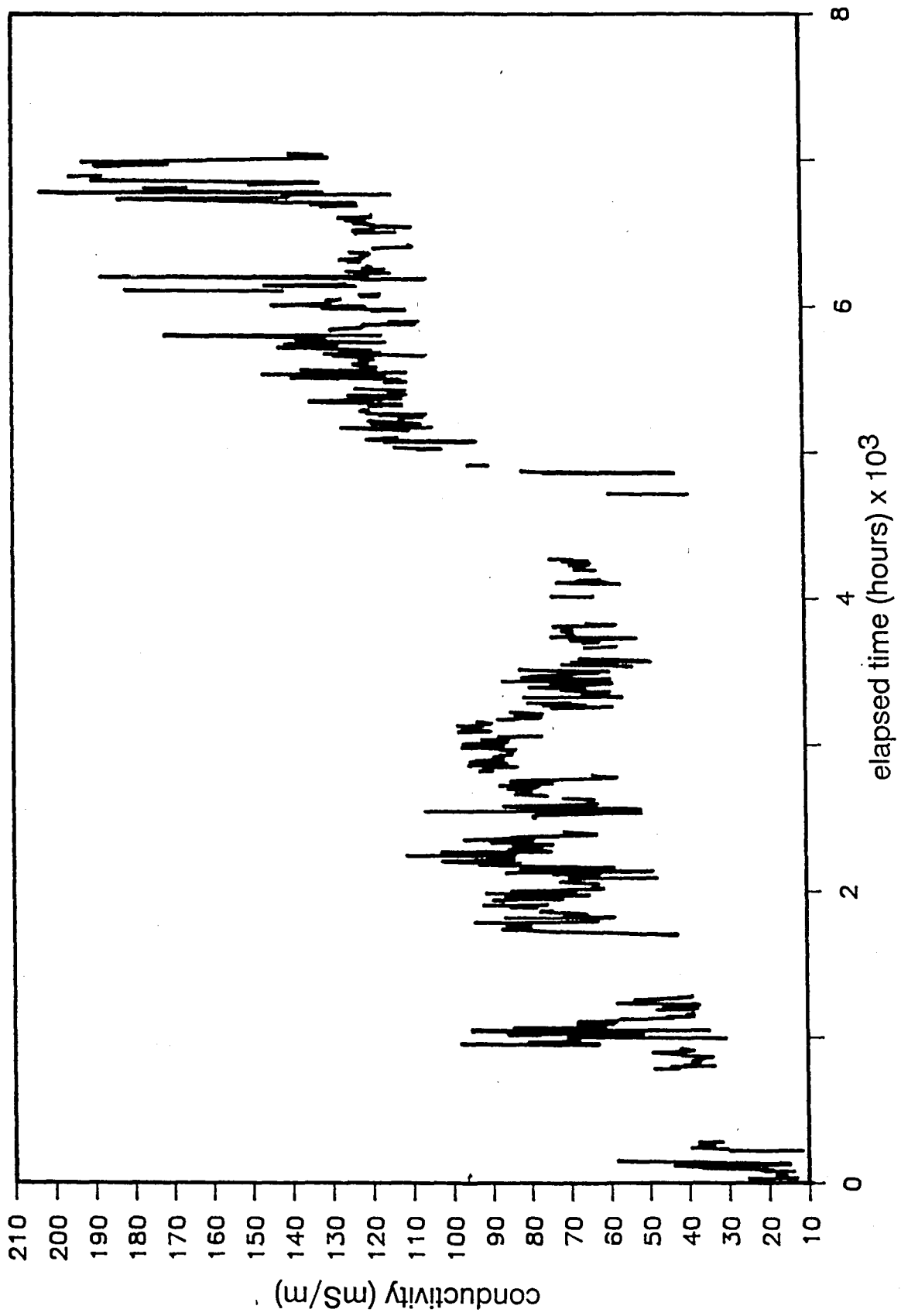
GRAPH 8A : MLT Product Conductivity - 1989
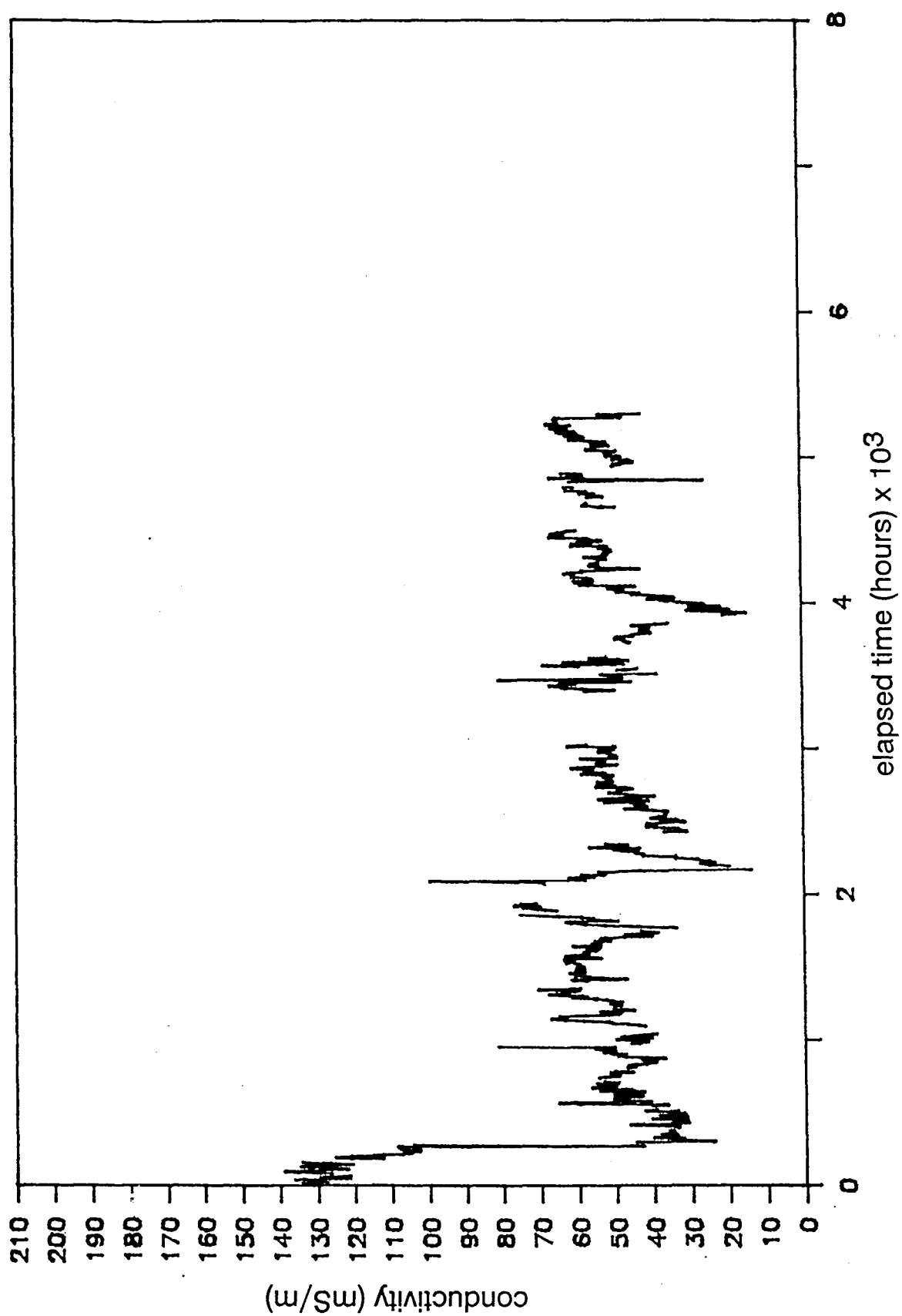
GRAPH 8B : MLT Product Conductivity - 1990
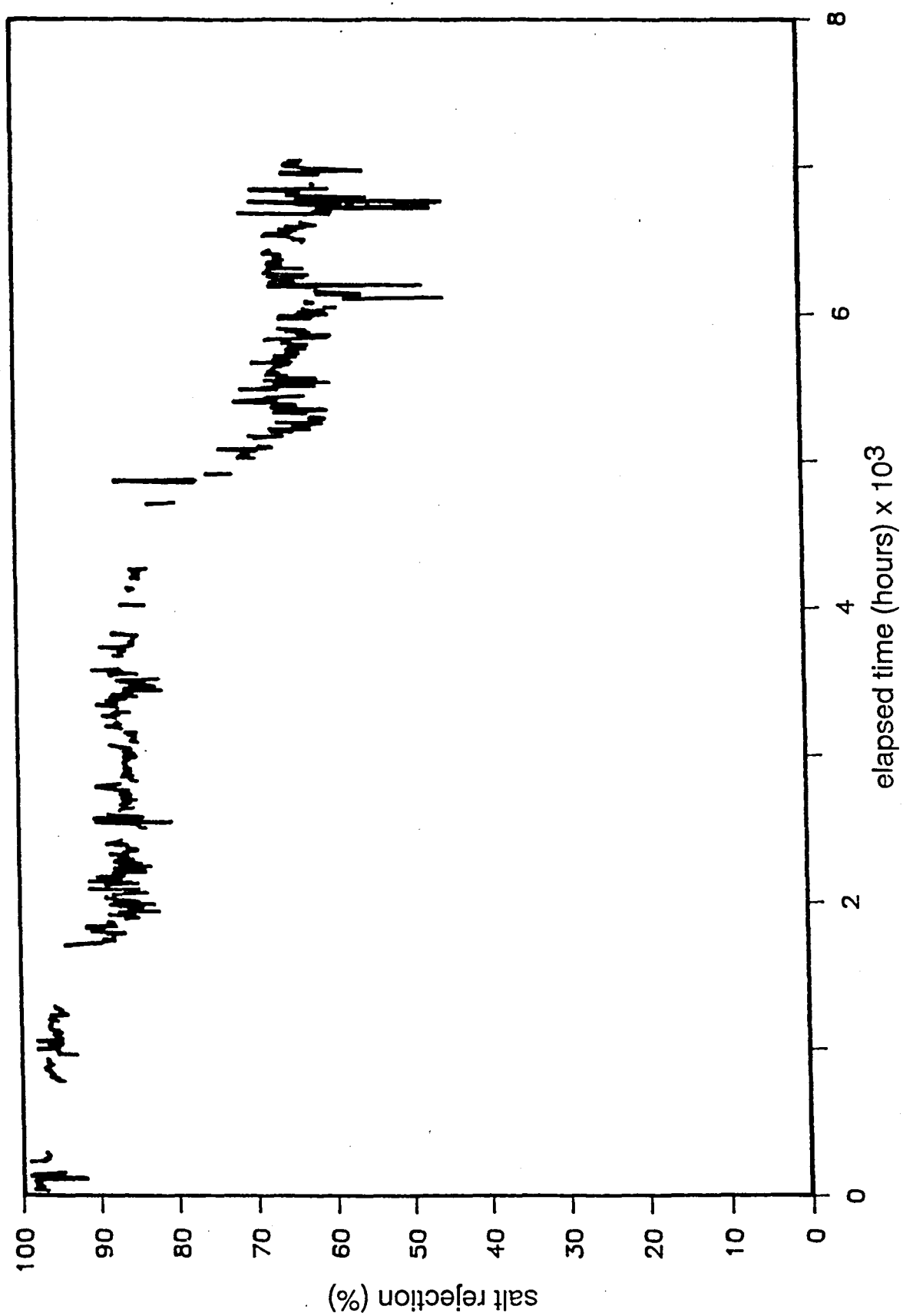
GRAPH 9A : MLT Rejection (wrt MLT Feed) - 1989
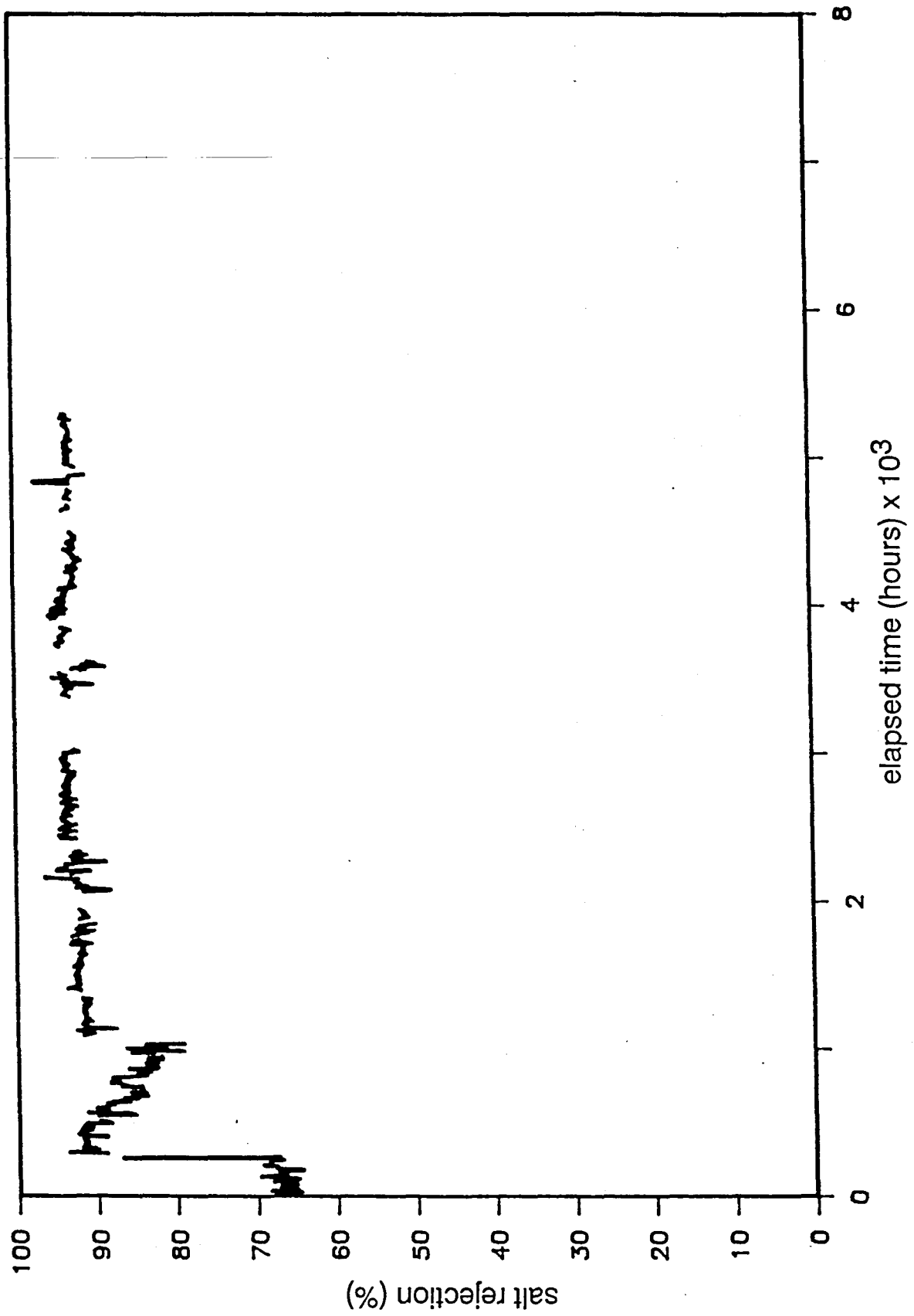
GRAPH 9B : MLT Rejection (wrt MLT Feed) - 1990

flux (ℓ.m2/d) x 10³
40 bar, 25°C

elapsed time (hours) x 10³
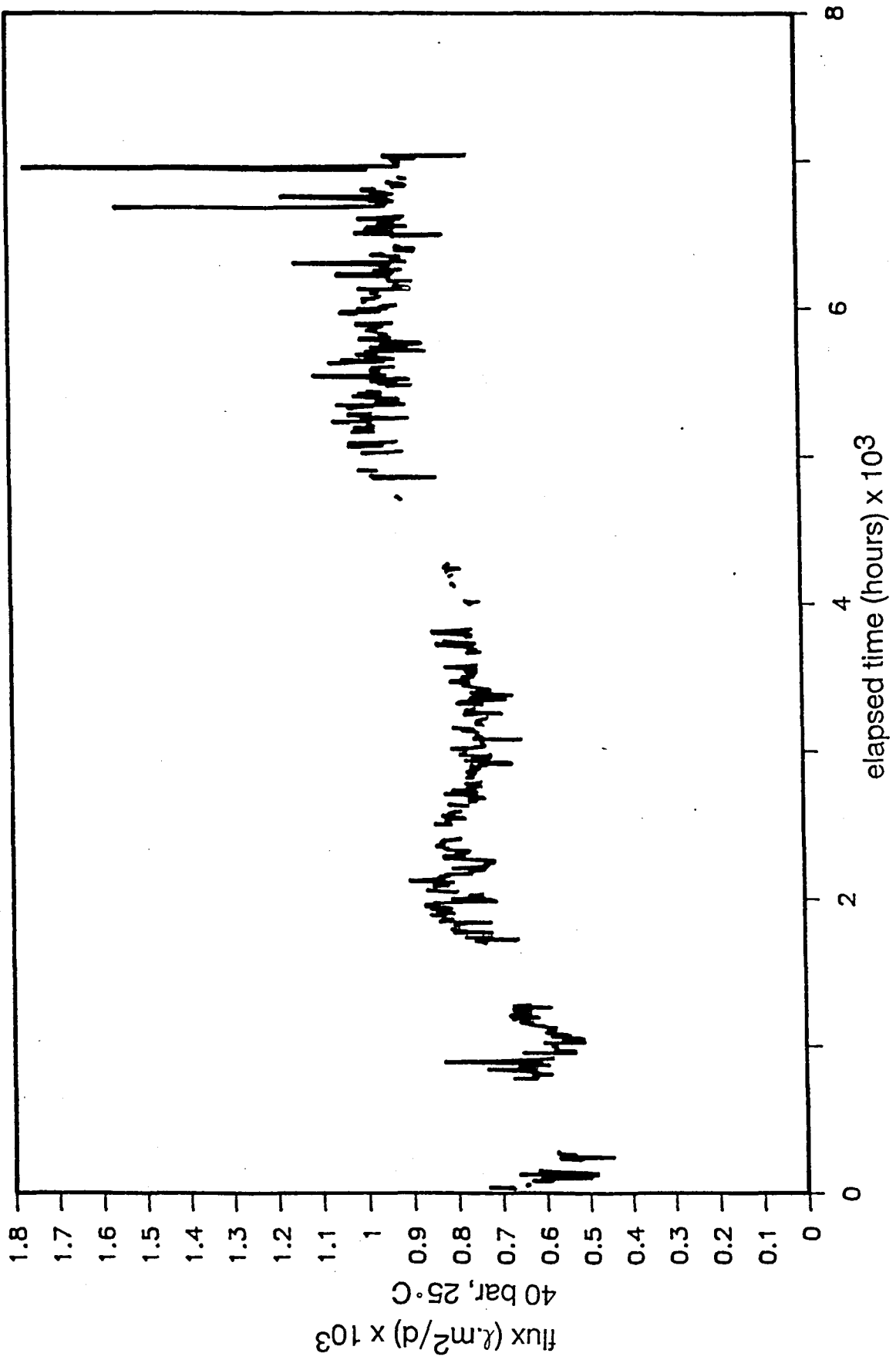
GRAPH 10A : MLT Corrected Flux - 1989
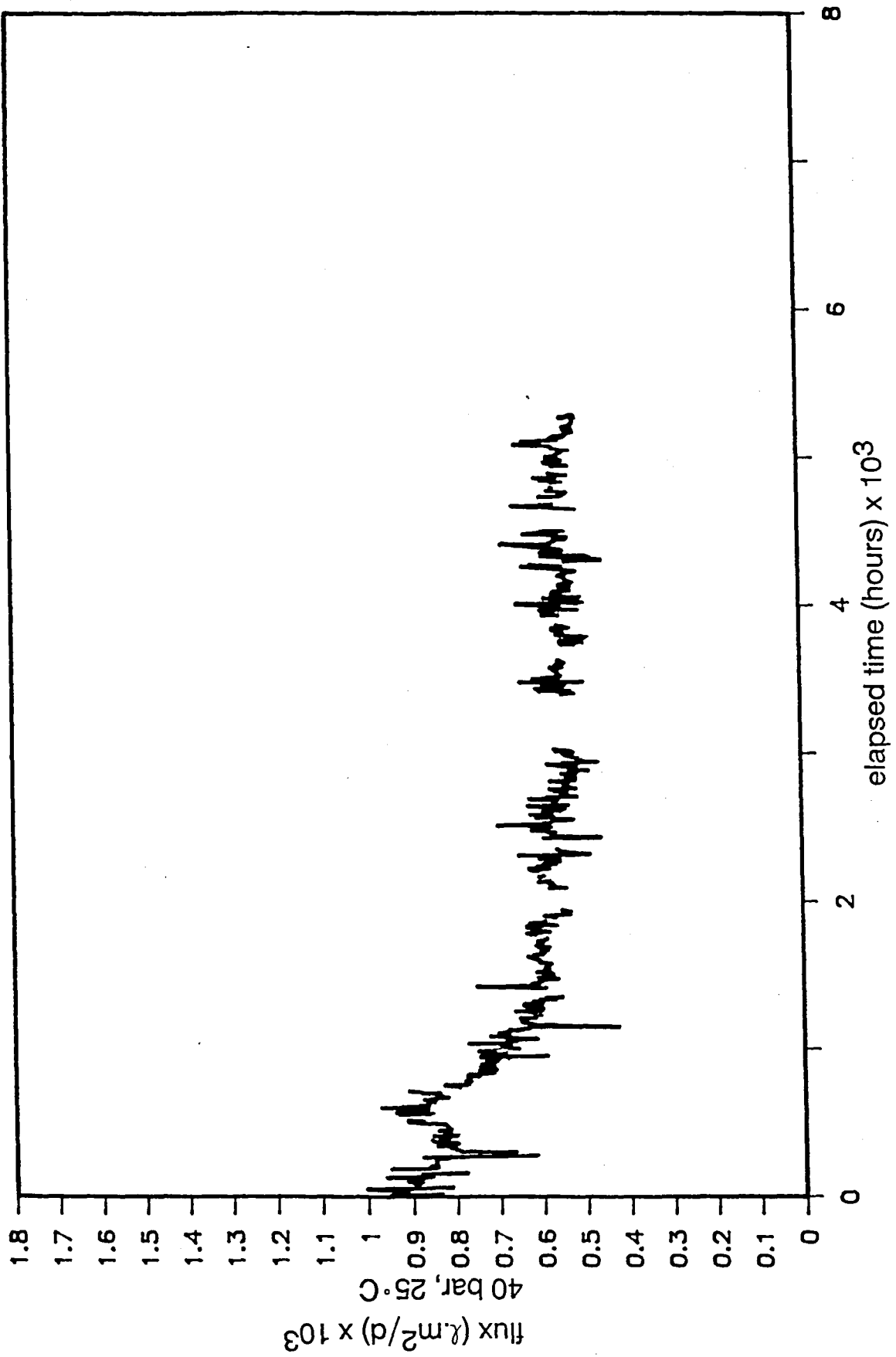
GRAPH 10B : MLT Corrected Flux - 1990
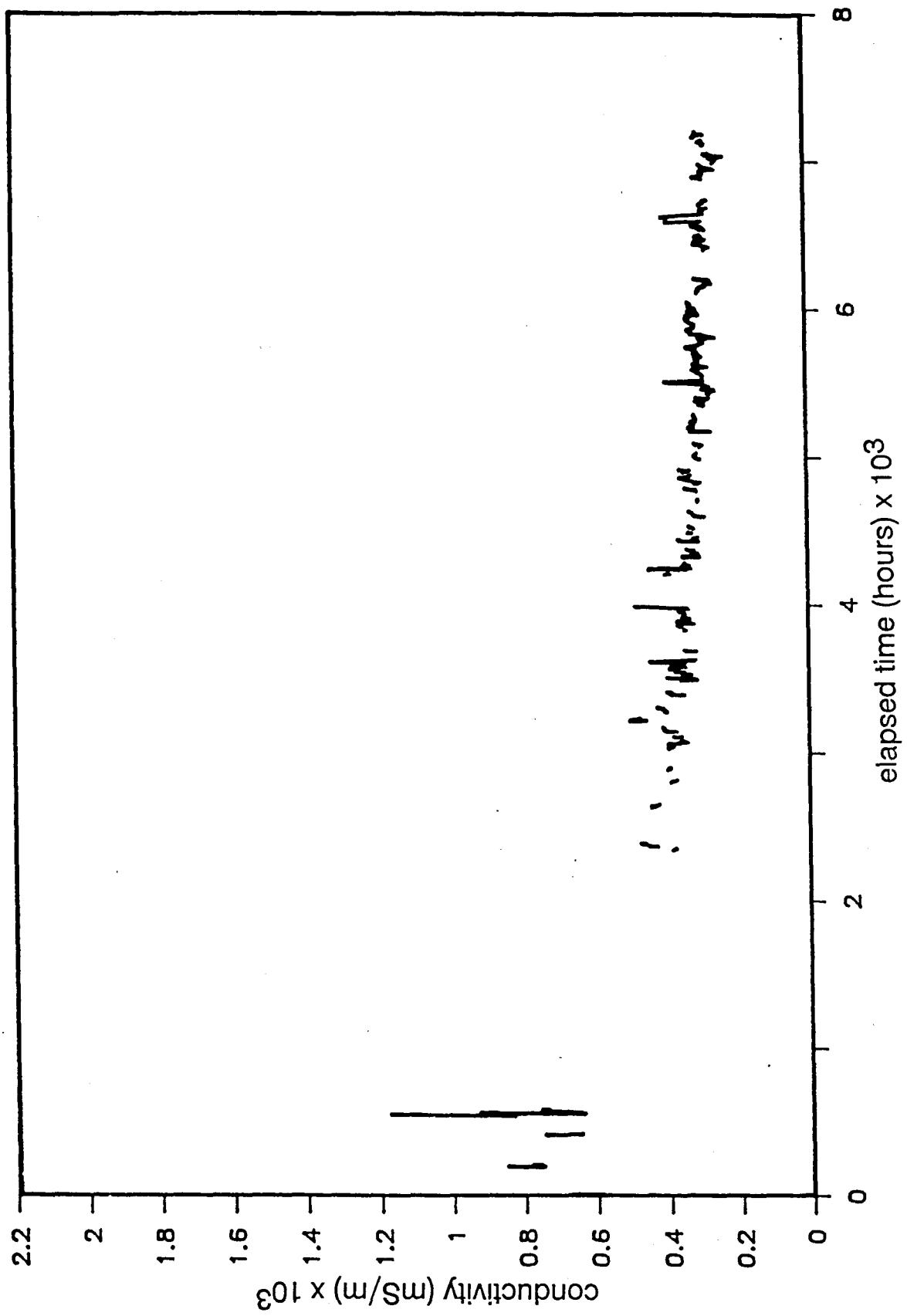
GRAPH 11A : SPARRO Feed Conductivity - 1989
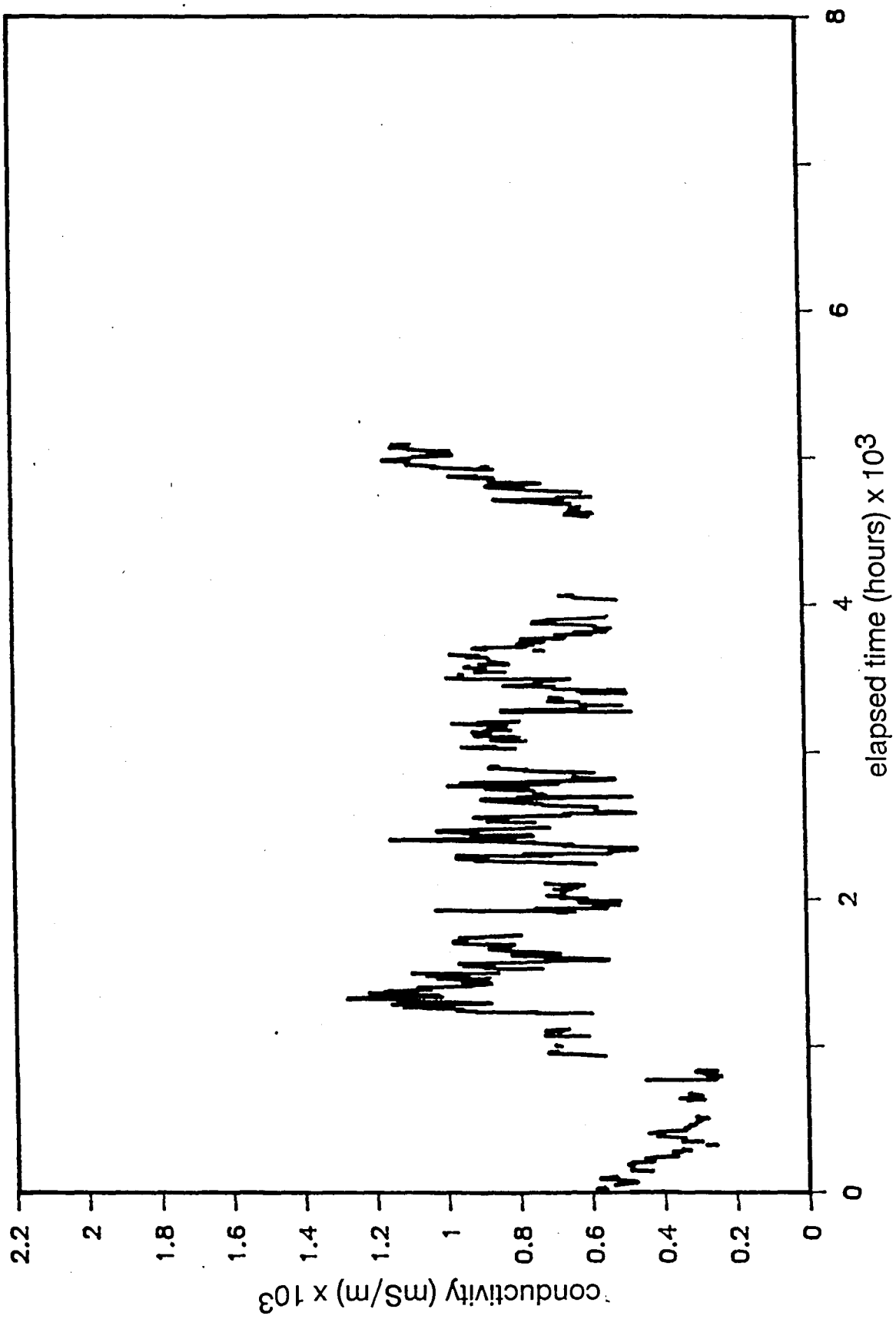
GRAPH 11B : SPARRO Feed Conductivity - 1990
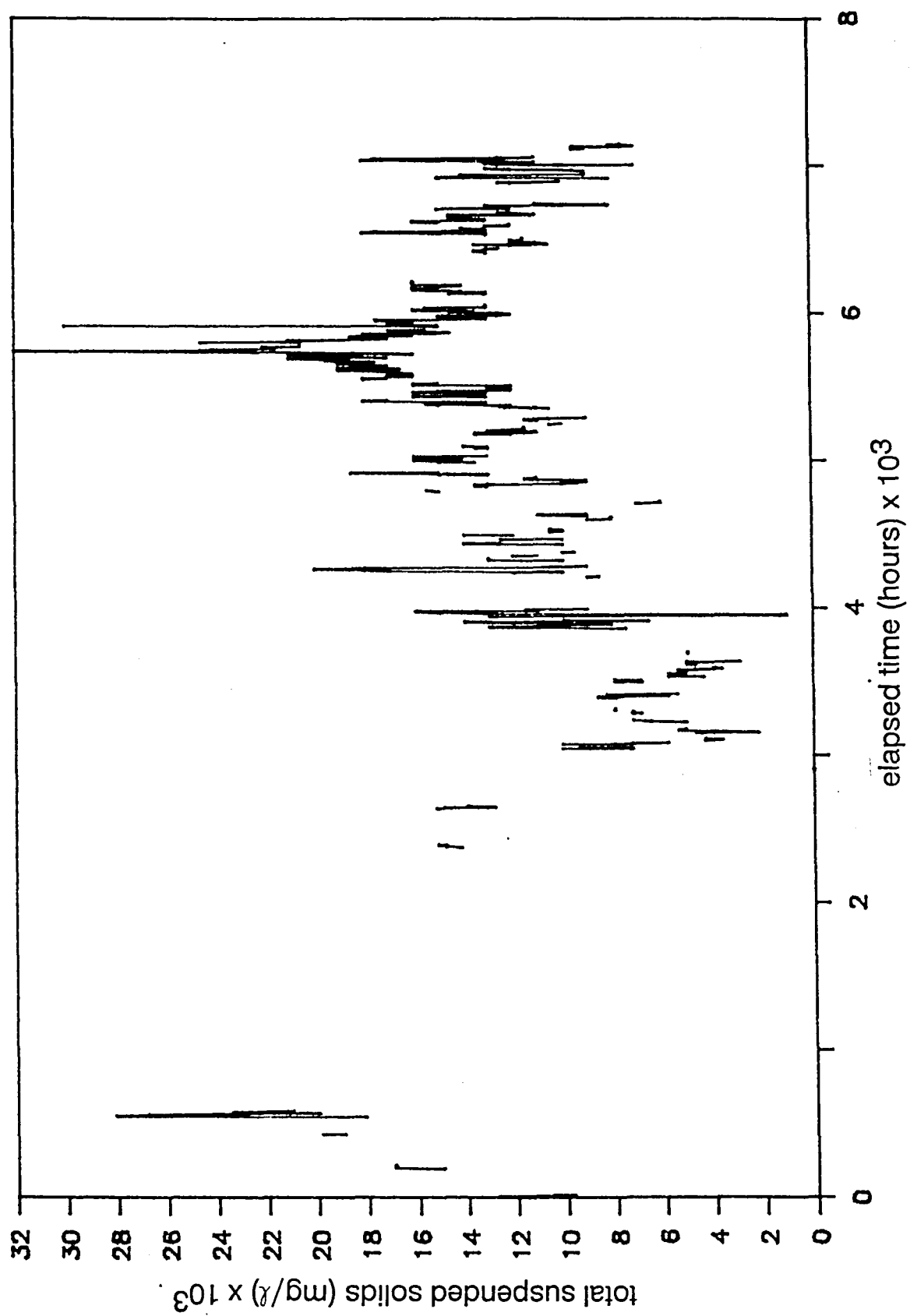
GRAPH 12A : SPARRO Feed Total Suspended Solids - 1989
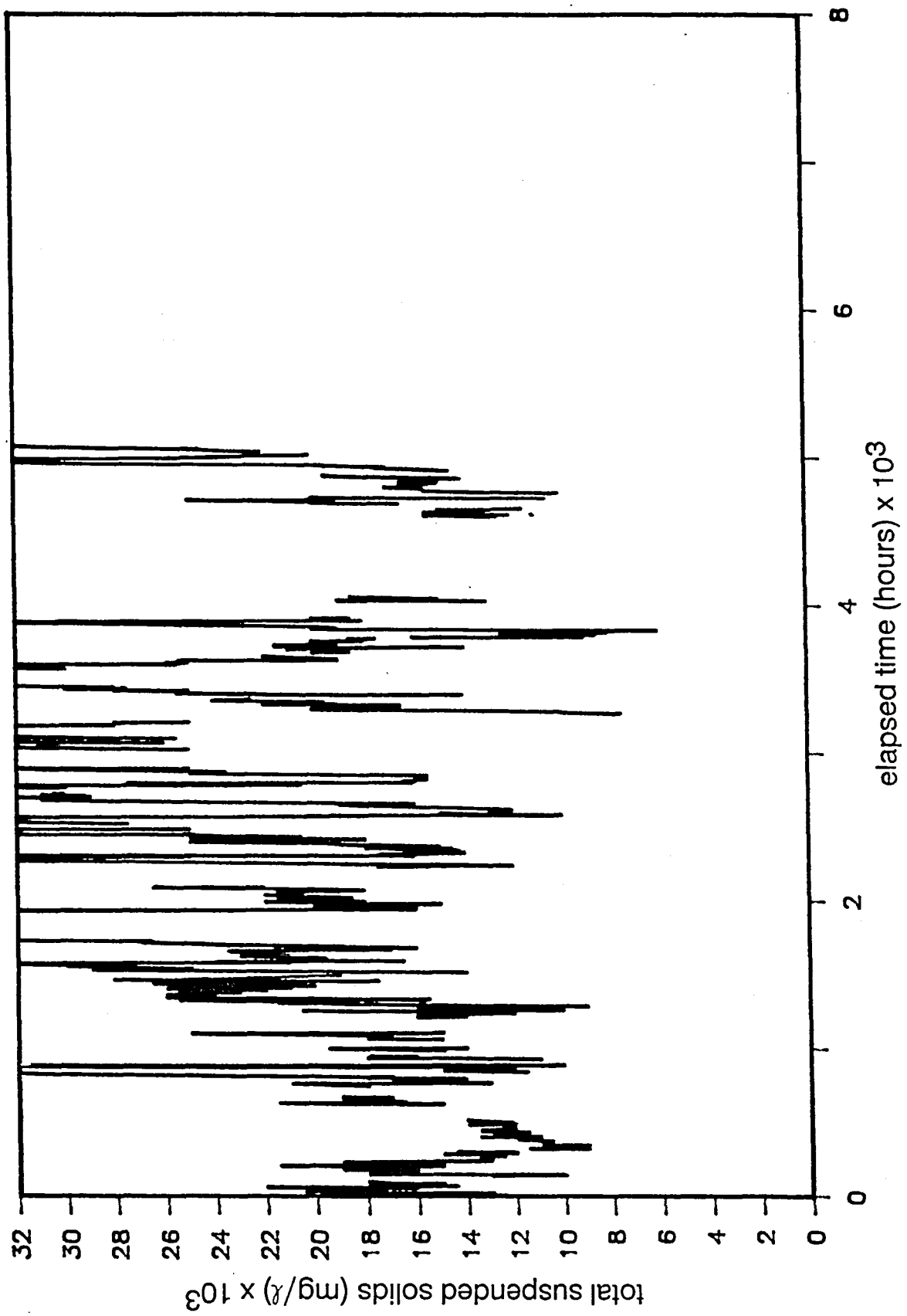
GRAPH 12B : SPARRO Feed Total Suspended Solids - 1990
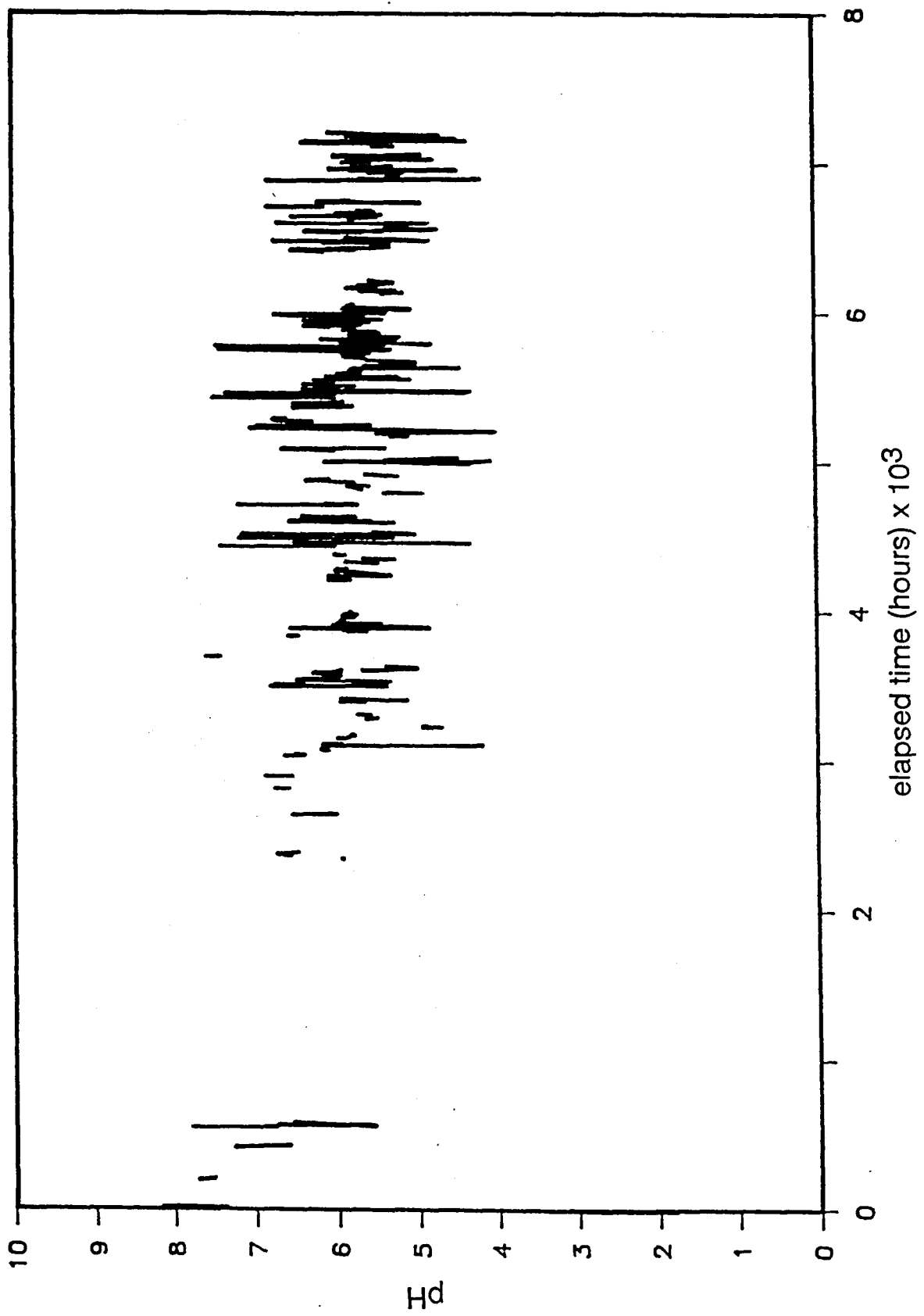
GRAPH 13A : SPARRO Feed pH - 1989
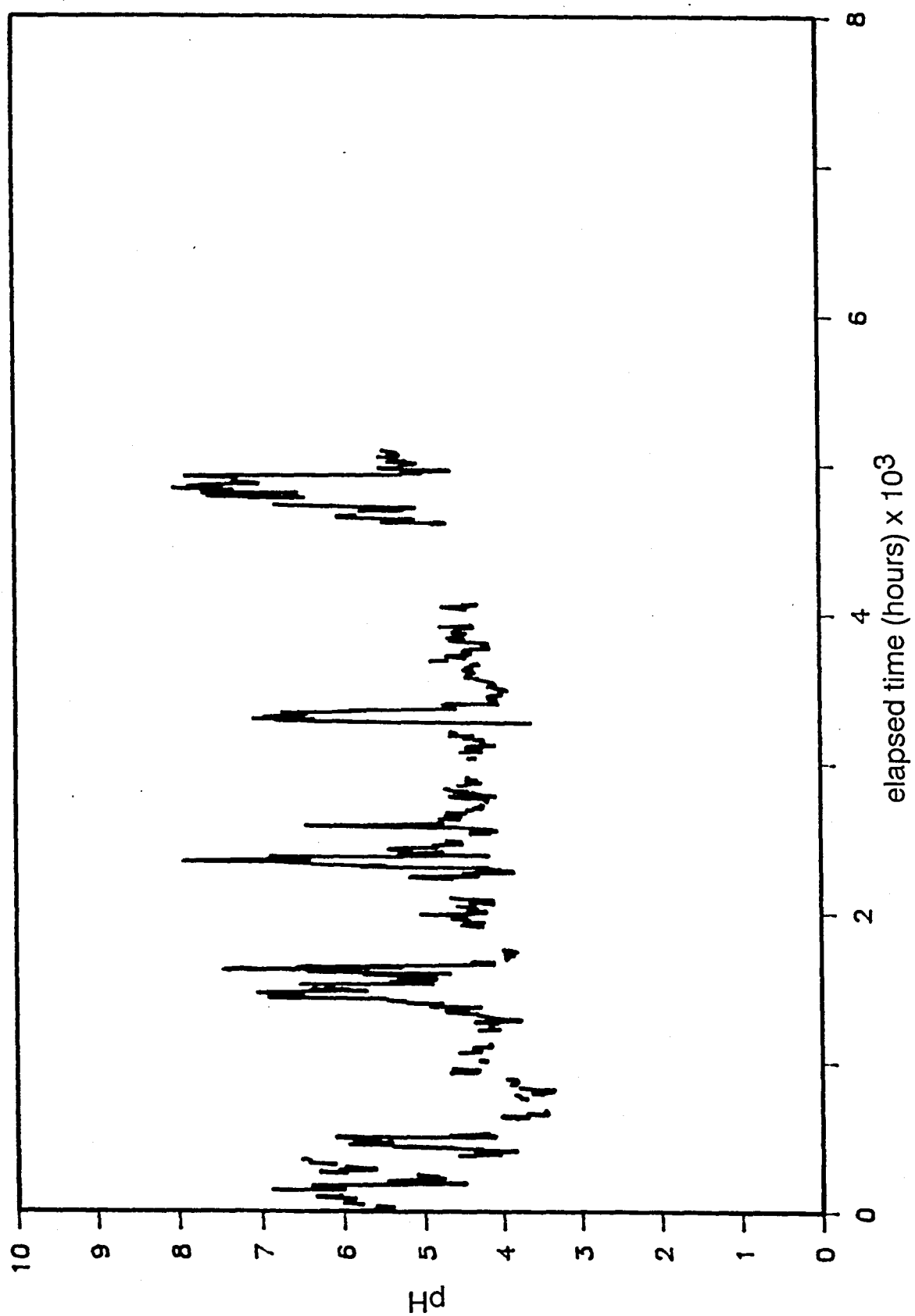
GRAPH 13B : SPARRO Feed pH - 1990
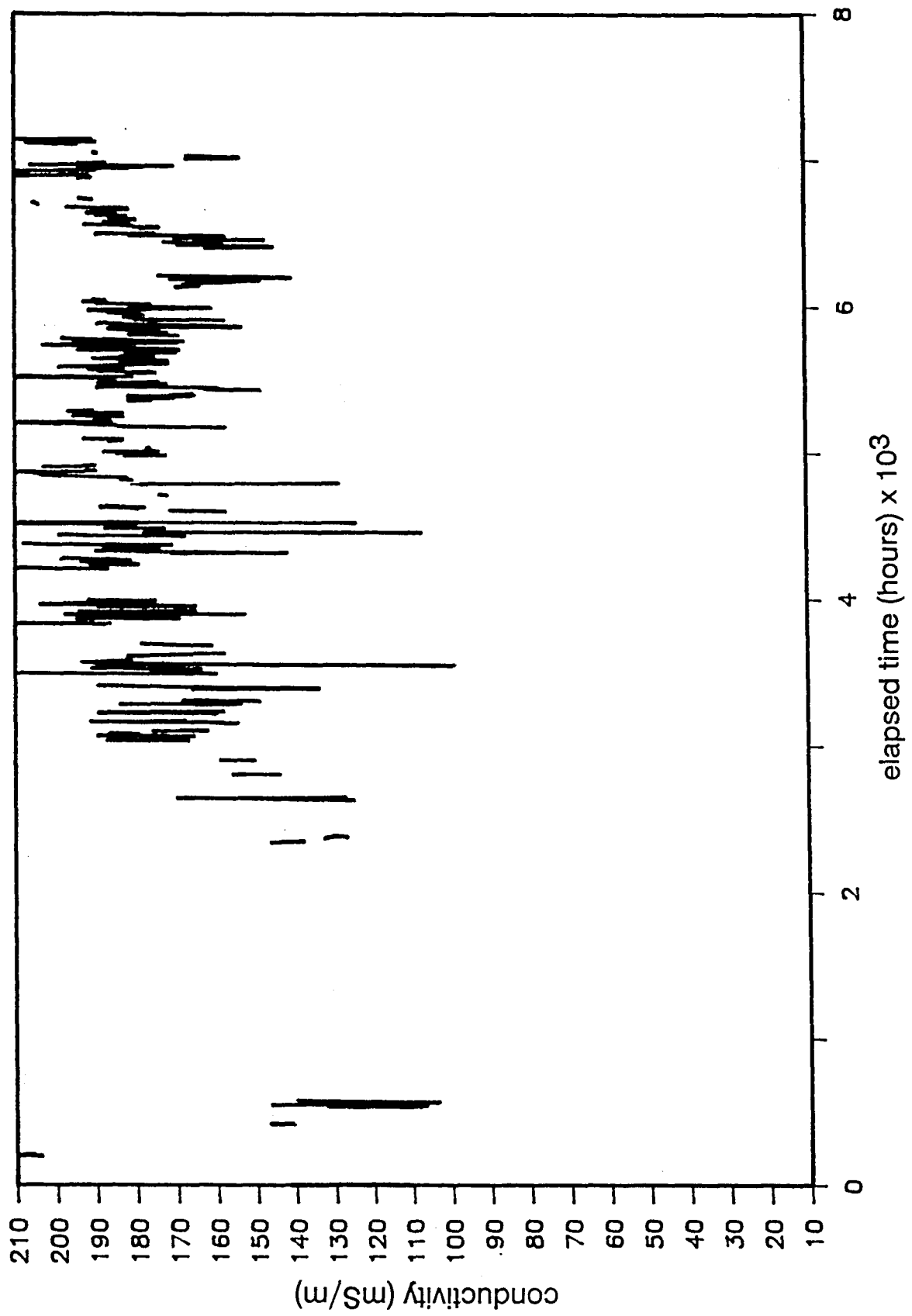
GRAPH 14A : SPARRO Product Conductivity - 1989
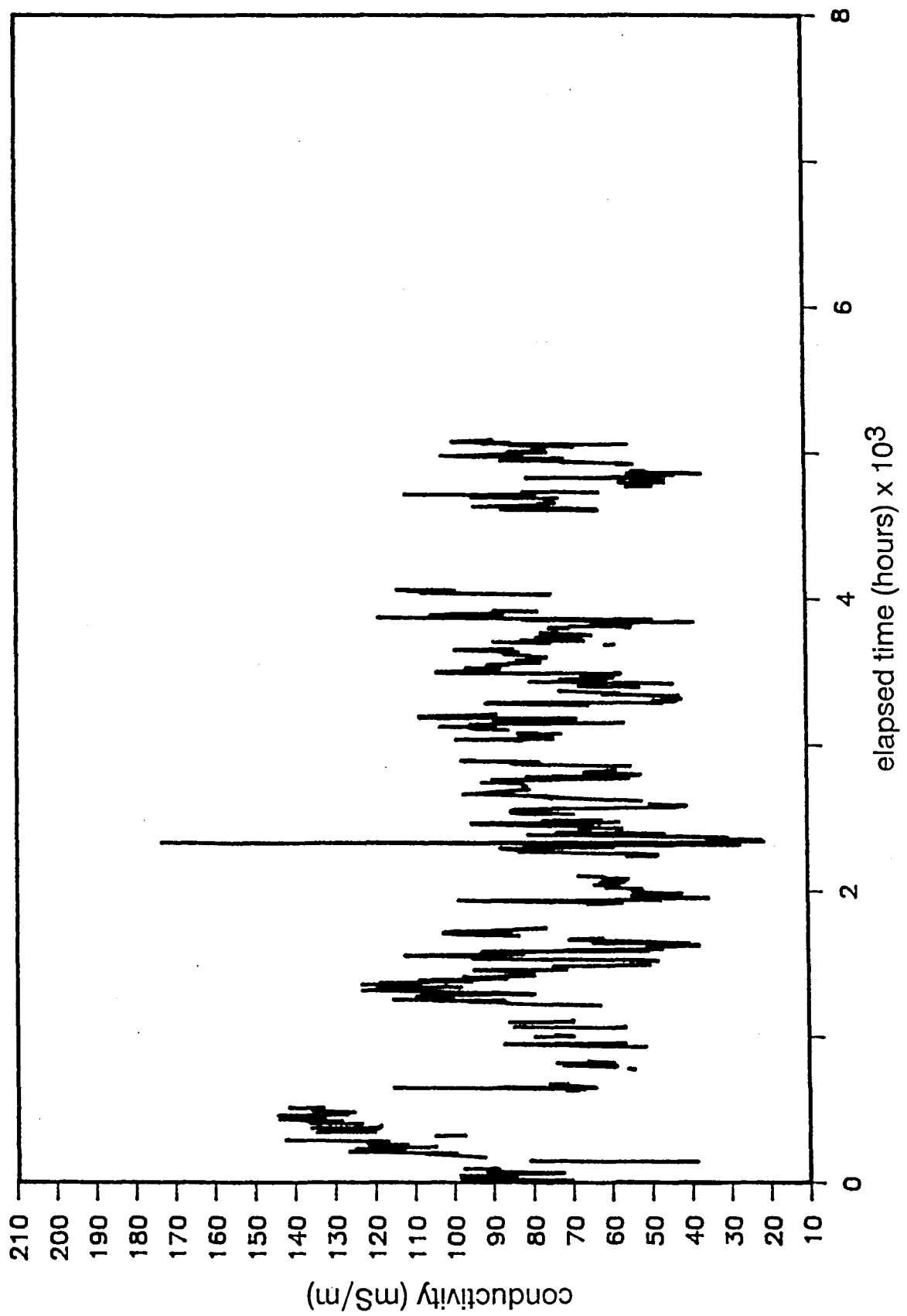
GRAPH 14B : SPARRO Product Conductivity - 1990
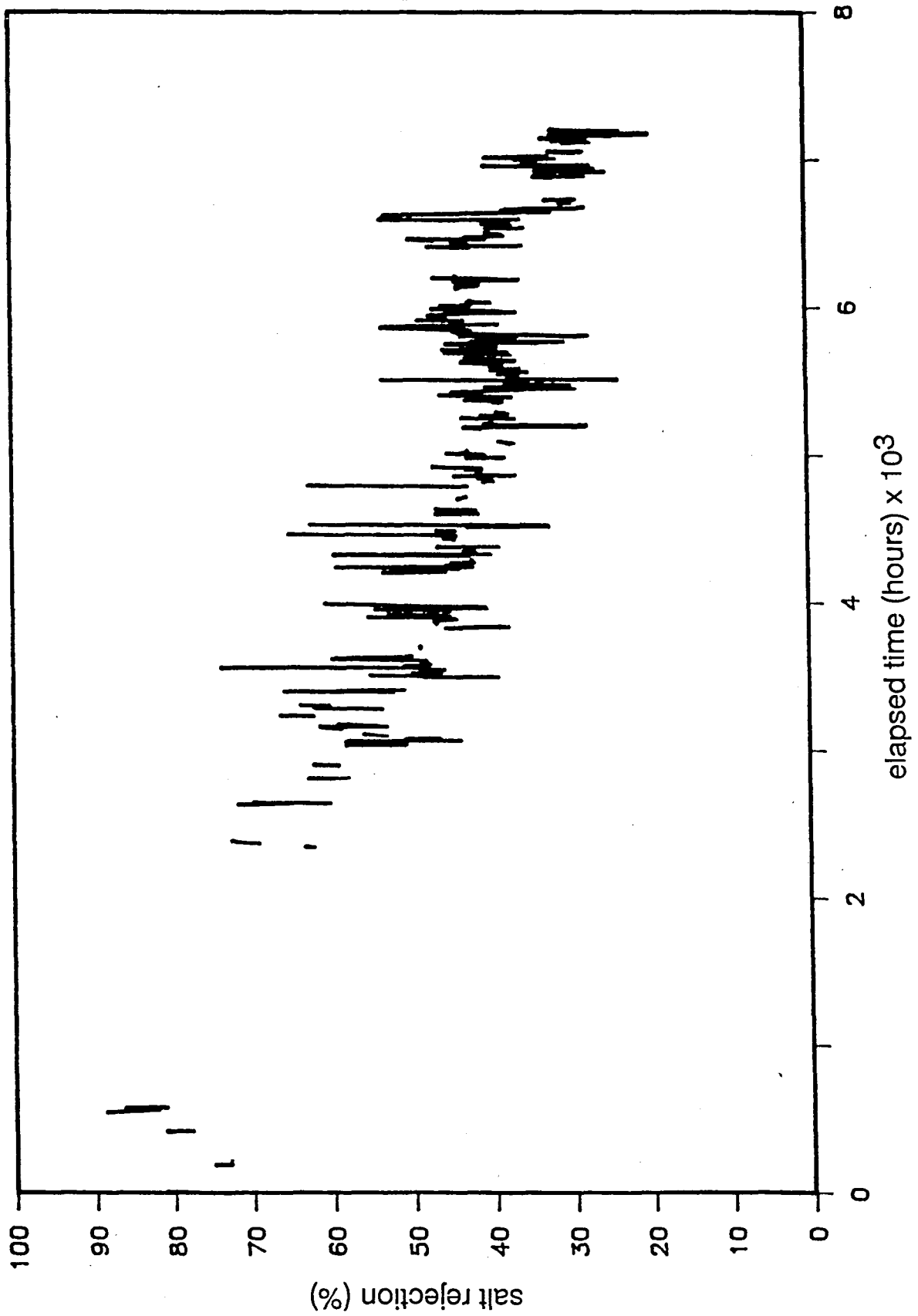
GRAPH 15A : SPARRO Rejection (wrt SPARRO Feed) - 1989
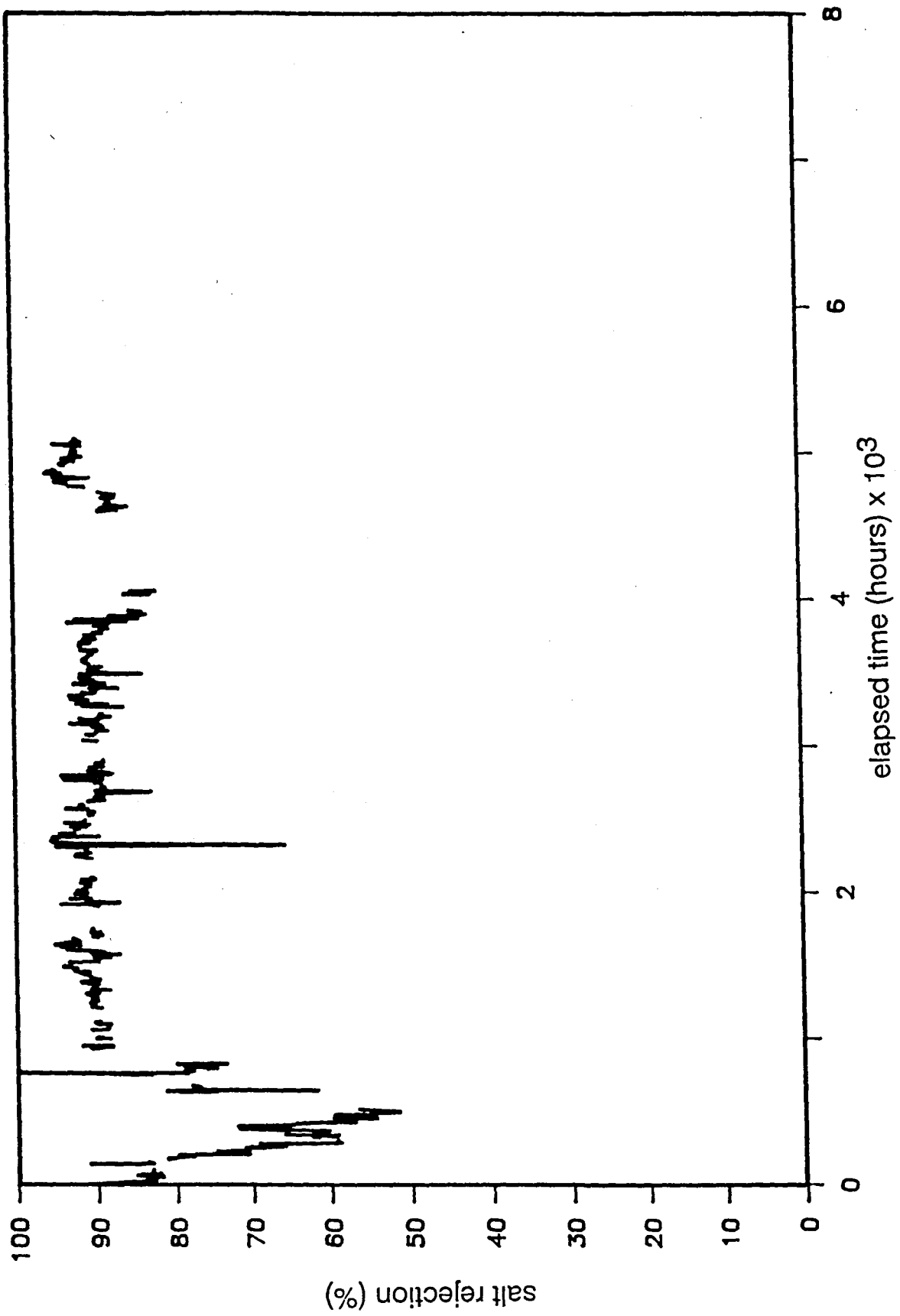
GRAPH 15B : SPARRO Rejection (wrt SPARRO Feed) - 1990

flux (λ.m2/d) x 10^3

40 bar, 25°C

elapsed time (hours) x 10^3
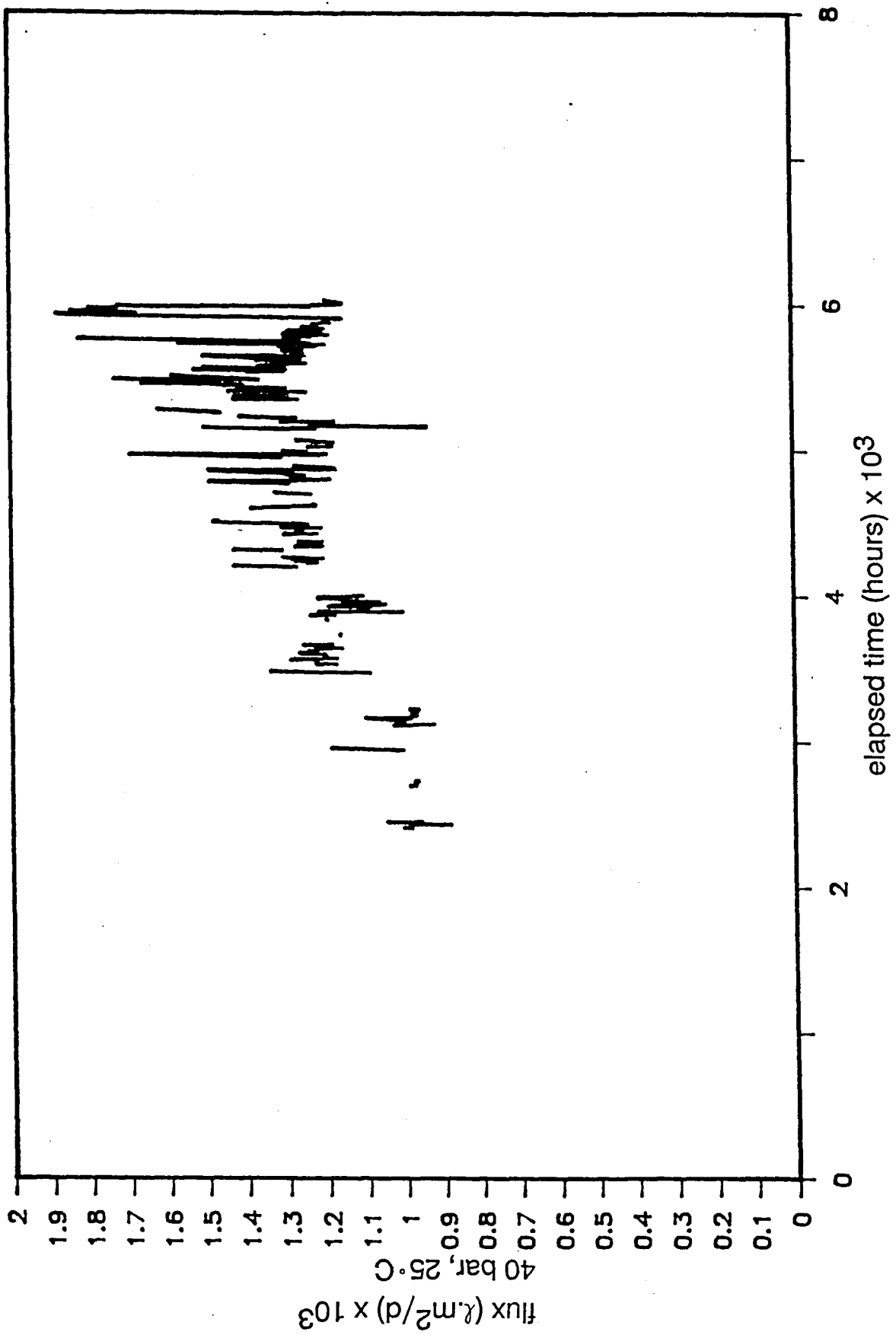
GRAPH 16A : SPARRO Corrected Flux - 1989

flux (ℓ.m2/d) x 10³
40 bar, 25·C

elapsed time (hours) x 10³
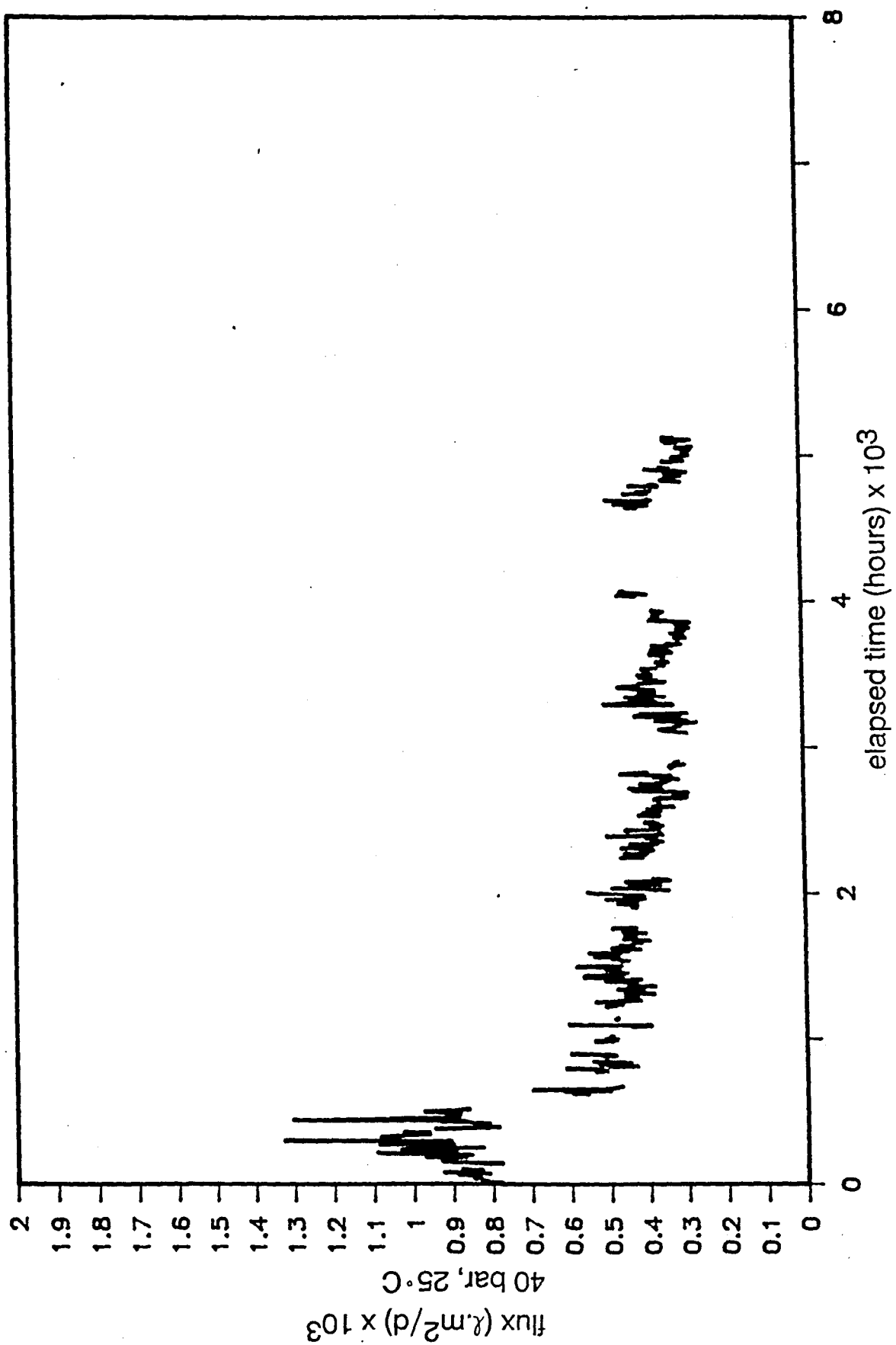
GRAPH 16B : SPARRO Corrected Flux - 1990

APPENDIX III   <u>REGISTER OF MODULES AND SALT REJECTIONS OF MODULES</u>
<u>INSTALLED ON MLT PLANT FROM MARCH 1989 TO AUGUST 1990</u>

APPENDIX III

MLT PLANT MODULE : REGISTER

POSITION NO. 1

DATE	PLANT HOURS	MODULE NO.	R COND. %	HOURS IN USE	FLUX ℓ/m².d
06.03.1989	0	881324	-		
01.06.1989	1047	890034	-	INSTALL 0	
01.06.1989	1047	890034	98	0	
22.06.1989	1472	890034	97	425	
28.07.1989	2190	890034	97	1143	
12.10.1989	3070	890034	83	2023	
13.11.1989	3686	890034	79,6	2639	
20.11.1989	3829	890034	74,5	2782	
30.11.1989	4003	890034	74,4	2956	
04.12.1989	4104	890034	79,5	3057	
11.12.1989	4218	890034	77,3	3171	
15.12.1989	4280	890034	75,1	3233	
22.12.1989	4370	890034	77,6	3323	
19.01.1990	4386	890034	76,9	3339	
29.01.1990	4592	890034	84,2	3545	
31.01.1990	4638	891035	-	INSTALL 0	
02.02.1990	4678	891035	98,1	40	
13.02.1990	4908	891035		270	
19.02.1990	5049	891035		411	
12.03.1990	5531	891035	94,47	893	
26.03.1990	5823	891035	94,75	1185	
11.04.1990	6190	891035	94,39	1552	
19.06.1990	7290	891035	93,87	2652	400
05.07.1990	7456	891035	95,99	2818	
13.07.1990	7636	891035	94,2	2998	
30.08.1990	8554	891035	91,3	3916	491

POSITION NO. 2

DATE	PLANT HOURS	MODULE NO.	R COND. %	HOURS IN USE	FLUX ℓ/m².d
06.03.1989	0	881343	-	INSTALL 0	
01.06.1989	1047	881343	90	1047	
22.06.1989	1472	881343	87	1472	
28.07.1989	2190	881343	86,5	2190	
12.10.1989	3070	881343	62	3070	
13.11.1989	3686	881343	59,3	3686	
20.11.1989	3829	881343	51,6	3829	
30.11.1989	4003	881343	48,7	4003	
04.12.1989	4104	881343	50,6	4104	
11.12.1989	4218	881343	46	4218	
15.11.1989	4280	881343	43,3	4280	
22.12.1989	4370	881343	47,5	4370	
19.01.1990	4386	881343	46,2	4386	
29.01.1990	4592	881343	54,3	4592	
31.01.1990	4638	891062	-	INSTALL 0	
02.02.1990	4678	891062	97,6	40	
13.02.1990	4908	891062		270	
19.02.1990	5049	891062		411	
12.03.1990	5531	891062	94,1	893	
26.03.1990	5823	891062	95,45	1185	
11.04.1990	6190	891062	94,60	1552	
19.06.1990	7290	891062	92,81	2652	542
05.07.1990	7456	891062	96,25	2818	
13.07.1990	7636	891062	94,2	2998	
30.08.1990	8554	891062	95,1	3916	653

POSITION	Position of module in stack 1 - 20
PLANT HOURS	Metered plant running time
MODULE NO.	Membratek serial number of module
R(COND)%	Salt rejection based on conductivity measurement
HOURS IN USE	Operating time elapsed since time of installation
FLUX	Measured flux in ℓ/m²/.d corrected to 25 ° C and 4 000 kPa.

POSITION NO. 3

DATE	PLANT HOURS	MODULE NO.	R COND. %	HOURS IN USE	FLUX $\ell/m^2.d$
06.03.1989	0	881094	-	INSTALL 0	
01.06.1989	1047	881094	87	1047	
22.06.1989	1472	881094	85	1472	
28.07.1989	2190	881094	83	2190	
12.10.1989	3070	881094	57	3070	
12.10.1989	3070	881510	-	INSTALL 0	
13.11.1989	3686	881510	88,3	616	
20.11.1989	3829	881510	83,9	759	
30.11.1989	4003	881510	67,4	933	
04.12.1989	4104	881510	88,8	1034	
11.12.1989	4218	881510	86,2	1148	
15.12.1989	4280	881510	84,8	1210	
22.12.1989	4370	881510	87,4	1300	
19.01.1990	4386	881510	86,6	1316	
29.01.1990	4592	881510	90,9	1522	
02.02.1990	4678	881510	91,3	1608	
13.02.1990	4908	881510		1838	
19.02.1990	5049	881510		1979	
12.03.1990	5531	881510	85,3	2461	
26.03.1990	5823	881510	86,67	2753	
11.04.1990	6190	881510	85,3	3120	
19.06.1990	7290	881510	84,02	4220	900
05.07.1990	7456	881510	90,02	4386	
13.07.1990	7636	881510	84,3	4566	
30.08.1990	8554	881510	86,6	5484	674

POSITION NO. 4

DATE	PLANT HOURS	MODULE NO.	R COND. %	HOURS IN USE	FLUX $\ell/m^2.d$
06.03.1989	0	881321	-	INSTALL 0	
01.06.1989	1047	881321	91	1047	
22.06.1989	1472	881321	86	1472	
28.07.1989	2190	881321	85	2190	
12.10.1989	3070	881321	64	3070	
13.11.1989	3686	881321	54,3	3686	
20.11.1989	3829	881321	51,6	3829	
30.11.1989	4003	881321	56,8	4003	
04.12.1989	4104.	881321	49,9	4104	
11.12.1989	4218	881321	46,2	4218	
15.12.1989	4280	881321	42,8	4280	
22.12.1989	4370	881321	45,7	4370	
19.01.1990	4386	881321	48,6	4386	
29.01.1990	4592	881321	54,1	4592	
31.01.1990	4638	891072	-	INSTALL 0	
02.02.1990	4678	891072	97,1	40	
13.02.1990	4908	891072		270	
19.02.1990	5049	891072		411	
12.03.1990	5531	891072	94,68	893	
26.03.1990	5823	891072	95,15	1185	
11.04.1990	6190	891072	94,57	1552	
11.06.1990	7044	900095	-	INSTALL 0	
19.06.1990	7290	900095	97,07	246	587
05.07.1990	7456	900095	98,38	412	
13.07.1990	7636	900095	97,5	592	
30.08.1990	8554	900095	96,8	1510	719

POSITION NO. 5

DATE	PLANT HOURS	MODULE NO.	R COND. %	HOURS IN USE	FLUX ℓ/m².d
06.03.1989	0	881320	-	INSTALL 0	
01.06.1989	1047	881320	91	1047	
02.06.1989	1061	890032	-	INSTALL 0	
22.06.1989	1472	890032	96	411	
28.07.1989	2190	890032	96	1129	
25.09.1989	2751	881492	-	INSTALL 0	
12.10.1989	3070	881492	93	319	
13.11.1989	3686	881492	88,6	935	
20.11.1989	3829	881492	86,7	1078	
30.11.1989	4003	881492	86,5	1252	
04.12.1989	4104	881492	89,7	1353	
11.12.1989	4218	881492	86,9	1467	
15.12.1989	4280	881492	86,7	1529	
22.12.1989	4370	881492	88,6	1619	
19.01.1990	4386	881492	87,8	1635	
29.01.1990	4592	881492	92,3	1841	
02.02.1990	4678	881492	92,2	1927	
13.02.1990	4908	881492		2157	
19.02.1990	5049	881492		2298	
12.03.1990	5531	881492	89,42	2780	
26.03.1990	5823	881492	90,13	3072	
11.04.1990	6190	881492	89,22	3439	
19.06.1990	7290	881492	88,61	4539	623
05.07.1990	7456	881492	92,32	4705	
13.07.1990	7636	881492	88,05	4885	
30.08.1990	8554	881492	90,0	5800	622

POSITION NO. 6

DATE	PLANT HOURS	MODULE NO.	R COND. %	HOURS IN USE	FLUX ℓ/m².d
06.03.1989	0	881351	-	INSTALL 0	
01.06.1989	1047	881351	91	1047	
22.06.1989	1472	881351	90	1472	
28.07.1989	2190	881351	88	2190	
12.10.1989	3070	881351	63,5	3070	
13.11.1989	3686	881351	58,6	3686	
20.11.1989	3829	881351	51,2	3829	
30.11.1989	4003	881351	65,2	4003	
04.12.1989	4104	881351	51	4104	
11.12.1989	4218	881351	46,2	4218	
15.12.1989	4280	881351	44,2	4280	
22.12.1989	4370	881351	48,5	4370	
19.01.1990	4386	881351	46,9	4386	
29.01.1990	4592	881351	57,8	4592	
31.01.1990	4638	890107	-	INSTALL 0	
02.02.1990	4678	890107	97,4	40	
09.02.1990	4838	891081	-.	INSTALL 0	
13.02.1990	4908	891081		70	
19.02.1990	5049	891081		211	
12.03.1990	5531	891081	94,47	693	
26.03.1990	5823	891081	94,90	985	
11.04.1990	6190	891081	94,56	1352	
04.05.1990	6504	900084	-	INSTALL 0	
19.06.1990	7290	900084	97,12	786	730
05.07.1990	7456	900084	98,33	952	
13.07.1990	7636	900084	97,03	1132	
30.08.1990	8554	900084	97,0	2050	625

POSITION NO. 7

DATE	PLANT HOURS	MODULE NO.	R COND. %	HOURS IN USE	FLUX $\ell/m^2.d$
06.03.1989	0	881344	-	INSTALL 0	
01.06.1989	1047	881344	90	1047	
22.06.1989	1472	881344	88	1472	
28.07.1989	2190	881344	86,5	2190	
12.10.1989	3070	881344	65,5	3070	
13.11.1989	3686	881344	56,2	3686	
20.11.1989	3829	881344	50,7	3829	
30.11.1989	4003	881344	88,9	4003	
04.12.1989	4104	881344	50,8	4104	
11.12.1989	4218	881344	46,4	4218	
15.12.1989	4280	881344	44,7	4280	
22.12.1989	4370	881344	49,8	4370	
19.01.1990	4386	881344	46,2	4386	
29.01.1990	4592	881344	51,9	4592	
31.01.1990	4638	891104	-	INSTALL 0	
02.02.1990	4678	891104	94,2	40	
13.02.1990	4908	891104		270	
19.02.1990	5049	891104		411	
12.03.1990	5531	891104	94,28	893	
26.03.1990	5823	891104	94,94	1185	
11.04.1990	6190	891104	94,33	1552	
19.06.1990	7290	891104	93,56	2652	702
05.07.1990	7456	891104	95,95	2818	
13.07.1990	7636	891104	93,9	2998	
30.08.1990	8554	891104	95,3	3916	529

POSITION NO. 8

DATE	PLANT HOURS	MODULE NO.	R COND. %	HOURS IN USE	FLUX $\ell/m^2.d$
06.03.1989	0	881348	-	INSTALL 0	
01.06.1989	1047	881348	88	1047	
22.06.1989	1472	881348	87	1472	
28.07.1989	2190	881348	85	2190	
12.10.1989	3070	881348	62,5	3070	
13.11.1989	3686	881348	52,8	3686	
20.11.1989	3829	881348	48,7	3829	
30.11.1989	4003	881348	89,7	4003	
04.12.1989	4104	881348	49,8	4104	
10.12.1989	4189	890017	-	INSTALL 0	
11.12.1989	4218	890017	93,8	29	
15.12.1989	4280	890017	93,2	91	
22.12.1989	4370	890017	94,2	181	
19.01.1990	4386	890017	92,9	197	
29.01.1990	4592	890017	92,6	403	
02.02.1990	4678	890017	94,9	489	
13.02.1990	4908	890017		719	
19.02.1990	5049	890017		860	
12.03.1990	5531	890017	89,44	1342	
26.03.1990	5823	890017	90,42	1634	
11.04.1990	6190	890017	89,43	2001	
19.06.1990	7290	890017	89,94	3101	623
05.07.1990	7456	890017	92,66	3267	
13.07.1990	7636	890017	88,9	3447	
30.08.1990	8554	890017	90,8	4365	686

POSITION NO. 9

DATE	PLANT HOURS	MODULE NO.	R COND. %	HOURS IN USE	FLUX $\ell/m^2.d$
06.03.1989	0	881298	-	INSTALL 0	
01.06.1989	1047	881298	88	1047	
22.06.1989	1472	881298	85	1472	
28.07.1989	2190	881298	85	2190	
12.10.1989	3070	881298	62,5	3070	
13.11.1989	3686	881298	61	3686	
20.11.1989	3829	881298	52,2	3829	
30.11.1989	4003	881298	53,8	4003	
04.12.1989	4104	881298	49,6	4104	
11.12.1989	4218	881298	44,2	4218	
15.12.1989	4280	881298	42,4	4280	
22.12.1989	4370	881298	46,2	4370	
19.01.1990	4386	881298	47,6	4386	
29.01.1990	4592	881298	54,1	4592	
31.01.1990	4638	891047	-	INSTALL 0	
02.02.1990	4678	891047	98,5	40	
13.02.1990	4908	891047		270	
19.02.1990	5049	891047		411	
12.03.1990	5531	891047	94,89	893	
26.03.1990	5823	891047	95,11	1185	
11.04.1990	6190	891047	94,3	1552	
19.06.1990	7290	891047	93,67	2652	604
05.07.1990	7456	891047	96,21	2818	
13.07.1990	7636	891047	94,05	2998	
30.08.1990	8554	891047	94,0	3916	565

POSITION NO. 10

DATE	PLANT HOURS	MODULE NO.	R COND. %	HOURS IN USE	FLUX $\ell/m^2.d$
06.03.1989	0	881295	-	INSTALL 0	
01.06.1989	1047	881295	88	1047	
22.06.1989	1472	881295	76,5	1472	
20.07.1989	1800(est)	890016	-	INSTALL 0	
28.07.1989	2190	890016	96	390	
12.10.1989	3070	890016	93	1270	
13.11.1989	3686	890016	80,8	1886	
20.11.1989	3829	890016	78,3	2029	
30.11.1989	4003	890016	77,9	2203	
04.12.1989	4104	890016	83,1	2304	
11.12.1989	4218	890016	79,4	2418	
15.12.1989	4280	890016	77,7	2480	
22.12.1989	4370	890016	80,5	2570	
19.01.1990	4386	890016	79,9	2586	
29.01.1990	4592	890016	85,1	2792	
02.02.1990	4678	890016	86,5	2878	
13.02.1990	4908	890016		3108	
19.02.1990	5049	890016		3249	
12.03.1990	5531	890016	83,09	3731	
26.03.1990	5823	890016	83,83	4023	
11.04.1990	6190	890016	83,48	4390	
30.04.1990	6458	900093	-	INSTALL 0	656
19.06.1990	7290	900093	96,66	832	
05.07.1990	7456	900093	97,95	998	
13.07.1990	7636	900093	96,9	1178	
30.08.1990	8554	900093	96,7	2096	833

POSITION NO. 11

DATE	PLANT HOURS	MODULE NO.	R COND. %	HOURS IN USE	FLUX ℓ/m².d
06.03.1989	0	881300	-	INSTALL 0	
01.06.1989	1047	881300	91	1047	
22.06.1989	1472	881300	86,5	1472	
28.07.1989	2190	881300	86,5	2190	
12.10.1989	3070	881300	61	3070	
13.11.1989	3686	881300	51,1	3686	
15.11.1989	3727	890445	-	INSTALL 0	
20.11.1989	3829	890445	91,9	102	
26.11.1989	3954	881451	-	(ex. 12)	
30.11.1989	4003	881451	42,8	49	
04.12.1989	4104	881451	31,9	150	
11.12.1989	4218	881451	27,6	264	
15.12.1989	4280	881451	25,5	326	
22.12.1989	4370	881451	29,3	416	
19.01.1990	4386	881451	29,5	432	
29.01.1990	4592	881451	37,3	638	
31.01.1990	4638	891097	-	INSTALL 0	
02.02.1990	4678	891097	97,5	40	
13.02.1990	4908	891097		270	
19.02.1990	5049	891097		411	
12.03.1990	5531	891097	93,76	893	
26.03.1990	5823	891097	94,65	1185	
11.04.1990	6190	891097	94,12	1552	
19.06.1990	7290	891097	94,18	2652	559
05.07.1990	7456	891097	96,10	2818	
13.07.1990	7636	891097	94,25	2988	
30.08.1990	8554	891097	95,8	3916	555

POSITION NO. 12

DATE	PLANT HOURS	MODULE NO.	R COND. %	HOURS IN USE	FLUX ℓ/m².d
06.03.1989	0	881451	-	INSTALL 0	
01.06.1989	1047	881451	84	1047	
22.06.1989	1472	881451	80	1472	
28.07.1989	2190	881451	79	2190	
12.10.1989	3070	881451	53	3070	
13.11.1989	3686	881451	43,2	3686	
15.11.1989	3727	880376	-	INSTALL 0	
20.11.1989	3829	880376	91,9	102	
30.11.1989	4003	880376	88,9	276	
04.12.1989	4104	880376	90,2	377	
11.12.1989	4218	880376	87,2	491	
15.12.1989	4280	880376	86,1	553	
22.12.1989	4370	880376	88,1	643	
19.01.1990	4386	880376	86,7	659	
29.01.1990	4592	880376	91,5	865	
02.02.1990	4678	880376	94,4	951	
13.02.1990	4908	880376		1181	
14.02.1990	4929	891094	-	INSTALL 0	
19.02.1990	5049	891094		120	
12.03.1990	5531	891094	95,25	602	
26.03.1990	5823	891094	95,70	894	
11.04.1990	6190	891094	95,13	1261	
19.06.1990	7290	891094	94,80	2361	600
05.07.1990	7456	891094	96,77	2527	
13.07.1990	7636	891094	95,00	2707	
20.07.1990	7805	900098		INSTALL 0	
30.08.1990	8554	900098	97,8	749	719

POSITION NO. 13

DATE	PLANT HOURS	MODULE NO.	R COND. %	HOURS IN USE	FLUX ℓ/m²·d
06.03.1989	0	881299	-	INSTALL 0	
01.06.1989	1047	881299	86	1047	
22.06.1989	1472	881299	85	1472	
28.07.1989	2190	881299	83	2190	
12.10.1989	3070	881299	57	3070	
13.11.1989	3686	881299	47,1	3686	
15.11.1989	3727	880379	-	INSTALL 0	
20.11.1989	3829	880379	94	102	
30.11.1989	4003	880379	89,4	276	
04.12.1989	4104	880379	90,8	377	
11.12.1989	4218	880379	87,8	491	
15.12.1989	4280	880379	86,9	553	
22.12.1989	4370	880379	88,8	643	
19.01.1990	4386	880379	87,6	659	
29.01.1990	4592	880379	92,1	865	
02.02.1990	4678	880379	91,5	951	
13.02.1990	4908	880379		1181	
19.02.1990	5049	880379		1322	
01.03.1990	5276	900020	-	INSTALL 0	
12.03.1990	5531	900020	96,22	255	
26.03.1990	5823	900020	96,58	547	
11.04.1990	6190	900020	96,19	914	
19.06.1990	7290	900020	95,89	2014	579
05.07.1990	7456	900020	96,95	2180	
13.07.1990	7636	900020	96,1	2360	
30.08.1990	8554	900020	96,7	3278	674

POSITION NO. 14

DATE	PLANT HOURS	MODULE NO.	R COND. %	HOURS IN USE	FLUX ℓ/m²·d
01.03.1989	0	881103	-	INSTALL 0	
01.06.1989	1047	881103	91	1047	
22.06.1989	1472	881103	89	1472	
28.07.1989	2190	881103	87	2190	
12.12.1989	3070	881103	69	3070	
13.11.1989	3686	881103	61,1	3686	
15.11.1989	3727	890686	-	INSTALL 0	
20.11.1989	3829	890686	91,6	102	
30.11.1989	4003	890686	90,6	276	
04.12.1989	4104	890686	92	377	
11.12.1989	4218	890686	90,4	491	
15.12.1989	4280	890686	89,7	553	
22.12.1989	4370	890686	90,9	643	
19.01.1990	4386	890686	90,5	659	
29.01.1990	4592	890686	93,7	865	
02.02.1990	4678	890686	93,1	951	
13.02.1990	4908	890686		1181	
19.02.1990	5049	890686		1322	
01.03.1990	5276	900023	-	INSTALL 0	
12.03.1990	5531	900023	96,15	255	
26.03.1990	5823	900023	96,65	547	
11.04.1990	6190	900023	96,33	914	
19.06.1990	7290	900023	96,03	2014	675
05.07.1990	7456	900023	97,20	2180	
13.07.1990	7636	900023	95,9	2360	
30.08.1990	8554	900023	96,5	3278	684

POSITION NO. 15

DATE	PLANT HOURS	MODULE NO.	R COND. %	HOURS IN USE	FLUX ℓ/m²·d
06.03.1989	0	881502	-	INSTALL 0	
01.06.1989	1047	881502	80	1047	
22.06.1989	1472	881502	75	1472	
20.07.1989	1800	890031	-	INSTALL 0	
28.07.1989	2190	890031	98	390	
26.09.1989	2756	881108	-	INSTALL 0	
12.10.1989	3070	881108	93,5	314	
13.11.1989	3686	881108	87,8	930	
15.11.1989	3727	890685	-	INSTALL 0	
20.11.1989	3829	890685	89,8	102	
30.11.1989	4003	890685	89,6	276	
04.12.1989	4104	890685	91,3	377	
11.12.1989	4218	890685	89,6	491	
15.12.1989	4280	890685	88,5	553	
22.12.1989	4370	890685	90,7	643	
19.01.1990	4386	890685	90,1	659	
29.01.1990	4592	890685	93,3	865	
02.02.1990	4678	890685	92,2	951	
13.02.1990	4908	890685		1181	
19.02.1990	5049	890685		1322	
12.03.1990	5531	890685	91,87	1864	
26.03.1990	5823	890685	95,24	2096	
11.04.1990	6190	890685	92,4	2463	
21.04.1990		900080	-	INSTALL 0	
22.04.1990	6303	900096	-	INSTALL 0	
19.06.1990	7290	900096	96,72	987	605
05.07.1990	7456	900096	97,82	1153	
13.07.1990	7636	900096	96,0	1333	
30.08.1990	8554	900096	96,5	2251	743

POSITION NO. 16

DATE	PLANT HOURS	MODULE NO.	R COND. %	HOURS IN USE	FLUX ℓ/m²·d
06.03.1989	0	881309	-	INSTALL 0	
01.06.1989	1047	881309	92,5	1047	
22.06.1989	1472	881309	90	1472	
28.07.1989	2190	881309	88	2190	
12.10.1989	3070	881309	69	3070	
13.11.1989	3686	881309	57,5	3686	
20.11.1989	3829	881309	53,7	3829	
30.11.1989	4003	881309	56,4	4003	
04.12.1989	4104	881309	53,6	4104	
11.12.1989	4218	881309	49,1	4218	
15.12.1989	4280	881309	48,9	4280	
22.12.1989	4370	881309	51,2	4370	
19.01.1990	4386	881309	49,2	4386	
29.01.1990	4592	881309	58,8	4592	
31.01.1990	4638	891085	-	INSTALL 0	
01.02.1990	4665	891082	-	INSTALL 0	
02.02.1990	4678	891082	96,9	13	
13.02.1990	4908	891082		243	
19.02.1990	5049	891082		384	
12.03.1990	5531	891082	23,05	866	
26.03.1990	5823	891082	93,53	1158	
11.04.1990	6190	891082	92,89	1525	
21.04.1990					
19.06.1990	7290	891082	93,05	2625	568
05.07.1990	7456	891082	95,44	2791	
13.07.1990	7636	891082	93,2	2791	
30.08.1990	8554	891082	95,2	3889	529

POSITION NO. 17

DATE	PLANT HOURS	MODULE NO.	R COND. %	HOURS IN USE	FLUX ℓ/m²,d
06.03.1989	0	881323	-	INSTALL 0	
01.06.1989	1047	881323	92	1047	
22.06.1989	1472	881323	90	1472	
28.07.1989	2190	881323	88,5	2190	
12.10.1989	3070	881323	67	3070	
13.11.1989	3686	881323	59	3686	
20.11.1989	3829	881323	55,6	3829	
30.11.1989	4003	881323	90,2	4003	
04.12.1989	4104	881323	56,1	4104	
11.12.1989	4218	881323	51,9	4218	
15.12.1989	4280	881323	48,7	4280	
22.12.1989	4370	881323	54	4370	
19.01.1990	4386	881323	51,8	4386	
29.01.1990	4592	881323	59,8	4592	
31.01.1990	4638	891092	-	INSTALL 0	
02.02.1990	4678	891092	93,6	40	
13.02.1990	4908	891092		270	
13.02.1990	4908	891091	-	INSTALL 0	
19.02.1990	5049	891091		141	
02.03.1990	5285	900034	-	INSTALL 0	
12.03.1990	5531	900034	96,31	246	
26.03.1990	5823	900034	96,55	538	
11.04.1990	6190	900034	96,22	905	
22.04.1990	6303	900099	-	INSTALL 0	
19.06.1990	7290	900099	97,02	987	779
05.07.1990	7456	900099	98,06	1153	
13.07.1990	7636	900099	97,25	1333	
30.08.1990	8554	900099	97,3	2251	719

POSITION NO. 18

DATE	PLANT HOURS	MODULE NO.	R COND. %	HOURS IN USE	FLUX ℓ/m²,d
06.03.1989	0	881319	-	INSTALL 0	
14.03.1989	125	881576	-	INSTALL 0	
01.06.1989	1047	881576	86	922	
22.06.1989	1472	881576	86	1347	
28.07.1989	2190	881576	81,5	2065	
12.10.1989	3070	881576	56,5	2945	
13.10.1989	3092	881490	-	INSTALL 0	
13.11.1989	3686	881490	90	594	
20.11.1989	3829	881490	89,5	737	
30.11.1989	4003	881490	93,7	911	
04.12.1989	4104	881490	92	1012	
11.12.1989	4218	881490	89,4	1126	
15.12.1989	4280	881490	89,2	1188	
22.12.1989	4370	881490	90,4	1278	
19.01.1990	4386	881490	90,4	1294	
29.01.1990	4592	881490	94,3	1500	
02.02.1990	4678	881490	75,6	1586	
13.02.1990	4908	881490		1816	
19.02.1990	5049	881490		1957	
12.03.1990	5531	881490	85,01	2439	
26.03.1990	5823	881490	85,38	2731	
11.04.1990	6190	881490	85,62	3098	
19.06.1990	7290	881490	86,47	4198	625
05.07.1990	7456	881490	89,51	4364	
13.07.1990	7636	881490	84,06	4544	
30.08.1990	8554	881490	87,3	5462	610

POSITION NO. 19

DATE	PLANT HOURS	MODULE NO.	R COND. %	HOURS IN USE	FLUX $\ell/m^2.d$
06.03.1989	0	881296	-	INSTALL 0	
29.04.1989	713	890024	-	INSTALL 0	
01.06.1989	1047	890024	95	334	
22.06.1989	1472	890024	95	759	
28.07.1989	2190	890024	93	1477	
12.10.1989	3070	890024	87	2357	
14.10.1989	3112	881342	-	INSTALL 0	
13.11.1989	3686	881342	89,7	574	
20.11.1989	3829	881342	91,7	717	
30.11.1989	4003	881342	93,8	891	
04.12.1989	4104	881342	92,2	992	
11.12.1989	4218	881342	90,2	1106	
15.12.1989	4280	881342	89,4	1168	
22.12.1989	4370	881342	91,2	1258	
19.01.1990	4386	881342	90,8	1274	
29.01.1990	4592	881342	94,2	1480	
02.02.1990	4678	891080	-	INSTALL 0	
02.02.1990	4678	891080	95,1	0	
13.02.1990	4908	891080		230	
19.02.1990	5049	891080		471	
12.03.1990	5531	891080	94,08	853	
26.03.1990	5823	891080	94,84	1145	
11.04.1990	6190	891080	94,09	1512	
19.06.1990	7290	891080	92,42	2612	578
05.07.1990	7456	891080	95,78	2778	
13.07.1990	7636	891080	93,5	2958	
30.08.1990	8554	891080	93,6	3876	608

POSITION NO. 20

DATE	PLANT HOURS	MODULE NO.	R COND. %	HOURS IN USE	FLUX $\ell/m^2.d$
06.03.1989	0	881297	-	INSTALL 0	
01.06.1989	1047	881297	88	1047	
22.06.1989	1472	881297	84,5	1472	
28.07.1989	2190	881297	82,5	2190	
12.10.1989	3070	881297	61,5	3070	
13.11.1989	3686	881297	47,9	3686	
20.11.1989	3829	881297	90,9	3829	
30.11.1989	4003	881297	63,5	4003	
04.12.1989	4104	881297	45,3	4104	
11.12.1989	4218	881297	41,9	4218	
15.12.1989	4280	881297	40,8	4280	
22.12.1989	4370	881297	43,9	4370	
19.01.1990	4386	881297	45,6	4386	
29.01.1990	4592	881297	51,1	4592	
31.01.1990	4638	891107	-	INSTALL 0	
02.02.1990	4678	891030	-	INSTALL 0	
02.02.1990	4678	891030	98,9	0	
13.02.1990	4908	891030		230	
19.02.1990	5049	891030		371	
12.03.1990	5531	891030	94,06	853	
26.03.1990	5823	891030	94,43	1145	
11.04.1990	6190	891030	93,91	1512	
19.06.1990	7290	891030	93,19	2612	574
05.07.1990	7456	891030	95,55	2778	
13.07.1990	7636	891030	95,60	2958	
30.08.1990	8554	891030	94,10	3876	672

APPENDIX IV   CALCIUM SULPHATE SEED PARTICLE SIZE CHARACTERISTICS

APPENDIX IV

MLT PLANT : PARTICLE SIZE OF SEED d$_{50}$ MICRONS

Date	Brine Reject	Cyclone Overflow	Cyclone Underflow	Feed	Gypsum
19.09.89	30	12	29	28	
20.09.89	37			44	
05.10.89	41	41	40		
11.10.89	39	28	42		
19.10.89	45	15	44		
25.10.89	42	20	44		
02.11.89	43	35	43		
08.11.89	42	23	43		
15.11.89	41	28	42		
22.11.89	40				
29.11.89	30	13	44		
07.12.89	37	25	37		
13.12.89	30				
19.12.89	40				
01.02.90	40	11	40		
08.02.90	45		50		
15.02.90	50	10	70		
22.02.90	40	12	45		
01.03.90	42	14	42		
07.03.90	32	11	40		
14.03.90	30	11	35	30	
15.03.90					40

SPARRO PLANT : PARTICLE SIZE OF SEED d_{50} MICRONS

Date	Brine Reject	Cyclone Overflow	Cyclone Underflow	Feed	Gypsum
19.09.89	68	35		64	75
05.10.89	66	37	67		
11.10.89	37	35	51		
19.10.89			25		
25.10.89	44	38	43		
02.11.89	49	37	48		
15.11.89	60	50	60		
22.11.89	65				
29.11.89	55	55	60		
07.12.89	60	70	62		
13.12.89	65				
01.02.90	60	50	60		
08.02.90	84	12	80		
15.02.90	71	11	90		
07.03.90	55	10	50		
14.03.90	50	50	50		

MLT Reject Particle Size Distribution
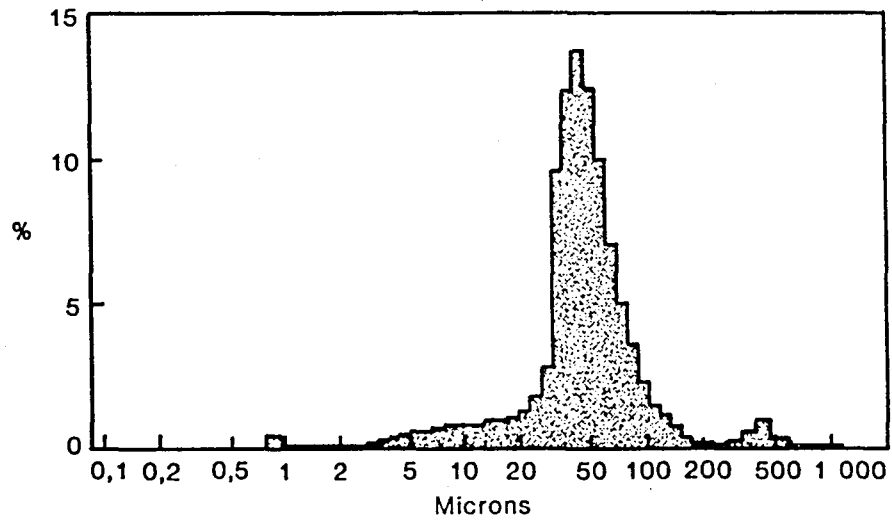
MTL Cyclone Underflow particle Size Distribution
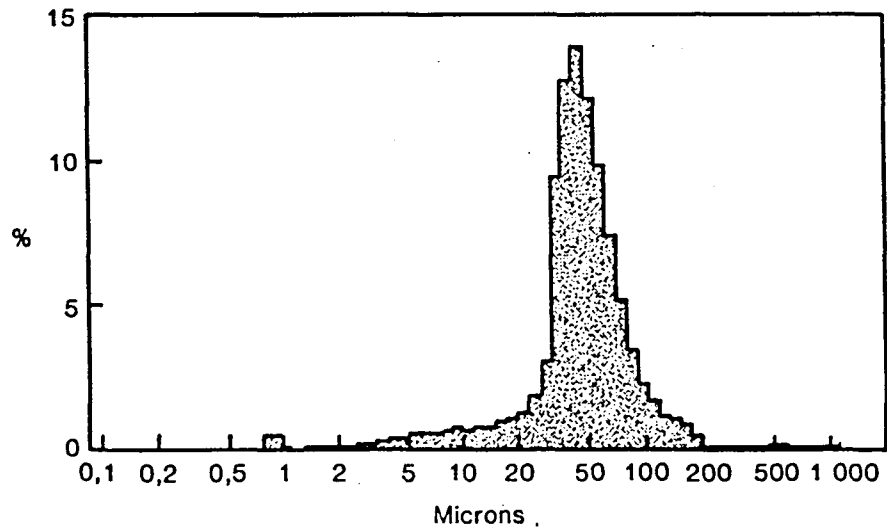
MLT Cyclone Overflow Particle Size Distribution
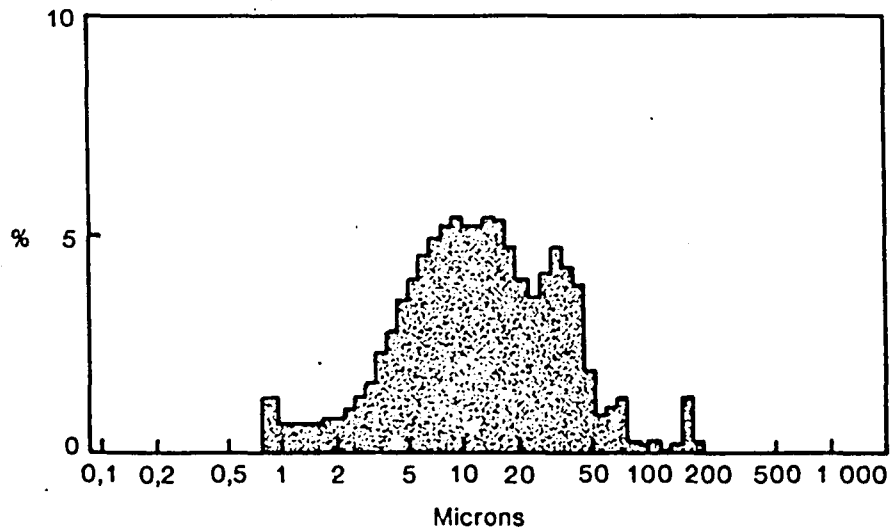
Sparro Reject Particle Size Distribution
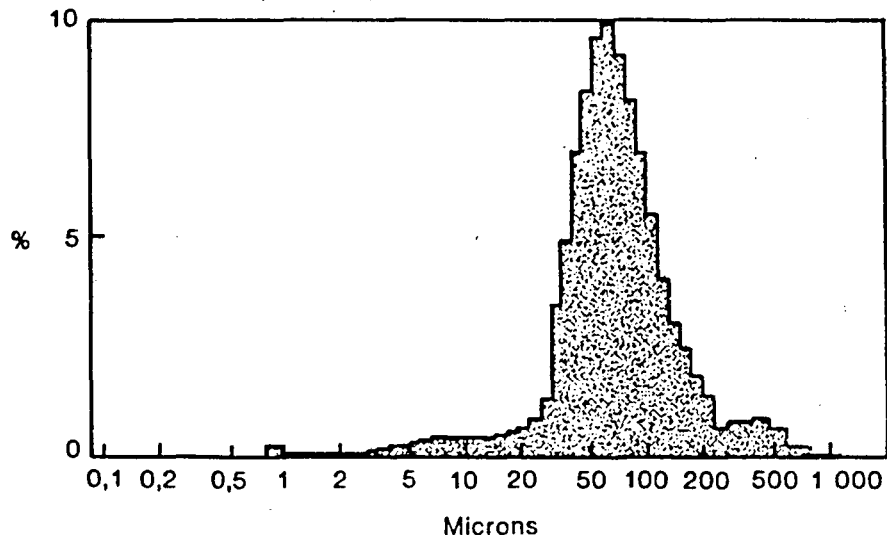
Sparro Cyclone Underflow Particle Size Distribution
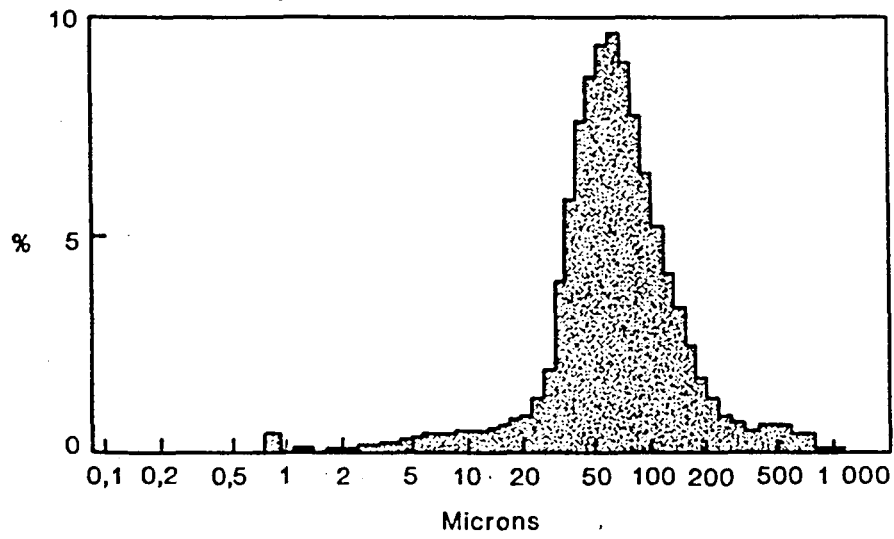
Sparro Cyclone Overflow Particle Size Distribution
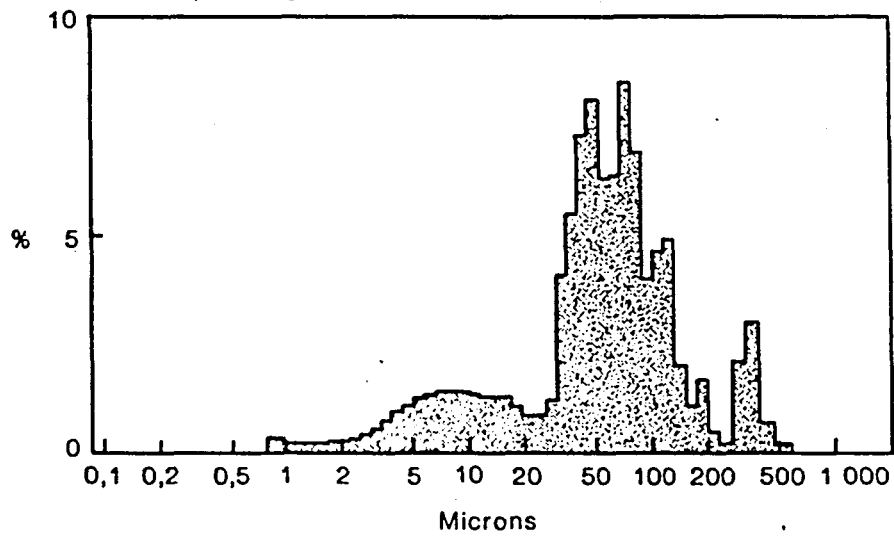
APPENDIX V <u>MICROSCOPE PHOTOGRAPHS OF CELLULOSE ACETATE MEMBRANE</u>
<u>THAT FAILED IN SPARRO PLANT</u>

APPENDIX V

MICROSCOPE PHOTOGRAPHS OF CELLULOSE ACETATE MEMBRANE THAT FAILED IN SPARRO PLANT
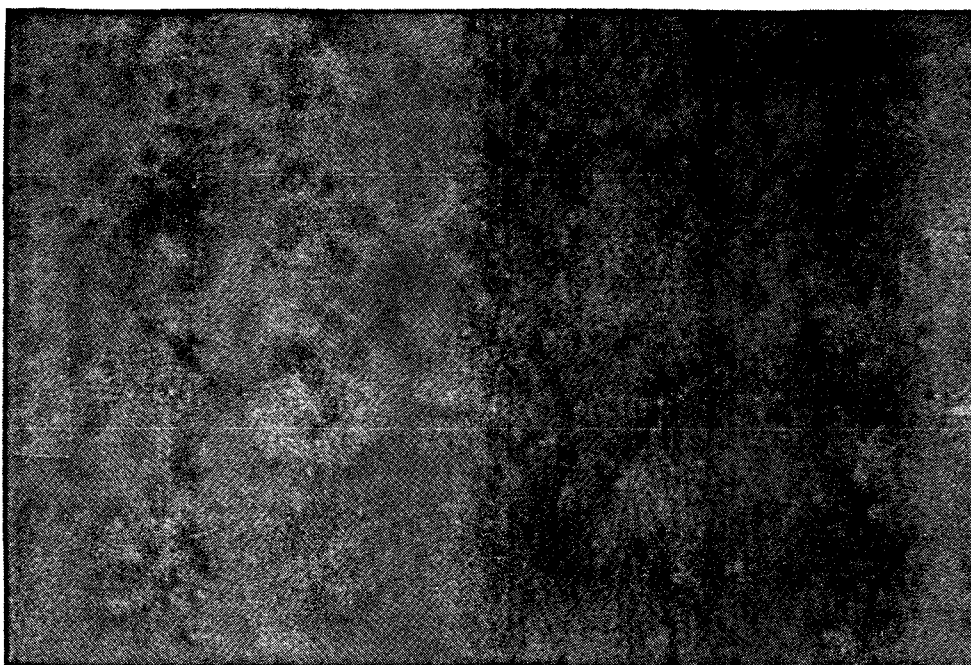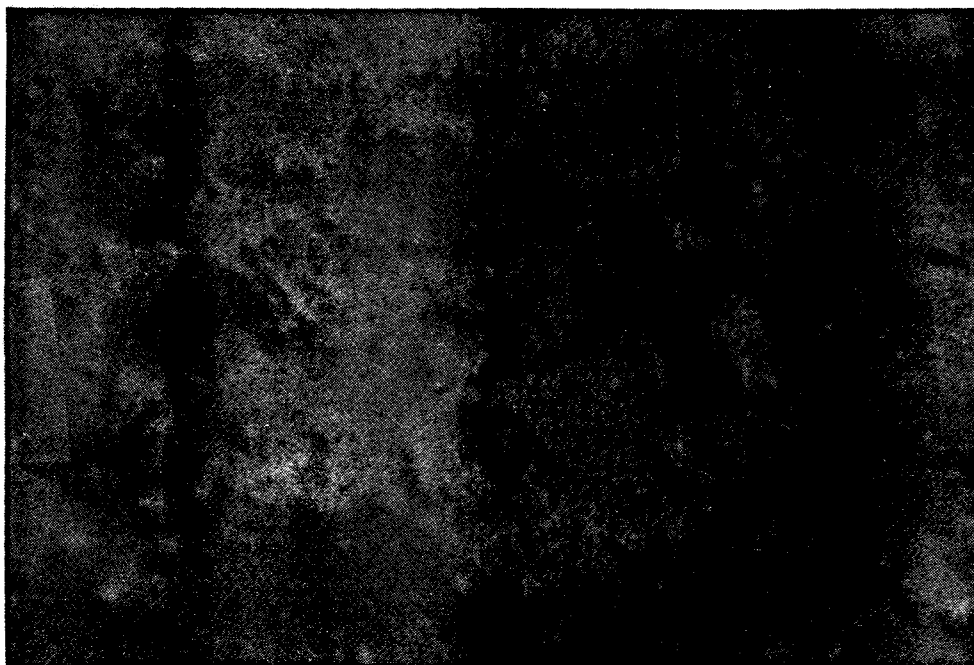
MICROSCOPE PHOTOGRAPHS OF CA MEMBRANE FROM MODULE EX BANK 4 (X 200) AFTER 285 HOURS OPERATION

APPENDIX VI   <u>MICROSCOPE PHOTOGRAPHS OF CALCIUM SULPHATE SEED CRYSTALS</u>
                   <u>FROM MLT PLANT AND COMMERCIAL GYPSUM</u>

APPENDIX VI

<u>MICROSCOPE PHOTOGRAPHS OF CALCIUM SULPHATE SEED CRYSTALS</u>

<u>CALCIUM SULPHATE SEED CRYSTALS EX MLT PLANT (X 200)</u>

<u>COMMERCIAL GRADE GYPSUM USED AS SEED (X 200)</u>

APPENDIX VIII

ANALYSIS OF COMRO TUBULAR CA MEMBRANES

INTRODUCTION

No chemical analyses were done, to determine the extent of possible hydrolysis of the COMRO
membranes received from MEMBRATEK. The titration techniques described in the literature for
determining the hydroxyl or acetyl content of a cellulose acetate polymer are regarded as
insufficiently sensitive and accurate at the levels at which chemical modification (due to
hydrolysis) of the membrane surface would have a serious effect on membrane performance.
For the same reason IR spectral analysis of the membrane material was not considered
worthwhile apart from the fact that the Institute itself does not possess the necessary analytical
equipment to perform any such quantitative tests.

The membrane samples were compared by means of optical microscopy and dye staining.
Samples were also preserved for comparison with membranes to be received at a later date.

REFLECTED-LIGHT DIC MICROSCOPY - MEMBRANE SURFACE DETERIORATION

This optical analytical technique is designed especially for the investigation of smooth-surfaced
objects. The method used highlights surface defects (deformations) and, for that reason, is
ideally suited to investigation of the topography of a membrane surface; scanning electron
microscopy is not suitable.

Sections were cut from the membranes received. The membrane films were not removed from
the support fabric, and the samples were mounted onto glass slides by means of double-sided
masking tape. The membranes were not rinsed clean during preparation of the samples, and
great care was taken not to damage the sample surfaces. Care was also taken to note the axial
cross-flow direction, and any force applied to the membrane surface during mounting of the
sample, was applied perpendicular to the direction of flow.

All the samples were gold-shadowed before microscopic analysis. Photographic records were
made of each of the different samples analysed. The photographs have a final magnification of
1 000x.

In order to have some sort of reference, samples of CA membranes that originated from two
other process applications were also obtained. As a control, fresh, unused CA membranes were
included in the study.

The following membranes were analysed:

1.   Set A: Unused membranes which were taken directly from production storage.

2. Set B: A set of membranes (taken from the inlet, centre and outlet sections of the module) was taken from a module in an RO pilot plant operating on filtered final effluent from an extended aeration sewage plant as feed. (These membranes have been subjected to sponge ball cleaning on occasions).

3. Set C: These membranes originated from an RO application in which small soft crystals of an organic acid are formed during concentration of the feed. No sponge ball cleaning was performed during the period of operation of these membranes.

4. Set 1: The COMRO membranes received as Sample No. 1 (881324).

5. Set 2: The COMRO membranes received as Sample No. 2 (881320).

SURFACE DEPOSITS - OPTICAL AND SEM ANALYSIS

Our Department of Physics has an EDAX facility coupled to their SEM, which would make elemental analysis of the surface deposits possible in principle. Non-adhering crystals were found to be present on the surfaces of the membrane samples investigated, but no evidence was found of fixed deposits or scale.

As an after thought, membrane samples could be rinsed clean with distilled water, the water evaporated, and the collected debris mounted on a carbon stub for elemental analysis. This would give an indication of the collective identity of substances of inorganic nature present within a membrane tube.

SURFACE STAINING - SIGNS OF MEMBRANE MODIFICATION

All the COMRO samples received were subjected to dye staining with an Identification Stain (Du Pont). No photographic records were made, as colour comparison of different membranes over a period of time would virtually be impossible, according to the photographic experts. However, it can be done if all the photographs were to be taken in a single session and the film processed in a single batch.

RESULTS

Microscopic Study

Figure 1 shows the surfaces of unused membranes. There is a marked difference between these membranes and those shown in Figures 4 and 5 which represent COMRO samples No. 1 and 2, respectively.

The streak lines on the membrane surface, caused by scraping of the sponge balls against the membrane, can be seen clearly in Figure 2. No other marks, except the scrape lines and dried bio-film, were present on any of the samples investigated.

Some collision of soft crystals with the membrane surface is evident from the three records shown in Figure 3. These membranes have apparently been operated for several months in a process in which crystals of an organic acid formed during concentration of the feed.

In comparison with Figure 3, Figures 4 and 5 show considerable surface deformation due to impingement of crystal. The direction of fluid-flow, which incidentally is the same on all the photographs, is clearly illustrated as along the length of the photograph.

It appears possible that continuous sustained exposure of the membrane surface to particle bombardment may eventually erode the top layer of the membrane and cause a drop in performance. It appears at present that the deformation which has taken place was purely plastic. However, although no evidence of surface puncturing could be found, the possibility that this has occurred cannot be ruled out completely, as some of the scouring marks noticeable are up to 0,5 μm wide.

Dye Staining

The membranes in both the COMRO sample Sets Nos. 1 and 2 (inlet, centre and outlet samples) stained the same light-yellow tint as did the MEMBRATEK set of unused control membranes.

Furthermore, the COMRO membranes all had radial indentations which corresponded to the parting line between the plastic pressure support disks of the tubular module. In addition to the light-yellow tint, the COMRO membranes also showed slight red discolouration along some of these indentation lines. An unused control membrane sample, which had been exposed to a 10 per cent NaOH solution for 5 minutes, stained a shade of green when it was subjected to a similar dye test. It is uncertain whether the red stain can be ascribed to a chemical or physical alteration of the membrane surface/material.

From fluid dynamic considerations it is however to be expected that concentration build-up in the indented areas would be higher than on the ridges between the indents. The likely occurrence of hydrolysis would, for the same reason, be higher in these areas.

Samples of the sets of membranes already received will be preserved and used for comparison in staining experiments to be conducted on future membranes to establish qualitatively whether the membrane actually deteriorates along the indentation lines.

SUGGESTION

The possibility that a protective coating might reduce or prevent erosion of the membrane surface could be considered.

Dr E P Jacobs
Institute for Polymer Science
University of Stellenbosch

24 July 1989
Report COMRO1

Figure 1   MICROGRAPHS (1000X MAGNIFICATION) OF THE SURFACE OF TUBULAR CA
            MEMBRANES - FRESH, UNUSED

Set A: Inlet, Centre and Outlet
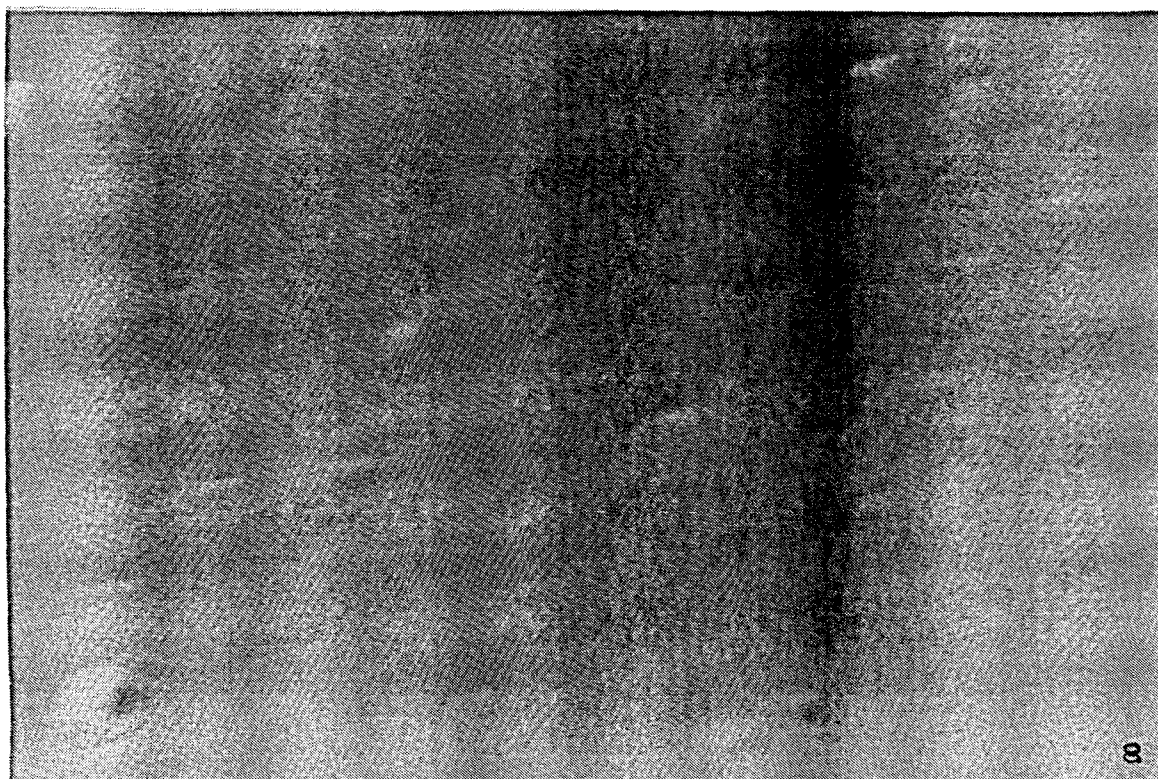
INLET

CENTRE

CONTINUED

Figure 1 <u>MICROGRAPHS (1000X MAGNIFICATION) OF THE SURFACE OF TUBULAR CA</u>
<u>MEMBRANES - FRESH, UNUSED</u>
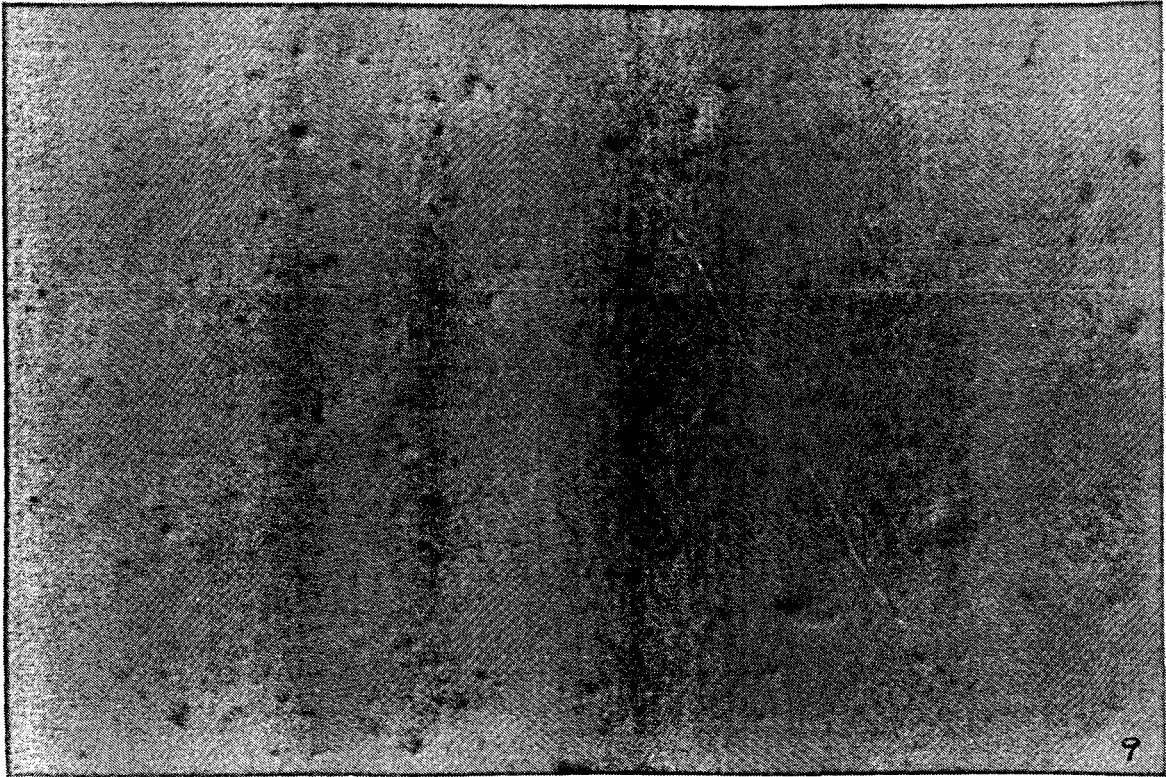
OUTLET

Figure 2   MICROGRAPHS (1000X MAGNIFICATION) OF THE SURFACE OF TUBULAR CA
MEMBRANES - TREATED SEWAGE

Set B: Inlet, centre and outlet

INLET

CENTRE

CONTINUED

Figure 2   <u>MICROGRAPHS (1000X MAGNIFICATION) OF THE SURFACE OF TUBULAR CA</u>
            <u>MEMBRANES - TREATED SEWAGE</u>

OUTLET

Figure 3   MICROGRAPHS (1000X MAGNIFICATION) OF THE SURFACE OF TUBULAR CA
MEMBRANES - ORGANIC ACID CRYSTALS PRESENT

Set C: Inlet, centre and outlet

INLET

CENTRE

CONTINUED

Figure 3   MICROGRAPHS (1000X MAGNIFICATION) OF THE SURFACE OF TUBULAR CA
            MEMBRANES - ORGANIC ACID CRYSTALS PRESENT

OUTLET

Figure 4   <u>MICROGRAPHS (1000X MAGNIFICATION) OF THE SURFACE OF TUBULAR CA</u>
<u>MEMBRANES - SEEDED SLURRY - COMRO MEMBRANES</u>

Set 1: Inlet, centre and outlet

INLET

CENTRE

CONTINUED

Figure 4   MICROGRAPHS (1000X MAGNIFICATION) OF THE SURFACE OF TUBULAR CA
            MEMBRANES - SEEDED SLURRY - COMRO MEMBRANES

OUTLET

Figure 5   MICROGRAPHS (1000X MAGNIFICATION) OF THE SURFACE OF TUBULAR CA MEMBRANES - SEEDED SLURRY - COMRO MEMBRANES

Set 2:   Inlet, centre and outlet
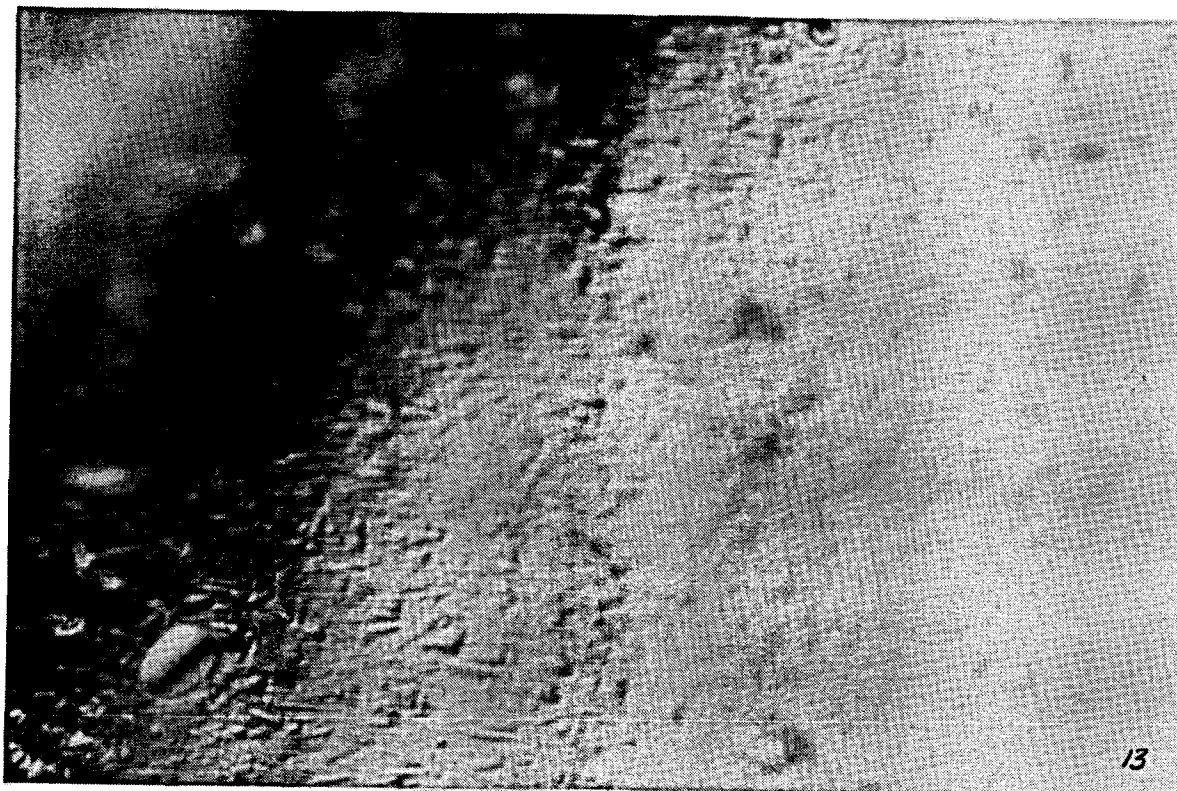
INLET
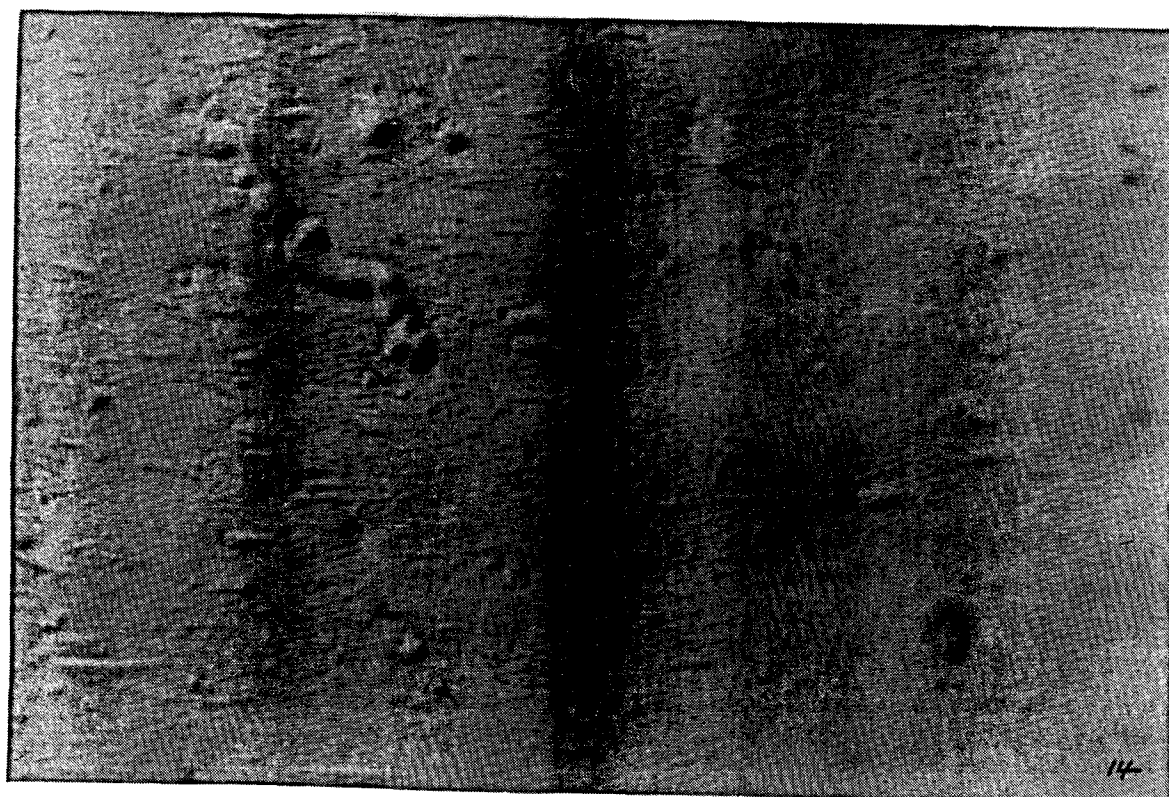
CENTRE

CONTINUED

Figure 5   <u>MICROGRAPHS (1000X MAGNIFICATION) OF THE SURFACE OF TUBULAR CA</u>
<u>MEMBRANES - SEEDED SLURRY - COMRO MEMBRANES</u>
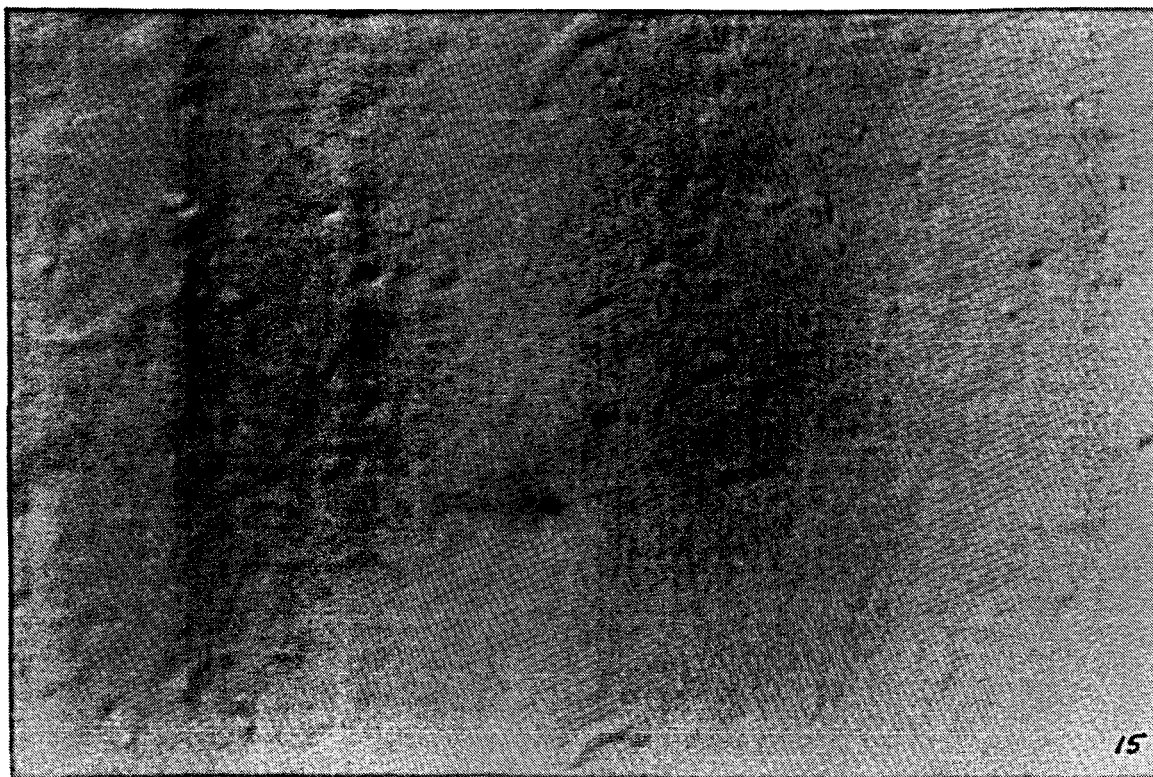
OUTLET

ANALYSIS OF MEMBRANE SAMPLES
SECOND MODULE SAMPLE SET

INTRODUCTION

Two sets of membrane samples were received from Membratek for analysis, one set marked Module 3 (881295) and the other Module 4 (881502); each set of membranes taken from the inlet, centre and outlet of each module.

OPTICAL MICROSCOPY - Differential Interference Contrast (DIC)

Sample Preparation

Samples were prepared for optical microscopy by cutting 6 cm-lengths from the various tubes. These samples were mounted on glass slides, and in order to get some indication of possible foulant deposits, the surfaces of the membrane samples were never touched by hand during sample preparation.

The samples were allowed to dry out naturally and were sputter-coated with gold before being analysed.

Observations

There were marked differences between the appearance of membranes from Modules 3 and 4 and those of Modules 1 and 2 received previously. Radial bands of up to 14 mm, and dull in contrast to the remainder of the membrane films which were still shiny in appearance, extended at intervals across the length of the samples analysed. Initially this was observed only after sputter-coating with gold. However, when once observed, it was also recognized on other samples once the surfaces of the membranes were wiped clean of any loose surface deposits or debris.

DIC micrographs were taken of sections of the various samples received (1000x magnification). As in the case of Modules 1 and 2 earlier investigated (Report COMRO1), erosion marks, caused by particle impingement, were again present as can be seen from Figure 1 (Module 3: Inlet, centre and outlet) and Figure 2 (Module 4: Inlet, centre and outlet).

Deposits were present in a greater or lesser extent on all of the samples analysed. (Module 3 seems to be less affected than Module 4). Cases were observed where deposits seem to have nucleated from scour marks left by larger-sized particle impingement on the membrane surface. (Figure 3 is an example of this occurring in Module 3: Inlet and centre sections). Figure 4 shows evidence of some scale deposit (Module 3: Centre and outlet).

Except for brief examination during EDAX analysis, the membranes were not investigated by means of SEM. During optical microscopy evaluation of the various samples, no obvious evidence was found of gross structural damage to the membrane body.

However, a strange phenomenon was noticed during the analysis of samples from Module 4 membranes. Previously, the marks on the membrane surfaces were all essentially unidirectional, and clearly in the axial direction of fluid flow. In Module 4 (see Figure 5), the membrane surface carried impressions which were clearly not unidirectional. A possible explanation for these randomly orientated marks is that they were formed by crystals of some sort, which had been forced into the membrane surface under the action of hydrostatic pressure. However, no evidence of the presence of long-shaped crystals could be found anywhere during microscopic analysis.

STAINING

Samples from the various membrane sets were rinsed clean with a 5 per cent acetic acid solution and rinsed thoroughly before being stained with identification stains obtained from Du Pont.

In comparison to membranes from the earlier received modules, membranes from Modules 3 and 4 differed in the way in which they stained under the action of the dye. This was regarded as some indication that the chemistry of the membrane material may have been affected.

FOURIER TRANSFORM INFRARED (FTIR)

To gain some proof for the above observation, membrane samples were taken for FTIR analysis. The samples were analysed using the ATR facility on the instrument as the membrane films abstracted from the support fabric were not clear. Unfortunately the spectra obtained during this part of the exercise were of little value in the end due to low emission levels.

However, during experiments to dissolve membrane films taken from Modules 3 and 4 and membrane films taken from freshly produced CA membranes (Membratek supplied) and virgin CA 398-10 cellulose di-acetate powder (IPS stock), differences in solubility behaviour was noticed.

Virgin membrane films and powder dissolved in acetone and swelled in chloroform. However, Module 3 and 4 samples only swelled in acetone, whereas chloroform left the films unaffected.

This was thought to be in further evidence that the chemistry of the membranes had been modified, although it could not be quantified due to the unavailability of the FTIR equipment.

EDAX ANALYSIS OF DEPOSITS ON MEMBRANE SURFACE

Specimen membranes were carbon-coated for elemental analysis of surface deposits by EDAX.

A representative elemental analysis of the deposits is shown in an EDAX printout (Figure 6). According to this analysis there is little presence of $CaSO_4$ in the deposit. Deposits appear mainly to consist of aluminium and silicon (probably aluminium silicates), and to a lesser extent iron and calcium (sulphates). (In retrospect, the tiny ($< 0,1$ μm) crystals that were seen during polarized light microscopy is therefore most probably of quartz origin).

CONCLUSION

Without the benefit of comparing the analysis given to that of a module that has accumulated the same number of operating hours, and which is still in good performance, the following can be said:

1. The surfaces of the membranes analysed appear to be eroded to a greater extent than those of Modules 1 and 2 (report COMRO1).

2. Surface deposits, consisting mainly of aluminium-silicates, were observed, especially in the case of Module 4.

3. According to solvent solubility differences, the COMRO samples are believed to be chemically different from the virgin membrane samples and powder analysed. (However, the latter is very much dependant on whether the same source and grade of material was used as reference material).

4. Based on the samples analysed from Modules 3 and 4, no reason, other than the possibility of hydrolysis, can be offered for the lower performance of the membrane specimens received.

SUGGESTIONS

1. The Institute will approach Membratek for 500 mm-sections of membranes from Modules 3 and/or 4. The membranes will be coated with supplemental polymers to establish whether it would be possible to restore the performance of the membranes. If positive results are obtained, arrangements can be made for module evaluation and dissemination of the results of the study.

2. The IPS can make tubular membrane test cells (400 - 500 mm long) available to COMRO, on either a hire or purchase basis, to allow close observation of single membrane performance. (Such cells can be piped into the end of a module train). This offers the advantage that single membranes can be removed for inspection at the first sign of performance deterioration. This might allow some insight into possible cause of membrane failure.

E P Jacobs
Institute for Polymer Science
University of Stellenbosch
02231/773172

Figure 1   <u>SURFACE EROSION PRESENT IN MODULE 3 (Inlet, centre and outlet)</u>
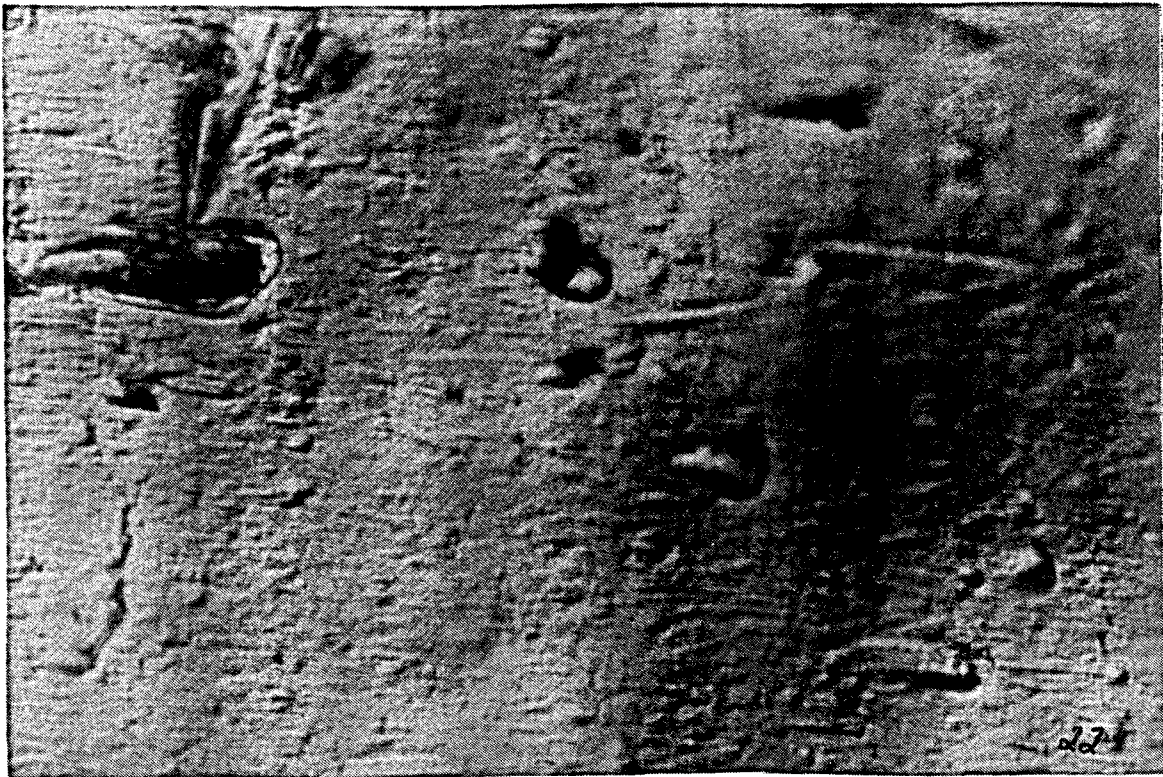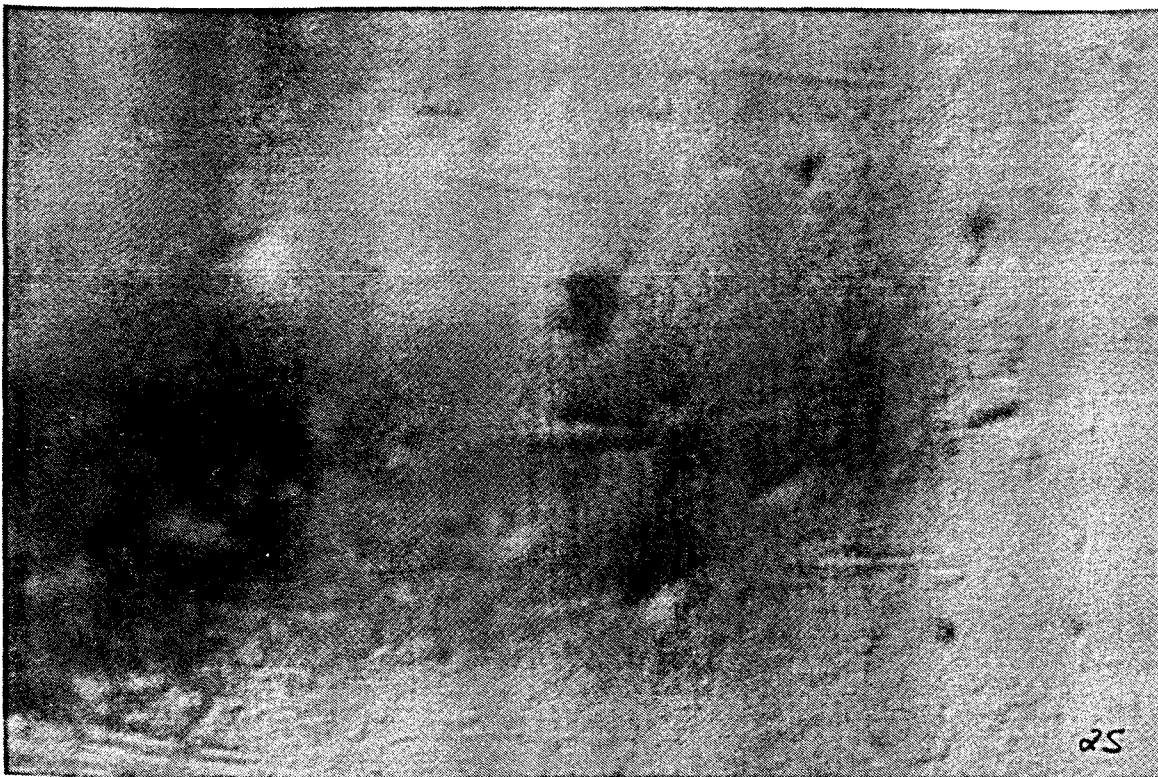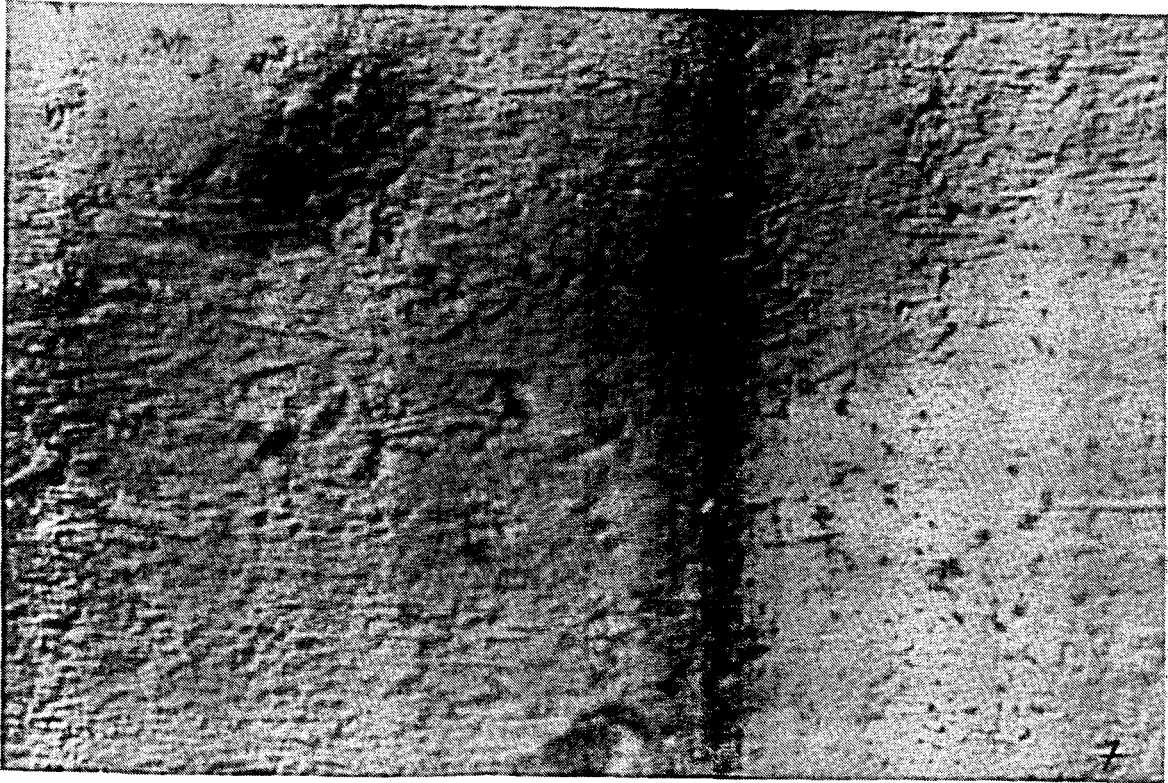
INLET

CENTRE

OUTLET

Figure 2   <u>SURFACE EROSION PRESENT IN MODULE 4 (Inlet, centre and outlet)</u>
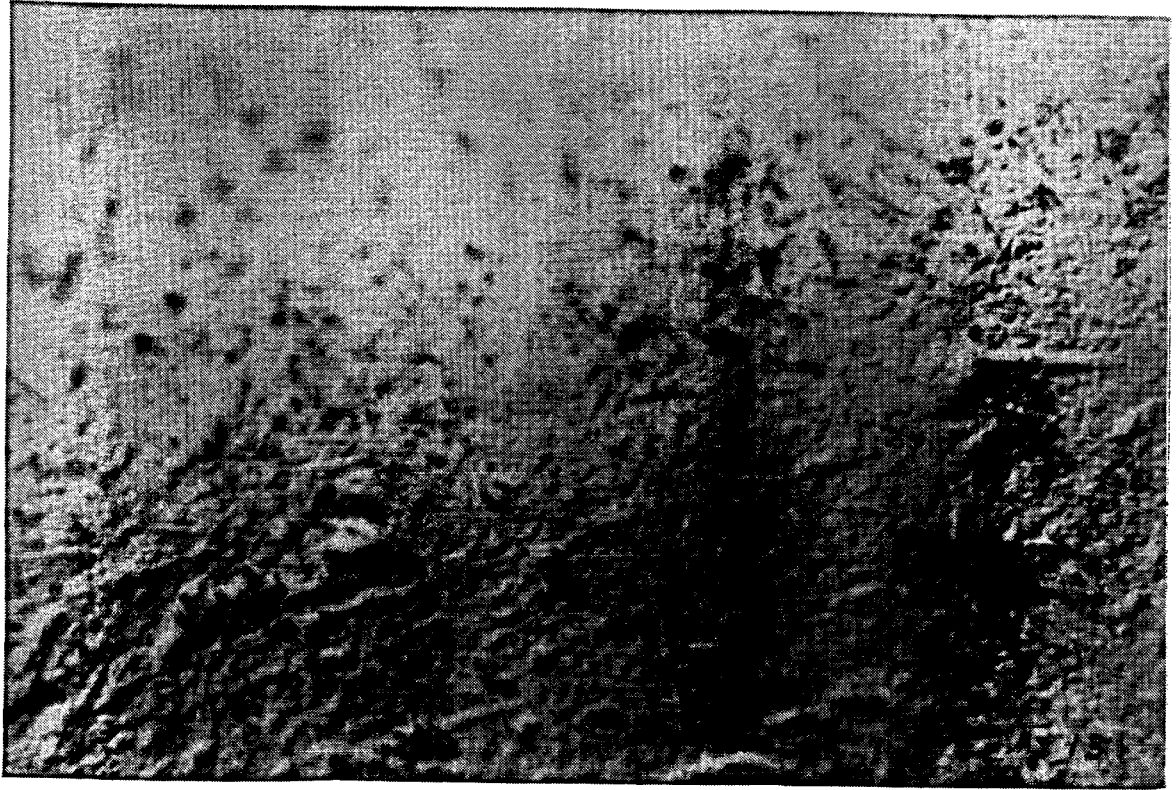
INLET

CENTRE

OUTLET

Figure 3   ALUMINIUM/SILICATE-RICH DEPOSITS NUCLEATING FROM SURFACE EROSION
MARKS (Module 3: Inlet, centre)
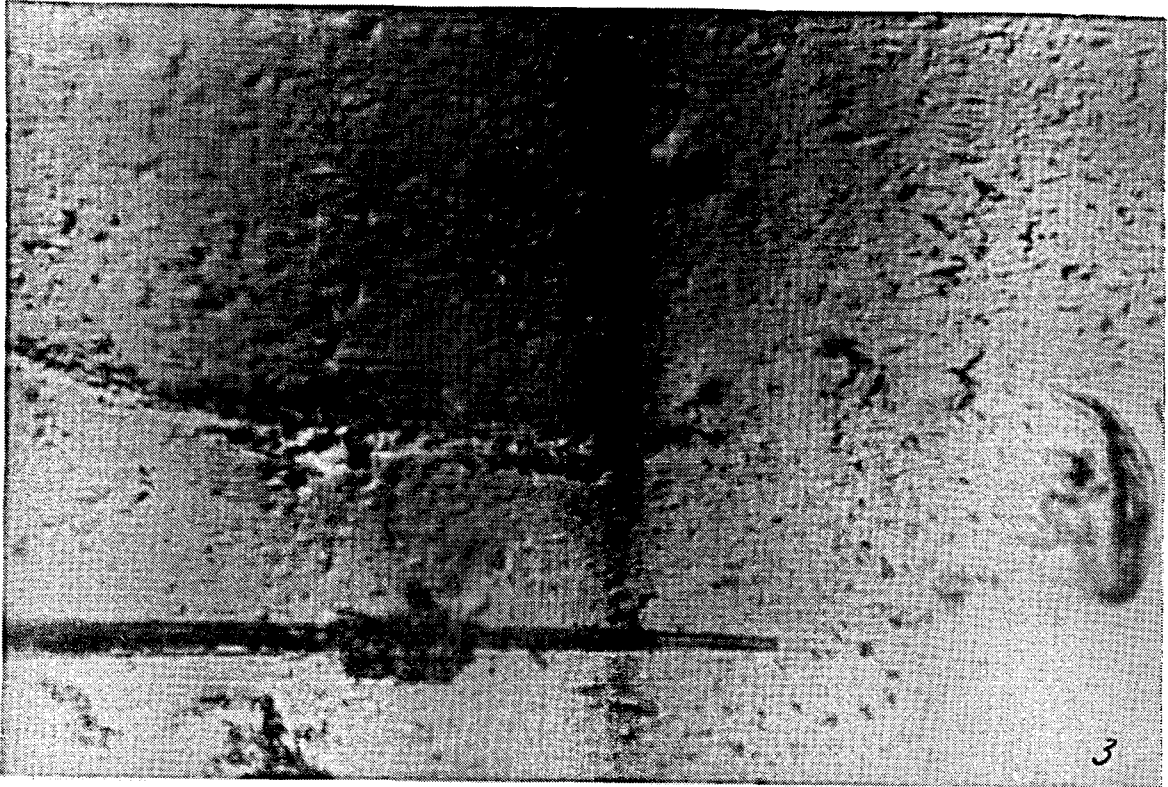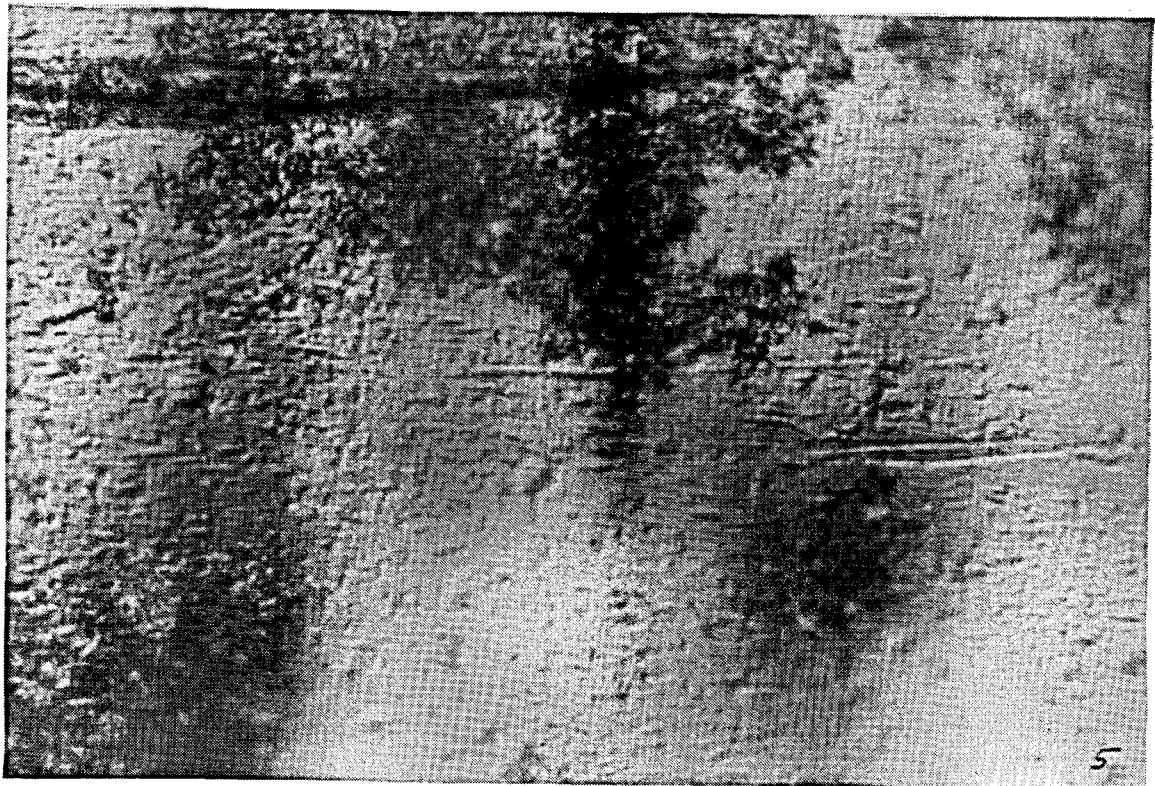
INLET

CENTRE

Figure 4   <u>SURFACE DEPOSITS FOUND PRESENT IN MODULE 3 AND 4 (Module 3: Inlet,</u>
<u>centre)</u>
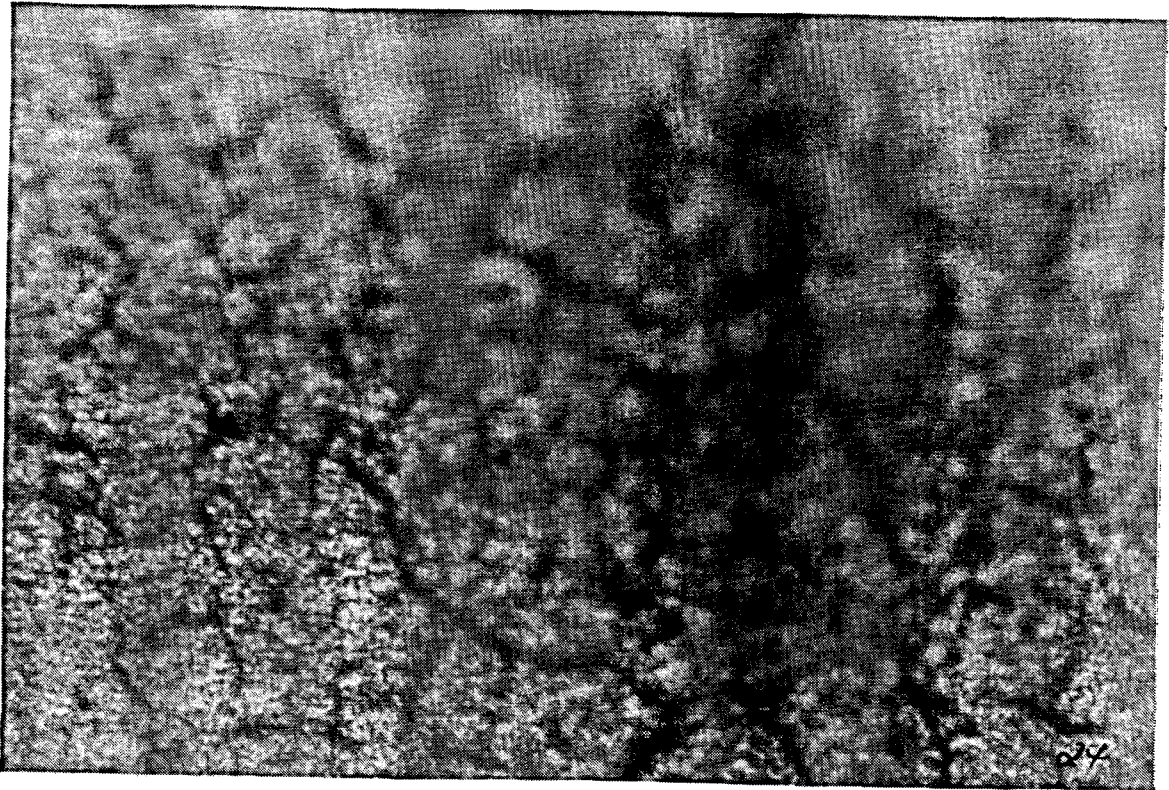
INLET

CENTRE

Figure 5   RANDOM DIRECTION IMPRESSIONS FOUND PREDOMINANTLY IN MODULE 4
(Module 4: Centre, Centre, Outlet)
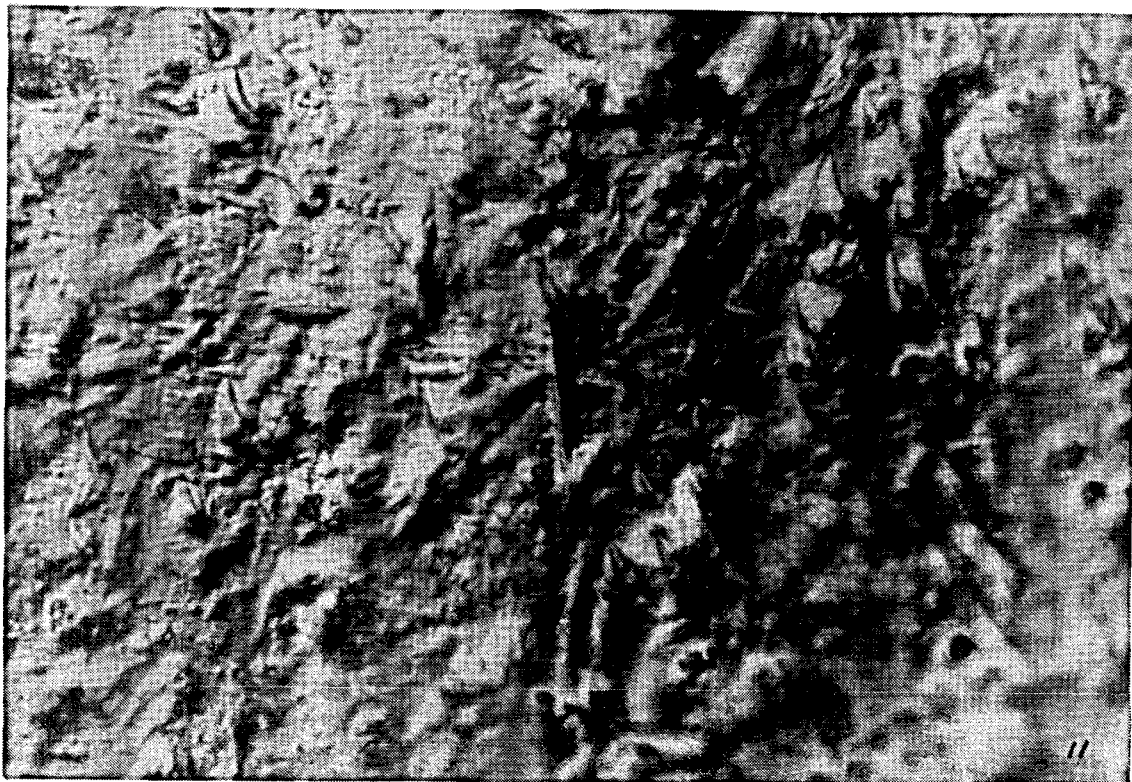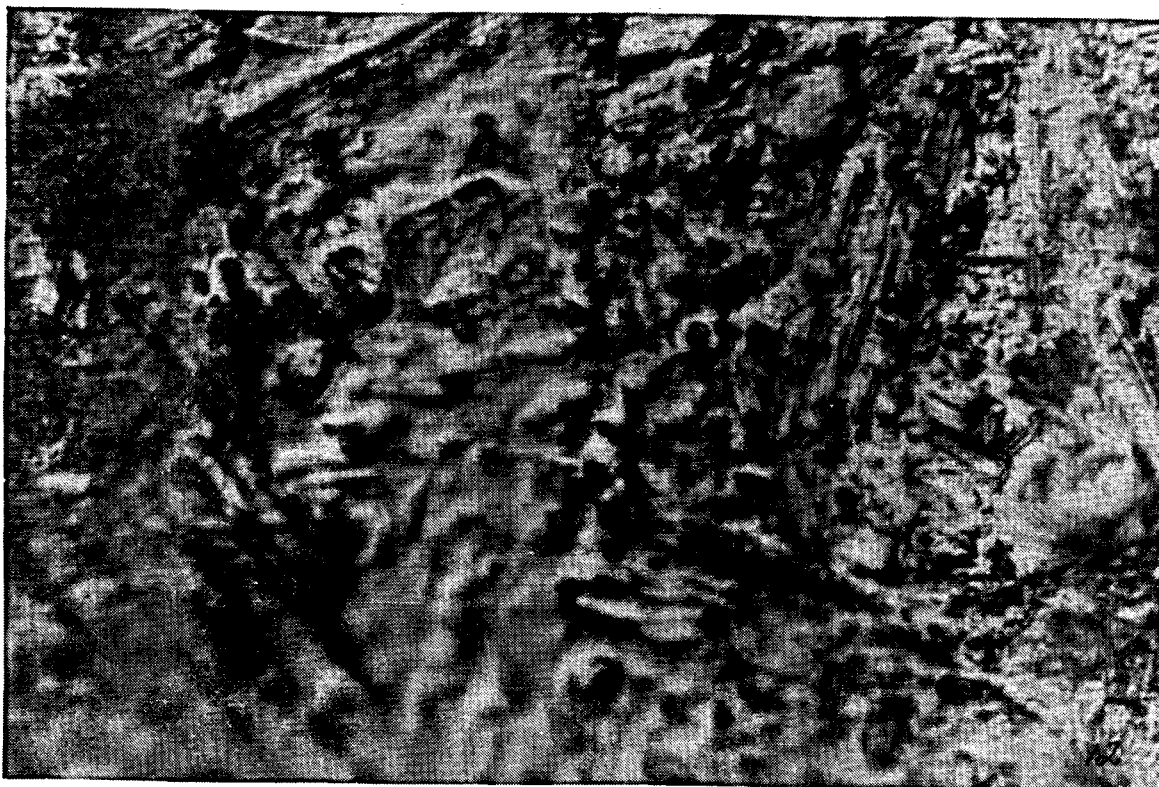
CENTRE

CENTRE
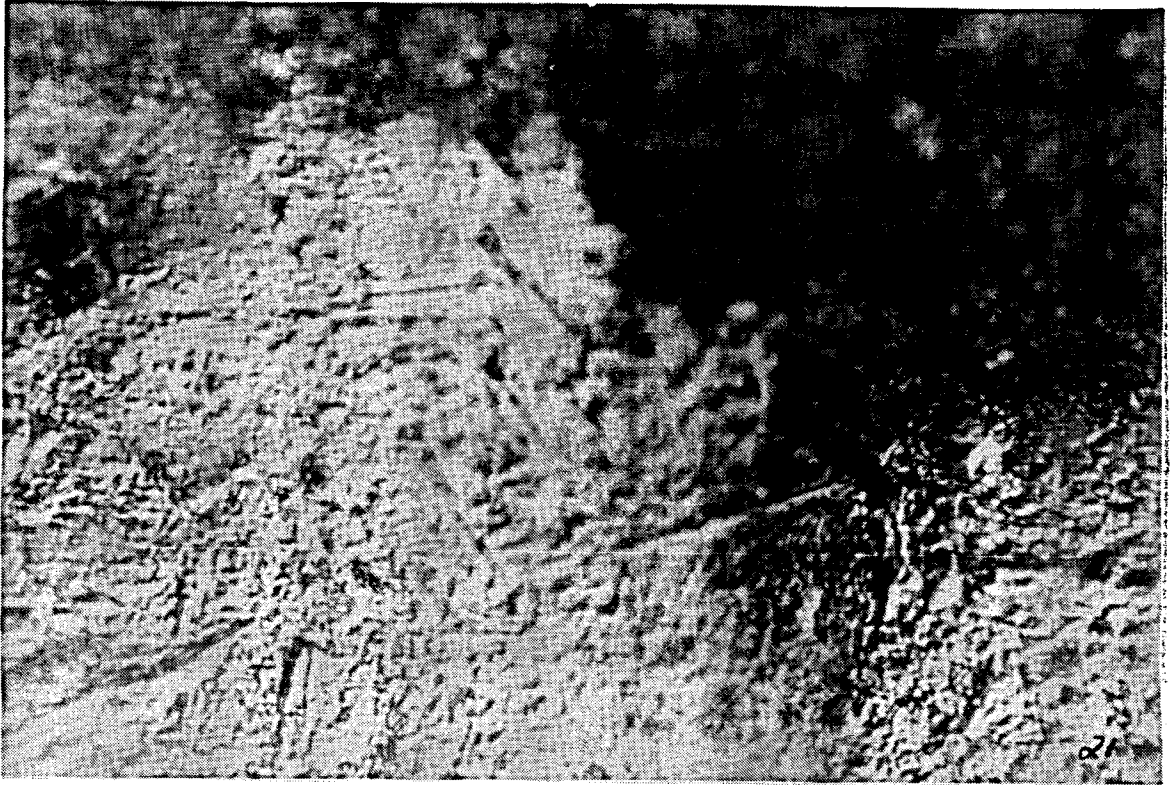
OUTLET

Figure 6   EDAX SPECTRA AND EXPLANATION OF ELEMENTAL ANALYSIS
            REPRESENTATIVE OF FOULANT LAYER FOUND IN MODULE 4
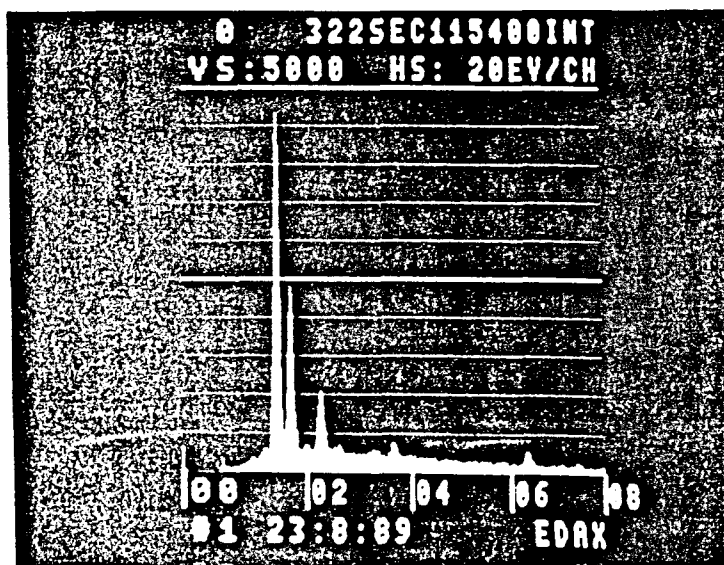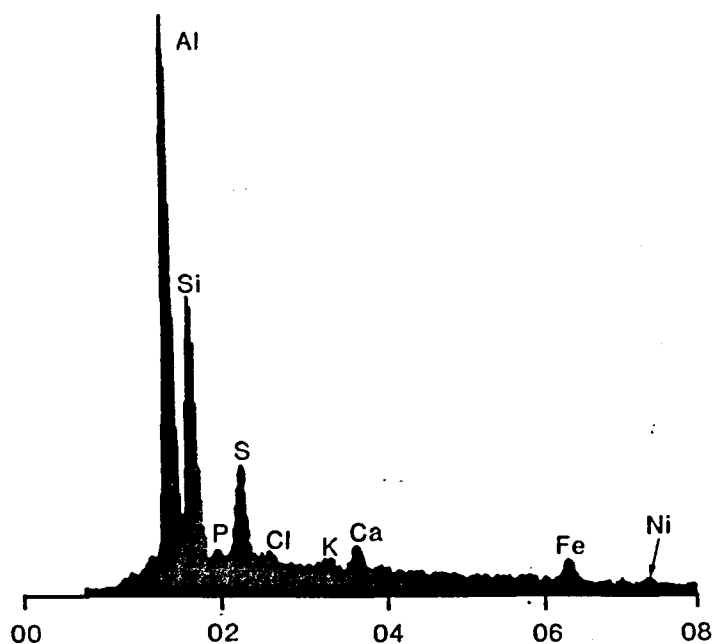
APPENDIX V

<u>MICROSCOPE PHOTOGRAPHS OF CELLULOSE ACETATE MEMBRANE THAT FAILED IN</u>
<u>SPARRO PLANT</u>
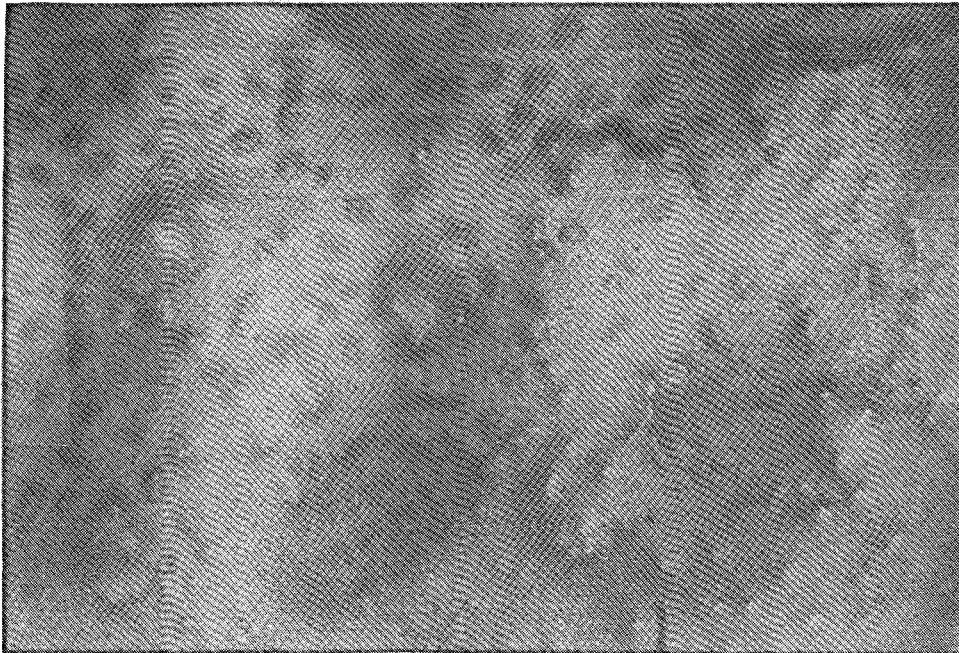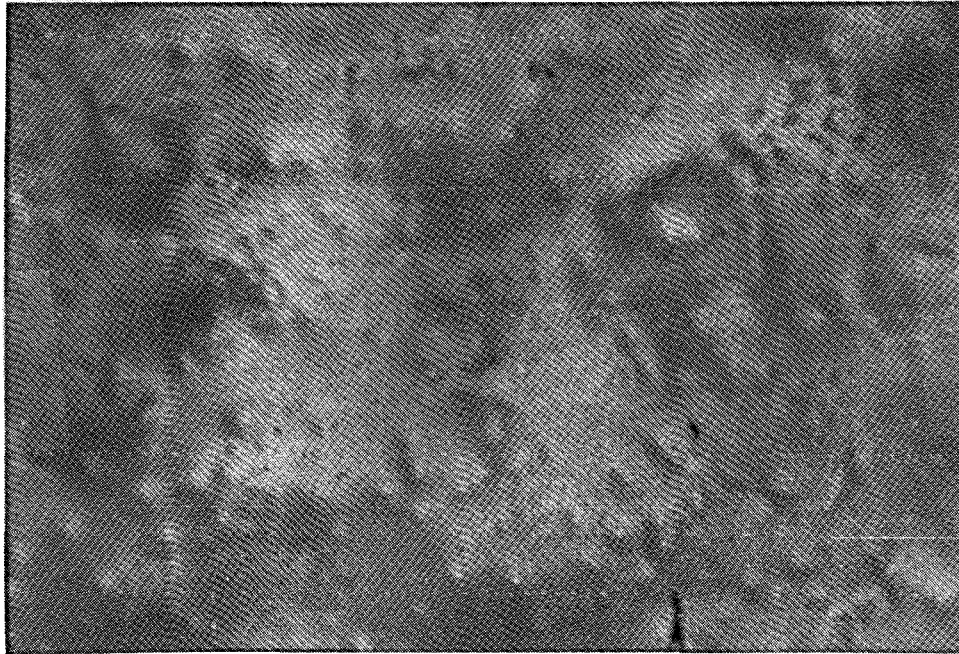
<u>MICROSCOPE PHOTOGRAPHS OF CA MEMBRANE FROM MODULE EX BANK 4 (X 200) AFTER</u>
<u>285 HOURS OPERATION</u>

APPENDIX VI

MICROSCOPE PHOTOGRAPHS OF CALCIUM SULPHATE SEED CRYSTALS
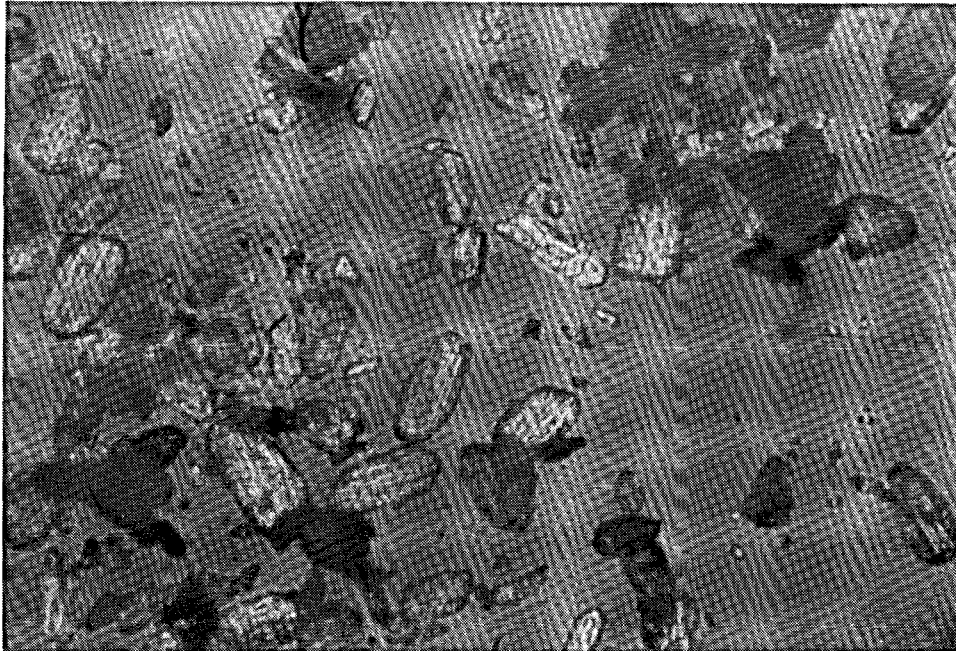
CALCIUM SULPHATE SEED CRYSTALS EX MLT PLANT (X 200)
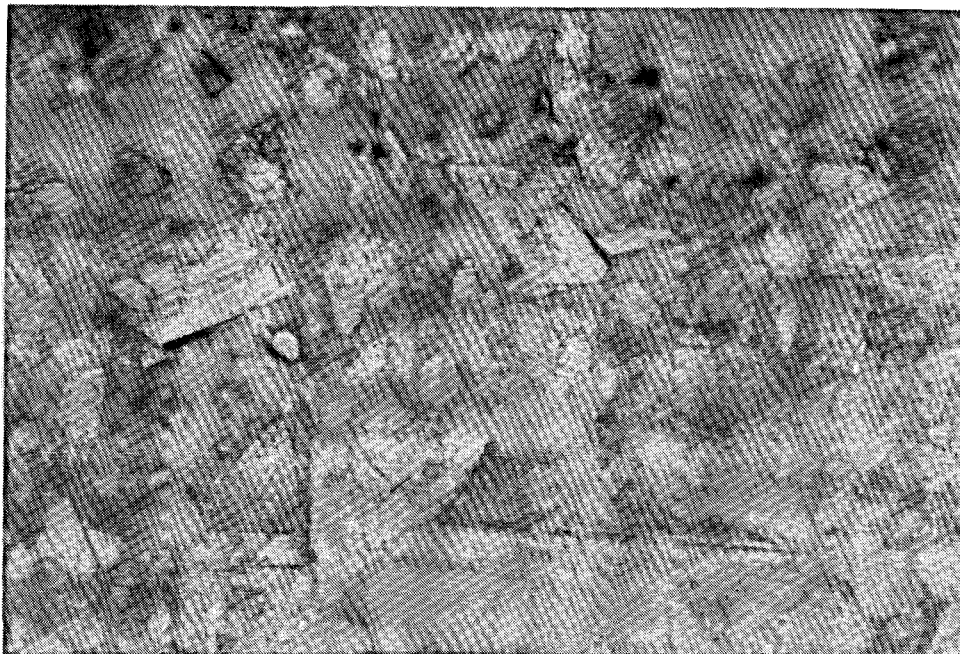
COMMERCIAL GRADE GYPSUM USED AS SEED (X 200)

Figure 1   <u>MICROGRAPHS (1000X MAGNIFICATION) OF THE SURFACE OF TUBULAR CA</u>
            <u>MEMBRANES - FRESH, UNUSED</u>

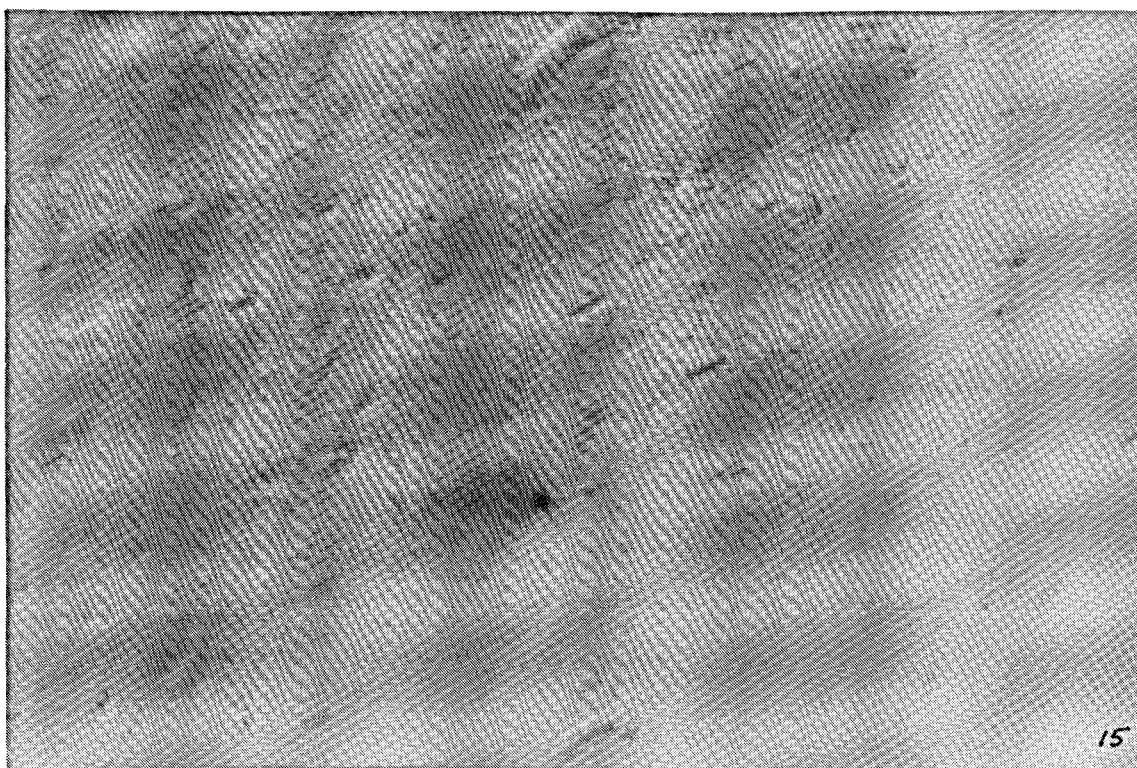Set A: Inlet, Centre and Outlet

INLET

CENTRE

CONTINUED

Figure 1   <u>MICROGRAPHS (1000X MAGNIFICATION) OF THE SURFACE OF TUBULAR CA</u>
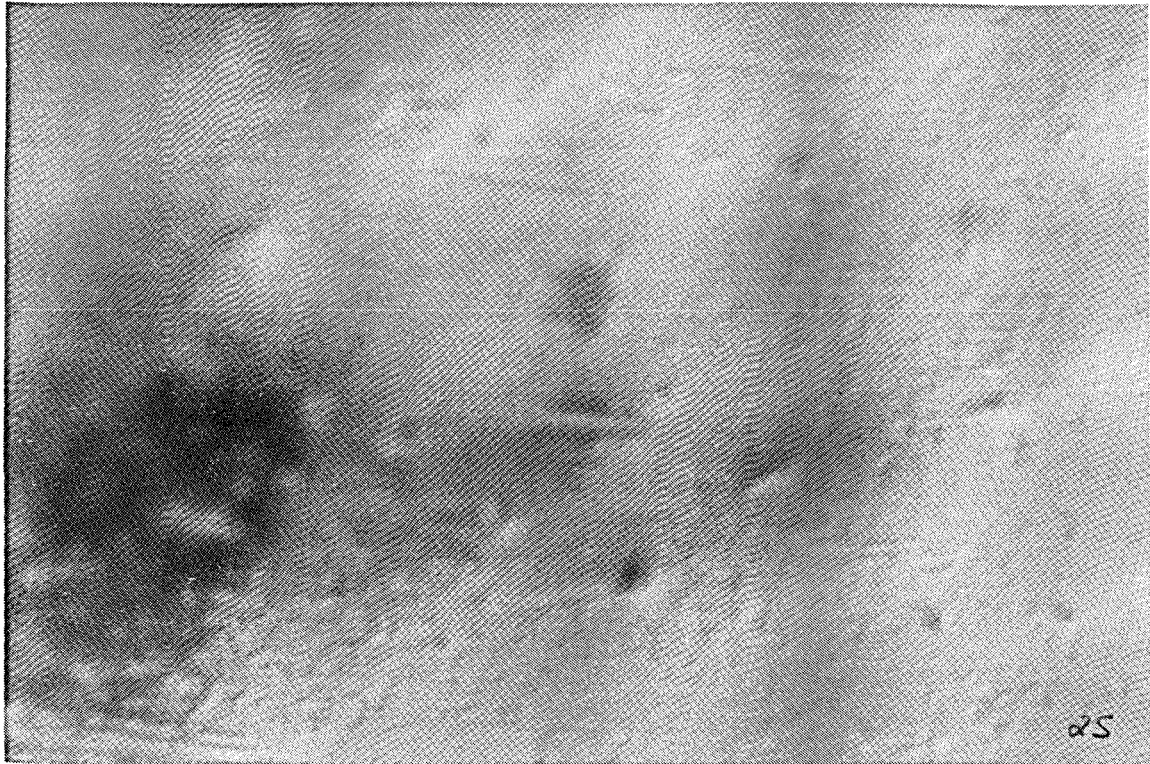   <u>MEMBRANES - FRESH, UNUSED</u>

OUTLET

125

Figure 2   <u>MICROGRAPHS (1000X MAGNIFICATION) OF THE SURFACE OF TUBULAR CA</u>
            <u>MEMBRANES - TREATED SEWAGE</u>

Set B: Inlet, centre and outlet

INLET

CENTRE

CONTINUED

Figure 2   <u>MICROGRAPHS (1000X MAGNIFICATION) OF THE SURFACE OF TUBULAR CA</u>
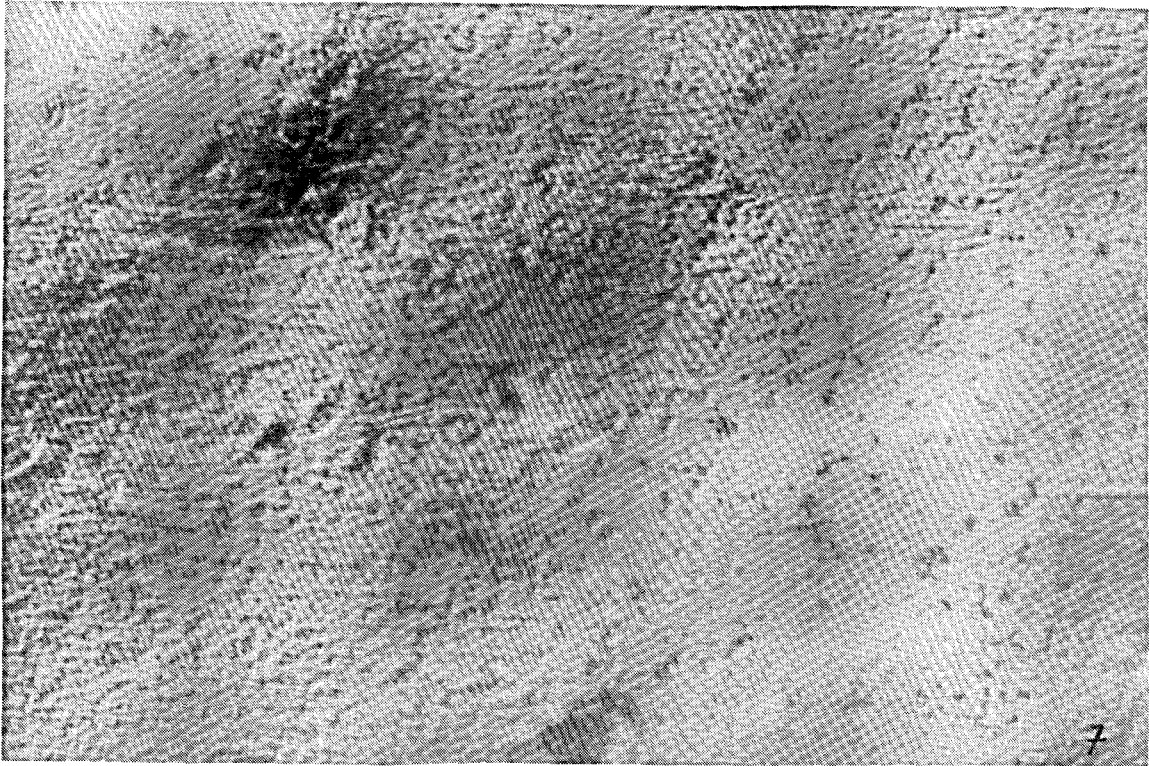<u>MEMBRANES - TREATED SEWAGE</u>

OUTLET

Figure 3   MICROGRAPHS (1000X MAGNIFICATION) OF THE SURFACE OF TUBULAR CA
MEMBRANES - ORGANIC ACID CRYSTALS PRESENT

Set C: Inlet, centre and outlet

INLET

CENTRE

CONTINUED

Figure 3   MICROGRAPHS (1000X MAGNIFICATION) OF THE SURFACE OF TUBULAR CA
            MEMBRANES - ORGANIC ACID CRYSTALS PRESENT

OUTLET

Figure 4   MICROGRAPHS (1000X MAGNIFICATION) OF THE SURFACE OF TUBULAR CA
            MEMBRANES - SEEDED SLURRY - COMRO MEMBRANES

Set 1: Inlet, centre and outlet

INLET

CENTRE

CONTINUED

Figure 4   <u>MICROGRAPHS (1000X MAGNIFICATION) OF THE SURFACE OF TUBULAR CA</u>
            <u>MEMBRANES - SEEDED SLURRY - COMRO MEMBRANES</u>

OUTLET

131

Figure 5   MICROGRAPHS (1000X MAGNIFICATION) OF THE SURFACE OF TUBULAR CA MEMBRANES - SEEDED SLURRY - COMRO MEMBRANES

Set 2:   Inlet, centre and outlet

INLET

CENTRE

CONTINUED

Figure 5   <u>MICROGRAPHS (1000X MAGNIFICATION) OF THE SURFACE OF TUBULAR CA
            MEMBRANES - SEEDED SLURRY - COMRO MEMBRANES</u>

OUTLET

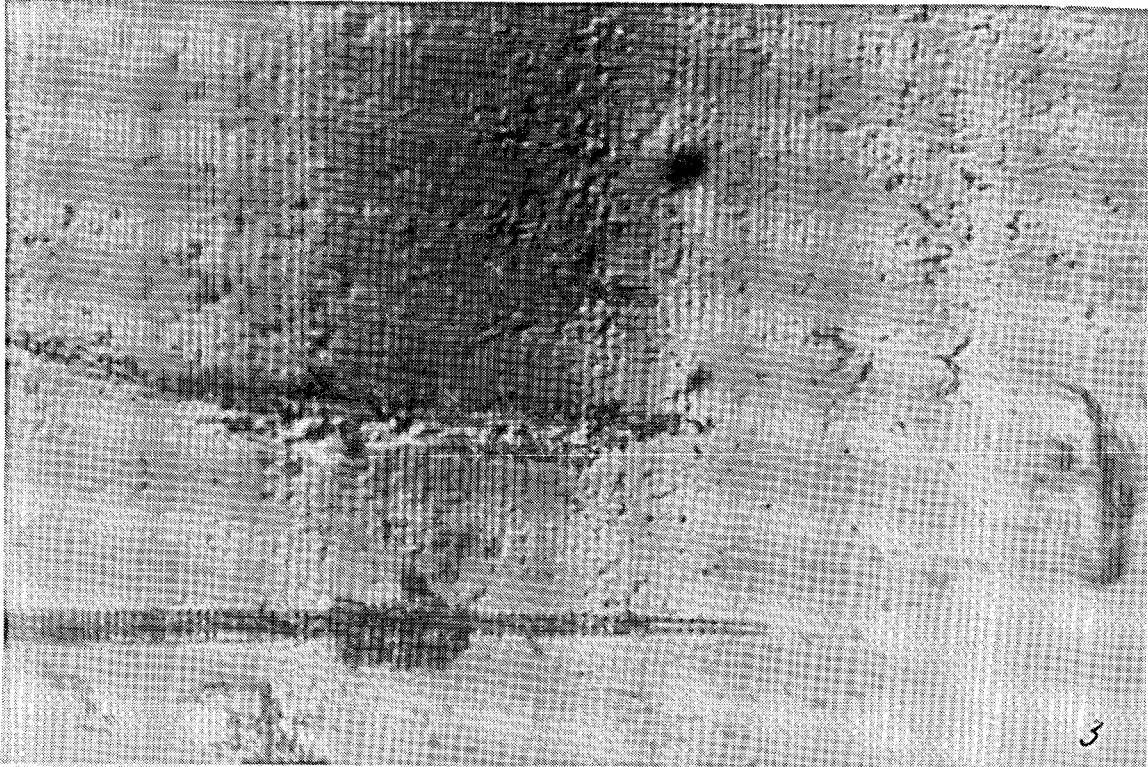Figure 1   <u>SURFACE EROSION PRESENT IN MODULE 3 (Inlet, centre and outlet)</u>

INLET

CENTRE

OUTLET

Figure 2   SURFACE EROSION PRESENT IN MODULE 4 (Inlet, centre and outlet)
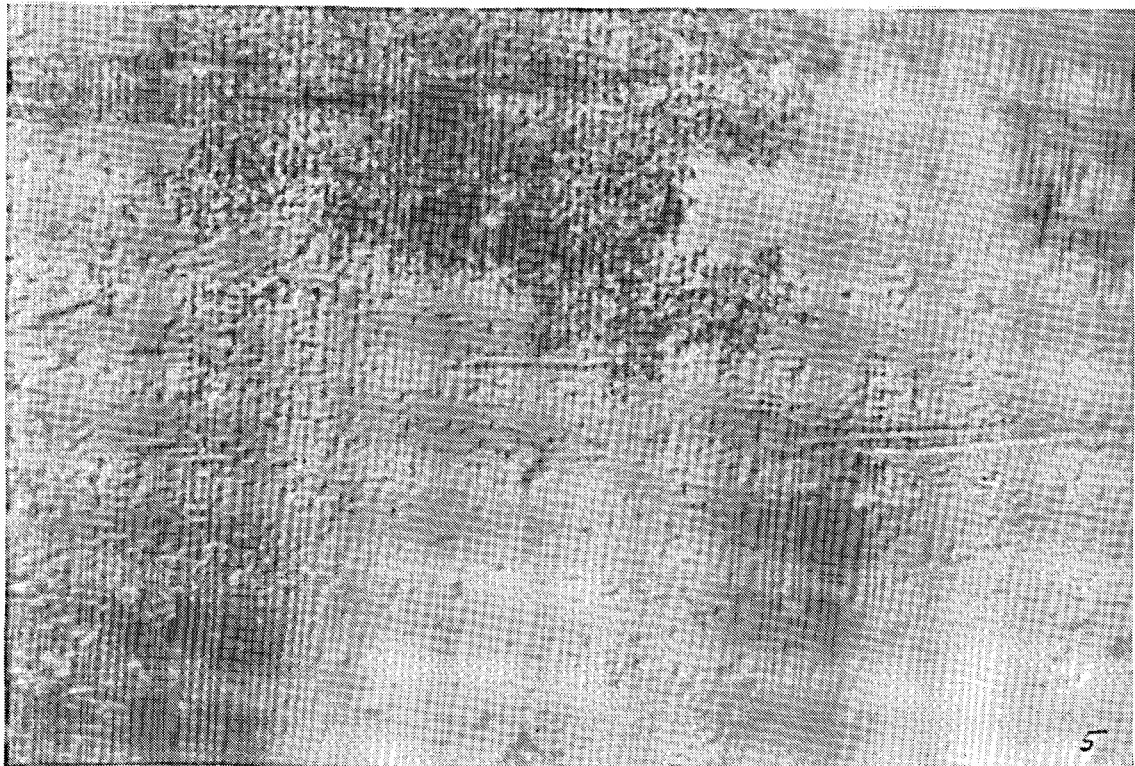

INLET

CENTRE

OUTLET

Figure 3   ALUMINIUM/SILICATE-RICH DEPOSITS NUCLEATING FROM SURFACE EROSION
            MARKS (Module 3: Inlet, centre)
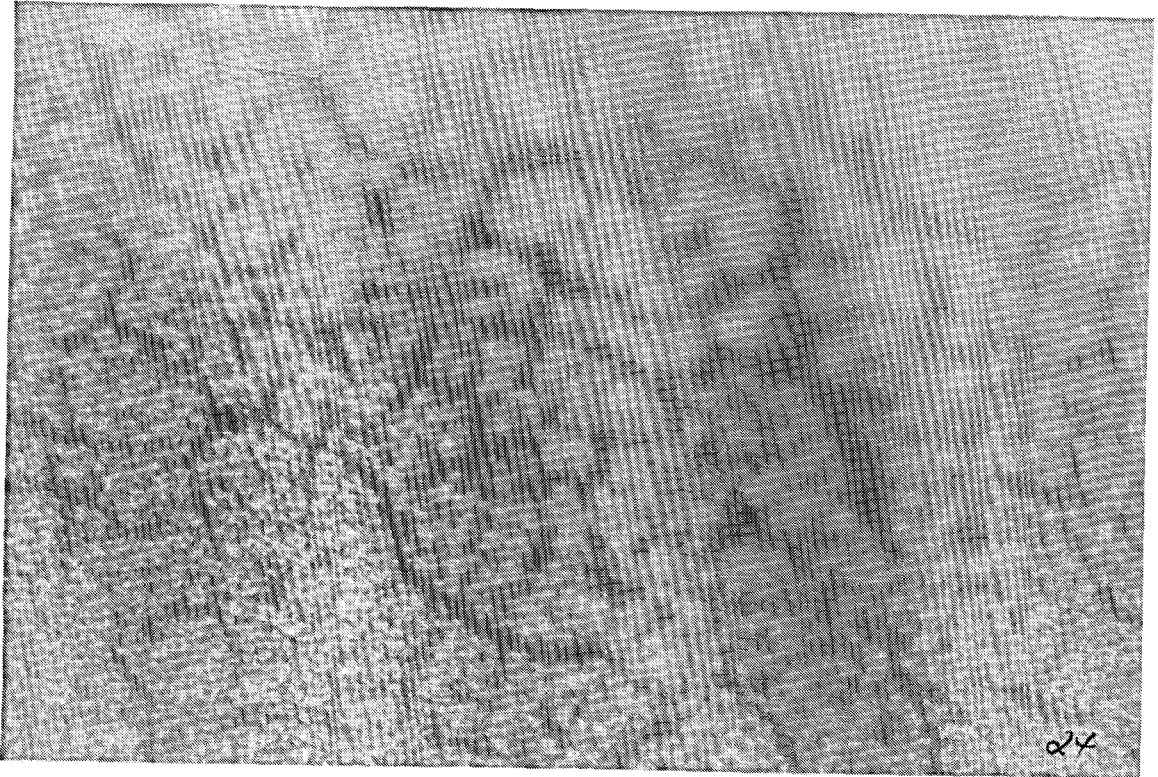

INLET

CENTRE

Figure 4   SURFACE DEPOSITS FOUND PRESENT IN MODULE 3 AND 4 (Module 3: Inlet, centre)
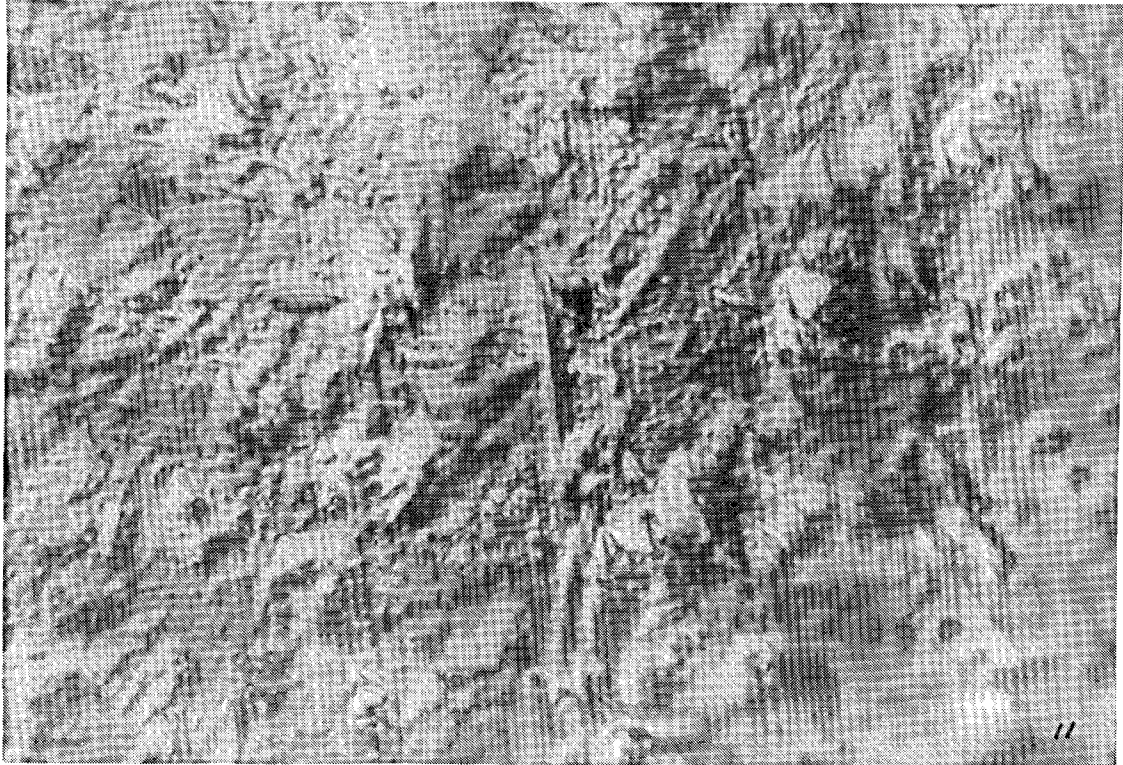

INLET

CENTRE

Figure 5   RANDOM DIRECTION IMPRESSIONS FOUND PREDOMINANTLY IN MODULE 4
(Module 4: Centre, Centre, Outlet)

CENTRE

CENTRE

OUTLET